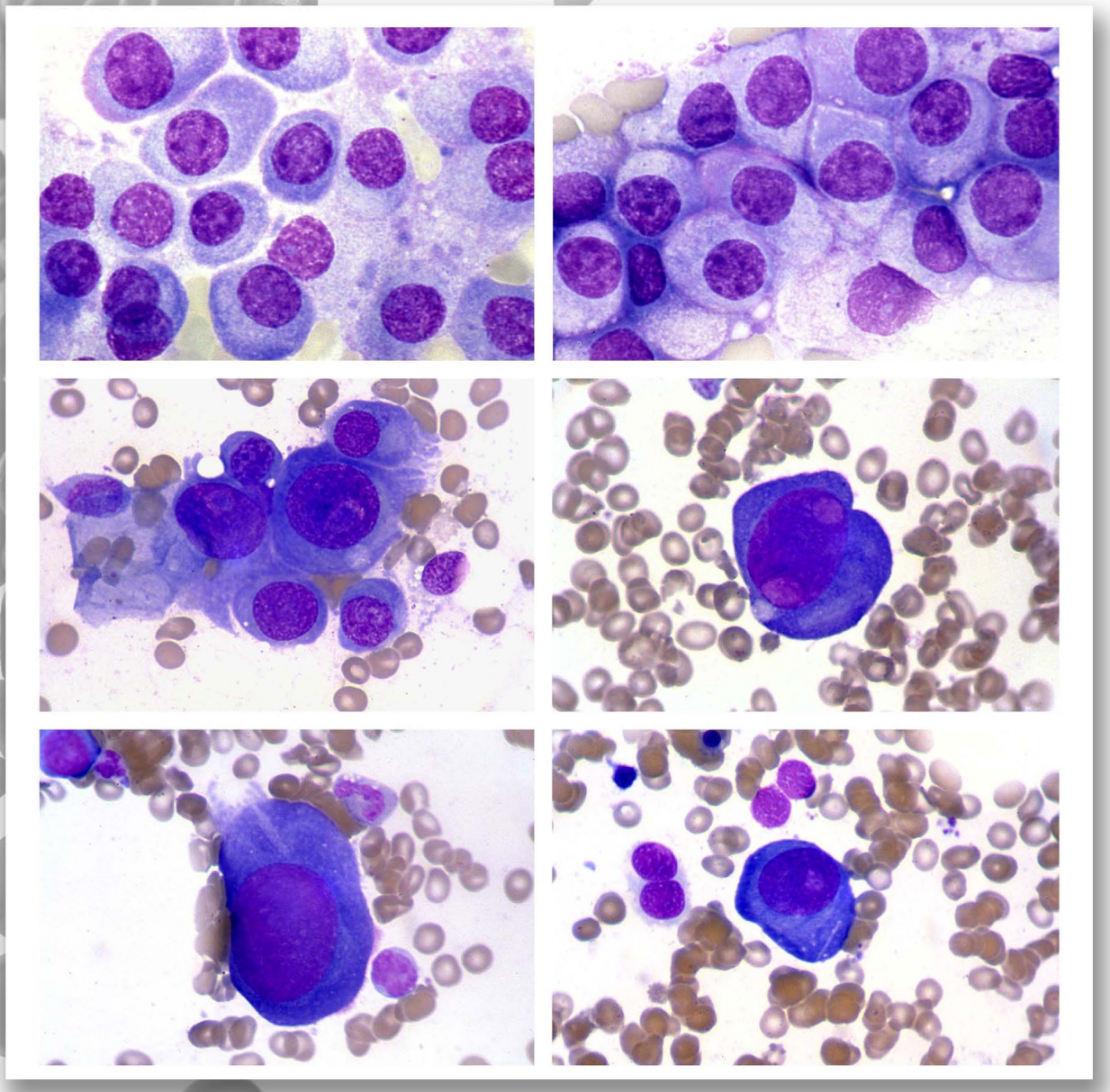
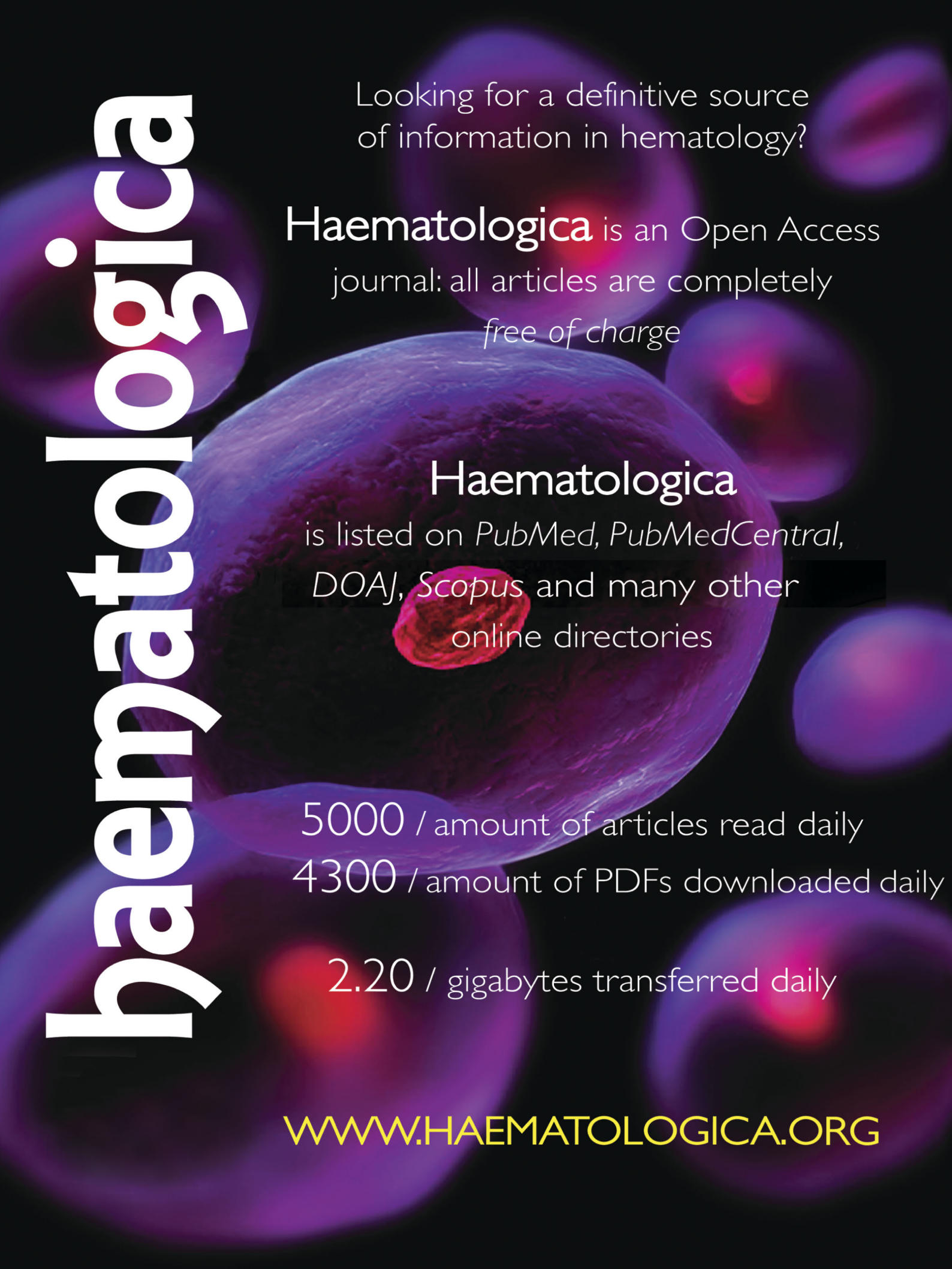
haematologica
Journal of The Ferrata Storti Foundation



ISSN 0390-6078
Volume 106
APRIL
2021 - 4

www.haematologica.org


haematologica
Looking for a definitive source of information in hematology?
Haematologica is an Open Access journal: all articles are completely free of charge
Haematologica is listed on PubMed, PubMedCentral, DOAJ, Scopus and many other online directories
5000 / amount of articles read daily
4300 / amount of PDFs downloaded daily
2.20 / gigabytes transferred daily
WWW.HAEMATOLOGICA.ORG

haematologica
Journal of the Ferrata Storti Foundation

Editor-in-Chief
Jacob M. Rowe (Haifa)

Deputy Editors
Carlo Balduini (Pavia), Jerry Radich (Seattle)

Managing Director
Antonio Majocchi (Pavia)

Associate Editors
Hélène Cavé (Paris), Monika Engelhardt (Freiburg), Steve Lane (Brisbane), PierMannuccio Mannucci (Milan), Simon Mendez-Ferrer (Cambridge), Pavan Reddy (Ann Arbor), David C. Rees (London), Francesco Rodeghiero (Vicenza), Davide Rossi (Bellinzona), Gilles Salles (New York), Aaron Schimmer (Toronto), Richard F Schlenk (Heidelberg), Sonali Smith (Chicago)

Assistant Editors
Anne Freckleton (English Editor), Britta Dorst (English Editor), Cristiana Pascutto (Statistical Consultant), Rachel Stenner (English Editor),

Editorial Board
Jeremy Abramson (Boston); Paolo Arosio (Brescia); Raphael Bejar (San Diego); Erik Berntorp (Malmö); Dominique Bonnet (London); Jean-Pierre Bourquin (Zurich); Suzanne Cannegieter (Leiden); Francisco Cervantes (Barcelona); Nicholas Chiorazzi (Manhasset); Oliver Cornely (Köln); Michel Delforge (Leuven); Ruud Delwel (Rotterdam); Meletios A. Dimopoulos (Athens); Inderjeet Dokal (London); Hervé Dombret (Paris); Peter Dreger (Hamburg); Martin Dreyling (München); Kieron Dunleavy (Bethesda); Dimitar Efremov (Rome); Sabine Eichinger (Vienna); Jean Feuillard (Limoges); Carlo Gambacorti-Passerini (Monza); Guillermo Garcia Manero (Houston); Christian Geisler (Copenhagen); Piero Giordano (Leiden); Christian Gisselbrecht (Paris); Andreas Greinacher (Greifswals); Hildegard Greinix (Vienna); Paolo Gresele (Perugia); Thomas M. Habermann (Rochester); Claudia Haferlach (München); Oliver Hantschel (Lausanne); Christine Harrison (Southampton); Brian Huntly (Cambridge); Ulrich Jaeger (Vienna); Elaine Jaffe (Bethesda); Arnon Kater (Amsterdam); Gregory Kato (Pittsburg); Christoph Klein (Munich); Steven Knapper (Cardiff); Seiji Kojima (Nagoya); John Koreth (Boston); Robert Kralovics (Vienna); Ralf Küppers (Essen); Ola Landgren (New York); Peter Lenting (Le Kremlin-Bicetre); Per Ljungman (Stockholm); Henk M. Lokhorst (Utrecht); John Mascarenhas (New York); Maria-Victoria Mateos (Salamanca); Giampaolo Merlini (Pavia); Anna Rita Migliaccio (New York); Mohamad Mohty (Nantes); Martina Muckenthaler (Heidelberg); Ann Mullally (Boston); Stephen Mulligan (Sydney); German Ott (Stuttgart); Jakob Passweg (Basel); Melanie Percy (Ireland); Rob Pieters (Utrecht); Stefano Pileri (Milan); Miguel Piris (Madrid); Andreas Reiter (Mannheim); Jose-Maria Ribera (Barcelona); Stefano Rivella (New York); Francesco Rodeghiero (Vicenza); Richard Rosenquist (Uppsala); Simon Rule (Plymouth); Claudia Scholl (Heidelberg); Martin Schrappe (Kiel); Radek C. Skoda (Basel); Gérard Socié (Paris); Kostas Stamatopoulos (Thessaloniki); David P. Steensma (Rochester); Martin H. Steinberg (Boston); Ali Taher (Beirut); Evangelos Terpos (Athens); Takanori Teshima (Sapporo); Pieter Van Vlierberghe (Gent); Alessandro M. Vannucchi (Firenze); George Vassiliou (Cambridge); Edo Vellenga (Groningen); Umberto Vitolo (Torino); Guenter Weiss (Innsbruck).

Editorial Office
Simona Giri (Production & Marketing Manager), Lorella Ripari (Peer Review Manager), Paola Cariati (Senior Graphic Designer), Igor Ebuli Poletti (Senior Graphic Designer), Marta Fossati (Peer Review), Diana Serena Ravera (Peer Review)

Affiliated Scientific Societies
SIE (Italian Society of Hematology, *www.siematologia.it*)
SIES (Italian Society of Experimental Hematology, *www.siesonline.it*)

haematologica
Journal of the Ferrata Storti Foundation

Information for readers, authors and subscribers

Haematologica (print edition, pISSN 0390-6078, eISSN 1592-8721) publishes peer-reviewed papers on all areas of experimental and clinical hematology. The journal is owned by a non-profit organization, the Ferrata Storti Foundation, and serves the scientific community following the recommendations of the World Association of Medical Editors (www.wame.org) and the International Committee of Medical Journal Editors (www.icmje.org).

Haematologica publishes editorials, research articles, review articles, guideline articles and letters. Manuscripts should be prepared according to our guidelines (www.haematologica.org/information-for-authors), and the Uniform Requirements for Manuscripts Submitted to Biomedical Journals, prepared by the International Committee of Medical Journal Editors (www.icmje.org).

Manuscripts should be submitted online at http://www.haematologica.org/.

Conflict of interests. According to the International Committee of Medical Journal Editors (http://www.icmje.org/#conflicts), "Public trust in the peer review process and the credibility of published articles depend in part on how well conflict of interest is handled during writing, peer review, and editorial decision making". The ad hoc journal's policy is reported in detail online (www.haematologica.org/content/policies).

Transfer of Copyright and Permission to Reproduce Parts of Published Papers. Authors will grant copyright of their articles to the Ferrata Storti Foundation. No formal permission will be required to reproduce parts (tables or illustrations) of published papers, provided the source is quoted appropriately and reproduction has no commercial intent. Reproductions with commercial intent will require written permission and payment of royalties.

Detailed information about subscriptions is available online at www.haematologica.org. Haematologica is an open access journal. Access to the online journal is free. Use of the Haematologica App (available on the App Store and on Google Play) is free.
For subscriptions to the printed issue of the journal, please contact: Haematologica Office, via Giuseppe Belli 4, 27100 Pavia, Italy (phone +39.0382.27129, fax +39.0382.394705, E-mail: info@haematologica.org).

Rates of the International edition for the year 2021 are as following:

	Institutional	*Personal*
Print edition	*Euro 700*	*Euro 170*

Advertisements. Contact the Advertising Manager, Haematologica Office, via Giuseppe Belli 4, 27100 Pavia, Italy (phone +39.0382.27129, fax +39.0382.394705, e-mail: marketing@haematologica.org).

Disclaimer. Whilst every effort is made by the publishers and the editorial board to see that no inaccurate or misleading data, opinion or statement appears in this journal, they wish to make it clear that the data and opinions appearing in the articles or advertisements herein are the responsibility of the contributor or advisor concerned. Accordingly, the publisher, the editorial board and their respective employees, officers and agents accept no liability whatsoever for the consequences of any inaccurate or misleading data, opinion or statement. Whilst all due care is taken to ensure that drug doses and other quantities are presented accurately, readers are advised that new methods and techniques involving drug usage, and described within this journal, should only be followed in conjunction with the drug manufacturer's own published literature.

Direttore responsabile: Prof. Carlo Balduini; Autorizzazione del Tribunale di Pavia n. 63 del 5 marzo 1955.
Printing: Press Up, zona Via Cassia Km 36, 300 Zona Ind.le Settevene - 01036 Nepi (VT)

Associated with USPI, Unione Stampa Periodica Italiana.
Premiato per l'alto valore culturale dal Ministero dei Beni Culturali ed Ambientali

haematologica
Journal of the Ferrata Storti Foundation

Table of Contents

Volume 106, Issue 4: April 2021

About the Cover

925 Images from the Haematologica Atlas of Hematologic Cytology: plasma cell myeloma
Rosangela Invernizzi
https://doi.org/10.3324/haematol.2021.278331

Editorials

926 Improving the safety of platelet transfusions by UV-C: let's go back to the bench
Daniele Prati
https://doi.org/10.3324/haematol.2020.275156

927 Understanding how retinoic acid derivatives induce differentiation in non-M3 acute myelogeneous leukemia
Martin Carroll
https://doi.org/10.3324/haematol.2020.275412

929 New option for improving hematological recovery: suppression of luteinizing hormone
Harold K. Elias and Marcel R.M. van den Brink
https://doi.org/10.3324/haematol.2020.274969

931 BETing on rational combination therapy in mutant *FLT3* acute myeloid leukemia
Richard M. Stone
https://doi.org/10.3324/haematol.2020.274753

Review Articles

933 The clinical role of the gut microbiome and fecal microbiota transplantation in allogeneic stem cell transplantation
Israel Henig et al.
https://doi.org/10.3324/haematol.2020.247395

947 Latest culture techniques: cracking the secrets of bone marrow to mass-produce erythrocytes and platelets *ex vivo*
Christian A. Di Buduo et al.
https://doi.org/10.3324/haematol.2020.262485

Articles

Hematologic cancers

958 Novel pyrrolobenzodiazepine benzofused hybrid molecules inhibit nuclear factor-κB activity and synergize with bortezomib and ibrutinib in hematologic cancers
Thomas Lewis et al.
https://doi.org/10.3324/haematol.2019.238584

Chronic Lymphocytic Leukemia

968 Combining ibrutinib and checkpoint blockade improves $CD8^+$ T-cell function and control of chronic lymphocytic leukemia in Eμ-TCL1 mice
Bola S. Hanna et al.
https://doi.org/10.3324/haematol.2019.238154

Cell Therapy & Immunotherapy

978 Immune reconstitution and associated infections following axicabtagene ciloleucel in relapsed or refractory large B-cell lymphoma
Jennifer M. Logue et al.
https://doi.org/10.3324/haematol.2019.238634

haematologica
Journal of the Ferrata Storti Foundation

987 CD28.OX40 co-stimulatory combination is associated with long *in vivo* persistence and high activity of CAR.CD30 T cells
Marika Guercio et al.
https://doi.org/10.3324/haematol.2019.231183

Acute Myeloid Leukemia

1000 The ASXL1^{G643W} variant accelerates the development of CEBPA mutant acute myeloid leukemia
Teresa D'Altri et al.
https://doi.org/10.3324/haematol.2019.235150

1008 Endogenous and combination retinoids are active in myelomonocytic leukemias
Orsola di Martino et al.
https://doi.org/10.3324/haematol.2020.264432

1022 A novel combination regimen of BET and FLT3 inhibition for FLT3-ITD acute myeloid leukemia
Lauren Y. Lee et al.
https://doi.org/10.3324/haematol.2020.247346

1034 Venetoclax combines synergistically with FLT3 inhibition to effectively target leukemic cells in FLT3-ITD+ acute myeloid leukemia models
Raghuveer Singh Mali et al.
https://doi.org/10.3324/haematol.2019.244020

1047 Immunophenotypic characterization of reactive and neoplastic plasmacytoid dendritic cells permits establishment of a ten-color flow cytometric panel for initial workup and residual disease evaluation of blastic plasmacytoid dendritic cell neoplasm
Wei Wang et al.
https://doi.org/10.3324/haematol.2020.247569

Acute Lymphoblastic Leukemia

1056 Phase II-like murine trial identifies synergy between dexamethasone and dasatinib in T-cell acute lymphoblastic leukemia
Yuzhe Shi et al.
https://doi.org/10.3324/haematol.2019.241026

1067 Combinatorial efficacy of entospletinib and chemotherapy in patient-derived xenograft models of infant acute lymphoblastic leukemia
Joseph P. Loftus et al.
https://doi.org/10.3324/haematol.2019.241729

Plasma Cell Disorders

1079 Carfilzomib, cyclophosphamide and dexamethasone for newly diagnosed, high-risk myeloma patients not eligible for transplant: a pooled analysis of two studies
Roberto Mina et al.
https://doi.org/10.3324/haematol.2019.243428

Blood Transfusion

1086 Efficacy of UVC-treated, pathogen-reduced platelets *versus* untreated platelets: a randomized controlled non-inferiority trial
Veronika Brixner et al.
https://doi.org/10.3324/haematol.2020.260430

Hematopoiesis

1097 Impact of luteinizing hormone suppression on hematopoietic recovery after intensive chemotherapy in patients with leukemia
Iman Abou Dalle et al.
https://doi.org/10.3324/haematol.2020.256453

1106 Oncogenic *Gata1* causes stage-specific megakaryocyte differentiation delay
Gaëtan Juban et al.
https://doi.org/10.3324/haematol.2019.244541

Non-Hodgkin Lymphoma

1120 Genetic lesions in *MYC* and *STAT3* drive oncogenic transcription factor overexpression in plasmablastic lymphoma
Julia Garcia-Reyero et al.
https://doi.org/10.3324/haematol.2020.251579

haematologica
Journal of the Ferrata Storti Foundation

Hodgkin Lymphoma

1129 Combining brentuximab vedotin with dexamethasone, high-dose cytarabine and cisplatin as salvage treatment in relapsed or refractory Hodgkin lymphoma: the phase II HOVON/LLPC Transplant BRaVE study
Marie José Kersten et al.
https://doi.org/10.3324/haematol.2019.243238

Hemostasis

1138 Sec22b determines Weibel-Palade body length by controlling anterograde endoplasmic reticulum-Golgi transport
Ellie Karampini et al.
https://doi.org/10.3324/haematol.2019.242727

Platelet Biology & its Disorders

1148 A multicenter study of romiplostim for chemotherapy-induced thrombocytopenia in solid tumors and hematologic malignancies
Hanny Al-Samkari et al.
https://doi.org/10.3324/haematol.2020.251900

Letters to the Editor

1158 Concomitant constitutive LNK and NFE2 mutation with loss of sumoylation in a case of hereditary thrombocythemia
Lukas Clemens Böckelmann et al.
https://doi.org/10.3324/haematol.2020.246587

1163 Targeting GLUT1 in acute myeloid leukemia to overcome cytarabine resistance
Hannah Åbacka et al.
https://doi.org/10.3324/haematol.2020.246843

1167 Anemia and hemodilution: analysis of a single center cohort based on 2,858 red cell mass measurements
Louis Drevon et al.
https://doi.org/10.3324/haematol.2020.249409

1172 Reveromycin A, a novel acid-seeking agent, ameliorates bone destruction and tumor growth in multiple myeloma
Keiichiro Watanabe et al.
https://doi.org/10.3324/haematol.2019.244418

1178 Infrequent “chronic lymphocytic leukemia-specific” immunoglobulin stereotypes in aged individuals with or without low-count monoclonal B-cell lymphocytosis
Andreas Agathangelidis et al.
https://doi.org/10.3324/haematol.2020.247908

1182 Isatuximab plus pomalidomide and dexamethasone in elderly patients with relapsed/refractory multiple myeloma: ICARIA-MM subgroup analysis
Fredrik Schjesvold et al.
https://doi.org/10.3324/haematol.2020.253450

1188 A homozygous missense variant in *UBE2T* is associated with a mild Fanconi anemia phenotype
Laura Schultz-Rogers et al.
https://doi.org/10.3324/haematol.2020.259275

1193 Bi38-3 is a novel CD38/CD3 bispecific T-cell engager with low toxicity for the treatment of multiple myeloma
Maxime Fayon et al.
https://doi.org/10.3324/haematol.2019.242453

1198 Effect of post-consolidation regimen on symptomatic osteonecrosis in three DCOG acute lymphoblastic leukemia protocols
Jenneke E. van Atteveld et al.
https://doi.org/10.3324/haematol.2020.257550

1202 Endoplasmic reticulum stress controls iron metabolism through *TMPRSS6* repression and hepcidin mRNA stabilization by RNA-binding protein HuR
Audrey Belot et al.
https://doi.org/10.3324/haematol.2019.237321

haematologica
Journal of the Ferrata Storti Foundation

1207 Sex-specific transcriptional profiles identified in β-thalassemia patients
Aikaterini Nanou et al.
https://doi.org/10.3324/haematol.2020.248013

1212 Lack of activation-induced cytidine deaminase expression in *in situ* follicular neoplasia
Tanu Goyal et al.
https://doi.org/10.3324/haematol.2020.249342

Case Reports

1216 Identification of biallelic germline variants of *SRP68* in a sporadic case with severe congenital neutropenia
Barbara Schmaltz-Panneau et al.
https://doi.org/10.3324/haematol.2020.247825

1220 Biallelic *IARS2* mutations presenting as sideroblastic anemia
Giulia Barcia et al.
https://doi.org/10.3324/haematol.2020.270710

Comment

1226 Comment on "Combining brentuximab vedotin with dexamethasone, high-dose cytarabine and cisplatin as salvage treatment in relapsed or refractory Hodgkin lymphoma: the phase II HOVON/LLPC Transplant BRaVE study."
Marco Picardi and Claudia Giordano
https://doi.org/10.3324/haematol.2020.278203

Errata Corrige

1228 A real world multicenter retrospective study on extramedullary disease from Balkan Myeloma Study Group and Barcelona University: analysis of parameters that improve outcome
Meral Beksac et al.
https://doi.org/10.3324/haematol.2020.278272

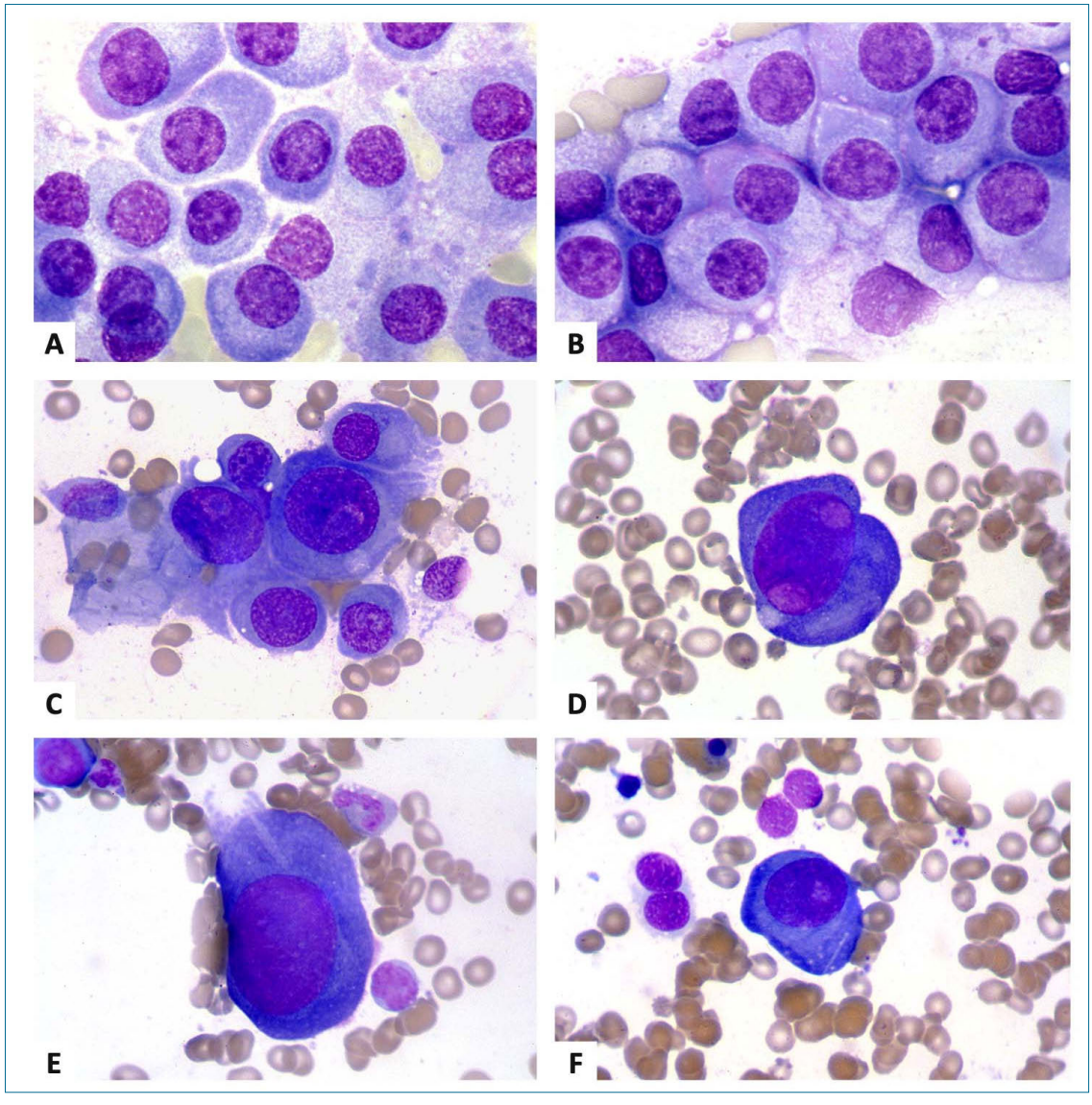
Images from the Haematologica Atlas of Hematologic Cytology: plasma cell myeloma

Rosangela Invernizzi

University of Pavia, Pavia, Italy

E-mail: ROSANGELA INVERNIZZI - rosangela.invernizzi@unipv.it

doi:10.3324/haematol.2021.278331



In plasma cell myeloma, the pleomorphism of plasma cells is mostly due to the fact that they are secretory cells and have abundant endoplasmic reticulum which may contain condensed or crystallized immunoglobulin. The Figure shows increased protein in the background with cellular debris (A); plasma cells with reticular cytoplasmic structures and pink-red periphery (center) (B); a group of plasmablasts with irregular cytoplasmic margins, cytoplasmic streamers and crystalline inclusions (C); a giant plasmablast with two macronucleoli and deeply basophilic cytoplasm with immunoglobulin accumulation in the form of amorphous substance or crystals (D). In Figure E and F, note the elongated lance-like and crystalline structures within the cytoplasm of giant plasmablasts.[1]

References

1. Invernizzi R. Mature B-cell neoplasms. Haematologica. 2020;105(Suppl 1):139-161.

Improving the safety of platelet transfusions by UV-C: let's go back to the bench

Daniele Prati

Department of Transfusion Medicine and Hematology, Fondazione IRCCS Ca' Granda Ospedale Maggiore Policlinico, Milano, Italy
E-mail: DANIELE PRATI - daniele.prati@policlinico.mi.it

doi:10.3324/haematol.2020.275156

Technologies for pathogen reduction in blood components have been under development for more than 30 years, with the aim of mitigating the infectious risks of blood transfusion. They are based on the principle of inactivating all nucleic acids in the blood unit (including intra-cellular), to prevent the replication of any possible pathogen. This is particularly desirable to protect platelet transfusion recipients, who are at higher risk of septic reactions. In fact platelets - differently from other blood products which are kept refrigerated or frozen - are stored at room temperature, thus increasing the risk of bacterial growth.

As recently outlined, designing and conducting clinical trials on pathogen reduced platelets is not straightforward.[1,2] In principle, studies should aim to demonstrate that pathogen-reduced platelets are more effective than standard platelets in preventing transfusion-transmitted infections. However, demonstrating such an advantage is considered unrealistic: given the unprecedented levels of blood safety, too many participants would need to be enrolled to achieve an adequate statistical power. Thus, the antimicrobial efficacy of these techniques is taken for granted from *in vitro* studies, and aims are set on the efficacy of platelet transfusion: *i.e.*, whether or not pathogen-reduced products retain their ability to increase platelet count, prevent bleeding and do not overly increase product need. Trials are generally based on a non-inferiority hypothesis, because pathogen-reduced platelets are not expected to provide better hemostatic efficacy than conventional platelets.[3]

Two pathogen-reduction techniques based on photochemical treatment of platelets, amotosalen plus UV-A light (Intercept, Cerus) and riboflavin plus UV light (Mirasol, TerumoBCT) – have already been tested in several randomized studies of prophylactic transfusion in thrombocytopenic patients. As summarized in a Cochrane systematic review the treatment with either of these two methods does not seem to cause higher rates of bleeding, death, or serious adverse events in recipients.[2] However, it is associated with approximately 20% lower post transfusion platelet count increments, shorter transfusion intervals and higher rates of refractoriness to platelet transfusions.[2,4] This, together with concerns about the long-term safety profile of amotosalen or riboflavin and cost, have hampered the widespread introduction of pathogen-reduction techniques in many countries.

Another pathogen reduction method, the Theraflex system (Macopharma S.A.S.), has more recently been developed. In contrast with Mirasol and Intercept, it is based on simple UV-C irradiation of platelets, without the addition of photoactive substances. The article by Brixner and colleagues in the current issue of *Haematologica*[5] reports the results of the first clinical study comparing the efficacy and safety of UV-C treated platelets to standard platelets (the CAPTURE trial). In a non-inferiority trial, the working group selected as primary endpoint the 1-hour corrected count increment (CCI), a measure of response to platelet transfusion that "corrects" the post-transfusion increase of platelet count for blood volume and number of platelets transfused, and set the acceptable inferiority margin at 30%.

From a methodological point of view, the trial was well designed and well conducted, and the authors should be commended for their effort. The main sponsor of the study was a non-commercial institution, the Research Foundation of the German Red Cross Blood Services. The working group successfully enrolled 175 patients (slightly more than the 166 planned), in 10 clinical centers. Patients were evaluated in up to eight per-protocol platelet transfusion episodes, and the percentage of off-protocol transfusions was kept low (about 5% in both arms). Both aphaeresis and buffy-coat derived platelet pools were used, reflecting the standard transfusion practice in Europe. Perhaps, the main limitation of the CAPTURE study was the choice of 1-hour CCI as primary endpoint. CCI is commonly used as a surrogate outcome for platelet transfusion efficacy, but its correlation with clinical efficacy has not been documented.[1] Theoretically, bleeding endpoints graded according to World Health Organisation system would have been more appropriate. However, reliable grading is not easy to standardise and apply, especially in a context of independent studies involving multiple evaluation sites.[1,3,6] However, CCI has been used in most previous trials on platelet concentrate pathogen-reduction,[2] which makes it acceptable for this initial evaluation of the Theraflex system.

The results of the CAPTURE trial are of great interest. In an intent-to-treat analysis, the mean 1-hour CCI was 12.7 (95% CI: 11.42-13.97) in the patients receiving UV-C treated products, and 15.53 (95% CI: 14.88-16.88) in those receiving conventional platelets. This accounted for a mean difference of 18.24% (95% CI: 6.4-30.8) between the two groups. Similar results were obtained using a per-protocol analysis. Thus, non-inferiority of pathogen-reduced platelets compared to the standard of care cannot be claimed, despite a narrow margin well below the pre-trial defined limit of 30%. In other words UV-C-treated platelets were clearly less effective than standard platelets in increasing post transfusion counts.[7] In addition, patients in the experimental treatment arm received 25% more platelet transfusions, seriously affecting treatment costs, and patients receiving pathogen-treated platelets had a higher frequency of low-grade transfusion-related adverse events (probably related to the higher transfusion requirements). No differences between the two treatment arms were observed with regards to the incidence of platelet alloimmunization and serious adverse events (including severe bleeding episodes), but it should be emphasized that the trial was not adequately powered for detecting them. Therefore, as correctly stated by the authors, no firm conclusions on safety could be drawn on the basis of the CAPTURE data.

Theraflex received the CE mark in 2009, but has not yet been commercialized. Certainly the evidence emerging from

the CAPTURE study mitigates the introduction of this new technology in clinical practice. Well designed clinical trials obtain their credibility from the definition of *a priori* hypotheses that helps researchers to avoid drawing wrong conclusions, and negative results are as useful as positive results in guiding medical treatments.

However, even when the primary outcome of a clinical trial fails, new research opportunities open up.[8] Hopefully, a careful analysis of the CAPTURE data will lead to future research in the field. Additional laboratory studies are probably required to i) gain further insight into the damage that UV-C irradiation causes to platelets apart from pathogen inactivation and to ii) develop strategies to improve the quality of Theraflex treated products.

Concerns regarding the possible transfusion transmission of SARS-CoV-2 at the beginning of the ongoing pandemic have revamped the interest in approaches capable of protecting the blood supply from known and newly emerging threats.[9] As Brixen and colleagues remind us, safe and effective pathogen reduction methods are still an unmet need.

Disclosures

DP sits on advisory boards, has received travel or research grants, as well as speaking and teaching fees from Macopharma, Ortho Clinical Diagnostics, Grifols, Terumo, Immucor, Diamed, Diatech Pharmacogenetics.

References

1. Heddle NM, Cardoso M, van der Meer PF. Revisiting study design and methodology for pathogen reduced platelet transfusions: a round table discussion. Transfusion. 2020;60(7):1604-1611.
2. Rebulla P, Garban F, van der Meer PF, Heddle NM, McCullough J. A crosswalk tabular review on methods and outcomes from randomized clinical trials using pathogen reduced platelets. Transfusion. 2020;60(6):1267-1277.
3. Rebulla P. The long and winding road to pathogen reduction of platelets, red blood cells and whole blood. Br J Haematol. 2019;186(5):655-667.
4. Estcourt LJ, Malouf R, Hopewell S, et al. Pathogen-reduced platelets for the prevention of bleeding. Cochrane Database Syst Rev. 2017;7(7):CD009072.
5. Brixner V, Bug G, Pohler P, et al. Efficacy of UVC-treated, pathogen-reduced platelets versus untreated platelets: a randomized controlled non-inferiority trial. Haematologica. 2021;106(4):1086-1096.
6. Rebulla P, Vaglio S, Beccaria F, et al. Clinical effectiveness of platelets in additive solution treated with two commercial pathogen-reduction technologies. Transfusion. 2017;57(5):1171-1183.
7. Mauri L, D'Agostino RB Sr. Challenges in the design and interpretation of noninferiority trials. N Engl J Med. 2017;377(14):1357-1367.
8. Pocock SJ, Stone GW. The primary outcome fails - what next? N Engl J Med. 2016;375(9):861-870.
9. Stanworth SJ, New HV, Apelseth TO, et al. Effects of the COVID-19 pandemic on supply and use of blood for transfusion. Lancet Haematol. 2020;7(10):e756-e764.

Understanding how retinoic acid derivatives induce differentiation in non-M3 acute myelogeneous leukemia

Martin Carroll

Division of Hematology and Oncology, University of Pennsylvania, Philadelphia, PA, USA

E-mail: MARTIN CARROLL - carroll2@pennmedicine.upenn.edu

doi:10.3324/haematol.2020.275412

Over 30 years ago, Huang and colleagues published the startling result that all trans-retinoic acid (ATRA) could induce clinical remissions without myelosuppression in patients with acute promyelocytic leukemia (APML).[1] Analysis in this report and subsequent analysis demonstrated that responses are due to induced differentiation of the leukemic clone and not the induction of cell death in the malignant cells. This work introduced the concept of differentiation therapy to the world of leukemia therapeutics. Other recently developed therapeutics for acute myeloid leukemia (AML) including FLT3 and IDH inhibitors in some patients with the targeted mutations are now known to induce differentiation.[2,3] However, there remain two outstanding questions in this field that stem from those original remarkable observations. First, what is the role of retinoic acid or its derivatives in controlling normal myeloid maturation? Second, how can this information be used to develop retinoic acid based therapeutics for non-M3 AML? di Martino and colleagues provide exciting new insights into these questions in this issue of Haematologica.[4]

To understand the complexity of these questions, it is valuable to first briefly introduce how retinoids and their derivatives function. Conceptually, retinoic acid (RA) functions through one of the retinoic acid receptors (RAR) which are members of the nuclear hormone receptor family. To simplify, binding of RA to the RAR induces binding to DNA. Commonly, this binding leads to recruitment of factors that promote gene transcription (such as histone acetyl transferases) and displacement of inhibitors of transcription such as nuclear receptor corepressor (NCOR1). There are many levels of complexity in these gene regulatory events.[5] Importantly, there are actually three isoforms of RAR. RAR can function as homodimers, heterodimers with themselves or heterodimers with other members of the nuclear hormone receptor superfamily including retinoic X receptors (RXR), Vitamin D receptors (VDR) and peroxisome proliferator activated receptor (PPAR). Thus, there are many combinatorial possibilities for gene targets and multiple levels of redundancy that have made defining the specific role of the nuclear hormone receptor superfamily in myeloid maturation and leukemia therapy challenging.

To address these questions, Di Martino and colleagues first use a murine model of AML induced using the KMT2A fusion protein, KMT2A-AF9. The leukemic cells were transduced with reporter constructs that are quite specific for activation by isoforms of RAR or RXR, trans-

planted into secondary recipients and reporter activation was used to determine if the leukemias have endogeneous expression of RXR or RAR ligands. These results show that the AML cells studied have spontaneous activation of RXRA which can be further stimulated with the RXR agonist, bexarotene. In contrast, there is minimal endogeneous activation of RARA. This is consistent with the group's previous report studying stress myelopoiesis.[6] To further study the role of RXRA and RXRB in this AML model the authors planned to induce leukemia in cells engineered to have a deletable form of the receptors. In a case of remarkably informative serendipity, the authors demonstrate robust selection in the leukemias for spontaneous deletion of RXRA and RXRB. Elegantly designed experiments validate that the RXR complex is a tumor suppressor in this model of AML. This better defines the biology of RXR in AML but targeting of RXR, as further discussed below, has not been adequate to induce a robust response in AML.

However, the authors continue on to studies that inform a pharmacologic approach to treatment of AML. Bexarotene is a small molecular agonist of RXR that Tsai and colleagues previously demonstrated to have modest activity in non-M3 AML.[7] diMartino and colleagues confirm that RXR activity stimulated by bexarotene has *in vitro* activity decreasing leukemic cell growth and that this is synergistically stimulated by simultaneous activation of RAR using ATRA or the more specific RARA ligand, BMS753.[8] They then use the RXRA deleted cells generated *in vivo*, re-introduce wild type or mutant RXRA and define the domains of RXRA necessary for suppressing leukemogenesis. This experiment is the most molecular robust definition of the requirement for RXR activation to reduce leukemogenesis to date and convincingly demonstrates that bexarotene effects are not off target effects. An interesting Figure 4 both validates this conclusion and demonstrates that the effects of retinoid/rexinoid combinations on leukemic cells depend strongly on the cell culture system. To further define the molecular effects of RAR and RXR on leukemic cells, the authors use reporter assays to show that RARA can have a strong interaction with the nuclear co-repressor, silencing mediator of retinoic acid and thyroid hormone receptor (SMRT). Overall, these data suggest that the therapeutic target complex in AML cells is a RARA/RXRA heterodimer which can act as a nuclear repressor. The ATRA-dependent release of co-repressor from the RARA:RXRA heterodimer may account for the synergy described. Simultaneous stimulation of both RARA with ATRA and RXR with bexarotene works best to induce this repressive activity and induce leukemic cell death or differentiation.

Importantly, for translational use, diMartino and colleagues go on to validate efficacy of the drug combination in multiple murine and human models of AML including primary human AML cells studied in culture. The clinical development of this drug combination is challenging. The authors have used, among other compounds, a bexarotene derivative, CW103-4 which has both RARA and RXRA agonist activity and, in theory, should be a potent anti-leukemic drug. However, CW103-4 is reported to be toxic in humans due to the induction of hypertriglyderidemia.[9] Of note, careful experiments shown here confirm that ATRA and bexarotene combinations are quite toxic in mice making it difficult to use the mouse model to test novel rexinoid drug combinations for AML therapy. However, the results here do suggest, for the first time, a way forward in this difficult area. Based on these studies, we can feel confident that the target complex in AML is a RARA: RXRA heterodimer. The therapeutic effects of the ATRA:bexarotene combination is likely achieved through changes in gene expression. Use of the carefully developed murine models shown here should allow for combinations of chromatin immunoprecipitation sequencing (ChiP-seq) and RNA seq studies that may define targets of the drug combination which can be pharmacologically targeted leading to non-toxic differentiation therapy for non-M3 AML. Alternatively, very careful drug binding studies may allow for dissociating the triglyceride regulating effects of retinoids and rexinoids from the myeloid effects. Either one of these approaches may bring us closer to the long-sought goal of differentiation therapy for non-M3 AML.

Disclosures

No conflicts of interest to disclose.

References

1. Huang ME, Ye YC, Chen SR, et al. Use of all-trans retinoic acid in the treatment of acute promyelocytic leukemia. Blood. 1988;72(2):567-572.
2. McMahon CM, Canaani J, Rea B, et al. Gilteritinib induces differentiation in relapsed and refractory FLT3-mutated acute myeloid leukemia. Blood Adv. 2019;3(10):1581-1585.
3. Fathi AT, DiNardo C, Kline I, et al. Differentiation syndrome associated with enasidenib, a selective inhibitor of mutant isocitrate dehydrogenase 2: analysis of a phase 1/2 study. JAMA Oncol. 2018;4(8):1106-1110.
4. di Martino O, Niu H, Hadwiger G, et al. Endogenous and combination retinoids are active in myelomonocytic leukemias. Haematologica. 2021;106(4):1008-1021.
5. le Maire A, Alvarez S, Shankaranarayanan P, de Lera AR, Bourguet W, Gronemeyer H. Retinoid receptors and therapeutic applications of RAR/RXR modulators. Curr Top Med Chem. 2012;12(6):505-527.
6. Niu H, Fujiwara H, di Martino O, et al. Endogenous retinoid X receptor ligands in mouse hematopoietic cells. Sci Signal. 2017;10(503):eaan1011.
7. Tsai DE, Luger SM, Andreadis C, et al. A phase I study of bexarotene, a retinoic X receptor agonist, in non-M3 acute myeloid leukemia. Clin Cancer Res. 2008;14(17):5619-5625.
8. Sanchez PV, Glantz ST, Scotland S, Kasner MT, Carroll M. Induced differentiation of acute myeloid leukemia cells by activation of retinoid X and liver X receptors. Leukemia. 2014;28(4):749-760.
9. Marshall PA, Jurutka PW, Wagner CE, et al. Analysis of differential secondary effects of novel rexinoids: select rexinoid X receptor ligands demonstrate differentiated side effect profiles. Pharmacol Res Perspect. 2015;3(2):e00122.

New option for improving hematological recovery: suppression of luteinizing hormone

Harold K. Elias and Marcel R.M. van den Brink

Department of Immunology and Department of Medicine, Memorial Sloan Kettering Cancer Center, New York, NY, USA

E-mail: MARCEL R.M. VAN DEN BRINK - vandenbm@mskcc.org

doi:10.3324/haematol.2020.274969

Current treatment modalities in leukemia are limited by bone marrow (BM) toxicity, a common adverse effect of cytotoxic chemotherapy and transplant-related conditioning regimens, resulting in an increased risk of bleeding and infections. Strategies to protect the BM from cytotoxic injury could augment hematopoietic recovery and improve overall patient outcomes.

Hematopoietic recovery following cytotoxic therapies and irradiation is dependent on the maintenance of a rare population of hematopoietic stem cells (HSCs) - which have the ability to sustain long-term hematopoietic recovery.[1,2] Following HSC transplant, there is evidence of decreased BM cellularity[3] and diminished colony-forming capacity[4-6] which could last up to approximately 5 years. Growing evidence attributes these functional defects to several intrinsic and extrinsic regulators which orchestrate radiation-induced senescent and pro-apoptotic programs, thereby dictating HSC fate.[7,8] Several radioprotective agents have been identified,[9] but very few mitigate radiation toxicity in the post-injury setting. Historically, mouse studies have informed post-irradiation strategies to promote HSC regeneration which are either cytokine-based, such as a combination of stem cell factor, FMS-like tyrosine kinase 3 ligand, megakaryocyte growth and development factor (MGDF) and Interleukin-3 (IL-3),[10] single agent IL-33,[11] or inhibitors targeting PTPσ[12] - none of which have been confirmed in the clinical setting. Cognate receptors for sex hormones and luteinizing hormone (LH)-releasing hormone (LHRH) have been identified on HSC and implicated in their function.[13-15] For example, LH can induce HSC expansion *in vitro*.[13] Moreover, preclinical studies targeting the sex-steroid axis, have demonstrated enhanced hematopoietic stem cell function and immune recovery, following sex-steroid ablation[16-18] and LHRH-antagonism.[13]

In this issue of *Haematologica*, Dalle and colleagues[19] provide clinical evidence of BM recovery and long-term hematopoietic reconstitution following targeted therapy of the sex-steroid axis. They conducted a retrospective

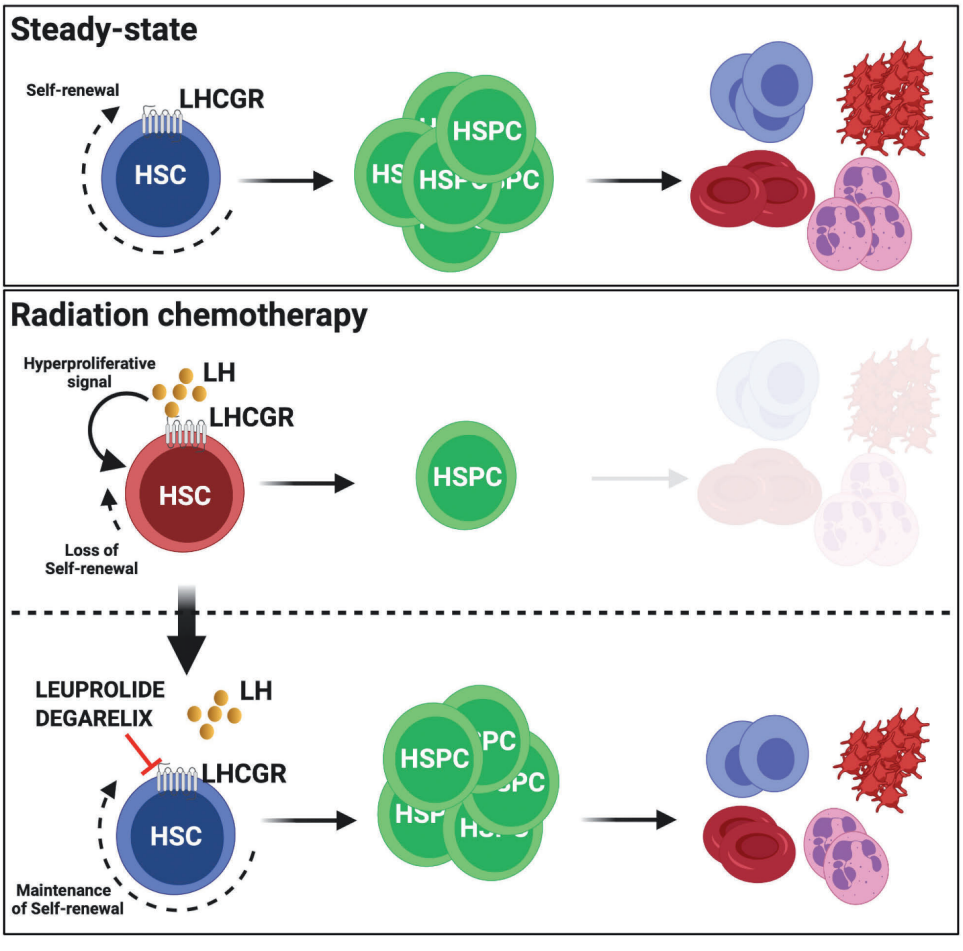


Figure 1. Schematic model of luteinizing hormone-releasing hormone antagonism mediated cytoprotection which promotes hematopoietic stem cell recovery following haematopoietic injury. Dalle *et al.*[19] provide clinical evidence for bone marrow recovery and long-term hematopoietic reconstitution with luteinizing hormone-releasing hormone (LHRH) antagonism (leuprolide) in leukemia patients following chemotherapy. HSC: hematopoietic stem cell; HSPC: hematopoietic stem and progenitor cell; LHCGR: luteinizing hormone/choriogonadotropin receptor; LH: luteinizing. hormone. Figure created with BioRender.com.

study of premenopausal women with leukemia treated with intensive chemotherapy and investigated the impact of leuprolide (gonadotropin-releasing hormone analogue) on long-term hematopoietic reconstituting ability. Their findings established an association between leuprolide use in leukemic patients and sustained recovery in blood counts. Additionally, patients with acute myeloid leukemia treated with leuprolide showed higher long-term hemoglobin levels and fewer blood transfusions. Notably, leuprolide treatment had no impact on either overall or event free survival. Finally, multivariate analysis confirmed that leuprolide administration showed an independent association with long-term hematological recovery.

This retrospective clinical study seeks to build upon previous work showing that sex steroid ablation and abrogation of LH can have beneficial effects on hematopoietic reconstitution in preclinical mouse models. However, the study raises several unanswered questions. Firstly, what would be an ideal clinical window and dosage for leuprolide administration following chemotherapy and whether that impacts association with recovery? The preclinical studies with LHRH-antagonists were protective when administered within 24 hours after radiation.[13] The current study was limited by sample size to determine statistical significance. Secondly, in relapse cases, where reinduction chemotherapy and irradiation is the standard of care, is additional leuprolide required to help boost hematological tolerance, thereby mitigating hematopoietic stress and temporary cytopenias? Thirdly, are the effects of leuprolide on hematopoietic recovery restricted to BM malignancies or could it be repurposed for treatment of other malignant and non-malignant diseases with BM involvement? Finally, from a mechanistic perspective, recent work demonstrating a role for estrogens in regulating HSC proliferation and function[14,15] begs the question: are these effects specific to LH or sex steroids? Considering the rationale for leuprolide to protect against chemoradiation induced premature ovarian failure,[20,21] preserved estrogen levels could explain the indirect beneficial effects of leuprolide on hematopoietic recovery. Hence, this warrants additional clinical studies accounting for ovarian failure, as that interpretation would restrict the potential utility of this therapy to a younger cohort. These findings also suggest a role of HSC extrinsic factors and raise the question whether leuprolide has a similar cytoprotective effect on the BM microenvironment?

In conclusion, the work by Dalle *et al.*[19] highlights a potential new therapeutic option for improving hematological recovery in patients undergoing intensive chemotherapy and transplant conditioning regimens, by boosting post-injury long-term hematopoietic reconstitution; although follow-up clinical investigations are warranted for the rational development of leuprolide as a stand-alone therapy, or in conjunction with other agents. This study also underscores the relevance of mouse models to explore additional markers and molecular underpinnings which confer survival advantage in post-irradiated HSC and BM, as those discoveries will direct us to novel non-cellular approaches to promote hematopoietic recovery and serve as effective therapies against BM toxicity.

Disclosures

MvdB has received research support and stock options from Seres; has received stock options from Notch Therapeutics; has received royalties from Wolters Kluwer; has consulted, received honorarium from or participated in advisory boards for Seres Therapeutics, Jazz Pharmaceuticals, Rheos, Therakos, WindMIL Therapeutics, Amgen, Merck & Co, Inc., Magenta Therapeutics, Frazier Healthcare Partners, Nektar Therapeutics, Notch Therapeutics, Forty Seven Inc., Priothera, Ceramedix, DKMS, Pharmacyclics (Spouse), Kite Pharmaceuticals (Spouse); has IP Licensing with Seres Therapeutics and Juno Therapeutics and holds a fiduciary role on the Foundation Board of DKMS (a nonprofit organization).

Contributions

HKE and MRMvdB have contributed equally.

References

1. Orkin SH, Zon LI. Hematopoiesis: an evolving paradigm for stem cell biology. Cell. 2008;132(4):631-644.
2. Bryder D, Rossi DJ, Weissman IL. Hematopoietic stem cells: the paradigmatic tissue-specific stem cell. Am J Pathol. 2006;169(2):338-346.
3. Arnold R, Schmeiser T, Heit W, et al. Hemopoietic reconstitution after bone marrow transplantation. Exp Hematol. 1986;14(4):271-277.
4. del Canizo C, Lopez N, Caballero D, et al. Haematopoietic damage persists 1 year after autologous peripheral blood stem cell transplantation. Bone Marrow Transplant. 1999;23(9):901-905.
5. Domenech J, Linassier C, Gihana E, et al. Prolonged impairment of hematopoiesis after high-dose therapy followed by autologous bone marrow transplantation. Blood. 1995;85(11):3320-3327.
6. Vellenga E, Sizoo W, Hagenbeek A, Lowenberg B. Different repopulation kinetics of erythroid (BFU-E), myeloid (CFU-GM) and T lymphocyte (TL-CFU) progenitor cells after autologous and allogeneic bone marrow transplantation. Br J Haematol. 1987;65(2):137-142.
7. Yukai Lu MH, Zihao Zhang, Yan Qi, Junping Wang. The regulation of hematopoietic stem cell fate in the context of radiation. Radiation Medicine and Protection. 2020;1(1):31-34.
8. Shao L, Wang Y, Chang J, Luo Y, Meng A, Zhou D. Hematopoietic stem cell senescence and cancer therapy-induced long-term bone marrow injury. Transl Cancer Res. 2013;2(5):397-411.
9. Koukourakis MI. Radiation damage and radioprotectants: new concepts in the era of molecular medicine. Br J Radiol. 2012;85(1012):313-330.
10. Drouet M, Mourcin F, Grenier N, et al. Single administration of stem cell factor, FLT-3 ligand, megakaryocyte growth and development factor, and interleukin-3 in combination soon after irradiation prevents nonhuman primates from myelosuppression: long-term follow-up of hematopoiesis. Blood. 2004;103(3):878-885.
11. Huang P, Li X, Meng Y, et al. Interleukin-33 regulates hematopoietic stem cell regeneration after radiation injury. Stem Cell Res Ther. 2019;10(1):123.
12. Zhang Y, Roos M, Himburg H, et al. PTPsigma inhibitors promote hematopoietic stem cell regeneration. Nat Commun. 2019;10(1):3667.
13. Velardi E, Tsai JJ, Radtke S, et al. Suppression of luteinizing hormone enhances HSC recovery after hematopoietic injury. Nat Med. 2018;24(2):239-246.
14. Mierzejewska K, Borkowska S, Suszynska E, et al. Hematopoietic stem/progenitor cells express several functional sex hormone receptors-novel evidence for a potential developmental link between hematopoiesis and primordial germ cells. Stem Cells Dev. 2015;24(8):927-937.
15. Nakada D, Oguro H, Levi BP, et al. Oestrogen increases haematopoietic stem-cell self-renewal in females and during pregnancy. Nature. 2014;505(7484):555-558.
16. Khong DM, Dudakov JA, Hammett MV, et al. Enhanced hematopoietic stem cell function mediates immune regeneration following sex steroid blockade. Stem Cell Reports. 2015;4(3):445-458.
17. Dudakov JA, Goldberg GL, Reiseger JJ, Chidgey AP, Boyd RL. Withdrawal of sex steroids reverses age- and chemotherapy-related defects in bone marrow lymphopoiesis. J Immunol. 2009;182(10):6247-6260.
18. Goldberg GL, Dudakov JA, Reiseger JJ, et al. Sex steroid ablation

enhances immune reconstitution following cytotoxic antineoplastic therapy in young mice. J Immunol. 2010;184(11):6014-6024.
19. Abou Dalle I, Paranal R, Zarka J, et al. Impact of luteinizing hormone suppression on hematopoietic recovery after intensive chemotherapy in patients with leukemia. Haematologica. 2021;106(4):1097-1105.
20. Poorvu PD, Barton SE, Duncan CN, et al. Use and effectiveness of gonadotropin-releasing hormone agonists for prophylactic menstrual suppression in postmenarchal women who undergo hematopoietic cell transplantation. J Pediatr Adolesc Gynecol. 2016;29(3):265-268.
21. Jadoul P, Kim SS, Committee IP. Fertility considerations in young women with hematological malignancies. J Assist Reprod Genet. 2012;29(6):479-487.

BETing on rational combination therapy in mutant *FLT3* acute myeloid leukemia

Richard M. Stone

Leukemia Division, Department of Medical Oncology, Dana-Farber Cancer Institute, Boston, MA, USA

E-mail: RICHARD M. STONE - rstone@partners.org

doi:10.3324/haematol.2020.274753

Acute myeloid leukemia (AML) is a heterogenous largely intrinsically resistant bone marrow stem cell malignancy.[1] While intensive therapies, including stem cell transplant, can cure some patients, these are difficult to apply and/or are ineffective in the many older patients who contract this disease. Individual patients have varying degrees of sensitivity to available agents which can be delineated based on cytogenetic and molecular disease features. About 30% of AML patients have malignant cells whose DNA harbors a mutation in the *FLT3* gene, encoding a transmembrane tyrosine kinase that transmits mitogenic signals from the extracellular space to the nucleus.[2] Three-quarters of the mutations encode a duplication of from 3 to 100 amino acids in the juxtamembrane region (which is associated with an adverse prognosis); the remaining mutations are point mutations in the tyrosine kinase domain.[2] Both mutations result in spontaneous dimerization and activation of the enzyme without the need for cognate ligand binding. Patients with mutant *FLT3* AML are routinely treated in the upfront setting with chemotherapy plus midostaurin, a multitargeted tyrosine kinase with FLT3 inhibitory activity.[3] Patients with relapsed or refractory mutant *FLT3* AML can be treated with gilteritinib, a more specific and relatively well-tolerated FLT3 inhibitor, based on results of a clinical trial showing superior survival with gilteritinb compared to conventional chemotherapy.[4]

Unfortunately, despite the successes with midostaurin and gilteritinib in clinical trials, patients with mutant *FLT3* AML frequently relapse after such therapies and are thus in need of new agents. The study of the mechanisms of resistance to FLT3 inhibitory therapy in AML is an important strategy to derive additional therapies. Patients who fail to respond or relapse after responding to gilteritinib frequently have mutations in the RAF-MAP-ERK downstream pathway.[5] While there are no inhibitors of this pathway in use for leukemia, this would be one strategy to employ in combination with FLT3 inhibitors to forestall or eliminate such resistance. Levis and colleagues have suggested that bromodomain inhibition in combination with FLT3 inhibition could potentially be a useful way to overcome resistance to single-agent FLT3 inhibitory therapy (*M Levis, personal observations, 2020*).

Bromodomain and extra-terminal domain (BET proteins) are master transcriptional regulators which activate a wide variety of genes[6] that are involved in cell cycle progression, leukemogenesis, and elaboration of stromal derived cytokines, the latter being important mechanisms of resistance to FLT3 inhibitors.[7] FLT3 inhibitors often clear peripheral blasts but fail to eliminate bone marrow blasts, presumably due to these pro-survival cytokines. Thus, inhibition of BET proteins, including BRD 2, 3 and 4 and BRD T could be useful in preventing FLT3 inhibitor resistance. BRD 4 may be the most relevant target since it recruits an important complex involved in transcription of MYC and other genes important in promoting cell division; this complex is called the positive transcription elongation factor complex (P-TEFb).

In this edition of Haematolgica, Lee *et al.* show that a novel BET inhibitor, PLX51107, achieved the goal of adequate MYC suppression in humans, thereby making it an attractive agent to combine with FLT3 inhibitors.[8] Could MYC downregulation with its associated decrease in cell cycle progression be useful in combination with FLT3 inhibitors such as the FLT3 ITD specific and potent agent, quizartinib?

Lee *et al.* make the important point that, while previous work had demonstrated synergistic cytotoxic effect of the BET inhibitor JQ1 and a FLT3 inhibitor, these experiments were performed in cell suspension culture which fails to faithfully reproduce the clinical situation. Blasts preferentially survive in the bone marrow stroma bathed in cytokines released by endothelial and other support cells. The authors of the current work showed that PXL51107 has single-agent activity against the FLT3 ITD containing human leukemia cell lines MV4-11 and MOLM14 in culture and *in vivo* in murine xenograft models but has no independent FLT3 inhibitory activity. This activity was synergistically increased when quizartinib was given in combination in the MV4-11 xenograft model or in primary AML cells co-cultured with bone marrow stroma. Further, plasma samples obtained from patients on a clinical trial of single-agent PLX51107 display MYC inhibition activity, suggesting that this agent possesses the requisite properties to achieve the goal of downregulation of pro-survival cytokines, making it a good candidate to combine with FLT3 inhibitors.

In summary, the preclinical work described by Lee *et al.*

supports an eventual trial of a BET inhibitor in combination with a FLT3 inhibitor in patients with mutant *FLT3* AML.[8] The idea is to injure the malignant cells with a FLT3 inhibitor and deprive them of their 'comfort zone' with the BET inhibitor. With an increase in potentially useful molecules in AML, the solid pre-clinical studies such as those described by Lee *et al.*[8] are needed to choose the most potentially useful combinations for clinical use.

Disclosures

RMS has sat on ad hoc boards and has had a consultancy role for Hoffman-LaRoche, Pfizer, Otsuka, Novartis, Jazz, Celgene, Astellas, Arog, Amgen, Agios, Actinum, Abbvie, Takeda, Macrogneics, Janssen, Gemoab, Daichii-Sanko, Biolinerx, Trovagene, Stemline, AStraZeneca, Elevate Bio, BerGenBio, Foghorn, Innate Pharma. GSK, Syndax, and Syros. He has been Principal Investigator for clinical research of his institution with Agios, Abbvie, Syndax, and Lilly. He has sat on the Data Safety and Monitoring Board for Celgene, Takeda, Argenix, and Syntax Clinical.

References

1. Dohner H, Estey E, Grimwade D, et al. Diagnosis and management of AML in adults: 2017 ELN recommendations from an international expert panel. Blood. 2017;129(4):424-447.
2. Daver N, Schlenk RF, Russell NH, Levis MJ. Targeting FLT3 mutations in AML: review of current knowledge and evidence. Leukemia. 2019;33(2):299-312.
3. Stone RM, Mandrekar SJ, Sanford BL, et al. Midostaurin plus chemotherapy for acute myeloid leukemia with a FLT3 mutation. N Engl J Med. 2017;377(5):454-464.
4. Perl AE, Martinelli G, Cortes JE, et al. Gilteritinib or chemotherapy for relapsed or refractory FLT3-mutated AML. N Engl J Med. 2019;381(18):1728-1740.
5. McMahon CM, Ferng T, Canaani J, et al. Clonal selection with RAS pathway activation mediates secondary clinical resistance to selective FLT3 inhibition in acute myeloid leukemia. Cancer Discov. 2019;9(8):1050-1063.
6. Shi J, Vakoc CR. The mechanisms behind the therapeutic activity of BET bromodomain inhibition. Mol Cell. 2014;54(5):728-736.
7. Yang X, Sexauer A, Levis M. Bone marrow stroma-mediated resistance to FLT3 inhibitors in FLT3-ITD AML is mediated by persistent activation of extracellular regulated kinase. Br J Haematol. 2014;164(1):61-72.
8. Lee L, Hizukuri Y, Severson P, et al. A novel combination regimen of BET and FLT3 inhibition for FLT3-ITD acute myeloid leukemia. Haematologica. 2021;106(4):1022-1033.

REVIEW ARTICLE

The clinical role of the gut microbiome and fecal microbiota transplantation in allogeneic stem cell transplantation

Ferrata Storti Foundation

Israel Henig,[1] Dana Yehudai-Ofir[1,2] and Tsila Zuckerman[1,2]

[1]Department of Hematology and Bone Marrow Transplantation, Rambam Health Care Campus and [2]The Ruth and Bruce Rappaport Faculty of Medicine, Technion - Israel Institute of Technology, Haifa, Israel

Haematologica 2021
Volume 106(4):933-946

ABSTRACT

Outcomes of allogeneic hematopoietic stem cell transplantation (allo-HSCT) have improved in the recent decade; however, infections and graft-*versus*-host disease remain two leading complications significantly contributing to early transplant-related mortality. In past years, the human intestinal microbial composition (microbiota) has been found to be associated with various disease states, including cancer, response to cancer immunotherapy and to modulate the gut innate and adaptive immune response. In the setting of allo-HSCT, the intestinal microbiota diversity and composition appear to have an impact on infection risk, mortality and overall survival. Microbial metabolites have been shown to contribute to the health and integrity of intestinal epithelial cells during inflammation, thus mitigating graft-*versus*-host disease in animal models. While the cause-and-effect relationship between the intestinal microbiota and transplant-associated complications has not yet been fully elucidated, the above findings have already resulted in the implementation of various interventions aiming to restore the intestinal microbiota diversity and composition. Among others, these interventions include the administration of fecal microbiota transplantation. The present review, based on published data, is intended to define the role of the latter approach in the setting of allo-HSCT.

Introduction

The past decades have witnessed important advances in the outcome of allogeneic hematopoietic stem cell transplantation (allo-HSCT),[1] mainly attributed to the reduction in non-relapse mortality.[2] Yet, the need for further improvement is compelling. Acute graft-*versus*-host disease (aGvHD) and infections are two of the main causes of early transplant-related mortality (TRM), jointly accounting for 36% and 43% of deaths by day 100 in matched related and matched unrelated transplants, respectively.[1]

One of the emerging and extensively explored allo-HSCT-associated issues is the change in the gut microbial flora, as well as its effect on the pathogenesis of transplant-related complications and association with transplant outcomes.

The human body hosts a hundred trillion microbial organisms; the majority of them are bacteria, predominantly colonizing the gut, with the lower intestine being most densely colonized (10^{11}-10^{12} organisms/g of intestinal content).[3] The composition of bacteria in the gut is referred to as the intestinal microbiota and their collective genome is termed the "intestinal microbiome".[3] The two main phyla constituting more than 90% of the gut microbiota are the *Firmicutes* and *Bacteroidetes* and among less dominant phyla are *Proteobacteria*, *Actinobacteria*, and *Verrucomicrobia*.[4] This composition is relatively flexible and can rapidly change in response to different environmental factors, adjusting the metabolic and immunologic performance accordingly.[5] Intestinal microbiota has been recently found to have a significant impact on both health and disease states. It appears to be crucial for the maturation and education of the immune system and has a role in intestinal cell proliferation, intestine vascularization and endocrine functions. Moreover, it produces energy, synthesizes vitamins, metabolizes bile acids and even inactivates drugs.[6-13] The microbiome has been reported to be associated with a variety of disorders such as

Correspondence:

TSILA ZUCKERMAN
t_zuckerman@rambam.health.gov.il

Received: May 23, 2020.
Accepted: August 28, 2020.
Pre-published: November 26, 2020.

https://doi.org/10.3324/haematol.2020.247395

©2021 Ferrata Storti Foundation

Material published in Haematologica is covered by copyright. All rights are reserved to the Ferrata Storti Foundation. Use of published material is allowed under the following terms and conditions: https://creativecommons.org/licenses/by-nc/4.0/legalcode. Copies of published material are allowed for personal or internal use. Sharing published material for non-commercial purposes is subject to the following conditions: https://creativecommons.org/licenses/by-nc/4.0/legalcode, sect. 3. Reproducing and sharing published material for commercial purposes is not allowed without permission in writing from the publisher.

obesity, type 2 diabetes, inflammatory bowel disease, rheumatoid arthritis and multiple sclerosis.[14-17] This association is also suggested to be true for cancer[18] and response to cancer immunotherapy.[19] The gut microbiota has a close and reciprocal relationship with the host immune system. Intestinal epithelial cells, goblet and paneth cells produce the luminal protective mucosal layer and antimicrobial peptides, allowing the transcellular transport of immunoglobulin A (IgA) antibodies. These functions regulate luminal microbial colonization.[20]

Homeostasis of the immune response in the gut mucosa is maintained by the balance between pro-inflammatory cells, which include T-helper 1 (Th1) cells producing interferon γ (IFNγ), Th17 cells producing IL-17A and IL-22, diverse innate lymphoid cells with cytokine effector features resembling those of Th2 and Th17 cells, the anti-inflammatory Foxp3+ regulatory T-cells (Tregs) and IgA-secreting B-cells. This homeostasis can be modulated by the gut microbiota.[21-23] In pre-clinical studies, intestinal microbiota has been shown to regulate the expression of pro-inflammatory cytokines, human leukocyte antigen (HLA) type I and type II molecules and increase T-cell proliferation.[18] Effects of the microbiota on cytokine expression and immune cell subsets are not limited to the gut, and are extended to regional mesenteric and systemic lymph nodes.[24] Furthermore, while some bacterial strains can induce pro-inflammatory intestinal Th17 cells,[25] others induce anti-inflammatory Tregs[26,27] and can thus ameliorate inflammatory colitis.[28] Moreover, human host gut microbiota has been shown to correlate with expression pattern of the cytokines secreted from peripheral blood mononuclear cells isolated from the host.[29] Microbial metabolites such as the short chain fatty acid (SCFA) butyrate or indole derivatives produced by tryptophan metabolism act to maintain the intestinal epithelial cell health, mucosal barrier, and to promote anti-inflammatory responses.[30,31]

Currently available molecular techniques allowing rapid and wide genomic sequencing enable extensive exploration of the microbiome. The most commonly used method is the 16S ribosomal RNA sequencing by PCR. Bioinformatics analysis tools assign the sequences to microbial taxon at different taxonomic levels. Other methods include shotgun next-generation metagenomics sequencing enabling massive and deeper genomic sequencing and allowing better identification of taxonomic species and potential functional pathways of the organisms, metatranscriptomics using high throughput RNA sequencing to profile gene expression, metaproteomics capable to provide large-scale characterization of the entire proteins in the environmental sample and metabolomics, identifying and quantifying all metabolites in the tested samples.[32,33] The two main microbiome features that have been widely characterized in health and disease are its diversity and the abundance of specific bacteria or bacterial subgroups.[34]

The revelation of significant relationship between the microbiome, the immune system and disease has led to interventional studies aiming to normalize the microbiome composition and diversity thus ameliorating disease conditions. One of such interventions is the use of fecal microbiota transplantation (FMT), the term referring to the transfer of the fecal microbial content from a healthy individual into the intestine of a diseased individual. FMT, the standard of care for refractory or recurrent *Clostridium difficile* infection (CDI), proved to be highly effective in this condition. At the same time, mixed results were demonstrated in the studies evaluating the use of FMT for the management of inflammatory bowel disease, irritable bowel syndrome and hepatic encephalopathy. To date, FMT application for indications other than CDI has been limited to the experimental setting only.[35,36]

The setting of allo-HSCT imposes a significant disruption on the gut microbiome homeostasis through a variety of mechanisms (all part of the transplantation procedure), such as the use of broad-spectrum antibiotics, dietary changes (restriction), gut epithelial damage by conditioning regimens and introduction of a donor immune system.

Data from clinical studies support the association of alterations in the gut microbiome profile, mainly loss of diversity and change in composition during allo-HSCT, with patient outcomes such as aGvHD, GvHD-related mortality, non-relapse mortality (NRM) and overall survival (OS).[37-40] Moreover, the gut microbial composition is reported to have an impact on infection risk, including CDI and blood stream infections (BSI), in this clinical setting.[38,41] Findings of these associations have led to a preponderance of research in this field,[42] and although the cause-and-effect relationship between the microbiome and transplant complications has not been unequivocally established, many ongoing clinical trials are implementing various interventions aiming to maintain microbiome diversity, thus potentially preventing transplant-related complications and treating aGvHD. These interventions include the use of probiotics,[43] prebiotics,[44] change in antibiotic prophylaxis[45] and administration of FMT.[46] This review appraises the currently available evidence on the association of gut microbiota and allo-HSCT and analyzes a potential role of FMT in allo-HSCT, by presenting two illustrative clinical cases, where effects on the gut microbiota composition could be employed either as a prophylactic or therapeutic measure.

Case 1

A 54-year old male, with mutated FLT3-ITD acute myeloid leukemia (AML) in complete remission (CR) after induction and re-induction chemotherapies, during which he acquired gut colonization with carbapenem-resistant *Klebsiella pneumoniae*. He underwent an allo-HSCT from a mismatched 9/10 unrelated female donor with myeloablative conditioning (busulfan, fludarabine) and received levofloxacin for infection prophylaxis. During the transplantation period, he had a BSI event with extended spectrum β lactamase *Escherichia coli* (*E. coli*) treated with meropenem for 10 days, followed by a CDI event treated with oral vancomycin. His neutrophils engrafted on day +15 and on day +33 he developed diarrhea and was diagnosed with grade 3 acute lower gastrointestinal (GI) GvHD that was steroid refractory.

This case raises a number of important questions related to the role of gut flora in allo-HSCT.

Is the microbiome already disrupted prior to allogeneic hematopoietic stem cell transplantation conditioning?

There is ample evidence suggesting that the pre-transplant patient microbiome is already disrupted. The insult to the microbiome starts with preceding chemotherapy and

antibiotic exposure. Galloway-Pena *et al.*[47] analyzed 487 stool samples from 30 AML patients and found that their pre-induction microbiome diversity was not significantly different from that of healthy volunteers participating in the Human Microbiome Project (HMP). However, following neutrophil recovery, patient microbiome composition changed, with a significant decrease in diversity. Importantly, this reduction in diversity was associated with an increased risk of infections. The use of carbapenem antibiotics for more than 3 days during induction elevated the risk for a subsequent loss of diversity.[47] Moreover, exposure to anti-anaerobic antibiotics, like piperacillin-tazobactam, ticarcillin, meropenem, clindamycin and metronidazole, within the 3 months preceding allo-HSCT was associated with a significant decrease in pre-transplant microbiome diversity.[38] With more courses of intensive chemotherapy, such as re-induction or salvage, the microbiome disruption was shown to enhance, leading to ecosystem instability and outgrowth of pathogenic bacteria like *Enterococcus*.[48] This disruption in patient microbiome continued up to the time of allo-HSCT, as shown in the largest to date inter-center effort, where 8,767 sequential stool samples were collected from 1,362 patients prior to and throughout the transplantation period and analyzed using 16S ribosomal RNA sequencing. The pre-transplant microbiome of patients obtained on days -30 to -6 (n=606), was compared to that of healthy volunteers (n=246), demonstrating a significant reduction in diversity in patient microbiome.[37] Additionally, evidence from another recently published study showed that the pre-transplant microbiome and the one derived from healthy controls differed in composition, displaying decreased abundance of beneficial bacteria of genera *Bifidobacterium* and butyrate producing genera such as *Faecalibacterium* and *Lachnospiraceae* in the former case.[49] To conclude, pre-transplant microbiome disruption is clearly evident.

What is the microbiome status during the transplantation period and at time of recovery?

Data from several studies demonstrate that during the transplantation course, the microbiome diversity significantly decreases and its composition changes.[37,50] The lower-diversity microbiome is reported to be characterized by abundance of pathogenic bacteria such as *Enterococcus*, *Klebsiella*, *Escherichia*, *Staphylococcus* and *Streptococcus*. The single taxonomic unit domination (abundance ≥30%) peaks at 1 week post-transplant, which is followed by a subsequent moderate decrease. The most common dominating taxonomic groups belong to the genera Enterococcus and Streptococcus.[37] Along the same lines, other studies have found the Enterococcus genus to be more prolific during the first month post-transplant, with significantly higher abundance in patients with active or subsequent aGvHD.[51,52] Following allo-HSCT, the microbiome recovery appears to be prolonged and incomplete. In a large cohort of patients (n=753), the post-transplant recovery of the gut microbiota has been reported to start around day +50, but even by day +100 the composition and bacterial abundance observed pre-transplant have not been fully achieved.[53] Moreover, in some patients, microbiota has remained disrupted even 1 year after HSCT, this being particularly the case with butyrate-producing bacteria and *Bifidobacterium*.[54] Eventually, the effect of environmental insult on the intestinal microbiota during allo-HSCT can be so severe that its recovery may require a long time.

Is the disrupted microbiome in allogeneic hematopoietic stem cell transplantation recipients clinically significant?

In the above-mentioned study by Peled *et al.*, reduced microbiome diversity both pre-transplant (days -30 to -6) and peri-engraftment (days +7 to 21), was shown to be significantly associated with lower 2-year OS, while a persistent decrease of this parameter in the latter period was also associated with higher 2-year treatment-related mortality (TRM). Moreover, lower peri-engraftment microbiome diversity in T-cell replete allo-HSCT corresponded to increased GvHD-related mortality, which was not observed in T-cell depleted transplantations. This difference suggests a connection between the microbiota and T-cell alloreactivity.[37] Liu *et al.* revealed a similar association of pre-transplant diversity with mortality as well as a correlation between post-transplant microbiome disruption and acute GI GvHD risk.[55] Furthermore, in a study of 66 patients whose stool specimens were analyzed weekly during the transplantation period up to day +100, Golob *et al.* found a trend of association between near-engraftment low microbiome diversity and the risk for grade 3-4 aGvHD.[56] Likewise, Mancini *et al.* evaluating a cohort of 100 patients, observed a significant connection between low microbiome diversity by day +10 and an increased risk for early (within 30 days) aGvHD.[38]

A number of studies also reported an impact of pre- or post-transplant bacterial abundance on patient outcomes (Table 1). Results of a two-cohort study (a total of 115 adult patients) conducted at the Memorial Sloan Kettering Cancer Center (MSKCC) demonstrated that increased abundance of the genus *Blautia*, including anaerobic commensal bacteria, observed 12 days post-transplant, was associated with reduced GvHD-related mortality and improved OS. At the same time, the use of antibiotics with anti-anaerobic activity and total parenteral nutrition (TPN) correlated with loss of *Blautia*.[57] In the pediatric setting, Biagi *et al.* reported an association of pre-transplant high abundance of *Blautia* and low abundance of *Fusobacterium* with diminished risk for grade 2-4 acute GI GvHD.[58] Additionally, pre-transplant *Enterobacteriaceae* abundance of >5% was associated with an increased risk of BSI and *Lachnospiraceae* abundance of ≤10% appeared to correspond to increased mortality.[38] In a large study from the MSKCC, very high abundance of a bacterial group, mainly composed of *Eubacterium limosum*, in pre-transplant samples or the presence of this group in peri-engraftment samples was found to correspond to a decreased relapse risk,[59] once again emphasizing the association of the microbiome and T-cell immunity. Furthermore, in the study from the Osaka University,[54] *Enterococcus* relative abundance of ≥1% at 1 month post-transplant appeared to be indicative of poor OS, with a 2-year survival of 83.9% for patients with relative abundance of *Enterococcus* <1% *versus* 47.6% for those in whom this parameter was ≥1%. It is noteworthy that none of the surviving patients at 1 year post-transplant displayed *Enterococcus* abundance higher than 1%, sug-

Table 1. Intestine microbial changes in diversity and abundance during pre-transplant and peri-engraftment periods, associated with outcomes of allogeneic hematopoietic stem cell transplantation

Outcome	Pre-transplant	Ref. #	Peri-engraftment	Ref. #
Overall survival ↓	Diversity ↓	37; 55	Diversity ↓	37
			Blautia (day +12) ↓	57
			Enterococcus RA ≥1% (day +30)	54
Transplant- related mortality ↑	*Lachnospiraceae* ≤ 10%	38	Peri-engraftment diversity ↓	37
			Engraftment diversity ↓	40
Acute gastrointestinal GvHD risk ↑	*Blautia ↓	58	≠Diversity ↓	56
	≠Diversity ↓	56	¥Diversity ↓ (day+10)	38
	*Fusobacterium ↑	58	*Lachnospiraceae* (day +10) ↓	38
			Staphylococcaceae (day +10) ↑	38
			Bacteroidaceae ↓	56
			Lachnospiraceae ↓	56
			Enterococcus ↑	52
			# Bacteroides ↑ (at engraftment)	58
GvHD-related mortality ↑			¶ Diversity ↓	37
			Blautia (on day +12) ↓	57
Blood stream infections ↑	*Enterobacteriaceae* (RA > 5%)	38	Enterococcus (RA ≥ 30%) -> VRE ↑	50
			Proteobacteria (RA ≥ 30%) -> GN ↑	50
Relapse ↓	**Eubacterium limosum ↑↑**	59	**Eubacterium limosum presence**	59

↓ represents a decrease in risk; ↑ represents an increase in risk; ↓next to diversity means loss of diversity; ↓ or ↑ next to a bacterial taxa represent decrease or increase in relative abundance, respectively. Different bacterial taxonomic rank is marked as follows: ***phyla*** (***bold and italics***), *family* (*italics*), genus (underlined) and **species** (**bold**). * taxa associated with grade 2-4 acute gastrointestinal graft-*versus*-host disease (GvHD). ≠ diversity associated with grade 3-4 acute GvHD (aGvHD). ¥ diversity associated with early aGvHD, by day 30. #a trend (P=0.05). ¶T-cell replete transplants. RA: relative abundance; VRE: vancomycin-resistant Enterococcus; GN: gram negative.

gesting that this cutoff could serve as a prognosticator of a long-term outcome in this clinical setting.[54] The above evidence suggests that the microbiota changes before and during allo-HSCT are significantly associated with transplant complications and outcomes and might even serve as a predictive marker in this setting.

Can prophylactic fecal microbiota transplantation reduce the risk of infections during allogeneic hematopoietic stem cell transplantation?

In allo-HSCT recipients, curtailment of infection risk is crucial for reducing TRM, particularly due to increased frequency of BSI with multidrug resistant (MDR) bacteria. MDR colonization is established to range between 16% for gram-negative bacteria and 39% for vancomycin-resistant *Enterococcus* (VRE). While BSI have been reported in 16-41% of patients colonized with MDR bacteria, findings regarding a possible association of such colonization with TRM or infection-related mortality are inconclusive.[60-62] In addition, MDR gram-negative colonization has neither been found to correspond to an increased risk for sepsis.[38,63] In the lack of clear evidence, proof-of-concept studies are becoming of increasing importance. Battipaglia *et al.*[64] have evaluated four patients colonized with MDR bacteria who had received FMT on days -46 to -9 before transplant with an aim to limit the risk for infectious complications during HSCT. All the four patients responded with decolonization of the MDR bacteria. One patient developed grade 3 acute gut GvHD on day +30 after transplant (day +51 after FMT) and two others developed bacteremia with sensitive bacteria. Notably, despite receiving broad-spectrum antibiotics during the transplantation period, none of the patients had recolonization of the gut with MDR bacteria.[64] Similar results were reported in a 63-year old HSCT recipient.[65]

The ongoing ODYSSEE trial (clinicaltrials gov. Identifier: 02928523) is aimed at reducing complications that may arise as a result of a loss of microbiota diversity, including infectious complications, poor nutritional status, prolonged hospitalization, as well as therapy discontinuation due to induction treatment-related toxicity in AML patients. Twenty newly diagnosed patients collected pre-induction autologous stools. This autologous FMT was later administered as enema after neutrophil recovery and prior to consolidation chemotherapy. Preliminary results demonstrated safety of this approach, with evidence of stool diversity restoration 10 days after FMT and reduction in antibiotic resistant gene copy count by 43%. Yet, clinical efficacy of this method still needs to be confirmed.[66]

An important pathogen to consider for intervention with FMT is *Clostridium difficile*. The incidence of CDI during allo-HSCT varies between 13% and 30%, mostly in the first month after transplant.[67-69] The disease is usually of mild-to-moderate severity, with good response to treatment; there is no association with TRM, and its possible correlation to subsequent acute GI GvHD is indefinite.[68-70] Given these facts, and the paucity of data on potential efficacy of prophylactic FMT in reducing the risk of CDI among *Clostridium difficile* carriers, FMT prophylaxis may not be required for this indication.

As for the treatment of recurrent CDI, results of three small studies demonstrate safety of FMT administration to a total of 16 patients with recurrent CDI after allo-HSCT, with only three patients recurring after the procedure.[71-73]

Currently available data are insufficient to definitively conclude that prophylactic FMT will reduce the infection rate in the allo-HSCT setting.

Can prophylactic fecal microbiota transplantation reduce the risk of acute graft-*versus*-host disease or transplant-related mortality?

The incidence of clinically significant aGvHD ranges between 22% in allo-HSCT from a matched related donor to 29% in case of a mismatched unrelated donor, with grade 3-4 disease incidence being 8.6% and 12%, respectively.[24] Whether any intervention that restores the microbiome composition could also decrease aGvHD rates is yet to be revealed. Hitherto, only two small studies have reported results of using prophylactic FMT in the post-engraftment period. In the study by Defillip *et al.*,[25] aiming to evaluate safety and feasibility of early restoration of the gut microbiome, frozen capsules of FMT derived from unrelated donors were administered to 13 allo-HSCT recipients 4 weeks after neutrophil engraftment. No FMT-related bacteremia events occurred and two cases of acute GI GvHD were registered. Analysis of stool composition indicated improvement in intestinal microbiome diversity after FMT that was mainly attributed to operational taxonomic units (OTU) originating from the FMT donor.[25] In the study by Taur *et al.*,[53] within 3-28 days of engraftment, patients not receiving broad-spectrum antibiotics, not critically ill and with low abundance of *Bacteroides* (<0.1% of the total 16S sequencing) at that time period, were randomized to either receive autologous FMT (n=14) or to a control group (n=11).

Solely the FMT group was found to reconstitute their microbiome diversity and composition to the pre-transplant state. Of note, the use of autologous FMT raises concern for disrupted microbiota due to prior antibiotic exposure.[53]

These data suggest feasibility and safety of prophylactic FMT; however, its clinical benefit has not been demonstrated yet.

Should additional interventions along with fecal microbiota transplantation aiming to attenuate mircobiome disruption be considered?

Given that a variety of factors could affect the microbiome diversity and composition during the transplantation course, their adequate control might potentially preclude such microbiome changes. The question remains whether FMT alone is sufficient enough or it should be combined with other interventions to provide the required control.

Transplant conditioning

Conditioning chemotherapy itself has a disruptive effect on the microbiome, as found by Montassier *et al.*[26] who evaluated eight lymphoma patients undergoing autologous HSCT with the BEAM (carmustine, etoposide, cytarabine arabine, melphalan) protocol. Since none of the patients received nasogastric tube nutrition, total parenteral nutrition, ciprofloxacin prophylaxis or systemic antibiotic treatment, only the chemotherapy effect on the microbiome was measured. Compared to pre-transplant samples, those drawn at 1 week post-conditioning demonstrated significantly reduced diversity, decreased abundance of *Firmicutes* and *Actinobacteria* and increased presence in bacteroides and proteobacteria, indicating chemotherapy-induced disruption of the intestinal microbiota.[26] Of note, this disruptive effect might be related to etoposide, which has bacterial inhibitory activity.[27,28] Remarkably, the post-transplant decrease in microbiome diversity appeared to be more profound when more intensive conditioning was applied.[74] However, reducing the conditioning intensity was not shown to consistently decrease the rate of aGvHD.[75] Moreover, it might increase the relapse rate and decrease long-term OS.[76,77] Therefore, changing the conditioning regimen in an attempt to attenuate the insult on the microbiome is not currently recommended.

Diet

Dietary interventions such as TPN, prebiotics and probiotics could potentially influence the microbiome composition before or during the transplantation course. TPN administration was reported to be associated with decreased recovery of post-transplant (up to day +120) diversity compared to enteral nutrition. In addition, SCFA levels in the gut content were found to be lower in the TPN group.[78] Iyama *et al.* retrospectively compared a group of patients whose diet was supplemented with prebiotics, i.e., glutamine, fiber and oligosaccharides (GFO) with a group that did not receive such supplementation. GFO was started 7 days before conditioning and continued up to day +28. In the GFO group, duration of diarrhea, mucositis and TPN requirement was shorter and the weight loss was also less prominent.[44] An ongoing prospective trial (clinicaltrials gov. Identifier: 02763033) is evaluating the efficacy of resistant potato starch supplementation between day -7 and day +100 in HSCT recipients. This starch is a non-absorbable carbohydrate that is metabolized by the anaerobic commensal bacteria to produce the SCFA butyrate,[79] shown to reduce the severity of acute GI GvHD in an experimental model.[31] Preliminary results demonstrate the feasibility of this approach in terms of patient compliance, increase in intestinal butyrate levels and abundance of butyrate producing bacteria.[80] As for probiotic supplementation, the available data do not suggest its influence on the microbiome composition or clinical outcomes. It is worth mentioning that the products used in the studies contained only one bacterial strain and not a diversity of bacteria,[43,81] and safety of probiotic administration is of concern in immunocompromised patients.[82]

The loss of diversity during the transplantation course is accompanied with microbiome domination by single taxonomic units such as *Enterococcus*.[37] This enterococcal expansion has been found to be most prominent in patients developing acute GI GvHD.[52] Stein-Thoeringer *et al.* have shown in a gnotobiotic mouse model of allo-HSCT that enterococcal expansion in the gut depends on lactose and its depletion decreases the enterococcal abundance and thus attenuates GvHD severity. Furthermore, in patients with a lactose malabsorption genotype, *Enterococcus* abundance appears to be higher than in patients without this genotype.[83] This finding may give rise to a new approach to dietary intervention during HSCT. Interestingly, in the study by Khandelwal *et al.*, where pediatric allo-HSCT patients under the age of 5 were treated with ready to eat human milk and breast feeding (n=24) or formula (n=14), plasma levels of IL6, IL10, and Reg3α were significantly lower in the group receiving human milk. The microbiome composition also

differed between the two groups, with an increase in pathogenic species such as *E. coli* in the formula-receiving group. Despite the fact that human milk oligosaccharides are metabolized to SCFA by the commensal bacteria, butyrate levels in the stool were similar in both groups. Moreover, no significant difference in the rate of grade 2-4 acute GI GvHD between the groups was revealed. However, the limited size of this study calls for cautious interpretation of these encouraging results.[84] Overall, dietary interventions emerge as a promising way to shape the intestinal microbiota during allo-HSCT. However, results are too preliminary and more research is required before implementing any of these methods.

Antibiotic treatment

The antibiotic treatment applied during the transplantation course is the main factor affecting the microbiome. Quinolone prophylaxis during afebrile neutropenia and systemic broad-spectrum antibiotic treatment with piperacillin-tazobactam or meropenem are widely accepted.[85-87] However, data demonstrate that the use of other antibiotics can better preserve gut beneficial commensals and is associated with improved outcomes.

The study from the University of Regensburg in Germany employed the non-absorbable antibiotic rifaximin and compared it to ciprofloxacin and metronidazole used in a historic cohort of patients for infection prophylaxis during allo-HSCT.[45] Antibiotics were given from day -8 up to engraftment. The urine 3-indoxyl sulfate (3-IS) level was measured as a marker of microbiome diversity.[88] In the rifaximin cohort, the pre-engraftment 3-IS levels were significantly higher without an increase in the sepsis rate or colonization with pathogenic bacteria. This group had significantly lower TRM, prolonged OS and the acute GI GvHD rate tended to be lower in these patients. The observed advantage remained evident even in patients who later received systemic antibiotics for neutropenic fever. [45]

Given the major role of microbiome diversity preservation during allo-HSCT and an association of impaired diversity with acute GI GvHD and adverse patient outcome, Weber *et al.* further compared the effects of various prophylactic and systemic antibiotics in an attempt to identify the ones that could spare commensal bacteria.[89] At 10 days post-transplant, the patient groups receiving rifaximin without systemic antibiotics or rifaximin with systemic antibiotics maintained their microbiome diversity and *Clostridia* abundance and had higher 3-IS levels compared to patients treated with ciprofloxacin/metronidazole ± systemic antibiotics. These results suggest that rifaximin could better preserve microbiome diversity even when systemic broad-spectrum antibiotics are administered during transplantation. Moreover, in the study conducted in two Canadian hospitals and assessing the effect of antibiotic prophylaxis or treatment given before day 0 on frequency of aGvHD and mortality, the authors compared the outcome of a cohort of patients exposed to antibiotics (n=239) to those who did not receive this therapy (n=261).[90] The antibiotic-receiving group demonstrated a significantly higher incidence of grade 2-4 aGvHD and significantly shorter OS at 1, 2 and 10 years post-transplant, indicating an association between the deleterious effect of such treatment on intestinal bacteria and inferior patient outcome.

Importantly, early start of systemic antibiotics (before engraftment) was found to be associated with a lower 3-IS urine level and decreased *Clostridia* abundance in the stool. Furthermore, the TRM rate in such cases was higher than in patients who did not require systemic antibiotics during HSCT or started them after engraftment.[91]

Similarly, systemic treatment with piperacillin-tazobactam and meropenem was reported to correlate with decreased microbiome diversity during the transplantation[37] and significant loss of commensal anaerobic bacteria.[92] In pediatric patients, Simms-Waldrip *et al.*[93] found that higher load of anti-anaerobic antibiotics was associated with a significant decrease in anti-inflammatory *Clostridia* (AIC) abundance, and in patients with aGvHD the abundance decrease was severe (10-log fold) compared to patients without GvHD. In a mouse allo-HSCT model, clindamycin administration was associated with AIC decrease and more severe GvHD, while re-administration of AIC increased its levels in the gut and improved survival.[93] Additionally, Lee *et al.*[94] compared patients who did not require any systemic antibiotic treatment during the transplantation course with those who received cefepime and those who were treated with carbapenem antibiotics. The carbapenem group displayed a significant loss of microbial diversity at engraftment and an increased rate of acute GI GvHD (32.1%) compared to the no-antibiotics group (11.6%). Interestingly, the cefepime group retained a diverse microbiome, demonstrating only a trend to a higher GI GvHD rate (26.4%).

Furthermore, a large multicenter study retrospectively evaluating 857 patients revealed that the use of piperacillin-tazobactam and imipenem-cilastatin was associated with increased 5-year GvHD-related mortality,[95] while this was not observed in patients receiving cefepime and aztreonam. The former antibiotics caused a significant decrease in abundance of *Bacteroidetes* and *Lactobacillus* compared to the latter ones. These results suggest that some antibiotics may be more beneficial than others in the setting of allo-HSCT, and that this beneficial effect is related to the antibiotic ability to be less detrimental to intestinal commensal bacteria.[95] Findings in the pediatric setting were consistent with these data, and exposure to anti-anaerobic antibiotics was reported to result in a significant decrease in butyrate-producing bacteria and the butyrate level in luminal content by day +14. Pediatric patients who later developed aGvHD had a significantly lower butyrate level at that time point than patients without GvHD.[96]

It was also demonstrated that specific antibiotic use during allo-HSCT could change the abundance of specific taxa which was associated with BSI risk. In a cohort of 94 patients, Taur Y *et al.*[50] found that domination of the gut microbiome (abundance ≥30%) by single bacterial taxa *Enterococcus* and *Streptococcus* occurred at the peri-engraftment period (days +10 to +20) in two thirds of the patients. However, treatment with metronidazole increased the risk for enterococcal domination by 3-fold, and this domination elevated the risk for VRE bacteremia by 9-fold. Altogether, these data establish an essential role of antibiotics in disrupting or preserving the intestinal microbiota during allo-HSCT.

Case 1: conclusions

Several issues should be considered in decision-making regarding the appropriate management of this case. This

Table 2. Clinical trials of fecal microbiota transplant in allogeneic hematopoietic stem cell transplantation.

FMT aim	Study (ref.) or ‡NCT number	Number of patients	Outcomes
Prophylactic			
Reduce pathogenic bacteria colonization pre-transplantation			
	Malard *et al.*[66]	20	Restoration of diversity, reduction in antibiotic-resistant gene copy count
	Battipaglia *et al.*[64]	4	All decolonized
	Innes *et al.*[65]	1	All decolonized
Restore microbiome diversity post-transplantation			
	Defillip *et al.*[25]	13	Increase in diversity
	Taur *et al.*[53]	Random: FMT 14 *vs.* control 11	Increase in diversity
Therapeutic			
Recurrent CDI			
	Webb *et al.*[71]	7	No recurrence in 6
	Moss *et al.*[72]	6	No recurrence in 4
	Bluestone *et al.*[73]	3	No recurrence in 1
Steroid refractory/dependent acute GI GvHD			
	Spindelboeck *et al.*[198]	3	2 CR, 1 PR, 3 died
	Kakihana *et al.*[146]	4	3 CR, 1 PR
	Kaito *et al.*[99]	1	CR
	Zhang *et al.*1[100]	1	CR
	Zhong *et al.*[101]	1	CR
	Shouval *et al.*[102]	7	2 CR, 1 PR, 4 died
	Malard *et al.*[103]	8	3 CR, 1 VGPR, 2 PR, 3 died
	Qi *et al.*[104]	8	8 ORR, 2 relapsed, 4 died
	van Lier *et al.*[105]	15	11 CR, 5 relapsed
	Bilinski *et al.*[106]	10	5 ORR, CR 4, SD 1
¶Ongoing clinical trials in GI acute GvHD			
	NCT04269850	¥20	Response and OS
	NCT03819803	¥15	Response
	NCT03812705	¥30	Response
	NCT04285424	¥30	Response
	NCT03359980 (HERACLES trial)	¥32	Response and OS

FMT: fecal microbiota transplant; ‡NCT number: clinicaltrials.gov Identifier. ¶Recruiting or completed from ClinicalTrials.gov; ¥Estimated enrollment; GI: gastrointestinal tract; GvHD: graft-*versus*-host disease; CR: complete remission; PR: partial remission; VGPR: very good partial remission; SD: stable disease; OS: overall survival; ORR: overall response rate.

patient has pre-transplant intestinal microbiota disruption and assumed colonization by MDR bacteria and probably by *Clostridium difficile*. His risk for aGvHD is high, since he has undergone allo-HSCT from a mismatched unrelated donor. Quinolone prophylaxis and meropenem treatment for BSI have further disrupted his intestinal microbiota. The existence of pre-transplant microbiota disruption, mainly attributed to the use of broad-spectrum antibiotics during intensive chemotherapy, is associated with increased TRM, shorter OS and GvHD-related mortality. Pre-transplant FMT can potentially enrich the microbiome diversity and eradicate MDR bacteria or *Clostridium difficile*; however, without controlling such factors as antibiotic prophylaxis and the type of systemic antibiotic therapy employed, the intervention by FMT may not completely achieve its goals.

So far, no data are available regarding a clinical benefit of prophylactic pre-transplant FMT.

While an association between peri-engraftment microbiome low diversity and patient outcome is established, implying potential feasibility of FMT use at that stage, data regarding FMT application before engraftment are not available, and for safety reasons this approach will probably not be attempted. Results of several small-scale studies suggest safety and feasibility of post-engraftment FMT in restoring microbiome diversity (Table 2); however, it remains unknown if this strategy could decrease the risk for aGvHD-related mortality and TRM.

As for dietary interventions at this period, their efficacy is still under investigation. Choosing a different antibiotic prophylaxis, such as rifaximin and systemic antibiotics such as cefepime, looks promising. Nevertheless, new strategies need to be tested to prove their non-inferiority in OS[85] and to establish less disruption for the microbiome (clinicaltrials gov. Identifier: 03078010), especially since fourth-generation cephalosporins have been found in one study to be associated with an increased risk for aGvHD.[97]

Case 1: recommendations

In this case, based on the currently available data, we do not recommend prophylactic administration of pre-transplant or post-engraftment FMT.

Case 2

A 25-year old female with intermediate-risk AML in CR underwent an allo-HSCT with BuCy myeloablative conditioning from her matched sibling. Her neutrophils engrafted by day +14. On day +34 she developed grade 3 aGvHD of the lower GI tract which was steroid refractory (SR). She did not respond to the addition of budesonide, extracorporeal photopheresis (ECP), mofetil mycophenolate or infliximab.

Can fecal microbiota transplantation mitigate prevailing acute gastrointestinal graft-*versus*-host disease?

The current data regarding the use of FMT for the treatment of acute GI GvHD are limited to case reports and small case series (Table 2). A total of 58 described patients were treated with FMT for SR GI grade 2-4 aGvHD. The FMT source was an unrelated donor in 36 cases, a related donor – in six cases and in eight cases a commercial pooled highly diverse FMT was used. FMT was processed and either given fresh within a few hours of collection or it was frozen and later thawed before administration. FMT was administered orally as packed capsules, through a nasogastric/nasoduodenal tube or an enema. Of 58 patients, 28 received FMT after two or more therapy lines, while 19 received it as second-line therapy right after steroid failure. Response was observed in 74% (43 of 58) of patients, with complete response in 57% (33 of 58) and partial response in 17% (10 of 58). Complete response was observed in 73% of patients receiving FMT as second-line therapy. Ten of the responding patients relapsed and 29 patients were alive at the last follow-up (54%; 29 of 54 patients with available data).

Response to treatment was seen within a median of 14 days (range: 3-28), with a median of two FMT (range: 1-7), and a median of 7 days between treatments (range: 2-60).[46,98-106]

Infectious complications occurred in 11 patients. Two had sepsis with bacteria not originating from FMT,[102] and one patient developed diarrhea due to Norovirus that was traced to FMT.[106] Other infections were attributed to the severe immunocompromised state of patients. However, a possible association with FMT could not be ruled out. In responding patients in whom the stool microbiome was sequenced post-FMT, it was found to be significantly more diverse and enriched with *Bacteroides*, *Lactobacillus*, *Bifidobacterium* and *Faecalibacterium* compared to pre-FMT microbiome.[46,98-101] Notably, the diversity increased only upon discontinuation of anti-anaerobic systemic antibiotic treatment, such as piperacillin-tazobactam. However, continuous use or re-initiating treatment with cefepime did not reduce FMT efficiency.[46,98,99]

These results are highly encouraging and support FMT therapy to be relatively safe and effective in SR GI aGvHD.

Case 2: conclusions

Available data suggest a potentially beneficial effect of FMT in acute lower GI GvHD. It should probably be used earlier rather than later, so that patients' response will not be overcome by infectious complications related to extensive immunosuppressive therapy. Discontinuation of antibiotic treatment prior to FMT administration appears to be an important factor contributing to successful response. If antibiotic treatment is required, using cefepime may allow attenuating microbiome insult while maintaining clinical response.

Current information is based on case reports and small series with a wide variability in patient selection, FMT preparation and mode of administration. However, the reported feasibility, safety and clinical benefit appear to be similar across the studies, implying that intestinal microbiota can be recovered with FMT, irrespective of its administration method. Safety remains a concern,[107] especially in advanced GI aGvHD, and if an infectious complication occurs post-FMT, the pathogen should be sequenced and traced to find out if it originates from the FMT.

Case 2: recommendations

Currently, ruxolitinib is the only FDA-approved drug for the treatment of SR aGvHD, while other modalities are also commonly used in this scenario (e.g., extracorporeal photopheresis). Thus, FMT could be recommended for patients with grade 2-4 steroid refractory or dependent aGVHD of the lower GI tract, albeit in the context of a clinical study only.[108-110] Other treatment approaches could also be considered, such as adding it to steroids as part of the first-line therapy (clinicaltrials gov. Identifier: 04269850).

Although clinical trials are still ongoing, given the grave prognosis of SR aGvHD with more than 50% mortality,[111] and the high rate of response to FMT, we recommend considering FMT as a therapeutic option in this setting.

Practical considerations for fecal microbiota transplantation treatment

As FMT has become the standard of care in recurrent and refractory CDI,[112,113] more and more centers are gaining access to FMT programs through either establishing their own stool banks or acquiring FMT from universal stool banks.[114,115]

One of the limiting factors to wider application of stool banks and FMT programs is the lack or variance of regulatory standards. In different countries, FMT is regulated as a drug, tissue or a combined product composed of both human cells and non-human components (microbial DNA and metabolites). Stool banks are recommended to operate under the designated authority in each country. In the absence of local directives, the scientific committee should be responsible for establishing regulatory protocols.[114]

FMT donor screening should follow national regulations and international recommendations.[114] Screening should include medical history related to the risk for transmitting infections, as well as medical conditions and treatments associated with perturbed microbiome (Table 3). Special considerations are to be applied when planning FMT use in allo-HSCT patients, such as testing the donor for Cytomegalovirus and Epstein-Barr virus IgG and IgM, and administering FMT from seronegative donors to seronegative patients. However, when weighing suitability of an FMT donor, one should be cognizant of the fact that no data are available to support the advantage of a particular

donor (a family member, an unrelated donor, or pooled stool from several unrelated donors).

As for autologous FMT, it has not been tested in the setting of aGvHD treatment. Since the microbiota composition of a patient is already disrupted prior to HSCT, using such stool in FMT preparation to be applied for diversity restoration may not be effective. In order to circumvent this problem, in AML patients, we recommend freezing self-stool before the beginning of induction chemotherapy.

In CDI, both fresh and frozen FMT have been shown to be efficient[116] as have been the two delivery routes – colonoscopy and oral capsules.[117] While there are no data pointing to the superiority of either method of preparation or administration for aGvHD treatment, frozen samples from a stool bank allow FMT to be readily available for immediate use without the need to wait for donor screening and FMT collection.

The basic principles of FMT preparation include weighing the sample, suspension in sterile solution (saline), adding glycerol in case the FMT is planned for freezing and storing, homogenization, filtering and aliquoting the suspension for fresh use or freezing (Table 3). The FMT product should be registered and labeled.[114]

Based on the available data (Table 2) we suggest evaluating clinical response at 7-14 days after FMT administration. If no response or only partial response is achieved, we recommend administering a second dose of FMT. Whether in such cases the use of FMT from another donor could provide a superior outcome is yet to be determined. In general, in order to consider FMT as an efficacious therapeutic approach for SR GI aGvHD management, an overall response rate of around 60-70%, with a complete response rate of 30-50% should be a desired target, as these rates are achieved with the use of the approved ruxolitinib treatment and in non-randomized FMT studies.[46,98-106,110]

As for the antibiotic treatment peri-FMT, if feasible, 24-48 hours prior to FMT, systemic antibiotics should be stopped or replaced by one with less anti-anaerobic activity such as rifaximin for prophylaxis or cefepime for febrile neutropenic treatment.[46,98,99]

Microbiome sequencing of donor and patient samples could help interpreting clinical outcomes. It could also be

Table 3. Practical aspects of fecal microbiota transplantation.

FMT stool bank[114]

- Center's own bank
- Acquiring FMT from stool banks of other centers or from a universal stool bank

Regulations[114]

- Set by the designated authority in each country
- Follow international guidelines and recommendations
- If local directives are not available, the center scientific committee should establish regulatory protocols
- FMT for SR GI aGvHD should be given within the setting of a clinical trial

FMT donor screening[114]*

Medical history for infections and risk for infections:

- HIV, hepatitis C, hepatitis B, syphilis, HTLV, other infections, malaria, tuberculosis, illegal drug use, unprotected sex, tissue/organ transplant, recent hospitalization, travel to high risk endemic countries, tattoo, piercing, earing, recent intestinal infection, recent vaccinations with live attenuated virus, blood transfusion, therapy with growth hormone.

Medical history for conditions and medications with risk for microbiota perturbation:

- Chronic gastrointestinal disease (e.g., inflammatory bowel disease, celiac disease), autoimmune disease, cancer, recent GI symptoms (e.g., diarrhea), neurologic disorders, psychiatric disorders, obesity, metabolic syndrome, diabetes, first degree relative with early colon cancer or polyposis. Antibiotic treatment in recent 3 months, chemotherapy, immunotherapy, prolonged use of proton-pump inhibitors, use of probiotics.

Blood tests:

- Hepatitis A, B and C, HTLV, HIV, treponema pallidum, strongyloides stercoralis, NAT for hepatitis B, C and HIV, ANCA (P and C), IgA antibodies level, anti-transglutaminase antibodies, antinuclear antibody, ASCA, liver enzymes, creatinine, calcium, albumin, cholesterol, triglycerides, complete blood count, thyroid function test.

Stool tests:

- Stool culture for *Shigella*, *Salmonella* and *Campylobacter*, direct smear for parasites from different occasions, *Clostridium difficile* antigen, vancomycin-resistant *Enterococci* (VRE), methicillin-resistant *Staphylococcus aureus* (MRSA), carbapenem-resistant *Enterobacteriaceae* (CRE), extended spectrum β lactamase producing *Enterobacteriaceae* (ESBL), *Biofire (Biofire FilmArray) multiplex PCR for *Yersinia enterocolitica*, EAEC (Enteroaggregative *E. coli*), EPEC (Enteropathogenic *E. coli*), ETEC (Enterotoxigenic *E. coli*), STEC (Shiga-like toxin producing *E. coli* stx1/stx2), *E. coli* O157, Shigella / EIEC (Enteroinvasive *E. coli*), *Cryptosporidium*, *Cyclospora cayetanensis*, *Entamoeba histolytica*, *Giardia lamblia*, Adenovirus F 40/41, Astrovirus, Norovirus, Rotavirus A, Sapovirus, *Campylobacter*, *Clostridium difficile* toxins A and B, *Plesiomonas shigelloides*, *Salmonella*, *Vibrio parahaemolyticus* and *vulnificus*, *Vibrio cholerae*.

Special considerations:

- Cytomegalovirus and Epstein-Barr virus serology (IgM and IgG) when administration to immunocompromised patients is planned.[114]
- Patients with severe food allergy should receive FMT from a donor who will avoid the allergy causing food for 72 hours prior to donation.*
- SARS-CoV-2 screening[120] following the FDA safety alert.[121]

Consent:

- Both donors and patients should sign appropriate informed consent.

continued on the next page

continued from previous page

FMT source[122]
- Fresh *versus* frozen: frozen is ready for immediate use.
- Unrelated donor, pooled stool from many unrelated donors, related donor, autologous collected while the patient was still healthy.

FMT preparation and storage[114,122]* (in brief)
- Donor stool collected into a sterile plastic container.
- If not done on site, it should be kept at -4°C until processing.
- Stool processing and storage should be done within 6 hours from collection.
- Processing should be done in a sterile hood
- Weigh the stool (25 g minimum for lower GI FMT and 12.5 g for upper GI FMT).
- Mix with sterile saline, homogenize, filter and centrifuge.
- Re-suspend the pellet with saline.
- If stored frozen, add glycerol to a concentration of 10%.
- Aliquot and label according to way of administration (capsules, tubes)
- Frozen FMT should be kept at -80°C and preferably used within 1 year from collection.

FMT administration[114,122]*

FMT preparation:
- Fresh FMT is given within 6-8 hours from collection.
- Frozen FMT is thawed at 37°C water bath and administered within 4-6 hours.
- Frozen capsules, thawed at room temperature for a few minutes.

Method of administration:
- Upper GI – gastroduodenoscopy, nasogastric tube, nasoduodenal tube, capsules.
- Lower GI - colonoscopy, enema.

Special considerations:
- If possible, to stop antibiotic treatment 24-48 hours prior to administration.
- Or replace current antibiotics with less anti-anaerobic antibiotics (e.g., rifaximin, cefepime)

Monitoring for clinical response in GI aGVHD
- In 7-14 days after administration.
- In case of no response or partial response, consider a second dose.

Stool sampling for later sequencing (16S ribosomal RNA sequencing or other)

From donor:
- A sample from the collected stool of each batch of donation.

From patient:
- A sample obtained before FMT, 1 week, 2 weeks and 4 weeks after FMT, at relapse/progression of GI aGvHD.

Monitoring for adverse events[122]*

Commonly reported:
- Aspiration (in upper GI administration), nausea, vomiting, constipation, diarrhea, bloating, abdominal pain, adverse events caused by the nasogastric tube insertion or colonoscopy procedure, fever.

Infections:
- Diarrhea, colitis, bacteremia, pneumonia.

*National and Institutional guidelines. FMT: fecal microbiota transplantation, SR: steroid refractory, GI: gastrointestinal, aGvHD: acute graft-*versus*-host disease, HIV: human immunodeficiency virus, HTLV: human T-cell leukemia virus, NAT: nucleic acid test, ANCA: anti-neutrophil cytoplasmic antibodies, ASCA: anti- saccharomyces cerevisiae antibodies, CMV: cytomegalovirus, EBV: Epstein-Bar virus.

valuable in distinguishing between the donor and the recipient as the source of post-FMT infection. However, currently there are no data suggesting that patient stool sequencing prior to FMT could guide its administration or affect the outcome. Therefore, given that the primary outcome should be the clinical response to treatment we recommend treating SR GI aGvHD patients with FMT even if the microbiome analysis is not available. Nonetheless, we do suggest storing stool samples from the donor and the patient (before and after FMT) for later sequencing if it becomes available.

Further accumulation of data on FMT for SR GI aGvHD will allow wider and more efficient application of this treatment approach.

Open challenges and future directions

Disruption of the intestinal microbiome during allo-HSCT is a multifaceted process with a cause-and-effect relationship between multiple factors such as conditioning, diet and antibiotic treatment. Lately, FMT has emerged as an intervention that can facilitate microbiome recovery and potentially intervene with the above interplay (Figure 1). The intestinal microbial disruption before and during allo-HSCT is clearly associated with transplant-related outcomes, mainly acute GvHD and mortality, and pre-clinical data demonstrate the key role of the intestinal microbiota in protecting the gut from inflammatory damage and in regulating the innate immune system to maintain a more tolerant state.[118]

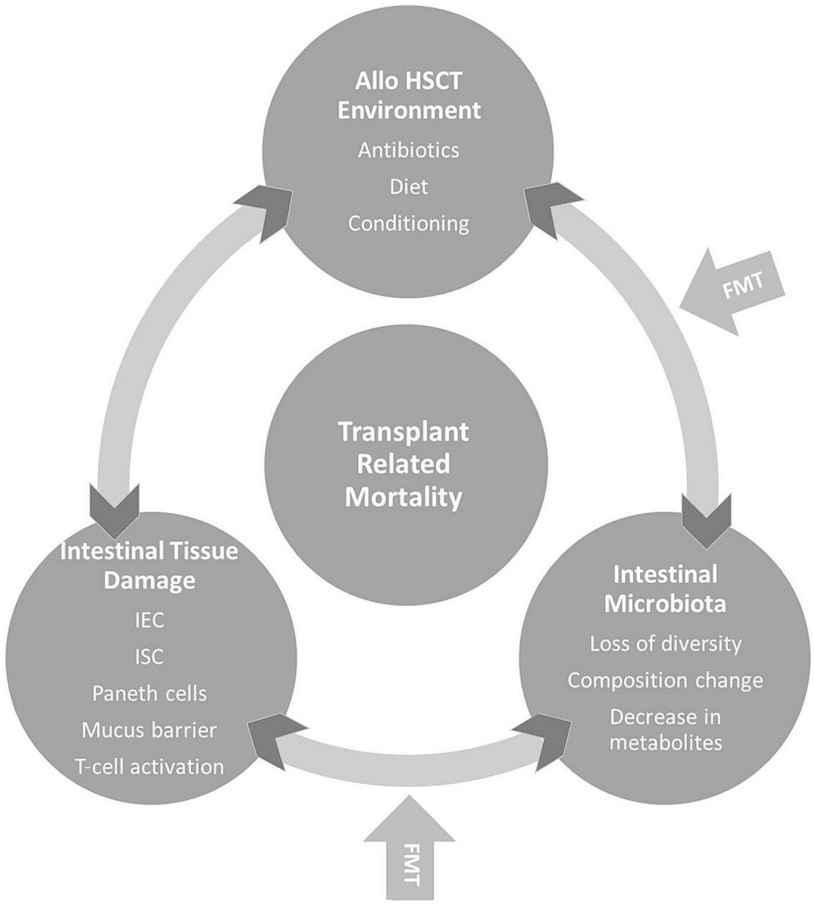


Figure 1. The multifactorial interplay between environmental factors, intestinal microbiota and tissue damage affects transplant-related outcomes. During allogeneic hematopoietic stem cell transplantation (allo-HSCT), conditioning chemotherapy causes damage to the intestinal mucosa cells such as intestinal epithelial cells, intestinal stem cells, paneth cells and mucus producing goblet cells. Gut microbiota is already disrupted before allo-HSCT and due to prophylactic and systemic antibiotic therapy the microbiota disruption worsens with loss of butyrate producing bacteria and other beneficial commensals, along with increase in pathogenic bacteria such as *Enterococcus*. Depletion of bacterial metabolites postpones epithelial cell repair and restoration of the mucus barrier. Pathogenic bacteria can disseminate through the damaged mucosa and cause blood stream infections, which will necessitate the administration of systemic antibiotics further disrupting the intestinal microbiota. This vicious cycle is associated with graft-*versus*-host disease (GvHD), increased mortality and diminished overall survival. The question remains whether fecal microbiota transplantation (FMT) and other interventions such as prebiotics and the use of antibiotics with less anti-anaerobic activity could eventually break the cycle and improve outcomes. IEC:– intestinal epithelial cells; ISC: intestinal stem cells.

While the addition of beneficial bacteria or their metabolites has been shown to ameliorate acute GvHD in animal allo-HSCT models, many challenges remain concerning the role of the intestinal microbiota in allo-HSCT in humans. A substantial amount of basic research is being conducted aiming to better understand the place of microbiome changes in the pathogenesis of acute GvHD. In addition, a large population microbiome analysis is ongoing attempting to delineate the interplay between other factors, such as antibiotics and diet, and the microbiota disruption, and to determine the optimal strategy allowing to preserve the microbiota intact.[119] However, while these issues are still under investigation, clinical trials evaluating the efficacy of FMT and other above-mentioned interventions in the HSCT setting are underway (Table 2). Joint efforts to further explore biological, correlative and recovery functions of the intestinal microbiota could ultimately lead to decreased transplant-related mortality, and even pave the way to personalized therapeutic strategies in HSCT.

Disclosures

No conflicts of interest to disclose.

Contributions

IH, DY-O and TZ wrote the paper.

Acknowledgements

The authors wish to thank Sonia Kamenetsky for her assistance in the preparation of this manuscript.

References

1. D'Souza A, Fretham C. Current uses and outcomes of hematopoietic cell transplantation (HCT): CIBMTR Summary Slides, 2019. Available at https://www.cibmtr.org. Accessed April, 2020. 2019.
2. Canaani J, Beohou E, Labopin M, et al. Trends in patient outcome over the past two decades following allogeneic stem cell transplantation for acute myeloid leukaemia: an ALWP/EBMT analysis. J Intern Med. 2019;285(4):407-418.
3. Turnbaugh PJ, Ley RE, Hamady M, Fraser-Liggett CM, Knight R, Gordon JI. The human microbiome project. Nature. 2007; 449(7164):804-810.
4. Eckburg PB, Bik EM, Bernstein CN, et al. Diversity of the human intestinal microbial flora. Science. 2005;308(5728):1635-1638.
5. Candela M, Biagi E, Maccaferri S, Turroni S, Brigidi P. Intestinal microbiota is a plastic factor responding to environmental changes. Trends Microbiol. 2012;20(8):385-391.
6. Fulde M, Hornef MW. Maturation of the enteric mucosal innate immune system during the postnatal period. Immunol Rev. 2014;260(1):21-34.
7. Ijssennagger N, Belzer C, Hooiveld GJ, et al. Gut microbiota facilitates dietary heme-induced epithelial hyperproliferation by opening the mucus barrier in colon. Proc Natl Acad Sci U S A. 2015;112(32):10038-10043.
8. Reinhardt C, Bergentall M, Greiner TU, et al. Tissue factor and PAR1 promote microbiota-induced intestinal vascular remodelling. Nature. 2012;483(7391):627-631.
9. Neuman H, Debelius JW, Knight R, Koren O. Microbial endocrinology: the interplay between the microbiota and the endocrine

system. FEMS Microbiol Rev. 2015;39(4):509-521.
10. Canfora EE, Jocken JW, Blaak EE. Short-chain fatty acids in control of body weight and insulin sensitivity. Nat Rev Endocrinol. 2015;11(10):577-591.
11. Yatsunenko T, Rey FE, Manary MJ, et al. Human gut microbiome viewed across age and geography. Nature. 2012;486(7402):222-227.
12. Devlin AS, Fischbach MA. A biosynthetic pathway for a prominent class of microbiota-derived bile acids. Nat Chem Biol. 2015;11(9):685-690.
13. Haiser HJ, Gootenberg DB, Chatman K, Sirasani G, Balskus EP, Turnbaugh PJ. Predicting and manipulating cardiac drug inactivation by the human gut bacterium Eggerthella lenta. Science. 2013;341(6143):295-298.
14. Turnbaugh PJ, Hamady M, Yatsunenko T, et al. A core gut microbiome in obese and lean twins. Nature. 2009;457(7228):480-484.
15. Qin J, Li Y, Cai Z, et al. A metagenome-wide association study of gut microbiota in type 2 diabetes. Nature. 2012;490(7418):55-60.
16. Kostic AD, Xavier RJ, Gevers D. The microbiome in inflammatory bowel disease: current status and the future ahead. Gastroenterology. 2014;146(6):1489-1499.
17. Forbes JD, Van Domselaar G, Bernstein CN. The gut microbiota in immune-mediated inflammatory diseases. Front Microbiol. 2016;7:1081.
18. Poore GD, Kopylova E, Zhu Q, et al. Microbiome analyses of blood and tissues suggest cancer diagnostic approach. Nature. 2020;579(7800):567-574.
19. Gopalakrishnan V, Spencer CN, Nezi L, et al. Gut microbiome modulates response to anti-PD-1 immunotherapy in melanoma patients. Science. 2018;359(6371):97-103.
20. Zama D, Biagi E, Masetti R, et al. Gut microbiota and hematopoietic stem cell transplantation: where do we stand? Bone Marrow Transplant. 2017;52(1):7-14.
21. Hooper LV, Littman DR, Macpherson AJ. Interactions between the microbiota and the immune system. Science. 2012;336(6086):1268-1273.
22. Zhao Q, Elson CO. Adaptive immune education by gut microbiota antigens. Immunology. 2018;154(1):28-37.
23. Honda K, Littman DR. The microbiota in adaptive immune homeostasis and disease. Nature. 2016;535(7610):75-84.
24. Shouval R, Fein JA, Labopin M, et al. Outcomes of allogeneic haematopoietic stem cell transplantation from HLA-matched and alternative donors: a European Society for Blood and Marrow Transplantation registry retrospective analysis. Lancet Haematol. 2019;6(11):e573-e584.
25. DeFilipp Z, Peled JU, Li S, et al. Third-party fecal microbiota transplantation following allo-HCT reconstitutes microbiome diversity. Blood Adv. 2018;2(7):745-753.
26. Montassier E, Batard E, Massart S, et al. 16S rRNA gene pyrosequencing reveals shift in patient faecal microbiota during high-dose chemotherapy as conditioning regimen for bone marrow transplantation. Microb Ecol. 2014;67(3):690-699.
27. Bodet CA, 3rd, Jorgensen JH, Drutz DJ. Antibacterial activities of antineoplastic agents. Antimicrob Agents Chemother. 1985;28(3):437-439.
28. Hamilton-Miller JM. Antimicrobial activity of 21 anti-neoplastic agents. Br J Cancer. 1984;49(3):367-369.
29. Schirmer M, Smeekens SP, Vlamakis H, et al. Linking the human gut microbiome to inflammatory cytokine production capacity. Cell. 2016;167(4):1125-1136.e8.
30. Swimm A, Giver CR, DeFilipp Z, et al. Indoles derived from intestinal microbiota act via type I interferon signaling to limit graft-versus-host disease. Blood. 2018;132(23):2506-2519.
31. Mathewson ND, Jenq R, Mathew AV, et al. Gut microbiome-derived metabolites modulate intestinal epithelial cell damage and mitigate graft-versus-host disease. Nat Immunol. 2016;17(5):505-513.
32. Sandhu SS, Pourang A, Sivamani RK. A review of next generation sequencing technologies used in the evaluation of the skin microbiome: what a time to be alive. Dermatol Online J. 2019;25(7):13030/qt3hv5z3q3.
33. Marchesi JR, Ravel J. The vocabulary of microbiome research: a proposal. Microbiome. 2015;3:31.
34. Rinninella E, Raoul P, Cintoni M, et al. What is the healthy gut microbiota composition? A Changing ecosystem across age, environment, diet, and diseases. Microorganisms. 2019;7(1):14.
35. Wortelboer K, Nieuwdorp M, Herrema H. Fecal microbiota transplantation beyond Clostridioides difficile infections. EBioMedicine. 2019;44:716-729.
36. Ooijevaar RE, Terveer EM, Verspaget HW, Kuijper EJ, Keller JJ. Clinical application and potential of fecal microbiota transplantation. Annu Rev Med. 2019;70:335-351.
37. Peled JU, Gomes ALC, Devlin SM, et al. Microbiota as predictor of mortality in allogeneic hematopoietic-cell transplantation. N Engl J Med. 2020;382(9):822-834.
38. Mancini N, Greco R, Pasciuta R, et al. Enteric microbiome markers as early predictors of clinical outcome in allogeneic hematopoietic stem cell transplant: results of a prospective study in adult patients. Open Forum Infect Dis. 2017;4(4):ofx215.
39. Staffas A, Burgos da Silva M, van den Brink MR. The intestinal microbiota in allogeneic hematopoietic cell transplant and graft-versus-host disease. Blood. 2017;129(8):927-933.
40. Taur Y, Jenq RR, Perales MA, et al. The effects of intestinal tract bacterial diversity on mortality following allogeneic hematopoietic stem cell transplantation. Blood. 2014;124(7):1174-1182.
41. Lee YJ, Arguello ES, Jenq RR, et al. Protective factors in the intestinal microbiome against clostridium difficile infection in recipients of allogeneic hematopoietic stem cell transplantation. J Infect Dis. 2017;215(7):1117-1123.
42. Andermann TM, Peled JU, Ho C, et al. The Microbiome and hematopoietic cell transplantation: past, present, and future. Biol Blood Marrow Transplant. 2018;24(7):1322-1340.
43. Ladas EJ, Bhatia M, Chen L, et al. The safety and feasibility of probiotics in children and adolescents undergoing hematopoietic cell transplantation. Bone Marrow Transplant. 2016;51(2):262-266.
44. Iyama S, Sato T, Tatsumi H, et al. Efficacy of enteral supplementation enriched with glutamine, fiber, and oligosaccharide on mucosal injury following hematopoietic stem cell transplantation. Case Rep Oncol. 2014;7(3):692-699.
45. Weber D, Oefner PJ, Dettmer K, et al. Rifaximin preserves intestinal microbiota balance in patients undergoing allogeneic stem cell transplantation. Bone Marrow Transplant. 2016;51(8):1087-1092.
46. Kakihana K, Fujioka Y, Suda W, et al. Fecal microbiota transplantation for patients with steroid-resistant acute graft-versus-host disease of the gut. Blood. 2016;128(16):2083-2088.
47. Galloway-Pena JR, Smith DP, Sahasrabhojane P, et al. The role of the gastrointestinal microbiome in infectious complications during induction chemotherapy for acute myeloid leukemia. Cancer. 2016;122(14):2186-2196.
48. Rashidi A, Kaiser T, Shields-Cutler R, et al. Dysbiosis patterns during re-induction/salvage versus induction chemotherapy for acute leukemia. Sci Rep. 2019;9(1):6083.
49. Kusakabe S, Fukushima K, Maeda T, et al. Pre- and post-serial metagenomic analysis of gut microbiota as a prognostic factor in patients undergoing haematopoietic stem cell transplantation. Br J Haematol. 2020;188(3):438-449.
50. Taur Y, Xavier JB, Lipuma L, et al. Intestinal domination and the risk of bacteremia in patients undergoing allogeneic hematopoietic stem cell transplantation. Clin Infect Dis. 2012;55(7):905-914.
51. Biagi E, Zama D, Nastasi C, et al. Gut microbiota trajectory in pediatric patients undergoing hematopoietic SCT. Bone Marrow Transplant. 2015;50(7):992-998.
52. Holler E, Butzhammer P, Schmid K, et al. Metagenomic analysis of the stool microbiome in patients receiving allogeneic stem cell transplantation: loss of diversity is associated with use of systemic antibiotics and more pronounced in gastrointestinal graft-versus-host disease. Biol Blood Marrow Transplant. 2014;20(5):640-645.
53. Taur Y, Coyte K, Schluter J, et al. Reconstitution of the gut microbiota of antibiotic-treated patients by autologous fecal microbiota transplant. Sci Transl Med. 2018;10(460):eaap9489.
54. Kusakabe S, Fukushima K, Yokota T, et al. Enterococcus: A Predictor of ravaged microbiota and poor prognosis after allogeneic hematopoietic stem cell transplantation. Biol Blood Marrow Transplant. 2020;26(5):1028-1033.
55. Liu C, Frank DN, Horch M, et al. Associations between acute gastrointestinal GvHD and the baseline gut microbiota of allogeneic hematopoietic stem cell transplant recipients and donors. Bone Marrow Transplant. 2017;52(12):1643-1650.
56. Golob JL, Pergam SA, Srinivasan S, et al. Stool microbiota at neutrophil recovery is predictive for severe acute graft vs host disease after hematopoietic cell transplantation. Clin Infect Dis. 2017;65(12):1984-1991.
57. Jenq RR, Taur Y, Devlin SM, et al. Intestinal Blautia is associated with reduced death from graft-versus-host disease. Biol Blood Marrow Transplant. 2015;21(8):1373-1383.
58. Biagi E, Zama D, Rampelli S, et al. Early gut microbiota signature of aGvHD in children given allogeneic hematopoietic cell transplantation for hematological disorders. BMC Med Genomics. 2019;12(1):49.
59. Peled JU, Devlin SM, Staffas A, et al. Intestinal microbiota and relapse after hematopoietic-cell transplantation. J Clin Oncol. 2017;35(15):1650-1659.
60. Forcina A, Lorentino F, Marasco V, et al. Clinical impact of pretransplant multidrug-resistant gram-negative colonization in autologous and allogeneic hematopoietic stem cell transplantation. Biol Blood Marrow Transplant. 2018;24(7):1476-1482.
61. Sadowska-Klasa A, Piekarska A, Prejzner W, Bieniaszewska M, Hellmann A.

Colonization with multidrug-resistant bacteria increases the risk of complications and a fatal outcome after allogeneic hematopoietic cell transplantation. Ann Hematol. 2018;97(3):509-517.
62. Bilinski J, Robak K, Peric Z, et al. Impact of gut colonization by antibiotic-resistant bacteria on the outcomes of allogeneic hematopoietic stem cell transplantation: a retrospective, single-center study. Biol Blood Marrow Transplant. 2016;22(6):1087-1093.
63. Oren I, Sprecher H, Finkelstein R, et al. Eradication of carbapenem-resistant Enterobacteriaceae gastrointestinal colonization with nonabsorbable oral antibiotic treatment: a prospective controlled trial. Am J Infect Control. 2013;41(12):1167-1172.
64. Battipaglia G, Malard F, Rubio MT, et al. Fecal microbiota transplantation before or after allogeneic hematopoietic transplantation in patients with hematologic malignancies carrying multidrug-resistance bacteria. Haematologica. 2019;104(8):1682-1688.
65. Innes AJ, Mullish BH, Fernando F, et al. Faecal microbiota transplant: a novel biological approach to extensively drug-resistant organism-related non-relapse mortality. Bone Marrow Transplant. 2017;52(10):1452-1454.
66. Malard F, Vekhoff A, Lapusan S, et al. The ODYSSEE study: Prevention of dysbiosis complications with autologous fecal microbiota transfer in acute myeloid leukemia patients undergoing intensive-treatment: Results of a prospective multicenter trial. Bone Marrow Transplant. 2019;54:OS16-11
67. Willems L, Porcher R, Lafaurie M, et al. Clostridium difficile infection after allogeneic hematopoietic stem cell transplantation: incidence, risk factors, and outcome. Biol Blood Marrow Transplant. 2012;18(8):1295-1301.
68. Alonso CD, Treadway SB, Hanna DB, et al. Epidemiology and outcomes of Clostridium difficile infections in hematopoietic stem cell transplant recipients. Clin Infect Dis. 2012;54(8):1053-1063.
69. Dubberke ER, Reske KA, Olsen MA, et al. Epidemiology and outcomes of Clostridium difficile infection in allogeneic hematopoietic cell and lung transplant recipients. Transpl Infect Dis. 2018;20(2):e12855.
70. Kinnebrew MA, Lee YJ, Jenq RR, et al. Early Clostridium difficile infection during allogeneic hematopoietic stem cell transplantation. PLoS One. 2014;9(3):e90158.
71. Webb BJ, Brunner A, Ford CD, Gazdik MA, Petersen FB, Hoda D. Fecal microbiota transplantation for recurrent Clostridium difficile infection in hematopoietic stem cell transplant recipients. Transpl Infect Dis. 2016;18(4):628-633.
72. Moss EL, Falconer SB, Tkachenko E, et al. Long-term taxonomic and functional divergence from donor bacterial strains following fecal microbiota transplantation in immunocompromised patients. PLoS One. 2017;12(8):e0182585.
73. Bluestone H, Kronman MP, Suskind DL. Fecal microbiota transplantation for recurrent Clostridium difficile infections in pediatric hematopoietic stem cell transplant recipients. J Pediatric Infect Dis Soc. 2018;7(1):e6-e8.
74. Han L, Zhang H, Chen S, et al. Intestinal microbiota can predict acute graft-versus-host disease following allogeneic hematopoietic stem cell transplantation. Biol Blood Marrow Transplant. 2019;25(10):1944-1955.
75. Kroger N, Iacobelli S, Franke GN, et al. Dose-reduced versus standard conditioning followed by allogeneic stem-cell transplantation for patients with myelodysplastic syndrome: A Prospective randomized phase III study of the EBMT (RICMAC Trial). J Clin Oncol. 2017;35(19):2157-2164.
76. Scott BL. Long-Term Follow up of BMT CTN 0901, a randomized phase III trial comparing myeloablative (MAC) to reduced intensity conditioning (RIC) prior to hematopoietic cell transplantation (HCT) for acute myeloid leukemia (AML) or myelodysplasia (MDS) (MAvRIC Trial). Biol Blood Marrow Transplant. 2020;26(3):S11.
77. Sengsayadeth S, Gatwood KS, Boumendil A, et al. Conditioning intensity in secondary AML with prior myelodysplastic syndrome/myeloproliferative disorders: an EBMT ALWP study. Blood Adv. 2018;2(16):2127-2135.
78. D'Amico F, Biagi E, Rampelli S, et al. Enteral nutrition in pediatric patients undergoing hematopoietic SCT promotes the recovery of gut microbiome homeostasis. Nutrients. 2019;11(12):2958.
79. Venkataraman A, Sieber JR, Schmidt AW, Waldron C, Theis KR, Schmidt TM. Variable responses of human microbiomes to dietary supplementation with resistant starch. Microbiome. 2016;4(1):33.
80. Riwes MM, Schmidt A, Braun T, et al. Rational modification of intestinal microbiome and metabolites after allogeneic hematopoietic stem cell transplantation with resistant starch: a pilot study. Blood. 2019;134(Suppl_1):3276.
81. Gorshein E, Wei C, Ambrosy S, et al. Lactobacillus rhamnosus GG probiotic enteric regimen does not appreciably alter the gut microbiome or provide protection against GVHD after allogeneic hematopoietic stem cell transplantation. Clin Transplant. 2017;31(5).
82. Boyle RJ, Robins-Browne RM, Tang ML. Probiotic use in clinical practice: what are the risks? Am J Clin Nutr. 2006;83(6):1256-1264; quiz 1446-1257.
83. Stein-Thoeringer CK, Nichols KB, Lazrak A, et al. Lactose drives Enterococcus expansion to promote graft-versus-host disease. Science. 2019;366(6469):1143-1149.
84. Khandelwal P, Andersen H, Romick-Rosendale L, et al. A pilot study of human milk to reduce intestinal inflammation after bone marrow transplant. Breastfeed Med. 2019;14(3):193-202.
85. Gafter-Gvili A, Fraser A, Paul M, et al. Antibiotic prophylaxis for bacterial infections in afebrile neutropenic patients following chemotherapy. Cochrane Database Syst Rev. 2012;1:CD004386.
86. Tomblyn M, Brunstein C, Burns LJ, et al. Similar and promising outcomes in lymphoma patients treated with myeloablative or nonmyeloablative conditioning and allogeneic hematopoietic cell transplantation. Biol Blood Marrow Transplant. 2008;14(5):538-545.
87. Averbuch D, Orasch C, Cordonnier C, et al. European guidelines for empirical antibacterial therapy for febrile neutropenic patients in the era of growing resistance: summary of the 2011 4th European Conference on Infections in Leukemia. Haematologica. 2013;98(12):1826-1835.
88. Weber D, Oefner PJ, Hiergeist A, et al. Low urinary indoxyl sulfate levels early after transplantation reflect a disrupted microbiome and are associated with poor outcome. Blood. 2015;126(14):1723-1728.
89. Weber D, Hiergeist A, Weber M, et al. Detrimental Effect of broad-spectrum antibiotics on intestinal microbiome diversity in patients after allogeneic stem cell transplantation: lack of commensal sparing antibiotics. Clin Infect Dis. 2019;68(8):1303-1310.
90. Routy B, Letendre C, Enot D, et al. The influence of gut-decontamination prophylactic antibiotics on acute graft-versus-host disease and survival following allogeneic hematopoietic stem cell transplantation. Oncoimmunology. 2017;6(1):e1258506.
91. Weber D, Jenq RR, Peled JU, et al. Microbiota disruption induced by early use of broad-spectrum antibiotics is an independent risk factor of outcome after allogeneic stem cell transplantation. Biol Blood Marrow Transplant. 2017;23(5):845-852.
92. Morjaria S, Schluter J, Taylor BP, et al. Antibiotic-induced shifts in fecal microbiota density and composition during hematopoietic stem cell transplantation. Infect Immun. 2019;87(9):e00206-e00219.
93. Simms-Waldrip TR, Sunkersett G, Coughlin LA, et al. Antibiotic-induced depletion of anti-inflammatory Clostridia is associated with the development of graft-versus-host disease in pediatric stem cell transplantation patients. Biol Blood Marrow Transplant. 2017;23(5):820-829.
94. Lee SE, Lim JY, Ryu DB, et al. Alteration of the intestinal microbiota by broad-spectrum antibiotic use correlates with the occurrence of intestinal graft-versus-host disease. Biol Blood Marrow Transplant. 2019;25(10):1933-1943.
95. Shono Y, Docampo MD, Peled JU, et al. Increased GVHD-related mortality with broad-spectrum antibiotic use after allogeneic hematopoietic stem cell transplantation in human patients and mice. Sci Transl Med. 2016;8(339):339ra371.
96. Romick-Rosendale LE, Haslam DB, Lane A, et al. Antibiotic exposure and reduced short chain fatty acid production after hematopoietic stem cell transplant. Biol Blood Marrow Transplant. 2018;24(12):2418-2424.
97. Nishi K, Kanda J, Hishizawa M, et al. Impact of the Use and type of antibiotics on acute graft-versus-host disease. Biol Blood Marrow Transplant. 2018;24(11):2178-2183.
98. Spindelboeck W, Schulz E, Uhl B, et al. Repeated fecal microbiota transplantations attenuate diarrhea and lead to sustained changes in the fecal microbiota in acute, refractory gastrointestinal graft-versus-host-disease. Haematologica. 2017;102(5):e210-e213.
99. Kaito S, Toya T, Yoshifuji K, et al. Fecal microbiota transplantation with frozen capsules for a patient with refractory acute gut graft-versus-host disease. Blood Adv. 2018;2(22):3097-3101.
100. Zhang J, Ren G, Li M, Lu P, Yi S. The effects of fecal donors with different feeding patterns on diarrhea in a patient undergoing hematopoietic stem cell transplantation. Case Rep Hematol. 2019;2019:4505238.
101. Zhong S, Zeng J, Deng Z, et al. Fecal microbiota transplantation for refractory diarrhea in immunocompromised diseases: a pediatric case report. Ital J Pediatr. 2019;45(1):116.
102. Shouval R, Youngster I, Geva M, et al. Repeated courses of orally administered fecal microbiota transplantation for the treatment of steroid resistant and steroid dependent intestinal acute graft vs. host disease: A pilot study (NCT 03214289). Blood. 2018;132(Suppl_1):2121.
103. Malard F, Legrand F, Cornillon J, et al. Successful and safe treatment of intestinal

graft-versus-host disease (GvHD) with pooled-donor full ecosystem microbiota biotherapeutics. Blood. 2019;134(Suppl_1): 1993.
104. Qi X, Li X, Zhao Y, et al. Treating steroid refractory intestinal acute graft-vs.-host disease with fecal microbiota transplantation: A pilot study. Front Immunol. 2018;9:2195.
105. van Lier YF, M D, Haverkate NJE, et al. Fecal microbiota transplantation can cure steroid-refractory intestinal graft-versus-host disease. Biol Blood Marrow Transplant 2019;25(3):S241.
106. Bilinski J, Lis K, Tomaszewska A, et al. Fecal microbiota transplantation as a treatment of severe steroid-resistant acute and chronic graft versus host disease. Spectrum of responses and complications. Blood. 2019;134(Suppl_1):5667.
107. DeFilipp Z, Bloom PP, Torres Soto M, et al. Drug-resistant E. coli bacteremia transmitted by fecal microbiota transplant. N Engl J Med. 2019;381(21):2043-2050.
108. Modemann F, Ayuk F, Wolschke C, et al. Ruxolitinib plus extracorporeal photopheresis (ECP) for steroid refractory acute graft-versus-host disease of lower GI-tract after allogeneic stem cell transplantation leads to increased regulatory T cell level. Bone Marrow Transplant. 2020;55(12): 2286-2293.
109. Drexler B, Buser A, Infanti L, Stehle G, Halter J, Holbro A. Extracorporeal photopheresis in graft-versus-host disease. Transfus Med Hemother. 2020;47(3):214-225.
110. Zeiser R, von Bubnoff N, Butler J, et al. Ruxolitinib for glucocorticoid-refractory acute graft-versus-host disease. N Engl J Med. 2020;382(19):1800-1810.
111. Srinagesh HK, Levine JE, Ferrara JLM. Biomarkers in acute graft-versus-host disease: new insights. Ther Adv Hematol. 2019;10:2040620719891358.
112. Bakken JS, Borody T, Brandt LJ, et al. Treating Clostridium difficile infection with fecal microbiota transplantation. Clin Gastroenterol Hepatol. 2011;9(12):1044-1049.
113. Davidovics ZH, Michail S, Nicholson MR, et al. Fecal microbiota transplantation for recurrent clostridium difficile infection and other conditions in children: A joint position paper from the North American Society for Pediatric Gastroenterology, Hepatology, and Nutrition and the European Society for Pediatric Gastroenterology, Hepatology, and Nutrition. J Pediatr Gastroenterol Nutr. 2019;68(1):130-143.
114. Cammarota G, Ianiro G, Kelly CR, et al. International consensus conference on stool banking for faecal microbiota transplantation in clinical practice. Gut. 2019;68(12): 2111-2121.
115. Panchal P, Budree S, Scheeler A, et al. Scaling safe access to fecal microbiota transplantation: past, present, and future. Curr Gastroenterol Rep. 2018;20(4):14.
116. Lee CH, Steiner T, Petrof EO, et al. Frozen vs fresh fecal microbiota transplantation and clinical resolution of diarrhea in patients with recurrent Clostridium difficile infection: a randomized clinical trial. JAMA. 2016;315(2):142-149.
117. Kao D, Roach B, Silva M, et al. Effect of oral capsule- vs colonoscopy-delivered fecal microbiota transplantation on recurrent Clostridium difficile infection: a randomized clinical trial. JAMA. 2017;318(20):1985-1993.
118. Riwes M, Reddy P. Microbial metabolites and graft versus host disease. Am J Transplant. 2018;18(1):23-29.
119. Nguyen CL, Gomes ALC, Peled JU, et al. Antibiotic exposures and dietary intakes are associated with changes in microbiota compositions in allogeneic hematopoietic stem cell transplant patients. Blood. 2019;134 (Suppl_1):597.
120. Ng SC, Chan FKL, Chan PKS. Screening FMT donors during the COVID-19 pandemic: a protocol for stool SARS-CoV-2 viral quantification. Lancet Gastroenterol Hepatol. 2020;5(7):642-643.
121. Safety alert regarding use of fecal microbiota for transplantation and additional safety protections pertaining to SARS-CoV-2 and COVID-19. Available at https://www.fda.gov/vaccines-blood-biologics/safety-availability-biologics/safety-alert-regarding-use-fecal-microbiota-transplantation-and-additional-safety-protections. Accessed on July 20, 2020.
122. Nicco C, Paule A, Konturek P, Edeas M. From donor to patient: Collection, preparation and cryopreservation of fecal samples for fecal microbiota transplantation. Diseases. 2020;8(2):9.

REVIEW ARTICLE

Latest culture techniques: cracking the secrets of bone marrow to mass-produce erythrocytes and platelets *ex vivo*

Christian A. Di Buduo,[1] Alicia Aguilar,[1] Paolo M. Soprano,[1] Alberto Bocconi,[1,2] Carolina P. Miguel,[1] Giovanna Mantica[1] and Alessandra Balduini[1,3]

[1]Department of Molecular Medicine, University of Pavia, Pavia, Italy; [2]Department of Chemistry, Materials and Chemical Engineering G. Natta, Politecnico di Milano, Milano, Italy and [3]Department of Biomedical Engineering, Tufts University, Medford, MA, USA

Ferrata Storti Foundation

Haematologica 2021
Volume 106(4):947-957

ABSTRACT

Since the dawn of medicine, scientists have carefully observed, modeled and interpreted the human body to improve healthcare. At the beginning there were drawings and paintings, now there is three-dimensional modeling. Moving from two-dimensional cultures and towards complex and relevant biomaterials, tissue-engineering approaches have been developed in order to create three-dimensional functional mimics of native organs. The bone marrow represents a challenging organ to reproduce because of its structure and composition that confer it unique biochemical and mechanical features to control hematopoiesis. Reproducing the human bone marrow niche is instrumental to answer the growing demand for human erythrocytes and platelets for fundamental studies and clinical applications in transfusion medicine. In this review, we discuss the latest culture techniques and technological approaches to obtain functional platelets and erythrocytes *ex vivo*. This is a rapidly evolving field that will define the future of targeted therapies for thrombocytopenia and anemia, but also a long-term promise for new approaches to the understanding and cure of hematologic diseases.

Introduction

The importance of three-dimensional (3D) tissue systems has grown substantively in recent years as laboratory tools that recapitulate the physiological architecture of native human tissues.[1] The bone marrow represents a challenging organ to reproduce because of its structure and complexity within the bone cavity.[2] Recent research in the field aims to overcome the problems by developing different 3D models for the *ex vivo* production of blood cells. These systems can be used to understand the process of hematopoiesis in normal conditions and disease states and as an innovative way to produce blood products for clinical needs.

More than 100 million units of blood are reported to be collected worldwide every year. Nevertheless, in no country does the contribution of volunteers succeed in coping with the growing demand, making it necessary to create alternative methods for the production of blood cells.[3] There is particular interest in the possibility of producing erythrocytes and platelets.

Platelets are needed more than other blood components because they are perishable. While erythrocytes can be refrigerated and used for up to 6 weeks and plasma can be frozen for as long as a year, platelets must be kept at room temperature to maintain their shape and function, which means that they have a shelf-life of only 5 days inside transfusion bags.[4] Overall, blood products for transfusion are often unavailable in low-income and middle-income countries.[5,6] Furthermore, even in developed countries, outside of large and medium-sized cities, hospitals can run out of platelets and erythrocytes when donation rates are down, which occurs mainly during the summer or public health emergencies, such as a pandemic. In the last few years, emerging infectious diseases have captured the attention of the transfusion medicine community and measures have been implemented to address

Correspondence:

CHRISTIAN A. DI BUDUO
christian.dibuduo@unipv.it

ALESSANDRA BALDUINI
alessandra.balduini@unipv.it

Received: September 25, 2020.
Accepted: December 11, 2020.
Pre-published: January 21, 2021.

https://doi.org/10.3324/haematol.2020.262485

©2021 Ferrata Storti Foundation

Material published in Haematologica is covered by copyright. All rights are reserved to the Ferrata Storti Foundation. Use of published material is allowed under the following terms and conditions: https://creativecommons.org/licenses/by-nc/4.0/legalcode. Copies of published material are allowed for personal or internal use. Sharing published material for non-commercial purposes is subject to the following conditions: https://creativecommons.org/licenses/by-nc/4.0/legalcode, sect. 3. Reproducing and sharing published material for commercial purposes is not allowed without permission in writing from the publisher.

concerns regarding potential transmission of prions and viruses.[7,8] The recent spread of Sars-CoV-2 has had a profound impact on the number of blood donations, blood component supplies, and safety.[9,10] The Sars-CoV-2 has a long incubation period and causes asymptomatic infections in most people, which poses enormous challenges in the recruitment of blood donors, necessitating the implementation of new screening guidelines for hemovigilance. Indeed, during the lockdown, blood transfusion centers experienced a dramatic drop in the number of volunteers almost worldwide. Furthermore, several agents first described decades ago still represent ongoing blood safety risks that have not been adequately addressed. These include several species of Babesia known to cause human infections, which are being reported more frequently every year, especially in the USA.[11]

Given all this background, *ex vivo* manufacture of erythrocytes and platelets is becoming an increasingly attractive approach for transfusion medicine. In this review, we discuss the most recent scientific knowledge about mechanisms of erythrocyte and platelet production and technological advances in the field of bioengineering, which together have led to the development of new laboratory tools that mimic human bone marrow with different levels of complexity. The breakthrough of these approaches will lead to the generation of highly defined and controlled microenvironments in a clinical-grade condition for producing blood cell units on demand for transfusions.

Looking inside the bone marrow: an overview on the origin of blood platelets and erythrocytes *in vivo*

The formation of blood cells from hematopoietic stem cells (HSC) occurs within the bone marrow through a series of ever more differentiated progenitors under the tight control of soluble and environmental factors that cooperate in a framework known as the hematopoietic niche.[12] Within this context, millions of platelets and erythrocytes are generated each day from a common megakaryocyte-erythroid progenitor cell that is recruited towards final differentiation by thrombopoietin or erythropoietin (Figure 1).[13] A subset of long-term HSC with restricted myeloid-repopulating activity committed to the erythro-megakaryocytic lineage has also been postulated.[14,15]

During their process of differentiation, both cell lineages undergo characteristic morphological changes that lead to the respective lineage consolidation. These include nuclear polyploidization and cellular enlargement with the development of cytoplasmic granules and the demarcation membrane system for megakaryocytes,[16] while cell size reduction and chromatin condensation accompanied by increased production of hemoglobin can be observed in erythroblasts.[17] Both cell lineages face one crucial final step at the end of their maturation. For megakaryocytes this is elongation of thin pseudopods, known as proplatelets, within the lumen of bone marrow sinusoids, where platelet detachment from the proplatelet shaft can be attributed mainly to turbulent blood hydrodynamics and fluid shear.[18] A recent study demonstrated that membrane budding also contributes to supply the platelet biomass.[19] For erythrocytes the crucial step entails expulsion of the nucleus from erythroblasts, which leads to the formation of reticulocytes, and the loss of organelles and ribosomes through autophagy/exosome-combined pathways.[20]

While cytokine-mediated priming is important to drive hematopoietic cell commitment, the final steps are strictly dependent on the interplay of different environmental cues, including cell-to-matrix and cell-to-cell interactions.[21,22] Both platelet and erythrocyte production are profoundly influenced by the composition and stiffness of the extracellular matrix, which can model cell behavior through mechanical and chemical signals via integrins and mechano-sensitive ion channels.[23-25] The protein tangle shaping the extracellular matrix is mainly composed of different types of collagen (I, II, III, V, XI), fibronectin, laminins, and glycosaminoglycans, continuously remodeled in physiology and disease through specific proteases, such as matrix metalloproteinases.[26] It has been demonstrated that the softest substrates of the extracellular matrix, such as fibronectin and type IV collagen, mainly located in the medullary cavity and around sinusoids, support megakaryocyte proliferation and proplatelet formation. In contrast, the endosteal surface, which is asymmetrically enriched with the stiff type I collagen, prevents platelet production.[27,28] Regarding erythropoiesis, the interaction with fibronectin also supports cell proliferation and protects from apoptosis.[29] Specialized niches localized throughout the intratrabecular space support erythrocyte maturation. Early erythroid progenitors are closely associated with perisinusoidal leptin receptor-positive stromal cells that secrete stem cell factor to support their maintenance,[30] while the process of enucleation takes place within erythroblastic islands, hematopoietic sub-compartments composed of erythroblasts surrounding a central macrophage.[31,32] Here, the interaction between macrophages and erythroblasts, mediated by the erythroblast-macrophage protein and integrins, is required to facilitate proliferation and differentiation and provide iron to the erythroblasts.[33]

In the light of all this knowledge, the top three challenges facing biomedical research today aimed at developing clinically relevant tools for *ex vivo* blood cell production are: (i) finding appropriate sources of stem cells; (ii) identifying efficient culture conditions for their commitment; (iii) mimicking relevant features of the bone marrow microenvironment to support the final stages of erythrocyte and platelet production.

The artificial cell and stem cell pipelines for obtaining functional platelets and erythrocytes *in vitro*

Artificial blood cell production and hematopoietic induction of stem cells have been studied to generate *in vitro* fully functional platelets and erythrocytes (Figure 2).

Synthetic platelets able to adhere to subendothelial structures have been constructed by functionalizing polymeric, liposomal or discoid albumin particles with recombinant glycoproteins or small peptides that bind to von Willebrand factor and collagen.[34] More recent advances in the field include: highly deformable microgel platelet-like particles, which tenaciously bind to fibrin fibers promoting clot contraction and stability;[35] platelet-like nanoparticles, whose discoidal shape and flexible exterior enhance platelet marginalization and aggregation;[36] and artificial dense granules consisting of liposomes that release factors

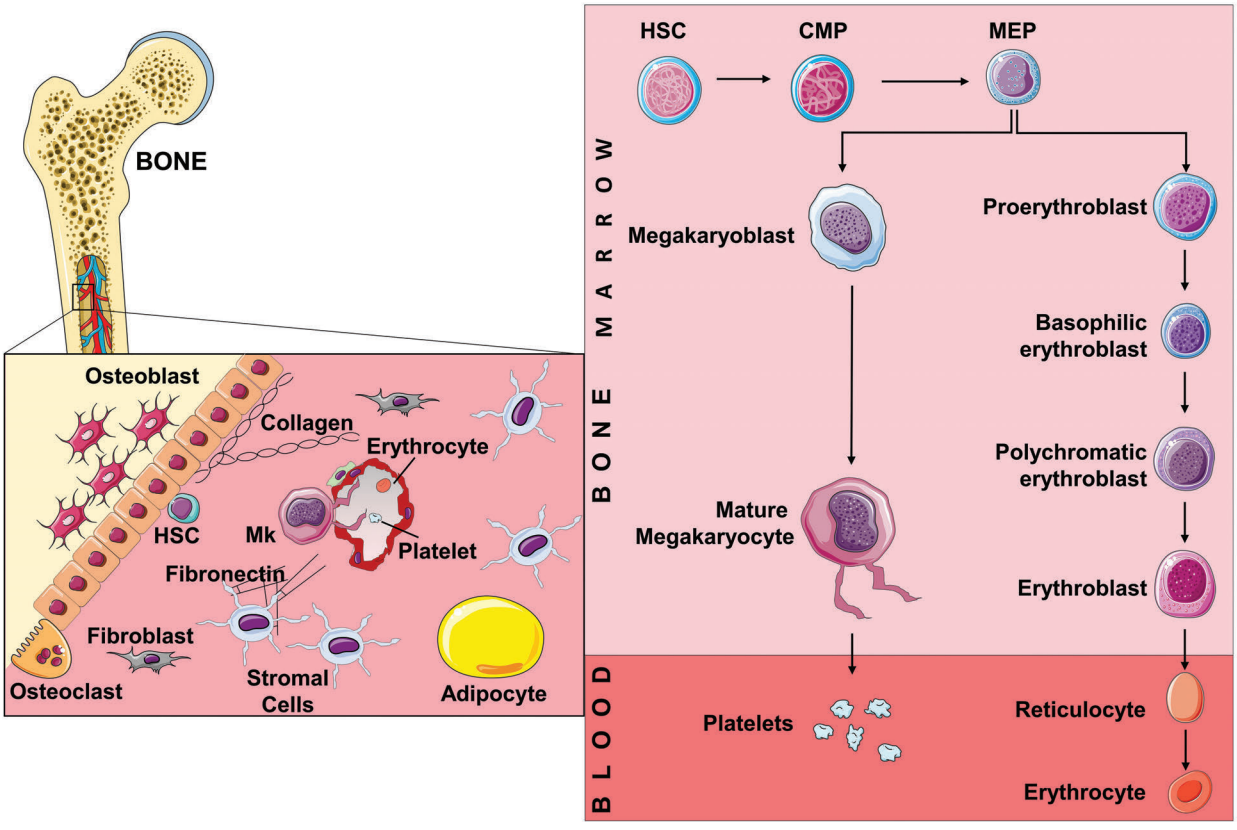


Figure 1. Bone marrow hematopoiesis. Schematic representation of the adult hematopoietic stem cell niche, showing various cell types and extracellular matrix components that influence the differentiation of blood progenitors. The hierarchical differentiation pathways of megakaryopoiesis and erythropoiesis are highlighted. Megakaryopoiesis is typically characterized by an increase in cell size and ploidy, resulting in the final extension of long pseudopods, called proplatelets, which release platelets into the bloodstream. Erythropoiesis entails several morphological and structural changes that give rise to basophilic, polychromatophilic and acidophilic erythroblasts. At the end of the terminal maturation reticulocytes are released into the bloodstream where they complete their maturation into mature erythrocytes. Mk: megakaryocyte; HSC: hematopoietic stem cell; CMP: common myeloid progenitor; MEP: megakaryocyte-erythroid progenitor. The figure was created using Servier Medical Art templates licensed under a Creative Commons Attribution 3.0 Unported License (*https://smart.servier.com*).

activating the coagulation cascade.[37]

Hemoglobin-based oxygen carriers, either human or bovine, have been proposed as erythrocyte surrogates, but none has been licensed by the Food and Drug Administration because of severe thrombotic adverse effects caused by the nitric oxide-scavenging effect of the hemoglobin molecule.[38] However, successful cases of compassionate usage have been reported,[39,40] and one of these products is currently used in South Africa in emergencies or when there is a clinical contraindication to blood transfusion.[41]

Engineered nanostructures that mimic biophysical actions of platelets and erythrocytes are therefore of interest. Advantages of their use would include no need of refrigeration and of blood grouping and matching, but they are not effective as native cells. Indeed, the functions of native cells are not easy to reproduce and thus much more effort has been focused on finding reliable sources of stem cells to be differentiated *in vitro*.

Animal models have been widely used. Megakaryocytes and erythrocytes can be obtained by flushing murine and rat femora or differentiated from murine fetal liver progenitors.[42,43] These are invaluable cell sources for studying the basic mechanisms of hematopoiesis and for providing proof of principle of new translational approaches for making blood cells available for transfusion. However, beyond ethical issues related to their intensive use in science, interspecies differences can render animals poor predictors of human physiology and their usage for clinical purposes is not conceivable.

Umbilical cord blood is a rapidly available source of human HSC that can be efficiently differentiated into primary cultures of erythroblasts or megakaryocytes.[44,45] Umbilical cord blood HSC have been used to establish immortalized human erythroid progenitor cell lines able to produce enucleated erythrocytes.[46] The main practical advantages of using umbilical cord blood are the relative ease of procurement, the lowest possibility of viral contamination and the absence of risk for mothers and donors. Nevertheless, active limitations remain the dependence on donors and the restricted availability to research teams. Finally, umbilical cord blood $CD34^+$ cells are stem cells of fetal/neonatal origin that give rise to cells that have distinct features from those of adult cells, such as a high proliferation rate and high percentages of fetal hemoglobin in the case of erythrocytes.[47-50]

Methods for obtaining human adult megakaryocytes from peripheral blood or bone marrow HSC have been tested and have provided invaluable data about mechanisms of platelet production in disease states due to inherited or acquired mutations in genes relevant for the control of megakaryopoiesis.[51] Giarratana *et al.* also used peripheral blood HSC to generate a homogeneous population of erythrocytes that were functional in terms of deformabil-

ity, enzyme content, capacity of their hemoglobin to fix/release oxygen, and expression of blood group antigens.[52] Nevertheless, these cell sources usually derive from clinical procedures and can be rare and difficult to obtain. They require a continuous supply of donors due to the limited expansion potential, making it difficult to hypothesize their usage for clinical applications. In this regard, Trakarnsanga *et al.* developed an alternative approach, immortalizing early bone marrow adult erythroblasts and generating a stable line functionally identical to adult donor erythrocytes.[53] This cell line revealed promising properties for manufacturing red blood cell products and as a research tool for the study of erythropoiesis in health and disease. Compared to umbilical cord blood-derived immortalized human erythroid progenitor cell lines, this source demonstrated better performance and recapitulation of adult erythropoiesis.[54]

The need for cells that could overcome the limits related to donor dependence have prompted researchers to use human embryonic stem cells (hESC) and human induced pluripotent stem cells (hiPSC). hESC have been grown either on stromal cells or in feeder-free and serum-free cultures to produce platelet-like particles displaying functional and morphological features comparable to peripheral blood platelets, but with limited long-term self-replication of megakaryocyte progenitors and consequent yield of platelets.[55] hESC have also been proposed as a source of stem cells to generate universal red blood cells,[56] but with some limitations in terms of cell survival and end-stage maturation.

Good outcomes have been obtained with hiPSC, which overcome ethical concerns related to the use of cells of embryonic origin. The physiological features of hiPSC-derived megakaryocytes resemble those of peripheral

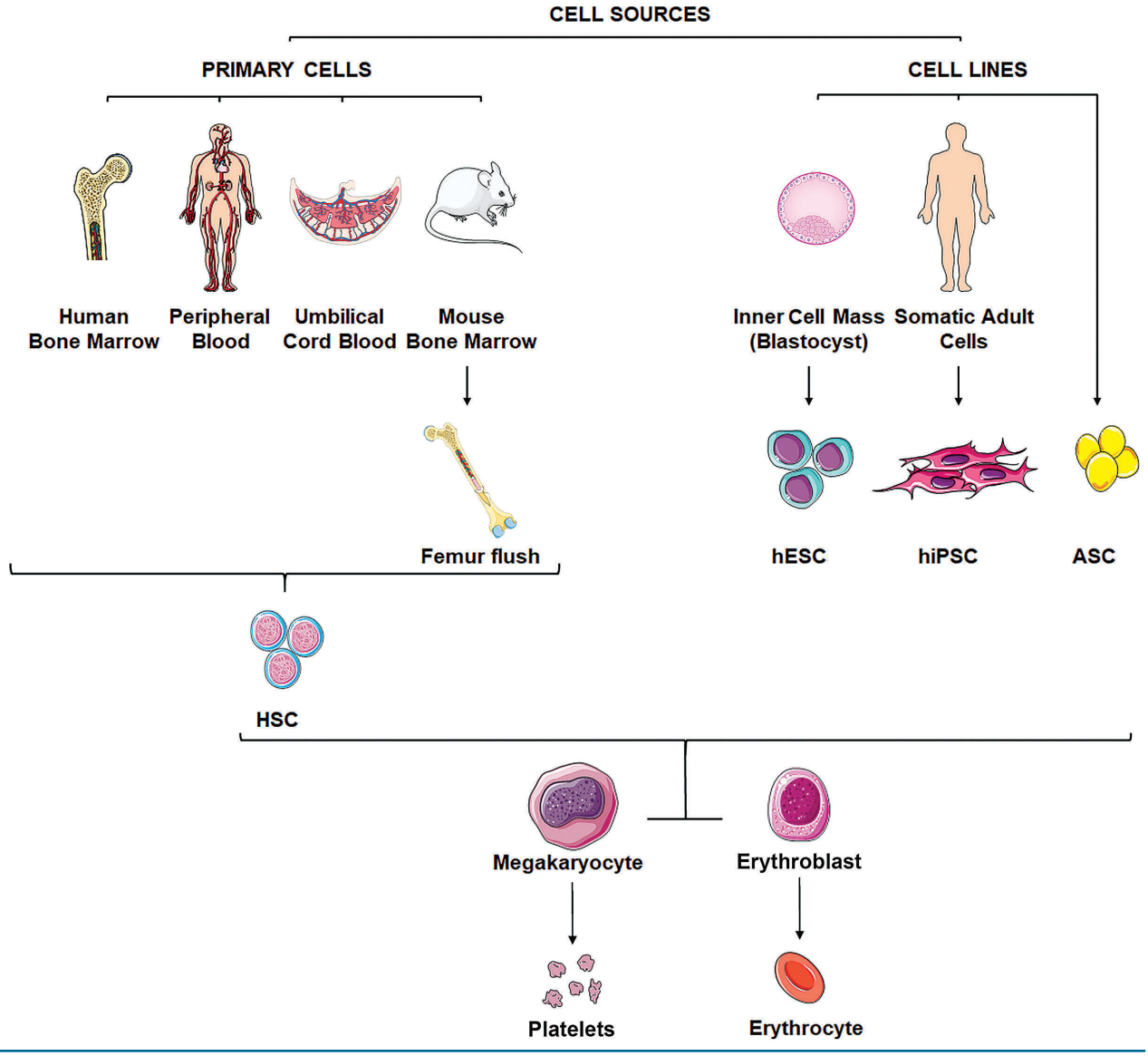


Figure 2. Overview of sources of stem cells for producing platelets and erythrocytes *in vitro*. Different stem cell sources have been studied for their potential to generate platelets and erythrocytes *in vitro*. Primary cells can be obtained either from human or mouse bone marrow, or derived from human peripheral blood and umbilical cord blood hematopoietic stem cells. Furthermore, immortalized cell lines have been generated from human embryonic stem cells, human-induced pluripotent stem cells and adipose-derived mesenchymal stromal/stem cell lines. HSC: hematopoietic stem cells; hESC: human embryonic stem cells; hiPSC: human-induced pluripotent stem cells, ASC: adipose-derived mesenchymal stromal/stem cells. The figure was created using Servier Medical Art templates licensed under a Creative Commons Attribution 3.0 Unported License (*https://smart.servier.com*).

blood platelets in many aspects, including morphology, expression of lineage-specific antigens, and ability to aggregate in response to agonists.[18,57] A major advantage of hiPSC is the possibility of using human leukocyte antigen-matched hiPSC or cells genetically engineered to lack certain antigens in order to produce platelets that would not be rejected by the recipient.[58] Alternatively, as hiPSC can be generated from any donor, they are theoretically suitable for generating a bank of phenotypically matched erythrocytes. Various research groups have published methods for generating red blood cells from hiPSC[59,60] albeit with some concerns about the expression of hemoglobin and enucleation potential, which could not be achieved in the context of *in vitro* differentiation, unless in the presence of feeder cells or after injection into mice recipients. Therefore, although very attractive, both hESC and hiPSC might not represent the best choice of stem cells for producing blood components. In most cases the differentiation protocols are long and expensive. Indeed, high costs for generating, validating, and maintaining these cell lines should be considered.[61] Finally, there is still the concern that any cellular product derived from them could be oncogenic or teratogenic,[62] given the potential genomic instability of these stem cell lines.

To overcome these limitations, the latest stem cell source to be investigated has been adipose tissue, which has the advantage of being ubiquitously available and easily accessible in large quantities with minimally invasive harvesting procedures. Ono-Uruga *et al.* recently demonstrated that the production of endogenous thrombopoietin is involved in megakaryocyte differentiation and platelet production from adipose-derived mesenchymal stromal/stem cell lines.[63] The lack of specific markers for the identification and isolation of this subset of stem cells and the absence of standardized isolation and culture protocols make it difficult to translate this approach into different laboratories.[64]

Finding the route towards differentiation: cytokines instruct but are not enough

It is conceivable that a regular, non-donor-derived supply of erythrocytes and platelets could be achieved in the near future, thus making it necessary to define the best culture conditions to maximize the yield of platelets generated per single megakaryocyte, as well as the number of enucleated erythrocytes obtained *in vitro* (Figure 3).

Recombinant human thrombopoietin is commonly used to produce megakaryocytes.[65-67] Thrombopoietin analogs, such as eltrombopag and romiplostim, have been tested in culture but their use for *ex vivo* platelet manufacturing is still limited because they can induce proliferation of immature progenitors.[68,69] Thrombopoietin and its analogs are combined with a wide variety of cytokines including stem cell factor and interleukins (e.g., IL-3, IL-6, IL-11) which synergize to produce very pure populations of mature megakaryocytes forming proplatelets without the need for serum supplementation or co-culture with

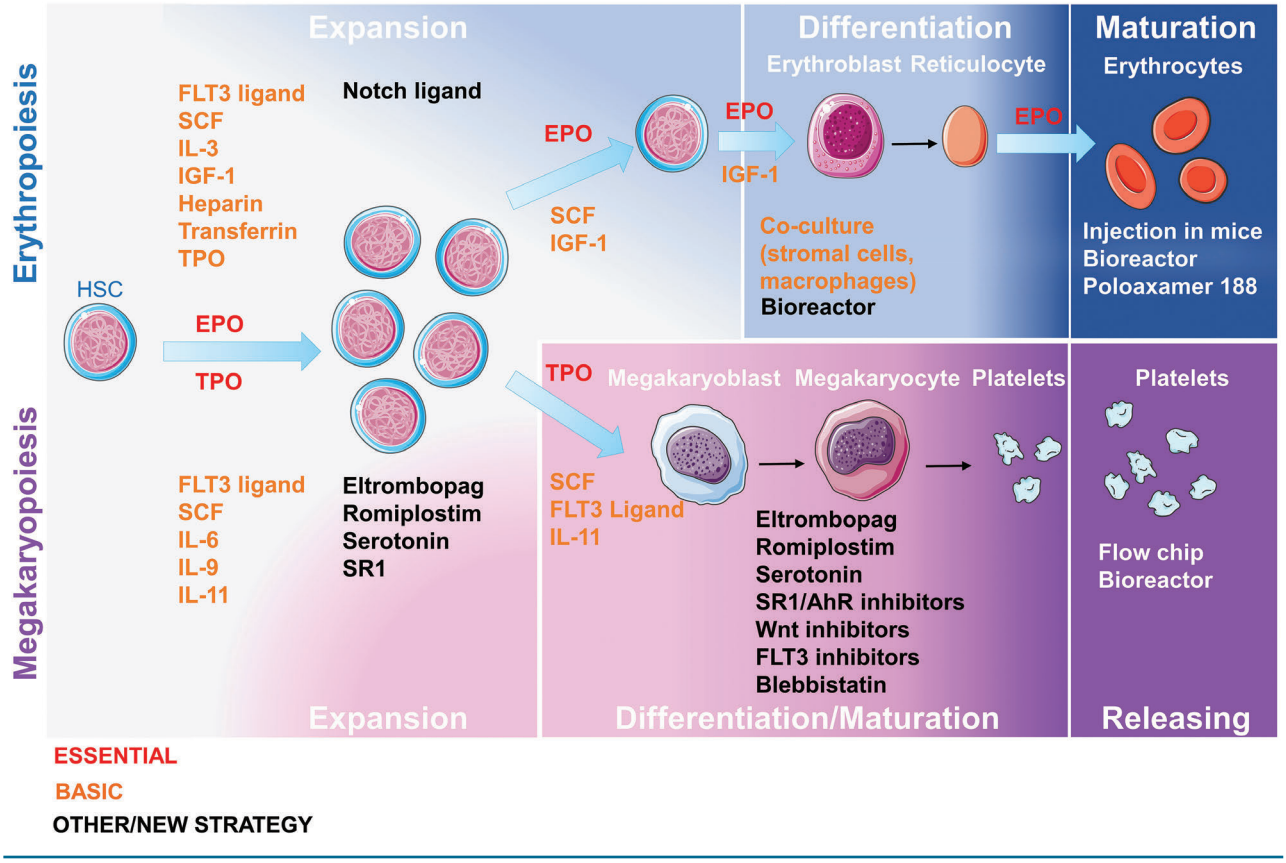


Figure 3. Overview of soluble factors used in the production of platelets and erythrocytes *in vitro*. Different cocktails of cytokines, pharmacological agents and/or co-culture with feeder cells have been used to generate platelets and erythrocytes *in vitro*. HSC: hematopoietic stem cell; FLT3: Fms related tyrosine kinase 3; SCF: stem cell factor; IL: interleukin; IGF-1: insulin-like growth factor-1; TPO: thrombopoietin; EPO: erythropoietin; SR1: stemRegenin 1; AhR: aryl hydrocarbon receptor. The figure was created using Servier Medical Art templates licensed under a Creative Commons Attribution 3.0 Unported License (*https://smart.servier.com*).

feeder cells.[65-67] Other strategies include the use of serotonin, which supports megakaryocyte maturation and proplatelet formation by activating biochemical pathways and through modulation of cytoskeleton dynamics.[70] The cytoskeleton is responsible for controlling membrane stiffness and resistance to deformation of megakaryocytes induced by environmental pressures. Inhibition of the actomyosin cytoskeleton by blebbistatin and Rho/ROCK inhibitors can soften the membrane and facilitate the fragmentation of megakaryocytes.[71,72] However, given the importance of cytoskeleton remodeling during the whole process of differentiation, such treatments should be administrated only to mature megakaryocytes at the stage of proplatelet formation. StemRegenin1, an antagonist of the aryl hydrocarbon receptor, was shown to specifically increase the expansion of $CD34^{+}CD41^{low}$ early megakaryocytic progenitors and to promote the capacity to generate proplatelets and platelet-like elements.[73] Subsequently, a high throughput screening by Seo *et al.* identified new inducers of megakaryocyte maturation and platelet production, such as CH223191, Wnt-C59 and TCS359, respectively inhibitors of the aryl hydrocarbon receptor and of the Wnt and Fms-like tyrosine kinase 3 pathways.[74] However, studies on their mechanisms of action are needed before a conceivable application for clinical purposes.

Most of the cited compounds have been studied in liquid cultures that lack the shear forces of blood flow to support the elongation process and platelet release. To face this challenge, microfluidic chips with flow chambers and fenestrated barriers functionalized with extracellular matrix components have been proposed.[75-77] Thon *et al.* established the first microfluidic chip. The device was made of transparent silicon and supported high-resolution live-cell microscopy and quantification of platelet production. It consisted of upper and lower microfluidic channels separated by a 2 μm fenestrated barrier. Megakaryocytes were seeded in the upper channel and extended proplatelets through the slits.[75] Later on, aiming to increase the yield of collected platelets, Avanzi *et al.* created an innovative bioreactor made of a pseudo-3D membrane, either a nanofiber membrane or a polyvinyl chloride filter, placed between two 3D-printed flow chambers. The upper side of the membrane housed megakaryocytes, and the lower compartment was a flow chamber destined to harvest platelets.[76] Blin *et al.* designed an evolution of these chips.[77] Their microfluidic device consisted of a microchannel textured with organized micropillar arrays coated with von Willebrand factor to anchor megakaryocytes while promoting platelet rolling into the flow. All these systems were able to provide a hydrodynamic shear supporting proplatelet elongation and fragmentation into platelets, but still with low efficiency in terms of numbers for clinical application because of their micro-scale nature.

Two- to four-phase cultures using combinations of erythropoietin and various growth factors, steroids and cytokines, with or without serum and/or feeder layers have been developed to reproduce complete erythropoiesis. A multistep process is needed to control the fine balance between cell expansion, differentiation and maturation. Cell expansion at the stage of stem cell progenitors has been carried out in the presence of stem cell factor, thrombopoietin and/or Fms-like tyrosine kinase 3.[78] Delta 1 Notch ligand increased the proliferation rate of early progenitors but the differentiation process was delayed in this culture.[79] Insulin-like growth factor 1 has been used to promote stem cell survival and to guide erythroid differentiation, and it has been validated as a promoter of nuclear condensation but not of enucleation.[80,81] Erythroblast enucleation is thought to be largely dependent on signals mediated by macrophages, but mimicking erythroblastic islands is challenging and different approaches have been proposed to enhance its occurrence *in vitro*. The basic method consists of seeding erythroid cells with feeder cells, such as murine and human stromal cells or human monocyte-derived macrophages, but differing effects on maturation and enucleation have been reported.[49,82,83] Recently, Lopez-Yrigoyen *et al.* established genetically programmed hiPSC-derived macrophages to develop an elegant approach of co-culture with umbilical cord blood- and hiPSC-derived erythroid cells that demonstrated efficient maturation and enucleation,[84] although the presence of feeder cells could make it difficult to isolate pure, non-contaminated erythrocytes. A second approach is to inject erythroid precursors into immunodeficient mice in order for the cells to complete their maturation, but this is clearly not applicable for obtaining cells for clinical purposes.[52] In a third approach different protocols have been developed to produce enucleated erythroblasts in the absence of feeder cells, including culture with a cytoprotective polymer called poloxamer 188 which increases membrane stability during the enucleation process.[85] The fourth approach involves seeding cells in agitated bioreactors systems. Timmins *et al.* used a commercially available device consisting of a rocking platform that guaranteed homogeneous mixing with low shear.[86] In this system feeder cells were not essential for proficient expansion and terminal differentiation of erythrocytes. The same results were obtained with a bottle-turning device culture system[87] and more recently with a stirred–tank bioreactor.[88] Culture in suspension is an approach that can be used for large-scale production of blood cells, including megakaryocytes. Constant agitation during culture, generated by a rotary cell culture system and stirred spinner flasks, demonstrated the ability to produce platelets.[89] More recently, the group of Koji Eto used big tank bioreactors to develop a scalable, controllable, turbulent flow-based system for platelet generation.[18] The breakthrough of the big bioreactors was their ability to guarantee appropriate oxygenation and prevent cell conglutination while providing dynamic flows mimicking those of the bloodstream.

In most of these conditions erythrocytes and platelets look immature; in particular, erythrocytes appear macrocytic with a large amount of fetal hemoglobin and platelets appear larger with immature granules. It is known that cultured megakaryocytes of any origin produce fewer platelets per single cell than do platelets *in vivo*. We can hypothesize that this is because they miss the physical environment of the bone marrow which drives maturation of HSC and the final production of erythrocytes and platelets *in vivo*. Thus, one of the major challenges in this field of research is to implement culture protocols with systems able to provide the most favorable conditions for mimicking the bone marrow hematopoietic niche.

The rise and perspectives of the three-dimensional bone marrow mimic

In the last decades, mechano-biological studies have consolidated the importance of the physical environment,

namely 3D structure, topography, local stiffness, and physical constraints, as a guiding cue for controlling *ex vivo* survival, migration, differentiation and maturation of different cell types.[90] In 2D cultures, cells are seeded in liquid medium in a monolayer in the presence of molecules and soluble factors diluted directly in the medium, but the complexity of 3D tissues is completely lost. Currently, the best approach to try to model the 3D complexity of native human tissues *ex vivo* is to exploit biomaterials. Indeed, 3D environments made of fibers/nanofibers, solid scaffolds, and hydrogels have demonstrated the possibility to enhance the culture area and to induce better expansion of HSC during long-term cultures. We now discuss different approaches that have been undertaken to support erythropoiesis and megakaryopoiesis *ex vivo*.

Erythropoiesis and erythrocyte production in three-dimensional cultures

The study of erythropoiesis in three dimensions remains marginal. Housler *et al.* customized a 3D compartmental hollow fiber perfused bioreactor.[91] The system was composed of a network of three independent bundles of capillaries, two of which were used for countercurrent medium perfusion and the third for oxygen and carbon dioxide transport. The bioreactor enabled expansion of erythrocyte progenitors and enucleation of erythroblasts. In an effort to try to maximize enucleation and recapitulate erythroblastic islands *ex vivo*, Lee *et al.* seeded late erythroblasts derived from umbilical cord blood-derived stem cells in different macroporous scaffolds and demonstrated the impact of the pore size on cell viability. Interestingly, they found clusters of mature erythroblasts, reminiscent of erythroblastic islands in the bone marrow, which in turn increased the maturation status and enucleation rate.[92] Fauzi *et al.* confirmed increased cell viability and proliferation, proposing a 3D alginate hydrogel associated with a rotating wall vessel system cultured with murine embryonic stem cells. This system demonstrated that early exposure to stem cell factor guides the differentiation of cells toward the erythroid lineage and allows a single-step culture for the production of definitive erythrocytes in 21 days.[93] Allenby *et al.* further demonstrated the importance of combining the 3D architecture with flow, developing a perfused 3D hollow fiber bioreactor.[94] Four ceramic hollow fibers were encased in a 3D polyurethane porous scaffold incorporated in a perfusion system that provided normoxic and hypoxic zones as in the bone marrow environment. Specific ports in the circuit enabled medium and egressed cell sampling for extracellular metabolic, protein, and cell analysis. The wall shear rate generated inside the system was estimated to be similar to that in murine bone marrow vasculature. The bone marrow-like environment of this bioreactor enabled cells to be seeded at high density to obtain continuous erythropoiesis. In addition to large-scale production these tools are candidates as models to study normal and abnormal erythropoiesis and for drug screening. Recently, a 3D model of erythropoiesis, made with polyurethane, was proposed to study erythroid failure in myelodysplastic syndromes.[95] To mimic the erythroblastic islands and enucleation process, primary bone marrow cells from healthy subjects and myelodysplastic patients were seeded in the 3D scaffold, which had a pore size and distribution close to that of bone marrow architecture. The 3D culture enabled continuous expansion and complete maturation of erythrocytes over 4 weeks. Most importantly, culture of $CD34^+$ cells in 3D scaffolds facilitated the greatest expansion and maturation of erythroid cells, including generation of erythroblastic islands and enucleated erythrocytes.

Megakaryopoiesis and platelet production in three-dimensional cultures

As already discussed, megakaryopoiesis is critically influenced by the mechanics and biochemical composition of bone marrow. In an attempt to mimic such a structure *in vitro*, Currao *et al.* produced 3D hyaluronan hydrogels functionalized with extracellular matrix components by photo-crosslinking.[96] When cultured inside such a structure, megakaryocytes demonstrated the ability to form platelets into a collagen type IV enriched environment, while this function was almost abrogated in the presence of collagen type I. The 3D culture in hydrogel also showed, for the first time, the impact of physical constraints on megakaryopoiesis and mechano-transduction pathways. In pullulan-dextran 3D hydrogel megakaryocytes were larger and had increased ploidy and expression of lineage-specific transcription factors.[97] Methylcellulose hydrogels showed that viability and maturation are directly linked to stiffness of the environment. Indeed, a stiff environment led to decreased survival and growth of megakaryocyte progenitors, while in a less stiff environment, megakaryocytes were more mature in terms of ploidy and morphology of the demarcation membrane system, which closely resembled that of bone marrow megakaryocytes. After recovery and transfer into the liquid medium, proplatelet production increased two-fold, due to the activation of mechano-transduction pathways and to a different actomyosin rearrangement.[98] Subsequently, Abbonante *et al.* demonstrated that the activation of TRPV4 (transient receptor potential cation channel subfamily V member 4), a membrane mechano-sensitive cation channel, regulates mechano-transduction pathways that, in turn, control thrombopoiesis on soft substrates.[23] Specifically, human megakaryocytes cultured on soft silk scaffolds (≤10 MPa) showed increased activation of TRPV4, leading to calcium influx and increased platelet production as a consequence of β1 integrin activation and internalization and of Akt phosphorylation.

By putting together all the pieces of information, scientists have been trying to develop flow bioreactors that mimic blood flow and allow better oxygenation and distribution of cytokines and nutrients during the 3D culture. The first platelet bioreactor was presented by Sullenbarger and colleagues. It was composed of a polycarbonate chamber with three disks of woven polyester or colloidal crystal hydrogel with medium flowing under and over the disks but not through them, thus limiting shear stress.[99] The culture of $CD34^+$ cells in this bioreactor allowed a long-term production of platelets and a higher number of collected platelets. Interestingly, when the oxygen concentration within the device was set at a low level (5%), HSC expansion was increased and platelet production was decreased. Contrariwise, culture at high oxygen tension (20%) increased the production of platelets but lowered HSC expansion.[100,101] A different combination of oxygen tensions at the beginning and at the end of the culture increased both HSC expansion and the final yield of platelets. More recently, Shepherd *et al.* developed a flow bioreactor based on a two-layer collagen scaffold.[102] The porous, structurally

graduated scaffold was meant to support megakaryocyte function by a bone marrow-like structure. To modulate the pore size of the collagen scaffold, a two-stage freezing technique was used, which created a variety of pore sizes with larger pores in the top layer and small pores at the bottom. Based on differential pore sizes this scaffold had a sieving capacity that enhanced the purity of the platelet output. Indeed, the bioreactor was conceived as a twin chamber culture system, whereby one side of the chamber allowed seeding of the cultured hiPSC-derived megakaryocytes into the scaffold, while cross-flow-generated shear forces were able to induce platelet release. In these conditions, platelet production was improved significantly compared to that in 2D cultures. Using a different approach, involving soft gel lithography, Kotha and colleagues were able to use collagen hydrogels as a scaffold to create a microvascular network.[103] Endothelial cells were seeded in the microvascular network to form endothelial vessels with a lumen, while megakaryocytes were encapsulated directly in the type I collagen hydrogel. Megakaryocytes were able to migrate to the microvascular network and to extend proplatelets. This bioengineered device provided a tool to study the vascular-megakaryocyte interface during thrombopoiesis. However, one limitation of this model was the size of the vessel (around 100 μm), which was bigger than sinusoid vessels.

The search for biomaterials that can be chemically and mechanically tailored to entrap bioactive molecules, such as growth factors and extracellular matrix components, while retaining bioavailability, has spawned research into the use of silk fibroin as scaffolds. Silk fibroin from *Bombyx mori* silkworm cocoons is a strong but elastic protein that is biocompatible, having low immunogenicity and low thrombogenicity.[104,105] Our group designed a silk tube functionalized with components of the extracellular matrix that support platelet production, such as fibronectin, type IV collagen and laminin, and stromal-derived factor-1α, surrounded by a type I collagen hydrogel and Matrigel or by a silk sponge.[105] The structure of the silk sponge was closer to the medullar topography and enhanced adhesion and migration of cells within the structure.[105] In the vascular compartment, the presence of stromal-derived factor-1α directed the migration of mature megakaryocytes towards the silk tube. Platelets collected with flow passing through the tube were functional and still alive 4 days after collection. It was also shown that co-culture with a monolayer of endothelial cells or functionalization of the silk tube with vascular endothelial growth factor and vascular cell adhesion molecule 1 increases the yield of platelets. This model could be easily adapted to study mechanisms of normal and pathological megakaryopoiesis and for drug screening.[69,105]

In an attempt to scale-up platelet production for transfusions, multi-porous silk sponges have been investigated.[106] These sponges were cultured within new modular flow chambers with flow passing through the different pores and megakaryocytes in direct contact with the flow. This enhanced the capacity of platelet production, because of the larger volume of perfusion that allowed an increase of the concentration of cells in the sponge and because of the softer environment functionalized with extracellular matrix components that support proplatelet formation.

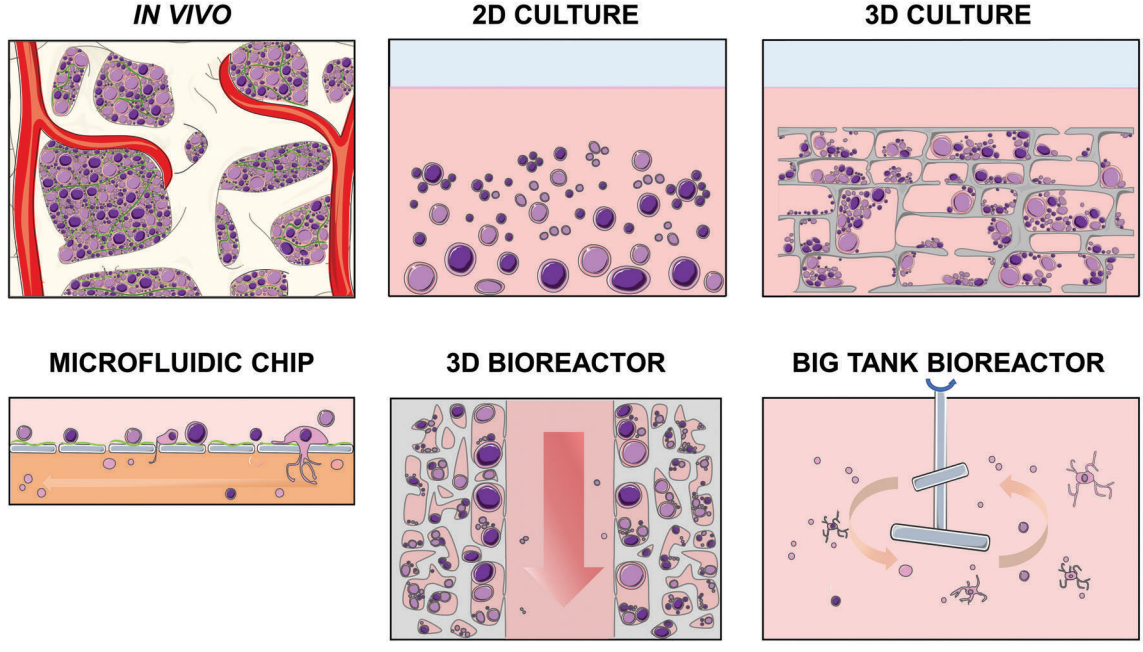


Figure 4. *In vivo versus in vitro*: an overview of different culture approaches for generating platelets and erythrocytes. *In vivo* cell maturation occurs in a complex environment in which cells experience different mechanical and biochemical cues due to cell-to-cell and cell-to matrix interactions. In the classical *in vitro* two-dimensional culture, cell contacts, confinement and environmental biomechanics are lost; moreover cells in contact with the plastic are artificially polarized. In the three-dimensional culture, topography and stiffness can be modeled to mimic the native environment. Only cell cultured in flow conditions can recapitulate blood hydrodynamics. Microfluidic devices have the ability to enable extension of proplatelets and the release of functional platelets. Three-dimensional bioreactors combine the advantages of a three-dimensional environment with flow through the scaffold: mature cells can migrate toward the perfused compartment to release either mature erythrocytes or platelets. Cell culture in agitated or stirred-tank bioreactors has been exploited to allow large-scale production of platelets or erythrocytes. 2D: two-dimensional; 3D: three-dimensional. The figure was created using Servier Medical Art templates licensed under a Creative Commons Attribution 3.0 Unported License (*https://smart.servier.com*).

Conclusions

Replicating erythrocyte and platelet production *ex vivo* is particularly challenging in the light of the unique architecture and composition of the native bone marrow microenvironment whose biochemical and mechanical signals influence progenitor cell differentiation and function.[12] Like building a house brick-by-brick, tissue-engineering approaches have combined all the knowledge collected over years of *in vivo* and *in vitro* research on hematopoiesis to develop bone marrow mimics with different levels of complexity (Figure 4). Nevertheless, there are aspects that still need to be addressed in order to increase the yield of cells produced and thereby enable clinical advances. Bone marrow mimics will need to be scaled-up several orders of magnitude to produce $3x10^{11}$ platelets,[107] the equivalent of one apheresis platelet unit, or $2x10^{12}$ erythrocytes, the number normally contained in one unit of blood. To achieve this, the whole process has to become more cost-efficient to match the current prices of high-quality blood products.[108] According to a current estimate, producing a number of erythrocytes in the desired range would cost thousands of dollars per unit just in consumables, without considering the investment in facilities, while the hospital costs for donated samples are in the order of magnitude of hundreds of dollars.[109, 110] Producing blood on a commercial scale will require substantial investment, and it will be challenging to maintain momentum in the direction of research and development of increasingly more efficient bone marrow models. Future advancement in this field will require scalable biomaterials and cell manufacturing techniques to produce blood cost-effectively in clinical-grade conditions. Costs could be reduced if specific culture components were to be produced in a bulk. The field is moving towards the discovery of novel agents, cytokines and/or chemically defined media that could be competitively priced compared to current reagents.[74,111,112] However, it is clear that optimization as well as research into safety and stability are needed before clinical application. Other approaches include genetic manipulation of human pluripotent stem cells to allow enhanced cell expansion but preserved differentiation, the decrease of device manufacturing costs, the reduction of total operating volume and cytokines, and optimization of methods for recovery and concentration of the final products.[113-115] However, in the short term the goal of this research is not to compete with the costs of blood donations. The most likely initial applications would be for the treatment of allo–immunized patients and those with rare blood groups. Indeed, gene therapies, with their potential to cure several benign and malignant hematologic diseases and develop cultured products to improve transfusion support for individuals with rare blood types, are currently in the therapeutic spotlight.[116] Optimized 3D culture systems could provide invaluable insight for studying disease mechanisms, supporting cell growth prior to gene manipulation and testing the safety of gene-edited blood products or new pharmacological treatments on patient-derived samples before *in vivo* use. This is a complex and multidisciplinary task that is focused on synergistic interactions between engineering, medicine and key biological processes. Bioengineering the complex structural and dynamic microenvironment of the bone marrow is on the verge of changing the landscape of healthcare in a revolution that is only just starting.

Disclosures

No conflicts of interest to disclose.

Contributions

AA, PMS, ABo, CPM and GM wrote the manuscript. CADB and ABa conceived the review, wrote the manuscript and gave overall direction.

Funding

This paper was supported by Cariplo Foundation (Grant 2017-0920) and by the European Commission (H2020-FETOPEN-1-2016-2017-SilkFusion, Grant Agreement 767309). The funders had no role in the design of the review, decision to publish it, or preparation of the manuscript.

References

1. Knight E, Przyborski S. Advances in 3D cell culture technologies enabling tissue-like structures to be created in vitro. J Anat. 2015;227(6):746-756.
2. Travlos GS. Normal structure, function, and histology of the bone marrow. Toxicol Pathol. 2006;34(5):548-565.
3. Dolgin E. Bioengineering: doing without donors. Nature. 2017;549(7673):S12-S15.
4. Hess JR. Conventional blood banking and blood component storage regulation: opportunities for improvement. Blood Transfus. 2010;8(Suppl 3):s9-15.
5. Custer B, Zou S, Glynn SA, et al. Addressing gaps in international blood availability and transfusion safety in low- and middle-income countries: a NHLBI workshop. Transfusion. 2018;58(5):1307-1317.
6. Allain JP. Current approaches to increase blood donations in resource-limited countries. Transfus Med. 2019;29(5):297-310.
7. Busch MP, Bloch EM, Kleinman S. Prevention of transfusion-transmitted infections. Blood. 2019;133(17):1854-1864.
8. Shander A, Goobie SM, Warner MA, et al. Essential role of patient blood management in a pandemic: a call for action. Anesth Analg. 2020;131(1):74-85.
9. Chang L, Yan Y, Wang L. Coronavirus disease 2019: coronaviruses and blood safety. Transfus Med Rev. 2020;34(2):75-80.
10. Stanworth SJ, New HV, Apelseth TO, et al. Effects of the COVID-19 pandemic on supply and use of blood for transfusion. Lancet Haematol. 2020;7(10):e756-e764.
11. Moritz ED, Winton CS, Tonnetti L, et al. Screening for Babesia microti in the U.S. blood supply. N Engl J Med. 2016;375(23):2236-2245.
12. Morrison SJ, Scadden DT. The bone marrow niche for haematopoietic stem cells. Nature. 2014;505(7483):327-334.
13. Laurenti E, Göttgens B. From haematopoietic stem cells to complex differentiation landscapes. Nature. 2018;553(7689):418-426.
14. Sanjuan-Pla A, Macaulay IC, Jensen CT, et al. Platelet-biased stem cells reside at the apex of the haematopoietic stem-cell hierarchy. Nature. 2013;502(7470):232-236.
15. Yamamoto R, Morita Y, Ooehara J, et al. Clonal analysis unveils self-renewing lineage-restricted progenitors generated directly from hematopoietic stem cells. Cell. 2013;154(5):1112-1126.
16. Machlus KR, Italiano JE. The incredible journey: from megakaryocyte development to platelet formation. J Cell Biol. 2013;201(6):785-796.
17. Nandakumar SK, Ulirsch JC, Sankaran VG. Advances in understanding erythropoiesis: evolving perspectives. Br J Haematol. 2016;173(2):206-218.
18. Ito Y, Nakamura S, Sugimoto N, et al. Turbulence activates platelet biogenesis to enable clinical scale ex vivo production. Cell. 2018;174(3):636-648.
19. Potts KS, Farley A, Dawson CA, et al. Membrane budding is a major mechanism of in vivo platelet biogenesis. J Exp Med. 2020;217(9):e20191206.
20. Moras M, Lefevre SD, Ostuni MA. From erythroblasts to mature red blood cells: organelle clearance in mammals. Front Physiol. 2017;8:1076.
21. Rieger MA, Hoppe PS, Smejkal BM, Eitelhuber AC, Schroeder T. Hematopoietic cytokines can instruct lineage choice. Science. 2009;325(5937):217-218.
22. Yu VW, Scadden DT. Hematopoietic stem cell and its bone marrow niche. Curr Top Dev Biol. 2016;118:21-44.
23. Abbonante V, Di Buduo CA, Gruppi C, et al. A new path to platelet production through matrix sensing. Haematologica. 2017;102(7):

1150-1160.
24. Leiva O, Leon C, Kah Ng S, Mangin P, Gachet C, Ravid K. The role of extracellular matrix stiffness in megakaryocyte and platelet development and function. Am J Hematol. 2018;93(3):430-441.
25. Ward CM, Ravid K. Matrix mechanosensation in the erythroid and megakaryocytic lineages. Cells. 2020;9(4):894.
26. Bonnans C, Chou J, Werb Z. Remodelling the extracellular matrix in development and disease. Nat Rev Mol Cell Biol. 2014;15(12):786-801.
27. Malara A, Gruppi C, Rebuzzini P, et al. Megakaryocyte-matrix interaction within bone marrow: new roles for fibronectin and factor XIII-A. Blood. 2011;117(8):2476-2483.
28. Balduini A, Pallotta I, Malara A, et al. Adhesive receptors, extracellular proteins and myosin IIA orchestrate proplatelet formation by human megakaryocytes. J Thromb Haemost. 2008;6(11):1900-1907.
29. Eshghi S, Vogelezang MG, Hynes RO, Griffith LG, Lodish HF. Alpha4beta1 integrin and erythropoietin mediate temporally distinct steps in erythropoiesis: integrins in red cell development. J Cell Biol. 2007;177(5):871-880.
30. Comazzetto S, Murphy MM, Berto S, Jeffery E, Zhao Z, Morrison SJ. Restricted hematopoietic progenitors and erythropoiesis require SCF from leptin receptor+ niche cells in the bone marrow. Cell Stem Cell. 2019;24(3):477-486.
31. Takaku T, Malide D, Chen J, Calado RT, Kajigaya S, Young NS. Hematopoiesis in 3 dimensions: human and murine bone marrow architecture visualized by confocal microscopy. Blood. 2010;116(15):e41-55.
32. Chasis JA, Mohandas N. Erythroblastic islands: niches for erythropoiesis. Blood. 2008;112(3):470-478.
33. de Back DZ, Kostova EB, van Kraaij M, van den Berg TK, van Bruggen R. Of macrophages and red blood cells; a complex love story. Front Physiol. 2014;5:9.
34. Modery-Pawlowski CL, Tian LL, Pan V, McCrae KR, Mitragotri S, Sen Gupta A. Approaches to synthetic platelet analogs. Biomaterials. 2013;34(2):526-541.
35. Brown AC, Stabenfeldt SE, Ahn B, et al. Ultrasoft microgels displaying emergent platelet-like behaviours. Nat Mater. 2014;13(12):1108-1114.
36. Anselmo AC, Modery-Pawlowski CL, Menegatti S, et al. Platelet-like nanoparticles: mimicking shape, flexibility, and surface biology of platelets to target vascular injuries. ACS Nano. 2014;8(11):11243-11253.
37. Donovan AJ, Kalkowski J, Szymusiak M, et al. Artificial dense granules: a procoagulant liposomal formulation modeled after platelet polyphosphate storage pools. Biomacromolecules. 2016;17(8):2572-2581.
38. Natanson C, Kern SJ, Lurie P, Banks SM, Wolfe SM. Cell-free hemoglobin-based blood substitutes and risk of myocardial infarction and death: a meta-analysis. JAMA. 2008;299(19):2304-2312.
39. Hardy JF, Bélisle S, Van der Linden P. Combined blood substitute and erythropoietin therapy in a severely injured Jehovah's witness. N Engl J Med. 2002;347(9):696-697;author reply 696-697.
40. Raff JP, Dobson CE, Tsai HM. Transfusion of polymerised human haemoglobin in a patient with severe sickle-cell anaemia. Lancet. 2002;360(9331):464-465.
41. Mer M, Hodgson E, Wallis L, et al. Hemoglobin glutamer-250 (bovine) in South Africa: consensus usage guidelines from clinician experts who have treated patients. Transfusion. 2016;56(10):2631-2636.
42. Merico V, Zuccotti M, Carpi D, et al. The genomic and proteomic blueprint of mouse megakaryocytes derived from embryonic stem cells. J Thromb Haemost. 2012;10(5):907-915.
43. Liu J, Zhang J, Ginzburg Y, et al. Quantitative analysis of murine terminal erythroid differentiation in vivo: novel method to study normal and disordered erythropoiesis. Blood. 2013;121(8):e43-49.
44. Jin H, Kim HS, Kim S, Kim HO. Erythropoietic potential of CD34+ hematopoietic stem cells from human cord blood and G-CSF-mobilized peripheral blood. Biomed Res Int. 2014;2014:435215.
45. Di Buduo CA, Abbonante V, Marty C, et al. Defective interaction of mutant calreticulin and SOCE in megakaryocytes from patients with myeloproliferative neoplasms. Blood. 2020;135(2):133-144.
46. Kurita R, Suda N, Sudo K, et al. Establishment of immortalized human erythroid progenitor cell lines able to produce enucleated red blood cells. PLoS One. 2013;8(3):e59890.
47. Liu ZJ, Sola-Visner M. Neonatal and adult megakaryopoiesis. Curr Opin Hematol. 2011;18(5):330-337.
48. Liu ZJ, Italiano J, Ferrer-Marin F, et al. Developmental differences in megakaryocytopoiesis are associated with up-regulated TPO signaling through mTOR and elevated GATA-1 levels in neonatal megakaryocytes. Blood. 2011;117(15):4106-4117.
49. Giarratana MC, Kobari L, Lapillonne H, et al. Ex vivo generation of fully mature human red blood cells from hematopoietic stem cells. Nat Biotechnol. 2005;23(1):69-74.
50. Zhang X, Ma YN, Zhang JW. Human erythroid progenitors from adult bone marrow and cord blood in optimized liquid culture systems respectively maintained adult and neonatal characteristics of globin gene expression. Biol Res. 2007;40(1):41-53.
51. Tomer A. Human marrow megakaryocyte differentiation: multiparameter correlative analysis identifies von Willebrand factor as a sensitive and distinctive marker for early (2N and 4N) megakaryocytes. Blood. 2004;104(9):2722-2727.
52. Giarratana MC, Rouard H, Dumont A, et al. Proof of principle for transfusion of in vitro-generated red blood cells. Blood. 2011;118(19):5071-5079.
53. Trakarnsanga K, Griffiths RE, Wilson MC, et al. An immortalized adult human erythroid line facilitates sustainable and scalable generation of functional red cells. Nat Commun. 2017;8:14750.
54. Daniels DE, Downes DJ, Ferrer-Vicens I, et al. Comparing the two leading erythroid lines BEL-A and HUDEP-2. Haematologica. 2020;105(8):e389-e394.
55. Takayama N, Nishikii H, Usui J, et al. Generation of functional platelets from human embryonic stem cells in vitro via ES-sacs, VEGF-promoted structures that concentrate hematopoietic progenitors. Blood. 2008;111(11):5298-5306.
56. Ma F, Ebihara Y, Umeda K, et al. Generation of functional erythrocytes from human embryonic stem cell-derived definitive hematopoiesis. Proc Natl Acad Sci U S A. 2008;105(35):13087-13092.
57. Moreau T, Evans AL, Vasquez L, et al. Large-scale production of megakaryocytes from human pluripotent stem cells by chemically defined forward programming. Nat Commun. 2016;7:11208.
58. Suzuki D, Flahou C, Yoshikawa N, et al. iPSC-derived platelets depleted of HLA class I are inert to anti-HLA class I and natural killer cell immunity. Stem Cell Reports. 2020;14(1):49-59.
59. Kobari L, Yates F, Oudrhiri N, et al. Human induced pluripotent stem cells can reach complete terminal maturation: in vivo and in vitro evidence in the erythropoietic differentiation model. Haematologica. 2012;97(12):1795-1803.
60. Razaq MA, Taylor S, Roberts DJ, Carpenter L. A molecular roadmap of definitive erythropoiesis from human induced pluripotent stem cells. Br J Haematol. 2017;176(6):971-983.
61. Huang CY, Liu CL, Ting CY, et al. Human iPSC banking: barriers and opportunities. J Biomed Sci. 2019;26(1):87.
62. Ben-David U, Benvenisty N. The tumorigenicity of human embryonic and induced pluripotent stem cells. Nat Rev Cancer. 2011;11(4):268-277.
63. Ono-Uruga Y, Tozawa K, Horiuchi T, et al. Human adipose tissue-derived stromal cells can differentiate into megakaryocytes and platelets by secreting endogenous thrombopoietin. J Thromb Haemost. 2016;14(6):1285-1297.
64. Baer PC. Adipose-derived mesenchymal stromal/stem cells: an update on their phenotype in vivo and in vitro. World J Stem Cells. 2014;6(3):256-265.
65. Bhatlekar S, Basak I, Edelstein LC, et al. Anti-apoptotic BCL2L2 increases megakaryocyte proplatelet formation in cultures of human cord blood. Haematologica. 2019;104(10):2075-2083.
66. Matsunaga T, Tanaka I, Kobune M, et al. Ex vivo large-scale generation of human platelets from cord blood CD34+ cells. Stem Cells. 2006;24(12):2877-2887.
67. Balduini A, Di Buduo CA, Malara A, et al. Constitutively released adenosine diphosphate regulates proplatelet formation by human megakaryocytes. Haematologica. 2012;97(11):1657-1665.
68. Currao M, Balduini CL, Balduini A. High doses of romiplostim induce proliferation and reduce proplatelet formation by human megakaryocytes. PLoS One. 2013;8(1):e54723.
69. Di Buduo CA, Currao M, Pecci A, Kaplan DL, Balduini CL, Balduini A. Revealing eltrombopag's promotion of human megakaryopoiesis through AKT/ERK-dependent pathway activation. Haematologica. 2016;101(12):1479-1488.
70. Ye JY, Liang EY, Cheng YS, et al. Serotonin enhances megakaryopoiesis and proplatelet formation via p-Erk1/2 and F-actin reorganization. Stem Cells. 2014;32(11):2973-2982.
71. Spinler KR, Shin JW, Lambert MP, Discher DE. Myosin-II repression favors pre/proplatelets but shear activation generates platelets and fails in macrothrombocytopenia. Blood. 2015;125(3):525-533.
72. Chang Y, Auradé F, Larbret F, et al. Proplatelet formation is regulated by the Rho/ROCK pathway. Blood. 2007;109(10):4229-4236.
73. Strassel C, Brouard N, Mallo L, et al. Aryl hydrocarbon receptor-dependent enrichment of a megakaryocytic precursor with a high potential to produce proplatelets. Blood. 2016;127(18):2231-2240.
74. Seo H, Chen SJ, Hashimoto K, et al. A β1-tubulin-based megakaryocyte maturation reporter system identifies novel drugs that promote platelet production. Blood Adv.

2018;2(17):2262-2272.
75. Thon JN, Mazutis L, Wu S, et al. Platelet bioreactor-on-a-chip. Blood. 2014;124(12): 1857-1867.
76. Avanzi MP, Mitchell WB. Ex vivo production of platelets from stem cells. Br J Haematol. 2014;165(2):237-247.
77. Blin A, Le Goff A, Magniez A, et al. Microfluidic model of the platelet-generating organ: beyond bone marrow biomimetics. Sci Rep. 2016;6:21700.
78. Migliaccio AR, Whitsett C, Papayannopoulou T, Sadelain M. The potential of stem cells as an in vitro source of red blood cells for transfusion. Cell Stem Cell. 2012;10(2):115-119.
79. Glen KE, Workman VL, Ahmed F, Ratcliffe E, Stacey AJ, Thomas RJ. Production of erythrocytes from directly isolated or Delta1 Notch ligand expanded CD34+ hematopoietic progenitor cells: process characterization, monitoring and implications for manufacture. Cytotherapy. 2013;15(9):1106-1117.
80. Ratajczak J, Zhang Q, Pertusini E, Wojczyk BS, Wasik MA, Ratajczak MZ. The role of insulin (INS) and insulin-like growth factor-I (IGF-I) in regulating human erythropoiesis. Studies in vitro under serum-free conditions-comparison to other cytokines and growth factors. Leukemia. 1998;12(3):371-381.
81. Muta K, Krantz SB, Bondurant MC, Wickrema A. Distinct roles of erythropoietin, insulin-like growth factor I, and stem cell factor in the development of erythroid progenitor cells. J Clin Invest. 1994;94(1):34-43.
82. Baek EJ, Kim HS, Kim S, Jin H, Choi TY, Kim HO. In vitro clinical-grade generation of red blood cells from human umbilical cord blood CD34+ cells. Transfusion. 2008;48(10):2235-2245.
83. Heideveld E, Masiello F, Marra M, et al. CD14+ cells from peripheral blood positively regulate hematopoietic stem and progenitor cell survival resulting in increased erythroid yield. Haematologica. 2015;100(11): 1396-1406.
84. Lopez-Yrigoyen M, Yang CT, Fidanza A, et al. Genetic programming of macrophages generates an in vitro model for the human erythroid island niche. Nat Commun. 2019;10(1):881.
85. Baek EJ, Kim HS, Kim JH, Kim NJ, Kim HO. Stroma-free mass production of clinical-grade red blood cells (RBCs) by using poloxamer 188 as an RBC survival enhancer. Transfusion. 2009;49(11):2285-2295.
86. Timmins NE, Athanasas S, Günther M, Buntine P, Nielsen LK. Ultra-high-yield manufacture of red blood cells from hematopoietic stem cells. Tissue Eng Part C Methods. 2011;17(11):1131-1137.
87. Zhang Y, Wang C, Wang L, et al. Large-scale ex vivo generation of human red blood cells from cord blood CD34(+) cells. Stem Cells Transl Med. 2017;6(8):1698-1709.
88. Bayley R, Ahmed F, Glen K, McCall M, Stacey A, Thomas R. The productivity limit of manufacturing blood cell therapy in scalable stirred bioreactors. J Tissue Eng Regen Med. 2018;12(1):e368-e378.
89. Yang Y, Liu C, Lei X, et al. Integrated biophysical and biochemical signals augment megakaryopoiesis and thrombopoiesis in a three-dimensional rotary culture system. Stem Cells Transl Med. 2016;5(2):175-185.
90. Ingber DE. From mechanobiology to developmentally inspired engineering. Philos Trans R Soc Lond B Biol Sci. 2018; 373(1759):20170323.
91. Housler GJ, Miki T, Schmelzer E, et al. Compartmental hollow fiber capillary membrane-based bioreactor technology for in vitro studies on red blood cell lineage direction of hematopoietic stem cells. Tissue Eng Part C Methods. 2012;18(2):133-142.
92. Lee E, Han SY, Choi HS, Chun B, Hwang B, Baek EJ. Red blood cell generation by three-dimensional aggregate cultivation of late erythroblasts. Tissue Eng Part A. 2015;21(3-4):817-828.
93. Fauzi I, Panoskaltsis N, Mantalaris A. Early exposure of murine embryonic stem cells to hematopoietic cytokines differentially directs definitive erythropoiesis and cardiomyogenesis in alginate hydrogel three-dimensional cultures. Stem Cells Dev. 2014;23(22):2720-2729.
94. Allenby MC, Panoskaltsis N, Tahlawi A, Dos Santos SB, Mantalaris A. Dynamic human erythropoiesis in a three-dimensional perfusion bone marrow biomimicry. Biomaterials. 2019;188:24-37.
95. Elvarsdóttir EM, Mortera-Blanco T, Dimitriou M, et al. A three-dimensional in vitro model of erythropoiesis recapitulates erythroid failure in myelodysplastic syndromes. Leukemia. 2020;34(1):271-282.
96. Currao M, Malara A, Di Buduo CA, Abbonante V, Tozzi L, Balduini A. Hyaluronan based hydrogels provide an improved model to study megakaryocyte-matrix interactions. Exp Cell Res. 2016;346(1):1-8.
97. Pietrzyk-Nivau A, Poirault-Chassac S, Gandrille S, et al. Three-dimensional environment sustains hematopoietic stem cell differentiation into platelet-producing megakaryocytes. PLoS One. 2015;10(8): e0136652.
98. Aguilar A, Pertuy F, Eckly A, et al. Importance of environmental stiffness for megakaryocyte differentiation and proplatelet formation. Blood. 2016;128(16): 2022-2032.
99. Sullenbarger B, Bahng JH, Gruner R, Kotov N, Lasky LC. Prolonged continuous in vitro human platelet production using three-dimensional scaffolds. Exp Hematol. 2009;37(1):101-110.
100. Lasky LC, Sullenbarger B. Manipulation of oxygenation and flow-induced shear stress can increase the in vitro yield of platelets from cord blood. Tissue Eng Part C Methods. 2011;17(11):1081-1088.
101. Mostafa SS, Miller WM, Papoutsakis ET. Oxygen tension influences the differentiation, maturation and apoptosis of human megakaryocytes. Br J Haematol. 2000; 111(3):879-889.
102. Shepherd JH, Howard D, Waller AK, et al. Structurally graduated collagen scaffolds applied to the ex vivo generation of platelets from human pluripotent stem cell-derived megakaryocytes: Enhancing production and purity. Biomaterials. 2018;182:135-144.
103. Kotha S, Sun S, Adams A, et al. Microvasculature-directed thrombopoiesis in a 3D in vitro marrow microenvironment. PLoS One. 2018;13(4):e0195082.
104. Omenetto FG, Kaplan DL. New opportunities for an ancient material. Science. 2010;329(5991):528-531.
105. Di Buduo CA, Wray LS, Tozzi L, et al. Programmable 3D silk bone marrow niche for platelet generation ex vivo and modeling of megakaryopoiesis pathologies. Blood. 2015;125(14):2254-2264.
106. Di Buduo CA, Soprano PM, Tozzi L, et al. Modular flow chamber for engineering bone marrow architecture and function. Biomaterials. 2017;146:60-71.
107. Blumberg N, Heal JM, Phillips GL. Platelet transfusions: trigger, dose, benefits, and risks. F1000 Med Rep. 2010;2:5.
108. Rousseau GF, Giarratana MC, Douay L. Large-scale production of red blood cells from stem cells: what are the technical challenges ahead? Biotechnol J. 2014;9(1):28-38.
109. Timmins NE, Nielsen LK. Blood cell manufacture: current methods and future challenges. Trends Biotechnol. 2009;27(7):415-422.
110. Zeuner A, Martelli F, Vaglio S, Federici G, Whitsett C, Migliaccio AR. Concise review: stem cell-derived erythrocytes as upcoming players in blood transfusion. Stem Cells. 2012;30(8):1587-1596.
111. Olivier EN, Zhang S, Yan Z, et al. PSC-RED and MNC-RED: albumin-free and low-transferrin robust erythroid differentiation protocols to produce human enucleated red blood cells. Exp Hematol. 2019;75:31-52.
112. Heshusius S, Heideveld E, Burger P, et al. Large-scale in vitro production of red blood cells from human peripheral blood mononuclear cells. Blood Adv. 2019;3(21):3337-3350.
113. Giani FC, Fiorini C, Wakabayashi A, et al. Targeted application of human genetic variation can improve red blood cell production from stem cells. Cell Stem Cell. 2016;18(1):73-78.
114. Bernecker C, Ackermann M, Lachmann N, et al. Enhanced ex vivo generation of erythroid cells from human induced pluripotent stem cells in a simplified cell culture system with low cytokine support. Stem Cells Dev. 2019;28(23):1540-1551.
115. Thon JN, Dykstra BJ, Beaulieu LM. Platelet bioreactor: accelerated evolution of design and manufacture. Platelets. 2017;28(5):472-477.
116. Reddy OL, Savani BN, Stroncek DF, Panch SR. Advances in gene therapy for hematologic disease and considerations for transfusion medicine. Semin Hematol. 2020;57(2): 83-91.

Ferrata Storti Foundation

Haematologica 2021
Volume 106(4):958-967

Novel pyrrolobenzodiazepine benzofused hybrid molecules inhibit nuclear factor-κB activity and synergize with bortezomib and ibrutinib in hematologic cancers

Thomas Lewis,[1] David B. Corcoran,[2] David E. Thurston,[2] Peter J. Giles,[1,3] Kevin Ashelford,[1,3] Elisabeth J. Walsby,[1] Christopher D. Fegan,[1] Andrea G. S. Pepper,[4] Khondaker Miraz Rahman[2#] and Chris Pepper[1,4#]

[1]Division of Cancer & Genetics, Cardiff University School of Medicine, Cardiff; [2]School of Cancer and Pharmaceutical Science, King's College London, Franklin-Wilkins Building, London; [3]Wales Gene Park, Heath Park, Cardiff and [4]Brighton and Sussex Medical School, University of Sussex, Brighton, UK

[#]KMR and CP contributed equally as co-senior authors.

ABSTRACT

Chronic lymphocytic leukemia (CLL) and multiple myeloma are incurable hematologic malignancies that are pathologically linked with aberrant nuclear factor-kappa B (NF-κB) activation. In this study, we identified a group of novel C8-linked benzofused pyrrolo[2,1-c][1,4]benzodiazepine monomeric hybrids capable of sequence-selective inhibition of NF-κB with low nanomolar LD_{50} values in CLL (n=46) and multiple myeloma cell lines (n=5). The lead compound, DC-1-192, significantly inhibited NF-κB DNA binding after just 4 h of exposure, demonstrating inhibitory effects on both canonical and non-canonical NF-κB subunits. In primary CLL cells, sensitivity to DC-1-192 was inversely correlated with RelA subunit expression (r^2=0.2) and samples with BIRC3 or NOTCH1 mutations showed increased sensitivity (*P*=0.001). RNA-sequencing and gene set enrichment analysis confirmed the over-representation of NF-κB regulated genes in the downregulated gene list. Furthermore, *in vivo* efficacy studies in NOD/SCID mice, using a systemic RPMI 8226 human multiple myeloma xenograft model, showed that DC-1-192 significantly prolonged survival (*P*=0.017). In addition, DC1-192 showed synergy with bortezomib and ibrutinib; synergy with ibrutinib was enhanced when CLL cells were co-cultured on CD40L-expressing fibroblasts in order to mimic the cytoprotective lymph node microenvironment (*P*=0.01). Given that NF-κB plays a role in both bortezomib and ibrutinib resistance mechanisms, these data provide a strong rationale for the use of DC-1-192 in the treatment of NF-κB-driven cancers, particularly in the context of relapsed/refractory disease.

Correspondence:

CHRIS PEPPER
c.pepper@bsms.ac.uk

Received: September 17, 2019.

Accepted: March 24, 2020.

Pre-published: May 7, 2020.

https://doi.org/10.3324/haematol.2019.238584

©2021 Ferrata Storti Foundation

Material published in Haematologica is covered by copyright. All rights are reserved to the Ferrata Storti Foundation. Use of published material is allowed under the following terms and conditions: https://creativecommons.org/licenses/by-nc/4.0/legalcode. Copies of published material are allowed for personal or internal use. Sharing published material for non-commercial purposes is subject to the following conditions: https://creativecommons.org/licenses/by-nc/4.0/legalcode, sect. 3. Reproducing and sharing published material for commercial purposes is not allowed without permission in writing from the publisher.

Introduction

Nuclear factor kappa B (NF-κB) denotes a family of homo- and heterodimeric transcription factors composed of five subunits: p65 (RelA), p50, RelB, p52 and c-Rel.[1] These subunits exert their effects via the canonical or non-canonical signaling pathways.[2] NF-κB is maintained in an inactive state in the cytoplasm but following IκB kinase (IKK) activation NF-κB is shuttled into the nucleus where it exerts its transcriptional effects.[3] NF-κB regulates the transcription of genes that are essential for cell survival, proliferation, inflammation and invasion/metastasis. These processes are commonly dysregulated in cancers, including CLL and multiple myeloma, leading to the constitutive aberrant activation of NF-κB.[2-4] Indeed, NF-κB has been shown to play a central role in disease progression and drug resistance in these hematologic cancers.[5,6] While treatment with currently established therapies, such as the proteasome inhibitor bortezomib or the BTK inhibitor ibrutinib,

are initially effective in a significant proportion of patients,[7,8] there is evidence to suggest that treatment with both of these agents causes an increase in NF-κB activation which has been linked to drug resistance and treatment failure.[9,10] Therefore, direct inhibition of NF-κB could potentially resensitize tumor cells, thus highlighting this transcription factor as a potential therapeutic target.[11-13]

Pyrrolo[2,1-c][1,4]benzodiazepines (PBD) are naturally occurring molecules produced by *Streptomyces* bacteria whose family members include anthramycin (Figure 1) and tomaymycin.[14,15] PBD are a class of sequence-specific covalent DNA minor groove binding agents that are selective for GC-rich sequences, and have been evaluated as potential chemotherapeutic agents in clinical trials.[16,17] More recently, members of the PBD family have been developed as cytotoxic payloads for attachment to antibodies to form antibody-drug conjugates, and a number of these are currently undergoing clinical evaluation for the treatment of leukemia and lung cancer.[18]

This study identified three lead compounds (DC-1-192, DC-1-92 and DC-1-170) (Figure 1) from a library screen of 87 novel synthetic C8-linked benzofused PBD monomeric hybrids based on their *in vitro* cytotoxicity. The compounds were then further evaluated for their biological properties, including differential toxicity, in malignant and age-matched normal B and T cells. In terms of their mechanism of action, PBD monomers can recognize and bind to specific sequences of DNA and therefore have the potential to act as competitive inhibitors of transcription factors. Previous research has shown that PBD monomers such as GWL-78 preferentially inhibit the transcription factor NF-Y,[19] while PBD monomers such as the DC-81-indole hybrid[20] and KMR-28-39 are potent NF-κB inhibitors.[21] The aim of this study was to determine the biological properties of these novel C8-linked benzofused PBD monomers by investigating their cytotoxic profiles in multiple myeloma cell lines, primary CLL cells and age-matched normal B- and T-lymphocytes. We went on to investigate their ability to inhibit NF-κB and whether they could potentiate the effects of the targeted agents bortezomib and ibrutinib, currently used in the treatment of myeloma and CLL, respectively.

Methods

Detailed methods can be found in the *Online Supplementary Appendix*.

Cell lines, primary chronic lymphocytic leukemia cells and normal lymphocytes

Primary CLL cell lines (n=46) and age-matched normal B and T cells were obtained with informed consent in accordance with the ethical approval granted by South East Wales Research Ethics Committee (02/4806). In addition, five multiple myeloma cell lines, JJN3, U266, OPM2, MM.1S and H929, were obtained from the *Deutsche Sammlung von Mikroorganismen und Zellkulturen*. The provenance of the cell lines was verified by multiplex polymerase chain reaction of minisatellite markers; all were certified mycoplasma-free.

Measurement of *in vitro* apoptosis

Apoptosis was assessed using annexin V and propidium iodide labeling. Samples were analyzed using an Accuri C6 flow cytometer with CFlow software (BD Biosciences).

Enzyme-linked immunosorbent assay for NF-κB subunits

Nuclear levels of p65, p50, p52 and RelB DNA binding were assessed in JJN3 and U266 cells treated for 4 h with DC-1-92, DC-1-170 (0nM 20 nM) and DC-1-192 (0nM 5 nM).

Synergy with bortezomib and ibrutinib

The synergy between the PBD monomers and bortezomib or ibrutinib was determined in JJN3 cells and primary CLL cells, respectively. Fixed molar ratios were derived from experimentally-determined median lethal dose (LD_{50}) values for each PBD and clinically achievable concentrations of bortezomib and ibrutinib.

RNA Isolation and sequencing

JJN3 cells were treated with 20 nM of either DC-1-170 or DC-1-192 for 4 h. RNA was extracted using an RNeasy mini-kit (Qiagen) in accordance with the manufacturer's instructions. Subsequently, 100-900 ng of high-quality total RNA (RNA integrity number >8) was depleted of ribosomal RNA, and sequencing libraries were prepared using the Illumina TruSeq Stranded Total RNA with Ribo-Zero Gold™ kit (Illumina Inc.).

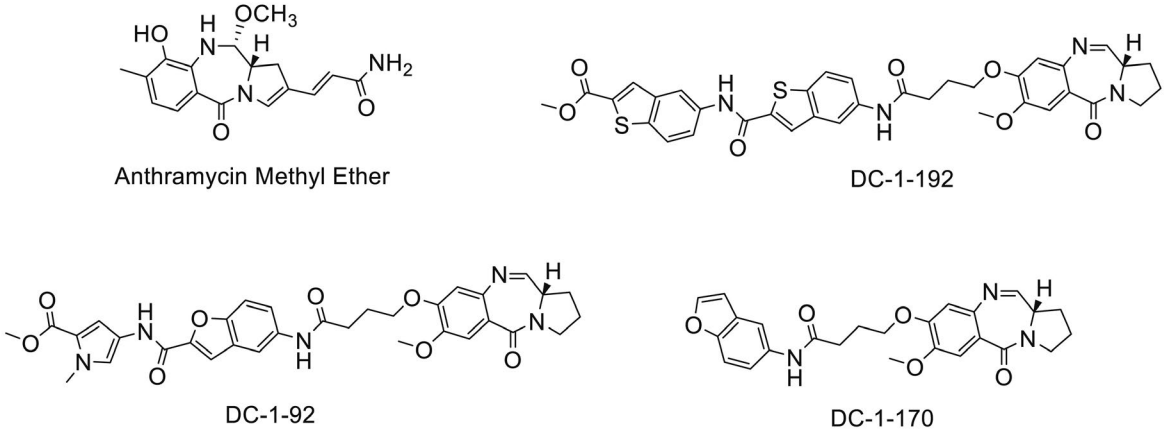


Figure 1. The structures of anthramycin and three structurally-related C8-linked benzofused PBD hybrids. Anthramycin (the first PBD to be isolated from a *Streptomyces* species), and the three synthetic PBD, DC-1-192, DC-1-92 and DC-1-170, identified as lead compounds in this study.

In vivo systemic xenograft model of myeloma in NOD/SCID mice

NOD/SCID mice were sublethally irradiated prior to tail vein inoculation with the human myeloma cell line RPMI8226 ($1x10^7$ cells) to initiate tumor development. The date of inoculation was denoted as day 0. Intravenous treatment with vehicle only; 0.05% dimethylsulfoxide in saline (n=7) or 1 mg/kg of DC-1-192 (n=7) was started at day 5. Survival was evaluated from the first day of treatment until death.

Statistical analysis

All statistical analyses were performed using Graphpad Prism 6.0 software (Graphpad Software). The normal distribution of the data was established using the omnibus K2 test. Univariate comparisons were made using the Student *t*-test for paired and unpaired observations. All toxicity data from drug treatment were used to produce sigmoidal dose-response curves from which LD_{50} values were calculated. Toxicity data from synergy experiments were processed using CalcuSyn software with the median effect method to subsequently calculate the combination index (CI) for each pair of agents; CI values less <1 were indicative of synergy.[22]

Results

Cytotoxic screening of pyrrolo[2,1-c][1,4]benzodiazepine compounds identified three lead compounds

Initial cytotoxicity screening (trypan blue exclusion assay) of a library of 87 novel synthetic C8-linked benzofused PBD monomeric hybrids was carried out using the multiple myeloma cell line, JJN3. Three lead compounds were selected for further investigation based on their cytotoxic effects at nanomolar concentrations. The chemical structures of all three compounds, together with that of anthramycin on which they are based, are shown in Figure 1.

In vitro and *in vivo* cytotoxicity of the lead pyrrolo[2,1-c][1,4]benzodiazepine compounds in multiple myeloma cell lines

The relative cytotoxicity of the three lead compounds was then assessed in five different multiple myeloma cell lines, JJN3, U266, OPM2, MM.1S and H929 using an annexin V/propidium iodide apoptosis assay. The cells were cultured for 48 h in increasing concentrations (1 nM-100 nM) of DC-1-92, DC-1-170 and DC-1-192 and were compared with untreated controls. Each compound showed a dose-dependent increase in apoptosis; a representative example of the data generated is shown in Figure 2A. The dose-response curves for each compound were compared in each cell line using overlaid sigmoidal plots (Figure 2B) and the mean LD_{50} values were then calculated for each treatment and plotted on the bar chart shown in Figure 2C. Although each cell line showed differential sensitivity to the three compounds, in every case DC-1-192 was the most cytotoxic PBD with DC-1-170 showing the least cytotoxicity (Figure 2D). The LD_{50} values for DC-1-192 were compared with the published NF-κB index value for each cell line.[23] The NF-κB index is the average of the $\log_2$ values for ten NF-κB-regulated genes (excluding *BIRC3/cIAP2*); the higher the index value, the more NF-κB-dependent the cell line is deemed to be. With the exception of JJN3 cells, sensitivity to DC-1-192 appeared to be inversely associated with the NF-κB index, a concept we went on to explore in subsequent experiments. In order to investigate the anti-tumor effects of DC-1-192 *in vivo*, we employed a systemic model of multiple myeloma in which NOD/SCID mice (2 groups of 7 mice) were inoculated with the human RPMI 8226 myeloma cell line ($1x10^7$ cells). Treatment was initiated 5 days after inocuation with either DC-1-192 (1 mg/kg) or vehicle control. DC-1-192 was administered once per day (5 days/week) for 3 weeks by intravenous injection and animals were monitored daily for morbidity and mortality. DC-1-192 significantly prolonged the survival of the mice; the median survival of the DC-1-192-treated mice was 68 days *versus* 56 days in untreated mice (hazard ratio [HR]=2.98; P=0.017) (Figure 2E).

Comparative cytotoxicity in primary chronic lymphocytic leukemia and normal B- and T-lymphocytes

Primary CLL cells and age-matched normal B- and T-lymphocytes obtained from healthy donors were treated with increasing concentrations of DC-1-92, DC-1-170 and DC-1-192. Apoptosis was measured using CD19/CD3/annexin V labeling to determine the percentage of apoptosis induced by the PBD compunds in $CD19^+$ B cells and $CD3^+$ T cells, as shown in *Online Supplementary Figure S1A*. *Online Supplementary Figure S1B* shows the comparative dose-responses for each of the cell types indicating that normal lymphocytes were less susceptible to the effects of the PBD. As was the case with the three multiple myeloma cell lines, DC-1-192 was the most potent cytotoxic agent in primary CLL cells. *Online Supplementary Figure S1C, D* shows that CLL cells were significantly more sensitive to the effects of the PBD than were age-matched normal B- and T-lymphocytes.

DC-1-192 shows preferential cytotoxicity in chronic lymphocytic leukemia cells carrying a *NOTCH1* or *BIRC3* mutation

All of the CLL samples treated with DC-1-192 (n=46) showed nanomolar LD_{50} values with a mean LD_{50} value for the entire CLL cohort of 3.8 nM (Figure 3A). We next examined whether sensitivity to DC-1-192 was associated with any of the known prognostic markers. There was no significant difference in mean LD_{50} value between *IGHV*-mutated and *IGHV*-unmutated samples (Figure 3B); CD38-positive and CD38-negative samples (≥/<20%) (Figure 3C) and samples with higher or lower β_2-microglobulin concentrations (≥/<3.5 mg/L) (Figure 3D). However, samples derived from patients with a BIRC3 (n=3) or NOTCH1 (n=11) mutation were significantly more sensitive to the effects of DC-1-192 (Figure 3E) suggesting that elevated NF-κB signaling may be a determinant of sensitivity.[24,25] In keeping with this concept, the nuclear expression of the NF-κB subunit p65 (RelA) was inversely correlated with DC-1-192 LD_{50} values (Figure 3F).

Nuclear localization of NF-κB subunits following treatment with pyrrolo[2,1-c][1,4]benzodiazepines

We have previously shown that PBD monomers, such as KMR-28-39, have NF-κB inhibitory effects.[21] We, therefore, determined the NF-κB inhibitory properties of this new series of compounds in two myeloma cell lines JJN3 and U266. JJN3 cells overexpress both the canonical and non-canonical NF-κB subunits and possess an *EFTUD2-NIK* fusion gene which lacks the TRAF3 binding domain resulting in the accumulation of a cytoplasmic EFTUD2-

NIK fusion protein. U266 cells exhibit a TRAF3 mutation causing stabilization of wild-type NIK protein.[23,24] Both cell lines were treated for 4 h with up to 20 nM of each agent and the relative change in nuclear p65 (RelA), p50, p52 and RelB DNA binding was determined as a function of the untreated control. Levels of c-Rel were not evaluated in this study as JJN3 cells show very low levels of this subunit relative to the dominant canonical subunits p65 and p50. In JJN3 cells, all the PBD showed significant inhibition of p65, p50 and Rel B but no significant reduction in p52 (Figure 4A). In contrast, U266 cells showed a significant reduction in the nuclear DNA binding of all four subunits (Figure 4B).

Transcriptional effects of DC-1-170 and DC-1-192 on JJN3 cells

As predicted, RNA-sequencing analysis of DC-1-170 and DC-1-192 revealed a dominant inhibitory effect on

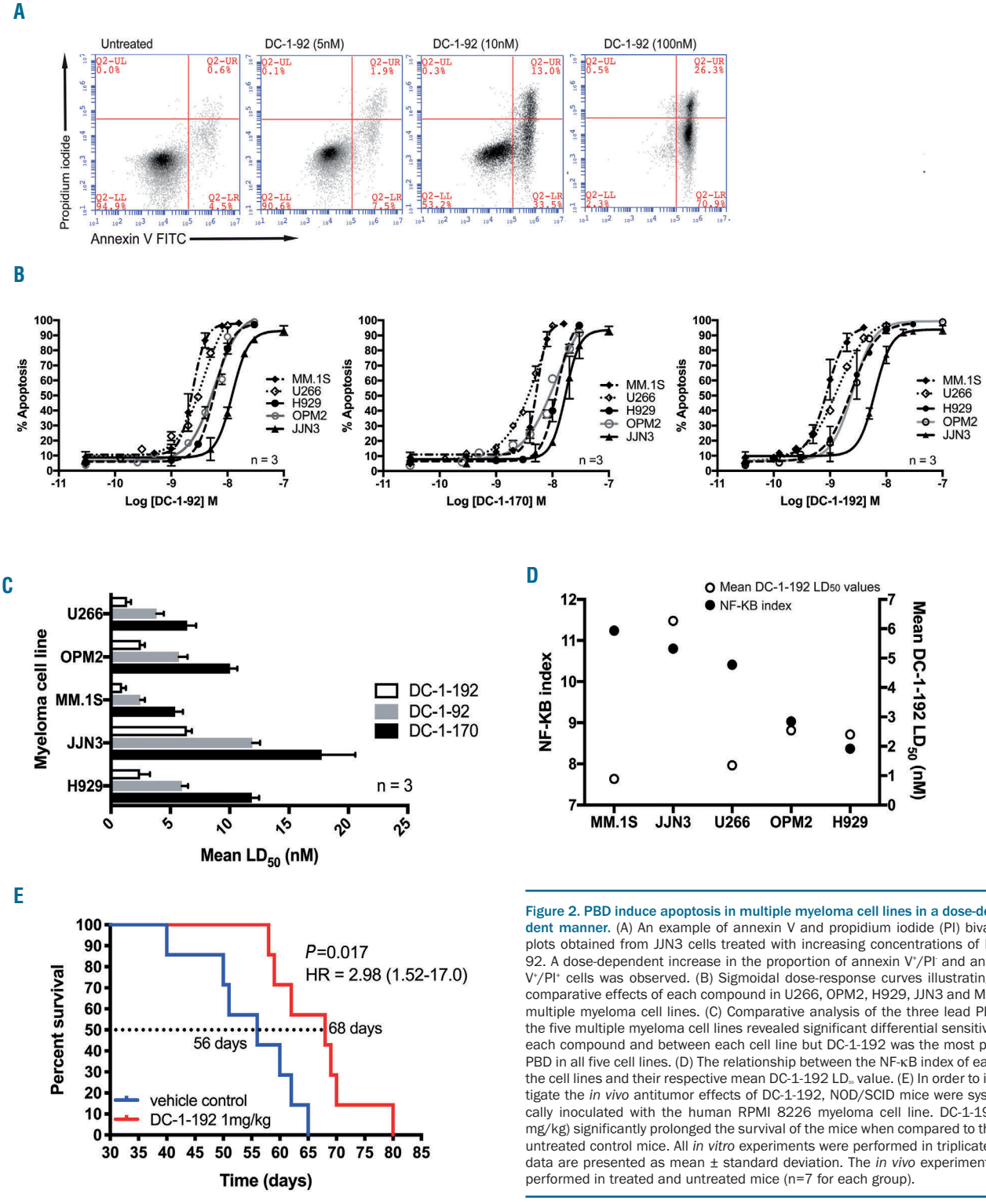


Figure 2. PBD induce apoptosis in multiple myeloma cell lines in a dose-dependent manner. (A) An example of annexin V and propidium iodide (PI) bivariate plots obtained from JJN3 cells treated with increasing concentrations of DC-1-92. A dose-dependent increase in the proportion of annexin V^+/PI^- and annexin V^+/PI^+ cells was observed. (B) Sigmoidal dose-response curves illustrating the comparative effects of each compound in U266, OPM2, H929, JJN3 and MM1.S multiple myeloma cell lines. (C) Comparative analysis of the three lead PBD in the five multiple myeloma cell lines revealed significant differential sensitivity to each compound and between each cell line but DC-1-192 was the most potent PBD in all five cell lines. (D) The relationship between the NF-κB index of each of the cell lines and their respective mean DC-1-192 LD_{50} value. (E) In order to investigate the *in vivo* antitumor effects of DC-1-192, NOD/SCID mice were systemically inoculated with the human RPMI 8226 myeloma cell line. DC-1-192 (1 mg/kg) significantly prolonged the survival of the mice when compared to that of untreated control mice. All *in vitro* experiments were performed in triplicate and data are presented as mean ± standard deviation. The *in vivo* experiment was performed in treated and untreated mice (n=7 for each group).

gene transcription with a smaller subset of genes showing increased transcription following exposure to the drug. In unsupervised hierarchical clustering, the samples clustered according to treatment condition (Figure 5A). Strikingly, 4,040/5,077 (80%) of the genes altered by exposure to the drugs were common to both PBD compounds (Figure 5B) suggesting that their structural similarity resulted in the inhibition of a conserved set of genes. Furthermore, gene set enrichment analysis, using WebGestalt (WEB-based GEne SeT AnaLysis Toolkit),[25] confirmed that NF-κB-regulated genes were significantly over-represented in the downregulated gene list, with a normalized enrichment score of -1.7750 (Figure 5C, D). These data suggest that inhibition of NF-κB target genes may contribute to the cytotoxicity of the PBD compounds.

Synergy between DC-1-192 in combination with bortezomib or ibrutinib

Overexpression of NF-κB is associated with chemotherapeutic drug resistance in both CLL and multiple myeloma.[26,27] Having established that DC-1-192 inhibited nuclear NF-κB DNA binding and downregulated NF-κB target genes, we set out to determine whether these inhibitory properties could enhance the killing effect of bortezomib and ibrutinib in the JJN3 myeloma cell line and primary CLL cells, respectively. To investigate syner-

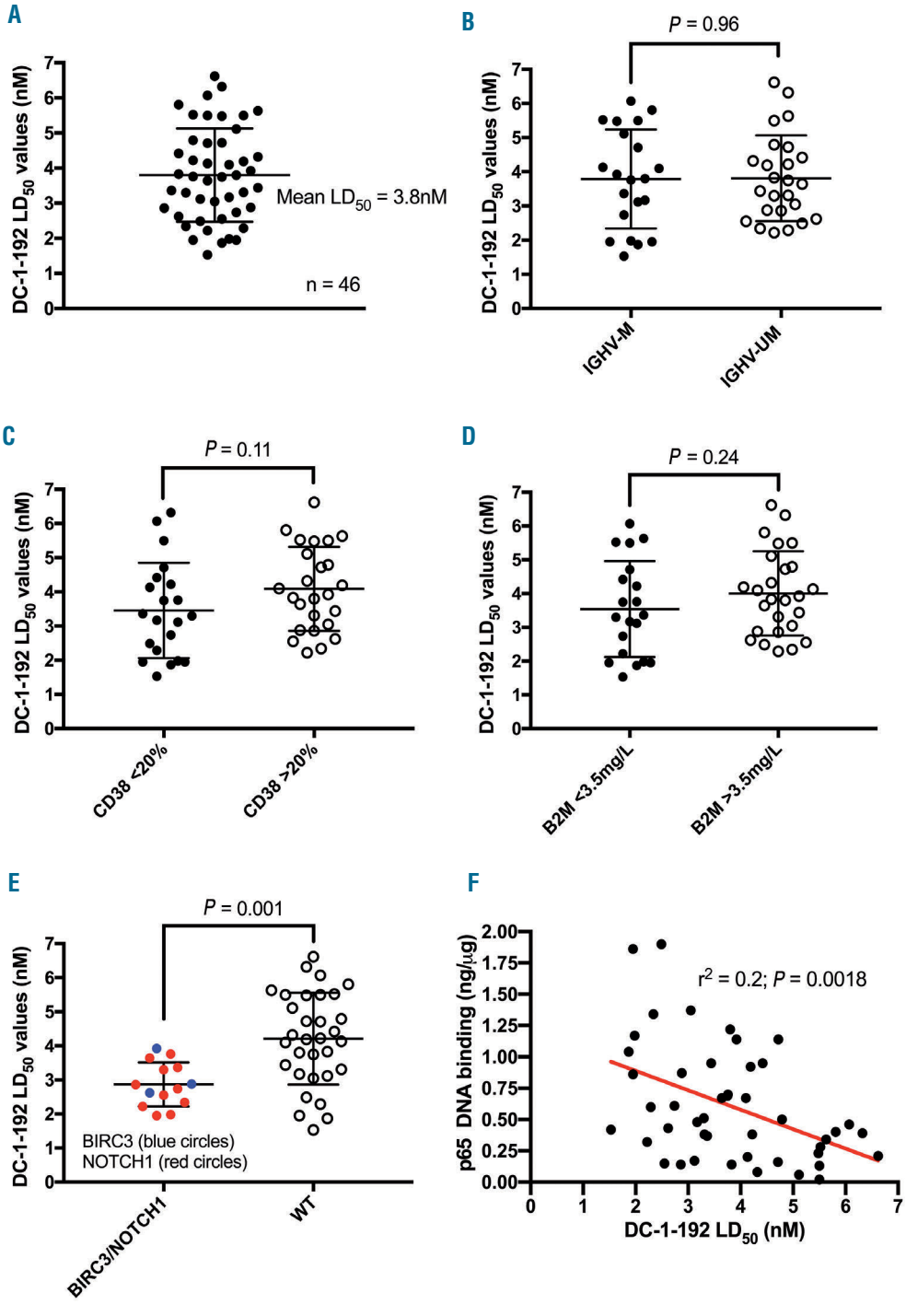


Figure 3. DC-1-192 was highly cytotoxic in primary chronic lymphocytic leukemia cells and showed preferential effects in BIRC3 and NOTCH1 mutated samples. (A) All 46 samples tested showed low nanomolar LD_{50} values when treated with DC-1-192. (B-D) Analysis of prognostic subsets revealed that DC-1-192 was equipotent in *IGHV* mutated and unmutated samples (B), CD38-positive and CD38-negative samples (C) and samples with high or low concentrations of β2-microglobulin (D). (E) In contrast, BIRC3 and NOTCH1 mutated samples showed significantly increased sensitivity to DC-1-192. (F) There was an inverse relationship between nuclear DNA binding of the canonical NF-κB subunit, p65, and DC-1-192 LD_{50} values.

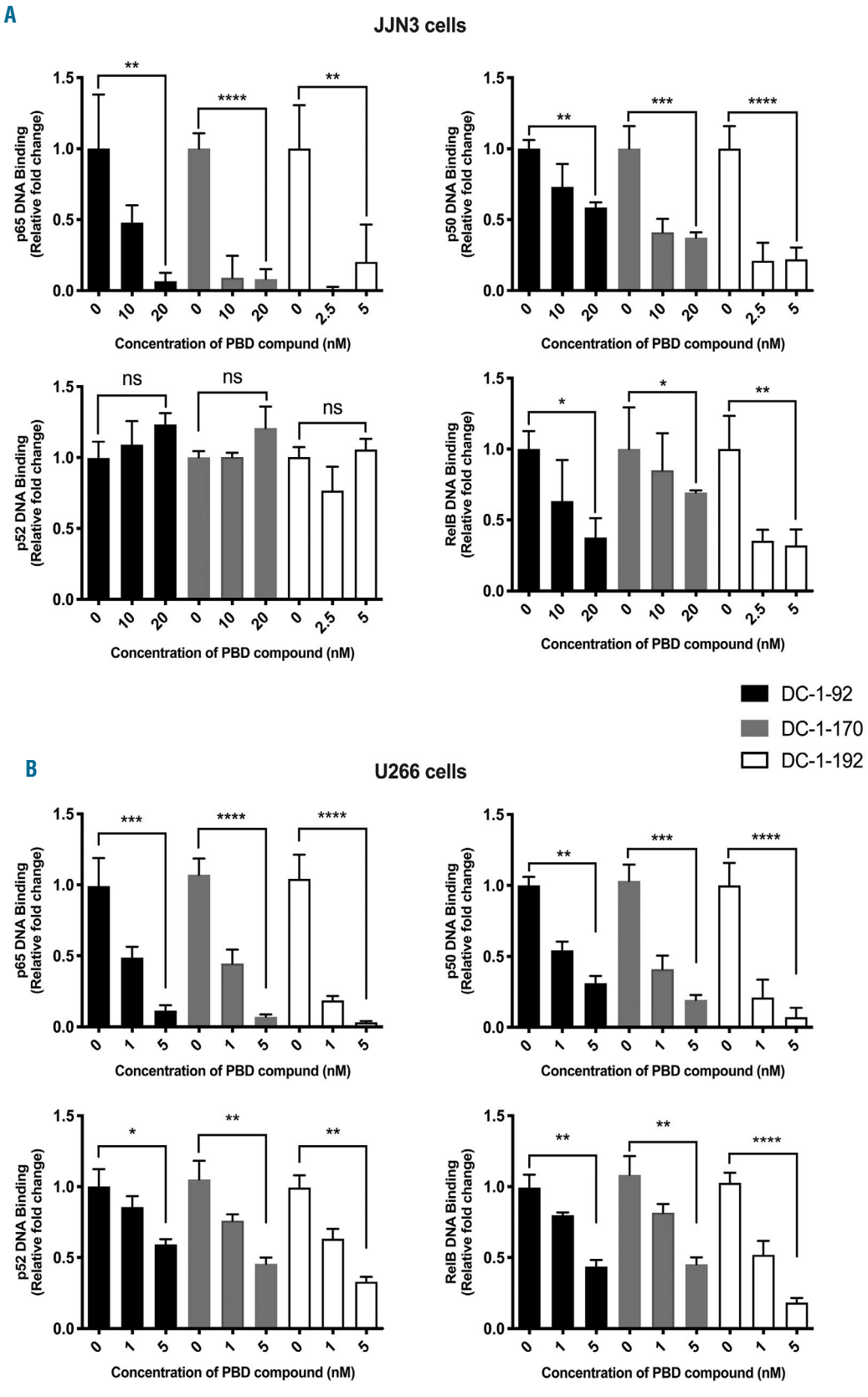
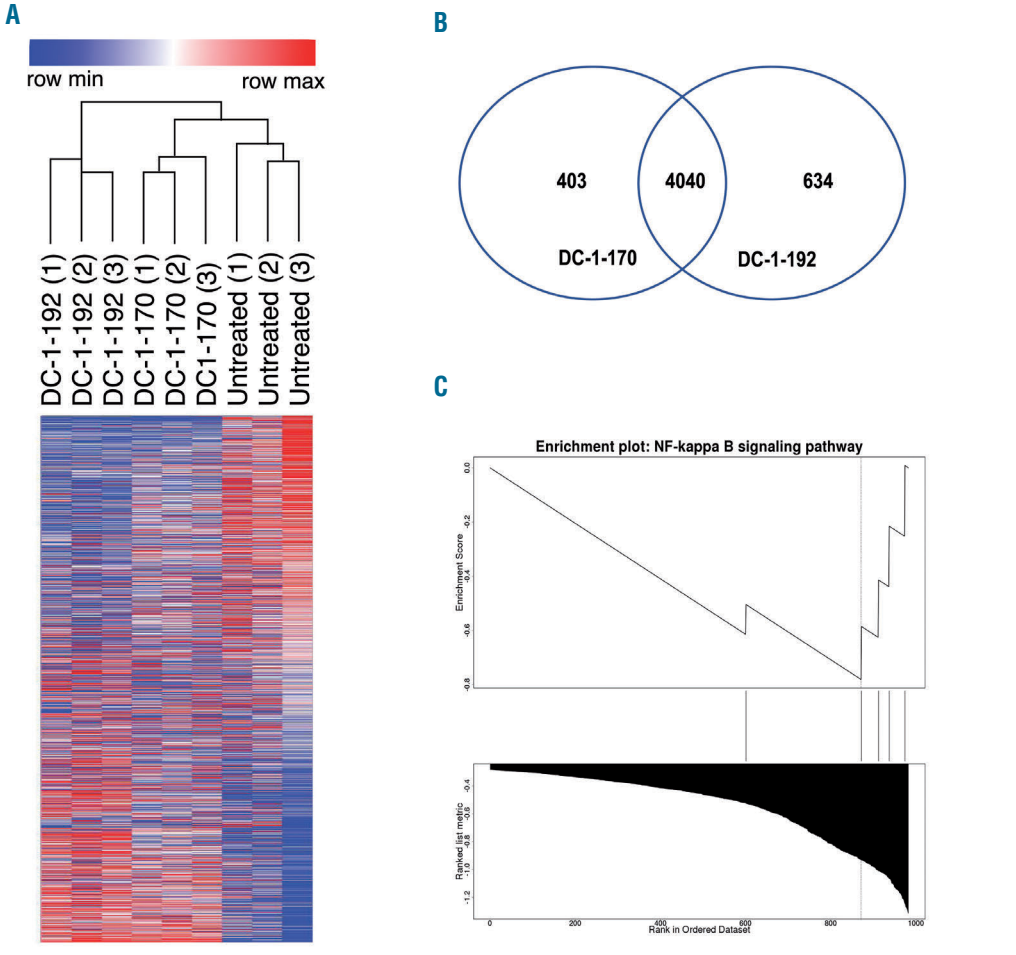


Figure 4. PBD show marked inhibitory effects on both canonical and non-canonical NF-κB subunits. JJN3 and U266 cells were treated with DC-1-92, DC-1-170 and DC-1-192 for 4 h. Nuclear extracts were then generated from these samples and the amounts of p65, p50, p52 and Rel B were quantified and expressed as relative fold-change as a function of the untreated controls. (A) JJN3 cells showed significant reductions in nuclear expression of p65, p50 and RelB NF-κB subunits but no change in p52 following exposure to DC-1-92, DC-1-170 and DC-1-192. (B) In contrast, U266 cells showed significant reductions in nuclear expression of all four NF-κB subunits. All experiments were performed in triplicate. *P<0.05, **P<0.01, ***P<0.001 and ****P<0.0001. ns: not statistically significant differences.

gy, JJN3 and primary CLL cells (n=5) were treated with increasing concentrations of DC-1-192 both alone and in combination with bortezomib in JJN3 cells and ibrutinib in CLL samples. The fixed molar ratios employed in the combination studies were determined experimentally using the LD_{50} values calculated from the previous toxicity data. The fraction affected plots and isobologram plots for the drugs and drug combinations in JJN3 cells (Figure 6A), and in primary CLL cells (Figure 6B) show that the cytotoxic effects of DC-1-192 are potentiated by the



D

GeneSet	Description	Enrichment Score	Normalized Enrichment Score	*P*-value	FDR
hsa04630	JAK-STAT signaling pathway	-0.6824	-1.9718	0.0012	0.0725
hsa05222	Small cell lung cancer	-0.7432	-1.7127	0.0013	0.1986
hsa04640	Hematopoietic cell lineage	-0.7257	-1.8594	0.0024	0.0642
hsa04064	NF-kappa B signaling pathway	-0.7806	-1.7750	0.0026	0.1348
hsa04080	Neuroactive ligand-receptor interaction	-0.5484	-1.8622	0.0053	0.0785
hsa05323	Rheumatoid arthritis	-0.6686	-1.7070	0.0062	0.1831
hsa04727	GABAergic synapse	-0.6176	-1.6455	0.0144	0.2779
hsa05133	Pertussis	-0.6619	-1.6262	0.0280	0.2904
hsa04150	mTOR signaling pathway	0.2546	1.0526	0.3760	0.6415
hsa05231	Choline metabolism in cancer	0.3838	1.0528	0.3765	0.6835
hsa00270	Cysteine and methionine metabolism	0.3715	1.0227	0.3816	0.6622
hsa04662	B cell receptor signaling pathway	0.2764	1.0024	0.4237	0.6656

Figure 5. RNA sequencing and gene set enrichment analysis revealed that DC-1-170 and DC-1-192 preferentially inhibited NF-κB target genes. (A) Unsupervised hierarchical clustering revealed a strong drug-associated transcriptional signature for both DC-1-170 and DC-1-192. (B) The majority 4,418/5,077 (87%) of the significantly altered transcripts were downregulated in response to drug. Strikingly, 4,040/5,077 (80%) of the changes were common to both DC-1-170 and DC-1-192. (C) Gene set enrichment analysis showed over-representation of NF-κB target genes in the gene list commonly downregulated by exposure to DC-1-170 and DC-1-192. (D) The top 12 over-represented pathways in the commonly downregulated gene list following exposure to DC-1-170 and DC-1-192 are shown. The table also shows the normalized enrichment scores, *P* values and false discovery rates (FDR) for each canonical gene set.

addition of bortezomib and ibrutinib, respectively. Furthermore, the combination of DC-1-192 with bortezomib and ibrutinib showed synergy (CI values <1) at the level of LD_{50}, LD_{75} and LD_{90} with an incremental increase in synergistic effect from LD_{50} to LD_{90} (Figure 6C). Furthermore, DC-1-192 showed increased synergy with ibrutinib when primary CLL cells were co-cultured on CD40L-expressing fibroblasts (Figure 6D) suggesting that these agents may be particularly effective in the treatment of tissue-resident CLL cells.

Discussion

NF-κB is a master regulator of a number of cellular processes that contribute to cancer progression, including cell survival and proliferation. Furthermore, it is often implicated in drug resistance, highlighting its potential as a therapeutic target.[12,13] The interest in small molecular DNA-binding agents, such as the PBD monomers, has increased in recent years due to their ability to selectively bind to specific sequences within the minor groove of DNA, a characteristic that separates them from traditional

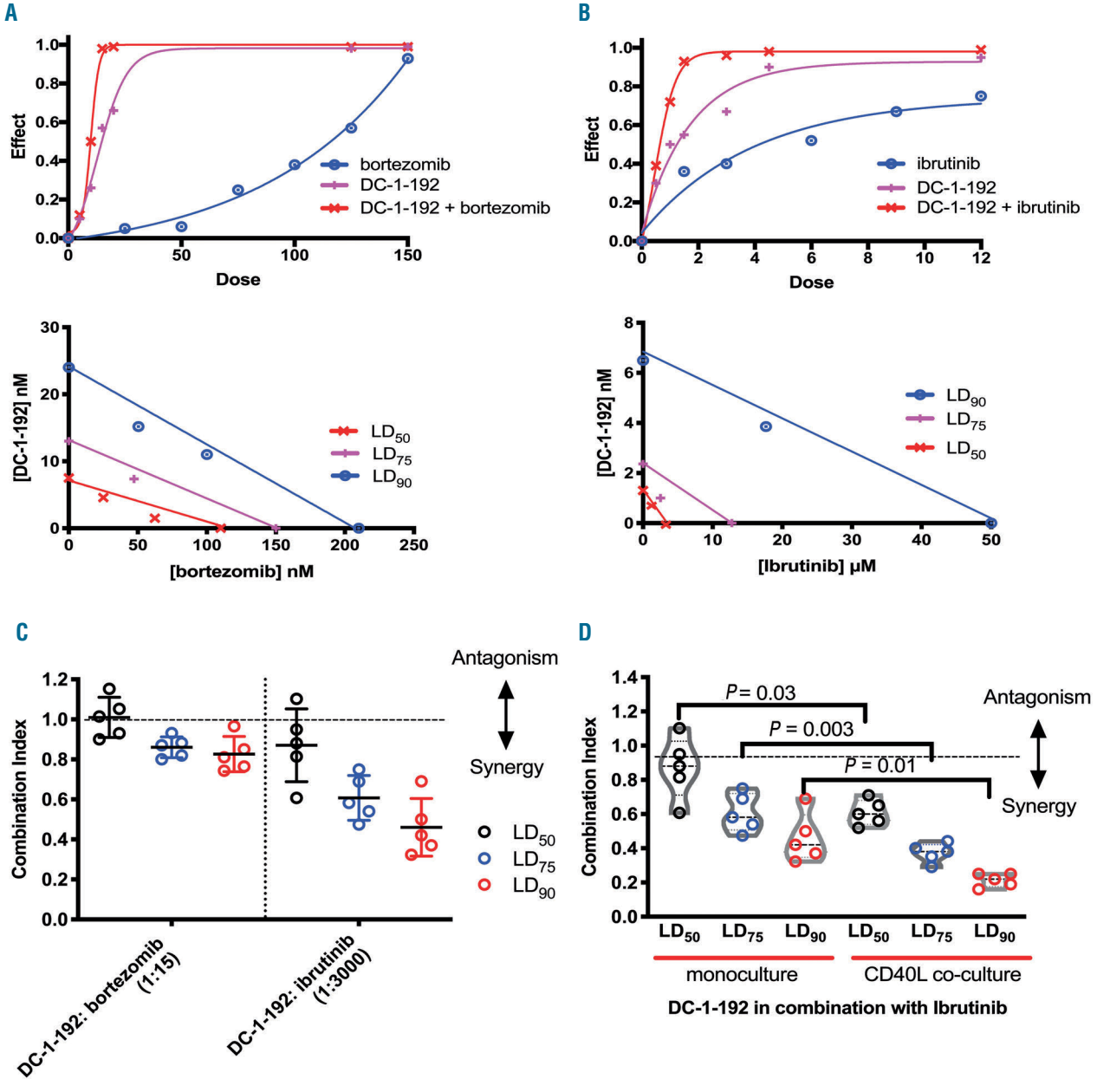


Figure 6. DC-1-192 demonstrates cytotoxic synergy with bortezomib and ibrutinib. Synergy between DC-1-192 and bortezomib was experimentally determined in JJN3 cells and between DC-1-192 and ibrutinib in primary chronic lymphocytic leukemia (CLL) cells. The fixed molar ratios for each combination were derived from the mean LD_{50} values for DC-1-192 and the clinically achievable doses of bortezomib and ibrutinib. Apoptosis was determined using the annexin V/propidium iodide assay. (A) The fraction affected plot and the isobologram plot for DC-1-192, bortezomib and their respective combination (1:15) in JJN3 cells. (B) The fraction affected plot and isobologram plot for DC-1-192, ibrutinib and their combination (1:3000) in primary cells. (C) The combination indices for the combination DC-1-192 with bortezomib and DC-1-192 with ibrutinib at the level of LD_{50}, LD_{75} and LD_{90} in primary CLL cells (n=5). (D) Comparison of the combination indices generated by the combination of DC-1-192 and ibrutinib in monoculture and CD40L-expressing co-culture. All JJN3 cell line experiments were performed in triplicate. All of the primary CLL experiments were performed on samples derived from five individual patients with data presented as the mean of duplicate experiments.

alkylating agents. This raises the possibility that they can selectively inhibit transcription factors,[16] so this study set out to determine the *in vitro* and *in vivo* biological effects of a series of novel C8-linked PBD-benzofused hybrids.

Initially library screening identified three lead compounds. All three PBD showed high potency in five different multiple myeloma cell lines with LD_{50} values in the low nanomolar range. Subsequently, the PBD showed similar high potency in a cohort of 46 primary CLL samples and significantly lower toxicity in normal age-matched B- and T-lymphocytes. The most cytotoxic PBD, DC-1-192, showed 2.4-fold and 4.6-fold differential toxicity in CLL cells suggesting that this compound has a positive therapeutic index. We went on to show that DC-1-192 was well tolerated in a systemic *in vivo* xenograft model of myeloma and significantly prolonged the survival of the mice.

Subset analysis of the CLL cohort data revealed that DC-1-192 was equipotent in poor prognostic groups including *IGHV* unmutated cases (P=0.96). Furthermore, samples derived from patients with BIRC3 or NOTCH1 mutations showed significantly increased sensitivity to DC-1-192. These mutations are known to cause aberrant activation of NF-κB signaling and are associated with resistance to chemoimmunotherapy and inferior clinical outcome.[28-32] Although these mutations are linked with non-canonical NF-κB activation, here we showed that nuclear expression of the canonical p65 subunit was a predictor of *in vitro* sensitivity to DC-1-192.

Given these findings, we plotted the previously published NF-κB index for each of the myeloma cell lines[23] against their respective LD_{50} for DC-1-192. Four of the five cell lines showed an inverse relationship between their NF-κB index and DC-1-192 LD_{50} value suggesting that response to DC-1-192 was influenced by how NF-κB-dependent the cell lines were. JJN3 cells were the exception to this rule; these cells had a high NF-κB index (10.8) but were relatively resistant, in comparison to the other four cell lines, to the cytotoxic effects of DC-1-192 (mean LD_{50} = 6 nM). The reasons for this are likely to be multiple and may be unrelated to NF-κB, but it is worthy of note that JJN3 cells possess a cytoplasmic *EFTUD2-NIK* fusion gene, which may alter p100 processing to p52. Indeed, when we assessed the impact of the PBD on nuclear NF-κB subunit DNA binding in JJN3 cells, all three compounds showed significant inhibition of the p65 and p50 canonical subunits as well as the non-canonical subunit RelB after 4 h. In contrast, no significant change in p52 was observed following treatment with the PBD. We subsequently repeated the experiments using the U266 cell line, which has a TRAF3 mutation leading to the cytoplasmic accumulation of NF-κB inducing kinase (NIK).[23,24] These cells showed a significant reduction in all four NF-κB subunits including p52 following short-term treatment with PBD.

The rapid reduction in nuclear NF-κB subunit expression indicates that NF-κB inhibition precedes apoptosis in these cells and may contribute to the efficacy of the PBD. Given the DNA binding characteristics of these compounds, it seems possible that they compete for NF-κB binding motifs, thereby inhibiting the transcription of NF-κB target genes. The reduction in nuclear NF-κB subunits observed in this study may have been caused by the shuttling of unbound NF-κB back to the cytoplasm and/or targeted degradation.[33,34]

Activation of NF-κB has also been implicated in the development of resistance to chemotherapeutic drugs in myeloma and CLL.[35] Several DNA-damaging agents, including melphalan and fludarabine, have been shown to induce the activity of NF-κB, thereby contributing to cellular resistance to the cytotoxic effects of these treatments.[6,36] In myeloma, bortezomib has been shown to re-sensitize malignant cells to the effects of chemotherapy.[37] However, the emergence of bortezomib-resistant subclones ultimately leads to relapse in many patients.[38] One putative mechanism of bortezomib resistance is the constitutive expression of NF-κB. Although bortezomib can prevent *de novo* activation of the canonical pathway, it has no significant effect on constitutive NF-κB activity.[27] In this study, we showed that direct competitive inhibition of NF-κB at the site of transcription led to the re-sensitization of multiple myeloma cells to the effects of bortezomib. This synergistic effect is likely to be multifactorial, but indicates that bortezomib and the PBD have different molecular targets.

Similarly, in CLL Bruton tyrosine kinase (BTK) has been shown to be a critical downstream mediator of B-cell receptor signaling that is often constitutively activated in CLL patients. The targeting of this kinase with the BTK inhibitor, ibrutinib, has shown notable effects in patients with relapsed CLL[39,40] and this is mediated, at least in part, by the distal inhibition of NF-κB.[41] However, emerging evidence of resistance mechanisms to ibrutinib strongly implicate NF-κB.[42] Here, we show that the combination of DC-1-192 with ibrutinib produced cytotoxic synergy suggesting that the PBD and ibrutinib target NF-κB through different mechanisms and/or that they have other, non-overlapping, molecular targets. Furthermore, synergy was enhanced when primary CLL cells were co-cultured on CD40L-expressing fibroblasts in order to mimic the lymph node microenvironment. This suggests that PBD may be particularly useful in targeting tissue-resident tumor cells.

In summary, the novel PBD compunds evaluated in this study showed low nanomolar toxicity in both primary CLL cells and myeloma cell lines. In addition, primary CLL cells carrying BIRC3 or NOTCH1 mutations were preferentially sensitive to the cytotoxic effects of DC-1-192 suggesting that this agent may be a potential therapeutic option for these poor-risk subsets. Mechanistically, the PBD demonstrated promising dual inhibitory properties on both the canonical and non-canonical NF-κB pathways, a characteristic that has been previously linked to significant antitumor effects in multiple myeloma.[43] Furthermore, the PBD showed *in vitro* synergy with bortezomib and ibrutinib in multiple myeloma and CLL, respectively, providing a strong rationale for the use of these agents in the treatment of relapsed/refractory B-cell neoplasms.

Disclosures

This work was supported by a grant (n. 12-1263/JGATCBR) from Worldwide Cancer Research (formerly AICR) to DET, KMR and CP in 2012. This support included a PhD studentship held by DBC, which enabled all of the novel medicinal chemistry. All of the authors declare that they have no material conflict of interests.

Contributions

TL performed experiments, analyzed data and drafted the

manuscript; DBC performed experiments, analyzed data and revised the manuscript; KMR and DET conceived and supervised the synthetic chemistry and revised the manuscript; PJG, KA, AGSP and EJW analyzed data and revised the manuscript; CDF provided vital reagents and revised the manuscript; CP conceived and supervised the cell biology experiments, analyzed data and revised the manuscript.

Acknowledgments

This work was supported by a grant (n. 12-1263/JGATCBR) from Worldwide Cancer Research (formerly AICR) to DET, KMR and CP in 2012. This support included a PhD studentship held by DBC, which enabled all of the novel medicinal chemistry. CP, CDF and AGSP are also supported by a Bloodwise Programme Continuity Grant (18005).

References

1. Zheng C, Yin Q, Wu H. Structural studies of NF-κB signaling. Cell Res. 2011;21(1):183-195.
2. Gasparini C, Celeghini C, Monasta L, Zauli G. NF-κB pathways in hematological malignancies. Cell Mol Life Sci. 2014;71(11):2083-2102.
3. Hoffmann A, Natoli G, Ghosh G. Transcriptional regulation via the NF-kappaB signaling module. Oncogene. 2006;25(51):6706-6716.
4. Braun T, Carvalho G, Fabre C, Grosjean J, Fenaux P, Kroemer G. Targeting NF-kappaB in hematologic malignancies. Cell Death Differ. 2006;13(5):748-758.
5. Abdi J, Chen G, Chang H. Drug resistance in multiple myeloma: latest findings and new concepts on molecular mechanisms. Oncotarget. 2013;4(12):2186-2207.
6. Hewamana S, Alghazal S, Lin TT, et al. The NF-kappaB subunit Rel A is associated with in vitro survival and clinical disease progression in chronic lymphocytic leukemia and represents a promising therapeutic target. Blood. 2008;111(9):4681-4689.
7. Merchionne F, Perosa F, Dammacco F. New therapies in multiple myeloma. Clin Exp Med. 2007;7(3):83-97.
8. Byrd JC, Brown JR, O'Brien S, et al. RESONATE Investigators. Ibrutinib versus ofatumumab in previously treated chronic lymphoid leukemia. N Engl J Med. 2014;371(3):213-223.
9. Hideshima T, Ikeda H, Chauhan D, et al. Bortezomib induces canonical nuclear factor-kappaB activation in multiple myeloma cells. Blood. 2009;114(5):1046-1052.
10. Ahn IE, Underbayev C, Albitar A, et al. Clonal evolution leading to ibrutinib resistance in chronic lymphocytic leukemia. Blood. 2017;129(11):1469-1479.
11. Wang CY, Mayo MW, Baldwin AS. TNF- and cancer therapy-induced apoptosis: potentiation by inhibition of NF-kappaB. Science. 1996;274(5288):784-787.
12. Hideshima T, Chauhan D, Richardson P, et al. NF-kappa B as a therapeutic target in multiple myeloma. J Biol Chem. 2002;277(19): 16639-16647.
13. Pepper C, Hewamana S, Brennan P, Fegan C. NF-kappaB as a prognostic marker and therapeutic target in chronic lymphocytic leukemia. Future Oncol. 2009;5(7):1027-1037.
14. Antonow D, Thurston DE. Synthesis of DNA-interactive pyrrolo[2,1-c [1,4]benzodiazepines (PBDs). Chem Rev. 2011;111(4): 2815-2864.
15. Gerratana B. Biosynthesis, synthesis, and biological activities of pyrrolobenzodiazepines. Med Res Rev. 2012;32(2):254-293.
16. Rahman KM, Vassoler H, James CH, Thurston DE. DNA sequence preference and adduct orientation of pyrrolo[2,1-c][1,4]benzodiazepine antitumor agents. ACS Med Chem Lett. 2010;1(8):427-432.
17. Puzanov I, Lee W, Chen AP, et al. Phase I pharmacokinetic and pharmacodynamic study of SJG-136, a novel DNA sequence selective minor groove cross-linking agent, in advanced solid tumors. Clin Cancer Res. 2011;17(11):3794-3802.
18. Mantaj J, Jackson PJ, Rahman KM, Thurston DE. From anthramycin to pyrrolobenzodiazepine (PBD)-containing antibody-drug conjugates (ADCs). Angew Chem Int Ed Engl. 2017;56(2):462-488.
19. Kotecha M, Kluza J, Wells G, et al. Inhibition of DNA binding of the NF-Y transcription factor by the pyrrolobenzodiazepine-polyamide conjugate GWL-78. Mol Cancer Ther. 2008;7(5):1319-1328.
20. Hu WP, Tsai FY, Yu HS, Sung PJ, Chang LS, Wang JJ. Induction of apoptosis by DC-81-indole conjugate agent through NF-kappaB and JNK/AP-1 pathway. Chem Res Toxicol. 2008;21(7):1330-1336.
21. Rahman KM, Jackson PJ, James CH, et al. GC-targeted C8-linked pyrrolobenzodiazepine-biaryl conjugates with femtomolar in vitro cytotoxicity and in vivo antitumor activity in mouse models. J Med Chem. 2013;56(7):2911-2935.
22. Chou TC. Drug combination studies and their synergy quantification using the Chou-Talalay method. Cancer Res. 2010;70(2): 440-446.
23. Demchenko YN, Glebov OK, Zingone A, Keats JJ, Bergsagel PL, Kuehl WM. Classical and/or alternative NF-kappaB pathway activation in multiple myeloma. Blood. 2010;115(17):3541-3552.
24. Keats JJ, Fonseca R, Chesi M, et al. Promiscuous mutations activate the noncanonical NF-kappaB pathway in multiple myeloma. Cancer Cell. 2007;12(2):131-144.
25. Zhang B, Kirov S, Snoddy J.WebGestalt: an integrated system for exploring gene sets in various biological contexts. Nucleic Acids Res. 2005;33(Web Server issue):W741-48.
26. Hertlein E, Byrd JC. Signalling to drug resistance in CLL. Best Pract Res Clin Haematol. 2010;23(1):121-131.
27. Markovina S, Callander NS, O'Connor SL, et al. Bortezomib-resistant nuclear factor-kappaB activity in multiple myeloma cells. Mol Cancer Res. 2008;6(8):1356-1364.
28. Diop F, Moia R, Favini C, et al. Biological and clinical implications of BIRC3 mutations in chronic lymphocytic leukemia. Haematologica. 2020;105(2):448-456.
29. Benedetti D, Tissino E, Pozzo F, et al. NOTCH1 mutations are associated with high CD49d expression in chronic lymphocytic leukemia: link between the NOTCH1 and the NF-κB pathways. Leukemia. 2018;32(3):654-662.
30. Asslaber D, Wacht N, Leisch M, Qi Y, et al. BIRC3 expression predicts CLL progression and defines treatment sensitivity via enhanced NF-κB nuclear translocation. Clin Cancer Res. 2019;25(6):1901-1912
31. Del Poeta G, Dal Bo M, Del Principe MI, et al. Clinical significance of c.7544-7545 del CT NOTCH1 mutation in chronic lymphocytic leukaemia. Br J Haematol. 2013; 160(3):415-418.
32. Rossi D, Rasi S, Fabbri G, et al. Mutations of NOTCH1 are an independent predictor of survival in chronic lymphocytic leukemia. Blood. 2012;119(2):521.
33. Hoffmann A, Levchenko A, Scott ML, Baltimore D. The IkappaB-NF-kappaB signaling module: temporal control and selective gene activation. Science. 2002;298 (5596):1241-1245.
34. Natoli G, Chiocca S. Nuclear ubiquitin ligases, NF-kappaB degradation, and the control of inflammation. Sci Signal. 2008;1(1):pe1.
35. Godwin P, Baird AM, Heavey S, Barr MP, O'Byrne KJ, Gately K. Targeting nuclear factor-kappa B to overcome resistance to chemotherapy. Front Oncol. 2013;3:120.
36. Baumann P, Mandl-Weber S, Oduncu F, Schmidmaier R. Alkylating agents induce activation of NFkappaB in multiple myeloma cells. Leuk Res. 2008;32(7):1144-1147.
37. San Miguel JF, Schlag R, Khuageva NK, et al. Bortezomib plus melphalan and prednisone for initial treatment of multiple myeloma. N Engl J Med. 2008;359(9):906-917.
38. Murray MY, Auger MJ, Bowles KM. Overcoming bortezomib resistance in 548 multiple myeloma. Biochem Soc Trans. 2014;42(4):804-808.
39. Woyach JA, Bojnik E, Ruppert AS, et al. Bruton's tyrosine kinase (BTK) function is important to the development and expansion of chronic lymphocytic leukemia (CLL). Blood. 2014;123(8):1207-1213.
40. Byrd JC, Furman RR, Coutre SE, et al. Targeting BTK with ibrutinib in relapsed chronic lymphocytic leukemia. N Engl J Med. 2013;369(1):32-42.
41. Herman SE, Mustafa RZ, Gyamfi JA, et al. Ibrutinib inhibits BCR and NF-κB signaling and reduces tumor proliferation in tissue-resident cells of patients with CLL. Blood. 2014;123(21):3286-3295.
42. Jayappa KD, Portell CA, Gordon VL, et al. Microenvironmental agonists generate de novo phenotypic resistance to combined ibrutinib plus venetoclax in CLL and MCL. Blood Adv. 2017;1(14):933-946.
43. Fabre C, Mimura N, Bobb K, et al. Dual inhibition of canonical and noncanonical NF-κB pathways demonstrates significant antitumor activities in multiple myeloma. Clin Cancer Res. 2012;18(17):4669-4681.

Ferrata Storti Foundation

Combining ibrutinib and checkpoint blockade improves CD8+ T-cell function and control of chronic lymphocytic leukemia in Eμ-TCL1 mice

Bola S. Hanna,[1] Haniyeh Yazdanparast,[1] Yasmin Demerdash,[1] Philipp M. Roessner,[1] Ralph Schulz,[1] Peter Lichter,[1] Stephan Stilgenbauer[2] and Martina Seiffert[1]

[1]Molecular Genetics, German Cancer Research Center (DKFZ), Heidelberg and [2]Internal Medicine III, University of Ulm, Ulm, Germany

Haematologica 2021
Volume 106(4):968-977

ABSTRACT

Ibrutinib is a Bruton's tyrosine kinase (BTK) inhibitor approved for the treatment of multiple B-cell malignancies, including chronic lymphocytic leukemia (CLL). In addition to blocking B-cell receptor signaling and chemokine receptor-mediated pathways in CLL cells, that are known drivers of disease, ibrutinib also affects the microenvironment in CLL via targeting BTK in myeloid cells and IL-2–inducible T-cell kinase (ITK) in T cells. These non-BTK effects were suggested to contribute to the success of ibrutinib in CLL. By using the Eμ-TCL1 adoptive transfer mouse model of CLL, we observed that ibrutinib effectively controls leukemia development, but also results in significantly lower numbers of CD8+ effector T cells, with lower expression of activation markers, as well as impaired proliferation and effector function. Using CD8+ T cells from a T-cell receptor (TCR) reporter mouse, we verified that this is due to a direct effect of ibrutinib on TCR activity, and demonstrate that co-stimulation via CD28 overcomes these effects. Most interestingly, combination of ibrutinib with blocking antibodies targeting PD-1/PD-L1 axis *in vivo* improved CD8+ T-cell effector function and control of CLL. In summary, these data emphasize the strong immunomodulatory effects of ibrutinib and the therapeutic potential of its combination with immune checkpoint blockade in CLL.

Correspondence:

MARTINA SEIFFERT
m.seiffert@dkfz.de

BOLA S. HANNA
b.hanna@dkfz.de

Received: September 11, 2019.

Accepted: March 3, 2020.

Pre-published: March 5, 2020.

https://doi.org/10.3324/haematol.2019.238154

©2021 Ferrata Storti Foundation

Material published in Haematologica is covered by copyright. All rights are reserved to the Ferrata Storti Foundation. Use of published material is allowed under the following terms and conditions: https://creativecommons.org/licenses/by-nc/4.0/legalcode. Copies of published material are allowed for personal or internal use. Sharing published material for non-commercial purposes is subject to the following conditions: https://creativecommons.org/licenses/by-nc/4.0/legalcode, sect. 3. Reproducing and sharing published material for commercial purposes is not allowed without permission in writing from the publisher.

Introduction

Within the last decade, a new era of therapeutic opportunities for patients with chronic lymphocytic leukemia (CLL) has begun.[1] Treatment responses, also in patients with relapsed and refractory disease or unfavorable genetic profile, have dramatically improved with the development and approval of kinase inhibitors that target B-cell receptor (BCR) signaling, a well-known driver of disease.[2,3] Ibrutinib is an orally bioavailable, irreversible inhibitor of Bruton's tyrosine kinase (BTK). Both *in vitro* and in patients, ibrutinib has been shown to potently inhibit BCR signaling, prevent lymphocyte adhesion and homing, and inhibit protective effects of the microenvironment, which yields high response rates and durable remissions in patients with CLL if applied continuously.[4,5]

In addition to pro-survival pathways in malignant cells, like BCR signaling, T cells represent an attractive therapeutic target in CLL. In patients and mouse models of CLL, T cells expand along with the disease course.[6,7] Our recent work has demonstrated a non-redundant role of CD8+ T cells in suppressing CLL progression in an IFNγ-dependent manner.[8] Yet chronic exposure to tumor-derived antigens in secondary lymphoid organs leads to their continuous activation, upregulation of inhibitory receptors, such as PD-1, and ultimately exhaustion.[8] Therefore, targeting inhibitory receptors, such as PD-1 and Lag3, offered novel opportunities of therapeutic reactivation of adaptive anti-tumor immunity by immune checkpoint blockade.[9,10] Notably, immune checkpoint blockade showed promising activity in a subgroup of CLL patients with Richter's transformation, suggesting that unleashing inhibited T cells results in better control of leukemia progression.[11] Besides its direct cytotoxic activity against malignant B cells, ibrutinib also exerts immunomodulatory effects (reviewed by Maharaj *et al.*).[12] Ibrutinib-mediated inhibition of STAT3 results in decreased expression of immunosuppressive molecules, such as PD-L1 and IL-10, by

CLL cells.[13] Gunderson *et al*. have demonstrated that BTK inhibition in tumor-associated myeloid cells reprograms them towards M1-like immunostimulatory phenotypes resulting in enhanced anti-tumoral T-cell activity.[14] In addition to modulating BTK-expressing cells in the microenvironment, ibrutinib has been shown to impact natural killer (NK)- and T-cell activity due to its non-BTK effects on IL-2-inducible T-cell kinase (ITK).[15,16] In a preclinical study, ITK inhibition by ibrutinib was shown to impair Fc receptor-mediated NK-cell functions and to antagonize cytotoxicity of rituximab.[16] However, NK-cell-mediated cellular cytotoxicity was significantly recovered 12 hours (h) after ibrutinib has been removed, which may be attributed to turnover of ITK.[17] Inhibition of ITK by ibrutinib was further shown to modulate TCR signaling in $CD4^+$ T cells and enhance Th1 response *in vitro*.[15] In addition, a reduced number or percentage of regulatory T cells in peripheral blood of ibrutinib-treated patients was reported.[18,19] Interestingly, ibrutinib was recently approved for the treatment of refractory chronic graft-*versus*-host-disease (cGvHD) after allogeneic hematopoietic stem cell transplantation, indicating its potent immunomodulatory effect *in vivo*.[20]

The strong immunomodulatory activity of ibrutinib encouraged several pre-clinical and clinical studies assessing its potential combination with other immunotherapeutic drugs, primarily immune checkpoint blockade.[21] The success of these immunotherapeutic approaches relies on enhancing the functional capacities and proliferation of anti-tumoral $CD8^+$ T cells. Despite a large body of evidence highlighting the immunomodulatory activity of ibrutinib, its exact impact on $CD8^+$ T cells in CLL remains less defined. While Long *et al*. observed an increase in $CD4^+$ and $CD8^+$ T-cell numbers in ibrutinib-treated patients,[19] a drop in T-cell numbers, activation, and proliferation was reported in another patient cohort.[22] Moreover, it was suggested that ibrutinib can enhance anti-tumoral $CD8^+$ T-cell function in CLL patients by fostering a switch of T-helper-cell polarization towards anti-tumoral Th1 cells.[15] However, this change in Th1 polarization could not be confirmed in a cohort of ibrutinib-treated patients.[19] Thus, in this study, we utilized the Eμ-TCL1 adoptive transfer (TCL1 AT) model of CLL to monitor $CD8^+$ T-cell differentiation and function under ibrutinib treatment. Through this, we observed that this drug reduces the functionality of $CD8^+$ T cells which could be overcome by combining ibrutinib with immune checkpoint blockade in the TCL1 AT model. The relevance of these findings for therapeutic applications has to be proven in ongoing clinical trials combining ibrutinib with anti(α)PD-L1 antibody durvalumab for treatment of B-cell lymphoma and CLL patients. (*Trial registered at clinicaltrials.gov identifiers: NCT02401048 and NCT02733042*).

Methods

Mouse models

Eμ-TCL1 (TCL1) mice on C57BL/6 background were kindly provided by Dr. Carlo Croce (Ohio State University, OH, USA).[23] C57BL/6 wild-type (WT) mice were purchased from Charles River Laboratories (Sulzfeld, Germany), and Nr4a1GFP mice[24] were kindly provided by Dr. Markus Feuerer (DKFZ, Heidelberg, Germany).

TCL1 tumor cells of C57BL/6N background were propagated once by adoptive transfer in C57BL/6N mice to ensure having enough tumor cells from the same donor for all treatment arms. Adoptive transfer of TCL1 tumors was performed as previously described.[9,25] Briefly, $1\text{-}2x10^7$ leukemic TCL1 splenocytes ($CD5^+CD19^+$ content of purified cells was typically above 90%) were transplanted by intraperitoneal (i.p.) injection into 2-3-month-old C57BL/6N WT females. All animal experiments were carried out according to governmental and institutional guidelines and approved by the local authorities (Regierungspräsidium Karlsruhe, permit numbers: G-36/14, G-123/14, G-16/15, and G-53/15).

In vivo treatment

Two to three weeks after tumor cell transplantation, tumor load in blood (defined as the number of $CD5^+CD19^+$ CLL cells/μL) was measured, and mice were assigned to different treatment arms to achieve comparable tumor load in all groups at baseline prior to treatment. Ibrutinib (provided by Pharmacyclics LLC, an AbbVie Company) was administered in drinking water containing sterile control vehicle (1% HP-β-CD) at a concentration of 0.16 mg/mL, as previously described.[26] For PD-1/PD-L1 blockade, mice were injected i.p. with 0.2 mg of αPD-1 (clone: RMP1-14), αPD-L1 (clone: 10F.9G2), or rat IgG2a isotype control antibody (clone: 2A3; all from BioXcell, West Lebanon, NH, USA) every 3 days for 4 weeks.

Flow cytometry and functional assays

Single cell suspensions from peripheral blood (PB) or lymphoid tissues were prepared and flow cytometric analyses of cell surface proteins and transcription factors were performed as detailed in the *Online Supplementary Appendix* and described before.[8,27] Gating strategies are depicted in the *Online Supplementary Appendix* and antibodies are listed in *Online Supplementary Table S1*.

Cytokine release, granzyme B production and degranulation capacity of $CD8^+$ T cells were assayed as previously described with minor modifications, as outlined in the *Online Supplementary Appendix*.[9]

Human PB mononuclear cells (PBMC) or mouse splenocytes were pre-treated for 30 minutes (min) with ibrutinib, CC-292 or ACP-196 (Selleckchem, Munich, Germany), then stimulated with 1 μg/mL αCD3 antibodies (clone HIT3a or 145-2C11, respectively) in 96-well round-bottom microtiter plates at a density of $2x10^6$/mL and incubated at 37°C and 5% CO_2 until analyzed by flow cytometry. For assessment of proliferation, cells were stained with 5 μM carboxyfluoresceinsuccinimidyl ester (CFSE; eBioscience) prior to drug treatment and stimulation as previously described.[28]

Statistical analysis

Sample size was determined based on expected variance of read-out. No samples or animals were excluded from the analyses. No randomization or blinding was used in animal studies. Data were analyzed using Prism 5.04 GraphPad software. Statistical tests of data were one-way ANOVA followed by multiple comparison test or unpaired Student *t*-test with Welch approximation to account for unequal variances. When appropriate, paired Student *t*-test was used. $P<0.05$ was considered to be statistically significant. All graphs show means±standard error of mean, unless otherwise indicated.

Results

Ibrutinib modulates effector $CD8^+$ T-cell differentiation and proliferation in the TCL1 adoptive transfer model

To investigate effects of ibrutinib on $CD8^+$ T cells *in vivo*,

we utilized the TCL1 AT model of CLL.[9,25] We transplanted C57BL/6 WT mice with TCL1 splenocytes, and after 2 weeks mice were assigned to treatment with ibrutinib or vehicle according to tumor load in PB. In line with published data,[29] ibrutinib treatment resulted in a significant decrease in CLL development in comparison to vehicle-treated mice, as evident by a decrease in $CD5^+CD19^+$ cell counts in PB and decreased splenomegaly and hepatomegaly (Figure 1A and B). Moreover, CLL cell proliferation was significantly reduced, as measured by Ki-67 staining (Figure 1C), confirming efficient cytotoxic activity of the drug.

We then evaluated the effect of ibrutinib on anti-tumoral $CD8^+$ T cells. We have recently shown that CLL development in TCL1 mice induces the differentiation of an anti-tumoral, oligoclonal effector $CD8^+$ T-cell population that controls tumor development in an IFNγ-dependent manner.[8] Accordingly, we analyzed the splenic $CD8^+$ T-cell composition using CD44 and CD127, which divide $CD8^+$ T cells into $CD127^{hi}CD44^{low}$ naïve, $CD127^{hi}CD44^{hi}$ memory, and $CD127^{low}CD44^{int\text{-}hi}$ effector subsets (Figure 1D). As expected, CLL development induced a sizable expansion of $CD127^{low}CD44^+$ effector T cells in vehicle-

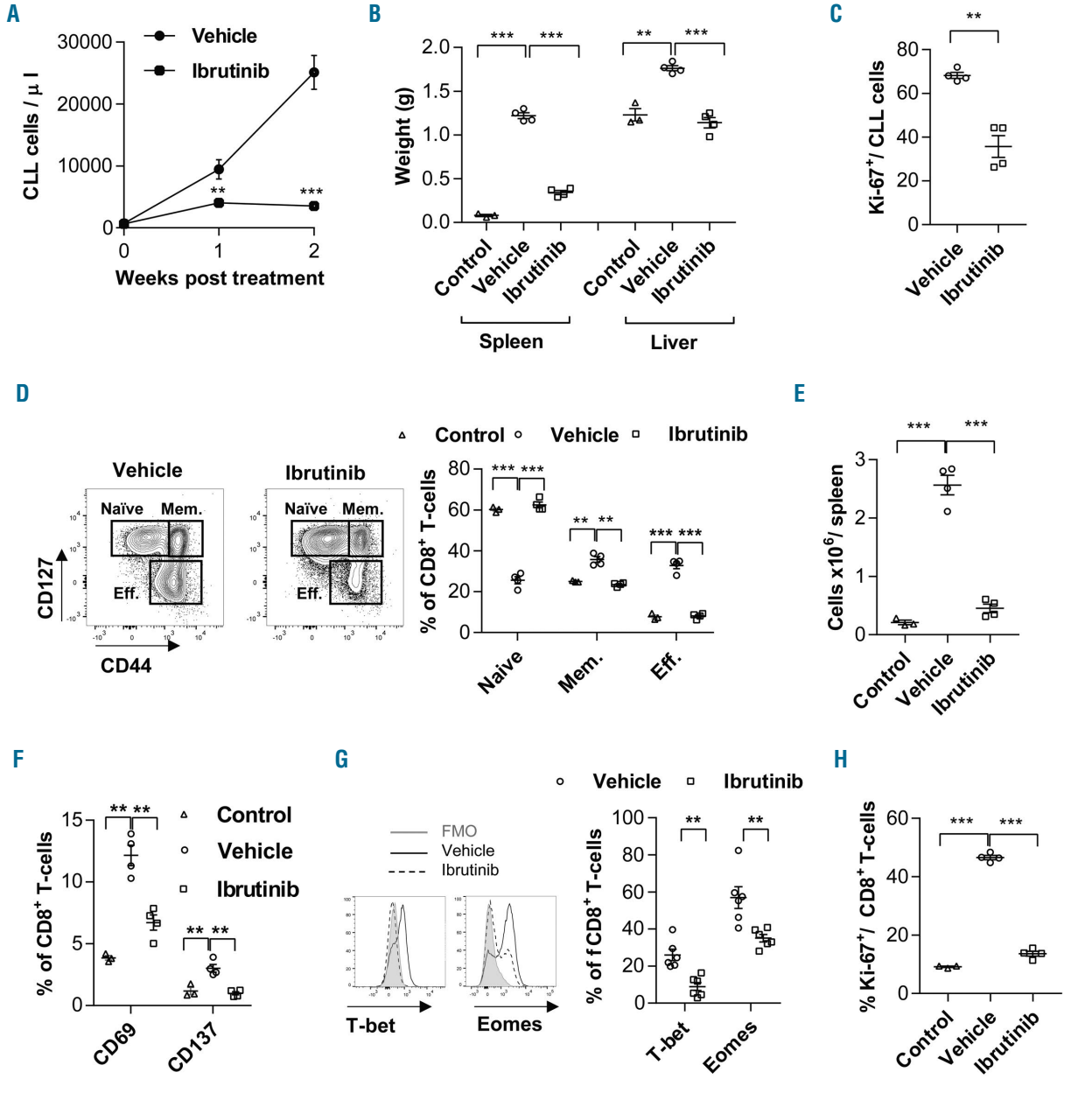


Figure 1. Ibrutinib modulates effector $CD8^+$ T-cell differentiation and proliferation in the TCL1 adoptive transfer model. C57BL/6 mice were transplanted with splenocytes from leukemic TCL1 mice, and after 2 weeks assigned to treatment with ibrutinib (0.16 mg/mL) or vehicle control in drinking water. Mice were sacrificed after 2 weeks of treatment. Untransplanted C57BL/6 mice (n=3) were used as controls. (A) Absolute numbers of $CD5^+CD19^+$ chronic lymphocytic leukemia (CLL) cells in peripheral blood analyzed by flow cytometry, and (B) spleen and liver weight of vehicle- or ibrutinib-treated mice (n=4). (C) Flow cytometric analysis of Ki-67 expression in $CD5^+CD19^+$ CLL cells in spleen from vehicle- or ibrutinib-treated mice (n=4). (D) Flow cytometric analysis of splenic $CD3^+CD8^+$ T cells from vehicle- or ibrutinib-treated mice (n=4). Cell subsets were defined as naïve ($CD127^{hi}CD44^{low}$), memory (Mem: $CD127^{hi}CD44^{hi}$), and effector (Eff: $CD127^{low}CD44^{int\text{-}hi}$) cells. (E) Absolute numbers of splenic $CD8^+$ Eff cells from control, vehicle- or ibrutinib-treated mice (n=4). (F) Flow cytometric analysis of CD69 and CD137, (G) T-bet and Eomes (FMO: fluorescence minus 1), and (H) Ki-67 expression on $CD8^+$ T cells from control, vehicle- or ibrutinib-treated mice (n=4). Results are representative of at least two independent experiments. Graphs show means±standard error of mean. $^{**}P<0.01$, $^{***}P<0.001$.

treated mice in comparison to untransplanted WT controls (Figure 1D and E). Interestingly, the percentage and absolute numbers of the effector population were lower in ibrutinib-treated mice (Figure 1D and E). This was accompanied by decreased expression of activation markers like CD69 and CD137 on CD8$^+$ T cells (Figure 1F), and decreased expression of transcription factors that regulate effector T-cell differentiation, such as T-box transcription factor T-bet and Eomesodermin (Eomes) (Figure 1G).[30] Furthermore, CD8$^+$ T-cell proliferation was significantly lower in ibrutinib- compared to vehicle-treated TCL1 mice, reaching levels similar to non-tumor control mice (Figure 1H). The drop in the effector population, activation markers and proliferation of CD8$^+$ T cells was also observed when treatment started at later stages of disease when all mice had more than 5,000 CLL cells/μL of blood, the leukemic threshold in CLL patients (*Online Supplementary Figure S1A*).

We next examined whether the observed changes in CD8$^+$ T cells are caused by a direct impact of ibrutinib on these cells or rather reflect a secondary normalization of the T-cell compartment due to the decrease in tumor load. Thus, we analyzed CD8$^+$ T cells in vehicle- and ibrutinib-treated mice having a similar disease load, as measured by CLL-cell infiltration in spleen and liver. While the vehicle-treated mice showed signs of overt leukemia with severe hepato-splenomegaly after 3 weeks of starting the treatment, ibrutinib successfully suppressed CLL development during that time. Nonetheless, mice continuously receiving ibrutinib succumbed to full-blown leukemia at week 4 post treatment exhibiting similar disease load to vehicle group at week 3 (*Online Supplementary Figure S1B*). Analysis of the spleen CD8$^+$ T-cell compartment of end-stage vehicle or ibrutinib-treated mice with comparable tumor load revealed a decrease in effector T-cell percentage and numbers, accompanied by a significant drop in activation marker expression and proliferation in the latter group (*Online Supplementary Figure S1C-E*). This suggests that the observed differences in CD8$^+$ T cells in ibrutinib-*versus* vehicle-treated mice were not secondary to changes in tumor load.

Ibrutinib modulates CD8$^+$ T-cell function in the TCL1 adoptive transfer model

We next examined the impact of ibrutinib treatment on the expression of inhibitory receptors like PD-1, CD244 and Lag3 on CD8$^+$ T cells. We observed a substantial drop in the expression of these markers in the ibrutinib cohort

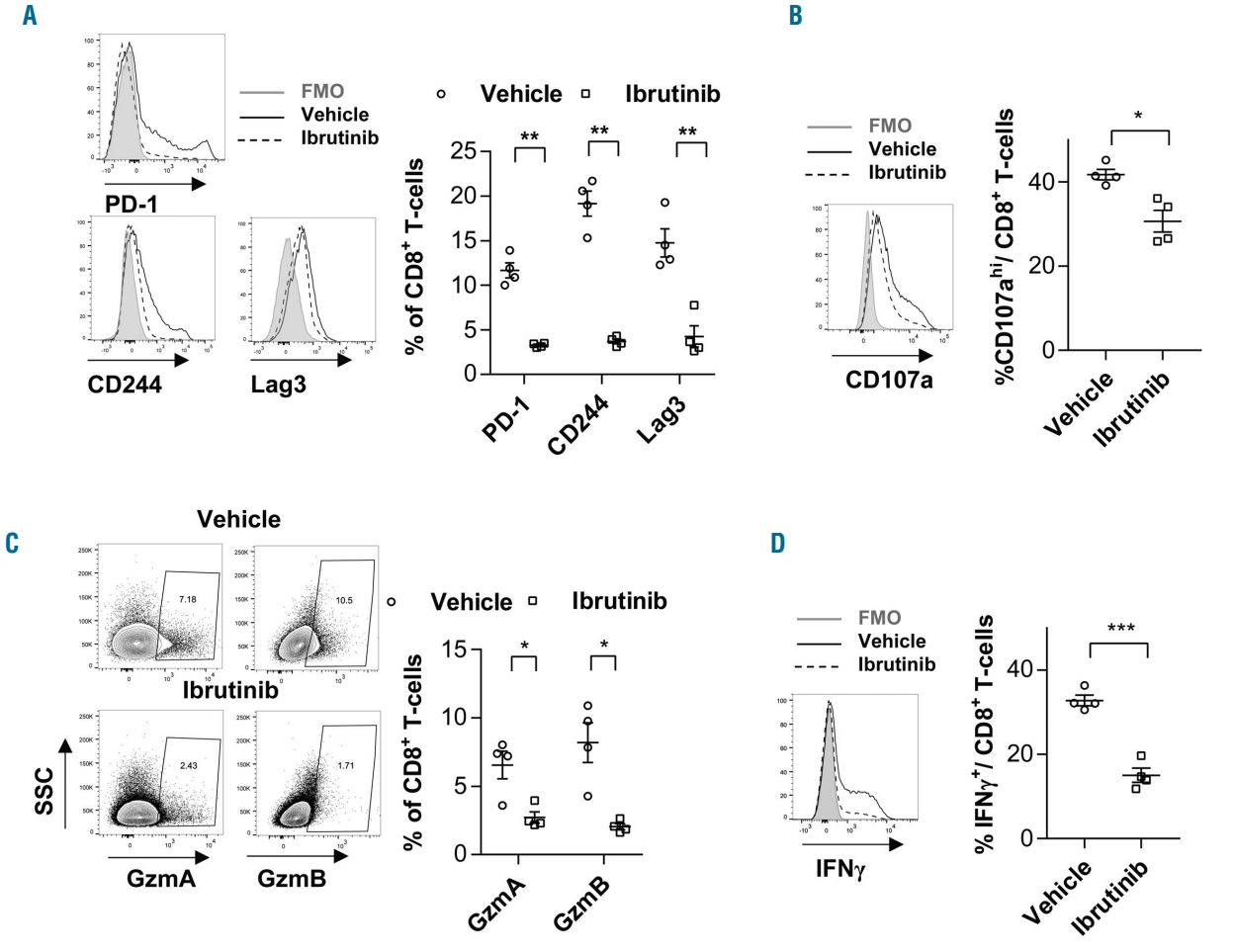


Figure 2. Ibrutinib modulates CD8$^+$ T-cell function in the TCL1 adoptive transfer model. C57BL/6 mice were transplanted with splenocytes from leukemic TCL1 mice, and after 2 weeks assigned to treatment with ibrutinib (0.16 mg/mL) or vehicle control in drinking water. Mice were sacrificed after 2 weeks of treatment. (A) Flow cytometric analysis of PD-1, CD244, and Lag3 expression on CD8$^+$ T cells from vehicle- or ibrutinib-treated mice (n=4). (B-D) Cytotoxic function of CD8$^+$ T cells was assessed by flow cytometric analysis of (B) degranulation capacity, as measured by CD107a expression on the cell surface, (C) GzmA and GzmB expression or (D) IFNγ production (n=4). Graphs show means±standard error of mean. *P<0.05, **P<0.01, ***P<0.001. nMFI: normalized median fluorescence intensity.

(Figure 2A). As T-cell inhibitory receptors are mainly induced upon activation of tumor-reactive T cells,[31] we evaluated whether the drop in their expression reflects an improvement in T-cell function or is rather a consequence of the drop in T-cell activation in ibrutinib-treated mice (Figure 1F). Thus, we analyzed the functional capacities of CD8$^+$ T cells using intracellular flow cytometric staining following mitogen PMA/ionomycin stimulation. CD8$^+$ T cells from ibrutinib-treated mice exhibited lower degranulation potential, as measured by CD107a presentation on the cell surface (Figure 2B). Furthermore, granzyme A (GzmA) and GzmB expression in CD8$^+$ T cells significantly dropped in these mice (Figure 2C). Moreover, production of IFNγ was significantly lower in CD8$^+$ T cells from ibrutinib-treated mice (Figure 2D), collectively indicating poor cytotoxic and effector function of these cells. The changes in cytokine production and cytolytic abilities were primarily attributed to the decrease in the effector CD8$^+$ fraction after ibrutinib treatment. Nonetheless, degranulation capacity, GzmA and GzmB levels were also decreased when focusing the analysis on the minor effector or PD-1$^+$ population in ibrutinib-treated mice (*Online Supplementary Figure S2A-F*). In summary, these data indicate that *in vivo* ibrutinib treatment alters activation, effector differentiation and function of CD8$^+$ T cells in the TCL1 AT model.

Ibrutinib modulates T-cell receptor signaling in CD8$^+$ T cells *in vitro*

We then investigated the mechanisms that control the above-mentioned changes in T-cell function. While ibrutinib can indirectly impact T cells through BTK inhibition in CLL cells or other antigen-presenting cells in the microenvironment, the drug can potentially affect T-cell function in a direct manner through its off-target effects on ITK. To examine these possibilities, we tested the effect of different BTK inhibitors on TCR signaling using a reporter mouse line for *Nr4a1*, an immediate target of TCR activation.[24] Splenocytes from *Nr4a1*-GFP mice were pre-treated with ibrutinib or dimethyl sulfoxide (DMSO) as control and then stimulated with αCD3 for 6 hours (h). We primarily used ibrutinib in a dose range of 100-1,000 nM, which results in ITK occupancy of up to 50% corresponding to the level observed *in vivo* in ibrutinib-treated CLL patients.[15] αCD3 stimulation resulted in a rapid increase of the *Nr4a1*-GFP signal in CD8$^+$ T cells in DMSO controls (Figure 3A). Interestingly, ibrutinib treatment resulted in a

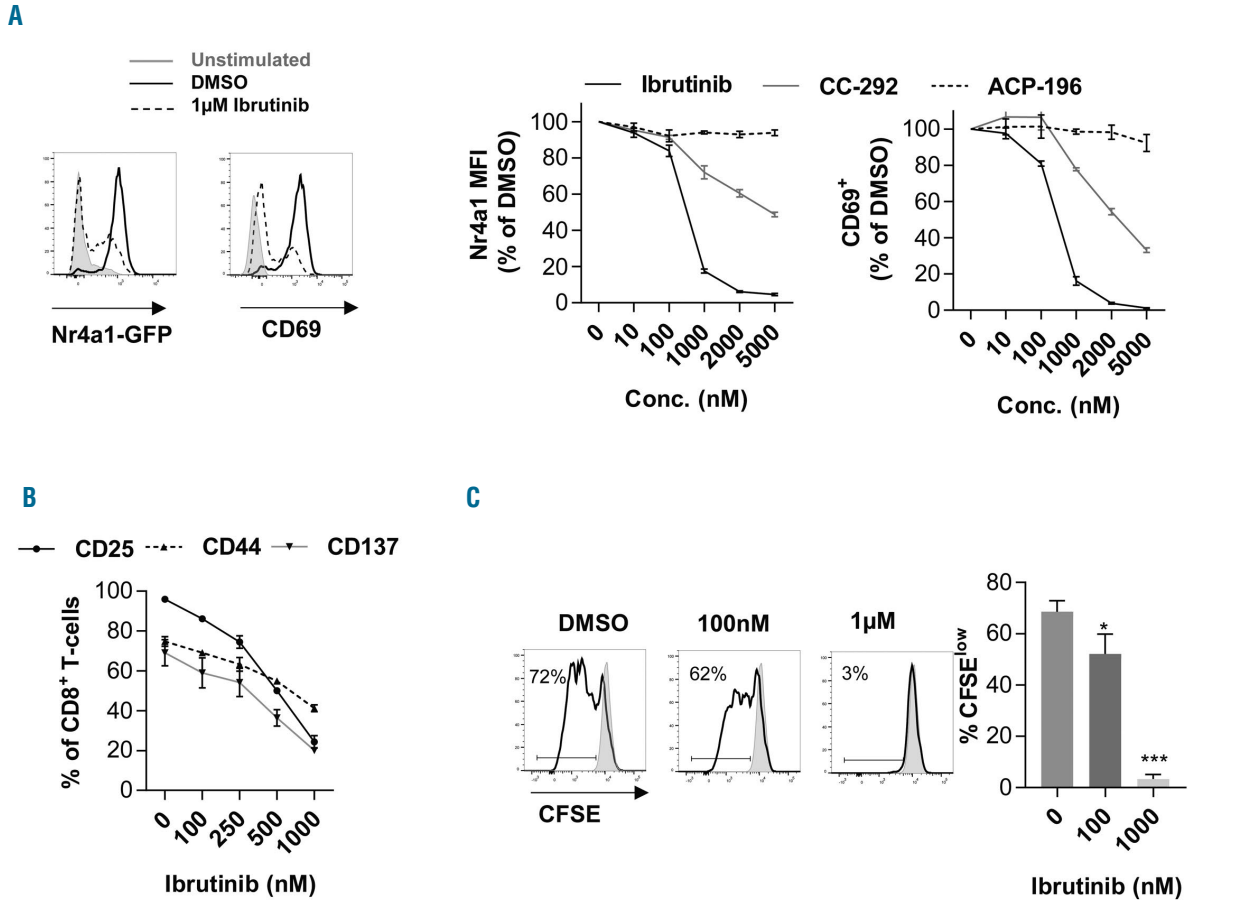


Figure 3. Ibrutinib modulates T-cell receptor signaling in CD8$^+$ T cells *in vitro*. (A) Splenocytes from *Nr4a1*-GFP transgenic mice (n=3) were pretreated with different concentrations of ibrutinib, ACP-196, CC-292 or DMSO for 30 minutes (min), and then stimulated with αCD3 antibody for 6 hours (h). *Nr4a1*-GFP (left panels) and CD69 (right panels) expression was analyzed by flow cytometry in viable, 7-aminoactinomycin D (7-AAD)-negative, single CD8$^+$ T cells. (Right) Relative percentages of *Nr4a1*-GFP- or CD69-positive cells. FMO: fluorescence minus 1. (B) Splenocytes from C57BL/6 mice (n=3) were pretreated with different concentrations of ibrutinib or DMSO for 30 min and then stimulated with αCD3 antibody. CD25, CD44 and CD137 expression was analyzed by flow cytometry in viable, 7-AAD-negative, single CD8$^+$ T cells after 24 h. (C) Peripheral blood mononuclear cells (PBMC) from healthy donors (n=5) were labeled with 5 μM carboxyfluorescein succinimidyl ester (CFSE), pretreated with different concentrations of ibrutinib or DMSO for 30 min and then stimulated with αCD3 antibody. Proliferation as measured by CFSE dilution after 72 h was analyzed by flow cytometry in viable, 7-AAD-negative, single CD8$^+$ T cells. Graphs show means±standard error of mean. **P*<0.05, ***P*<0.01, ****P*<0.001; MFI: median fluorescence intensity.

15% decrease in the *Nr4a1*-GFP MFI at 100 nM and abrogation of *Nr4a1*-GFP induction in most of the cells at a concentration of 1 μM (Figure 3A). Similarly, the induction of early activation marker CD69 was significantly reduced at a concentration of 100 nM or higher (Figure 3A). We compared these effects to the more specific BTK inhibitors, CC-292 and ACP-196, which have ITK IC_{50} values of 24 and 1,000 nM, respectively, compared to that of 4.9 nM of ibrutinib.[32] Interestingly, we observed that the decrease in *Nr4a1*-GFP and CD69 signals was less pronounced in CC-292 and was entirely absent upon ACP-196 treatment (Figure 3A), indicating that these effects are BTK-independent. In line with these results, ibrutinib, but not ACP-196 treatment of mouse splenocytes, inhibited the expression of other activation markers like CD25, CD44 and CD137 on $CD8^+$ T cells in response to αCD3 stimulation (Figure 3B and *Online Supplementary Figure S3A-C)*. In addition, CFSE dilution assays showed that ibrutinib, but not ACP-196, inhibited $CD8^+$ T-cell proliferation (*Online Supplementary Figure S3D*). Similar to murine splenocytes, treatment of human PMBC with ibrutinib resulted in a dose-dependent decrease in proliferation of $CD8^+$ T cells in response to αCD3 stimulation (Figure 3C). Collectively, these data suggest that ibrutinib can modulate $CD8^+$ T-cell response to TCR stimulation in a BTK-independent manner.

Strong co-stimulatory signals can rescue $CD8^+$ T cells from inhibitory effects of ibrutinib *in vitro*

We next evaluated potential approaches to unleash $CD8^+$ T cells from ibrutinib's inhibitory effects. Previous work has shown that CD28 signaling is intact in the absence of ITK.[33] Thus, we hypothesized that strong CD28 co-stimulation can hijack ibrutinib inhibitory effects on $CD8^+$ T cells. Therefore, we evaluated the effect of the drug on murine $CD8^+$ T cells stimulated with αCD3 alone or αCD3 plus αCD28. The addition of αCD28 antibody had no impact on the drop of *Nr4a1*-GFP signal after ibrutinib treatment (Figure 4A), which is in line with previous work demonstrating that *Nr4a1* induction by TCR

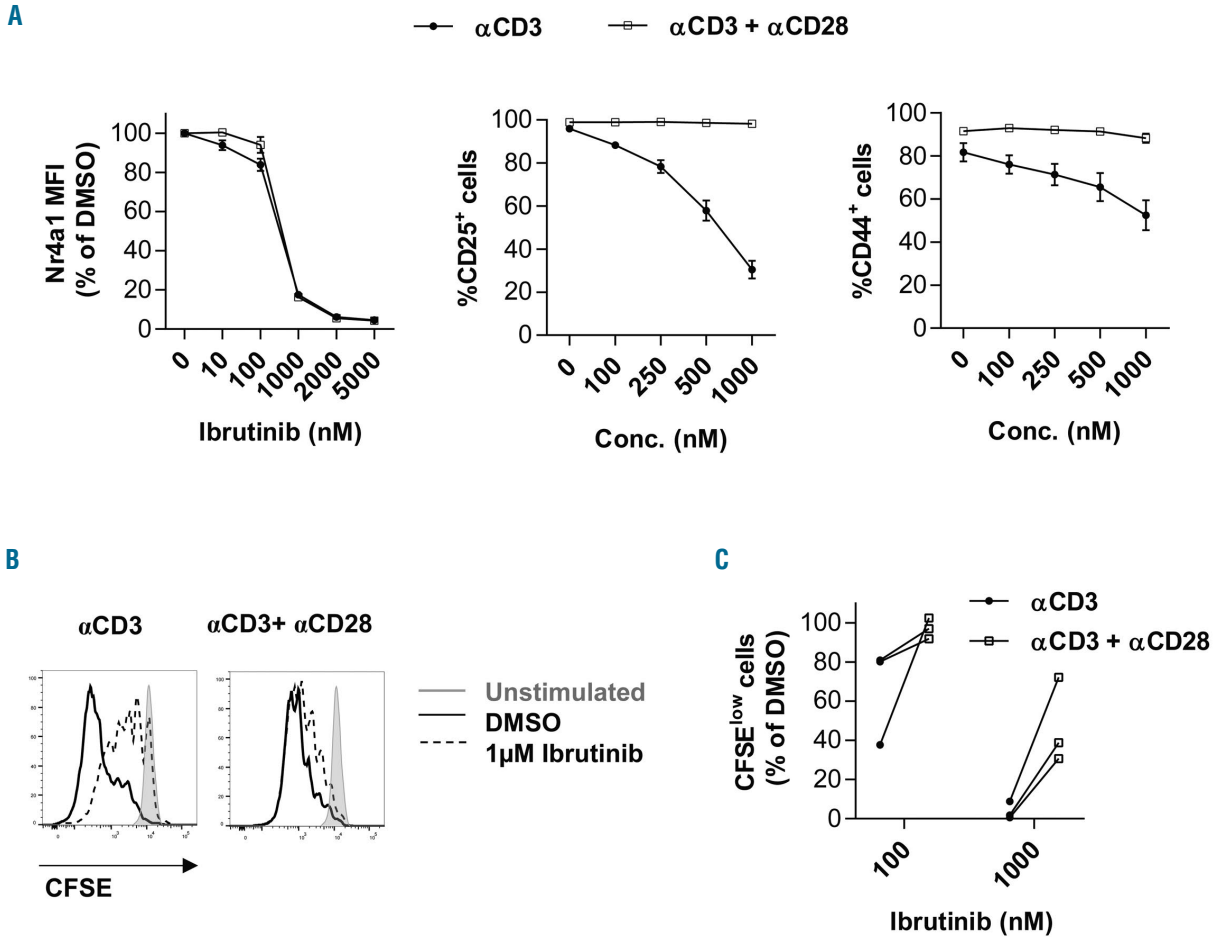


Figure 4. Strong co-stimulatory signals can rescue $CD8^+$ T cells from inhibitory effects of ibrutinib *in vitro*. (A) (Left) Splenocytes from *Nr4a1*-GFP transgenic mice (n=3) were pretreated with different concentrations (Conc.) of ibrutinib or dimethyl sulfoxide (DMSO) for 30 minutes (min), and then stimulated with either αCD3 or αCD3 plus αCD28 antibodies for 6 hours (h). *Nr4a1*-GFP, expression was analyzed by flow cytometry in viable, 7-aminoactinomycin D (7-AAD)-negative, single $CD8^+$ T cells. (Middle and right panels) Splenocytes from C57BL/6 mice (n=4) were pretreated with different concentrations of ibrutinib or DMSO for 30 min and then stimulated with either αCD3 or αCD3 plus αCD28 antibodies. CD25, and CD44 expression were analyzed by flow cytometry in $CD8^+$ T cells after 24 h. (B) Splenocytes from C57BL/6 mice (n=4) were labeled with carboxyfluorescein succinimidyl ester (CFSE), pretreated with different concentrations of ibrutinib or DMSO for 30 min and then stimulated with αCD3 or αCD3 plus αCD28 antibodies. Proliferation as measured by CFSE dilution after 48 h was analyzed by flow cytometry in viable, 7-AAD-negative, single $CD8^+$ T cells. (C) Peripheral blood mononuclear cells (PBMC) from healthy donors (n=3) were labeled with CFSE, pretreated with different concentrations of ibrutinib or DMSO for 30 min and then stimulated with αCD3 or αCD3 plus αCD28 antibodies. Proliferation as measured by CFSE dilution after 72 h was analyzed by flow cytometry in viable, 7-AAD-negative, single $CD8^+$ T cells. Graphs show means±standard error of mean. MFI: median fluorescence intensity.

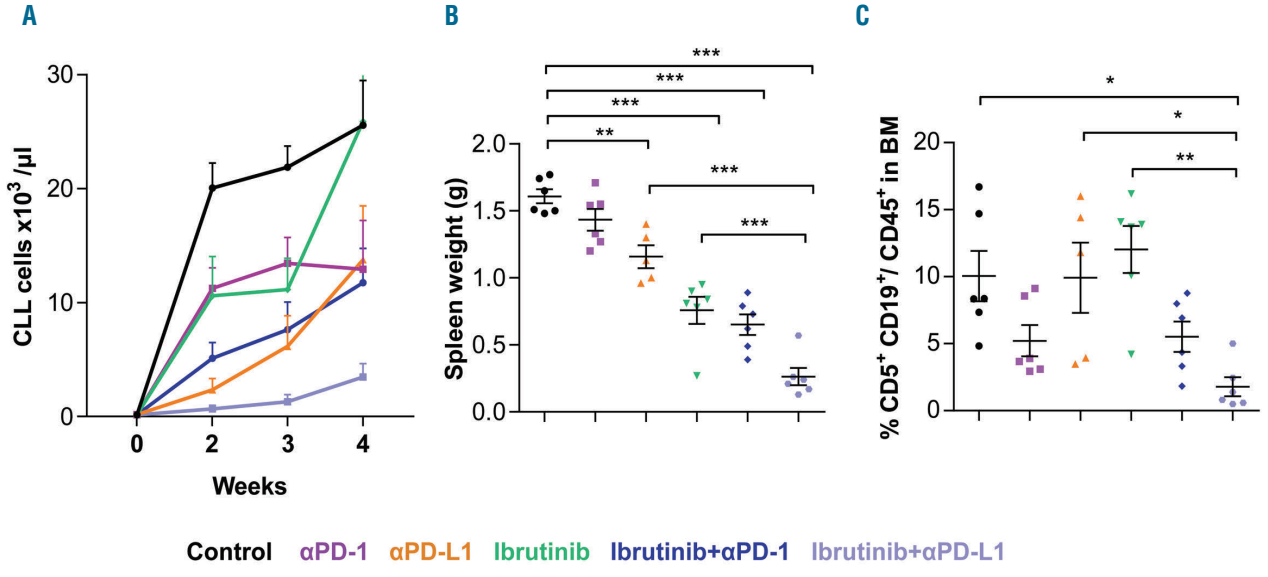


Figure 5. Blocking PD-1/PD-L1 axis enhances the anti-leukemic activity of ibrutinib. C57BL/6 mice were transplanted with splenocytes from leukemic TCL1 mice, and after 2 weeks assigned to treatment with isotype antibody plus vehicle (control), αPD-1, αPD-L1, ibrutinib, αPD-1 + ibrutinib, or αPD-L1 + ibrutinib. Mice were sacrificed after 4 weeks of treatment (n=6). (A) Absolute numbers of $CD5^+CD19^+$ chronic lymphocytic leukemia (CLL) cells in peripheral blood over time analyzed by flow cytometry, and (B) spleen weight of different treatment arms at the end-point (n=6). (C) Tumor load, defined as percentage of $CD5^+CD19^+$ CLL cells out of $CD45^+$ cells in bone marrow (BM) (n=4-6). Graphs show means±standard error of mean. **P*<0.05, ***P*<0.01, ****P*<0.001.

stimulation is independent of CD28 co-stimulation and remains intact in *cd28*$^{-/-}$ mice.[24] Interestingly, CD28 co-stimulation completely abolished the inhibition of activation marker expression that is caused by ibrutinib (Figure 4A). Moreover, $CD8^+$ T-cell proliferation was rescued to normal levels when co-stimulated by αCD28 (Figure 4B). Similar results were observed by addition of αCD28 antibody to human $CD8^+$ T cells (Figure 4C), confirming that strong co-stimulatory signals can circumvent the TCR inhibitory effects of ibrutinib.

Blocking the PD-1/PD-L1 axis enhances the anti-leukemic activity of ibrutinib

In the subsequent experiments, we investigated possible immunomodulatory drugs that can recapitulate the *in vitro* effects of αCD28 antibodies and thereby reverse the block of $CD8^+$ T-cell differentiation in the TCL1 AT model. In light of recent results showing CD28 signaling as the primary target of PD-1 blockade,[34,35] we reasoned that blocking the PD-1/PD-L1 axis can enhance anti-tumoral T-cell activity and improve therapeutic efficacy of ibrutinib. Thus, we treated CLL-bearing mice with ibrutinib alone or in combination with αPD-1 or αPD-L1 antibodies. As shown in *Online Supplementary Figure S4*, all treatment groups had comparable tumor load at the start of the treatment. Consistent with our previous work, blocking the PD-1/PD-L1 axis by αPD-L1 resulted in delayed CLL development in PB, spleen and bone marrow (BM) (Figure 5A-C). The effects were more pronounced for αPD-L1 compared to αPD-1 treatment, which is likely due to the additional effects of αPD-L1 antibodies on tumor-associated myeloid cells, as shown by us and others.[9,36] Interestingly, combination of ibrutinib with PD-1 or PD-L1 blocking antibodies resulted in enhanced disease control in PB, spleen and BM, which was most pronounced in the αPD-L1/ibrutinib combination (Figure 5A-C), confirming a therapeutic efficacy of this combination.

Blocking the PD-1/PD-L1 axis expands the effector population and enhances the functional capacity of $CD8^+$ T cells

We then examined the effect of PD-1/PD-L1 combination with ibrutinib on $CD8^+$ T-cell activity. We restricted our analysis to αPD-1 plus ibrutinib treatment as these mice had more comparable tumor load to the ibrutinib single arm (Figure 5A-C), and thereby we could exclude changes in T cells that are caused by differences in disease load. In line with our previous data, ibrutinib reduced the percentage of effector population, and decreased activation, proliferation and functional capacities of $CD8^+$ T cells (Figure 6A-D). Interestingly, combination of ibrutinib with αPD-1 resulted in a significant increase in effector $CD8^+$ T-cell percentages (Figure 6A), which was accompanied by an increase in activation marker expression on $CD8^+$ T cells (Figure 6B). Moreover, $CD8^+$ T-cell functional capacity was improved by the combination treatment, as shown by a significant increase in degranulation capacity and IFNγ production (Figure 6C and D). The increase in degranulation capacity and IFNγ production was also observed when focusing the analysis on the $CD8^+$ effector T-cell population (*Online Supplementary Figure S5A* and *B*). Collectively, these data show that blocking the PD-1/PD-L1 pathway can improve $CD8^+$ T-cell function and enhance CLL control after ibrutinib treatment.

Discussion

Ibrutinib has been approved as a successful inhibitor of BTK for treatment of CLL and other B-cell lymphomas. In addition, it was also the first clinically available inhibitor of ITK.[15] ITK is expressed in T cells in which, as a major player in TCR signaling, it is responsible for calcium mobilization, cytoskeleton reorganization, synapse formation and adhesion.[37] Deletion or inhibition of ITK in

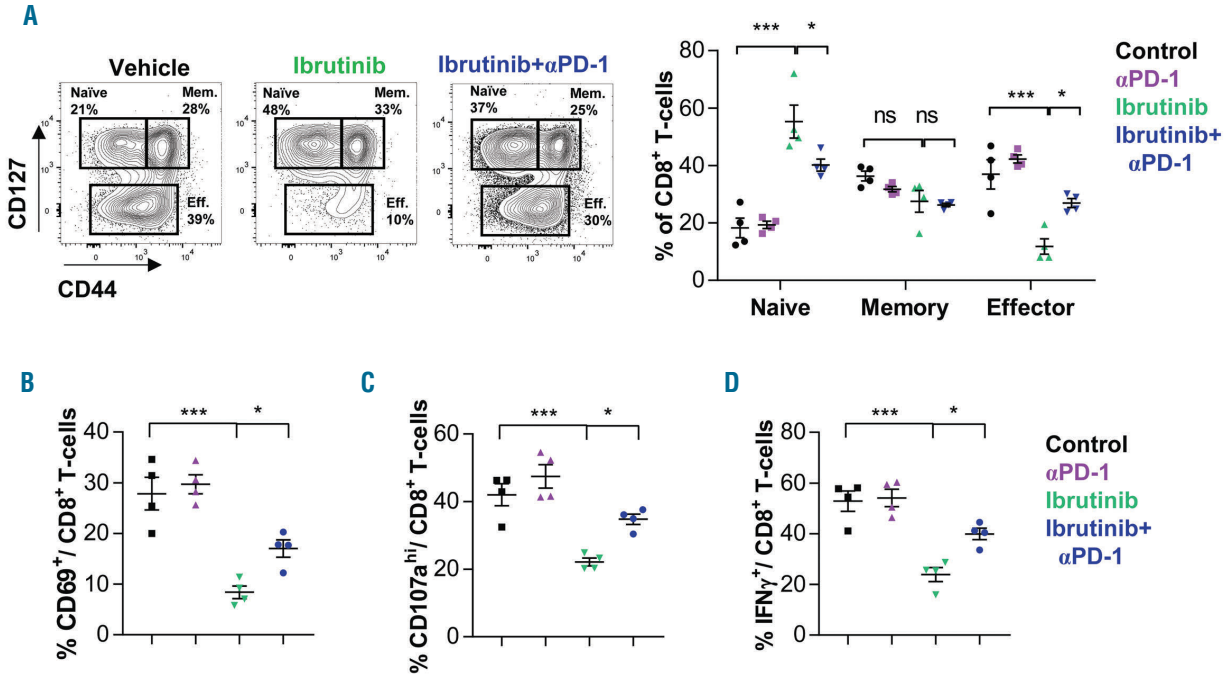


Figure 6. Blocking the PD-1/PD-L1 axis expands the effector population and enhances the functional capacity of CD8⁺ T cells. C57BL/6 mice were transplanted with splenocytes from leukemic TCL1 mice, and after 2 weeks assigned to treatment with isotype antibody plus vehicle (control), αPD-1, ibrutinib, or αPD-1 + ibrutinib. Mice were sacrificed after 4 weeks of treatment. (A) Flow cytometric analysis of splenic $CD3^+CD8^+$ T cells from different treatment arms (n=4). Cell subsets were defined as naïve ($CD127^{hi}CD44^{low}$), memory (Mem: $CD127^{hi}CD44^{hi}$), and effector (Eff: $CD127^{low}CD44^{int-hi}$) cells. (B) Flow cytometric analysis of CD69 expression. (C and D) Cytotoxic function of $CD8^+$ T cells was assessed by flow cytometric analysis of (C) degranulation capacity, as measured by CD107a expression on the cell surface, and (D) IFNγ production (n=4). Graphs show means±standard error of mean. *P<0.05, ***P<0.001, ns: not significant.

$CD8^+$ T cells results in their decreased expansion, delayed expression of cytolytic effector molecules, and defective degranulation upon TCR activation.[38] This leads to a global defect in the cytolysis of pathogens, and as a consequence, to reduced viral clearance. In line with this, dramatic *in vivo* immunomodulation by ibrutinib has led to its approval for the treatment of refractory cGvHD,[20] but the mechanisms underlying this clinical efficacy are poorly understood.

So far, modulating effects of ibrutinib on the differentiation of $CD4^+$ T cells, like Th1, Th2, Th17 and Treg cells, have been described.[15,19,22] In the current study, we observed a negative impact of ibrutinib on $CD8^+$ T-cell proliferation and function in the TCL1 AT model, which reduces their phenotype to a level of tumor naïve control mice. As our *in vitro* data confirmed $CD8^+$ T-cell inhibition by ibrutinib, but not the specific BTK inhibitor ACP-196, this effect is BTK-independent and most likely mediated by inhibition of ITK downstream of the TCR. Along this line, CC-292, an inhibitor with a higher selectivity for BTK, had a lower impact on T-cell activity *in vitro*, and has been previously shown not to impair T-cell function in the TCL1 AT model.[39] But as these drugs might have different efficacies in patients, caution must be exercised when extrapolating clinical effects from these pre-clinical observations. Our observations in the TCL1 AT model seem to be in contrast to published data describing an increase of $CD8^+$ T-cell numbers and their reduced expression of inhibitory receptors, like PD-1, in CLL patients after 8-20 weeks of treatment with ibrutinib.[19] The results of this study suggest that this may be due to diminished activation-induced cell death of T cells through ITK inhibition. As our data demonstrate that inhibition of ITK by ibrutinib decreases TCR signaling and thereby activation of T cells, a consequence of that is not only reduced functional properties, as we show, but also diminished activation-induced cell death, confirming the observations of Long *et al.* in CLL patients.[19] A further study documented that ibrutinib decreases CD8 T-cell proliferation and activation in patients 8 weeks after treatment start.[22] However, these results have been largely viewed as a sign of favorable immune normalization under ibrutinib treatment, rather than a direct side effect of the drug. In light of our *in vitro* and *in vivo* results, it is more likely that these findings in CLL patients are due to the off-target effects of ibrutinib on ITK. In a further study that investigated T cells in CLL patients before and after 1 year of treatment with ibrutinib, disease-associated, elevated T-cell numbers and T-cell-related cytokine levels in PB had normalized, and T-cell repertoire diversity had increased significantly in treated patients.[40] Considering the broad effects of BTK blockade on functional properties of many immune cell types, these changes in the T-cell compartment might be due to ibrutinib's ability to rewire the carefully constructed, supportive microenvironmental network in CLL, which presumably contributes to the therapeutic success of this drug.[41] But as ibrutinib, first-of-all, considerably redistributes malignant B cells from lymph nodes to blood, which ultimately results in a reduction of tumor burden, this suggests that normalization of the T-cell compartment under ibrutinib treatment is secondary to the effect of the drug on CLL-cell numbers and their localization. This is supported by our previous results as well as published data of others showing that T-cell expansion and exhaustion positively correlates with tumor load and predominantly occurs in secondary lymphoid organs.[7-9] Along this

line, enhanced engraftment and efficacy of CLL patient-derived chimeric antigen receptor (CAR) T cells after more than 1 year of treatment with ibrutinib can be also explained by a normalization of T cells associated with a reduction of exhaustion phenotype, secondary to the effective control of CLL by the drug.[42] In this study, the authors further show that *ex vivo* treatment of CLL CAR T cells with ibrutinib does not impact on their proliferation or function. Our data here clearly show that this observation is due to a commonly used stimulation protocol for T cells *in vitro* in which αCD3 and αCD28 antibodies are combined as stimuli. Co-stimulation of $CD8^+$ T cells with αCD28 was also used by Dubovsky *et al*. who describe that ibrutinib does not affect TCR signaling and function of these cells.[15] This observation was in contrast to results obtained in ITK-deficient mice which show impaired TCR-dependent signaling and $CD8^+$ T-cell effector function in response to viral infections.[43] We now show that inhibition of T-cell activity by ibrutinib can be overcome by co-stimulatory signaling mediated by CD28, which is known to be independent of ITK.[33] In line with our findings, stimulation of ITK-deficient $CD8^+$ T cells with αCD3 only leads to impaired expansion and activity.[43]

Considering our observations that ibrutinib negatively impacts on the activity of $CD8^+$ T cells, one needs to investigate whether patients under long-term ibrutinib treatment have reduced adaptive immunity. In early clinical studies and applications of ibrutinib, this was hard to assess, as treated patients were relapsed and refractory, as well as high-risk CLL who have a profound immune suppression and perturbation of both innate and adaptive immunity, and therefore an increased susceptibility to infections is likely to be caused by the disease.[44] Only more recently, with the approval of ibrutinib as first-line therapy for CLL, have high rates of infectious complications in patients on ibrutinib monotherapy and in combination with other drugs been observed.[45] However, in comparison to the severe effects chemotherapy has on the immune system of patients, ibrutinib is reasonably well-tolerated, and by monitoring the impact of ibrutinib on patients' immune status, or by preventing immunosuppressive adverse effects by rational combination treatment approaches with drugs that improve T-cell effector function, outcome for patients can be even further improved. Recent data of clinical trials with the highly selective BTK inhibitor acalabrutinib showed overall response rates of 85% in treatment-naïve CLL patients and 94% in relapsed/refractory cases.[46,47] Most adverse events (AE) observed in these trials were mild or moderate (grade 1-2) and were most commonly diarrhea and headache. It was hypothesized that due to its greater selectivity for BTK, acalabrutinib has favorable pharmacokinetic properties and an improved toxicity profile than ibrutinib. Considering, however, the short history of acalabrutinib treatment compared to ibrutinib, and the lack of a head-to-head comparison of the two drugs in CLL patients, it remains unclear whether the long-term immune side effects of the drugs are comparable.

Interestingly, the immunomodulatory effect of ibrutinib can be even of therapeutic advantage, as shown in patients with relapsed CLL after allogeneic hematopoietic stem cell transplantation, in which ibrutinib was tolerable and effective.[48]

Our data in the TCL1 AT model show that combining ibrutinib with immune checkpoint blockade leads to enhanced $CD8^+$ T-cell function and reduced CLL progression. Both αPD-1 and αPD-L1 treatment improved the therapeutic effect of ibrutinib, with better results observed with αPD-1. As PD-L1 is expressed by CLL and myeloid cells in this model,[25] this antibody has a broader activity compared to αPD-1. Besides blocking the interaction with PD-1, αPD-L1 but not αPD-1 antibodies were shown to modulate myeloid cell subsets within the tumor microenvironment via activating Fcγ receptors.[36] Furthermore, blocking PD-L1 directly on tumor cells dampens their glycolysis, leaving more available glucose in the extracellular tumor milieu for T cells, which enhances their activity.[49]

Testing the combination of ibrutinib with immune checkpoint blockade in the mouse model allowed us to monitor tumor load in all organs affected by disease. In line with observations in CLL patients, ibrutinib as single-agent was not able to reduce malignant cells in the BM, which explains why patients and mice relapse if therapy is discontinued. Interestingly, if combined with αPD-1 or αPD-L1, tumor control in the BM was as efficient as in spleen and blood, suggesting that the combination of ibrutinib with checkpoint blockade might be able to eradicate CLL cells more efficiently, eventually leading to a cure.

Disclosures

No conflicts of interest to disclose.

Contributions

BSH designed the study, performed experiments, analyzed and interpreted data, prepared figures, and wrote the manuscript; HY, YD, PMR and RS performed experiments, analyzed and interpreted data. SS and PL critically advised the study and reviewed the manuscript; MS designed and supervised the study, interpreted data, and wrote the manuscript.

Funding

This study was supported by the German José Carreras Foundation (13R/2018), the German Cancer Aid (grant number 112069), the BMBF-Network "PRECiSe" (031L0076A), the ERA-NET TRANSCAN-2 program JTC 2014–project FIRE-CLL, and the Cooperation Program in Cancer Research of the DKFZ and Israel's Ministry of Science, Technology and Space. SS was supported by the DFG (SFB1074 subproject B1).

References

1. Burger JA, O'Brien S. Evolution of CLL treatment - from chemoimmunotherapy to targeted and individualized therapy. Nat Rev Clin Oncol. 2018;15(8):510-527.
2. Wiestner A. The role of B-cell receptor inhibitors in the treatment of patients with chronic lymphocytic leukemia. Haematologica. 2015;100(12):1495-1507.
3. Farooqui MZH, Valdez J, Martyr S, et al. Ibrutinib for previously untreated and relapsed or refractory chronic lymphocytic leukaemia with *TP53* aberrations: a phase 2, single-arm trial. Lancet Oncol. 2015; 16(2):169-176.
4. Badar T, Burger JA, Wierda WG, O'Brien S. Ibrutinib: a paradigm shift in management of CLL. Exp Rev Hematol. 2014;7(6):705-717.
5. Davids MS, Brown JR. Ibrutinib: a first in class covalent inhibitor of Bruton's tyrosine kinase. Future Oncol. 2014;10(6):957-967.
6. Hofbauer JP, Heyder C, Denk U, et al. Development of CLL in the TCL1 transgenic mouse model is associated with severe skewing of the T-cell compartment homologous to human CLL. Leukemia. 2011;25(9):1452-1458.
7. Riches JC, Davies JK, McClanahan F, et al. T cells from CLL patients exhibit features

of T-cell exhaustion but retain capacity for cytokine production. Blood. 2013; 121(9):1612-1621.
8. Hanna BS, Roessner PM, Yazdanparast H, et al. Control of chronic lymphocytic leukemia development by clonally-expanded CD8+ T cells that undergo functional exhaustion in secondary lymphoid tissues. Leukemia. 2019;33(3):625-637.
9. McClanahan F, Hanna B, Miller S, et al. PD-L1 checkpoint blockade prevents immune dysfunction and leukemia development in a mouse model of chronic lymphocytic leukemia. Blood. 2015;126(2):203-211.
10. Wierz M, Pierson S, Guyonnet L, et al. Dual PD1/LAG3 immune checkpoint blockade limits tumor development in a murine model of chronic lymphocytic leukemia. Blood. 2018;131(14):1617-1621.
11. Ding W, LaPlant BR, Call TG, et al. Pembrolizumab in patients with CLL and Richter transformation or with relapsed CLL. Blood. 2017;129(26):3419-3427.
12. Maharaj K, Sahakian E, Pinilla-Ibarz J. Emerging role of BCR signaling inhibitors in immunomodulation of chronic lymphocytic leukemia. Blood Adv. 2017;1(21):1867-1875.
13. Kondo K, Shaim H, Thompson PA, et al. Ibrutinib modulates the immunosuppressive CLL microenvironment through STAT3-mediated suppression of regulatory B-cell function and inhibition of the PD-1/PD-L1 pathway. Leukemia. 2018;32(4):960-970.
14. Gunderson AJ, Kaneda MM, Tsujikawa T, et al. Bruton tyrosine kinase-dependent immune cell cross-talk drives pancreas cancer. Cancer Discov. 2016;6(3):270-285.
15. Dubovsky JA, Beckwith KA, Natarajan G, et al. Ibrutinib is an irreversible molecular inhibitor of ITK driving a Th1-selective pressure in T lymphocytes. Blood. 2013;122(15):2539-2549.
16. Kohrt HE, Sagiv-Barfi I, Rafiq S, et al. Ibrutinib antagonizes rituximab-dependent NK cell-mediated cytotoxicity. Blood. 2014;123(12):1957-1960.
17. Ng PP, Lu DK, Sukbuntherng J, et al. Ibrutinib enhances the activity of anti-CD20 antibodies in an MCL mouse model: effect of drug at clinically relevant concentrations on ADCC and ADCP. Blood. 2015; 126(23):3998-3998.
18. Podhorecka M, Goracy A, Szymczyk A, et al. Changes in T-cell subpopulations and cytokine network during early period of ibrutinib therapy in chronic lymphocytic leukemia patients: the significant decrease in T regulatory cells number. Oncotarget. 2017;8(21):34661-34669.
19. Long M, Beckwith K, Do P, et al. Ibrutinib treatment improves T cell number and function in CLL patients. J Clin Invest. 2017;127(8):3052-3064.
20. Miklos D, Cutler CS, Arora M, et al. Ibrutinib for chronic graft-versus-host disease after failure of prior therapy. Blood. 2017;130(21):2243-2250.
21. Sagiv-Barfi I, Kohrt HE, Czerwinski DK, et al. Therapeutic antitumor immunity by checkpoint blockade is enhanced by ibrutinib, an inhibitor of both BTK and ITK. Proc Natl Acad Sci U S A. 2015;112(9):E966-972.
22. Niemann CU, Herman SEM, Maric I, et al. Disruption of in vivo chronic lymphocytic leukemia tumor–microenvironment interactions by ibrutinib - findings from an investigator-initiated Phase II study. Clin Cancer Res. 2016;22(7):1572-1582.
23. Bichi R, Shinton SA, Martin ES, et al. Human chronic lymphocytic leukemia modeled in mouse by targeted TCL1 expression. Proc Natl Acad Sci U S A. 2002;99(10):6955-6960.
24. Moran AE, Holzapfel KL, Xing Y, et al. T cell receptor signal strength in Treg and iNKT cell development demonstrated by a novel fluorescent reporter mouse. J Exp Med. 2011;208(6):1279-1289.
25. Hanna BS, McClanahan F, Yazdanparast H, et al. Depletion of CLL-associated patrolling monocytes and macrophages controls disease development and repairs immune dysfunction in vivo. Leukemia. 2016;30(3):570-579.
26. Chang BY, Huang MM, Francesco M, et al. The Bruton tyrosine kinase inhibitor PCI-32765 ameliorates autoimmune arthritis by inhibition of multiple effector cells. Arthritis Res Ther. 2011;13(4):R115.
27. Haderk F, Schulz R, Iskar M, et al. Tumor-derived exosomes modulate PD-L1 expression in monocytes. Sci Immunol. 2017; 2(13):eaah5509.
28. Quah BJ, Warren HS, Parish CR. Monitoring lymphocyte proliferation in vitro and in vivo with the intracellular fluorescent dye carboxyfluorescein diacetate succinimidyl ester. Nat Protoc. 2007; 2(9):2049-2056.
29. Ponader S, Chen SS, Buggy JJ, et al. The Bruton tyrosine kinase inhibitor PCI-32765 thwarts chronic lymphocytic leukemia cell survival and tissue homing in vitro and in vivo. Blood. 2012;119(5):1182-1189.
30. Kaech SM, Cui W. Transcriptional control of effector and memory CD8+ T cell differentiation. Nat Rev Immunol. 2012; 12(11):749-761.
31. Fuertes Marraco SA, Neubert NJ, Verdeil G, Speiser DE. Inhibitory receptors beyond T cell exhaustion. Front Immunol. 2015; 6:310.
32. Barf T, Covey T, Izumi R, et al. Acalabrutinib (ACP-196): a covalent Bruton tyrosine kinase inhibitor with a differentiated selectivity and in vivo potency profile. J Pharmacol Exp Ther. 2017;363(2):240-252.
33. Li C-R, Berg LJ. Cutting Edge: Itk is not essential for CD28 signaling in naive T cells. J Immunol. 2005;174(8):4475-4479.
34. Kamphorst AO, Wieland A, Nasti T, et al. Rescue of exhausted CD8 T cells by PD-1-targeted therapies is CD28-dependent. Science. 2017;355(6332):1423-1427.
35. Hui E, Cheung J, Zhu J, et al. T cell costimulatory receptor CD28 is a primary target for PD-1-mediated inhibition. Science. 2017;355(6332):1428-1433.
36. Dahan R, Sega E, Engelhardt J, et al. FcγRs modulate the anti-tumor activity of antibodies targeting the PD-1/PD-L1 axis. Cancer Cell. 2015;28(3):285-295.
37. Bunnell SC, Diehn M, Yaffe MB, et al. Biochemical interactions integrating Itk with the T cell receptor-initiated signaling cascade. J Biol Chem. 2000;275(3):2219-2230.
38. Kapnick SM, Stinchcombe JC, Griffiths GM, Schwartzberg PL. Inducible T cell kinase regulates the acquisition of cytolytic capacity and degranulation in CD8+ CTLs. J Immunol. 2017;198(7):2699-2711.
39. Lee-Vergés E, Hanna BS, Yazdanparast H, et al. Selective BTK inhibition improves bendamustine therapy response and normalizes immune effector functions in chronic lymphocytic leukemia. Int J Cancer. 2019;144(11):2762-2773.
40. Yin Q, Sivina M, Robins H, et al. Ibrutinib therapy increases T cell repertoire diversity in patients with chronic lymphocytic leukemia. J Immunol. 2017;198(4):1740-1747.
41. Bachireddy P, Wu CJ. Arresting the inflammatory drive of chronic lymphocytic leukemia with ibrutinib. Clin Cancer Res. 2016;22(7):1547-1549.
42. Fraietta JA, Beckwith KA, Patel PR, et al. Ibrutinib enhances chimeric antigen receptor T-cell engraftment and efficacy in leukemia. Blood. 2016;127(9):1117-1127.
43. Atherly LO, Brehm MA, Welsh RM, Berg LJ. Tec kinases Itk and Rlk are required for CD8+ T cell responses to virus infection independent of their role in CD4+ T cell help. J Immunol. 2006;176(3):1571-1581.
44. Kipps TJ, Stevenson FK, Wu CJ, et al. Chronic lymphocytic leukaemia. Nat Rev Dis Primers. 2017;3:16096.
45. Tillman BF, Pauff JM, Satyanarayana G, Talbott M, Warner JL. Systematic review of infectious events with the Bruton tyrosine kinase inhibitor ibrutinib in the treatment of hematologic malignancies. Eur J Haematol. 2018;100(4):325-334.
46. Sharman JP, Banerji V, Fogliatto LM, et al. ELEVATE TN: Phase 3 study of acalabrutinib combined with obinutuzumab (O) or alone vs O plus chlorambucil (Clb) in patients (Pts) with treatment-naive chronic lymphocytic leukemia (CLL). Blood. 2019;134(Suppl 1):31.
47. Byrd JC, Wierda WG, Schuh A, et al. Acalabrutinib monotherapy in patients with relapsed/refractory chronic lymphocytic leukemia: updated phase 2 results. Blood. 2020;135(15):1204-1213.
48. Ryan CE, Sahaf B, Logan AC, et al. Ibrutinib efficacy and tolerability in patients with relapsed chronic lymphocytic leukemia following allogeneic HCT. Blood. 2016;128(25):2899-2908.
49. Chang C-H, Qiu J, O'Sullivan D, et al. Metabolic competition in the tumor microenvironment is a driver of cancer progression. Cell. 2015;162(6):1229-1241.

Ferrata Storti Foundation

Haematologica 2021
Volume 106(4):978-986

Immune reconstitution and associated infections following axicabtagene ciloleucel in relapsed or refractory large B-cell lymphoma

Jennifer M. Logue,[1,2*] Elisa Zucchetti,[3*] Christina A. Bachmeier,[1] Gabriel S. Krivenko,[1] Victoria Larson,[2] Daniel Ninh,[1] Giovanni Grillo,[3] Biwei Cao,[4] Jongphil Kim,[4] Julio C. Chavez,[2,5] Aliyah Baluch,[2,6] Farhad Khimani,[1,2] Aleksandr Lazaryan,[1,2] Taiga Nishihori,[1,2] Hien D. Liu,[1,2] Javier Pinilla-Ibarz,[2,5] Bijal D. Shah,[2,5] Rawan Faramand,[1,2] Anna E. Coghill,[7] Marco L. Davila,[1,2] Bhagirathbhai R. Dholaria,[1,8] Michael D. Jain[1,2#] and Frederick L. Locke[1,2#]

[1]Department of Blood and Marrow Transplant and Cellular Immunotherapy, H. Lee Moffitt Cancer Center and Research Institute, Tampa, FL, USA; [2]Morsani College of Medicine, University of South Florida, Tampa, FL, USA; [3]Divisione di Ematologia, Centro Trapianti di Midollo, ASST Grande Ospedale Metropolitano Niguarda, Milan, Italy; [4]Department of Biostatistics and Bioinformatics, H. Lee Moffitt Cancer Center and Research Institute, Tampa, FL, USA; [5]Department of Malignant Hematology, H. Lee Moffitt Cancer Center and Research Institute, Tampa, FL, USA; [6]Department of Infectious Diseases, H. Lee Moffitt Cancer Center and Research Institute, Tampa, FL, USA; [7]Cancer Epidemiology Program, H. Lee Moffitt Cancer Center and Research Institute, Tampa, FL, USA and [8]Department of Hematology-Oncology, Vanderbilt University Medical Center, Nashville, TN, USA

*JML and EZ contributed equally as co-first authors.
#MDJ and FLL contributed equally as co-senior authors

ABSTRACT

CD19 chimeric antigen receptor T (CAR T)-cell therapy with axicabtagene ciloleucel (axi-cel) for relapsed or refractory (R/R) large B-cell lymphoma (LBCL) may lead to durable remissions, however, prolonged cytopenias and infections may occur. In this single center retrospective study of 85 patients, we characterized immune reconstitution and infections for patients remaining in remission after axi-cel for LBCL. Prolonged cytopenias (those occurring at or after day 30 following infusion) were common with ≥grade 3 neutropenia seen in 21 of 70 (30%) patients at day 30 and persisting in 3 of 31 (9.7%) patients at 1 year. B cells were undetectable in 30 of 34 (88.2%) patients at day 30, but were detected in 11 of 19 (57.9%) at 1 year. Median immunoglobulin G levels levels reached a nadir at day 180. By contrast, CD4 T cells decreased from baseline and were persistently low with a median CD4 count of 155 cells/μL at 1 year after axi-cel (n=19, range: 33– 269). In total, 23 of 85 (27.1%) patients received intravenous immunoglobulins after axi-cel, and 34 of 85 (40%) received granulocyte-colony stimulating factor. Infections in the first 30 days occurred in 31 of 85 (36.5%) patients, of which 11 of 85 (12.9%) required intravenous antibiotics or hospitalization ("severe") and were associated with cytokine release syndrome, neurotoxicity, tocilizumab use, corticosteroid use, and bridging therapy on univariate analyses. After day 30, seven severe infections occurred, with no late deaths due to infection. Prolonged cytopenias are common following axi-cel therapy for LBCL and typically recover with time. Most patients experience profound and prolonged CD4 T-cell immunosuppression without severe infection.

Correspondence:

FREDERICK L. LOCKE
frederick.locke@moffitt.org

MICHAEL D. JAIN
michael.jain@moffitt.org

Received: September 21, 2019.

Accepted: April 2, 2020.

Pre-published: April 23, 2020.

https://doi.org/10.3324/haematol.2019.238634

©2021 Ferrata Storti Foundation

Material published in Haematologica is covered by copyright. All rights are reserved to the Ferrata Storti Foundation. Use of published material is allowed under the following terms and conditions: https://creativecommons.org/licenses/by-nc/4.0/legalcode. Copies of published material are allowed for personal or internal use. Sharing published material for non-commercial purposes is subject to the following conditions: https://creativecommons.org/licenses/by-nc/4.0/legalcode, sect. 3. Reproducing and sharing published material for commercial purposes is not allowed without permission in writing from the publisher.

Introduction

Axicabtagene ciloleucel (axi-cel) can lead to long term disease control for patients with R/R LBCL, including diffuse (DLBCL), primary mediastinal (PMBCL), and transformed follicular lymphoma (tFL). In the pivotal ZUMA-1 trial, axi-cel led to a best objective response rate (ORR) of 82% and complete response (CR) rate of 54%, with 2-year follow-up data reporting durable responses and median overall

survival not reached.[1,2] Major acute side effects of chimeric antigen receptor T (CAR T)-cell therapy include cytokine release syndrome (CRS) and neurologic toxicities, which are treated with anti-IL-6 receptor blockade and/or corticosteroids.

In the ZUMA-1 trial, grade 3 or higher cytopenias were common in the first 30 days following CAR T-cell therapy, and this is typically attributed to fludarabine and cyclophosphamide given for lymphodepletion prior to CAR T-cell infusion.[3,4] However, cytopenias may persist, and at 3 months or later, 17% of ZUMA-1 patients experienced one or more grade 3 or higher cytopenia, including 11% with neutropenia, 7% with thrombocytopenia, and 3% with anemia.[1] Late cytopenias were seen without evidence of marrow dysplasia or relapse. In addition, B-cell aplasia occurred due to on-target elimination of CD19-expressing normal B cells, with resultant hypogammaglobulinemia, and use of intravenous immunoglobulins (IVIG) in 31%. Overall, 28% of patients had ≥grade 3 infections on the ZUMA-1 trial.

The presence of early and late cytopenias, corticosteroid treatment for CRS and neurotoxicity, and reconstitution of B and T lymphocytes after CAR T therapy may put patients at risk of infection. This study aimed to characterize immune reconstitution after axi-cel therapy and identify early and late infections in patients with R/R LBCL receiving treatment with axi-cel. We examined cytopenias, lymphocyte reconstitution, and infection data up to 1 year following infusion of axi-cel.

Methods

Patients and data collection

We retrospectively reviewed data from the medical records of patients with R/R LBCL who were treated with axi-cel at the Moffitt Cancer Center between February 1, 2016, and February 28, 2019. This study was approved by the Institutional Review Board. Data extracted from the electronic medical record included patient demographics, prior therapies, baseline disease status, CAR T-cell product, dates of treatment and disease progression or last follow-up, occurrence and grade of CRS and neurotoxicity, complete blood counts (CBC), immunoglobulin levels, infection data, pathology reports, and drug administration. B-, T- and natural killer-lymphocyte subsets were quantified from fresh peripheral blood samples using a validated flow cytometry panel in the clinical lab. All data was censored at date of progression, development of a new malignancy requiring systemic treatment, death, or last follow-up, in order to understand the effect of axi-cel therapy independent of disease progression. Immunoglobulin levels were censored after a patient was treated with IVIG. Adverse events were graded per the Common Terminology Criteria for Adverse Events (CTCAE) v4.03. CRS was scored based on modified Lee grading system.[5] Neurologic toxicity was scored based on CAR-related encephalopathy syndrome/CAR T toxity (CRES/CAR-TOX) grading system or individual terms for CTCAE neurotoxicity.[6] Disease status at apheresis was defined as: primary refractory, never achieving end of treatment CR; refractory, not primary refractory and no response to the most recent therapy; relapsed, responded to most recent therapy and progressed. Bridging therapy was defined as any lymphoma-specific therapy administered after leukapheresis and before conditioning chemotherapy. Cyclophosphamide and fludarabine conditioning followed by axi-cel infusion were performed as in ZUMA-1. Prophylaxis policies were adapted from our institution's autologous stem cell transplant procedures. Our institutional standard for antimicrobial prophylaxis includes starting antibacterial prophylaxis with a fluoroquinolone and antifungal prophylaxis with fluconazole on the morning of axi-cel infusion or earlier if the patient is neutropenic, with discontinuation in afebrile patients free of infection after neutrophil recovery. The standard empiric treatment for neutropenic fever included cefepime or piperacillin/tazobactam. *Pneumocystis jiroveci pneumonia* (PJP) prophylaxis is started on day 30 following axi-cel infusion and included sulfamethoxazole-trimethoprim in patients without cytopenias, with inhaled pentamidine, dapsone or atovaquone prophylaxis used in cytopenic patients. Duration of PJP prophylaxis was physician dependent and was typically provided for 6-12 months, or until recovery of CD4 count over 200 cells/μL. Varicella zoster virus (VZV) reactivation prophylaxis is provided for a minimum of 12 months, typically using acyclovir. Herpes simplex virus (HSV) 1/2 immunoglobulin G (IgG) testing was by ARUP laboratories (Salt Lake City, UT).

Definition of infection

An episode of infection was defined as a viral, bacterial, or fungal finding based on microbiological data or a clinical syndrome, which was found based on retrospective chart review. Severe infection was defined as an infection which required intravenous (IV) antibiotics or hospitalization. Standard follow-up at our institution includes clinic appointments on days 30, 90, 180, 270, and 360. Patients were expected to call if they developed any infectious symptoms in the interim.

Statistical analysis

Patient characteristics were summarized using descriptive statistics including median and range for continuous measures and proportions and frequencies for categorical measures. Chi-square test or Fisher exact test was used to explore the association between categorical variables. Dunnett's test was used to make pairwise comparisons with Day 0, and Kruskal-Wallis test has been used to compare total white blood cells (WBC), neutrophils (N), CD3 positive cells, CD56 positive cells, CD8 positive cells, CD4 positive cells, CD19 positive cells, and IgG levels up to 1 year following axi-cel. When comparing characteristics to infection/severe infection, the associations between categorical variables were evaluated using χ^2 tests or Fisher's exact tests when the expected frequency was less than 5. In addition, infection incidence per 1,000 person-days at day 30, 90, 180, 270, and 360 was computed to incorporate the multiple infections per patient. The cumulative incidence of first infection was estimated by competing risk approach, where death or progression were considered as competing events. The association between continuous variables and infection were assessed using Wilcoxon tests. Categorical variable levels for overall survival (OS) were compared using the Log-rank test. Kaplan-Meier curves were used to show progression free survival (PFS) and OS for all patients in the study. Statistical significance was defined as two-sided *P*-value of <0.05.

Results

The majority of acute toxicities are known to resolve before day 30 after CAR T, which also is the time of first disease assessment.[7] Therefore, we separately analyzed immune reconstitution and infections prior to day 30 and after day 30 after axi-cel infusion. Further, in order to focus on survivorship we censored patients from the analysis at the time of lymphoma relapse. Of 85 infused patients, we censored 11 for analysis beyond day 30 due to early progressive disease or death, and an additional 4 patients

Table 1. Patient characteristics and clinical outcomes.

	Analysis up to day 30 (n=85)	Analysis after day 30 (n=70)
Axi-cel		
Standard of Care	63 (74.1%)	48 (68.6%)
Clinical trial	22 (25.9%)	22 (31.4%)
Age, years		
Median (range)	64 (28-79)	63 (28-79)
≥65	40 (47·1%)	29 (41·4%)
Sex		
Female	34 (40·0%)	27 (38·6%)
ECOG at apheresis		
0	28 (32·9%)	26 (37·1%)
1	38 (44·7%)	34 (48·6%)
2	16 (18·8%)	9 (12·9%)
3	3 (3·5%)	1 (1·4%)
Disease stage at apheresis		
I or II	18 (21·2%)	17 (24·3%)
III or IV	67 (78·8%)	53 (75·7%)
International Prognostic Index score at apheresis		
0-2	28 (32·9%)	27 (38·6%)
3-5	57 (67·1%)	43 (61·4%)
Presence of bulky disease	20 (23·5%)	13 (18·6%)
Disease type		
Diffuse large B-cell lymphoma	56 (65·9%)	47 (67·1%)
Transformed follicular lymphoma	26 (30·6%)	20 (28·6%)
Primary mediastinal B-cell lymphoma	3 (3·5%)	3 (4·3%)
Prior lines of therapies		
Median (range)	3 (1-8)	3 (1-7)
1	3 (3·5%)	3 (4·3%)
2	26 (30·6%)	25 (35·7%)
≥3	56 (65·9%)	42 (60·0%)
Prior autologous stem cell transplant	21 (24·7%)	17 (24·3%)
Prior allogeneic stem cell transplant	2 (2·4%)	2 (2·9%)
Bridging therapy	48 (56·5%)	36 (51·4%)
Disease status		
Primary refractory	26 (30·6%)	22 (31·4%)
Refractory	31 (36·5%)	25 (35·7%)
Relapsed	28 (32·9%)	23 (32·9%)
Cytokine release syndrome maximum grade		
0	6 (7·1%)	4 (5·7%)
1	36 (42·4%)	34 (48·6%)
2	35 (41·2%)	29 (41·4%)
3-4	8 (9·4%)	3 (4·3%)
CAR T-cell related encephalopathy syndrome maximum grade		
0	28 (32·9%)	25 (35·7%)
1-2	31 (36·5%)	28 (40·0%)
3-4	26 (30·6%)	17 (24·3%)
Treatment for toxicity		
Steroid use	39 (45·9%)	27 (38·6%)
Tocilizumab use	39 (45·9%)	28 (40·0%)
30-day response		
ORR	68 (80·0%)	64 (91·4%)
CR	41 (48·2%)	38 (54·3%)
PR	27 (31·8%)	26 (37·1%)
SD	9 (10·6%)	6 (8·6%)
PD	7 (8·2%)	0 (0·0%)
No response assessment	1 (1·2%)	0 (0·0%)

Patient baseline characteristics prior to axi-cel and clinical outcomes following axi-cel infusion for patients analyzed prior to and after day 30. axi-cel: axicabtagene ciloleucel; IQR: interquartile range; ECOG: Eastern Cooperative Oncology Group performance status; Bulky disease: any mass diameter greater than 10 cm; ORR: overall response rate (calculated as complete response [CR] + partial response [PR]); SD: stable disease; PD: progressive disease; CAR T: chimeric antigen receptor T . Disease status at apheresis was defined as: primary refractory, never achieving end of treatment CR; refractory, not primary refractory and no response to the most recent therapy; relapsed, responded to most recent therapy and progressed.

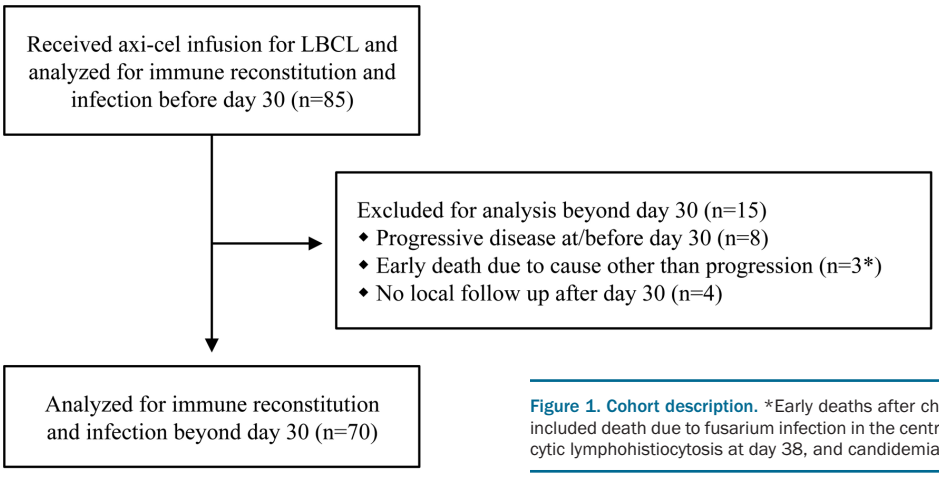


Figure 1. Cohort description. *Early deaths after chimeric antigen receptor T (CAR T) therapy included death due to fusarium infection in the central nervous system at day 39, hemophagocytic lymphohistiocytosis at day 38, and candidemia at day 40.[19]

Table 2. Cytopenias following axicabtagene ciloleucel (axi-cel).

	Apheresis	Day 30	Day 90	Day 180	Day 270	Day 360
Grade 3-4 Leukopenia	3.5% (3/85)	28.6% (20/70)	10.7% (6/56)	16.7% (7/42)	9.4% (3/32)	3.2% (1/31)
Any Grade Leukopenia	23.5% (20/85)	85.7% (60/70)	64.3% (36/56)	64.3% (27/42)	56.3% (18/32)	51.6% (16/31)
Grade 3-4 Neutropenia	3.5% (3/85)	30.0% (21/70)	12.5% (7/56)	11.9% (5/42)	9.4% (3/32)	9.7% (3/31)
Any Grade Neutropenia	14.1% (12/85)	71.4% (50/70)	37.5% (21/56)	42.9% (18/42)	37.5% (12/32)	25.8% (8/31)
Grade 3-4 Anemia	7.1% (6/85)	7.1% (5/70)	3.6% (2/56)	7.1% (3/42)	3.1% (1/32)	3.2% (1/31)
Any Grade Anemia	57.6% (49/85)	87.1% (61/70)	44.6% (25/56)	31.0% (13/42)	31.3% (10/32)	22.6% (7/31)
Grade 3-4 Thrombocytopenia	5.9% (5/85)	25.7% (18/70)	5.4% (3/56)	4.8% (2/42)	3.1% (1/32)	3.2% (1/31)
Any Grade Thrombocytopenia	28.2% (24/85)	80% (56/70)	51.8% (29/56)	45.2% (19/42)	43.8% (14/32)	38.7% (12/31)
Any Grade 3-4 Cytopenia	14.1% (12/85)	44.3% (31/70)	14.3% (8/56)	19.0% (8/42)	9.4% (3/32)	9.7% (3/31)
Any Grade Cytopenia	72.9% (62/85)	100.0% (70/70)	83.9% (47/56)	81.0% (34/42)	71.9% (23/32)	67.7% (21/31)

Clinical complete blood count and differential results were graded using clinical trial criteria (CTCAE v4.03). Grade 3-4 leukopenia = white blood cell count (WBC) <2,000/mm^3; grade 3-4 neutropenia = neutrophil (N) count <1,000/mm^3; grade 3-4 anemia = hemoglobin (Hb) <8 g/dL; grade 3-4 thrombocytopenia = platelet (PLT) count <50,000/mm^3. For any grade cytopenia, patients had at least grade 1 leukopenia, neutropenia, anemia, or thrombocytopenia, defined as WBC <4,000/mm^3, N <1,800/mm^3, Hb <11.4 g/dl, and PLT <143,000/mm^3, based on the lower limits of normal set by the clinical laboratory at our institution. Information is shown as % (#patients/total number of non-relapsing patients with follow-up at that time point).

because they followed up outside of our institution (Figure 1). Median follow-up from time of axi-cel infusion was 12.8 months (range: 0.8-42.4). The median time from apheresis to axi-cel infusion was 27 days (range: 20-42). Patient characteristics are shown in Table 1. Severe (grade 3 or higher) CRS occurred in 9.4% of patients, and severe neurotoxicity occurred in 30.6%. Median duration of corticosteroid treatment for toxicity was 7 days (range: 1–62). ORR at day 30 was 80%, and CR at day 30 was 48.2%. Kaplan-Meier curves of PFS and OS are shown in the *Online Supplementary Figure S1*.

In order to describe cytopenias after axi-cel, we graded cytopenias based on the clinical CBC and differential using clinical trial criteria (CTCAE v4.03; Table 2). At baseline (time of apheresis) prior to axi-cel, 14.1% of patients had grade 3 or 4 cytopenias. At day 30 after axi-cel, grade 3 or 4 leukopenia, neutropenia, or thrombocytopenia was found in 28.6%, 30%, and 25.7% of patients, respectively, for a cumulative grade 3 or 4 cytopenia rate of 44.3%. All patients at day 30 had at least one grade 1 cytopenia. Most patients recovered counts over subsequent months, although a proportion of patients (3 of 31; 9.7%) still had neutrophil counts below 1,000/mL at 1 year after axi-cel infusion.

Cellular and humoral reconstitution was evaluated over time using the clinical CBC and a flow cytometry panel that quantifies B-, T-, and NK-cell subsets (Figure 2). Median leukocyte and neutrophil counts decreased after axi-cel therapy and remained significantly below baseline levels at 1 year after therapy. Similarly, peripheral blood CD4 T cells were low at a median of 220 cells/μL (range: 34–1,720) prior to axi-cel and remained persistently low after axi-cel, with a median CD4 count of 155 cells/μL (range: 33–269) at 1 year. Multiple comparison testing and means are provided in the *Online Supplementary Table S1*. CD19 positive B cells were detectable in 28 of 58 (48.3%) patients at baseline prior to axi-cel and in 4 of 34 (11.8%) patients at day 30. The proportion of patients with detectable levels at day 90, 180, and 360, were 22.6% (7 of 31), 46.2% (12 of 26), and 57.9% (11 of 19), respectively; B cells had significantly increased from baseline by 1 year (P=0.05). At baseline 9 of 58 (15·5%) patients had IgG <300 mg/dL, 16 of 58 (27.6%) patients had IgG <400 mg/dL, and 27 of 58 (46.6%) patients had IgG <500 mg/dL. IgG levels decreased after axi-cel infusion with a nadir at 6 months. By 1 year, excluding patients censored for receipt of IVIG, 9 of 17 (52.9%) had IgG levels above 400 mg/dL and 7 of 17 (41·2%) patients had IgG levels above 500 mg/dL. Of the patients with IgG ≥500 mg/dL at baseline, new hypogammaglobulinemia occurred in 10 of 17 (58.8%) that were measured at day 30 and 20 of 27 (74.1%) in total at any time. We also followed quantitative titers of HSV antibodies in 17 patients (*Online Supplementary Figure S2*). While quantitative levels

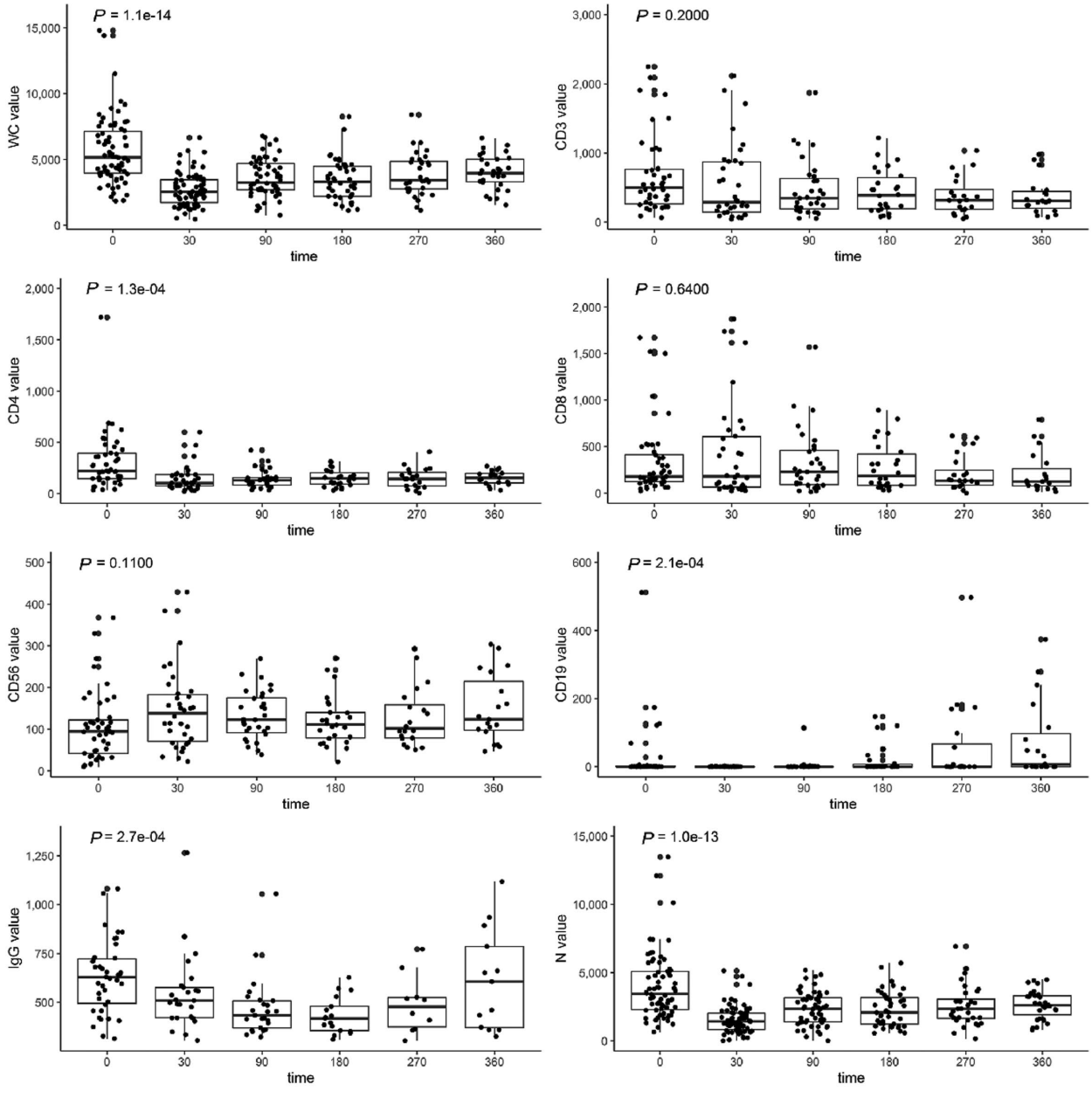


Figure 2. Cellular and humoral immune reconstitution after axicabtagene ciloleucel (axi-cel). Box and whisker plots demonstrating cellular and immune reconstitution following treatment with axi-cel. White blood cells (WC) and neutrophils (N) were measured by complete blood counts with differential at baseline (n=85), day 30 (n=70), day 90 (n=56), day 180 (n=42), day 270 (n=32), and day 360 (n=31). CD3 T cells, CD4 T cells, CD8 T cells, CD56 natural killer cells, and CD19 B cells were measured by flow cytometry at baseline (n=58) and at day 30 (n=34), 90 (n=31), 180 (n=26), 270 (n=20) and 360 (n=19). Also shown are serum mmunoglobulin G (IgG) levels at baseline (n=58) and at day 30 (n=34), 90 (n=31), 180 (n=19), 270 (n=17) and 360 (n=17) after treatment with axi-cel. Boxes demonstrate first quartile, median and third quartile values. Whiskers show the data ranges. Dots represent individual patients. *P*-values are calculated by the Kruskal-Wallis test to assess significant differences in the indicated cell type after axi-cel infusion.

decreased, no patient fell below the minimum titer for a positive test during the follow-up period. In total, 23 of 85 (27.1%) patients required IVIG after axi-cel. 34 of 85 (40·0%) patients required G-CSF due to severe neutropenia.

A proportion of patients had bone marrow biopsies done pre-treatment and after axi-cel therapy (Table 3). The median pre-treatment marrow occurred at day -179 (range: -1551 to -7). Before axi-cel, 21.5% of patients had a hypocellular marrow, 60% of patients had a normocellular marrow, no patients had dysplasia, 10.8% had mild to moderate fibrosis, and16·9% had a clonal population. Of marrows with a clonal population, four showed DLBCL, three follicular lymphoma (FL), one marginal zone lymphoma (MZL), one chronic lymphocytic leukemia (CLL), one monoclonal plasma cell proliferation in the setting of monoclonal gammopathy of undetermined significance, and one had monoclonal $CD5^+$ B cells. Of these patients, seven went on to have repeat bone marrow biopsies after treatment with axi-cel, and no patients showed persistence of the clonal population at the time of repeat biopsy. Within the first 100 days after axi-cel, 16 patients had bone marrow biopsies done in the absence of lymphoma progression, occurring at median day 31

Table 3. Bone marrow biopsy findings

	Pre-axi-cel	Day 1-100	Day 101-360
Median Day (range)	-179 (-1551 to -7)	31 (6 to 100)	202 (102 to 289)
Hypocellular marrow	21·5% (14/65)	87·5% (14/16)	50·0% (3/6)
Normocellular marrow	60·0% (39/65)	12·5% (2/16)	50·0% (3/6)
Hypercellular marrow	18·5% (12/65)	0·0% (0/16)	0·0% (0/6)
Dysplasia Present	0·0% (0/65)	6·3% (1/16)	33·3% (2/6)
Fibrosis Present	10·8% (7/65)	31·3% (5/16)	33·3% (2/6)

axi-cel: axicabtagene ciloleucel. Bone marrow cellularity as designated by the clinical pathologist. Clinical criteria account for patient age and are defined as hypocellular with a cell-to-fat ratio of 1:3 or less and hypercellular with a cell-to-fat ratio of 3:1 or greater.[20]

(range: 6-100). Of these, 87.5% showed hypocellularity, 6.3% had evidence of dysplasia, and 31.3% displayed mild fibrosis. Beyond the first 100 days after axi-cel, six bone marrow biopsies were done at median day 202 (range: 102-289). Of these, three were hypocellular and three were normocellular. Dysplasia and fibrosis were observed in four patients, with two patients having both dysplasia and fibrosis on biopsy, one patient with fibrosis only, and one patient with dysplasia only.

In the first 30 days, infection occurred in 31 of 85 patients (36.5%). Of these, 12 patients had *Clostridium difficile* (14.1%), and 10 patients had a respiratory virus (11.8%) (Figure 3A, *Online Supplementary Table S2A*). At the time of *Clostridium difficile* detection, one patient was on fluoroquinolone prophylaxis, while eight were receiving broad spectrum antibiotics for neutropenic fever and three patients were not on any antibiotics. We further classified the infections as severe or non-severe on the basis of whether IV antibiotics were required or if hospitalization was warranted, and 11 patients (12.9%) had at total of 13 severe infections in the first 30 days. Two patients experienced two severe infections each. These severe infections included six cases of bacteremia, one cellulitis, one acute cholecystitis, one urinary tract infection, two fungal infections (candidemia and fusariosis) and two viremias (adenovirus and cytomegalovirus). For the case of candidemia, cultures drawn on day 38 post axi-cel eventually became positive for *Candida krusei* (5 days later on day 43). The patient was on antifungal prophylaxis with fluconazole, and autopsy revealed disseminated candidemia. The case of *Fusarium* was only discovered upon autopsy; the patient did not have positive fungal cultures and had received antifungal prophylaxis starting with fluconazole, and at the time of death, micafungin. Neither patient who experienced a fungal infection had a prior allogeneic stem cell transplant. Both patients received five prior lines of therapy before axi-cel and were treated with prolonged steroids for neurotoxicity after axi-cel. For the two cases of viremia, both patients received antiviral prophylaxis with acyclovir. The most common organisms were gram positive and the fungal isolates were not susceptible to fluconazole (*Online Supplementary Table S3*).

Severe infections before day 30 were associated on univariate analyses with severe CRS, severe neurotoxicity, tocilizumab use, steroid use, and bridging therapy (P=0.007, P=0.007, P=0.03, P=0.004, and P=0.02, respectively) (Figure 3B-C, *Online Supplementary Table S4*). The presence of infection was associated with a higher baseline total white blood cell (WBC) and neutrophil count (P=0.03 and P=0.02, respectively) (*Online Supplementary Table S5*).

After 30 days from time of axi-cel infusion, we identified 32 infections in 31 of 70 (44.3%) patients (*Online Supplementary Table S2B*). Of these, 25 infections were non-severe with 19 cases of upper respiratory viruses, one case of bacterial pneumonia, two cases of bacterial sinusitis, one case of *Clostridium difficile*, one cellulitis, and one groin abscess, all managed with oral antibiotics. The remaining seven cases were severe, including five cases of pneumonia, one case of sepsis due to methicillin-resistant *Staphylococcus aureus* bacteremia, and one case of neutropenic fever resolving with IV antibiotics.

In total, infection was a contributor to death in three cases (3.5%), all early after axi-cel, including both cases of fungal infection and one case of *Streptococcus mitis* bacteremia co-occurring with rapid lymphoma progression. All other deaths on this study occurred after lymphoma progression.

On a rate basis, infection incidence decreased from 11.7 incident infections per 1,000 person-days in the first 30 days to 2.3 incident infections per 1,000 person-days between day 31 and day 90, and incidence continued to decrease over time (Figure 4A). However, estimates are affected by the competing risk of lymphoma progression or death (Figure 4B).

We evaluated if cytopenias and/or poor immune reconstitution at day 30 were associated with infection after day 30 (*Online Supplementary Figure S3*). CD4 and CD8 T-cell counts were not significantly lower at day 30 in patients who would go on to develop infection compared to those who remained infection-free. Similarly, day 30 IgG levels were not lower in patients who went on to develop infection compared to those who did not.

Discussion

Patients with lymphoma receiving fludarabine and cyclophosphamide followed by CD19 CAR T-cell therapy are at risk of acute and chronic immunosuppression. This is due to tumor-related immunosuppression, residual effects of prior lines of lymphoma therapy, lymphodepletion due to fludarabine and cyclophosphamide, B-cell aplasia with hypogammaglobulinemia, immunosuppressive corticosteroids needed for toxicity treatment, and prolonged cytopenias possibly due to cytokine and/or chemokine effects.[8-11] Here we have characterized immune reconstitution and associated infections in a retrospective cohort of patients receiving a single CAR T product, axi-cel, in patients with LBCL.

First, we confirm that cytopenias are common after axi-cel therapy and may persist for months after therapy. On bone marrow biopsy the typical finding is of a normocellular to hypocellular marrow, although cases of myelodysplastic syndrome have been reported after axi-cel.[12] Attribution of bone marrow changes to axi-cel is unclear

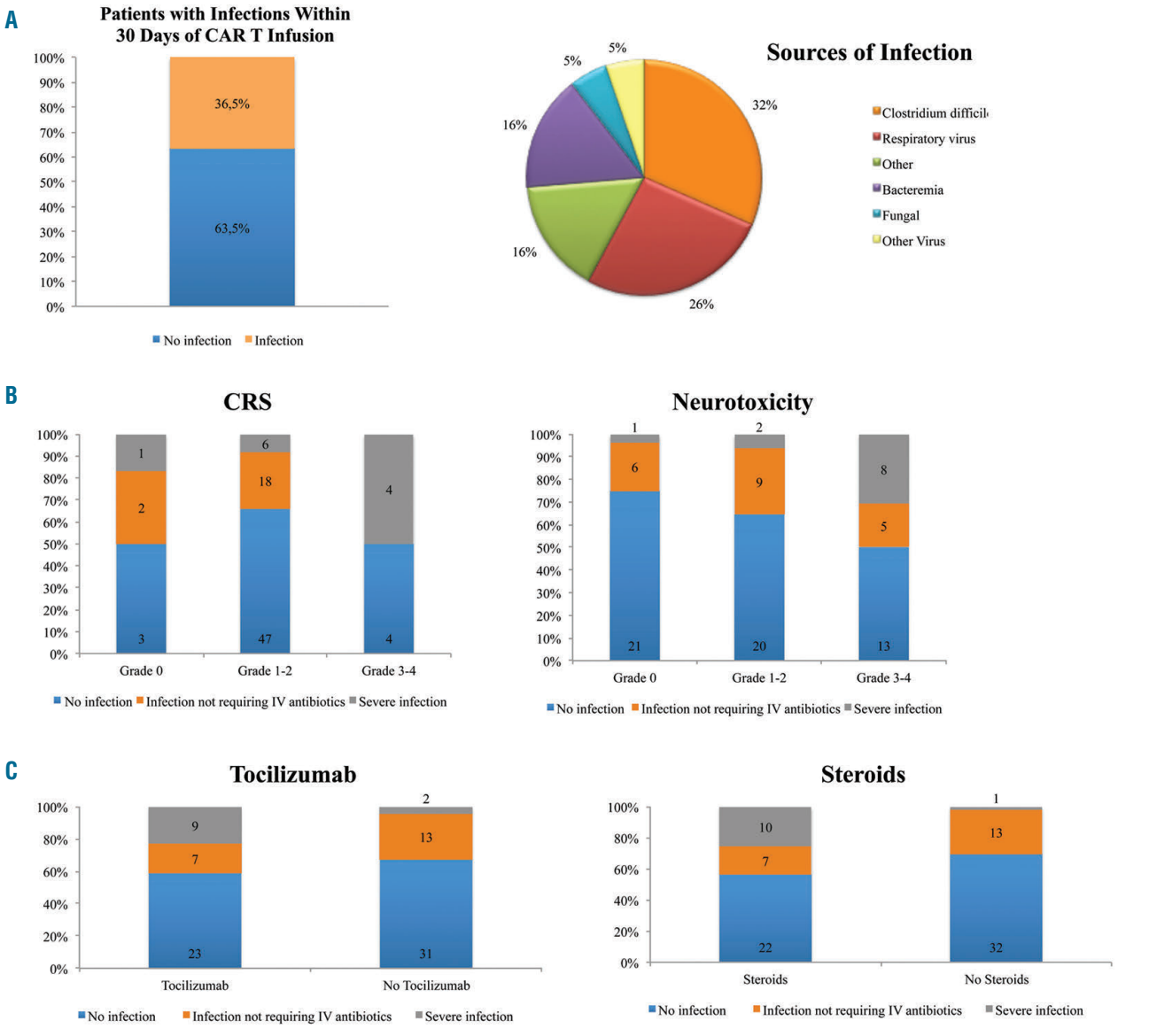


Figure 3. Infections in the first 30 days after axi-cel therapy for aggressive B-cell lymphoma. (A) Rate and type of infection observed in 85 patients in the first 30 days after axi-cel infusion. (B) Infection by grade of cytokine release syndrome (CRS) or neurotoxicity. (C) Non-severe and severe infections in the first 30 days by receipt of anti-IL-6R therapy (tocilizumab) or steroid therapy. CRS: cytokine release syndrome.

given that 65.9% of the original cohort received at least 3 prior lines of therapy. However a limitation of this study is that there is no standardized schedule for bone marrow biopsies at our institution before or after treatment with axi-cel. Rather, biopsies were done at the discretion of the attending physician with the primary reason for bone marrow biopsy after axi-cel being prolonged cytopenias. Therefore, this data set may not capture all dysplasia or fibrosis events that occur pre- or post-axi-cel therapy. Ultimately, a prospective study including bone marrow biopsies would be helpful.

The mechanism for prolonged cytopenias after CAR T-cell therapy is unclear. Purine analogues such as fludarabine are often associated with prolonged cytopenias, but responding patients generally recover lymphocyte counts and cytopenias within weeks to months after fludarabine and cyclophosphamide, even after six cycles such as is given in CLL.[13,14] Fried *et al.* studied 38 pediatric and adult patients after CD19 CAR T therapy for B-cell lymphomas or acute lymphoblastic leukemia (ALL) in the first 2 months after therapy and found a moderate correlation between neutrophil counts and soluble SDF-1.[8] Our data suggest that although patients may have hypocellular bone marrows and severe cytopenias in the months after axi-cel, supportive care is effective as patients generally recover their counts over subsequent months.

In our cohort, 36.5% of patients were diagnosed with infections within 30 days after axi-cel, and 44.3% of patients had infections between days 31 and 360. Hill and colleagues previously reported on infections following treatment with a CD19/4-1BB/CD3z/EGFRt CAR T-cell therapy for ALL, CLL, and non-Hodgkin lymphoma on clinical trials.[3] They saw that 23% of patients had infections within 28 days, and 14% of patients had infections between days 29 and 90. Park and colleagues reported on infections occurring after treatment with a

CD19/CD28/CD3z CAR in R/R B-ALL treated through a phase I trial and found that 42% of patients had infections during the first 30 days after axi-cel infusion, while 31% of surviving patients had infections between day 31 and day 180.[15] Overall, infection rates in our cohort were similar to that reported on these trials, although we characterized most of these infections as non-severe.

In the cohort of lymphoma patients described here, most of the infections in the first 30 days were due to *Clostridium difficile* colitis or respiratory viruses and were manageable. The rate of *Clostridium difficile* is likely influenced by our choice of fluoroquinolone prophylaxis for all CAR T patients. Severe infections occurred in 12.9% of patients, and in 3.5% of patients, infection was a contributor to death. We find that early severe infections almost always occur in patients that have severe CRS and/or neurotoxicity and receive treatment with tocilizumab, corticosteroids, and/or had bridging therapy. At baseline, total WBC and neutrophil counts were counterintuitively higher in patients with infection compared to those who do not experience infection. Speculatively, patients with higher neutrophil counts at baseline may have adverse lymphoma biology and a greater degree of tumor-related immunosuppression.[16,17] We also noted that the majority of bacterial isolates in severe infection were gram positive, which may also be related to our use of fluoroquinolone prophylaxis to prevent gram negative infections. The two fungal infections were not susceptible to our prophylactic fluconazole. Clinically, patients who require steroids for toxicity management are at a higher infection risk. There is an overall lack of data to guide prophylaxis policies following treatment with CAR T-cell therapy, and further study is needed to optimize infection prophylaxis and prevent infection in this group.

We also report that CD4 T-cell levels remain persistently low for months after axi-cel. Indeed, we observed that CD4 counts remain significantly low even at 1 year after treatment. Despite profound and prolonged T-cell immunosuppression, severe infections remain rare. Our low rate of severe infection is in agreement with the smaller study published by Kochenderfer and colleagues, in which only 1 of 7 patients (14·3%) had a severe infection requiring hospitalization after treatment with CD19 CAR T-cells for LBCL.[10] Longer follow-up is needed to determine how CD4 counts recover beyond 1 year and the degree to which prophylaxis and vigilance for CD4 recovery are necessary. In our institution we currently provide PJP prophylaxis and VZV reactivation prophylaxis for a minimum of 6 months or until recovery of CD4 count over 200 cells/μL, although there is physician variability in duration of prophylaxis and also with respect to the provision of IVIG to clinically asymptomatic patients. While we did not observe any PJP or *Mycobacterium avium-intracellulare* in our cohort, the level of CD4 suppression after CAR T-cell therapy may provide an impetus for prolonged or alternative prophylaxis in some patients. During the dates of this cohort study we typically revaccinated patients starting at 3 months post-CAR T-cell therapy in a manner analogous to our practice after autologous stem cell transplant. However, in this study we found that immunoglobulin levels nadir at 6 months and recover thereafter and we also noted recovery of B-cell aplasia and immunoglobulin levels while maintaining lymphoma remission, as is reported in other studies.[1,10,11] This suggests that CD19 CAR T-cell therapy does not lead to a permanent loss of humoral immunity, which may account for a lower rate of opportunistic infections. Moreover, the available data presented here on HSV titers suggests that patients may not lose full protection against some infections. Similarly, Hill *et al.*[18] recently reported on antiviral humoral immunity in 39 adults receiving CD19 CAR-T cell therapy and found that anti-measles IgG levels remained stable over time, possibly because long-lived plasma cells do not express CD19.[18] Further study is required on the efficacy and optimal timing of infectious prophylaxis and vaccination after CAR T therapy.

Given the low rate of severe infections, this study is limited in that it cannot generate a risk prediction model for severe infection using baseline factors. A larger, ideally multicenter, cohort is needed to identify patients at risk of infection and to consider modifying treatment. Another issue is that we censored patients at the time of disease progression in order to reduce confounding introduced by subsequent therapy. However, cytopenias and poor immune reconstitution may interfere with therapies given for post-CAR T relapse and further study is needed to

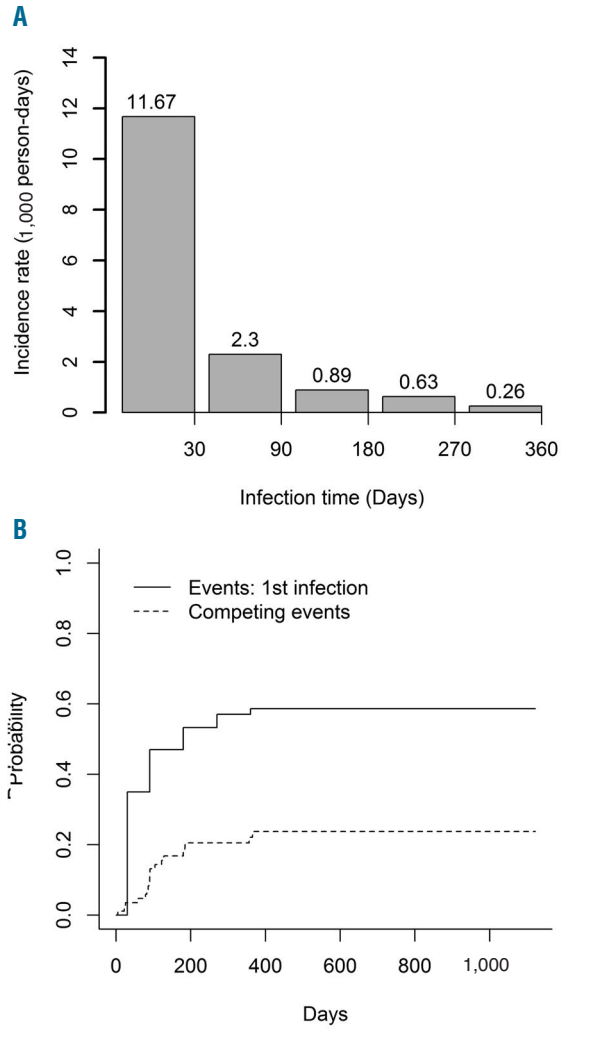


Figure 4. Infections occurring post-axi-cel. (A) Incidence rate of infection over time per 1,000 person-days, with time from axi-cel infusion on the X-axis. (B) Competing risk plot of the cumulative incidence of a patient's first infection. Death or progression were considered as competing events. axi-cel: axicabtagene ciloleucel.

identify if patients relapsing post-CAR T have unique infectious risks.

CAR T-cell therapy provides durable remissions in 40-50% of R/R LBCL patients. As more patients receive this therapy and have prolonged remissions, we will need to understand and manage the unique survivorship issues that occur. Here we report that patients in remission after axi-cel have prolonged immunosuppression, with CD4 T-cell counts in particular remaining low for at least 1 year, and are at risk of infection in the short and long term.

Disclosures

CB sits on the Advisory Board for Kite/Gilead; JCCh sit on the Advisory Board for Kite/Gilead, Novartis, Bayer, Genetech and is a member of the Speaker Bureau for Genetech; BDS has is a consultant for Celgene/Juno, Adaptive, Kite/Gilead, Novartis, Pharmacyclics, Spectrum/Acroteca and AstraZeneca and has received research funding from Jazz and Incyte; JP-I is a consultant for Takeda, Abbvie, Janssen, Novartis, Gilead and Teva; MLD has received research funding from Celgene, Novartis, Atara and other financial support from Novartis, Precision Biosciences, Celyad, Bellicum, GlaxoSmithKline and holds stock options from Precision Biosciences, Adaptive Biotechnologies, Anixa Biosciences; FLL is a Consultant for Cellular Biomedicine Group, Inc. and a scientific advisor for Kite/Gilead, Novartis, and MDJ is consultant for Kite/Gilead and Novartis.

Contributions

MDJ and FLL designed and supervised the research; KML, EZ, CAB, GSK, VL and DN collected and analyzed data; GG, BC and JK provided statistical analysis; JCC, AB, FK, AL, TN, HDL, JP, BDS, RF, AEC, MLD and BRD provided patient information and data.

All authors contributed to the writing of the manuscript.

Funding

This work was supported by NCI P30 CA076292 and NCI K23-CA201594.

References

1. Locke FL, Ghobadi A, Jacobson CA, et al. Long-term safety and activity of axicabtagene ciloleucel in refractory large B-cell lymphoma (ZUMA-1): a single-arm, multicentre, phase 1-2 trial. Lancet Oncol. 2019; 20(1):31-42.
2. Neelapu SS, Locke FL, Bartlett NL, et al. Axicabtagene ciloleucel CAR T-cell therapy in refractory large B-cell lymphoma. N Engl J Med. 2017;377(26):2531-2544.
3. Hill JA, Li D, Hay KA, et al. Infectious complications of CD19-targeted chimeric antigen receptor-modified T-cell immunotherapy. Blood. 2018;131(1):121-130.
4. Jain MD, Davila ML. Concise review: emerging principles from the clinical application of chimeric antigen receptor T cell therapies for B cell malignancies. Stem Cells. 2018;36(1):36-44.
5. Lee DW, Gardner R, Porter DL, et al. Current concepts in the diagnosis and management of cytokine release syndrome. Blood. 2014; 124(2):188-195.
6. Neelapu SS, Tummala S, Kebriaei P, et al. Chimeric antigen receptor T-cell therapy - assessment and management of toxicities. Nat Rev Clin Oncol. 2018;15(1):47-62.
7. Locke FL, Go WY, Neelapu SS. Development and use of the anti-CD19 chimeric antigen receptor T-cell therapy axicabtagene ciloleucel in large B-cell lymphoma: a review. JAMA Oncol. 2019:1-10.
8. Fried S, Avigdor A, Bielorai B, et al. Early and late hematologic toxicity following CD19 CAR-T cells. Bone Marrow Transplant. 2019;54(10):1643-1650.
9. Shalabi H, Shah NN, Fry TJ, Yates B, Delbrook C. Chimeric antigen receptor induced cytopenia differs from chemotherapy induced myelosuppression. Blood. 2017; 130(Suppl 1):S5048.
10. Kochenderfer JN, Somerville RPT, Lu T, et al. Long-duration complete remissions of diffuse large B cell lymphoma after anti-CD19 chimeric antigen receptor T cell therapy. Mol Ther. 2017;25(10):2245-2253.
11. Schuster SJ, Svoboda J, Chong EA, et al. Chimeric antigen receptor T cells in refractory B-cell lymphomas. N Engl J Med. 2017;377(26):2545-2554.
12. Locke FL, Neelapu SS, Bartlett NL, et al. Phase 1 results of ZUMA-1: a multicenter study of KTE-C19 anti-CD19 CAR T cell therapy in refractory aggressive lymphoma. Mol Ther. 2017;25(1):285-295.
13. Joffe E, Ariela Arad N, Bairey O, et al. Persistently low lymphocyte counts after FCR therapy for chronic lymphocytic leukemia are associated with longer overall survival. Hematol Oncol. 2018;36(1):128-135.
14. Ysebaert L, Gross E, Kuhlein E, et al. Immune recovery after fludarabine-cyclophosphamide-rituximab treatment in B-chronic lymphocytic leukemia: implication for maintenance immunotherapy. Leukemia. 2010;24(7):1310-1316.
15. Park JH, Romero FA, Taur Y, et al. Cytokine release syndrome grade as a predictive marker for infections in patients with relapsed or refractory B-cell acute lymphoblastic leukemia treated with chimeric antigen receptor T cells. Clin Infect Dis. 2018;67(4):533-540.
16. Annibali O, Hohaus S, Marchesi F, et al. The neutrophil/lymphocyte ratio >/=3.5 is a prognostic marker in diffuse large B-cell lymphoma: a retrospective analysis from the database of the Italian regional network 'Rete Ematologica del Lazio per i Linfomi' (RELLI). Leuk Lymphoma. 2019; 60(14): 3386-3394.
17. Porrata LF, Ristow K, Habermann T, et al. Predicting survival for diffuse large B-cell lymphoma patients using baseline neutrophil/lymphocyte ratio. Am J Hematol. 2010;85(11):896-899.
18. Hill JA, Krantz EM, Hay KA, et al. Durable preservation of antiviral antibodies after CD19-directed chimeric antigen receptor T-cell immunotherapy. Blood Adv. 2019;3(22):3590-3601.
19. Hashmi H, Bachmeier C, Chavez JC, et al. Haemophagocytic lymphohistiocytosis has variable time to onset following CD19 chimeric antigen receptor T cell therapy. Br J Haematol. 2019;187(2):e35-e38.
20. Nonomura Y, Yasumoto M, Yoshimura R, et al. Relationship between bone marrow cellularity and apparent diffusion coefficient. J Magn Reson Imaging. 2001;13(5):757-760.

ARTICLE

CD28.OX40 co-stimulatory combination is associated with long *in vivo* persistence and high activity of CAR.CD30 T cells

Marika Guercio,[1] Domenico Orlando,[1] Stefano Di Cecca,[1] Matilde Sinibaldi,[1] Iolanda Boffa,[1] Simona Caruso,[1] Zeinab Abbaszadeh,[1] Antonio Camera,[1] Biancamaria Cembrola,[1] Katia Bovetti,[1] Simona Manni,[1] Ignazio Caruana,[1] Roselia Ciccone,[1] Francesca Del Bufalo,[1] Pietro Merli,[1] Luciana Vinti,[1] Katia Girardi,[1] Annalisa Ruggeri,[1] Cristiano De Stefanis,[1] Marco Pezzullo,[1] Ezio Giorda,[1] Marco Scarsella,[1] Rita De Vito,[2] Sabina Barresi,[3] Andrea Ciolfi,[3] Marco Tartaglia,[3] Lorenzo Moretta,[4] Franco Locatelli,[1,5#] Concetta Quintarelli[1,6#] and Biagio De Angelis[1#]

[1]Department of Onco-Hematology and Cell and Gene Therapy, Bambino Gesù Children's Hospital, IRCCS, Rome; [2]Department of Laboratories, Pathology Unit, Bambino Gesù Children's Hospital, IRCCS, Rome; [3]Genetics and Rare Diseases Research Division, Ospedale Pediatrico Bambino Gesù IRCSS, Rome; [4]Department of Immunology, Bambino Gesù Children's Hospital, IRCCS, Rome; [5]Department of Pediatrics, Sapienza, University of Rome, Rome and [6]Department of Clinical Medicine and Surgery, Federico II University, Naples, Italy

[#]FL, CQ and BDA contributed equally as co-senior authors.

Ferrata Storti Foundation

Haematologica 2021
Volume 106(4):987-999

ABSTRACT

The prognosis of many patients with chemotherapy-refractory or multiply relapsed CD30$^+$ non-Hodgkin lymphoma (NHL) or Hodgkin lymphoma (HL) still remains poor, and novel therapeutic approaches are warranted to address this unmet clinical need. In light of this consideration, we designed and pre-clinically validated a chimeric antigen receptor (CAR) construct characterized by a novel anti-CD30 single-chain variable-fragment cassette, linked to CD3ζ by the signaling domains of two co-stimulatory molecules, namely CD28.4-1BB or CD28.OX40. We found that CAR.CD30 T cells exhibit remarkable cytolytic activity *in vitro* against both HL and NHL cell lines, with sustained proliferation and pro-inflammatory cytokine production, even after multiple and sequential lymphoma-cell challenges. CAR.CD30 T cells also demonstrated anti-lymphoma activity in two *in vivo* xenograft immune-deficient mouse models of metastatic HL and NHL. We observed that administration of CAR.CD30 T cells, incorporating the CD28.OX40 co-stimulatory domains and manufactured in the presence of interleukin 7 and interleukin 15, were associated with the best overall survival in the treated mice, along with establishment of a long-term immunological memory able to protect mice from further tumor re-challenge. Our data indicate that, in the context of *in vivo* systemic metastatic xenograft mouse models, the co-stimulatory machinery of CD28.OX40 is crucial for improving persistence, *in vivo* expansion and proliferation of CAR.CD30 T cells upon tumor encounter. The CD28.OX40 co-stimulatory combination is ultimately responsible for the anti-tumor efficacy of the approach, paving the way to translate this therapeutic strategy into clinical use for patients with CD30$^+$ HL and NHL.

Introduction

Use of chimeric antigen receptor (CAR) T cells is a new promising approach of adoptive cancer cell immunotherapy, combining antigen recognition by a monoclonal antibody with the effector function of T cells.[1] CAR T cells directed against CD19 have been shown to induce sustained complete responses in patients with relapsed/refractory B-cell non-Hodgkin (NHL) lymphomas, particularly diffuse

Correspondence:

BIAGIO DE ANGELIS
biagio.deangelis@opbg.net

FRANCO LOCATELLI
franco.locatelli@opbg.net

Received: July 8, 2019.
Accepted: March 24, 2020.
Pre-published: May 7, 2020.

https://doi.org/10.3324/haematol.2019.231183

©2021 Ferrata Storti Foundation

Material published in Haematologica is covered by copyright. All rights are reserved to the Ferrata Storti Foundation. Use of published material is allowed under the following terms and conditions: https://creativecommons.org/licenses/by-nc/4.0/legalcode. Copies of published material are allowed for personal or internal use. Sharing published material for non-commercial purposes is subject to the following conditions: https://creativecommons.org/licenses/by-nc/4.0/legalcode, sect. 3. Reproducing and sharing published material for commercial purposes is not allowed without permission in writing from the publisher.

large B-cell lymphoma.[2,3] However, alternative targets are needed for other types of lymphoma lacking CD19 expression, including diseases such as classical Hodgkin lymphoma (HL), anaplastic large-cell lymphoma and other T-cell lymphomas.

Although most patients with HL or NHL are cured with first-line therapies, a relevant proportion of them have primary refractory disease or experience relapse after initial response to treatment.[4] The standard of care for patients who relapse after first-line treatment is intensive chemotherapy followed, in responders, by autologous stem cell transplantation. Although autologous transplantation offers the potential to cure about half of patients, the prognosis of subjects relapsing after the autograft or not eligible for transplantation is poor.[5] Novel therapies are, therefore, desirable for patients with relapsed/refractory lymphoma.

Despite biological differences, HL and NHL have proven to be good targets for immunotherapy: indeed, both occur in the immune-rich lymphoid tissues and are easily accessible to antibody- and cell-based immunotherapy.[5] Moreover, CD30, a cell-membrane protein belonging to the tumor-necrosis-factor receptor superfamily 8, can be found on the cell-surface of both HL and selected NHL including anaplastic large-cell lymphoma, diffuse large B-cell lymphoma, primary mediastinal B-cell lymphoma,[6] peripheral T-cell lymphoma,[7] and adult T-cell leukemia/lymphoma,[8] as well as in rare solid tumors,[9] including embryonal carcinomas[10] and seminomas.[11] Its restricted expression on a subset of normal, activated T and B cells[12,13] renders CD30 an excellent candidate for immune-based therapies, with a low risk of off-tumor, on-target toxicity.

CD30 has been extensively explored as a target for antibody-based therapy. The most remarkable results have been achieved with brentuximab-vedotin, an antibody-drug conjugate directed against CD30, shown to be well tolerated and associated with relevant activity in HL and anaplastic large-cell lymphoma.[14] Although brentuximab-vedotin appears to induce excellent responses.[15,16] this antibody-drug conjugate is also associated with adverse events leading to treatment discontinuation in a significant proportion of patients.[17] To overcome the challenges presented by antibody-based therapy, namely limited response durability and reduced tumor penetration.[18] CAR T cells have been explored.

Immunotherapeutic approaches with CAR targeting CD30 have shown efficacy in preclinical models,[19,20] and these results have been translated into the clinic in two trials based on second-generation CD30.CAR T cells, including either CD28 or 4-1BB co-stimulatory domains.[21,22] The clinical efficacy of these second-generation CD30.CAR T cells was, however, suboptimal, as inconsistent responses were observed, most patients having either stable disease after multiple CAR T-cell infusions, or no response at all. Overall, lymph nodes showed better responses than extranodal lesions and CAR T cells did not persist longer than 60 days after infusion. Notably, two studies with CD30.CAR T cells supported several other clinical observations in different settings,[23,24] showing a correlation between CAR T-cell persistence and patients' outcome. We therefore sought to optimize the CAR.CD30 T-cell approach by using a novel single-chain variable fragment (scFv), as well as a novel third-generation construct.

We demonstrate that, with our CAR.CD30 T-cell approach, the use of the novel scFv, the combination of the co-stimulatory molecules CD28 and OX40, as well as a production process based on the addition of interleukin 7 (IL7) and interleukin 15 (IL15), are all relevant to drive high *in vivo* proliferation/expansion, long-term persistence and establishment of the immunological memory necessary to control lymphoma recurrence.

Methods

Generation of retroviral vectors and transduction method of T cells

The scFv for CAR.CD30 molecules is derived from the AC10 monoclonal antibody.[25] The details of the constructs are provided in Figure 1A, *Online Supplementary Figure S1A*, *Online Supplementary Materials* and *Online Supplementary Table S1*, which report the amino-acid sequences for all the construct components. Retroviral supernatant was generated in 293T-cells[19,26,27] and quantified using a Retro-X™ qRT-PCR Titration Kit (Takara) to be used at 10^9 retrovirus-copies/0.5x10^6 T cells. The supernatant was used to transduce primary T cells derived from peripheral blood mononuclear cells of healthy donors (Ethical Committee approval n. 969/2015 protocol n. 669LB). More details on transduction are provided in the *Online Supplementary Materials*.

Phenotypic analysis

The following monoclonal antibodies were used: CD3, CD4, CD8, CD45RA, CD45RO, CD62L, CD223, CD274, CD279, and TIM3 (BD Pharmigen, USA). The expression of CAR.CD30 on T cells was evaluated using anti-CD34 antibody (R&D, USA) or the Pierce Recombinant Biotinylated Protein L.[28] (Thermo Fisher Scientific, USA). The gating strategy is reported in *Online Supplementary Figure S2*.

In vitro anti-lymphoma activity

CAR T-cell cytotoxicity was evaluated using a ^{51}Cr-release assay.[20] For co-culture experiments, T cells and lymphoma-cell lines (Ethical Committee approval n. 652/2018 protocol n. GR-2016-02364546), were plated for 7 days, and residual tumor analyzed by fluorescent activated cell sorting (FACS). For "stressed" co-cultures, tumor cells were added on days 0, 5, 10, 15 and 20 at an effector:target (E:T) ratio of 1:1. The residual tumor cells and persisting T cells were analyzed by FACS 5 days after each tumor addition.

Cytokine analysis

Supernatant collected from 24 h co-culture experiments was analyzed by an enzyme-linked lectin assay (ELLA) (R&D System).

In vivo experiments

In vivo experiments were approved by the Italian Health Ministry (n. 88/2016-PR). Specifically, 6-week old NSG (NOD.Cg-Prkdcscid Il2rgtm1Wjl/SzJ; from Charles River) mice were engrafted intravenously (i.v.) with 0.2x10^6 CD30$^+$ Karpas299-eGFP-FFLuc (NHL model) or 2x10^6 CD30$^+$ L428-eGFP-FFLuc (HL model). After tumor engraftment, mice received an i.v. injection of effector T cells (10x10^6/mouse). Tumor growth was evaluated using an IVIS imaging system (Perkin Elmer, USA).[27] For tumor re-challenge, mice of the NHL model surviving until day +140, were infused i.v. with 0.2x10^6 Karpas299-eGFP-FFLuc cells. Mice were followed for an additional 110 days, without effector T-cell administration.

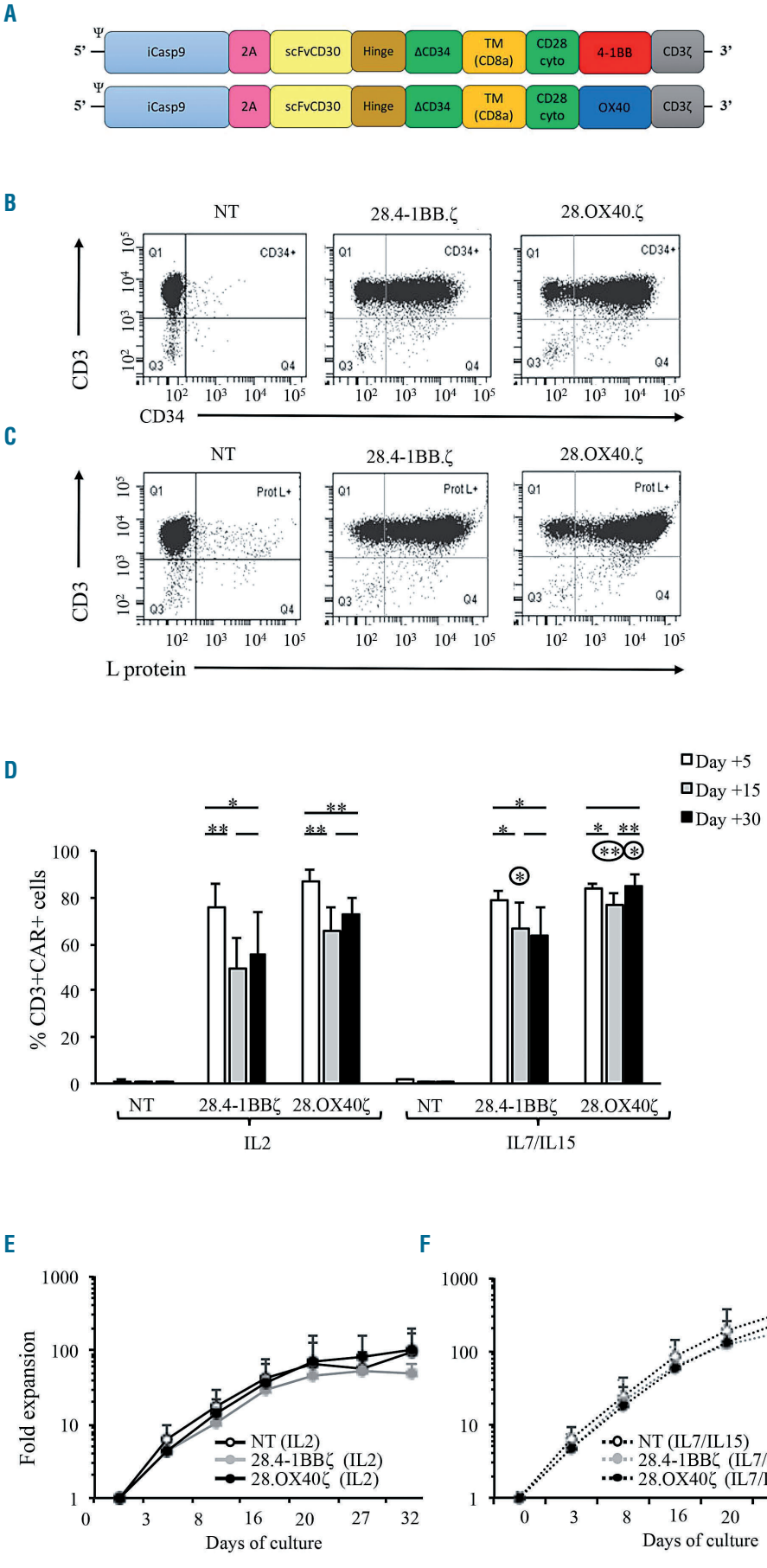


Figure 1. CAR.CD30 T cells with CD28.OX40 or CD28.4-1BB co-stimulation exhibit similar transduction levels and *in vitro* proliferation upon cytokine stimulation. **(A)** Diagram of the expression cassette of two third-generation CAR.CD30. The single-chain variable fragment (scFv) of CD30 was cloned in frame with CD8aTM, CD28 cytoplasmic moiety, and a second co-stimulatory domain represented by either 4-1BB or OX40, as well as the signaling domain CD3-zeta chain (ζ). As a trackable marker, we added a peptide derived from human CD34 (ΔCD34). A safety switch, namely inducible caspase-9 (iCasp9), was also included in the vector constructs. (B) Flow-cytometry analyses in a representative donor showing chimeric antigen receptor (CAR) expression by detection of membrane CD34 in non-transduced (NT) T cells (negative control; left panel), T cells genetically modified with CAR.CD30.ΔCD34.28.4.1BB.ζ (28.4.1BB.ζ; middle panel) and T cells genetically modified with CAR.CD30.ΔCD34.CD28.OX40.ζ (28.OX40.ζ; right panel). (C) Flow-cytometry analyses in a representative donor showing CAR expression using L protein to detect the scFv in NT T cells (negative control; left panel), T cells genetically modified with 28.4.1BB.ζ (middle panel) and T cells genetically modified with 28.OX40.ζ (right panel). (D) Percentage of CAR$^+$ CD3$^+$ T cells during the time course of prolonged *in vitro* culture (day +5 white bars; day +15 gray bars; day +30 black bars), in NT, 28.4.1BB.ζ and 28.OX40.ζ grown in interleukin (IL)2 or in IL7/IL15. (E, F) Fold expansion of NT (empty circle), 28.4.1BB.ζ (gray circle) and 28.OX40.ζ (black circle) grown in IL2 (E) or IL7/IL15 (F) (dotted lines). Data from seven healthy donors are expressed as average ± standard deviation. *P≤0.05; **P≤0.01; ***P≤0.001. Circled asterisks refer to the difference between the T-cell populations grown in IL2 or in IL7/IL15.

Results

Characterization of CAR.CD30 T-cell *in vitro* activity

CAR.CD30 molecules, either second-generation or third-generation (II-CAR or III-CAR), did not induce any proliferative changes in genetically modified T cells as compared to control non-transduced (NT) T cells (*Online Supplementary Figure S1B*). Moreover, regardless of the high level of CAR expression, detected with either anti-CD34 (Figure 1B) or protein L (Figure 1C, *Online Supplementary Figure S1C*), *in vitro* co-culture experiments showed that II-CAR.CD30.4-1BB was characterized by the worst anti-tumor activity compared to all the other configurations (*Online Supplementary Figure S3A* and *B*). The II-CAR.CD30.CD28 exerts a similar anti-lymphoma activity as the III-CAR also including the OX40 co-stimulatory domain; however, at a very low E:T ratio (1:8 effector T cells *vs.* L428 target cells), we observed that only the III-CAR showed significant anti-lymphoma activity compared to NT T cells (*Online Supplementary Figure S3B*). Moreover, we observed a superior trend, although not statistically significant, of a higher percentage of CAR$^+$ T cells (*Online Supplementary Figure S1D*) and interferon-γ production upon CD30$^+$ tumor encounter (*Online Supplementary Figure S3C* and *D*) in CAR.CD30.CD28.OX40 T cells with respect to II-CAR. Considering these data, together with the clinical evidence of the unsatisfactory outcome of patients receiving II-CAR.CD30 therapy,[21,22] we continued our study focusing on III-CAR.CD30.

CAR.CD30 T cells did not exert fratricidal activity

The percentage of CD30$^+$ T cells is high after *in vitro* stimulation, but then declines over time, with no significant difference between NT and CAR.CD30 T cells (*Online Supplementary Figure S4A*), indicating that CAR.CD30 T cells do not exert fratricidal activity. Moreover, CAR.CD30 T cells did not proliferate when stimulated by irradiated autologous activated T/CAR cells (*Online Supplementary Figure S4B*). Notably, mean fluorescence intensity (MFI) of CD30 in lymphoma cells was significantly higher with respect to activated T cells (*Online Supplementary Figure S4C*).

Characterization of third-generation CAR.CD30 T cells in extended *ex vivo* culture

We sought to verify whether different culture conditions could influence the percentage of total CAR$^+$ T cells during standard and prolonged *in vitro ex vivo* expansion (day 30) to stress the system. CAR.CD30 T cells expanded in IL2 showed a significant reduction of CAR during extended *in vitro* culture (Figure 1D). The percentage of CAR.CD30.CD28.4-1BB decreased from 76.09% ± 9.80% (day +5) to 49.20% ± 13.35 (day +15, P=0.002), and to 55.93% ± 18.09% after long-term culture (day +30, P=0.027 with respect to day +5). Similar results were also observed for CAR.CD30.CD28.OX40 T cells: 87.27% ± 5.07% (day +5), 65.15% ± 10.92% (day +15, P=0.003); and 73.05% ± 6.41% (day +30, P=0.009 compared to day +5). Moreover, IL7/IL15, compared to the IL2 condition, significantly improved the total percentage of CAR$^+$ T cells at day +15 (a standard time for CAR T-cell manufacturing); 76.84% ± 5.45% CAR.CD30.CD28.OX40 and 66.44% ± 10.95% CAR.CD30.CD28.4-1BB; P=0.004 and P=0.02, respectively).

While CAR.CD30 T cells did not show a significant proliferative advantage over NT T cells (Figure 1E and F), IL7/IL15 improved the expansion rate compared to IL2 (*Online Supplementary Figure S5A-C*), without any predominant T-cell receptor Vβ family selection (*Online Supplementary Figure S6A* and *B*). Independently of the co-stimulatory combination used, we did not observe a significant difference in the suicide gene inducible caspase 9 (iCasp9) activity, either *in vitro* (*Online Supplementary Figure S7A*) or *in vivo* (*Online Supplementary Figure S7B-E*). Details are provided in the *Online Supplementary Results*.

CAR.CD30.CD28.OX40 T cells exert a superior *in vitro* anti-lymphoma activity compared to CAR.CD30.CD28.4-1BB T cells

Both types of III-CAR.CD30 T cells significantly lysed the Karpas-299 NHL cell line (Figure 2A), as well as two HL cell lines (namely, HDML-2 and L428) (Figure 2B and C, respectively). Cytotoxicity was specific, since negligible lysis was observed against CD30-negative BV173 cells (Figure 2D). The anti-lymphoma activity was also confirmed in a 7-day co-culture assay (Figure 2E-G).

Interestingly, at a very low E:T ratio, the anti-tumor activity of CAR.CD30.CD28.OX40 was superior to that exerted by CAR.CD30.CD28.4-1BB T cells: E:T ratio 1:8 T cells:Karpas-299 cells; P=0.03 (Figure 2E) and E:T ratios 1:16 and 1:32 T cells:HDML2 cells; P=0.03 and P=0.01, respectively (Figure 2F). The enhanced activity of CAR.CD30.CD28.OX40 T cells compared to that of CAR.CD30.CD28.4-1BB T cells was also demonstrated considering IFNγ production upon stimulation by Karpas-299 cells (Figure 2H) and HDML2 cells (Figure 2I). However, IFNγ production was comparable when we used the cell line L428 as the target (Figure 2J).

Long-term tumor control and CAR.CD30 T-cell selection in a "stressed" co-culture model

To evaluate the lytic potential of CAR.CD30 T cells, we "stressed" the co-culture conditions by re-challenging Karpas-299 cells every 5 days (Figure 3A). At each time-point, we evaluated the percentage of residual tumor, CAR expression and its relative MFI, the relative production of IFNγ, TNFα, IL2 and IL10 (24 h after each tumor re-challenge), the CD4$^+$/CD8$^+$ distribution and the memory/exhaustion profile.

Both types of III-CAR.CD30 T cells exhibited high tumor control even after multiple exposures to Karpas-299. Although we did not observe significant differences in the *in vitro* anti-tumor activity between constructs, CAR.CD30.CD28.4-1BB T cells showed high intra-donor variability in terms of tumor elimination. By contrast, CAR.CD30.CD28.OX40 T cells were endowed with more stable and predictable lymphoma recognition and killing (residual tumor cells at day +20: 8.6% ± 5.3% for 28.OX40.ζ and 27.9% ± 29.5% for 28.4-1BB.ζ T cells) (Figure 3B). Interestingly, while the percentage of CAR$^+$ cells increased after the first tumor encounter, subsequent tumor re-challenging negatively affected the percentage of residual CAR.CD30.CD28.4-1BB T cells in the *in vitro* culture (93.8% ± 2.7% at day +5 and 63.0% ± 32.30% at day +20; P=0.041) (Figure 3C); by contrast, the percentage of CAR.CD30.CD28.OX40 T cells remained stable over time (Figure 3C). This phenomenon led to a significant difference of CAR$^+$ cells at day +20 between the two types of CAR T cells (P=0.043) (Figure 3C).

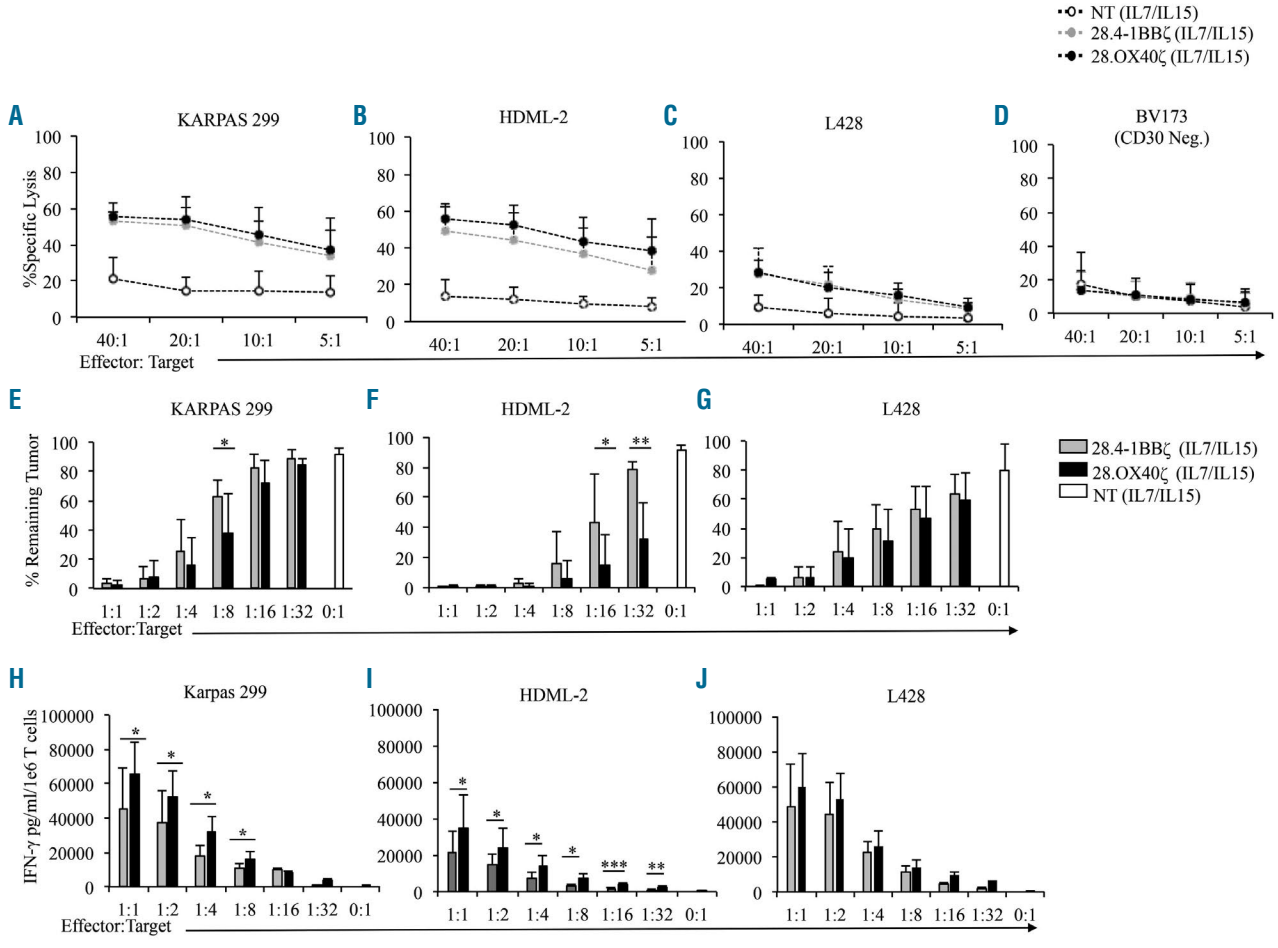


Figure 2. 28.OX40.ζ CAR T cells exert more efficient lymphoma control compared to 28.4-1BB.ζ CAR T cells at low effector:target ratios. (A-D) *In vitro* ^{51}Cr cytotoxic assay to evaluate cytolytic activity of non-transduced (NT) T cells (empty circle), 28.4-1BB.ζ T cells (gray circle) and 28.OX40.ζ T cells (black circle), on CD30$^+$ lymphoma cell lines, namely Karpas-299 (A), HDML-2 (B) and L428 (C) cells, as well as on the CD30$^-$ leukemia cell line BV173 (D). (E-G) The long-term 7-day co-culture assay was performed at decreasing effector:target ratios, from 1:1 to 1:32. In particular, 28.4-1BB.ζ (gray bars), 28.OX40.ζ (black bars) and NT (white bar) T cells were co-cultured with CD30$^+$ Karpas-299 (E), HDML-2 (F) and L428 (G) cell lines. (H-J) Interferon-gamma (IFN-γ) production after 24 h of co-culture was measured. Data from seven healthy donors are expressed as average ± standard deviation. *P≤0.05; **P≤0.01; ***P≤0.001 and ****P≤0.0001.

Similarly, the higher CAR MFI observed since day 0 in CAR.CD30.CD28.OX40 T cells compared to CAR.CD30.CD28.4-1BB T cells was retained stably over time during "stressed" co-culture experiments (Figure 3D).

Furthermore, CAR.CD30.CD28.OX40 T cells showed a significantly higher activation profile over time after tumor exposure compared to CAR.CD30.CD28.4-1BB T cells, in terms of cytokine production (Figure 3E-G), with a lower level of IL10 (produced by Karpas-299 cells, as shown by the red bar in Figure 3H.

Dynamic evolution of memory and exhaustion profiles in response to cytokine or tumor stimulation in CAR.CD30 T cells

At day +15 after transduction, most expanded CAR T cells cultured with IL2 had an effector memory (EM) phenotype (Figure 4A), with no substantial differences observed when compared with NT T cells. IL7/IL15 significantly reduced the central memory (CM) compartment, in favor of EM and effector terminal (EMRA) cells in both CAR.CD30. Interestingly, the "stressed" co-culture significantly changed the profile of CAR T cells. After 5 days of co-culture the naïve compartment decreased rapidly from 26.1% ± 13.0% to 2.6% ± 1.3% for 28.OX40.ζ (P=0.029) and from 30.1% ± 16.5% to 4.0% ± 3.0% for 28.4-1BB.ζ T cells (P=0.034). Tumor-cell encounter significantly modulated CAR T-cell subsets, while the profile of NT T cells compared to day 0 remained stable. In particular, the naïve subset was significantly reduced in both CAR T-cell types, whereas the CM subset increased from day 0 to day +20 (see Figure 4B).

We sought to evaluate the exhaustion profile modulation of CAR T cells after tumor challenge. Although no difference was recorded at day 0 (Figure 4C), we observed a significant upregulation of LAG3, TIM3, and PD-1 receptors after the first tumor-cell exposure, with CAR.CD30.CD28.OX40 T cells showing higher expression of TIM3 over time compared to CAR.CD30.CD28.4-1BB cells. Nevertheless, TIM3 was also significantly upregulated in NT T cells upon tumor exposure (Figure 4D). Interestingly, no differences were observed between III-CAR-T-cell types in terms of percentage of exhausted cells with triple positivity for LAG3/TIM3/PD-1 (Figure 4D).

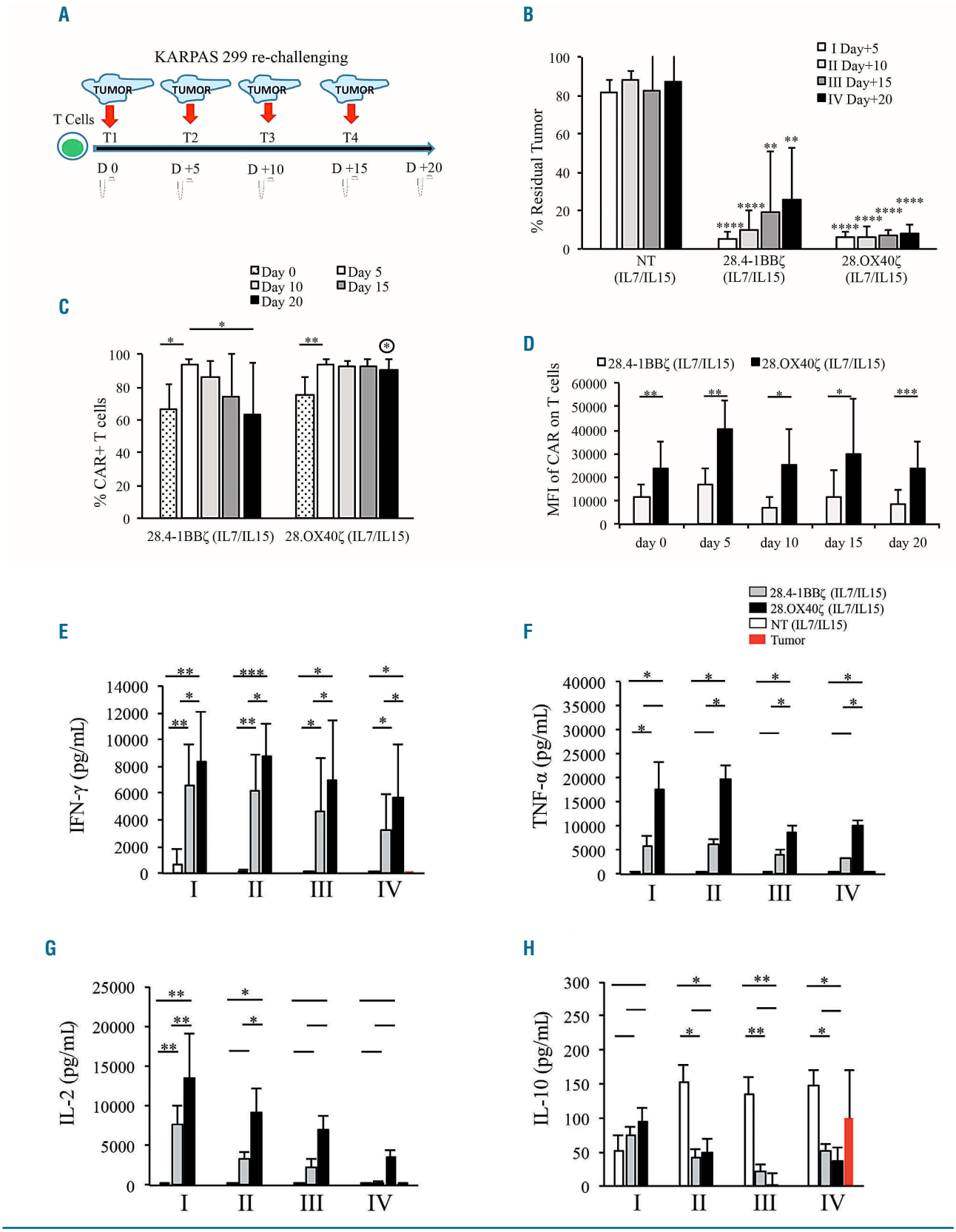
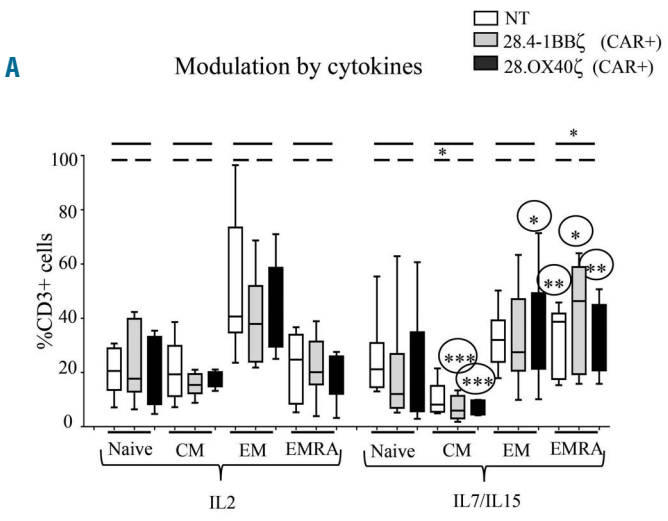
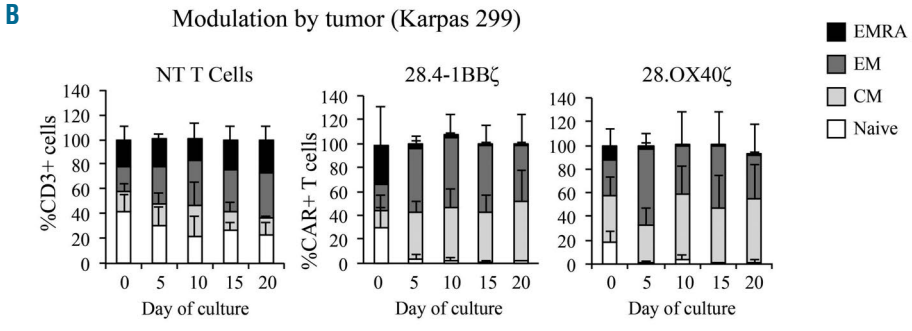
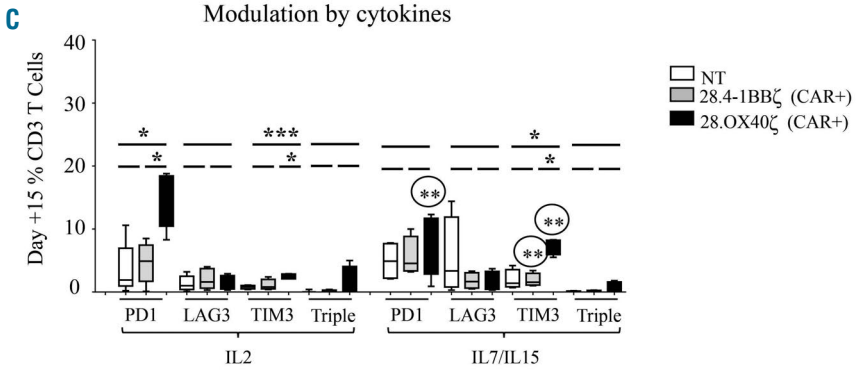


Figure 3. Long-term tumor control and CAR.CD30 T-cell selection in the "stressed" co-culture *in vitro* assay model. (A) The panel shows the experimental design of the "stressed" co-culture. (B) Residual CD30$^+$ tumor cells were quantified during the "stressed" co-culture after addition of tumor cells every 5 days. Data are shown for day +5 (white bars), day +10 (light gray bars), day +15 (dark gray bars) and day +20 (black bars). (C) The percentage of CAR$^+$ T cells was quantified during the "stressed" co-culture. Data are shown for day 0 (dotted bars, referring to the percentage of CAR$^+$ T cells before the first addition of tumor cells), day +5 (white bars), day +10 (light gray bars), day +15 (dark gray bars) and day +20 (black bars). (D) Mean fluorescence intensity (MFI) analysis of CAR expression on 28.4-1BB.ζ T cells (gray bars) and 28.0X40.ζ T cells (black bars). (E) Interferon (IFN)-γ, (F) tumor necrosis factor (TNF)-α, (G) interleukin (IL)-2 and (H) IL-10 production was analyzed in supernatants collected 24 h after addition of tumor cells to the culture. Data from seven healthy donors are expressed as average ± standard deviation. *P≤0.05; **P≤0.01; ***P≤0.001 and ****P≤0.0001. Circled asterisks refer to the difference between 28.0X40.ζ and 28.4-1BB.ζ T cells.







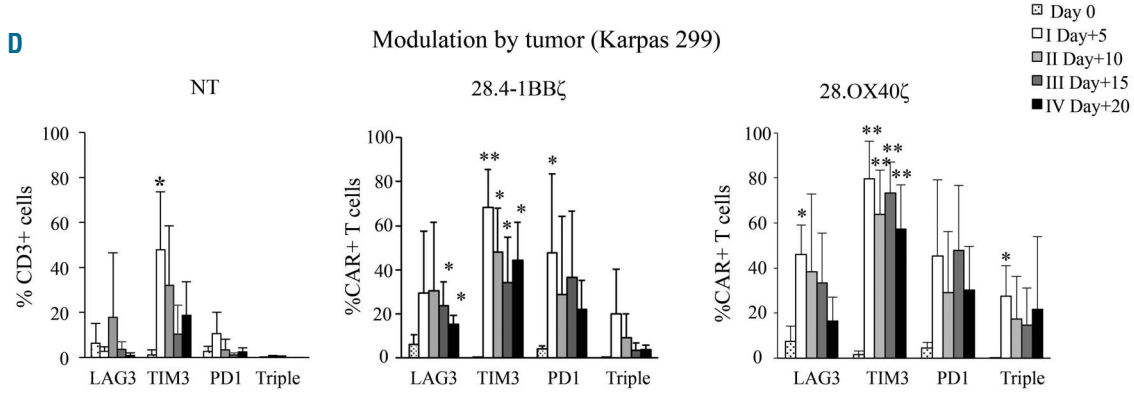


Figure 4. Memory and exhaustion profiles in CAR.CD30 T cells. (A) Non-transduced (NT; white bars), 28.4.1BB.ζ (light gray bars) or 28.0X40.ζ (dark gray bars) T cells, expanded in interleukin (IL)2 or IL7/IL15 cytokines were analyzed by flow-cytometry at day +15 of *in vitro* culture to establish the percentage of naïve, central memory (CM), effector memory (EM) and effector terminal (EMRA) CD3+ cell subsets. (B) Analysis of naïve (white bars), CM (light gray bars), EM (dark gray bars) and EMRA (black bars) CD3+ cell subsets in the long-term "stressed" co-culture for NT (left panel), 28.4-1BB.ζ (middle panel) and 28.0X40.ζ (right panel) T cells. (C) NT (white bars), 28.4.1BB.ζ (light gray bars) or 28.0X40.ζ (dark gray bars) T cells expanded in IL2 or IL7/IL15 cytokines were analyzed to assess their exhaustion profile by the expression of the three markers PD1, LAG3 and TIM3. (D) Analysis of the exhaustion profile in NT (left panel), 28.4.1BB.ζ (middle panel) and 28.0X40.ζ (right panel) T cells during the long-term "stressed" co-culture assay at day 0 (white dotted bars), Time I: day +5 (white bars), time II: day +10 (light gray bars), time III: day +15 (dark gray bars) and time IV: day +20 (black bars). Data from four healthy donors are expressed as average ± standard deviation. **P*<0.05; ***P*<0.001. Circled asterisks refer to the difference between the T-cell population grown in IL2 or in IL7/IL15.

Dynamic evolution of the CD4/CD8 ratio in response to cytokine or tumor stimulation of CAR.CD30 T cells

We also evaluated the dynamic evolution of $CD4^+$ and $CD8^+$ T cells during prolonged *in vitro* culture in the presence of either cytokine stimulation (days +5, +15 and +30 after transduction) or exposure to tumor cells. As shown by CFSE analysis, we observed that $CD8^+$ T cells had a proliferative advantage compared to $CD4^+$ T cells, whether stimulated with IL2 (Figure 5A) or IL7/IL15 (Figure 5B). This observation correlated with the evidence that, during prolonged *in vitro* culture, in the presence of cytokine stimulation, the CAR.CD30 T-cell population was significantly enriched for $CD8^+$ cells (Figure 5C and D). Indeed, irrespectively of cytokine usage (IL2 or IL7/IL15) or choice of co-stimulatory domains (28.OX40 *vs*. 28.4-1BB), $CD4^+$ T-cell percentage decreased over time up to day +30 of culture, compared with the percentage on day +5. Notably, the $CD4^+/CD8^+$ T-cell ratio remained stable over time when CAR.CD30 T cells were exposed to sequential re-challenge with Karpas-299 (Figure 5E and F), suggesting that repeated tumor stimulation induces equal expansion of CD4 and CD8 CAR^+ T cells.

Evaluation of the efficacy of CAR.CD30 T-cells in a mouse model of Hodgkin lymphoma

We next assessed whether the choice of the co-stimulatory combination or cytokines used during *in vitro* expansion might influence the *in vivo* activity of CAR.CD30 T cells against L428 cells (Figure 6A). Bioluminescence in HL-tumor-bearing mice, treated with NT T cells, rapidly increased up to 5 log in less than 50 days (Figure 6B and C) and mice either died or were sacrificed due to poor conditions. Macroscopic analysis of sacrificed mice showed large tumor masses located preferentially in the liver. HL-tumor-bearing mice treated with 28.4-1BB.ζ (IL2) survived on average significantly longer (79 ± 10 days) compared with mice treated with NT (IL2) (Figure 6D; 52 ± 9 days, P=0.008). The use of IL7/IL15 did not improve the anti-tumor effect of 28.4-1BB.ζ, in terms of both bioluminescence signal (Figure 6B and C) and overall survival (Figure 6D). The median survival of HL-tumor-bearing mice treated with 28.OX40.ζ (IL2) was significantly better than that of mice treated with either NT (IL2) (P=0.009) or 28.4-1BB.ζ (IL2) (P=0.008). Notably, the best outcome was observed in mice given 28.OX40.ζ T cells grown in the presence of IL7/IL15, as three out of five mice were still alive at the experimental end-point of day +165 (Figure 6D).

Although mice treated with NT T cells showed a significant increase in human circulating $CD45^+CD3^+$ cells with a peak evaluated at day +56 (Figure 6E), we did not observe any tumor control. Only in mice given 28.OX40.ζ T cells did we observe a long-lasting persistence of circulating CAR T cells up to day +130 (Figure 6F). The percentage of circulating 28.OX40.ζ T cells (Figure 6F) remained stable during the first 100 days. On day +165, we found residual circulating T cells in only two out of four treated mice (0.06% ± 0.02%) although all four mice were cured at this time. In these two mice, circulating CAR.CD30 T cells were equally distributed between $CD4^+$ and $CD8^+$, as CM and EM (*Online Supplementary Figure S8*). These data further confirmed *in vitro* results about the superiority of IL7/IL15 over IL2 in expanding CAR T cells. Moreover, 28.4-1BB.ζ T cells showed only slight *in vivo* expansion and persistence (Figure 6F). We also correlated the kinetics of tumor growth (bioluminescence) and CAR T-cell expansion, observing that mice receiving 28.OX40.ζ T cells showed a significant reduction of tumor burden concomitant with the $CD3^+$ peak (*Online Supplementary Figure S9A* and *B*). By contrast, in mice treated with 28.41BB.ζ, the kinetics of circulating T cells ($CD45^+CD3^+$), as well as of CAR^+ T cells, did not correlate with bioluminescence signaling (*Online Supplementary Figure S9C* and *D*).

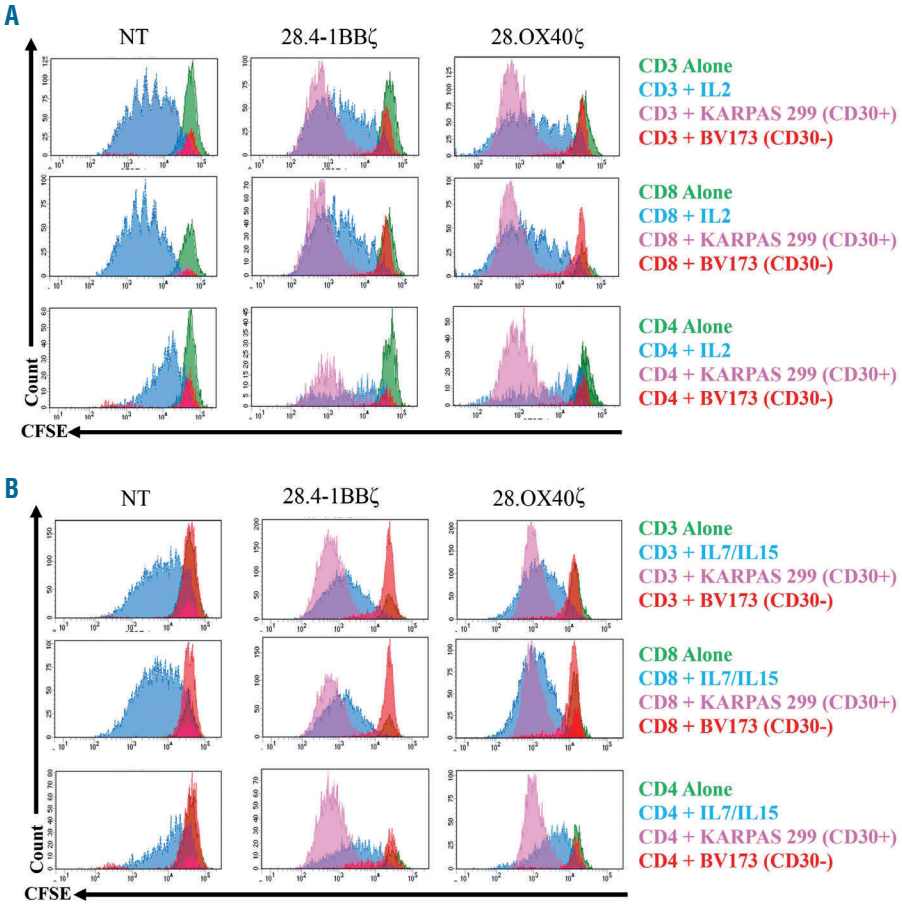
Evaluation of persistence and establishment of long-term immunological memory in the re-challenged mouse model of non-Hodgkin lymphoma

We then evaluated *in vivo* efficacy, persistence and establishment of long-term memory of CAR.CD30 T cells (IL7/IL15) in a Karpas-299 xenograft model with tumor re-challenge (Figure 7A). While tumor bioluminescence in the group treated with NT T cells progressively increased up to 5 log in less than 40 days (Figure 7B and C), in mice receiving 28.OX40.ζ T cells we observed significant tumor control (P=0.0075) as measured by reduction of the bioluminescence signal. The median survival of mice treated with NT T cells was 45.5 days, while 30% of mice given 28.4-1BB.ζ and 60% of mice given 28.OX40.ζ experienced long-term tumor control (Figure 7D). In particular, the median survival of mice treated with 28.4-1BB.ζ was 58 days (P=0.05), and undetermined for mice given 28.OX40.ζ (P=0.0002) (Figure 7D).

After 140 days, cured mice were re-challenged i.v. with Karpas-299 cells, and followed for an additional 100 days. Bioluminescence analysis showed rapid progression of the tumor in control mice (CTR mice), as well as in 28.4-1BB.ζ-treated mice. In contrast, in 28.OX40.ζ-treated mice, after an initial expansion of the tumor for the first 40 days, at day +100 (at day +240 overall), four of six mice were tumor-free, which translated into a statistically significant survival benefit (Figure 7D). To confirm the establishment of long-term immunological memory, we analyzed circulating $CD45^+CD3^+$ human cells over time in treated mice. We observed significantly greater expansion of circulating T cells in the first week after effector T-cell infusion in mice treated with 28.OX40.ζ CAR T cells (2.49% ± 1.03%) (Figure 7E) compared to mice given 28.4-1BB.ζ CAR T cells (0.27% ± 0.11%; P<0.001) or NT T cells (0.35% ± 0.07%; P=0.005).

Interestingly, at day +132 (before the second infusion of tumor cells), the number of circulating CAR T cells was negligible in all cohorts. Forty days after tumor re-challenge (day +180), we observed a significant and impressive expansion of circulating human $CD45^+CD3^+$ cells in mice treated with 28.OX40.ζ T cells (Figure 7E) compared to that in mice receiving 28.4-1BB.ζ T cells. After re-expansion, $CD3^+$ cells were significantly enriched in 28.OX40.ζ CAR^+ T cells (Figure 7F, *Online Supplementary Figure S10A-H*). This enrichment was tumor-specific, since the complete eradication of the second tumor infusion was associated with a simultaneous decline of circulating 28.OX40.ζ T cells to an undetectable percentage, as measured at day +221 (Figure 7E, *Online Supplementary Figure S10A-H*).

Finally, while human CAR.CD30 T cells were found to infiltrate tumor (*Online Supplementary Figure S11A*) independently of the co-stimulatory combination present in the CAR construct, the infiltration observed in 28.OX40.ζ (IL7/15) T-cell-treated mice was greater than that in all other conditions (*Online Supplementary Figure S11B* and *C*).



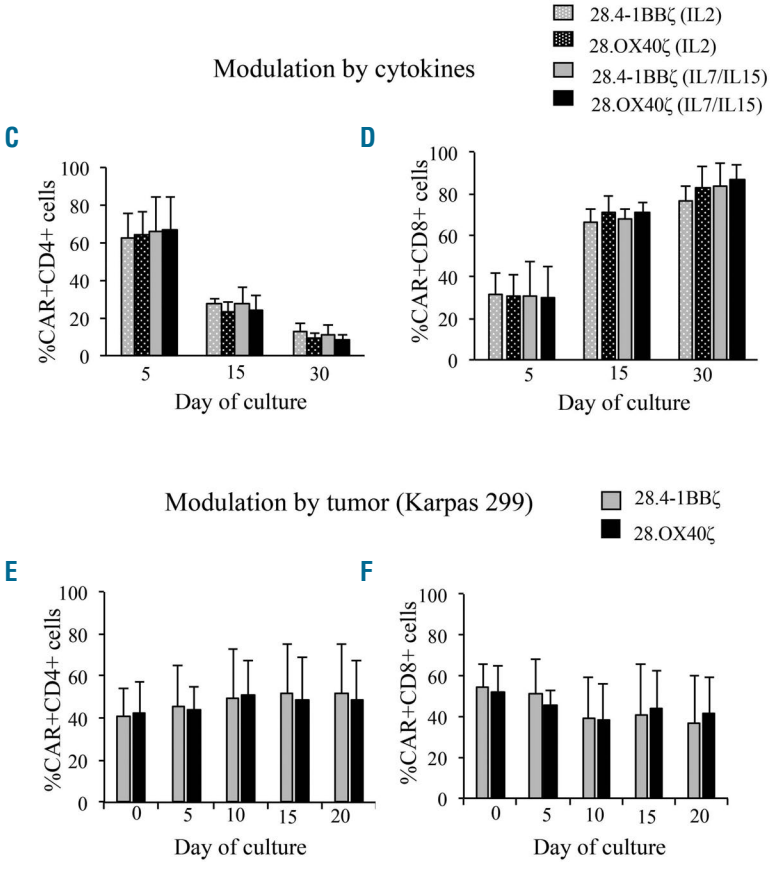


Figure 5. The CD4/CD8 CAR.CD30 T-cell ratio is modulated by both cytokines and CD30+ tumor cells. (A) Analysis of the proliferation of non-transduced (NT, left panels), 28.4.1BB.ζ (middle panels) or 28.OX40.ζ (right panels) T cells, unstimulated (green histograms), stimulated with interleukin (IL)2 cytokine (blue histograms), stimulated with CD30+ Karpas-299 cells (pink histograms) and stimulated with CD30- BV173 cells (red histograms). (B) Analysis of the proliferation of NT (left panels), 28.4.1BB.ζ (middle panels) or 28.OX40.ζ (right panels) T cells, unstimulated (green histograms), stimulated with IL7-IL15 cytokine (blue histograms), stimulated with CD30+ Karpas-299 cells (pink histograms) and stimulated with CD30- BV173 cells (red histograms). (C, D) Flow cytometric analysis of CD4+ and CD8+ CAR+ T-cell percentage evaluated during *in vitro* exposure to IL2 (28.4.1BB.ζ, dotted gray bars; 28.OX40.ζ, dotted black bars), or IL7-IL15 (28.4.1BB.ζ, gray bars; 28.OX40.ζ, black bars). (E, F) Flow cytometric analysis of CD4+ and CD8+ T-cell percentage in CAR.CD30 T cells evaluated during long-term "stressed" co-culture for 28.4.1BB.ζ (gray bars) and 28.OX40.ζ (black bars). Data from seven healthy donors are expressed as average ± standard deviation.

Discussion

To date, clinical trials conducted in adults with relapsed/refractory CD30$^+$ lymphoma, using II-CAR.CD30 T cells, led to suboptimal outcomes.[21,22] As in patients with B-cell acute lymphocytic leukemia receiving CAR.CD19 T cells,[29] a clear correlation between CAR T-cell persistence in peripheral blood and clinical benefit was reported in HL and NHL,[21,30] highlighting the need for further optimization. We, therefore, attempted to include a novel scFv, derived from the high-affinity anti-CD30 mouse AC10 monoclonal antibody, in our CAR construct.[25] In the context of high-affinity CAR, major concerns are related to CAR T-cell overstimulation, induction

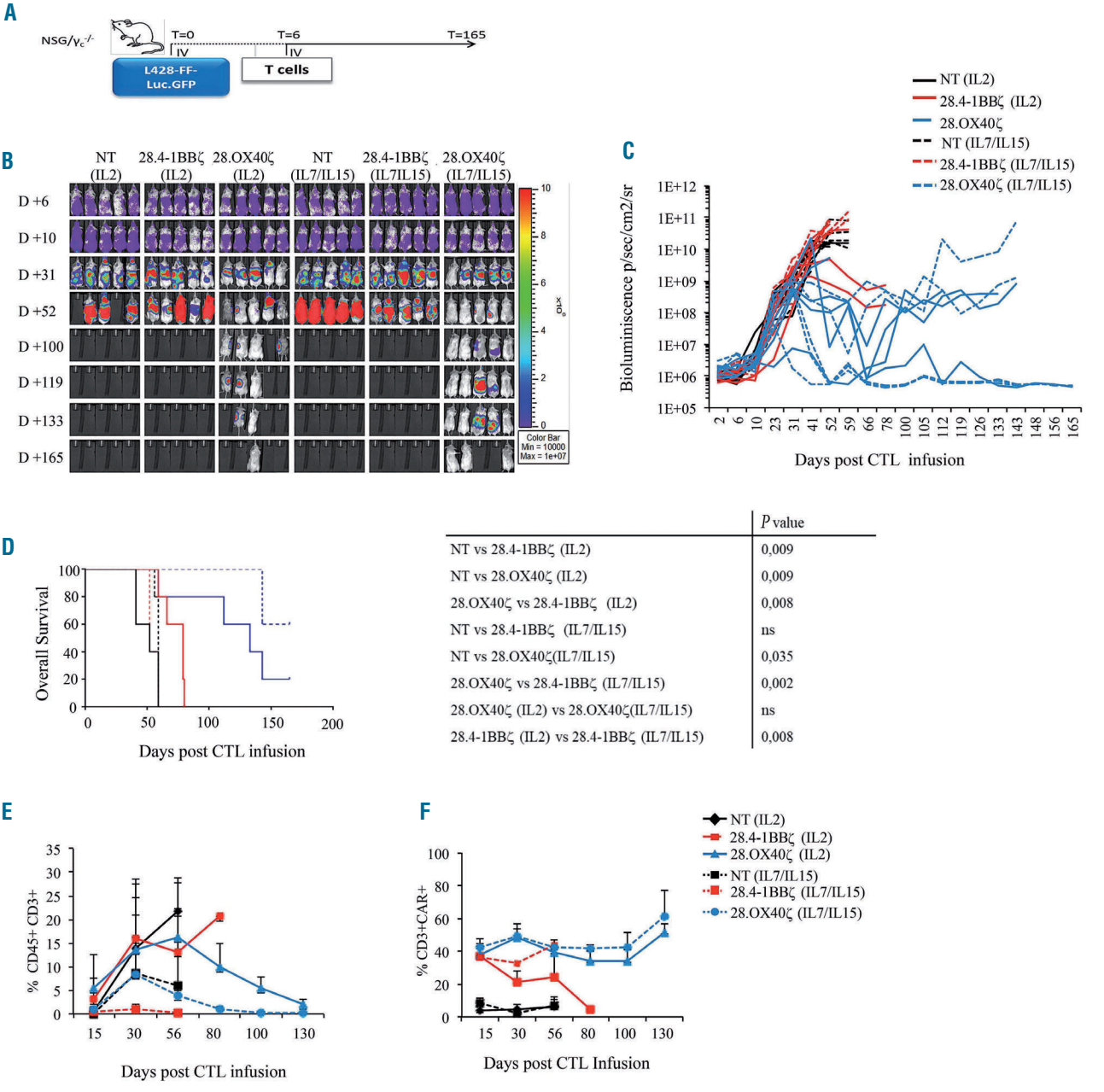


Figure 6. Mouse model of Hodgkin lymphoma to evaluate anti-lymphoma activity of CAR.CD30 T cells generated and expanded in the presence of interleukin-2 or interleukin-7/interleukin-15. (A) The schema shows the *in vivo* xenograft immunodeficient mouse model, in which Hodgkin lymphoma (HL) L428-eGFP-FFLuc cells were systemically infused into NSG mice. Effector cells were infused intravenously at the time of tumor establishment (day +6), as assessed by IVIS imaging. Blood was collected periodically from the mice. (B) IVIS imaging of tumor growth from day +6 to day +165 (end of experiment). (C) Bioluminescence of each single xenograft mouse treated with non-transduced (NT) T cells and interleukin (IL)2 (black line; 5 mice); 28.4-1BBζ T cells (IL2) (red line; 5 mice); 28.0X40ζ T cells (IL2) (blue line; 5 mice); NT T cells (IL7/IL15) (dotted black line; 5 mice); 28.4-1BBζ T cells (IL7/IL15) (dotted red line; 5 mice) and 28.0X40ζ T cells (IL7/IL15) (dotted blue line; 5 mice). (D) Kaplan-Meier survival curve analysis of tumor-bearing mice treated with NT (IL2) (black line; 5 mice), 28-0X40ζ (IL2) (blue line; 5 mice), 28-41BBζ (IL2) (red line; 5 mice), NT (IL7/IL15) (dotted black line; 5 mice), 28-0X40ζ (IL7/IL15) (dotted blue line; 5 mice) and 28-41BBζ (IL7/IL15) (dotted red line; 5 mice). *P*-values are reported in the table. (E) Average percentages of circulating human CD45$^+$ CD3$^+$ T cells in mice treated with NT (IL2) (black line; 5 mice), 28-0X40ζ (IL2) (blue line; 5 mice), 28-41BBζ (IL2) (red line; 5 mice), NT (IL7/IL15) (dotted black line; 5 mice), 28-0X40ζ (IL7/IL15) (dotted blue line; 5 mice) and 28-41BBζ (IL7/II15) (dotted red line; 5 mice). (F) Average percentages of circulating human CD3$^+$ CAR$^+$ T cells in mice treated with NT (IL2) (black line; 5 mice), 28-0X40ζ (IL2) (blue line; 5 mice), 28-41BBζ (IL2) (red line; 5 mice), NT (IL7/IL15) (dotted black line; 5 mice), 28-0X40ζ (IL7/IL15) (dotted blue line; 5 mice) and 28-41BBζ (IL7/II15) (dotted red line; 5 mice).

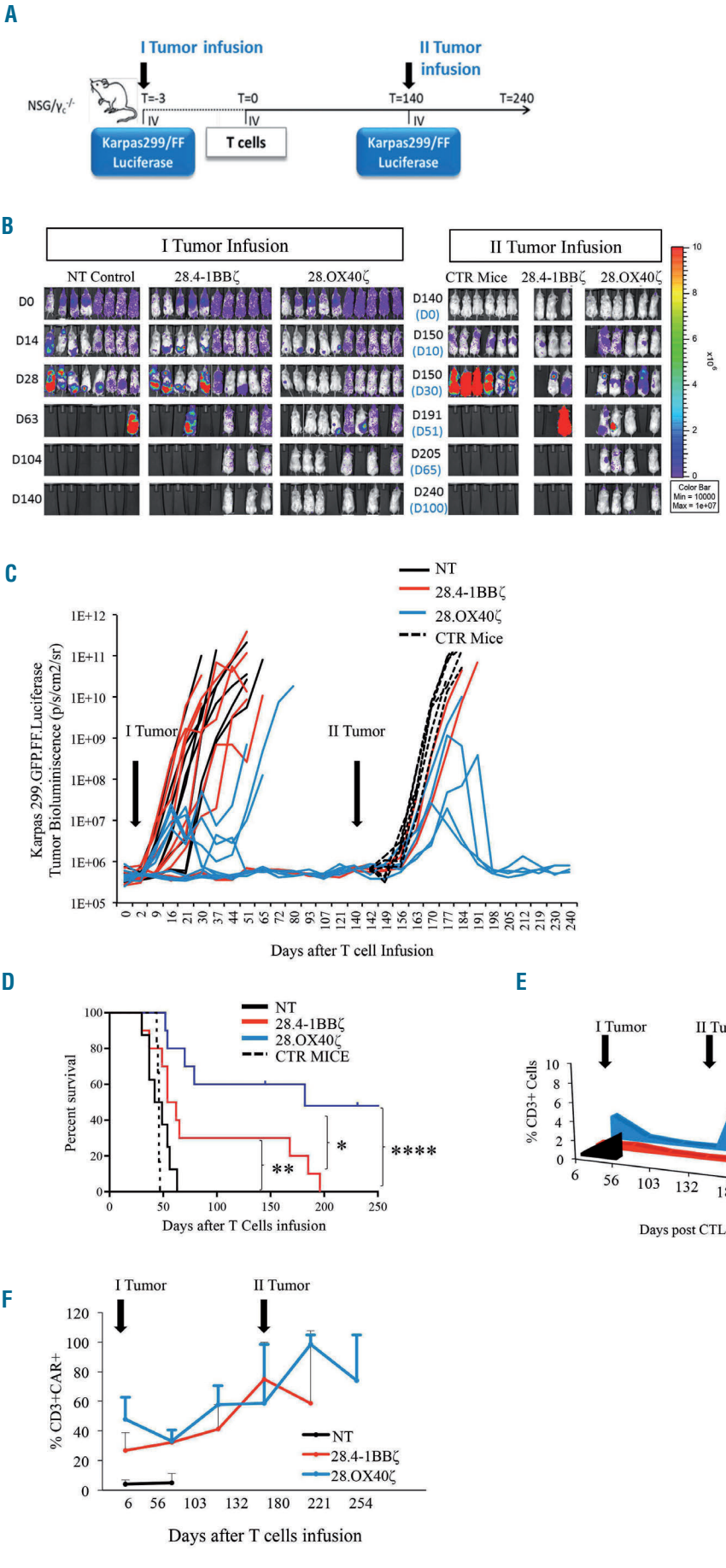


Figure 7. Re-challenge of the non-Hodgkin lymphoma mouse model to evaluate long-term anti-lymphoma activity of CAR.CD30 T cells in generating an efficient immunological memory. (A) The schema shows the *in vivo* xenograft immunodeficient re-challenge mouse model, in which non-Hodgkin lymphoma Karpas-299-eGFP-FFLuc cells were systemically infused into NSG mice, at day -3 and day +140. Effector cells were infused intravenously only once, at the time of tumor establishment (day 0) assessed by IVIS imaging. Blood was collected periodically from the mice. (B) IVIS imaging of tumor growth from day 0 to day +240 (end of experiment). At day +140, surviving mice treated with CAR.CD30 T cells (2 mice treated with 28-41BBζ and 4 mice with 28.OX40ζ T cells) received the second intravenous infusion of tumor. As a control, six mice were given only Karpas-299-eGFP-FFLuc cells (CTR Mice). Days from the tumor re-challenge are shown in blue. (C) Bioluminescence of each single xenograft mouse treated with NT (black lines; 8 mice); 28.4-1BBζ T cells (red lines; 10 mice); 28.OX40ζ T cells (blue line; 10 mice). Bioluminescence in the control cohort of the tumor re-challenge (CTR Mice) is shown by black dotted lines. Tumor infusions are represented by black arrows. (D) Kaplan-Meier survival curve analysis of tumor-bearing mice treated with non-transduced (NT, black line), 28.4-1BBζ (red line), 28.OX40ζ (blue line). Overall survival of control mice is shown by a dotted black line. *P<0.05; **P<0.001; ***P<0.0001; ****P<0.00001. (E) Three-dimensional area graph showing the percentage of circulating human CD3+ T cells during long-term *in vivo* experiments of mice treated with NT (black area), 28.4-1BBζ T cells (red area) and 28.OX40ζ T cells (blue area). Tumor infusions are represented by black arrows. (F) Average percentages of circulating human CD3+/CAR+ T cells in mice treated with NT (black line), 28.4-1BBζ T cells (red line) and 28.OX40ζ T cells (blue line). Black arrows represent tumor infusions.

of exhaustion and limited *in vivo* persistence. Moreover, in the case of CAR.CD30, the low CD30 expression on CD3$^+$ T cells could also cause chronic antigen stimulation and the occurrence of cellular fratricide.[31]

Our experimental data indicate that the inclusion of an AC10-derived scFv in the CAR construct, independently of the co-stimulatory domains, was not associated with exhaustion, even after multiple CD30$^+$ lymphoma-cell stimulations. Furthermore, we did not observe fratricidal activity among CAR.CD30 T-cell populations. With respect to co-stimulatory domains, we comparatively evaluated two III-CAR.CD30, incorporating either CD28.OX40 or CD28.4-1BB. The clinical impact of combining co-stimulatory domains has not yet been clearly established, and it may be construct- and disease-specific.[32,33] However, in the setting of repetitive antigen engagement, driving T-cell maturation to terminally differentiated cells associated with loss of CCR7, the combined CD28ζ-OX40 signaling CAR rescued CCR7$^-$ T cells from apoptosis resulting, in turn, in more efficient antitumor efficacy.[34] For early clinical development, trial designs comparing two CAR T cells simultaneously administered to the same patient have provided invaluable evidence of the pharmacokinetic effect of co-stimulatory domains.[35-37] Ultimately, experimental evidence[38,39] suggests that the positioning of co-stimulatory domains within the endodomain of a CAR can influence CAR T-cell activity, and no algorithm, up to now, has been able to predict which co-stimulatory combination is optimal for a specific CAR construct, making the search for optimized activity strictly dependent on experimental conditions. We recently showed the advantage of using the CD28.4-1BB co-stimulatory domain to optimize CAR T-cell therapy targeting GD2$^+$ neuroblastoma.[40] In the current study, however, we observed an *in vivo* superiority of the CAR.CD30 construct incorporating the CD28.OX40 co-stimulatory domains, in terms of both anti-lymphoma activity and CAR T-cell persistence. We also confirmed the *in vitro* data in an *in vivo* model, showing greater stability of the CAR.CD30.CD28.OX40 T-cell population, both in terms of CAR$^+$ cell percentage and CAR expression (MFI), even after repeated/prolonged exposures to tumor. CAR.CD30.CD28.OX40 T-cell activation profile correlates with efficient tumor control, stable expression of CAR molecule on the cell membrane and high production of IFN-γ, TNF-α and IL2 cytokines (Th1 profile). Evaluation of the cytokine activation profile is especially relevant in the context of lymphoma. Indeed, HL malignant cells express high levels of PDL1 and produce the immunosuppressive IL10, TGFβ, galectin 1 and prostaglandin E2 molecules, which inhibit T-cell effector functions and induce apoptosis of activated Th1 and CD8$^+$ T cells.[41,42] We demonstrated that CAR.CD30.CD28.OX40 T cells and, in particular, the CD8$^+$ fraction, exert significant and prolonged anti-lymphoma activity even in this strongly immune-modulating environment.

Importantly, we confirmed that the manufacturing process based on IL7/IL15 is crucial for optimizing CAR T-cell activity also in the lymphoma setting. In particular, we proved, both *in vitro* and *in vivo*, that CAR.CD30 T cells (IL7/IL15) systematically exposed to CD30$^+$ lymphoma cells were significantly enriched in CM and EM subpopulations, in both CD4$^+$ and CD8$^+$ T-cell subsets. Moreover, in a NHL xenograft mouse model, in which we mimic lymphoma relapse through tumor re-challenge, CAR.CD30.CD28.OX40 T cells were able to re-expand significantly and exert tumor control. We also showed that the number of CAR.CD30.CD28.OX40 T cells declined in peripheral blood upon lymphoma eradication. Thorough characterization of mouse tissues after long-term *in vivo* experiments (day +240) revealed the presence of CAR.CD30.CD28.OX40 T cells in several organs, including bone marrow, lymph nodes, kidney, liver, spleen and thyroid.

The inclusion of the inducible "safety switch" iCasp9[43] is crucial to render the therapeutic approach safer, controlling potential unwanted side effects in the context of CAR T cells. We showed both *in vitro* and *in vivo* that AP1903 is able to significantly reduce iCasp9.CAR.CD30 cells. However, the persistence, albeit at very low levels, of genetically modified T cells with a low expression of CAR.CD30 after AP1903 treatment cannot be excluded.

Overall, the significant *in vivo* reactivity, the high potency, the negligible toxicity in animals and the long persistence of CAR.CD30.CD28.OX40 T cells contribute to the value of this CAR design, which will be tested in a clinical trial for patients with relapsed/refractory HL and anaplastic large-cell lymphoma.

Disclosures

No conflicts of interest to disclose. A patent application has been made (n. 102018000003464).

Contributions

MG, CQ, BDA and FL designed experimental studies, supervised the conduction of the project, analyzed the data and wrote the manuscript. MG, DO, SDC, MS, SC, IB, ZA, AC, BC, KB, IC, CDS, MP, EG, MS, SM, RC and RDV performed the in vitro experiments. CDS and MP performed immunohistochemistry assays. MG, IB, BDA and CQ performed the in vivo experiments. DO, MG and BDA cloned the retroviral vector. MG, EG, MS and MS performed FACS analysis. AR, FDB, PM, LV, KG, RDV, LM and FL provided patients' samples, medical advice and expertise in pediatric lymphoma. SB, ACi and MT analyzed data. All authors read and approved the final version of the manuscript.

Acknowledgments

We are grateful to Bellicum Pharmaceuticals for kindly providing the AP1903 dimerizing drug.

Funding

The experimental work was supported by grants awarded by Ricerca Finalizzata GR-2016-02364546 (to BDA), Associazione Italiana Ricerca per la Ricerca sul Cancro (AIRC)-Special Project 5×1000 n. 9962 (to FL), AIRC IG 2018 id. 21724 (to FL), Ricerca Finalizzata GR-2013-02359212 (to CQ), Ricerca Corrente (to CQ and BDA). Progetto Ministeriale CAR-T (to FL), and Associazione "Raffaele Passarelli" Onlus (to BDA).

References

1. Sadelain M. Chimeric antigen receptors: driving immunology towards synthetic biology. Curr Opin Immunol. 2016;41:68-76.
2. Schuster SJ, Svoboda J, Chong EA, et al. Chimeric antigen receptor T cells in refractory B-cell lymphomas. N Engl J Med. 2017;377(26):2545-2554.
3. Locke FL, Ghobadi A, Jacobson CA, et al. Long-term safety and activity of axicabtagene ciloleucel in refractory large B-cell lymphoma (ZUMA-1): a single-arm, multicentre, phase 1-2 trial. Lancet Oncol. 2019;20(1):31-42.
4. Rezvani AR, Storer B, Maris M, et al. Nonmyeloablative allogeneic hematopoietic cell transplantation in relapsed, refractory, and transformed indolent non-Hodgkin's lymphoma. J Clin Oncol. 2008;26(2):211-217.
5. von Tresckow B, Moskowitz CH. Treatment of relapsed and refractory Hodgkin lymphoma. Semin Hematol. 2016;53(3):180-185.
6. Steidl C, Gascoyne RD. The molecular pathogenesis of primary mediastinal large B-cell lymphoma. Blood. 2011;118(10):2659-2669.
7. Sabattini E, Pizzi M, Tabanelli V, et al. CD30 expression in peripheral T-cell lymphomas. Haematologica. 2013;98(8):e81-82.
8. Bossard C, Dobay MP, Parrens M, et al. Immunohistochemistry as a valuable tool to assess CD30 expression in peripheral T-cell lymphomas: high correlation with mRNA levels. Blood. 2014;124(19):2983-2986.
9. Berger GK, Gee K, Votruba C, McBride A, Anwer F. Potential application and prevalence of the CD30 (Ki-1) antigen among solid tumors: a focus review of the literature. Crit Rev Oncol Hematol. 2017;113:8-17.
10. Pallesen G, Hamilton-Dutoit SJ. Ki-1 (CD30) antigen is regularly expressed by tumor cells of embryonal carcinoma. Am J Pathol. 1988;133(3):446-450.
11. Hittmair A, Rogatsch H, Hobisch A, Mikuz G, Feichtinger H. CD30 expression in seminoma. Hum Pathol. 1996;27(11):1166-1171.
12. de Bruin PC, Gruss HJ, van der Valk P, Willemze R, Meijer CJ. CD30 expression in normal and neoplastic lymphoid tissue: biological aspects and clinical implications. Leukemia. 1995;9(10):1620-1627.
13. Agrawal B, Reddish M, Longenecker BM. CD30 expression on human CD8+ T cells isolated from peripheral blood lymphocytes of normal donors. J Immunol. 1996;157(8):3229-3234.
14. Bonthapally V, Wu E, Macalalad A, et al. Brentuximab vedotin in relapsed/refractory Hodgkin lymphoma post-autologous transplant: meta-analysis versus historical data. Curr Med Res Opin. 2015;31(5):993-1001.
15. Chen R, Gopal AK, Smith SE, et al. Five-year survival and durability results of brentuximab vedotin in patients with relapsed or refractory Hodgkin lymphoma. Blood. 2016;128(12):1562-1566.
16. Pro B, Advani R, Brice P, et al. Five-year results of brentuximab vedotin in patients with relapsed or refractory systemic anaplastic large cell lymphoma. Blood. 2017;130(25):2709-2717.
17. Moskowitz CH, Nademanee A, Masszi T, et al. Brentuximab vedotin as consolidation therapy after autologous stem-cell transplantation in patients with Hodgkin's lymphoma at risk of relapse or progression (AETHERA): a randomised, double-blind, placebo-controlled, phase 3 trial. Lancet. 2015;385(9980):1853-1862.
18. Thurber GM, Schmidt MM, Wittrup KD. Antibody tumor penetration: transport opposed by systemic and antigen-mediated clearance. Adv Drug Deliv Rev. 2008;60(12):1421-1434.
19. Savoldo B, Rooney CM, Di Stasi A, et al. Epstein Barr virus specific cytotoxic T lymphocytes expressing the anti-CD30zeta artificial chimeric T-cell receptor for immunotherapy of Hodgkin disease. Blood. 2007;110(7):2620-2630.
20. Di Stasi A, De Angelis B, Rooney CM, et al. T lymphocytes coexpressing CCR4 and a chimeric antigen receptor targeting CD30 have improved homing and antitumor activity in a Hodgkin tumor model. Blood. 2009;113(25):6392-6402.
21. Wang CM, Wu ZQ, Wang Y, et al. Autologous T cells expressing CD30 chimeric antigen receptors for relapsed or refractory Hodgkin lymphoma: an open-label phase I trial. Clin Cancer Res. 2017;23(5):1156-1166.
22. Ramos CA, Ballard B, Zhang H, et al. Clinical and immunological responses after CD30-specific chimeric antigen receptor-redirected lymphocytes. J Clin Invest. 2017;127(9):3462-3471.
23. Louis CU, Savoldo B, Dotti G, et al. Antitumor activity and long-term fate of chimeric antigen receptor-positive T cells in patients with neuroblastoma. Blood. 2011;118(23):6050-6056.
24. Heczey A, Louis CU, Savoldo B, et al. CAR T cells administered in combination with lymphodepletion and PD-1 inhibition to patients with neuroblastoma. Mol Ther. 2017;25(9):2214-2224.
25. Wahl AF, Klussman K, Thompson JD, et al. The anti-CD30 monoclonal antibody SGN-30 promotes growth arrest and DNA fragmentation in vitro and affects antitumor activity in models of Hodgkin's disease. Cancer Res. 2002;62(13):3736-3742.
26. Quintarelli C, Orlando D, Boffa I, et al. Choice of costimulatory domains and of cytokines determines CAR T-cell activity in neuroblastoma. Oncoimmunology. 2018;7(6):e1433518.
27. Di Stasi A, De Angelis B, Savoldo B. Gene therapy to improve migration of T cells to the tumor site. Methods Mol Biol. 2010;651:103-118.
28. Zheng Z, Chinnasamy N, Morgan RA. Protein L: a novel reagent for the detection of chimeric antigen receptor (CAR) expression by flow cytometry. J Transl Med. 2012;10:29.
29. Zhu Y, Tan Y, Ou R, et al. Anti-CD19 chimeric antigen receptor-modified T cells for B-cell malignancies: a systematic review of efficacy and safety in clinical trials. Eur J Haematol. 2016;96(4):389-396.
30. Turtle CJ, Hanafi LA, Berger C, et al. Immunotherapy of non-Hodgkin's lymphoma with a defined ratio of CD8+ and CD4+ CD19-specific chimeric antigen receptor-modified T cells. Sci Transl Med. 2016;8(355):355ra116.
31. Hombach AA, Rappl G, Abken H. Blocking CD30 on T cells by a dual specific CAR for CD30 and colon cancer antigens improves the CAR T cell response against CD30(-) tumors. Mol Ther. 2019;27(10):1825-1835.
32. Weinkove R, George P, Dasyam N, McLellan AD. Selecting costimulatory domains for chimeric antigen receptors: functional and clinical considerations. Clin Transl Immunol. 2019;8(5):e1049.
33. Hombach AA, Rappl G, Abken H. Arming cytokine-induced killer cells with chimeric antigen receptors: CD28 outperforms combined CD28-OX40 "super-stimulation". Mol Ther. 2013;21(12):2268-2277.
34. Hombach AA, Chmielewski M, Rappl G, Abken H. Adoptive immunotherapy with redirected T cells produces CCR7- cells that are trapped in the periphery and benefit from combined CD28-OX40 costimulation. Hum Gene Ther. 2013;24(3):259-269.
35. Cheng Z, Wei R, Ma Q, et al. In vivo expansion and antitumor activity of coinfused CD28- and 4-1BB-engineered CAR-T cells in patients with B cell leukemia. Mol Ther. 2018;26(4):976-985.
36. Savoldo B, Ramos CA, Liu E, et al. CD28 costimulation improves expansion and persistence of chimeric antigen receptor-modified T cells in lymphoma patients. J Clin Invest. 2011;121(5):1822-1826.
37. Ramos CA, Rouce R, Robertson CS, et al. In vivo fate and activity of second- versus third-generation CD19-specific CAR-T cells in B cell non-Hodgkin's lymphomas. Mol Ther. 2018;26(12):2727-2737.
38. Pule MA, Straathof KC, Dotti G, Heslop HE, Rooney CM, Brenner MK. A chimeric T cell antigen receptor that augments cytokine release and supports clonal expansion of primary human T cells. Mol Ther 2005;12(5):933-941.
39. Hombach AA, Heiders J, Foppe M, Chmielewski M, Abken H. OX40 costimulation by a chimeric antigen receptor abrogates CD28 and IL-2 induced IL-10 secretion by redirected CD4(+) T cells. Oncoimmunology. 2012;1(4):458-466.
40. Orlando D, Miele E, De Angelis B, et al. Adoptive immunotherapy using PRAME-specific T cells in medulloblastoma. Cancer Res. 2018;78(12):3337-3349.
41. Wein F, Kuppers R. The role of T cells in the microenvironment of Hodgkin lymphoma. JJ Leukoc Biol. 2016;99(1):45-50.
42. Wein F, Weniger MA, Hoing B, et al. Complex immune evasion strategies in classical Hodgkin lymphoma. Cancer Immunol Res. 2017;5(12):1122-1132.
43. Gargett T, Brown MP. The inducible caspase-9 suicide gene system as a "safety switch" to limit on-target, off-tumor toxicities of chimeric antigen receptor T cells. Front Pharmacol. 2014;5:235.

Ferrata Storti Foundation

The ASXL1-G643W variant accelerates the development of CEBPA mutant acute myeloid leukemia

Teresa D'Altri,[1,2,3] Anna S. Wilhelmson,[1,2,3] Mikkel B. Schuster,[1,2,3] Anne Wenzel,[1,2,3] Adrija Kalvisa,[1,2,3] Sachin Pundhir,[1,2,3] Anne Meldgaard Hansen[1,2,3] and Bo T. Porse[1,2,3]

[1]The Finsen Laboratory, Rigshospitalet, Faculty of Health Sciences, University of Copenhagen; [2]Biotech Research and Innovation Centre (BRIC), University of Copenhagen and [3]Danish Stem Cell Center (DanStem) Faculty of Health Sciences, University of Copenhagen, Copenhagen, Denmark

Haematologica 2021
Volume 106(4):1000-1007

ABSTRACT

ASXL1 is one of the most commonly mutated genes in myeloid malignancies, including myelodysplastic syndrome (MDS) and acute myeloid leukemia (AML). In order to further our understanding of the role of ASXL1 lesions in malignant hematopoiesis, we generated a novel knockin mouse model carrying the most frequent *ASXL1* mutation identified in MDS patients, *ASXL1* p.G643WfsX12. Mutant mice neither displayed any major hematopoietic defects nor developed any apparent hematological disease. In AML patients, *ASXL1* mutations co-occur with mutations in *CEBPA* and we therefore generated compound *Cebpa* and *Asxl1* mutated mice. Using a transplantation model, we found that the mutated *Asxl1* allele significantly accelerated disease development in a CEBPA mutant context. Importantly, we demonstrated that, similar to the human setting, *Asxl1* mutated mice responded poorly to chemotherapy. This model therefore constitutes an excellent experimental system for further studies into the clinically important question of chemotherapy resistance mediated by mutant ASXL1.

Correspondence:

BO PORSE
bo.porse@finsenlab.dk

Received: August 16, 2019.

Accepted: March 19, 2020.

Pre-published: May 7, 2020.

https://doi.org/10.3324/haematol.2019.235150

©2021 Ferrata Storti Foundation

Material published in Haematologica is covered by copyright. All rights are reserved to the Ferrata Storti Foundation. Use of published material is allowed under the following terms and conditions: https://creativecommons.org/licenses/by-nc/4.0/legalcode. Copies of published material are allowed for personal or internal use. Sharing published material for non-commercial purposes is subject to the following conditions: https://creativecommons.org/licenses/by-nc/4.0/legalcode, sect. 3. Reproducing and sharing published material for commercial purposes is not allowed without permission in writing from the publisher.

Introduction

Additional sex comb-like 1 (*ASXL1*) is a frequently mutated gene in myeloid malignancies including myelodysplastic syndrome (MDS) and acute myeloid leukemia (AML).[1,2] Moreover, *ASXL1* mutations are also highly prevalent in premalignant states such as clonal hematopoiesis of indeterminate potential (CHIP), demonstrating that *ASXL1* lesions are early driver events with the potential to predispose for further malignant transformation.[3,4] The vast majority of *ASXL1* mutations are located in the last exon and are deletions, insertions, or substitutions resulting in stop codon mutations and truncation of the ASXL1 protein.[1,2] Mutations are always monoallelic and mRNA expression levels are variable. Due to difficulties in detecting ASXL1 in human samples, *ASXL1* mutations were originally believed to be loss of function lesions and consequently haploinsufficient.[5] However, in a more recent work, the truncated protein can indeed be detected, raising the possibility that *ASXL1* mutations may act as dominant negative or gain of function variants.[6]

Mechanistically, ASXL1 is a dual function epigenetic regulator. Specifically, it interacts directly with the BRCA1-associated protein 1 (BAP1) to form a complex which de-ubiquitinates H2AK119Ub, a repressive histone mark deposited by the polycomb repressive complex 1 (PRC1).[5,7,8] Moreover, ASXL1 interacts with the components of the polycomb repressive complex 2 (PRC2) which deposits the H3K27me3 repressive mark.[5,9]

The interest in the role of ASXL1 in malignant hematopoiesis has spurred the development of several *Asxl1* knockout mouse models[10-12] (for a recent review, see[13]) Although these models do not result in identical phenotypes, they all show phenotypes consistent with human MDS. Interestingly, overexpression of a truncated form of *Asxl1* yielded similar results suggesting that the mutations found in patients

result in a dominant-negative version of the protein.[6] In line with these findings, several reports have indicated that truncated ASXL1 enhances BAP1 complex activity, thereby promoting depletion of the H2AK119Ub mark and aberrant myeloid differentiation.[14,15] More refined modeling of ASXL1 function in hematological malignancies has been performed by knockin of patient-specific ASXL1 lesions into the murine *Asxl1* locus.[16,17] These knockin mice generally exhibit more subtle phenotypes compared to the complete deletion of the gene. Although heterozygous knockin mice do no develop MDS or AML, the knockin alleles collaborate with other leukemic drivers such as MN1 and RUNX1 or accelerate AML development in an insertional mutagenesis setting.[16,17]

CEBPA is a key myeloid transcription factor which is mutated in approximately 10% of AML patients and biallelic CEBPA mutant AML constitutes a specific AML subtype.[18-20] These patients either harbor biallelic N-terminal lesions or, more frequently, combine these lesions with a C-terminal mutation. Whereas the N-terminal lesions promote the expression of the N-terminally truncated p30 isoform, C-terminal mutations result in variants that are unable to dimerize and are consequently inactive. Hence, the genetic lesions in biallelic CEBPA mutant AML converge at the expression of the N-terminally truncated p30 isoform in the form of CEBPA-p30 homodimers.[20] In stark contrast to full-length CEBPA, CEBPA-p30 is not able to repress E2F-mediated cell cycle progression[21] and recent work has also identified specific downstream targets of this oncogenic CEBPA variant.[22] Importantly, mice in which CEBPA-p30 expression is driven from the endogenous *Cebpa* locus develop AML within the first year of their lives.[21] Interestingly, mutations in ASXL1 are frequent in biallelic CEBPA mutant AML, but how these two sets of lesions interact functionally is currently unknown.[23,24]

In the present work, we generated a novel *Asxl1* knockin line by introducing the most common disease-associated mutation (p.G643WfsX12) into the murine *Asxl1* allele.[2,25] In order to assess the importance of *Asxl1* lesions in the context of biallelic CEBPA mutated AML, we combined lesions in these two proteins and found that the ASXL1 mutation accelerated the development of CEBPA-p30 driven AML. Gene expression analysis yielded potential drivers of the accelerated phenotype. Interestingly, ASXL1 mutated AML were largely refractory to chemotherapy, thereby paralleling the findings from the human setting.

Methods

Generation of the *Asxl1*^{G643W} knockin mice

The *Asxl1G*^{643W} knockin line was generated using the double nicking CRISPR-Cas9 system in embryonic stem cells (ESC), followed by blastocyst injection. Two pspCas9n-2A-Puro constructs containing the two Asxl1 target sequences were electroporated into C57BL/6N ESCs together with a 141-mer single stranded (ss) DNA correction template containing the desired mutation. ESC clones were screened for the presence of the mutation and correctly targeted clones were injected into mouse blastocysts. Please refer to the *Online Supplementary Appendix* for additional details.

F1 offspring were backcrossed into C57BL/6 and maintained on that background. Animals were housed in a specific-pathogen-free facility and all procedures were approved by the Danish Animal Ethical Committee.

In vivo acute myeloid leukemia development

Bone marrow (BM) cells were retrieved and frozen in fetal calf serum (FCS) with 10% DMSO. For leukemic experiments, stored BM was thawed and 2 million viable cells were transplanted into lethally irradiated (900 Gy) recipients by tail vein injection. Three weeks later, recipients were subjected to three intraperitoneal injections with poly-IC (0.3 mg in 200 μL PBS, GE Healthcare) separated by 48 hours. Recipient mice were monitored for leukemic development and euthanized when moribund. Please refer to the *Online Supplementary Appendix* for additional details.

For the chemotherapy experiments, we transplanted cohorts of sublethally irradiated recipients with frozen secondary AML. Three weeks after transplant half the mice in each cohort were treated for 3 days with cytarabine 50 mg/kg and doxorubicine 1 mg/kg and for 2 days with cytarabine 50 mg/kg. The remaining mice received PBS as vehicle treatment. 25-30 μL of blood were harvested for analysis three days after the last injection. Leukemic cell numbers were determined by combining cell counting with CD45.1 (recipient)/ CD45.2 (donor) flow cytometry. For the survival study, the mice were observed for signs of disease and euthanized when moribund.

Flow cytometry analysis and cell sorting

For blood analysis, 50 μL blood was collected from the facial vein. Erythrocytes were depleted with BD PharmLyse. For BM analysis, cells were collected by crushing tibia, femur and ilium and filtered. Blood or BM nucleated cells were washed in PBS with 3% FCS and stained for 15 min at 4°C. Please refer to the *Online Supplementary Appendix* for additional details (antibodies and marker combinations).

Statistics

Unpaired t-test was used to compare values in the different groups. Log-rank (Mantel-Cox) test was used to compare survival distributions. For the chemotherapy data in Figure 5B a one-tailed Mann-Whitney U test was used.

RNA sequencing

Donor derived AML blasts (CD45.2, Ter119-, B220-, CD3-, Mac1low, Gr1low, c-Kit^{+}) were sorted from frozen BM samples into RLT lysis buffer (Qiagen) and RNA was extracted using the RNA Microkit (Qiagen). 100 ng RNA was used for the library generation, using TruSeq-V2 kit (Illumina). The libraries were analyzed by Qbit (ThermoFisher) and Bioanalyzer (Agilent) and pooled in equimolar amounts. Multiplexed samples were sequenced on a NextSeq 500 (Illumina) yielding approximately 35-45 million reads per sample. Please refer to the *Online Supplementary Appendix* for additional details.

Results

Generation of the *Asxl1*^{G643W} knockin mouse line

In order to model the role of ASXL1 lesions in hematopoietic malignancies in the best possible manner, we decided to generate a mouse line expressing the most common ASXL1 mutation (G643WfsX12, from hereon G643W) found in MDS patients.[2,25] Specifically, we used a double nicking CRISPR-Cas9 system in combination with a 141 bp ssDNA donor strand to introduce the c.1934dupG mutation into the endogenous *Asxl1* locus. This approach results in the insertion of a G within a stretch of eigth G located in the last exon of *Asxl1* which in turn generates a frameshift and an in-frame stop codon

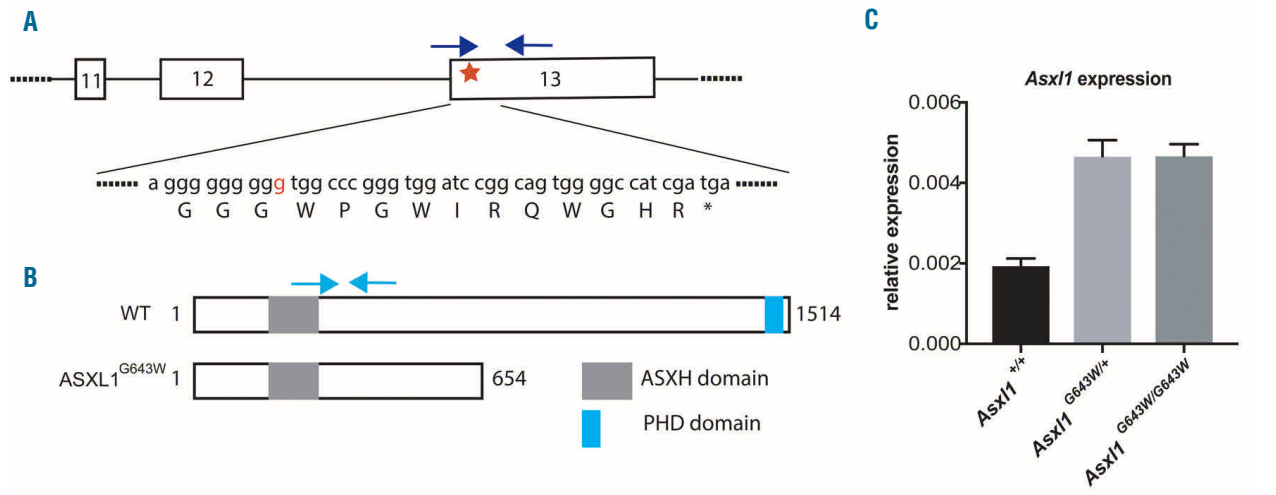


Figure 1. Generation of the *Asxl1*^{G643W} mutant mouse line. (A) Schematic representation of the three last exons of the *Asxl1* gene. The red star represents the G643W mutation. The "g" inserted in the mutated allele is indicated in red. The protein sequence is in capitals and the asterisk represents the stop codon generated as a result of the frameshift. The blue arrows represent primers used for genotyping (two forward primers have been used to selectively anneal the wild-type [WT] and mutated sequence, respectively). (B) Schematic representation of WT and G643W mutant ASX1 proteins. The major plant homeodomain (PHD) and additional sex combs homology domain (ASXH) are indicated. Amino acids are numbered. The light blue arrows represent the primers used for quantitative RT-PCR. (C) The relative expression of *Asxl1* cDNA in *Asxl1*+/+, *Asxl1*$^{G643W/+}$ and *Asxl1*$^{G643W/G643W}$ BM cells, determined by quantitative RT-PCR (n=3 mice in each experimental group).

12 codons downstream, thereby precisely mimicking the human situation (Figure 1A). The mutated *Asxl1*^{G643W} allele expresses a truncated form of ASXL1 lacking the C-terminal plant homeodomain (Figure 1B). Both *Asxl1*$^{G643W/+}$ and *Asxl1*$^{G643W/G643W}$ mice express elevated levels of Asxl1, demonstrating that the mutated allele escapes nonsense-mediated mRNA decay (Figure 1C). This is in line with the previously observed expression of truncated ASXL1 in patient cells.[6] The increased levels of the mutated mRNA could potentially be the result of a feedback mechanism.

The *Asxl1*^{G643W} variant has minimal impact on normal hematopoiesis

We next assessed the impact of the G643W mutation in the context of normal hematopoiesis. Both *Asxl1*$^{G643W/+}$ and *Asxl1*$^{G643W/G643W}$ mice were born at the expected Mendelian ratios and showed a normal lifespan. This suggests that the ASXL1^{G643W} variant has no impact on embryonic development or aging.

We next analyzed peripheral blood for the relative frequencies of the major blood lineages. Six-month old *Asxl1*$^{G643W/+}$ and *Asxl1*$^{G643W/G643W}$ mice displayed no major changes within the peripheral blood compared to wild-type (WT) controls (Figure 2A). However, at 18 months, we observed a skewing towards the myeloid lineage in ASXL1 mutated mice (Figure 2B-C, *Online Supplementary Figure S1A*). The age-dependent skewing was accompanied by a mild splenomegaly (Figure 2G).

Consistent with the lack of changes in the peripheral blood in young mice, 6-month old *Asxl1*$^{G643W/+}$ and *Asxl1*$^{G643W/G643W}$ neither displayed any changes within the hematopoietic stem cell (HSC) and multipotent progenitor (MPP) compartment, nor within the distribution of mature blood lineages in the bone marrow (Figure 2D-F, *Online Supplementary Figure S1B*). Competitive transplantation of ASXL1-mutated BM cells revealed a significant but minor reduction in the ability of *Asxl1*$^{G643W/G643W}$ BM to reconstitute hematopoiesis, suggesting that HSC functionality is only mildly affected (Figure 2H).

Collectively, these findings show that mutation of ASXL1 leads to a mild and age-dependent perturbation of the hematopoietic system in mice.

The ASXL1^{G643W} variant accelerates the development of CEBPA mutant acute myeloid leukemia

Mutations in *ASXL1* and *CEBPA* are frequently co-occurring in AML patients.[23,24] In order to test the potential functional interplay between these factors, we crossed all three Asxl1 genotypes onto either a *Cebpa*$^{fl/p30}$; *Mx1Cre* or *Cebpa*$^{fl/+}$; *Mx1Cre* background resulting in a total of six genotypes. We subsequently transplanted BM from these mice into lethally irradiated recipients and 3 weeks later induced the deletion of the conditional *Cebpa* allele by injections with polyinosinic:polycytidylic (pIpC) acid (Figure 3A). This strategy facilitates the deletion of the full-length *Cebpa* allele, thereby allowing the *Cebpa*^{p30} allele to exert its oncogenic function. Consistent with previous findings, *Asxl1*$^{+/+}$; *Cebpa*$^{\Delta/p30}$ donor cells sustain the development of AML with a median latency of 43 weeks (Figure 3B).[26] Interestingly, both heterozygous and homozygous expression of the ASXL1^{G643W} variant significantly accelerated CEBPA mutant driven AML development, with median disease latencies of 37 and 38 weeks, respectively. In contrast, none of the control *Cebpa*$^{\Delta/+}$ genotypes lead to AML, irrespective of their *Asxl1* mutation status.

Given that *Asxl1*$^{G643W/G643W}$ animals, compared to their heterozygous counterparts, displayed a somewhat more pronounced phenotype during steady-state hematopoiesis, we decided to focus on this genotype in the context of CEBPA mutant AML. Whereas *Asxl1*$^{+/+}$; *Cebpa*$^{\Delta/p30}$ and *Asxl1*$^{G643W/G643W}$; *Cebpa*$^{\Delta/p30}$ leukemias appeared morphologically identical, the latter displayed a trend towards increased levels of c-Kit (Figure 3C-E, *Online Supplementary Figure S2*). This suggests that the *Asxl1* mutation, at least in the context of CEBPA mutant AML, could result in a slightly more immature leukemic phenotype which would be consistent with the more aggressive nature of ASXL1 mutant AML.

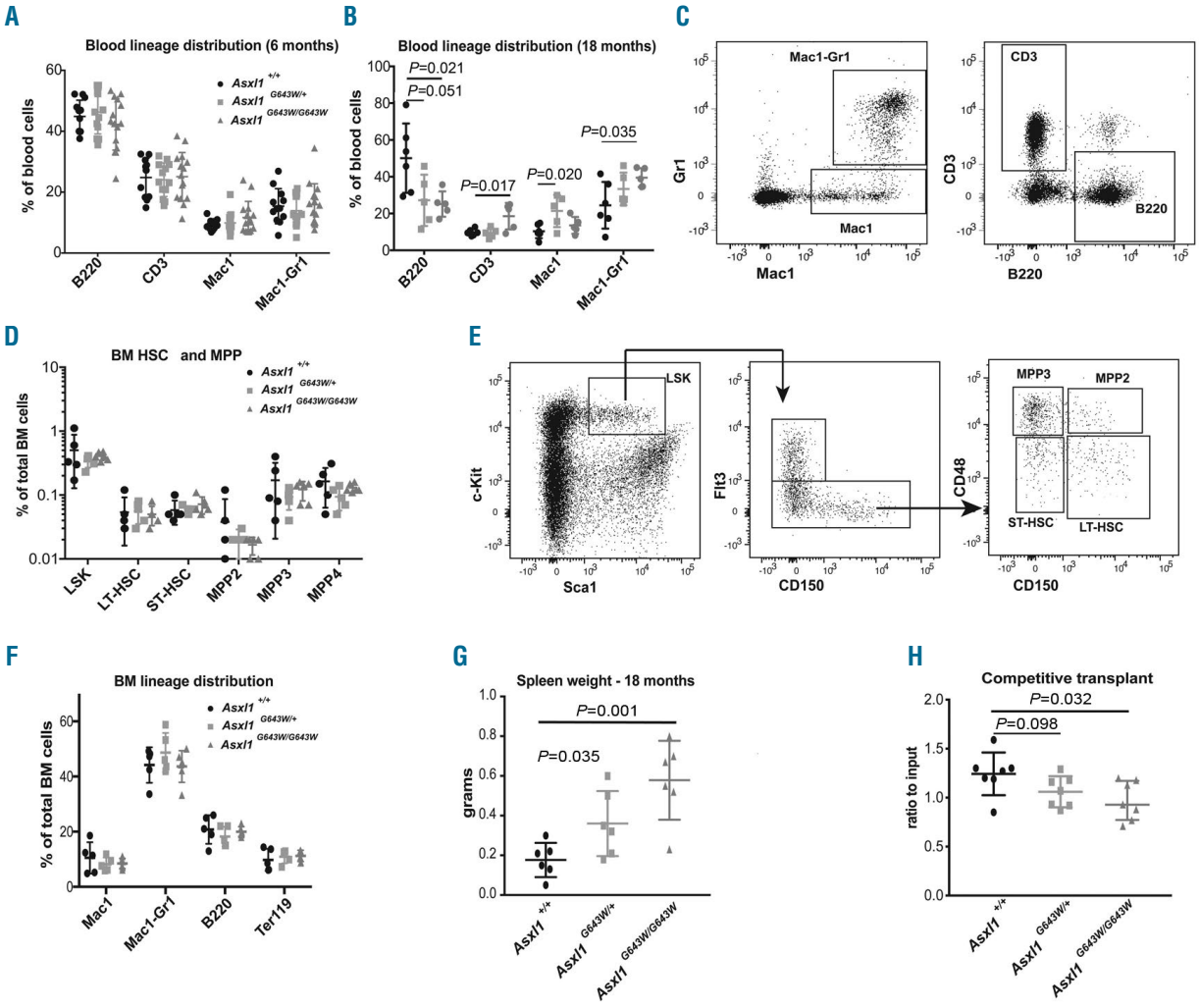


Figure 2. The ASXL1^{G643W} variant has minimal impact on normal hematopoiesis. (A) Fluorescence-activated cell sorting (FACS)-based analysis of the peripheral blood of 6-month old *Asxl1*$^{+/+}$, *Asxl1*$^{G643W/+}$ and *Asxl1*$^{G643W/G643W}$ mice (n>11 mice in each experimental group). The relative distribution of B cells (B220), T cells (CD3), neutrophilic granulocytes (Mac1-Gr1) and other monocytic/granulocytic cells (Mac1) was analyzed. (B) FACS-based analysis of the peripheral blood of 18-month old *Asxl1*$^{+/+}$, *Asxl1*$^{G643W/+}$ and *Asxl1*$^{G643W/G643W}$ mice (n>5 mice in each experimental group). The relative distribution of B cells (B220), T cells (CD3), neutrophilic granulocytes (Mac1-Gr1) and other monocytic/granulocytic cells (Mac1) was analyzed. (C) Representative FACS profiles of the data from (A-B) with the gating strategy indicated. The FACS profile represents an *Asxl1*$^{+/+}$ control mouse. See the *Online Supplementary Figure S1* for representative FACS plots of *Asxl1*$^{G643W/+}$ and *Asxl1*$^{G643W/G643W}$ animals. (D) FACS-based analysis of bone marrow hematopoietic stem cell (HSC) and multipotent progenitor (MPP) subsets in 6-month old *Asxl1*$^{+/+}$, *Asxl1*$^{G643W/+}$ and *Asxl1*$^{G643W/G643W}$ mice (n>5 mice in each experimental group). (E) Representative FACS profiles of the data from (D) with the gating strategy indicated. The FACS profile represents an *Asxl1*$^{+/+}$ control mouse. See the *Online Supplementary Figure S1* for representative FACS plots of *Asxl1*$^{G643W/+}$ and *Asxl1*$^{G643W/G643W}$ animals. (F) Lineage distribution of mature bone marrow (BM) subsets in 6-month old *Asxl1*$^{+/+}$, *Asxl1*$^{G643W/+}$ and *Asxl1*$^{G643W/G643W}$ mice (n>5 mice in each experimental group). The relative distribution of B cells (B220), T cells (CD3), neutrophilic granulocytes (Mac1-Gr1) and other monocytic/granulocytic cells (Mac1) was analyzed. (G) Spleen weights of 18-month old *Asxl1*$^{+/+}$, *Asxl1*$^{G643W/+}$ and *Asxl1*$^{G643W/G643W}$ mice (n>5 mice in each experimental group). (H) Competitive BM transplantation of 1:1 mixtures of CD45.2 donor BM cells from 6-month old *Asxl1*$^{+/+}$, *Asxl1*$^{G643W/+}$or *Asxl1*$^{G643W/G643W}$ mice and CD45.1 competitor cells into lethally irradiated CD45.1 recipient mice. The ratio of CD45.2 to CD45.1 in peripheral blood is depicted (n>7 mice in each experimental group).

Collectively, these findings agree with the observed co-occurrence of *ASXL1* and *CEBPA* mutations in human AML and suggest that these lesions co-operate in the development of AML.

The ASXL1^{G643W} variant affects the expression of leukemia relevant pathways

In order to understand the molecular underpinnings of the functional co-operation between *ASXL1* and *CEBPA* mutations, we isolated leukemic blasts from *Asxl1*$^{+/+}$; *Cebpa*$^{\Delta/p30}$ and *Asxl1*$^{G643W/G643W}$; *Cebpa*$^{\Delta/p30}$ donor-derived AML and subjected them to gene expression profiling. This analysis revealed that in the context of CEBPA mutant AML, the *Asxl1*$^{G643W/G643W}$ genotype was associated with the upregulation of 177 genes and the down-regulation of 279 genes (adjusted *P*-value <0.05; Figure 4A, *Online Supplementary Table S1, Online Supplementary Figure S3A*). Interestingly, 18 of 30 of the most upregulated genes encoded pseudogenes, perhaps reflecting a role for ASXL1 in mediating their repression. Gene set enrichment analysis (GSEA) identified gene ontology processes associated with mitosis (chromosome condensation, metaphase/ anaphase transition of mitotic cell cycle and others; Figure 4B and *Online Supplementary Table S2*) to be up-regulated in the *Asxl1*$^{G643W/G643W}$ genotype likely reflecting the recent finding of ASXL1 being involved in maintaining sister chromatid separation.[27] Furthermore, GSEA identified gene ontology terms associated with ribosome biosynthesis (ribosome biogenesis), DNA damage (regulation of DNA damage response, signal transduction by

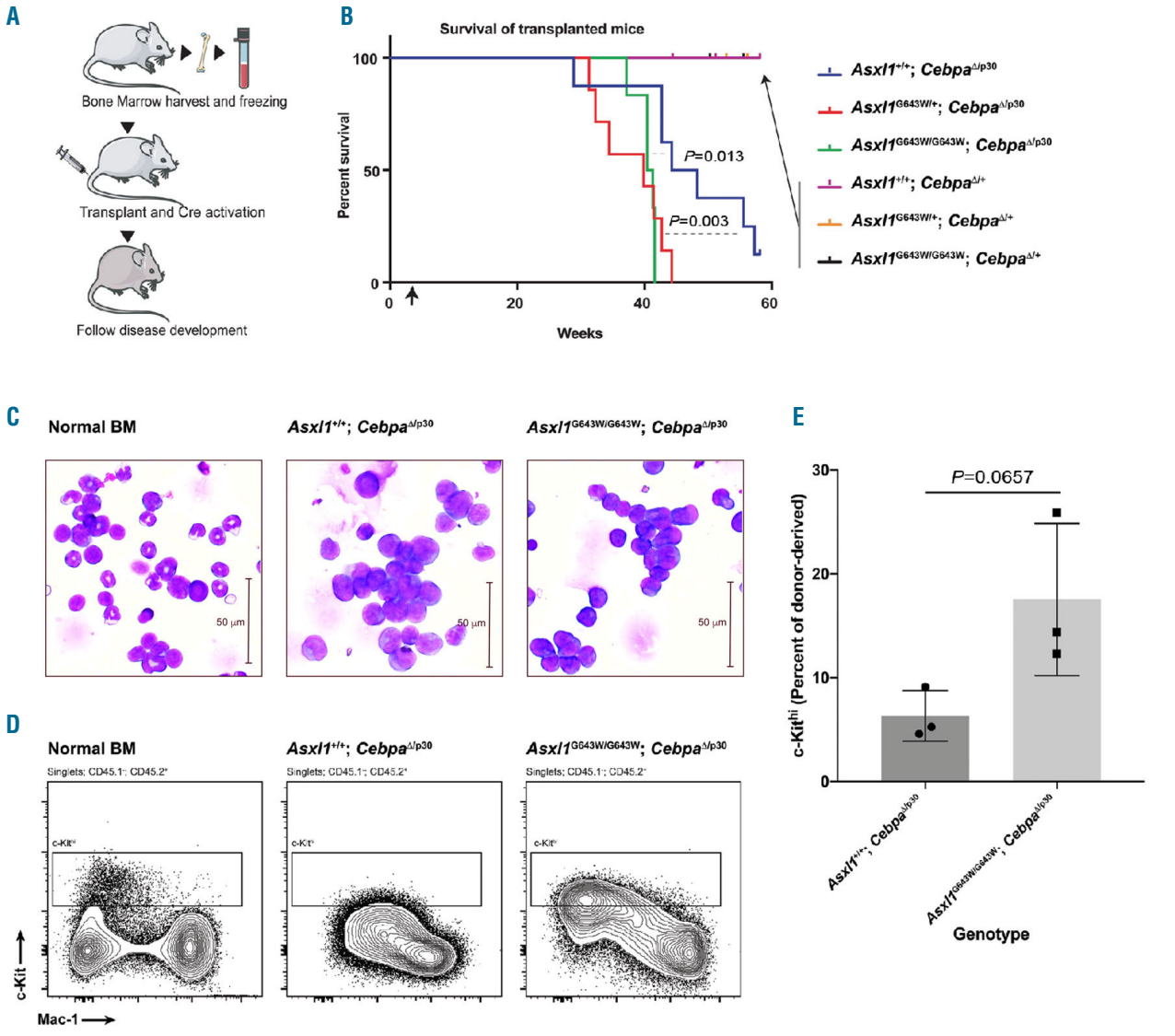


Figure 3. The ASXL1^{G643W} variant accelerate CEBPA mutant acute myeloid leukemia. (A) Schematic outline of the experiment. Briefly, bone marrow (BM) was harvested from mice with different genotypes and then transplanted into cohorts of irradiated recipients. Three weeks after the transplant, mice were injected with plpC and subsequently observed for signs of disease development over a period of 60 weeks. (B) Kaplan-Meyer survival curve of transplanted mice. The arrow indicates the time point for injection with plpC. We used a Log-rank (Mantel-Cox) test to determine statistical significance (n>7 mice in each experimental group). (C) Giemsa staining of Asxl1$^{+/+}$; Cebpa$^{\Delta/p30}$ or Asxl1$^{G643W/G643W}$; Cebpa$^{\Delta/p30}$ leukemic blasts isolated from the BM of moribund mice. A normal aged-matched mouse was included as a control. (D) Fluorescence-activated cell sorting (FACS) analysis of Asxl1$^{+/+}$; Cebpa$^{\Delta/p30}$ or Asxl1$^{G643W/G643W}$; Cebpa$^{\Delta/p30}$ leukemic blast isolated from transplanted mice. The plot shows the amount of donor-derived c-Kit positive cells. A normal aged-matched mouse was included as a control. (E) Quantification of the data from (D) (n=3 mice in each experimental group).

p53 class mediator) and immune activation (antigen processing a presentation of exogenous antigen) to be down-regulated in the *Asxl1*$^{G643W/G643W}$ genotype (Figure 4C). These findings do not only point to changes in the overall metabolic status of ASXL1 mutant cells, but may also indicate a reduced activation of the immune system as well as a decreased response to genomic insults.

Focusing on individual genes, we noticed a marked up-regulation of *Traip* in the *Asxl1*$^{G643W/G643W}$ genotype ($\log_2$ fold change =6.7; Figure 4A, *Online Supplementary Figure S3A*). TRAIP is an E3 ubiquitin ligase which has been shown to be involved in the regulation of the NF-κB pathway, cell proliferation, regulation of the spindle assembly checkpoint, DNA replication fork recovery and more recently as a master regulator of DNA crosslink repair.[28-32]

Finally, in order to understand the epigenetic characteristics of the genes deregulated in the *Asxl1*$^{G643W/G643W}$ genotype, we overlaid published ChIP-seq data from *Cebpa*$^{\Delta/p30}$ AML[22] with promoter coordinates from deregulated and constant genes, identified in our gene expression analysis described above. In these ASXL1 proficient cells, the promoters of genes that were upregulated following mutation of *Asxl1* (in the context of CEBPA mutant AML), were characterized by low levels of "activating" histone modifications H3K4me3 and H3K27ac as well as by high level of the repressive histone mark H3K27me3 (Figure 4D, *Online Supplementary Figure S3B-C*). This combination of epigenetic marks is consistent with the low expression of these genes and previous work has demonstrated that loss of ASXL1 activity is associated with upregulation of PRC2-repressed genes.[5,9] Genes that are down-regulated in the *Asxl1*$^{G643W/G643W}$

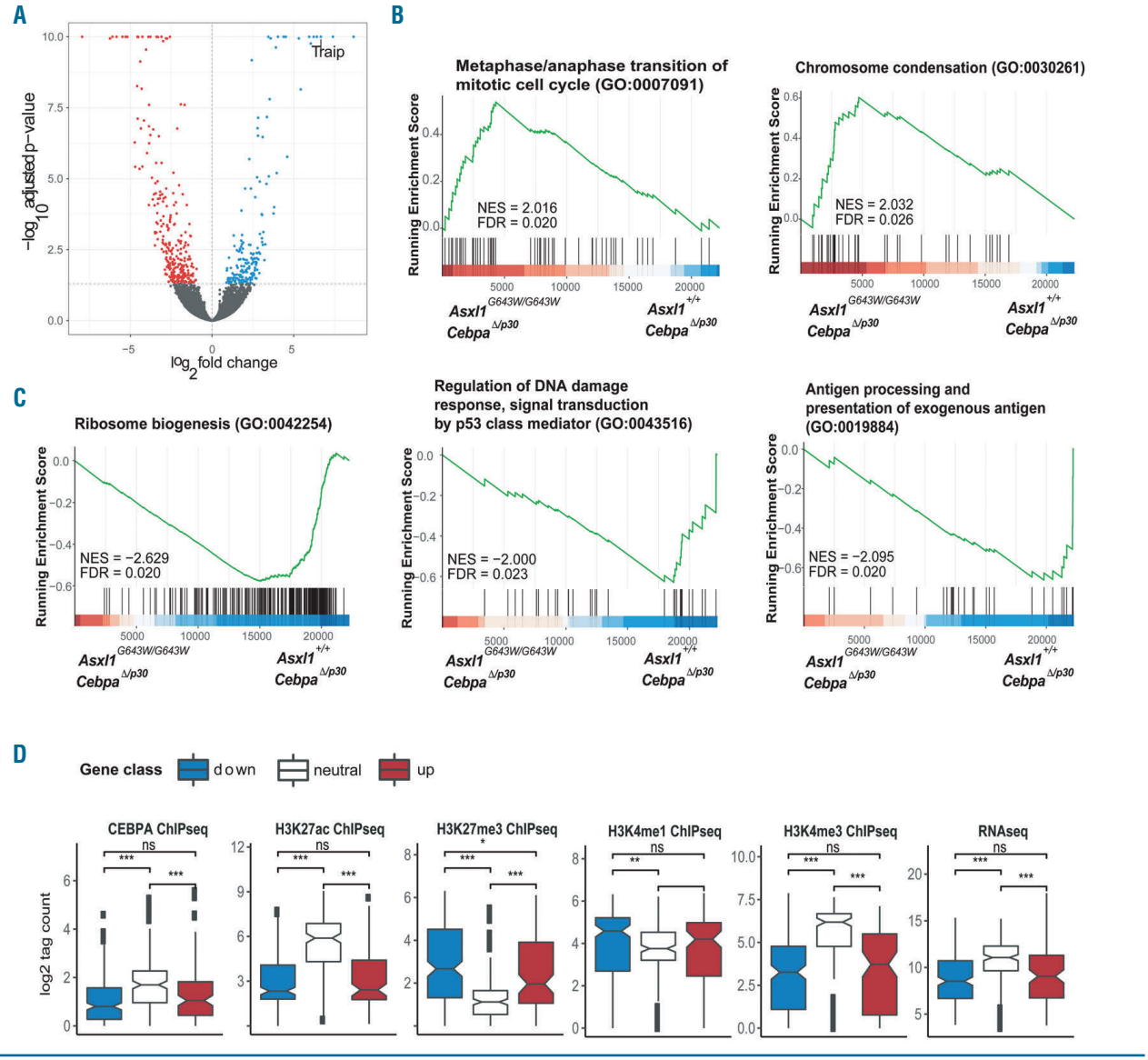


Figure 4. The ASXL1^{G643W} variant affects the expression of leukemia relevant pathways. (A). Volcano plot depicting gene expression changes in *Asxl1*$^{G643W/G643W}$; *Cebpa*$^{\Delta/p30}$ *vs.* Asxl1$^{+/+}$; *Cebpa*$^{\Delta/p30}$ leukemic blasts. (B-C). GSEA plots for selected gene sets which are either upregulated (B) or downregulated (C) in *Asxl1*$^{G643W/G643W}$; *Cebpa*$^{\Delta/p30}$ *versus* Asxl1$^{+/+}$; *Cebpa*$^{\Delta/p30}$ leukemic blasts. (D) Boxplots showing the CHIP-signal levels of selected marks surrounding the TSS (+/- 500 bp) for genes that are either up- or downregulated in *Asxl1*$^{G643W/G643W}$; *Cebpa*$^{\Delta/p30}$ vs. Asxl1$^{+/+}$; *Cebpa*$^{\Delta/p30}$ leukemic blasts (*Online Supplementary Table S1*). The data is derived from a previous CEBPA mutant (*Cebpa*$^{p30/p30}$, *Asxl1 WT*) dataset.[22] Gene expression levels as determined by RNA sequencing are also indicated. Up: upregulated genes in *Asxl1*$^{G643W/G643W}$ *vs.* Asxl1$^{+/+}$ leukemic blasts (false discovery rate [FDR] 0.05, log.FC>0, baseMean>10, n=105), down: downregulated genes in *Asxl1*$^{G643W/G643W}$ *vs.* Asxl1$^{+/+}$; (FDR 0.05, log.FC <0, baseMean >10, n=201), neutral: neutral genes (-0.01 < log.FC<0.01, baseMean>10, n=165) in *Asxl1*$^{G643W/G643W}$ *vs.* Asxl1$^{+/+}$. *P*-values levels **P*<0.05s, ***P*=0.01, ****P*=0.001 are indicated

genotype are also weakly expressed and display a similar epigenetic signature. The downregulation of these genes could potentially be due to a global decrease in H3K4me3 which has previously been found to be associated with the expression of a C-terminally truncated ASXL1 variant.[17]

Collectively, these data suggest that expression of the ASXL1^{G643W} variant affects the expression of a number of leukemic relevant genes and pathways, consistent with the role of ASXL1 as a broad epigenetic modifier.

The ASXL1^{G643W} variant is associated with increased resistance to chemotherapy in the context of CEBPA mutant acute myeloid leukemia

Failure to respond to chemotherapy is a major determinant of overall survival in AML and genomic stratification has associated ASXL1 mutations with adverse outcome in human AML.[33-35] This raises the possibility that AML-associated mutations in ASXL1 specifically impact on the cellular response to chemotherapy. In order to test this possibility, we used our well-defined experimental set-up to assess the impact of the *Asxl1*$^{G643W/G643W}$ genotype on the response to induction chemotherapy in the context of CEBPA mutant AML. To this end, we transplanted *Asxl1*$^{+/+}$*; Cebpa*$^{\Delta/p30}$ and *Asxl1*$^{G643W/G643W}$; *Cebpa*$^{\Delta/p30}$ secondary AML (a total of seven clones) into recipient mice and subjected them to low-dose induction chemotherapy 3 weeks post transplantation (Figure 5A, *Online Supplementary Figure S4*). Compared to the ASXL1^{WT} cohort, ASXL1^{G643W} mice displayed reduced response to chemotherapy as

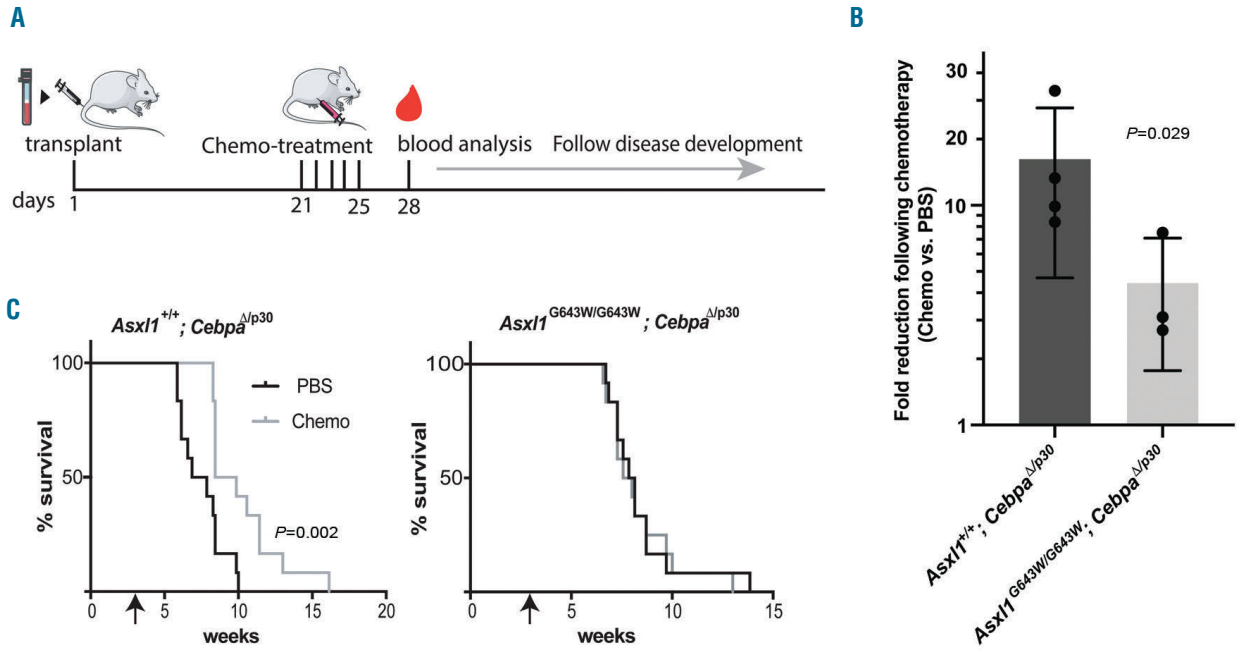


Figure 5. The ASXL1^{G643W} variant is associated with increased resistance to chemotherapy. (A) Schematic outline of the chemotherapy treatment set-up. Briefly, sub-lethally irradiated recipient mice were transplanted with bone marrow (BM) cells harvested from leukemic mice. Twenty-one days after transplant, recipient mice were treated with standard induction chemotherapy for 5 days. Three days later, blood was harvested for analysis and leukemic mice were subsequently monitored for disease development. (B) Analysis of peripheral leukemic numbers in mice after chemotherapy/vehicle treatment. Each data point represents the fold change difference between the vehicle-treated and chemotherapy-treated groups for a given clone (n=12 mice per clone). The two different genotypes, Asx*l1*$^{+/+}$; *Cebpa*$^{\Delta/p30}$ and Asxl1G643W/G643W *Cebpa*$^{\Delta/p30}$, were represented by four and three clones, respectively. The responses of individual clones are indicated in the *Online Supplementary Figure S4*. A one-tailed Mann-Whitney U test was used to assess statistical significance. (C) Kaplan-Meyer survival curves of leukemic mice after chemotherapy/vehicle treatment. The data represent the aggregate of two different leukemic clones (n=6 recipients of each clone, clones 1-2 and 5-6) for each of the two different genotypes (Asx*l1*$^{+/+}$; *Cebpa*$^{\Delta/p30}$ and Asxl1G643W/G643W; *Cebpa*$^{\Delta/p30}$).

measured by the decrease of leukemic cells in the peripheral blood 3 days post-treatment cessation (Figure 5B). This translated into an increased latency for the treated ASXL1^{WT} cohort whereas chemotherapy had no impact on survival of the ASXL1^{G643W} mutant cohort (Figure 5C).

Taken together, these findings demonstrate that mutation of ASXL1 renders CEBPA mutated AML largely resistant to chemotherapy.

Discussion

Myeloid diseases such as AML are developing from pre-malignant clones which mostly harbor lesions in epigenetic regulators.[3,4] One of these regulators is ASXL1 which is consequently frequently mutated in both MDS and AML as well as in premalignant settings such as CHIP. This mutational profile raises the question whether ASXL1 plays a functional role in full-blown AML or whether it merely provides a fertile ground in which AML can evolve.

There has been considerable confusion concerning the molecular mechanisms by which ASXL1 mutations sustain AML development or hematological deficiencies, specifically whether ASXL1 mutations act as dominant negatives. Some of this confusion is related to the inherent difficulties in detecting ASXL1 by western blotting (issues which we also experienced) thus making it nearly impossible to determine whether the mutated protein is present or not. However, overexpression of ASXL1 variants was associated with hematological malignancies raising the possibility that the mutated protein could act as a dominant negative.[6,14,15] Our analysis of heterozygous and homozygous *Asxl1*^{G643W} mice in the context of normal hematopoiesis suggests that the *Asxl1*^{G643W} variant has a dose-dependent impact in this context. Given that complete loss of *Asxl1* leads to more pronounced hematopoietic phenotypes, the most restrained explanation from the *in vivo* work is that the ASXL1^{G643W} variant is hypomorphic or, alternatively, that it exerts a combination of dominant negative and hypomorphic effects.[10-12]

Expression of the *Asxl1*^{G643W} variant in the context of CEBPA mutant AML significantly accelerated AML development and was associated with marked resistance to induction chemotherapy. These findings are not only in perfect alignment with the co-occurrence of *CEBPA* and *ASXL1* lesions in human AML, but also with the overall poor prognosis of ASXL1 mutated human AML. Hence the resistance towards chemotherapy is likely underlying the poor prognosis of AXL1 mutated AML.[33-35] It would be interesting to test if other mouse models can recapitulate this behavior beyond CEBPA mutant AML.

Interestingly, gene expression analysis demonstrated that *Asxl1*$^{G643W/G643W}$; *Cebpa*$^{\Delta/p30}$ exhibited downregulation of signatures associated with immune activation perhaps reflecting that the *Asxl1* lesion renders the developing leukemia less visible to the immune system. We also observed a reduction in activation of the DNA damage pathways in ASXL1 mutated cells which could potentially reflect efficient clearing of ongoing genomic insults. Here our finding of the marked upregulation of *Traip* is of particular interest as the corresponding protein has recently been identified as a master regulator of DNA crosslink repair.[32] Thus, our data strongly suggest that *Asxl1* lesions have functional conse-

quences in the context of CEBPA mutant AML and that they therefore provide more than a fertile ground for AML development.

To summarize, we have generated a novel ASXL1^{G643W} mouse model mimicking the most commonly observed *ASXL1* lesion mutation in human MDS and AML patients. Consistent with the co-occurrence of *CEBPA* and *ASXL1* lesions in AML, the ASXL1^{G643W} variant accelerates AML development in the context of CEBPA mutant AML. Finally, the observed resistance towards chemotherapy conferred by the ASXL1^{G643W} variant provides us with an experimental handle for future experiments aimed at its reversal.

Disclosures

No conflicts of interest to disclose

Contributions

TD, MBS, AMH and ASW carried out the experiments; TD, AW, AK, SP and BTP analyzed data; TDA and BP drafted the manuscript which was proofread by all authors; BTP directed the research.

Acknowledgments

We thank Javier Martín Gonzalez and the Transgenic Core Facility for the generation of the mutant strain.

Funding

This work was supported by a grant from the Danish Cancer Society (to Teresa D'Altri) and through a center grant from the Novo Nordisk Foundation (Novo Nordisk Foundation Center for Stem Cell Biology, DanStem; Grant Number NNF17CC0027852). The present work is also part of the Danish Research Center for Precision Medicine in Blood Cancers funded by the Danish Cancer Society grant no. R223-A13071 and Greater Copenhagen Health Science Partners.

References

1. Gelsi-Boyer V, Trouplin V, Adelaide J, et al. Mutations of polycomb-associated gene ASXL1 in myelodysplastic syndromes and chronic myelomonocytic leukaemia. Br J Haematol. 2009;145(6):788-800.
2. Bejar R, Stevenson K, Abdel-Wahab O, et al. Clinical effect of point mutations in myelodysplastic syndromes. N Engl J Med. 2011;364(26):2496-2506.
3. Jaiswal S, Fontanillas P, Flannick J, et al. Age-related clonal hematopoiesis associated with adverse outcomes. N Engl J Med. 2014; 371(26):2488-2498.
4. Genovese G, Kahler AK, Handsaker RE, et al. Clonal hematopoiesis and blood-cancer risk inferred from blood DNA sequence. N Engl J Med. 2014;371(26):2477-2487.
5. Abdel-Wahab O, Adli M, LaFave LM, et al. ASXL1 mutations promote myeloid transformation through loss of PRC2-mediated gene repression. Cancer Cell. 2012; 22(2):180-193.
6. Inoue D, Matsumoto M, Nagase R, et al. Truncation mutants of ASXL1 observed in myeloid malignancies are expressed at detectable protein levels. Exp Hematol. 2016;44(3):172-176.1.
7. Dey A, Seshasayee D, Noubade R, et al. Loss of the tumor suppressor BAP1 causes myeloid transformation. Science. 2012; 337(6101):1541-1546.
8. Scheuermann JC, de Ayala Alonso AG, Oktaba K, et al. Histone H2A deubiquitinase activity of the Polycomb repressive complex PR-DUB. Nature. 2010;465(7295):243-247.
9. Abdel-Wahab O, Dey A. The ASXL-BAP1 axis: new factors in myelopoiesis, cancer and epigenetics. Leukemia. 2013;27(1):10-15.
10. Abdel-Wahab O, Gao J, Adli M, et al. Deletion of Asxl1 results in myelodysplasia and severe developmental defects in vivo. J Exp Med. 2013;210(12):2641-2659.
11. Fisher CL, Pineault N, Brookes C, et al. Loss-of-function additional sex combs like 1 mutations disrupt hematopoiesis but do not cause severe myelodysplasia or leukemia. Blood. 2010;115(1):38-46.
12. Wang J, Li Z, He Y, et al. Loss of Asxl1 leads to myelodysplastic syndrome-like disease in mice. Blood. 2014;123(4):541-553.
13. Asada S, Fujino T, Goyama S, Kitamura T. The role of ASXL1 in hematopoiesis and myeloid malignancies. Cell Mol Life Sci. 2019;76(13):2511-2523.
14. Asada S, Goyama S, Inoue D, et al. Mutant ASXL1 cooperates with BAP1 to promote myeloid leukaemogenesis. Nat Commun. 2018;9(1):2733.
15. Balasubramani A, Larjo A, Bassein JA, et al. Cancer-associated ASXL1 mutations may act as gain-of-function mutations of the ASXL1-BAP1 complex. Nat Commun. 2015; 6:7307.
16. Hsu YC, Chiu YC, Lin CC, et al. The distinct biological implications of Asxl1 mutation and its roles in leukemogenesis revealed by a knock-in mouse model. J Hematol Oncol. 2017;10(1):139.
17. Nagase R, Inoue D, Pastore A, et al. Expression of mutant Asxl1 perturbs hematopoiesis and promotes susceptibility to leukemic transformation. J Exp Med. 2018;215(6):1729-1747.
18. Pabst T, Mueller BU, Zhang P, et al. Dominant-negative mutations of CEBPA, encoding CCAAT/enhancer binding protein-alpha (C/EBPalpha), in acute myeloid leukemia. Nat Genet. 2001;27(3):263-270.
19. Papaemmanuil E, Gerstung M, Bullinger L, et al. Genomic classification and prognosis in acute myeloid leukemia. N Engl J Med. 2016;374(23):2209-2221.
20. Ohlsson E, Schuster MB, Hasemann M, Porse BT. The multifaceted functions of C/EBPalpha in normal and malignant haematopoiesis. Leukemia. 2016;30(4):767-775.
21. Kirstetter P, Schuster MB, Bereshchenko O, et al. Modeling of C/EBPalpha mutant acute myeloid leukemia reveals a common expression signature of committed myeloid leukemia-initiating cells. Cancer Cell. 2008;13(4):299-310.
22. Jakobsen JS, Laursen LG, Schuster MB, et al. Mutant CEBPA directly drives the expression of the targetable tumor-promoting factor CD73 in AML. Sci Adv. 2019; 5(7):eaaw4304.
23. Rose D, Haferlach T, Schnittger S, Perglerova K, Kern W, Haferlach C. Subtype-specific patterns of molecular mutations in acute myeloid leukemia. Leukemia. 2017; 31(1):11-17.
24. Su L, Tan Y, Lin H, et al. Mutational spectrum of acute myeloid leukemia patients with double CEBPA mutations based on next-generation sequencing and its prognostic significance. Oncotarget. 2018; 9(38):24970-24979.
25. Chou WC, Huang HH, Hou HA, et al. Distinct clinical and biological features of de novo acute myeloid leukemia with additional sex comb-like 1 (ASXL1) mutations. Blood. 2010;116(20):4086-4094.
26. Schuster MB, Frank A-K, Bagger FO, Rapin N, Vikesaa J, Porse BT. Lack of the p42 form of C/EBPα leads to spontaneous immortalization and lineage infidelity of committed myeloid progenitors. Exp Hematol. 2013; 41(10):882-893.e16.
27. Li Z, Zhang P, Yan A, et al. ASXL1 interacts with the cohesin complex to maintain chromatid separation and gene expression for normal hematopoiesis. Sci Adv. 2017;3(1):e1601602.
28. Chapard C, Hohl D, Huber M. The role of the TRAF-interacting protein in proliferation and differentiation. Exp Dermatol. 2012; 21(5):321-326.
29. Chapard C, Meraldi P, Gleich T, Bachmann D, Hohl D, Huber M. TRAIP is a regulator of the spindle assembly checkpoint. J Cell Sci. 2014;127(Pt 24):5149-5156.
30. Feng W, Guo Y, Huang J, Deng Y, Zang J, Huen MS. TRAIP regulates replication fork recovery and progression via PCNA. Cell Discov. 2016;2:16016.
31. Hoffmann S, Smedegaard S, Nakamura K, et al. TRAIP is a PCNA-binding ubiquitin ligase that protects genome stability after replication stress. J Cell Biol. 2016;212(1):63-75.
32. Wu RA, Semlow DR, Kamimae-Lanning AN, et al. TRAIP is a master regulator of DNA interstrand crosslink repair. Nature. 2019;567(7747):267-272.
33. Schnittger S, Eder C, Jeromin S, et al. ASXL1 exon 12 mutations are frequent in AML with intermediate risk karyotype and are independently associated with an adverse outcome. Leukemia. 2013;27(1):82-91.
34. Paschka P, Schlenk RF, Gaidzik VI, et al. ASXL1 mutations in younger adult patients with acute myeloid leukemia: a study by the German-Austrian Acute Myeloid Leukemia Study Group. Haematologica. 2015; 100(3):324-330.
35. Pratcorona M, Abbas S, Sanders MA, et al. Acquired mutations in ASXL1 in acute myeloid leukemia: prevalence and prognostic value. Haematologica. 2012;97(3):388-392.

Ferrata Storti Foundation

Haematologica 2021
Volume 106(4):1008-1021

Endogenous and combination retinoids are active in myelomonocytic leukemias

Orsola di Martino,[1] Haixia Niu,[2] Gayla Hadwiger,[1] Heikki Kuusanmaki,[3] Margaret A. Ferris,[4] Anh Vu,[1] Jeremy Beales,[1] Carl Wagner,[5] María P. Menéndez-Gutiérrez,[6] Mercedes Ricote,[6] Caroline Heckman[3] and John S. Welch[1]

[1]Department of Internal Medicine, Washington University, St Louis, MO, USA; [2]Division of Experimental Hematology and Cancer Biology, Cancer and Blood Diseases Institute, Cincinnati Children's Hospital Medical Center, Cincinnati, OH, USA; [3]Institute for Molecular Medicine Finland, Helsinki Institute of Life Science, University of Helsinki, Helsinki, Finland; [4]Department of Pediatrics, Washington University, St Louis, MO, USA; [5]School of Mathematical and Natural Sciences, Arizona State University, Phoenix, AZ, USA and [6]Myocardial Pathophysiology Area, Centro Nacional de Investigaciones Cardiovasculares (CNIC), Madrid, Spain

ABSTRACT

Retinoid therapy transformed response and survival outcomes in acute promyelocytic leukemia (APL) but has demonstrated only modest activity in non-APL forms of acute myeloid leukemia (AML). The presence of natural retinoids *in vivo* could influence the efficacy of pharmacologic agonists and antagonists. We found that natural RXRA ligands, but not RARA ligands, were present in murine *MLL-AF9*-derived myelomonocytic leukemias *in vivo* and that the concurrent presence of receptors and ligands acted as tumor suppressors. Pharmacologic retinoid responses could be optimized by concurrent targeting of RXR ligands (e.g., bexarotene) and RARA ligands (e.g., all-trans retinoic acid), which induced either leukemic maturation or apoptosis depending on cell culture conditions. Co-repressor release from the RARA:RXRA heterodimer occurred with RARA activation, but not RXRA activation, providing an explanation for the combination synergy. Combination synergy could be replicated in additional, but not all, AML cell lines and primary samples, and was associated with improved survival *in vivo*, although tolerability of bexarotene administration in mice remained an issue. These data provide insight into the basal presence of natural retinoids in leukemias *in vivo* and a potential strategy for clinical retinoid combination regimens in leukemias beyond APL.

Correspondence:

JOHN S. WELCH
jwelch@wustl.edu

Received: June 26, 2020.

Accepted: November 16, 2020.

Pre-published: February 4, 2021.

https://doi.org/10.3324/haematol.2020.264432

©2021 Ferrata Storti Foundation

Material published in Haematologica is covered by copyright. All rights are reserved to the Ferrata Storti Foundation. Use of published material is allowed under the following terms and conditions: https://creativecommons.org/licenses/by-nc/4.0/legalcode. Copies of published material are allowed for personal or internal use. Sharing published material for non-commercial purposes is subject to the following conditions: https://creativecommons.org/licenses/by-nc/4.0/legalcode, sect. 3. Reproducing and sharing published material for commercial purposes is not allowed without permission in writing from the publisher.

Introduction

The retinoic acid receptors (RAR) and retinoid X receptors (RXR) are ligand-activated transcription factors that influence hematopoietic stem cell self-renewal and differentiation.[1-3] Transcriptional activation of the retinoid receptors is ligand dependent.[4] Therefore, the potential activity of retinoid receptors in leukemogenesis may be altered depending on the availability of natural ligands within a leukemic population, and retinoid receptors might act as either tumor suppressors or oncogenes depending on the ligand context. However, in leukemia, it is not known whether these receptors are exposed to natural activating ligands *in vivo*, or whether different forms of leukemia might contain different quantities of functional ligands.

There are three different RAR and RXR isoforms (α, β, and γ) that are differently expressed in hematopoietic cells.[5,6] RARA and RXRA expression are dynamically regulated during myeloid maturation, with highest mRNA expression in mature neutrophils.[7] RAR function as obligate heterodimers with RXR, whereas RXR can form either homodimers or heterodimers with other orphan nuclear receptors (e.g., peroxisome proliferator-activated receptors [PPAR], liver X receptors [LXR], etc.).[4] RAR-RXR dimers bind DNA with high affinity at specific retinoic acid response elements (RARE) in target gene promoters/enhancers.[8] RAR-RXR acts as a transcriptional repressor by binding co-repressor complexes composed by nuclear receptor

co-repressor (N-CoR) and the silencing mediator for retinoid and thyroid hormone receptors (SMRT) and recruiting histone deacetylases (HDAC). Local histone deacetylation then facilitates chromatin condensation and gene silencing. Ligand binding alters the heterodimer conformation, displacing the co-repressors and facilitating binding of co-activator complexes composed by p160 family (TIF-2/SRC-1/RAC3) with histone acetylase activity (HAT). Local histone acetylation then facilitates chromatin decondensation and gene transcription activation.[9,10]

All-trans retinoic acid (ATRA) has been proposed as the natural ligand for RAR. Multiple natural ligands have been proposed for RXR, including modified retinoic acids (9-cis retinoic acid and 9-cis-13,14-dihydroretinoic acid) and long-chain fatty acids (C22:6, C22:5; C20:4, and C24:5), which are available in diverse tissues as well as in serum.[11-15] Natural RXRA, but not RARA, ligands are present in normal hematopoietic cells *in vivo* under steady-state conditions, with preferential distribution in myeloid cells ($Gr1^+$) and following myeloid stress resulting from granulocyte-colony stimulating factor (GCSF) treatment.[14]

ATRA (tretinoin) has transformed the outcomes of M3-acute promyelocytic leukemia (APL).[16,17] However, outcomes with ATRA in non-APL AML have yielded mixed results.[18] Bexarotene is a pan-RXR-activating ligand, which is approved for the treatment of cutaneous T-cell lymphoma (CTCL).[19] In small exploratory studies of non-APL AML, bexarotene demonstrated evidence of activity, but only in a small proportion of patients.[20,21]

We used an *in vivo* reporter assay to explore whether retinoid receptors in leukemia cells are transcriptionally active (and therefore might be best targeted with antagonists) or transcriptionally inactive (and therefore might be best targeted with agonists). Our results show that natural ligands for RXRA, but not RARA, are present at low levels *in vivo* in primary mouse myelomonocytic leukemia cells where they exhibit tumor suppressor phenotypes.

Methods

Hematopoietic cell culture

Mouse BM Kit^+ cells were isolated using an Automacs Pro (Miltenyl Biotec, San Diego, CA, USA) and plated in RPMI 1640 medium, 15% fetal bovine serum (FBS), Scf (50 ng/mL), IL3 (10 ng/mL), Flt3 (25 ng/mL), Tpo (10 ng/mL), L-glutamine (2 mM), sodium pyruvate (1 mM), HEPES buffer (10 mM), penicillin/streptomycin (100 units/mL), β-mercaptoethanol (50 μM). *MLL-AF9* leukemia was cultured in a similar media, but without Flt3, or Tpo. MOLM-13 were grown in RPMI1640 and 20% FBS; THP-1 in RPMI1640, 10% FBS, 0.05 mM MetOH; MONOMAC-6 in RPMI1640, 10% FBS, 2 mM L-glutamine, 2 mM NEAA, 1 mM sodium pyruvate, 10 ug/mL human insulin; OCI-AML-3 in α-MEM and 20% FBS. Fluorescence was detected on a FACS Scan, Gallios instrument (Beckman Coulter, Brea, CA, USA) or ZE5 Cell Analyzer (Biorad, Hercules, CA, USA).

Primary acute myeloid leukemia samples

All cryopreserved AML samples were collected as part of a study approved by the University of Helsinki after patients provided informed consent in accordance with the Declaration of Helsinki. Thawed BM mononuclear cells were suspended in 87.5% RPMI 1640 medium plus 12.5% HS5 stromal cells conditioned media, and supplemented with 10% FBS, L-glutamine (2 mM) and penicillin/streptomycin (100 units/mL). 10,000 cells/well in 25 μL were plated on 384-well plates containing bexarotene and ATRA. The cells were incubated with the drugs for 96 h after which cell viability was measured with CellTiter-Glo (Promega, Madison, WI, USA).

Mice

UAS-GFP and *Mx1-Cre x* $Rxra^{flox/flox}$ *x* $Rxrb^{flox/flox}$ mice were bred as previously described.[22,23] pIpC treatment was intraperitoneal injection (IP) with 300 μg/mouse; four doses were given every other day. *Rxra* and *Rxrb* deletion were confirmed by polymerase chain reaction (PCR). Bexarotene was administrated by oral gavage, suspended in sterile α-tocopherol suspension or in corn oil, 1 mg per mouse per day for 5 days/week. *Lox-stop-Lox* YFP mice were a gift from Todd Fehniger, Washington University. Dnmt3a-R878H/FLT3-ITD mouse leukemia cells were generated by Angela Verdoni and were a gift from Timothy Ley, Washington University (*T Ley, unpublished material, 2019*). To generate this line, hematopoietic cells derived from Dnmt3a R878H mosaic mice were transduced with an MSCV-FLT3-ITD-IRES-GFP retrovirus, and transplanted into multiple recipient mice. AML developing in these mice were confirmed to express the R878H allele by RNA-seq, with approximately 50% of all reads coming from the mutant allele (*T Ley, personal communication 2019*). The AML sample (AML-1) examined in these studies is associated with rapid lethality in secondary transplants (median 48 days in syngeneic B6 animals) and an immature myeloid immunophenotype ($Cd117^+$ and partial expression of Gr-1 and Cd11b) (*O di Martino personal observation, 2020*). Tet2-KO/FLT3-ITD leukemia cells were a gift from Ross Levine, Memorial Sloan Kettering Cancer Center. The Washington University Animal Studies Committee approved all animal experiments.

Study approval

All animal procedures were approved by the Institutional Animal Care and Use Committee of Washington University. All cryopreserved human AML samples were collected as part of a study approved by the University of Helsinki after patients provided informed consent in accordance with the Declaration of Helsinki.

Results

RXRA natural ligands are present in MLL-AF9 myeloid leukemia cells *in vivo*

RARA and *RXRA* are preferentially expressed in mature myeloid cells and this pattern is reflected in a biased expression in M4/M5 AML where *RARA* and *RXRA* expression correlates with markers of maturation[7] (*Online Supplementary Figure S1*). Therefore, we hypothesized that the availability of natural retinoids in hematopoietic malignancies might also be myeloid biased.

We evaluated *in vivo* retinoid ligand availability using a retroviral model of myelomonocytic leukemia and a reporter assay we had previously characterized.[14,22] *UAS-GFP* bone marrow (BM) cells first were transduced with a retrovirus expressing *MLL-AF9* and transplanted into sublethally irradiated recipient mice (see Figure 1A). Once leukemia emerged (i.e., *UAS-GFP x MLL-AF9*), these cells were transduced with a second retrovirus (*MSCV*-Flag-Gal4 DBD-RXRA LBD-IRES-mCherry) and subsequently transplanted into sublethally irradiated recipients. Using this strategy, leukemia cells with active, natural RXRA ligands express GFP (*Online Supplementary Figure S2A* and *B*). *Ex vivo*, the reporter was sensitive to

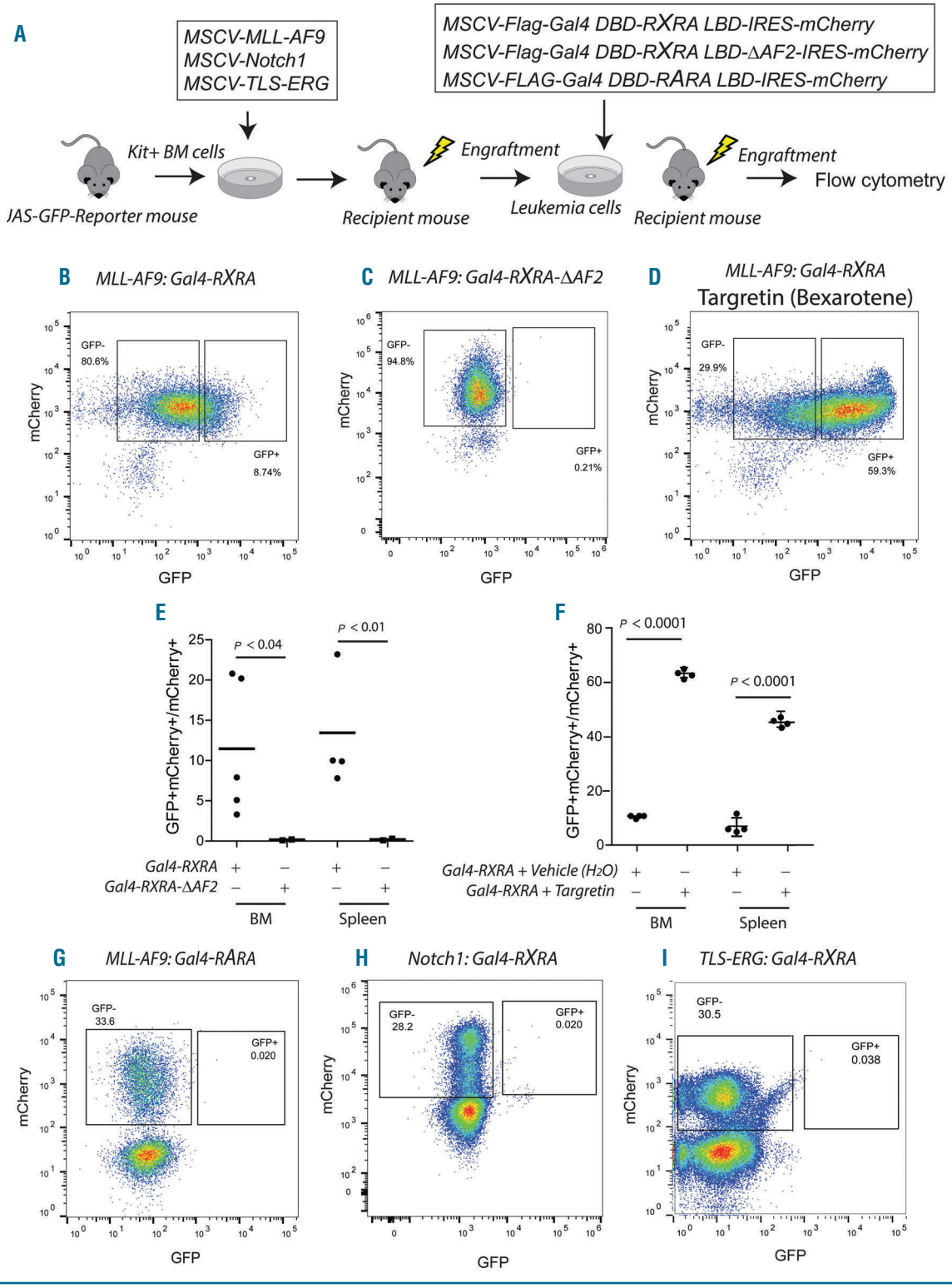


Figure 1. Retinoid X receptors (RXR) natural ligands are present in MLL-AF9 myeloid leukemia *in vivo*. (A) Schema for bone marrow (BM) transplant procedure. Kit$^+$ cells isolated from the BM of UAS-GFP mice using magnetic-activated cell sorting (MACS) were transduced with MSCV-MLL-AF9, MSCV-Notch1 or MSCV-TLS-ERG retroviruses and then injected into sublethally irradiated recipient mice. When leukemia emerged, recipient mice were sacrificed and their leukemic cells harvested. Leukemia cells were transduced with *MCSV-Flag-Gal4-RXRA-IRES-mCherry* (Gal4-RXRA), *MSCV-Flag-Gal4-RXRA-ΔAF2-IRES-mCherry* (Gal4-RXRA-ΔAF2), or *MSCV-Flag-Gal4-RARA-IRES-mCherry* (Gal4-RARA) and then injected into sublethally irradiated recipient mice. After leukemia engraftment, leukemia cells were harvested and the ratio of mCherry$^+$GFP$^+$ *versus* total mCherry$^+$ cells was evaluated by flow cytometry. (B and C) Representative data showing GFP and mCherry intensity in *MLL-AF9* leukemia cells. (D) Representative GFP and mCherry expression in mice transplanted with *MLL-AF9*-derived leukemic cells transduced with Gal4-RXRA and treated with Targretin (bexarotene, 50 mg/kg) by oral gavage administration for 2 days. (E) Combined results from mice transplanted with *MLL-AF9*-derived leukemia transduced with Gal4-RXRA (circles; n=5 recipient mice) or RXRA-ΔAF2 (squares; n=3 recipient mice). (F) Combined results from mice transplanted with *MLL-AF9*-derived leukemia cells transduced with Gal4-RXRA and gavaged with bexarotene (Targretin) (squares; n=4 recipient mice) or water (vehicle) (circles; n=4 recipient mice). (G) Representative GFP and mCherry intensity in *MLL-AF9*-derived leukemia cells transduced with Gal4-RARA and transplanted into recipient mice (n=3 recipient mice). (H and I) Representative GFP and mCherry intensity in leukemia cells derived with MSCV-Notch1 (n=5 recipient mice) or MSCV-TLS-ERG (n=4 recipient mice) retroviruses, transduced with Gal4-RXRA, and transplanted into recipient mice. *t*-test with Welch's correction.

low nM concentrations of retinoids and exhibited specificity between RARA and RXRA ligands (*Online Supplementary Figure S2D-F*). Although the RXRA LBD is used in this assay, the ligand-binding pocket is highly conserved between RXRA, RXRB, and RXRG, and no RXR subtype-specific compounds have yet been identified, suggesting that natural ligands that activate RXRA are likely to cross-react with RXRB and RXRG.[25] We noted the presence of mCherry^{+}GFP^{+} cells in both BM and spleen from multiple mice transplanted using three different primary *MLL-AF9* leukemias and engrafted into a total of five different recipients (Figure 1B and E). As a negative control, we transduced *UAS-GFP x MLL-AF9* leukemia cells with a retrovirus expressing Gal4-RXRA-ΔAF2,

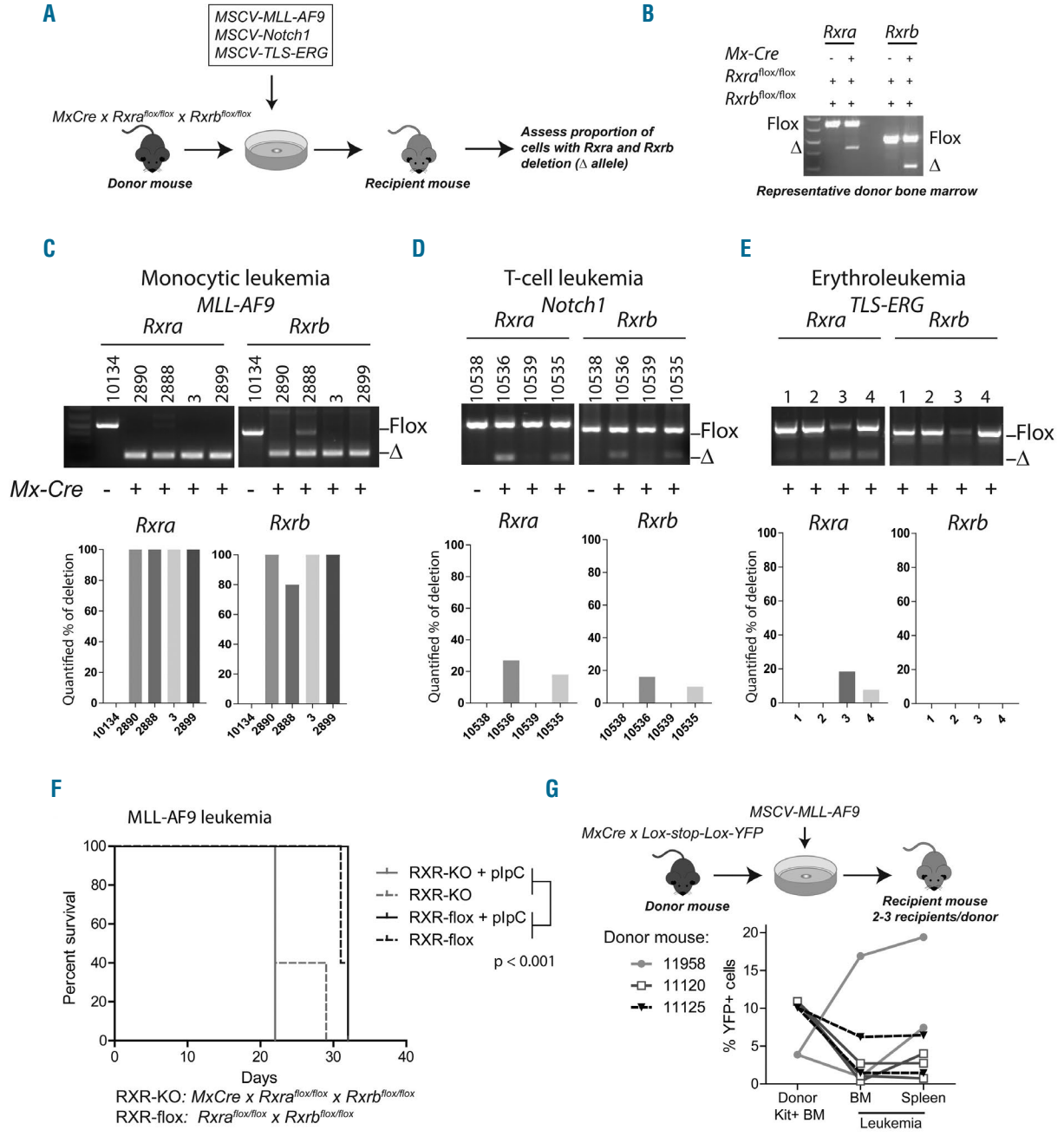


Figure 2. Retinoid X receptors (RXR) act as tumor suppressors in mouse MLL-AF9 leukemias. (A) Schema for leukemia transplant procedure. *Rxra$^{flox/flox}$ x Rxrb$^{flox/flox}$ x Mx-Cre* bone marrow (BM) cells were collected from the donor mice and transduced as indicated and injected into sublethally irradiated recipient mice. Upon leukemia engraftment, the proportion of *Rxra* and *Rxrb* deletion was assessed by polymerase chain reaction (PCR). (B) PCR results from representative donor BM cells with "Flox" indicating the retained and "Δ" the deleted allele. (C-E) PCR analysis of *Rxra* and *Rxrb* alleles from leukemias that emerged from individual mice. Bar graphs display the quantified percentage of deleted alleles in each unique leukemia. ImageJ software was used for quantification analysis. (F) Kaplan-Meier survival curve of mice injected with *Rxra$^{flox/flox}$ x Rxrb$^{flox/flox}$ x Mx-Cre MLL-AF9* leukemic cells (RXR-KO) or *Rxra$^{flox/flox}$ x Rxrb$^{flox/flox}$* MLL-AF9 leukemic cells (RXR-flox). Each cohort consisted of five mice. Indicated cohorts were treated with three doses of pIpC on days 5-10 (solid lines). (G) Schema for BM transplant procedure of *Lox-stop-Lox-YFP x Mx-Cre* mice and YFP evaluation of the hematopoietic cell. Kit^{+} BM cells from *Lox-stop-Lox-YFP x Mx-Cre* donor mice were harvested (n=3 donor mice) and transduced with *MSCV-MLL-AF9* retrovirus, then injected into sublethally irradiated recipient mice (n=7 recipient mice). The percentage of yellow fluorescent protein (YFP) was quantified by flow cytometry in BM cells before transduction and after leukemia emerged. Each line represents results from an individual recipient mouse.

which contains a deletion of the RXRA C-terminal helix 12 (AF2 domain); this mutation is able to bind to RXR ligands, but does not transactivate the reporter (Figure 1C and E, and *Online Supplementary Figure S2C*).[14]

In vivo, a significative proportion of cells remained mCherry^{+}GFP^{-} (Figure 1B). To determine whether RXRA transactivation could be further stimulated, leukemic RXRA reporter mice were orally gavaged for 2 days with 50 mg/kg bexarotene using a clinical formulation with improved solubility (Targretin). Bexarotene is a pan-RXR agonist and results were compared with vehicle control (water). We observed that bexarotene treatment further augmented RXRA-dependent GFP expression (Figure 1D and F). In contrast, we did not observe evidence of natural

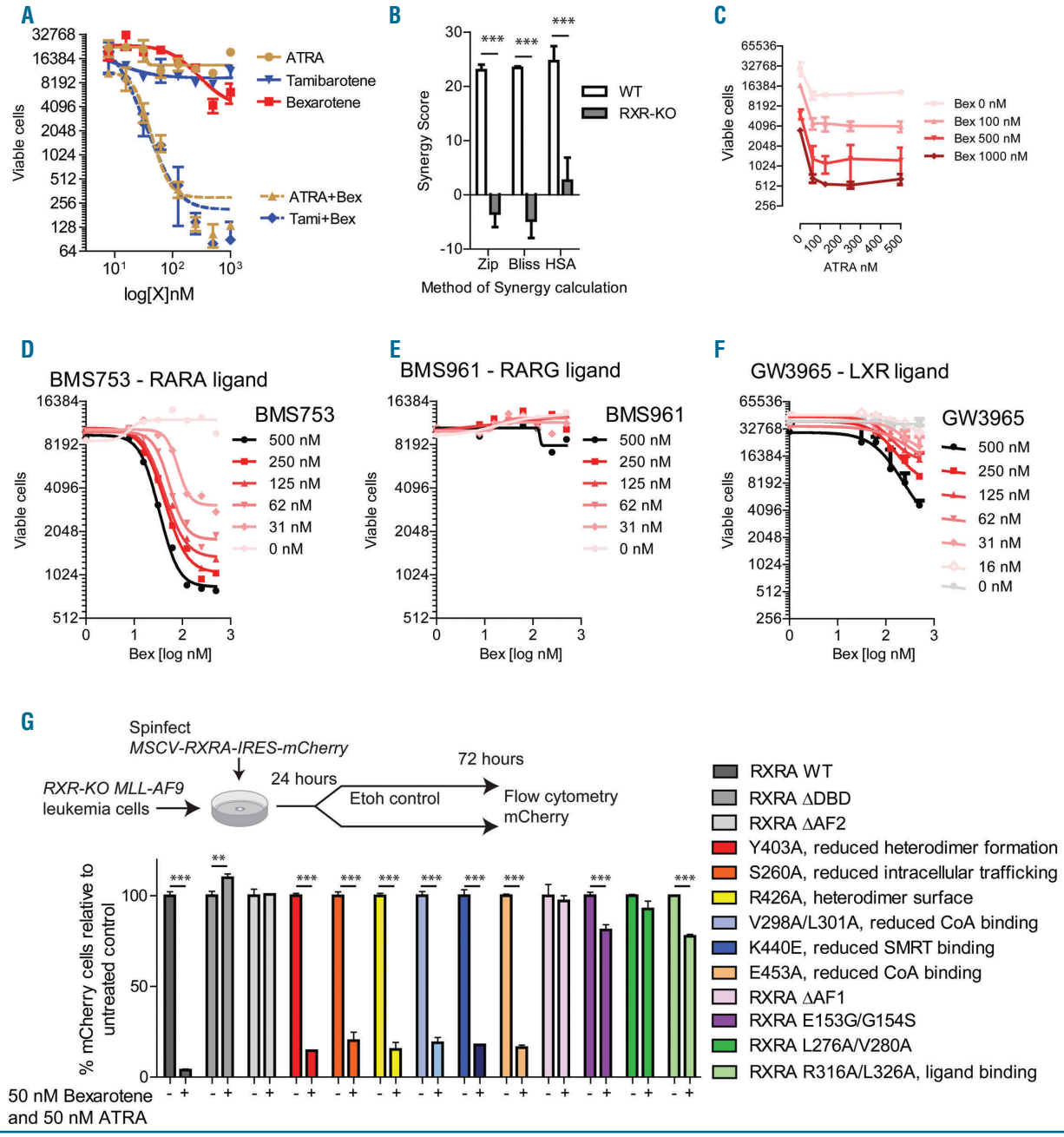


Figure 3. Pharmacologic targeting of natural retinoic acid receptor (RAR)A and retinoid X receptor (RXR)A ligands blocks MLL-AF9 proliferation *in vitro*. (A) *MLL-AF9* leukemia cells derived from *UAS-GFP* bone marrow (BM) and transduced with *MSCV-Flag-Gal4-RXRA-IRES-mCherry* retrovirus (*MLL-AF9 Gal4-RXRA* cells) were treated as indicated, replated after 48 hours (h), and total viable cells in 50 μL assessed in duplicate after 96 total h of treatment at indicated doses. (B) *MLL-AF9* RXR-flox (wild-type, WT) or RXR-KO (*Rxra/Rxrb* deficient) leukemia cells (see Figure 2) were treated with all-trans retinoic acid (ATRA) and bexarotene for 96 total h and the synergy was calculated by SynergyFinder software[24] using three different mathematical calculators for synergy *versus* additive effects (Zip, Bliss, and HAS). In these calculations, results >1 suggest mathematical synergy, although larger values are typically required for biologically relevant synergy. (C) *MLL-AF9 Gal4-RXRA* cells were treated as indicated, replated after 48 h, and total viable cells in 50 μL were assessed in duplicate after 96 total h of treatment. (D-F) *MLL-AF9* leukemia cells were treated as indicated, replated after 48 h, and total viable cells in 50 μL assessed in duplicate after 96 h of total treatment. (G) *Rxra/Rxrb* deficient MLL-AF9 leukemia cells (RXR-KO) were transduced with retrovirus encoding *MSCV-RXRA* (full length)-*IRES-mCherry* or retrovirus with indicated RXRA mutations. Mutations and published mutation effects are indicated. 24 h after retroviral transduction, cells were treated in triplicate with 50 nM ATRA/bexarotene, and the proportion of mCherry^{+} cells was assessed relative to untreated control population after 72 h. ***P*<0.01, ****P*<0.001, *t*-test with Welch's correction relative to control.

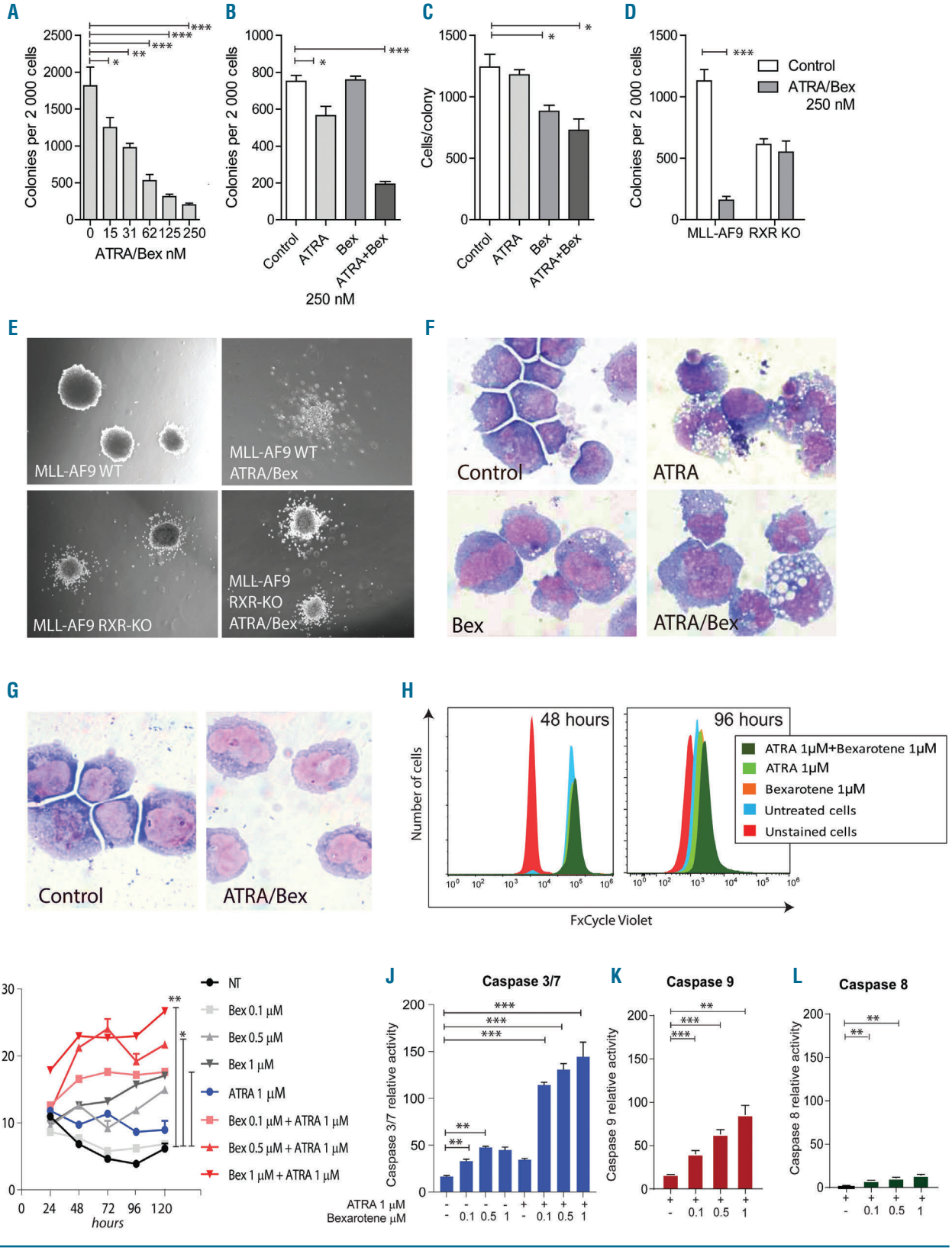


Figure 4. Differentiation and apoptosis induced by all-trans retinoic acid (ATRA)/bexarotene. (A-D) Colony forming units (CFU) in methylcellulose per 2,000 *MLL-AF9* leukemia cells treated as indicated and assessed in triplicate. (E) Photographs of *MLL-AF9* colonies treated as indicated for 7 days. (F) Cytospin preparation of *MLL-AF9* leukemia cells treated with or without ATRA and bexarotene for 96 hours (h) stained with Wright-Giemsa. (G) Cytospin preparation of *MLL-AF9* leukemia cells that remains after treatment with ATRA/bexarotene and stained with Wright-Giemsa. (H) Cell division analysis of *MLL-AF9* leukemia. On day 0, cells were stained with FxCycle Violet, and retained dye was assessed at indicated time points by flow cytometry. (I) Annexin V staining of *MLL-AF9* leukemia cells after 24, 48, 72, 96, and 120 h of ATRA and bexarotene treatment in triplicate. (J-L) Relative activity of caspases 3/7, 9, and 8 in *MLL-AF9* leukemia cells after 48 h of ATRA and bexarotene treatment in triplicate. *P<0.05, **P<0.01, ***P<0.001, t-test with Welch's correction relative to control.

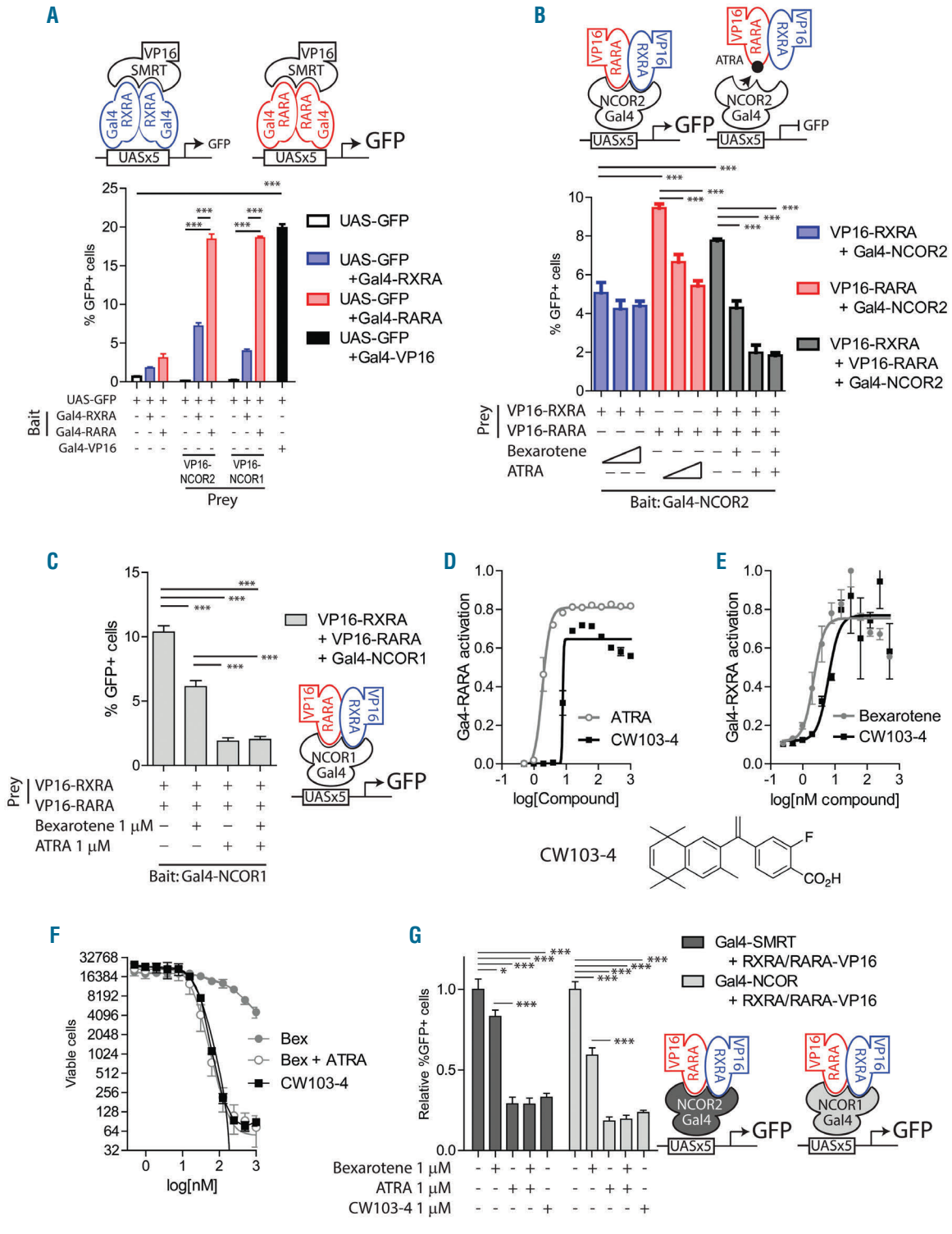


Figure 5. Interaction of co-repressors NCOR and SMRT with natural retinoic acid receptor (RAR)A : retinoid X receptor (RXR)A heterodimers. (A) Mammalian two-hybrid assay schema. 293T cells co-transfected with plasmids encoding the reporter: *UAS-GFP*; "bait": *Gal4-RXRA* or *Gal4-RARA*; and "prey": *VP16-SMRT* or *VP16-NCOR*. The percentage of GFP$^+$ cells was assessed 48 hours (h) after transfection by flow cytometry in triplicate. A vector encoding *Gal4-VP16* fusion was used as a positive control. (B) Reversely, 293T cells were co-transfected with plasmids encoding the reporter: *UAS-GFP*; "bait": *Gal4-SMRT*; and "prey": *VP16-RARA* and/or *VP16-RXRA*. Cells were treated with increasing concentrations of all-trans retinoic acid (ATRA) and bexarotene (0, 100 nM and 1 μM) in triplicate. The percentage of GFP$^+$ cells was assessed 48 h after transfection by flow cytometry. (C) 293T cells were co-transfected with plasmids encoding the reporter: *UAS-GFP*; "bait": *Gal4-NCOR*; and "prey": *VP16-RARA* and/or *VP16-RXRA*. Cells were treated with ATRA and bexarotene (1 μM) in triplicate. The percentage of GFP$^+$ cells was assessed 48 h after transfection by flow cytometry. (D and E) *MLL-AF9* leukemia cells derived from UAS-GFP bone marrow and transduced with *MSCV-Flag-Gal4-RXRA-IRES-mCherry* retrovirus (*MLL-AF9 Gal4-RXRA* cells) or *MSCV-Flag-Gal4-RARA-IRES-mCherry* retrovirus (*MLL-AF9 Gal4-RARA* cells) were treated as indicated, replated and total viable cells in 50 μL assessed after 96 total h of treatment in duplicate. (F) *MLL-AF9* cells were treated as indicated, replated and total viable cells in 50 μL assessed after 96 total h of treatment in duplicate. (G) 293T cells were co-transfected with plasmids encoding the reporter: UAS-GFP; "bait": *Gal4-NCOR* or *Gal4-SMRT*; and "prey": *VP16-RARA* and/or *VP16-RXRA*. Cells were treated with ATRA, bexarotene, and CW103-4 as indicated in triplicate. The percentage of GFP$^+$ cells was assessed 48 h after transfection by flow cytometry. *P<0.05, ***P<0.001, *t*-test with Welch's correction.

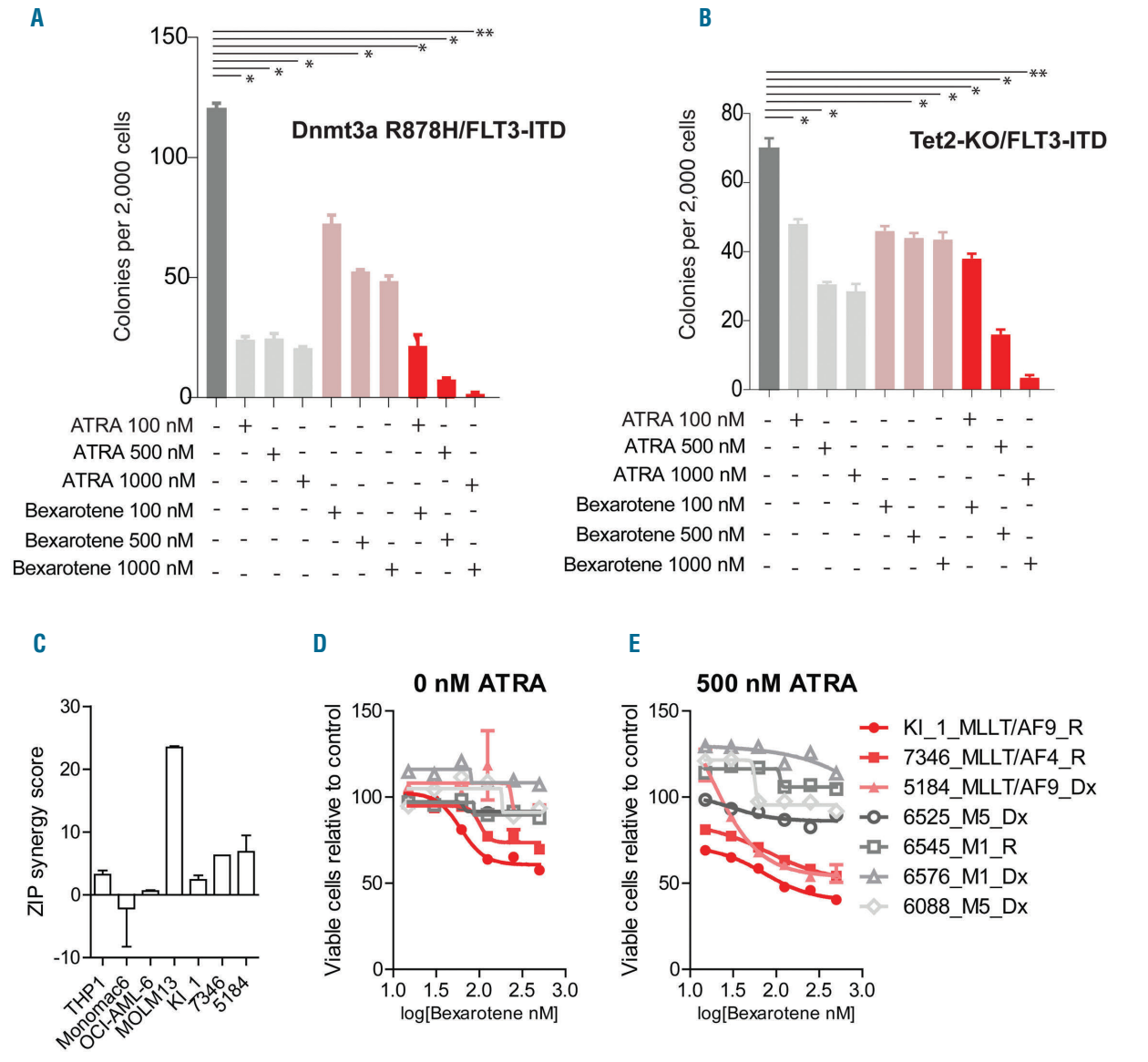


Figure 6. All-trans retinoic acid (ATRA)/bexarotene in different leukemia cell lines and in human acute myeloid leukemia (AML) *ex vivo*. (A and B) Colony forming units (CFU) in methylcellulose per 2,000 *Dnmt3a* R878H/*FLT3*-ITD and *Tet2-KO/FLT3*-ITD leukemia cells treated as indicated for 7 days in duplicate. (C) Zip synergy score of ATRA and bexarotene interactions calculated by SynergyFinder.[24] (D and E) Cell viability of primary human AML leukemia samples treated for 96 hours *ex vivo* with ATRA and bexarotene at indicated concentrations assessed in duplicate by CellTiter-Glo (CTG). Dx: sample acquired at initial diagnosis; R: sample acquired at relapse. *P<0.05, **P<0.01, *t*-test relative to control.

RARA ligands following transplantation of *UAS-GFP x MLL-AF9* leukemia cells transduced with Gal4-RARA (Figure 1G), suggesting the absence of RARA ligands, in *MLL-AF9* leukemia cells *in vivo*.

To determine whether natural RXRA ligands were present in other forms of murine leukemia, we repeated these studies in leukemias derived using activated *Notch1* (T-cell leukemia)[26] and *TLS-ERG* (erythroleukemia).[27] In neither was the presence of mCherry^{+}GFP^{+} cells observed (Figure 1H and I).

RXR acts as tumor suppressors in mouse MLL-AF9 leukemias

Given the presence of natural RXRA ligands in *MLL-AF9* leukemia, we sought to determine whether activated endogenous mouse Rxrs contribute to leukemic growth *in vivo*. We transduced *Mx-Cre x Rxra$^{flox/flox}$ x Rxrb$^{flox/flox}$* BM cells with *MLL-AF9* retrovirus, transplanted these into sublethally irradiated recipient mice, and derived subsequent leukemias (see Figure 2A). Of note, *Rxrg* expression is low to absent in hematopoietic cells (*Online Supplementary Figure S1G*).[28] We performed our initial retroviral transduction and transplantation in the absence of polyinosinic:polycytidylic acid (pIpC) treatment. However, low levels of native interferons induced Mx-Cre activity in a subset of cells, and a small proportion of BM cells exhibited *Rxra* and *Rxrb* deletion prior to transduction and transplantation (Figure 2B).[23] Unexpectedly, all *MLL-AF9*-derived primary leukemias emerged with almost 100% deletion of both *Rxra* and *Rxrb* alleles even in the absence of any pIpC injections (Figure 2C), suggesting a strong positive selection for the Δ/Δ (deleted) alleles. In

contrast, repeat experiments deriving *Notch1* T-cell leukemia and TLS-ERG erythroleukemias showed near complete retention of *Rxra*$^{flox/flox}$ *and Rxrb*$^{flox/flox}$ alleles (Figure 2D and E). We performed secondary transplantation of *MLL-AF9* leukemia cells derived from *Mx-Cre x Rxra*$^{flox/flox}$ *x Rxrb*$^{flox/flox}$ and from *Rxra*$^{flox/flox}$ *x Rxrb*$^{flox/flox}$ mice using 1x10^6 leukemia cells per recipient. Because these tumors were transplanted immediately, we were unaware of their deletion status and separately treated cohorts of mice with pIpC or control intending to determine whether the deleted allele augmented growth. We subsequently noted that primary tumors derived from Mx-Cre$^+$ mice already carried deleted alleles and that these *Rxra/Rxrb* null (RXR-KO) leukemias resulted in shorter latency than tumors derived from Mx-Cre$^-$ mice, and that further stimulation by pIpC did not impact survival (Figure 2F). This suggests that RXR-KO leukemia cells grow more quickly *in vivo* than their wild-type counterparts, and could, therefore, have outgrown the wild-type populations during the primary transplantations. To exclude the possibility that *MLL-AF9* leukemogenesis or hematopoietic transplantation could non-specifically activate *Mx-Cre* and induce deletion of the *Rxr* alleles, we crossed *Mx-Cre* mice with *Lox-stop-Lox-YFP* reporter mice and derived seven independent *MLL-AF9* leukemias using three individual donors. The leukemia cells that emerged were not associated with increased YFP expression, suggesting that Mx-Cre activation does not routinely occur following viral *MLL-AF9* leukemogenesis and transplantation (Figure 2G).

Pharmacologic targeting RXRA and RARA *in vitro*

In vitro, bexarotene exerted dose-dependent growth inhibition in *UAS-GFP x MLL-AF9 x Gal4-RXRA* leukemia cells, although the effect was modest (2-4 fold) (Figure 3A, red line). Because Rxrs act as heterodimers with other orphan receptors, we screened for interactions with additional ligands. The combination of bexarotene with either ATRA or tamibarotene (an RARA-specific agonist) lead to profound, dose-dependent growth inhibition while single-agent RARA ligands resulted in only modest (2-4 fold) growth inhibition (Figure 3A, blue and brown lines). Response and synergy were absent in RXR-KO *MLL-AF9* leukemia cells (Figure 3B). The effect of ATRA on leukemic growth inhibition reached a plateau at 60-100 nM, whereas increasing concentrations of bexarotene were associated with increasing growth reduction up to 1 μM (Figure 3C). After 5 days of retinoids, we noted the proportion of GFP$^+$ cells and the GFP median fluorescence intensity (MFI) was significantly reduced (*Online Supplementary Figure S3A* and *B*), suggesting that the most RXR responsive cells experienced the greatest negative selection by retinoid treatment.

We tested a series of additional nuclear receptor ligands for anti-leukemic activity. A broad range of RXR ligands cooperated with ATRA to induce anti-leukemic activity and again displayed only modest single-agent activity (*Online Supplementary Figure S4A* and *B*). The RARA-specific agonist BMS753, but not the RARG-specific agonist BMS961, cooperated with bexarotene to inhibit MLL-AF9 cell growth (Figure 3D and E). RXR weak agonists and antagonists (LG100754 and HX531) were insufficient to cooperate with ATRA or tamibarotene (RARA specific agonist) and the pan-RAR inverse agonist BMS493 inhibited the effect of combination ATRA and bexarotene (*Online Supplementary Figure S4C* and *D*). Finally, the PPARA agonist GW7647, PPARG agonist pioglitazone, and the LXR agonist GW3965 had modest effects with bexarotene (Figure 3F and *Online Supplementary Figure S4E* and *F*).

RXRA domains required for retinoid sensitivity

To map the structural domains of RXRA required for anti-leukemic activity, we retrovirally re-expressed RXRA in RXR-KO *MLL-AF9* leukemia cells (Figure 3G). mCherry expression identified transduced cells. A series of *RXRA* deletions and mutations were generated and the position of the *LBD* mutations are highlighted within an available RXRA crystal structure (Protein Database: 4K4J) (*Online Supplementary Figure S5A* and *B*). The expression of the RXRA mutants was confirmed by western blot (*Online Supplementary Figure S5C*). In cells transduced with full-length RXRA, bexarotene and ATRA induced a strong decrease in the proportion of mCherry$^+$ cells after 48 h (Figure 3G), consistent with a strong retinoid sensitivity among cells expressing wild-type RXRA. We found that mutants lacking the AF1, DBD, or AF2 domain and mutations reported to: disrupt the DNA binding zinc finger (E153G/G154S),[29] reduce co-activator binding (L276A/V280A),[30] or abrogate ligand binding (R316A/L326A),[31] were unresponsive to retinoids (Figure 3G). Additional mutations reported to: reduce co-activator binding (E453A, V298A/L301A),[32] reduce intracellular trafficking of RXRA (S260A),[33] obstruct the heterodimer interface (Y402A, R426A)[34] or reduce co-repressor binding to RXRA (K440E),[32] largely retained sensitivity to retinoids (Figure 3G). These data demonstrate the necessity of specific, functional RXRA domains (AF1, DBD, and AF2), as well as RXRA co-activator-interacting moieties for the activity of the RARA:RXRA heterodimer.

Maturation and apoptosis induced by ATRA/bexarotene

Retinoids have been associated with myeloid maturation programs.[35-38] We observed that different culture conditions influenced the effect of retinoid-induced maturation and apoptosis in *MLL-AF9* leukemia. When grown in methylcellulose, combination ATRA/bexarotene reduced colony-forming capacity in a dose-dependent manner (Figure 4A); these effects were associated with changes in the number of colonies, the size of the colonies (smaller), colony morphology (diffusion of cell clustering), and cellular cytomorphology (acquisition of vacuoles), consistent with loss of self-renewal and maturation (Figure A-F). Again, these phenotypes were absent in RXR-KO leukemia cells and single-agent retinoids resulted in modest effects. However, when *MLL-AF9* leukemia cells were grown in liquid culture, retinoid combinations did not induce cytomorphologic changes or cell cycle exit, but rather, they induced time- and dose-dependent apoptosis and activation of intrinsic caspase pathways (Caspases 3/7 and 9) (Figure 4G-L).

Co-repressor binding to RARA:RXRA heterodimers

The synergy observed between ATRA and bexarotene suggests different effects within the RARA:RXRA heterodimer. In the absence of retinoids, the RARA:RXRA heterodimer binds to co-repressors such as the nuclear receptor co-repressor (NCOR1) and silencing mediator of retinoic acid and thyroid hormone receptor (SMRT, aka NCOR2).[39-42] Using a mammalian two-hybrid assay in 293T cells,[43] we noted that RARA resulted in greater tran-

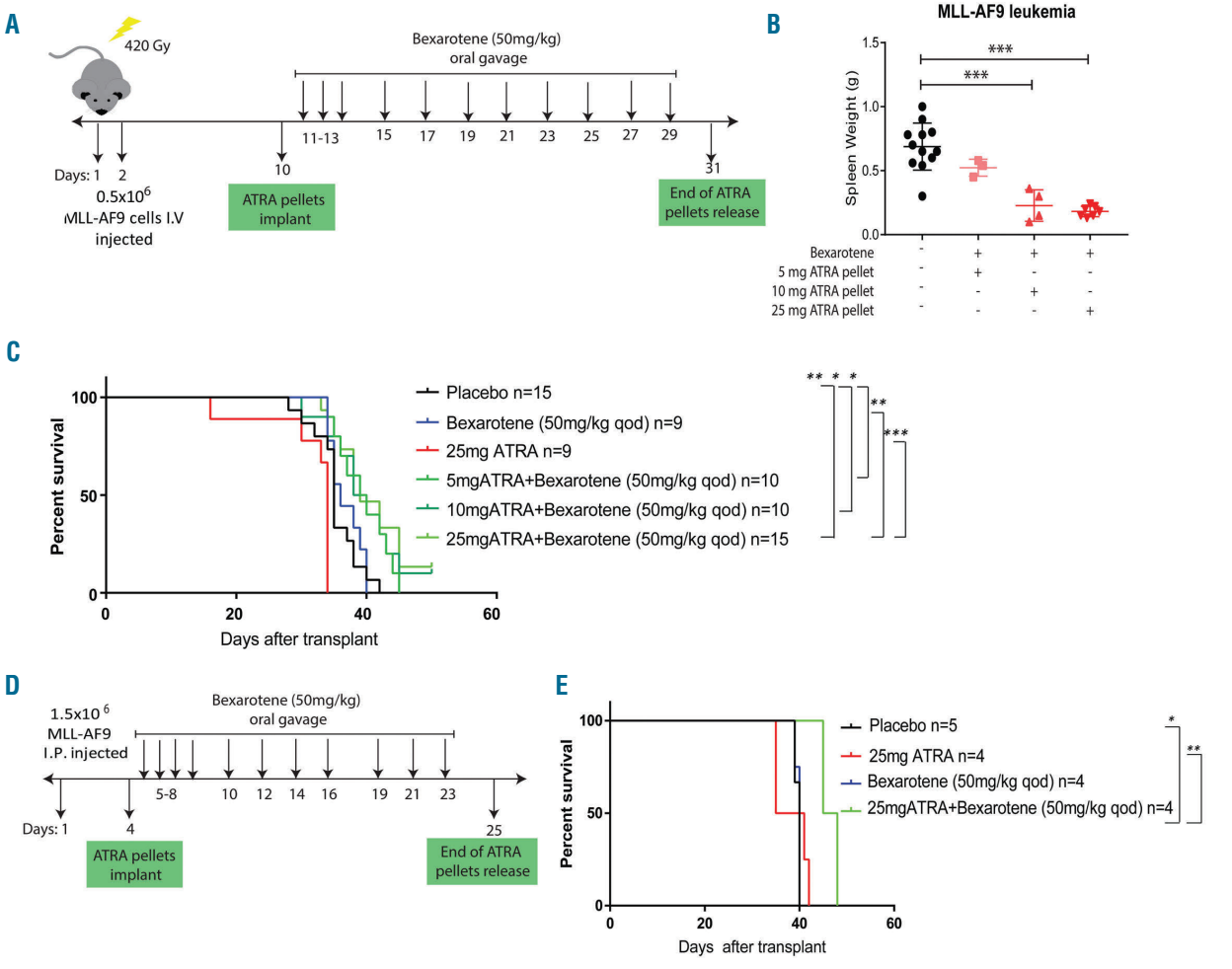


Figure 7. Concurrent all-trans retinoic acid (ATRA)/bexarotene treatment reduces MLL-AF9 leukemia burden *in vivo*. (A) Schema for leukemia transplant procedure and *in vivo* treatment. Sublethally irradiated FVB mice were transplanted with 0.5x10^6 *MLL-AF9* leukemia cells. Ten days later the mice were divided in four different cohorts and treated with 21-day release ATRA pellets. 5 mg: n=5 (~0.23 mg/day), 10 mg: n=5 (~0.5 mg/day), and 25 mg: n=8 (~1.2 mg/day). One day after pellet implantation, bexarotene (50 mg/kg) was delivered by oral gavage as indicated. A control cohort was implanted with placebo pellets and treated with the vehicle gavage (n=12). IV: intravenous. (B) The mice were sacrificed 21 days from pellet implantation and the spleen weight analyzed. (C) Kaplan-Meier survival curve analysis of mice transplanted with MLL-AF9 cells and treated as indicated in (A). (D) Schema for leukemia transplant procedure and mice treatment. FVB mice were transplanted with 1.5x10^6 *MLL-AF9* leukemia cells by intraperitoneal (IP) injection. Five days later the mice were divided in four different cohorts and implanted with 21-day release ATRA pellets 25 mg (~1.2 mg/day) or placebo pellets. One day after pellet implantation, bexarotene (Targretin, 50 mg/kg) was delivered by oral gavage as indicated. (E) Kaplan-Meier survival curve analysis of mice transplanted with MLL-AF9 cells and treated as indicated in (E). **P*<0.05, ***P*<0.01, ****P*<0.001, *t*-test.

scriptional activity with either co-repressor (SMRT) *versus* RXRA, suggesting a stronger affinity of RARA to co-repressors than RXRA (Figure 5A). Similarly, when the bait and prey strategy was reversed (Figure 5B), ATRA led to greater reporter inhibition than bexarotene, with as great an effect as the combination of ATRA and bexarotene (Figure 5B). Similar results were noted using NCOR as bait (Figure 5C), suggesting that co-repressor interactions with RARA:RXRA heterodimers are dominated by interactions with RARA.

A bexarotene derivative (CW103-4) had been identified with potential dual RARA/RXRA activity.[44-46] CW103-4 has improved murine pharmacokinetics compared with bexarotene (peak plasma concentration of 152,955.83 *vs.* 18,633.33 ng/mL and area under the curve of 51,531 *vs.* 8,523 ng/mL).[43] However, this is associated with a 5-fold increase in triglycerides 24 h after treatment,[43] making it an interesting tool compound, but not an obvious clinical therapy. We assessed this compound to determine whether its dual-affinity might provide single-agent activity *in vitro*. Indeed, CW103-4 exhibited dual RARA and RXRA activation in *UAS-GFP x MLL-AF9* leukemia cells, and was capable of ATRA-independent anti-leukemic activity (Figure 5D-F and *Online Supplementary Figure S6A-D*). Specifically, CW103-4 induced proliferative capacity reduction and apoptosis mediated by caspases 3/7 activation (*Online Supplementary Figure S6A-D*). Interestingly, CW103-4 also induced consistent single-agent co-repressor release (Figure 5G). To determine whether these effects might occur through LXRs or PPARD, we assessed reporter activation and found no evidence of cross-reactivity with these receptors (*Online Supplementary Figure S6E-G*). These results suggest that single-agent bexarotene is ineffective to induce co-repressor release from the RARA:RXRA heterodimer, and that co-repressor release results primarily from RARA activation, providing an explanation for the anti-leukemic combination synergy (Figure 3A and B).

ATRA/bexarotene responses in diverse acute myeloid leukemias

To determine whether retinoid combination efficacy was limited to MLL-AF9 models or might extend to other leukemias, we examined the effect of combination ATRA/bexarotene on the proliferative capacity of two additional primary murine AML. The first was derived in the Timothy Ley lab using a *Dnmt3a* R878H knock-in allele and BM cells transduced with MSCV-FLT3-ITD virus containing GFP (Dnmt3a R878H/FLT3-IT (*T Ley, unpublished observations, 2019*). The second was derived in the Ross Levine lab using germline *Tet2* deficiency crossed with a germline FLT3-ITD allele (*Tet2-KO x FLT3-ITD*).[47] Both primary mouse leukemias could be grown transiently in methylcellulose, and we observed anti-leukemic activity of combination retinoids, with limited effects by single agents (Figure 6A and B). We examined cell growth of several human AML cell lines and primary human AML following ATRA/bexarotene treatment, noting low nM IC_{50} combination ATRA/bexarotene in THP1, Monomac6, OCI-AML-3, and MOLM13 (1.3±1.2, 19.2±1.7, 5.0±1.1, and 15.8±1.2, respectively), with evidence of synergy in THP1 and MOLM13, both of which contain MLL translocations (Figure 6C). Slightly higher IC_{50} values were observed for CW103-4 (8±1.1, 43±1.2, 20±1.1, and 24±1.4, respectively). We also assessed retinoid responses in a series of primary AML samples collected at diagnosis or relapse and noted evidence of response and modest synergy in samples with MLL translocations (KI_1, 7346, and 5184) (Figure 6D and E).

ATRA/bexarotene activity *in vivo*

To determine whether retinoid combinations could be transitioned into *in vivo* activity, we first assessed the potential tolerability of the combination on normal hematopoiesis. Two cohorts of 5 wild-type mice were treated with ATRA/bexarotene by oral gavage or vehicle control. No differences were noted in the peripheral blood counts after 3 weeks of treatment (*Online Supplementary Figure S7A-E*), suggesting tolerance of the combination by normal hematopoiesis.

Subsequently, we tested the effect of combination retinoids on MLL-AF9 leukemia *in vivo*. In our first studies, we engrafted MLL-AF9 leukemia cells using sublethal irradiation and we treated mice with slow-release ATRA/bexarotene pellets implanted subcutaneously. However, this lead to wound dehiscence and loss of the pellets (*data not shown*). Second, four cohorts of mice were treated with 21 days ATRA release pellets (placebo, 5 mg, 10 mg, and 25 mg, which provide an average of 0.23 mg, 0.5 mg, and 1.2 mg/day, respectively). The day after pellet implantation, all ATRA cohorts received bexarotene by oral gavage (in α-tocopherol, 50 mg/kg, which is reported to be better tolerated as a vehicle than corn oil during serial administration)[48] (Figure 7A). However, tolerance of the combination by the mice was quite poor, as they exhibited reduced activity the day after gavage, ruffled fur, weight loss, and poor wound healing, and bexarotene could be administered only every other day (qod) (*Online Supplementary Figure S7F*). After 21 days from pellet implantation, the mice were sacrificed and the spleen weight was analyzed. This end-point was designed to isolate leukemic growth from confounding factors of toxicity. We observed a significant dose-dependent effect of combination retinoid treatment in reducing the tumor burden (spleen weight) of treated mice compared to the control cohort (Figure 7B). Of note, the *in vivo* steady-state serum concentration of ATRA resulting from 10 mg 21-day release pellets is reported as 100-220 nM,[49] and the 5 mg pellets did not provide a sufficient dose to inhibit leukemic growth.

Third, we suspected that some of the toxicity might be due to retinoid-induced radiation recall, a known complication of retinoids,[50,51] and tolerability might be improved using a micronized formula of bexarotene found in the clinical Targretin formulation.[52] We found that *MLL-AF9* leukemia cells engrafted consistently following IP injection without irradiation conditioning, with improved fur ruffling, improved wound healing, and no weight loss (*Online Supplementary Figure S7G*). However, the mice again exhibited reduced activity the day after gavage and administration was again reduced to qod due to tolerability. Despite this, the combination of ATRA/bexarotene was associated with improved survival (Figure 7D and E). This study was repeated a fourth time with similar modest, but significant, improvement in survival and tolerability issues that persisted (*data not shown*). Thus, retinoid delivery to mice in the context of leukemic models remains a challenge, but is still associated with a statistical and reproducible survival advantage, although modest.

Discussion

Retinoid therapy has transformed the treatment of APL.[16,17] Retinoids have been explored in different clinical trials in non-APL, and their action has repeatedly been shown, although never to the extent seen in APL.[18]

We previously found that natural RXRA ligands are present in mouse hematopoietic cells *in vivo*, that they are biased toward myeloid cells and dynamically regulated under myeloid stress (e.g., GCSF treatment).[14] Consistent with those findings, in this study we found also that a malignant myeloid stressor (*MLL-AF9* transformation) was associated with natural *in vivo* RXRA ligands. *In vivo* natural RXRA ligands resulted in incomplete reporter activation, and pharmacologic doses of ligands could activate the reporter further under both basal conditions[14] and leukemic stress (Figure 1). In contrast to these RXRA results, we have been unable to detect natural RARA ligands (Figure 1G).[14,22]

We found that *MLL-AF9* cells that carried deleted *Rxra* and *Rxrb* alleles had a competitive advantage during MLL-AF9 leukemogenesis (Figure 2C and F). Whereas Notch-derived T-cell leukemias and TLS-ERG-derived erythroleukemia were not associated with *in vivo* natural RXRA ligands, and also were not associated with a competitive advantage among cells with *Rxra* or *Rxrb* deletion (Figures 1 and 2). Thus, the presence *versus* absence of active natural ligands may determine whether RXR exert tumor suppressor activity.

RXR form heterodimers with a wide range of orphan nuclear receptors. Other groups have reported co-operativity of RXR ligands with either RARA ligands[37] or LXR ligands.[53] MLL-AF9 leukemia cells appeared most sensitive to the combination of RARA and RXR ligands (Figure 3). Culture conditions influenced retinoid responses, and we observed that combinations of retinoids induced either maturation or apoptosis depending on whether the leukemia cells were grown in methylcellulose or liquid

culture (Figure 4). The relevant cell signals that influence retinoid responses in these two settings still have to be defined.

The synergy of ATRA and bexarotene can be understood within the context of co-repressor interactions with the RARA:RXRA heterodimer. Other studies of the RARA:RXRA heterodimer identified a subordinate role for RXR.[32,39,41,42] Consistent with those results, mammalian two-hybrid assays demonstrated that RARA bound more effectively to co-repressors, that ATRA was more efficient than bexarotene at releasing co-repressors from RARA:RXRA, and that these limitations could be overcome using a bexarotene-derivative compound with dual RARA/RXRA activity (CW103-4) (Figure 5). Thus, the ATRA-dependent release of co-repressor from the RARA:RXRA heterodimer may account for the synergy observed between ATRA and bexarotene.

Within the RARA:RXRA heterodimer, specific RXRA domains appear necessary for anti-leukemic effects, including the AF1, DBD, and AF2, as well as amino acids responsible for ligand-binding and co-activator recruitment (Figure 3G). Thus, although ligand activation of RXR may be subordinate to RAR, RXR play an active, not a passive role in anti-leukemic response to ligands.

Other studies have suggested that biomarkers may identify subsets of retinoid-sensitive patients.[54,55] We note that expression of *RARA* and *RXRA* are co-ordinately regulated in AML with highest expression in M4/M5-FAB AML (*Online Supplementary Figure S1*). Cell lines and primary AML samples suggest that combination retinoids may be active in leukemias beyond the mouse MLL-AF9 model and a potential bias in sensitivity within this group of patients (Figure 6). Larger studies will be required to accurately determine the specificity and sensitivity of these biomarkers as predictors of retinoid responses in non-APL AML. We have established an on-going *ex vivo* biomarker study of primary AML samples (*clinicaltrials.gov identifier: NCT04263181*) to further address this issue.

Although both ATRA and bexarotene are well-tolerated orally-available compounds, approved by the US Food and Drug Administration, we found it difficult to provide mice with a sufficient dose to enable us to observe any big effects (Figure 7). Both oral ATRA and bexarotene are poorly soluble, have short serum half-lives (1 and 7 h, respectively), and their BM concentrations may be locally reduced by stroma expression of P450 enzymes.[56] Given the short serum half-life of bexarotene, our administration of bexarotene (given every other day) is likely associated with a suboptimal area under the curve and incomplete receptor activation *in vivo*. Although ATRA is highly active against APL, administration and *in vivo* activity of ATRA in mouse models of APL have been surprisingly modest. For example, across multiple mouse models, ATRA improved median survival in secondary transplants: 53 days *versus* 31 days,[57] 35 *versus* 25 days,[58] approximately 90 days *versus* approximately 50 days,[59] approximately 75 days *versus* approximately 35 days,[60] approximately 45 days *versus* approximately 35 days,[61] and approximately 130 days *versus* approximately 85 days.[49] In contrast, Westervelt *et al*. found that a liposomal formulation of ATRA (that is now no longer commercially available) resulted in much higher levels of ATRA in mice than ATRA slow-release pellets, and in 88% long-term survival. Therefore, additional chemical or formulaic modifications may be required to optimize *in vivo* retinoids as anti-leukemic therapeutics, and the combination of free acid ATRA and bexarotene is not sufficient to overcome these limitations.

In summary, we find evidence of natural RXRA, but not RARA ligands in myelomonocytic MLL-AF9 mouse leukemia *in vivo* where the concurrent presence of receptors and active ligands acts as tumor suppressors. RARA and RXRA are co-ordinately expressed in myelomonocytic leukemias, and optimal retinoid activation appears to require concurrent activation of both elements in the RARA:RXRA heterodimer, providing a further step toward improved retinoid therapeutics in AML.

Disclosures

No conflicts of interest to disclose.

Contributions

JSW and OdM designed experiments, performed experiments, and wrote the manuscript; HN, GH, HK, MAF, AV, JB, CW, MPM, MR and CH designed and performed experiments.

Acknowledgments

We thank the Alvin J. Siteman Cancer Center at Washington University School of Medicine and Barnes-Jewish Hospital in St. Louis, MO, USA for the use of the Flow Cytometry Core. The Siteman Cancer Center is supported in part by an NCI Cancer Center Support Grant P30 CA91842. We thank High-Throughput Screening Center at Washington University School of Medicine in St. Louis, MO, USA. We thank Deborah Laflamme, Conner York, and Julie Richie for technical assistance.

Funding

This work was supported by NIH R01 HL128447 (to JSW), NIH P50 CA171963 (Project 1, to JSW and DRP) by the Siteman Investment Program (to JSW), and grants from the Spanish Ministerio de Ciencia e Innovación (MCI) (SAF2015-71878-REDT-NurCaMeIn, RTI2018-095928-B100) (to MR). The CNIC is supported by the MCI and the Pro CNIC Foundation and is a Severo Ochoa Center of Excellence (SEV-2015-0505).

References

1. Bushue N, Wan YJ. Retinoid pathway and cancer therapeutics. Adv Drug Deliv Rev. 2010;62(13):1285-1298.
2. Oren T, Sher JA, Evans T. Hematopoiesis and retinoids: development and disease. Leuk Lymphoma. 2003;44(11):1881-1891.
3. Kastner P, Lawrence HJ, Waltzinger C, Ghyselinck NB, Chambon P, Chan S. Positive and negative regulation of granulopoiesis by endogenous RARalpha. Blood. 2001;97(5):1314-1320.
4. Evans RM, Mangelsdorf DJ. Nuclear receptors, RXR, and the Big Bang. Cell. 2014; 157(1):255-266.
5. Purton LE, Dworkin S, Olsen GH, et al. RARgamma is critical for maintaining a balance between hematopoietic stem cell self-renewal and differentiation. J Exp Med. 2006;203(5):1283-1293.
6. Lefebvre P, Benomar Y, Staels B. Retinoid X receptors: common heterodimerization partners with distinct functions. Trends Endocrinol Metab. 2010;21(11):676-683.
7. Network TCGAR. Genomic and epigenomic landscapes of adult de novo acute myeloid leukemia. N Engl J Med. 2013; 368(22):2059-2074.
8. Loinder K, Soderstrom M. The nuclear receptor corepressor (N-CoR) modulates basal and activated transcription of genes controlled by retinoic acid. J Steroid

Biochem Mol Biol. 2003;84(1):15-21.
9. Martino OD, Welch JS. Retinoic acid receptors in acute myeloid leukemia therapy. Cancers (Basel). 2019;11(12):1915.
10. Altucci L, Gronemeyer H. The promise of retinoids to fight against cancer. Nat Rev Cancer. 2001;1(3):181-193.
11. Arnold SL, Amory JK, Walsh TJ, Isoherranen N. A sensitive and specific method for measurement of multiple retinoids in human serum with UHPLC-MS/MS. J Lipid Res. 2012;53(3):587-598.
12. Jones JW, Pierzchalski K, Yu J, Kane MA. Use of fast HPLC multiple reaction monitoring cubed for endogenous retinoic acid quantification in complex matrices. Anal Chem. 2015;87(6):3222-3230.
13. Lengqvist J, Mata De Urquiza A, Bergman AC, et al. Polyunsaturated fatty acids including docosahexaenoic and arachidonic acid bind to the retinoid X receptor alpha ligand-binding domain. Mol Cell Proteomics. 2004;3(7):692-703.
14. Niu H, Fujiwara H, di Martino O, et al. Endogenous retinoid X receptor ligands in mouse hematopoietic cells. Sci Signal. 2017;10(503):eaan1011.
15. Ruhl R, Krzyzosiak A, Niewiadomska-Cimicka A, et al. 9-cis-13,14-dihydroretinoic acid is an endogenous retinoid acting as RXR ligand in mice. PLoS Genet. 2015;11(6):e1005213.
16. Lo-Coco F, Avvisati G, Vignetti M, et al. Retinoic acid and arsenic trioxide for acute promyelocytic leukemia. N Engl J Med. 2013;369(2):111-121.
17. Wang ZY, Chen Z. Acute promyelocytic leukemia: from highly fatal to highly curable. Blood. 2008;111(5):2505-2515.
18. Brown G, Hughes P. Retinoid differentiation therapy for common types of acute myeloid leukemia. Leuk Res Treatment. 2012;2012:939021.
19. Querfeld C, Rosen ST, Guitart J, et al. Comparison of selective retinoic acid receptor- and retinoic X receptor-mediated efficacy, tolerance, and survival in cutaneous T-cell lymphoma. J Am Acad Dermatol. 2004;51(1):25-32.
20. Tsai DE, Luger SM, Andreadis C, et al. A phase I study of bexarotene, a retinoic X receptor agonist, in non-M3 acute myeloid leukemia. Clin Cancer Res. 2008;14(17):5619-5625.
21. Welch JS, Niu H, Uy GL, et al. A phase I dose escalation study of oral bexarotene in combination with intravenous decitabine in patients with AML. Am J Hematol. 2014;89(8):E103-108.
22. Niu H, Chacko J, Hadwiger G, Welch JS. Absence of natural intracellular retinoids in mouse bone marrow cells and implications for PML-RARA transformation. Blood Cancer J. 2015;5:e284.
23. Menendez-Gutierrez MP, Roszer T, Fuentes L, et al. Retinoid X receptors orchestrate osteoclast differentiation and postnatal bone remodeling. J Clin Invest. 2015;125(2):809-823.
24. Ianevski A, He L, Aittokallio T, Tang J. SynergyFinder: a web application for analyzing drug combination dose-response matrix data. Bioinformatics. 2017;33(15):2413-2415.
25. Alvarez S, Alvarez R, Khanwalkar H, et al. Retinoid receptor subtype-selective modulators through synthetic modifications of RARgamma agonists. Bioorg Med Chem. 2009;17(13):4345-4359.
26. Pear WS, Aster JC, Scott ML, et al. Exclusive development of T cell neoplasms in mice transplanted with bone marrow expressing activated Notch alleles. J Exp Med. 1996;183(5):2283-2291.
27. Carmichael CL, Metcalf D, Henley KJ, et al. Hematopoietic overexpression of the transcription factor Erg induces lymphoid and erythro-megakaryocytic leukemia. Proc Natl Acad Sci U S A. 2012;109(38):15437-15442
28. Ricote M, Snyder CS, Leung HY, Chen J, Chien KR, Glass CK. Normal hematopoiesis after conditional targeting of RXRalpha in murine hematopoietic stem/progenitor cells. J Leukoc Biol. 2006;80(4):850-861.
29. Temple KA, Cohen RN, Wondisford SR, Yu C, Deplewski D, Wondisford FE. An intact DNA-binding domain is not required for peroxisome proliferator-activated receptor gamma (PPARgamma) binding and activation on some PPAR response elements. J Biol Chem. 2005;280(5):3529-3540.
30. Leo C, Yang X, Liu J, Li H, Chen JD. Role of retinoid receptor coactivator pockets in cofactor recruitment and transcriptional regulation. J Biol Chem. 2001;276(25):23127-23134.
31. Hiromori Y, Aoki A, Nishikawa J, Nagase H, Nakanishi T. Transactivation of the human retinoid X receptor by organotins: use of site-directed mutagenesis to identify critical amino acid residues for organotin-induced transactivation. Metallomics. 2015;7(7):1180-1188.
32. Ghosh JC, Yang X, Zhang A, et al. Interactions that determine the assembly of a retinoid X receptor/corepressor complex. Proc Natl Acad Sci U S A. 2002;99(9):5842-5847.
33. Jusu S, Presley JF, Kremer R. Phosphorylation of human retinoid X receptor alpha at Serine 260 impairs its subcellular localization, receptor interaction, nuclear mobility, and 1alpha,25-dihydroxyvitamin D3-dependent DNA binding in Ras-transformed keratinocytes. J Biol Chem. 2017;292(4):1490-1509.
34. Vivat-Hannah V, Bourguet W, Gottardis M, Gronemeyer H. Separation of retinoid X receptor homo- and heterodimerization functions. Mol Cell Biol. 2003;23(21):7678-7688.
35. Welch JS, Klco JM, Varghese N, Nagarajan R, Ley TJ. Rara haploinsufficiency modestly influences the phenotype of acute promyelocytic leukemia in mice. Blood. 2011;117(8):2460-2468.
36. Kastner P, Chan S. Function of RARalpha during the maturation of neutrophils. Oncogene. 2001;20(49):7178-7185.
37. Kizaki M, Dawson MI, Heyman R, et al. Effects of novel retinoid X receptor-selective ligands on myeloid leukemia differentiation and proliferation in vitro. Blood. 1996;87(5):1977-1984.
38. Collins SJ. Retinoic acid receptors, hematopoiesis and leukemogenesis. Curr Opin Hematol. 2008;15(4):346-351.
39. Altucci L, Rossin A, Hirsch O, et al. Rexinoid-triggered differentiation and tumor-selective apoptosis of acute myeloid leukemia by protein kinase A-mediated desubordination of retinoid X receptor. Cancer Res. 2005;65(19):8754-8765.
40. Lammi J, Perlmann T, Aarnisalo P. Corepressor interaction differentiates the permissive and non-permissive retinoid X receptor heterodimers. Arch Biochem Biophys. 2008;472(2):105-114.
41. Pogenberg V, Guichou JF, Vivat-Hannah V, et al. Characterization of the interaction between retinoic acid receptor/retinoid X receptor (RAR/RXR) heterodimers and transcriptional coactivators through structural and fluorescence anisotropy studies. J Biol Chem. 2005;280(2):1625-1633.
42. Hu X, Li Y, Lazar MA. Determinants of CoRNR-dependent repression complex assembly on nuclear hormone receptors. Mol Cell Biol. 2001;21(5):1747-1758.
43. Zhang J, Hu X, Lazar MA. A novel role for helix 12 of retinoid X receptor in regulating repression. Mol Cell Biol. 1999;19(9):6448-6457.
44. Hanish BJ, Hackney Price JF, Kaneko I, et al. A novel gene expression analytics-based approach to structure aided design of rexinoids for development as next-generation cancer therapeutics. Steroids. 2018;135:36-49.
45. Jurutka PW, Kaneko I, Yang J, et al. Modeling, synthesis, and biological evaluation of potential retinoid X receptor (RXR) selective agonists: novel analogues of 4-[1-(3,5,5,8,8-pentamethyl-5,6,7,8-tetrahydro-2-naphthyl)ethynyl]benzoic acid (bexarotene) and (E)-3-(3-(1,2,3,4-tetrahydro-1,1,4,4,6-pentamethylnaphthalen-7-yl)-4-hydroxypheny l)acrylic acid (CD3254). J Med Chem. 2013;56(21):8432-8454.
46. Marshall PA, Jurutka PW, Wagner CE, et al. Analysis of differential secondary effects of novel rexinoids: select rexinoid X receptor ligands demonstrate differentiated side effect profiles. Pharmacol Res Perspect. 2015;3(2):e00122.
47. Shih AH, Jiang Y, Meydan C, et al. Mutational cooperativity linked to combinatorial epigenetic gain of function in acute myeloid leukemia. Cancer Cell. 2015;27(4):502-515.
48. Neophytou CM, Constantinou AI. Drug delivery innovations for enhancing the anticancer potential of vitamin E isoforms and their derivatives. Biomed Res Int. 2015;2015:584862.
49. Westervelt P, Pollock JL, Oldfather KM, et al. Adaptive immunity cooperates with liposomal all-trans-retinoic acid (ATRA) to facilitate long-term molecular remissions in mice with acute promyelocytic leukemia. Proc Natl Acad Sci U S A. 2002;99(14):9468-9473.
50. Malik SM, Collins B, Pishvaian M, Ramzi P, Marshall J, Hwang J. A phase I trial of bexarotene in combination with docetaxel in patients with advanced solid tumors. Clin Lung Cancer. 2011;12(4):231-236.
51. Noble S, Wagstaff AJ. Tretinoin. A review of its pharmacological properties and clinical efficacy in the topical treatment of photodamaged skin. Drugs Aging. 1995;6(6):479-496.
52. Tesseur I, Lo AC, Roberfroid A, et al. Comment on "ApoE-Directed Therapeutics Rapidly Clear β-Amyloid and Reverse Deficits in AD Mouse Models". Science. 2013;340(6135):924-e.
53. Sanchez PV, Glantz ST, Scotland S, Kasner MT, Carroll M. Induced differentiation of acute myeloid leukemia cells by activation of retinoid X and liver X receptors. Leukemia. 2014;28(4):749-760.
54. McKeown MR, Corces MR, Eaton ML, et al. Super-enhancer analysis defines novel epigenomic subtypes of non-APL AML including an RARalpha dependency targetable by SY-1425, a potent and selective RARalpha agonist. Cancer Discov. 2017;7(10):1136-1153.
55. Mugoni V, Panella R, Cheloni G, et al. Vulnerabilities in mIDH2 AML confer sensitivity to APL-like targeted combination therapy. Cell Res. 2019;29(6):446-459.

56. Hernandez D, Palau L, Norsworthy K, et al. Overcoming microenvironment-mediated protection from ATRA using CYP26-resistant retinoids. Leukemia. 2020;34(11):3077-3081.
57. Keeshan K, Vieugue P, Chaudhury S, et al. Co-operative leukemogenesis in acute myeloid leukemia and acute promyelocytic leukemia reveals C/EBPalpha as a common target of TRIB1 and PML/RARA. Haematologica. 2016;101(10):1228-1236.
58. Lu Y, Yan JS, Xia L, et al. 2-bromopalmitate targets retinoic acid receptor alpha and overcomes all-trans retinoic acid resistance of acute promyelocytic leukemia. Haematologica. 2019;104(1):102-112.
59. Lallemand-Breitenbach V, Guillemin MC, Janin A, et al. Retinoic acid and arsenic synergize to eradicate leukemic cells in a mouse model of acute promyelocytic leukemia. J Exp Med. 1999;189(7):1043-1052.
60. Omidvar N, Maunakea ML, Jones L, et al. PML-RARalpha co-operates with Sox4 in acute myeloid leukemia development in mice. Haematologica. 2013;98(3):424-427.
61. Coltella N, Valsecchi R, Ponente M, Ponzoni M, Bernardi R. Synergistic leukemia eradication by combined treatment with retinoic acid and HIF inhibition by EZN-2208 (PEG-SN38) in preclinical models of PML-RARalpha and PLZF-RARalpha-driven leukemia. Clin Cancer Res. 2015;21(16):3685-3694.

Ferrata Storti Foundation

A novel combination regimen of BET and FLT3 inhibition for FLT3-ITD acute myeloid leukemia

Lauren Y. Lee,[1] Yoshiyuki Hizukuri,[2] Paul Severson,[3] Benjamin Powell,[3] Chao Zhang,[3] Yan Ma,[3] Maiko Narahara,[2] Hiroyuki Sumi,[2] Daniela Hernandez,[1] Trivikram Rajkhowa,[1] Gideon Bollag[3] and Mark Levis[1]

[1]Sidney Kimmel Comprehensive Cancer Center, Johns Hopkins University, Baltimore, MD, USA; [2]Daiichi Sankyo Co. Ltd., Tokyo, Japan and [3]Plexxikon Inc., Berkeley, CA, USA

Haematologica 2021
Volume 106(4):1022-1033

ABSTRACT

Acute myeloid leukemia (AML) patients with FLT3-ITD mutations have a high risk of relapse and death. FLT3 tyrosine kinase inhibitors improve overall survival, but their efficacy is limited and most patients who relapse will ultimately die of the disease. Even with potent FLT3 inhibition, the disease persists within the bone marrow (BM) microenvironment, mainly due to BM stroma activating parallel signaling pathways that maintain pro-survival factors. BET inhibitors suppress pro-survival factors such as MYC and BCL2, but these drugs thus far have shown only limited single-agent clinical potential. We demonstrate here, using pre-clinical and clinical correlative studies, that the novel 4-azaindole derivative, PLX51107, has BET-inhibitory activity *in vitro* and *in vivo*. The combination of BET and FLT3 inhibition induces a synergistic anti-leukemic effect in a murine xenograft model of FLT3-ITD AML, and against primary FLT3-ITD AML cells co-cultured with BM stroma. Using suppression of MYC as a surrogate for BET inhibition, we demonstrate BET inhibition in human patients. The short plasma half-life of PLX51107 results in intermittent target inhibition to promote tolerability while overcoming the protective effect of the microenvironment. Mechanistically, the synergistic cytotoxicity is associated with suppression of key survival genes such as MYC. These data provide the scientific rationale for a clinical trial of a BET plus FLT3 inhibitor for the treatment of relapsed/refractory FLT3-ITD AML. A clinical trial of PLX51107 as monotherapy in patients with different malignancies is underway and will be reported separately.

Correspondence:

MARK LEVIS
levisma@jhmi.edu

Received: January 16, 2020.

Accepted: November 9, 2020.

Pre-published: January 28, 2021.

https://doi.org/10.3324/haematol.2020.247346

©2021 Ferrata Storti Foundation

Material published in Haematologica is covered by copyright. All rights are reserved to the Ferrata Storti Foundation. Use of published material is allowed under the following terms and conditions: https://creativecommons.org/licenses/by-nc/4.0/legalcode. Copies of published material are allowed for personal or internal use. Sharing published material for non-commercial purposes is subject to the following conditions: https://creativecommons.org/licenses/by-nc/4.0/legalcode, sect. 3. Reproducing and sharing published material for commercial purposes is not allowed without permission in writing from the publisher.

Introduction

Internal tandem duplication (ITD) mutations of the receptor tyrosine kinase FLT3 are associated with a poor prognosis in acute myeloid leukemia (AML), both at diagnosis and in the relapsed/refractory setting.[1-3] Several FLT3 tyrosine kinase inhibitors (TKI) have recently been approved for use in this disease subtype at various stages of the disease, and outcomes for patients with FLT3-mutated AML are now improving.[4] Unfortunately, relapses still occur, and the presence of a FLT3-ITD mutation is one of the worst prognostic factors at relapse, with few patients achieving cure.[5,6] FLT3 inhibitors such as gilteritinib and quizartinib only prolong survival and very few relapsed patients are cured.[7,8] In relapsed FLT3-ITD AML patients treated with these drugs, circulating peripheral blasts are eliminated, but marrow blasts persist,[9,10] and resistance-conferring FLT3 point mutations or RAS-pathway mutations soon emerge.[11-13] Combinations with chemotherapy and hypomethylating agents are under investigation, but a combination with a more targeted agent might represent a better option.

We and others have previously reported that marrow blasts are protected from the FLT3 inhibition *via* signaling through stromal-derived cytokines.[9,10,14,15] Rather than target individual cytokines, we looked further downstream at the convergence of their signaling pathways, which drive transcription of pro-survival genes such as MYC. This led us to explore the inhibition of bromodomain and extra-terminal domain (BET) proteins, which are master transcription regulators.[16] This family of proteins includes BRD2, BRD3, BRD4 and BRDT. They associate with acetylated

chromatin to control transcriptional activation and cell cycle progression in leukemogenesis.[17] Of the four BET family members, BRD4 has been of particular interest in drug development as it directly recruits positive transcription elongation factor complex b (P-TEFb) to promote transcription of MYC and other proto-oncogenes.[18]

Previous work revealed that the combination of BET inhibition and FLT3 inhibition led to synergistic cytotoxicity in FLT3-ITD AML cells.[19] Although this was an important proof-of-principle, these studies were carried out using cells in suspension culture, which does not address the fundamental problem of microenvironment-mediated resistance to FLT3 inhibition. Furthermore, in order to translate this *in vitro* combination appropriately into the clinic, a BET inhibitor is needed that can achieve adequate MYC suppression in humans. We report here that the combination of PLX51107,[20] a structurally novel BET inhibitor currently in early phase clinical studies, and quizartinib, a highly selective FLT3 inhibitor, results in synergistic cytotoxic effects in FLT3-ITD AML blasts on bone marrow (BM) stroma, and that this combination represents a clinically viable strategy to overcome microenvironment-mediated resistance to FLT3 inhibition.

Methods

FLT3 and BET inhibitors

PLX51107 was synthesized at Plexxikon Inc. (Berkeley, CA, USA), a Daiichi Sankyo subsidiary. Quizartinib was obtained from LC Laboratories (Woburn, MA, USA). Stock solutions in dimethyl sulfoxide (DMSO) were stored at -20°C. Dilutions from the stock solutions were prepared in RPMI (Gibco, Waltham, MA, USA) with 10% fetal bovine serum (FBS) (Gemini Bio Products, Sacramento, CA, USA), penicillin/streptomycin, and 2 M L-glutamine (Gibco, Waltham, MA, USA). The final concentration of DMSO in all experiments was ≤0.1%.

Patients' samples

Patients' leukemia samples, as well as plasma and BM from healthy donors, were acquired under an institutional review board-approved protocol from the Johns Hopkins Tumor and Cell Procurement Bank. Patients gave informed consent according to the Declaration of Helsinki.

Cell cultures

Cell lines and primary leukemia cells were cultured in RPMI with 10% FBS, penicillin/streptomycin, and L-glutamine at 37°C in 5% CO_2. OCI-AML3 (expressing a wild-type FLT3 gene, an NPM1 gene mutation [type A], and a DNMT3A R882C mutation) and Molm14 cells (expressing a 21 bp FLT3-ITD mutation) were purchased from Deutsche Sammlung von Mikroorganismen and Zellkulturen, Braunschweig, Germany. MV4-11 cells (FLT3-ITD mutated) were from American Type Culture Collection, Manassas, VA, USA.

Cytotoxicity assays

Primary co-cultures in 96-well plates were incubated with specified drug treatments for 72 hours (h) prior to the assessment of cytotoxicity by a dimethyl-thiazole diphenol tetrazolium bromide (MTT) assay (Roche Diagnostics, Indianapolis, IN, USA) as described.[21] Experimental duplicates were also concurrently counted for cell viability by trypan blue exclusion under light microscopy.

Immunoblotting

The antibodies to probe for MYC and β-actin were obtained from Cell Signaling Technologies (#5605, Danvers, MA, USA) and β-actin (13E5, Danvers, MA, USA).

Plasma inhibitory activity assays

Plasma for the plasma inhibitory activity (PIA) assays was collected from patients enrolled in a phase Ib/IIa dose-escalation/expansion study of PLX51107 (*clinicaltrials.gov identifier: NCT02683395*). Plasma samples were collected from cycle 1 on day (d)1 at 0, 0.5, 1, 2, 3, 5, 7, and 9 h, and pre-dose on d2 (i.e., 24 h post d1 dose). The samples were stored at -80°C and used within 12 months of collection for the PIA assays.

The PIA assay was adapted from a previously described approach.[22] OCI-AML3 cells were incubated with each plasma sample for 3 h at 37°C in microcentrifuge tubes. Each OCI-AML3 sample was then centrifuged and washed a total of five times each in phosphate buffered saline (PBS) prior to cell lysis. Lysates were cleared by centrifugation. 50 μg of lysates were subjected to sodium dodecyl sulphate-polyacrylamide gel electrophoresis (SDS-PAGE) and immunoblot, as described above. Membranes were probed for antibodies against MYC and β-actin, as described above.

Colony-forming assays

Colony-forming assays of normal human BM progenitors were performed as described.[23]

Information concerning primary stromal culture and leukemic cell co-culture, xenograft studies, RNA sequencing and quantitative-polymerase chain reaction (PCR) is available in the *Online Supplementary Methods*.

Results

Previous work demonstrated a synergistic cytotoxic effect of the BET inhibitor JQ1 and FLT3 inhibition in FLT3-ITD AML cells in suspension culture.[19] To pursue this concept *in vivo*, we first tested it in a mouse model of FLT3-ITD AML. JQ1 is poorly suited to *in vivo* application. However, PLX51107 is a structurally distinct BET inhibitor that exhibits low nanomolar affinity and a unique binding position,[20] and is rationally designed for therapeutic use in humans. PLX51107, which has no activity as a FLT3 inhibitor (*Online Supplementary Figure S1*), potently inhibited the *in vitro* growth of two AML cell lines harboring FLT3 ITD mutations, MV4-11 and MOLM-14, with IC_{50} values of 62 and 79 nM, respectively (*Online Supplementary Figure S2*), suggesting that these cell lines are susceptible to BET inhibition. Despite its short plasma half-life, oral administration of PLX51107 led to significant transcriptional changes of a BET target gene HEXIM1 in MV4-11 cells xenografted in female SCID mice, confirming target engagement *in vivo*.[20] Here we used the same model but extended the duration of the study to examine the *in vivo*-efficacy of PLX51107 as a single agent or in combination with quizartinib in treating FLT3-ITD AML.

We first evaluated three oral doses (10, 20 and 40 mg/kg daily) of PLX51107 for efficacy in blocking MV4-11 xenograft growth. PLX51107 treatments demonstrated dose-dependent suppression of tumor growth (Figure 1A), achieving >50% tumor growth inhibition at 10 mg/kg dose (corresponding $AUC_{0\text{-}24}$ = 29,300 ng x h/mL) and above. PLX51107 dosed at 40 mg/kg resulted in tumor regression between d4 and d13 of dosing. By d14 (the last

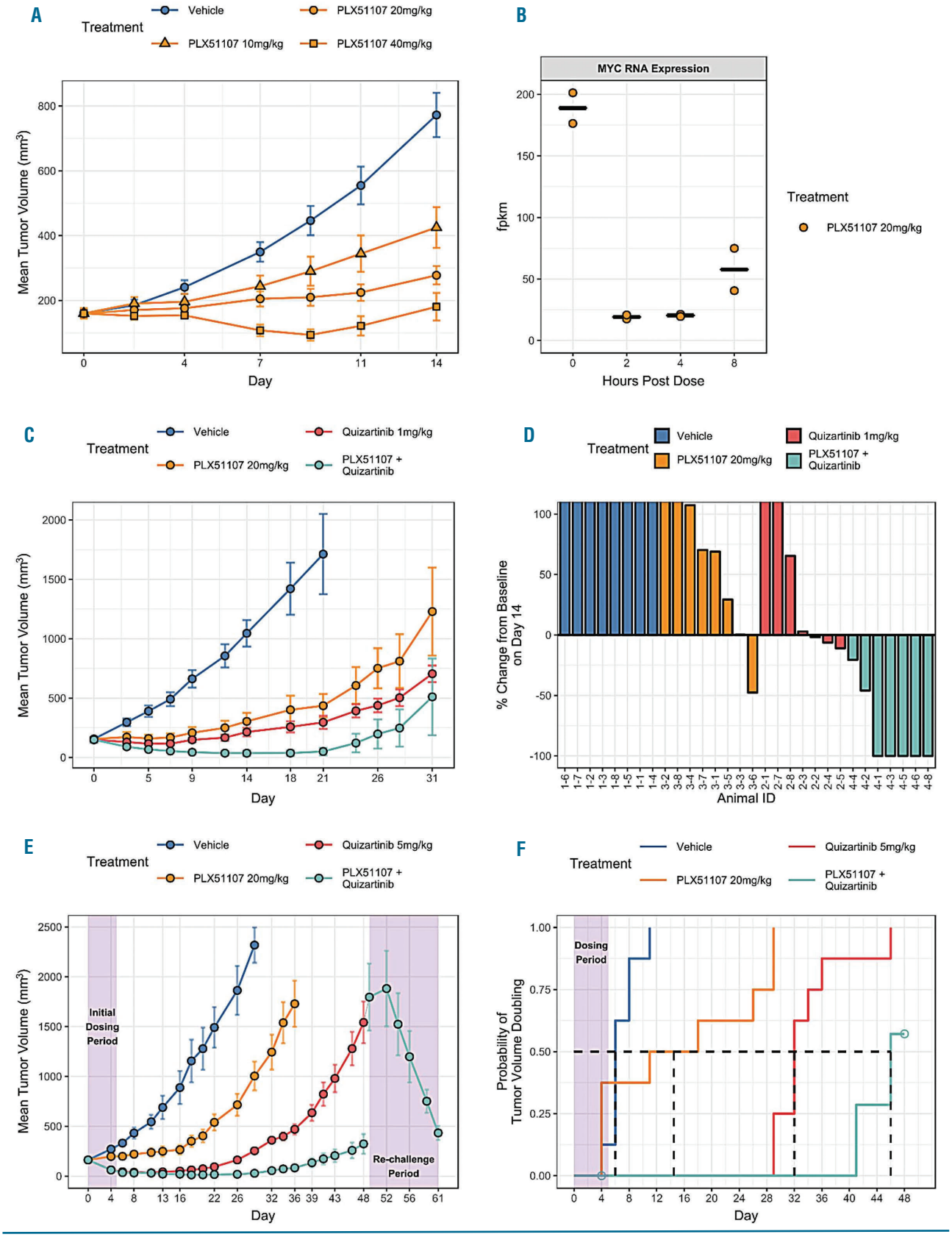


Figure 1. ***In vivo*** **efficacy of PLX51107 and quizartinib in MV4-11 xenograft models.** (A) Dose-response relationship of PLX51107 single agent activity after 14-day treatment; (B) MYC gene expression measured pre-dose, 2, 4 and 8 hours after a single 20 mg/kg dose of PLX51107. Two mice were taken down at each time point for the gene expression profiling. (C and D) 20 mg/kg PLX51107 were combined with low-dose (1 mg/kg) quizartinib in a continuous (25-day) dosing regimen. Treatment of MV4-11 xenografts with quizartinib and/or PLX51107 results in tumor control, particularly in the combination arm. (D) 5 of 7 mice treated with the combination had no measurable tumor on day 14. (E and F) 20 mg/kg PLX51107 was combined with high-dose (5 mg/kg) quizartinib for 5 days. On day 49, following regrowth of tumors in the short-term single-agent quizartinib arm, treatment was restarted with 20 mg/kg PLX51107 plus 5 mg/kg quizartinib to monitor further tumor control.

day of dosing and tumor measurement), PLX51107 treatment groups showed 57%, 81%, and 97% tumor growth inhibition (%TGI) at 10, 20, and 40 mg/kg doses, respectively. These results indicate that PLX51107 has single agent activity against AML *in vivo*. No adverse effects were observed at doses of 10 and 20 mg/kg. The high dose (40 mg/kg) was also tolerated but exhibited some toxicity (e.g., body weight loss in some animals) which recovered over time. The toxicity is likely due to the high exposure of PLX51107 at this dose ($AUC_{0\text{-}24}$ = 211,000 ng x h/mL). Based on in-life tolerability and body weight changes, the maximum dose without body weight loss in this study was 20 mg/kg with corresponding $AUC_{0\text{-}24}$ of 78,800 ng x h/mL. In the same model, we tested whether the PLX51107 treatment had any effect of MYC gene expression. Mice were given a single dose of 20 mg/kg PLX51107 and MYC RNA was measured in the tumor tissues after 2, 4 and 8 h (Figure 1B). Relative to pre-dose MYC expression, we observed a 90% decrease in MYC gene expression between 2 and 4 h post dose that only partially rebounded at 8 h post dose.

We next evaluated efficacy of the quizartinib-PLX51107 combination in the MV4-11 xenograft model using two different dosing regimens (PLX51107 at 20 mg/kg was used in both cases). The first experiment examined the effect of PLX51107 in combination with continuous (25 days), low-dose (1 mg/kg) quizartinib (Figure 1C). d0 is first day of dosing. On d5, PLX51107 alone almost completely suppressed tumor growth (TGI=98%) while quizartinib monotherapy and quizartinib-PLX51107 combination caused tumor regression (22% and 55%, respectively). Tumors in mice in the single agent quizartinib group progressed on d9 whereas mice in the combination group had maintained tumor regression until d26. On d14, 5 out of 7 animals in the quizartinib-PLX51107 group had no measurable tumors (100% decrease) (Figure 1D).

The third MV4-11 xenograft study examined the effect of PLX51107 on the duration of response after short-term (5 days) co-administration with high-dose (5 mg/kg) quizartinib (Figure 1E and F). By d4, PLX51107 alone delayed tumor growth (%TGI=68%) while quizartinib monotherapy and quizartinib-PLX51107 combination caused significant tumor regression (61% and 62%, respectively). The benefit of adding PLX51107 became evident when the durations of response were compared. Mice in the 5 mg/kg quizartinib group progressed on d26 (22 days after the last quizartinib dose) whereas mice in the quizartinib-PLX51107 group maintained tumor regression until d39. Two out of eight animals in the combination group achieved complete remission (CR) by d4 and six achieved CR by d18, while no animal in the single agent groups experienced a CR. Furthermore, tumors in mice that relapsed after short-term, single-agent quizartinib treatment decreased in size when challenged with quizartinib + PLX51107 on d49.

Taken together, these studies showed that, in a mouse xenograft model, PLX51107 enhanced the response of AML cells to continuous, low-dose quizartinib treatment and significantly improved the duration of response to short-term, high-dose quizartinib treatment without attendant toxicity. In addition, PLX51107 showed activity against AML not controlled by prior quizartinib treatment.

The efficacy observed in the xenograft studies reflects primarily the synergy between two cytotoxic agents acting at different levels of oncogenic signaling (i.e., proximal and downstream) in malignant cells not associated with BM stroma. In the clinical setting, BET inhibition could reduce the level of survival factors such as MYC in blasts on stromal cells, thereby undermining the resistance to the effects of FLT3 inhibition conferred by the microenvironment. Before we could test this hypothesis using co-culture of primary blast samples with mesenchymal stromal cells, it was necessary to determine the concentration of PLX51107 in culture medium that would give rise to a pharmacodynamic effect comparable to that observed in humans at clinically achievable drug exposure. To that end, we developed a surrogate assay modeled on the one we had previously used to estimate FLT3 inhibition *in vivo*.[22] A phase I dose escalation study of PLX51107 in patients with solid tumors and hematologic malignancy (*clinicaltrials.gov identifier: NCT02683395*) is underway, and the results of this trial will be published separately. Plasma samples collected from patients on this study were incubated with OCI-AML3 cells (NPM1-mutated, FLT3-wild-type). The degree and duration of MYC inhibition were quantified by immunoblotting and densitometry. We refer to this value as the plasma inhibitory activity for MYC (or MYC PIA). The OCI-AML3 cell line was selected because MYC expression is suppressed by PLX51107 (Figure 2A and B) but not by quizartinib (Figure 2C). Such specificity makes it possible to use the developed assay to measure the BET-mediated (FLT3-independent) effect in a quizartinib-PLX51107 combination trial.

Six dose levels of PLX51107 were evaluated in cancer patients. The MYC PIA assay showed that suppression of MYC appeared at 30 mg/day and peaked at 120 mg/day (Figure 3A). A further increase in dose to 160 mg/day did not lead to enhanced MYC suppression. For each plasma sample that was used to assay for MYC PIA, the plasma concentration of PLX51107 within that sample was measured. When the MYC PIA results are plotted against concentrations of the drug, the points align with the standard curve (see Figure 2B) of PLX51107 in plasma (Figure 3B). We also plotted all MYC PIA values from the 120 mg/day cohort (Figure 3C), from which we estimate the duration of MYC inhibition to be approximately 6 h at this dose. The mean plasma concentration over the first 6 h is 3.3 µM, which achieves approximately 80% inhibition of MYC in the PIA. An equivalent effect is achieved in regular culture medium by PLX51107 at a concentration of 250 nM.

Even potent FLT3 inhibitors such as gilteritinib and quizartinib are unable to eradicate FLT3-ITD AML blasts on BM stroma as single agents (Figure 4A), which we and others have observed previously.[9,10,14,15] Having established that PLX51107 could achieve target inhibition and tumor control *in vivo*, we next asked if stromal-mediated resistance to FLT3 inhibition *in vitro* could be overcome with the addition of BET inhibition. In previous studies, the concentration of quizartinib necessary to achieve complete FLT3 inhibition in blasts on BM stroma was established to be 50 nM (in culture medium).[24,25] From the above experiments, the plasma concentration of PLX51107 in patients (Figure 3B) that resulted in MYC inhibition can be achieved by 250 nM PLX51107 in cell culture medium (Figure 2A). Therefore, primary blast samples from patients with FLT3-ITD AML were co-cultured with mesenchymal stromal cells obtained from healthy marrow donors in the presence of 50 nM quizartinib, 250 nM PLX51107, or the combination, for 72 h, and then the cells were assayed for viability compared with untreated con-

trol (Figure 4B). There was inter-sample variation in the cytotoxic response to quizartinib (consistent with that previously observed; see Figure 4A), while PLX51107 by itself induced minimal cytotoxicity. The drugs induced no apparent effect on the proliferation of the stromal cells, either alone or in combination (*data not shown*). Importantly, the combination of the two drugs resulted in a synergistic cytotoxic effect against the patient-derived blasts (Figure 4B). We used ten samples in this fashion (the clinical data for these ten patients are detailed in *Online Supplementary Table S1*) and averaged the responses in an MTT assay to demonstrate a consistent synergy by median effect analysis (Figure 4C). We confirmed these results by performing direct cell counts using Trypan Blue exclusion to identify viable cells (*data not shown*). However, this synergistic effect was the result of continuous exposure to BET inhibition. The PIA data (see Figure 3) indicated that BET inhibition only lasted for approximately 6 h per day in patients. Therefore, we modeled this intermittent BET inhibition by incubating the blasts with PLX51107 for 6 h per day during the 3-day exposure period, with quizartinib continuously present (Figure 4D). Interestingly, the degree of cytotoxicity with intermittent exposure to BET inhibition was similar to that observed with continuous exposure. The explanation for this may be that the effects of PLX51107 on transcription persist for several hours after exposure to the drug, at least as seen in the mouse xenograft studies (Figure 1) and as observed by others.[20] We repeated the combination experiment using a different FLT3 inhibitor, gilteritinib, to confirm that the synergy was due to a FLT3 TKI class effect (*Online Supplementary Figure S3*).

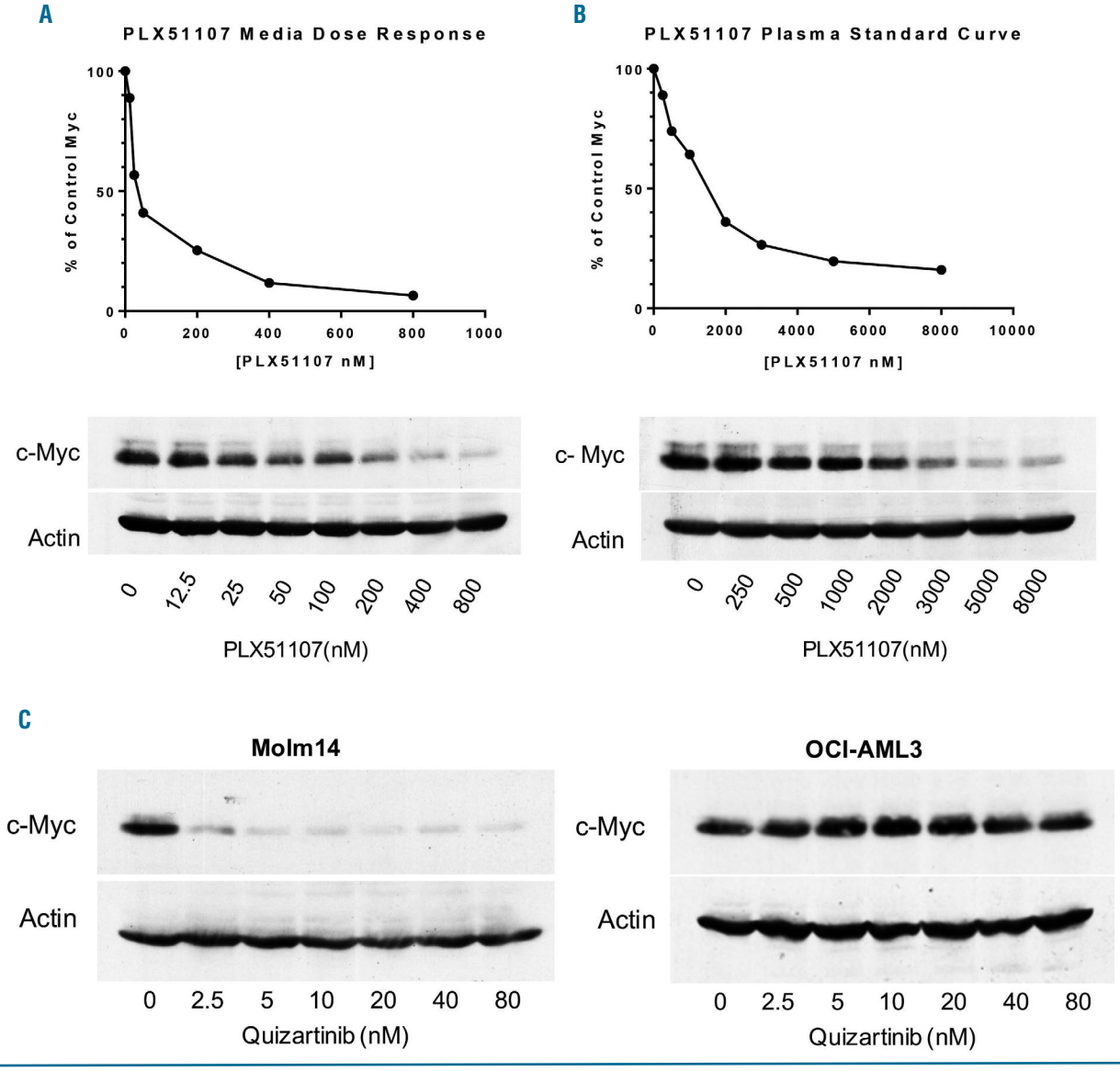


Figure 2. *In vitro* and *in vivo* correlative analysis of PLX51107 pharmacodynamic effect. OCI-AML3 cells were treated with increasing concentrations of PLX51107 for 3 hours (h) in either (A) RPMI/10% fetal bovine serum media or (B) control human plasma. Cells were then lysed and probed for MYC by immunoblotting. The quantitative analyses were performed by densitometry. The dose response curves in the graphs were generated from the average densitometry values of three separate experiments. Representative blots from both media and plasma conditions are shown. (C) Molm14 (FLT-ITD FLT3 receptor) and OCI-AML3 (wild-type FLT3 receptor) cells were treated with quizartinib for 3 h. Cells were then lysed and analyzed for MYC protein expression by immunoblotting, as described in the Methods section.

We repeated the combination treatments using three different primary AML samples on stroma and analyzed gene expression patterns at different time points using RNA sequencing. Using a false discovery rate (FDR) cut-off of 0.05 in transcript level, global changes in gene expression were minimal with quizartinib at 6 h and modest at 24 h (Figure 5A). Not surprisingly, the addition of PLX51107 resulted in more dramatic changes in gene expression at both 6 h and 24 h. The effects of BET inhibition on gene expression were transient, as a 6-h (e.g.,

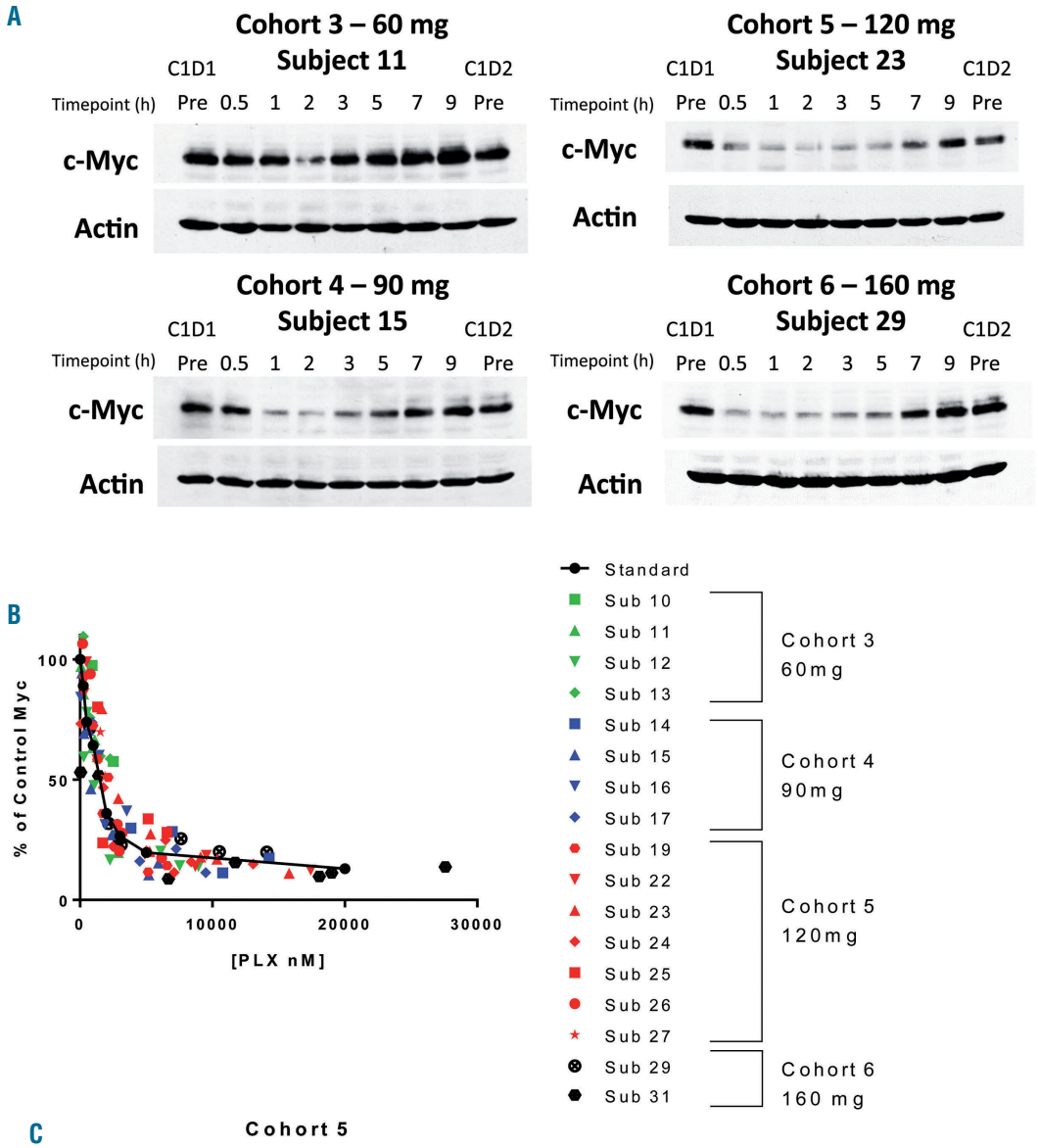


Figure 3. Plasma inhibitory activity (PIA) assays for MYC. (A) PIA assays for MYC were performed on patients' plasma samples collected at different time points throughout cycle 1 day 1 in a dose escalation study of PLX51107. Out of six cohorts, only the samples from the four cohorts receiving the highest doses exhibited MYC suppression in the MYC surrogate assay (shown here). Cohorts 5 and 6, receiving 120 mg or 160 mg of PLX51107 per day, produced the maximal MYC suppressive effect, which lasted for approximately 6 hours (h). (B) A total of 17 patients' plasma sets were analyzed by the PIA assay. Each symbol represents a time point for a particular patient. The MYC PIA result for each point is plotted against the concentration of PLX51107 measured in that sample. The plasma standard curve (solid black line) was generated from OCI-AML3 dose responses in Figure 1A. (C) PIA assays for cohort 5 are plotted against time after dosing. Values for MYC expression were obtained through densitometry and the 6-h length of MYC suppression is indicated by the bracket.

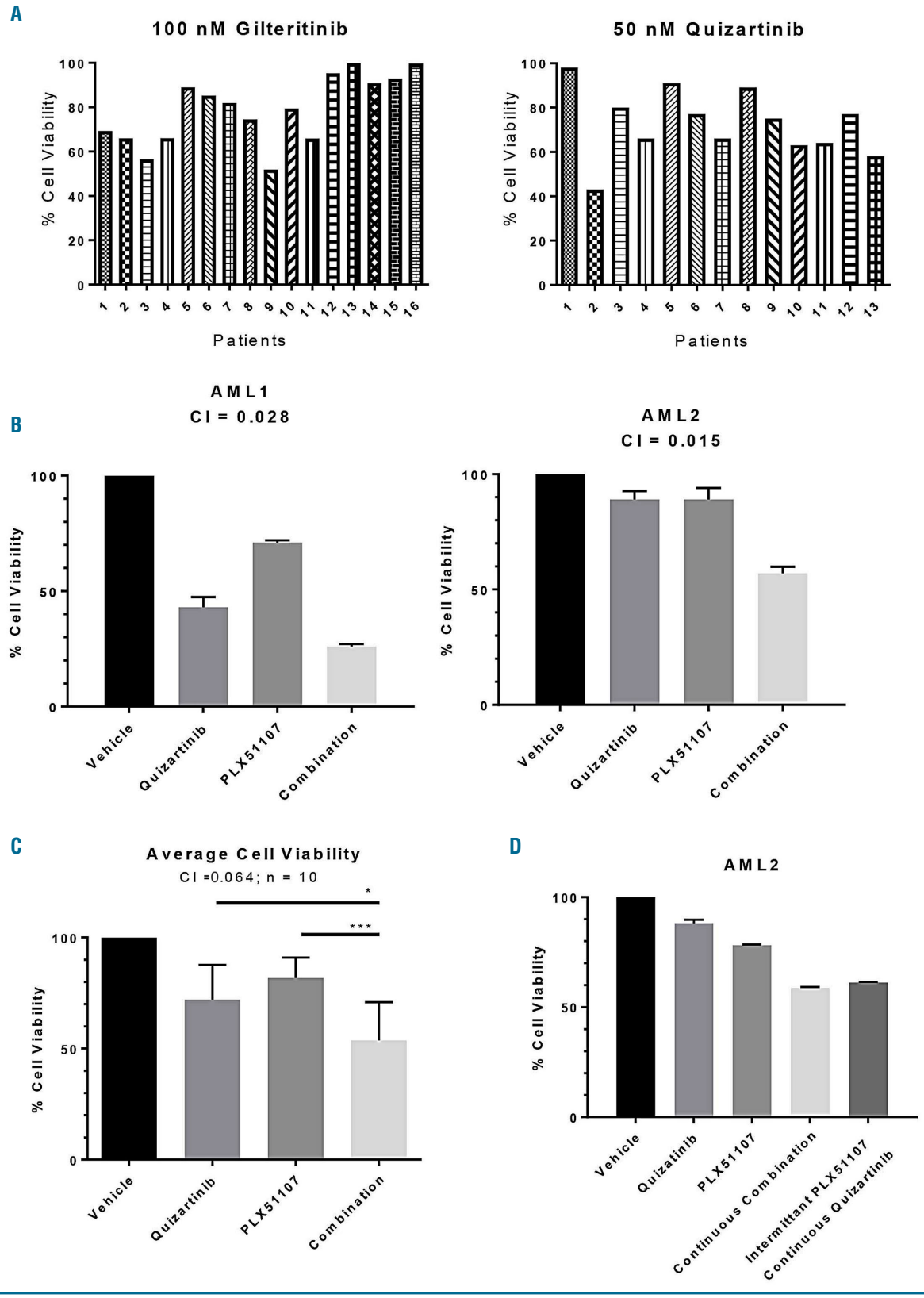


Figure 4. Synergistic cytotoxicity of PLX51107 and quizartinib in primary acute myeloid leukemia samples on bone marrow stroma. (A) Primary blasts from patients with relapsed or refractory FLT3-ITD AML were co-cultured with BM stromal cells in the presence of the clinically achievable doses of either 100 nM gilteritinib (left) or 50 nM quizartinib (right) for 72 hours (h) and cell viability was assessed by a dimethyl-thiazole diphenol tetrazolium bromide (MTT) assay. Sample numbers in the gilteritinib series do not correspond to those in the quizartinib series, as they were assayed at different times. (B) Relapsed or refractory FLT3-ITD AML patients' samples were co-cultured with BM stroma and treated with 50 nM quizartinib, 250 nM PLX51107, or a combination (50 nM quizartinib and 250 nM PLX51107) for 72 h prior to assessment for cell viability by MTT. Overall, a total of ten AML samples were screened. AML1 and AML2 are two representative cases. Patients' characteristics for AML1 and AML2 are provided in *Online Supplementary Table S1*. (C) Averages of each condition from the ten primary samples are shown, with standard deviations represented by error bars. *P<0.05, **P<0.01; two-tailed Student *t*-test. (D) Sample AML2 exposed to quizartinib and PLX51107 as in (B), but for this experiment, PLX51107 was washed out after 6 h exposure for each of the 3 days of exposure.

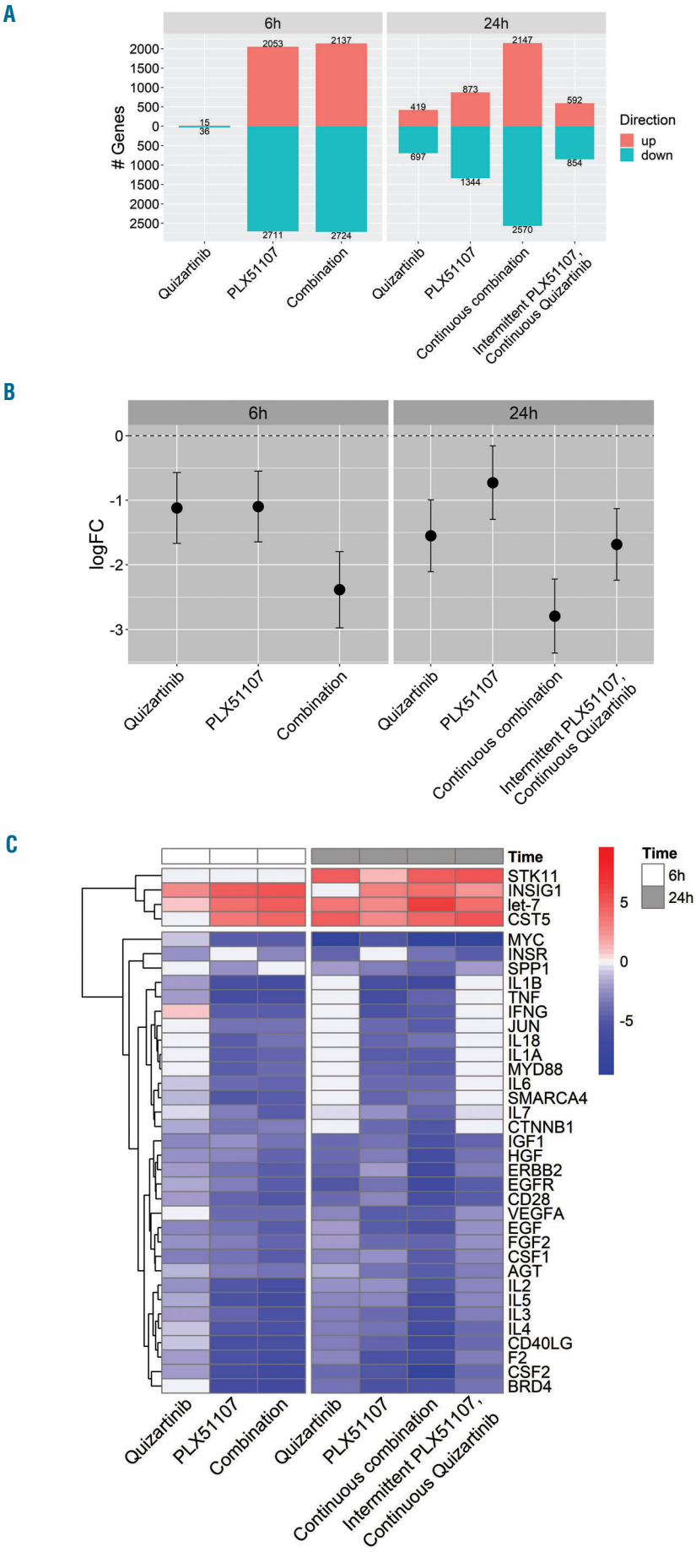


Figure 5. Legend on following page.

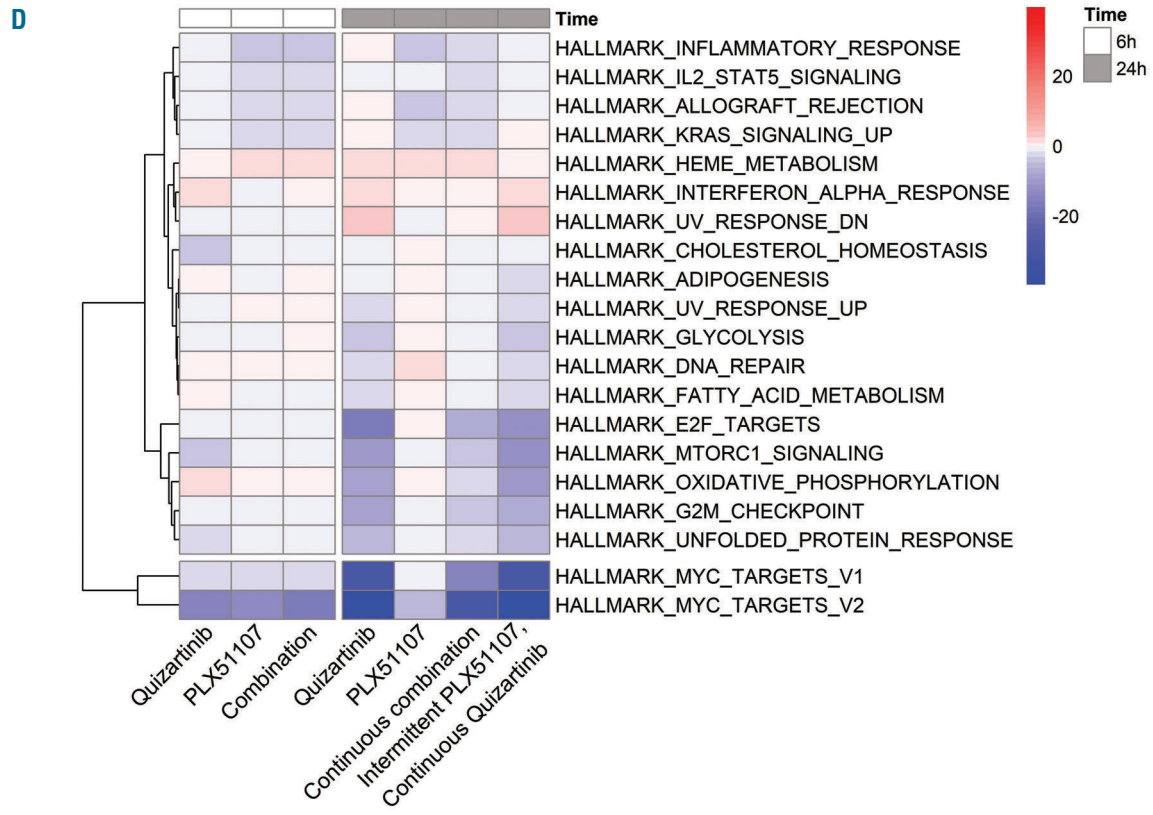


Figure 5. Gene expression. (A) Differentially expressed genes. Three different primary blasts from relapsed FLT3-ITD acute myeloid leukemia (AML) patients were treated with 50 nM quizartinib, 250 nM PLX51107, a continuous combination of both (50 nM quizartinib and 250 nM PLX51107), or intermittent dosing (6 hours [h]) of 250 nM PLX51107 and continuous 50 nM quizartinib. Cells were collected at both 6-h and 24-h time points for the transcriptome analysis. In each condition, the number of differentially expressed genes (averaged for the three samples) with false discovery rate (FDR) values <0.05 is shown. (B) Average expression of MYC for the three samples in (A) for each treatment condition compared to its time-matched baseline control. logFC values from the baseline are shown. (C) Heat map representation of the Ingenuity Pathway Analysis using the differentially expressed genes in each condition. Genes detected in (A) were used as input data. From the generated upstream factors, those that are not a single gene or miRNA were excluded. Upstream factors that had the highest activation z-scores in absolute value >4.5 were extracted. The color on the heat map indicates the activation z-scores and the heat map data are clustered by row. (D) Camera gene set enrichment analysis was performed on the three AML samples using MSigDB Hallmark gene sets. From the hallmark gene sets, those with -$\log_{10}$ (FDR) scores >2 were analyzed. Downregulated gene sets are indicated by negative values. Red: upregulated; blue: downregulated.

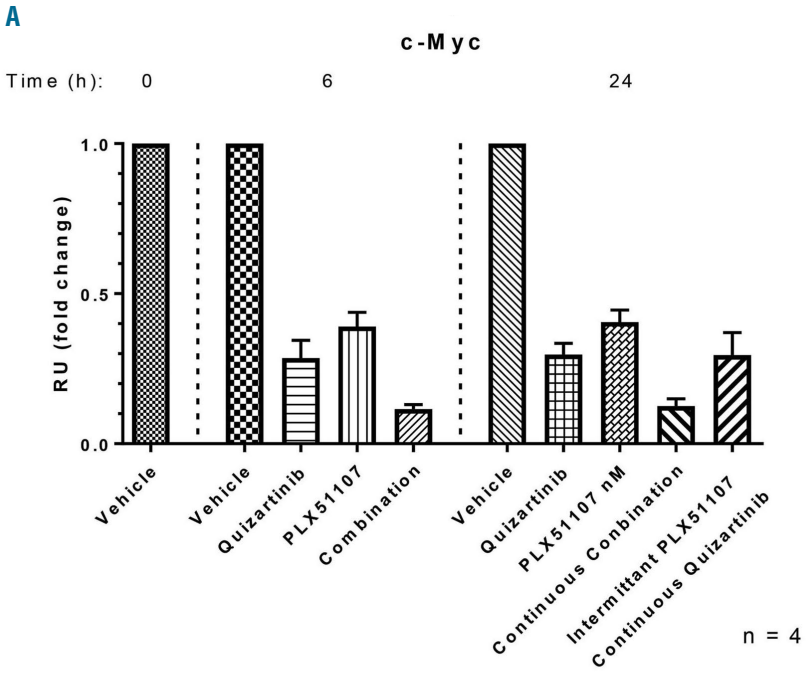
intermittent) exposure to PLX51107 in combination with continuous exposure to quizartinib yielded a pattern that was similar to that of quizartinib alone. Using both a simple iterative approach and a gene set enrichment analysis (GSEA), we identified MYC as one of the genes most affected by the combination of the two drugs (Figure 5B). We then used the upstream analysis function in the ingenuity pathway analysis (IPA) to analyze the changes induced by the drug exposure. The IPA confirmed that MYC-associated genes displayed the highest level of downregulation, even in cells that were intermittently exposed to BET inhibition (Figure 5C). Camera GSEA was also consistent with IPA upstream analysis (Figure 5D).

We confirmed that MYC RNA levels and protein were directly suppressed in these primary samples co-cultured on stroma using quantitative-PCR and immunoblotting (Figure 6A and B). Six-hour exposure to BET inhibition resulted in augmented suppression of MYC transcript and protein, which resolved by 24 h (i.e., after 18 h of washout). The synergistic cytotoxic effects were apparently the result of suppressing MYC expression for just 6 h.

The implications of the above findings are that combination therapy with approximately 120 mg/day PLX51107 and 60 mg/day quizartinib will be a more effective therapy for relapsed FLT3-ITD AML than 60 mg/day of quizartinib alone. However, quizartinib is myelosuppressive at doses higher than 60 mg/day[23,26,27] and it is possible that the addition of PLX51107 will lead to greater marrow suppression. To investigate this possibility, we performed colony assays using normal BM-derived progenitor cells exposed to these two drugs. PLX51107 alone at concentrations below 1,000 nM had no discernible effect on erythroid or granulocyte-macrophage colony forming activity, even with 10-14 days of continuous exposure (Figure 7A). In the presence of 50 nM quizartinib, 500 nM PLX51107 did suppress colony formation (Figure 7B). However, in this experiment, the progenitor cells were exposed to BET inhibition continuously for 10-14 days, rather than the intermittent exposures used in the cytotoxicity assays. We predict that intermittent BET inhibition with continuous FLT3 inhibition would not cause intolerable myelosuppression in AML patients.

Discussion

The BM microenvironment protects blasts against toxins through diverse mechanisms, including expression of



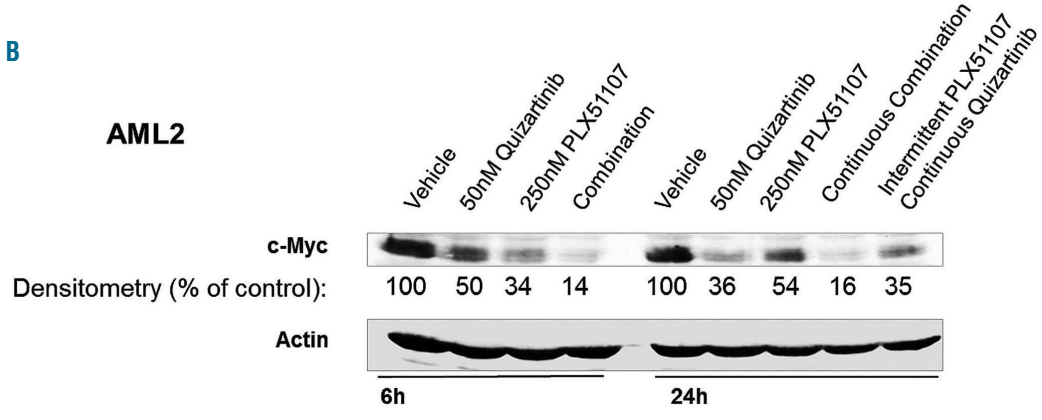


Figure 6. Primary samples co-cultured on stroma using quantitative-polymerase chain reaction (qPCR) and immunoblotting. (A) MYC expression in primary acute myeloid leukemia (AML) blasts by qPCR. Primary blasts from a patient with relapsed FLT3-ITD AML were co-cultured on stroma and treated under the specified condition. RNA was isolated from cells at 6-hour (h) and 24-h time points and analyzed as described in the Methods section. (B) MYC protein expression in primary AML blasts by immunoblotting. A primary FLT3-ITD AML sample (AML2, from Figure 4B) was treated with drug for 3 h, lysed, and probed for MYC as described in the Methods section. β-actin was used as control for protein loading. Protein expression levels were quantified by densitometry.

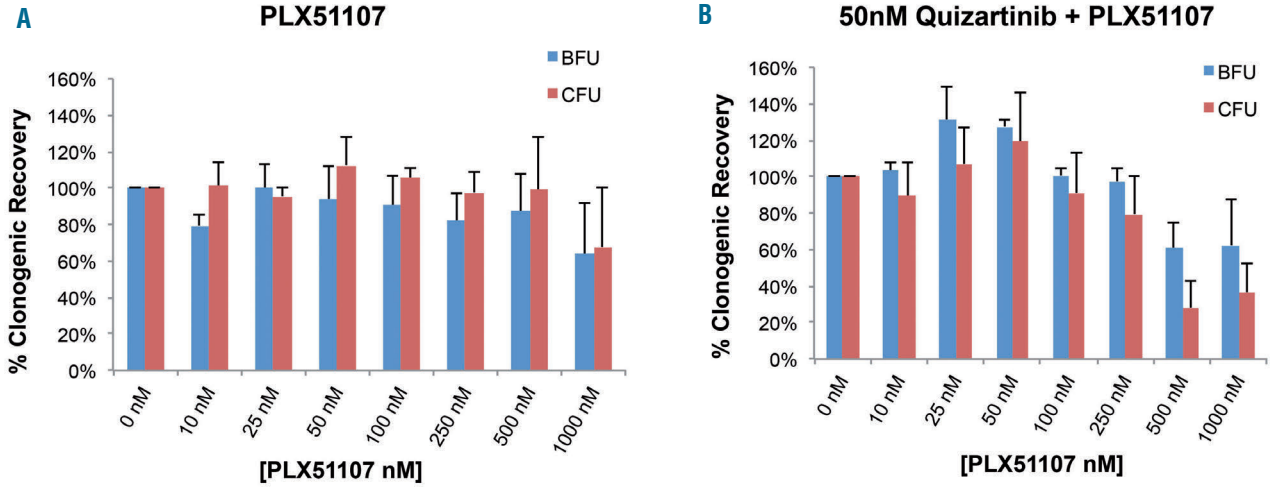


Figure 7. Colony forming cell assays. Colony assays were performed using normal bone marrow progenitor cells from healthy donors. Cells were cultured either with (A) PLX51107 alone or (B) with 50 nM quizartinib and increasing concentrations of PLX51107 for 10-14 days prior to assessment by microscopy. Averages of three individual experiments (three different donors) are shown; standard error of mean is shown as error bars. BFU: burst-forming unit; CFU: colony-forming unit.

cytochrome P450 enzymes within stromal cells and the production of cytokines that activate pro-survival pathways within the leukemia cells.[10,28] Overcoming the protective effect of marrow could lower disease burden in responding patients, and either directly prolong survival or allow more successful application of allogeneic transplantation.

We have turned to BET inhibitors to undermine the stroma-derived maintenance of pro-survival proteins in blasts within the marrow. BET inhibitors have attracted considerable interest as potential therapies for different diseases, but it seems unlikely that sustained suppression of BET protein activity would be tolerated in humans, a concern that has largely been borne out by early studies of first generation BET inhibitors.[29,30] However, PLX51107 has a relatively short plasma half-life in human patients, and our *ex vivo* surrogate PIA assay for MYC indicates effective BET inhibition can be achieved with this drug even at modest daily doses. Using the MYC PIA assay, in combination with the FLT3 PIA assay, a plasma sample from a patient taking both a BET and FLT3 inhibitor can be assayed for each drug effect separately, using OCI-AML3 cells for BET inhibition and MOLM-14 cells for the FLT3 inhibition. Even though intermittent, the BET inhibition induced by PLX51107 still results in synergistic cytotoxicity in combination with FLT3 inhibition against blasts on BM stromal cells. BET inhibition is expected to affect MYC and a myriad of other key genes, any number of which could contribute to the synergistic effect.[18] Our use of MYC in the PIA assay is primarily a surrogate for BET activity, and, indeed, our data indicate that it is likely to be the most appropriate.

In designing a clinical protocol for this combination regimen, we will need to choose a clinically validated FLT3 inhibitor. Both gilteritinib and quizartinib prolong survival for relapsed FLT3-ITD AML, and both are synergistic with BET inhibition. FLT3-TKD mutations emerge in response to monotherapy with quizartinib,[11] while RAS mutations emerge in response to gilteritinib therapy,[31] so neither drug offers a particular advantage in this regard. Quizartinib is more myelosuppressive than gilteritinib,[27] but, at least in our colony assays, the addition of BET inhibition does not seem to increase this. On the other hand, quizartinib, as a type II inhibitor, is more selective than gilteritinib, and its combination with another small molecule inhibitor may result in fewer off-target effects.

In summary, this work provides the scientific foundation for a clinical trial of a BET plus FLT3 inhibitor for the treatment of relapsed/refractory FLT3-ITD AML. The PIA assays for MYC and FLT3 can provide laboratory correlates to quantify *in vivo* inhibition of both targets in the dose escalation and expansion cohorts.

Disclosures

ML is a consultant to Daiichi-Sankyo, Astellas, Novartis, FujiFilm, Amgen, and Agios, and receives research funding from Astellas, FujiFilm, and Novartis; PS, BP, CZ, YM and GB are employees of Plexxikon, whose product, PLX51107, is a subject of this research; YH, MN and HS are employees of Daiichi-Sankyo, whose product, quizartinib, is a subject of this research; LL, DH and TR have no conflict of interest to disclose.

Contributions

LL performed experiments, analyzed data and wrote the manuscript; YH, PS, BP, CZ, YM, MN, HS, DH, TR and GR performed experiments, analyzed data and edited the manuscript; ML designed the study, analyzed data and wrote the manuscript.

References

1. Papaemmanuil E, Gerstung M, Bullinger L, et al. Genomic classification and prognosis in acute myeloid leukemia. N Engl J Med. 2016;374(23):2209-2221.
2. Levis M. FLT3 mutations in acute myeloid leukemia: what is the best approach in 2013? Hematology Am Soc Hematol Educ Program. 2013;2013:220-226.
3. Wattad M, Weber D, Dohner K, et al. Impact of salvage regimens on response and overall survival in acute myeloid leukemia with induction failure. Leukemia. 2017; 31(6):1306-1313.
4. Daver N, Schlenk RF, Russell NH, Levis MJ. Targeting FLT3 mutations in AML: review of current knowledge and evidence. Leukemia. 2019;33(2):299-312.
5. Chevallier P, Labopin M, Turlure P, et al. A new Leukemia Prognostic Scoring System for refractory/relapsed adult acute myelogeneous leukaemia patients: a GOELAMS study. Leukemia. 2011;25(6):939-944.
6. Ravandi F, Kantarjian H, Faderl S, et al. Outcome of patients with FLT3-mutated acute myeloid leukemia in first relapse. Leuk Res. 2010;34(6):752-756.
7. Cortes J, Perl AE, Dohner H, et al. Quizartinib, an FLT3 inhibitor, as monotherapy in patients with relapsed or refractory acute myeloid leukaemia: an open-label, multicentre, single-arm, phase 2 trial. Lancet Oncol. 2018;19(7):889-903.
8. Perl AE, Altman JK, Cortes J, et al. Selective inhibition of FLT3 by gilteritinib in relapsed or refractory acute myeloid leukaemia: a multicentre, first-in-human, open-label, phase 1-2 study. Lancet Oncol. 2017; 18(8):1061-1075.
9. Sexauer A, Perl A, Yang X, et al. Terminal myeloid differentiation in vivo is induced by FLT3 inhibition in FLT3/ITD AML. Blood. 2012;120(20):4205-4214.
10. Yang X, Sexauer A, Levis M. Bone marrow stroma-mediated resistance to FLT3 inhibitors in FLT3-ITD AML is mediated by persistent activation of extracellular regulated kinase. Br J Haematol. 2014;164(1):61-72.
11. Smith CC, Wang Q, Chin CS, et al. Validation of ITD mutations in FLT3 as a therapeutic target in human acute myeloid leukaemia. Nature. 2012;485(7397):260-263.
12. Piloto O, Wright M, Brown P, Kim KT, Levis M, Small D. Prolonged exposure to FLT3 inhibitors leads to resistance via activation of parallel signaling pathways. Blood. 2007; 109(4):1643-1652.
13. Zhang H, Savage S, Schultz AR, et al. Clinical resistance to crenolanib in acute myeloid leukemia due to diverse molecular mechanisms. Nat Commun. 2019;10(1):244.
14. Parmar A, Marz S, Rushton S, et al. Stromal niche cells protect early leukemic FLT3-ITD+ progenitor cells against first-generation FLT3 tyrosine kinase inhibitors. Cancer Res. 2011;71(13):4696-4706.
15. Traer E, Martinez J, Javidi-Sharifi N, et al. FGF2 from marrow microenvironment promotes resistance to FLT3 inhibitors in acute myeloid leukemia. Cancer Res. 2016;76(22): 6471-6482.
16. Winter GE, Mayer A, Buckley DL, et al. BET bromodomain proteins function as master transcription elongation factors independent of CDK9 recruitment. Mol Cell. 2017; 67(1):5-18.
17. Shi J, Vakoc CR. The mechanisms behind the therapeutic activity of BET bromodomain inhibition. Mol Cell. 2014;54(5):728-736.
18. Delmore JE, Issa GC, Lemieux ME, et al. BET bromodomain inhibition as a therapeutic strategy to target c-Myc. Cell. 2011; 146(6):904-917.
19. Fiskus W, Sharma S, Qi J, et al. BET protein antagonist JQ1 is synergistically lethal with FLT3 tyrosine kinase inhibitor (TKI) and overcomes resistance to FLT3-TKI in AML cells expressing FLT-ITD. Mol Cancer Ther. 2014;13(10):2315-2327.
20. Ozer HG, El-Gamal D, Powell B, et al. BRD4 profiling identifies critical chronic lymphocytic leukemia oncogenic circuits and reveals sensitivity to PLX51107, a novel structurally distinct BET inhibitor. Cancer Discov. 2018;8(4):458-477.
21. Pratz KW, Sato T, Murphy KM, Stine A, Rajkhowa T, Levis M. FLT3-mutant allelic burden and clinical status are predictive of response to FLT3 inhibitors in AML. Blood. 2010;115(7):1425-1432.
22. Levis M, Brown P, Smith BD, et al. Plasma

inhibitory activity (PIA): a pharmacodynamic assay reveals insights into the basis for cytotoxic response to FLT3 inhibitors. Blood. 2006;108(10):3477-3483.
23. Galanis A, Ma H, Rajkhowa T, et al. Crenolanib is a potent inhibitor of FLT3 with activity against resistance-conferring point mutants. Blood. 2014;123(1):94-100.
24. Cortes JE, Kantarjian H, Foran JM, et al. Phase I study of quizartinib administered daily to patients with relapsed or refractory acute myeloid leukemia irrespective of FMS-like tyrosine kinase 3-internal tandem duplication status. J Clin Oncol. 2013; 31(29):3681-3687.
25. Levis MJ, Cortes JE, Gammon GM, Trone D, Kang D, Li J. Laboratory and clinical investigations to identify the optimal dosing strategy for quizartinib (AC220) monotherapy in FLT3-ITD-positive (+) relapsed/refractory (R/R) acute myeloid leukemia (AML). Blood. 2016;128(22):4042-4042.
26. Galanis A, Levis M. Inhibition of c-Kit by tyrosine kinase inhibitors. Haematologica. 2015;100(3):e77-79.
27. Lee LY, Hernandez D, Rajkhowa T, et al. Preclinical studies of gilteritinib, a next-generation FLT3 inhibitor. Blood. 2017; 129(2):257-260.
28. Chang YT, Hernandez D, Alonso S, et al. Role of CYP3A4 in bone marrow microenvironment-mediated protection of FLT3/ITD AML from tyrosine kinase inhibitors. Blood Adv. 2019;3(6):908-916.
29. Berthon C, Raffoux E, Thomas X, et al. Bromodomain inhibitor OTX015 in patients with acute leukaemia: a dose-escalation, phase 1 study. Lancet Haematol. 2016; 3(4):e186-195.
30. Amorim S, Stathis A, Gleeson M, et al. Bromodomain inhibitor OTX015 in patients with lymphoma or multiple myeloma: a dose-escalation, open-label, pharmacokinetic, phase 1 study. Lancet Haematol. 2016; 3(4):e196-204.
31. McMahon CM, Ferng T, Canaani J, et al. Clonal selection with Ras pathway activation mediates secondary clinical resistance to selective FLT3 inhibition in acute myeloid leukemia. Cancer Discov. 2019;9(8):1050-1063.

Ferrata Storti Foundation

Haematologica 2021
Volume 106(4):1034-1046

Venetoclax combines synergistically with FLT3 inhibition to effectively target leukemic cells in FLT3-ITD+ acute myeloid leukemia models

Raghuveer Singh Mali,[1] Qi Zhang,[2] Rosa Anna DeFilippis,[3] Antonio Cavazos,[2] Vinitha Mary Kuruvilla,[2] Jayant Raman,[3] Vidhi Mody,[4] Edna F. Choo,[4] Monique Dail,[5] Neil P. Shah,[3,6] Marina Konopleva,[2] Deepak Sampath[1°#] and Elisabeth A. Lasater[1#]

[1]Department of Translational Oncology, Genentech, Inc., South San Francisco, CA; [2]Department of Leukemia, The University of Texas M.D. Anderson Cancer Center, Houston, TX; [3]Department of Medicine, Division of Hematology and Oncology, University of California, San Francisco, CA; [4]Department of Drug Metabolism and Pharmacokinetics, Genentech, Inc., South San Francisco, CA; [5]Oncology Biomarker Development, Genentech, Inc., South San Francisco, CA and [6]Helen Diller Comprehensive Cancer Center, University of California, San Francisco, CA, USA

[#]DS and EAL contributed equally as co-senior authors.
[°]Current address: Ultragenyx Pharmaceutical, Novato, CA, USA.

ABSTRACT

FLT3 internal tandem duplication (*FLT3-ITD*) mutations account for approximately 25% of adult acute myeloid leukemia (AML) cases and are associated with poor prognosis. Venetoclax, a selective BCL-2 inhibitor, has limited monotherapy activity in relapsed/refractory AML with no responses observed in a small subset of *FLT3-ITD*+ patients. Further, *FLT3-ITD* mutations emerged at relapse following venetoclax monotherapy and combination therapy suggesting a potential mechanism of resistance. Therefore, we investigated the convergence of FLT3-ITD signaling on the BCL-2 family proteins and determined combination activity of venetoclax and FLT3-ITD inhibition in preclinical models. *In vivo*, venetoclax combined with quizartinib, a potent FLT3 inhibitor, showed greater anti-tumor efficacy and prolonged survival compared to monotherapies. In a patient-derived *FLT3-ITD*+ xenograft model, cotreatment with venetoclax and quizartinib at clinically relevant doses had greater anti-tumor activity in the tumor microenvironment compared to quizartinib or venetoclax alone. Use of selective BCL-2 family inhibitors further identified a role for BCL-2, BCL-X_L and MCL-1 in mediating survival in *FLT3-ITD*+ cells *in vivo* and highlighted the need to target all three proteins for greatest anti-tumor activity. Assessment of these combinations *in vitro* revealed synergistic combination activity for quizartinib and venetoclax but not for quizartinib combined with BCL-X_L or MCL-1 inhibition. FLT3-ITD inhibition was shown to indirectly target both BCL-X_L and MCL-1 through modulation of protein expression, thereby priming cells toward BCL-2 dependence for survival. These data demonstrate that FLT3-ITD inhibition combined with venetoclax has impressive anti-tumor activity in FLT3-ITD+ AML preclinical models and provides strong mechanistic rational for clinical studies.

Correspondence:

ELISABETH A. LASATER
lasater.elisabeth@gene.com

DEEPAK SAMPATH
dsampath@ultragenyx.com

Received: December 5, 2019.

Accepted: May 14, 2020.

Pre-published: May 15, 2020.

https://doi.org/10.3324/haematol.2019.244020

©2021 Ferrata Storti Foundation

Material published in Haematologica is covered by copyright. All rights are reserved to the Ferrata Storti Foundation. Use of published material is allowed under the following terms and conditions: https://creativecommons.org/licenses/by-nc/4.0/legalcode. Copies of published material are allowed for personal or internal use. Sharing published material for non-commercial purposes is subject to the following conditions: https://creativecommons.org/licenses/by-nc/4.0/legalcode, sect. 3. Reproducing and sharing published material for commercial purposes is not allowed without permission in writing from the publisher.

Introduction

Fms-like tyrosine kinase 3 (*FLT3*) is one of the most commonly mutated genes in adult acute myeloid leukemia (AML) with internal tandem duplication (*FLT3-ITD*) mutations identifiable in approximately 25% of cases[1] and activating tyrosine kinase domain (*FLT3-TKD*) mutations occurring in about 7% of cases.[2] Both FLT3-ITD and FLT3-TKD are ligand-independent, constitutively activated kinases that signal through the canonical downstream pathways phosphoinositide 3-kinase (PI3K) and mitogen-activated protein kinases (RAS-MAPK)[3] and broadly impact cell

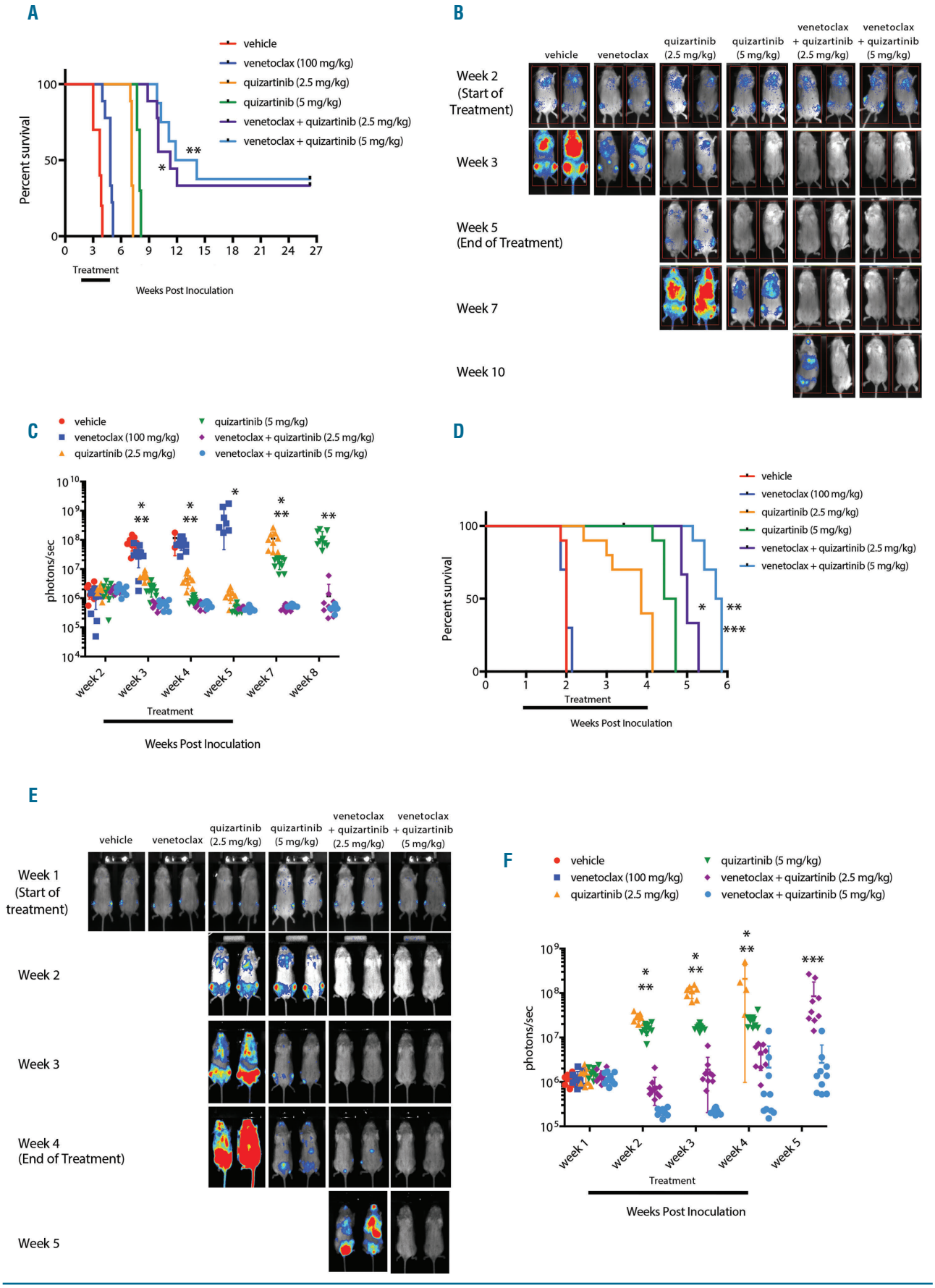


Figure 1. Legend on following page.

Figure 1 (previous page). Venetoclax combined with quizartinib prolongs survival and reduces tumor burden in FLT3-ITD+ xenograft models. NOD/SCID/IL-2Rγ^{null} (NSG) mice were engrafted with luciferase expressing MV4;11 or Molm13 cells and leukemic cell engraftment was confirmed by bioluminescence imaging (BLI) and treatment began 14 days post-inoculation for the MV4;11 model and 7 days post-inoculation in the Molm13 model. Mice were treated orally with 100 mg/kg venetoclax, 2.5 mg/kg or 5 mg/kg quizartinib, or the combination once daily for 21 continuous days and overall survival and disease burden was assessed. (A) Kaplan-Meier survival curve for MV4;11-engrafted mice. N=8-10 animals/group and median survival and statistical significance were determined by log-rank test: **P*<0.0001 for venetoclax + 2.5 mg/kg quizartinib *vs.* 2.5 mg/kg quizartinib; ***P*<0.0001 for venetoclax + 5 mg/kg quizartinib *vs.* 5 mg/kg quizartinib. (B) Representative BLI for MV4;11-engrafted mice for each group at indicated time point. (C) Quantitation of the BLI signal from MV4;11-engrafted mice in each group at indicated time post-inoculation: **P*<0.0001, *P*=0.0002, *P*=0.001 and *P*=0.0004 for venetoclax + 2.5 mg/kg quizartinib *vs.* 2.5 mg/kg quizartinib for week 3, 4, 5 and 7, respectively, by unpaired t-test for each time point; ***P*=0.0004, *P*=0.0247, *P*<0.0001 and *P*=0.0001 for venetoclax + 5 mg/kg quizartinib *vs.* 5 mg/kg quizartinib for week 3, 4, 7 and 8, respectively, by unpaired t-test for each time point. (D) Kaplan-Meier curve for Molm13-engrafted mice. N=10 animals/group and survival and statistical significance were determined by log-rank test: **P*<0.0001 for venetoclax + 2.5 mg/kg quizartinib *vs.* 2.5 mg/kg quizartinib; ***P*<0.0001 for venetoclax + 5 mg/kg quizartinib *vs.* 5 mg/kg quizartinib; and ****P*<0.0001 for venetoclax + 5 mg/kg quizartinib *vs.* venetoclax + 2.5 mg/kg quizartinib. (E) Representative BLI for Molm13-engrafted mice at indicated time point. (F) Quantitation of BLI signal from Molm13-engrafted mice at indicated time point post-inoculation: **P*<0.0001, *P*<0.0001 and *P*=0.0086 for venetoclax + 2.5 mg/kg quizartinib *vs.* 2.5 mg/kg quizartinib for week 2, 3 and 4, respectively, by unpaired t test for each timepoint; ***P*<0.0001 for venetoclax + 5 mg/kg quizartinib *vs.* 5 mg/kg quizartinib for week 2, 3 and 4 by unpaired t-test for each timepoint; and ****P*=0.0129 for venetoclax + 5 mg/kg quizartinib *vs.* venetoclax + 2.5 mg/kg quizartinib at week 5 by unpaired t-test.

proliferation, differentiation, and survival. Notably, FLT3-ITD also activates STAT5, a distinguishing feature from FLT3-TKD and ligand-stimulated wild-type (WT) FLT3.[4,5]

Intrinsic apoptosis regulates survival through balancing anti- and pro-apoptotic proteins. The BCL-2 family of anti-apoptotic proteins includes B-cell lymphoma 2 (BCL-2), B-cell lymphoma-extra-large (BCL-X_L) and myeloid cell leukemia 1 (MCL-1) that bind and neutralize pro-apoptotic BCL-2 homology 3 (BH3)-only proteins and pro-apoptotic effector proteins, BCL-2-associated X protein (BAX) and BCL-2 antagonist/killer (BAK),[6] preventing induction of apoptosis. The development of BH3 mimetic compounds, including venetoclax (ABT-199/GDC-0199), that specifically target individual BCL-2 family members has helped clarify dependence of cancer cells on BCL-2,[7] BCL-X_L[8,9] and/or MCL-1[10,11] and also revealed mechanisms of venetoclax resistance, including upregulation of BCL-X_L and/or MCL-1.[12]

Venetoclax, a highly potent, specific inhibitor of BCL-2, has preclinical and clinical activity across a range of hematologic malignancies.[13-17] In AML, while venetoclax has limited monotherapy activity,[14] venetoclax combined with low-dose cytarabine (LDAC) or hypomethylating agents (HMA) has broad activity across mutation subsets.[18,19] In the venetoclax monotherapy trial,[14] new *FLT3-ITD* mutations emerged at progression in 4 of 15 patients with initial venetoclax response and 3 of 3 patients with baseline *FLT3-ITD* mutations showed no measurable reduction in bone marrow (BM) blasts.[20] Initial molecular analysis of samples from the venetoclax combination trials revealed that relapse may also be associated with *FLT3-ITD* mutations.[21] In 25 patients evaluated at relapse, *FLT3-ITD* mutations expanded in three patients treated with venetoclax plus HMA and new *FLT3-ITD* mutations were detected in two patients treated with venetoclax plus LDAC. While patient numbers reported in these studies are low, the association of *FLT3-ITD* mutations with primary resistance and emergence of *FLT3-ITD* mutations at relapse suggests that mutant FLT3 may influence sensitivity to venetoclax and warrants further investigation.

Resistance to apoptosis can be achieved through oncogenic signaling or transcriptional regulation that alter expression of apoptotic proteins. RAS-MAPK, PI3K and the Janus kinase (JAK)-STAT pathways can all regulate anti- and pro-apoptotic proteins.[22-24] As such, STAT5, a known transcriptional regulator of BCL-X_L and BCL-2,[25] can also regulate MCL-1 expression in FLT3-ITD+ cells.[26] Given that FLT3-ITD regulates multiple survival pathways and is linked to increased BCL-X_L[27-30] and MCL-1[26,29] expression, which can promote venetoclax resistance, there is strong scientific rationale to investigate BH3 mimetics combined with FLT3-ITD inhibition. Ma *et al.* described combination activity of venetoclax and the FLT3 inhibitors midostaurin and gilteritinib in FLT3-ITD+ AML models.[31] However, direct comparison of BCL-2, BCL-X_L and MCL-1 inhibition in reducing survival when combined with FLT3-ITD inhibition has not been investigated, nor has the role of individual signaling pathways downstream of FLT3-ITD in regulating BCL-2 family members. Therefore, we aimed to thoroughly investigate the combined efficacy of FLT3-ITD and BCL-2 family inhibition using potent and selective pharmacologic inhibitors in pre-clinical models of FLT3-ITD+ AML. We describe herein the superiority of targeting BCL-2, rather than BCL-X_L or MCL-1, in combination with FLT3 inhibition in FLT3-ITD+ AML. Given that venetoclax is presently being tested in AML clinical trials, our preclinical data provides a strong mechanistic rational for further evaluation of venetoclax combinations with FLT3-ITD inhibitors for the treatment of FLT3-ITD+ patients.

Methods

Orthotopic cell line xenograft models

Cell line xenograft studies were approved by Genentech's Institutional Animal Care and Use Committee (IACUC) and adhere to the Eighth Edition of the Guide for the Care and Use of Laboratory Animals (NRC 2011). NOD/SCID/IL-2Rγ^{null} (NSG) mice (Jackson Laboratory, Bar Harbor, ME) were housed in autoclaved individually ventilated cages. Eight to 10 week old mice were pre-conditioned with busulfan (20 mg/kg; Sigma) by intraperitoneal administration 24 hours prior to cell line inoculation. Luciferase-positive AML cell lines ($2x10^6$ cells) were suspended in Hanks' balanced salt solution (HBSS) and injected via tail vein. Engraftment of leukemic cells and disease burden was determined by bioluminescence imaging (BLI). Equally engrafted mice were grouped out based on BLI at 7 (Molm13) or 14 days (MV4;11) post inoculation and treated as described for 21 continuous days. Animals were monitored for signs of disease progression and euthanized at first measurement of greater than 20% weight loss or when reaching any humane endpoint.

Primary patient-derived xenograft models

Primary patient samples were collected and utilized at the M.D. Anderson Cancer Center (MDACC). All patients gave informed consent in accord with the Declaration of Helsinki under Institutional Review Board-approved protocols. Studies were approved by the MDACC IACUC and adhere to the Eighth Edition of the Guide for the Care and Use of Laboratory Animals (NRC 2011). Seven week old NSG mice were pre-conditioned by

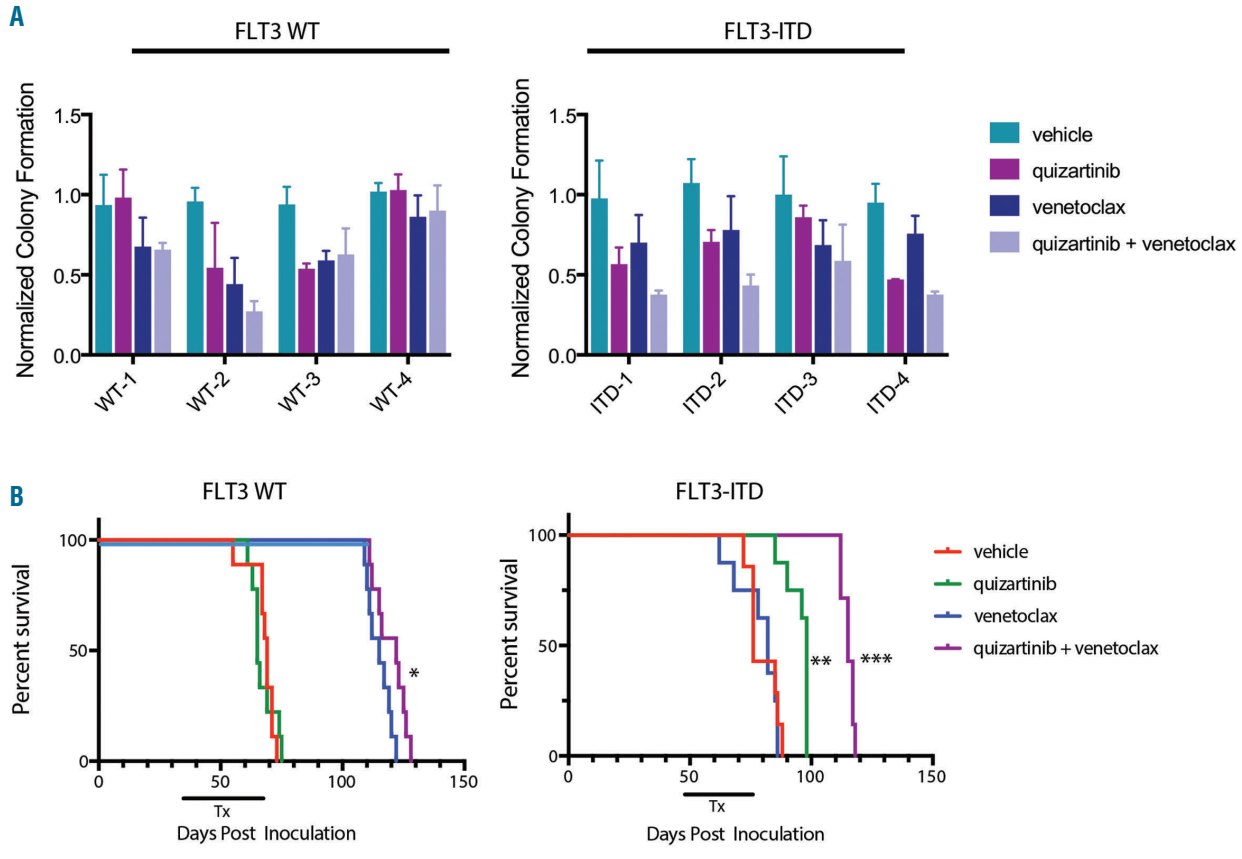


Figure 2. Venetoclax combined with quizartinib has greater anti-tumor efficacy against primary FLT3-ITD+ acute myeloid leukemia models. (A) Primary patient samples were treated with 20 nM quizartinib, 50 nM venetoclax or the combination in methylcellulose in triplicate for 14 days and colony forming units were counted. Data were normalized to the median colony number for the vehicle-treated cells for each sample and plotted as mean + standard deviation. (B) NOD/SCID/IL-2Rγ^{null} (NSG) mice were engrafted with primary samples from Fms-like tyrosine kinase 3 wild-type (FLT3-WT) or *FLT3* internal tandem duplication (FLT3-ITD+) patients and treated orally with 5 mg/kg quizartinib, 100 mg/kg venetoclax or the combination once daily for 28 days and efficacy was assessed. Kaplan-Meier survival curve for FLT3-WT and FLT3-ITD+ models. N=7-9 animals/group and median survival and statistical significance were determined by log-rank test: *P<0.0001 for venetoclax *vs.* vehicle or quizartinib in FLT3-WT model. **P=0.0004 for quizartinib *vs.* vehicle or venetoclax and ***P=0.0003 for quizartinib + venetoclax *vs.* quizartinib in the FLT3-ITD+ model.

sublethal irradiation (250 cGY) 24 hours prior to cell inoculation. FLT3 WT or FLT3-ITD+ primary patient samples (1x10^6 cells) were suspended in Phosphate-buffered saline (PBS) and inoculated through tail vein injection. Engraftment and disease burden were determined by co-staining for human and murine anti-CD45 (BioLegend, San Diego, CA) in peripheral blood samples. Mice were grouped out based upon engraftment (WT average 2.2% engraftment; ITD average 0.8% engraftment) and treated as described for 28 continuous days. Animals were monitored for signs of disease progression and euthanized at first measurement of greater than 20% weight loss or when reaching any humane endpoint.

BLISS analysis

Details are provided in the *Online Supplementary Appendix*.

BH3 profiling

Details are provided in the *Online Supplementary Appendix*.

Statistical analysis

Statistical comparisons included unpaired t-test or one-way ANOVA with Tukey *post hoc* test or Dunnett post-test, as indicated with P<0.05 considered statistically significant. Kaplan-Meier survival analysis was used for *in vivo* studies and significance was determined by log-rank test with P<0.05 considered significant. All analyses were completed using Prism software package (version 7; Graphpad Software, La Jolla, CA, USA).

Results

Venetoclax combined with FLT3-ITD inhibition prolonged survival of FLT3-ITD+ leukemic mice *in vivo*

In order to explore the impact FLT3-ITD on venetoclax activity, we assessed venetoclax treatment in combination with the selective FLT3 inhibitor quizartinib (AC220)[32] in FLT3-ITD+ cell line xenograft models (MV4;11 and Molm13). Mice with established leukemia were treated orally with vehicle, venetoclax (100 mg/kg), quizartinib (2.5 or 5 mg/kg), or the combination for 21 continuous days. Consistent with clinical data, venetoclax alone demonstrated little to no efficacy based on survival with marginal improvement in the MV4;11 model (Figure 1A-C) and no anti-tumor activity in the Molm13 model (Figure 1D-F), while quizartinib significantly reduced disease burden and increased survival compared to vehicle in both models (Figure 1A-F). Venetoclax combined with quizartinib led to further improvement in survival and reduction in tumor burden compared to quizartinib alone (Figure 1A-F). Additionally, in the MV4;11 model a subset

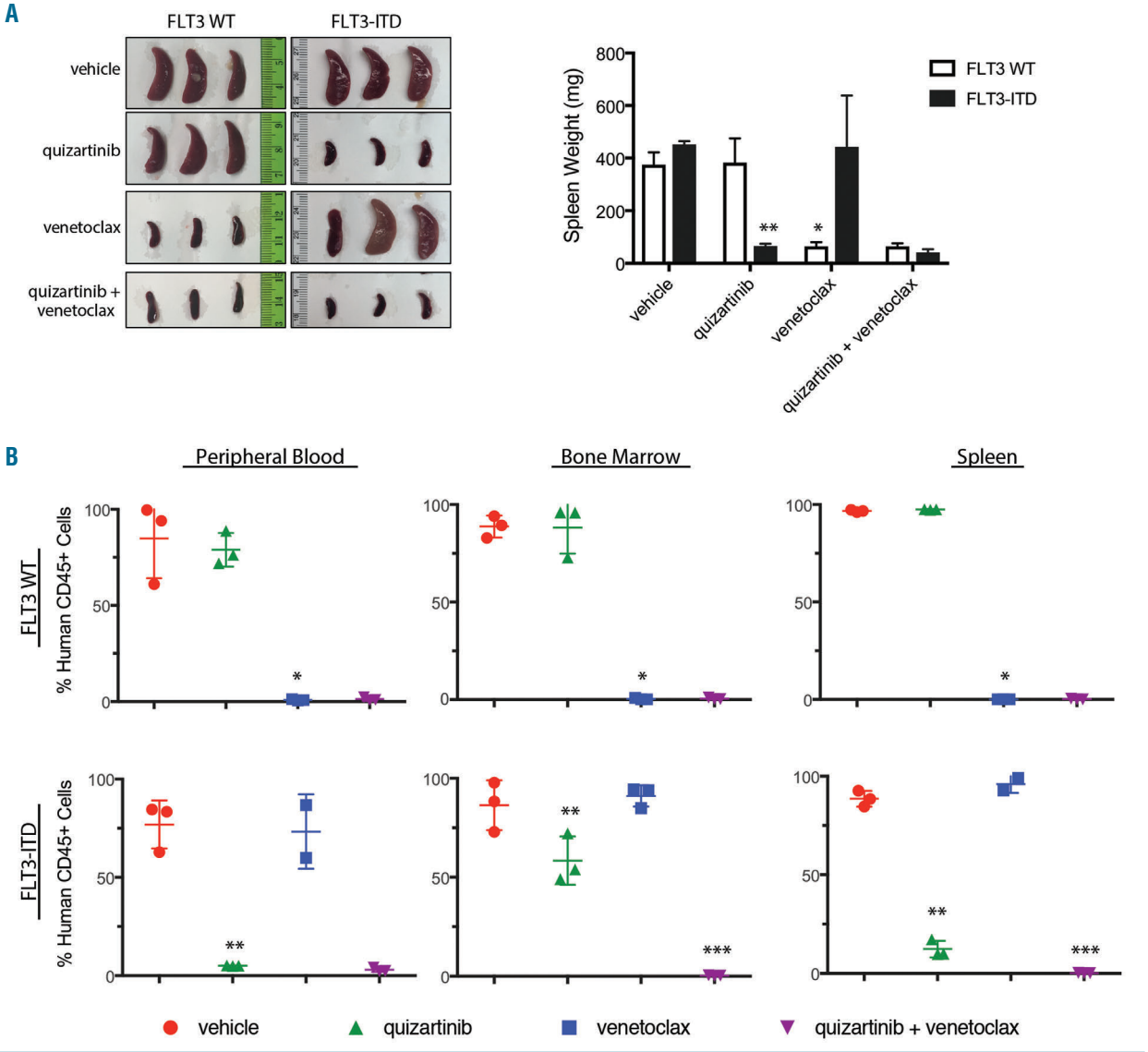


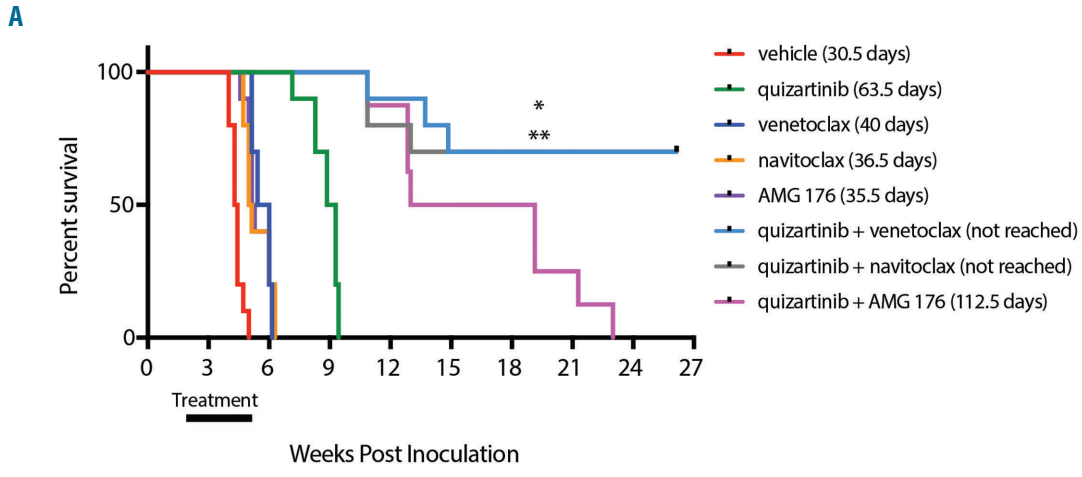
Figure 3. Venetoclax combined with quizartinib to reduce disease burden in the tumor microenvironment of patient-derived FLT3-ITD+ xenograft models. NOD/SCID/IL-2Rγ^{null} (NSG) mice were engrafted with primary samples from Fms-like tyrosine kinase 3 wild-type (FLT3-WT) or *FLT3* internal tandem duplication (FLT3-ITD+) patients and were treated orally with 5 mg/kg quizartinib, 100 mg/kg venetoclax or the combination once daily for 28 days. (A) Spleen images and spleen weight at the end of 28 days of dosing. Data is represented as average + standard deviation (n=3). **P*=0.0004 for venetoclax *vs.* quizartinib for FLT3-WT model and ***P*=0.0068 for quizartinib *vs.* venetoclax for FLT3-ITD+ model by one-way ANOVA with Tukey *post hoc* test. (B) Percentage of human CD45^{+} cells in peripheral blood, bone marrow and spleen at the end of dosing. Data is represented as average + standard deviation (n=3). **P*<0.0001 for venetoclax *vs.* quizartinib in the FLT3-WT model in the peripheral blood, bone marrow and spleen; ***P*=0.0005, *P*=0.01 and *P*<0.0001 for quizartinib *vs.* venetoclax for peripheral blood, bone marrow and spleen, respectively, for FLT3-ITD+ model; and *** *P*=0.0002 and *P*=0.0159 for quizartinib + venetoclax *vs.* quizartinib for bone marrow and spleen, respectively, for FLT3-ITD+ model by one-way ANOVA with Tukey *post hoc* test.

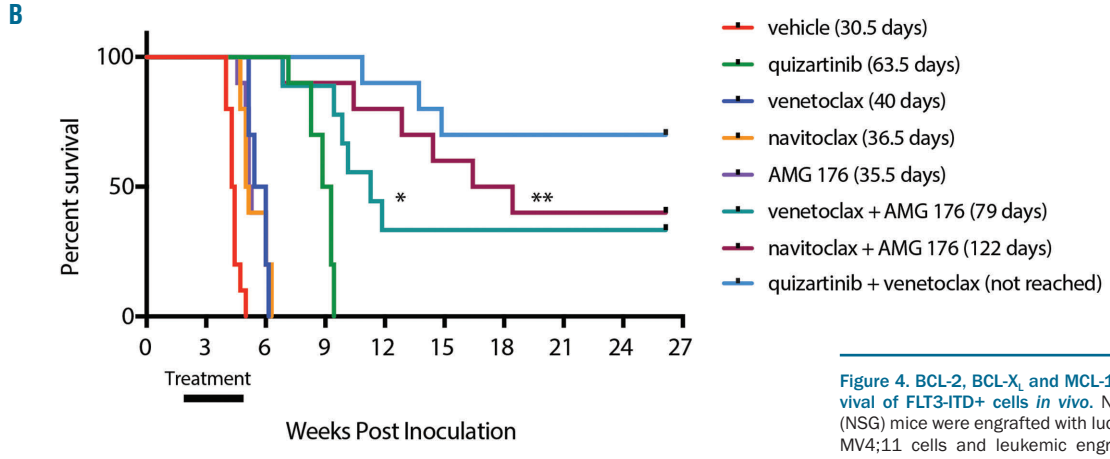
of mice remained disease-free showing long-term survival following combination treatment with venetoclax that was not observed with quizartinib monotherapy. All drug treatments were well tolerated based on minimal changes in body weight (*Online Supplementary Figure S1*). Importantly, combination activity was demonstrated at clinically relevant doses, as 5 mg/kg dose of quizartinib achieved Cmax of ~1 μM in NSG mice (*Online Supplementary Figure S2*), similar to the clinically efficacious dose of 60 mg/day in patients.[33]

FLT3-ITD inhibition combines with venetoclax in primary patient samples

Studies were expanded to primary AML patient samples to confirm combination activity *ex vivo*. FLT3-WT and FLT3-ITD+ primary samples were treated with quizartinib, venetoclax or the combination of both drugs and colony forming units were determined after 14 days. In 3 of 4 FLT3-ITD+ samples, venetoclax plus quizartinib impaired colony formation greater than each agent alone (Figure 2A), suggesting that the co-treatment targeted more FLT3-ITD+ progenitor cells, which is an important factor related to greater clinical response.

In vivo efficacy of quizartinib and venetoclax was also investigated in FLT3-WT and FLT3-ITD+ patient-derived xenograft (PDX) models (see *Online Supplementary Figure S3A* for cytogenetic characteristics). Following engraftment, mice were treated orally with vehicle, venetoclax (100 mg/kg), quizartinib (5 mg/kg), or the combination for 28 continuous days. Quizartinib prolonged survival of the





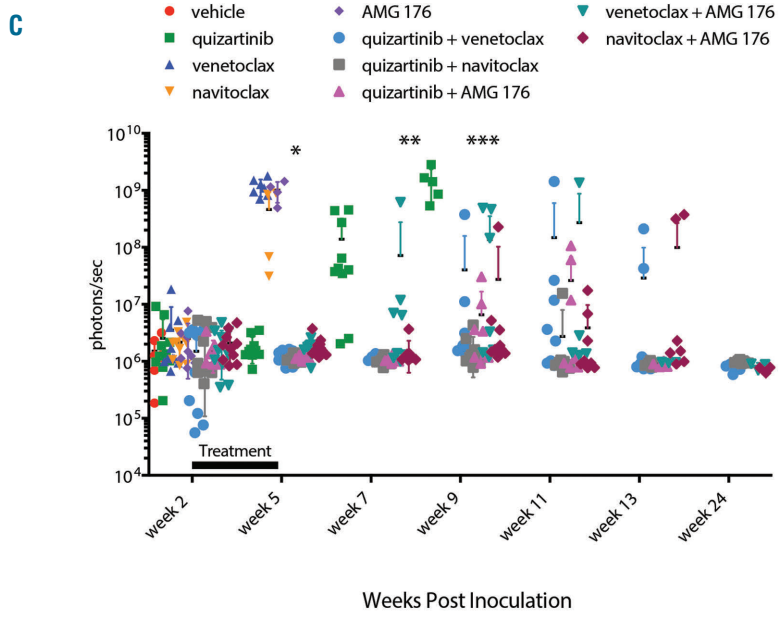


Figure 4. BCL-2, BCL-X_L and MCL-1 contribute to survival of FLT3-ITD+ cells *in vivo*. NOD/SCID/IL-2Rγ^{null} (NSG) mice were engrafted with luciferase expressing MV4;11 cells and leukemic engraftment was confirmed by BLI and treatment began 14 days post inoculation. Mice were treated orally with 5 mg/kg quizartinib, 100 mg/kg venetoclax, 100 mg/kg navitoclax or 10 mg/kg AMG 176 as single agents or in combinations as indicated once daily for 21 days. All treatment groups were run concurrently, however for clarity survival data has been split between panels A and B and vehicle, quizartinib, venetoclax, navitoclax and AMG 176 single agent groups have been plotted in both panels for reference. (A) Kaplan-Meier survival curves for quizartinib in combination with AMG 176, venetoclax or navitoclax. N=8-10 animals/group. Median survival and statistics were determined by log-rank test: *P=0.0059 for quizartinib + venetoclax *vs.* quizartinib + AMG 176; and **P=0.0095 for quizartinib + navitoclax *vs.* quizartinib + AMG 176. (B) Kaplan-Meier survival curves for AMG 176 in combination with venetoclax or navitoclax. N=8-10 animals/group. Median survival and statistics were determined by log-rank test: *P=0.0008 for venetoclax + AMG 176 *vs.* quizartinib; and **P=0.0002 for navitoclax + AMG 176 *vs.* quizartinib. (C) Quantitation of the bioluminescence imaging (BLI) signal from MV4;11-engrafted mice in each group at indicated time post-inoculation: *P<0.005 for quizartinib single agent and all combinations *vs.* venetoclax, AMG 176 or navitoclax single agents at week 5 by one-way ANOVA with Tukey post-test; **P<0.05 for quizartinib + venetoclax, quizartinib + navitoclax, quizartinib + AMG 176 and navitoclax + AMG 176 vs. quizartinib single agent on week 7 by one-way ANOVA with Dunnett post-test; ***P=0.0001 for quizartinib + venetoclax, quizartinib + navitoclax, quizartinib + AMG 176, venetoclax + AMG 176 and navitoclax + AMG 176 *vs.* single agent quizartinib at week 9 by one-way ANOVA with Dunnett post-test.

FLT3-ITD+ model whereas venetoclax prolonged survival of the FLT3-WT model (Figure 2B). Venetoclax combined with quizartinib further improved survival of the FLT3-ITD+ model compared to quizartinib alone, while no combination effect was observed in the FLT3-WT model (Figure 2B). Analysis of leukemia cells from vehicle-treated mice showed that FLT3-WT cells had elevated BCL-2 protein expression relative to BCL-X_L or MCL-1, which may account for venetoclax sensitivity. Conversely, the FLT3-ITD+ cells showed elevated MCL-1 expression compared to BCL-2 or BCL-X_L, consistent with the lack of single agent venetoclax activity (*Online Supplementary Figure S3B*).

A cohort of drug-treated mice (n=3/group) were assessed at the end of dosing. Venetoclax reduced splenomegaly and leukemic cells in peripheral blood (PB), BM and spleen (Figure 3A-B; *Online Supplementary Figure S3C*) in the FLT3-WT model. In the FLT3-ITD+ model, quizartinib treatment significantly reduced splenomegaly and leukemic blasts in the PB, BM and spleen while venetoclax demonstrated little activity (Figure 3A-B; *Online Supplementary Figure S3C*). Although quizartinib monotherapy profoundly reduced FLT3-ITD+ PB blasts, significant blasts were still present in the BM (~50%) and spleen (~12%; Figure 3B; *Online Supplementary Figure S3C*). Notably, the addition of venetoclax to quizartinib reduced leukemic cells in the BM and spleen to less than 1% (Figure 3B; *Online Supplementary Figure S3C*). Treatment was well tolerated as determined by minimal changes in body weight (*Online Supplementary Figure S3D*). These results further demonstrate that venetoclax, when combined with quizartinib, is more efficacious than either single agent alone in FLT3-ITD+ primary AML localized within a biologically relevant tumor microenvironment at clinically achievable doses.

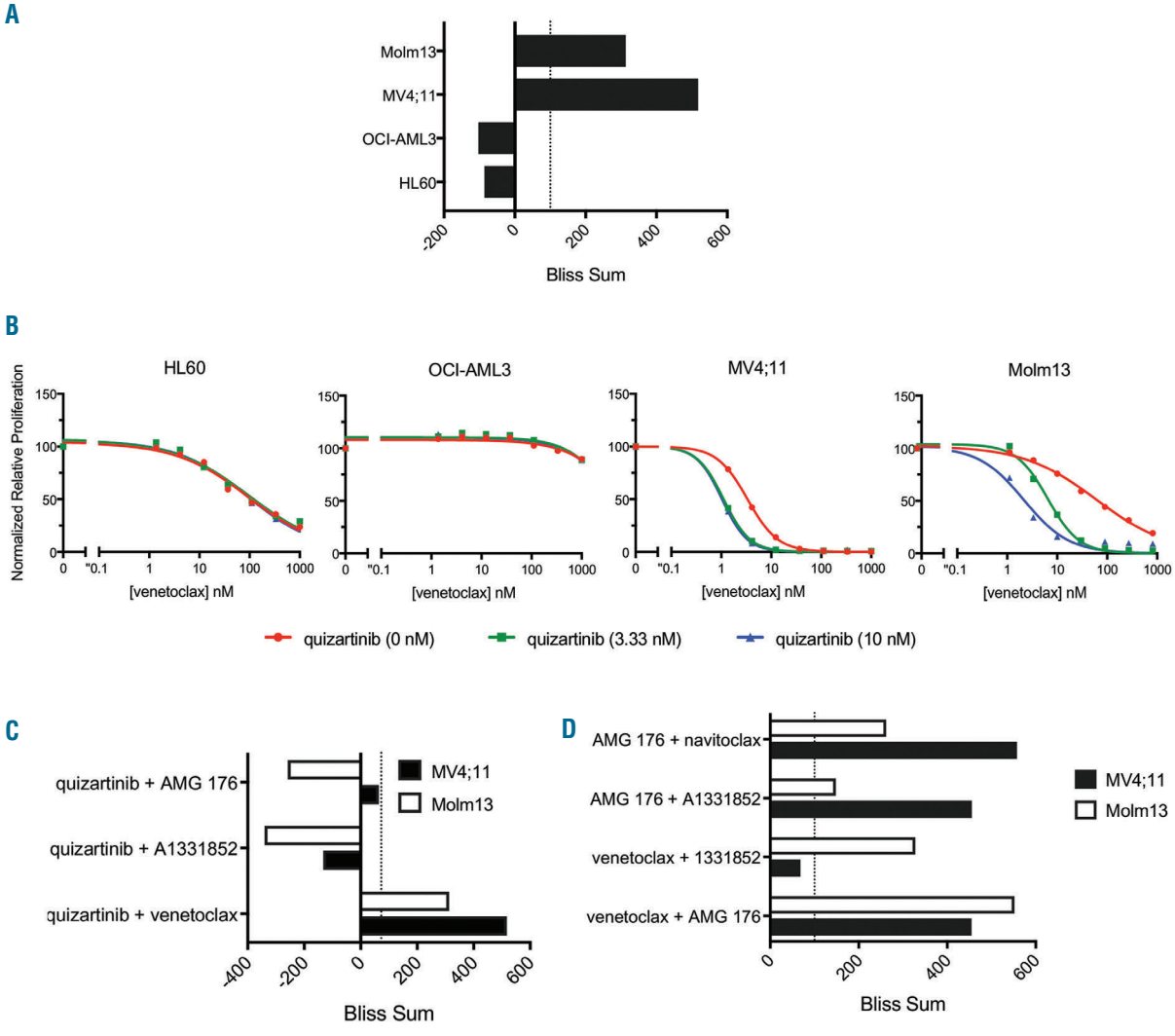


Figure 5. Venetoclax synergistically combined with quizartinib in FLT3-ITD+ cell lines. (A) Cell lines were treated for 48 hours with venetoclax, quizartinib or the combination at indicated concentrations. ATP content was determined by CellTiter-Glo and Bliss sums were calculated and plotted for each cell line. Bliss sum of >100 is highly synergistic. (B) Cell lines were treated for 48 hours with quizartinib, venetoclax or the combination as indicated and cell viability was assessed by CellTiter-Glo. Values are normalized to the average of the untreated samples for each cell line. (C) Fms-like tyrosine kinase 3 (FLT3) internal tandem duplication (FLT3-ITD+) cell lines were treated for 48 hours with combinations of quizartinib and venetoclax, AMG 176 or A1331852 as indicated. ATP content was determined by CellTiter-Glo and Bliss sums were calculated and plotted for each cell line. (D) FLT3-ITD+ cell lines were treated for 48 hours with combinations of venetoclax, AMG 176, A1331852 or navitoclax as indicated. ATP content was determined by CellTiter-Glo and Bliss sums were calculated and plotted for each cell line.

BCL-2, BCL-X_L and MCL-1 promote survival of FLT3-ITD+ cells *in vivo*

In order to understand the role of BCL-X_L and MCL-1 in FLT3-ITD mediated survival *in vivo*, we utilized selective inhibitors to pharmacologically assess the contributions of the anti-apoptotic proteins. Drug combinations of quizartinib, venetoclax, navitoclax (dual BCL-2/BCL-X_L inhibitor)[8] and AMG 176 (MCL-1 inhibitor)[11] were tested in the MV4;11 model at well-tolerated and clinically relevant doses. AMG 176 dosed at 10 mg/kg achieved a C_{max} of ~2 μM in peripheral blood of NSG mice (*Online Supplementary Figure S2*), which is within the cumulative weekly dose range recently reported[11] and 100 mg/kg dose of navitoclax overlaps with clinically achievable exposure.[8,9] Other than quizartinib, single agents targeting the anti-apoptotic proteins showed minimal improvement in survival compared to vehicle control while all combinations with quizartinib enhanced its single agent activity.

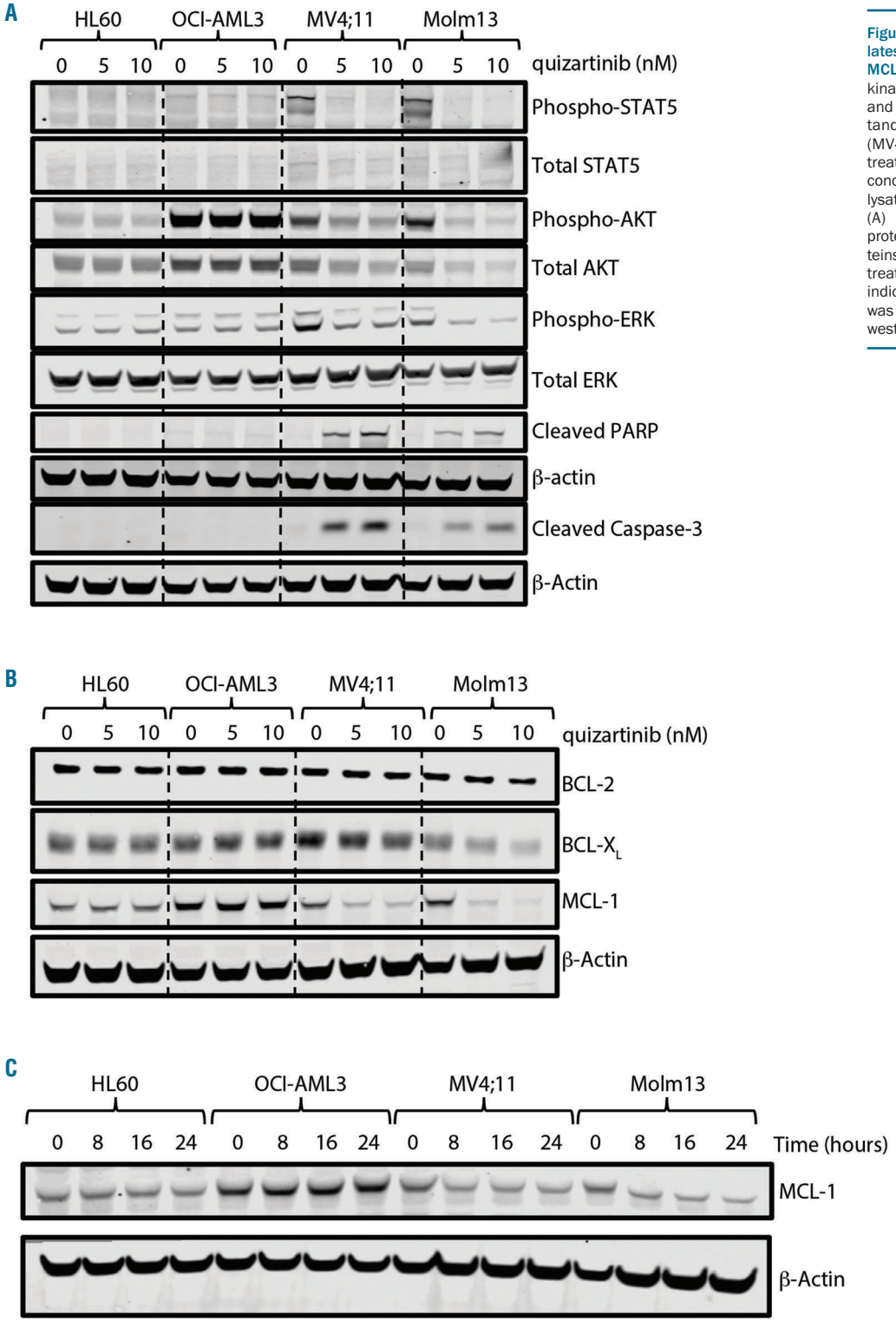


Figure 6. FLT3-ITD signaling regulates the expression of BCL-X_L and MCL-1 *in vitro*. Fms-like tyrosine kinase 3 wild-type (FLT3-WT) (HL60 and OCI-AML3) and *FLT3* internal tandem duplication (FLT3-ITD+) (MV4;11 and Molm13) cell lines treated for 24 hours with indicated concentration of quizartinib and cell lysates analyzed by western blot for (A) FLT3-ITD downstream effector proteins and (B) BCL-2 family proteins as indicated. (C) Cell lines were treated with 10 nM quizartinib for indicated time and MCL-1 expression was assessed in whole cell lysate by western blot.

While MCL-1 inhibition (AMG 176) plus quizartinib improved survival, the response was inferior to venetoclax or navitoclax (BCL-2/BCL-X_L) combined with quizartinib (Figure 4 A,C), demonstrating that inhibition of BCL-2 promotes enhanced anti-tumor efficacy compared to targeting MCL-1 in combination with FLT3-ITD inhibition. Co-targeting of BCL-2 and MCL-1 (venetoclax + AMG 176) resulted in shorter median survival compared with inhibition of BCL-2, BCL-X_L and MCL-1 (navitoclax + AMG 176; Figure 4B-C) indicating that in order to achieve maximum efficacy in the MV4;11 model *in vivo*, inhibition of all three anti-apoptotic proteins may be required. Quizartinib plus venetoclax was superior to navitoclax plus AMG 176, suggesting that FLT3-ITD inhibition

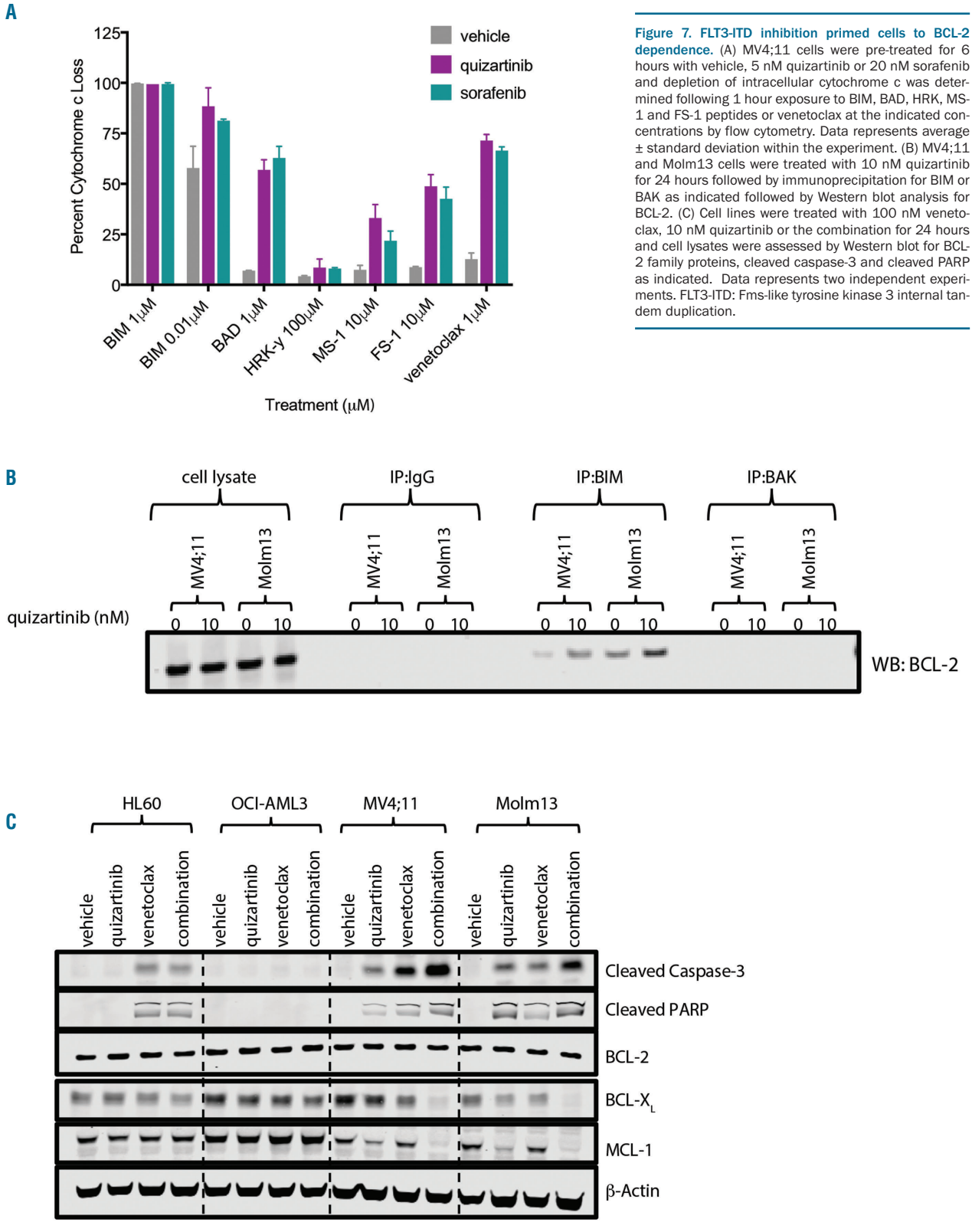


Figure 7. FLT3-ITD inhibition primed cells to BCL-2 dependence. (A) MV4;11 cells were pre-treated for 6 hours with vehicle, 5 nM quizartinib or 20 nM sorafenib and depletion of intracellular cytochrome c was determined following 1 hour exposure to BIM, BAD, HRK, MS-1 and FS-1 peptides or venetoclax at the indicated concentrations by flow cytometry. Data represents average ± standard deviation within the experiment. (B) MV4;11 and Molm13 cells were treated with 10 nM quizartinib for 24 hours followed by immunoprecipitation for BIM or BAK as indicated followed by Western blot analysis for BCL-2. (C) Cell lines were treated with 100 nM venetoclax, 10 nM quizartinib or the combination for 24 hours and cell lysates were assessed by Western blot for BCL-2 family proteins, cleaved caspase-3 and cleaved PARP as indicated. Data represents two independent experiments. FLT3-ITD: Fms-like tyrosine kinase 3 internal tandem duplication.

blocked additional pro-survival nodes. Treatments were well tolerated based on minimal changes in body weight (*Online Supplementary Figure S4*). These data underscore the need to target all three BCL-2 family members to robustly induce FLT3-ITD+ leukemia cell death *in vivo*.

Maximum efficacy is demonstrated *in vitro* when simultaneously inhibiting BCL-2, BCL-X_L and MCL-1 in FLT3-ITD+ cell lines

In order to further dissect the combination of venetoclax and quizartinib, survival and signaling pathways were pharmacologically investigated *in vitro*. FLT3-ITD+ and FLT3-WT (HL60 and OCI-AML3) cell lines were treated in a dose matrix with quizartinib and venetoclax and analyzed by the Bliss independence model[34] to determine synergy. Bliss scores added within a cell line are referred to as a Bliss sum and > 100 was considered highly synergistic. Only the FLT3-ITD+ cell lines showed positive Bliss scores, indicating the combination is synergistic *in vitro* (Figure 5A; *Online Supplementary Figure S5A*). Confirming the Bliss analysis, co-treatment with low dose quizartinib and venetoclax reduced proliferation and increased apoptosis in the FLT3-ITD+ cell lines (Figure 5B; *Online Supplementary Figure S5B*). Venetoclax combined with sorafenib or midostaurin also reduced viability (*Online Supplementary Figure S5C*) while no combination effect was observed in FLT3-WT cell lines (*Online Supplementary Figure S5B-C*) indicating FLT3-ITD-specific response. In order to pharmacologically assess the contribution of MCL-1 and BCL-X_L *in vitro*, AMG 176 and A1331852 (BCL-X_L specific)[9] were utilized in combination with quizartinib. Bliss analysis demonstrated that quizartinib combined with AMG 176 or A1331852 was not synergistic *in vitro* (Figure 5C).

In order to understand the dependence of FLT3-ITD+ cell lines on BCL-2, BCL-X_L and MCL-1 *in vitro*, combinations of venetoclax, navitoclax (BCL-2/BCL-X_L), A1331852 (BCL-X_L) and AMG 176 (MCL-1) were tested. In both cell lines, co-inhibition of BCL-2, BCL-X_L and MCL-1 (AMG 176 + navitoclax) was as synergistic as quizartinib plus venetoclax highlighting that all three proteins mediated survival. However, differential responses between cell lines were observed for other combinations. For the Molm13 cell line, venetoclax plus A1331852 (BCL-X_L) or AMG 176 (MCL-1) showed comparable or more synergy than quizartinib plus venetoclax, respectively and AMG 176 plus A1331852 (MCL-1 and BCL-X_L inhibition) was least synergistic (Figure 5D; *Online Supplementary Figure S6A*). These data suggest that BCL-2 may play an important survival role in Molm 13 cells and needs to be co-targeted. The combination of navitoclax plus AMG 176 was less effective than venetoclax plus AMG 176, which could be a result of the reduced potency of navitoclax toward BCL-2 compared to venetoclax.[9] This is reflected by the combination activity observed at lower doses of venetoclax (<4 nM) when combined with AMG 176 compared to navitoclax plus AMG 176 (*Online Supplementary Figure S6A*).

For the MV4;11 cell line, synergy scores were similar for venetoclax plus AMG 176 (MCL-1) and AMG 176 plus A1331852 (MCL-1 and BCL-X_L inhibition) indicating that MCL-1 inhibition is synergistic with BCL-2 or BCL-X9 inhibition *in vitro* (Figure 5D; *Online Supplementary Figure S6A*). Interestingly, *in vitro* venetoclax plus AMG 176 and navitoclax plus AMG 176 responses were similar whereas *in vivo* navitoclax plus AMG 176 was superior to venetoclax plus AMG 176 (Figure 4B). Assessment of protein expression in cells grown *in vitro versus in vivo* revealed increased BCL-X_L expression and decreased BCL-2 expression *in vivo* (*Online Supplementary Figure S6B*) which could account for the greater dependence on BCL-X_L for survival *in vivo*. Venetoclax plus A1331852 (BCL-X_L) was not synergistic *in vitro* (Figure 5D), consistent with minimal navitoclax activity *in vivo* (Figure 4B). These data further demonstrate the need for simultaneous inhibition of BCL-2, BCL-X_L and MCL-1 in order to achieve maximal anti-tumor activity in FLT3-ITD+ models as each of these proteins appear to mediate survival.

BCL-X_L and MCL-1 expression is regulated by FLT3-ITD *in vitro*

Given that BCL-X_L and MCL-1 are described to be downstream of FLT3-ITD, we evaluated the effect of FLT3 inhibition on protein expression. Quizartinib treatment resulted in kinase inhibition only in FLT3-ITD+ cell lines as confirmed by reduced phosphorylation of downstream effectors ERK, AKT and STAT5 (Figure 6A). While protein levels remained unchanged in FLT3-WT cells, quizartinib reduced BCL-X_L protein by 20-40% and MCL-1 protein by 60-80%, but did not alter BCL-2 expression in FLT3-ITD+ cell lines (Figure 6B; *Online Supplementary Figure S7A*). Sorafenib and midostaurin also reduced MCL-1 protein in the FLT3-ITD+ cell lines (*Online Supplementary Figure S7B*), confirming FLT3-ITD specificity and consistent with reported data.[31] A shorter treatment period demonstrated maximum MCL-1 downregulation as early as 8 hours post FLT3-ITD inhibition (Figure 6C; *Online Supplementary Figure S7C*) reflective of the short half-life for MCL-1 (~2 hours).[35] Assessment of gene expression showed minimal decrease in mRNA expression following quizartinib treatment (*Online Supplementary Figure S7D*), suggesting post-transcriptional regulation. Further, proteasome (MG132) but not caspase (Z-VAD-FMK) inhibition rescued loss of MCL-1 protein induced by quizartinib (*Online Supplementary Figure S7E*). Given the long half-life of BCL-X_L (~20 hours[36]) and toxicity associated with MG132, BCL-X_L protein changes were not captured. However, these data support that BCL-X_L and MCL-1 are indirectly regulated post-transcriptionally downstream of FLT3-ITD.

FLT3-ITD+ cells become BCL-2 dependent following quizartinib treatment

In order to determine if FLT3-ITD inhibition altered survival dependence, dynamic BH3 profiling was utilized. MV4;11 cells were pre-treated with quizartinib or sorafenib followed by treatment with BH3 domain mimetic peptides and assessed for mitochondrial cytochrome c (Cytc) loss.[37] FLT3-ITD inhibition primed cells toward apoptosis as determined by increased Cytc loss when co-treated with low-dose BIM peptide (0.01 μM) compared to vehicle-treated (Figure 7A). FLT3-ITD inhibition increased Cytc loss when co-treated with BAD, MS-1 and FS-1 peptides, suggesting dependence on BCL-2/BCL-X_L, MCL-1 and BCL2-related protein A1 (A1) proteins, respectively, with BAD (BCL-2/BCL-X_L) peptide showing greatest activity (Figure 7A). Co-treatment with HRK peptide (BCL-X_L) demonstrated little activity, while venetoclax combined with FLT3-ITD inhibition resulted in Cytc loss similar to BAD peptide confirming shifted survival dependency to BCL-2 *in vitro* (Figure 7A). Further,

quizartinib treatment increased BIM:BCL-2 complexes in FLT3-ITD+ cell lines (Figure 7B), and co-treatment of cells with quizartinib and venetoclax caused greater reduction in BCL-X_L and MCL-1 protein expression in FLT3-ITD+ cell lines (Figure 7C) compared to single agents. Therefore, FLT3-ITD inhibition switched survival dependence to BCL-2 *in vitro*, providing mechanistic rationale for the synergistic activity of quizartinib and venetoclax.

BCL-X_L and MCL-1 expression is maintained *in vitro* by multiple FLT3-ITD downstream pathways

In order to determine the FLT3-ITD signaling pathways regulating expression of BCL-2, BCL-X_L and MCL-1, selective kinase inhibitors pictisilib (PI3K), cobimetinib (MEK) or ruxolitinib (JAK) were utilized. BCL-X_L and BCL-2 protein were unchanged by any treatment in the FLT3-ITD+ cell lines while PI3K inhibition slightly reduced MCL-1 protein across all cell lines and JAK inhibition reduced MCL-1 protein only in FLT3-ITD+ cell lines (*Online Supplementary Figure S8A-B*). In order to pharmacologically test dependence on these pathways, Bliss analysis was performed. PI3K and BCL-2 co-inhibition was the most synergistic in the FLT3-ITD+ cell lines followed by MEK and BCL-2 co-inhibition. Although ruxolitinib reduced MCL-1 protein expression, the combination was not synergistic in FLT3-ITD+ cell lines (*Online Supplementary Figure S8C*). All Bliss sums ranked less than quizartinib plus venetoclax. The reduced synergy and inability of individual downstream pathways to modulate BCL-X_L and MCL-1 protein support directly targeting FLT3-ITD rather than downstream effectors in combination with venetoclax. Together, the data presented here demonstrated that the combination of quizartinib and venetoclax targets all three anti-apoptotic proteins through indirect regulation of BCL-X_L and MCL-1 by FLT3-ITD inhibition and potent inhibition of BCL-2 by venetoclax.

Discussion

Although minimally active as a monotherapy, venetoclax combined with HMA or LDAC is efficacious in AML patients who are unfit for high intensity chemotherapy across diverse mutation subsets.[18,19] Given this activity, there is clinical rationale for developing combination regimens that maximize efficacy while minimizing toxicity. With this in mind, we provide strong mechanistic rationale for a combination regimen of FLT3-ITD inhibition and venetoclax to be tested clinically.

FLT3 inhibitors became standard of care in FLT3-mutant AML with midostaurin plus chemotherapy in frontline AML and gilteritinib monotherapy in relapsed/refractory AML receiving Food and Drug Administration approval. However, duration of response is often short-lived and patients can relapse with aggressive disease. Therefore, combining FLT3 inhibitors with agents that potently induce apoptosis has the potential to achieve more durable responses for FLT3-ITD+ patients. Combination activity of midostaurin or gilteritinib and venetoclax in preclinical FLT3-ITD+ models has recently been described.[31] However, the role of BCL-X_L in FLT3-ITD+ cells or the contribution of FLT3-ITD downstream pathways in mediating BCL-2 family dependence was not explored in depth. Here we have demonstrated that BCL-2, BCL-X_L and MCL-1 all promote survival of FLT3-ITD+ cells *in vivo* and that targeting of single pathways downstream of FLT3-ITD is insufficient to modulate BCL-X_L and MCL-1. We have provided a more thorough investigation of BCL-2 family dependencies *in vitro* and *in vivo* and demonstrate robust anti-leukemia activity of venetoclax combined with FLT3 inhibitors in FLT3-ITD+ preclinical AML models. The data presented here demonstrated that FLT3-ITD+ inhibition indirectly modulated BCL-X_L and MCL-1 expression while venetoclax potently inhibited BCL-2 resulting in simultaneous targeting of all three anti-apoptotic proteins. Importantly, our studies utilized clinically achievable concentrations of inhibitors and demonstrated *in vivo* anti-tumor activity in models of established leukemia.

We identified that inhibition of individual signaling pathways downstream of FLT3-ITD was insufficient in modulating anti-apoptotic proteins, suggesting that multiple downstream pathways need to be simultaneously inhibited to induce apoptosis. Such functional co-operation has been described for BCR-ABL, where RAS, STAT5 and PI3K individually contribute to survival and provide overlapping anti-apoptotic signals.[38] Potently targeting FLT3-ITD presents an opportunity to inhibit multiple downstream pathways to indirectly reduce BCL-X_L and MCL-1 expression and switch survival dependence to BCL-2. This switch in survival dependence sensitizes mutant cells to venetoclax treatment as demonstrated by enhanced anti-tumor activity of quizartinib plus venetoclax compared to monotherapies. While mechanisms of resistance to the combination of FLT3-ITD inhibition and venetoclax were not explored here, resistance to FLT3 inhibitors is well-described and includes acquired inhibitor-resistant point mutations,[39] suboptimal drug concentrations in the BM, bypass of FLT3-ITD signaling,[40] and alteration of apoptotic proteins.[41] Additionally, mutations in BCL-2 have been identified in chronic lymphocytic leukemia patients following relapse as a mechanism of venetoclax resistance.[42,43] Based on the indirect regulation of BCL-X_L and MCL-1 by FLT3-ITD signaling described here, potential resistance mechanisms to the combination of venetoclax and FLT3-ITD inhibition could include inhibitor-resistant point mutations that interfere with FLT3-ITD signaling inhibition or activating mutations in parallel signaling pathways, both of which would likely alter BCL-2 family expression. Investigation into resistance mechanisms is the focus of future work.

Importantly, venetoclax plus quizartinib combination activity was demonstrated *in vivo* in FLT3-ITD heterozygous (Molm13) and homozygous (MV4;11) preclinical models. Superior long-term survival and disease free state was observed in the MV4;11 xenograft model, which could reflect stronger FLT3-ITD addiction in the homozygous model as described by Pratz *et al.*[44] or result from different secondary mutations in the models. Combination activity was also demonstrated in a PDX model (*Online Supplementary Figure S3A*) with co-occurring *FLT3/DNMT3A/NPM1* mutations, a subset associated with heavy disease burden and poor event free survival compared to non-triplet mutant patients.[45,46] Notably, gilteritinib improved survival in *FLT3/DNMT3A/NPM1* mutant patients compared to chemotherapy[47] and our data indicate venetoclax may further enhance gilteritinib activity in this subset. While additional studies are required to parse out biological differences between FLT3-ITD heterozygous and homozygous mutations and the role of co-

occurring mutations, the data presented here describes combination activity for venetoclax and FLT3 inhibition in multiple FLT3-ITD+ preclinical models.

The BM microenvironment can provide protection from cytotoxic agents and secreted factors in conditioned media from immortalized BM stromal cells increased BCL-X_L (*BCL2L1*) mRNA expression and decreased *BCL2* in primary AML samples, correlating to loss of venetoclax sensitivity compared to samples cultured in normal media.[48] This altered expression was also observed in MV4;11 cells grown *in vivo versus in vitro* (*Online Supplementary Figure S6B*). As seen in this and other studies,[13,49] the Molm13 and MV4;11 cell lines are sensitive to venetoclax *in vitro*, however, when grown *in vivo* sensitivity is greatly lost (Figure 1). Therefore, the contribution of anti-apoptotic proteins in promoting survival may be underestimated outside of the tumor microenvironment. In support, quizartinib monotherapy eliminated tumor cells from the periphery (<5% hCD45+ cells) but not the spleen or BM of the FLT3-ITD+ PDX model while quizartinib plus venetoclax more completely eliminated leukemic cells from the tumor microenvironment (Figure 3B). Importantly, anti-tumor activity was achieved with clinically relevant doses of both venetoclax and quizartinib.

Together, the preclinical data presented here provides strong mechanistic rationale for the combination of venetoclax and FLT3 inhibitors in FLT3-ITD+ AML. Indeed, clinical investigation has been initiated through a phase 1b multi-center study of venetoclax and gilteritinib in R/R AML (*clinicaltrials gov. Identifier: 03625505*) and a phase 1b/II study of quizartinib and venetoclax in R/R FLT3-mutated AML (*clinicaltrials gov. Identifier: 03735875*). Perl *et al*. recently reported that the combination of venetoclax and gilteritinib is well-tolerated with febrile neutropenia (47%), anemia (27%), thrombocytopenia and neutropenia (each 7%) being the most common treatment-related adverse events. In the dose escalation portion of this study, the drug combination showed high response rates, with 90% of FLT3 mutant patients demonstrating blast clearance.[50] The data collected from these on-going trials will be important to define the mechanistic activity and safety of venetoclax combined with FLT3-ITD inhibition in patients.

Disclosures

Venetoclax is developed in collaboration between Genentech, Inc. and AbbVie. RSM, VM, EFC, MD, DS and EAL are current or former employees of Genentech, Inc.. NPS received research funding from Bristol-Myers Squibb. MK is a consultant for AbbVie, Genentech, F. Hoffman La-Roche; served as advisory board member for F. Hoffman La-Roche and AbbVie; holds shares from Reata Pharmaceuticals; honoraria from Amgen, Abbvie, Genentech; research funding from AbbVie, Genentech, Eli Lilly, Cellectis, Calithera, Stemline, Threshold, Flexus Biosciences, Novartis, Ablynx, Agios and Amgen. All other authors declare no conflicts of interest.

Contributions

RSM, QZ, RD, EFC, MD, NPS, MK, DS and EAL designed experiments and analyzed data; RSM, EAL, QZ, RD, VMK, AC, VM and JR performed experiments; RSM, MD, DS and EAL wrote the manuscript. All authors reviewed and edited the manuscript.

Acknowledgments

The authors acknowledge Kyle Edgar for support on the Bliss analysis, and Aaron Logan and colleagues at the UCSF tissue bank for providing primary patient samples (supported by the UCSF Cancer Center Support Grant). The authors also acknowledge and thank the Genentech dosing core, cell line core group, animal resources personnel and veterinary staff for their assistance and contributions to this project.

References

1. Levis M, Small D. FLT3: ITDoes matter in leukemia. Leukemia. 2003;17(9):1738-1752.
2. Yamamoto Y, Kiyoi H, Nakano Y, et al. Activation mutation of D835 within the activation loop of FLT3 in human hematologic malignancies. Blood. 2001;97(8):2434-2439.
3. Choudhary C, Muller-Tidow C, Berdel WE, Serve H. Signal transduction of oncogenic Flt3. Int J Hematol. 2005;82(2):93-99.
4. Hayakawa F, Towatari M, Kiyoi H, et al. Tandem-duplicated Flt3 constitutively activates STAT5 and MAP kinase and introduces autonomous cell growth in IL3-dependent cell lines. Oncogene. 2000; 19:624-631.
5. Mizuki M, Fenski R, Halfter H, et al. Flt3 mutations from patients with acute myeloid leukemia induce transformation of 32D cells mediated by the Ras and STAT5 pathways. Blood. 2000;96(12):3907-3914.
6. Czabotar PE, Lessene G, Strasser A, Adams JM. Control of apoptosis by the BCL-2 protein family: implications for physiology and therapy. Nat Rev Mol Cell Biol. 2014;15(1):49-63.
7. Souers AJ, Leverson JD, Boghaert ER, et al. ABT-199, a potent and selective BCL-2 inhibitor, achieves antitumor activity while sparing platelets. Nat Med. 2013;19(2):202-208.
8. Tse C, Shoemaker AR, Adickes J, et al. ABT-263: a potent and orally bioavailable Bcl-2 family inhibitor. Cancer Res. 2008;68(9):3421-3428.
9. Leverson JD, Phillips DC, Mitten MJ, et al. Exploiting selective BCL-2 family inhibitors to dissect cell survival dependencies and define improved strategies for cancer therapy. Sci Transl Med. 2015;7(279):279ra240.
10. Kotschy A, Szlavik Z, Murray J, et al. The MCL1 inhibitor S63845 is tolerable and effective in diverse cancer models. Nature. 2016;538(7626):477-482.
11. Caenepeel S, Brown SP, Belmontes B, et al. AMG 176, a selective MCL1 inhibitor, is effective in hematologic cancer models alone and in combination with established therapies. Cancer Discov. 2018;8(12):1582-1597.
12. Bose P, Gandhi V, Konopleva M. Pathways and mechanisms of venetoclax resistance. Leuk Lymphoma. 2017;58(9):1-17.
13. Pan R, Hogdal LJ, Benito JM, et al. Selective BCL-2 inhibition by ABT-199 causes on-target cell death in acute myeloid leukemia. Cancer Discov. 2014;4(3):362-375.
14. Konopleva M, Pollyea DA, Potluri J, et al. Efficacy and biological correlates of response in a Phase II Study of Venetoclax monotherapy in Patients with acute myelogenous leukemia. Cancer Discov. 2016;6(10):1106-1117.
15. Punnoose EA, Leverson JD, Peale F, et al. Expression profile of BCL-2, BCL-XL, and MCL-1 predicts pharmacological response to the BCL-2 selective antagonist venetoclax in multiple myeloma models. Mol Cancer Ther. 2016;15(5):1132-1144.
16. Kumar S, Kaufman JL, Gasparetto C, et al. Efficacy of venetoclax as targeted therapy for relapsed/refractory t(11;14) multiple myeloma. Blood. 2017;130(22):2401-2409.
17. Stilgenbauer S, Eichhorst B, Schetelig J, et al. Venetoclax for patients with chronic lymphocytic leukemia With 17p deletion: results from the full population of a Phase II pivotal Trial. J Clin Oncol. 2018;36(19):1973-1980.
18. Pollyea DA, Pratz KW, Jonas BA, et al. Venetoclax in combination with hypomethylatling agents induces rapid, deep, and durable responses in patients with AML ineligible for intensive therapy. Blood. 2018;132(Suppl_1):285.
19. Wei AH, Montesinos P, Ivanov V, MD, et al. Venetoclax plus LDAC for patients with untreated AML ineligible for intensive chemotherapy: phase 3 randomized placebo-controlled trial. Blood. 2020; 135(24): 2137-2145.
20. Chyla B, Daver N, Doyle K, et al. Genetic biomarkers of sensitivity and resistance to venetoclax monotherapy in patients With relapsed acute myeloid leukemia. Am J Hematol. 2018;93(6):E202-E205.
21. DiNardo CD, Tiong IS, Quaglieri A, et al.

Molecular patterns of response and treatment failure after frontline venetoclax combinations in older patients with AML. Blood. 2020;135(11):791-803.
22. Fulda S. Modulation of mitochondrial apoptosis by PI3K inhibitors. Mitochondrion. 2013;13(3):195-198.
23. Thomas LW, Lam C, Edwards SW. Mcl-1; the molecular regulation of protein function. FEBS Lett. 2010;584(14):2981-2989.
24. Grad JM, Zeng X-R, Boise LH. Regulation of Bcl-XL: a little bit of this and a little bit of STAT. Curr Opin Oncol. 2000;12(6):543-549.
25. Alvarez J, Frank D. Genome-wide analysis of STAT target genes: elucidating the mechanism of STAT-mediated oncogenesis. Cancer Biol Ther. 2004;3(11):1045-1050.
26. Yoshimoto G, Miyamoto T, Jabbarzadeh-Tabrizi S, et al. FLT3-ITD up-regulates MCL-1 to promote survival of stem cells in acute myeloid leukemia via FLT3-ITD-specific STAT5 activation. Blood. 2009; 114(24):5034-5043.
27. Minami Y, Yamamoto K, Kiyoi H, Ueda R, Saito H, Naoe T. Different antiapoptotic pathways between wild-type and mutated FLT3: insights into therapeutic targets in leukemia. Blood. 2003;102(8):2969-2975.
28. Spiekermann K, Dirschinger RJ, Schwab R, et al. The protein tyrosine kinase inhibitor SU5614 inhibits FLT3 and induces growth arrest and apoptosis in AML-derived cell lines expressing a constitutively activated FLT3. Blood. 2003;101(4):1494-1504.
29. Kasper S, Breitenbuecher F, Heidel F, et al. Targeting MCL-1 sensitizes FLT3-ITD-positive leukemias to cytotoxic therapies. Blood Cancer J. 2012;2(3):e60.
30. Bagrintseva K, Geisenhof S, Kern R, et al. FLT3-ITD-TKD dual mutants associated with AML confer resistance to FLT3 PTK inhibitors and cytotoxic agents by overexpression of Bcl-x(L). Blood. 2005; 105(9):3679-3685.
31. Ma J, Zhao S, Qiao X, et al. Inhibition of Bcl-2 synergistically enhances the antileukemic activity of midostaurin and gilteritinib in preclinical models of FLT3-mutated acute myeloid leukemia. Clin Cancer Res. 2019; 25(22):6815-6826.
32. Zarrinkar PP, Gunawardane RN, Cramer MD, et al. AC220 is a uniquely potent and selective inhibitor of FLT3 for the treatment of acute myeloid leukemia (AML). Blood. 2009;114(14):2984-2992.
33. Levis MJ, Cortes JE, Gammon GM, Trone D, Kang D, Li J. Laboratory and clinical investigations to identify optimal dosing strategy for quizartinib (AC220) monotherapy in FLT3-ITD positive relapsed/refractory acute myeloid leukemia. Blood. 2016; 128(22): 4042.
34. Foucquier J, Guedj M. Analysis of drug combinations: current methodological landscape. Pharmacol Res Perspect. 2015; 3(3):e00149.
35. Yang T, Kozopas KM, Craig RW. The intracellular distribution and pattern of Mcl-1 overlap with, but are not identical to, those of Bcl-2. J Cell Biol. 1995;128(6):1173-1184.
36. Rooswinkel RW, van de Kooij B, de Vries E, et al. Antiapoptotic potency of Bcl-2 proteins primarily relies on their stability, not binding selectivity. Blood. 2014; 123(18): 2806-2815.
37. Del Gaizo Moore V, Letai A. BH3 profiling--measuring integrated function of the mitochondrial apoptotic pathway to predict cell fate decisions. Cancer Lett. 2013;332(2):202-205.
38. Sonoyama J, Matsumura I, Ezoe S, et al. Functional cooperation among Ras, STAT5, and phosphatidylinositol 3-kinase is required for full oncogenic activities of BCR/ABL in K562 cells. J Biol Chem. 2002; 277(10):8076-8082.
39. Smith CC, Wang Q, Chin CS, et al. Validation of ITD mutations in FLT3 as a therapeutic target in human acute myeloid leukaemia. Nature. 2012;485(7397):260-263.
40. McMahon CM, Ferng T, Canaani J, et al. Clonal selection with RAS pathway activation mediates secondary clinical resistance to selective FLT3 inhibition in acute myeloid leukemia. Cancer Discov. 2019;9(8):1050-1063.
41. Naqvi K, Konopleva M, Ravandi F. Targeted therapies in acute myeloid leukemia: a focus on FLT-3 inhibitors and ABT199. Expert Rev Hematol. 2017;10(10):863-874.
42. Blombery P, Anderson MA, Gong J-n, et al. Acquisition of the recurrent Gly101Val mutation in BCL2 confers resistance to venetoclax in patients with progressive chronic lymphocytic leukemia. Cancer Discov. 2019;9(3):342-353.
43. Tausch E, Close W, Dolnik A, et al. Venetoclax resistance and acquired *BCL2* mutations in chronic lymphocytic leukemia. Haematologica. 2019;104(9):434-437.
44. Pratz KW, Sato T, Murphy KM, Stine A, Rajkhowa T, Levis M. FLT3-mutant allelic burden and clinical status are predictive of response to FLT3 inhibitors in AML. Blood. 2010;115(7):1425-1432.
45. Loghavi S, Zuo Z, Ravandi F, et al. Clinical features of de novo acute myeloid leukemia with concurrent DNMT3A, FLT3 and NPM1 mutations. J Hematol Oncol. 2014;7:74.
46. Bezerra MF, Lima AS, Piqué-Borràs M-R, et al. Co-occurrence of DNMT3A, NPM1, FLT3 mutations identifies a subset of acute myeloid leukemia with adverse prognosis. Blood. 2020;135(11):870-875.
47. Perl AE, Martinelli G, Cortes JE, et al. Gilteritinib or chemotherapy for relapsed or refractory FLT3-mutated AML. N Engl J Med. 2019;381(18):1728-1740.
48. Karjalainen R, Pemovska T, Popa M, et al. JAK1/2 and BCL2 inhibitors synergize to counteract bone marrow stromal cell-induced protection of AML. Blood. 2017; 130(6):789-802.
49. Niu X, Wang G, Wang Y, et al. Acute myeloid leukemia cells harboring MLL fusion genes or with the acute promyelocytic leukemia phenotype are sensitive to the Bcl-2-selective inhibitor ABT-199. Leukemia. 2014;28(7):1557-1560.
50. Perl AE, Daver NG, Pratz KW, et al. Venetoclax in combination with gilteritinib in patients with relapsed/refractory acute myeloid leukemia: a Phase 1b study. Blood. 2019;134(Supp_1):3910.

ARTICLE

Immunophenotypic characterization of reactive and neoplastic plasmacytoid dendritic cells permits establishment of a ten-color flow cytometric panel for initial workup and residual disease evaluation of blastic plasmacytoid dendritic cell neoplasm

Wei Wang,[1] Joseph D. Khoury,[1] Roberto N. Miranda,[1] Jeffrey L. Jorgensen,[1] Jie Xu,[1] Sanam Loghavi,[1] Shaoying Li,[1] Naveen Pemmaraju,[2] Than Nguyen,[1] L. Jeffrey Medeiros[1] and Sa A. Wang[1]

[1]Department of Hematopathology, The University of Texas MD Anderson Cancer Center, and [2]Department of Leukemia, The University of Texas MD Anderson Cancer Center, Houston, TX, USA

Ferrata Storti Foundation

Haematologica 2021
Volume 106(4):1047-1055

ABSTRACT

Blastic plasmacytoid dendritic cell neoplasm (BPDCN) is a rare hematopoietic neoplasm whose immunophenotype remains incompletely characterized, particularly with regards to its distinction from reactive plasmacytoid dendritic cells (PDC). This limitation complicates detection of low-level involvement by BPDCN as well as minimal residual disease (MRD) assessment following therapy. We conducted the current study to characterize the immunophenotype of BPDCN in a cohort of 39 patients, and compared it to that of reactive PDC. We found that, in addition to CD56 expression (97%), BPDCN showed a number of aberrancies, including decreased/negative CD38 (82%), positive CD7 (64%), negative CD2 (81%), negative CD303 (56%), increased HLA-DR (69%) and decreased CD123 (78%) expression. Although BPDCN cells were characterized by CD56 expression, reactive PDC consistently included a $CD56^+$ subset, ranging from 1.3%-20% (median 4.5%) of all PDC, challenging the detection of MRD. These $CD56^+$ reactive PDC were, however, consistently positive for CD2 and CD303, brightly positive for CD38, and negative for CD7, distinctively different from BPDCN. Based on these findings, we set up a ten-color flow cytometry assay for BPDCN and validated it to a sensitivity of 0.01%. This panel was prospectively tested in 19 bone marrow samples from seven patients with BPDCN, and it effectively distinguished BPDCN cells from background reactive PDC in all cases. In summary, by understanding the immunophenotype of reactive and neoplastic PDC, BPDCN can be effectively detected by flow cytometry to a very low level using a panel of markers in addition to CD56. Such an assay could be used for initial bone marrow workup as well as MRD detection after therapy.

Introduction

Blastic plasmacytoid dendritic cell neoplasm (BPDCN) is a rare, clinically aggressive neoplasm derived from non-activated precursors of plasmacytoid dendritic cells (PDC).[1,2] Patients often present with a widespread disease involving multiple anatomic sites, most commonly the skin, followed by bone marrow (BM), peripheral blood and lymph nodes.[1,3-5] BPDCN can occur at any age, but mostly affects patients in their seventh decade of life.

The diagnosis of BPDCN relies on morphology in combination with immunophenotypic studies.[6] BPDCN cells are medium-sized with immature chromatin, resembling lymphoblasts or myeloblasts. They often show cytoplasmic vacuoles and pseudopodia, but these are neither sensitive nor specific features as they may also be present in a variety of other hematolymphoid neoplasms.[7]

Correspondence:

WEI WANG
wwang13@mdanderson.org

SA A. WANG
swang5@mdanderson.org

Received: January 16, 2020.

Accepted: March 26, 2020.

Pre-published: April 2, 2020.

https://doi.org/10.3324/haematol.2020.247569

©2021 Ferrata Storti Foundation

Material published in Haematologica is covered by copyright. All rights are reserved to the Ferrata Storti Foundation. Use of published material is allowed under the following terms and conditions: https://creativecommons.org/licenses/by-nc/4.0/legalcode. Copies of published material are allowed for personal or internal use. Sharing published material for non-commercial purposes is subject to the following conditions: https://creativecommons.org/licenses/by-nc/4.0/legalcode, sect. 3. Reproducing and sharing published material for commercial purposes is not allowed without permission in writing from the publisher.

Immunophenotypically, BPDCN cells are typically positive for CD4, CD56, CD123, HLA-DR, TCL1, and TCF4, and are negative for lineage-specific antigens for B cells (e.g., CD19), T cells (surface and cytoplasmic CD3) as well as myeloid cells (myeloperoxidase).[3,8] Monocytic markers such as CD64 are also negative. Our group has recently demonstrated that co-expression of CD123 and TCF4, as determined by immunohistochemistry constitutes a highly reliable marker for BPDCN.[9]

Despite significant advances in immunophenotypic characterization of BPDCN at baseline, data regarding the distinction between reactive/normal PDC and BPDCN cells remain limited. This limitation raises diagnostic challenges particularly in the evaluation of BM samples with a minimal disease burden, either at presentation in patients with predominantly extramedullary disease or after therapy in patients evaluated for measurable/minimal residual disease (MRD). With advances in treatment options for BPDCN patients and the importance of achievement of disease remission for allogeneic stem cell therapy, the need for reliable and reproducible criteria to assess BM samples for potential low-level BPDCN involvement has gained increased attention. An assay that can reliably distinguish neoplastic PDC from background reactive PDC becomes important. Variable numbers of reactive PDC are detected routinely in the BM by flow cytometry immunophenotyping and/or immunohistochemistry. Similar to their neoplastic counterparts, reactive PDC are positive for CD4, CD123, CD303, HLA-DR and TCF4, and they lack expression of lineage-specific antigens. CD56, a marker frequently expressed in BPDCN, is the only marker being used to date to distinguish neoplastic from reactive PDC. However, CD56 expression can be found in a small subset of reactive PDC.[10-12] Thus, distinguishing CD56$^+$ BPDCN from CD56$^+$ reactive PDC becomes quite challenging in the assessment of post treatment BM specimens, which often contain reactive PDC.

In this study, our aim was to characterize the immunophenotype of BPDCN, with particular focus on the differences between BPDCN and normal/reactive PDC. From understanding these differences, we developed and validated a ten-color clinical-grade flow cytometry immunophenotyping panel and compared its performance to that of orthogonal tools for residual disease evaluation.

Methods

Study group

We identified all patients with BPDCN diagnosed at The University of Texas MD Anderson Cancer Center between 2010 and 2019. All patients fulfilled the diagnostic criteria for BPDCN as defined in the World Health Classification. Patients for whom flow cytometry immunophenotyping had been performed on BM specimens were included in this study. A control group of patients who had BM evaluation by flow cytometry immunophenotyping were also included to study reactive PDC; this group included patients who underwent BM staging for lymphoma or had hematologic diseases other than BPDCN and were in complete remission with or without stem cell transplantation. This study was approved by the University of Texas MD Anderson Cancer Center Institutional Review Board and was conducted in accordance with the Declaration of Helsinki.

Table 1. The list of antibodies used in our flow cytometric panels.

Panel #	Antibody list
Panel #1	Tube 1: CD7/CD33/CD19/CD34/CD13/CD2/CD38/CD45 Tube 2: HLA-DR/CD117/CD4/CD34/CD123/CD38/CD45 Tube 3: CD41/CD36/CD56/CD34/CD64/HLA-DR/CD14/CD45 Tube 4: CD5/CD25/CD22/CD34/CD38/CD15/CD45 Tube 5: TdT/MPO/CD34/CD3/cytoCD3/CD45 (cyto tube)
Panel #2	HLA-DR/CD64/CD4/CD33/CD56/CD45/CD303/CD123
Panel #3	CD2/CD4/CD7/CD38/CD45/CD56/CD64/CD123/CD303/ HLA-DR

Flow cytometric immunophenotypic analysis

BM aspirate specimens were collected in EDTA anticoagulant tubes, and processed within 12 h of collection using a standard lyse/wash technique (PharmLyse™, BD Biosciences, San Diego, CA, USA). For each analysis a minimum of 200,000 events was acquired on FACSCanto II instruments (8-color and 10-color, BD Biosciences).

At the time of initial diagnosis, a comprehensive panel designed for the workup of acute leukemia was performed routinely (panel #1 in Table 1). This panel included lineage-defining markers for B, T, myeloid, and monocytic cells, as well as markers (CD4, CD123, HLA-DR, CD56) necessary for initial screening of BPDCN. When a diagnosis of BPDCN was suspected from panel #1 analysis, an additional panel (panel #2 in Table 1) was used for further characterization and confirmation.

Based on the findings of the current study, a one-tube, ten-color assay (panel #3 in Table 1) was subsequently constructed and validated for distinguishing BPDCN cells from reactive PDC.

Immunohistochemistry

Immunohistochemical studies were performed using formalin-fixed, paraffin-embedded BM core biopsy or aspirate clot specimens.[13] TCF4/CD123 double staining was performed using a previously described protocol.[9]

Results

Immunophenotype of blastic plasmacytoid dendritic cell neoplasm

A total of 39 patients with a diagnosis of BPDCN were studied, including 30 men and 9 women with a median age of 69 years (range, 3-87 years). Flow cytometry immunophenotyping was performed using panel #1 (Table 1) and the more recent cases were also tested using panel #2 (Table 1). The median number of BPDCN cells detected by the flow cytometry was 18% (range, 0.1-91%). The immunophenotype of BPDCN in these 39 cases is summarized in Figure 1 and *Online Supplementary Table S1*.

BPDCN cells were positive for CD45, falling into the "blast" gate on CD45/SSC in all cases (39/39, 100%). CD45 expression was often present at a similar level as, or slightly higher than, that of granulocytes (Figure 2A) with the exception of three cases (8%) which showed significantly lower CD45 expression (dimmer than granulocytes) (Figure 2B). HLA-DR as well as CD123 expression was uniformly positive in all cases. Cells were positive for CD4 in all 38 cases assessed, uniform in 34 (89%) and partially in four (11%) cases. BPDCN cells were positive for CD56 in 97% (36/37) of cases, with mostly (92%, 33/36) uniform and occasionally partial (3/36, 8%) expression. The only case in which CD56 was not expressed was a 3-

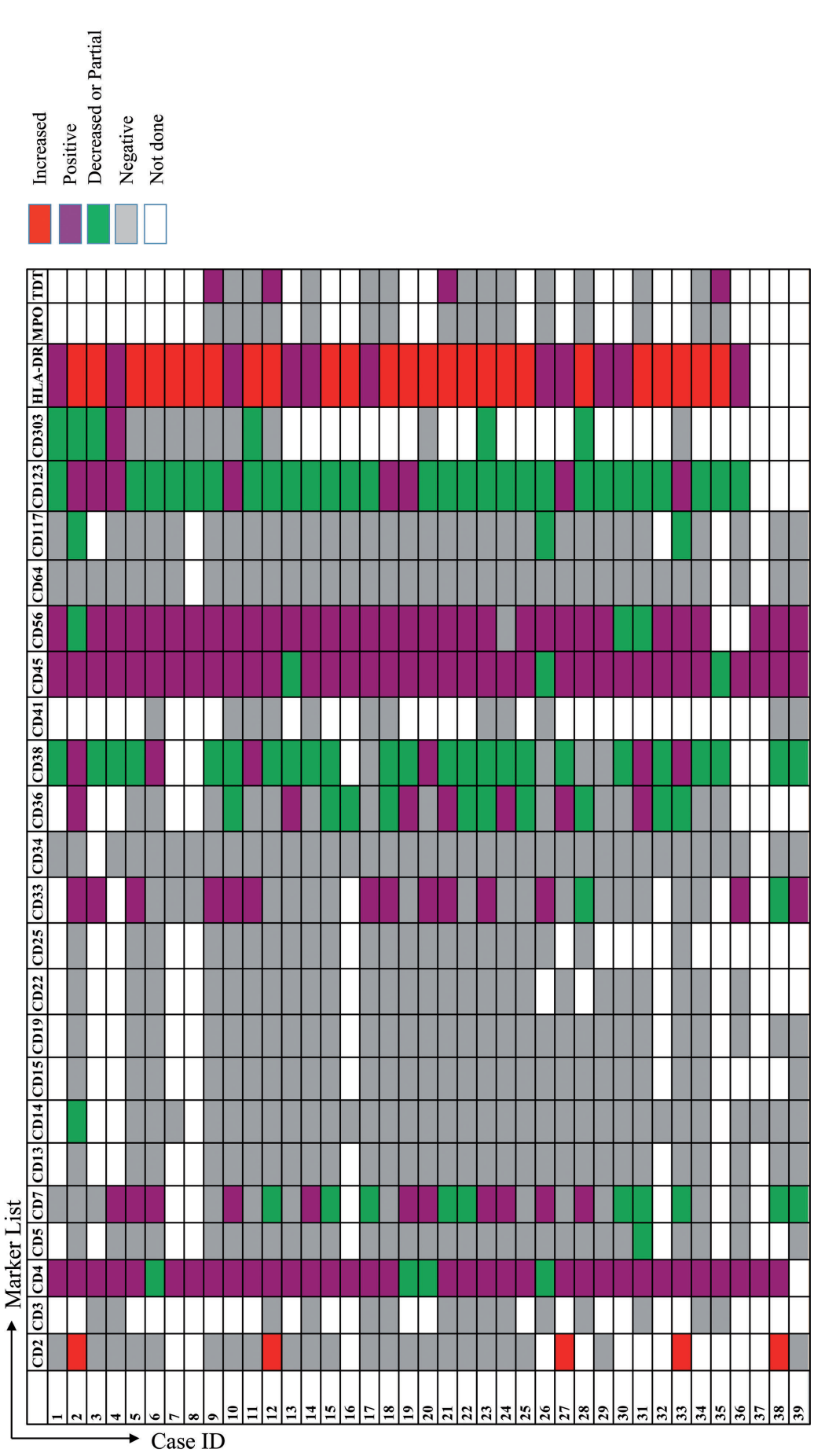


Figure 1. The immunophenotype of blastic plasmacytoid dendritic cell neoplasm. The figure summarizes the immunophenotype of blastic plasmacytoid dendritic cell neoplasms in 39 patients. Different colors represent different levels of expression.

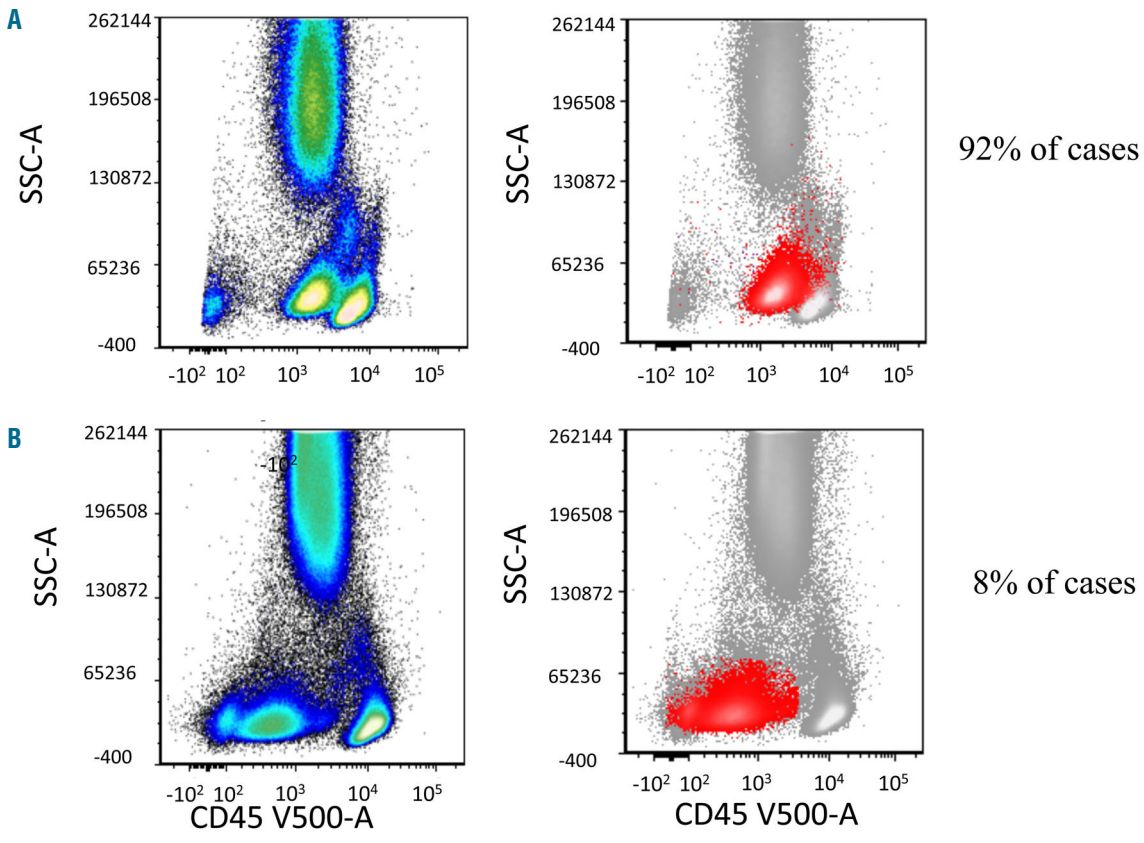


Figure 2. The location of blastic plasmacytoid dendritic cell neoplasm cells on CD45/SSC plots. (A): Most (92%) cases of blastic plasmacytoid dendritic cell neoplasm (BPDCN) show CD45 expression at a level similar to or slightly higher than that detected in granulocytes. (B) A small subset (8%) of cases shows lower CD45 expression. The red population represents BPDCN cells.

year old girl who otherwise had a typical immunophenotype of BPDCN. CD303, a marker which showed a high diagnostic value for BPDCN in some previous studies,[14,15] was expressed in 44% (7/16) of cases. Additionally, cells were positive for CD7 in 64% (21/33) of cases, with uniform expression in 11 and partial expression in ten cases. CD38 was variably expressed in 88% (30/34) of cases. Cells were positive for CD2 in 5/27 (19%) cases and all positive cases showed bright expression. CD33 was expressed in 48% (16/33) of cases. CD36 was expressed in 57% (17/30) of cases, with the expression being uniform in seven (41%) and partial in ten (59%) cases. CD117 was partially expressed in three of 34 (9%) cases. CD5 expression was uncommon, only being observed in one of 30 (3%) cases. Partial CD14 without CD64 expression was detected in one (3%, 1/34) case and TdT expression was detected in 25% (4/16) of cases. All cases were negative for CD3 (surface and cytoplasmic), CD13, CD15, CD19, CD22, CD25, CD34, CD41, CD64 and myeloperoxidase.

Immunophenotype of normal/reactive plasmacytoid dendritic cells

The immunophenotype of normal/reactive PDC was studied in BM samples from 22 patients without BPDCN, including 11 samples that were submitted for lymphoma staging, four cases of B-lymphoblastic leukemia in remission and seven post-transplant samples from patients with B-lymphoblastic leukemia or acute myeloid leukemia. In these cases, normal/reactive PDC represented 0.11% (median) of total nucleated cells (range, 0.01% to 0.43%) as determined by flow cytometry.

Similar to BPDCN cells, normal/reactive PDC were consistently positive for CD123 and HLA-DR and negative for CD64. They were all positive for CD4, CD45, and CD303. Likewise, they were all positive for CD38, which was brightly expressed in all cases, and CD33, which was expressed uniformly in 12 of 21 (57%) cases and partially in the remaining (43%, 9/21). Of note, although positive, CD33 expression in normal/reactive PDC was lower than that of monocytes and basophils (Figure 3D). CD2 expression by normal/reactive PDC showed a bimodal pattern with a spectrum from completely negative cells to positive cells in all cases (Figure 4A). CD7 expression was consistently positive in a small subset of normal/reactive PDC with a median of 13% (range, 0.3% to 21%). Of note, these CD7$^+$ PDC were negative for CD56 (Figure 4A).

The immunophenotype of CD56$^+$ normal/reactive plasmacytoid dendritic cells

CD56 expression was observed in a subset of normal/reactive PDC in all 22 non-BPDCN cases described above, with a median of 4.5% (range, 1.3% to 20%) of total PDC. This CD56$^+$ subset of PDC showed substantial immunophenotypic overlap with BPDCN in PDC-defining markers, including being positive for CD4, CD123, HLA-DR, and CD303; and the panel (panel #2, Table 1) initially designed for BPDCN was incapable of distinguishing these cells from BPDCN.

This population of CD56$^+$ PDC was further studied with

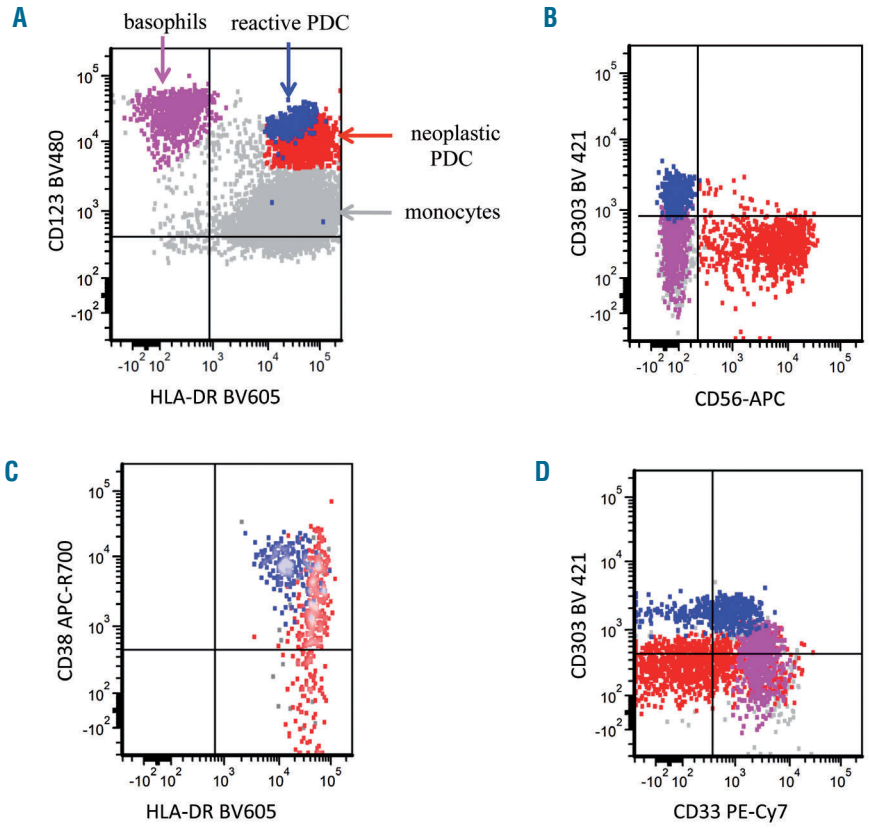


Figure 3. Differential immunophenotypic characteristics of blastic plasmacytoid dendritic cell neoplasm and reactive plasmacytoid dendritic cells. Blastic plasmacytoid dendritic cell neoplasm (BPDCN) cells often show increased HLA-DR, decreased CD123, decreased CD303, decreased CD38, and positive CD56 expression. Pink: basophils; blue: reactive plasmacytoid dendritic cells (PDC); red, neoplastic PDC; and gray: monocytes. (A) Both basophils and PDC are bright for CD123. Basophils are negative whereas PDC are positive for HLA-DR. In comparison to reactive PDC (blue), neoplastic PDC (red) often show decreased CD123 and increased HLA-DR expression. Monocytes (gray) are also positive for CD123 and HLA-DR, but their CD123 level is much lower than that of PDC. (B) Neoplastic PDC are positive for CD56 and negative for CD303. CD303 is positive in reactive PDC. (C) Neoplastic PDC often show decreased CD38 expression when compared to reactive PDC. (D) Reactive PDC are positive for CD33, and approximately half of BPDCN cases are negative for CD33.

an expanded panel of markers, and demonstrated a remarkably consistent pattern. They were positive for CD2 (100%), negative for CD7 (100%), and showed bright CD38 (100%) expression in all 22 cases tested (Table 2). CD303 expression was also positive in all cases (100%), uniform in 13 (59%) and partial in nine (41%). A representative case of CD56$^+$ reactive PDC is shown in Figure 4A.

Of note, the expression of CD56 in normal/reactive PDC is not limited to BM samples. We analyzed a reactive PDC proliferation using immunohistochemistry in a patient who had a self-limited skin lesion, likely an insect bite, which had CD56 expression and had presented a diagnostic challenge at initial encounter (Figure 5).

Differential immunophenotypic characteristics of blastic plasmacytoid dendritic cell neoplasm and reactive plasmacytoid dendritic cells

The immunophenotype of BPDCN was compared to that of reactive PDC. In addition to being "positive" and "negative", the markers of expression were also scored as "increased" or "decreased/partial" if the intensity difference was greater than one-third on a log scale (Figure 1). This comparison was facilitated by the presence of reactive PDC in some cases of BPDCN at initial diagnosis and in many cases of BPDCN following therapy. Compared with reactive PDC, BPDCN cells showed brighter HLA-DR expression in 25 of 36 (69%) cases (Figure 3A), and lower CD123 expression in 28 of 36 (78%) cases (Figure 3A). In the latter cases, although decreased, CD123 levels in BPDCN were still higher than those of monocytes (Figure 3A). CD303, a marker that is consistently positive in normal/reactive PDC, was only positive in seven of 16 (44%) BPDCN cases, of which six showed decreased expression and only one (6% in total) had a normal level of CD303 (Figure 3B). In contrast to bright CD38 expression in reactive PDC, CD38 expression was frequently downregulated in BPDCN cells, being decreased in 24 of 34 (70%) and negative in four of 34 (12%) (Figures 1 and 3C). While CD33 expression was positive in all cases of reactive PDC, it was only positive in 48% (16/33) of BPDCN cases.

We next focused on the difference between BPDCN and reactive CD56$^+$ PDC. Unlike CD56$^+$ reactive PDC that were uniformly positive for CD2, bright for CD38 and consistently negative for CD7, BPDCN cells were frequently negative for CD2 (81%), positive for CD7 (64%) and with decreased or negative (82%) expression of CD38 (Figure 4B) (Table 2). In contrast to the 100% positivity of reactive PDC for CD303, only 44% of BPDCN cases were positive. Using a combination of markers (CD2, CD7, CD56, CD303, CD38), none of the 39 BPDCN cases showed an immunophenotype exactly the same as that of CD56$^+$ reactive PDC, which were CD56$^+$/CD2$^+$/CD7$^-$/CD303$^+$/CD38$^{+bright}$.

Establishment and validation of a flow cytometry assay for minimal residual disease

Based on these findings, a one-tube, ten-color assay CD2/CD7/CD38/CD303/CD123/HLA-DR/CD64/CD4/CD45/CD56 was constructed (panel #3, Table 1). Detailed information, including the antibody clones and the fluorochrome attached to each antibody, is listed in *Online Supplementary Table S2*. CD123, HLA-DR, CD45, and CD64 were included to identify PDC that were CD123^{bright}/HLA-DR$^+$/CD64$^-$/CD45^{dim+}. In patients who received targeted therapy to CD123, an alternative gating strategy was also used to examine PDC that were

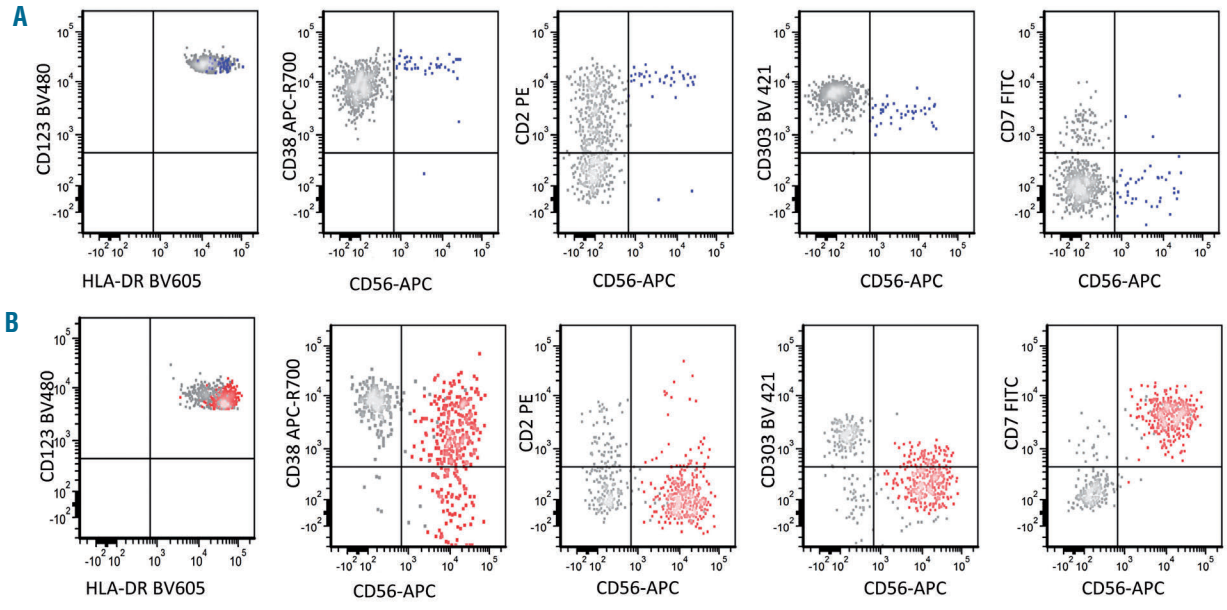


Figure 4. Representative cases of reactive and neoplastic CD56⁺ plasmacytoid dendritic cells. Gray: CD56⁻ reactive plasmacytoid dendritic cells (PDC); blue: CD56⁺ reactive PDC; red: CD56⁺ neoplastic PDC. (A) CD56⁺ reactive PDC are consistently positive for CD2 and CD303, negative for CD7. CD38 expression is bright. (B) In contrast, neoplastic CD56⁺ neoplastic PDC are often negative for CD2 with decreased to negative CD303 expression. CD7 expression is often positive and CD38 expression level is often decreased. Focusing on CD56⁻ PDC (gray) in both panels (A) and (B), these cells are positive for CD303 and CD38. CD2 shows a bimodal pattern of expression (both negative and positive cells present). A small subset of reactive PDC is CD7⁺ and these CD7⁺ reactive PDC are negative for CD56.

Table 2. The major immunophenotypic differences between CD56-positive reactive plasmacytoid dendritic cells and blastic plasmacytoid dendritic cell neoplasm.

	CD2 positive	CD7 positive	CD38 bright	CD303 positive
CD56-positive reactive PDC	100%	0%	100%	100%
BPDCN	19%	64%	18%	44%

PDC: plasmacytoid dendritic cells; BPDCN: blastic plasmacytoid dendritic cell neoplasm.

$CD4^+CD64^-CD56^+HLA\text{-}DR^+CD45^{dim+}$. Representative cases to illustrate our gating strategy are shown in *Online Supplementary Figures S1* and *S2*. The sensitivity of this panel was validated to be 0.01% according to the MRD testing guideline from the College of American Pathologists (*Online Supplementary Figure S3*).

The ten-color MRD panel was tested prospectively in 19 BM samples from seven patients who had a confirmed diagnosis of BPDCN. These 19 samples included one for initial BM diagnosis and 18 samples for evaluation of residual disease during the course of treatment. Using this flow cytometry panel, 12 (63%) samples were positive for BPDCN and the median number of aberrant cells was 0.05% of total nucleated cells (range, 0.008% to 56.5%). Of the 12 positive samples, one was detected as early relapse after stem cell transplant, with 0.01% of aberrant PDC. Of note, all samples had mixed reactive PDC in the background, serving as an internal comparison. All positive cases showed a similar immunophenotype to that identified in the original diagnostic specimen and no significant immunophenotypic shift was observed. For patients who received anti-CD123 targeted therapy, CD123 expression was still maintained in BPDCN as well as normal PDC.

Flow cytometry *versus* immunohistochemistry in the assessment of minimal residual disease

We compared flow cytometry immunophenotyping and dual-color immunohistochemistry for TCF4/CD123 to determine the relative performance of these assays in BM evaluation in the context of BPDCN after therapy. To achieve this, we first systematically assessed the number, distribution, and morphological characteristics of TCF4/CD123 dual-positive cells in 18 BM samples from patients without BPDCN. In such cases, PDC were few and often scattered, with a broad range of morphological characteristics that ranged from mature plasmacytoid forms to others with increased nucleus-to-cytoplasm ratio and occasional nuclear membrane convolutions. Although occasional loose PDC aggregates were identified, none of the cases had tight PDC aggregates or sheets of PDC. Next, we performed TCF4/CD123 double-stain immunohistochemistry in 14 cases with a history of BPDCN who had been evaluated for residual disease by flow cytometry immunophenotyping. In these cases, TCF4/CD123 highlighted scattered PDC but could not reliably distinguish reactive from neoplastic PDC. As shown in Figure 5, the TCF4/CD123 immunostain highlighted scattered PDC in a case of BPDCN prior to (Figure 6A) and after stem cell transplant in remission (Figure 6B), in both cases accounting for around 1-2% of the total cells in the BM. It is uncertain from the TCF4/CD123 immunostain whether these are aberrant or not. Flow cytometry, on the other hand, was capable of differentiating them: it detected neoplastic PDC mixed with normal PDC in the pre-transplant specimen (Figure 6C), whereas only reactive PDC but no aberrant PDC were detected in the post-transplant specimen (Figure 6D).

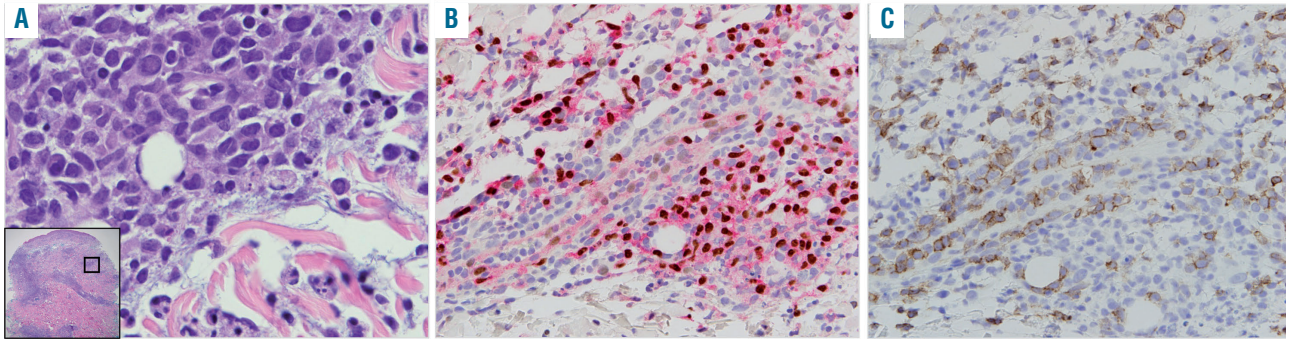


Figure 5. A case of reactive plasmacytoid dendritic cell proliferation positive for CD56 by immunohistochemistry. (A) A skin biopsy shows small clusters of plasmacytoid dendritic cells (PDC), some with plasmacytoid morphology in a self-limited skin lesion, likely caused by an insect bite. The insert shows the low-power view of the skin biopsy. (B) Double staining for CD123/TCF4 highlights scattered and loosely clustered PDC. (C) CD56 immunostaining shows that many PDC are positive.

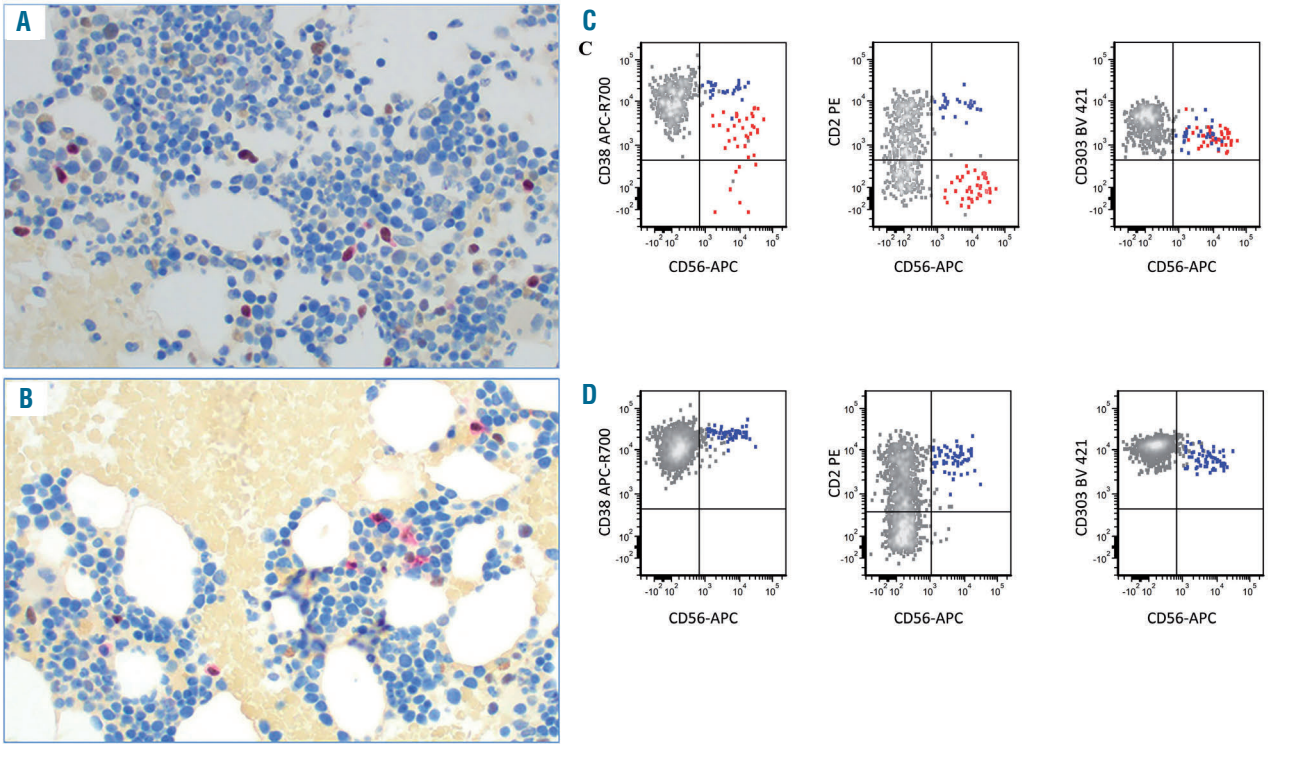


Figure 6. Immunostain and flow cytometric analysis of a case of blastic plasmacytoid dendritic cell neoplasm before and after transplantation. (A, B) Immunostain using a dual-color TCF4/CD123 double stain showed scattered plasmacytoid dendritic cells (PDC) in both samples, before (A) and after (B) transplantation. (C, D) Flow cytometric analysis showed that a subset of PDC (red) in the pre-transplant sample (C) was aberrant (decreased CD38, negative CD2, decreased CD303 expression) whereas all PDC in the post-transplant sample (D) showed a normal immunophenotype. CD56$^+$ reactive PDC are highlighted blue in (C) and (D).

Discussion

In this study, we investigated the immunophenotype of BPDCN in a large cohort of 39 patients and compared it to that of reactive PDC. This study is the first to go beyond a simple characterization of the BPDCN immunophenotype, but to understand the immunophenotypic aberrancy/alterations of BPDCN. Of particular interest, we show that CD56 is expressed in a small subset of normal/reactive PDC and therefore, CD56 alone is insufficient to differentiate BPDCN from reactive PDC, especially when the tumor burden is low. Through further characterization of these CD56$^+$ normal PDC, we identified a combination of markers that can detect BPDCN and distinguish neoplastic from non-neoplastic PDC in BM with a sensitivity of 0.01%.

The diagnosis of BPDCN at the time of initial presentation, typically with a high tumor burden, is often straightforward as BPDCN cells show a distinct immunophenotype, being positive for HLA-DR, CD123 (bright), CD4, CD56, and absence of myeloperoxidase and monocytic markers as well as B- and T-cell lineage-defining markers. The neoplastic infiltrate can be further confirmed by immunohistochemical studies using CD123, TCL1 or a more specific TCF4/CD123 double stain. Basophils often have a similar level of CD123 expression but they are negative for HLA-DR. Monocytes, some hematopoietic precursors and acute myeloid leukemia blasts are positive

for both CD123 and HLA-DR,[16] but their level of CD123 expression is substantially lower than that of PDC.

More challenging is the evaluation of MRD status after treatment or staging assessment of BM specimens with a low tumor burden. This challenge is attributable to the immunophenotypic overlap between BPDCN cells and reactive PDC, especially, the CD56$^+$ subset of reactive PDC. In fact, an initial panel designed for BPDCN MRD detection (panel #2, Table 1) failed to distinguish BPDCN from normal PDC. An immunohistochemical study with TCF4/CD123 was able to highlight PDC, but was incapable of differentiating BPDCN from reactive PDC. These problems prompted us to study the immunophenotype of reactive PDC, and explore the immunophenotypic difference between neoplastic and reactive PDC.

Although both reactive PDC and BPDCN cells were uniformly positive for CD123 and HLA-DR, BPDCN cells tended to have brighter HLA-DR and lower CD123 expression. While all reactive PDC were positive for CD33, 52% of BPDCN cases did not express this marker. All reactive PDC were positive for CD2 with a bimodal pattern, whereas only 19% of BPDCN cases were positive for CD2. With regards to other lymphoid antigens, CD7 expression in BPDCN was very frequent (64%), whereas CD5 was only observed in less than 5% of cases. CD303, a marker considered specific for PDC, was reported to be expressed in 90%,[14] 63%[17] and 53%[18] of BPDCN cases as determined by immunohistochemistry. According to flow cytometry analysis, CD303 was expressed in 75%[15] and 64%[19] of cases. Of note, various anti-CD303 antibodies have been used in previous studies, including clone DDX0043 (Dendritics, Dardilly, France),[14,17] rabbit anti-cytoplasmic CD303,[18] and AC144.[15] In our study, using clone 201A from Biolegend, all reactive PDC were positive for CD303, whereas only 44% of BPDCN cases were positive. Of the CD303$^+$ BPDCN cases, many showed a decreased level of expression compared to that of the internal control-normal PDC. Recently, Huang and colleagues reported decreased or absent CD303 expression in early stages of plasmacytotoid maturation in their series of myeloid neoplasms with PDC differentiation.[20] The lower CD303 intensity in BPDCN might reflect the immaturity of tumor cells as they derived from less mature/precursors of PDC. Nonetheless, this altered level of expression of CD303 in BPDCN facilitates the identification of neoplastic cells in a background of normal PDC, and contributes to MRD detection.

We further confirmed that CD56 was normally expressed in a subset of normal PDC, ranging from 1.3% to 20% of total PDC. A similar observation was previously made in peripheral blood and BM samples from healthy people.[10-12] These CD56$^+$ PDC have been proposed to be precursors as well as the cell of origin of BPDCN. We show here that the CD56$^+$ subset of normal PDC are positive for CD2 and CD303, negative for CD7,[10-12] and retained a high level of CD38. This immunophenotypic pattern is distinctively different from that of CD56$^+$ BPDCN cells, which are often CD2$^-$ (81%), CD7$^+$ (64%), CD303$^-$ (56%), and show decreased or negative CD38 expression (82%). Based on the immunophenotypic differences, we designed a new flow cytometric panel composed of these markers. This panel was capable of detecting BPDCN cells to a level of 0.01% and, prospectively tested in 19 BM samples from seven patients, was able to reliably distinguish BPDCN cells from reactive PDC in all samples. Of note, every BM sample contained reactive PDC, which served as internal controls for comparison. Other markers that could be explored in the future to distinguish BPDCN cells from normal PDC include CD5, CD13, CD22, and CD33. BCL2 is also potentially valuable as it is expressed in BPDCN but often negative in reactive PDC.[5]

In this study, the flow cytometry assay for MRD detection was not compared to mutational analysis for a number of reasons. First, not every case of BPDCN had detectable mutations using our current next-generation sequencing analysis covering 81 frequently mutated genes in myeloid/lymphoid neoplasms. Second, the mutations frequently found in BPDCN, such as *TET2*, *ASXL1*, *TP53* and *NRAS*, are also commonly found in myeloid neoplasms. It is well known that myeloid neoplasms such as myelodysplastic syndrome and chronic myelomonocytic leukemia frequently co-occur with BPDCN.[8,21] Thus the detection of these mutations by next-generation sequencing cannot differentiate a BPDCN clone and a myeloid clone in such cases. Last, the sensitivity of next-generation sequencing is about 1%, which is unable to reach the 0.01% level of sensitivity of flow cytometry.

In summary, we have provided the immunophenotypic characteristics of BPDCN in detail in this study. We have also defined "immunophenotypic aberrancies" of BPDCN in comparison with normal/reactive PDC. It is imperative to recognize that reactive PDC usually include a small subset of CD56$^+$ cells, which should not be misinterpreted as BPDCN. These CD56$^+$ PDC have an immunophenotypic profile distinctively different from that of BPDCN, which allowed us to develop a flow cytometric assay that has a high sensitivity and specificity for the detection of MRD. Such laboratory tests are much in need in the era of targeted therapy and precision medicine. This flow cytometry panel is valuable for disease monitoring during treatment and also enables early detection of relapse in BPDCN patients who have undergone allogeneic stem cell transplant, allowing for early intervention. The significance of positive MRD prior to and following stem cell transplantation is of great interest in BPDCN, and deserves future studies.

Disclosures

No conflicts of interest to disclose.

Contributions

WW and SAW designed and wrote the manuscript. TN performed the experiments. JX, SL, SL, JDK, RNM, JLJ, NP and LJM offered suggestions, wrote and reviewed the manuscript.

References

1. Khoury JD. Blastic plasmacytoid dendritic cell neoplasm. Curr Hematol Malig Rep. 2018;13(6):477-483.
2. Beird HC, Khan M, Wang F, et al. Features of non-activation dendritic state and immune deficiency in blastic plasmacytoid dendritic cell neoplasm (BPDCN). Blood Cancer J. 2019;9(12):99.
3. Facchetti F, Petrella T, Pileri S. Blastic plasmacytoid dendritic cell neoplasm. In: Swerdlow S, Campo E, Harris N, et al., eds. WHO Classification of Tumours of Haematopoietic and Lymphoid Tissues. Revised 4th edition. Lyon, 2017:174-177.
4. Venugopal S, Zhou S, El Jamal SM, Lane

AA, Mascarenhas J. Blastic plasmacytoid dendritic cell neoplasm-current insights. Clin Lymphoma Myeloma Leuk. 2019;19 (9):545-554.
5. Sapienza MR, Pileri A, Derenzini E, et al. Blastic plasmacytoid dendritic cell neoplasm: state of the art and prospects. Cancers (Basel). 2019;11(5).
6. Garnache-Ottou F, Vidal C, Biichle S, et al. How should we diagnose and treat blastic plasmacytoid dendritic cell neoplasm patients? Blood Adv. 2019;3(24):4238-4251.
7. Lyapichev KA, Sukswai N, Konoplev S, Khoury JD. Blastic plasmacytoid dendritic cell neoplasm with unusual lymphoid features and macrovacuoles. Ann Hematol. 2019;98(9):2221-2222.
8. Alayed K, Patel KP, Konoplev S, et al. TET2 mutations, myelodysplastic features, and a distinct immunoprofile characterize blastic plasmacytoid dendritic cell neoplasm in the bone marrow. Am J Hematol. 2013;88(12): 1055-1061.
9. Sukswai N, Aung PP, Yin CC, , et al. Dual expression of TCF4 and CD123 is highly sensitive and specific for blastic plasmacytoid dendritic cell neoplasm. Am J Surg Pathol. 2019;43(10):1429-1437.
10. Comeau MR, Van der Vuurst de Vries AR, Maliszewski CR, Galibert L. CD123bright plasmacytoid predendritic cells: progenitors undergoing cell fate conversion? J Immunol. 2002;169(1):75-83.
11. Osaki Y, Yokohama A, Saito A, et al. Characterization of CD56+ dendritic-like cells: a normal counterpart of blastic plasmacytoid dendritic cell neoplasm? PLoS One. 2013;8(11):e81722.
12. Petrella T, Comeau MR, Maynadie M, et al. 'Agranular CD4+ CD56+ hematodermic neoplasm' (blastic NK-cell lymphoma) originates from a population of CD56+ precursor cells related to plasmacytoid monocytes. Am J Surg Pathol. 2002;26(7):852-662.
13. Khoury JD, Wang WL, Prieto VG, et al. Validation of Immunohistochemical assays for integral biomarkers in the NCI-MATCH EAY131 clinical trial. Clin Cancer Res. 2018;24(3):521-531.
14. Boiocchi L, Lonardi S, Vermi W, Fisogni S, Facchetti F. BDCA-2 (CD303): a highly specific marker for normal and neoplastic plasmacytoid dendritic cells. Blood. 2013;122 (2):296-297.
15. Garnache-Ottou F, Feuillard J, Ferrand C, et al. Extended diagnostic criteria for plasmacytoid dendritic cell leukaemia. Br J Haematol. 2009;145(5):624-636.
16. Arcangeli S, Rotiroti MC, Bardelli M, et al. Balance of Anti-CD123 chimeric antigen receptor binding affinity and density for the targeting of acute myeloid leukemia. Mol Ther. 2017;25(8):1933-1945.
17. Julia F, Dalle S, Duru G, et al. Blastic plasmacytoid dendritic cell neoplasms: clinico-immunohistochemical correlations in a series of 91 patients. Am J Surg Pathol. 2014;38(5):673-680.
18. Jaye DL, Geigerman CM, Herling M, Eastburn K, Waller EK, Jones D. Expression of the plasmacytoid dendritic cell marker BDCA-2 supports a spectrum of maturation among CD4+ CD56+ hematodermic neoplasms. Mod Pathol. 2006;19(12):1555-1562.
19. Tsagarakis NJ, Kentrou NA, Papadimitriou KA, et al. Acute lymphoplasmacytoid dendritic cell (DC2) leukemia: results from the Hellenic Dendritic Cell Leukemia Study Group. Leuk Res. 2010;34(4):438-446.
20. Huang Y, Wang Y, Chang Y, et al. Myeloid neoplasms with elevated plasmacytoid dendritic cell differentiation reflect the maturation process of dendritic cells. Cytometry A. 2020;97(1):61-69.
21. Brunetti L, Di Battista V, Venanzi A, et al. Blastic plasmacytoid dendritic cell neoplasm and chronic myelomonocytic leukemia: a shared clonal origin. Leukemia. 2017;31(5):1238-1240.

Ferrata Storti Foundation

Haematologica 2021
Volume 106(4):1056-1066

Phase II-like murine trial identifies synergy between dexamethasone and dasatinib in T-cell acute lymphoblastic leukemia

Yuzhe Shi,[1] Melanie C. Beckett,[1] Helen J. Blair,[1] Ricky Tirtakusuma,[1] Sirintra Nakjang,[1] Amir Enshaei,[1] Christina Halsey,[2] Josef Vormoor,[3] Olaf Heidenreich,[1,3] Anja Krippner-Heidenreich[3#] and Frederik W. van Delft[1#]

[1]Wolfson Childhood Cancer Research Centre, Northern Institute for Cancer Research, Newcastle University, Newcastle upon Tyne, UK; [2]Wolfson Wohl Cancer Research Centre, Institute of Cancer Sciences, College of Medical, Veterinary and Life Sciences, University of Glasgow, Glasgow, UK and [3]Prinses Máxima Centrum voor Kinderoncologie, Utrecht, the Netherlands

[#]*AKH and FWvD contributed equally as co-senior authors.*

ABSTRACT

T-cell acute lymphoblastic leukemia (T-ALL) is frequently characterized by glucocorticoid (GC) resistance, which is associated with inferior outcomes, thus highlighting the need for novel therapeutic approaches for GC-resistant T-ALL. The pre-T-cell receptor (pTCR)/TCR signaling pathways play a critical role in cell fate decisions during physiological thymocyte development, with an interplay between TCR and glucocorticoid receptor (GR) signaling determining the T-lymphocyte selection process. We performed an shRNA screen *in vitro* and *in vivo* in T-ALL cell lines and patient-derived xenograft (PDX) samples to identify vulnerabilities in the pTCR/TCR pathway and identified a critical role for the lymphocyte cell-specific kinase (LCK) in cell proliferation. LCK knockdown or inhibition with dasatinib (DAS) caused cell cycle arrest. Combination of DAS with dexamethasone (DEX) resulted in significant drug synergy leading to cell death. The efficacy of this drug combination was underscored in a randomized phase II-like murine trial, recapitulating an early phase human clinical trial. T-ALL expansion in immunocompromised mice was significantly impaired using this drug combination, compared to mice receiving control vehicle or single drug treatment, highlighting the immediate clinical relevance of this drug combination for high-risk T-ALL patients. Our results thus provide a strategy to improve the efficacy of current chemotherapy platforms and circumvent GC resistance.

Correspondence:

FREDERIK W. VAN DELFT
frederik.van-delft@newcastle.ac.uk

Received: October 21, 2019.

Accepted: March 4, 2020.

Pre-published: March 5, 2020.

https://doi.org/10.3324/haematol.2019.241026

©2021 Ferrata Storti Foundation

Material published in Haematologica is covered by copyright. All rights are reserved to the Ferrata Storti Foundation. Use of published material is allowed under the following terms and conditions: https://creativecommons.org/licenses/by-nc/4.0/legalcode. Copies of published material are allowed for personal or internal use. Sharing published material for non-commercial purposes is subject to the following conditions: https://creativecommons.org/licenses/by-nc/4.0/legalcode, sect. 3. Reproducing and sharing published material for commercial purposes is not allowed without permission in writing from the publisher.

Introduction

Current minimal residual disease (MRD)-stratified chemotherapy protocols for patients with T-cell acute lymphoblastic leukemia (T-ALL) result in 5-year event-free survival rates of 80% and 50% for pediatric and adult patients, respectively.[1,2] Induction failure, early relapse, and isolated central nervous system (CNS) involvement are more common in T- than B-lineage ALL.[3] Moreover, resistance to conventional chemotherapy including glucocorticoid (GC) is a frequent feature of relapsed and refractory T-ALL, reducing the second remission rate and long-term outcomes.[4] GC are an instrumental component of ALL therapy and induce apoptosis in lymphoid malignancies.[5-7] Resistance to GC is a critical factor influencing treatment response and outcome.[5,8-11] Amongst ALL subtypes, GC resistance is more frequently observed in infant ALL and T-ALL.[5,9,11,12]

Endogenous GC can induce apoptosis during the selection process of T lymphocytes in the thymus, an effect which can be constrained by crosstalk with T-cell receptor (TCR) signaling.[13,14] Whilst mature T-cell maintenance requires tonic TCR signaling, inappropriate TCR expression has been shown to give rise to T-cell malignancies in mouse model systems.[15,16]

The immature pre-T-cell receptor (pTCR) consists of a complex of alpha (pTCRα) and beta (TCRβ) peptide chains complexed with CD3δε and CD3γε heterodimers.

Activation of this complex occurs through the SRC family kinase (SFK) members lymphocyte cell-specific protein-tyrosine kinase (LCK) and FYN. They are critical modulators of T-cell development and activation.[17] LCK phosphorylates the plasma membrane-associated TCR complex[18] and ZAP70.[19] ZAP70 in turn phosphorylates the linker for activation of T cells (LAT) leading to the activation of downstream signaling cascades. The overall activity of LCK is regulated by the phosphorylation status of the activating and inhibitory tyrosine residues 394 and 505, respectively.[20] LCK activation correlates with Y416SRC (also Y394LCK) phosphorylation, as the latter over-rides the inhibitory effects of Y505 phosphorylation.[21]

We hypothesized, therefore, that T-ALL continues to rely on proliferative and survival stimuli inherent to the TCR signaling pathway, which, if inhibited, may enhance GC sensitivity. A targeted shRNA screen directed against components of the TCR signaling initiation complex identified a crucial role for LCK in T-ALL proliferation, both *in vitro* and *in vivo*. The anti-proliferative effects of LCK knockdown could be replicated by using the small molecule inhibitor dasatinib (DAS). Drug synergy was observed using DAS in combination with dexamethasone (DEX) on patient-derived xenograft (PDX) cell survival *in vitro*. Mirroring the design of early phase human trials, a murine phase II-like trial demonstrated significantly impaired leukemia progression *in vivo* using combination treatment. Our results present a clear rationale for using DAS in conjunction with DEX to enhance conventional chemotherapeutic treatment and revert GC resistance in pediatric T-ALL patients.

Methods

Patient samples

The patient-derived material was collected as part of diagnostic investigations of patients at the Great North Children's Hospital, Department of Paediatric Haematology and Oncology, Newcastle upon Tyne, UK. The material was collected and stored with informed consent obtained from all subjects in accordance with the Declaration of Helsinki.

Samples with explicit written consent for *in vivo* studies were requested from the Newcastle Biomedicine Biobank, Newcastle University, UK, and used according to approvals given by the Newcastle Biomedicine Biobank (NHB application NHB-008) and the local institutional review board Newcastle & North Tyneside Ethics Committee (REC reference: 07/H0906/109).

Drug matrix assays

Dasatinib (9 nM – 30 μM) (DC Chemicals, Shanghai, China) was titrated on T-ALL cell lines ($4x10^4$/well) in 96-well plates (Corning, NY, USA). Cell viability was assessed after 3 days using Cell Counting Kit 8 (NBS Biologicals, Cambridgeshire, UK). Absorbance was measured at OD450 nm using a POLARstar Omega plate reader (BMG LABTECH, Bucks, UK). IC_{50} values were determined by GraphPad Prism. Assays were performed in triplicate and at least three independent repeats were performed.

For DAS/DEX combination treatments DAS (80 nM – 50 μM) and DEX (0.09 nM – 600 nM) were titrated in 2-dimensions on T-ALL cell lines ($4x10^4$ cells per well in 96-well plate) or *ex vivo* expanded PDX cells ($8x10^4$ cells per well in 96-well plate). *Ex vivo* expansion was achieved after co-culture with OP9-DL1 for 1 week, after which cells were separated from their feeders by repetitive transfer and subsequently plated. After 72 hours (h) of culture, the plates were developed as above. Drug synergy was determined using Combenefit software (v.2.021).[22]

Phase II-like murine trial

For each of the ten PDX samples, $8x10^6$ cells were intrafemorally (IF) injected into four NSG mice (40 mice in total) under isoflurane anesthesia. The four NSG mice derived from one PDX sample were matched for gender and age. T-ALL engraftment in mouse peripheral blood was monitored weekly by tail vein bleeds (20 μL blood/mouse). The four mice of each PDX were randomized to receive control vehicle, DAS (35 mg/kg), DEX (1 mg/kg) or DEX/DAS combination by intraperitoneal (IP) injection upon engraftment, defined as ≥0.5% peripheral blood $hCD45^+/hCD7^+$ cells. The median treatment duration of these mice was 15 days, depending on their clinical status. When any of the four mice displayed signs of ill health or weight loss, all four mice derived from this PDX were killed at the same time to assess leukemia engraftment in bone marrow, blood, spleen, liver and CNS. Spleen size and weight were recorded. Statistical analyses were performed using RStudio (Boston, MA, USA) with linear mix model. The final analysis excluded the four mice derived from patient sample LK214, as all mice succumbed to T-ALL before treatment was initiated.

See the *Online Supplementary Appendix* for further details of the methods used.

Results

A targeted shRNA screen of T-cell receptor pathway components identifies an essential role for lymphocyte cell-specific kinase in T-cell acute lymphoblastic leukemia cell line and patient-derived xenograft proliferation *in vitro*

To explore the importance of the pTCR/TCR signaling complex in proliferation and survival of malignant T cells, we performed a limited shRNA screen targeting six genes with three shRNAs per gene, including *LCK, ZAP70, PTCRA, FYN, CD3E* and *LAT* in four T-ALL cell lines (HPB-ALL, CUTLL1, MOLT4, SUPT1), and included 18 control shRNAs (see *Online Supplementary Methods and Online Supplementary Table S1A*). *In silico* analysis using the Cancer Cell Line Encyclopedia (CCLE) demonstrated that these six genes are highly expressed in a panel of T-ALL cell lines (*Online Supplementary Figure S1A*). *LCK* and *PTCRA* expression was confirmed by targeted gene expression analysis in T-ALL cell lines and patient samples (Figure 1B) (*Online Supplementary Figure S1B*). The limited shRNA screen revealed the shLCK#3 construct targeting *LCK* was the only construct significantly depleted in all four cell lines, when compared with base line shRNA integration, underlining an important role for LCK in T-ALL cell line proliferation and/or survival (Figure 1A and *Online Supplementary Figure S1C* and *D*). The shLCK#1, shZAP70#1 and shPTCRA#2 constructs were lost in 3 out of 4 cell lines. Constructs targeting *FYN, CD3E,* or *LAT* were significantly depleted in one cell line only, suggesting that these molecules do not play an universal role in T-ALL cell proliferation. ShRNAs against essential ribosomal genes were predictably depleted, whilst all three shRNA constructs targeting the tumor suppressor *PTEN* were enriched as expected. Repeated sampling at 16, 30 and 40 days after transduction demonstrated progressive depletion of shRNA constructs targeting *LCK* and *ZAP70* (*Online Supplementary Table S2 and Online Supplementary Figure S1E*). PDX LK203 showed

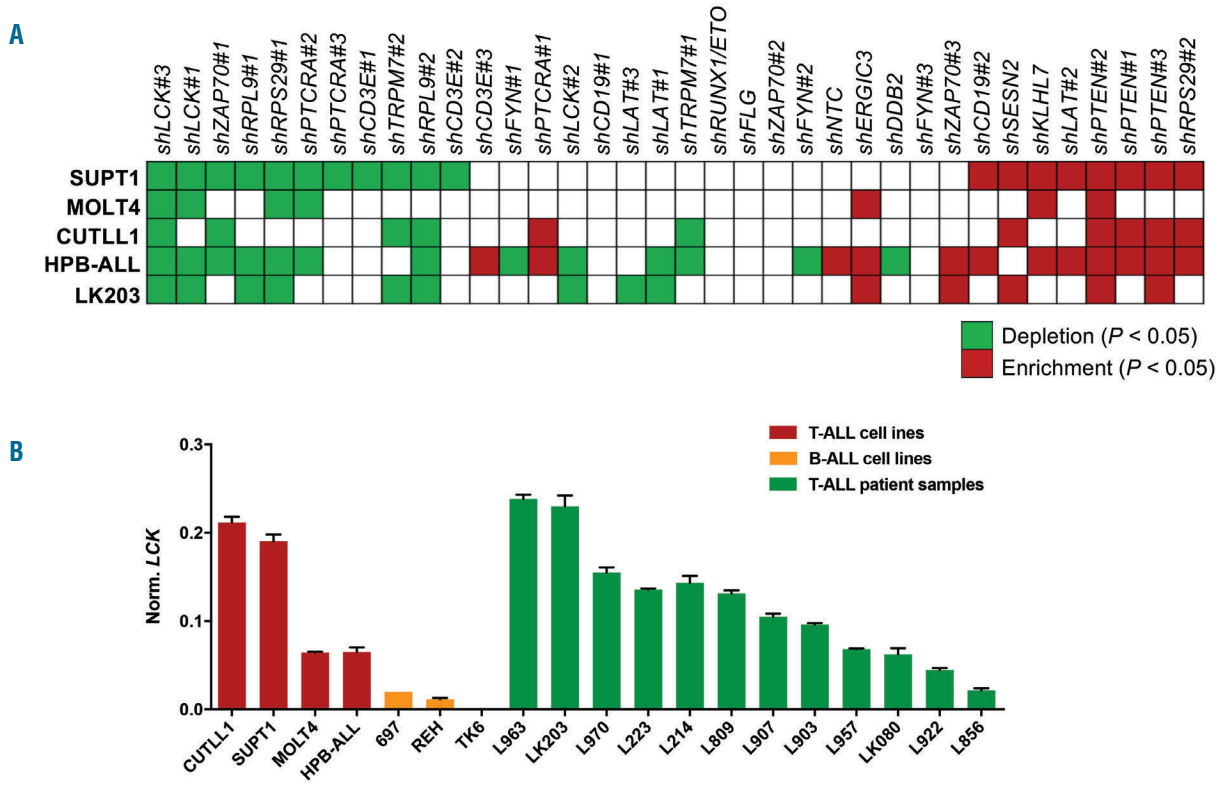


Figure 1. A targeted shRNA screen reveals lymphocyte cell-specific kinase (LCK) is essential for *in vitro* proliferative potential. (A) T-cell acute lymphoblastic leukemia (T-ALL) cell lines (SUPT1, MOLT4, HBP-ALL, CUTLL1) and PDX LK203 were subjected to a functional screen using a pLKO5-shRNA library containing 36 constructs targeting selected pre-T-cell receptor (pTCR)/TCR signaling complex components (PTCRA, CD3E, FYN, ZAP70, LCK, LAT), positive (PTEN, RPS29, RPL9), negative controls (KLHL7, CD19, DDB2, ERGIC3, FLG, RUNX1-ETO, SESN2, TRPM7) and a non-targeting control (NTC). Genomic DNA was sampled and barcoded. Enriched and depleted shRNAs were identified by next generation sequencing (NGS). The heatmap depicts statistically significant gains (red) or losses (green) of shRNA constructs after *in vitro* culture of four T-ALL cell lines (40 days) and PDX LK203 (30 days). (B) Relative gene expression of *LCK* in seven cell lines and 12 PDX samples. *LCK* expression was determined in four T-ALL cell lines, 697 and REH (B-lineage ALL cell lines [B-ALL]), TK6 (lymphoblastoid cell line), and 12 PDX samples by real time quantitative-polymerase chain reaction. GAPDH served as reference gene for normalization.

good viability (≥75%) and proliferation potential (T_d = 2.8 days) in co-culture with human mesenchymal stem cells (hMSC), hence subjected to shRNA screening. ShRNA sequencing 30 days after transduction confirmed all constructs targeting *LCK* were significantly depleted (Figure 1A, *Online Supplementary Table S3 and Online Supplementary Figure S1F*).

Knockdown of lymphocyte cell-specific kinase in T-cell acute lymphoblastic leukemia cell lines confirms an essential role for lymphocyte cell-specific kinase *in vitro* propagation

To confirm the role of LCK and other components of the pTCR/TCR signaling complex in cell proliferation, competitive outgrowth assays were performed. SUPT1, MOLT4 and CUTLL1 cells were transduced with lentiviral shRNAs targeting *LCK, ZAP70, FYN, PTCRA* or non-targeting control shRNAs. Successfully transduced cells expressing green fluorescence protein (GFP) were seeded in a 1:1 ratio with parental cells.

Three shRNAs were used to silence *LCK*, of which shLCK#3 achieved the greatest degree of knockdown. Lentiviral knockdown with shLCK#3 led to significant reduction in mRNA in SUPT1 (75%KD), MOLT4 (55% KD), and CUTLL1 (45% KD) cells (Figure 2A). In general, greater knockdown was associated with more pronounced impairment of *in vitro* proliferation (*Online Supplementary Figure S2A*). LCK expression was confirmed at protein level, demonstrating ubiquitous expression of LCK in cell lines (*Online Supplementary Figure S1G*). In line with mRNA downregulation, knockdown of *LCK* led to a decrease in total LCK protein expression (Figure 2A). Non-transduced cells consistently outcompeted *LCK* knockdown cells resulting in a pronounced loss of over 70% transduced GFP^+ cells in all three cell lines, underlining the critical and universal role of LCK in T-ALL cell line maintenance (Figure 2B and C, and *Online Supplementary Figure S2A and C*).

A similar but less significant observation was made for *ZAP70* knockdown in SUPT1, MOLT4 and CUTLL1 cells. Efficient *ZAP70* knockdown correlated with a pronounced proliferation defect (*Online Supplementary Figure S2A and C*). Knockdown of *PTCRA* affected proliferation in $pTCR\alpha^+$ MOLT4 and SUPT1, but not in pTCRα- CUTLL1 (*Online Supplementary Figure S2A and C*). Moreover, *FYN* knockdown did not affect proliferation in any of the cell lines despite efficient knockdown (*Online Supplementary Figure S2B*).

Knockdown of lymphocyte cell-specific kinase in T-cell acute lymphoblastic leukemia cell lines and patient-derived xenograft samples impairs leukemia propagation *in vivo*

To confirm a functional role for LCK *in vivo*, PDX L963 cells were transduced with our shRNA library and transplanted into six NSG mice (Figure 3A and *Online*

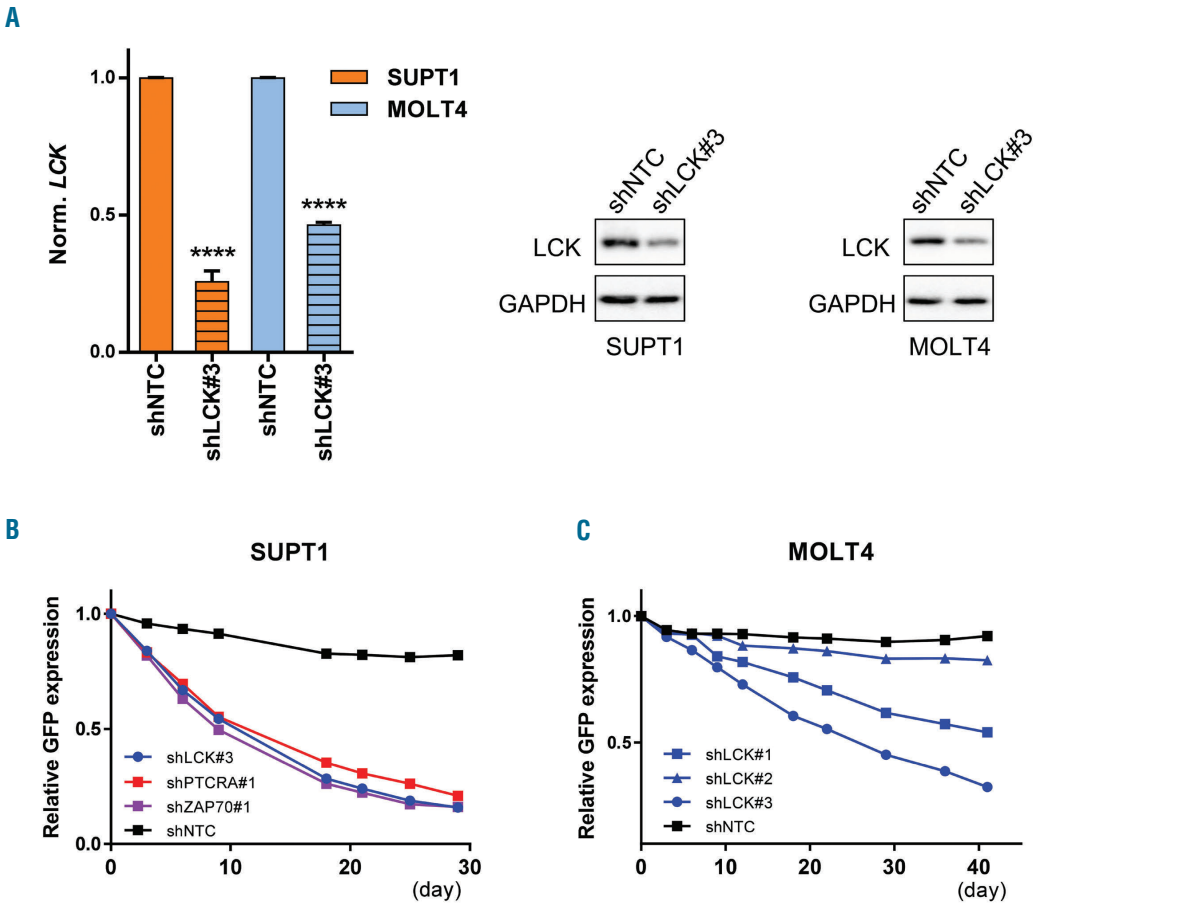


Figure 2. Knockdown of lymphocyte cell-specific kinase (LCK) reduces propagation of T-cell acute lymphoblastic leukemia (T-ALL) cell lines *in vitro*. SUPT1 (A and B) and MOLT4 (A and C) cells were lentivirally transduced with shNTC (non-targeting control), shLCK#1, shLCK#2, shLCK#3, shPTCRA#1, or shZAP70#1 expression constructs. (A) Knockdown efficiency of LCK at mRNA level (left) and protein level (right) after 6 days. Whole cell lysates were probed for total LCK and GAPDH in western blot analysis. (B and C) T-ALL cell lines SUPT1 (B) and MOLT4 (C) transduced with GFP-expressing shLCK (blue), shZAP70 (purple), shPTCRA (red) or shNTC (black) constructs were seeded in a 1:1 ratio with non-transduced parental cells *in vitro*. Cells were cultured and analyzed repetitively by flow cytometry for the presence of GFP$^+$ cells over a time period of 30 and 40 days for SUPT1 and MOLT4, respectively. A relative GFP expression of 1 denotes a mixture of 50% GFP$^+$ cells with 50% parental cells (ratio 1:1). A value of 0.5 refers to 25% of GFP$^+$ cells and 75% parental cells (ratio 1:4). Student's *t*-test: ****P<0.001.

Supplementary Figure S3A). Genomic DNA (gDNA) was extracted from L963 cells isolated from bone marrow and spleen after mice became symptomatic (week 11). ShRNA sequencing indicated that shLCK#3 represented the most significantly depleted shRNA construct *in vivo* (Figure 3A, *Online Supplementary Table S3 and Online Supplementary Figure S3B*).

To assess the effect of *LCK* knockdown on engraftment fitness, MOLT4 cells were transduced with lentiviral vectors encoding either red fluorescent protein RFP/shNTC (non-targeting control) or GFP/shLCK#3. Equal proportions of cell populations were transplanted into NSG mice (n=5). Leukemia cells were isolated from spleen, bone marrow and liver once mice were symptomatic (day 26). Flow cytometric analysis of the leukemic cell population established that cells carrying shNTC had a clear competitive engraftment advantage over cells with *LCK* knockdown in all mice tissues sampled (Figure 3B and *Online Supplementary Figure S3C*).

Knockdown of lymphocyte cell-specific kinase leads to cell cycle arrest in T-cell acute lymphoblastic leukemia cell lines and patient-derived xenograft samples

Next we investigated the mechanisms underlying the defect in proliferation, survival and engraftment observed after *LCK* knockdown. Jurkat, MOLT4 and SUPT1 cells were transduced with shLCK#1/#3 and cell cycle analyses performed. In all cell lines, we observed significant cell cycle arrest with an increase in G_0/G_1 phase and decrease in S phase after *LCK* knockdown (Figure 4A-C and *Online Supplementary Figure S4A*).

ShLCK#3 led to decreased protein levels of total LCK and activated p-Y416^{SRC} in cell lines, suggesting activation status of LCK is associated with cell cycle arrest. In PDX L963, *LCK* knockdown led to a 45% reduction in total LCK expression, as well as a 71% reduction in p-Y416^{SRC} as assessed by Phosflow (Figure 4D). This knockdown resulted in a decrease in S phase over time compared to control (*Online Supplementary Figure S4B*). The proliferative behavior of PDX cells was analyzed after labeling with cell trace violet (CTV). PDX L963 cells were transduced with shRNA constructs targeting *LCK* or a non-targeting control (NTC) and co-cultured with OP9-DL1 feeder cells for 13 days. The *LCK* knockdown cells showed restricted proliferation compared to the control cells (Figure 4E). Confirmatory siRNA knockdown of *LCK* was undertaken in PDX samples LK203 and L963. Knockdown of total and activated LCK was confirmed by Phosflow. Cell cycle

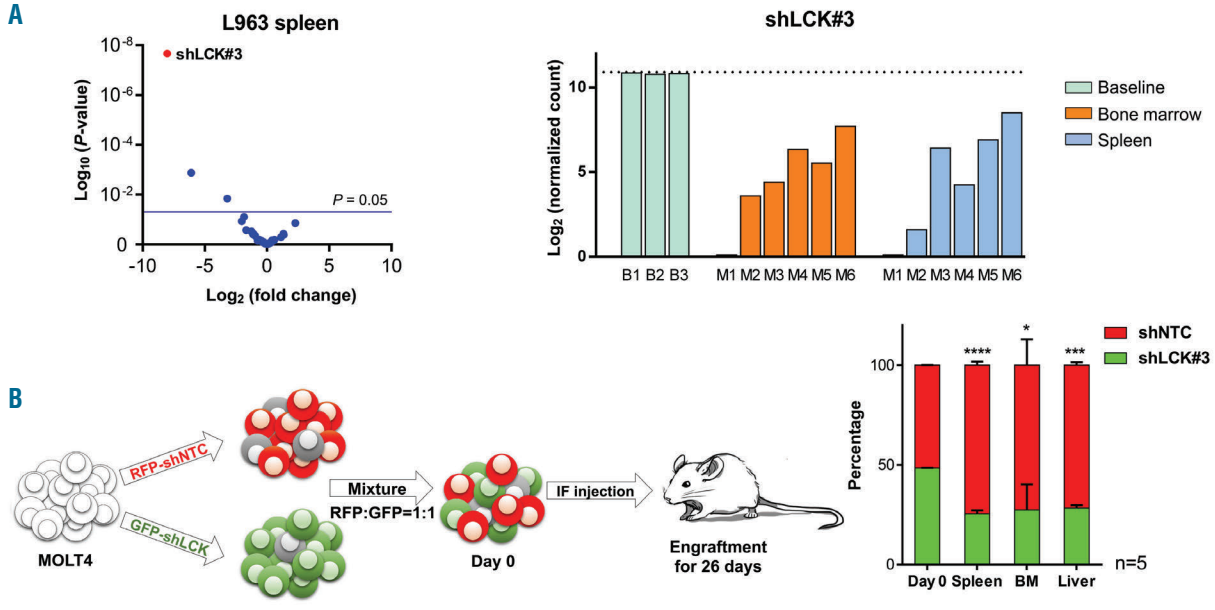


Figure 3. Loss of lymphocyte cell-specific kinase (LCK) negatively effects propagation potential of the T-cell acute lymphoblastic leukemia (T-ALL) cell line MOLT4 and patient-derived xenograft (PDX) L963 *in vivo*. (A) Volcano plot derived from the functional *in vivo* screen representing the magnitude of the fold change (log_2) in shRNA abundance derived from leukemia cells isolated from the spleen of PDX L963 on the x-axis. Each dot represents an individual shRNA construct. The y-axis represents the significance in enrichment or depletion of shRNA constructs (log_{10} scale). Three dots (shLCK#3, shRPL9#1 and shCD19#2) above the blue line are significantly depleted ($P<0.05$). Bar plot of the normalized shLCK#3 sequencing reads (log_2) in leukemic cells derived from the bone marrow (orange) or spleen (blue) of six individual mice (M1-6), relative to the frequency of these reads before transplantation (green, base line B1-3). (B) Schematic representation of the *in vivo* competitive outgrowth assay. MOLT4 cells were lentivirally transduced with shNTC (red fluorescent protein, RFP) or shLCK#3 (GFP) and intrafemorally injected into five NSG mice in a 1:1 ratio. Mice were culled once symptomatic and the ratio of RFP : GFP positive human leukemic cells in spleen (n=5), bone marrow (n=3) or liver (n=3) determined by flow cytometry. In all mice, the MOLT4 cells carrying shLCK#3 were outcompeted by shNTC cells during engraftment in spleen, marrow and liver. Student's *t*-test: *$P<0.05$, ***$P<0.005$, ****$P<0.001$.

arrest was observed, corroborating our earlier findings (*Online Supplementary Figure S4C and D*).

Knockdown of *LCK* was analyzed for early apoptosis induction in CUTLL1, MOLT4, SUPT1 and Jurkat. Although a clear increase in Annexin V staining was observed in MOLT4, suggesting *LCK* knockdown led to apoptosis, this was not observed in CUTLL1, Jurkat or SUPT1 (*Online Supplementary Figure S4E*). This suggests that cell cycle arrest, rather than apoptosis induction, is the predominant effect leading to diminished cell expansion *in vitro* and reduced propagation *in vivo* after LCK knockdown.

Tyrosine kinase inhibitor dasatinib blocks lymphocyte cell-specific kinase function and leads to cell cycle arrest while lymphocyte cell-specific kinase activation levels predict response to its inhibition

The tyrosine kinase inhibitor DAS is a dual SRC/ABL inhibitor known to effectively inhibit LCK.[21] The effect of DAS on LCK protein expression and activation status was assessed by western blot, after demonstrating near universal LCK activation as evidenced by tyrosine residue 416 phosphorylation in cell lines (*Online Supplementary Figure S1G*). We confirmed that DAS effectively abolished activated p-Y416^{SRC} in all four T-ALL cell lines tested, whilst slightly decreasing total LCK protein levels. Furthermore, dephosphorylation of inhibitory p-Y505^{LCK} was noted, as well as a decrease in p-Y783$^{PLC\gamma1}$ and p-Y493^{ZAP70}, two downstream targets of LCK (Figure 5A and *Online Supplementary Figure S5A*). As knockdown of LCK leads to cell cycle arrest, we performed cell cycle analyses after administration of DAS. Cell cycle arrest was observed in all six T-ALL cell lines tested, with a significant increase in G_0/G_1 and decrease in S phase (Figure 5A and *Online Supplementary Figure S5B*). In parallel, PDX cells supported by *in vitro* co-culture with OP9-DL1 were exposed to DAS. In line with our cell line data, DAS abolished activated p-Y416^{SRC} levels in all six PDX samples (Figure 5B and *Online Supplementary Figure S5C*) and cell cycle arrest was observed in all three PDX samples tested (Figure 5B and *Online Supplementary Figure S5D*).

The *in vitro* sensitivity of a panel of nine T-ALL cell lines to DAS was determined. The IC_{50} observed ranged from 5 nM (HSB2) to 15 μM (MOLT16) (Figure 5C). The cell line HSB2 not only demonstrated the highest sensitivity to DAS but also the highest p-Y416^{SRC} activation level as determined by Phosflow. This observation can be explained by the presence of a t(1;7)(p34;q34) translocation leading to LCK activation by TCRβ enhancer elements in HSB2. We thus hypothesized that the level of activated LCK might represent a biomarker for DAS responsiveness. Phosflow was used to quantify and calculate the ratio between p-Y416^{SRC} and total LCK. A strong and significant correlation was observed between the IC_{50} for DAS and the ratio of activated Y416^{SRC} in T-ALL cell lines (R_2=0.778, P=0.004) (Figure 5C). The sensitivity of PDX cells to DAS ranged from GI_{50} of 23.8 nM to 19.7 μM (median of 1.2 μM). However, in this setting, no significant correlation between the GI_{50} and p-Y416^{SRC}/LCK ratio was identified, suggesting that DAS sensitivity of patient-derived cells is dependent on additional factors (*Online Supplementary Figure S5E*).

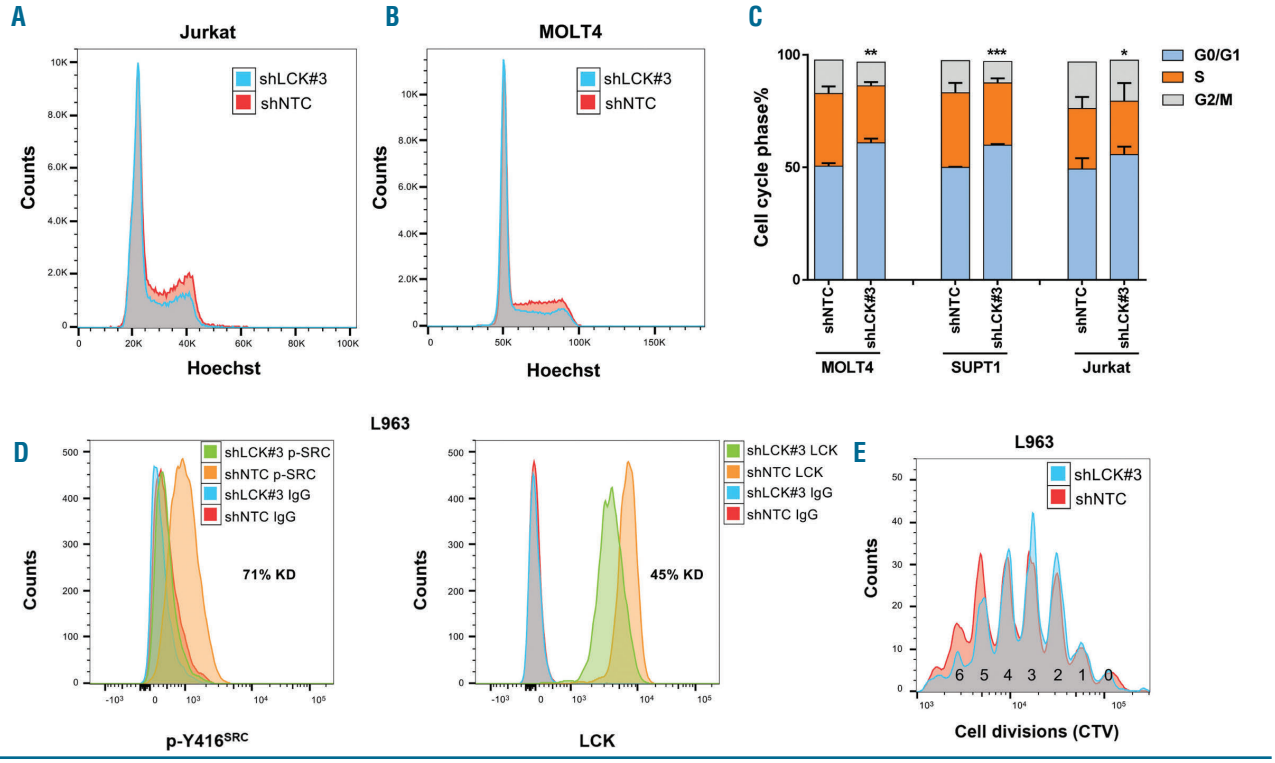


Figure 4. Lymphocyte cell-specific kinase (LCK) knockdown leads to cell cycle arrest in T-cell acute lymphoblastic leukemia (T-ALL) cell lines and patient-derived xenograft (PDX) cells. (A-C) Cell cycle status was determined by flow cytometry using Hoechst 33342 in cell lines Jurkat (A and C), MOLT4 (B and C), and SUPT1 (C) 7 days after transduction with shLCK#3 or shNTC expression vectors. (D) PDX L963 cells were lentivirally transduced with shLCK#3 or shNTC expression constructs. Phosflow analysis of total LCK and p-Y416^{SRC} was performed 8 days later. (E) shLCK#3 and shNTC transduced PDX L963 cells were loaded with CTV and cultured for 13 days. Flow cytometric analysis of CTV incorporation (cell divisions) was performed and demonstrated progressive reduction in cell number after 4-6 cell divisions after LCK knockdown relative to control knockdown. Student's *t*-test: **P*<0.05, ***P*<0.01, ****P*<0.005.

Dasatinib re-sensitizes dexamethasone resistance in T-cell acute lymphoblastic leukemia cell lines and patient-derived xenograft samples

DAS leads to complete inhibition of p-Y416^{SRC} and cell cycle arrest in T-ALL cell lines and PDX cells, suggesting that DAS treatment of T-ALL has a cytostatic effect. In clinical practice, effective eradication of T-ALL relies on the application of combinatorial treatment. LCK inhibition has previously been shown to sensitize chronic lymphoid leukemia (CLL) to DEX and induce cell death.[23] We thus went on to investigate potential synergy between LCK inhibition and DEX, as DEX is universally used for treatment of ALL. The cell viability of SUPT1 and CUTLL1, in the presence of DEX, was evaluated after knockdown of LCK. Whereas the cell viability of mock transduced and non-targeting control cells was minimally affected by DEX treatment, LCK knockdown increased DEX sensitivity suggesting that LCK protein and/or activity levels play a crucial role in GC resistance (Figure 6A and *Online Supplementary Figure S6A*).

A more detailed analysis of the potency of the combination of DEX and LCK inhibition was examined by using DAS instead of the LCK knockdown. DEX (0-600 nM) and DAS (0-50 μM) were titrated along a dose matrix and cell viability was determined. Synergy for individual drug combinations was determined using Combenefit.[22] The matrix revealed drug synergy at concentrations which are clinically achieved, i.e., 100 nM for DEX and 264 nM for DAS (Figure 6B and *Online Supplementary Figure S6B*).[24,25] Bioinformatic analysis of all ten T-ALL cell lines revealed a statistically significant enrichment of drug synergy at clinically relevant concentrations. This synergy was observed at 8-110 nM of DEX and 0.223-4.5 μM of DAS (*Online Supplementary Figure S6C and D*).

Subsequently, PDX cells were expanded *ex vivo* for 1 week and exposed to the same drug combinations in dose matrices. These assays verified the synergistic action of DEX+DAS in a wide range of PDX cells, whilst confirming that increased DAS concentrations and resultant LCK inhibition augmented the response to DEX (Figure 6C and *Online Supplementary Figure S6E*). Combined analysis of all drug matrices with PDX cells again revealed a statistically significant enrichment of drug synergy at clinically relevant concentrations (*Online Supplementary Figure S6F*). Moreover, the combination of DEX+DAS induced more cell death compared with control vehicle or single drugs as revealed by Annexin V/PI staining (Figure 6C).

DEX has a wide range of actions, including genomic and non-genomic effects. Genomic effects are the result of nuclear translocation of the GC receptor and subsequent transactivation or repression of genes containing a GC response element (GRE), as exemplified by the Glucocorticoid-Induced Leucine Zipper (GILZ) gene. Accordingly, we observed strong induction of *GILZ* gene expression after DEX exposure in the T-ALL cell line Jurkat and five PDX samples tested (Figure 6D and *Online Supplementary Figure S6G*). This response was significantly enhanced when combining DEX with knockdown of *LCK* (Figure 6D) or DEX+DAS in a range of T-ALL cell lines and PDX samples, suggesting that LCK inactivation augments DEX-induced gene transcription and reverses DEX resistance (Figure 6D and *Online Supplementary Figure S6G*).

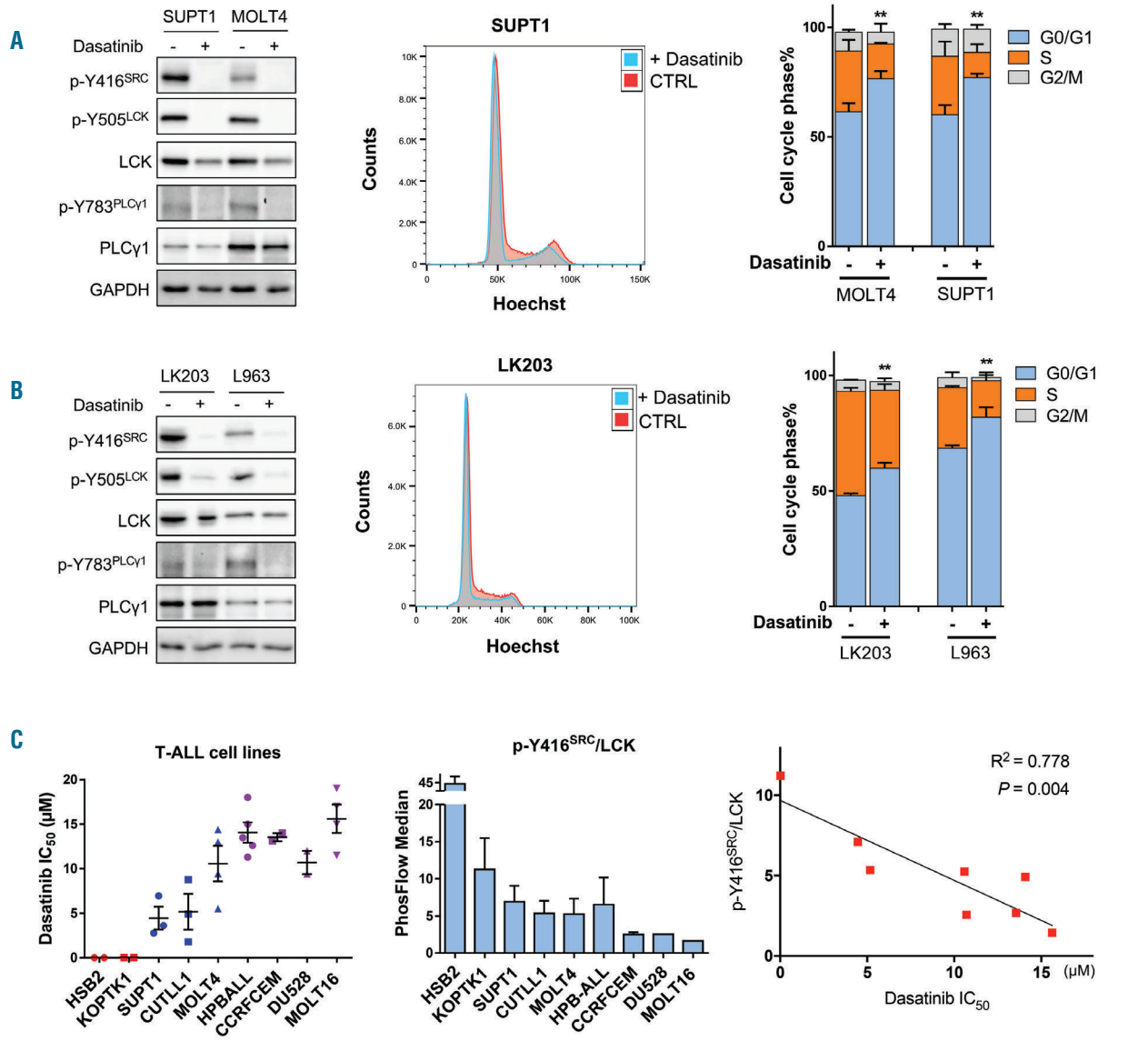


Figure 5. Dasatinib (DAS) inhibits lymphocyte cell-specific kinase (LCK) and leads to cell cycle arrest. (A) SUPT1 and MOLT4 cells were treated with vehicle control or DAS (2 μM) for 24 hours (h) and expression of total LCK, activated p-Y416^{SRC}, total PLCγ1 and activated p-Y783^{PLCγ1} was assessed in western blot analysis (left) or cells were stained with Hoechst and analyzed for cell cycle status (middle and right). (B) Patient-derived xenograft (PDX) LK203 and L963 cells were treated for 24 h with 1 μM of DAS. LCK and PLCγ1 total protein and activating phospho-sites at Y416 and Y783 were assessed in western blot analyses or PDX were stained with Hoechst and analyzed for cell cycle status. (C) The *in vitro* sensitivity of a panel of T-ALL cell lines to DAS was investigated and IC_{50} calculated. Phosflow was used to determine the ratio of activated p-Y416^{SRC}/total LCK. This ratio was correlated with *in vitro* sensitivity to DAS (R^2=0.778, *P*=0.004). Student's *t*-test: ***P*<0.01. NB HSB2 was excluded from this analysis, as the extreme sensitivity to DAS was caused by the presence of a unique translocation absent in all other sensitive cell lines.

Phase II-like trial *in vivo* demonstrates significant reduction in leukemia burden after combination treatment with dexamethasone and dasatinib

To test the efficacy of DEX and DAS *in vivo*, we conducted a phase II-like trial in mice (Figure 7A).[26] Ten PDXs were engrafted in four mice each. The four mice derived from one single patient sample were randomly assigned to treatment arms, namely control vehicle, DEX (1 mg/kg), DAS (35 mg/kg) or DEX+DAS (1 mg/kg DEX + 35 mg/kg DAS). After IF injection, mice tail vein blood was monitored weekly for human CD7/CD45 and murine CD45 expression to monitor peripheral blood engraftment. Representative PDX L809 commenced treatment 46 days after injection for a total duration of 3 weeks; the four mice were culled 72 days after injection (Figure 7B). L809 cells engrafted in the spleens of the four mice showed greatly reduced levels of total LCK and dephosphorylation of LCK (p-Y416^{SRC} and p-Y505^{LCK}) after DAS or DEX+DAS combination treatment (Figure 7C). Western blot analysis of positively selected viable human cells again demonstrated decreased protein expression of LCK and p-Y416^{SRC} after DAS treatment. The number of residual viable human cells after effective DEX+DAS treatment was not sufficient to categorically confirm reduced protein expression (*Online Supplementary Figure S7F*). One mouse in the DAS arm (LK080) developed uterine prolapse before dosing commenced and the mice derived from PDX LK214 succumbed during the first week of treatment. These five were excluded from the final analysis. Combining the results of 35 mice derived from nine patient samples, DEX+DAS treatment significantly impaired leukemia progression more than single drug DEX, DAS or control vehi-

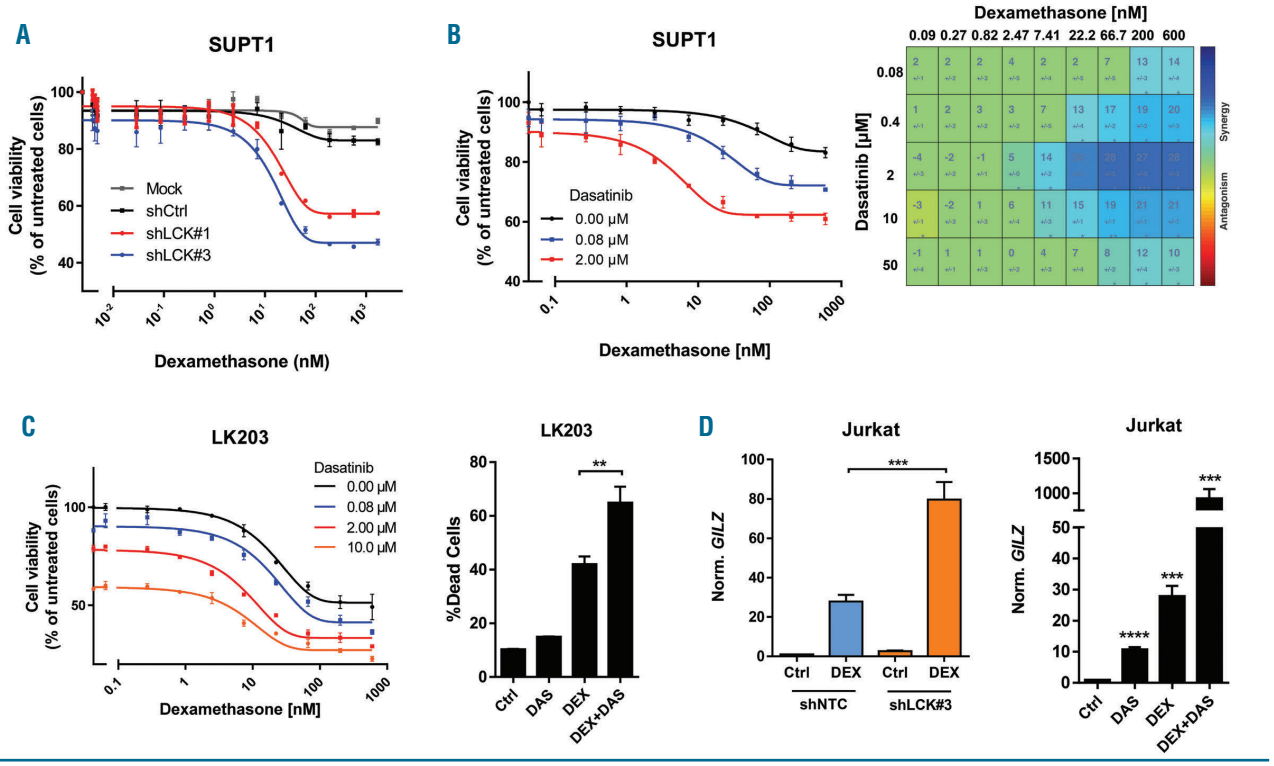


Figure 6. Dexamethasone (DEX) and dasatinib (DAS) act synergistically to induce cell death in T-cell acute lymphoblastic leukemia (T-ALL). (A) Cell viability of parental SUPT1 cells (mock), shCtrl (NTC), shLCK#1 or shLCK#3 transduced SUPT1 cells upon treatment with increasing DEX concentrations (0-1699 nM). (B) Cell viability of SUPT1 with and without DAS (left; black line, no DAS; blue line, 0.8 µM; red line, 2.0 µM) in combination with increasing concentrations of DEX (0-600 nM) as derived from the drug matrix with titration of DEX (0-600 nM) and DAS (0 - 50 uM; right). (Right) Combenefit analysis of drug matrix demonstrates drug synergy in SUPT1 cells at clinically relevant drug concentrations. (C) (Left) LK203 cells were expanded *ex vivo* on OP9-DL1 feeder cells for 1 week prior to treatment with and without DAS (black line, no DAS; blue line, 0.08 µM; red line, 2.0 µM; orange line, 10 µM) in combination with increasing concentrations of DEX (0-600 nM) as derived from a drug matrix with DEX (0-600 nM) and DAS (0 - 50 uM) (*Online Supplementary Figure S6E*). (Right) Cell death analysis in LK203 cells exposed to control (Ctrl) conditions, DAS (1 µM), DEX (100 nM) or DAS+DEX combination treatment. (D) (Left) Normalized *GILZ* mRNA expression in Jurkat cells after transduction with shNTC or shLCK#3 with or without DEX exposure (100 nM). (Right) Normalized *GILZ* mRNA expression in Jurkat cells after exposure to Ctrl conditions, DAS (2 µM), DEX (100 nM) or DAS+DEX combination treatment at the same concentrations. Student's *t*-test: ***P*<0.01, ****P*<0.005, *****P*<0.001.

cle as measured by hCD45 or hCD7 engraftment in peripheral blood, bone marrow, spleen and CNS (Figure 7D-F and *Online Supplementary Figure S7A*). Single agent DEX reduced CNS leukemia burden in 7 out of 9 samples, reflecting its proven efficacy in reducing CNS relapses,[27] whilst DAS showed some reduction in CNS burden in 4 out of 8 samples (*Online Supplementary Figure S7B*). Combination therapy was particularly effective, with complete eradication of measurable CNS leukemia in five patient samples and evidence of an additive effect with DEX in 3 out of 4 of the remaining patient samples (*Online Supplementary Figure S7B*). When considering the cohort of nine patient samples overall, combination treatment significantly reduced leukemic infiltrates compared to control (P=0.02). Representative histology images are shown in Figure 7G. Spleen weight was substantially reduced in mice receiving combination treatment, compared with the single or control treatment arms (*Online Supplementary Figure S7C and D*). DEX+DAS also significantly reduced hCD45$^+$ or hCD7$^+$ leukemia cell engraftment in liver tissue of all six PDX samples analyzed (*Online Supplementary Figure S7E*). The initial therapeutic advantage of DEX+DAS in mice derived from PDX LK080 was lost at the end of the experiment, most likely because these mice were kept alive for 3 weeks after completion of treatment. In the case of L907, however, the benefit of combination treatment was not observed until the last time point (*Online Supplementary Figure S7G*).

Discussion

Using a phase II-like murine trial, we demonstrate here the efficacy of the drug combination DEX+DAS in impairing expansion of human T-ALL samples. This effect is apparent in an unselected, biologically heterogeneous, cohort of PDX samples. This trial format recapitulates early phase human clinical trials and indicates that this drug combination could be widely applicable in the treatment of T-ALL. Studies by Serafin *et al.* first proposed a role for this drug combination.[28] Our murine trial extends these initial observations with an extensive cohort consisting of nine different PDX demonstrating treatment advantage for both DEX sensitive and resistant T-ALL.

Significant superiority of DEX+DAS was demonstrated even after exclusion of mice who reached their clinical end points prematurely. These untoward events highlight the practicalities of performing murine trials.

We propose that the impaired *in vivo* expansion results from a combination of cell cycle arrest as well as cell death. Several mechanisms could provide plausible explanations for the occurrence of cell cycle arrest. DAS is a protein tyrosine kinase inhibitor which targets Abl and SFK family members. We have confirmed that DAS effectively inhibits activity of the SFK member LCK by preventing phosphorylation, leading to G_0/G_1 arrest. DAS has previously been shown to inhibit cyclin dependent kinase 1 (CDK1), which plays a central role in G1/S and G2/M

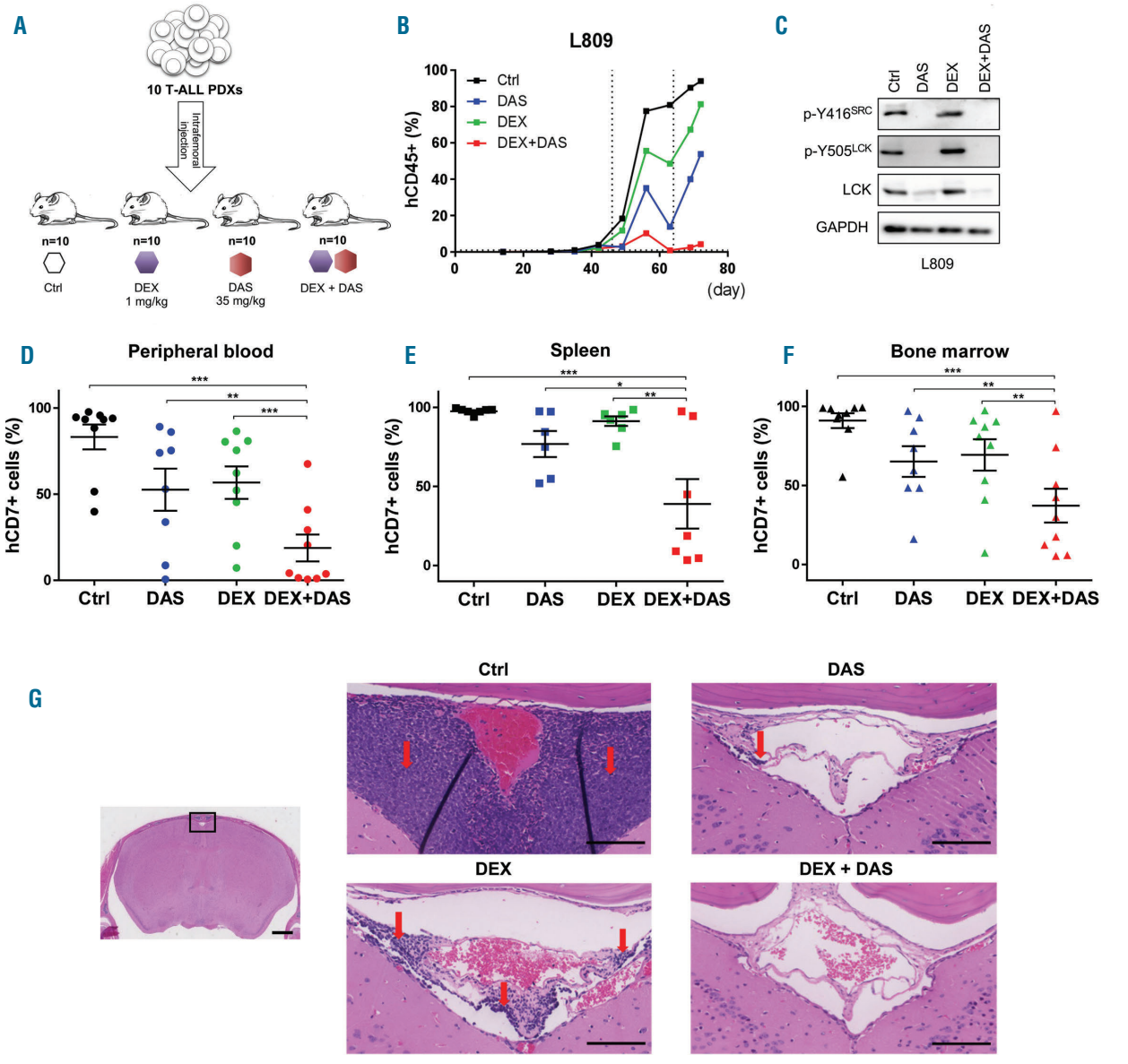


Figure 7. Dexamethasone (DEX) + dasatinib (DAS) synergize to impair leukemia engraftment in a Phase II-like murine trial. (A) Layout of the *in vivo* trial using ten different patient-derived xenograft (PDX) samples. PDX samples were engrafted into four mice each and treated with control vehicle (Ctrl), DEX (1 mg/kg), DAS (35 mg/kg) or DEX+DAS (1 mg/kg DEX + 35 mg/kg DAS). Mice were dosed once daily, 5 times per week, for 2-3 weeks depending on clinical status of the mice. (B) Engraftment of hCD45$^+$ cells (%) was determined weekly in peripheral blood derived from four mice injected with PDX L809. Engraftment levels are shown starting from day of injection (day 0) in mice receiving control vehicle (Ctrl, black), DAS (blue), DEX (green), or DEX+DAS (red). Vertical dotted lines indicate the treatment window (3 weeks) starting on day 46 and completing on day 64. Mice were culled on day 72 and analyzed for hCD45/hCD7 engraftment. (C) Western blotting of total and phosphorylated lymphocyte cell-specific kinase (LCK) protein levels of whole cell lysates derived from the spleens of four mice injected with PDX L809 under four different treatment arms (Ctrl, DAS, DEX or DEX+DAS) relative to the housekeeper GAPDH. (D-F) Summary of final human CD7$^+$ engraftment (%) in peripheral blood (D), spleen (E), and bone marrow (F) of mice treated with Ctrl (black), DAS (blue), DEX (green), or DEX+DAS (red). *P<0.05, **P<0.01, ***P<0.001. (G) Photomicrographs of whole brain-skull sections stained with Hematoxylin & Eosin from PDX L809. (Left) Low power scout view of whole brain with area shown in all other images marked by black box. (Centre and right) High power view (x20 objective) of meninges around the central venous sinus in mice receiving Ctrl, DAS, DEX or DEX+DAS treatment. Red arrows mark the leukemic infiltrate. Scale bar marks 1 mm on scout view and 100 μm on high power images.

transition.[29] Furthermore, G1 cell cycle arrest, through upregulation of the cyclin-dependent kinase inhibitors p21CIP1 (CDKN1A) and p27KIP1 (CDKN1B), has been observed after DAS treatment in acute myeloid leukemia.[30] We propose that LCK is the predominant target of DAS in this disease setting, as our shRNA screen identified a critical role for LCK in cell proliferation in cell lines and PDX samples. Moreover, LCK is the proposed DAS target when blocking T-cell activation.[21] Competitive assays confirmed defective proliferation of T-ALL cells after LCK knockdown *in vitro* and *in vivo*. We have shown that LCK knockdown leads to G_0/G_1 cell cycle arrest in cell lines and PDX. This effect was more pronounced using DAS, a finding which could potentially be explained by incomplete knockdown of LCK or the wide spectrum of kinases targeted by DAS.

As reported earlier and confirmed in our studies, DAS is cytotoxic to a small subset of T-ALL samples with IC_{50} values in the low nanomolar range.[31] These observations were made in T-ALL samples without kinase activating mutations, which are seen very infrequently in T-ALL. To the best of our knowledge, our cohort includes only one

PDX with such an activating genetic lesion (LK287, *FIP1L1-PDGFRA*). Cytotoxicity to DAS is significantly increased upon combination with DEX. Our data indicate drug synergy between DAS and DEX at clinically relevant concentrations. A previous, mostly *in vitro*, study advocated the use of DEX+DAS in GC resistant T-ALL.[28] Our extended studies indicate DEX+DAS act synergistically in the majority of cell lines and PDX tested independent of their prior sensitivity to DEX. The potential of DEX+DAS to revert GC resistance is an exciting observation. GC resistance is frequently observed in relapsed/refractory T-ALL,[4] and DEX+DAS provide a clinically actionable approach to re-sensitize T-ALL resistant to DEX.

The implementation of DAS into clinical management would benefit from the identification of a reliable response biomarker. Although LCK activation status (ratio p-Y416^{SRC}/LCK) strongly correlates with DAS sensitivity in cell lines, we were unable to corroborate this observation in PDX cells. Sample size and intricacies of *in vitro* assays using PDX cells could provide possible explanations for these inconsistencies. Nevertheless, *in vivo* drug synergy was observed in the majority of samples tested. Of interest, drug response profiling of T-ALL samples suggested SRC pathway activation may represent a response biomarker.[31]

The mechanism underlying the observed drug synergy remains to be fully elucidated. T-cell activation can be blocked by using clinically relevant concentrations of the tyrosine kinase inhibitor DAS, which binds to the ATP-binding pocket of LCK thereby preventing the phosphorylation of the activating loop of the kinase domain p-Y416^{SRC}.[21,32] When DEX is combined with DAS, physiological CD3^{+} T-cell proliferation is reduced in an additive way.[33,34] Furthermore, it has been previously suggested that the Calcineurin/NFAT/IL-4 axis is activated in patients exhibiting a prednisone poor response.[28] We have shown here that combination of DEX+DAS significantly increases *GILZ* gene expression, reflecting increased transcriptional activity of the GC receptor. We thus hypothesize that inhibition of LCK disrupts the TCR-GR complex and established crosstalk between the TCR and GR pathways leading to dissociation and transcriptional activation of the GR.[13]

To conclude, drug resistant T-ALL continues to represent an unmet clinical need. We provide further support for the inclusion of DAS in the treatment of T-ALL. It has been reported that DAS in combination with conventional chemotherapy is safe and well tolerated in children and young adults, although hematologic toxicity was significant.[35] Thus, the DEX+DAS combination should be considered in the early phase setting to evaluate toxicity and efficacy in patients with GC resistant disease with or without cerebral spinal fluid involvement.

Disclosures

No conflicts of interest to disclose.

Contributions

FWvD, AKH and YS designed the research; YS performed the research; YS, MCB, HJB, OH and RT designed and performed the in vivo experiments; FWvD, AKH and YS analyzed the data and wrote the paper; SN and AE performed the bioinformatics analysis; CH performed brain histology and imaging; JV, OH and CH reviewed the manuscript.

Acknowledgments

The authors would like to thank patients, parents, and hospital staff at the Great North Children's Hospital, Newcastle upon Tyne, UK, for their valuable collaboration. The authors would like to thank Lynn Stevenson and Clare Orange, University of Glasgow, for brain histology and imaging. The brain histology slides were scanned by Glasgow University slide scanning and image analysis service at the Queen Elizabeth University Hospital, Glasgow. CH was funded by the Chief Scientist Office (ETM/374).

Funding

This work was supported by a Newcastle University Research Fellowship (to FWvD), Chinese Scholarship Council (CSC) (to YS), JGW Patterson Foundation (to MCB), North of England Children's Cancer Research, Action Medical Research (to FWvD).

References

1. Marks DI, Paietta EM, Moorman AV, et al. T-cell acute lymphoblastic leukemia in adults: clinical features, immunophenotype, cytogenetics, and outcome from the large randomized prospective trial (UKALL XII/ECOG 2993). Blood. 2009;114(25):5136-5145.
2. Patrick K, Wade R, Goulden N, et al. Outcome for children and young people with early T-cell precursor acute lymphoblastic leukaemia treated on a contemporary protocol, UKALL 2003. Br J Haematol. 2014;166(3):421-424.
3. Goldberg JM, Silverman LB, Levy DE, et al. Childhood T-cell acute lymphoblastic leukemia: the Dana-Farber Cancer Institute acute lymphoblastic leukemia consortium experience. J Clin Oncol. 2003;21(19):3616-3622.
4. Raetz EA, Borowitz MJ, Devidas M, et al. Reinduction platform for children with first marrow relapse of acute lymphoblastic leukemia: a Children's Oncology Group study[corrected]. J Clin Oncol. 2008;26(24):3971-3978.
5. Inaba H, Pui CH. Glucocorticoid use in acute lymphoblastic leukaemia. Lancet Oncol. 2010;11(11):1096-1106.
6. Pui CH, Carroll WL, Meshinchi S, Arceci RJ. Biology, risk stratification, and therapy of pediatric acute leukemias: an update. J Clin Oncol. 2011;29(5):551-565.
7. Pui CH, Mullighan CG, Evans WE, Relling MV. Pediatric acute lymphoblastic leukemia: where are we going and how do we get there? Blood. 2012;120(6):1165-1174.
8. Dordelmann M, Reiter A, Borkhardt A, et al. Prednisone response is the strongest predictor of treatment outcome in infant acute lymphoblastic leukemia. Blood. 1999;94(4):1209-1217.
9. Hongo T, Yajima S, Sakurai M, Horikoshi Y, Hanada R. In vitro drug sensitivity testing can predict induction failure and early relapse of childhood acute lymphoblastic leukemia. Blood. 1997;89(8):2959-2965.
10. Kaspers GJ, Wijnands JJ, Hartmann R, et al. Immunophenotypic cell lineage and in vitro cellular drug resistance in childhood relapsed acute lymphoblastic leukaemia. Eur J Cancer. 2005;41(9):1300-1303.
11. Klumper E, Pieters R, Veerman AJ, et al. In vitro cellular drug resistance in children with relapsed/refractory acute lymphoblastic leukemia. Blood. 1995;86(10):3861-3868.
12. Pieters R, den Boer ML, Durian M, et al. Relation between age, immunophenotype and in vitro drug resistance in 395 children with acute lymphoblastic leukemia-implications for treatment of infants. Leukemia. 1998;12(9):1344-1348.
13. Jamieson CA, Yamamoto KR. Crosstalk pathway for inhibition of glucocorticoid-induced apoptosis by T cell receptor signaling. Proc Natl Acad Sci U S A. 2000;97(13):7319-7324.
14. Ashwell JD, King LB, Vacchio MS. Crosstalk between the T cell antigen receptor and the glucocorticoid receptor regulates thymocyte development. Stem Cells. 1996;14(5):490-500.
15. Cui Y, Onozawa M, Garber HR, et al. Thymic expression of a T-cell receptor targeting a tumor-associated antigen coexpressed in the thymus induces T-ALL.

Blood. 2015;125(19):2958-2967.
16. Serwold T, Hochedlinger K, Swindle J, Hedgpeth J, Jaenisch R, Weissman IL. T-cell receptor-driven lymphomagenesis in mice derived from a reprogrammed T cell. Proc Natl Acad Sci U S A. 2010;107(44):18939-18943.
17. Palacios EH, Weiss A. Function of the Src-family kinases, Lck and Fyn, in T-cell development and activation. Oncogene. 2004;23(48):7990-8000.
18. Iwashima M, Irving BA, van Oers NS, Chan AC, Weiss A. Sequential interactions of the TCR with two distinct cytoplasmic tyrosine kinases. Science. 1994;263(5150):1136-1139.
19. van Oers NS, Killeen N, Weiss A. Lck regulates the tyrosine phosphorylation of the T cell receptor subunits and ZAP-70 in murine thymocytes. J Exp Med. 1996;183(3):1053-1062.
20. Nyakeriga AM, Garg H, Joshi A. TCR-induced T cell activation leads to simultaneous phosphorylation at Y505 and Y394 of p56(lck) residues. Cytometry A. 2012;81(9):797-805.
21. Lee KC, Ouwehand I, Giannini AL, Thomas NS, Dibb NJ, Bijlmakers MJ. Lck is a key target of imatinib and dasatinib in T-cell activation. Leukemia. 2010;24(4):896-900.
22. Di Veroli GY, Fornari C, Wang D, et al. Combenefit: an interactive platform for the analysis and visualization of drug combinations. Bioinformatics. 2016;32(18):2866-2868.
23. Harr MW, Caimi PF, McColl KS, et al. Inhibition of Lck enhances glucocorticoid sensitivity and apoptosis in lymphoid cell lines and in chronic lymphocytic leukemia. Cell Death Differ. 2010;17(9):1381-1391.
24. Liston DR, Davis M. Clinically relevant concentrations of anticancer drugs: a guide for nonclinical studies. Clin Cancer Res. 2017;23(14):3489-3498.
25. Yang L, Panetta JC, Cai X, et al. Asparaginase may influence dexamethasone pharmacokinetics in acute lymphoblastic leukemia. J Clin Oncol. 2008;26(12):1932-1939.
26. Townsend EC, Murakami MA, Christodoulou A, et al. The Public Repository of Xenografts enables discovery and randomized Phase II-like trials in mice. Cancer Cell. 2016;30(1):183.
27. Mitchell CD, Richards SM, Kinsey SE, Lilleyman J, Vora A, Eden TO; Medical Research Council Childhood Leukaemia Working P. Benefit of dexamethasone compared with prednisolone for childhood acute lymphoblastic leukaemia: results of the UK Medical Research Council ALL97 randomized trial. Br J Haematol. 2005;129(6):734-745.
28. Serafin V, Capuzzo G, Milani G, et al. Glucocorticoid resistance is reverted by LCK inhibition in pediatric T-cell acute lymphoblastic leukemia. Blood. 2017;130(25):2750-2761.
29. Kruewel T, Schenone S, Radi M, et al. Molecular characterization of c-Abl/c-Src kinase inhibitors targeted against murine tumour progenitor cells that express stem cell markers. PLoS One. 2010;5(11):e14143.
30. Guerrouahen BS, Futami M, Vaklavas C, et al. Dasatinib inhibits the growth of molecularly heterogeneous myeloid leukemias. Clin Cancer Res. 2010;16(4):1149-1158.
31. Frismantas V, Dobay MP, Rinaldi A, et al. Ex vivo drug response profiling detects recurrent sensitivity patterns in drug-resistant acute lymphoblastic leukemia. Blood. 2017;129(11):e26-e37.
32. Schade AE, Schieven GL, Townsend R, et al. Dasatinib, a small-molecule protein tyrosine kinase inhibitor, inhibits T-cell activation and proliferation. Blood. 2008;111(3):1366-1377.
33. Nerreter T, Distler E, Kochel C, Einsele H, Herr W, Seggewiss-Bernhardt R. Combining dasatinib with dexamethasone long-term leads to maintenance of antiviral and antileukemia specific cytotoxic T cell responses in vitro. Exp Hematol. 2013;41(7):604-614.e4.
34. Smith LK, Cidlowski JA. Glucocorticoid-induced apoptosis of healthy and malignant lymphocytes. Prog Brain Res. 2010;182:1-30.
35. Slayton WB, Schultz KR, Kairalla JA, et al. Dasatinib plus intensive chemotherapy in children, adolescents, and young adults with Philadelphia chromosome-positive acute lymphoblastic leukemia: results of Children's Oncology Group trial AALL0622. J Clin Oncol. 2018;36(22):2306-2314.

ARTICLE

Combinatorial efficacy of entospletinib and chemotherapy in patient-derived xenograft models of infant acute lymphoblastic leukemia

Joseph P. Loftus,[1*] Anella Yahiaoui,[2*] Patrick A Brown,[3] Lisa M. Niswander,[1] Asen Bagashev,[1] Min Wang,[2] Allyson Shauf,[2] Stacey Tannheimer[2] and Sarah K. Tasian[1,4]

[1]Division of Oncology and Center for Childhood Cancer Research, Children's Hospital of Philadelphia, Philadelphia, PA; [2]Gilead Sciences, Foster City, CA; [3]Department of Pediatrics, Division of Pediatric Hematology/Oncology, Johns Hopkins University and Sidney Kimmel Comprehensive Cancer Center, Baltimore, MD and [4]Department of Pediatrics and Abramson Cancer Center, University of Pennsylvania Perelman School of Medicine, Philadelphia, PA, USA

**JPL and AY contributed equally as co-first authors.*

Ferrata Storti Foundation

Haematologica 2021
Volume 106(4):1067-1078

ABSTRACT

Survival of infants with *KMT2A*-rearranged acute lymphoblastic leukemia (ALL) remains dismal despite intensive chemotherapy. We observed constitutive phosphorylation of spleen tyrosine kinase (SYK) and associated signaling proteins in infant ALL patient-derived xenograft (PDX) model specimens and hypothesized that the SYK inhibitor entospletinib would inhibit signaling and cell growth *in vitro* and leukemia proliferation *in vivo*. We further predicted that combined entospletinib and chemotherapy could augment anti-leukemia effects. Basal kinase signaling activation and *HOXA9/MEIS1* expression differed among *KMT2A*-rearranged (*KMT2A-AFF1* [n=4], *KMT2A-MLLT3* [n=1], *KMT2A-MLLT1* [n=4]) and non-*KMT2A*-rearranged [n=3] ALL specimens and stratified by genetic subgroup. Incubation of *KMT2A*-rearranged ALL cells *in vitro* with entospletinib inhibited methylcellulose colony formation and SYK pathway signaling in a dose-dependent manner. *In vivo* inhibition of leukemia proliferation with entospletinib monotherapy was observed in RAS-wild-type *KMT2A-AFF1, KMT2A-MLLT3*, and *KMT2A-MLLT1* ALL PDX models with enhanced activity in combination with vincristine chemotherapy in several models. Surprisingly, entospletinib did not decrease leukemia burden in two *KMT2A-AFF1* PDX models with *NRAS* or *KRAS* mutations, suggesting potential RAS-mediated resistance to SYK inhibition. As hypothesized, superior inhibition of ALL proliferation was observed in *KMT2A-AFF1* PDX models treated with entospletinib and the MEK inhibitor selumetinib *versus* vehicle or inhibitor monotherapies ($P<0.05$). In summary, constitutive activation of SYK and associated signaling occurs in *KMT2A*-rearranged ALL with *in vitro* and *in vivo* sensitivity to entospletinib. Combination therapy with vincristine or selumetinib further enhanced treatment effects of SYK inhibition. Clinical study of entospletinib and chemotherapy or other kinase inhibitors in patients with *KMT2A*-rearranged leukemias may be warranted.

Introduction

B-cell acute lymphoblastic leukemia (B-ALL) is the most common childhood cancer and is characterized by recurrent somatic cytogenetic and molecular abnormalities. While modern risk-adapted chemotherapy regimens for children and adolescents/young adults (AYA) have achieved overall survival rates exceeding 90%,[1,2] optimal salvage therapy for the 10-15% of children and >60% of adults with B-ALL who relapse remains a major unmet medical need.[3-5]

Patients with B-ALL harboring rearrangements in lysine-specific methyltrans-

Correspondence:
SARAH K. TASIAN
tasians@chop.edu

Received: October 28, 2019.
Accepted: May 8, 2020.
Pre-published: May 15, 2020.

https://doi.org/10.3324/haematol.2019.241729

©2021 Ferrata Storti Foundation

Material published in Haematologica is covered by copyright. All rights are reserved to the Ferrata Storti Foundation. Use of published material is allowed under the following terms and conditions: https://creativecommons.org/licenses/by-nc/4.0/legalcode. Copies of published material are allowed for personal or internal use. Sharing published material for non-commercial purposes is subject to the following conditions: https://creativecommons.org/licenses/by-nc/4.0/legalcode, sect. 3. Reproducing and sharing published material for commercial purposes is not allowed without permission in writing from the publisher.

ferase 2A (*KMT2A, formerly mixed lineage leukemia* [*MLL*]; located at chromosome 11q23) are at higher risk of relapse and have inferior overall survival.[6-8] *KMT2A* rearrangements occur in approximately 10% of childhood and adult B-ALL cases with highest frequency (75%) in infants diagnosed with leukemia at <365 days old.[8,9] Children with *KMT2A*-rearranged (*KMT2A*-R) ALL have a poor prognosis with 5-year event-free survival (EFS) of 20-50% in infants[9-12] and approximately 58% in older children.[13] Age <6 months at diagnosis, hyperleukocytosis with white blood cell count >300x10^9/L, and poor response to prednisone prophase chemotherapy have been associated with worst clinical outcomes and dismal long-term survival amongst infants with *KMT2A*-R ALL.[10,11] Adults with *KMT2A*-R ALL have similarly poor outcomes with <50% 5-year EFS.[14]

Wild-type *KMT2A* is required for normal hematopoiesis and post-natal hematopoietic cell maintenance.[15] Disruption of *KMT2A* via chromosomal translocation in acute lymphoid and myeloid leukemias was first described nearly three decades ago.[16,17] In ALL, these translocations result in fusion of *KMT2A* to one of >100 currently known translocation partner genes, leading to production of fusion proteins which disrupt normal regulation of gene expression by wild-type *KMT2A*.[18-20] Recruitment of the super elongation complex (SEC) and the H3K79 histone methyltransferase DOT1L by the fusion proteins consequently leads to new fusion-dependent functions of *KMT2A*.[21] While numerous partner genes have been reported, five translocations account for the majority of *KMT2A* rearrangements in ALL across the age spectrum. These include t(4;11)(q21;q23) with *KMT2A-AFF1* fusion (60%), t(11;19)(q23;p13.3) with *KMT2A-MLLT1* fusion (18%), t(9;11)(p21;q23) with *KMT2A-MLLT3* fusion (12%), t(10;11)(p12;q23) with *KMT2A-MLLT10* fusion (3%), and t(6;11)(q27;q23) with *KMT2A-MLLT4* fusion (1%).[8,22-24]

Preclinical studies of murine models and primary patient specimens demonstrate that *KMT2A*-R ALL cells harbor gene expression signatures with distinct arrest in B-cell development at the pro-B and pre-B cell stages. Recent publications have reported a strong link between increased expression of the HOX cluster of transcription factor genes (particularly *HOXA9*) and its co-factor *MEIS1* in accelerating *KMT2A*-R leukemia development via upregulation of spleen tyrosine kinase (SYK),[21,25] as well as constitutive activation of SYK signaling in several B-ALL subtypes.[2,26] There specific mechanisms by which *KMT2A* translocations contribute to SYK signaling in B-ALL and their role in leukemogenesis and maintenance have not been completely characterized.

SYK is expressed in hematopoietic cells and involved in multiple signal transduction pathways downstream of the B-cell receptor (BCR). SYK is autophosphorylated and activated when its two tandem Src homology 2 (SH2) domains bind to immunoreceptor tyrosine based activation motifs (ITAM).[27] This binding then initiates downstream signal transduction via activation of effector molecules, including phospholipase C gamma (PLCγ), B-cell linker protein (BLNK), phosphatidylinositol 3 kinase (PI3K), and mitogen activated protein kinase (MAPK) that converge to activate multiple downstream signaling pathways involved in B-cell malignancies. This makes SYK an attractive potential therapeutic target.[28,29] *In vitro* and *in vivo* activity of SYK inhibition in preclinical B-ALL models has been previously established[26,30,31] and several SYK inhibitors (e.g., entospletinib, fostamatinib) are under evaluation in patients with relapsed/refractory solid tumors, hematologic malignancies, or autoimmune diseases.

Entospletinib (ENTO, formerly GS-9973)[32] is a potent and highly selective SYK inhibitor under current clinical investigation in adults with relapsed acute leukemias (*clinicaltrials.gov identifiers: NCT02343939 and NCT02404220*). Interim analysis of a phase Ib/II study of ENTO and chemotherapy showed complete responses in two patients with relapsed KMT2A-R acute myeloid leukemia (AML) treated with ENTO monotherapy for 14 days, suggesting potential for particular clinical activity in *KMT2A*-rearranged leukemias.[33] Translating the efficacy of SYK inhibition with ENTO and depth of response in combination with standard-of-care chemotherapy agents warrants further investigation at a molecular level. In the current study, we assessed the therapeutic potential of ENTO monotherapy and in combination with chemotherapy or other kinase inhibitors in preclinical infant *KMT2A*-R and non-*KMT2A*-R ALL patient-derived xenograft (PDX) models to delineate the potential anti-leukemic utility of SYK inhibition in this high-risk childhood leukemia subtype.

Methods

KMT2A-rearranged acute lymphoblastic leukemia patient specimens and xenotransplantation models

Viably cryopreserved leukemia cells from infants with *de novo KMT2A*-R (n=4; corresponding relapse, n=3) and non-*KMT2A*-R ALL (n=3) enrolled on the Children's Oncology Group (COG) trial AALL0631 were obtained via informed consent as previously described.[34] Additional specimens from an infant with relapsed *KMT2A*-R (n=1; ALL3103) and an adult with *de novo KMT2A*-R ALL (n=1; ALL3113) were obtained from the University of California, San Francisco and University of Pennsylvania leukemia biorepositories under approved institutional research protocols after informed consent in accordance with the Declaration of Helsinki (Table 1). PDX models were established in NOD.Cg-*Prkdcscid Il2rgtm1Wjl/SzJ* (NSG) mice via an Institutional Animal Use and Care Committee-approved protocol at the Children's Hospital of Philadelphia as described with serial transplantation of human ALL cells into secondary or tertiary recipients for experimental studies.[35-38] Additional established non-*KMT2A*-R ALL PDX models (primarily of the Philadelphia chromosome-like [Ph-like] subtype)[15,37-39] (*Online Supplementary Table S1*) were used as negative controls.

Kinase inhibitors and chemotherapy

The selective SYK inhibitor entospletinib (ENTO)[32] was provided as a dispersible powder for *in vitro* studies and in rodent chow formulation in 0.03%, 0.05%, and 0.07% concentrations for *in vivo* animal studies by Gilead Sciences Inc. (Foster City, CA, USA). Rodent chow concentrations were selected and optimized based upon PK levels achieved in ENTO-treated adult patients with acute leukemia (*clinicaltrials.gov identifiers: NCT02404220 and NCT02343939*).[33] Vincristine and dexamethasone were purchased from the Children's Hospital of Philadelphia investigational pharmacy (Philadelphia, PA, USA). The MEK inhibitor selumetinib, SYK inhibitor fostamatinib, and multi-kinase inhibitor dasatinib were purchased from Selleckchem (Houston, TX, USA) or LC Labs (Woburn, MA, USA). Cell viability and phosphoflow cytom-

Table 1. Molecular and cytogenetic characteristics of acute lymphoblastic leukemia (ALL) patient-derived xenograft (PDX) models.

ALL PDX model	COG USI	*KMT2A* status	Translocation	Disease status	Other genetic alterations
ALL185GD	PAVVRD	wild-type	*P2RY8-CRLF2*, *PAX5-AUTS2*	*De novo*	*JAK2* mut, *CDKN2A/B* del
ALL83GD	PAUFHC	wild-type	*P2RY8-CRLF2*, *PAX5-C20orf112*	*De novo*	*JAK2* del, *CDKN2A/B* del, *RTEL* del
ALL132GD	PAUXSA	wild-type	t(1;19) (q23;p13) with *TCF3-PBX1*	*De novo*	*KRAS* mut, *WHSC1* mut, gain *CCND3, MYB, ESR1*
ALL150MD	PAVEDG	*KMT2A-AFF1*	t(4;11) (q21;q23)	*De novo*	*KRAS* mut
ALL142MD	PAVBRV	*KMT2A-AFF1*	t(4;11) (q21;q23)	*De novo*	*NRAS* mut
ALL142MR	PAVBRV	*KMT2A-AFF1*	t(4;11) (q21;q23)	Relapse	*NRAS* mut, *IKZF1* del, cnLOH of chr22
ALL3113MR	n/a	*KMT2A-AFF1*	t(4;11) (q21;q23)	*De novo*	*JAK2* mut, *TP53* 17p del, *IKZF1* 7p del
ALL3103MR	n/a	*KMT2A-MLLT3*	t(9;11) (p21;q23)	Relapse	None identified
ALL135MD	PAUYJT	*KMT2A-MLLT1*	t(11;19) (q23;p13.3)	*De novo*	None identified
ALL135MR	PAUYJT	*KMT2A-MLLT1*	t(11;19) (q23;p13.3)	Relapse	None identified
ALL26MD	PASHFM	*KMT2A-MLLT1*	t(11;19) (q23;p13.3)	*De novo*	None identified
ALL26MR	PASHFM	*KMT2A-MLLT1*	t(11;19) (q23;p13.3)	Relapse	Partial 10q del, including *PTEN*

COG USI: Children's Oncology Group unique specific identifier; cnLOH: copy-neutral loss of heterozygosity; del: deletion; mut: mutation; n/a: not available.

etry signaling analyses of human B-ALL cell lines and PDX model cells treated with vehicle, kinase inhibitors, or chemotherapy (*in vitro* or *in vivo*) are detailed in the *Online Supplementary Methods* with data shown in *Online Supplementary Figures S1-S6*.

In vivo drug testing in patient-derived xenograft models

Animal studies were conducted under a CHOP Institutional Animal Use and Care Committee (IACUC)-approved protocol in accordance with the Panel on Euthanasia of the American Veterinary Medical Association's guidelines. After flow cytometric (FC) confirmation of ≥1% $CD45^+$ $CD19^+$ human ALL (fluorochrome-conjugated antibodies from EBioscience) in murine peripheral blood, engrafted ALL PDX models were randomized to treatment with vehicle, ENTO chow orally *ad libitum*, vincristine 0.1 mg/kg intraperitoneally (IP) weekly, or both ENTO and vincristine for 72 hours (pharmacokinetic [PK] and pharmacodynamics [PD] studies) or up to 28 days (treatment efficacy studies) as described.[37,38] Vincristine dosing was previously optimized in ALL cell line and PDX models (*not shown*). Additional studies in some ALL PDX models assessed selumetinib 100 mg/kg administered orally twice daily[40] 5 days/week as (ALL135MR and ALL3113) or dexamethasone 1 mg/kg PO once daily 5 days/week (ALL3113, ALL83GD) as monotherapy or in combination with ENTO. Further details about *in vivo* drug testing in ALL PDX models and conduction of all other experimental studies are included in the *Online Supplementary Methods*.

Results

Characterization of constitutive SYK pathway activation in infant *KMT2A*-R acute lymphoblastic leukemia patient-derived xenograft models

Constitutive SYK pathway activation was detected across a genetic spectrum of infant ALL and some non-infant Philadelphia chromosome-like (Ph-like) ALL control specimens using harvested murine spleens from well-engrafted PDX models (Table 1). Assessment of phosphorylated and total SYK levels revealed that expression of high basal phosphorylated SYK (pSYK) was seen in the majority of infant non-*KMT2A*-R and *KMT2A*-R ALL specimens (Figure 1, left). pSYK levels were also elevated in some Ph-like ALL specimens and absent in splenic tissue from non-leukemia-injected NSG mice (Figure 1, right). Total SYK expression was relatively consistent across all models. The observed constitutive basal pSYK levels, coupled with a previously suggested role of upregulated SYK as a driver in AML models with high *HOXA9* and *MEIS1* expression,[25] and early reports of clinical responses in adults with relapsed *KMT2A*-R leukemias treated with entospletinib[42,43] led us to investigate the role of SYK signaling and therapeutic potential of ENTO specifically in infant *KMT2A*-R ALL PDX models.

Entospletinib decreases leukemic burden and inhibits kinase signaling in *KMT2A*-R acute lymphoblastic leukemia

SYK plays a pivotal role upstream of several key leukemia-associated signaling pathways,[26,29] including RAS/MAPK, PI3K/AKT/mTOR, and JAK/STAT. SYK inhibition by ENTO has the potential to impact multiple signal transduction pathways in ALL (*Visual Abstract*), leading to potential anti-leukemic efficacy. Given our initial demonstration of constitutive SYK and other signaling pathway activation in infant ALL specimens by Simple Western, we first assessed leukemia cell growth inhibitory effects of ENTO *in vitro* using methylcellulose colony assays. Viably cryopreserved harvested *KMT2A*-R PDX ALL cells (model ALL3103 with *KMT2A-MLLT3* fusion) were grown under anchorage-independent (non-adherent) conditions in serum-free methylcellulose and treated with a clinically-relevant dose range of ENTO for 14 days (Figure 2A). ENTO maximally inhibited colony formation (89% inhibition; $P<0.0001$ by *t*-test), suggesting that SYK plays a central role upstream of signaling pathways essential to proliferation and survival.

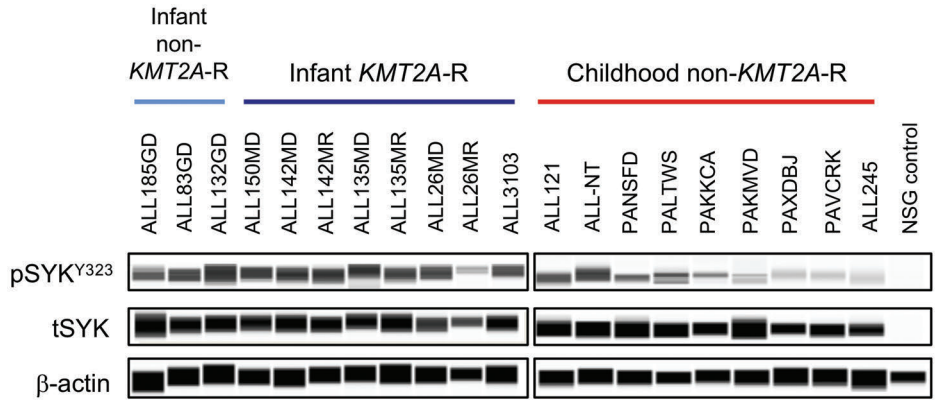


Figure 1. Constitutive SYK signaling occurs in infant acute lymphoblastic leukemia (ALL). Simple Western analysis of splenic lysates from human ALL patient-derived xenograft (PDX) models demonstrated high basal phosphorylated SYK (pSYK) levels in the majority of infant non-*KMT2A*-rearranged (R) (light blue) and *KMT2A*-R (dark blue) ALL specimens. pSYK levels were lower in most childhood non-*KMT2A*-R ALL specimens (red) and absent in splenic tissue from non-leukemia-injected NSG mice (gray). Total SYK levels were similar across all models. ALL PDX model names are specified above corresponding Simple Western data.

We then assessed the ability of ENTO to inhibit leukemia proliferation *in vivo* in ALL3103 and NH011 (Ph-like ALL with *NUP214-ABL1* fusion) PDX mice. ENTO 0.03% and 0.07% chow concentrations administered for 28 days both potently decreased human $CD45^+$ $CD19^+$ ALL cell counts in peripheral blood measured weekly by quantitative flow cytometry and in end-study spleens (Figure 2B and C and *Online Supplementary Figure S7*). Terminal PK evaluation of ENTO in the periphery confirmed that high levels of ENTO could be achieved by continuous chow administration (Figure 2D) without statistical difference between the 0.03% and 0.07% treatment groups. Simple Western analysis of highly leukemia-engrafted splenic lysates from individual ENTO-treated mice demonstrated marked inhibition of pSYK Y323, cMYC and pERK T202/Y204 as compared to control chow-treated animals after 4 weeks of treatment (Figure 2E) and high correlation between ENTO levels and pSYK and pERK inhibition in well-engrafted ALL3103 PDX mice treated in pharmacodynamic studies for 72 hours with entospletinib (*Online Supplementary Figure S8*). These results confirmed the on-target inhibition of pSYK and key downstream signaling phosphoproteins by ENTO, suggesting that an achieved dose level of 3330-7900 nM *in vivo* was sufficient to inhibit constitutive pSYK signaling and decrease *in vivo* leukemia proliferation in an aggressive relapsed infant *KMT2A*-R ALL PDX model.

In vitro pharmacodynamic inhibition of signaling proteins in infant *KMT2A*-R models

To extend our observation of ALL cell SYK dependency for proliferation and survival in other *KMT2A*-R fusion types, we evaluated ENTO in another aggressive multiply-relapsed infant ALL PDX model with *KMT2A-MLLT1* fusion (ALL135MR) in short-term *in vitro* cultures and observed dose-dependent inhibition of pERK1/2, $pAKT^{S473}$, pSTAT5, and cMYC (Figure 3A). Interestingly, similar *in vitro* incubation of leukemia cells from an infant ALL PDX model with *KMT2A-AFF1* fusion and concomitant $NRAS^{G12D}$ mutation (ALL142MR) with ENTO showed little to no inhibition of the same key pathways (Figure 3B). These data suggest differential signaling effects potentially related to specific *KMT2A* fusion partner and/or RAS-mutant status.

Evaluation of expression signatures in *KMT2A*-R acute lymphoblastic leukemia subtypes

KMT2A-R ALL has been shown to have distinct gene expression signatures that define B-cell developmental arrest at either the pro-B- and pre-B-cell stages.[22] Understanding the signaling pathway dependencies of different *KMT2A*-R fusion proteins in infant ALL cells may lead to more effective therapeutic targeting strategies for this high-risk patient population. To assess potential differential gene expression signatures, we evaluated the transcription factors *HOXA9* and *MEIS1*, which are known downstream targets of *KMT2A*. As hypothesized, *HOXA9* and *MEIS1* expression levels correlated with both KMT2A-R fusion status and specific gene partner (Figure 4A). Infant ALL specimens with *KMT2A-MLLT3* and *KMT2A-MLLT1* fusions expressed both high *HOXA9* and *MEIS1*, while *KMT2A-AFF1* models had high *MEIS1* and normal *HOXA9* expression. Conversely, infant non-*KMT2A*-R samples had normal expression levels of *HOXA9* and *MEIS1*. These distinct expression signatures exhibited amongst *KMT2A*-R samples with different fusion partners are concordant with reports of differential chromatin binding of *KMT2A*-R fusion proteins leading to distinct gene expression profiles and potentially differential clinical outcomes.[1,21]

Given the observed stratification of *HOXA9* and *MEIS1* expression signatures among the *KMT2A* subgroups, we next assessed protein expression signatures in these samples to evaluate potential correlation. Simple Western analysis of splenic lysates from *KMT2A*-R and non-*KMT2A*-R ALL PDX models (Figure 4B) demonstrated that leukemias with different *KMT2A* fusion partners induced different patterns of signaling activation. High levels of cMYC were detected only in *KMT2A*-AFF1 models, while *KMT2A*-MLLT1 models had high SRC, absent PTEN, and high pAKT levels. Regulation of both SRC and PI3K pathways are known to be potentially SYK-dependent, concordant with data from our *in vitro* studies in ENTO-treated ALL135MR cells (Figure 3A). Overall, differential gene expression signatures between *KMT2A*-R and non-*KMT2A*-R ALL subtypes (*Online Supplementary Figure S9A*) and differences between gene and protein expression signatures among the *KMT2A* fusion subtypes (Figure 4B and *Online Supplementary Figure S9B*) showed unique signaling

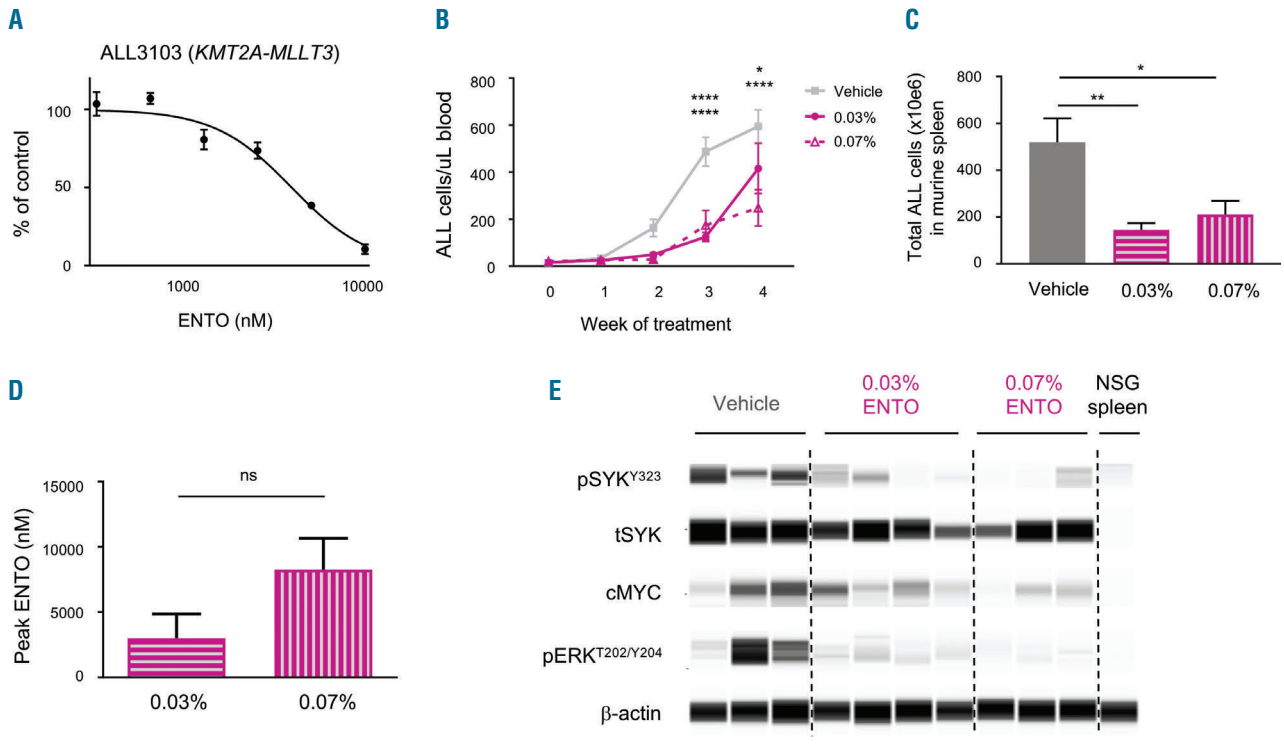


Figure 2. Activity and dose optimization of entospletinib monotherapy in *KMT2A*-R acute lymphoblastic leukemia (ALL). (A) Viably cryopreserved harvested human *KMT2A*-R ALL cells from murine PDX spleens (model ALL3103 with *KMT2A-MLLT3* fusion) demonstrated dose-dependent inhibition of colony formation *in vitro* in methylcellulose colony assays after ENTO treatment for 14 days. Samples were plated in triplicate in methylcellulose-based medium and grown in 10% leukocyte-conditioned medium with 25% FBS and 2% BSA. Data are displayed as mean ± SEM. (B) ALL3103 PDX mice were treated with vehicle (control) or ENTO chow at the specified concentrations for 4 weeks. Human $CD45^+$ $CD19^+$ ALL flow cytometric analysis of murine blood at weekly time points and (C) spleens at study endpoint demonstrated significant inhibition of ALL proliferation with ENTO treatment (mean ± SEM). No difference in ALL burden was observed in 0.03% *versus* 0.07% ENTO-treated animals. (D) Terminal blood was collected from animals after 4 weeks of continuous ENTO chow consumption and evaluated for entospletinib levels. Data from individual animals are plotted as median interquartile range. ns: not significant by t-test. (E) Terminal spleens from individual mice were harvested, viably cryopreserved, lysed, and evaluated for levels of pSYK, SYK, cMYC, pERK and β-actin by Simple Western. *P<0.05, **P<0.01, ****P<0.0001 as compared to control chow-fed mice by ANOVA with Tukey's post-test.

dependencies that may relate to their differential ENTO sensitivity.

Entospletinib potently inhibits *in vivo* acute lymphoblastic leukemia proliferation with enhanced efficacy in combination with chemotherapy

We then investigated the extent to which ENTO could inhibit *in vivo* leukemia proliferation in ALL PDX models when administered as monotherapy or in combination with vincristine (VCR) chemotherapy. We observed that combined ENTO and VCR treatment resulted in superior inhibition of ALL proliferation in a *KMT2A-MLLT3* (ALL3103) model and a *KMT2A-MLLT1* (ALL135MR) model (both RAS wild-type) than was observed with single-agent ENTO or VCR (P<0.001 and P<0.05, respectively) (Figure 5A). Superior leukemic cell depletion with ENTO and VCR combination was confirmed by quantitative CD19 IHC in harvested murine spleens and bone marrow (see *Online Supplementary Figure S10* for representative ALL3103 data). Conversely, drug treatment of two *RAS*-mutant *KMT2A*-R ALL PDX models (Figure 5B) showed marked vincristine-induction reduction of leukemic burden (ALL142MR, P<0.0001; ALL150MD, P<0.001) but no effects of ENTO monotherapy or additional treatment effect of combined ENTO and VCR. Evaluation of an adult RAS wild-type *KMT2A-AFF1* ALL PDX model (ALL3113) showed significant treatment effects of ENTO alone and in combination with VCR (P<0.0001 for both) (Figure 5C), contrasting with effects observed in the RAS-mutant models. Taken together, these data indicate that RAS mutations in *KMT2A*-R subtypes may overcome or prevent potential anti-leukemia activity of ENTO.

We then explored treatment effects of ENTO in a control non-*KMT2A*-R ALL PDX model with t(1;19) resulting in *TCF3-PBX1* fusion and a $KRAS^{G12D}$ mutation (ALL132GD), which we expected to be sensitive to ENTO given typical pre-BCR expression on this more mature B-ALL subtype[42,43] and confirmed by positive FC immunoglobulin μ-heavy chain staining on AALL132GD cells (*data not shown*). However, we saw no response to single-agent ENTO or in combination with VCR, further substantiating the potential impact of RAS mutations upon ENTO insensitivity (Figure 5D). Finally, we tested ENTO and VCR in two RAS wild-type non-*KMT2A*-R ALL PDX models (ALL185GD and ALL83GD) (Figure 5E). We observed sensitivity of model ALL185GD to ENTO monotherapy (P<0.05) and in combination with VCR (P<0.0001), although the latter effects did not differ from those of VCR monotherapy. Model ALL83GD was not sensitive to ENTO alone, but showed significant combinatorial treatment efficacy *versus* ENTO or VCR monotherapy (P<0.0001 and P<0.05, respectively). Interestingly, we discovered that the ALL185GD and ALL83GD non-*KMT2A*-R models have *P2RY8-CRLF2* fusions with expected constitutive activation of JAK/STAT signaling (Figure 4B). Our group recently reported an essential role

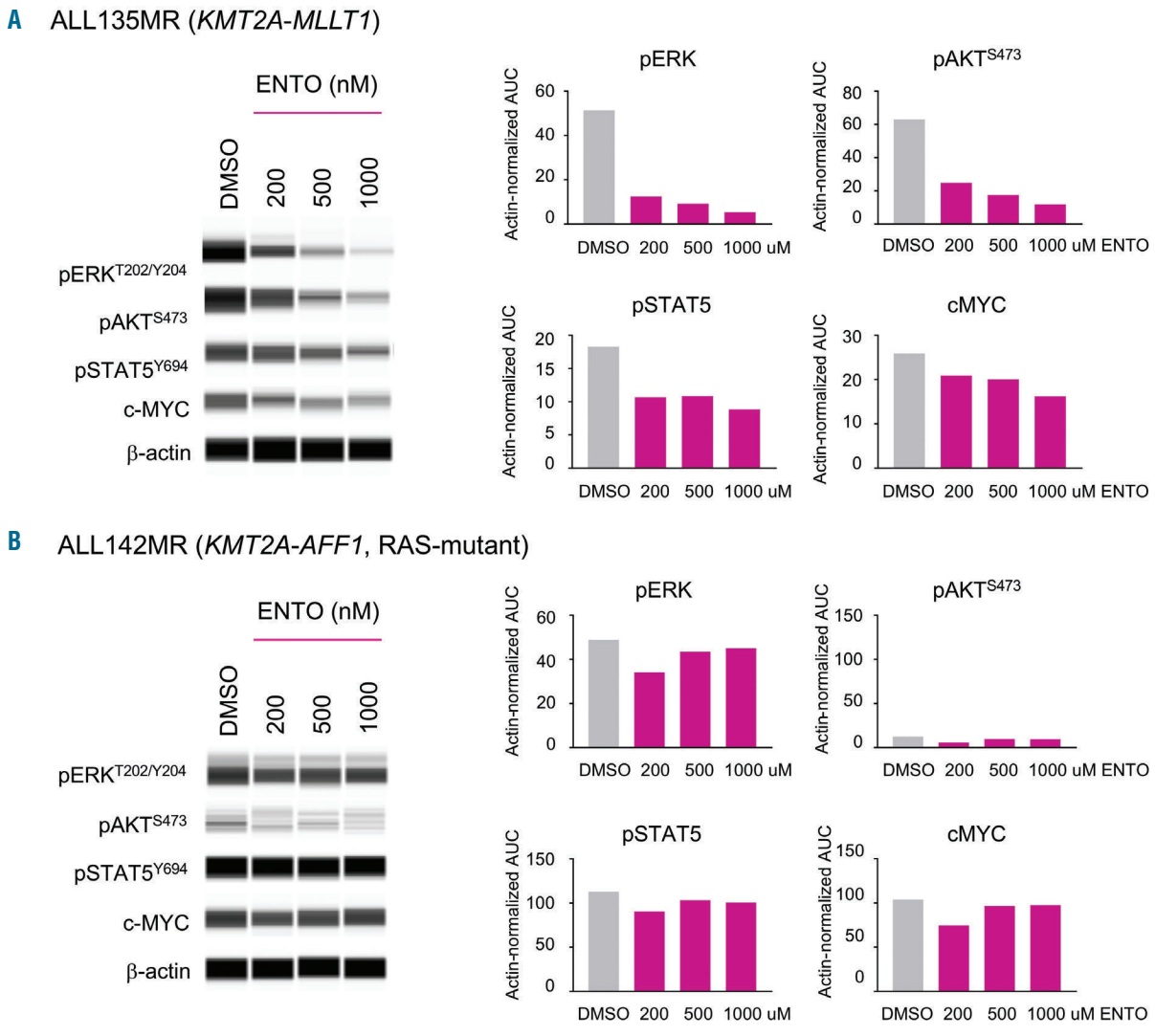


Figure 3. *In vitro* activity of entospletinib in *KMT2A*-R acute lymphoblastic leukemia (ALL). Viably cryopreserved KMT2A-R ALL PDX cells were exposed *in vitro* to 0.1% DMSO (vehicle control) or increasing concentrations of entospletinib (200 nM, 500 nM, 1 uM) for 2 hours, then lysed and analyzed by Simple Western. Additional untreated (baseline) cells were lysed immediately following sample thaw. (A) Dose-dependent inhibition of the specified phosphoproteins was observed with ENTO in the ALL135MR PDX model (*KMT2A-MLLT1*, RAS wild-type), while (B) no treatment effect was seen in the 142MR PDX model (*KMT2A-AFF1*, *NRAS*-mutant).

of SFK signaling in *CRLF2*-rearranged Ph-like ALL with *in vitro* and *in vivo* sensitivity to the kinase inhibitor dasatinib[44,45] and hypothesize that the observed ENTO sensitivity in our *CRLF2*-R infant ALL models could be due to a similar mechanism and signaling dependency.

Superior preclinical activity of combined SYK and MEK inhibition in *KMT2A*-R acute lymphoblastic leukemia patient-derived xenograft models

Given the surprising observed lack of ENTO activity in our RAS-mutant *KMT2A-AFF1* infant ALL PDX models, we hypothesized that dual treatment with ENTO and a MEK inhibitor (MEKi) would have superior therapeutic effects. To test this prediction, we treated RAS-mutant (ALL142MR; infant) and RAS wild-type (ALL3113MR; adult) *KMT2A-AFF1* ALL PDX models with ENTO, selumetinib (SEL), or both kinase inhibitors and quantified ALL cell counts in peripheral blood during treatment and in end-study spleens. As expected,[40,46] single-agent SEL treatment of the RAS-mutant ALL142MR model appreciably decreased leukemia burden and augmented anti-ALL effects in combination with ENTO (Figure 6A). Despite its lack of RAS mutation, the ALL3113 model was surprisingly sensitive to SEL monotherapy[41,48] and potent *in vivo* activity with near-complete leukemia clearance was observed with dual ENTO and SEL treatment (Figure 6B). These *in vivo* efficacy data in both RAS-mutant and wild-type models, and our additional demonstration of constitutive pERK levels and *ex vivo* signaling inhibition in end-study spleens of both ALL142MR and ALL3113 models (Figure 6C), suggest that MEK inhibition may be a relevant therapeutic strategy for *KMT2A*-R ALL irrespective of RAS mutation status and may augment SYK inhibitor effectiveness.

Discussion

SYK pathway activation plays a central role in the proliferation and survival of malignant B cells, implicating

SYK as a potential therapeutic target. Preclinical studies have shown that SYK inhibition can attenuate the growth of B-ALL *in vitro* and *in vivo* regardless of pre-BCR expression or genetic subtype.[26,29] Mohr *et al*. also recently reported that *HOXA9/MEIS1*-induced upregulation of SYK is a major driver of leukemogenesis in AML.[25] Several early phase clinical trials are now testing the safety and potential efficacy of ENTO in combination with chemotherapy in adults with relapsed or refractory leukemias (*clinicaltrials.gov identifiers: NCT02404220, NCT02343939, NCT03135028*). Interim results from these studies have reported manageable adverse events and remarkable response rates, particularly in patients with KMT2A-R AML (*clinicaltrials.gov identifier: NCT02343939*).[33]

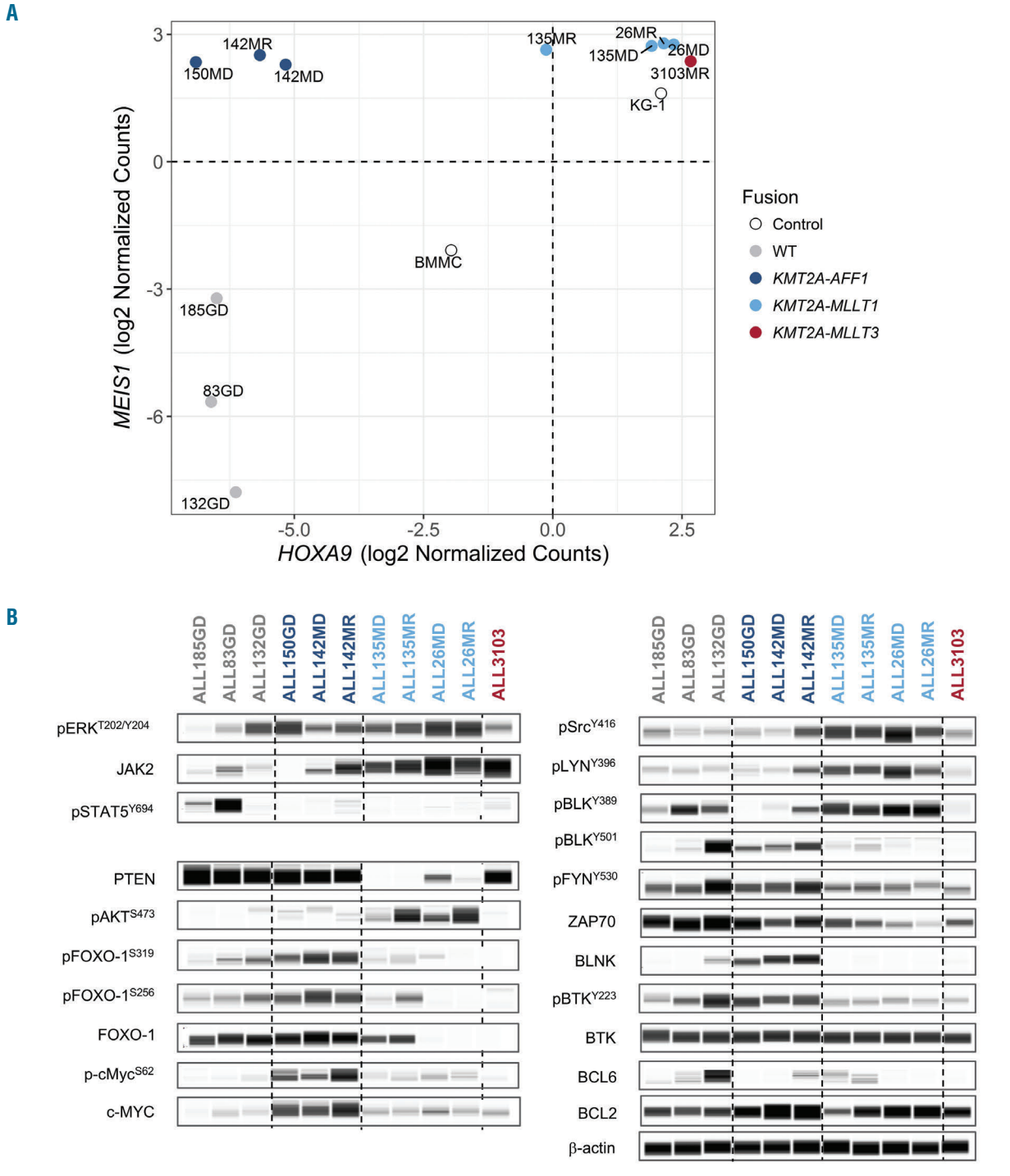


Figure 4. *HOXA9* and *MEIS1* expression signatures of *KMT2A*-R and non-*KMT2A*-R acute lymphoblastic leukemia (ALL) patient-derived xenograft (PDX) specimens. (A) Splenic PDX samples were analyzed for expression of mRNA for *HOXA9* and *MEIS1* by NanoString, with human bone marrow mononuclear cells (BMMC) and KG-1 cell line as negative and positive controls, respectively. Increased *MEIS1* and/or *HOXA9* expression was seen in *KMT2A*-R ALL PDX models *versus* non-*KMT2A*-R (WT) models and generally clustered by genetic subtype. (B) Total and phosphorylated signal transduction proteins from murine splenic lysates were evaluated using Simple Western. Basal kinase signaling activation differed among *KMT2A*-R and non-*KMT2A*-R ALL samples and stratified by genetic subgroup (*KMT2A-AFF1, KMT2A-MLLT1, KMT2A-MLLT3*, and non-*KMT2A*-R). β-actin was used as a protein loading control.

Chemotherapy resistance and subsequent relapse remain a major cause of childhood cancer mortality, especially for infants with *KMT2A*-R B-ALL who have extremely poor EFS. In one study, Pieters *et al.* reported 3-fold higher risk of relapse or death in infants with *KMT2A*-R ALL (irrespective of *KMT2A* rearrangement subtype) *versus* those without *KMT2A* rearrangements.[10] Outcomes for infants with the *KMT2A-AFF1* subtype from t(4;11) are particularly poor, although differences in associated HOX family gene expression and presence or absence of reciprocal *AFF1-KMT2A* fusions may contribute to differential clinical outcomes, as shown recently by Agras-Doblas and Bueno *et al.* in a large analysis of infant ALL specimens from the European co-operative groups' Interfant-99 and -06 trials[47-49] and reviewed by Slany.[20]

Several groups have hypothesized that addition of targeted inhibitors to frontline chemotherapy could decrease relapse risk and improve survival for infants with ALL, as has been shown with tyrosine kinase inhibitors (TKI) for patients with *BCR-ABL1*-rearranged (Ph^+) ALL. Unfortunately, addition of the FMS-like tyrosine kinase 3

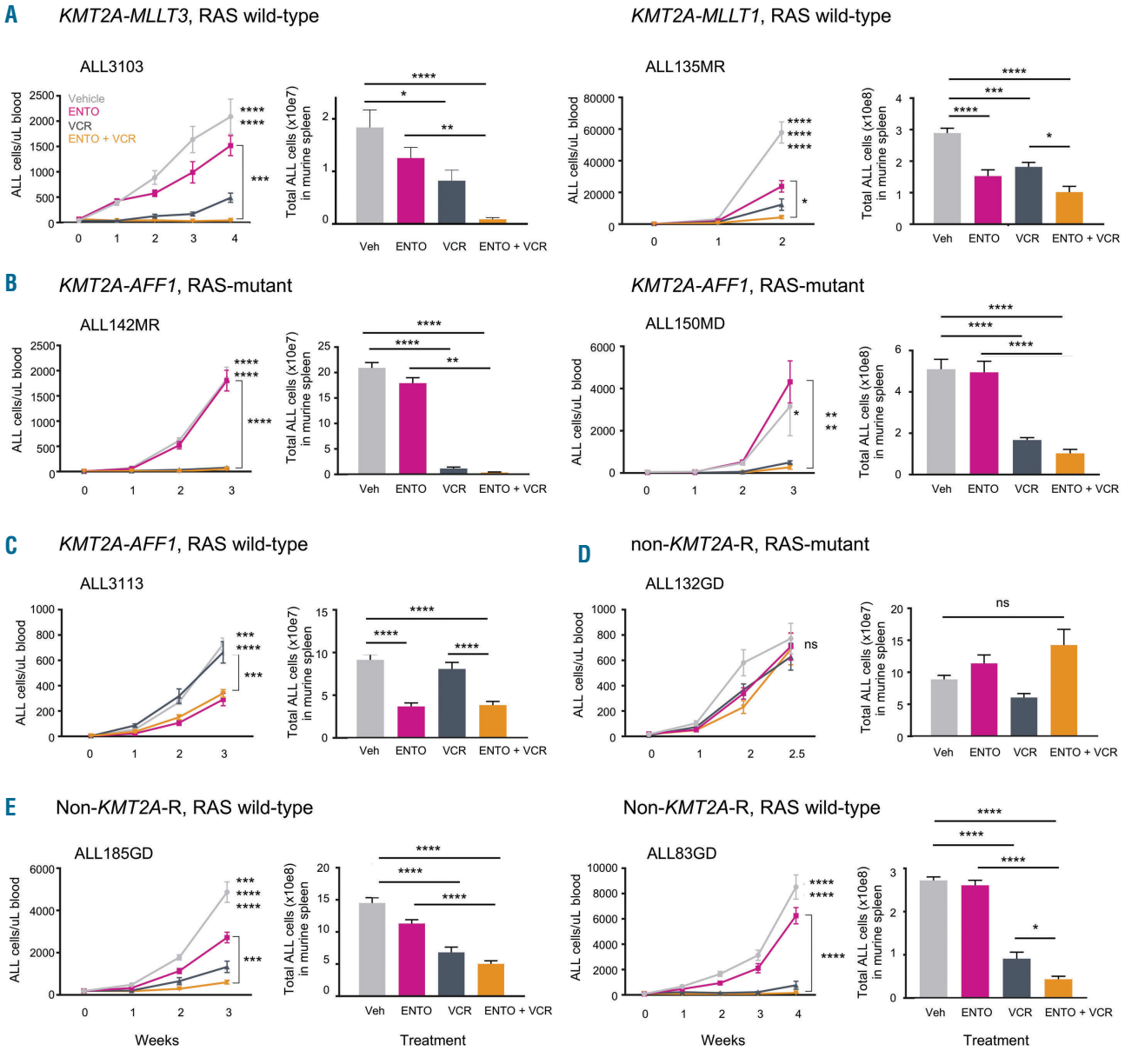


Figure 5. Entospletinib potently inhibits *in vivo* acute lymphoblastic leukemia (ALL) proliferation with enhanced efficacy in combination with chemotherapy. Animals engrafted with *KMT2A*-R (ALL3103, ALL135MR, ALL142MR, ALL150MD, ALL3113) or non-*KMT2A*-R (ALL132GD, ALL185GD, ALL83GD) ALL were treated with control chow, 0.05% ENTO chow, 0.1 mg/kg vincristine (VCR) IP weekly, or both ENTO and VCR. Human $CD45^+CD19^+$ ALL cells were quantified by flow cytometry in end-of-study murine spleens and peripheral blood. (A) Combined ENTO+VCR significantly inhibited leukemia proliferation with enhanced activity compared to ENTO and/or VCR monotherapies in *KMT2A*-R PDX models without RAS mutations. (B) Conversely, potent VCR effects were observed in *KMT2A*-R ALL PDX models with *NRAS* or *KRAS* mutations without additional activity of combination treatment. (C) A *KMT2A*-R RAS wild-type ALL PDX model was sensitive to ENTO and not to VCR. (D) No treatment effects of ENTO or VCR were observed in a non-*KMT2A*-R *KRAS*-mutant ALL PDX model, while single-agent activity of VCR and/or ENTO and enhanced effects of combination treatment were detected in (E) non-*KMT2A*-R RAS wild-type PDX control models with other ALL-associated translocations. Data were analyzed by one-way ANOVA with Tukey's post-test for multiple comparisons. **P*<0.05, ***P*<0.01, ****P*<0.001, *****P*<0.0001.

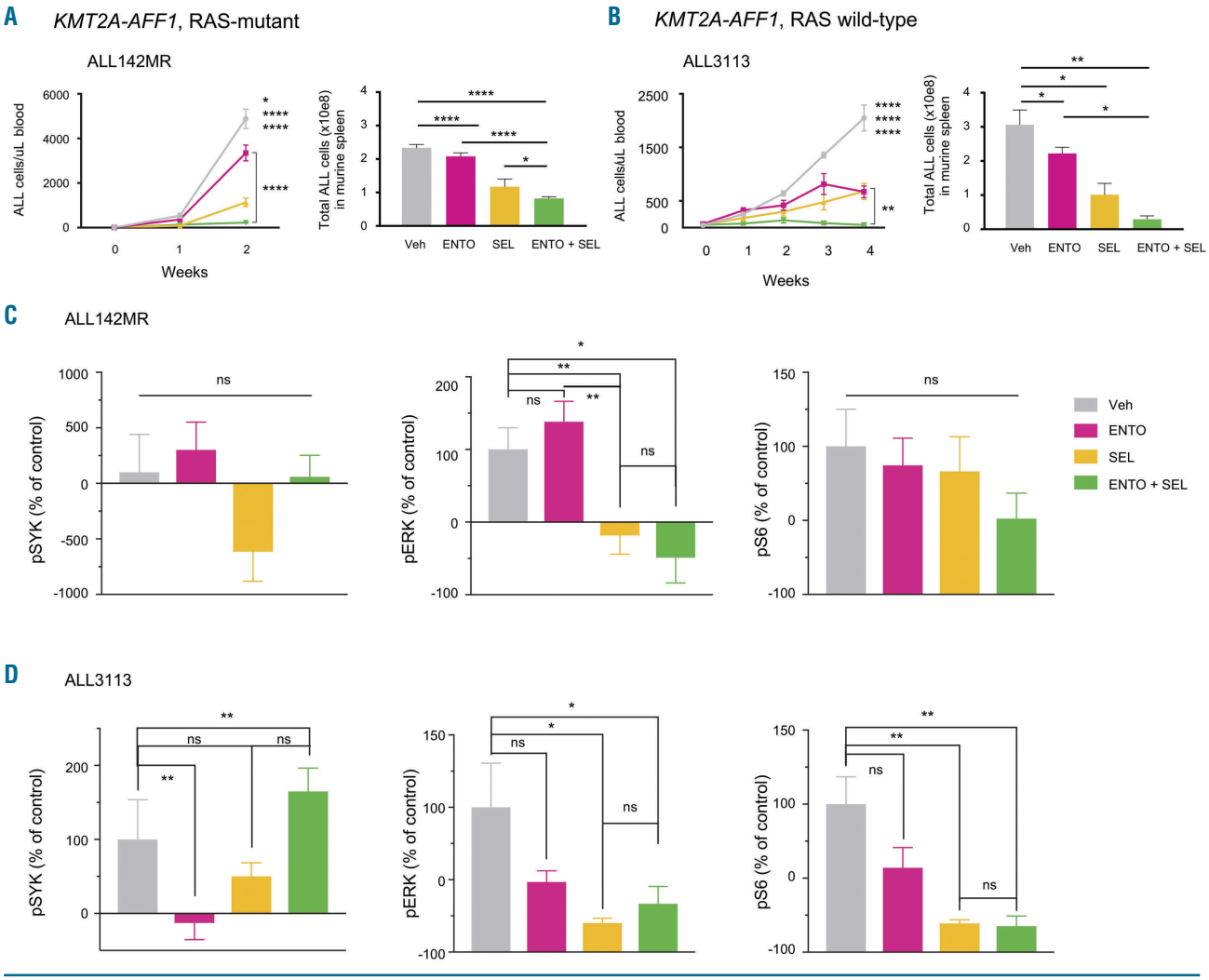


Figure 6. Superior preclinical activity of entospletinib and selumetinib in *KMT2A*-R acute lymphoblastic leukemia (ALL) patient-derived xenograft (PDX) models. (A) PDX models 142MR (*KMT2A-AFF1*, *NRAS*-mutant) and (B) ALL3113 (*KMT2A-AFF1*, RAS wild-type) were treated with vehicle control chow, 0.05% ENTO chow, 100 mg/kg selumetinib (SEL) via oral gavage twice daily 5 days/week, or both ENTO and SEL for 2 or 4 weeks. Human CD45$^+$ CD19$^+$ ALL cells were quantified by flow cytometry in peripheral blood and end-study murine spleens. Enhanced anti-leukemia efficacy was observed in both models with combined ENTO and SEL treatment *versus* ENTO or SEL alone, as measured by one-way ANOVA with post Tukey's post-test for multiple comparisons. *P<0.05, **P<0.01, ****P<0.0001. (C) *Ex vivo* phosphoflow cytometry analysis of gated human CD19$^+$ CD45$^+$ ALL cells in end-study murine spleens after 2 weeks (ALL142MR) or 4 weeks (ALL3113) of ENTO and/or SEL treatment demonstrate inhibition of pSYK, pERK, and/or pS6 *versus* vehicle control (gray). ns: not significant, *P<0.05, **P<0.01 by one-way ANOVA with post Tukey's post-test for multiple comparisons.

inhibitor (FLT3i) lestaurtinib did not improve EFS for infants with *KMT2A*-R B-ALL (which usually have high FLT3 receptor [CD135] surface expression) in the COG trial AALL0631, which was likely in part attributable to insufficient PD target inhibition observed by correlative plasma inhibitory activity (PIA) assays.[50,51] Similarly, no appreciable efficacy of the FLT3i quizartinib (AC220) was observed in children with relapsed *KMT2A*-R ALL in the TACL2009-004 phase I clinical trial (*clinicaltrials.gov identifier: NCT011411267*), although complete responses occurred in 3 of 7 patients with relapsed *FLT3*-mutant AML with 94-100% FLT3 inhibition by PIA assay seen in all studied patients.[52] Despite promising preclinical data,[53,54] clinical activity of DOT1L inhibitors (e.g., pinemetostat [EPZ-5676]) targeting the KMT2A complex was similarly disappointing in children with relapsed KMT2A-R leukemias (*clinicaltrials.gov identifier: NCT02141828*),[55] again potentially due to insufficient achievable drug levels considered necessary for response. Menin inhibitors targeting the KMT2A complex have shown exciting preclinical activity and may have superior pharmacologic properties, but have not yet entered clinical testing. Finally, current or planned trials are assessing the potential activity of 5-azacytidine priming (COG AALL15P1; *clinicaltrials.gov identifier: NCT02828358*) or blinatumomab[56] specifically in infants with *KMT2A*-R ALL; however, results of these approaches are not yet known.

Our current study sought to define the potential activity of the selective SYK inhibitor ENTO specifically in preclinical infant *KMT2A*-R ALL PDX models. Our demonstration of *in vitro* and *in vivo* anti-leukemia activity of ENTO with enhanced effects in combination with VCR or dexamethasone (critical and commonly-used anti-ALL chemotherapy agents) provides a rationale for further evaluation of SYK inhibition as a therapeutic strategy for this high-risk leukemia subtype. Interestingly, we observed minimal activity of ENTO alone or with VCR in *KMT2A*-R leukemias harboring concomitant RAS muta-

tions. This observation extended to a control non-*KMT2A*-R infant ALL model with a *TCF3-PBX1* fusion from t(1;19), which had a concomitant *KRAS* mutation and was also insensitive to ENTO. Prior studies have shown that RAS mutations occur significantly more frequently in infants with B-ALL, particularly in those with the most common *KMT2A-AFF1* subtype. Data do not agree as to whether ALL-associated RAS mutations confer higher relapse risk and inferior overall survival.[8,24,57,58]

The potential role of RAS mutations in conferring insensitivity to SYK inhibition in ALL was further extended by evaluation of ENTO in combination with the clinically-available MEK inhibitor selumetinib in two *KMT2A*-R ALL PDX models. As predicted,[40,59] we observed significant inhibition of leukemia proliferation with SEL treatment of a RAS-mutant *KMT2A-AFF1* infant ALL model with superior activity of ENTO and SEL combination. However, SEL monotherapy and combined SEL/ENTO therapy was also quite efficacious in a RAS wild-type KMT2A-AFF1 adult ALL model with high basal pERK levels. These data contrast somewhat with earlier preclinical data from Irving *et al*. demonstrating preferential activity of SEL (monotherapy or in combination with dexamethasone) in RAS-mutant ALL,[40,46] an approach now under clinical investigation in children with relapsed/refractory RAS-mutant ALL via the SeluDex phase I/II trial (*clinicaltrials.gov identifier: NCT03705507*), but are concordant with data from Kerstjens *et al*. reporting preclinical MEK inhibitor activity in both RAS-mutant and wild-type ALL.[59] Cremer *et al*. also recently reported that MAPK pathway activation is a major mechanism of entospletinib or fostamatinib resistance in AML and can be overcome with dual SYK and MEK inhibition.[60]

In summary, our studies show constitutive activation of SYK and associated kinase signaling in preclinical infant *KMT2A*-R and childhood Ph-like ALL PDX models. We report potent *in vitro* and *in vivo* effects of selective SYK inhibition with enhanced activity with chemotherapy in non-RAS-mutant *KMT2A*-R ALL models. We also observed combinatorial activity of ENTO with the MEK inhibitor selumetinib in two *KMT2A*-R ALL PDX models with RAS mutation or pathway activation. Our findings warrant further evaluation of efficacy and toxicity of ENTO/SEL dual therapy in additional PDX models, potentially in combination with steroids or other traditional chemotherapy agents. Taken together, our preclinical studies demonstrate activity of ENTO in *KMT2A*-R ALL in combination with anti-ALL chemotherapy or MEK inhibition and suggest a potential for clinical evaluation of SYK inhibitor-based therapies in children and adults with these high-risk leukemias.

Disclosures

AY, MW, AS and ST are current or former employees of Gilead Sciences and have equity ownership in Gilead Sciences. SKT received research funding from Gilead Sciences. The remaining authors declare no relevant conflicts of interest.

Contributions

JPL and AY designed and performed research, analyzed data, and contributed to writing the manuscript; PAB contributed vital new reagents, and analyzed and interpreted data; LMN, AB, MW and AS performed research and analyzed data; ST and SKT oversaw the study, designed research, analyzed and interpreted data, and wrote the manuscript; SKT was responsible for revision of the manuscript; all authors approved the final version of the manuscript.

Acknowledgments

We acknowledge Dr Ann Forslund and Ms Chelsea Mullins formerly at Gilead Sciences for study protocol management and data analysis, and Dr Emer Clarke at ReachBio Research Labs for assistance with experimental studies. We also thank Dr Christian Hurtz at the University of Pennsylvania for assistance with experimental studies and scientific discussion. These studies were supported by Gilead Sciences. Specimen banking for patients enrolled on the COG AALL0631 trial (clinicaltrials.gov identifier: NCT00557193) was supported by NIH/NCI U10CA180886 and U10CA098543. Infant and childhood ALL patient-derived xenograft model creation was also supported by the Gabrielle's Angel Foundation for Cancer Research Foundation, the Rally Foundation for Childhood Cancer Research, the SchylerStrong Foundation in memory of Schyler Anna Herman, the Simutis family childhood leukemia research fund in memory of Andrew David Simutis, and Team Nate and the Viands family childhood leukemia research fund in honor of Nathaniel J Viands. LMN was supported by NIH/NCI 5T32HD43021-15. SKT was supported by NIH/NCI K08CA184418 and 1U01CA232486 awards and Department of Defense Translational Team Science Award CA180683P1.

Funding

These studies were supported by Gilead Sciences. Specimen banking for patients enrolled on the COG AALL0631 trial ((clinicaltrials.gov identifier: NCT00557193) was supported by NIH/NCI U10CA180886 and U10CA098543. Infant and childhood ALL patient-derived xenograft model creation was also supported by the Gabrielle's Angel Foundation for Cancer Research Foundation, the Rally Foundation for Childhood Cancer Research, the SchylerStrong Foundation in memory of Schyler Anna Herman, the Simutis family childhood leukemia research fund in memory of Andrew David Simutis, and Team Nate and the Viands family childhood leukemia research fund in honor of Nathaniel J Viands. LMN was supported by NIH/NCI 5T32HD43021-15. SKT was supported by NIH/NCI K08CA184418 and 1U01CA232486 awards and Department of Defense Translational Team Science Award CA180683P1.

References

1. Pui CH, Yang JJ, Hunger SP, et al. Childhood acute lymphoblastic leukemia: progress through collaboration. J Clin Oncol. 2015;33(27):2938-2948.
2. Geng H, Hurtz C, Lenz KB, et al. Self-enforcing feedback activation between BCL6 and pre-B cell receptor signaling defines a distinct subtype of acute lymphoblastic leukemia. Cancer Cell. 2015;27(3):409-425.
3. Nguyen K, Devidas M, Cheng SC, et al. Factors influencing survival after relapse from acute lymphoblastic leukemia: a Children's Oncology Group study. Leukemia. 2008;22(12):2142-2150.
4. Teachey DT, Hunger SP. Predicting relapse risk in childhood acute lymphoblastic leukaemia. Brit J Haematol. 2013;162(5):606-620.
5. Sun W, Malvar J, Sposto R, et al. Outcome of children with multiply relapsed B-cell acute lymphoblastic leukemia: a therapeutic advances in childhood leukemia and lymphoma study. Leukemia. 2018;32(11):2316-2325.
6. Marks DI, Moorman AV, Chilton L, et al. The clinical characteristics, therapy and

outcome of 85 adults with acute lymphoblastic leukemia and t(4;11)(q21;q23)/MLL-AFF1 prospectively treated in the UKALLXII/ECOG2993 trial. Haematologica. 2013;98(6):945-952.
7. Behm FG, Raimondi SC, Frestedt JL, et al. Rearrangement of the MLL gene confers a poor prognosis in childhood acute lymphoblastic leukemia, regardless of presenting age. Blood. 1996;87(7):2870-2877.
8. Winters AC, Bernt KM. MLL-rearranged leukemias-an update on science and clinical approaches. Front Pediatr. 2017;5:4.
9. Brown P. Treatment of infant leukemias: challenge and promise. Hematology Am Soc Hematol Educ Program. 2013; 2013:596-600.
10. Pieters R, Schrappe M, De Lorenzo P, et al. A treatment protocol for infants younger than 1 year with acute lymphoblastic leukaemia (Interfant-99): an observational study and a multicentre randomised trial. Lancet. 2007;370(9583):240-250.
11. Driessen EMC, de Lorenzo P, Campbell M, et al. Outcome of relapsed infant acute lymphoblastic leukemia treated on the interfant-99 protocol. Leukemia. 2017; 31(12):2854.
12. Brown P, Pieters R, Biondi A. How I treat infant leukemia. Blood. 2019;133(3):205-214.
13. Vrooman LM, Blonquist TM, Harris MH, et al. Refining risk classification in childhood B acute lymphoblastic leukemia: results of DFCI ALL Consortium Protocol 05-001. Blood Advances. 2018;2(12):1449-1458.
14. Lafage-Pochitaloff M, Baranger L, Hunault M, et al. Impact of cytogenetic abnormalities in adults with Ph-negative B-cell precursor acute lymphoblastic leukemia. Blood. 2017;130(16):1832-1844.
15. Iacobucci I, Li Y, Roberts KG, et al. Truncating erythropoietin receptor rearrangements in acute lymphoblastic leukemia. Cancer Cell. 2016;29(2):186-200.
16. Tkachuk DC, Kohler S, Cleary ML. Involvement of a homolog of Drosophila trithorax by 11q23 chromosomal translocations in acute leukemias. Cell. 1992;71(4):691-700.
17. Gu Y, Nakamura T, Alder H, et al. The t(4;11) chromosome translocation of human acute leukemias fuses the ALL-1 gene, related to Drosophila trithorax, to the AF-4 gene. Cell. 1992;71(4):701-708.
18. Zangrando A, Dell'Orto MC, te Kronnie G, Basso G. MLL rearrangements in pediatric acute lymphoblastic and myeloblastic leukemias: MLL specific and lineage specific signatures. BMC Med Genomics. 2009;2(1):36.
19. de Boer J, Walf-Vorderwulbecke V, Williams O. In focus: MLL-rearranged leukemia. Leukemia. 2013;27(6):1224-1228.
20. Slany RK. MLL fusion proteins and transcriptional control. Biochim Biophys Acta Gene Regul Mech. 2020;1863(3):194503.
21. Lin S, Luo RT, Ptasinska A, et al. Instructive role of MLL-fusion proteins revealed by a model of t(4;11) pro-B acute Lymphoblastic Leukemia. Cancer Cell. 2016;30(5):737-749.
22. Krivtsov AV, Armstrong SA. MLL translocations, histone modifications and leukaemia stem-cell development. Nat Rev Cancer. 2007;7(11):823-833.
23. Meyer C, Burmeister T, Groger D, et al. The MLL recombinome of acute leukemias in 2017. Leukemia. 2018;32(2):273-284.
24. Andersson AK, Ma J, Wang J, et al. The landscape of somatic mutations in infant MLL-rearranged acute lymphoblastic leukemias. Nat Genet. 2015;47(4):330-337.
25. Mohr S, Doebele C, Comoglio F, et al. Hoxa9 and Meis1 cooperatively induce addiction to Syk signaling by suppressing miR-146a in acute myeloid leukemia. Cancer Cell. 2017;31(4):549-562.e11.
26. Perova T, Grandal I, Nutter LM, et al. Therapeutic potential of spleen tyrosine kinase inhibition for treating high-risk precursor B cell acute lymphoblastic leukemia. Sci Transl Med. 2014;6(236):236ra62.
27. Mócsai A, Ruland J, Tybulewicz VLJ. The SYK tyrosine kinase: a crucial player in diverse biological functions. Nat Rev Immunol. 2010;10:387.
28. Efremov DG, Laurenti L. The Syk kinase as a therapeutic target in leukemia and lymphoma. Expert Opin Investig Drugs. 2011;20(5):623-636.
29. Sharman J, Di Paolo J. Targeting B-cell receptor signaling kinases in chronic lymphocytic leukemia: the promise of entospletinib. Ther Adv Hematol. 2016;7(3):157-170.
30. Kohrer S, Havranek O, Seyfried F, et al. Pre-BCR signaling in precursor B-cell acute lymphoblastic leukemia regulates PI3K/AKT, FOXO1 and MYC, and can be targeted by SYK inhibition. Leukemia. 2016;30(6):1246-1254.
31. Loftus JP, Yahiaoui A, Shen F, et al. Enhanced efficacy of the SYK inhibitor entospletinib and vincristine in KMT2A-rearranged acute lymphoblastic leukemia. EHA Annual Congress. 2018:abstract PF164.
32. Currie KS, Kropf JE, Lee T, et al. Discovery of GS-9973, a selective and orally efficacious inhibitor of spleen tyrosine kinase. J Med Chem. 2014;57(9):3856-3873.
33. Walker AR, Byrd JC, Bhatnagar B, et al. Results of a phase 1b/2 study of entospletinib (GS-9973) monotherapy and in combination with induction chemotherapy in newly diagnosed patients with acute myeloid leukemia. EHA Annual Congress. 2018:abstract S118.
34. Salzer WL, Jones TL, Devidas M, et al. Decreased induction morbidity and mortality following modification to induction therapy in infants with acute lymphoblastic leukemia enrolled on AALL0631: a report from the Children's Oncology Group. Pediatr Blood Cancer. 2015; 62(3):414-418.
35. Maude SL, Tasian SK, Vincent T, et al. Targeting JAK1/2 and mTOR in murine xenograft models of Ph-like acute lymphoblastic leukemia. Blood. 2012; 120(17):3510-3518.
36. Maude SL, Dolai S, Delgado-Martin C, et al. Efficacy of JAK/STAT pathway inhibition in murine xenograft models of early T-cell precursor (ETP) acute lymphoblastic leukemia. Blood. 2015;125(11):1759-1767.
37. Tasian SK, Teachey DT, Li Y, et al. Potent efficacy of combined PI3K/mTOR and JAK or ABL inhibition in murine xenograft models of Ph-like acute lymphoblastic leukemia. Blood. 2017;129(2):177-187.
38. Tasian SK, Hurtz C, Wertheim GB, et al. High incidence of Philadelphia chromosome-like acute lymphoblastic leukemia in older adults with B-ALL. Leukemia. 2017;31(4):981-984.
39. Ding YY, Stern JW, Jubelirer TF, et al. Clinical efficacy of ruxolitinib and chemotherapy in a child with Philadelphia chromosome-like acute lymphoblastic leukemia with GOLGA5-JAK2 fusion and induction failure. Haematologica. 2018:103(9):e427-e431.
40. Irving J, Matheson E, Minto L, et al. Ras pathway mutations are prevalent in relapsed childhood acute lymphoblastic leukemia and confer sensitivity to MEK inhibition. Blood. 2014;124(23):3420-3430.
41. Walker AR, Byrd JC, Blachly JS, et al. Entospletinib in combination with induction chemotherapy in previously untreated acute myeloid leukemia: response and predictive significance of HOXA9 and MEIS1 expression. Clin Cancer Res. 2020; 26(22):5852-5859.
42. Kohrer S, Havranek O, Seyfried F, et al. Pre-BCR signaling in precursor B-cell acute lymphoblastic leukemia regulates PI3K/AKT, FOXO1 and MYC, and can be targeted by SYK inhibition. Leukemia. 2016;30(6):1246-1254.
43. van der Veer A, van der Velden VHJ, Willemse ME, et al. Interference with pre-B-cell receptor signaling offers a therapeutic option for TCF3-rearranged childhood acute lymphoblastic leukemia. Blood Cancer J. 2014;4(2):e181.
44. Hurtz C, Tasian SK, Wertheim GB, et al. Redundant JAK, SRC and PI3 kinase signaling pathways regulate cell survival in human Ph-like ALL cell lines and primary cells. Blood. 2017;130(Suppl 1):717.
45. Hurtz C, Wertheim GB, Loftus JP, et al. Oncogene-independent adaptation of pre-B cell receptor signaling confers drug resistance and signaling plasticity in Ph-like ALL. Blood. 2019;134(S1):747.
46. Matheson EC, Thomas H, Case M, et al. Glucocorticoids and selumetinib are highly synergistic in RAS pathway mutated childhood acute lymphoblastic leukemia through upregulation of BIM. Haematologica. 2019;104(9):1804-1811.
47. Agraz-Doblas A, Bueno C, Bashford-Rogers R, et al. Unraveling the cellular origin and clinical prognostic markers of infant B-cell acute lymphoblastic leukemia using genome-wide analysis. Haematologica. 2019;104(6):1176-1188.
48. Marschalek R. Another piece of the puzzle added to understand t(4;11) leukemia better. Haematologica. 2019;104(6):1098-1100.
49. Bueno C, Calero-Nieto FJ, Wang X, et al. Enhanced hemato-endothelial specification during human embryonic differentiation through developmental cooperation between AF4-MLL and MLL-AF4 fusions. Haematologica. 2019;104(6):1189-1201.
50. Levis M, Brown P, Smith BD, et al. Plasma inhibitory activity (PIA): a pharmacodynamic assay reveals insights into the basis for cytotoxic response to FLT3 inhibitors. Blood. 2006;108(10):3477-3483.
51. Brown PA, Kairalla J, Hilden JM, et al. FLT3 inhibitor correlative laboratory assays impact outcomes in KMT2A-rearranged infant acute lymphoblastic leukemia (ALL) patients treated with lestaurtinib: AALL0631, a Children's Oncology Group Study. Blood. 2019;134(S1):1293.
52. Cooper TM, Cassar J, Eckroth E, et al. A phase I study of quizartinib combined with chemotherapy in relapsed childhood leukemia: a therapeutic advances in Childhood Leukemia and Lymphoma (TACL) Study. Clin Cancer Res. 2016;22 (16):4014-4022.
53. Bernt KM, Zhu N, Sinha AU, et al. MLL-rearranged leukemia is dependent on aberrant H3K79 methylation by DOT1L. Cancer Cell. 2011;20(1):66-78.
54. Daigle SR, Olhava EJ, Therkelsen CA, et al.

Selective killing of mixed lineage leukemia cells by a potent small-molecule DOT1L inhibitor. Cancer Cell. 2011;20(1):53-65.
55. Shukla N, Wetmore C, O'Brien MM, et al. Final report of phase 1 study of the DOT1L inhibitor, pinometostat (EPZ-5676), in children with relapsed or refractory MLL-r acute leukemia. Blood. 2016;128(22):2780.
56. von Stackelberg A, Locatelli F, Zugmaier G, et al. Phase I/phase II study of blinatumomab in pediatric patients with relapsed/refractory acute lymphoblasticl eukemia. J Clin Oncol. 2016;34(36):4381-4389.
57. Driessen EM, van Roon EH, Spijkers-Hagelstein JA, et al. Frequencies and prognostic impact of RAS mutations in MLL-rearranged acute lymphoblastic leukemia in infants. Haematologica. 2013;98(6):937-944.
58. Prelle C, Bursen A, Dingermann T, Marschalek R. Secondary mutations in t(4;11) leukemia patients. Leukemia. 2013;27(6):1425-1427.
59. Kerstjens M, Driessen EM, Willekes M, et al. MEK inhibition is a promising therapeutic strategy for MLL-rearranged infant acute lymphoblastic leukemia patients carrying RAS mutations. Oncotarget. 2017; 8(9):14835-14846.
60. Cremer A, Ellegast JM, Alexe G, et al. Resistance mechanisms to SYK inhibition in acute myeloid leukemia. Cancer Discov. 2020; 10(2):214-231.

ARTICLE

Carfilzomib, cyclophosphamide and dexamethasone for newly diagnosed, high-risk myeloma patients not eligible for transplant: a pooled analysis of two studies

Roberto Mina,[1] Francesca Bonello,[1] Maria Teresa Petrucci,[2] Anna Marina Liberati,[3] Concetta Conticello,[4] Stelvio Ballanti,[5] Pellegrino Musto,[6°] Attilio Olivieri,[7] Giulia Benevolo,[8] Andrea Capra,[1] Milena Gilestro,[1] Piero Galieni,[9] Michele Cavo,[10] Agostina Siniscalchi,[11] Antonio Palumbo,[1°] Vittorio Montefusco,[12] Gianluca Gaidano,[13] Paola Omedé,[1] Mario Boccadoro[1] and Sara Bringhen[1]

[1]Myeloma Unit, Division of Hematology, University of Torino, Azienda Ospedaliero-Universitaria Città della Salute e della Scienza di Torino, Torino; [2]Division of Hematology, Department of Cellular Biotechnologies and Hematology, Sapienza University of Rome, Rome; [3]Università degli Studi di Perugia, Struttura Complessa Universitaria Oncoematologia - Azienda Ospedaliera Santa Maria di Terni, Terni; [4]Division of Hematology, AOU Policlinico-OVE, University of Catania, Catania; [5]Reparto di Ematologia con TMO, Ospedale Santa Maria della Misericordia, Perugia; [6]Hematology Unit, IRCCS-CROB, Rionero in Vulture (PZ); [7]Clinica di Ematologia, Università Politecnica delle Marche, Ancona; [8]Hematology, Città della Salute e della Scienza, Turin; [9]Division of Hematology, Ospedale "C. e G. Mazzoni", ASUR Marche-AV5, Ascoli Piceno; [10]"Seràgnoli" Institute of Hematology, Bologna University School of Medicine, Bologna; [11]UOC Ematologia, Ospedale S. Eugenio, ASLRM2, Rome; [12]Hematology Department, Fondazione IRCCS Istituto Nazionale Tumori, Milano and [13]Division of Hematology, Department of Translational Medicine, Università del Piemonte Orientale, Novara, Italy

°PM is currently at the Department of Emergency and Organ Transplantation, "Aldo Moro" University School of Medicine, Unit of Hematology and Stem Cell Transplantation, AOU Consorziale Policlinico, Bari.

°AP is currently a GlaxoSmithKline AG employee.

Ferrata Storti Foundation

Haematologica 2021
Volume 106(4):1079-1085

ABSTRACT

Despite remarkable advances in the treatment of multiple myeloma (MM) in the last decades, the prognosis of patients harboring high-risk cytogenetic abnormalities remains dismal as compared to that of standard-risk patients. Proteasome inhibitors have been demonstrated to partially ameliorate the prognosis of high-risk patients. We pooled together data from two phase I/II trials on transplant-ineligible patients with MM receiving upfront carfilzomib cyclophosphamide and dexamethasone followed by carfilzomib maintenance. The aim of this analysis was to compare treatment outcomes in patients with standard-risk *versus* high-risk cytogenetic abnormalities detected by fluorescence *in situ* hybridization (FISH) analysis. High risk was defined by the presence of at least one chromosomal abnormality, including t(4;14), del17p and t(14;16). Overall, 94 patients were included in the analysis: 57 (61%) in the standard-risk and 37 (39%) in the high-risk group. Median follow-up was 38 months. In standard-risk *versus* high-risk patients, we observed similar progression-free survival (PFS) (3-year PFS: 52% *vs.* 43%, respectively; *P*=0.50), overall survival (OS) (3-year OS: 78% *vs.* 73%; *P*=0.38), and overall response rate (88% *vs.* 95%; *P*=0.47), with no statistical differences between the two groups. No difference in terms of PFS was observed between patients with or without del17p. Carfilzomib, used both as induction and maintenance agent for transplant-ineligible newly diagnosed MM patients, mitigated the poor prognosis carried by high-risk cytogenetics and resulted in similar PFS and OS as in standard-risk patients. (Registered at *clinicaltrials.gov identifiers: NCT01857115 [IST-CAR-561] and NCT01346787 [IST-CAR-506].*)

Correspondence:

SARA BRINGHEN
sarabringhen@yahoo.com

Received: November 21, 2019.

Accepted: February 19, 2020.

Pre-published: February 27, 2020.

https://doi.org/10.3324/haematol.2019.243428

©2021 Ferrata Storti Foundation

Material published in Haematologica is covered by copyright. All rights are reserved to the Ferrata Storti Foundation. Use of published material is allowed under the following terms and conditions: https://creativecommons.org/licenses/by-nc/4.0/legalcode. Copies of published material are allowed for personal or internal use. Sharing published material for non-commercial purposes is subject to the following conditions: https://creativecommons.org/licenses/by-nc/4.0/legalcode, sect. 3. Reproducing and sharing published material for commercial purposes is not allowed without permission in writing from the publisher.

Introduction

Multiple myeloma (MM) is a plasma cell dyscrasia with a heterogeneous prognosis ranging from a few years to over a decade, according to both disease-related factors (such as albumin and β–2 microglobulin levels, cytogenetic abnormalities [CA] or presence of extramedullary disease) and patient-related factors (age, comorbidities, frailty status).[1-3] To date, one of the most powerful prognostic markers in MM is the presence of either primary (translocations) or secondary (deletions or amplifications) recurrent CA detected by fluorescence *in situ* hybridization (FISH). Deletions of chromosome 17p and TP53 have been reported in 5-20% of MM patients according to the cut-off adopted by laboratories and have been clearly associated with a dismal prognosis.[4] Another adverse CA is t(4;14), which is carried by 12-15% of MM patients and leads to the deregulation of fibroblast growth factor receptor 3 (FGFR3) and multiple myeloma SET domain (MMSET).[5,6] Eventually, the occurrence of t(14;16) has been associated to worse progression-free survival (PFS) and overall survival (OS) in a study published by the Mayo Clinic,[7] although some doubts have been cast by another study by Intergroupe Francophone du Myélome (IFM)[8] and conflicting results have been thereafter reported even in patients treated in the novel agent era. The presence of at least one of these three abnormalities identifies a subgroup of patients at high risk of relapse and death.[9]

MM is mainly a disease of the elderly, with a median age at diagnosis of 69 years.[10] Older patients are usually considered not eligible for high-dose chemotherapy and autologous stem cell transplantation (ASCT). In this patient population, the initial therapeutic approach includes either a triplet proteasome inhibitor (PI)-based regimen (bortezomib-melphalan-prednisone, VMP), a two-drug regimen containing an immunomodulatory agent (IMiD; lenalidomide-dexamethasone, Rd), or a combination of both a PI and an IMiD (bortezomib-lenalidomide-dexamethasone, VRD).[11] In the VISTA study that led to the approval of the VMP combination, the median PFS was 19.8 months in high-risk (HiR) patients by FISH and 23 months in standard-risk (SR) patients (HR:1.29).[12,13] In the FIRST study, among patients receiving continuous Rd, the median PFS was 8.4 months in HiR patients *versus* 31.1 in SR patients.[14,15]

Carfilzomib is a second-generation PI currently approved for relapsed and/or refractory (RR)MM patients. In the phase III ENDEAVOR trial comparing carfilzomib-dexamethasone (Kd) to bortezomib-dexamethasone (Vd), the PFS and OS advantage of Kd observed in the overall population was also retained in HiR patients (median PFS in HiR patients treated with Kd *vs.* Vd: 8.8 *vs.* 6.0 months; P=0.007).[16] Similarly, in the phase III ASPIRE trial, the triplet carfilzomib-lenalidomide-dexamethasone (KRd) proved to be superior to Rd also in patients with HiR CA (median PFS in HiR patients treated with KRd *vs.* Rd: 23.1 *vs.* 13.9 months; P=0.08).[17] Taken together, these results suggest that carfilzomib-based regimens might at least partially overcome the negative impact of HiR cytogenetics in MM patients.

We previously published the results of two phase I/II trials showing that the combination carfilzomib-cyclophosphamide-dexamethasone (KCyd), followed by carfilzomib maintenance, was effective and well tolerated in newly diagnosed (ND) elderly MM patients (NDMM).[18,19] Here we report the results of a pooled analysis of patient data from the two trials aiming at evaluating the efficacy of a carfilzomib-based therapy in SR and HiR patients.

Methods

Study design and treatment

We pooled together data from two phase I/II (IST-CAR-561; *clinicaltrials.gov identifier: NCT01857115*) and phase II (IST-CAR-506; *clinicaltrials.gov identifier: NCT01346787*) studies. Both trials enrolled NDMM patients over 65 years of age or younger but not eligible for ASCT. Ethics committees or institutional review boards at the study sites approved both studies, which were carried out in accordance with the Declaration of Helsinki. All patients provided written informed consent.

Details of study procedures have been published previously.[18-20] Briefly, in both trials treatment consisted of nine 28-day cycles of KCyD followed by maintenance with single-agent carfilzomib until disease progression or intolerance. Carfilzomib was administered once weekly (70 mg/m^2) in the IST-CAR-561 study and twice weekly (36 mg/m^2) in the IST-CAR-506 study. The same doses and schedules of cyclophosphamide (oral 300 mg on days 1, 8 and 15) and dexamethasone (40 mg on days 1, 8, 15 and 22) were used in both studies.

Endpoints

The aim of our analysis was to compare treatment efficacy, in terms of response to therapy, PFS, PFS-2 and OS in patients with SR *versus* HiR cytogenetics receiving carfilzomib-based regimens.

Cytogenetic risk was centrally assessed by FISH analysis and t(4;14), t(11;14), t(14;16), del13 and del17p were evaluated in both studies. A 15% cut-off point was used for detection of translocations and a 10% cut-off point for deletions. FISH analysis was performed on CD138$^+$ purified plasma cells. According to the Revised International Staging System (R-ISS) criteria proposed by the International Myeloma Working Group (IMWG) in 2015, high cytogenetic risk was defined by the presence of at least one CA among del17p, t(4;14) or t(14;16).[21] Patients' fitness was defined according to the IMWG frailty score,[2] and patients were classified as either fit, intermediate fit or unfit.

Statistical analysis

Data from the two trials were pooled together and analyzed. Comparisons between different patient groups were performed using Fisher's exact test. PFS was calculated from the date of enrollment to the date of progression or death, or the date the patient was last known to be in remission. PFS-2 was calculated from the date of enrollment to the date of second relapse/progression or death or the date the patient was last known to be in remission. OS was calculated from the date of enrollment to the date of death or the date the patient was last known to be alive.

Time-to-event data were analyzed using the Kaplan-Meier method; survival curves were compared with the log-rank test. The Cox proportional hazards model was used to estimate the hazard ratio (HR) values and the 95% confidence intervals (CI). All reported P-values were two-sided at the conventional 5% significance level. In order to account for potential confounders, the comparison SR *versus* HiR was adjusted for age, International Staging System (ISS), IMWG Frailty Score and trial (once- *vs.* twice-weekly carfilzomib).

Data were analyzed using R software (version 3.5.1).

Table 1. Patients' characteristics at baseline.

	All patients n=94	Standard-risk patients n=57	High-risk patients n=37
Age			
Median (range)	72 (68-75)	72 (68-75)	72 (68-74)
≥75 years, n (%)	24 (26%)	16 (28%)	8 (22%)
Sex, n (%)			
Male	40 (43%)	24 (42%)	16 (43%)
Female	54 (57%)	33 (58%)	21 (57%)
ISS, n (%)			
I	28 (30%)	19 (33%)	9 (24%)
II	32 (34%)	17 (30%)	15 (41%)
III	34 (36%)	21 (37%)	13 (35%)
FISH, n (%)			
t(4;14)	12 (13%)	–	12 (32%)
t(14;16)	4 (4%)	–	4 (11%)
del17p	22 (23%)	–	22 (59%)
≥2 CA*	1 (1%)	–	1 (3%)
Frailty Score, n (%)			
Fit	53 (56%)	34 (60%)	19 (51%)
Intermediate	29 (31%)	18 (32%)	11 (30%)
Frail	12 (13%)	5 (9%)	7 (19%)
LDH [UI/mmol]			
Median (range)	282.5 (168-361)	288 (198-359)	274 (154-386)
Missing	18 (19%)	13 (23%)	5 (14%)

ISS: International Staging System; FISH: fluorescence *in situ* hybridization; LDH: lactate dehydrogenase; n: number; CA: cytogenetic abnormalities. *At least two cytogenetic abnormalities among t(4;14), t(14;16) and del17p.

Results

Among the 121 patients enrolled in the two trials (63 patients from IST-CAR-561 and 58 patients from IST-CAR-506), complete cytogenetic data were available for 94 patients: 57 patients (61%) in the SR and 37 (39%) in the HiR group according to FISH analysis. Among patients in the HiR group, t(4;14) was present in 12 patients (13%), t(14;16) in four patients (4%), and del17p in 22 (23%) patients. The median percentage of plasma cells with t(4;14) was 80% (range: 15-99), with t(14;16) was 85%, and with del17p was 34% (range: 10-95).

Baseline characteristics were well balanced between SR and HiR patients and are summarized in Table 1. Median age at enrollment was 72 years (range: 60-86) for the entire population; no significant differences in terms of age, sex, ISS stage or frailty status were observed between the two groups.

Median follow-up was 38 months for the entire cohort. Ninety-two of 94 patients started the induction phase (1 withdrew consent and 1 was lost to follow-up before commencing therapy): 56 of 57 in the SR and 36 of 37 in the HiR group. Seventy patients (74%) started the maintenance phase: 42 (74%) in the SR and 28 (76%) in the HR group (P=1.00). The median duration of treatment was 16.9 months in SR patients and 14.6 months in HiR patients.

Responses to therapy are shown in Table 2. No significant differences in terms of overall response rate (ORR) were observed between SR and HiR patients both after the induction phase (86% and 92%, respectively; P=0.52) and overall (induction and maintenance phases; 88% and 95%, respectively; P=0.47). In addition, the rate of complete response (CR) after the induction phase (19% *vs.* 22%; P=0.80) and the maintenance phase (23% *vs.* 24%; P=1) was similar in SR and in HiR patients.

Median PFS was similar between SR (not reached [NR]) and HiR (27.8 months) patients (HR 0.81, 95%CI: 0.44-1.48; P=0.50); at 3 years, 52% and 43% of patients were alive and free from progression in the two groups, respectively. Median PFS-2 was NR and 44.1 months, respectively (HR 0.67, 95%CI: 0.32-1.39; P=0.28). No significant differences were observed in median OS in SR and HiR patients, respectively (median OS: NR *vs.* NR, HR 0.72, 95%CI: 0.34-1.52; P=0.38), with 78% of patients in the SR and 73% in the HiR group alive at 3 years from diagnosis (Figure 1A-C).

No significant differences in terms of median PFS, PFS-2 and OS were observed among patients with or without del17p (PFS: 35 *vs.* 35.7 months, HR 0.92, 95%CI: 0.47-1.82, P=0.82; PFS-2: 44.1 months *vs.* NR, HR 1.20, 95%CI: 0.55-2.64, P=0.65; OS: 47.5 months *vs.* NR, HR 1.17, 95% CI: 0.52-2.62, P=0.70) (Figure 2). When adopting a higher cut-off for del17p positivity (>20%), no significant difference in PFS was reported between del17p-negative and del17p-positive patients (median: 35.7 *vs.* 35 months).

Discussion

The aim of our analysis was to evaluate whether a carfilzomib-based upfront treatment could abrogate the

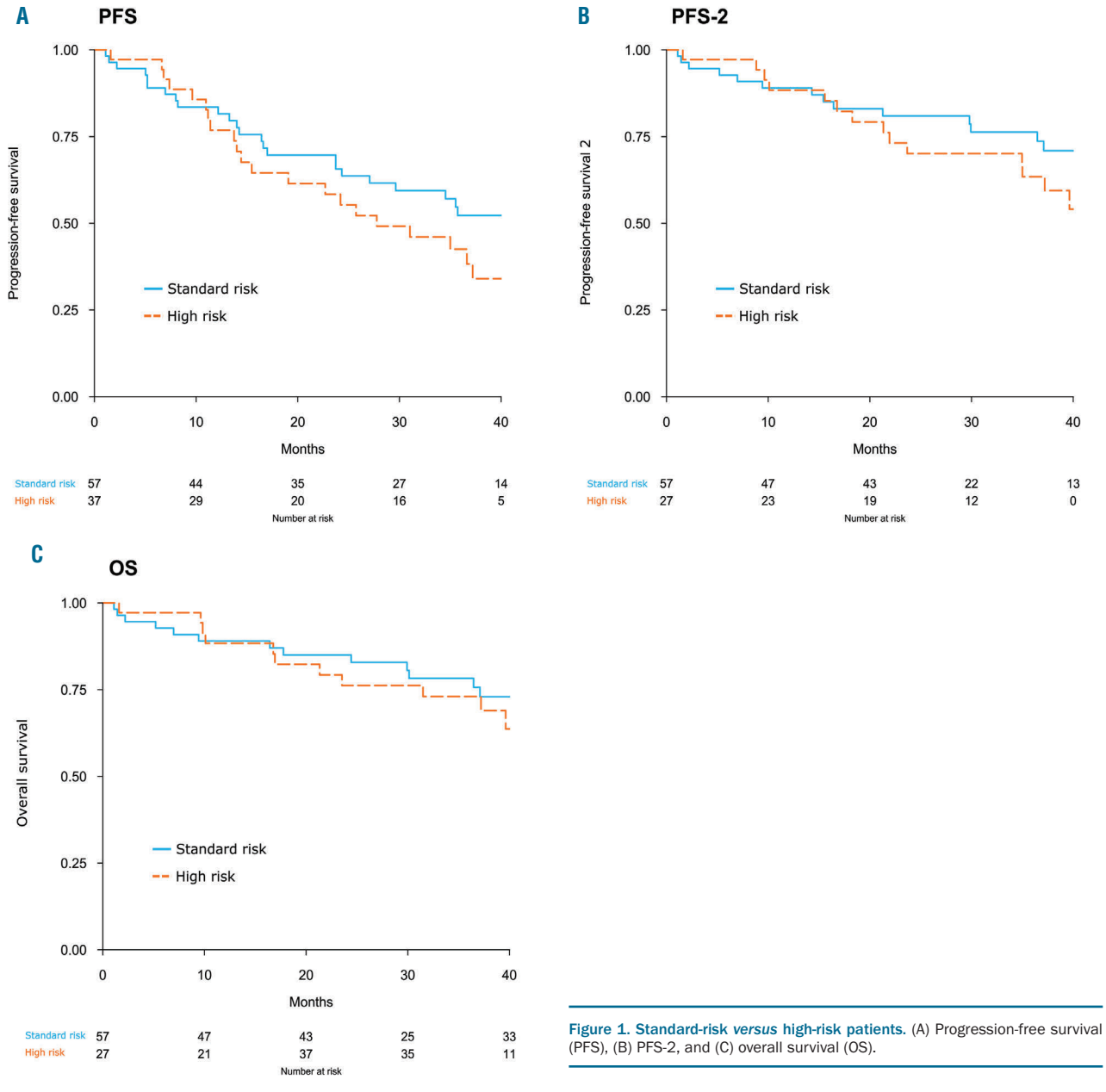


Figure 1. Standard-risk *versus* high-risk patients. (A) Progression-free survival (PFS), (B) PFS-2, and (C) overall survival (OS).

negative impact of HiR cytogenetics and ameliorate the prognosis of transplant-ineligible MM patients carrying HiR CA.

Our results showed similar ORR and CR/stringent CR rates between SR and HiR patients according to the cytogenetic profile, as well as no significant differences in terms of PFS, PFS-2 and OS between the two groups. Furthermore, KCyd seemed to mitigate the poor prognosis conferred by del17p in terms of PFS, PFS-2 and OS.

In Europe, Rd and VMP are currently the first-line regimens of choice for the treatment of older NDMM patients. To date, however, no prospective data on the comparison of VMP and Rd have been published, and the results of the first prospective, phase IV trial comparing these two standards of care are awaited (*clinicaltrials.gov identifier: NCT03829371*). However, we have recently published a pooled analysis of two phase III studies in which patients were treated either with VMP or Rd plus lenalidomide maintenance (Rd-R), showing a PFS (HR: 0.54) and OS (HR: 0.73) advantage in HiR patients receiving bortezomib upfront.[22] These results were in line with those generated in another phase III study in the transplant setting, in which bortezomib partially improved the poor prognosis of HiR patients carrying t(4;14) and/or del17p.[23]

In the ASPIRE trial, the addition of carfilzomib to Rd (KRd) improved the median PFS of approximatively 10 months compared to Rd in patients with HiR cytogenetics, although median PFS in HiR patients treated with KRd (23 months) remained approximatively 6 months shorter than in SR patients (29 months).[17] In the ENDEAVOR trial, the doublet Kd proved to be superior to Vd in HiR patients (HR for PFS: 0.64, 95%CI: 0.45-0.92; *P*=0.007), although median PFS was inferior in HiR *versus* SR patients receiving Kd (8.8 months *vs.* NR, respectively).[16] In HiR RRMM patients, ixazomib in combination with Rd also proved to be effective as compared to Rd (HR 0.54, 95%CI: 0.32-0.91; *P*=0.021), with similar median PFS in HiR and SR patients treated with this triplet (21.4 and 20.6 months,

Table 2. Best response after induction phase and overall (induction and maintenance).

	All patients n=94	Standard-risk patients n=57	High-risk patients n=37
Response after induction			
ORR, n (%)	83 (88%)	49 (86%)	34 (92%)
sCR/CR	19 (20%)	11 (19%)	8 (22%)
VGPR	42 (45%)	25 (44%)	17 (46%)
PR	22 (23%)	13 (23%)	9 (24%)
SD	6 (6%)	4 (7%)	2 (5%)
NA	5 (5%)	4 (7%)	1 (3%)
Response, induction and maintenance			
ORR, n (%)	85 (90%)	50 (88%)	35 (95%)
sCR/CR	22 (23%)	13 (23%)	9 (24%)
VGPR	42 (45%)	25 (44%)	17 (46%)
PR	21 (22%)	12 (21%)	9 (24%)
SD	4 (4%)	3 (5%)	1 (3%)
NA	5 (5%)	4 (7%)	1 (3%)

ORR: overall response rate; CR: complete response; sCR: stringent CR; VGPR: very good partial response; PR: partial response; SD: stable disease; NA: not available; n: number.

respectively).[24] The efficacy of newer PI in HiR patients may be even more pronounced in the upfront setting, in which the probability of HiR patients treated with KRd of achieving at least a very good partial response (≥VGPR) or a CR was similar to that of SR patients.[25] In the phase II FORTE study, similar ≥VGPR rates (79% *vs.* 86%) and minimal residual disease negativity (62% *vs.* 49%) were obtained with eight cycles of KRd irrespective of ASCT in both SR and HiR disease according to the R-ISS.[26] These results confirmed the efficacy in HiR patients that we observed with carfilzomib in the non-transplant setting.

The IMWG recommends the inclusion of a PI in the upfront treatment of HiR NDMM patients.[21] Our results are in line with the evidence that PI, especially those of the second generation such as carfilzomib, can at least partially abrogate the adverse impact of high-risk CA and ameliorate the prognosis of HiR patients.

As we mentioned above, current approved treatment options in transplant-ineligible NDMM patients include Rd, VMP with or without daratumumab and VRD, with Dara-Rd coming soon. Despite the pitfalls of cross-trial comparisons, the median PFS and OS observed in HiR patients receiving carfilzomib-based therapy in our analysis compare favorably with those observed in HiR patients receiving Rd in the FIRST trial[15] (PFS: 8.4 months; OS: 29.3 months) and VMP in the VISTA study[12] (median PFS: 19.8 months), with results similar to those observed in HiR patients treated with Dara-Rd in the phase III MAIA study.[27] Daratumumab, combined to either VMP or Rd, will represent the new standard of care in the upfront treatment of patients ineligible for transplant. The median PFS of patients treated with Dara-VMP was 36.4 months in the recently updated ALCYONE study and NR at 30 months in the MAIA study with Dara-Rd.[28,29] Despite these impressive results, the PFS benefit seemed striking in SR patients (HR 0.39 for Dara-VMP and 0.49 for Dara-Rd), while it was less evident in HiR patients (HR 0.78 for Dara-VMP and 0.85 for Dara-Rd). In the era of anti-CD38-based first-line regimens, HiR genetic lesions are still an unfavorable prognostic factor and HiR patients continue to represent an unmet medical need.

Our analysis has some limitations. First of all, the small

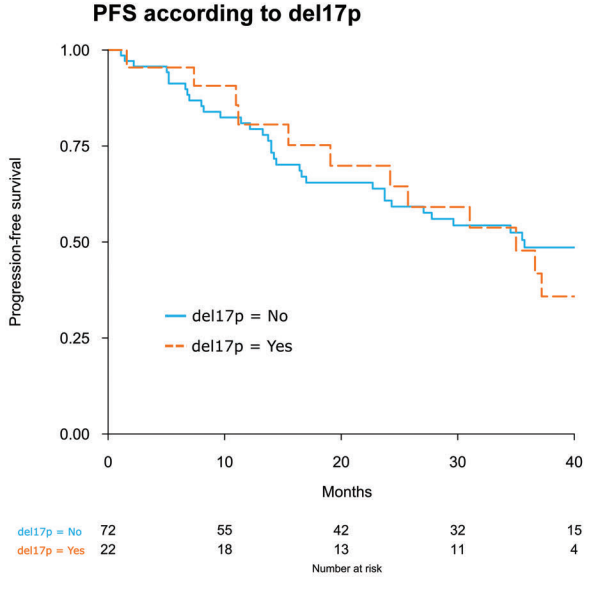


Figure 2. Median progression-free survival (PFS) according to del17p status.

number of patients analyzed does not allow definite conclusions to be drawn on this issue, but prompts further evaluation of carfilzomib as induction therapy in transplant-ineligible patients. We used a 10% cut-off to define the positivity or negativity for del17p, even though the median percentage of plasma cells with del17p was slightly higher (34%; range: 17-80). The exact cut-off to be used to define del17p positivity is a matter of controversy. While the Mayo Clinic group showed no correlation between PFS and OS and the mutational burden in del17p patients, a recent study published by Thakurta *et al.* showed a positive correlation between a high cancer clonal fraction and survival outcomes.[30,31] Remarkably, our results remained consistent when a higher cut-off for del17p positivity was adopted (>20%, as in the ENDEAVOR trial). At the same time as the two trials included in our analysis were being designed, the impact of other HiR

genetic features, such as bi-allelic inactivation, was still unknown, and therefore it could not be addressed in our work.

The prolonged use of carfilzomib in our study may have had a beneficial role in HiR patients. The available evidence suggests that continuous therapy could be superior to fixed duration therapy and could be of particular benefit to HiR patients. However, continuous therapy is not sufficient to overcome the poor prognosis of adverse CA. For example, in the FIRST study, the median PFS of HiR patients treated with continuous Rd was only 9 months.[14,15] In our analysis, the median duration of therapy was similar between SR and HiR patients (16.9 *vs.* 14.6 months), meaning that both groups of patients benefited from prolonged treatment. In conclusion, the results of our pooled analysis suggest that a carfilzomib-based treatment is effective as upfront treatment for HiR, transplant-ineligible MM patients. Carfilzomib may contribute to fill the gap between SR and HiR patients, thus improving the poor prognosis of the latter. Our results provide the basis for a further investigation of carfilzomib as upfront therapy for the treatment of HiR MM patients.

Disclosures

RM has received honoraria from Sanofi, Celgene, Takeda and Janssen; has served on the advisory boards for Sanofi, Takeda, and Janssen; has received consultancy fees from Janssen; MTP has received honoraria from Celgene, Janssen-Cilag, BMS, Takeda, and Amgen, has served on the advisory boards for Celgene, Janssen-Cilag, BMS, Takeda, and Amgen; AML has received honoraria from Janssen, Celgene, Bristol-Myers Squibb, and Servier, has received clinical trial support from Novartis, AbbVie, Roche, Amgen, and Celgene, has served on the advisory boards for AbbVie, Amgen, Takeda, and Servier, and has undertaken consultancy for Incyte; StB has received honoraria for attending meetings from Janssen and Celgene; PM has received personal fees from Amgen, Novartis, BMS, Celgene, Janssen, and Takeda; GB has served on the advisory boards for Novartis, Celgene, and Amgen; MC has received grants from Janssen and Celgene; has received personal fees from Janssen, Celgene, Amgen, BMS, and Takeda; AP is currently a GlaxoSmithKline AG employee; VM has received speaking fees from and served on the advisory boards for Amgen, Celgene, Janssen, and Takeda; GG has served on the advisory boards for Janssen, AbbVie, Astra-Zeneca, and Sunesys, has served on the speakers' bureaus for Janssen, Gilead, and AbbVie; PO has served on the advisory boards for Janssen; MB has received honoraria from Sanofi, Celgene, Amgen, Janssen, Novartis, Bristol-Myers Squibb, and AbbVie; has served on the advisory boards for Janssen and GSK; has received research funding from Sanofi, Celgene, Amgen, Janssen, Novartis, Bristol-Myers Squibb, and Mundipharma; SB has received honoraria from Bristol-Myers Squibb, Celgene, Amgen and Janssen, has served on the advisory boards for Amgen, Karyopharm, Janssen and Celgene, and has received consultancy fees from Takeda and Janssen. The remaining authors have no conflicts of interest to disclose.

Contributions

RM, FB, PO, MB and SB made substantial contributions to the conception or design of the analysis; all authors are responsible for the acquisition, analysis or interpretation of data; RM, FB, AC, MG, PO and SB made the first draft of the manuscript; AC carried out the statistical analysis; MB and SB supervised the analysis; all authors critically revised the manuscript for important intellectual content; all authors gave their final approval of the version to be published; all authors agree to be accountable for all aspects of the work in ensuring that questions related to the accuracy or integrity of any part of the work are appropriately investigated and resolved.

Acknowledgments

We thank the patients who took part in these studies and their families, the study co-investigators, nurses and co-ordinators at each of the clinical sites. We would also like to thank the nurses Rosalia Capobianco and Giacomo Castorina, and the data managers Debora Caldarazzo and Federica Leotta.

Funding

The IST-CAR-561 (NCT01857115) study was sponsored by Stichting Hemato-Oncologie voor Volwassenen Nederland (HOVON, the Netherlands), in collaboration with Fondazione Neoplasie Sangue ONLUS (Italy). The IST-CAR-506 (NCT01346787) study was sponsored by the HOVON Foundation and co-sponsored by Fondazione Neoplasie Sangue ONLUS. Both trials were supported by funding from AMGEN (Onyx Pharmaceuticals), which had no role in study design, data collection, data analysis, data interpretation, writing of the report or publication of this article. The corresponding author had full access to all the data in the two studies, and had final responsibility for the decision to prepare and submit this manuscript for publication, together with the other authors.

References

1. Greipp PR, San Miguel J, Durie BGM, et al. International staging system for multiple myeloma. J Clin Oncol. 2005;23(15):3412-3420.
2. Palumbo A, Bringhen S, Mateos M-V, et al. Geriatric assessment predicts survival and toxicities in elderly myeloma patients: an International Myeloma Working Group report. Blood. 2015;125(13):2068-2074.
3. Larocca A, Dold SM, Zweegman S, et al. Patient-centered practice in elderly myeloma patients: an overview and consensus from the European Myeloma Network (EMN). Leukemia. 2018;32(8):1697-1712.
4. Fonseca R, Bergsagel PL, Drach J, et al. International Myeloma Working Group molecular classification of multiple myeloma: spotlight review. Leukemia. 2009;23(12):2210-2221.
5. Moreau P, Attal M, Garban F, et al. Heterogeneity of t(4;14) in multiple myeloma. Long-term follow-up of 100 cases treated with tandem transplantation in IFM99 trials. Leukemia. 2007;21(9):2020-2024.
6. Gertz MA, Lacy MQ, Dispenzieri A, et al. Clinical implications of t(11;14)(q13;q32), t(4;14)(p16.3;q32), and -17p13 in myeloma patients treated with high-dose therapy. Blood. 2005;106(8):2837-2840.
7. Fonseca R, Blood E, Rue M, et al. Clinical and biologic implications of recurrent genomic aberrations in myeloma. Blood. 2003;101(11):4569-4575.
8. Avet-Loiseau H, Malard F, Campion L, et al. Translocation t(14;16) and multiple myeloma: is it really an independent prognostic factor? Blood. 2011;117(6):2009-2011.
9. Palumbo A, Avet-Loiseau H, Oliva S, et al. Revised International Staging System for Multiple Myeloma: a report from International Myeloma Working Group. J Clin Oncol. 2015;33(26):2863-2869.
10. Howlader N, Noone A, Krapcho M, et al. Cancer Statistics Review, 1975-2015, National Cancer Institute. Based on November 2018 SEER data submission, posted to the SEER web site, April 2019. https://seer.cancer.gov/csr/1975_2015/ [Last accessed 7 Jan 2019]
11. Moreau P, San Miguel J, Sonneveld P, et al. Multiple myeloma: ESMO Clinical Practice Guidelines for Diagnosis, Treatment and Follow-up. Ann Oncol. 2017;28(Suppl 4):iv52-iv61.
12. San-Miguel JF, Schlag R, Khuageva NK, et al. Bortezomib plus melphalan and prednisone for initial treatment of multiple myeloma. N

Engl J Med. 2008;359(9):906-917.
13. San-Miguel JF, Schlag R, Khuageva NK, et al. Persistent overall survival benefit and no increased risk of second malignancies with bortezomib-melphalan-prednisone versus melphalan-prednisone in patients with previously untreated multiple myeloma. J Clin Oncol. 2013;31(4):448-455.
14. Benboubker L, Dimopoulos MA, Dispenzieri A, et al. Lenalidomide and dexamethasone in transplant-ineligible patients with myeloma. N Engl J Med. 2014; 371(10):906-917.
15. Facon T, Dimopoulos MA, Dispenzieri A, et al. Final analysis of survival outcomes in the phase 3 FIRST trial of up-front treatment for multiple myeloma. Blood. 2018;131(3):301-310.
16. Chng W-J, Goldschmidt H, Dimopoulos MA, et al. Carfilzomib-dexamethasone vs bortezomib-dexamethasone in relapsed or refractory multiple myeloma by cytogenetic risk in the phase 3 study ENDEAVOR. Leukemia. 2017;31(6):1368-1374.
17. Avet-Loiseau H, Fonseca R, Siegel D, et al. Carfilzomib significantly improves the progression-free survival of high-risk patients in multiple myeloma. Blood. 2016;128(9):1174-1180.
18. Bringhen S, Petrucci MT, Larocca A, et al. Carfilzomib, cyclophosphamide, and dexamethasone in patients with newly diagnosed multiple myeloma: a multicenter, phase 2 study. Blood. 2014;124(1):63-69.
19. Bringhen S, D'Agostino M, De Paoli L, et al. Phase 1/2 study of weekly carfilzomib, cyclophosphamide, dexamethasone in newly diagnosed transplant-ineligible myeloma. Leukemia. 2018;32(4):979-985.
20. Bringhen S, Mina R, Petrucci MT, et al. Once-weekly versus twice-weekly carfilzomib in patients with newly diagnosed multiple myeloma: a pooled analysis of two phase I/II studies. Haematologica. 2019; 104(8):1640-1647.
21. Sonneveld P, Avet-Loiseau H, Lonial S, et al. Treatment of multiple myeloma with high-risk cytogenetics: a consensus of the International Myeloma Working Group. Blood. 2016;127(24):2955-2962.
22. Larocca A, Mina R, Offidani M, et al. First-line therapy with either bortezomib-melphalan-prednisone or lenalidomide-dexamethasone followed by lenalidomide for transplant-ineligible multiple myeloma patients: a pooled analysis of two randomized trials. Haematologica. 2020; 105(4):1074-1080.
23. Sonneveld P, Goldschmidt H, Rosiñol L, et al. Bortezomib-based versus nonbortezomib-based induction treatment before autologous stem-cell transplantation in patients with previously untreated multiple myeloma: a meta-analysis of phase III randomized, controlled trials. J Clin Oncol. 2013;31(26):3279-3287.
24. Avet-Loiseau H, Bahlis NJ, Chng W-J, et al. Ixazomib significantly prolongs progression-free survival in high-risk relapsed/refractory myeloma patients. Blood. 2017; 130(24):2610-2618.
25. Gay F, Cerrato C, Scalabrini DR, et al. Carfilzomib-lenalidomide-dexamethasone (KRd) induction-autologous transplant (ASCT)-Krd consolidation vs KRd 12 cycles vs carfilzomib-cyclophosphamide-dexamethasone (KCd) induction-ASCT-KCd consolidation: analysis of the randomized FORTE trial in newly diagnosed multiple myeloma (NDMM). Blood. 2018;132(Suppl 1):Abstract #121 [ASH 2018 60th Meeting].
26. Gay F, Rota Scalabrini D, Belotti A, et al. Updated efficacy and MRD data according to risk status in newly diagnosed myeloma patients treated with carfilzomib plus lenalidomide or cyclophosphamide: results from the FORTE trial. HemaSphere. 2018;2(S1):6 [Abstract #S109, EHA 2018 23rd Congress].
27. Facon T, Kumar SK, Plesner T, et al. Phase 3 randomized study of daratumumab plus lenalidomide and dexamethasone (D-Rd) versus lenalidomide and dexamethasone (Rd) in patients with newly diagnosed multiple myeloma (NDMM) ineligible for transplant (MAIA). Blood. 2018;132(Suppl 1):Abstract #LBA-2 [ASH 2018 60th Meeting].
28. Facon T, Kumar S, Plesner T, et al. Daratumumab plus lenalidomide and dexamethasone for untreated myeloma. N Engl J Med. 2019;380(22):2104-2115.
29. Mateos M-V, Dimopoulos MA, Cavo M, et al. Daratumumab plus bortezomib, melphalan, and prednisone for untreated myeloma. N Engl J Med. 2018;378(6):518-528.
30. Lakshman A, Painuly U, Rajkumar SV, et al. Impact of acquired del(17p) in multiple myeloma. Blood Adv. 2019;3(13):1930-1938.
31. Thakurta A, Ortiz M, Blecua P, et al. High subclonal fraction of 17p deletion is associated with poor prognosis in multiple myeloma. Blood. 2019;133(11):1217-1221.

Ferrata Storti Foundation

Haematologica 2021
Volume 106(4):1086-1096

Efficacy of UVC-treated, pathogen-reduced platelets *versus* untreated platelets: a randomized controlled non-inferiority trial

Veronika Brixner,[1*] Gesine Bug,[2*] Petra Pohler,[3*] Doris Krämer,[4] Bernd Metzner,[4] Andreas Voß,[4] Jochen Casper,[4] Ulrich Ritter,[5] Stefan Klein,[6] Nael Alakel,[7] Rudolf Peceny,[8] Hans G. Derigs,[9] Frank Stegelmann,[10] Martin Wolf,[11] Hubert Schrezenmeier,[12] Thomas Thiele,[13] Erhard Seifried,[1] Hans-Hermann Kapels,[14] Andrea Döscher,[14] Eduard K. Petershofen,[14] Thomas H. Müller[3] and Axel Seltsam[3,15]

[1]German Red Cross Blood Transfusion Service and Goethe University Clinics, Frankfurt/Main; [2]Department of Hematology and Oncology, University Hospital Frankfurt, Goethe University, Frankfurt/Main; [3]German Red Cross Blood Service NSTOB, Springe; [4]Department of Oncology and Hematology, University Hospital, Oldenburg; [5]Department of Hematology and Oncology, Municipal Hospital Bremen, Bremen; [6]Department of Hematology and Oncology, University Hospital, Mannheim; [7]Medical Clinic I, Department of Hematology and Oncology, University Hospital, Carl Gustav Carus Faculty of Medicine, Dresden; [8]Department of Hematology and Oncology, Municipal Hospital, Osnabrück; [9]Medical Clinic I, Department of Hematology and Oncology, Carl Gustav Carus Faculty of Medicine, University Hospital, Dresden; [10]Department of Internal Medicine III, University Hospital, Ulm; [11]Department of Hematology and Oncology, Municipal Hospital, Kassel; [12]Institute for Transfusion Medicine, University Hospital Ulm, Ulm; and Institute for Clinical Transfusion Medicine and Immunogenetics Ulm, German Red Cross Blood Service Baden-Württemberg - Hessia, Ulm; [13]Institute for Immunology and Transfusion Medicine, Department of Medicine, University of Greifswald, Greifswald; [14]German Red Cross Blood Service NSTOB, Oldenburg and [15]Bavarian Red Cross Blood Service, Nuremberg, Germany

**VB, GB and PP contributed equally as co-first authors*

ABSTRACT

Pathogen reduction (PR) technologies for blood components have been established to reduce the residual risk of known and emerging infectious agents. THERAFLEX UV-Platelets, a novel ultraviolet C (UVC) light-based PR technology for platelet concentrates, works without photoactive substances. This randomized, controlled, double-blind, multicenter, non-inferiority trial was designed to compare the efficacy and safety of UVC-treated platelets to that of untreated platelets in thrombocytopenic patients with hematologic-oncologic diseases. The primary objective was to determine non-inferiority of UVC-treated platelets, assessed by the 1-hour corrected count increment (CCI) in up to eight per-protocol platelet transfusion episodes. Analysis of the 171 eligible patients showed that the defined non-inferiority margin of 30% of UVC-treated platelets was narrowly missed as the mean differences in 1-hour CCI between standard platelets *versus* UVC-treated platelets for intention-to-treat and per-protocol analyses were 18.2% (95% Confidence Interval [CI]: 6.4-30.1) and 18.7% (95% CI: 6.3-31.1), respectively. In comparison to the control, the UVC group had a 19.2% lower mean 24-hour CCI and was treated with an about 25% higher number of platelet units, but the average number of days to the next platelet transfusion did not differ significantly between both treatment groups. The frequency of low-grade adverse events was slightly higher in the UVC group and the frequencies of refractoriness to platelet transfusion, platelet alloimmunization, severe bleeding events, and red blood cell transfusions were comparable between groups. Our study suggests that transfusion of pathogen-reduced platelets produced with the UVC technology is safe but non-inferiority was not demonstrated. (*clinicaltrials gov. Identifier: DRKS00011156*).

Correspondence:

AXEL SELTSAM
a.seltsam@blutspendedienst.com

Received: May 26, 2020.

Accepted: November 6, 2020.

Pre-published: February 4, 2021.

https://doi.org/10.3324/haematol.2020.260430

©2021 Ferrata Storti Foundation

Material published in Haematologica is covered by copyright. All rights are reserved to the Ferrata Storti Foundation. Use of published material is allowed under the following terms and conditions: https://creativecommons.org/licenses/by-nc/4.0/legalcode. Copies of published material are allowed for personal or internal use. Sharing published material for non-commercial purposes is subject to the following conditions: https://creativecommons.org/licenses/by-nc/4.0/legalcode, sect. 3. Reproducing and sharing published material for commercial purposes is not allowed without permission in writing from the publisher.

Introduction

Improvements in donor screening, Good Manufacturing Practice (GMP) and viral marker testing have significantly reduced the incidence of transfusion-transmitted infections. However, the blood supply remains under threat from various disease-causing agents, including known pathogens which are often not assayed in conventional blood screening protocols, i.e., bacteria and human cytomegalovirus, low-titer viruses that escape detection early after infection, and novel emerging transfusion-transmissible pathogens such as Zika virus and hepatitis E virus.[1,2] While techniques reducing the biological activities of pathogens in red blood cells are still under development, techniques for platelet and plasma products have been introduced or are under consideration as additional safety measure in an increasing number of countries.[3,4] Current methods for platelets use chemical reagents (amotosalen or riboflavin) in combination with ultraviolet (UV) light.[5] However, chemical additives and/or their photoproducts potentially increase the risk of adverse effects, such as immune reactions or toxicity, especially in polytransfused patients.

The THERAFLEX UV-Platelets (Macopharma, Mouvaux, France) method for pathogen reduction (PR) of platelet products is based on treatment with UVC light alone, without any photoactive substances.[6] UVC is absorbed by nucleic acids, resulting in the formation of pyrimidine dimers, which block the elongation of nucleic acid transcripts. It was shown that UVC treatment significantly reduces the infectivity of platelet concentrates (PC) contaminated by pathogenic viruses, bacteria and parasites.[7-12] Moreover, this technique was shown in a mouse model to achieve sufficient white cell inactivation to prevent transfusion-associated graft-*versus*-host disease (TA-GvHD).[13] Several studies have shown that UVC-treated platelets meet the quality requirements for PC.[14-16] This randomized controlled non-inferiority trial evaluated the clinical efficacy and safety of pathogen-reduced PC produced using UVC illumination technology compared to that of conventional untreated PCs in thrombocytopenic hematology-oncology patients.

Methods

Study design

CAPTURE (Clinical Assessment of Platelets Treated with UVC in Relation to Established Preparations) was designed as a randomized, double-blind, parallel controlled, non-inferiority trial. The trial protocol was approved by a the central ethic committee. Ten hematology/oncology centers in Germany participated in the study. The treatment period started on the day of the first study platelet transfusion and continued for a maximum of 28 days. A safety follow-up period began after the treatment period and continued for 30 days or until the day of early withdrawal, loss to follow-up, or death of the subject, depending on which occurred first (*Online Supplementray Figure S1* in the *Online Supplementary Appendix*).

Adult patients with hematologic or oncologic diseases and with thrombocytopenia or who were expected to become thrombocytopenic after chemotherapy or due to underlying active disease were eligible to participate in the study if they were expected to receive at least one platelet transfusion. All individuals involved in the clinical care, assessment and trial management of the patients were blinded.

Treatment

Reference and UVC-treated platelet products were either collected by apheresis or prepared from five buffy coats and resuspended in platelet additive solution (PAS). PR of PC was performed within 6 hours after apheresis platelet collection or 6 hours after preparation of the pooled platelet unit using the THERAFLEX UV-Platelets system.[6] Reference platelets were left untreated or were γ-irradiated if indicated. UVC-treated products generally were not γ-irradiated. Patients in both treatment arms received platelet transfusions prophylactically (trigger 10,000/μL) or for treatment of bleeding.

Study endpoints

The primary efficacy endpoint, the 1-hour CCI, was measured 30-90 minutes post-transfusion for each of a maximum of eight per-protocol platelet transfusion episodes per patient administered within the treatment period. The patient's pre-transfusion platelet count, which was used for this calculation, had to be measured within 12 hours before the start of transfusion. CCI was calculated using the formula:

$$CCI = \frac{Post-precount \times 10^9 L \; Platelet\; dose\; tranfused \times 10^{11} \times BSA}{}$$

$$BSA\,(Body\; Surface\; Area) = 0.20247 \times Height\; m^{0.725} \times Weight\; kg^{0.425}$$

Secondary efficacy endpoints included the variables 24-hour CCI, 1-hour count increment (CI), 24-hour CI (specimens collected 18-30 hours post-transfusion were considered time compliant), number of platelet transfusions per patient, number of red blood cell (RBC) transfusions per patient, and interval between study platelet transfusions. Secondary safety endpoints included adverse events, clinical and immunological refractoriness, severe bleeding events (World Health Organization [WHO] grade 3 and 4), and alloimmunization to UVC-induced neoantigens on platelets.

Statistical analyses

The study was designed as a one-sided non-inferiority trial comparing the 1-hour CCI of UVC-treated PC transfusions with those of untreated PC transfusions to test the null-hypothesis and demonstrate that pathogen-reduced platelets are non-inferior to control platelets. The non-inferiority criterion was met if the upper limit of the 95% Confidence Interval (CI) of the mean difference in 1-hour CCI between the control and UVC groups was below the lower limit of the zone of non-inferiority (based on the results of previous studies with alternative PR methods[17-25] an up to 30% reduction of 1-hour CCI was considered non-inferior). A total of 166 patients were required (83 per arm).

Results

Patients

Out of a total of 177 patients screened at 10 study sites between October 2016 and January 2019, 175 were enrolled in the study and randomized to the UVC arm (n=89) or control arm (n=86) (Figure 1). Two patients in each arm did not receive the first platelet transfusion within the specified time period of 6 weeks after randomization and were excluded from the study. The intention-to-treat (ITT) analyses were thus performed on 171 patients. After excluding patients who received off-protocol transfusions and/or study platelet transfusions from the wrong treatment arm or who met exclusion criteria, the data set

Table 1. Baseline characteristics of study patients.

Parameter		UVC	Control	P
Patients	n	87	84	
Male/female	n/n	55/32	52/32	0.876
Age	Years, mean ± SD	56.67 ± 14.11	54.79 ± 11.90	0.348
Ethnicity				0.377
Caucasian	n (%)	85 (97.70)	84 (100.00)	
Asian	n (%)	1 (1.15)	0 (0.00)	
Other	n (%)	1 (1.15)	0 (0.00)	
Body surface area	m^2, mean ± SD	1.95 ± 0.20	1.97 ± 0.23	0.525
Previous pregnancy	n/total n of women (%)	27/32 (84.38)	23/32 (71.88)	0.365
Treatment modality				
Inpatients	n (%)	86 (98.85)	83 (98.81)	1.000
Outpatients	n (%)	1 (1.15)	1 (1.19)	
Primary diagnosis				0.105
Acute lymphoblastic leukemia	n (%)	7 (8.05)	2 (2.38)	
Acute myeloid leukemia	n (%)	40 (45.98)	30 (35.71)	
Chronic leukemia	n (%)	1 (1.15)	0 (0.00)	
Multiple myeloma	n (%)	22 (25.29)	26 (30.95)	
Non-Hodgkin lymphoma	n (%)	9 (10.34)	16 (19.05)	
Hodgkin lymphoma	n (%)	0 (0.00)	3 (3.57)	
Other	n (%)	8 (9.20)	7 (8.33)	
Treatment				0.118
Autologous stem cell transplantation	n (%)	29 (33.33)	41 (48.81)	
Allogenic stem cell transplantation	n (%)	6 (6.90)	5 (5.95)	
Chemotherapy only	n (%)	52 (59.77)	38 (45.24)	
Transfusion history				
Platelets	n (%)	55 (63.22)	45 (53.57)	0.217
Red blood cells	n (%)	54 (62.07)	57 (67.86)	0.522
Laboratory values prior (< 12 hours) to 1st transfusion				
Platelet count	10^9/L, mean ± SD	59.05 ± 75.21	52.04 ± 61.05	
Hemoglobin	g/L, mean ± SD	91.15 ± 14.04	93.54 ± 13.92	
International normalized ratio	mean ± SD	1.02 ± 0.11	1.04 ± 0.15	
Activated partial thromboplastin time	s, mean ± SD	28.66 ± 5.98	28.44 ± 5.28	
Prothrombin time	%, mean ± SD	97.41 ± 15.49	97.79 ± 16.44	
Fibrinogen	g/L, mean ± SD	3.16 ± 1.23	3.29 ± 0.90	
D-Dimer	ng/mL, mean ± SD	2935.75 ± 4086.45	1347.63 ± 357.09	

UVC: ultraviolet C; SD: standard deviation: INR: international normailzed ratio; s: seconds.

for the PP analyses consisted of 146 patients. One UVC arm patient who withdrew his informed consent after the first platelet transfusion but agreed to further documentation of adverse events was included in the ITT and PP populations. The planned safety follow-up could not be carried out in a total of six patients. There were no significant differences in the patient characteristics of the two study groups (Table 1).

Transfusions

In the ITT set, a total of 568 platelet units were transfused, 320 to patients in the UVC arm and 248 to those in the control arm. In the PP set, a total of 432 platelet units were transfused, 249 to patients in the UVC arm and 183 to those in the control arm (Tables 2-4). Most of the transfusions were platelets administered as single units given prophylactically and were performed with apheresis platelet units due to higher recruitment rates in study centers that were using apheresis platelets only (Table 2). The mean pre-transfusion platelet count was about $12x10^9$/L and did not differ between the two arms. In the control arm, the majority of transfused platelet units (ITT: 77.8%; PP: 78.1%) were γ-irradiated. Only 4% of platelet transfusions in the UVC arm and 5% in the control arm were off-protocol transfusions (*Online Supplementary Table S1*). Platelet characteristics were similar between study arms.

Platelet transfusion efficacy

All patients in the UVC arm and 96% (81 of 84) of the controls were evaluable for analysis in the ITT population. The mean 1-hour CCI value, the primary outcome, was 12.70% (95% CI: 11.42-13.97) in the UVC group and 15.53% (95% CI: 14.18-16.88) in the control group. The mean difference in 1-hour CCI between the control and

Table 2. Platelet transfusion characteristics and pre-transfusion count (based on intention-to-treat anlysis).

Parameter		UVC	Control	P
Platelet transfusions	n	320	248	**0.041**
Apheresis platelets	n	223	166	0.060
Buffy-coat platelets	n	97	82	0.396
Transfusion episodes*	n	316	245	**0.038**
Single dose	n (%)	312 (98.73)	242 (98.78)	
Multi-dose	n (%)	4 (1.27)	3 (1.22)	
Indication for platelet transfusion†				0.211
Trigger based	n (%)	302 (98.69)	236 (100.00)	
Prior to intervention	n (%)	3 (0.98)	0 (0.00)	
Treatment of active bleeding	n (%)	1 (0.33)	0 (0.00)	
ABO incompatibility†				0.353
Major	n (%)	32 (10.46)	22 (9.32)	
Minor	n (%)	82 (26.80)	52 (22.03)	
Major and minor	n (%)	10 (3.27)	13 (5.51)	
No mismatch	n (%)	182 (59.48)	149 (63.14)	
Platelet dose per single transfusion†	x 10^{11}, mean ± SD	3.26 ± 0.37	3.30 ± 0.37	0.242
Storage time†	Days, mean ± SD	2.87 ± 1.18	2.93 ± 1.23	0.488
Mean pre-transfusion platelet count*	10^9/L, mean ± SD	12.58 ± 6.64	12.14 ± 7.70	0.544

*Transfusion episode = two or more platelet transfusions on the same day, whereby the interval between two consecutive transfusion is less than 2 hours †Only per-protocol transfusions were included in these analyses. UVC: ultraviolet C; SD: standard deviation.

UVC groups was 18.24% (95% CI: 6.40-30.08). For analysis in the PP population, 75 patients in the UVC arm and 71 patients in the control arm were evaluable. The mean 1-hour CCI value was 13.18% (95% CI: 11.80-14.56) in the UVC group and 16.21% (95% CI: 14.73-17.70) in the control group. The mean difference in 1-hour CCI between the control and UVC groups was 18.70% (95% CI: 6.33-31.07). Thus, the upper bounds of the 95% CI slightly exceeded the specified margin of 30% with both ITT and PP approaches, indicating that non-inferiority cannot be claimed (Tables 3 -4, Figure 2). Results for all secondary efficacy endpoints are given in Tables 3-4. For the ITT population, the mean values for platelet count increment parameters were lower in the UVC group than in the control group: 18.5% for 1-hour CI, 20.4% for 24-hour CI and 19.2% for 24-hour CCI. Patients in the UVC arm received about 25% more platelet transfusions than patients in the control arm. Accordingly, the mean total dose of platelets transfused per patient was significantly higher in the UVC arm than in the control arm. The mean time interval between platelet transfusions and the mean number of RBC transfusions did not differ significantly between arms. Comparable results were obtained for the PP analysis.

Alloimmunization and refractoriness

Antibodies against platelet antigens were detected in 10.3% and 8.3% of patients of the UVC arm and control arm, respectively, prior to the first study platelet transfusion. Platelet antibodies developed in six patients who tested negative at the beginning of the study: one patient in the UVC arm (human leukocyte antigen [HLA] class I) and five patients in the control arm were affected (three HLA class I, one human platelet antigen [HPA], one HLA class I plus HPA; *data not shown*). The number of refractory episodes and the number of patients with refractory episodes did not differ significantly between groups (Table 5). Immunological refractoriness due to HLA class I antibodies was determined in two patients in the UVC arm and one patient in the control arm; the HLA antibodies were detectable prior to the first study platelet transfusion in all three cases. Platelet antibodies to UVC-related neoantigens were not detected in this study.

Safety

A total of 1,374 adverse events were documented, 741 in the UVC arm and 633 in the control arm (Table 6). At least one adverse event occurred in 85 patients in the UVC group and in 80 patients in the control arm (*Online Supplementary Table S2*). The majority of adverse events were non-serious grade 1 and 2 events that were unrelated to the platelet transfusions. The number of mild grade 1 and 2 non-serious adverse events related to platelet transfusion was significantly higher in the UVC arm than in the control arm. The difference between arms was still of only borderline significance when we compared the ratios per platelet transfusion and patient that were calculated to account for the higher number of platelet transfusions in the UVC arm. The symptoms of the reported transfusion-related adverse events were mainly those known to be associated with platelet transfusions, such as chills, pyrexia, hypersensitivity (allergic reactions), refractoriness and rash (*Online Supplementary Table S3*). Ten serious adverse events were recorded in each treatment arm; they affected ten patients in the UVC arm and eight in the control arm; none of these serious adverse events were related to the platelet transfusions. Severe bleeding (WHO grade 3 and 4) was observed in one patient in the control arm but in none in the UVC arm. There was no statistically significant difference in mortality between arms (Table 6).

Discussion

This multicenter, randomized controlled study was designed to evaluate the efficacy and safety of pathogen-

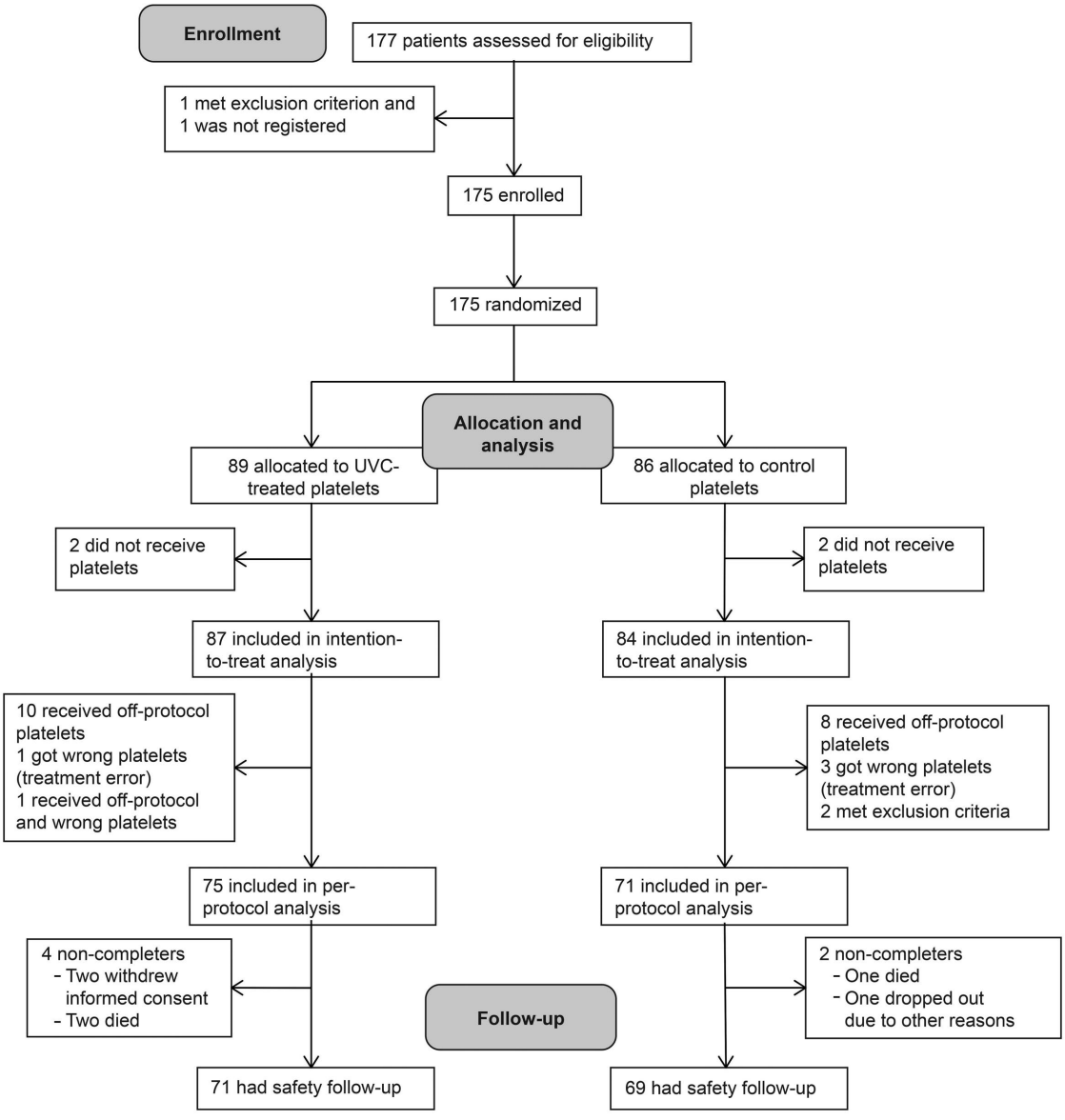


Figure 1. CAPTURE/CONSORT study flow diagram. Off-protocol platelet transfusions were defined as transfusions of conventional platelet units, and treatment errors were defined as transfusions with study platelet products from the wrong treatment arm.

reduced platelets produced by THERAFLEX UV-Platelets PR technology in thrombocytopenic patients with hematologic or oncologic malignancies. One-hour CCI was frequently used as a primary or secondary outcome in previous clinical studies with standard and pathogen-reduced platelets.[17-26] With one exception,[24] the transfusion of pathogen-reduced platelets in these studies resulted in a reduction of mean 1-hour CCI, ranging from 12% to 31% for amotosalen/UVA-treated PC and from 30% to 38% for riboflavin/UV-treated PC. Based on these findings obtained with two alternative PR methods, we set the non-inferiority margin for the mean 1-hour CCI at 30%. This margin is supported by the result of the PLADO trial investigating single transfusions with platelet doses between $1.1x10^{11}$ and $4.4x10^{11}$ per square meter of body-surface area in the prophylactic transfusion setting.[26] The median 4-hour post transfusion CCI in the low dose platelet group of PLADO was 10 (interquartile range, 5-15) and in the medium dose group also 10 (interquartile range, 6-16). The frequency and severity of bleeding events (WHO grade ≥2) in both groups were not higher than that in patients in the high dose group. With a mean platelet dose of $1.7x10^{11}/m^2$ in pathogen-reduced PC in our trial, a CCI reduction by 30% corresponds to a mean dose of $1.2x10^{11}/m^2$ which is still within the range of the PLADO trial. The about 18% lower mean 1-hour CCI, which is very consistent with the result of a radiolabeling study,[16] and the 19% lower mean 24-hour CCI in our study suggest a reduced transfusion efficacy for UVC-treated platelets compared to untreated platelets. There are other product-related factors such as the use of a platelet additive solution (PAS) and γ-irradiation that also affect CCI outcome.[24,27] In our study, UVC-treated platelets were generally not γ-irradiated and PAS was used for preparation of both test and control platelet units. Therefore, the lower CCI for UVC-treated platelet transfusions are likely due to

Table 3. Efficacy endpoints (based on intention-to-treat analysis).

Parameter		UVC	Control	*P*
Patients	n	87	84	
Platelet transfusions	n	320	248	**0.041**
Platelet transfusion episodes*	n	316	245	**0.038**
Primary endpoint†				
1-hour CCI	mean ± SD	12.70 ± 5.98	15.53 ± 6.09	
	CI 95%	11.42 - 13.97	14.18 - 16.88	
	mean difference (CI 95%)	2.83 (0.99-4.67)		
	mean difference (%) (CI 95%)	18.24 (6.40-30.08)		
Secondary endpoints†				
1-hour CI	mean ± SD	22.05 ± 11.35	27.06 ± 12.25	
	CI 95%	19.63 - 24.47	24.35 - 29.76	
24-hour CI	mean ± SD	15.07 ± 9.65	18.94 ± 11.69	
	CI 95%	13.01 - 17.12	16.37- 21.51	
24-hour CCI	mean ± SD	8.77 ± 5.52	10.85 ± 6.16	
	CI 95%	7.59 - 9.94	9.50 - 12.21	
Platelet transfusions per patient	n, mean ± SD	3.68 ± 2.38	2.95 ± 2.22	**0.041**
Platelet transfusion episodes per patient*	n, mean ± SD	3.47 ± 2.16	2.77 ± 1.95	**0.030**
Total dose of platelets transfused per patient‡	x 10^{11}, mean ± SD	11.45 ± 7.23	9.27 ± 6.50	**0.040**
Interval between platelet transfusions	Days, mean ± SD	2.62 ± 1.75	2.80 ± 1.97	0.586
Red cell transfusions per patient	n, mean ± SD	2.71 ± 2.39	2.20 ± 2.37	0.163

*Transfusion episode, two or more platelet transfusions on the same day, whereby the interval between two consecutive transfusions is less than 2 hours; †The mean corrected count increment (CCI) and count increment (CI) values were calculated as the mean of the average CCI/CI of all transfusions per patient. ‡ Only per-protocol transfusions were included in this analysis. UVC: ultraviolet C; SD: standard deviation; CI: Confidence Interval.

effects on the platelets, such as increased activation, as described for the other PR methods.[28]

Despite the difference in mean 1-hour CCI of less than 20% between control and UVC-treated platelets, the non-inferiority margin of 30% was narrowly missed with upper bounds of 30.1% for the ITT-analysis and 31.1% for the PP-analysis. Although the 1-hour CCI results of this study do not allow to claim non-inferiority of UVC-treated platelets compared to untreated reference platelets, they are well within the range of those reported for the other PR methods.[29] In addition, despite lower mean post-transfusion count increments of UVC-treated platelets, the mean 1-hour and 24-hour CCI values are far above the thresholds that have been established to define successful transfusion.[30]

As platelet transfusions are used to treat and prevent bleeding, there is an obvious need for clinical trials of pathogen-reduced platelet products to assess their efficacy with regard to clinically relevant bleeding. However, the results of previous studies consistently suggest that it is probably unlikely that transfusion studies comparing the clinical efficacy of two different platelet preparations can show a significant difference in the prevention of clinically relevant bleeding unless the products differ substantially.[5] The PLADO trial demonstrated that when following a prophylactic platelet transfusion strategy, which is still the standard of care for most hematology-oncology patients, products with reduced count increments may increase the transfusion frequency but do not necessarily increase the number of clinically relevant bleeding events.[26] In addition, even large studies investigating prophylactic *versus* therapeutic platelet transfusion therapy for hematological cancers in up to 300 patients per arm were too small to detect differences in clinically more relevant bleeding of WHO grade 3 and 4.[31,32] All completed studies of pathogen-reduced platelets, including our trial, followed a prophylactic transfusion regimen and tested products with count increments that were lower than those of the reference product. As expected, a recent Cochrane review and two recently published clinical trials investigating the effectiveness of pathogen-reduced platelets for the prevention of bleeding did not find a difference in the risk of developing clinically severe bleeding compared to standard platelets, although a slight increase in clinically irrelevant WHO grade 2 bleeding was detected in patients in the PR arms.[25,33,34]

It is an ongoing discussion whether CCI can be used as surrogate efficacy marker in platelet transfusion studies.[29] However, in the absence of a suitable relevant bleeding outcome for platelet transfusion studies, we decided to use the 1-hour CCI as primary efficacy endpoint in our study.[35] It is at least a measure for the availability of circulating platelets and was used in almost all previous clinical studies with pathogen-reduced platelets, allowing comparison between the different products.[29]

In accordance with previous studies of pathogen-reduced platelets,[17,18,20,23,25,34] the transfusion of UVC-treated platelets was associated with an increased rate of platelet product utilization. The explanation for the higher usage of pathogen-reduced platelet products compared to the reference products may be that, due to a lower platelet increment, the transfusion trigger was met sooner. It remains to be elucidated whether the lower levels of recovery of pathogen-reduced platelets in the circulation could be the result of the early removal of damaged platelets or of the rapid utilization of activated platelets at sites of injury. However, the fact that there was no significant difference in RBC usage between study arms sug-

Table 4. Efficacy endpoints (based on per-protocol anlysis).

Parameter		UVC	Control	P
Patients	n	75	71	
Platelet transfusions	n	249	183	0.030
Platelet transfusion episodes*	n	245	181	0.028
Primary endpoint†				
1-hour CCI	mean ± SD	13.18 ± 5.98	16.21 ± 6.18	
	CI 95%	11.80 - 14.56	14.73 - 17.70	
	mean difference (CI 95%)	3.03 (1.03-5.04)		
	mean difference (%) (CI 95%)	18.70 (6.33-31.07)		
Secondary endpoints†				
1 hour-CI	mean ± SD	22.94 ± 11.23	28.36 ± 12.65	
	CI 95%	20.36 - 25.53	25.33 - 31.40	
24-hour CI	mean ± SD	15.76 ± 9.82	20.37 ± 11.96	
	CI 95%	13.50 - 18.02	17.50- 23.24	
24-hour CCI	mean ± SD	9.18 ± 5.65	11.62 ± 6.24	
	CI 95%	7.88 - 10.47	10.12 - 13.12	
Platelet transfusions per patient	n, mean ± SD	3.32 ± 2.22	2.58 ± 1.85	0.030
Platelet transfusion episodes per patient*	n, mean ± SD	3.27 ± 2.10	2.55 ± 1.79	0.028
Total dose of platelets transfused per patient‡	x 10^{11}, mean ± SD	10.82 ± 7.13	8.54 ± 6.04	0.040
Interval between platelet transfusions	Days, mean ± SD	2.70 ± 1.80	3.06 ± 2.14	0.372
Red cell transfusions per patient	n, mean ± SD	2.47 ± 2.19	2.10 ± 2.25	0.312

*A transfusion episode was defined as two or more platelet transfusions on the same day where the interval between two consecutive transfusions was less than 2 hours. †Mean corrected count increment (CCI) and count increment (CI) values were calculated as the mean of the average CCI/CI of all transfusions per patient. ‡Only per-protocol transfusions were included in this analysis. UVC: ultraviolet C; SD: standard deviation; CI: Confidence Interval.

Table 5. Refractoriness to platelet transfusions (based on intention-to-treat analysis).

Parameter		UVC	Control	P
Refractory episodes*	n	15	6	0.055
Patients with at least one refractory episode	n (%)	14 (16.09)	6 (7.14)	0.095
Single episode of refractoriness	n (%)	13 (92.86)	6 (100.00)	
Multiple episodes of refractoriness	n (%)	1 (7.14)	0 (0.00)	
Immunological refractoriness†	n (%)	2 (14.29)	1 (16.67)	1.000
Antibodies to HLA class I	n (%)	2 (100.00)	1 (100.00)	
Antibodies to HPA	n (%)	0 (0.00)	0 (0.00)	
Antibodies to UVC-related neoantigens	n (%)	0 (0.00)	0 (0.00)	

*Episode of "clinical" refractoriness, defined as two consecutive transfusions, each with a 1-hour CCI < 7.5. †Episode of "clinical" refractoriness in the presence of platelet antibodies. No immunologic refractoriness due to seroconversion was recorded. UVC: ultrviolet C; HLA: human leukocyte antigen; HLP: human platelet antigen.

gests that the hemostatic function of UVC-treated and reference platelets was equivalent.

An increase in the utilization of platelet units due to reduced increments of pathogen-reduced platelets would have clinically and economically relevant effects. While randomized controlled clinical trials consistently report that pathogen-reduced platelets are associated with a higher number of transfusions per patient, surveillance studies did not show increased usage of PC after universal adaption of a routinely used PR technology.[36,37] This contradictory result may be explained by the fact that PR implementation in routine practice is often associated with changes in PC specifications and platelet supply logistics that can impact platelet quality. In routine practice, the requirement for generally higher platelet contents in pathogen-reduced PC compared to untreated PC may be a feasible strategy to compensate for the lower recovery of pathogen-reduced platelets, although this could require more blood donations in several settings.[38]

Adverse events overall occurred at similar frequencies and severities in the treatment and control groups. In particular, transfusion-related adverse events were infrequent and mainly low-grade, in line with current hemovigilance data.[39,40] The higher number of such low-grade transfusion-related adverse events in the UVC arm is due to the fact that episodes of platelet refractoriness, which were more frequently observed in patients receiving UVC-treated platelets, were recorded as transfusion-related low grade 1 and 2 adverse events at some study sites. No unusual adverse events were associated with the transfusion of UVC-treated platelets. Rates of platelet antibodies were low and similar in both arms. Most of the patients with platelet antibodies were pre-immunized prior to the first study platelet transfusion. Similar to the findings reported for other DNA-targeted PR systems, UVC treatment was previously shown to impair direct antigen presentation of antigen-presenting cells in PC, which may possibly reduce alloimmunization in transfusion recipients.[13]

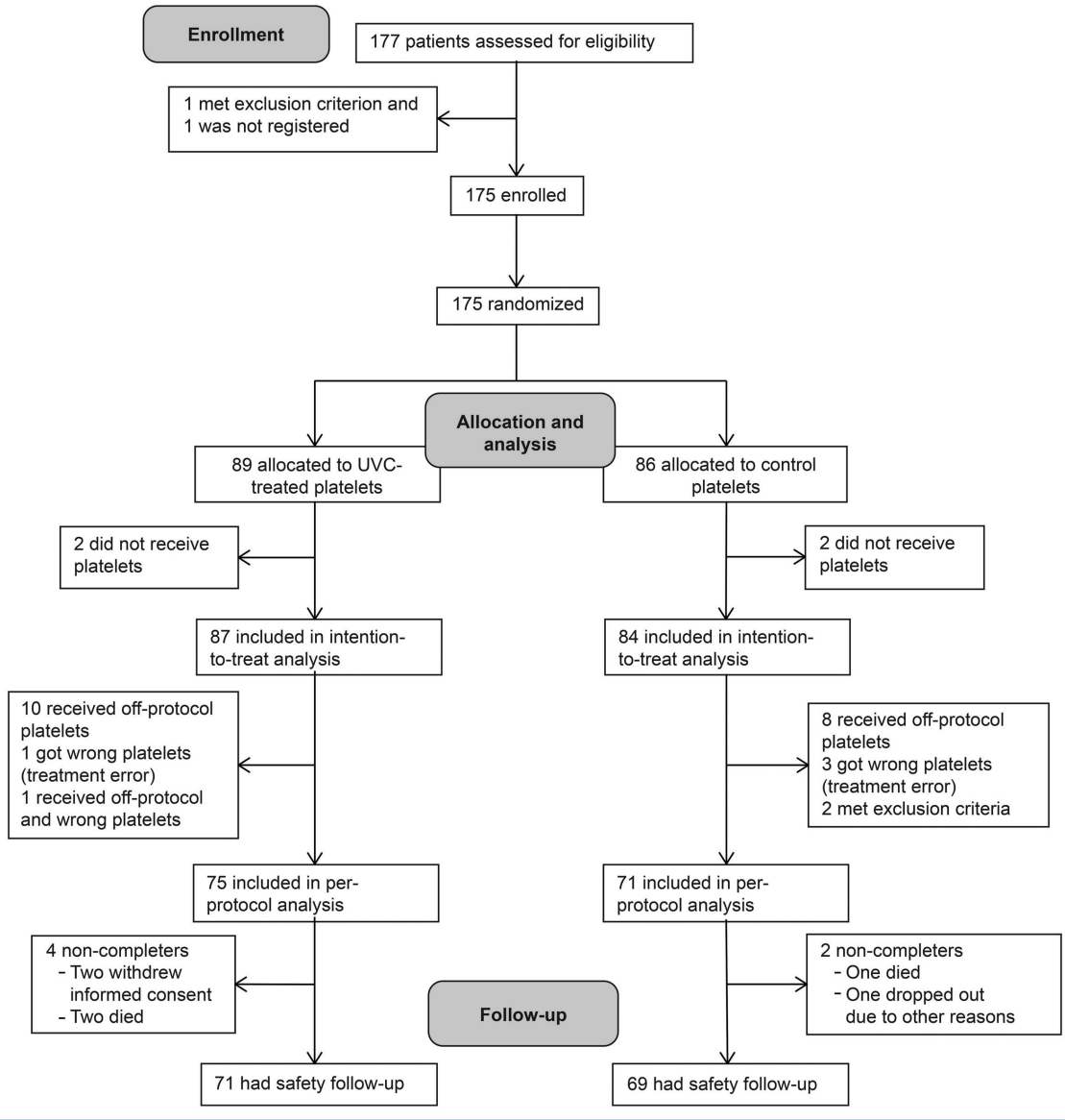


Figure 2. Primary endpoint results. Non-inferiority plot comparing the difference in percentage of the 1-hour corrected count increment (CCI) between the control and UVC (test) arms. The point estimates of the difference in percentage and their 95% Confidence intervals are displayed for the per-protocol (PP) analysis and the intention-to-treat (ITT) analysis. The dotted vertical line shows the predefined non-inferiority margin of 30.0%. For both analyses, the 95% Confidence Interval slightly exceeds the non-inferiority margin.

Reduced immunogenicity of pathogen-reduced treated platelets produced using the riboflavin/UV technology was described in animal studies, but this effect was not observed in clinical studies.[41-43] The low percentage of immunized patients in our study was too small for any conclusion on the immunogenicity of UVC-treated platelets. A systematic review of the data from 2,075 randomized patients enrolled in 12 studies revealed with high-quality evidence that pathogen-reduced platelets increase the risk of platelet refractoriness in adult cancer patients.[33] We also found a higher rate of platelet refractoriness in the test arm of our study, which may be explained, at least in part, by the lower mean CCI of the UVC-treated platelets. As also observed for other pathogen-reduced platelets, the lower CCI translates into a higher portion of transfusions with a platelet recovery below the threshold that indicates successful transfusion.[30]

The THERAFLEX UV-Platelets PR technology was developed for platelets suspended in plasma with SSP+PAS, which has been in routine use in Germany for more than a decade. Although limited data is available in the literature, the CCI of platelets stored in this solution seem to be comparable to those of platelets stored in plasma.[44] Moreover, some evidence obtained with the riboflavin/UV PR system suggests that the use of SSP+ or a similar additive solution protects platelet quality after PR treatment and results in transfusion success rates which are comparable to those of platelets stored in plasma.[45,46] Thus, we expect that the results obtained with UVC-treated platelets compared to untreated platelets in additive solution may also be extended to the comparison with untreated plasma platelets, which are traditionally used as the reference standard.

There are several limitations of our study. The relationship between CCI and clinically significant bleeding has never been shown. In addition, it is a general limitation to

Table 6. Adverse events (based on intention-to-treat analysis).

		UVC	Control	P
Any adverse events*	n	741	633	0.328
Related to platelet transfusion	n (%)	34 (4.59)	11 (1.74)	0.034
Rate per transfusion episode and patient	mean	0.09	0.05	0.127
Unrelated to platelet transfusion	n (%)	707 (95.41)	622 (98.26)	0.457
Non-serious adverse events	n (%)	731 (98.65)	623 (98.42)	0.326
Related to platelet transfusion	n (%)	34 (4.65)	11 (1.77)	0.034
Rate per transfusion episode and patient	Mean	2.69	3.38	0.159
Unrelated to platelet transfusion	n (%)	697 (95.35)	612 (98.23)	0.454
Grade 1 or 2 adverse events	n (%)	617 (84.40)	510 (81.86)	0.255
Related to platelet transfusion	n (%)	33 (5.35)	10 (1.96)	0.031
Rate per transfusion episode and patient	mean	0.09	0.03	0.047
Unrelated to platelet transfusion	n (%)	584 (94.65)	500 (98.04)	0.376
Grade 3 or 4 adverse events	n (%)	114 (15.60)	113 (18.14)	0.895
Related to platelet transfusion	n (%)	1 (0.88)	1 (0.88)	0.987
Unrelated to platelet transfusion	n (%)	113 (99.12)	112 (99.12)	0.897
Serious adverse events	n (%)	10 (1.35)	10 (1.58)	
Related to platelet transfusion	n (%)	0 (0.00)	0 (0.00)	
Unrelated to platelet transfusion	n (%)	10 (100.00)	10 (100.00)	0.940
Patients with severe bleeding (WHO grades 3 and 4)	n (%)	0 (0.00)	1 (1.19)	0.491
Death n (%)	2 (2.30)	2 (2.38)	1.000	

*The causal relationship of an adverse event to a platelet transfusion was classified by the investigators using the imputability levels 'excluded', 'unlikely', 'possible', 'likely/probable', and 'certain'. Adverse events classified as 'excluded' or 'unlikely' were considered as unrelated, while adverse events classified as 'possible', 'likely/probable' or 'certain' were considered as related. UVC: ultrviolet C; WHO: World Health Organisation.

this and other transfusion studies with new platelet products that a consensual non-inferiority margin does not exist. Other trials with pathogen-reduced platelets using the 1-hour CCI as primary endpoint set different non-inferiority margins (e.g., 20% for the MIRACLE trial).[19] However, the suitability of bleeding as efficacy outcome in non-inferiority clinical trials with pathogen-reduced platelets is also under debate.[35] It is a general limitation for clinical trials with pathogen-reduced products that testing the impact of a PR method on blood safety is unfeasible due to the extremely low frequency of infectious transmissions. Nevertheless, the decision to implement a pathogen-reduced product will have to be based on the balance of increased safety for established and emerging pathogens and clinical efficacy, which may be influenced by PR treatment. Randomized controlled trials are generally limited to small numbers of patients and usually focus on patient groups with defined demographic characteristics and treatment indications. In addition, results regarding prophylactic platelet transfusion in adult patients with thrombocytopenia and hematologic diseases are no substitute for clinical studies of pathogen-reduced platelets in pediatric medicine and other clinical contexts, such as post-traumatic coagulopathy. Only postmarketing studies collecting clinical information from standard medical practice in a large number and wide range of patients receiving pathogen-reduced platelet transfusions may allow for a meaningful assessment of rare adverse effects resulting from the use of pathogen-reduced blood products.[47]

Disclosures

VB received grants from the Research Foundation of the German Red Cross Blood Services (Forschungsgemeinschaft der Blutspendedienste des Deutschen Roten Kreuzes) and Macopharma for the development of the UVC-based PI technology for platelets and from CERUS for a clinical trial on PI technology for Red Blood Cells. GB received departmental research funding from Novartis, travel grants from Celgene, Gilead, Neovii and Sanofi and honoraria for advisory board memberships for Celgene, Eurocept, Gilead, Hexal, Novartis, Pfizer and Jazz. PP received grants from the Research Foundation of the German Red Cross Blood Services (Forschungsgemeinschaft der Blutspendedienste des Deutschen Roten Kreuzes) and Macopharma for the development of the UVC-based PI technology for platelets. JC received consultancy fee from Pfizer, Merck, Ipsen, Medac; speaker's bureau fees from Pfizer, Merck, Ipsen, Medac; served as consultant for Pfizer, Merck, Ipsen, Medac; received research funding from Ipsen, Medac; reports membership of the Federal Joint Committee (G-BA) Public Policy and Strategy Committee (non-profit). UR received department honoraria for advisory board memberships for Pfizer, Daiichi-Sankyo, Jazz, Servier and Novartis. NA received speaker's bureau fees from Basilea Pharmaceutica, honoraria for advice from Gilead, MSD Sharp & Dohme GmbH, Pfizer, Amgen and travel grants from Gilead, MSD Sharp & Dohme GmbH, Pfizer, Amgen. RP received consulting fee from Sanofi Genzyme and Pfizer, and received travel and accommodation expenses from Bristol-Myers Squibb. TT received personal fees from Bristol Myers Squibb, Bayer, Daichii Sankyo, Pfizer, Novo Nordisk, Chugai Pharma and Novartis. THM received grants from the Research Foundation of the German Red Cross Blood Services (Forschungsgemeinschaft der Blutspendedienste des Deutschen Roten Kreuzes) and Macopharma for the development of the UVC-based PI technology for platelets, and reports membership for advisory boards (non-profit) for three German Blood Services (Jena, Rostock, Suhl). AS received grants from the Research Foundation of the German Red Cross Blood Services (Forschungsgemeinschaft der Blutspendedienste des Deutschen

Roten Kreuzes) and Macopharma for the development of the UVC-based PI technology for platelets, and honoraria for advisory board memberships for Grifols, Quotient and Imusyn. DK, BM, AV, SK, HGD, FS, MW, HS, ES, H-HK, AD and EKP have no conflicts of interest to disclose.

Contributions

AS, GB, THM, PP, VB contributed to the conception and design of the study; GB, VB, DK, BM, AV, JC, UR, SK, NA, RP, HGD, FS, MW, HS, TT, H-H K, AD, EKP contributed to the acquisition of data; AS, THM, PP analyzed and interpreted the data and wrote the manuscript; GB and ES contributed to the interpretation of the data. All authors critically reviewed and revised the manuscript content and checked the final version of the manuscript. All authors are accountable for all aspects of the work.

Acknowledgments

We are very grateful to all patients who agreed to participate in the CAPTURE trial. Most sincere thanks to Jana Reins, Sabrina Pigur and Doreen Chudziak for study monitoring, to the nursing staff at all participating hospitals for their support, and to Andreas Greinacher (chairman DSMB), Hannes Wandt (member DSMB), and Thomas Kohlmann (member DSMB) for safety oversight. Many thanks to Nancy Heddle for her scientific advice on the design of the study.

Moreover, we wish to thank all blood bank personnel from the German Red Cross Blood Transfusion Service in Frankfurt, Germany and the German Red Cross Blood Service NSTOB in Oldenburg and Springe, Germany for their assistance in the collection, processing, quality monitoring and distribution of the platelet products, and give special thanks to Sarah Dombos, Mesut Karatas, Sebastian Haase, Maren Schepers, Katrin Dahse, Hagen Baume, Ute Gravemann and Anke Wenk. Thanks also to Franz Wagner, Irene Mardt, Nicola Gökbuket and Ina Müller for assessing and processing the serious adverse events.

Thanks to all data managers and statisticians from the Alcedis, Contract Research Organization in Gießen, Germany, particularly Marina Mangold, Sascha Wurmbach, Philipp Schnecko and Claudia Lorenz-Schlüter, and to Macopharma for technical support.

Funding

This work was supported by the Research Foundation of the German Red Cross Blood Services (Forschungsgemeinschaft der Blutspendedienste des Deutschen Roten Kreuzes) and Macopharma S.A.S. Macopharma had no role in data collection, study management or data analyses.

References

1. Stramer SL. Current perspectives in transfusion-transmitted infectious diseases: emerging and re-emerging infections. ISBT Sci Ser. 2014;9(1):30-36.
2. Lanteri MC, Kleinman SH, Glynn SA, et al. Zika virus: a new threat to the safety of the blood supply with worldwide impact and implications. Transfusion. 2016;56(7):1907-1914.
3. Jutzi M, Mansouri Taleghani B, Rueesch M, Amsler L, Buser A. Nationwide implementation of pathogen inactivation for all platelet concentrates in Switzerland. Transfus Med Hemother. 2018;45(3):151-156.
4. Godbey EA, Thibodeaux SR. Ensuring safety of the blood supply in the United States: donor screening, testing, emerging pathogens, and pathogen inactivation. Semin Hematol. 2019;56(4):229-235.
5. Seltsam A, Muller TH. Update on the use of pathogen-reduced human plasma and platelet concentrates. Br J Haematol. 2013; 162(4):442-454.
6. Seltsam A, Muller TH. UVC irradiation for pathogen reduction of platelet concentrates and plasma. Transfus Med Hemother. 2011;38(1):43-54.
7. Mohr H, Gravemann U, Bayer A, Muller TH. Sterilization of platelet concentrates at production scale by irradiation with shortwave ultraviolet light. Transfusion. 2009;49(9):1956-1963.
8. Castro E, Gonzalez LM, Rubio JM, Ramiro R, Girones N, Montero E. The efficacy of the ultraviolet C pathogen inactivation system in the reduction of Babesia divergens in pooled buffy coat platelets. Transfusion. 2014;54(9):2207-2216.
9. Eickmann M, Gravemann U, Handke W, et al. Inactivation of Ebola virus and Middle East respiratory syndrome coronavirus in platelet concentrates and plasma by ultraviolet C light and methylene blue plus visible light, respectively. Transfusion. 2018;58(9):2202-2207.
10. Faddy HM, Fryk JJ, Prow NA, et al. Inactivation of dengue, chikungunya, and Ross River viruses in platelet concentrates after treatment with ultraviolet C light. Transfusion. 2016;56(6):1548-1555.
11. Steinmann E, Gravemann U, Friesland M, et al. Two pathogen reduction technologies--methylene blue plus light and shortwave ultraviolet light--effectively inactivate hepatitis C virus in blood products. Transfusion. 2013;53(5):1010-1018.
12. Gravemann U, Handke W, Muller TH, Seltsam A. Bacterial inactivation of platelet concentrates with the THERAFLEX UV-Platelets pathogen inactivation system. Transfusion. 2019;59(4):1324-1332.
13. Pohler P, Muller M, Winkler C, et al. Pathogen reduction by ultraviolet C light effectively inactivates human white blood cells in platelet products. Transfusion. 2015;55(2):337-347.
14. Pohler P, Lehmann J, Veneruso V, et al. Evaluation of the tolerability and immunogenicity of ultraviolet C-irradiated autologous platelets in a dog model. Transfusion. 2012;52(11):2414-2426.
15. Thiele T, Pohler P, Kohlmann T, et al. Tolerance of platelet concentrates treated with UVC-light only for pathogen reduction--a phase I clinical trial. Vox Sang. 2015;109(1):44-51.
16. Bashir S, Cookson P, Wiltshire M, et al. Pathogen inactivation of platelets using ultraviolet C light: effect on in vitro function and recovery and survival of platelets. Transfusion. 2013;53(5):990-1000.
17. van Rhenen D, Gulliksson H, Cazenave JP, et al. Transfusion of pooled buffy coat platelet components prepared with photochemical pathogen inactivation treatment: the euroSPRITE trial. Blood. 2003;101(6):2426-2433.
18. McCullough J, Vesole DH, Benjamin RJ, et al. Therapeutic efficacy and safety of platelets treated with a photochemical process for pathogen inactivation: the SPRINT Trial. Blood. 2004;104(5):1534-1541.
19. Cazenave JP, Folléa G, Bardiaux L, et al. A randomized controlled clinical trial evaluating the performance and safety of platelets treated with MIRASOL pathogen reduction technology. Transfusion. 2010;50(11):2362-2375.
20. Kerkhoffs JL, van Putten WL, Novotny VM, et al. Clinical effectiveness of leucoreduced, pooled donor platelet concentrates, stored in plasma or additive solution with and without pathogen reduction. Br J Haematol. 2010;150(11):209-217.
21. Janetzko K, Cazenave JP, Kluter H, et al. Therapeutic efficacy and safety of photochemically treated apheresis platelets processed with an optimized integrated set. Transfusion. 2005;45(9):1443-1452.
22. Lozano M, Knutson F, Tardivel R, et al. A multi-centre study of therapeutic efficacy and safety of platelet components treated with amotosalen and ultraviolet A pathogen inactivation stored for 6 or 7 d prior to transfusion. Br J Haematol. 2011;153(3):393-401.
23. Rebulla P, Vaglio S, Beccaria F, et al. Clinical effectiveness of platelets in additive solution treated with two commercial pathogen-reduction technologies. Transfusion. 2017;57(5):1171-1183.
24. Sigle JP, Infanti L, Studt JD, et al. Comparison of transfusion efficacy of amotosalen-based pathogen-reduced platelet components and gamma-irradiated platelet components. Transfusion. 2013;53(8):1788-1797.
25. van der Meer PF, Ypma PF, van Geloven N, et al. Hemostatic efficacy of pathogen-inactivated vs untreated platelets: a randomized controlled trial. Blood. 2018;132(2):223-231.
26. Slichter SJ, Kaufman RM, Assmann SF, et al. Dose of prophylactic platelet transfusions and prevention of hemorrhage. N Engl J Med. 2010;362(7):600-613.
27. Seigeot A, Desmarets M, Rumpler A, et al. Factors related to the outcome of prophylactic platelet transfusions in patients with

hematologic malignancies: an observational study. Transfusion. 2018;58(6):1377-1387.
28. Magron A, Laugier J, Provost P, Boilard E. Pathogen reduction technologies: the pros and cons for platelet transfusion. Platelets. 2018;29(1):2-8.
29. Rebulla P, Garban F, van der Meer PF, Heddle NM, McCullough J. A crosswalk tabular review on methods and outcomes from randomized clinical trials using pathogen reduced platelets. Transfusion. 2020;60(6):1267-1277.
30. Kerkhoffs JL, Eikenboom JC, Schipperus MS, et al. A multicenter randomized study of the efficacy of transfusions with platelets stored in platelet additive solution II versus plasma. Blood. 2006;108(9):3210-3215.
31. Wandt H, Schaefer-Eckart K, Wendelin K, et al. Therapeutic platelet transfusion versus routine prophylactic transfusion in patients with haematological malignancies: an open-label, multicentre, randomised study. Lancet. 2012;380(9850):1309-13016.
32. Stanworth SJ, Estcourt LJ, Powter G, et al. A no-prophylaxis platelet-transfusion strategy for hematologic cancers. N Engl J Med. 2013;368(19):1771-1780.
33. Estcourt LJ, Malouf R, Hopewell S, et al. Pathogen-reduced platelets for the prevention of bleeding. Cochrane Database Syst Rev. 2017;7(7):CD009072.
34. Garban F, Guyard A, Labussiere H, et al. Comparison of the hemostatic efficacy of pathogen-reduced platelets vs untreated platelets in patients with thrombocytopenia and malignant hematologic diseases: a randomized clinical trial. JAMA Oncol. 2018;4(4):468-475.
35. Heddle NM, Cardoso M, van der Meer PF. Revisiting study design and methodology for pathogen reduced platelet transfusions: a round table discussion. Transfusion. 2020;60(7):1604-1611.
36. Osselaer JC, Doyen C, Defoin L, et al. Universal adoption of pathogen inactivation of platelet components: impact on platelet and red blood cell component use. Transfusion. 2009;49(7):1412-1422.
37. Amato M, Schennach H, Astl M, et al. Impact of platelet pathogen inactivation on blood component utilization and patient safety in a large Austrian Regional Medical Centre. Vox Sang. 2017;112(1):47-55.
38. Richtlinie zur Gewinnung von Blut und Blutbestandteilen und zur Anwendung von Blutprodukten (Richtlinie Hämotherapie). In: Bundesärztekammer, ed.2019:1-103.
39. Daurat A, Roger C, Gris J, et al. Apheresis platelets are more frequently associated with adverse reactions than pooled platelets both in recipients and in donors: a study from French hemovigilance data. Transfusion. 2016;56(6):1295-1303.
40. Bolton-Maggs PH. SHOT conference report 2016: serious hazards of transfusion - human factors continue to cause most transfusion-related incidents. Transfus Med. 2016;26(6):401-405.
41. Slichter SJ, Pellham E, Bailey SL, et al. Leukofiltration plus pathogen reduction prevents alloimmune platelet refractoriness in a dog transfusion model. Blood. 2017; 130(8):1052-1061.
42. Jackman RP, Muench MO, Inglis H, et al. Reduced MHC alloimmunization and partial tolerance protection with pathogen reduction of whole blood. Transfusion. 2017;57(2):337-348.
43. Saris A, Kerkhoffs JL, Norris PJ, et al. The role of pathogen-reduced platelet transfusions on HLA alloimmunization in hemato-oncological patients. Transfusion. 2019; 59(2):470-481.
44. Tardivel R, Vasse J, Gaucheron S, Lebaudy J-P, Lamy de la Chapelle T, Semana G. A comparative study of the efficiency of plasma and additive solution preserved platelet concentrates. Vox Sang. 2012;103 (Suppl 1):S247.
45. van der Meer PF, Bontekoe IJ, Daal BB, de Korte D. Riboflavin and UV light treatment of platelets: a protective effect of platelet additive solution? Transfusion. 2015;55(8):1900-1908.
46. Drawz SM, Marschner S, Yanez M, et al. Observational study of corrected count increments after transfusion of platelets treated with riboflavin pathogen reduction technology in additive solutions. Transfusion. 2015;55(7):1745-1751.
47. Corash L, Benjamin RJ. The role of hemovigilance and postmarketing studies when introducing innovation into transfusion medicine practice: the amotosalen-ultraviolet A pathogen reduction treatment model. Transfusion. 2016;56 (Suppl 1):S29-38.

ARTICLE

Impact of luteinizing hormone suppression on hematopoietic recovery after intensive chemotherapy in patients with leukemia

Iman Abou Dalle,[1,2] Ronald Paranal,[3] Jabra Zarka,[1] Shilpa Paul,[4] Koji Sasaki,[1] Wen Li,[5] Jing Ning,[6] Nicholas J. Short,[1] Maro Ohanian,[1] Jorge E. Cortes,[7] Elias J. Jabbour[1] and Ghayas C. Issa[1]

[1]Department of Leukemia, The University of Texas MD Anderson Cancer Center, Houston, TX, USA; [2]Division of Hematology and Oncology, American University of Beirut, Beirut, Lebanon; [3]Department of Medicine, Baylor College of Medicine, Houston, TX, USA; [4]Department of Clinical Pharmacy, The University of Texas MD Anderson Cancer Center, Houston, TX, USA; [5]Division of Clinical and Translational Sciences, Department of Internal Medicine, The University of Texas McGovern Medical School at Houston, Houston, TX, USA; [6]Department of Biostatistics, The University of Texas MD Anderson Cancer Center, Houston, TX, USA and [7]Georgia Cancer Center, Augusta University, Augusta, GA, USA

Ferrata Storti Foundation

Haematologica 2021
Volume 106(4):1097-1105

ABSTRACT

Treatment of acute leukemia with intensive chemotherapy leads to an increased risk of myelosuppression. Luteinizing hormone (LH) blockade improves hematopoietic recovery in mice after radiation or chemotherapy, through protection of the hematopoietic stem cells which express the LH receptor. We hypothesized that LH blockade improves hematopoietic recovery following intensive chemotherapy in patients with leukemia. We conducted a retrospective analysis on pre-menopausal women with acute myeloid leukemia (AML) or acute lymphoblastic leukemia (ALL) who received intensive chemotherapy and leuprolide given for abnormal uterine bleeding prevention or treatment. Given that leuprolide is more commonly administered in younger patients, we performed propensity score matching between the leuprolide (AML n=64; ALL n=49) and control groups (AML n=128; ALL n=98 patients). Patients with AML who received leuprolide had an additional increase of 13.8x10^9/L/year in their platelet count, and a 0.19x 10^9/L/year increase in their lymphocyte count after chemotherapy compared to control (P=0.02; P=0.03 respectively). Those with ALL who received leuprolide had an additional increase of 0.37x10^9/L/year in their absolute neutrophil count (P=0.02). In AML, leuprolide was associated with higher long-term hemoglobin levels (P<0.001) and less blood transfusions (mean, 23.9 *vs.* 34.7 units; P=0.002) compared to control. In a multivariate analysis, leuprolide was identified as an independent factor predicting improved hemoglobin levels, lymphocyte and platelet counts in AML. In conclusion, leuprolide use in leukemia patients receiving intensive chemotherapy was associated with improved long-term blood count recovery and with decreased transfusion requirements in AML.

Introduction

Hematopoiesis is an uninterrupted process of self-renewal, proliferation and differentiation of hematopoietic stem cells (HSC) in order to produce mature blood cells.[1] Maintenance of HSC is essential for regeneration of all bone marrow elements particularly following injuries such as ionizing radiation and/or chemotherapy. Treatment of acute leukemia with intensive cytotoxic chemotherapy results in acute hematopoietic suppression, leading to increased risks of infection and bleeding, especially in older patients where the induction mortality can reach up to 20-30%.[2-4] In addition to decreased blood counts, chemotherapy induces HSC senescence causing long-term bone marrow damage and, in some

Correspondence:
GHAYAS C. ISSA
gcissa@mdanderson.org

Received: April 23, 2020.
Accepted: November 6, 2020.
Pre-published: December 3, 2020.

https://doi.org/10.3324/haematol.2020.256453

©2021 Ferrata Storti Foundation

Material published in Haematologica is covered by copyright. All rights are reserved to the Ferrata Storti Foundation. Use of published material is allowed under the following terms and conditions: https://creativecommons.org/licenses/by-nc/4.0/legalcode. Copies of published material are allowed for personal or internal use. Sharing published material for non-commercial purposes is subject to the following conditions: https://creativecommons.org/licenses/by-nc/4.0/legalcode, sect. 3. Reproducing and sharing published material for commercial purposes is not allowed without permission in writing from the publisher.

instances, secondary myeloid malignancies.[5,6] There is an unmet need to develop strategies aimed at selectively protecting HSC from the damaging effects of chemotherapy, and maintaining the HSC pool especially for cancer survivors. Growing evidence suggests that the luteinizing hormone/choriogonadotropin receptor (LHCGR) is expressed on human HSC and that LH is implicated in HSC self-renewal.[7,8] In preclinical murine models, LH suppression using an LH-releasing hormone (LHRH) antagonist improved hematopoietic recovery after chemotherapy or lethal dose radiation.[9-11] Leuprolide, a gonadotropin-releasing hormone (GnRH) agonist, has been widely used in cancer patients during intensive chemotherapy and allogeneic stem cell transplantation in order to reduce the incidence of abnormal uterine bleeding and for fertility preservation.[12-14] In this study, we conducted a retrospective analysis aimed at evaluating the effect of leuprolide on hematopoietic recovery following intensive cytotoxic chemotherapy in acute leukemia.

Table 1. Baseline characteristics.

Characteristics	Before propensity matching N (%), median [range]			After propensity matching N (%), median [range]		
	Leuprolide	Control	*P*	Leuprolide	Control	*P*
A. AML cohort						
N	66	388		64	128	
Age, years	33 [19-54]	47 [18-56]	<0.001	33 [19-54]	35 [18-56]	0.7
ECOG PS						1
0-1	58 (91)	326 (87)	0.4	58 (91)	117 (91)	
≥2	6 (9)	51 (13)		6 (9)	11 (9)	
WBC x10^9/L	7.1 [0.7-160]	6.6 [0.5-390]	0.7	7.2 [0.7-160]	6.6 [0.5-80]	0.6
Plt x10^9/L	38.5 [3-271]	42.0 [1-676]	0.8	37 [3-271]	35.5 [2-575]	0.7
LDH UI/L	786 [297-18,336]	920 [200-14,701]	0.1	789 [297-18,336]	886 [322-14,701]	0.1
AMML/AMOL	22 (33)	120 (31)	0.8	22 (34)	31 (24)	0.2
ELN Risk			0.1			0.9
Favorable	21 (32)	78 (20)		21 (33)	39 (31)	
Intermediate	27 (41)	194 (50)		26 (41)	53 (41)	
Adverse	18 (27)	116 (30)		17 (26)	36 (28)	
Treatment*			0.04			0.4
Doublet	23 (35)	205 (53)		22 (35)	54 (42)	
Triplet	37 (56)	171 (44)		36 (56)	67(52)	
Other	6 (9)	12 (3)		6 (9)	7 (6)	
FLT3 Inhibitor	14 (21)	41 (11)	0.02	14 (22)	10 (9)	0.009
Transplant	27 (41)	110 (28)	0.04	20 (31)	37 (29)	0.7
B. ALL cohort						
N	65	192		49	98	
Age, years	31 [18-49]	41 [18-56]	<0.001	32 [18-49]	32 [18-55]	0.6
ECOG PS			1			1
0-1	50 (85)	145 (84)		42 (86)	85 (87)	
≥2	9 (15)	28 (16)		7 (14)	13 (13)	
WBC x10^9/L	5.8 [0.6-316]	5.4 [0.5-420]	0.9	7.6 [0.6-316]	7 [0.6-420]	0.5
Plt x10^9/L	51 [0-495]	29 [2-393]	0.1	54 [0-495]	50 [5-395]	0.8
LDH UI/L	1,096 [284-28,015]	1,256 [238-37,602]	0.5	1,109 [284-28,015]	1,125 [268-37,602]	0.8
Adverse CG**	32 (54)	87 (50)	0.6	25 (51)	47 (48)	0.7
B-ALL	58 (89)	178 (93)	0.4	44 (90)	89 (91)	1
T-ALL	7 (11)	14 (7)		5 (10)	9 (9)	
Treatment			0.001			0.07
HyperCVAD	43 (66)	169 (88)		34 (69)	83 (85)	
AugBFM	18 (28)	23 (12)		13 (27)	15 (15)	
Transplant	24 (37)	37 (19)	0.006	19 (39)	19 (19)	0.02

Propensity score matching included all the above baseline characteristics. * Doublet chemotherapy: idarubicin and cytarabine (IA); triplet chemotherapy: IA plus a nucleoside analog (i.e., cladribine, clofarabine, or fludarabine). **Adverse cytogenetics: complex karyotype (≥ 5 abnormalities) t(9;22), t(4;11), and low hypodiploidy/near-triploidy. AML: acute myeloid leukemia; ALL: acute lymphoblastic leukemia; N: number; ECOG PS: Eastern Cooperative Oncology Group performance status; WBC: white blood cell; Plt: platelet count; LDH: lactate dehydrogenase level; AMML/AMOL: acute myelomonocytic leukemia and monocytic leukemia; HyperCVAD: hyperfractionated cyclophosphamide, vincristine, adriamycin, dexamethasone; AugBFM: Augmented BFM regimen; ELN: European LeukemiaNet.

Methods

Patient selection

We screened adult female patients younger than 55 years at The University of Texas MD Anderson Cancer Center (Houston, TX) with newly diagnosed acute myeloid leukemia (AML) or acute lymphoblastic leukemia (ALL), treated with intensive chemotherapy between January 2000 and December 2017. We identified those who received at least one leuprolide injection for prevention or treatment of abnormal uterine bleeding with intensive chemotherapy (leuprolide received between day -7 and day 90 of induction chemotherapy start). The control group consisted of patients who had never received leuprolide (Figure 1). Baseline variables including age, types of treatment, laboratory parameters as well as clinical outcomes were collected and analyzed. All peripheral blood counts, performed between the start of treatment with induction chemotherapy until the date of last follow-up, were extracted from the electronic medical records and analyzed. We compared short and long-term count recovery, transfusion requirements and survival between the leuprolide and control groups.

This study was performed in accordance with the Declaration of Helsinki and was approved by the MD Anderson Institutional Review Board.

Statistical analysis

Patient characteristics were summarized using median (range) for continuous variables and frequency (percentage) for categorical variables. Fisher's exact test and Wilcoxon rank-sum test were used to assess differences in categorical and continuous variables.

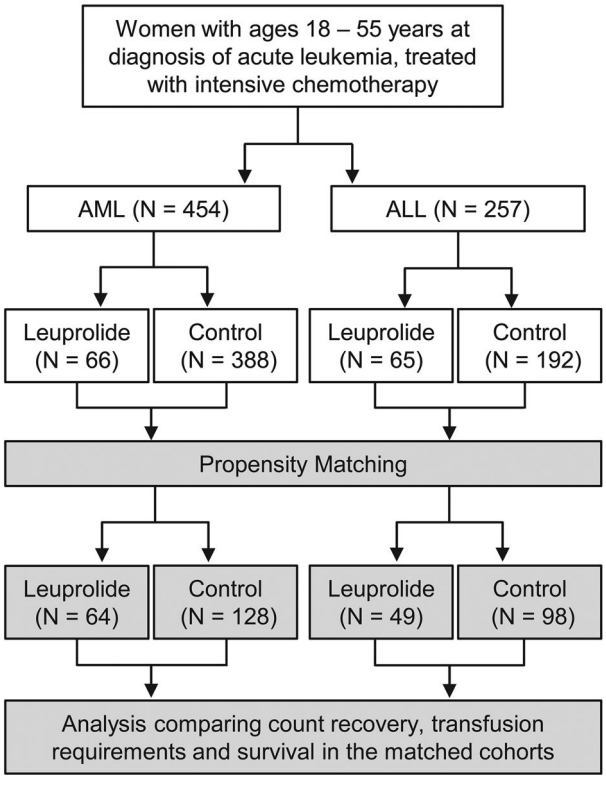


Figure 1. Patient selection. Control cohorts consisted of patients who had never received leuprolide. Propensity matching was done to adjust for covariate imbalances including the age difference between the respective case and control groups. All subsequent analyses were done comparing matched cohorts. AML: acute myeloid leukemia; ALL: acute lymphoblastic leukemia.

Given that leuprolide was more commonly given in younger patients, propensity score matching was used to adjust for covariate imbalances including the age difference between the respective case and control groups (Figure 1). Using the nearest-neighbor algorithm, patients from the leuprolide groups were matched to control at a 1:2 ratio.[15] A logistic regression model was used to estimate propensity scores. All subsequent analyses including count recovery, transfusion requirements and survival were performed on matched cohorts. Absolute neutrophil count (ANC) and platelet recovery were defined as achievement of an ANC ≥$1x10^9$/L, and a platelet count ≥$100x10^9$/L after first induction chemotherapy. Scatterplots of all peripheral blood cell counts for each patient, collected between induction chemotherapy (day 0) and last follow-up date, were extracted from health records, plotted and compared between leuprolide and control matched groups. Lowess smooth curves were used for indicating longitudinal trajectories of counts and differences were assessed using the generalized estimation equation model.[16,17] The probabilities of recovery were estimated using the Kaplan-Meier method. Overall survival (OS) was calculated as the time interval from treatment start date to the date of death, and was censored at the last follow-up date for patients who were alive. Event free survival (EFS) was defined as the time interval between the date of response and the date of relapse or death, whichever was first and was censored at last follow-up in patients alive and in remission. The Kaplan-Meier method was used to estimate the probability of OS and EFS, and log-rank test was used to compare survival between matched cohorts. Univariate and multivariate analyses were performed to determine the differential effect of leuprolide on count recovery and the interaction with baseline characteristics, treatment type, and relapse status. All computations were done in R version 3.4.4.

Results

Patient population

We identified 454 pre-menopausal women with AML and 257 with ALL, newly diagnosed and treated with intensive chemotherapy. Among those patients, 66 with AML and 65 with ALL had received leuprolide (Figure 1). Those who never received leuprolide were used as control cohorts and included 388 patients with AML and 192 patients with ALL (Figure 1; Table 1). Among patients with AML who received leuprolide, 33 (52%) received it between day -7 and day 15 of induction chemotherapy start, compared to 22 patients (45%) with ALL who received leuprolide during this time interval (*Online Supplementary Table S2*). Leuprolide was given in various dosage forms either through subcutaneous or intramuscular injections depending on the platelet count at time of administration. The median cumulative dose of leuprolide per patient, given throughout cycles of chemotherapy was 22.5 mg (range, 3–78.75 mg) for those with AML and 22.5 mg (range, 11.25–135 mg) for those with ALL (*Online Supplementary Table S2*). Patients who received leuprolide were significantly younger than the control cohorts (AML: 33 years *vs.* 47 years, $P<0.001$; ALL: 31 years *vs.* 41 years, $P<0.001$). Baseline characteristics were well balanced after propensity score matching (Table 1). For patients with AML, the most commonly given treatment regimens consisted of triplets including the backbone of idarubicin and cytarabine in addition to a nucleoside analog (cladribine, clofarabine or fludarabine).[18-20] The rest of the patients received a combination of idarubicin and cytarabine.

Targeted therapy was added by the treating physicians when indicated (*Online Supplementary Table S1* includes mutations identified in the AML matched cohorts). Patients in the ALL cohorts received either HyperCVAD (alternating cycles of hyperfractionated cyclophosphamide, vincristine, doxorubicin, dexamethasone and methotrexate and cytarabine) or Augmented Berlin–Frankfurt–Münster (AugBFM) regimens.[21]

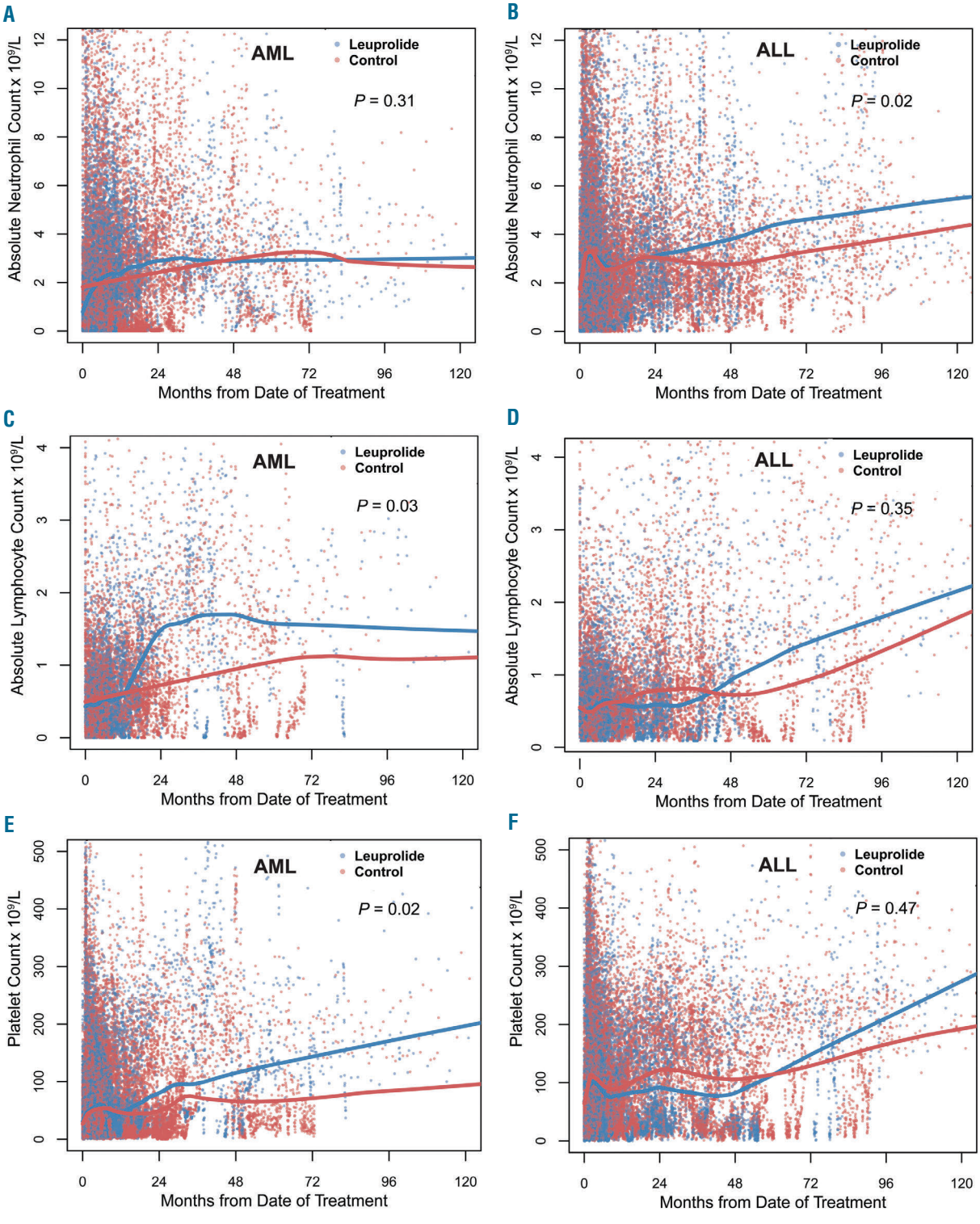


Figure 2. Long-term peripheral blood count recovery following chemotherapy with and without leuprolide. Scatterplots of all corresponding peripheral blood laboratory data extracted from health records, collected after induction chemotherapy (day 0) where each dot represents a single value (blue for leuprolide, red for control). (A-B) Change in absolute neutrophil count. (C-D) Change in absolute lymphocyte count. (E-F) Change in platelet count. Lowess smooth curves were used for indicating longitudinal trajectories of counts and differences were assessed using the generalized estimation equation model. AML: acute myeloid leukemia; ALL: acute lymphoblastic leukemia.

Table 2. Multivariate analysis of factors predicting long-term count recovery.

	ANC		ALC		Platelets		Hemoglobin	
	10^6/L/year (95% CI)	P	10^6/L/year (95% CI)	P	10^6/L/year (95% CI)	P	10^3 g/dL/year (95% CI)	P
AML								
PS ≤1	–	–	-20 (-37, -3)	0.02	-557 (-1,505, 390)	0.25	–	–
Adverse risk	–	–	–	–	-1391 (-2,375, -408)	0.006	–	–
BM blast %							0.1 (-0.1, 0.3)	0.4
FLT3 inhibitor	–	–	–	–	-1641 (-2,633, -650)	0.001	–	–
Triplet therapy	–	–	20 (8, 32)	0.001	–	–	5 (-9, 18)	0.5
Relapse	–	–	-17 (-32, -2)	0.02	–	–	-35 (-48, -23)	<0.001
Leuprolide	–	–	16 (5, 26)	0.003	1412 (433, 2,390)	0.005	14 (2, 26)	0.02
ALL								
PS ≤1	–	–	2 (-6, 9)	0.7	–	–	–	–
Adverse risk	–	–	–	–	–	–	9 (-5, 23)	0.2
B *vs.* T ALL	–	–	4 (-28, 36)	0.8	–	–	–	–
HyperCVAD	-68 (-97, -40)	<0.001	7 (-6, 19)	0.3				
Transplant	31 (8, 55)	0.01						
Relapse	32 (4, 61)	0.02	–	–	–	–	–	–
Leuprolide	28 (0.1, 56)	0.049	0.2 (-11, 12)	1	–	–	2 (-8, 12)	0.7

Values shown represent effect of variable on change in count per year (95% Confidence Interval [CI]). ANC: absolute neutrophil count; ALC: absolute lymphocyte count; PS: Eastern Cooperative Oncology Group performance status, assessed as PS ≤1 *vs.* PS≥2; Adverse risk in AML according to the European LeukemiaNet risk stratification, adverse risk in ALL corresponds to complex karyotype (≥ 5 abnormalities) t(9;22), t(4;11), and low hypodiploidy/near-triploidy, assessed as adverse *vs.* non-adverse; BM blasts: bone marrow blasts, assessed a continuous variable; Triplet chemotherapy: idarubicin and cytarabine plus a nucleoside analog (i.e., cladribine, clofarabine, or fludarabine), compared to doublet chemotherapy. Transplant corresponds to an allogeneic hematopoietic stem cell transplant; HyperCVAD: hyperfractionated cyclophosphamide, vincristine, adriamycin, dexamethasone, compared to all other treatments. Relapse and transplant were assessed as time-dependent variables. AML: acute myeloid leukemia; ALL: acute lymphoblastic leukemia.

Hematopoietic recovery

We evaluated whether leuprolide administration was associated with an improved blood count recovery following intensive chemotherapy in propensity matched cohorts. There was no difference in immediate count recovery following initial cycles of treatment when comparing those who received leuprolide to those who did not from the respective matched cohorts (*Online Supplementary Figure S1*). The median times to ANC and platelet count recovery were 25 days (95% Confidence Interval [CI]: 23-27) and 22 days (95% CI: 21-24) for AML matched patients who received leuprolide *versus* 25 days (95% CI: 24-28, *P*=0.47) and 23 days (95% CI: 22-24, *P*=0.2) for those who didn't receive leuprolide respectively. Matched patients with ALL who received leuprolide had a median time to ANC and platelet count recovery of 19 days (95% CI: 17-21) and 20 days (95% CI: 18-22) compared to 17 days (95% CI: 16-18, *P*=0.32) and 19 days (95% CI: 18-20, *P*=0.25) respectively. Given that preclinical data indicated an impact of LH suppression on the earliest hematopoietic stem cell progenitors, we evaluated the effect of leuprolide on long-term count recovery. Patients with ALL from matched cohorts who received leuprolide had an additional increase of their ANC of $0.37x10^9$/L/year compared to those who did not receive leuprolide (*P*=0.02) (Figure 2A-B). We also found that lymphocyte count recovery significantly differed between the two matched groups in the AML cohort with an additional increase in the ALC of $0.19x10^9$/L/year in patients who received leuprolide compared to control (*P*=0.03) (Figure 2C-D). Similarly, for platelet count recovery, patients with AML from matched cohorts who received leuprolide had an additional increase of $13.8x10^9$/L/year following chemotherapy compared with those in the control group (*P*=0.02) (Figure 2E-F). We found an association between long-term improvement of red blood cell parameters including hemoglobin and hematocrit levels in addition to red blood cell count and leuprolide in AML (*P*<0.001 and *P*=0.004, respectively) (*Online Supplementary Figure S2*). Patients with AML who received leuprolide had an additional increase in their hemoglobin level of 0.03 g/dL/year (*P*<0.001) (Figure 3A-B). These differences were most evident 2-4 years after the initial date of chemotherapy.

Transfusion requirements

Patients with AML treated with leuprolide received less packed red blood cells (pRBC) transfusions compared to the matched control group with an average of 23.9 units *versus* 34.7 units (*P*=0.002), given at any time following start of chemotherapy, which was concordant with the count recovery analysis for this group (Figure 3C). These patients also had less platelet transfusions with an average of 24.4 units compared to 32.8 units in the matched control group (*P*=0.06, respectively) (Figure 3C). This difference in transfusion requirements was less pronounced in the ALL matched cohorts where patients in the leuprolide

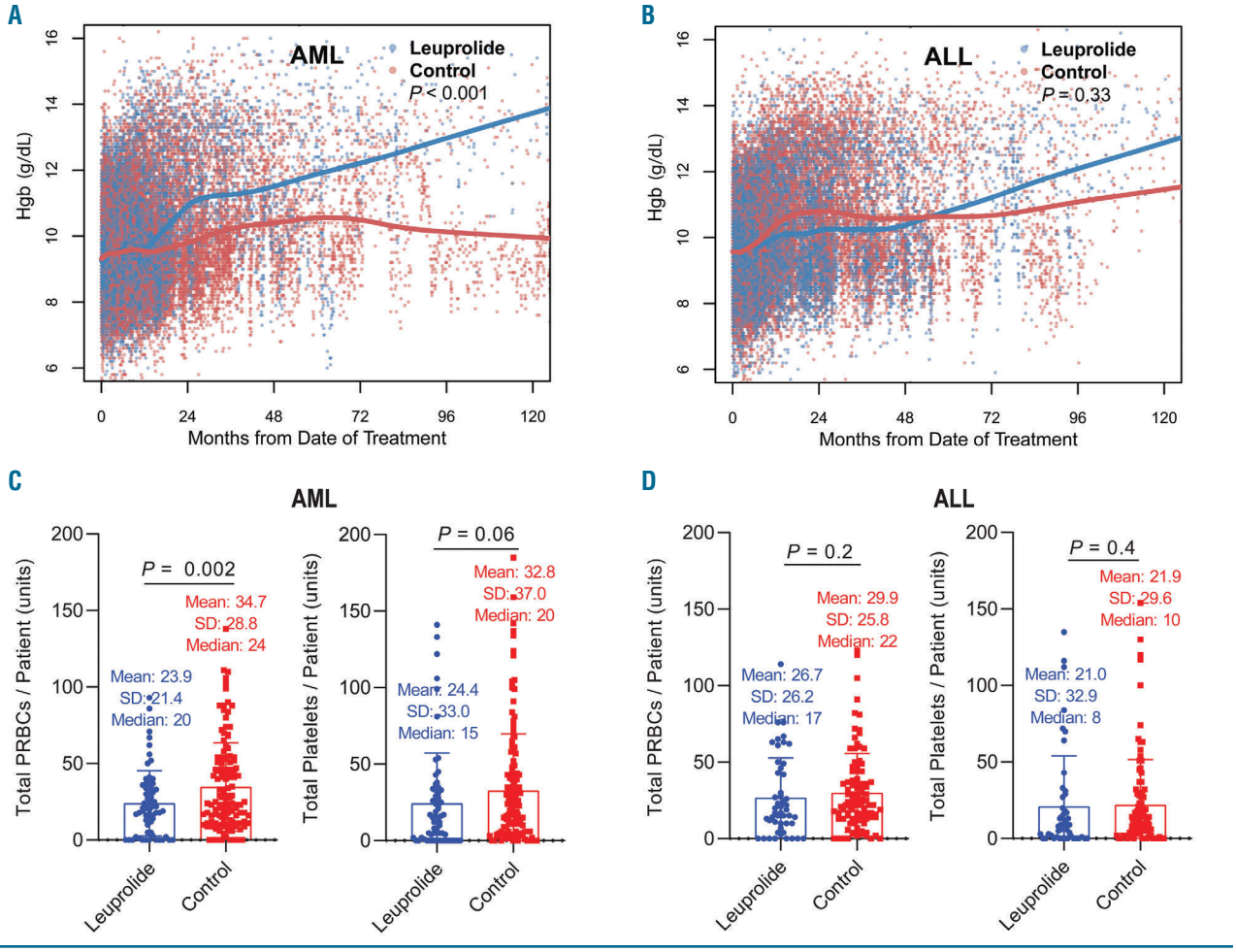


Figure 3. Long-term changes in hemoglobin levels and transfusion requirements with and without leuprolide. (A-B) Scatterplots of all corresponding peripheral blood hemoglobin (Hgb) levels extracted from health records, collected between induction chemotherapy (day 0) and last follow-up date where each dot represents a single value (blue for leuprolide, red for control). (A) Acute myeloid leukemia (AML) matched cohorts and (B) acute lymphoblastic leukemia (ALL) matched cohorts. Lowess smooth curves were used for indicating longitudinal trajectories of counts and differences were assessed using the generalized estimation equation model. (C-D) Transfusion requirements: differences in the mean number of blood and platelet units given between induction chemotherapy date (day 0) and last follow-up date in AML (C) and ALL (D) comparing matched leuprolide and control cohorts. Each value represents the total number of transfusion units given during this time period for each patient.

group had on average 26.7 units of pRBC compared to 29.9 units in the matched control group (P=0.24), and an average of 21.0 units of pRBC compared to 21.9 units in the same respective groups (P=0.44) (Figure 3D).

Multivariate analysis

Given that numerous factors such dose of leuprolide, age or relapse status for example could affect count recovery and the possible association with leuprolide, we performed a univariate analysis followed by a multivariate analysis for significant factors impacting long-term count recovery. We examined whether leuprolide dosing (higher cumulative leuprolide dose) or timing of administration of leuprolide (between day -7 and day 15 of induction chemotherapy compared to leuprolide given later) correlated with long-term count recovery and found no statistically significant associations in the univariate analysis (*Online Supplementary Table S3*). Patients with AML who received FMS-like tyrosine kinase 3 (FLT3) inhibitors in addition to their chemotherapy had lower platelet recovery (P<0.001). Relapse status, investigated as a time dependent variable, was associated with lower long-term lymphocyte count and hemoglobin levels in AML (P=0.04 and P=0.01 respectively) and higher neutrophil count recovery in ALL (P=0.001). The full results of the univariate analysis are included in *Online Supplementary Table S3*. We next sought to assess the differential impact of leuprolide on count recovery when all co-factors are considered. We found that leuprolide administration was independently associated with long-term hemoglobin levels, lymphocyte and platelet counts in AML (P=0.02, P=0.003, and P=0.005, respectively) and ANC levels in ALL (P=0.049) (Table 2). Additional independent co-factors identified in this analysis for AML included performance status, adverse risk according to the European LeukemiaNet classification, relapse status, and receipt of a FLT3 inhibitor or triplet chemotherapy. For ALL, independent factors included relapse or whether patients had an allogeneic stem cell transplant or were treated with HyperCVAD.

Impact on survival

We found that patients in the leuprolide groups were significantly younger than the respective control groups (Table 1). This was also associated with an improved OS

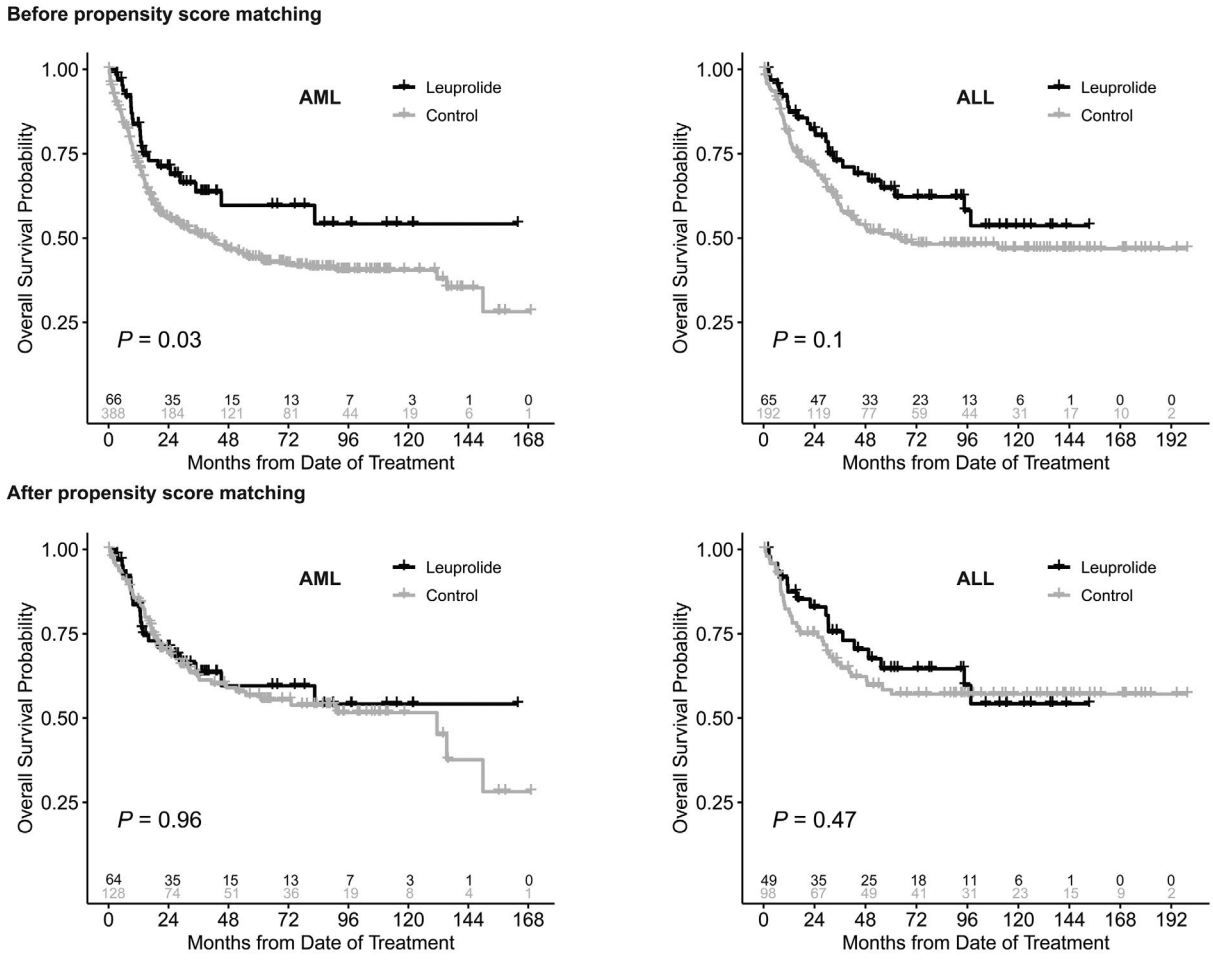


Figure 4. Overall survival in acute myeloid leukemia and acute lymphoblastic leukemia patients with and without leuprolide before and after propensity score matching. AML: acute myeloid leukemia; ALL: acute lymphoblastic leukemia.

in the leuprolide groups compared to the control groups prior to propensity score matching (Figure 4A-B). However, after propensity score matching there was no association between leuprolide administration and survival outcomes. The 5-year OS for patients with AML who had received leuprolide was 60% (95% CI: 47-76) compared to 57% (95% CI: 48-67) in the matched control cohort (P=0.96) (Figure 4C). The 5-year OS for patients with ALL who had received leuprolide was 65% (95% CI: 52-81) compared to 58% (95% CI: 49-70) in the matched control cohort (P=0.47) (Figure 4D). Similarly, there was no difference in EFS comparing patients with AML with leuprolide and the matched control group (P=0.29) (*Online Supplementary Figure S3*) and no difference in ALL patients with leuprolide and their matched control group (P=0.85) (*Online Supplementary Figure S3*).

Discussion

In this study, we show that use of leuprolide in premenopausal women with acute leukemia receiving chemotherapy was associated with less transfusions and better long-term count recovery. Bone marrow suppression caused by cytotoxic chemotherapy is a common dose limiting adverse event in cancer treatment, especially in hematologic malignancies. It leads to increased morbidity and mortality because of the higher risk of infection and bleeding. Myelosuppression is caused by apoptosis of highly proliferative multipotent and hematopoietic progenitors.[22,23] Moreover, use of cytotoxic chemotherapy can lead to long-term bone marrow damage by various mechanisms including induction of apoptosis, senescence of HSC, or damage to bone marrow stromal cells.[6,24] After chemotherapy insult, dormant HSC transiently proliferate to replenish blood cells and sustain hematopoietic homeostasis.[25] An unbalanced HSC proliferation and exit from dormancy could lead to long-term bone marrow suppression, and an increased risk of DNA damage.[26,27] Therefore, there is a critical need to limit the damaging effects of cytotoxic chemotherapy on HSC and preserve the HSC pool.

There is growing evidence that several pituitary hormone receptors including LH, follicle-stimulating hormone, prolactin, and growth hormone receptors, are expressed by human HSC and are directly implicated in HSC self-renewal, proliferation and differentiation.[7,8,28] Notably, patients with history of germ cell tumors have an increased risk of developing myeloid neoplasms.[29-31] While this had been attributed in some cases to therapy-related leukemogenesis, recent genomic analysis demonstrated that these neoplasms could be clonally related, thus indicating shared ancestry between the corresponding tissues

of origin.[32] Use of leuprolide was found to enhance T-cell recovery following allogeneic bone marrow transplantation in a mouse model through enhanced thymic reconstitution.[33] Velardi and colleagues demonstrated that LH blockade protects HSC from the damaging effects of chemotherapy or radiation in mice. LHRH antagonism led to quiescence in early hematopoietic progenitors. The HSC pool was maintained by preventing early progenitors from entering the cell cycle thus protecting them from chemotherapy or radiation damage.[9] This mechanism is very similar to the fertility preserving effect of leuprolide.[34] LHRH blockade in preclinical models halted recruitment of primordial quiescent follicles after treatment with chemotherapy thereby preserving the functional potential of the ovary. This has been validated in clinical studies and is now one of the strategies to preserve fertility in women receiving chemotherapy.[35,36] It is plausible that this observed protective effect on HSC seen with leuprolide is mediated through a downstream effect on estrogen or other sex hormones.[7,37] In a mouse model, estrogen increased hematopoietic stem-cell self-renewal in females and during pregnancy.[37] However, levels of these hormones were not assessed in patients included in our analysis.

We report the first clinical evidence indicating a correlation between use of leuprolide and improved transfusion requirements in addition to improved long-term blood count recovery in women with acute leukemia receiving intensive chemotherapy. We observed an improvement in neutrophil, lymphocyte and platelet counts mostly when the corresponding lineage was not affected by leukemia. Some of the improvement in transfusion requirements could be related to a decrease in uterine bleeding through the hormonal suppression induced by LH blockade. However, we were unable to accurately quantify bleeding episodes from corresponding medical records. We also could not determine whether patients prone to bleeding preferentially received leuprolide which could affect the interpretation of ours results, however we tried to correct for selection bias through propensity score matching and the multivariate analysis. We found in our analysis that patients who received leuprolide and a FLT3 inhibitor added to their induction chemotherapy had a reduced platelet count recovery. Given that the FLT3 receptor is expressed by immature hematopoietic cells, and is restricted in normal bone marrow to early progenitors, targeting FLT3 could affect normal hematopoiesis leading to thrombocytopenia and delayed count recovery after chemotherapy.[38] Thrombocytopenia is reported in 12-46% of patients receiving sorafenib, the FLT3 inhibitor most commonly used in this cohort. Sorafenib is a multi-kinase inhibitor that could affect numerous other pathways important for normal hematopoiesis and platelet generation from long-term HSC, therefore explaining this observation.[39] There was no effect of LH blockade on rates of leukemia relapse or death in both AML and ALL cohorts, indicating that the theoretical risk of leuprolide protecting leukemia stem cells potentially expressing the LH receptor was not clinically meaningful in our study. Prospective studies are needed in order to confirm our findings and evaluate the effect of LH blockade on safety and count recovery following intensive chemotherapy in all hematologic malignancies. There are several ongoing clinical trials evaluating the effect of leuprolide on immune function following bone marrow transplantation (clinicaltrials gov. Identifier: 00275262, 01746849 and 01338987).

Repurposing old approved drugs in the field of cancer is gaining more importance given the high global burden of cancer and its substantial costs.[40] LH antagonism, which allows for a reversible ablation of this hormonal axis, has a strong safety profile in other cancers such as breast and prostate cancer. Our findings potentially add another indication for use of leuprolide in women receiving high doses of chemotherapy by (i) minimizing uterine bleeding, (ii) decreasing the risk of ovarian failure and preserving fertility and (iii) protecting HSC from damage and improving long-term count recovery. Another hypothesis worth testing is whether LH blockade would reduce expansion of clonal hematopoiesis of indeterminate potential (CHIP) cells following chemotherapy or radiation, thus reducing the risk of therapy-related myeloid malignancies (assuming CHIP clones express the LHCGR).[41]

In summary, use of leuprolide in patients with newly diagnosed acute leukemia receiving intensive chemotherapy was associated with decreased transfusion requirements and improved long-term blood count recovery. Further studies are needed to validate these findings.

Disclosures

NJS received research funding from Takeda Oncology, consultancy fees from AstraZeneca, Takeda Oncology and Amgen. JEC received research funding from Ambit BioSciences, ARIAD, Arog, Astellas Pharma, AstraZeneca, Bristol-Myers Squibb, Celator, Celgene, Novartis, Pfizer, Sanofi, Sun Pharma, Teva; consultant fees from Ambit BioSciences, ARIAD, Astellas Pharma, BiolineRx, Bristol-Myers Squibb, Novartis; Pfizer. EJJ received research funding and consultancy fees from Takeda, BMS, Adaptive, Amgen, AbbVie, Pfizer and Cyclacel LTD. GCI received research funding from Celgene, Syndax and Novartis and served on an advisory board for Novartis.

Contributions

IA wrote the manuscript; IA, RMP, JZ, SP, KS, NJS, MO, JEC, EJJ contributed to data collection and analysis; WL and JN analyzed the data and performed the statistical analysis; GCI designed the study, supervised the analysis and wrote the manuscript.

Funding

The study was supported by Leukemia Texas (PI – Issa GC), the National Cancer Institute K12 Paul Calabresi Clinical Scholarship Award (NIH/NCI K12 CA088084 to Issa GC) and the Cancer Center Support Grant (NCI Grant P30 CA016672).

References

1. Orkin SH, Zon LI. Hematopoiesis: an evolving paradigm for stem cell biology. Cell. 2008;132(4):631-644.
2. Tilly H, Castaigne S, Bordessoule D, et al. Low-dose cytarabine versus intensive chemotherapy in the treatment of acute nonlymphocytic leukemia in the elderly. J Clin Oncol. 1990;8(2):272-279.
3. Menzin J, Lang K, Earle CC, et al. The outcomes and costs of acute myeloid leukemia among the elderly. Arch Intern Med. 2002;162(14):1597-1603.
4. Kantarjian H, O'Brien S, Cortes J, et al. Results of intensive chemotherapy in 998 patients age 65 years or older with acute

myeloid leukemia or high-risk myelodysplastic syndrome: predictive prognostic models for outcome. Cancer. 2006; 106(5):1090-1098.
5. Wang Y, Probin V, Zhou D. Cancer therapy-induced residual bone marrow injury-Mechanisms of induction and implication for therapy. Curr Cancer Ther Rev. 2006;2(3):271-279.
6. Shao L, Wang Y, Chang J, et al. Hematopoietic stem cell senescence and cancer therapy-induced long-term bone marrow injury. Transl Cancer Res. 2013;2(5):397-411.
7. Mierzejewska K, Borkowska S, Suszynska E, et al. Hematopoietic stem/progenitor cells express several functional sex hormone receptors-novel evidence for a potential developmental link between hematopoiesis and primordial germ cells. Stem Cells Dev. 2015;24(8):927-937.
8. Abdelbaset-Ismail A, Suszynska M, Borkowska S, et al. Human haematopoietic stem/progenitor cells express several functional sex hormone receptors. J Cell Mol Med. 2016;20(1):134-146.
9. Velardi E, Tsai JJ, Radtke S, et al. Suppression of luteinizing hormone enhances HSC recovery after hematopoietic injury. Nat Med. 2018;24(2):239-246.
10. Khong DM, Dudakov JA, Hammett MV, et al. Enhanced hematopoietic stem cell function mediates immune regeneration following sex steroid blockade. Stem Cell Reports. 2015;4(3):445-458.
11. Dudakov JA, Goldberg GL, Reiseger JJ, et al. Sex steroid ablation enhances hematopoietic recovery following cytotoxic antineoplastic therapy in aged mice. J Immunol. 2009;183(11):7084-7094.
12. Quaas AM, Ginsburg ES. Prevention and treatment of uterine bleeding in hematologic malignancy. Eur J Obstet Gynecol Reprod Biol. 2007;134(1):3-8.
13. Jadoul P, Kim SS, Committee IP. Fertility considerations in young women with hematological malignancies. J Assist Reprod Genet. 2012;29(6):479-487.
14. Poorvu PD, Barton SE, Duncan CN, et al. Use and effectiveness of gonadotropin-releasing hormone agonists for prophylactic menstrual suppression in postmenarchal women who undergo hematopoietic cell transplantation. J Pediatr Adolesc Gynecol. 2016;29(3):265-268.
15. Ho DE, Imai K, King G, Stuart EA. MatchIt: nonparametric preprocessing for parametric causal inference. J Stat Software. 2011; 42(8):1-28.
16. Cleveland WS. Robust locally weighted regression and smoothing scatterplots. J Am Stat Association. 1979;74(368):829-836.
17. Liang KY, Zeger SL. Longitudinal data analysis using generalized linear models. Biometrika. 1986;73(1):13-22.
18. Jabbour E, Short NJ, Ravandi F, et al. A randomized phase 2 study of idarubicin and cytarabine with clofarabine or fludarabine in patients with newly diagnosed acute myeloid leukemia. Cancer. 2017;123(22):4430-4439.
19. Nazha A, Kantarjian H, Ravandi F, et al. Clofarabine, idarubicin, and cytarabine (CIA) as frontline therapy for patients </=60 years with newly diagnosed acute myeloid leukemia. Am J Hematol. 2013;88(11):961-966.
20. Jain P, Kantarjian HM, Ravandi F, et al. Cladribine combined with idarubicin and Ara-C (CLIA) as frontline and salvage treatment for young patients (≤65 yrs) with acute myeloid leukemia. Blood. 2016; 128(22):1639-1639.
21. Rytting ME, Jabbour EJ, Jorgensen JL, et al. Final results of a single institution experience with a pediatric-based regimen, the augmented Berlin-Frankfurt-Munster, in adolescents and young adults with acute lymphoblastic leukemia, and comparison to the hyper-CVAD regimen. Am J Hematol. 2016;91(8):819-823.
22. Shao L, Sun Y, Zhang Z, et al. Deletion of proapoptotic Puma selectively protects hematopoietic stem and progenitor cells against high-dose radiation. Blood. 2010; 115(23):4707-4714.
23. Yu H, Shen H, Yuan Y, et al. Deletion of Puma protects hematopoietic stem cells and confers long-term survival in response to high-dose gamma-irradiation. Blood. 2010;115(17):3472-3480.
24. Mauch P, Constine L, Greenberger J, et al. Hematopoietic stem cell compartment: acute and late effects of radiation therapy and chemotherapy. Int J Radiat Oncol Biol Phys. 1995;31(5):1319-1339.
25. Wilson A, Laurenti E, Oser G, et al. Hematopoietic stem cells reversibly switch from dormancy to self-renewal during homeostasis and repair. Cell. 2008;135(6):1118-1129.
26. Walter D, Lier A, Geiselhart A, et al. Exit from dormancy provokes DNA-damage-induced attrition in haematopoietic stem cells. Nature. 2015;520(7548):549-552.
27. Fabiani E, Falconi G, Fianchi L, et al. Clonal evolution in therapy-related neoplasms. Oncotarget. 2017;8(7):12031-12040.
28. Bujko K, Cymer M, Adamiak M, et al. An overview of novel unconventional mechanisms of hematopoietic development and regulators of hematopoiesis - a roadmap for future investigations. Stem Cell Rev Rep. 2019;15(6):785-794.
29. Nichols CR, Roth BJ, Heerema N, et al. Hematologic neoplasia associated with primary mediastinal germ-cell tumors. N Engl J Med. 1990;322(20):1425-1429.
30. Hartmann JrT, Fossa SD, Nichols CR, et al. Incidence of metachronous testicular cancer in patients with extragonadal germ cell tumors. J Natl Cancer Inst. 2001; 93(22):1733-1738.
31. Nichols CR, Hoffman R, Einhorn LH, et al. Hematologic malignancies associated with primary mediastinal germ-cell tumors. Ann Intern Med. 1985;102(5):603-609.
32. Taylor J, Donoghue MTA, Ho C, et al. Germ cell tumors and associated hematologic malignancies evolve from a common shared precursor. J Clin Invest. 2020;130 (12):6668-6676.
33. Goldberg GL, King CG, Nejat RA, et al. Luteinizing hormone-releasing hormone enhances T cell recovery following allogeneic bone marrow transplantation. J Immunol. 2009;182(9):5846-5854.
34. Ataya KM, McKanna JA, Weintraub AM, et al. A luteinizing hormone-releasing hormone agonist for the prevention of chemotherapy-induced ovarian follicular loss in rats. Cancer Res. 1985;45(8):3651-3656.
35. Munhoz RR, Pereira AA, Sasse AD, et al. Gonadotropin-releasing hormone agonists for ovarian function preservation in premenopausal women undergoing chemotherapy for early-stage breast cancer: a systematic review and meta-analysis. JAMA Oncol. 2016;2(1):65-73.
36. Oktay K, Harvey BE, Partridge AH, et al. Fertility preservation in patients with cancer: ASCO Clinical Practice Guideline update. J Clin Oncol. 2018;36(19):1994-2001.
37. Nakada D, Oguro H, Levi BP, et al. Oestrogen increases haematopoietic stem-cell self-renewal in females and during pregnancy. Nature. 2014;505(7484):555-558.
38. Gilliland DG, Griffin JD. The roles of FLT3 in hematopoiesis and leukemia. Blood. 2002;100(5):1532-1542.
39. Daver N, Schlenk RF, Russell NH, et al. Targeting FLT3 mutations in AML: review of current knowledge and evidence. Leukemia. 2019;33(2):299-312.
40. Pushpakom S, Iorio F, Eyers PA, et al. Drug repurposing: progress, challenges and recommendations. Nat Rev Drug Discov. 2019;18(1):41-58.
41. Takahashi K, Wang F, Kantarjian H, et al. Preleukaemic clonal haemopoiesis and risk of therapy-related myeloid neoplasms: a case-control study. Lancet Oncol. 2017; 18(1):100-111.

Ferrata Storti Foundation

Haematologica 2021
Volume 106(4):1106-1119

Oncogenic *Gata1* causes stage-specific megakaryocyte differentiation delay

Gaëtan Juban,[1a*] Nathalie Sakakini,[1,2b*] Hedia Chagraoui,[1] David Cruz Hernandez,[1,2] Qian Cheng,[3] Kelly Soady,[1,2] Bilyana Stoilova,[1,2] Catherine Garnett,[1,2] Dominic Waithe,[3] Georg Otto,[1c] Jessica Doondeea,[1,2] Batchimeg Usukhbayar,[1,2] Elena Karkoulia,[4] Maria Alexiou,[5d] John Strouboulis,[4e] Edward Morrissey,[5] Irene Roberts,[1,2,6] Catherine Porcher[1#] and Paresh Vyas[1,2,7#]

[1]MRC Molecular Hematology Unit WIMM, University of Oxford, Oxford, UK; [2]Haematology Theme Oxford Biomedical Research Center, Oxford, UK; [3]Center for Computational Biology WIMM, University of Oxford, Oxford, UK; [4]Institute of Molecular Biology and Biotechnology, Foundation of Research & Technology-Hellas, Heraklion, Crete Greece; [5]Biomedical Sciences Research Center "Alexander Fleming", Vari, Greece; [6]Department of Pediatrics University of Oxford, Oxford, UK and [7]Department of Hematology, Oxford University Hospitals NHS Foundation Trust, Oxford, UK

**GJ and NS contributed equally as co-first authors.*
#CP and PV contributed euqally as co-senior authors.

[a]Current address: Institut NeuroMyoGène, Université Claude Bernard Lyon 1, CNRS UMR 5310, INSERM U1217, Université Lyon, Lyon, France.

[b]Current address: Cambridge Stem Cell Institute, Cambridge, UK.

[c]Current address: Genetics and Genomic Medicine, University College London Institute of Child Health, London, UK.

[d]Current address: Department of Dentistry, University of Alberta, Edmonton, Alberta, Canada.

[e]Current address: Rayne Institute School of Cancer & Pharmaceutical Sciences, King's College London, London, UK

ABSTRACT

The megakaryocyte/erythroid transient myeloproliferative disorder (TMD) in newborns with Down syndrome (DS) occurs when N-terminal truncating mutations of the hemopoietic transcription factor GATA1, that produce GATA1short protein (GATA1s), are acquired early in development. Prior work has shown that murine GATA1s, by itself, causes a transient yolk sac myeloproliferative disorder. However, it is unclear where in the hemopoietic cellular hierarchy GATA1s exerts its effects to produce this myeloproliferative state. Here, through a detailed examination of hemopoiesis from murine GATA1s embryonic stem cells (ESC) and GATA1s embryos we define defects in erythroid and megakaryocytic differentiation that occur late in hemopoiesis. GATA1s causes an arrest late in erythroid differentiation *in vivo*, and even more profoundly in ESC-derived cultures, with a marked reduction of Ter-119 cells and reduced erythroid gene expression. In megakaryopoiesis, GATA1s causes a differentiation delay at a specific stage, with accumulation of immature, kit-expressing CD41^{hi} megakaryocytic cells. In this specific megakaryocytic compartment, there are increased numbers of GATA1s cells in S-phase of the cell cycle and a reduced number of apoptotic cells compared to GATA1 cells in the same cell compartment. There is also a delay in maturation of these immature GATA1s megakaryocytic lineage cells compared to GATA1 cells at the same stage of differentiation. Finally, even when GATA1s megakaryocytic cells mature, they mature aberrantly with altered megakaryocyte-specific gene expression and activity of the mature megakaryocyte enzyme, acetylcholinesterase. These studies pinpoint the hemopoietic compartment where GATA1s megakaryocyte myeloproliferation occurs, defining where molecular studies should now be focused to understand the oncogenic action of GATA1s.

Correspondence:

PARESH VYAS
paresh.vyas@imm.ox.ac.uk

GAËTAN JUBAN
gaetan.juban@univ-lyon1.fr

Received: December 8, 2019.

Accepted: May 20, 2020.

Pre-published: June 11, 2020

https://doi.org/10.3324/haematol.2019.244541

©2021 Ferrata Storti Foundation

Material published in Haematologica is covered by copyright. All rights are reserved to the Ferrata Storti Foundation. Use of published material is allowed under the following terms and conditions: https://creativecommons.org/licenses/by-nc/4.0/legalcode. Copies of published material are allowed for personal or internal use. Sharing published material for non-commercial purposes is subject to the following conditions: https://creativecommons.org/licenses/by-nc/4.0/legalcode, sect. 3. Reproducing and sharing published material for commercial purposes is not allowed without permission in writing from the publisher.

Introduction

The X-chromosome-encoded hematopoietic transcription factor GATA1 is essential for normal erythroid and megakaryocytic differentiation.[1-3] Clonal mutations acquired in fetal life, leading to loss of the N-terminal 84 amino acids of GATA1, occur in approximately 28% of newborns with Downs syndrome (DS) and are associated with either a clinically overt, or clinically silent, myeloproliferative disorder known as transient myeloproliferative disorder (TMD).[4-7] The mutant truncated GATA1 protein is known as GATA1short or GATA1s. In most neonates with DS the mutant fetal GATA1s clone disappears by 3 months of age[7] (and Roberts and Vyas unpublished data). In approximately 3% of all neonates the TMD clone acquires additional mutations[8,9] that transform the clone resulting in megakaryoblast-erythroid leukemia known as myeloid leukemia of Down syndrome (ML-DS). Germline mutations resulting in GATA1s, in disomic individuals and families also cause disease, but rather than being oncogenic cause cytopenia[10] including the clinical phenotype of Diamond-Blackfan anemia.[11]

In order to begin to understand how GATA1s perturbs hemopoiesis, a mouse model of GATA1s has been studied.[12] These mice develop a transient megakaryoblastic myeloproliferative disorder that resolves *in utero* and likely originates from yolk sac hemopoiesis. Interestingly, these mice are anemic *in utero* leading to embryonic loss. Mice that survive then have minimal hemopoietic defects in adult life. Consistent with this human induced pluripotent stem cells (iPSC) derived from GATA1s-expressing TMD cells failed to complete erythropoiesis.[13]

This suggests that the N-terminal of GATA1 has a specific developmental role in restraining megakaryocyte production and is required for terminal red cell maturation. However, it is unclear which developmental hemopoietic cell populations require the N-terminus of GATA1 and the cellular and molecular mechanisms responsible for perturbed hemopoiesis in GATA1s cells.

In order to identify the cellular populations most perturbed by GATA1s, we studied hemopoietic differentiation from both ESC culture-derived embryoid bodies (that recapitulate yolk sac hemopoiesis) and murine yolk sacs in GATA1s and control wild-type GATA1 mice. We define specific stages in megakaryocyte maturation, where GATA1s megakaryocytic cells are significantly increased in overall number, exhibit decreased apoptosis, have increased numbers of cells in S-phase, exhibit a delay in terminal maturation and mature abnormally. Importantly, this population affected by GATA1s mutations is also observed in human TMD samples.

Methods

Creation of gene targeted embryonic stem cells (ESC), growth and differentiation of murine ESC, characterisation of ESC, flow cytometry, gene expression analysis, cell staining and microscopy, acetylcholinesterase staining quantitation, cell cycle and apoptosis assays

Details are stated in the *Online Supplementary Appendix*. Antibody clones and colours are listed in the *Online Supplementary Table S1*. Raw RNA sequencing data have been deposited in Arrayexpress (*https://www.ebi.ac.uk/arrayexpress/*) with accession number E-MTAB-8968. Western blotting was performed as previously described.[14]

Mice

Animal studies were approved by the University of Oxford's Ethics Committee and conducted in accordance with the UK Home Office regulations (PPL n°PA7C92A40). Embryos were processed as set out in the *Online Supplementary Appendix*.

Human samples

Parents gave written informed consent in accordance with the Declaration of Helsinki, and the study was approved by the Thames Valley Research Ethics Committee (06MRE12-10; NIHR portfolio no. 6362).

Statistical analyses

All experiments were performed using at least three different cultures or animals in independent experiments. The Student's *t*-test was used for statistical analyses. $P<0.05$ was considered significant.

Results

Differentiation of bioGATA1 (bioG1) and bioGATA1s (bioG1s) cells

Murine bioGata1 and bioGata1s alleles were created in male BirA ligase-expressing ESC[15] by gene targeting of X-chromosome encoded Gata1 (*Online Supplementary Figure 1A-B*). Correct targeting was verified by Southern blot analysis (*Online Supplementary Figure 1C*) and PCR (*Online Supplementary Figure 1D-E*). We generated three ESC types: BirA-bioGATA1s (hereafter, bioG1s) and as controls parental BirA (hereafter, BirA) and BirA-bioGATA1 (hereafter, bioG1).

In order to study the mGATA1s megakaryocyte phenotype, we used a 12 day megakaryocyte *in vitro* ESC differentiation protocol[16] (Figure 1A). ESC were differentiated into embryoid bodies (EB), EB disaggregated at day 6 (d6), then $CD41^+$ hemopoietic cells isolated by bead-enrichment and $kit^{hi}CD41^+$ cells fluorescence-activated cell sorting (FACS)-purified (*Online Supplementary Figure S1F-G*) for further 6-day culture on OP9 stromal cells with cytokines to promote megakaryocyte differentiation. Western blot analysis of d6 $CD41^+$ cells confirmed bioG1 cells expressed only a single higher molecular weight full-length bioGATA1 isoform, whereas bioG1s cells only expressed a single lower weight bioGATA1s isoform (Figure 1B). We next confirmed expression of *Gata1* exon 3 (common to both Gata1 and Gata1s) in BirA, bioG1 and bioG1s cells and appropriately detected cDNA spanning *Gata1* exon 2-3 only in BirA and bioG1 and not bioG1s cells (Figure 1C).

Next, we tested the lineage characteristics of cells produced by the 12 day culture. First, we took all cells at day 12 (d12) and confirmed expression of megakaryocyte genes *gpIIB, gpVI, mpl* and *p-selectin* in BirA, bioG1 and bioG1s cells but not in ESC (Figure 1C). Next, by staining d12 cells with megakaryocyte-specific acetylcholinesterase stain (Figure 1D) we confirmed megakaryocyte production. Interestingly, bioG1s cultures produced significantly fewer megakaryocytes providing a first clue that megakaryocyte differentiation is impaired by GATA1s.

In order to obtain a more complete initial view of megakaryocyte differentiation we analysed kit (marker of

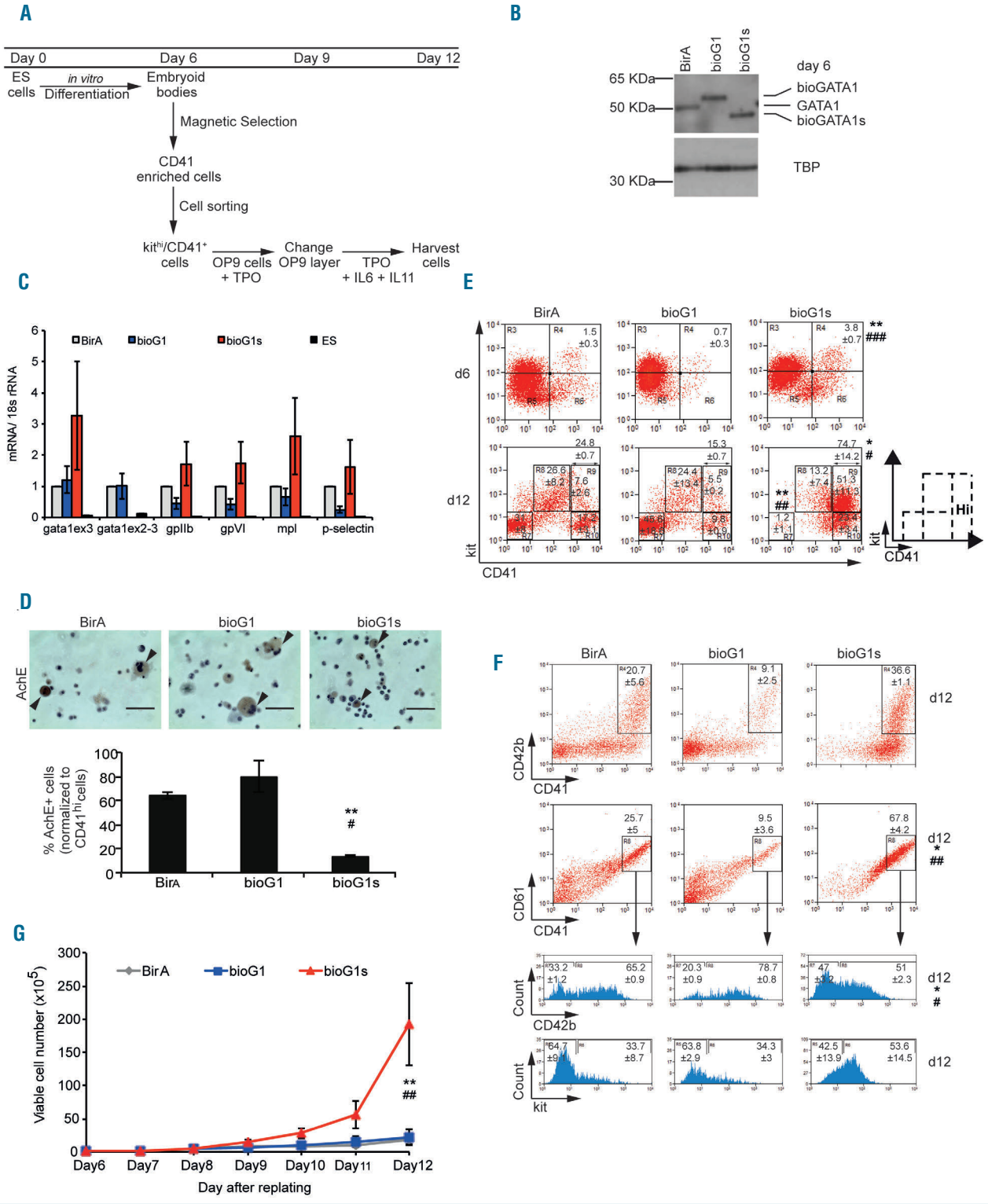


Figure 1. Gata1s embryonic stem cell-derived hematopoietic progenitors generate more immature megakaryocytes. (A) Protocol of *in vitro* megakaryocyte differentiation from embryonic stem cells (ESC). Top, day of culture. Below, sequential steps in the culture. TPO: thrombopoietin; IL6: interleukin 6; IL11: interleukin 11. (B) Western blot probed with anti-mGATA1 antibody (top panel) and anti-TBP antibody (bottom panel) using nuclear extracts from day 6 (d6) $CD41^+$ cells from *in vitro* cultures. Genotype of cells is indicated above the blot. (C) Expression analysis of indicated genes in three independent day 12 (d12) embryoid bodies (EB)-derived megakaryocyte cultures from BirA (grey bar), bioG1 (blue bar) and bioG1s (red bar) cells or from undifferentiated ESC (black bar). (D) Top, photomicrographs of acetylcholinesterase (AChE) stained megakaryocytes (arrows) from d12 of culture. Scale bars indicate 100 μm. Below, bar plot of percentages of $AChE^+$ cells (relative to $CD41^{hi}$ cells) in three different cultures. (E) Flow cytometry showing expression of kit and CD41 on cells produced at d6 (above) or d12 (below) of *in vitro* culture. Left, BirA cells, middle, bioG1 cells and right, bioG1s cells. Figures in each gate show the mean ±1 standard deviation (SD) percentage of cells within the gate (five independent experiments). Position of $CD41^{hi}$ cells is indicated on the right of the d12 plot. (F) Flow cytometry showing expression of CD42b and CD41 (top) and CD61 and CD41 (middle) at d12 of culture. Bottom, CD42b and kit expression in $CD41^+CD61^+$ cells. Left, BirA cells, middle, bioG1 cells and right, bioG1s cells. Figures in each gate show the mean ±1SD percentage of cells within the gate (three independent experiments). (G) Viable cell count (y-axis) from d6 to d12 in culture (x-axis) when $kit^{hi}CD41^+$ cells from BirA (grey line), bioG1 (blue line) and bioG1s (red line) EB were replated on OP9 layer with cytokines (three independent experiments). Dead cells were excluded by trypan blue staining. *P<0.05 and **P<0.01 *vs.* BirA. $^{\#}P$<0.05, $^{\#\#}P$<0.01 and $^{\#\#\#}P$<0.001 *vs.* bioG1.

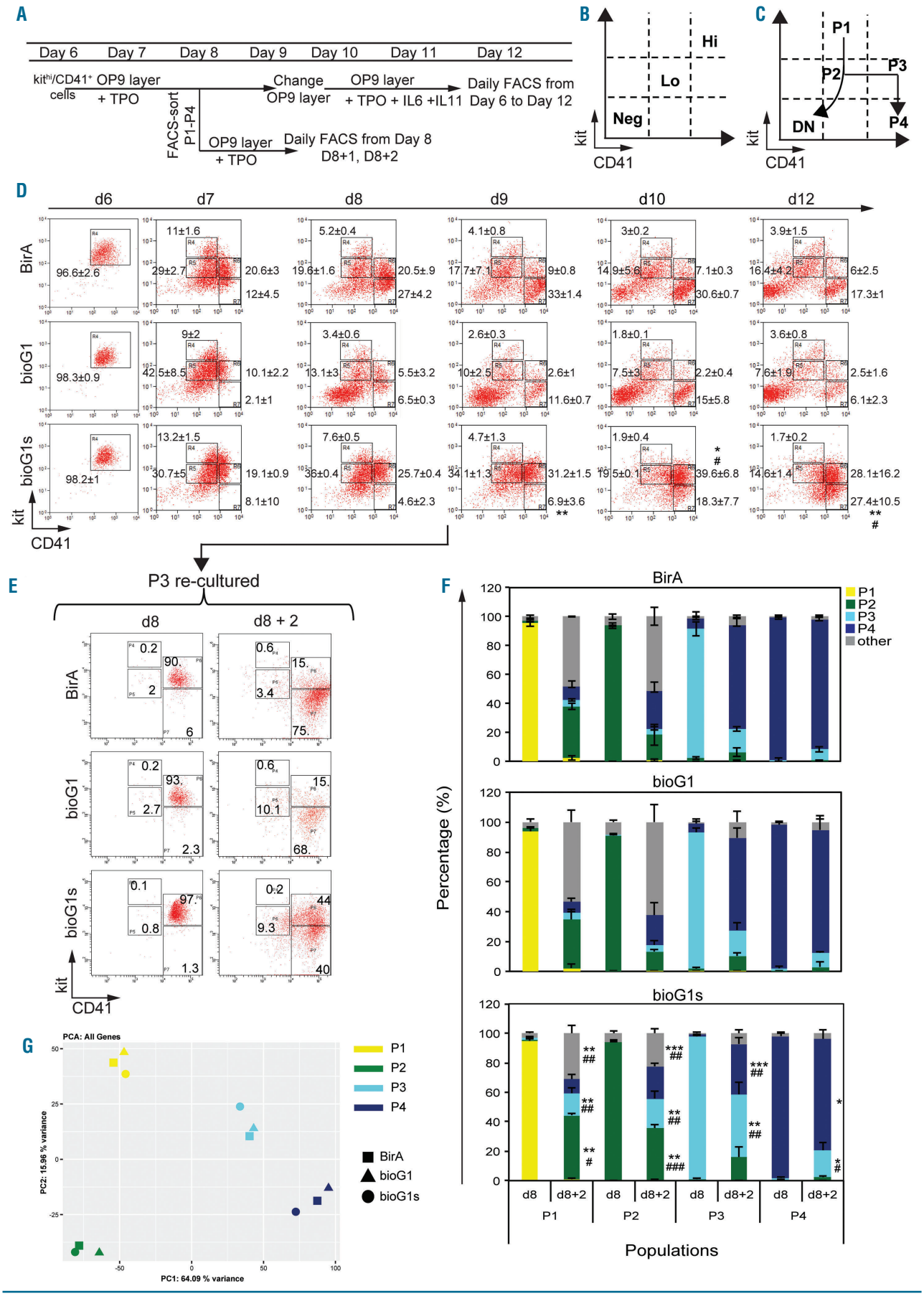


Figure 2. Legend on following page.

Figure 2. (previous page) Gata1s hemopoietic cells have abnormal differentiation kinetics. (A) Schematic of experiment. Hemopoietic cells ($kit^{hi}CD41^{lo}$) from BirA, bioG1 and bioG1s day 6 (d6) embryoid bodies (EB) were cultured for another 6 days (up to day 12 [d12]). Aliquots of culture were analysed daily for kit and CD41 expression by fluorescence-activated cell sorting (FACS). In parallel, at d8, populations P1-P4 (see panel B-C) cells were purified by FACS-sorting, from cultures of three genotypes, re-cultured for 2 days and kit and CD41 analysed by FACS analysis. (B) Schematic of levels of kit and CD41 expression detected by flow cytometry. Neg: negative; lo: low and hi: high. Different levels of kit and CD41 expression define different hemopoietic cell populations in panels C-E. (C) Schematic summary of the data from panel (D), showing the two branches of hemopoietic differentiation undertaken by the initial $kit^{hi}CD41^{lo}$ (P1 population). P1 cells differentiate into P2 cells ($kit^{lo}CD41^{lo}$). P2 cells then differentiate into either DN (double negative, $kit^{-}CD41^{-}$) cells or into P3 ($kit^{lo}CD41^{hi}$) cells. P3 cells differentiate into P4 ($kit^{-}CD41^{hi}$) cells. (D) Representative FACS plots showing the differentiation of d6 hemopoietic cells ($kit^{hi}CD41^{lo}$, termed P1 population) from BirA (top), bioG1 (middle) and bioG1s (bottom) cultures from d7 to d12 monitored by kit and CD41 expression. Numbers within gates are the mean percentage ± 1 standard deviation of cells within the gate from three independent experiments. (E) Example of the re-culturing of FACS-purified d8 populations for two additional days. Here, P3 cells were FACS-purified from BirA cultures (top), bioG1 (middle) and bioG1s (bottom) cultures and re-cultured for 2 days. Left, FACS plots of post-sort purity checks of sorted P3 cell population. Right, expression of kit and CD41 expression after two days of culture. (F) Quantitation of the different populations generated by FACS-sorted d8 P1, P2, P3 and P4 populations after an additional 2 days of culture (three independent experiments for BirA and bioG1, four independent experiments for bioG1s). (G) Principal component analysis (PCA) plot showing P1 to P4 populations (each dot corresponds to the average of the four replicates) from each genotype using all genes analysed by RNA sequencing. Percentage variance for each PC is shown. $*P<0.05$, $**P<0.01$ and $***P<0.001$ *vs.* BirA. $^{\#}P<0.05$, $^{\#\#}P<0.01$ and $^{\#\#\#}P<0.001$ *vs.* bioG1.

immature hemopoietic cells) and CD41 (marker of megakaryocyte maturation) expression at d6 and d12 of culture (Figure 1E; *Online Supplementary Figure S1F*). D6 bioG1s EB produced significantly more $kit^{+}CD41^{+}$ (hemopoietic) cells. By d12, there were significantly more $CD41^{hi}$ cells in bioG1s cultures than bioG1 and BirA cultures but most bioG1s $CD41^{hi}$ cells still expressed the immaturity marker, kit. Finally, there were significantly fewer non-megakaryocyte $kit^{-}CD41^{-}$ cells in bioG1s compared to bioG1 and BirA cultures.

In order to further characterize megakaryocyte marker expression, we confirmed that $CD41^{+}$ megakaryocytes also co-expressed the mature megakaryocyte markers CD42b and CD61 at d12 (Figure 1F; *Online Supplementary Figure S1H*), paradoxically even in kit expressing cells in bioG1s cells. Interestingly, there were significantly greater percentage of $CD41^{+}CD61^{+}$ cells in bioG1s cultures compared to control bioG1 and BirA cultures. Finally, bioG1s cells also expressed lower levels of the maturity marker CD42b on $CD41^{+}CD61^{+}$ cells.

Finally, we measured cell growth by counting viable cell numbers daily from d6 to d12 (Figure 1G). Numbers of cells in BirA, bioG1 and bioG1s were similar from d6 to d9 but then increased significantly in bioG1s cultures and were 10-fold greater at d12 compared to both BirA and bioG1 cultures.

In summary, the cultures produced both megakaryocyte and non-megakaryocyte cells. Compared to wild-type GATA1 hemopoietic cells, bioG1s cells were more proliferative, producing more immature megakaryocytes and fewer non-megakaryocytic cells.

In order to characterize the kinetics of abnormal differentiation we sampled cultures daily from d6 to d12 (Figure 2A-D). Starting with FACS-purified d6 $kit^{hi}CD41^{lo}$ cell population (termed P1), we monitored maturation (lower the level of kit expression the more mature the cells) and acquisition of the megakaryocyte lineage (increasing CD41 expression).

The temporal sequence of flow cytometric plots suggested that control cells (BirA and bioG1) first showed a decrease in kit expression level, generating a $kit^{lo}CD41^{lo}$ population (termed P2) (seen at d7). Cells in P2 then divided into two differentiation branches (Figure 2B-D; *Online Supplementary Figures S2A, S3A*). In one branch, cells progressively lost expression of both kit and CD41 (d8 onwards) to generate a $kit^{-}CD41^{-}$ population (double negative [DN] cells). This DN population was mainly composed of erythroid cells (see below). In the other branch, P2 cells also differentiated towards the megakaryocytic lineage with an increase in CD41 expression level ($kit^{lo}CD41^{hi}$ population, called P3) (d7 onwards) followed by loss of kit expression ($kit^{-}CD41^{hi}$ population, called P4) (d8 onwards).

In contrast, there were two marked differences in bioG1s cultures (Figure 2D). First, they generated far fewer DN cells. Second, bioG1s cells showed enhanced differentiation into the P3 population (d9-10) but with a delay of differentiation into P4 (best seen at d8-9, more cells in P4 in control cultures). In contrast, there were more cells in bioG1s in P4 at d12.

Though this temporal analysis was suggestive of two differentiation branches and hierarchical relationships between P2, P3, P4 and P2 and DN (Figure 2C), in order to provide more definitive proof we FACS-sorted each population (P1, P2, P3, P4) individually at d8 and re-cultured them for 2 days. During re-culture we analyzed kit and CD41 expression in the progeny produced (Figure 2E, re-culture of P3, Figure 2F, data summary; *Online Supplementary Figures S2B, S3B*). FACS-sorted P1 generated all the other populations. Purified P2 generated all the populations except P1. P3 differentiated primarily into P3 and P4 only but not DN cells. Finally, re-culturing of P4 cells generated principally P4 cells. These data were consistent with the differentiation branches and hierarchical relationships in Figure 2C. Finally, we performed RNAseq on sorted populations and showed that they were transcriptionally distinct. A PCA plot using all expressed genes revealed that each population form a separate cluster, regardless of their genotype. Moreover P3 and P4 populations segregated along PC1, suggesting they related to each other (Figure 2G). Analyses have also been run using the top most variant genes across all populations, ranging from 100 to 10,000 genes and revealed a similar pattern (*Online Supplementary Figure S3C*).

Comparing the differentiation potential of FACS-sorted bioG1s populations to control BirA and bioG1 cells (Figure 2F), bioG1s P1 cells also generated significantly more P2 and P3 cells than BirA and bioG1 P1 cells. BioG1s P2 cells also generated significantly more P2 and P3 cells than BirA and bioG1 P2 cells. Finally, bioG1s P3 cells generated more P3 but fewer P4 cells compared to BirA and bioG1 P3 cells.

Taken together, $kit^{hi}CD41^{lo}$ hemopoietic progenitors differentiate either into non-megakaryocytic DN cells or megakaryocytic cells with increased CD41 expression and loss of kit expression. BioG1s mutant cells have a reduced ability to differentiate into DN cells but generate more megakaryocytic cells but with a partial differentiation delay at the P3 population stage.

Reduced erythroid differentiation by bioGATA1s hemopoietic cells

In order to confirm the identity of $kit^{-}CD41^{-}$ cells (DN), we analyzed morphology, cell surface markers and mRNA

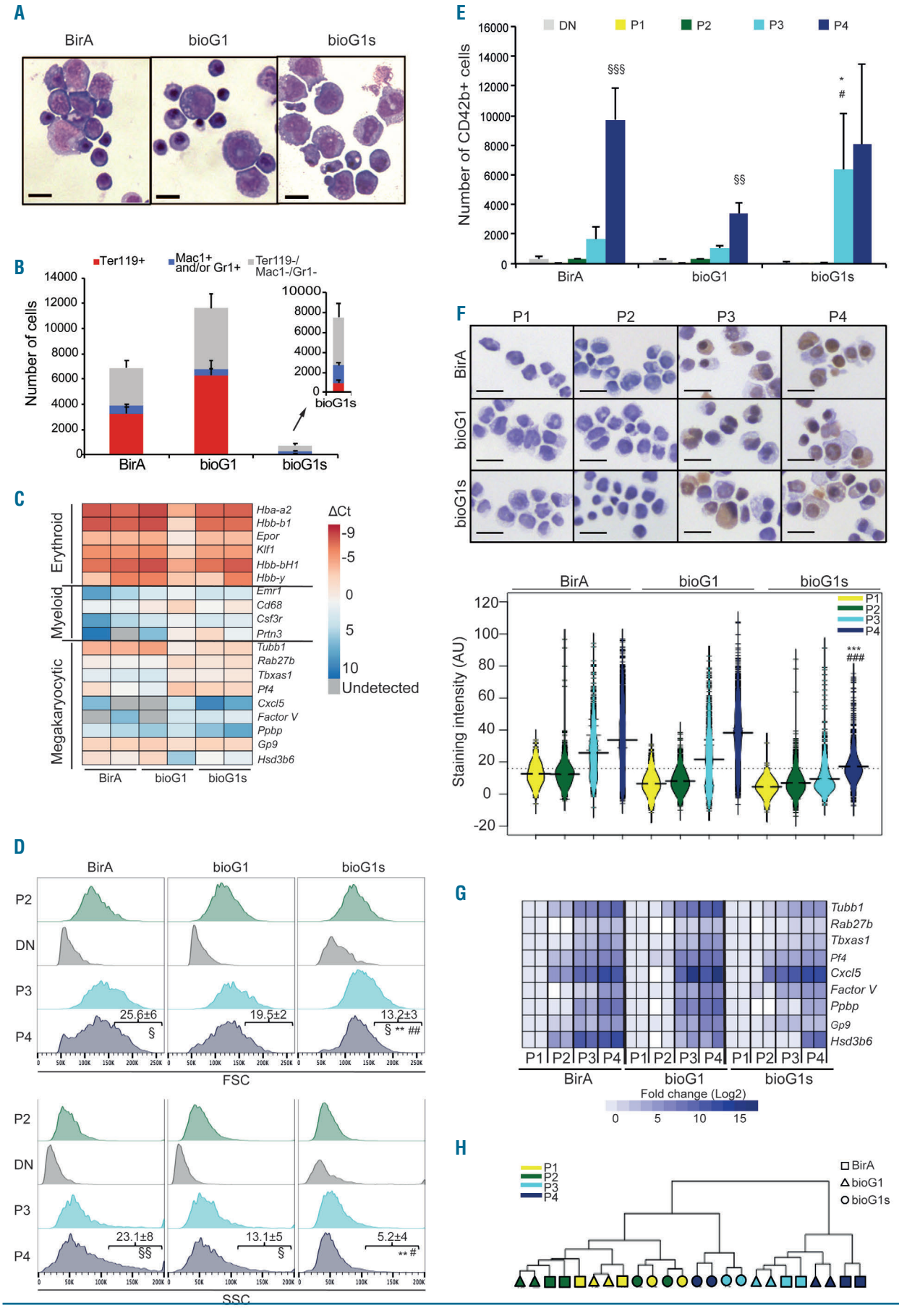


Figure 3. Legend on following page.

Figure 3. (previous page) Gata1s cells fail to produce erythroid cells and mature megakaryocytes. (A) Micrographs of May-Grunwald-Giemsa-stained cytospins of fluorescence-activated cell sorting (FACS)-purified double negative (DN) (kit$^-$CD41$^-$) cells at day 10 (d10). Genotype of cells is indicated above. Scale bars represent 25 μm. (B) Bar plot of number of erythroid cells (Ter119$^+$) and myeloid cells (Gr1$^+$ and/or Mac1$^+$) within the DN population at d10 of culture in BirA, bioG1 and bioG1s cultures. 250,000 total cells analysed by FACS in each case. (C) Heatmap of mRNA expression of selected erythroid (top), myeloid (middle) and megakaryocytic (bottom) genes (in rows) in DN BirA (left), bioG1 (middle) and bioG1 (right) cells at d10. Data from two independent biological replicates is shown. (D) Representative histogram (three independent experiments were performed) showing size (forward scatter [FSC-A], top panel) and granularity (side scatter [SSC-A], bottom panel) assessed by flow cytometry. Data from BirA (left), bioG1 (middle), bioG1s (right) from P2, DN, P3, P4 populations is shown. In P4, numbers indicate the mean percentage ±1 standard deviation (SD) of cells within the gate. (E) Bar plot showing the number of cells expressing CD42b at d12 from DN, P1, P2, P3 and P4 populations from genotypes indicated (three independent experiments). (F) Top, representative micrographs of acetylcholinesterase (AChE) staining of FACS-purified P1 to P4 d10 BirA, bioG1 and bioG1s populations. Scale bars represent 10 μm. Bottom, quantitation of AChE staining, from 500 cells, analyzed from three independent experiments. Bean-plot of staining intensity expressed in arbitrary units (AU) (y-axis) for each population (P1 to P4) from BirA, bioG1 and bioG1s cells. (G) Heatmap showing the fold change in expression of selected megakaryocytic genes (indicated on the right) in FACS-purified P1, P2, P3 and P4 at d10 (columns). Data from two independent biological replicates is shown. Genotype of the cells is indicated below the heatmap. (H) Hierarchical clustering using mRNA data from (G). *P<0.05, **P<0.01 and ***P<0.001 between bioG1s and BirA. $^{\#}P$<0.05, $^{\#\#}P$<0.01 and $^{\#\#\#}P$<0.001 between bioG1s and bioG1. $^{\S}P$<0.05 and $^{\S\S}P$<0.01 between P4 and P2. $^{\$\$}P$<0.01 and $^{\$\$\$}P$<0.001 between P4 and P3.

expression profile of FACS-purified cells (Figure 3A-C; *Online Supplementary Figure S4A-F*). Morphologically, DN cells were primarily erythroid cells, at different stages of maturation, with hardly any granulated myeloid cells (Figure 3A). Approximately 50% of BirA and bioG1 DN cells were Ter119$^+$ and 5% were Mac1$^+$, Gr1$^+$ or both Mac1$^+$Gr1$^+$ (Figure 3B; *Online Supplementary Figure S4A-C*). The DN population was markedly reduced in bioG1s cultures compared to bioG1 (24-fold) and BirA cultures (16-fold) and with more myeloid than erythroid cells. In all three genotypes approximately 50-60% DN cells were Ter119$^-$Gr1$^-$Mac1$^-$. Given FACS-purified DN cells showed higher mRNA expression of erythroid genes and lower expression of myeloid and megakaryocytic genes (Figure 3C; *Online Supplementary Figure S3D-F*), one possible lineage assignment for the Ter119$^-$Gr1$^-$Mac1$^-$ cells could be immature Ter119$^-$ erythroid cells.

Altered megakaryocytic maturation of bioGATA1s cells

During differentiation, megakaryocytes enlarge considerably, acquire granules and develop a demarcation membrane system for proplatelet formation. We used multiple approaches to study megakaryocyte maturation as cells progressed from P2 to P4. First, morphologically, cells in populations P1 and P2 were small, with a blast morphology (*Online Supplementary Figure S5A*). In contrast, cells in P3 and P4 were larger, particularly P4 which were maturing megakaryocytes. In order to quantify these changes, we measured cell size (forward scatter[FSC-A]) and granularity (side scatter [SSC-A]) by flow cytometry (Figure 3D). Concordantly, there was a progressive increase of size and granularity from P2 to P3 and P4. A similar trend was also seen in the mutant cells, but to a lower extent. Closer inspection of FSC and SSC profiles showed a lower proportion of larger and more granular cells in the P4 population in bioG1s compared to control BirA and bioG1 populations. Finally, as expected the erythroid-dominant DN cells showed decreased cell size and granularity compared to P2 cells.

Next, we studied CD42b expression in DN, P1 to P4 populations at d12 (Figure 3E; *Online Supplementary Figure S5B-E*). As expected, very few cells in DN, P1 and P2 expressed CD42b (<4%; absolute numbers <200 cells). In contrast, and as expected, the absolute number (Figure 3E) and proportion (*Online Supplementary Figure S5E*) of CD42b$^+$ cells in P3 and P4 were significantly much higher than in DN, P1 and P2. Importantly, there were significant differences between bioG1s and BirA and bioG1. Absolute numbers of CD42b$^+$ in P3 (Figure 3E) were significantly greater in bioG1s compared to BirA and bioG1 supporting the hypothesis that compared to wild-type GATA1, GATA1s promotes proliferation of kit^{lo} immature megakaryocytes (P3). In contrast, the absolute numbers of mature kit$^-$CD42b$^+$ P4 bioG1s cells were no different compared to bioG1 and BirA.

Furthermore, the absolute number and ratio of CD42b$^+$ cells in P4 relative to P3 was greater in BirA and bioG1. In contrast, in bioG1s the absolute number and ratio of CD42b$^+$ cells was not significantly different between P3 and P4 (Figure 3E; *Online Supplementary Figure S5E*). This supports the hypothesis that GATA1s, compared to wild-type GATA1, is less effective at driving maturation of P3 megakaryocytic cells to P4 megakaryocytic cells.

Next, we measured activity of acetylcholinesterase, an enzyme whose activity increases with megakaryocyte maturation, by quantitating intensity of an acetylcholinesterase driven cytochemical reaction in purified P1, P2, P3 and P4 populations (Figure 3F). The intensity of acetylcholinesterase-induced cytochemical staining was low in P1 and P2 and increased in P3 cells, and increased further, in P4 cells. Importantly, there was significantly lower cytochemical staining in P3 and P4 in bioG1s compared to control BirA and bioG1 cells, which may reflect the smaller size of P3 and P4 bioG1s cells and/or difference in maturation state of bioG1s cells.

Finally, we tested mRNA expression of megakaryocyte specific genes in P1-P4 in all three genotypes (Figure 3G; *Online Supplementary Figure S4E-F*). There was reduced expression of megakaryocyte genes in P3 and P4 in bioG1s compared to BirA and bioG1 cells (*Tubb1, Factor V, Pbbp, Gp9* and *Hsd3b6*). Hierarchical clustering analysis confirmed that bioG1s P3 and P4 cells were transcriptionally more closely related to the more immature P1 and P2 cell populations than P3 and P4 from GATA1 wild-type cells (Figure 3H; *Online Supplemental Figure S5F*).

Taken together, these data confirm megakaryocytes mature from P1 to P4. BioG1s produce more immature megakaryocytes (P3) but they fail to differentiate as efficiently into the most mature megakaryocyte population (P4) compared to wild-type cells.

Decreased apoptosis and increased proliferation in mutant P3 population

In order to understand why the number of bioG1s cells increased during megakaryocytic differentiation (Figure 1G; Figure 3E), we asked if this was due to reduced apoptosis (Figure 4A-B) and/or increased cycling of cells (Figure 4C-D) in bioG1s compared to control BirA cells. We performed flow analyses in P1-P4 sub-populations at d8 (for apoptosis) or d9 (for cell cycle) (2 or 3 days after re-culture of kit^{hi}CD41^{lo}). There was a significant, and specific, decrease in Annexin V$^+$ cells in bioG1s P3 cells. There was

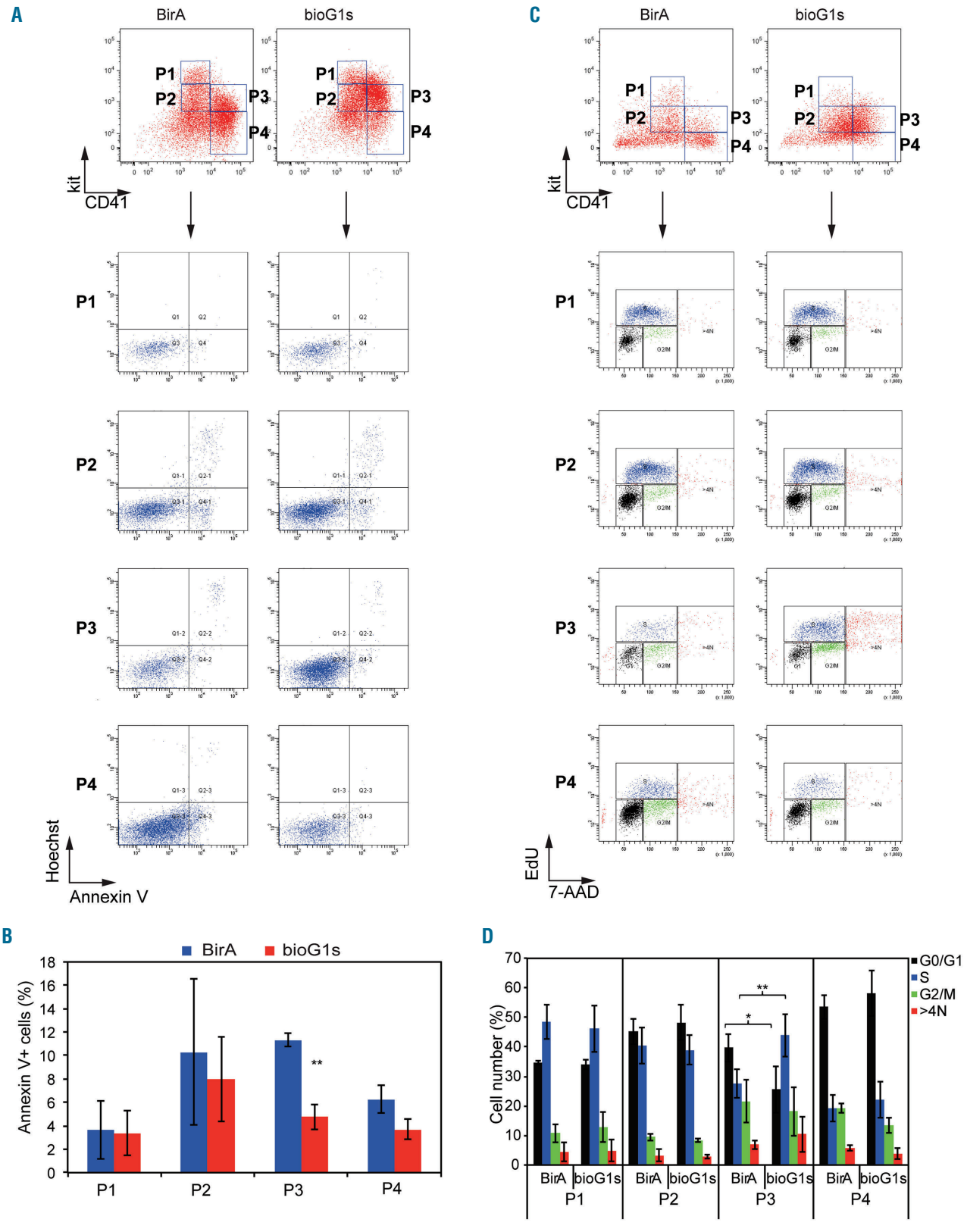


Figure 4. Increased proliferation and decreased apoptosis in GATA1s P3 cells. (A) Flow cytometry analysis, from one representative experiment (of three independent experiments) at day 8 (d8), showing kit and CD41 expression of BirA (left) and bioG1s (right) cells (top). P1 to P4 populations indicated. Below, Annexin V and Hoechst staining within P1 to P4 populations. (B) Bar plot of data from all three experiments showing mean percentage ±1 standard deviation (SD) of AnnexinV$^+$ cells in BirA and bioG1s cultures. (C) Representative flow cytometry analysis, from one experiment (of three independent experiments) at d9. Details as set out in (A). Below, cell cycle analysis determined by EdU incorporation and 7-AAD staining. (D) Bar plot from all three experiments showing mean percentage ±1SD of cells in G0/G1, S, G2/M phases of cell cycle and cells with >4N ploidy, in BirA and bioG1s cultures. *P<0.05 and **P<0.01 between bioG1s and BirA

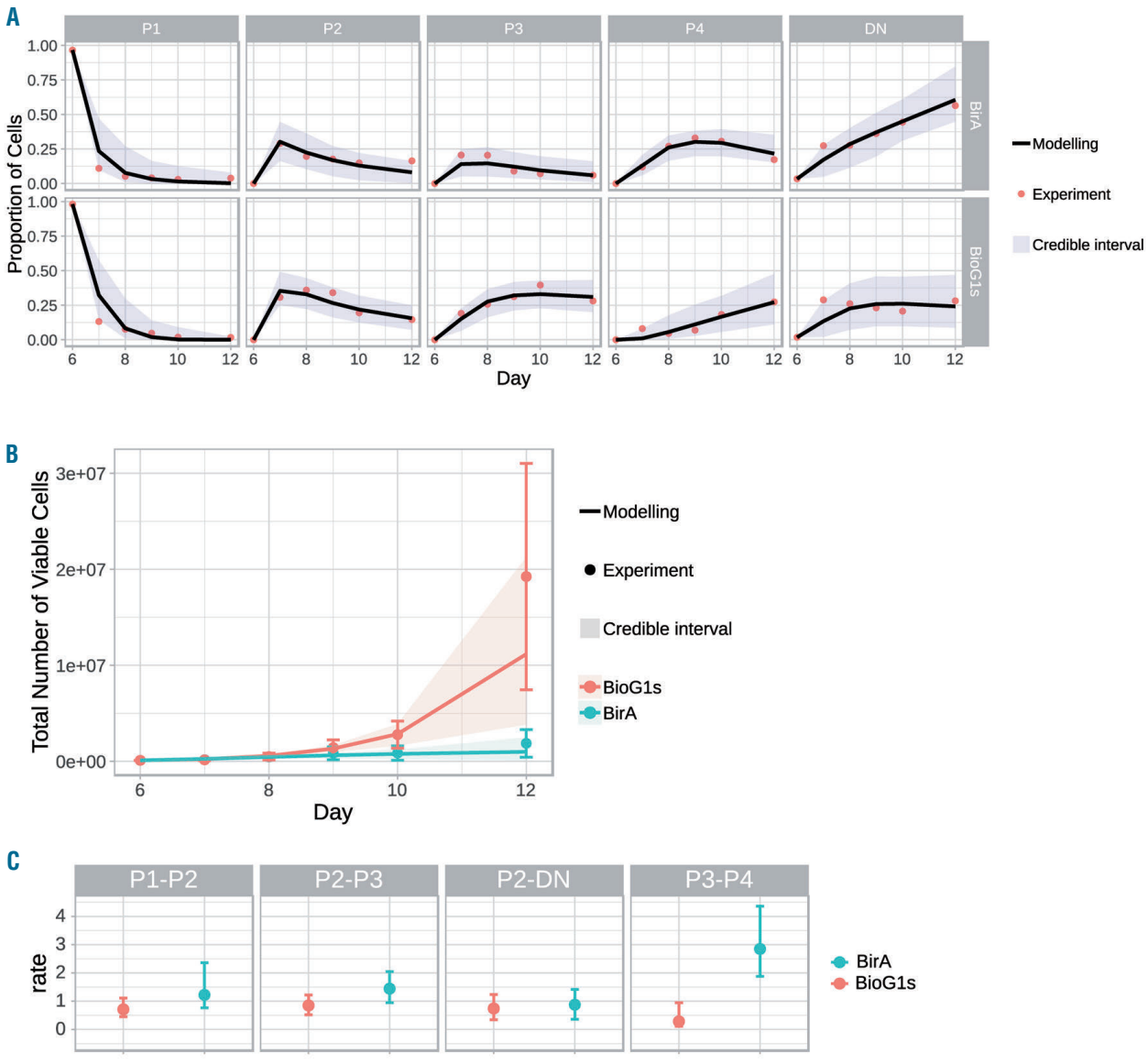


Figure 5. Cell fate modeling suggests GATA1s enhances cell division in P3 cells and reduces commitment to P4. (A) Fit of the mathematical model to the proportions of cells in each population (three independent experiments for BirA, four independent experiments for bioG1s). Top, BirA cells, below, bioG1s cells. The points are the data taken from Figure 2 and the solid line is the model fit. The shaded region is the 95% Confidence Interval (CI) for the data – i.e., 95% of the data should lie within the shaded region. (B) Growth curve for the total number of cells modeled from the model fit. Top, BirA cells, below, bioG1S cells. Note the difference in scale of the y-axis. The error bars of the data are two-times the standard deviation of the replicates. Note the rate of transition of P3 to P4 is much lower for bioG1s. (C) Inferred cell transition rates between the populations and their 95% CI.

also a specific, and significant, increase of bioG1s P3 cells in S-phase and decrease in G1/G0 phase.

Modeling transitions through differentiation

Using the kinetic data of differentiation (Figure 2), together with absolute cell numbers produced per initial cell numbers and the cell cycle and apoptosis data (Figure 4) we have developed a mathematical model (see the *Online Supplementary Appendix*) to study the rates at which the cells transition between P1 to all other populations and how Gata1s mutation alters the kinetics of transition. The fit of the model to the data can be seen in Figure 5A and the modeled cell numbers in culture (Figure 5B) closely mirrors the actual cell numbers produced in culture (Figure 1G). Comparing the rates of transition between the different populations, for BirA and bioG1s cells, only the rate of transition of P3 and P4 was different between BirA and bioG1s cells. Here, bioG1s showed statistically markedly reduced transition between P3 and P4 compared to BirA cells (Figure 5C). This slower transition from P3 to P4 produces an accumulation of cells in P3, where cells are proliferating more than in P4. This provides a likely explanation for the large increase in cell numbers seen in Figure 1G for bioG1s cells from d10 to d12.

GATA1s phenotype is recapitulated *in vivo*

Next, we asked if the *in vitro* EB-derived P1-P4 populations were present in mouse development. EB hemopoiesis mimics yolk sac hemopoiesis[17,18] in that it first produces kit$^+$CD41$^+$CD16$^-$CD32$^-$ primitive yolk sac erythroid progenitors with myeloid and megakaryocytic potential,[17,19] followed by kit$^+$CD41$^+$CD16$^+$32$^+$ definitive ery-

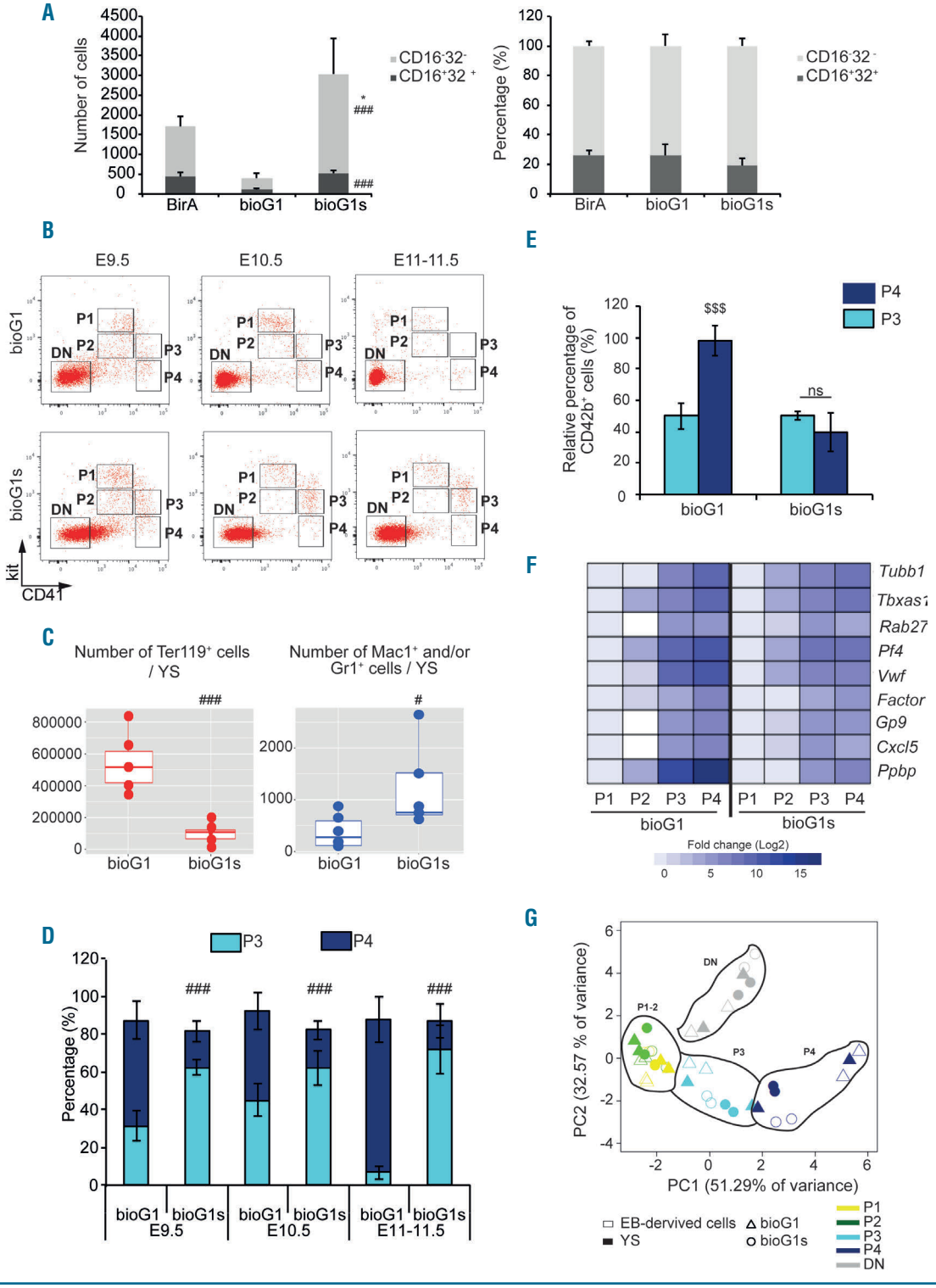


Figure 6. Hemopoietic populations in the yolk-sac. Expansion of GATA1s P3 relative to P4 populations. (A) Bar plot of absolute number (left) and percentage (right) of primitive progenitors with myeloid potential (CD16-CD32-) and definitive erythro-myeloid progenitors ($CD16^+CD32^+$) in day 6 (d6) EB-derived $kit^{hi}CD41^{lo}$ cells. Shown are mean percentage ±1 standard deviation (SD) from three independent experiments. Cell genotype is indicated. (B) Representative flow cytometry analysis plot of kit and CD41 expression from bioG1 (top) and bioG1s (bottom) at E9.5 (left), E10.5 (middle) and E11-11.5 (right) (n=5-7 yolk sacs analyzed individually for each genotype). P1-P4 and DN populations indicated. (C) Box plot of absolute number/yolk sac of erythroid (left, $Ter119^+$) and myeloid (right, $Mac1^+$ and/or $Gr1^+$) in bioG1 and bioG1s. Each dot represents one yolk sac analyzed at E10.5 (n=5/genotype). (D) Ratio of P3/P4 cells expressed as a percentage (y-axis) in bioG1 and bioG1s yolk sacs at different time points (x-axis). The ratios were calculated using the data shown in B, considering only the $CD41^{hi}$ fraction. (E) Mean percentage ±1SD of $CD42b^+$ E10.5 yolk sac cells in P3 and P4 in bioG1 and bioG1s (n=5 for each genotype). (F) Heatmap of fold change of mRNA expression of megakaryocytic genes (rows) in E10.5 yolk sac cells purified from P1 to P4 from bioG1 (left) and bioG1s (right). Cells purified from two independent litters for each genotype, in two independent experiments. (G) Two dimensional principal component analysis (2D-PCA) plot of mRNA expression of 23 genes from either yolk sac cells (shaded symbols) or from embryoid bodies (EB)-derived *in vitro* cultures (open symbols), from bioG1 (triangles) and bioG1s (circles) genotypes, from P1 to P4 and double negative (DN) cells (colour coded as indicated below the figure). Conditions were performed in biological duplicates. Data taken from the *Online Supplementary Figure S5F* (EB-derived cultures) and *Online Supplementary Figure S6H* (yolk sac). **P*<0.05 and ****P*<0.001 between bioG1s and BirA. $^{\#}P$<0.05 and $^{\#\#\#}P$<0.001 between bioG1s and bioG1. $^{\$\$\$}P$<0.01 between P4 and P3.

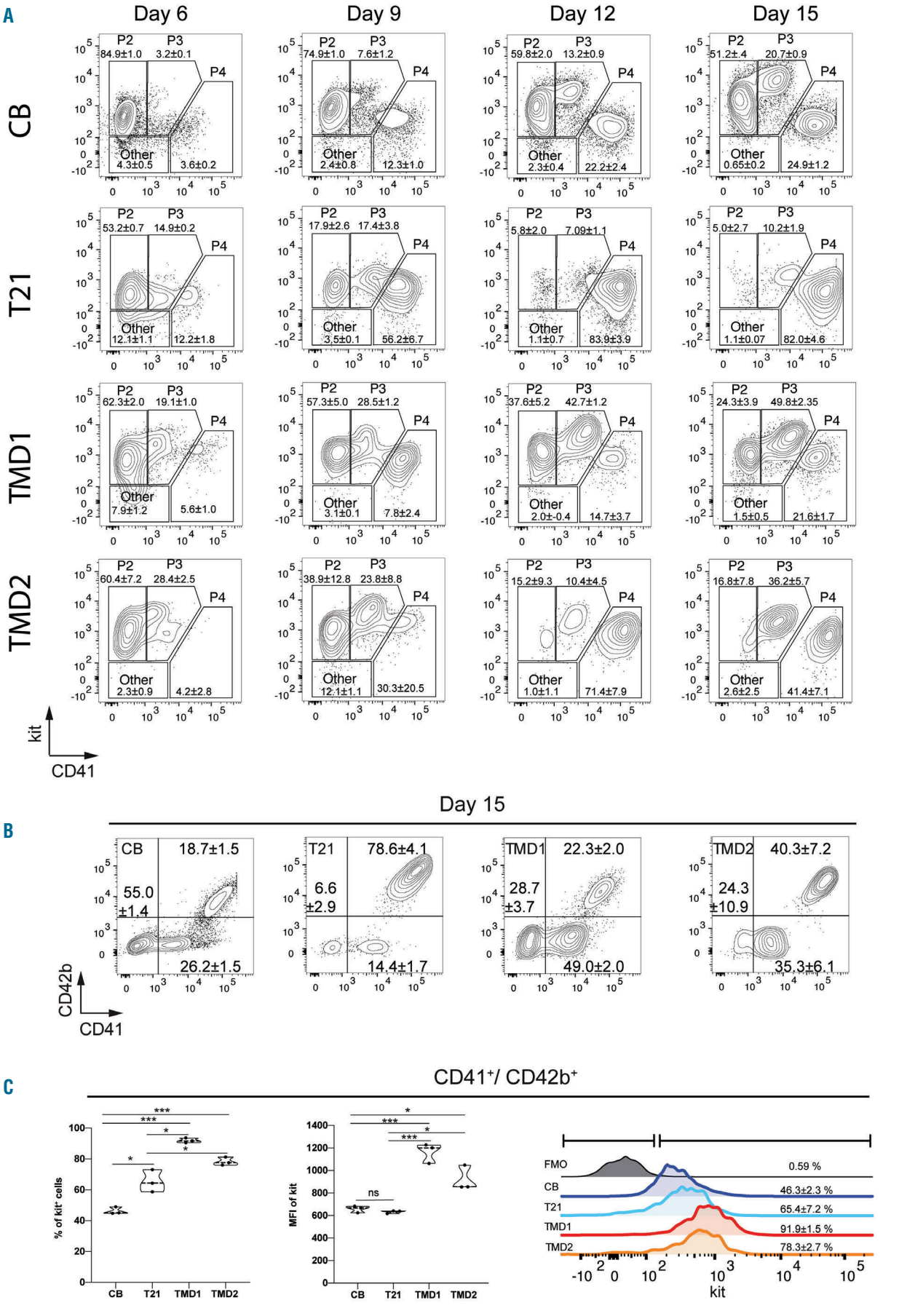


Figure 7. Legend on following page.

Figure 7. (previous page) Megakaryocytic maturation defect is recapitulated in patients with transient myeloproliferative disorder. (A) Representative contour flow cytometry plots of live, CD235a negative cells at day 6 (d6), d9, d12 and d15 of megakaryocytic differentiation assessed by kit (y-axis) and CD41 (x-axis) expression. CB refers to human neonatal GATA1 wild-type (WT) cells ; T21 refers to trisomy for chromosome 21 (T21) and GATA1 WT; TMD1 refers to T21 with a GATA1s mutation (exon2:c.G220C:p.V74L), variant allel frequency (VAF)=10.3 % of mononuclear cells (MNC); TMD2 refers to T21 with a GATA1s mutation (exon2:c.108_109del:p.S36fs), VAF=9.2% of MNC. Numbers within gates are the mean percentage ± 1 standard devaitaion (SD) of cells from three culture experiments performed in parallel for each sample. (B) Representative contour plots of live, CD235a negative cells at d15 of megakaryocytic maturation assessed by CD42b (y-axis) and CD41 (x-axis) expression for (from left to right) CB, T21, TMD1 and TMD2. Numbers within gates are as in A. (C) Plots comparing the percentage of kit positive cells (left), the mean fluorescence intensity (MFI) (middle) or both (right) in mature megakaryocytes defined as $CD41^{+}CD42b^{+}$ in the same set of samples. The unpaired *t*-test was used for statistical analysis. **P*<0.05, ***P*<0.01 and *P****<0.001.

throid-myeloid progenitors (EMP).[20] In d6 EB cultures, the majority of $kit^{hi}CD41^{lo}$ hemopoietic cells were $CD16^{+}CD32^{-}$ primitive erythroid progenitors with myeloid potential (Figure 6A; *Online Supplementary Figure S6A-C*) consistent with previous reports.[20]

Next, we analyzed hemopoietic cells from E9.5 to E11.5 yolk sac for kit and CD41 expression (Figure 6B). In E9.5 yolk sac, we identified populations with the same immunophenotypic profile as P1 to P4 and DN ($kit^{-}CD41^{-}$) populations seen *in vitro* in cultures, in both bioG1 and bioG1s embryos. From E9.5 to E11.5, the DN population was sustained in both bioG1 and bioG1s yolk sac. We then purified this population and quantitated the absolute number of cells/yolk sac (Figure 6C; *Online Supplementary Figure S6D-F*). Absolute numbers of DN cells were far lower in bioG1s yolk sac, with a significantly marked reduction in $Ter119^{+}$ cells and increase in $Mac1^{+}/Gr1^{+}$ cells consistent with data from EB-derived cultures.

Turning to P1-P4 populations, there was a reduction of P1-P2 populations at E10.5, which virtually disappeared by E11-11.5 with mainly P3 and P4 populations present. Importantly, in bioG1s, there was a significant increase in P3 relative to P4 at each time point (E9.5-E11.5) and sustained higher levels of P3 cells at E11-11.5, mirroring *in vitro* culture data (Figure 6B, D). Purified P3 and P4 populations contained $CD42b^{+}$ cells (Figure 6E; *Online Supplementary Figure S6D, E, G*). In control bioG1 cells there were significantly more $CD42b^{+}$ cells in P4 than P3, consistent with megakaryocyte maturation in P4. This was not the case in bioG1s P4 cells, consistent with aberrant, reduced megakaryocyte maturation. We also tested mRNA expression in purified E10.5 P1-P4 cells (Figure 6F). In bioG1 cells megakaryocytic gene expression (most noticeable for *Ppbp, Vwf, Pf4, Tbxas1*) increased progressively from P1/P2 to P3 then to P4. In contrast, in bioG1s cells expression of these genes did not increase from P3 to P4 cells, consistent with a megakaryocyte maturation defect. In order to ultimately confirm that the populations derived from the yolk sac were related to the ones identified from the EB model we performed a two-dimensional principal component analysis (PCA) (Figure 6G). Expression profiles of a panel of genes were interrogated by Fluidigm in DN and P1-P4 EB- and yolk sac-derived populations in both bioG1 and bioG1s (*Online Supplementary Figures S5F, S6H*). The genes were carefully selected for their well known role in specific hemopoietic lineages (*Online Supplementary Table S2*). The PCA was first performed on the EB population using prcomp function (PCA analysis using TRUE for the scale parameter). The yolk sac populations were then projected using the function predict. The most important finding was that yolk-sac and EB-derived DN and P1-P4 populations clustered together, consistent with the notion that the yolk sac and EB populations are transcriptionally similar. Principal component 1 (PC1) (51% of variance) separated the P3 and P4 populations (genes whose expression contributed most to variance were the megakaryocyte genes – *Tubb1, Factor V, Gp9* and *Pf4*) whereas PC2 (32% of variance) separated the P1-P2 and DN populations (genes whose expression contributed most to variance were the erythroid genes – *Klf1, Epor*, and globin genes).

Altered megakaryocytic differentiation is recapitulated in transient myeloproliferative disease samples

Finally, we asked if the amplified immature megakaryocytic population observed in *in vitro* EB-derived Gata1s cells was also present in TMD patients (*Online Supplementary Table S3*). We analyzed the megakaryocytic differentiation of human cord blood $CD34^{+}$ cells cultured in presence of thrombopoietin (TPO) and stem cell factor (SCF) (Figure 7; *Online Supplementary Figure S7*). Cells from disomic cord blood gave rise to $kit^{hi}CD41^{lo}CD42b^{-}$ cells that then matured into a $kit^{lo}CD41^{hi}CD42b^{+}$ population (Figure 7A-B). Cells from T21 cord blood showed an exacerbated megakaryocytic differentiation, as most of the cells were $kit^{lo}CD41^{hi}CD42b^{+}$ by d12, in accordance with a previous report.[21] Interestingly, cells derived from both TMD cord blood (harbouring a Gata1s mutation in around 10% of mononuclear cell [MNC]) showed an accumulation of the immature $kit^{hi}CD41^{lo}CD42b^{-}$ population with a decreased maturation into $kit^{lo}CD41^{hi}CD42b^{+}$ cells compared to T21-derived cells. Moreover, $kit^{lo}CD41^{hi}CD42b^{+}$ cells derived from both TMD samples harboured an increased level of kit expression compared to controls (Figure 7C), suggesting an altered megakaryocytic maturation.

Discussion

Our studies of a new knock-in GATA1s allele, in hemopoiesis from ESC and in murine yolk sacs, define the cellular mechanisms leading to a developmental-stage specific megakaryocyte myeloproliferation that likely contributes to the oncogenic effect of GATA1s. GATA1s results in a 10-fold increase in megakaryocytic cells from ESC cultures compared to control. Though prior work on GATA1s TMD-derived iPSC also demonstrated erythroid differentiation arrest and enhanced megakaryocyte differentiation, the stage in hemopoiesis where perturbed differentiation occurs was unclear.[13] We now demonstrate that accumulation of megakaryocytic lineage cells occurs predominantly late in megakaryopoiesis, at an immature megakaryocyte precursor stage (where most cells are 2N), within a specific compartment (termed P3), characterized

by high CD41 expression and low level of kit expression ($kit^{lo}CD41^{hi}$). Importantly, we showed the accumulation of a similar immature megakaryocytic population in samples from TMD patients, though its immunophenotype slightly differs between mouse and human.

A number of mechanisms may contribute to increased number of GATA1s P3 cells. Hemopoietic cells have a range of cell fate options including differentiation (with or without entering cell cycle), entering cell cycle without differentiating, apoptosis and quiescence. Our data shows that GATA1s P3 cells have increased number of cells in S-phase, reduced number in G0/G1 and a lower number of apoptotic cells compared to GATA1 P3 cells. Detailed kinetic studies of ES-derived hemopoiesis demonstrate a delay in exiting the P3 compartment into the next, more mature megakaryocyte compartment (termed P4) where cells have lost kit expression and presumably lost the proliferative drive afforded by kit signaling. For a 10-fold increase in cell number there need only just over three more cell divisions to account for the increase in GATA1s cell number.

Three major, open questions arise out of our work that provides a platform for future studies. The first two related questions are, what molecular mechanisms explain how GATA1s causes differentiation delay and why does differentiation delay specifically occur in the megakaryocyte lineage? Though the answers to these questions are unclear, prior data suggests that sustained elevated expression of GATA2 in GATA1s cells may play a role.[22] Chromatin occupancy by GATA2/E-box proteins/LMO2/FLI1/ERG/RUNX1 heralds megakaryocyte lineage priming and sustained GATA2 repression of specific loci is correlated with terminal megakaryocyte maturation[23] and indirectly modulates megakaryocyte cell progression in GATA1 deficient megakaryocytes.[24] However, proof that GATA2 is pivotal for GATA1s oncogenicity is still required and if GATA2 is needed, the mechanism by which it delays megakaryocyte differentiation in GATA1s cells requires further work.

Prior work has also suggested that GATA1 may directly interface with cell cycle.[25] Consistent with this, one report has shown that GATA1 directly binds pRB/E2F2 via amino acid residues in the N-terminal GATA1 domain that is deleted in GATA1s.[26] Normally, GATA1/pRB/E2F2 restrain uncommitted murine hemopoietic cell proliferation whereas GATA1s fails to bind pRB/E2F2 and fails to do this.

Our data also confirm that erythroid maturation is reduced in GATA1s cells consistent with prior work.[13] One mechanism for this may be reduced GATA1s binding to cis-elements of erythroid genes which was demonstrated in an erythroid-megakaryocyte cell line model[27] that may cause a failure of terminal erythroid maturation, resulting in activation of an apoptotic program which is normally forestalled by GATA1 and erythropoietin.[28]

The third question is why does GATA1s exert a developmental-stage specific myeloproliferative effect? One possible explanation is that fetal liver-restricted IGF-1 signaling promotes E2F-induced erythro-megakaryocyte proliferation and that the extent of this proliferation is restrained by GATA1, but not GATA1s.[29] Additionally, post-natal bone marrow-specific type 1 interferon signaling may actively suppress GATA1s megakaryocyte-erythroid progenitor growth promoting resolution of TMD in the post-natal period.[30]

In summary, our work now establishes the stage to test the role of previously identified molecular players (GATA1s, GATA2, E2F proteins, pRB, IGF-1 and interferon signaling) and possibly new determinants that regulate transition into and out of P3-like compartment *in vivo* and regulate the commitment of P2-like cells into either megakaryocytic or non-megakaryocytic paths of differentiation.

Disclosures

No conflicts of interest to disclose.

Contributions

GJ and NS conceived, designed and performed experiments, analyzed and interpreted the data, wrote the manuscript; HC and DCH performed experiments and analyzed the data; QC performed modeling analyses; KS, BS, CG assisted with experiments; EK, MA generated ESC and mouse line bioG1; DW wrote the script to analyze staining data; GO performed computational analyses for RNAseq; JD, BU managed mouse colonies; QC, HC, DCH, BS and DW contributed to editing the manuscript; EM, IR, JS, CP, and PV designed the study, analyzed and interpreted the data, wrote the manuscript and academically drove the project.

Funding

PV and IR are supported by Bloodwise Specialist Programme Grant 13001 and by the NIHR Oxford Biomedical Centre Research Fund. PV and CP are supported by programme grants from the MRC Molecular Haematology Unit (MC_UU_12009/11). CG is supported by a Wellcome Trust Clinical Training Fellowship.

References

1. Fujiwara Y, Browne CP, Cunniff K, Goff SC, Orkin SH. Arrested development of embryonic red cell precursors in mouse embryos lacking transcription factor GATA-1. Proc Natl Acad Sci U S A. 1996;93(22):12355-12358.
2. Shivdasani RA, Fujiwara Y, McDevitt MA, Orkin SH. A lineage-selective knockout establishes the critical role of transcription factor GATA-1 in megakaryocyte growth and platelet development. EMBO J. 1997; 16(13):3965-3973.
3. Vyas P, Ault K, Jackson CW, Orkin SH, Shivdasani RA. Consequences of GATA-1 deficiency in megakaryocytes and platelets. Blood. 1999;93(9):2867-2875.
4. Wechsler J, Greene M, McDevitt MA, et al. Acquired mutations in GATA1 in the megakaryoblastic leukemia of Down syndrome. Nat Genet. 2002;32(1):148-152.
5. Rainis L, Bercovich D, Strehl S, et al. Mutations in exon 2 of GATA1 are early events in megakaryocytic malignancies associated with trisomy 21. Blood. 2003; 102(3):981-986.
6. Ahmed M, Sternberg A, Hall G, et al. Natural history of GATA1 mutations in Down syndrome. Blood. 2004;103(7):2480-2489.
7. Roberts I, Alford K, Hall G, et al. GATA1-mutant clones are frequent and often unsuspected in babies with Down syndrome: identification of a population at risk of leukemia. Blood. 2013;122(24):3908-3917.
8. Yoshida K, Toki T, Okuno Y, et al. The landscape of somatic mutations in Down syndrome-related myeloid disorders. Nat Genet. 2013;45(11):1293-1299.
9. Labuhn M, Perkins K, Papaemmanuil E, et al. Mecanisms of progression of myeloid preleukemia to transformed myeloid leukemia in children with Down syndrome. Cancer Cell. 2019; 36(2):123-138.
10. Hollanda LM, Lima CS, Cunha AF, et al. An inherited mutation leading to production of only the short isoform of GATA-1 is associated with impaired erythropoiesis. Nat Genet. 2006;38(7):807-812.
11. Sankaran VG, Ghazvinian R, Do R, et al. Exome sequencing identifies GATA1 muta-

tions resulting in Diamond-Blackfan anemia. J Clin Invest. 2012;122(7):2439-2443.
12. Li Z, Godinho FJ, Klusmann JH, Garriga-Canut M, Yu C, Orkin SH. Developmental stage-selective effect of somatically mutated leukemogenic transcription factor GATA1. Nat Genet. 2005;37(6):613-619.
13. Byrska-Bishop M, VanDorn D, Campbell AE, et al. Pluripotent stem cells reveal erythroid-specific activities of the GATA1 N-terminus. J Clin Invest. 2015;125(3):993-1005.
14. Hamlett I, Draper J, Strouboulis J, Iborra F, Porcher C, Vyas P. Characterization of megakaryocyte GATA1-interacting proteins: the corepressor ETO2 and GATA1 interact to regulate terminal megakaryocyte maturation. Blood. 2008;112(7):2738-2749.
15. Driegen S, Ferreira R, van Zon A, et al. A generic tool for biotinylation of tagged proteins in transgenic mice. Transgenic Res. 2005;14(4):477-482.
16. Nishikii H, Eto K, Tamura N, et al. Metalloproteinase regulation improves in vitro generation of efficacious platelets from mouse embryonic stem cells. J Exp Med. 2008;205(8):1917-1927.
17. Palis J, Robertson S, Kennedy M, Wall C, Keller G. Development of erythroid and myeloid progenitors in the yolk sac and embryo proper of the mouse. Development. 1999;126(22):5073-5084.
18. Keller G, Kennedy M, Papayannopoulou T, Wiles MV. Hematopoietic commitment during embryonic stem cell differentiation in culture. Mol Cell Biol. 1993;13(1):473-486.
19. Tober J, Koniski A, McGrath KE, et al. The megakaryocyte lineage originates from hemangioblast precursors and is an integral component both of primitive and of definitive hematopoiesis. Blood. 2007;109(4):1433-1441.
20. McGrath KE, Frame JM, Fegan KH, et al. Distinct sources of hematopoietic progenitors emerge before HSCs and provide functional blood cells in the mammalian embryo. Cell Rep. 2015;11(12):1892-1904.
21. Roy A, Cowan C, Mead A, et al. Perturbation of fetal liver hematopoietic stem and progenitor cell development by trisomy 21. Proc Natl Acad Sci U S A. 2012;109(43):17579-17584.
22. Bourquin JP, Subramanian A, Langebrake C, et al. Identification of distinct molecular phenotypes in acute megakaryoblastic leukemia by gene expression profiling. Proc Natl Acad Sci U S A. 2006;103(9):3339-3344.
23. Pimkin M, Kossenkov AV, Mishra T, et al. Divergent functions of hematopoietic transcription factors in lineage priming and differentiation during erythro-megakaryopoiesis. Genome Res. 2014;24(12):1932-1944.
24. Huang Z, Dore LC, Li Z, et al. GATA-2 reinforces megakaryocyte development in the absence of GATA-1. Mol Cell Biol. 2009;29(18):5168-5180.
25. Dubart A, Romeo PH, Vainchenker W, Dumenil D. Constitutive expression of GATA-1 interferes with the cell-cycle regulation. Blood. 1996;87(9):3711-3721.
26. Kadri Z, Shimizu R, Ohneda O, et al. Direct binding of pRb/E2F-2 to GATA-1 regulates maturation and terminal cell division during erythropoiesis. PLoS Biol. 2009;7(6):e1000123.
27. Chlon TM, McNulty M, Goldenson B, Rosinski A, Crispino JD. Global transcriptome and chromatin occupancy analysis reveal the short isoform of GATA1 is deficient for erythroid specification and gene expression. Haematologica. 2015;100(5):575-584.
28. Gregory T, Yu C, Ma A, Orkin SH, Blobel GA, Weiss MJ. GATA-1 and erythropoietin cooperate to promote erythroid cell survival by regulating bcl-xL expression. Blood. 1999;94(1):87-96.
29. Klusmann JH, Godinho FJ, Heitmann K, et al. Developmental stage-specific interplay of GATA1 and IGF signaling in fetal megakaryopoiesis and leukemogenesis. Genes Dev. 2010;24(15):1659-1672.
30. Woo AJ, Wieland K, Huang H, et al. Developmental differences in IFN signaling affect GATA1s-induced megakaryocyte hyperproliferation. J Clin Invest. 2013;123(8):3292-3304.

Ferrata Storti Foundation

Genetic lesions in *MYC* and *STAT3* drive oncogenic transcription factor overexpression in plasmablastic lymphoma

Julia Garcia-Reyero,[1,2] Nerea Martinez Magunacelaya,[2] Sonia Gonzalez de Villambrosia,[3] Sanam Loghavi,[4] Angela Gomez Mediavilla,[2] Raul Tonda,[5] Sergi Beltran,[5] Marta Gut,[5] Ainara Pereña Gonzalez,[2] Emmanuel D'Ámore,[6] Carlo Visco,[7] Joseph D. Khoury[4] and Santiago Montes-Moreno[1,2]

[1]Anatomic Pathology Service, Hospital Universitario Marqués de Valdecilla/IDIVAL, Universidad de Cantabria, Santander, Spain; [2]Translational Hematopathology Laboratory, IDIVAL, Centro de Investigación Biomédica en Red de Cáncer (CIBERONC), Santander, Spain; [3]Cytogenetics Unit, Department of Hematology, HUMV, Santander, Spain; [4]Hematopathology Department, MD Anderson Cancer Center, Houston, TX, USA; [5]Centre Nacional d'Anàlisi Genòmica. Barcelona Institute of Science and Technology (BIST). Universitat Pompeu Fabra, Barcelona, Spain; [6]Departments of Pathology and Hematology, San Bortolo Hospital, Vicenza, Italy and [7]Department of Medicine, Section of Hematology, University of Verona, Verona, Italy

Haematologica 2021
Volume 106(4):1120-1128

ABSTRACT

The mutational profile of plasmablastic lymphoma has not been described. We performed a targeted, exonic next-generation sequencing analysis of 30 plasmablastic lymphoma cases with a B-cell lymphoma-dedicated panel and fluorescence *in situ* hybridization for the detection of *MYC* rearrangements. Complete phenotyping of the neoplastic and microenvironmental cell populations was also performed. We identified an enrichment in recurrent genetic events in *MYC* (69% with *MYC* translocation or amplification and three cases with missense point mutations), *PRDM1*/Blimp1 and *STAT3* mutations. These gene mutations were more frequent in Epstein-Barr virus (EBV)-positive disease. Other genetic events included mutations in *BRAF*, *EP300*, BCR (*CD79A* and *CD79B*), NOTCH pathway (*NOTCH2*, *NOTCH1* and *SGK1*) and *MYD88p*L265P. Immunohistochemical analysis showed consistent MYC expression, which was higher in cases with *MYC* rearrangements, together with phospho-STAT3 (Tyr705) overexpression in cases with STAT3 SH2 domain mutations. Microenvironmental cell populations were heterogeneous and unrelated to EBV, with enrichment of tumor-associated macrophages (TAM) and PD1-positive T cells. PD-L1 was expressed in all cases in the TAM population but only in the neoplastic cells in five cases (4 of 14 EBV-positive cases). HLA expression was absent in the majority of cases of plasmablastic lymphoma. In summary, the mutational profile of plasmablastic lymphoma is heterogeneous and related to EBV infection. Genetic events in *MYC*, *STAT3* and *PRDM1*/Blimp1 are more frequent in EBV-positive disease. An enrichment in TAM and PD1 reactive T lymphocytes is found in the microenvironment of plasmablastic lymphoma and a fraction of the neoplastic cells express PD-L1.

Correspondence:

SANTIAGO MONTES MORENO
santiago.montes@scsalud.es

Received: March 1, 2020.

Accepted: April 9, 2020.

Pre-published: April 9, 2020.

https://doi.org/10.3324/haematol.2020.251579

©2021 Ferrata Storti Foundation

Material published in Haematologica is covered by copyright. All rights are reserved to the Ferrata Storti Foundation. Use of published material is allowed under the following terms and conditions: https://creativecommons.org/licenses/by-nc/4.0/legalcode. Copies of published material are allowed for personal or internal use. Sharing published material for non-commercial purposes is subject to the following conditions: https://creativecommons.org/licenses/by-nc/4.0/legalcode, sect. 3. Reproducing and sharing published material for commercial purposes is not allowed without permission in writing from the publisher.

Introduction

Plasmablastic lymphoma (PBL) is an aggressive type of non-Hodgkin B-cell lymphoma defined as a high-grade large B-cell neoplasm with plasma cell phenotype (i.e., loss of B-cell antigens with downregulation of CD20 and PAX5 expression and overexpression of PRDM1/Blimp1 and XBP1s).[1-4]

Epstein-Barr virus (EBV) infection is found in the majority of cases but is not required for the development of a plasmablastic phenotype since clear-cut PBL can be negative for EBV.[3-5] In addition, recent evidence suggests that EBV or human immunodeficiency virus (HIV) status does not influence the gene expression profile

patterns of PBL.[6] However EBV positivity in PBL has been found to be associated with increased expression of the programmed death ligand 1 (PD-L1) protein as well as other immune escape markers,[7,8] and decreased expression of major histocompatibility class II (MHCII)/human leukocyte A (HLA)-DR molecules by the neoplastic cells.[9] This has recently been found to be associated with increased antiviral cytotoxic immunity involving different immune cell populations.[7]

The genetic landscape of somatic mutations in PBL is unclear. So far, *MYC-IGH* translocations have been the most commonly detected alterations, being present in 60% of cases.[10,11] Concurrent mutations in *PRDM1*/Blimp1 have been found in half of these cases.[12] Very recently, exome sequencing of a series of HIV-positive cases of PBL showed somatic mutations involving components of the non-canonical NFκB pathway as well as genes involved in immune response,[13] but the data remain limited.

Our aim was to characterize the genetic profile of a series of PBL cases using targeted exonic next-generation sequencing (NGS) and correlate the findings with EBV infection and the expression status of immune checkpoint proteins in both the population of neoplastic cells and cells in the microenvironment. In addition, we quantified the components of the microenvironment and searched for skewed T-cell populations in this tumor. We found that the mutational profile of PBL was related to EBV infection in the tumor cells and identified recurrent genetic events in *MYC*, *STAT3* and *PRDM1*/Blimp1 that were more frequent in EBV-positive disease. In addition, we identified PD-L1 expression on tumor cells in a subset of cases as well as enrichment of tumor-associated macrophages (TAM) and programmed death 1 (PD1) reactive T cells in the microenvironment of PBL cases.

Methods

Case selection

Twenty-eight new cases were retrieved from the files of the Pathology Department of Universitario Marqués de Valdecilla Hospital (Santander, Spain), ten samples from the files of the University of Texas MD Anderson Cancer Center Hematopathology Department (Houston, TX, USA) and four cases from the Pathology Department of San Bortolo Hospital (Vicenza, Italy). Material transfer agreements were signed by the Instituto de Investigación Marqués de Valdecilla (IDIVAL) and corresponding institutions to share the material in the project. The study and sample collection were approved by the local ethics committee (CEIC Cantabria, Institutional Review Board code 2016.168) and complied with the Declaration of Helsinki. All cases were diagnosed according to the World Health Organization (WHO) classification of Hematolymphoid Neoplasms.[14] All cases had to be negative for pan-B-cell markers (CD20), HHV-8 and ALK in order to be included in the study. The phenotype of the cases was consistent with a plasma cell differentiation program.[4,15] The clinical features of the cases were recorded and a summary is available in *Online Supplementary Table S1*.

Immunohistochemistry and *in situ* hybridization

Immunohistochemical reactions were performed following conventional automated procedures.Chromogenic *in situ* hybridization for EBV and its encoding RNA (EBER) and fluorescence *in situ* hybridization (FISH) for the detection of *MYC* rearrangements were also done.

Quantification of the cellular composition of the tumor and transcription factor abundance

The different lymphoid and histiocytic/dendritic subpopulations, identified with CD3, CD8, PD1, CD163, PD-L1 and MHCII/HLA DP/DR and the absolute number of nuclei showing expression of MYC and phospho-STAT3 (Tyr705) were quantified.

Next-generation sequencing using amplicon-based library generation

DNA was extracted from formalin-fixed paraffin-embedded samples using the PicoPure™ DNA Isolation Kit (ThermoFisher Scientific) and was quantified by an Qbit fluorometer (ThermoFisher Scientific). All samples subjected to NGS analysis were required to have >50% of neoplastic cells, identified by morphology (hematoxylin & eosin).

A TruSeq® Custom Amplicon Low Input Library containing exonic regions of 35 selected genes of interest was used to isolate the DNA for sequencing (Illumina). The selected genes were *CARD11*, *ARID1A*, *NOTCH1*, *TCF3*, *SMARCA4*, *STAT6*, *EP300*, *CREBBP*, *MLL2*, *BTK*, *NOTCH2*, *TNFRSF14*, *ATM*, *FOXO1*, *B2M*, *PLCG2*, *CD79B*, *TP53*, *STAT3*, *BCL2*, *MEF2B*, *CD79A*, *CXCR4*, *PTPN1*, *MYD88*, *FAT2*, *PRDM1*, *TNFAIP3*, *SGK1*, *CCND3*, *PIM1*, *EZH2*, *BRAF*, *MYC* and *NOTHC2*. Of note, variants occurring in regions outside the coverage of our targeted design were not explored using this approach. Details about library preparation can be found in the *Online Supplementary Material*.

Sequencing was performed using a HiSeq instrument (Illumina, paired end, 2x150) at the National Genomic Analysis Center (CNAG, Barcelona, Spain).

Sequencing data interpretation and reporting

Only variants in which both libraries had a coverage ≥300 reads and had the same genotype were selected for downstream analysis. Subsequently only missense, frameshift, and nonsense somatic mutations with a variant frequency >10% were considered (*Online Supplementary Table S2*). Single nucleotide polymorphisms were filtered out using variant allele frequency criteria, and with comparison with dbSNP and an in-house database of germline variants. Finally, 34 somatic mutations (31 missense, 3 nonsense) in 14 genes were considered (Table 1).

Further details on the methods are provided in the *Online Supplementary Material*.

Results

The mutational profile of plasmablastic lymphoma is heterogeneous and correlates with Epstein-Barr virus infection in the neoplastic cells

After targeted NGS with a lymphoma-dedicated panel, somatic missense and nonsense mutations were identified in 18 out of 30 PBL cases (60%). EBV-negative cases tended to show a higher rate of mutations, as compared to EBV-positive cases (87.5% *vs.* 54%, respectively; χ^2 test, $P>0.05$) (Figure 1).

Interestingly the pattern of mutations was also different

Table 1. Summary of the mutations found in 18 out 30 cases (60%) of plasmablastic lymphoma analyzed by targeted exonic next-generation sequencing.

ID	Gene	Location chromosome	Domain	Allele	cDNA position	Codons	AA change		Consequence*	Existing_variation
4	*STAT3*	17	---	A	2009	Gac/Tac	566	D/Y	deleterious	COSM220689
4	*EP300*	22	---	A	7249	atG/atA	2010	M/I	tolerated	---
11	*MYC*	8	---	G	578	aCc/aGc	23	T/S	tolerated	---
11	*MYC*	8	---	A	775	Tac/Aac	89	Y/N	tolerated	---
11	*MYC*	8	---	C	899	tTc/tCc	130	F/S	deleterious	COSM4171775
11	*MYC*	8	---	G	945	atC/atG	145	I/M	deleterious	---
14	*STAT3*	17	SH2	A	2255	Atg/Ttg	648	M/L	tolerated	---
14	*STAT3*	17	SH2	A	2232	tAc/tTc	640	Y/F	probably damaging	COSM1155743
17	*STAT3*	17	SH2	G	2165	Ggc/Cgc	618	G/R	deleterious	COSM1166777
17	*PRDM1*	6	PR	G	843	gaC/gaG	203	D/E	neutral	rs811925*, COSM4160094
28	*PRDM1*	6	PR	G	843	gaC/gaG	203	D/E	neutral	rs811925*, COSM4160094
7	*MYC*	8	---	T	1085	tAc/tTc	192	Y/F	probably damaging	---
7	*CD79B*	17	---	T	175	Gac/Aac	34	D/N	tolerated	---
8	*SMARCA4*	19	---	A	3295	cGa/cAa	1005	R/Q	deleterious	---
8	*PRDM1*	6	Ac	A	2546	gGc/gAc	771	G/D	tolerated	---
2	*STAT3*	17	SH2	A	2253	aAc/aTc	647	N/I	deleterious	COSM1155744
2	*NOTCH1*	9	EGF-like	A	1278	cCc/cTc	401	P/L	deleterious	COSM4745915
5	*STAT3*	17	SH2	A	2232	tAc/tTc	640	Y/F	probably damaging	COSM1155743
10	*PRDM1*	6	Pro-rich	A	1295	aGc/aAc	354	S/N	tolerated	rs143040512,COSM4406870
10	*CD79A*	19	---	A	413	tgG/tgA	76	W/*	---	COSM5493940
26	*PRDM1*	6	PR	G	843	gaC/gaG	203	D/E	neutral	rs811925*, COSM4160094
27	*PRDM1*	6	PR	G	843	gaC/gaG	203	D/E	neutral	rs811925*, COSM4160094
3	*ARID1A*	1	---	A	762	Ggg/Agg	131	G/R	deleterious	---
3	*ARID1A*	1	---	C	6526	tGc/tCc	2052	C/S	deleterious	---
3	*MYD88*	3	TIR	C	794	cTg/cCg	265	L/P	deleterious	COSM85940
15	*BRAF*	7	ATP binding site	G	1467	gGa/gCa	469	G/A	deleterious	COSM460
18	*SGK1*	6	---	A	1950	tCc/tTc	451	S/F	deleterious	---
18	*SGK1*	6	---	A	1737	gCt/gTt	380	A/V	tolerated	---
9	*NOTCH2*	1	PEST	A	7418	Cga/Tga	2400	R/*	deleterious	COSM36210
1	*MYC*	8	---	T	747	agC/agT	79	S/	---	---
1	*EP300*	22	---	A	6411	cGc/cAc	1731	R/H	deleterious	---
1	*BRAF*	7	STKc_Raf	T	1860	gTg/gAg	600	V/E	deleterious	COSM476
1	*SGK1*	6	---	A	1004	Aag/Tag	136	K/*	deleterious	---
13	*TP53*	17	---	T	1008	cGt/cAt	273	R/H	possibly damaging	COSM10660

Gene name, exonic location, cDNA position, single nucleotide change observed, and amino acid change predicted, together with consequences predicted using three different algorithms are shown. In addition, the dbSNP and the COSMIC identity is provided when available. ID: identity; AA: amino acid.

between EBV-positive and EBV-negative cases. Recurrent somatic mutations restricted to EBV-positive cases were found in *PRDM1*/Blimp1 in six cases and in *STAT3* in five cases. Notably, a recurrent *PRDM1*/Blimp1 variant, D203E, was identified in four out of six cases, involving the PR domain of the protein.

STAT3 mutations were found in five out of 30 cases (16%), all EBV-positive. Interestingly all but one (*STAT3p*D566Y) of the mutations involve the SH2 domain of STAT3 protein (*STAT3p*Y640F, *STAT3p*M648L, *STAT3p*G618R, *STAT3p*N647I) (Figure 2) and lead to phosphoSTAT3 (Tyr705) protein overexpression (see below).

The majority of PBL cases (16 out of 23 tested, 69%) harbored structural abnormalities at the *MYC* locus. Fourteen cases were found to have a *MYC* translocation (60%) using break apart probes. *MYC-IGH* was confirmed in seven of nine cases tested (77%). *MYC* was found to be amplified by FISH in two additional cases (Figure 1). Thus, in cases with *MYC* rearrangements, *MYC-IGH* was the most frequent alteration. Although there was a clear trend for an association between EBV positivity and *MYC* rearrangement the difference was not statistically significant (χ^2 test, P=0.06).

Furthermore, *MYC* was found to be mutated in three cases with all but one of the mutations involving exon 2 and consisting of transversions and transitions at C: G pairs (4 out of 7 mutations) (Table 1). Furthermore, the *MYCp*79S mutation involves the WRCY consensus motif. All these features are consistent with a mechanism related with aberrant somatic hypermutation, as described in early reports.[16]

Mutations common mutations diffuse large B-cell lymphoma (DLBCL), not otherwise specified (NOS), involving B-cell receptor (BCR) activation, TLR/NFκB, histone-mod-

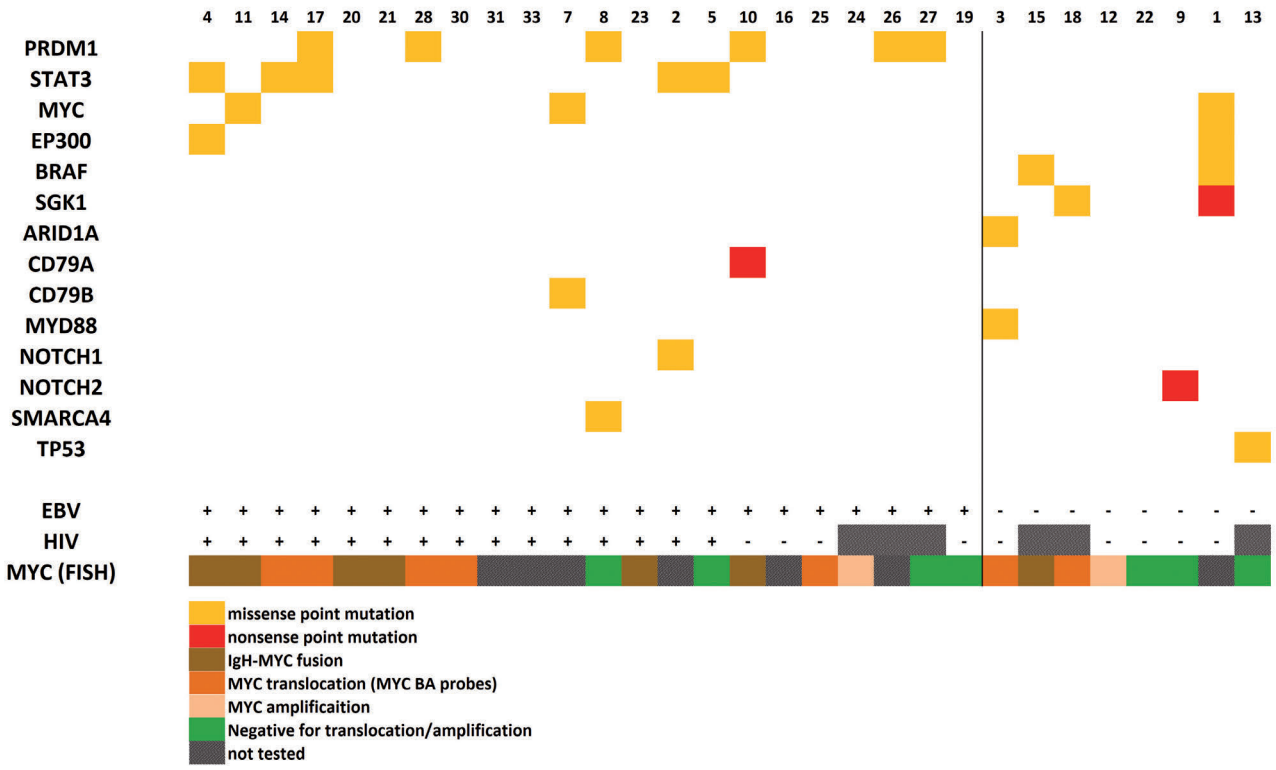


Figure 1. Summary of the mutations found in 18 out of 30 cases (60%) analyzed by targeted exonic next-generation sequencing. Epstein-Barr virus (EBV) positivity of tumor cells and human immunodeficiency virus (HIV) infection by the patient are shown, together with the status of the *MYC* gene as determined by interphase fluorescence *in situ* hybridization (FISH). The pattern of somatic mutations is heterogeneous with a trend to a higher rate of mutations in EBV-positive cases. The most common genetic events in plasmablastic lymphoma are mutations (including translocations, amplifications and point mutations) in the *MYC* gene. Previously undescribed abnormalities in plasmablastic lymphoma such as *STAT3* (16% of cases), *BRAF*, *MYD88*, *NOTCH2* and *TP53* mutations were also identified (see details in Table 1).

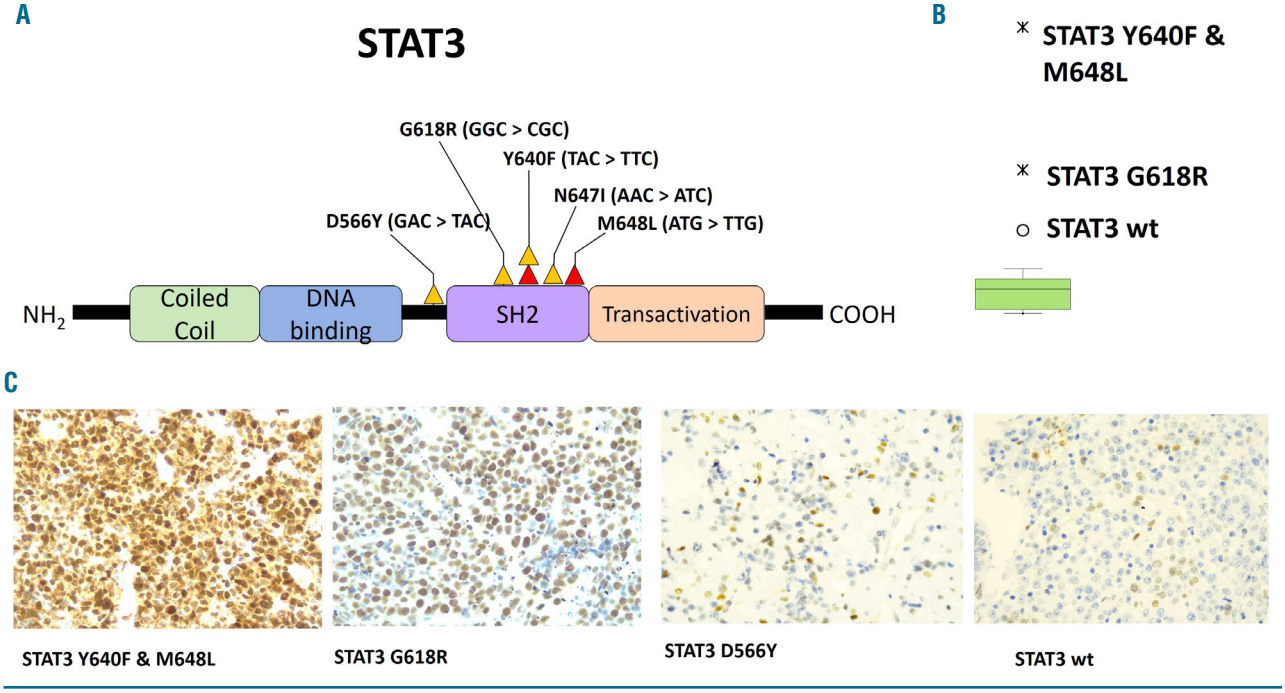


Figure 2. *STAT3* mutations in plasmablastic lymphoma. (A) *STAT3* mutations were found in five cases (16%), all of which were positive for Epstein-Barr virus. Interestingly all but one (*STAT3*pD566Y) of the mutations involved the SH2 domain of the STAT3 protein. (B) The mean phosho-STAT3 expression for SH2 domain-mutated cases (2 cases with available mutational and immunohistochemical data) was 249 nuclei per high power field (40x), whereas that for STAT3 wild-type cases was 28 nuclei per high power field. Thus, STAT3 SH2 domain mutations led to phosphoSTAT3 (Tyr705) protein overexpression. (C) Representative microphotographs of phosphoSTAT3 (Tyr705) protein expression in plasmablastic lymphoma.

ifying genes and the NOTCH pathway were found in eight cases (Table 1, Figure 1). These mutations involved *CD79p*AW76*, *CD79Bp*D34N, *MYD88p*L265P, *NOTCH1p*P401L, *NOTCH2p*R2400*, *SGK1Kp*136*and *EP300p*M2010I/*EP300p*R1731H. The NOTCH pathway was affected by somatic mutations in NOTCH2 (1 case), NOTCH1 (1 case) and SGK1 (2 cases). Other mutations found were *SMARCA4p*R1005Q and *TP53p*R273H. Of note, two cases, both EBV-negative, had mutations in the *BRAF* gene, one case with the canonical activating *BRAFp*V600E mutation and the other with a *BRAFp*G469A mutation in the ATP binding site.

STAT3 mutations are associated with constitutive phospho-STAT3 (Tyr705) activation and MYC protein overexpression is related to *MYC* rearrangement status

Expression of phospho-STAT3 (Tyr705) protein was quantified immunohistochemically in 20 cases with available mutational data. Mean phospho-STAT3 expression was 48 nuclei per high power field (HPF; 40x) in these 20 cases. Mean expression for two out of four SH2 domain-mutated cases with available immunohistochemical data was 249 nuclei per HPF. Mean phosho-STAT3 expression for *STAT3* wild-type cases was 28 nuclei per HPF. Mean phospho-STAT3 expression for the single non-SH2 *STAT3*-mutated sample was 40 nuclei per HPF. Thus, *STAT3* SH2 domain mutations (*STAT3p*Y640F, *STAT3p*M648L, *STAT3p*G618R, *STAT3p*N647I) were associated with overexpression of phospho-STAT3, as determined by immunohistochemistry of tissue samples (Figure 2B).

MYC protein was consistently expressed in all the cases (range, 59-236 nuclei per HPF; mean 236), irrespective of the presence of *MYC* translocations, as previously reported.[12,17] However, significant differences in the level of MYC expression were found, according to *MYC* gene status. *MYC*-translocated (14 cases) and -amplified cases (2 cases) had, as expected, higher MYC protein expression than cases without *MYC* rearrangements (7 cases). The mean number of positive nuclei per HPF was 109 in non-rearranged cases *versus* 282 in *MYC*-rearranged cases (Mann-Whitney test, $P<0.0001$) (Figure 3).

Mean MYC protein expression in 22 cases with available data was 236 nuclei per HPF, which was significantly higher than the mean 48 nuclei per HPF in the cases of phospho-STAT3 protein expression (Wilcoxon test, $P<0.001$). There was no correlation between the levels of expression of the two proteins (Pearson test, non-significant). Due to the high prevalence of *MYC* translocations and amplification in PBL and the relatively low levels of phospho-STAT3 expression and absence of correlation between the proteins, it is unlikely that STAT3 activation contributed to MYC overexpression in most cases. However, one of our cases with *STAT3* SH2 domain mutations and absence of *MYC* translocation by FISH showed high levels of both phospho-STAT3 and MYC proteins, without detectable PRDM1/Blimp1 mutations, suggesting that MYC overexpression might be related with STAT3 activation by mutations in rare cases of PBL.

In summary, MYC protein overexpression is due to rearrangements involving *MYC* in a significant proportion of cases of PBL (69% in our series). Most translocations fuse *MYC* to *IGH* and a few cases may show amplifications of the *MYC* gene. Both alterations lead to MYC protein overexpression. Genetic alterations in the *MYC* regulatory domains of *PRDM1*/Blimp1 may also contribute to its overexpression.[12] In addition here we show that a frac-

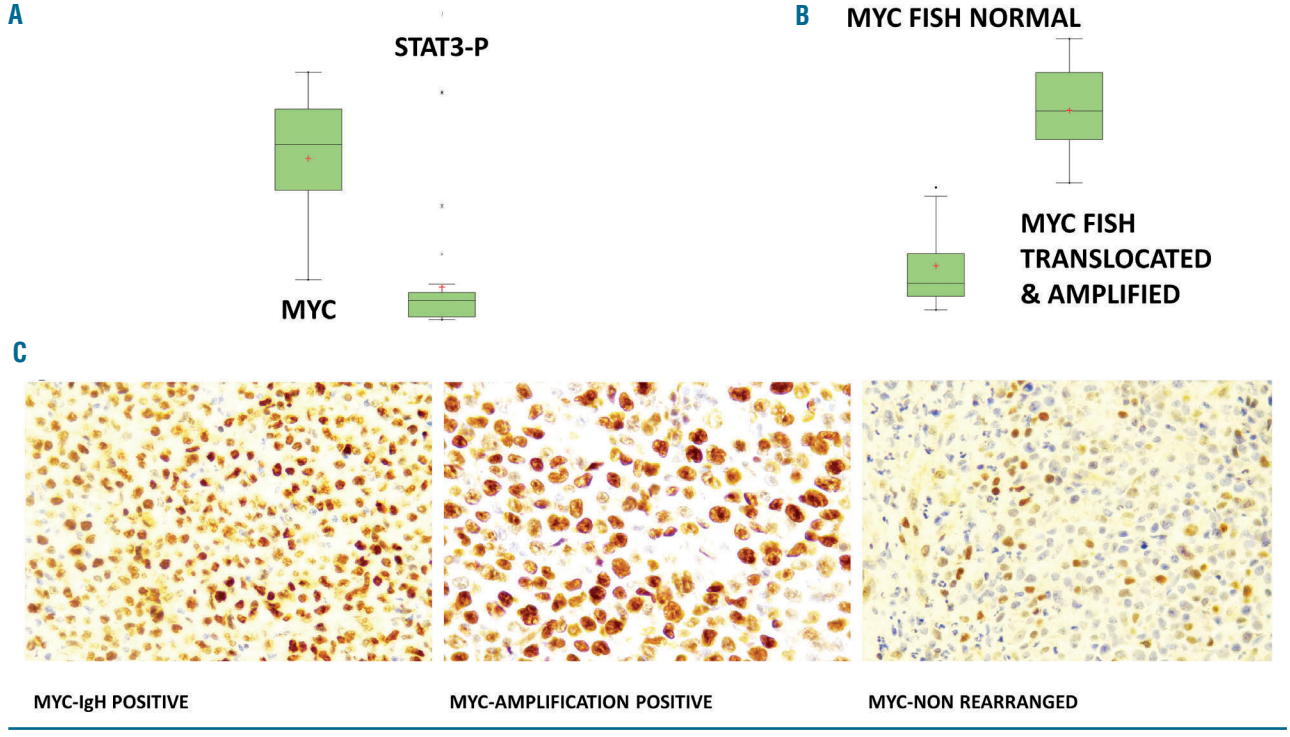


Figure 3. MYC protein expression in plasmablastic lymphoma. (A) MYC protein was consistently expressed in the cases of plasmablastic lymphoma. (A) Mean MYC protein expression in 22 cases with available data was 236 nuclei per high power field (HPF), which was significantly higher than the mean of 48 nuclei per HPF in the case of phospho-STAT3 protein expression (Wilcoxon test, $P<0.001$). *MYC* translocated cases (n=14) and *MYC* amplified cases (n=2) had higher MYC protein expression than cases without *MYC* rearrangements (n=7) (Mann-Whitney test, $P<0.0001$). (C) Representative microphotographs of MYC protein expression in plasmablastic lymphoma.

tion of PBL cases has STAT3 activation due to somatic mutations in the *STAT3*-SH2 domain that may increase MYC expression, as previously described in DLBCL[18] (Figure 4).

Phenotype of the immune microenvironment and neoplastic cells in plasmablastic lymphoma

We quantified the expression of CD163 and PD-L1 in histiocytic/dendritic cells in the cases of PBL. The mean expression of PDL1 was 33 nuclei per HPF (range, 1.67-61) and the mean expression of CD163 was 38 nuclei per HPF (range, 2-84) (Figure 5). The correlation between CD163 and PD-L1 expression was statistically significant (Pearson 0.6, $P<0.05$), suggesting that PD-L1-positive cells are histiocytes in PBL. There was not a significant difference in the content or distribution of CD163 and PD-L1-positive histiocytes between EBV-positive and EBV-negative cases (Mann-Whitney test, $P>0.05$).

CD8-positive and PD1-positive T-cell subpopulations were quantified. The mean number of CD8-positive lymphocytes was 52 nuclei per HPF (range, 1-117) and the mean number of PD1-positive lymphocytes was 32 nuclei per HFP (range, 0-76). There was a significant difference in the distribution of CD8 and PD1-positive cell subsets (Wilcoxon test, $P<0.001$) consistent with different cell populations. The Pearson correlation value was however statistically significant (Pearson 0.59, $P<0.05$). There was no significant difference in the content and distribution of CD8 or PD1-positive lymphocytes between EBV-positive and EBV-negative cases (Mann-Whitney test, $P>0.05$) (Figure 5).

PD-L1 was expressed by tumor cells in five out of 24 (20%) cases evaluated (mean 59 nuclei per HPF; range, 25-98). Four out of five PD-L1-positive cases (in the neoplastic cells) were EBV-positive. Fourteen EBV-positive PBL cases were negative for PD-L1 in the tumor cells. Thus four out of 18 (22%) EBV-positive PBL cases were PD-L1-positive, while one out of six (16%) EBV-negative cases was PD-L1-positive. Thus, there was no association between EBV infection by tumor cells and PD-L1 expression, since most of the EBV-positive cases were PD-L1-negative (P=non-significant) (Figure 5). Interestingly one case with *STAT3* SH2 mutations showed concurrent PD-L1 and phospho-STAT3 (Tyr705) expression. PD-L1 expression data were not available for the other *STAT3* SH2-mutated cases to test this association.

Consistent with previously published data,[9] MHCII protein/HLA (DP, DR) was virtually absent in PBL. Only three cases out of 25 tested were positive (12%, mean 349 nuclei per HPF; range, 284-440). Two cases showed a membranous and cytoplasmic granular pattern and the other a membranous pattern. All three cases were EBV-positive. The other 22 cases were completely negative for HLA expression in tumor cells (Figure 5).

Discussion

In this study we characterized the genetic profile of a series of cases of PBL using targeted exonic NGS, any correlations with EBV infection and the expression of immune checkpoint proteins in both the neoplastic population and tumor microenvironment. We found that genetic abnormalities (including translocations, amplifications and point mutations) in the *MYC* gene were the most common genetic event in PBL. In addition to previously described translocations, involving *IGH* and *MYC*,[10,11] here we found that a few cases may have *MYC* amplification, confirming our previous observations.[12] Both *MYC* translocations and amplifications lead to a significantly increased expression of MYC protein. Interestingly we also identified *MYC* point mutations, mainly consisting of transversions and transitions at C:G pairs and involving exon 2 and, in the case of *MYC*p79S mutation, the WRCY consensus motif. All these features are consistent with a mechanism related to aberrant somatic hypermutation.[16] The oncogenic effect of these point mutations does, however, remain unclear.

We also found that 16% of our cases (5 cases) carried recurrent somatic mutations in the oncogene *STAT3*, preferentially involving the SH2 domain of the protein. Interestingly these mutations were restricted to EBV-positive PBL. Here we demonstrate that these mutations led to increased expression of phospho-STAT3 (Tyr705).

STAT3 mutations and phospho-STAT3 overexpression have been found very rarely in DLBCL NOS (6% according to Ohgami *et al.*[19]). In cases of ALK-positive large B-cell lymphomas, which commonly show a plasmablastic phe-

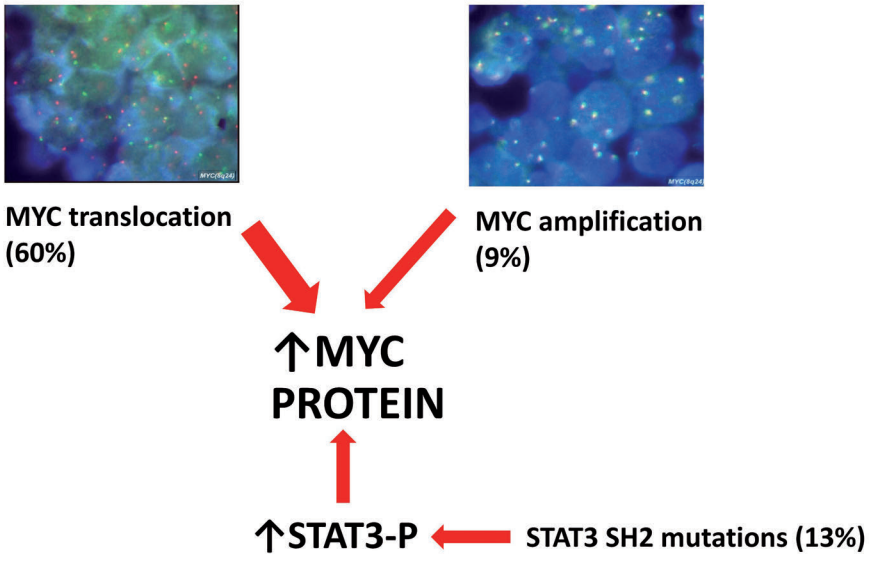


Figure 4. MYC protein overexpression in plasmablastic lymphoma. MYC protein overexpression is due to rearrangements involving *MYC* in a significant proportion of cases of plasmablastic lymphoma (69% in these series). Most translocations fuse *MYC* to *IGH* and a few cases may show amplifications of the *MYC* gene. In addition, we found that some cases of plasmablastic lymphoma have STAT3 activation due to somatic mutations in the *STAT3*-SH2 domain which may increase MYC expression.

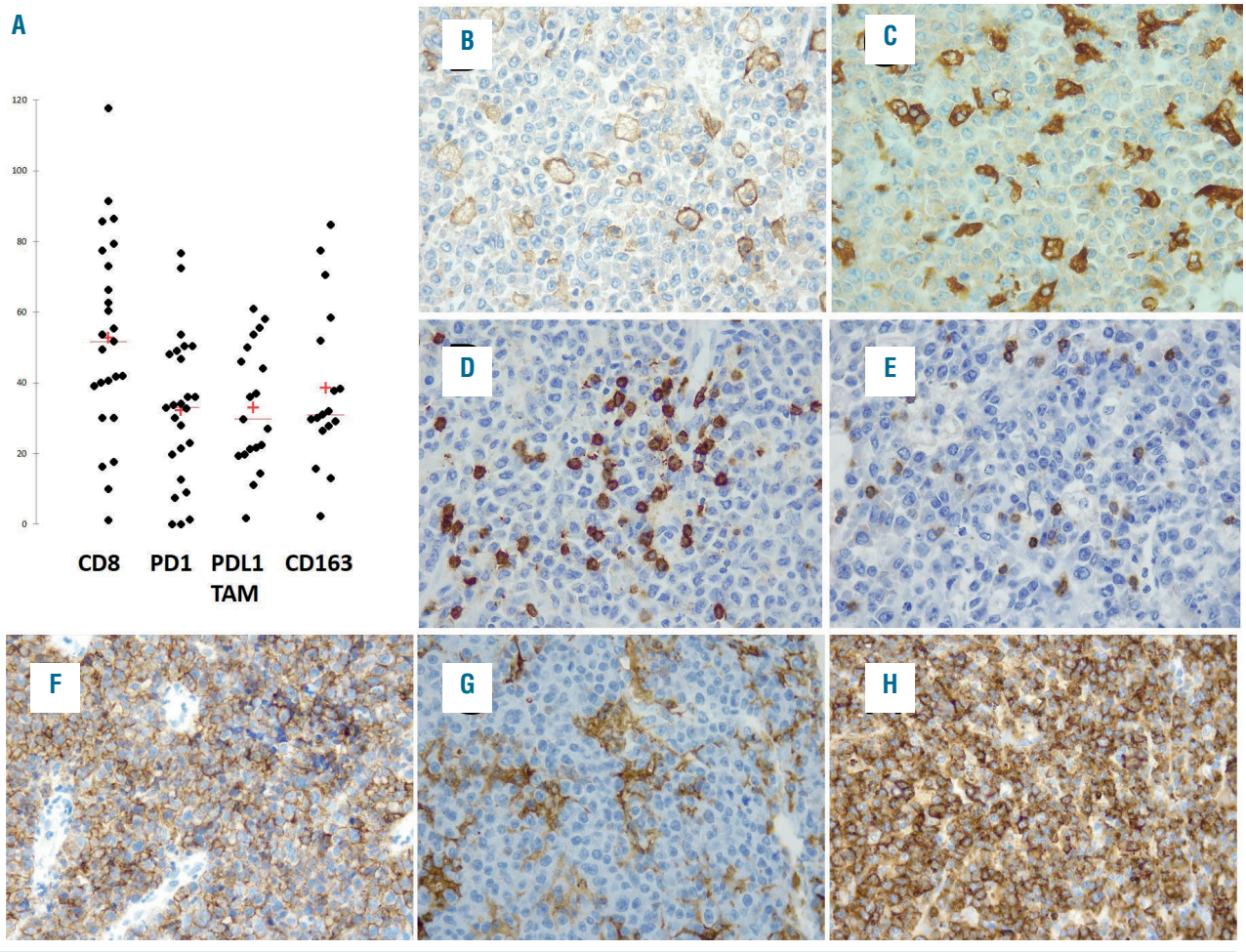


Figure 5. Phenotype of microenvironmental and neoplastic cells in plasmablastic lymphoma. (A) Scattergram illustrating the mean and range of expression values after quantification of the immunohistochemical expression of CD8, PD1 in lymphocytes and PD-L1 and CD163 in histiocyte/dendritic cell populations. (B) Representative image of a case with a mean of 36 PD-L1-positive non-neoplastic cells. (C) The same case showed a mean of 37 CD163-positive histiocytes. (D) The mean expression of CD8-positive cells in this representative case was 53. (E) PD1 identified a different T-cell subpopulation (mean of 36 PD1-positive cells in this representative example, case n. 25). (F) PD-L1 expression by neoplastic cells was identified in five out of 24 cases evaluated (20%). (G) MHCII protein/HLA (DP, DR) was, in most cases, restricted to histiocyte and endothelial cell populations. (H) MHCII protein/HLA (DP, DR) expression was identified in the neoplastic cells in three out of 25 cases tested (12%). Two of the three cases showed cytoplasmic granular and membranous staining (as illustrated in the figure) and one case had a membranous pattern.

notype, phospho-STAT3 expression has been found to be associated with the presence of ALK rearrangements and overexpression.[20] Importantly, STAT3 activation, due to somatic mutations in the *STAT3*-SH2 domain may contribute to MYC overexpression, as previously described in DLBCL.[18] In addition, one case in our series showed concurrent *STAT3* SH2 mutations and phospho-STAT3 (Tyr705) expression and PD-L1 overexpression, confirming previous results in other lymphoma types suggesting that STAT3 activation triggers PD-L1 overexpression.[21]

STAT3 somatic mutations in PBL have not been previously described so far and may have therapeutic implications for the clinical testing of STAT3 inhibitors in these patients.

Interestingly the pattern of somatic mutations in EBV-negative disease was more heterogeneous. Mutations involving BCR activation, TLR/NFκB, histone modifying genes and the NOTCH pathway were found in eight cases (Table 1, Figure 1). *MYD88p*L265P mutation, involving the TIR domain of the *MYD88* gene, has been previously described in activated B-cell-type DLBCL, in primary central nervous system lymphoma and in other DLBCL in immune privileged sites[22,23] as well as in lymphoplasmacytic lymphoma/Waldenström macroglobulinemia[24] and leads to downstream activation of the IRAK4/IRAK1/TRAF6 complex and NFκB activation. The pattern of mutations in *CD79A/B* in PBL cases was distinct from that found in DLBCL NOS. Mutations in *CD79A/B* were found located outside the ITAM domains related with constitutive BCR activation in activated B-cell-type DLBCL.[25] NOTCH pathway genes that were mutated were *NOTCH2*, *NOTCH1* and *SGK1*. *NOTCH2p*R2400* is a nonsense mutation that truncates the PEST domain of the NOTCH2 protein and has already been described in B-cell non-Hodgkin lymphomas, including DLBCL NOS.[26] PEST domain-truncating mutations have been found in multiple tumor types and functional studies suggest that this class of mutations can be targeted with Notch inhibitors including γ secretase inhibitors.[27] *NOTCH1p*P401L was reported in chronic lymphocytic leukemia in a previous study[28] and lies within the calcium-binding EGF-like domains repeat. Mutations in *SGK1* involved the *SGK1p*S451F and *SGK1p*A380V point mutations and the *SGK1p*K136* truncating mutation. These

mutations have not been previously described in DLBCL NOS.[26] SGK1 has been suggested to be a negative regulator of NOTCH signaling, enhancing NOTCH protein degradation and reducing its activation by γ-secretase.[29] Other mutations found were *SMARCA4p*R1005Q and *TP53p*R273H.

Of note MAPK/ERK pathway-activating mutations involving *BRAF* (*BRAFp*V600E, *BRAFp*G469A) were found in two cases, both EBV-negative. *BRAF* mutations have been observed, rarely, in related neoplasms such as multiple myeloma. Previous studies found *BRAF* mutations in 4% of cases of multiple myeloma;[30] they were associated with aggressive clinical features, a plasmablastic phenotype and clonal evolution,[31,32] with obvious clinical implications for targeted therapy.

In addition to the genetic profile of the cases, we also explored the composition of the tumor microenvironment and the expression of immune-checkpoint markers in both the neoplastic and other lymphoid and histiocytic/dendritic populations. Our results confirm those of previous studies showing an enrichment in TAM that express CD163 and PD-L1. The PBL also had a significant population of CD8-positive T cells, irrespective of the almost absent expression of MHCII/HLA by the neoplastic cells.[9] Importantly, together with CD8-positive T cells, there was a distinct population of PD1-positive T cells. In the PBL cases that we studied, EBV did not influence the immune populations, with regards to the content of TAM and CD8-positive and PD1-positive T cells quantified in the tissue. Furthermore, in our series, PD-L1 expression by the neoplastic cells was found in 20% of the cases analyzed, similarly to previously published series,[8] and there was no association between EBV infection by tumor cells and PD-L1 expression, since PD-L1 was found in both EBV-positive and EBV-negative variants and most of the EBV-positive cases were PD-L1-negative. These findings are in agreement with previously published data on PBL, with variable expression of PD-L1 ranging from 20 to 44%, by the neoplastic population.[8,33] In our series, however, we did not confirm an association between EBV infection and PD-L1 expression, suggested by others.[8] This difference may be due to a combination of factors, including different clones used for the detection of PD-L1 expression (22C3 clone in this study, SP142 in others[8]) and different quantification and statistical methods used. In addition another biological factor related to the uncommon PD-L1 expression in PBL cases could be related to the usual latency pattern found in these cases, since PD-L1 expression in EBV-positive post-transplant lymphoproliferative disorder has been strongly associated with EBV latency patterns 2 and 3[34] while PBL cases usually have EBV latency pattern 1.[7] Notably one of our cases points to STAT3 activation as a potential cause for PD-L1 overexpression in PBL. Collectively our results on the microenvironment and immune-checkpoint expression in PBL indicate a potential for immune checkpoint interference in patients with this type of lymphoma.

In summary, in this study we found that the mutational profile of PBL was related to EBV infection in the tumor cells and identified recurrent genetic events in *MYC*, *STAT3* and *PRDM1*/Blimp1 that were associated with EBV-positive disease. *MYC* genetic alterations (including translocations and amplification) and SH2 domain *STAT3* mutations led to *MYC* and phospho-STAT3 (Tyr705) protein overexpression, respectively. Other somatic mutations including *BRAFp*V600E, *MYD88p*L265P, *NOTCH2p*R2400* and *TP53p*R273H, appeared in EBV-negative disease, suggesting an overlapping mutational profile with both multiple myeloma and DLBCL NOS. Furthermore, the tumor microenvironment in PBL was characterized by an enrichment in PD-L1-positive TAM and PD1 reactive T lymphocytes with expression of PD-L1 by the neoplastic tumor cells in a fraction of cases. Novel molecular targets derived from the present study include MYC and STAT3 activation, MAPK/ERK and NOTCH2 pathway mutations and immune-checkpoint interference.

Disclosures

No conflicts of interest to disclose.

Contributions

JGR and NMM performed research, analyzed data and approved the paper. SGV, RT, SB and MG analyzed data and approved the paper. SL and EDA performed research, provided clinical data and approved the paper. AGM and AGP performed research and approved the paper. CV and JK provided clinical data and approved the paper. SMM designed and performed research, analyzed data, and wrote and approved the paper.

Funding

This study was supported by grants from MINECO (PI16/1397, SMM, Principal Investigator) and IDIVAL (NEXTVAL 15/09, SMM, Principal Investigator). NMM was supported by Asociación Española contra el Cancer (AECC).

Acknowledgments

The authors acknowledge the Valdecilla Tumor Biobank Unit (Tissue Node, PT13/0010/0024) for their skillful handling and processing of tissue samples and all their clinical colleagues and pathologists who provided clinical data and samples for this research study.

References

1. Swerdlow S, Campo E, Harris NL, et al. (Editors). WHO Classification of Tumours of Haematopoietic and Lymphoid Tissues. Fourth edition. IARC 2008.
2. Campo E, Swerdlow SH, Harris NL, Pileri S, Stein H, Jaffe ES. The 2008 WHO classification of lymphoid neoplasms and beyond: evolving concepts and practical applications. Blood. 2011;117(19):5019-5032.
3. Delecluse HJ, Anagnostopoulos I, Dallenbach F, et al. Plasmablastic lymphomas of the oral cavity: a new entity associated with the human immunodeficiency virus infection. Blood. 1997;89(4):1413-1420.
4. Montes-Moreno S, Gonzalez-Medina AR, Rodriguez-Pinilla SM, et al. Aggressive large B-cell lymphoma with plasma cell differentiation: immunohistochemical characterization of plasmablastic lymphoma and diffuse large B-cell lymphoma with partial plasmablastic phenotype. Haematologica. 2010;95(8):1342-1349.
5. Colomo L, Loong F, Rives S, et al. Diffuse large B-cell lymphomas with plasmablastic differentiation represent a heterogeneous group of disease entities. Am J Surg Pathol. 2004;28(6):736-747.
6. Chapman J, Gentles AJ, Sujoy V, et al. Gene expression analysis of plasmablastic lymphoma identifies downregulation of B-cell receptor signaling and additional unique transcriptional programs. Leukemia. 2015;29(11):2270-2273.
7. Gravelle P, Péricart S, Tosolini M, et al. EBV infection determines the immune hall-

marks of plasmablastic lymphoma. Oncoimmunology. 2018;7(10):e1486950.
8. Laurent C, Fabiani B, Do C, et al. Immune-checkpoint expression in Epstein-Barr virus positive and negative plasmablastic lymphoma: a clinical and pathological study in 82 patients. Haematologica. 2016;101(8):976-984.
9. Schmelz M, Montes-Moreno S, Piris M, Wilkinson ST, Rimsza LM. Lack and/or aberrant localization of major histocompatibility class II (MHCII) protein in plasmablastic lymphoma. Haematologica. 2012;97(10):1614-1616.
10. Valera A, Balagué O, Colomo L, et al. IG/MYC rearrangements are the main cytogenetic alteration in plasmablastic lymphomas. Am J Surg Pathol. 2010;34(11):1686-1694.
11. Taddesse-Heath L, Meloni-Ehrig A, Scheerle J, Kelly JC, Jaffe ES. Plasmablastic lymphoma with MYC translocation: evidence for a common pathway in the generation of plasmablastic features. Mod Pathol. 2010;23(7):991-999.
12. Montes-Moreno S, Martinez-Magunacelaya N, Zecchini-Barrese T, et al. Plasmablastic lymphoma phenotype is determined by genetic alterations in MYC and PRDM1. Mod Pathol. 2017;30(1):85-94.
13. Munevver C, Rong HR, Chineke I, et al. Genetic analysis of plasmablastic lymphomas in HIV (+) patients reveals novel driver regulators of the noncanonical NF-κB pathway. Blood. 2018;132(Suppl 1):1565.
14. Swerdlow SH, Campo E, Harris NL, et al. (Editors). WHO Classification of Tumours of Haematopoietic and Lymphoid Tissues. Revised fourth edition. IARC. Lyon 2017.
15. Montes-Moreno S, Martinez-Magunacelaya N, Zecchini-Barrese T, et al. Plasmablastic lymphoma phenotype is determined by genetic alterations in MYC and PRDM1. Mod Pathol. 2017;30(1):85-94.
16. Pasqualucci L, Neumeister P, Goossens T, et al. Hypermutation of multiple proto-oncogenes in B-cell diffuse large-cell lymphomas. Nature. 2001;412(6844):341-346.
17. Loghavi S, Alayed K, Aladily TN, et al. Stage, age, and EBV status impact outcomes of plasmablastic lymphoma patients: a clinicopathologic analysis of 61 patients. J Hematol Oncol. 2015;8:65.
18. Sarosiek KA, Malumbres R, Nechushtan H, Gentles AJ, Avisar E, Lossos IS. Novel IL-21 signaling pathway up-regulates c-Myc and induces apoptosis of diffuse large B-cell lymphomas. Blood. 2010;115(3):570-580.
19. Ohgami RS, Ma L, Monabati A, Zehnder JL, Arber DA. STAT3 mutations are present in aggressive B-cell lymphomas including a subset of diffuse large B-cell lymphomas with CD30 expression. Haematologica. 2014;99(7):e105-107.
20. Valera A, Colomo L, Martinez A, et al. ALK-positive large B-cell lymphomas express a terminal B-cell differentiation program and activated STAT3 but lack MYC rearrangements. Mod Pathol. 2013;26(10):1329-1337.
21. Tabanelli V, Corsini C, Fiori S, et al. Recurrent PDL1 expression and PDL1 (CD274) copy number alterations in breast implant-associated anaplastic large cell lymphomas. Hum Pathol. 2019;90:60-69.
22. Ngo VN, Young RM, Schmitz R, et al. Oncogenically active MYD88 mutations in human lymphoma. Nature. 2011;470(7332):115-119.
23. Chapuy B, Roemer MG, Stewart C, et al. Targetable genetic features of primary testicular and primary central nervous system lymphomas. Blood. 2016;127(7):869-881.
24. Treon SP, Xu L, Yang G, et al. MYD88 L265P somatic mutation in Waldenstrom's macroglobulinemia. N Engl J Med. 2012;367(9):826-833.
25. Davis RE, Ngo VN, Lenz G, et al. Chronic active B-cell-receptor signalling in diffuse large B-cell lymphoma. Nature. 2010;463(7277):88-92.
26. Karube K, Enjuanes A, Dlouhy I, et al. Integrating genomic alterations in diffuse large B-cell lymphoma identifies new relevant pathways and potential therapeutic targets. Leukemia. 2018;32(3):675-684.
27. Wang K, Zhang Q, Li D, et al. PEST domain mutations in Notch receptors comprise an oncogenic driver segment in triple-negative breast cancer sensitive to a γ-secretase inhibitor. Clin Cancer Res. 2015;21(6):1487-1496.
28. Sutton LA, Ljungström V, Mansouri L, et al. Targeted next-generation sequencing in chronic lymphocytic leukemia: a high-throughput yet tailored approach will facilitate implementation in a clinical setting. Haematologica. 2015;100(3):370-376.
29. Mo JS, Ann EJ, Yoon JH, et al. Serum- and glucocorticoid-inducible kinase 1 (SGK1) controls Notch1 signaling by downregulation of protein stability through Fbw7 ubiquitin ligase. J Cell Sci. 2011;124(Pt 1):100-112.
30. Chapman MA, Lawrence MS, Keats JJ, et al. Initial genome sequencing and analysis of multiple myeloma. Nature. 2011;471(7339):467-472.
31. Bohn OL, Hsu K, Hyman DM, Pignataro DS, Giralt S, Teruya-Feldstein J. BRAF V600E mutation and clonal evolution in a patient with relapsed refractory myeloma with plasmablastic differentiation. Clin Lymphoma Myeloma Leuk. 2014;14(2):e65-68.
32. Andrulis M, Lehners N, Capper D, et al. Targeting the BRAF V600E mutation in multiple myeloma. Cancer Discov. 2013;3(8):862-869.
33. Chen BJ, Chapuy B, Ouyang J, et al. PD-L1 expression is characteristic of a subset of aggressive B-cell lymphomas and virus-associated malignancies. Clin Cancer Res. 2013;19(13):3462-3473.
34. Veloza L, Teixido C, Castrejon N, et al. Clinicopathological evaluation of the programmed cell death 1 (PD1)/programmed cell death-ligand 1 (PD-L1) axis in post-transplant lymphoproliferative disorders: association with Epstein-Barr virus, PD-L1 copy number alterations, and outcome. Histopathology. 2019;75(6):799-812.

ARTICLE

Combining brentuximab vedotin with dexamethasone, high-dose cytarabine and cisplatin as salvage treatment in relapsed or refractory Hodgkin lymphoma: the phase II HOVON/LLPC Transplant BRaVE study

Marie José Kersten,[1,2*] Julia Driessen,[1*] Josée M. Zijlstra,[2,3] Wouter J. Plattel,[2,4] Franck Morschhauser,[5] Pieternella J. Lugtenburg,[2,6] Pauline Brice,[7] Martin Hutchings,[8] Thomas Gastinne,[9] Roberto Liu,[1] Coreline N. Burggraaff,[3] Marcel Nijland,[2,4] Sanne H. Tonino,[1,2] Anne I.J. Arens,[10] Roelf Valkema,[11] Harm van Tinteren,[12] Marta Lopez-Yurda,[12] Arjan Diepstra,[2,13] Daphne De Jong[2,14] and Anton Hagenbeek[1,2]

[1]Department of Hematology, Amsterdam UMC, University of Amsterdam, LYMMCARE (Lymphoma and Myeloma Center Amsterdam), Cancer Center Amsterdam, Amsterdam, the Netherlands; [2]HOVON and Lunenburg Lymphoma Phase I/II Consortium (LLPC), the Netherlands; [3]Department of Hematology, Amsterdam UMC, Vrije Universiteit Amsterdam, Cancer Center Amsterdam, Amsterdam, the Netherlands; [4]Department of Hematology, University of Groningen, University Medical Center Groningen, Groningen, the Netherlands; [5]Department of Hematology, Centre Hospitalier Universitaire, Lille, [6]Department of Hematology, Erasmus MC Cancer Institute, Erasmus University Medical Center, Rotterdam, the Netherlands; [7]Department of Hematology, Hopital Saint Louis, Paris, France; [8]Department of Hematology, Rigshospitalet, Copenhagen, Denmark; [9]Department of Hematology, Centre Hospitalier Universitaire, Nantes, France; [10]Department of Radiology and Nuclear Medicine, Radboud University Medical Center, Nijmegen, the Netherlands; [11]Department of Radiology and Nuclear Medicine, Erasmus University Medical Center, Rotterdam, the Netherlands; [12]Department of Biometrics, Netherlands Cancer Institute, Amsterdam, the Netherlands; [13]Department of Pathology and Medical Biology, University of Groningen, University Medical Center Groningen, Groningen, the Netherlands and [14]Department of Pathology, Amsterdam UMC, Vrije Universiteit Amsterdam, Cancer Center Amsterdam, Amsterdam, the Netherlands; HOVON Pathology Facility and Biobank, Amsterdam, the Netherlands

*MJK and JD contributed equally as co-first authors.

Ferrata Storti Foundation

Haematologica 2021
Volume 106(4):1129-1137

ABSTRACT

Achieving a metabolic complete response (mCR) before high-dose chemotherapy (HDC) and autologous peripheral blood stem cell transplant (auto-PBSCT) predicts progression-free survival (PFS) in relapsed/refractory classical Hodgkin lymphoma (R/R cHL). We added brentuximab vedotin (BV) to DHAP (dexamethasone, high-dose cytarabine, cisplatin) to improve the mCR rate. In a phase I dose-escalation part of the study in 12 patients, we showed that BV-DHAP is feasible. This phase II study included 55 R/R cHL patients (23 primary refractory). Treatment consisted of three 21-day cycles of BV 1.8 mg/kg on day 1, and DHAP (dexamethasone 40 mg days 1-4, cisplatin 100 mg/m^2 day 1 and cytarabine 2x2 g/m^2 day 2). Patients with a metabolic partial response (mPR) or mCR proceeded to HDC/auto-PBSCT. Based on independent central [^{18}F]fluorodeoxyglucose (FDG) - positron emission tomography (PET) - computed tomography (CT) scan review, 42 of 52 evaluable patients (81% [95%CI: 67-90]) achieved an mCR before HDC/auto-PBSCT, five had an mPR and five had progressive disease (3 were not evaluable). After HDC/auto-PBSCT, four patients with an mPR converted to an mCR. Two-year PFS was 74% [95%CI: 63-86] and overall survival 95% [95%CI: 90-100]. Toxicity was manageable and mainly consisted of grade 3/4 hematologic toxicity, fever, nephrotoxicity, ototoxicity (grade 1/2), and transiently elevated liver enzymes during BV-DHAP. Eighteen patients developed new onset peripheral neuropathy (maximum grade 1/2); all recovered. In conclusion, BV-DHAP is a very effective salvage regimen in R/R cHL patients, but patients should be monitored closely for toxicity. (*clinicaltrials.gov identifier: NCT02280993*).

Correspondence:

MARIE JOSÉ KERSTEN
m.j.kersten@amsterdamumc.nl

Received: November 18, 2019.

Accepted: March 19, 2020.

Pre-published: April 9, 2020.

https://doi.org/10.3324/haematol.2019.243238

©2021 Ferrata Storti Foundation

Material published in Haematologica is covered by copyright. All rights are reserved to the Ferrata Storti Foundation. Use of published material is allowed under the following terms and conditions: https://creativecommons.org/licenses/by-nc/4.0/legalcode. Copies of published material are allowed for personal or internal use. Sharing published material for non-commercial purposes is subject to the following conditions: https://creativecommons.org/licenses/by-nc/4.0/legalcode, sect. 3. Reproducing and sharing published material for commercial purposes is not allowed without permission in writing from the publisher.

Introduction

Salvage chemotherapy followed by high-dose chemotherapy (HDC) and autologous peripheral blood stem cell transplant (auto-PBSCT) has been the standard of care for patients with relapsed or refractory classical Hodgkin lymphoma (R/R cHL) for decades.[1,2] With this treatment, cure rates of 40-60% can be achieved. Patients failing this treatment and those relapsing after second-line treatment generally have a very poor prognosis.[3-5]

Response to salvage treatment is one of the most important predictors of outcome after auto-PBSCT, with metabolic active residual disease, as assessed by [^{18}F]fluorodeoxyglucose (FDG) - positron emission tomography (PET) - computed tomography (CT) scan, before HDC/auto-PBSCT conferring an inferior prognosis.[6-8] Therefore, higher cure rates may be achieved by improving the metabolic complete response (mCR) rate before HDC/auto-PBSCT. Conventional salvage chemotherapy regimens result in mCR rates of about 50-60%.[6,9-11] DHAP (dexamethasone, high-dose cytarabine, cisplatin) is one of the most commonly used salvage regimens for R/R cHL in Europe.[12]

Brentuximab vedotin (BV) is targeted high-dose intracellular chemotherapy, consisting of an anti-CD30 antibody conjugated to the potent anti-microtubule agent monomethyl auristatin-E.[13,14] Several phase II studies have shown promising clinical activity of BV in R/R cHL, both as monotherapy and combined with chemotherapy.[15-20] Toxicities of BV include infusion-related reaction (IRR), myelosuppression, and peripheral neuropathy, the latter being reversible in the majority of patients.[15,16,18,20,21]

In the current prospective, multicenter, international phase I/II Transplant BRaVE study we investigated the efficacy and safety of BV-DHAP followed by HDC (BEAM: carmustine, etoposide, cytarabine, melphalan) and auto-PBSCT in R/R cHL patients.

Results of the phase I part of this study in 12 patients have been published previously and showed that the combination of BV-DHAP is feasible with acceptable toxicity.[22] The recommended dose level was established at full dose of all drugs with BV dosed at 1.8 mg/kg.[22] The primary endpoints for the phase II single arm part were the fraction of patients achieving an mCR as judged by independent review of PET-CT scan after the third cycle of BV-DHAP, and the rate of grade 3/4 non-hematologic adverse events (AE), including neurotoxicity, during BV-DHAP.

Methods

Patients

The study enrolled patients aged ≥18 years with histologically confirmed CD30 positive cHL by local pathology assessment, either having primary refractory disease or a first relapse after first-line chemotherapy. *Online Supplementary Table S1* shows the complete list of inclusion and exclusion criteria. Central pathology review was performed by two experienced hematopathologists (DDJ, AD).

All patients provided written informed consent. The study protocol was approved by the Ethical Review Committee (ERC) of all participating centers. The study was carried out in accordance with the principles of the Declaration of Helsinki.

Study design and treatment

Transplant BRaVE (*clinicaltrials.gov identifier: NCT02280993*) is a prospective, open-label study conducted at eight centers in the Netherlands (n=5), France (n=3) and Denmark (n=1). An independent Data Safety Monitoring Board (DSMB) evaluated the general progress and safety aspects of the study at predefined intervals.

Baseline assessment included a lymph node and bone marrow biopsy, and a PET-CT scan. Patients filled in a neurotoxicity questionnaire at study entry, prior to each cycle, and at three months after auto-PBSCT.

Patients were treated with three 21-day cycles of BV (1.8 mg/kg, i.v., day 1), dexamethasone (40 mg orally or intravenous [i.v.], days 1-4), cisplatin (100 mg/m^2, continuous i.v. [24 hours], day 1) and cytarabine (2x2 g/m^2 q12 hours, 3 hours for each infusion, day 2). After cycle 2, stem cells were mobilized and harvested using granulocyte colony-stimulating factor (G-CSF). A PET-CT scan was performed after cycle 3. Patients with progressive disease (PD) went off study, whereas patients with a partial response (mPR) or mCR proceeded to BEAM (carmustine, 300 mg/m^2, day -7; etoposide, 100 mg/m^2 and cytarabine, 100 mg/m^2, 2x/day, days -6, -5, -4 and -3; and melphalan, 140 mg/m^2, day -2), followed by auto-PBSCT (on day 0). Six weeks after auto-PBSCT, response evaluation was performed by PET-CT. G-CSF was recommended to prevent long-lasting neutropenia.

Endpoints

All endpoints and their definitions are described in *Online Supplementary Table S2*. Responses were determined according to the 2014 Lugano criteria.[23] All PET-CT scans were centrally reviewed by two independent nuclear medicine physicians (AA, RV) and a third adjudicator (OH) in case of discrepancies. Visual assessment was performed using the Deauville score (DS), assessing DS1-3 as mCR. Toxicity was reported according to the Common Terminology Criteria for Adverse Events (CTCAE) version 4.03.

Statistical analysis

Details about the study design and statistical analysis are provided in *Online Supplementary Appendix 1*. Efficacy analysis was performed among all evaluable patients. Primary safety analysis was performed among all patients who received at least one dose of study medication. Response rates and their corresponding 95% two-sided exact confidence intervals (CI) were calculated. AE were analyzed descriptively. The Kaplan-Meier method was used for time-to-event analysis. An exploratory analysis with a Cox proportional hazards regression was performed on all phase II patients, and six patients from the phase I part of the study who were treated at the recommended dose level. The Kaplan-Meier method and log-rank test were used to analyze univariable associations with progression-free survival (PFS). All statistical analyses were performed using R software version 3.6.1 and SAS software version 9.4.

Results

Patients and treatment

Between May 2014 and July 2017, a total of 67 patients with R/R cHL were enrolled for the entire Transplant BRaVE phase I/II study (n=12 in phase I and n=55 in phase II). Due to withdrawal of consent of two patients after one cycle of BV-DHAP and three patients not completing all BV-DHAP cycles, five more patients were enrolled in phase II than planned according to the sample size calculations (n=50) to ensure a sufficient number of evaluable patients in the primary analysis.

Patients' characteristics for the phase II patients are summarized in Table 1. Median age was 29 years, and 27 patients were female (49%). Twenty-three patients (43%) had primary refractory disease and 16 patients (29%) had relapsed within one year of first-line treatment. Among the first 20 patients of phase II (stage 1), enough responses were observed (16 mCR) with acceptable toxicity (7 patients experienced significant toxicity) for the DSMB to approve proceeding to stage 2.

Of the 55 enrolled patients, 49 (89%) completed all three cycles of BV-DHAP, and 47 (85%) underwent BEAM and auto-PBSCT (Figure 1). Two patients withdrew consent after cycle 1 due to psychological issues, and two patients had PD after cycle 2. In cycle 3, two patients did not receive BV due to toxicity. One of these patients received VIM (ifosfamide, mitoxantrone and etoposide) in cycle 3 because of hepatotoxicity and was not evaluable for response. However, this patient still proceeded successfully to BEAM and auto-PBSCT. The other patient received DHAP without BV because of an anaphylactic shock following BV infusion in cycle 2. This patient went off study thereafter because of toxicity and a mixed response by local PET-CT assessment (which was eventually considered mCR by central PET-CT review) and proceeded to auto-PBSCT after additional treatment with miniBEAM.

Besides the two patients who did not receive BV in cycle 3, dose reductions or delays included three delays of cycle 2 due to infection (n=1), venous thrombosis (n=1), or neutropenia (n=1), and three delays of BV infusion due to IRR (grade 1/2). Cycle 3 was delayed in two patients (malaise and neutropenia), and there were two delays of BV infusion (IRR: one grade 2 and one grade 3). Furthermore, eight patients switched from cisplatin to carboplatin due to ototoxicity (n=7; grade 1/2) or nephrotoxicity (n=1; grade 3, recovered completely), and one patient received no cisplatin and cytarabine in cycle 3 due to electrolyte disorder and sepsis.

Efficacy and stem cell harvest

Three patients were not evaluable for response after three cycles of BV-DHAP: two patients withdrew consent after cycle 1, and one patient did not have a PET-CT scan after cycle 3. By independent central PET-CT review, 42 of 52 evaluable patients achieved an mCR (81% [95%CI: 67-90]) and five patients an mPR (10%), resulting in an overall response rate of 90% (95%CI: 79-97). A total of five patients had PD (10%) and did not proceed to BEAM. Two of those patients showed PD on a CT scan after cycle 2 and three had PD on the PET-CT scan after cycle 3 (Figure 1). After auto-PBSCT, four out of five patients with mPR converted to mCR. One patient had a persisting mPR and received additional radiotherapy according to the local physician's decision, and is still in mCR thereafter.

There were no significant differences in baseline characteristics (i.e., age, time to relapse and first-line treatment) between patients with mCR or mPR. The mCR rate was lower for patients with primary refractory disease compared to patients with a later relapse, but this was not statistically significant (mCR rate 73% [95%CI: 69-96] *vs.* 86% [95%CI: 50-89]; *P*=0.29, respectively).

Stem cell harvest after cycle 2 was successful using G-CSF in all patients, with one apheresis session in 43 patients and two apheresis sessions in nine patients, of whom two patients received plerixafor (3 patients went off study before apheresis). The median yield was $5.3x10^6$ $CD34^+$/kg (range: 1.8-22.7).

Table 1. Patients' characteristics.

	Phase II patients (n=55) N of patients (%)
Age, years	
Median [range]	29 [19-71]
Female	27 (49)
Ann Arbor stage at baseline	
I	8 (15)
II	16 (29)
III	10 (18)
IV	20 (36)
Unknown	1 (2)
ECOG PS at baseline	
0	35 (64)
1	17 (31)
Unknown	3 (5)
Baseline B symptoms	20 (36)
Bone marrow involvement	2 (4)
First-line treatment	
ABVD	40 (73)
BEACOPP baseline	2 (4)
Escalated BEACOPP	8 (15)
Other	5 (9)
Prior radiotherapy	9 (16)
Response to first-line treatment	
CR	32 (58)
PR	10 (18)
SD	2 (4)
PD	11 (20)
Time from response to first-line treatment to relapse	
Primary refractory disease*	23 (42)
Relapse within 1 year	16 (29)
Relapse after 1 year	16 (29)
Median time, months [range])	5 [0-160]

*Primary refractory disease is defined as failure to obtain a complete response with front-line therapy. N: number; ECOG PS: Eastern Cooperative Oncology Group Performance Score; ABVD: adriamycin, bleomycin, vinblastine, and dacarbazine; BEACOPP: bleomycin, etoposide, adriamycin, cyclophosphamide, vincristine, procarbazine, and prednisone; CR: complete response; PR: partial response; SD: stable disease; PD: progressive disease.

Safety

During BV-DHAP treatment, 20 patients (36%) experienced one or more AE that met the dose-limiting toxicity criteria (considered significant toxicity).

Grade 3/4 neutropenia and thrombocytopenia were common (*Online Supplementary Table S3*). After BEAM/auto-PBSCT, the median recovery time to an absolute neutrophil count (ANC) ≥$0.5x10^9$/L was 12 days (range: 8-29), and the median recovery time to platelets ≥$20x10^9$/L was 15 days (range: 6-46) (*Online Supplementary Table S3*).

During BV-DHAP, febrile neutropenia (n=14) was the most common non-hematologic grade 3/4 toxicity, followed by elevated liver enzymes (n=10) and electrolyte disorders (n=6) (Table 2). After BEAM/auto-PBSCT, one

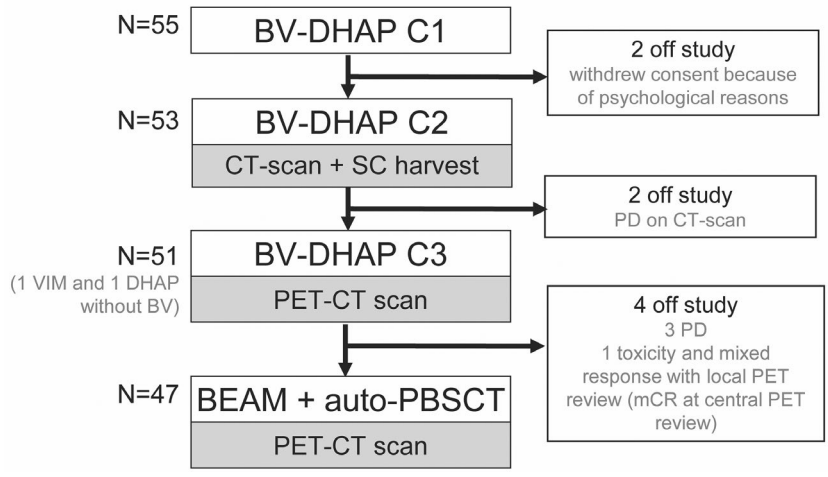


Figure 1. Consort diagram. Number of patients in the full analysis set going through the protocol treatment including reasons for exclusion. BV: brentuximab vedotin; DHAP: dexamethasone, high-dose cytarabine, cisplatin; C: cycle; N: number; CT: computed tomography; SC: stem cell; PD: progressive disease; VIM: ifosfamide, mitoxantrone, etoposide; PET: positron emission tomography; mCR: metabolic complete response; BEAM: carmustine, etoposide, cytarabine, melphalan; auto-PBSCT: autologous peripheral blood stem-cell transplant.

patient developed veno-occlusive disease (VOD) that was fatal. This patient already had elevated levels of alanine aminotransferase (ALT), aspartate aminotransferase (AST) and gamma-glutamyl transferase (GGT) during BV-DHAP and very high levels of AST (2400 U/L), ALT (970 U/L), lactate dehydrogenase (LDH; 1,400 U/L), GGT (900 U/L) and direct bilirubin (660 μmol/L) during the VOD after BEAM/auto-PBSCT.

Peripheral neuropathy grade 1/2 was present before study entry in 11 patients (n=1 grade 2) but did not worsen during BV-DHAP treatment. During BV-DHAP treatment, 15 (27%) and three (5%) patients developed novel onset grade 1 and 2 peripheral neuropathy, respectively, but all recovered. Of all patients, regardless of the presence of peripheral neuropathy at baseline, 12 patients reported transient muscle weakness (grade 1/2) in the neurotoxicity questionnaire, of whom 11 recovered without sequelae. No grade 3/4 neuropathy has occurred (*Online Supplementary Table S4*).

In total, seven patients experienced ototoxicity (n=3 grade 1, n=4 grade 2) and switched from cisplatin to carboplatin in cycle 2 or 3. Three patients recovered without sequelae, and three patients had continuing ototoxicity (hearing loss or tinnitus) 6 months after auto-PBSCT (1 patient unknown).

Serious AE (SAE) grade 3/4 following BV-DHAP treatment are described in Table 3. In total, 18 (33%) patients experienced one or more SAE during BV-DHAP. SAE that occurred in more than one patient were febrile neutropenia (n=9), infections (n=2), and renal function disorder (n=2). Most SAE recovered, except for the two renal function disorders which recovered with sequelae (persisting grade 1 or 2 nephrotoxicity, e.g., decreased glomerular filtration rate or persisting high levels of creatinine). One additional nephrotoxicity grade 3 was not considered an SAE because of rapid recovery without hospitalization.

Survival

After a median follow-up of 27 months, the 2-year PFS by intention-to-treat for all 55 patients was 73.5% (95%CI: 62.6-86.4) (events=14/55) and the 2-year overall survival (OS) was 94.9% (95%CI: 89.5-00.0) (events=3/55) (Figure 2A and B).

Three patients died during the study period: one patient died of encephalitis (exact cause remained unknown despite a brain autopsy, the patient did not recover from seizures; brain autopsy did not show cerebral localization of lymphoma or infection), and one patient died due to VOD. Both deaths occurred within four months after BEAM/auto-PBSCT. The third patient died of an unrelated head trauma, nine months after BEAM/auto-PBSCT while in mCR. One patient who withdrew consent after cycle 1 went off study and later died from PD; this patient was censored at the time of withdrawal of consent.

Patients with progression after treatment in this study received salvage treatment according to the treating physician's choice. Four patients received BV monotherapy, two of whom had a complete response, but all progressed again and needed a third salvage regimen.

Exploratory analysis of survival

For an exploratory analysis of PFS, six patients from phase I who were treated at the recommended dose level were added to the analysis, to a total of 61 patients.[22]

Patients with mPR after three cycles showed a significantly lower PFS compared to patients with mCR. Two-year PFS rates of patients with mPR (n=5) *versus* patients with mCR (n=48) were 40% (95%CI: 14-100) *versus* 87% (95%CI: 78-97): log-rank *P*=0.004, hazard ratio (HR) 6.02 (95%CI: 1.50-24.2; *P*=0.011), respectively (Figure 3A and *Online Supplementary Table S5*). A multivariable Cox analysis showed that patients with an mPR had a significantly increased risk of progression, independently of primary refractory status (*Online Supplementary Table S5*). Patients with relapsed disease (n=37) had a lower risk of progression compared to patients with primary refractory disease (n=24), with 2-year PFS rates of 86% (95%CI: 75-98) *versus* 63% (95%CI: 46-85): log-rank *P*=0.036, HR 0.33 (95%CI: 0.11-0.98; *P*=0.046), respectively (Figure 3B and *Online Supplementary Table S5*). Univariable analysis did not show significant associations for other baseline risk factors (i.e., B symptoms, age, stage and first-line treatment regimen) (*Online Supplementary Table S5*).

Central pathology review

Based on morphology, immunophenotype, and molecular clonality analysis if needed, central pathology review confirmed cHL (according to the World Health Organization classification 2016[24]) in 59 of all 67 patients (88%) of the complete phase I (cHL confirmed in 10 of 12 patients in total) and phase II (cHL confirmed in 49 of 55 patients in total) part of the study. In all cases with equivo-

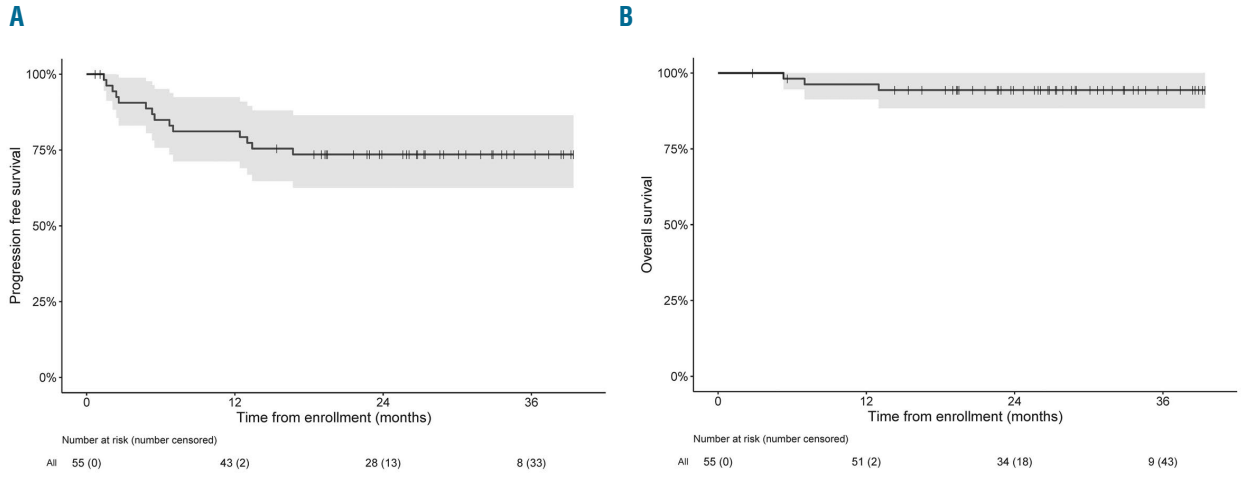


Figure 2. Kaplan-Meier survival analysis. Kaplan-Meier survival analysis for all 55 phase II patients by intention-to-treat, including the number of patients at risk at 1, 2 and 3 years with regard to (A) progression-free survival and (B) overall survival, measured from enrollment.

cal morphological and/or immunohistochemical features, including cases with high numbers of Epstein Barr virus-encoded RNA (EBER)-positive atypical large cells and/or small lymphocytes (n=16), extensive immunohistochemical and molecular T-cell receptor and immunoglobulin heavy and light chain gene rearrangement assays (BIOMED) were performed (*Online Supplementary Table S6*). In eight patients, cHL could not be confirmed. Of these, five patients were diagnosed with peripheral T-cell lymphoma (PTCL) not otherwise specified (NOS), one patient with angioimmunoblastic T-cell lymphoma (AITL), and one patient with immunodeficiency-associated B-lymphoproliferative disorder (IA-B-LPD).[25] In one patient, a classifying diagnosis could not be made due to lack of representative material in the biopsy sample. Additionally, in one patient, a composite lymphoma of cHL and lymphoplasmacytic lymphoma (LPL) was diagnosed. In all cases, high CD30 expression was present. Of the seven patients with PTCL, AITL or IA-B-LPD, six had an mCR after three cycles of BV-DHAP. One patient with PTCL had PD after cycle 2, one with AITL had PD after auto-PBSCT, and one patient with PTCL died due to unrelated head-trauma. When excluding the patient with unrelated death, there was no significant difference in PFS between patients with confirmed cHL *versus* patients with another diagnosis (2-year PFS 81% *vs.* 67%, log-rank *P*=0.36).

Discussion

In this international, prospective phase II study, we investigated the efficacy and safety of BV-DHAP as first salvage treatment for patients with R/R cHL. This study is the first to investigate this combination. Treatment with BV-DHAP resulted in a high proportion of patients with an mCR prior to HDC/auto-PBSCT, and toxicity was mostly reversible.

Data on FDG-PET-CT results following treatment with DHAP are scarce, but generally only about 25% of patients achieved a CR as assessed by CT scan.[4,26] Other trials have recently investigated BV in combination with other salvage chemotherapy combinations, such as bendamustine, ICE (ifosfamide, carboplatin, etoposide) or ESHAP (etoposide, methylprednisolone, high-dose cytarabine and cisplatin), and have shown mCR rates up to 76% prior to HDC/auto-PBSCT.[15-18,27] The administration schedule of BV differed among these studies, and most studies used more than three administrations of BV in total.[15-18,27] In the current study, three cycles of BV-DHAP resulted in a high mCR rate with only three administrations of BV. This makes it a less 'financially toxic' therapy than using BV in first line for all patients or to use it as consolidation therapy after auto-PBSCT.

In R/R cHL patients treated with salvage chemotherapy followed by HDC and auto-PBSCT, historical studies demonstrate a 5-year PFS of approximately 50%.[1-4,26,28,29] In 97 patients treated with ICE, 2-year event-free survival was 70%.[6] Another regimen consisting of bendamustine, gemcitabine and vinorelbine (in 59 patients) resulted in a 2-year PFS of 63%.[30] With the present treatment protocol, we have been able to achieve a high 2-year PFS rate of 74%. A total of 14 events occurred (including 3 deaths), and at the present median follow-up of 27 months, no relapses have occurred beyond 18 months from enrollment. Longer follow-up is needed to confirm that the majority of patients in remission after 2 years are indeed cured.[3,28,31]

The unprecedented high response rate and prolonged PFS of this treatment regimen were achieved at the cost of higher toxicity in comparison to other salvage regimens. However, most of the observed toxicities, including neutropenia, thrombocytopenia, fever, nausea/vomiting, ototoxicity and nephrotoxicity are toxicities of specific concern during treatment with DHAP.[4,26,32,33] Other regimens of BV with bendamustine, nivolumab, ICE or ESHAP seem to induce fewer AE, with most toxicities consisting of hematologic toxicity.[15,16,18,19,34] While the occurrence of grade 3/4 non-hematologic toxicity was low with BV-bendamustine, a substantial proportion of the patients (25%) did not undergo auto-PBSCT, resulting in a lower 2-year PFS of 62.6%.[16] Another recent study with BV-bendamustine in 40 patients had a 3-year PFS of 67.3%, and 82.5% of patients underwent auto-PBSCT.[19] The combination of BV with nivolumab resulted in an mCR rate of 61% with almost all patients experiencing grade 1/2 toxicity and 31% having grade 3/4 toxicity; however, these AE were also manageable.[34]

Table 2. Adverse events grade 3 or 4 during brentuximab vedotin and dexamethasone, high-dose cytarabine and cisplatin, high-dose cytarabine, cisplatin.

Adverse event	Cycle 1 (n=55)		Cycle 2 (n=53)		Cycle 3 (n=51)		Total* (n=55)	
CTCAE grade (n)	**3**	**4**	**3**	**4**	**3**	**4**	**3**	**4**
Febrile neutropenia	7	1	2	0	3	1	12 (22%)	2 (4%)
Elevated liver enzymes	3	0	5	1	1	0	9 (16%)	1 (2%)
Electrolyte disorders	2	1	0	1	2	0	4 (7%)	2 (4%)
Nausea/vomiting	1	0	3	0	2	0	4 (7%)	0 (0%)
Fever	0	0	1	0	2	0	3 (5%)	0 (0%)
Renal function disorder	1	0	0	0	2	0	3 (5%)	0 (0%)
Sepsis	0	0	1	1	1	0	2 (4%)	1 (2%)
Bone pain	2	0	0	0	0	0	2 (4%)	0 (0%)
Diarrhea	1	0	1	0	0	0	2 (4%)	0 (0%)
Epistaxis	0	0	1	0	1	0	2 (4%)	0 (0%)
Infection	0	0	1	0	1	0	2 (4%)	0 (0%)
Infusion-related reaction	0	0	2	0	0	0	2 (4%)	0 (0%)
Malaise	1	0	1	0	0	0	1 (2%)	0 (0%)
Abdominal pain	1	0	0	0	0	0	1 (2%)	0 (0%)
Back pain	0	0	0	0	1	0	1 (2%)	0 (0%)
Constipation	0	0	0	0	1	0	1 (2%)	0 (0%)
Headache	1	0	0	0	0	0	1 (2%)	0 (0%)
Myalgia shoulder	1	0	0	0	0	0	1 (2%)	0 (0%)
Periodic paralysis (hypokalemia)	1	0	0	0	0	0	1 (2%)	0 (0%)
Syncope	0	0	0	0	1	0	1 (2%)	0 (0%)
Total	**22**	**2**	**18**	**3**	**18**	**1**	**55**	**6**
Individual patients†	17	2	14	2	11	1	29	5
Individual patients total‡	18 (33%)		15 (28%)		11 (22%)		30 (55%)	

*Patients with a specific toxicity in more than one cycle were only counted once in the column representing the total toxicity. †Total of patients who experienced one or more grade 3 or 4 toxicity during the cycle concerned. ‡Total of patients who experienced one or more grade 3 or 4 toxicity during the cycle concerned. Patients who experienced both a grade 3 and grade 4 toxicity were only counted once. n: number; CTCAE: Common Terminology Criteria for Adverse Events.

A sequential approach of BV monotherapy followed by chemotherapy in PET-positive patients is interesting, since some patients could be spared the toxicity of salvage chemotherapy without losing efficacy. However, only a minority of patients achieved a PET-negative response after BV monotherapy.[15] The ESHAP regimen is similar to DHAP, except that it contains methylprednisolone instead of dexamethasone, and cisplatin is given over 4 days of 25 mg/m^2/day compared to 100 mg/m^2 in one day with the DHAP regimen.[18] Hematologic toxicity was comparable between BV-ESHAP and BV-DHAP with about 50% of patients experiencing grade 3/4 thrombocytopenia and neutropenia. For BV-ESHAP, grade 3 fever and mucositis were the most frequent non-hematologic grade 3/4 toxicities whereas DHAP was also associated with fever, but not with mucositis. In contrast, only grade 1/2 renal dysfunction occurred with BV-ESHAP, and no cases of elevated liver enzymes or ototoxicity are described.[18]

In ten patients, a transient grade 3/4 increase in liver enzymes was observed during BV-DHAP treatment (n=1 grade 4), which was reversible in all patients. One patient developed a fatal VOD after BEAM/auto-PBSCT. Additionally, one patient treated in the phase I part of this study also developed a grade 3 VOD, which, however, recovered without sequelae. Both patients already had elevated liver enzymes during BV-DHAP treatment. This complication has previously been described in patients receiving high-dose alkylating agents such as melphalan or cyclophosphamide.[35]

BV as consolidation therapy has been shown to prolong PFS in high-risk R/R cHL patients who have undergone HDC/auto-PBSCT.[36] Whether BV before auto-PBSCT in combination with chemotherapy, or as consolidation after auto-PBSCT will be more effective is unknown. Of note, with BV consolidation, peripheral neuropathy occurred in 67% of patients, including 13% (n=22) grade 3 peripheral neuropathy. With BV-DHAP, the incidence of peripheral neuropathy was lower, was mostly reversible, and no grade 3/4 occurred, probably because only three administrations of BV were given.

In-depth pathology workup and reclassification were performed to exclude lymphomas that are known as cHL mimickers such as AITL and PTCL (with follicular helper T-cell immunophenotype with secondary cHL-like blasts), as well as immunodeficiency-associated B-cell lymphoproliferative disorders (IA-B-LPD).[37-39] In retrospect, seven cases were identified as cHL-mimickers with central pathology review. Awareness for cHL-mimickers is important because patients with T-cell lymphoma generally have a worse prognosis.[40] In this cohort of patients, no significant differences in response rates or PFS were observed between patients with confirmed or unconfirmed cHL, although the number of patients is too small to validate this finding.

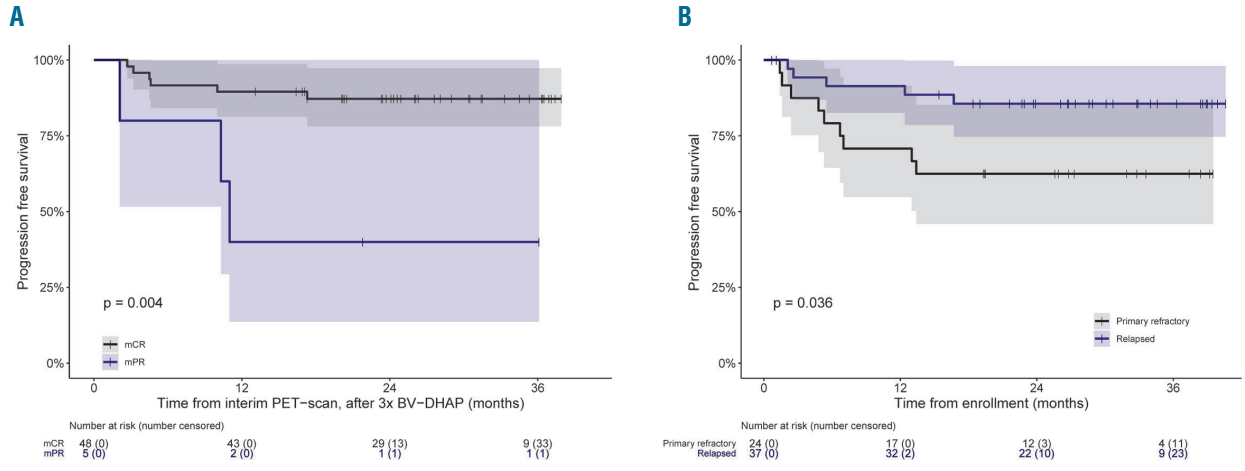


Figure 3. Kaplan-Meier exploratory analysis. Kaplan-Meier exploratory analysis for all 55 phase II patients and six patients from phase I who were treated at the same dose level, including the number of patients at risk at 1, 2 and 3 years with regard to (A) progression-free survival (PFS) stratified for patients with a metabolic complete response (mCR; n=48) or partial response (mPR; n=5) on the positron emission tomography-computed tomography (PET-CT) scan after three cycles of BV-DHAP, measured from the time of that PET-CT scan, and (B) PFS stratified for relapsed patients (n=37; defined as recurrent disease after having reached a complete response on first-line treatment) *versus* patients with primary refractory disease (n=24; no complete response on first-line treatment), measured from enrollment. BV: brentuximab vedotin; DHAP: dexamethasone, high-dose cytarabine, cisplatin.

Table 3. Serious adverse events grade 3 or 4 during brentuximab vedotin and dexamethasone, high-dose cytarabine and cisplatin.

Serious adverse event	Cycle 1 (n=55)		Cycle 2 (n=53)		Cycle 3 (n=51)		Total** (n=55)		Recovered
CTCAE grade (n)	**3**	**4**	**3**	**4**	**3**	**4**	**3**	**4**	
Febrile neutropenia	5	1	0	0	3	0	8	1	All
Infection	0	0	1	0	1	0	2	0	All
Renal function disorder	0	0	0	0	2	0	2	0	With sequela*
Sepsis	0	0	0	1	1	0	1	1	All
Epistaxis	0	0	1	0	0	0	1	0	All
Fever	0	0	0	0	1	0	1	0	All
Elevated liver enzymes	0	0	0	1	0	0	0	1	All
Infusion-related reaction	0	0	1	0	0	0	1	0	All
Malaise	1	0	1	0	0	0	1	0	All
Nausea/vomiting	1	0	0	0	1	0	1	0	All
Periodic paralysis (hypokalemia)	1	0	0	0	0	0	1	0	All
Total	**8**	**1**	**4**	**2**	**9**	**0**	**19**	**3**	
Individual patients†	7	1	4	2	7	0	15	3	
Individual patients total‡	8 (15%)		6 (11%)		7 (14%)		18 (33%)		

*Persisting grade 1 or 2 nephrotoxicity (e.g., decreased glomerular filtration rate or persisting high levels of creatinine). **Patients with a specific toxicity in more than one cycle were only counted once in the column representing the total toxicity. †Total of patients who experienced one or more grade 3 or 4 toxicity during the concerning cycle. ‡Total of patients who experienced one or more grade 3 or 4 toxicity during the concerning cycle. n: number; CTCAE: Common Terminology Criteria for Adverse Events.

An exploratory analysis on PFS showed that patients with an mPR prior to BEAM/auto-PBSCT have a higher risk of relapse, despite conversion to an mCR after auto-PBSCT. This finding is in line with other trials investigating risk factors for relapse after auto-PBSCT.[5-7] PET-adapted therapy could probably further improve outcome by intensifying treatment for high-risk patients with new agents, such as checkpoint inhibitors in addition to BV. Moreover, a group of patients at low-risk for relapse, might possibly be cured with a combination of new drugs only, without the toxic consequences of HDC and auto-PBSCT. Risk stratification based on the PET-CT scan at relapse could also be further improved by quantitative analysis and the assessment of metabolic tumor volume.[41,42]

The addition of BV to salvage treatment has not yet been investigated in a randomized phase III trial. However, several phase II studies have now shown that BV in combination with chemotherapy results in high mCR rates prior to HDC/auto-PBSCT. A combined pooled analysis of all of these studies is planned to give more insight into the effect of BV on response rates and toxicity in this setting.

In conclusion, in R/R cHL, three cycles of BV-DHAP is a highly effective salvage regimen resulting in an mCR rate of 81% prior to HDC/auto-PBSCT as shown by independent central PET-CT review. Patients should be monitored closely for toxicity, especially hematologic toxicity, nephrotoxicity and liver toxicity.

Disclosures

The study drug (BV) was provided for the study and the study was funded by Takeda. Takeda did not have any influence on the analysis of the data or the interpretation of the results. AH received consultancy fees, honoraria, and research funding from Millennium/Takeda. MJK: Millennium/Takeda: Honoraria, Research Funding; Celgene: Honoraria, Research Funding; Roche: Honoraria, Research Funding; Gilead: Honoraria; Kite Pharma: Honoraria; Novartis: Honoraria. FM: Janssen: Scientific Lectures; BMS: Membership on an entity's Board of Directors or advisory committees; Epizyme: Consultancy; Gilead: Consultancy, Membership on an entity's Board of Directors or advisory committees; Roche: Membership on an entity's Board of Directors or advisory committees; Celgene: Consultancy, Membership on an entity's Board of Directors or advisory committees. PJL: Millennium/Takeda: Consultancy, Research Funding; Servier: Consultancy, Research Funding; Roche: Consultancy; BMS: Consultancy; Sandoz: Consultancy; Genmab: Consultancy. AD: Millennium/Takeda: Consultancy, Honoraria, Research Funding. PB: Millennium/Takeda: Honoraria, Research Funding, Scientific Advisory Board; Roche: Honoraria; BMS: Honoraria, Scientific Advisory Board; MSD: Honoraria, Scientific Advisory Board; Jansen: Honoraria. MH: Consultant/advisor: Roche, Takeda, Celgene, Genmab; Research support: Roche, Takeda, Celgene, Genmab, Novartis, Janssen, Incyte, Genentech. TG: Millennium/Takeda: Honoraria, Gilead, Roche, MSD. JMZ: Consultant/advisor: Gilead, Roche, Takeda; Honoraria: Gilead, Roche, Takeda, Janssen. DDJ: Consultant/advisor: Takeda. All remaining authors have declared no conflicts of interest.

Contributions

MJK and AH designed the study; all authors collected the data; JD, MLY and HvT analyzed the data; JD and MJK wrote the manuscript with contributions from all authors, who also interpreted the data, read, commented on, and approved the final version of the manuscript; DdJ and AD performed the central pathology review; JZ, CB, AA and RV organized and performed the central FDG-PET-CT review; MJK and AH supervised the study.

Acknowledgments

The authors would like to thank all patients who participated in the trial, the Transplant BRaVE-trial team of the Trial Office of the Amsterdam UMC, location AMC, for their efforts in trial management and central data management, and the members of the Data Safety and Monitoring Board. The authors thank Marjolein Spiering, Edith van Dijkman, the data managers, trial nurses, lab and pharmacy personnel for their essential assistance with collecting and managing the study data. The authors thank Prof. Dr. Otto S. Hoekstra and Drs. Gerben J.C. Zwezerijnen for reviewing discrepancies in the central FDG-PET-CT review and Nathalie Hijmering, HOVON Pathology Facility and Biobank for biopsy collection and support of central pathology review.

Funding

This work was supported by research funding from Takeda.

References

1. Schmitz N, Pfistner B, Sextro M, et al. Aggressive conventional chemotherapy compared with high-dose chemotherapy with autologous haemopoietic stem-cell transplantation for relapsed chemosensitive Hodgkin's disease: a randomised trial. Lancet. 2002;359(9323):2065-2071.
2. Linch DC, Winfield D, Goldstone AH, et al. Dose intensification with autologous bone-marrow transplantation in relapsed and resistant Hodgkin's disease: results of a BNLI randomised trial. Lancet. 1993; 341(8852):1051-1054.
3. Majhail NS, Weisdorf DJ, Defor TE, et al. Long-term results of autologous stem cell transplantation for primary refractory or relapsed Hodgkin's lymphoma. Biol Blood Marrow Transplant. 2006;12(10):1065-1072.
4. Josting A, Rudolph C, Mapara M, et al. Cologne high-dose sequential chemotherapy in relapsed and refractory Hodgkin lymphoma: results of a large multicenter study of the German Hodgkin Lymphoma Study Group (GHSG). Ann Oncol. 2005;16(1):116-123.
5. Moskowitz CH, Nimer SD, Zelenetz AD, et al. A 2-step comprehensive high-dose chemoradiotherapy second-line program for relapsed and refractory Hodgkin disease: analysis by intent to treat and development of a prognostic model. Blood. 2001; 97(3):616-623.
6. Moskowitz CH, Matasar MJ, Zelenetz AD, et al. Normalization of pre-ASCT, FDG-PET imaging with second-line, non-cross-resistant, chemotherapy programs improves event-free survival in patients with Hodgkin lymphoma. Blood. 2012;119(7):1665-1670.
7. Moskowitz CH, Yahalom J, Zelenetz AD, et al. High-dose chemo-radiotherapy for relapsed or refractory Hodgkin lymphoma and the significance of pre-transplant functional imaging. Br J Haematol. 2010; 148(6):890-897.
8. Devillier R, Coso D, Castagna L, et al. Positron emission tomography response at the time of autologous stem cell transplantation predicts outcome of patients with relapsed and/or refractory Hodgkin's lymphoma responding to prior salvage therapy. Haematologica. 2012;97(7):1073-1079.
9. Smeltzer JP, Cashen AF, Zhang Q, et al. Prognostic significance of FDG-PET in relapsed or refractory classical Hodgkin lymphoma treated with standard salvage chemotherapy and autologous stem cell transplantation. Biol Blood Marrow Transplant. 2011;17(11):1646-1652.
10. Santoro A, Magagnoli M, Spina F, et al. Ifosfamide, gemcitabine, and vinorelbine: a new induction regimen for refractory and relapsed Hodgkin's lymphoma. Haematologica. 2007;92(1):35-41.
11. Labrador J, Cabrero-Calvo M, Perez-Lopez E, et al. ESHAP as salvage therapy for relapsed or refractory Hodgkin's lymphoma. Ann Hematol. 2014;93(10):1745-1753.
12. Eichenauer DA, Aleman BMP, Andre M, et al. Hodgkin lymphoma: ESMO Clinical Practice Guidelines for diagnosis, treatment and follow-up. Ann Oncol. 2018;29(Suppl 4):iv19-iv29.
13. Younes A, Bartlett NL, Leonard JP, et al. Brentuximab vedotin (SGN-35) for relapsed CD30-positive lymphomas. N Engl J Med. 2010;363(19):1812-1821.
14. Falini B, Pileri S, Pizzolo G, et al. CD30 (Ki-1) molecule, a new cytokine receptor of the tumor necrosis factor receptor superfamily as a tool for diagnosis and immunotherapy. Blood. 1995;85(1):1-14.
15. Moskowitz AJ, Schröder H, Yahalom J, et al. PET-adapted sequential salvage therapy with brentuximab vedotin followed by augmented ifosfamide, carboplatin, and etoposide for patients with relapsed and refractory Hodgkin's lymphoma: a non-randomised, open-label, single-centre, phase 2 study. Lancet Oncol. 2015;16(3):284-292.
16. LaCasce AS, Bociek RG, Sawas A, et al. Brentuximab vedotin plus bendamustine: a highly active first salvage regimen for relapsed or refractory Hodgkin lymphoma. Blood. 2018;132(1):40-48.
17. Chen R, Palmer JM, Martin P, et al. Results of a multicenter phase II trial of brentuximab vedotin as second-line therapy before autologous transplantation in relapsed/refractory Hodkgin lymphoma. Biol Blood Marrow Transplant. 2015; 21(12):2136-2140.
18. Garcia-Sanz R, Sureda A, de la Cruz F, et al. Brentuximab vedotin and ESHAP is highly effective as second-line therapy for Hodgkin lymphoma patients (long-term results of a trial by the Spanish GELTAMO Group). Ann Oncol. 2019;30(4):612-620.
19. Broccoli A, Argnani L, Botto B, et al. First salvage treatment with bendamustine and brentuximab vedotin in Hodgkin lymphoma: a phase 2 study of the Fondazione Italiana Linfomi. Blood Cancer J. 2019; 9(12):100.
20. Herrera AF, Palmer J, Martin P, et al. Autologous stem-cell transplantation after second-line brentuximab vedotin in relapsed or refractory Hodgkin lymphoma. Ann

Oncol. 2018;29(3):724-730.
21. Younes A, Gopal AK, Smith SE, et al. Results of a pivotal phase II study of brentuximab vedotin for patients with relapsed or refractory Hodgkin's lymphoma. J Clin Oncol. 2012;30(18):2183-2189.
22. Hagenbeek A, Mooij H, Zijlstra J, et al. Phase 1 dose-escalation study of brentuximab-vedotin combined with dexamethasone, high-dose cytarabine and cisplatin, as salvage treatment in relapsed/refractory classical Hodgkin lymphoma: the Transplant BRaVE study. Haematologica. 2018; 104(4):e151-e153.
23. Cheson BD, Fisher RI, Barrington SF, et al. Recommendations for initial evaluation, staging, and response assessment of Hodgkin and non-Hodgkin lymphoma: the Lugano classification. J Clin Oncol. 2014; 32(27):3059-3068.
24. Swerdlow SH, Campo E, Pileri SA, et al. The 2016 revision of the World Health Organization classification of lymphoid neoplasms. Blood. 2016;127(20):2375-2390.
25. Natkunam Y, Gratzinger D, Chadburn A, et al. Immunodeficiency-associated lymphoproliferative disorders: time for reappraisal? Blood. 2018;132(18):1871-1878.
26. Josting A, Muller H, Borchmann P, et al. Dose intensity of chemotherapy in patients with relapsed Hodgkin's lymphoma. J Clin Oncol. 2010;28(34):5074-5080.
27. Moskowitz AJ, Schoder H, Gavane S, et al. Prognostic significance of baseline metabolic tumor volume in relapsed and refractory Hodgkin lymphoma. Blood. 2017; 130(20):2196-2203.
28. Sureda A, Constans M, Iriondo A, et al. Prognostic factors affecting long-term outcome after stem cell transplantation in Hodgkin's lymphoma autografted after a first relapse. Ann Oncol. 2005;16(4):625-633.
29. Hahn T, McCarthy PL, Carreras J, et al. Simplified validated prognostic model for progression-free survival after autologous transplantation for Hodgkin lymphoma. Biol Blood Marrow Transplant. 2013; 19(12):1740-1744.
30. Santoro A, Mazza R, Pulsoni A, et al. Bendamustine in combination with gemcitabine and vinorelbine is an effective regimen as induction chemotherapy before autologous stem-cell transplantation for relapsed or refractory Hodgkin lymphoma: final results of a multicenter phase II study. J Clin Oncol. 2016;34(27):3293-3299.
31. Arai S, Fanale M, DeVos S, et al. Defining a Hodgkin lymphoma population for novel therapeutics after relapse from autologous hematopoietic cell transplant. Leuk Lymphoma. 2013;54(11):2531-2533.
32. Sorigue M, Sancho JM, Pineda A, et al. Incidence and prognostic significance of nephrotoxicity in patients receiving eshap as salvage therapy for lymphoma. Leuk Res. 2017;58:98-101.
33. McKeage M. Comparative adverse effect profiles of platinum drugs. Drug Safety. 1995;13(4):228-244.
34. Herrera AF, Moskowitz AJ, Bartlett NL, Vose JM, Ramchandren R, Feldman T. Interim results of brentuximab vedotin in combination with nivolumab in patients with relapsed or refractory Hodgkin lymphoma. Blood. 2018;131(11):1183-1194.
35. Coppell JA, Richardson PG, Soiffer R, et al. Hepatic veno-occlusive disease following stem cell transplantation: incidence, clinical course, and outcome. Biol Blood Marrow Transplant. 2010;16(2):157-168.
36. Moskowitz CH, Nademanee A, Masszi T, et al. Brentuximab vedotin as consolidation therapy after autologous stem-cell transplantation in patients with Hodgkin's lymphoma at risk of relapse or progression (AETHERA): a randomized, double-blind, placebo-controlled, phase 3 trial. Lancet. 2015;385(9980):1853-1862.
37. Sarkozy C, Copie-Bergman C, Damotte D, et al. Gray-zone lymphoma between cHL and large B-cell lymphoma. A histopathologic series from the LYSA. Am J Surg Pathol. 2019;43(3):341-351.
38. Pilichowska M, Pittaluga S, Ferry JA, et al. Clinicopathologic consensus study of gray zone lymphoma with features intermediate between DLBCL and classical HL. Blood Advances. 2017;1(26):2600-2609.
39. Jiang M, Bennani NN, Feldman AL. Lymphoma classification update: T-cell lymphomas, Hodgkin lymphomas, and histiocytic/dendritic cell neoplasms. Expert Rev Hematol. 2017;10(3):239-249.
40. Vose J, Armitage J, Weisenburger D, International TCLP. International peripheral T-cell and natural killer/T-cell lymphoma study: pathology findings and clinical outcomes. J Clin Oncol. 2008;26(25):4124-4130.
41. Mettler J, Muller H, Voltin CA, et al. Metabolic tumour volume for response prediction in advance-stage Hodgkin lymphoma. J Nucl Med. 2019;60(2):207-211.
42. El-Galaly TC, Villa D, Gormsen LC, Baech J, Lo A, Cheah CY. FDG-PET/CT in the management of lymphomas: current status and future directions. J Intern Med. 2018; 284(4):358-376.

Ferrata Storti Foundation

Sec22b determines Weibel-Palade body length by controlling anterograde endoplasmic reticulum-Golgi transport

Ellie Karampini,[1] Petra E. Bürgisser,[2] Jenny Olins,[1] Aat A. Mulder,[3] Carolina R. Jost,[3] Dirk Geerts,[4] Jan Voorberg[1,5] and Ruben Bierings[1,2]

[1]Molecular and Cellular Hemostasis, Sanquin Research and Landsteiner Laboratory, Amsterdam University Medical Center, University of Amsterdam, Amsterdam; [2]Hematology, Erasmus MC, University Medical Center Rotterdam, Rotterdam; [3]Molecular Cell Biology, Leiden University Medical Center, Leiden and [4]Medical Biology Amsterdam University, Medical Center, University of Amsterdam, Amsterdam and [5]Experimental Vascular Medicine, Amsterdam University Medical Center, University of Amsterdam, Amsterdam, the Netherlands

Haematologica 2021
Volume 106(4):1138-1147

ABSTRACT

Von Willebrand factor (VWF) is a multimeric hemostatic protein that is synthesized in endothelial cells, where it is stored for secretion in elongated secretory organelles called Weibel-Palade bodies (WPB). The hemostatic activity of VWF is strongly related to the length of these bodies, but how endothelial cells control the dimensions of their WPB is unclear. In this study, using a targeted short hairpin RNA screen, we identified longin-SNARE Sec22b as a novel determinant of WPB size and VWF trafficking. We found that Sec22b depletion resulted in loss of the typically elongated WPB morphology together with disintegration of the Golgi and dilation of rough endoplasmic reticulum cisternae. This was accompanied by reduced proteolytic processing of VWF, accumulation of VWF in the dilated rough endoplasmic reticulum and reduced basal and stimulated VWF secretion. Our data demonstrate that the elongation of WPB, and thus adhesive activity of their cargo VWF, is determined by the rate of anterograde transport between endoplasmic reticulum and Golgi, which depends on Sec22b-containing SNARE complexes.

Correspondence:

RUBEN BIERINGS
r.bierings@erasmusmc.nl

Received: November 11, 2019.

Accepted: March 24, 2020.

Pre-published: March 26, 2020.

https://doi.org/10.3324/haematol.2019.242727

©2021 Ferrata Storti Foundation

Material published in Haematologica is covered by copyright. All rights are reserved to the Ferrata Storti Foundation. Use of published material is allowed under the following terms and conditions: https://creativecommons.org/licenses/by-nc/4.0/legalcode. Copies of published material are allowed for personal or internal use. Sharing published material for non-commercial purposes is subject to the following conditions: https://creativecommons.org/licenses/by-nc/4.0/legalcode, sect. 3. Reproducing and sharing published material for commercial purposes is not allowed without permission in writing from the publisher.

Introduction

Endoplasmic reticulum (ER)-to-Golgi transport is the first step in the secretory pathway.[1] As eukaryotic cells are extremely compartmentalized, ER is the first stop in protein production as well as the initial quality check point of whether proteins are correctly folded.[2] Correctly folded proteins are then trafficked to the Golgi where they are additionally modified before being directed to their appropriate destination: endo/lysosome, plasma membrane or secretion.[3] At the *trans*-Golgi network (TGN), proteins will either enter the "constant" constitutive pathway for unimpeded release, or will be temporarily stored in secretory vesicles, often of the family of lysosome-related organelles, for regulated secretion. Storage and regulated secretion allow the immediate discharge of larger quantities of protein in a correct physiological setting.[4]

The biogenesis of lysosome-related organelles is crucial for the proper function of a wide variety of cells, their importance being well-highlighted by the fact that defective formation of these organelles results in the manifestation of a large number of clinical abnormalities including bleeding, immunodeficiency, hypopigmentation and neurological defects.[5] Within the family of lysosome-related organelles, Weibel-Palade bodies (WPB) are the storage organelles of endothelial cells.[6,7] WPB primarily contain von Willebrand factor (VWF), a large multimeric hemostatic protein that serves a critical role in platelet adhesion and as a chaperone for coagulation factor VIII.[8] The biogenesis of WPB is directly dependent on the synthesis and correct post-translational processing of VWF.[9-12] WPB have a distinct, elongated morphology that is intrinsically linked to the inherent ability of VWF multimers to self-organize in

tubules when exposed to the internal milieu of the TGN.[13-15] Quantitative or qualitative defects of VWF, for instance due to mutations in *VWF*, cause von Willebrand disease (VWD), the most common inherited bleeding disorder.[16] *VWF* mutations that affect the synthesis or processing of the protein often result in altered WPB morphology, with WPB being either round or short.[17] Upon regulated, explosive release from WPB, VWF unfurls into strings up to 1 mm long that are anchored on the apical side of the endothelium.[18-20] VWF strings create an adhesive platform for platelets to initiate the formation of the initial platelet plug at the site of vascular damage.[21,22] The adhesive capacity of VWF towards platelets and self-associating plasma VWF is proportional to WPB size.[23] In turn, WPB size is determined before budding from the TGN by incorporation of so-called "VWF quanta" and it was previously shown that reduced VWF synthesis or unlinking of Golgi stacks affects WPB length.[24] However, how endothelial cells control WPB size and thus hemostatic activity of VWF is largely unknown.

Due to the distinctive shape of their WPB, endothelial cells are an excellent model system for elucidating how cells manage formation and morphology of lysosome-related organelles. As WPB formation is driven by VWF, monitoring intracellular VWF trafficking can be used as a tool to study the complex mechanisms involved. VWF undergoes extensive post-translational modification during its journey through the endothelial secretory pathway.[25] VWF enters the ER as a single pre-pro-polypeptide chain that forms tail-to-tail dimers by formation of disulfide bonds between the C-terminal cysteine knot (CTCK) domains of two proVWF monomers.[26] After dimerization-dependent exit from the ER, proVWF dimers are transported to the Golgi, where VWF propeptide is cleaved from the proVWF chain. Inter-dimer disulfide bonds between cysteines in the D3 domains lead to formation of head-to-head VWF multimers.[27] VWF multimers are then condensed into tubules that are packaged into newly forming WPB that emerge from the TGN.[28,29]

Trafficking of proteins during formation and maturation of subcellular organelles, such as WPB, is dependent on membrane fusion, which is universally controlled by SNARE proteins.[30] The SNARE complex consists of a v-SNARE on the vesicle membrane and t-SNARE on the acceptor membrane which together form a four-helix bundle that allows the membranes to fuse. Although several SNARE have been associated with WPB exocytosis,[7] the SNARE that take part in the biogenesis of lysosome-related organelles and WPB are not known. The subfamily of longin-SNARE (VAMP7, YKT6 and Sec22b), which derives its name from an N-terminal self-inhibitory longin-domain that can fold back on the SNARE domain, controls membrane fusion events that traffic proteins to and from the Golgi.[31]

In this study we addressed the role of longin-SNARE in the formation of WPB. Using a targeted short hairpin (sh)RNA screen of longin-SNARE in primary endothelial cells we identified Sec22b as a novel determinant of WPB morphology. Sec22b silencing resulted in short WPB, disintegration of the Golgi complex, reduced proVWF processing and retention of proVWF in a dilated ER. Our data suggest that the distinctive morphology of WPB and thus the adhesive activity of their main cargo VWF is determined by the rate of membrane fusion between ER and Golgi, which is dependent on Sec22b-containing SNARE complexes.

Methods

Antibodies

The antibodies used in this study are listed in *Online Supplementary Table S1*.

Cell culture, lentiviral transfection and transduction

Pooled, cryopreserved primary human umbilical vein endothelial cells (HUVEC) were obtained from Promocell (Heidelberg, Germany). HUVEC were cultured in EGM-18 medium, i.e., EGM-2 medium (CC-3162, Lonza, Basel, Switzerland) supplemented with 18% fetal calf serum (Bodinco, Alkmaar, the Netherlands). Human embryonic kidney 293T (HEK293T) cells were obtained from the American Type Cell Culture (Wessel, Germany) and were grown in Dulbecco modified Eagle medium containing D-glucose and L-glutamine (Lonza, Basel, Switzeland) supplemented with 10% fetal calf serum, 100 U/mL penicillin and 100 µg/mL streptomycin. HEK293T cells were seeded on collagen-coated plates or flasks and were transfected with third-generation lentiviral packaging plasmids pMD2.G, pRSV-REV and pMDLg/pRRE (Addgene, Cambridge, MA, USA) using transit-LT1 (Mirus Bio LLC, Madison, WI, USA) following the supplier's protocol. After incubation for 6-8 h, the medium was exchanged for EGM-18. Virus particles were collected 24 and 48 h following transfection and were filtered through 0.45 µm pore filters in EGM-18. Two batches of virus were used to transduce HUVEC, cord blood outgrowth endothelial cells or HEK293T cells for a period of 48 h. Transduced endothelial cells were selected by puromycin (0.5 µg/mL), which was added to the medium for 72 h after the second virus installment.

DNA constructs for shRNA silencing of longin-SNARE, CRISPR editing and mEGFP-Sec22b-ΔSNARE

The LKO.1-puro-CMV-mEGFP-U6-shC002 vector, which simultaneously expresses monomeric enhanced green fluorescent protein (mEGFP) and a non-targeting control shRNA from the cytomegalovirus (CMV) and U6 promoter, respectively, was described previously.[32] shRNA targeting Sec22b, VAMP7 and YKT6 were obtained from the MISSION® shRNA library developed by TRC at the Broad Institute of MIT and Harvard and distributed by Sigma-Aldrich (*Online Supplementary Table S2*). Fragments containing the shRNA expression cassette from the shRNA library were transferred to the LKO.1-puro-CMV-mEGFP-U6 vector by *Sph*I-EcoRI subcloning. CRISPR-mediated depletion of Sec22b in HUVEC was performed essentially as described previously.[33] LentiCRISPR_v2 (a gift from Dr. Feng Zhang; Addgene #52961), a lentiviral vector which simultaneously expresses Cas9 endonuclease and guide (g)RNA has been described previously.[34] gRNA were designed to target exon 1 of the *SEC22B* gene using the CRISPOR Design tool (*http://crispor.tefor.net/*)[35] by submitting the DNA sequence of *SEC22B* exon 1 flanked by 100 bp up- and downstream (chromosome 1: 120,1501898-120,176,515 reverse strand) (*Online Supplementary Figure 2A*). gRNA sequences that have a high predicted efficiency with limited off-target effects were selected. The gRNA used in this study are shown in *Online Supplementary Table S3* and were cloned as hybridized complementary oligos (with *Bsm*BI restriction site-compatible overhangs on either side) into *Bsm*BI-digested LentiCRISPR_v2 plasmid. LVX-mEGFP-LIC has been described previously.[36] To construct a human Sec22b variant that lacks its SNARE domain (Gly135-Lys174), a synthetic Sec22b fragment was generated by gene synthesis in which codons 135-174 were removed from the 214-codon Sec22b coding sequence and was flanked by *Bsr*GI and *Not*I sites. The resulting Sec22b-ΔSNARE fragment was cloned in frame behind

mEGFP in LVX-mEGFP-LIC by subcloning between the *BsrGI* and *NotI* sites. All constructs were sequence verified. Lentiviral plasmids were produced in Stbl3 bacteria.

Further details on materials and methods are provided in the *Online Supplementary Data*.

Results

Weibel-Palade body length is significantly reduced upon Sec22b silencing

To determine the role of longin-SNARE in WPB biogenesis we performed a targeted shRNA screen against VAMP7, YKT6 and Sec22b in HUVEC and evaluated WPB morphology by VWF immunostaining. As shown in Figure 1A, in shCTRL, shVAMP7 and shYKT6 transduced cells, VWF was primarily stored in typical cigar-shaped WPB. However, upon Sec22b silencing (shSec22b) (*Online Supplementary Figure S1*), WPB lost their characteristic elongated morphology and appeared short and "stubby". Quantification of WPB length in control and knockdown (KD) cells showed a significant reduction in WPB length after Sec22b KD, whereas no difference was found in the absence of VAMP7 or YKT6 (Figure 1B). To further substantiate the role of Sec22b in WPB formation we used CRISPR-mediated *SEC22B*-editing of HUVEC (*Online Supplementary Figure S2A-C*). Cells depleted of Sec22b were identified by Sec22b staining (*Online Supplementary*

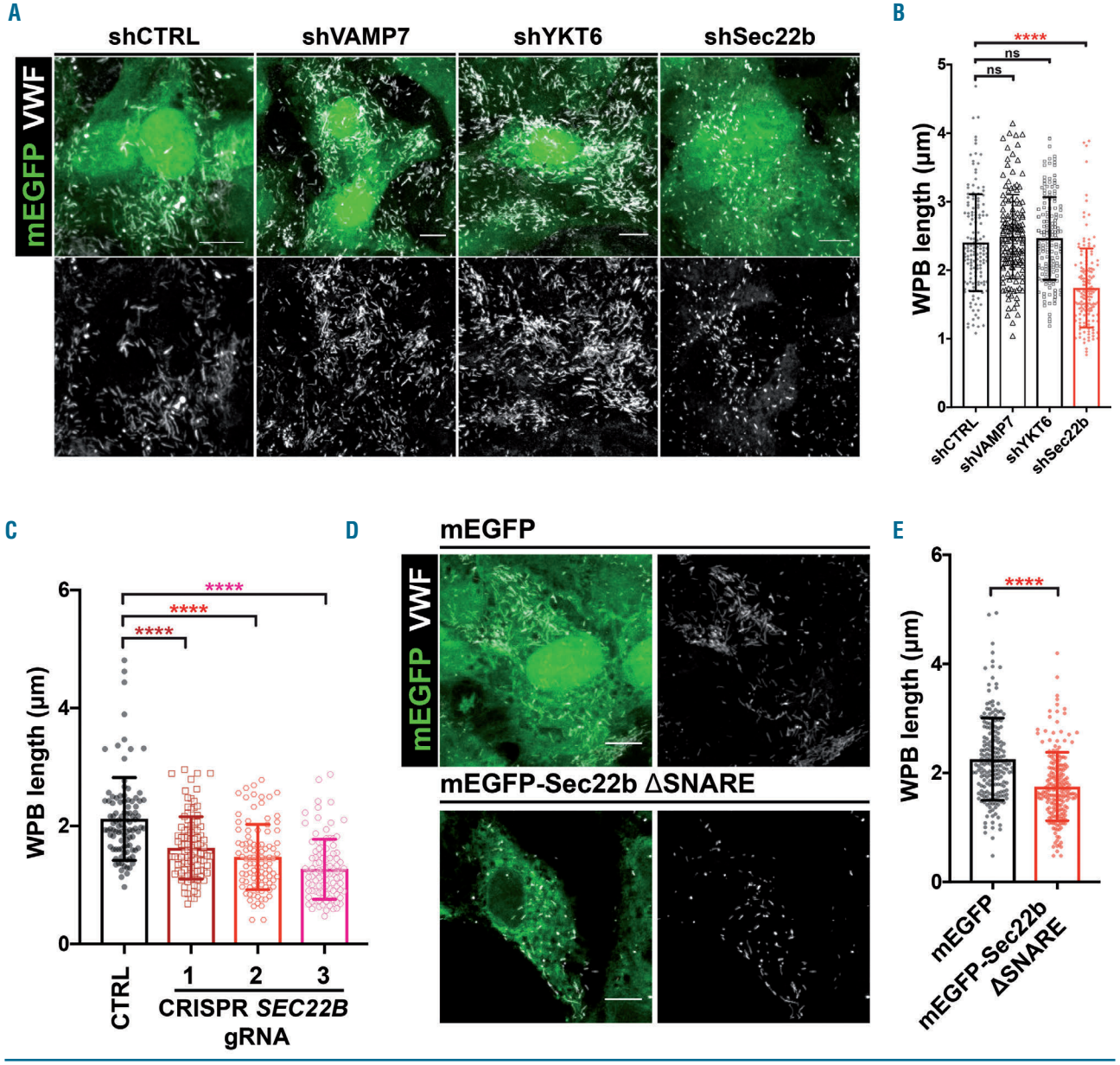


Figure 1. Sec22b depletion and fusogenic function affects Weibel-Palade body elongation. (A) von Willebrand factor (VWF) immunostaining in endothelial cells (EC) transduced with shCTRL, shVAMP7, shYKT6 or shSec22b (green channel: mEGFP-expressing EC). (B) Quantification of Weibel-Palade body (WPB) length in shCTRL, shVAMP7, shYKT6 and shSec22b EC (n=3, one-way analysis of variance [ANOVA] with the Dunnett multiple comparisons test, ****P<0.0001). (C) WPB length in control and CRISPR *SEC22B* knockout EC (n=3, one-way ANOVA with the Dunnett multiple comparisons test, ****P<0.0001). (D) VWF immunostaining in mEGFP and mEGFP-Sec22b-ΔSNARE expressing EC (both in green). (E) WPB length in mEGFP and mEGFP-Sec22b-ΔSNARE expressing EC (n=3, t-test with Welch correction, ****P<0.0001).

Figure S2D). A similar reduction of WPB length was observed in endothelial cells targeted with three separate gRNA directed to exon 1 of Sec22b (Figure 1B, *Online Supplementary Figure S2E*). As a third, independent strategy we also determined WPB morphology after expression of an mEGFP-tagged non-fusogenic Sec22b variant (mEGFP-Sec22b-ΔSNARE), which lacks the SNARE domain responsible for fusion and compared these with mEGFP-expressing cells (Figure 1D). We found that the ΔSNARE construct had a dominant-negative effect on WPB size, with these WPB being significantly shorter than the mEGFP control (Figure 1E). To investigate whether the size reduction extends to other (post-Golgi) organelles, we determined the localization of the tetraspanin CD63. CD63 normally cycles between plasma membrane, endolysosomal organelles and WPB in an AP-3-dependent manner.[37] Silencing of Sec22b did not lead to apparent changes in the morphology of CD63$^+$ endolysosomal organelles, nor did it impede the trafficking of CD63 to shorter WPB (*Online Supplementary Figure S3*). Together these results identify Sec22b as a determinant of secretory organelle size in endothelial cells.

Sec22b silencing results in unlinked Golgi ribbon

Since the size of nascent WPB is regulated by incorporation of multiple so-called VWF quanta from the TGN,[24] we investigated TGN morphology in Sec22b-depleted cells. TGN46 immunostaining showed that while the TGN in control cells had a compact morphology, shSec22b-treated cells exhibited a dispersed TGN morphology, consistent with an unlinked Golgi ribbon (Figure 2A and B). Quantification of the area that encompassed the entire TGN46 immunoreactivity in shSec22b and shCTRL cells revealed that, due to their fragmentation, TGN in Sec22b-depleted cells extended to a significantly larger intracellular area than the compact TGN in control cells (Figure 2C). The crucial role for Sec22b in maintaining Golgi integrity is not limited to endothelial cells, as illustrated by a similar effect on Golgi morphology in Sec22b-depleted HEK293T cells (*Online Supplementary Figure S4*). It has previously been described that unlinking Golgi stacks using depletion of Golgi matrix proteins or nocodazole gives rise to shorter WPB.[24] When evaluating WPB length in shSec22b cells with compact *versus* dispersed TGN we also observed that in those cells in which the Golgi was dispersed, WPB were on average shorter than in those with intact Golgi (Figure 2D), which suggests that the reduction in WPB length after Sec22b depletion is (at least partly) a consequence of Golgi disintegration.

Sec22b silencing results in decreased von Willebrand factor trafficking to the Golgi and retention of von Willebrand factor in the endoplasmic reticulum

As Sec22b has been associated with membrane fusion events during anterograde and retrograde trafficking between the ER and Golgi,[31] we evaluated VWF traffick-

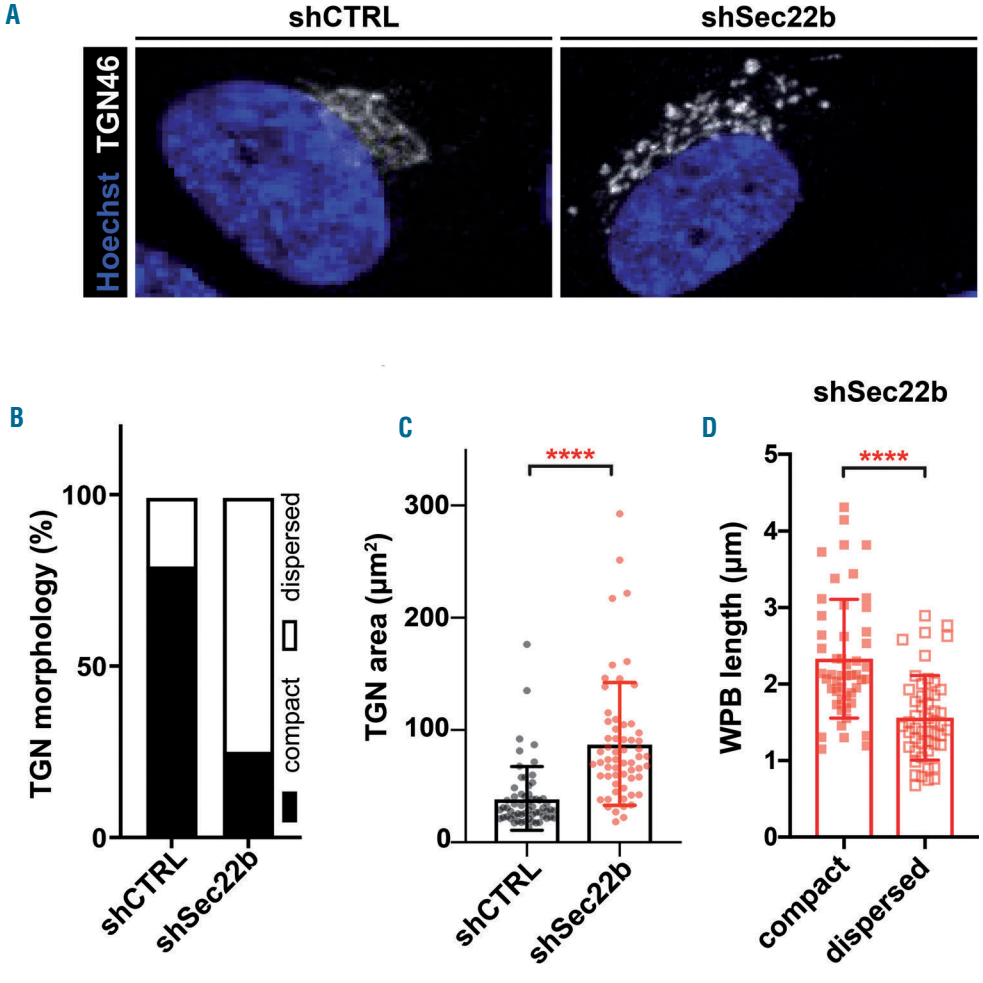


Figure 2. Sec22b depletion results in *trans*-Golgi network fragmentation. (A) Immunofluorescent staining of *trans*-Golgi network (TGN46) in control and Sec22b-depleted cells (blue channel: Hoechst nuclear staining). (B) Quantification of TGN dispersal in control and Sec22b knockdown (KD) endothelial cells (EC). (C) Quantification of TGN area coverage in shCTRL and shSec22b EC (n=5, *t*-test with Welch correction, ****P<0.001). (D) Weibel-Palade body (WPB) length in Sec22b KD EC with compact *versus* dispersed TGN (n=3, *t*-test with Welch correction, ****P<0.0001).

ing in the endothelial early secretory pathway. A key step during VWF biosynthesis is the proteolytic cleavage of proVWF into VWF propeptide and mature VWF, which takes place upon its arrival in the Golgi.[38] We used the intracellular ratio between the two distinct forms of VWF, proVWF (ER) and mature VWF (Golgi and post-Golgi), as a measure of ER and Golgi transport by estimating the amount of proVWF and VWF in shCTRL and shSec22b endothelial cells (Figure 3A). While the total amount of mature VWF was markedly reduced in shSec22b cells, the proportion of VWF in the unprocessed proVWF form was increased. Therefore, the proVWF:VWF ratio was significantly increased in the Sec22b KD endothelial cells (Figure 3B). This suggests that proteolytic processing of proVWF is reduced in the absence of Sec22b, possibly due to a reduced flux of VWF from the ER. Consistent with this we observed increased VWF immunoreactivity in reticular perinuclear structures resembling the ER after Sec22b silencing (Figure 3C). Simultaneous with - but independent of - proteolytic processing, VWF dimers oligomerize into long VWF multimers in the Golgi.[10,38] VWF multimer analysis using sodium dodecylsulfate-agarose gel electrophoresis showed that Sec22b silencing did not affect multimerization *per se*, as evidenced by high molecular weight VWF multimers in lysates of shCTRL and shSec22b endothelial cells. However, the increased proportion of VWF dimers in the Sec22b KD cells indicates that VWF is retained in the ER (Figure 3D and E). Together this points to a reduction of anterograde ER-Golgi trafficking of VWF in the absence of Sec22b.

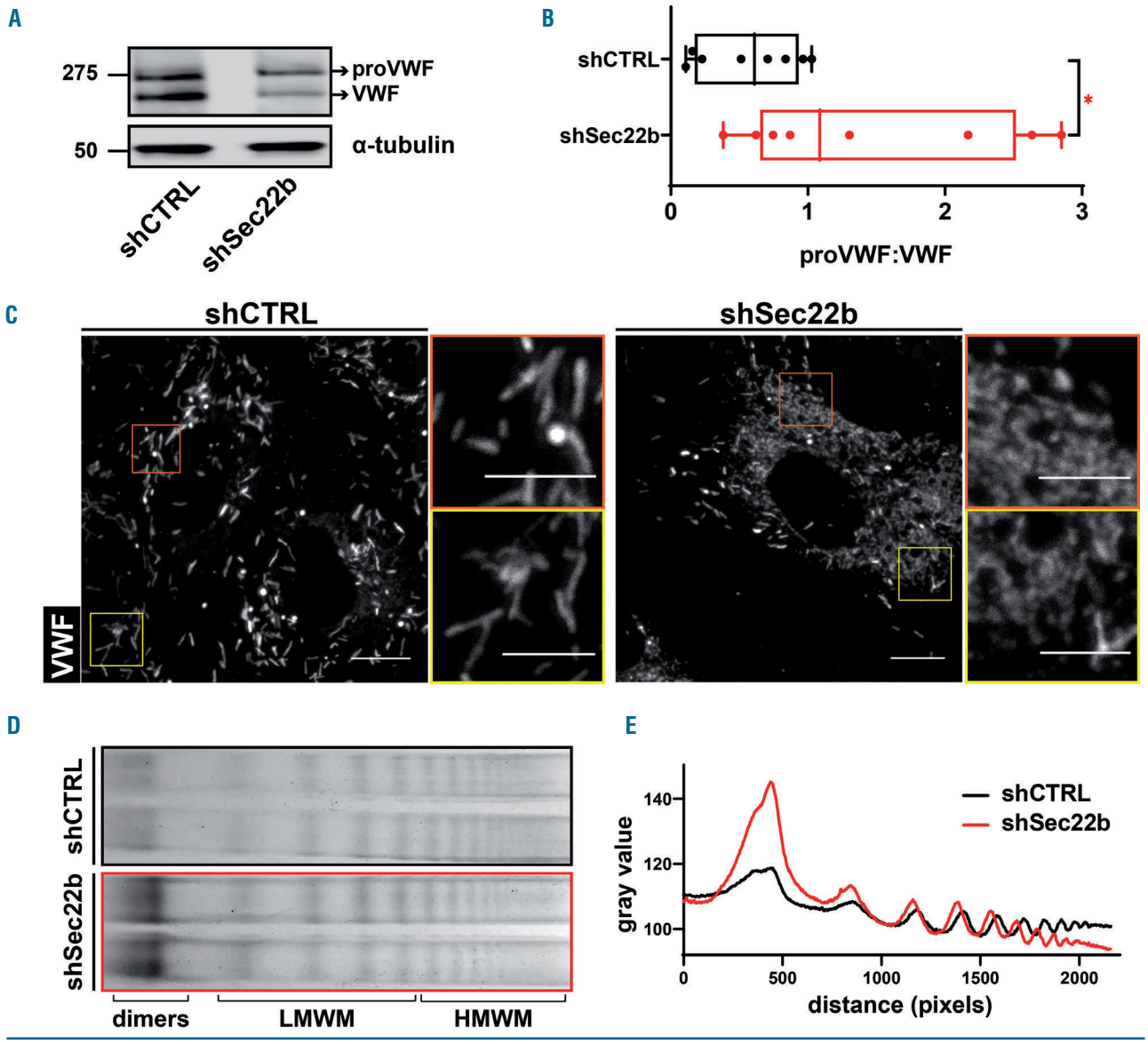


Figure 3. Sec22b depletion results in retention of von Willebrand factor in the endoplasmic reticulum. (A) Western blot analysis of monomeric von Willebrand factor (VWF) under reducing conditions in control and Sec22b knockdown (KD) endothelial cells (EC). Uncleaved (proVWF) and cleaved (VWF) forms are indicated by arrows. α-tubulin was used as a loading control. Molecular weight standards are indicated on the left (kDa). (B) ProVWF:VWF ratio in control and shSec22b EC (n=8, paired *t*-test, *P<0.05). (C) Immunofluorescent staining of VWF in shCTRL and shSec22b human umbilical vein EC (boxed areas are shown magnified on the right, size bar corresponds to 10 μm for images or 5 μm for boxed areas). (D) VWF multimer blot (4 samples from 2 independent experiments) in control and Sec22b KD EC. (E) Line graph of the densitometry of VWF multimer bands. LMWM: low molecular weight multimers; HMWM: high molecular weight multimers

Sec22b silencing results in accumulation of von Willebrand factor in dilated rough endoplasmic reticulum

Since VWF was retained in the ER, potentially along with other proteins, we used electron microscopy to examine the impact of reduced anterograde trafficking on the ER (Figure 4A). When Sec22b was silenced the rough ER (rER) appeared enlarged and ribosome-studded, membrane-limited, rounded structures developed, with electron-dense content. These rER structures represent severely dilated ER cisternae as they often retained a membranous connection to the rER. The dilated rER phenotype was observed in the majority of Sec22b-depleted cells (72.9%) (Figure 4B). Closer examination of the rER morphology revealed that apart from the round rER structures, the luminal width of ER sheets was significantly increased in Sec22b KD cells (0.29 μm ± 0.18 μm) when compared to control cells (0.10 μm ± 0.01 μm) (Figure 4C). This suggests that upon removal of Sec22b the rER expands in size dramatically, possibly to facilitate the accumulation of secretory proteins such as VWF. Indeed, immunogold staining for VWF in Sec22b KD endothelial cells localized within dilated rER and was prominently found in the round, dense rER structures (Figure 4D). Taken together this shows that VWF exits the ER in a Sec22b-dependent manner and upon Sec22b silencing is retained in rER-derived structures.

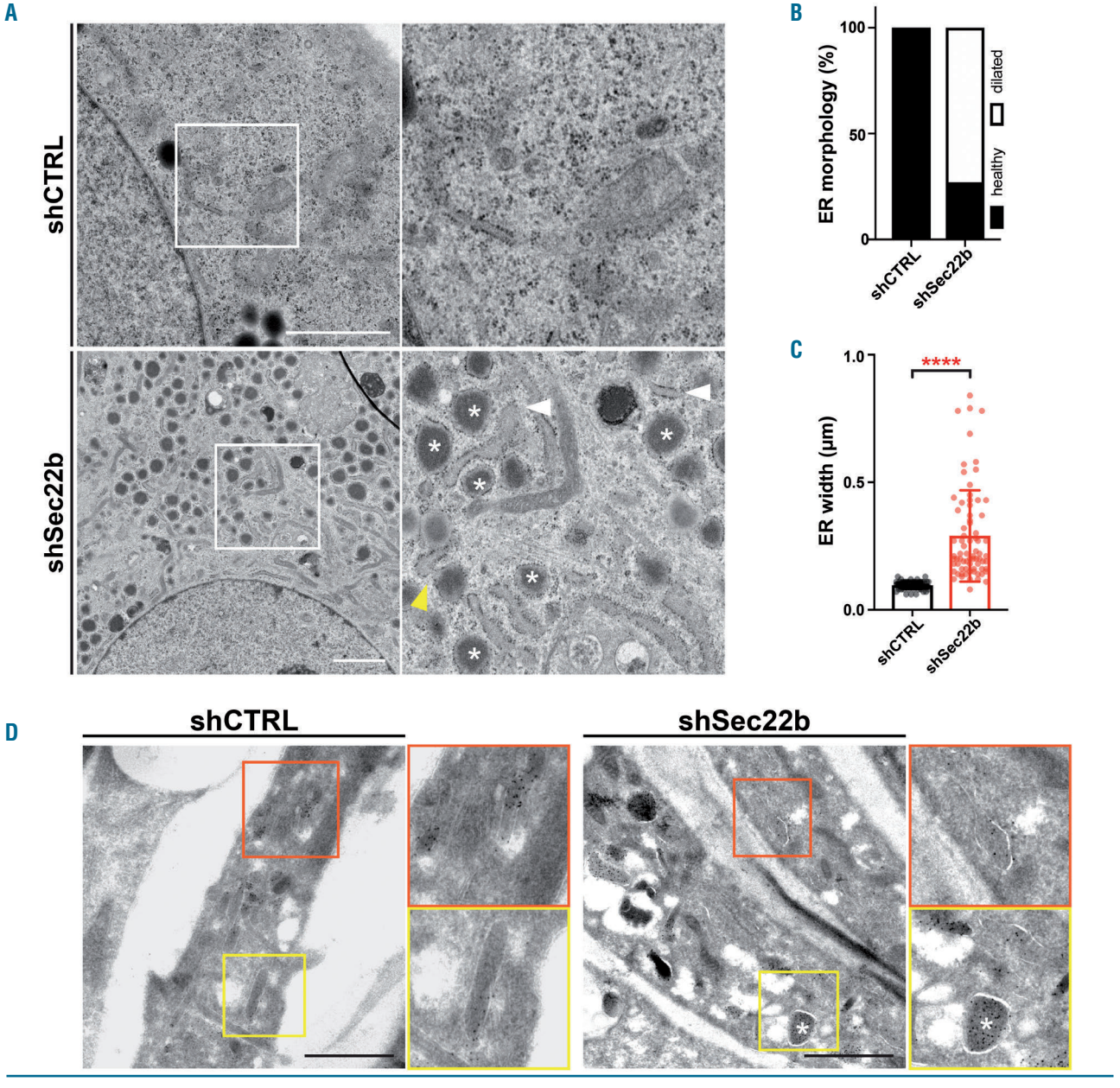


Figure 4. von Willebrand factor accumulation in dilated rough endoplasmic reticulum in Sec22b-depleted endothelial cells. (A) Electron microscopy of control and Sec22b knockdown (KD) endothelium cells (EC) (dilated rough endoplasmic reticulum [ER] shown by white arrowheads, ribosome-studded dilated ER by white asterisks, and the connection of ER structures to rough ER sheets by a yellow arrowhead; scale bar corresponds to 2 μm). (B) Quantification of healthy *versus* dilated ER in control and Sec22b KD cells. (C) Quantification of ER width in control and Sec22b KD cells (*t*-test with Welch correction, ****P<0.0001). (D) von Willebrand factor immunogold staining (10 nm gold particles) in control and Sec22b KD EC (boxed regions are magnified on the right side with the corresponding color; scale bar represents 1 μm).

Retention of von Willebrand factor in the endoplasmic reticulum results in reduced von Willebrand factor secretion in Sec22b-depleted cells

The lack of mature VWF, as well as the shorter WPB, prompted us to investigate how much VWF is stored and secreted in the absence of Sec22b. We observed that in the Sec22b-depleted cells, intracellular VWF levels were slightly increased when compared to the levels in control cells (Figure 5A), potentially because of VWF entrapment in the ER. On the other hand, basal secretion was significantly decreased in Sec22b-silenced cells (Figure 5B). Basal secretion primarily originates from unstimulated WPB release,[39,40] suggesting that this compartment is smaller upon Sec22b depletion. In line with this, VWF release through histamine-induced WPB exocytosis was also significantly reduced (Figure 5C). WPB acquire secretion competence during maturation by recruiting Rab GTPases and Rab-effectors,[7] so this decrease could potentially be attributed to defects in WPB maturation in Sec22b-depleted cells. We assessed whether two maturation-dependent components of the exocytotic machinery, Rab27A and Slp4-a,[41,42] were recruited to WPB but found no difference between shSec22b and shCTRL cells (*Online Supplementary Figure S5*). Thus, the simplest explanation for reduction in (stimulated) VWF secretion is failure of sufficient VWF to progress to a stimulus-sensitive compartment, i.e. the WPB, because it is retained in the ER.

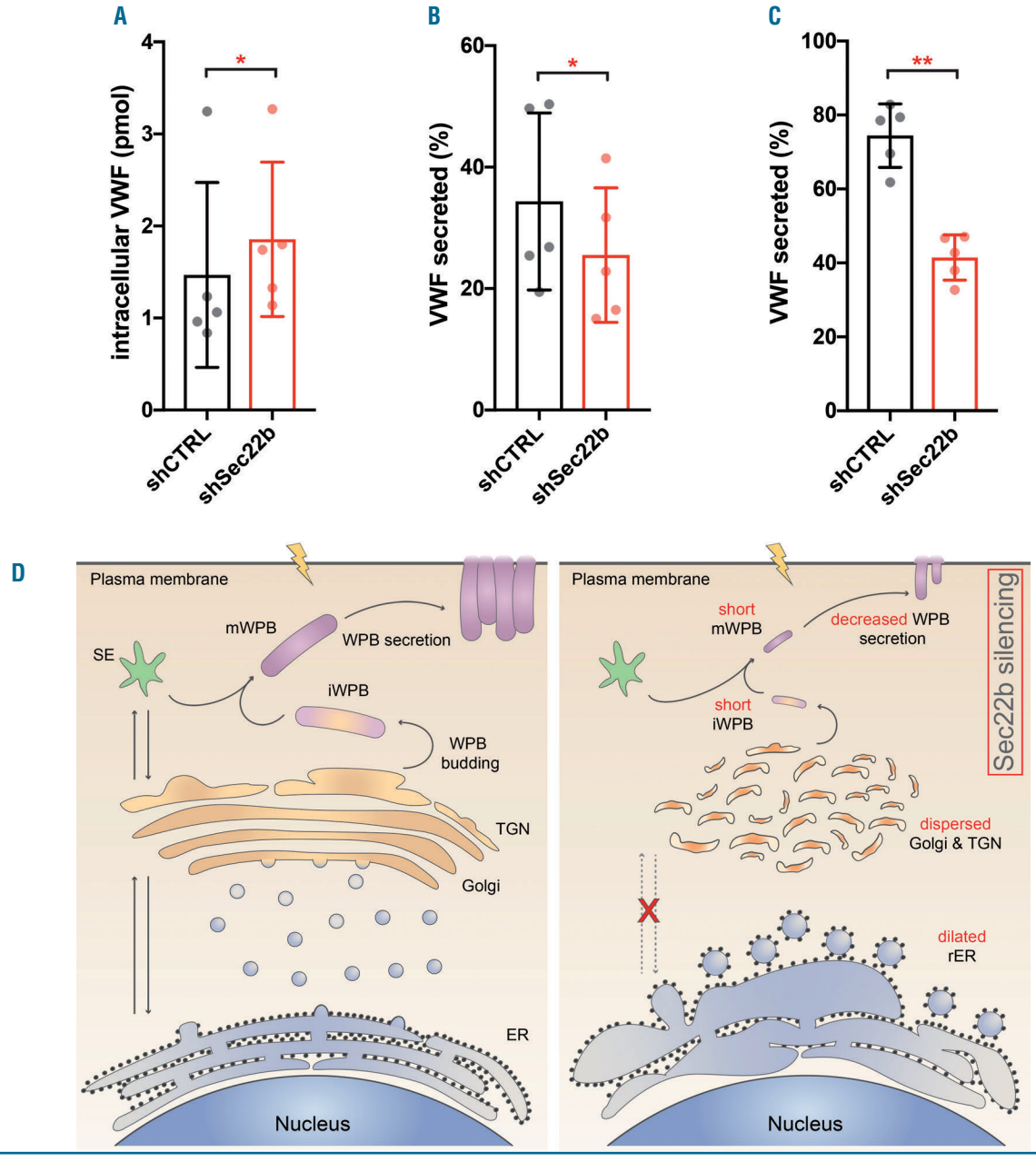


Figure 5. Sec22b silencing results in reduced basal and stimulated secretion. (A) Intracellular von Willebrand factor (VWF) content in control and Sec22b-silenced endothelial cells measured by enzyme-linked immunosorbent assay (n=5, paired *t*-test, **P*<0.05). (B) Basal VWF release presented as percentage of intracellular VWF content (n=5, paired *t*-test, **P*<0.05) (C) Histamine-stimulated VWF release presented as percentage of intracellular VWF content (n=3 independent experiments, paired *t*-test, ***P*<0.01). (D) Proposed model of Sec22b-dependent VWF trafficking and Weibel-Palade body size control. SE: sorting endosome; WPB: Weibel-Palade body; iWPB: immature WPB; mWPB: mature WPB; ER: endoplasmic reticulum; rER: rough ER; TGN: *trans*-Golgi network.

Discussion

SNARE proteins are key drivers of membrane fusion that initiate and regulate specificity of membrane docking and bilayer mixing.[30] There is a subcategory of SNARE, known as longin-SNARE (YKT6, VAMP7 and Sec22b), which generally participate in fusion events during biogenesis, maturation and exocytosis of secretory organelles in eukaryotic cells.[43-47] In this study, using a shRNA screen targeting longin-SNARE we identified Sec22b as a novel regulator of WPB formation and VWF trafficking, its depletion leading to short and "stubby" WPB that were accompanied by Golgi disintegration and retention of VWF in the ER.

Sec22b is a known participant in anterograde transport of cargo in the early secretory pathway.[48,49] Overexpression of the Sec22b-ΔSNARE variant led to a dominant-negative effect resulting in smaller WPB, corroborating experiments that used RNA interference and CRISPR strategies to deplete Sec22b expression. This is most probably a consequence of Sec22b-ΔSNARE outcompeting endogenous Sec22b while failing to properly bind with its cognate SNARE due to the lack of the SNARE helix,[50] which precludes formation of a complete *trans*-SNARE complex and subsequent membrane fusion. The importance of a functional, fusion-competent Sec22b has also been highlighted by mutations in the SNARE domain of the *Drosophila* homolog of Sec22b, which caused disruption of ER-Golgi transport and resulted in cargo retention in the ER and abnormal ER morphology.[51] Similar ER cargo retention is likely at play in Sec22b-depleted EC in our study (Figures 3 and 4). Congestion of anterograde flux from the ER limits the supply of VWF to the Golgi and as WPB formation is driven by condensation of multimeric VWF in the TGN, we assume this reduction is (at least partly) responsible for the smaller size of WPB.

The smaller WPB phenotype is likely further exacerbated by fragmentation of the TGN (Figure 2), which was previously proposed to limit the possibility of adjacent VWF quanta co-packaging into a single, extended WPB.[24] Interestingly, that study also demonstrated that experimental reduction of VWF trafficking by small interfering RNA silencing of VWF synthesis led to reduction of WPB length without affecting overall Golgi morphology. The data we present here suggest that a Sec22b-dependent trafficking pathway is used both by VWF and by components that establish or maintain Golgi ribbon integrity. This is in line with previous studies of Sec22b in other models, such as an *Arabidopsis* mutant deficient for the Sec22b homolog, which displayed comparable TGN disruption.[52] The observed phenotype may be a consequence of defective trafficking of direct regulators of Golgi morphology, such as Golgi reassembly stacking proteins (GRASP)[53] or golgins.[54] Indeed, Golgi fragmentation and the concomitant reduction in the length of WPB has also been observed after depletion of Golgi tethering proteins (GM130, GRASP55 and giantin).[24] TGN fragmentation may also merely result from the induced imbalance in trafficking, as the phenotype was also reported after disruption of retrograde trafficking from early endosomes or within the Golgi.[55,56] While further investigation is required to decipher the precise role of Sec22b in the maintenance of TGN morphology, the resulting consequences highlight its indispensable function in ensuring adequate trafficking of VWF and WPB biogenesis.

Upon Sec22b silencing, dilated ER cisternae were observed, accompanied by electron-dense, ribosome-studded rER structures that contained VWF aggregates. There was a striking resemblance with the dilated ER morphology that is observed in response to VWD-causing mutations in VWF that affect the protein's ability to dimerize and leave the ER.[57,58] Sec22b is recruited onto ER-derived COPII vesicles that transfer proteins from the ER to the Golgi, through interactions of its longin domain with Sec23/Sec24 of the COPII-coating complex.[59,60] Similar dilated ER phenotypes and ER retention of secretory proteins have been described in chondrocytes from *sec24d*-deficient zebrafish[61] and in pancreatic acinar cells from Sec23$^{lgt/lgt}$ mice that additionally display lack of zymogen granules.[62] This suggests that the rate of COPII-mediated, anterograde ER-Golgi traffic underpins the ability of endothelial cells to shape WPB to their typical elongated morphology.

A recent study identified GBF1 as a dynamic regulator of anterograde VWF trafficking and WPB morphology that, dependent on external/environmental cues, controls the flux of proteins (including VWF) from the ER to Golgi.[63] Similar to what we observed after Sec22b silencing, depletion of GBF1 led to accumulation of VWF in the ER and a reduction in the overall state of VWF proteolytic processing. However, a number of important phenotypic differences suggest that GBF1 and Sec22b operate through different mechanisms. Unlike Sec22b, GBF1 depletion did not affect Golgi morphology and, unexpectedly, resulted in unusually large WPB that remained associated with or in close vicinity of the Golgi. Despite their reduction in length, WPB in Sec22b-depleted cells normally recruited exocytotic components such as Rab27A and Slp4-a (*Online Supplementary Figure S5*), contrary to the enlarged WPB in GBF1-ablated cells which failed to acquire post-Golgi cargo and Rab27A and which were secretion incompetent.[63] Although their short WPB were still responsive to agonists, Sec22b-depleted EC secreted reduced amounts of VWF through the regulated and basal secretory pathway (Figure 4B and C), which we presume is due to a reduction in WPB pool size. These discrepancies emphasize that future studies are needed to clarify how such opposing effects on WPB formation and secretion can arise from defects in anterograde ER-Golgi transport.

In conclusion, we identified Sec22b as a new regulatory component of the endothelial secretory pathway that controls VWF trafficking and the morphology of its carrier organelle the WPB. We propose a model (Figure 5D) in which secretory proteins such as VWF and components that control Golgi morphology utilize a Sec22b-dependent pathway to arrive at the Golgi, where VWF is packaged in elongated WPB with dimensions that are proportional to the size of the Golgi. The reduction in WPB length in the absence of Sec22b is explained by a combination of retention of VWF in the ER and disintegration of the Golgi. Reduced flux of VWF through the secretory pathway ultimately decreases the amount of VWF that can be secreted by EC that lack Sec22b function. This highlights the importance of efficient transport of VWF through the secretory pathway prior to its packaging in WPB and identifies Sec22b as a potential determinant of plasma VWF levels. Future studies should address the impact of components of this protein complex on VWF plasma levels in patients with bleeding and thrombotic disorders.

Disclosures

No conflicts of interest to disclose.

Contributions

EK, PB, JO and AAM performed research and analyzed data; CRJ and DG contributed vital reagents and expertise; EK, JV and RB designed the research; EK, JV and RB wrote the paper.

Funding

This study was supported by grants from the Landsteiner Stichting voor Bloedtransfusie Research (LSBR-1517 and LSBR-1707), the Netherlands Ministry of Health (PPOC-2015-24P) and the Dutch Thrombosis Foundation (TSN 2017-01).

References

1. Gomez-Navarro N, Miller E. Protein sorting at the ER-Golgi interface. J Cell Biol. 2016;215(6):769-778.
2. Araki K, Nagata K. Protein folding and quality control in the ER. Cold Spring Harb Perspect Biol. 2011;3(11):1-25.
3. Kienzle C, von Blume J. Secretory cargo sorting at the trans-Golgi network. Trends Cell Biol. 2014;24(10):584-593.
4. Halban PA, Irminger JC. Sorting and processing of secretory proteins. Biochem J. 1994;299(1):1-18.
5. Huizing M, Helip-Wooley A, Westbroek W, Gunay-Aygun M, Gahl WA. Disorders of lysosome-related organelle biogenesis: clinical and molecular genetics. Annu Rev Genomics Hum Genet. 2008;9:359-386.
6. Weibel ER, Palade GE. New cytoplasmic components in arterial endothelia. J Cell Biol. 1964;23(1):101-112.
7. Schillemans M, Karampini E, Kat M, Bierings R. Exocytosis of Weibel–Palade bodies: how to unpack a vascular emergency kit. J Thromb Haemost. 2019;17(1):6-18.
8. Sadler JE. Biochemistry and genetics of von Willebrand factor. Annu Rev Biochem. 1998;67:395-424.
9. Wagner DD, Saffaripour S, Bonfanti R, et al. Induction of specific storage organelles by von Willebrand factor propolypeptide. Cell. 1991;64(2):403-413.
10. Voorberg J, Fontijn R, Calafat J, Janssen H, van Mourik JA, Pannekoek H. Biogenesis of von Willebrand factor-containing organelles in heterologous transfected CV-1 cells. EMBO J. 1993;12(2):749-758.
11. Groeneveld DJ, van Bekkum T, Dirven RJ, et al. Angiogenic characteristics of blood outgrowth endothelial cells from patients with von Willebrand disease. J Thromb Haemost. 2015;13(10):1854-1866.
12. Schillemans M, Kat M, Westeneng J, et al. Alternative trafficking of Weibel-Palade body proteins in CRISPR/Cas9-engineered von Willebrand factor-deficient blood outgrowth endothelial cells. Res Pract Thromb Haemost. 2019;3(4):718-732.
13. Michaux G, Abbitt KB, Collinson LM, Haberichter SL, Norman KE, Cutler DF. The physiological function of von Willebrand's factor depends on its tubular storage in endothelial Weibel-Palade bodies. Dev Cell. 2006;10(2):223-232.
14. Huang R-H, Wang Y, Roth R, et al. Assembly of Weibel Palade body-like tubules from N-terminal domains of von Willebrand factor. Proc Natl Acad Sci U S A. 2008;105(2):482-487.
15. Berriman JA, Li S, Hewlett LJ, et al. Structural organization of Weibel-Palade bodies revealed by cryo-EM of vitrified endothelial cells. Proc Natl Acad Sci U S A. 2009;106(41):17407-17412.
16. Leebeek FWG, Eikenboom JCJ. Von Willebrand's disease. N Engl J Med. 2016;375(21):2067-2080.
17. Valentijn KM, Eikenboom J. Weibel-Palade bodies: a window to von Willebrand disease. J Thromb Haemost. 2013;11(4):581-592.
18. Conte IL, Cookson E, Hellen N, Bierings R, Mashanov G, Carter T. Is there more than one way to unpack a Weibel-Palade body? Blood. 2015;126(18):2165-2167.
19. Dong JF, Moake JL, Nolasco L, et al. ADAMTS-13 rapidly cleaves newly secreted ultralarge von Willebrand factor multimers on the endothelial surface under flowing conditions. Blood. 2002;100(12):4033-4039.
20. Zheng Y, Chen J, López JA. Flow-driven assembly of VWF fibres and webs in in vitro microvessels. Nat Commun. 2015;6(1):7858.
21. De Ceunynck K, De Meyer SF, Vanhoorelbeke K. Unwinding the von Willebrand factor strings puzzle. Blood. 2013;121(2):270-277.
22. Sadler JE. von Willebrand factor assembly and secretion. J Thromb Haemost. 2009;7(Suppl 1):24-27.
23. Ferraro F, da Silva ML, Grimes W, et al. Weibel-Palade body size modulates the adhesive activity of its von Willebrand factor cargo in cultured endothelial cells. Sci Rep. 2016;6(1):32473.
24. Ferraro F, Kriston-Vizi J, Metcalf DJ, et al. A two-tier Golgi-based control of organelle size underpins the functional plasticity of endothelial cells. Dev Cell. 2014;29(3):292-304.
25. Springer TA. von Willebrand factor, Jedi knight of the bloodstream. Blood. 2014;124(9):1412-1426.
26. Zhou Y-F, Eng ET, Nishida N, Lu C, Walz T, Springer TA. A pH-regulated dimeric bouquet in the structure of von Willebrand factor. EMBO J. 2011;30(19):4098-4111.
27. Purvis AR, Gross J, Dang LT, et al. Two Cys residues essential for von Willebrand factor multimer assembly in the Golgi. Proc Natl Acad Sci U S A. 2007;104(40):15647-15652.
28. Zenner HL, Collinson LM, Michaux G, Cutler DF. High-pressure freezing provides insights into Weibel-Palade body biogenesis. J Cell Sci. 2007;120(Pt 12):2117-2125.
29. Mourik MJ, Faas FGA, Zimmermann H, Voorberg J, Koster AJ, Eikenboom J. Content delivery to newly forming Weibel-Palade bodies is facilitated by multiple connections with the Golgi apparatus. Blood. 2015;125(22):3509-3516.
30. Jahn R, Scheller RH. SNAREs - engines for membrane fusion. Nat Rev Mol Cell Biol 2006;7(9):631-643.
31. Daste F, Galli T, Tareste D. Structure and function of longin SNAREs. J Cell Sci. 2015;128(23):4263-4272.
32. Lenzi C, Stevens J, Osborn D, Hannah MJ, Bierings R, Carter T. Synaptotagmin 5 regulates Ca 2+ -dependent Weibel–Palade body exocytosis in human endothelial cells. J Cell Sci. 2019;132(5):jcs221952.
33. Schillemans M, Karampini E, van den Eshof BL, et al. Weibel-palade body localized syntaxin-3 modulates von Willebrand factor secretion from endothelial cells. Arterioscler Thromb Vasc Biol. 2018;38(7):1549-1561.
34. Sanjana NE, Shalem O, Zhang F. Improved vectors and genome-wide libraries for CRISPR screening. Nat Methods. 2014;11(8):783-784.
35. Haeussler M, Schönig K, Eckert H, et al. Evaluation of off-target and on-target scoring algorithms and integration into the guide RNA selection tool CRISPOR. Genome Biol. 2016;17(1):148.
36. van Breevoort D, Snijders AP, Hellen N, et al. STXBP1 promotes Weibel-Palade body exocytosis through its interaction with the Rab27A effector Slp4-a. Blood. 2014;123(20):3185-3194.
37. Karampini E, Schillemans M, Hofman M, et al. Defective AP-3-dependent VAMP8 trafficking impairs Weibel-Palade body exocytosis in Hermansky-Pudlak syndrome type 2 blood outgrowth endothelial cells. Haematologica. 2019;104(10):2091-2099.
38. Vischer U, Wagner D. von Willebrand factor proteolytic processing and multimerization precede the formation of Weibel-Palade bodies. Blood. 1994;83(12):3536-3544.
39. Giblin JP, Hewlett LJ, Hannah MJ. Basal secretion of von Willebrand factor from human endothelial cells. Blood. 2008;112(4):957-964.
40. Lopes da Silva M, Cutler DF. von Willebrand factor multimerization and the polarity of secretory pathways in endothelial cells. Blood. 2016;128(2):277-285.
41. Hannah MJ, Hume AN, Arribas M, et al. Weibel-Palade bodies recruit Rab27 by a content-driven, maturation-dependent mechanism that is independent of cell type. J Cell Sci. 2003;116(Pt 19):3939-3948.
42. Bierings R, Hellen N, Kiskin N, et al. The interplay between the Rab27A effectors Slp4-a and MyRIP controls hormone-evoked Weibel-Palade body exocytosis. Blood. 2012;120(13):2757-2767.
43. Jani RA, Purushothaman LK, Rani S, Bergam P, Setty SRG. STX13 regulates cargo delivery from recycling endosomes during melanosome biogenesis. J Cell Sci. 2015;128(17):3263-3276.
44. Koseoglu S, Peters CG, Fitch-Tewfik JL, et al. VAMP-7 links granule exocytosis to actin reorganization during platelet activation. Blood. 2015;126(5):651-660.
45. Kweon Y, Rothe A, Conibear E, Stevens TH. Ykt6p is a multifunctional yeast R-SNARE that is required for multiple membrane transport pathways to the vacuole. Mol Biol Cell. 2003;14(5):1868-1881.
46. Matsui T, Jiang P, Nakano S, Sakamaki Y, Yamamoto H, Mizushima N. Autophagosomal YKT6 is required for fusion with lysosomes independently of syntaxin 17. J Cell Biol. 2018;217(8):2633-2645.
47. Dai J, Lu Y, Wang C, et al. Vps33b regulates Vwf-positive vesicular trafficking in

megakaryocytes. J Pathol. 2016;240(1):108-119.
48. Zhang T, Wong SH, Tang BL, Xu Y, Hong W. Morphological and functional association of Sec22b/ERS-24 with the pre-Golgi intermediate compartment. Mol Biol Cell. 1999;10(2):435-453.
49. Liu Y, Barlowe C. Analysis of Sec22p in endoplasmic reticulum/Golgi transport reveals cellular redundancy in SNARE protein function. Mol Biol Cell. 2002;13(9):3314-3324.
50. Liu Y, Flanagan JJ, Barlowe C. Sec22p export from the endoplasmic reticulum Is independent of SNARE pairing. J Biol Chem. 2004;279(26):27225-27232.
51. Zhao X, Yang H, Liu W, et al. Sec22 regulates endoplasmic reticulum morphology but not autophagy and is required for eye development in Drosophila. J Biol Chem. 2015;290(12):7943-7951.
52. El-Kasmi F, Pacher T, Strompen G, et al. Arabidopsis SNARE protein SEC22 is essential for gametophyte development and maintenance of Golgi-stack integrity. Plant J. 2011;66(2):268-279.
53. Xiang Y, Wang Y. GRASP55 and GRASP65 play complementary and essential roles in Golgi cisternal stacking. J Cell Biol. 2010;188(2):237-251.
54. Wang T, Grabski R, Sztul E, Hay JC. p115-SNARE interactions: a dynamic cycle of p115 binding monomeric SNARE motifs and releasing assembled bundles. Traffic. 2015;16(2):148-171.
55. Shitara A, Shibui T, Okayama M, et al. VAMP4 is required to maintain the ribbon structure of the Golgi apparatus. Mol Cell Biochem. 2013;380(1-2):11-21.
56. Zolov SN, Lupashin V V. Cog3p depletion blocks vesicle-mediated Golgi retrograde trafficking in HeLa cells. J Cell Biol. 2005;168(5):747-759.
57. Wang J-W, Valentijn KM, de Boer HC, et al. Intracellular storage and regulated secretion of von Willebrand factor in quantitative von Willebrand disease. J Biol Chem. 2011;286(27):24180-24188.
58. Wang JW, Groeneveld DJ, Cosemans G, et al. Biogenesis of Weibel-Palade bodies in von Willebrand's disease variants with impaired von Willebrand factor intrachain or interchain disulfide bond formation. Haematologica. 2012;97(6):859-866.
59. Mancias JD, Goldberg J. The transport signal on Sec22 for packaging into COPII-coated vesicles Is a conformational epitope. Mol Cell. 2007;26(3):403-414.
60. Adolf F, Rhiel M, Hessling B, et al. Proteomic profiling of mammalian COPII and COPI vesicles. Cell Rep. 2019;26(1):250-265.
61. Ohisa S, Inohaya K, Takano Y, Kudo A. sec24d encoding a component of COPII is essential for vertebra formation, revealed by the analysis of the medaka mutant, vbi. Dev Biol. 2010;342(1):85-95.
62. Tao J, Zhu M, Wang H, et al. SEC23B is required for the maintenance of murine professional secretory tissues. Proc Natl Acad Sci U S A. 2012;109(29):E2001-2009.
63. Lopes-da-Silva M, McCormack JJ, Burden JJ, Harrison-Lavoie KJ, Ferraro F, Cutler DF. A GBF1-dependent mechanism for environmentally responsive regulation of ER-Golgi transport. Dev Cell. 2019;49(5):786-801.e6.

Ferrata Storti Foundation

Haematologica 2021
Volume 106(4):1148-1157

A multicenter study of romiplostim for chemotherapy-induced thrombocytopenia in solid tumors and hematologic malignancies

Hanny Al-Samkari,[1,2] Aric D. Parnes,[2,3,4] Katayoon Goodarzi,[1,2] James I. Weitzman,[2,5] Jean M. Connors[2,3,4] and David J. Kuter[1,2]

[1]Division of Hematology Oncology, Massachusetts General Hospital, Boston, MA; [2]Harvard Medical School, Boston, MA; [3]Hematology Division, Brigham and Women's Hospital, Boston, MA; [4]Department of Medical Oncology, Dana-Farber Cancer Institute, Boston, MA and [5]Division of Hematology Oncology, Newton-Wellesley Hospital, Newton, MA, USA

ABSTRACT

Chemotherapy-induced thrombocytopenia (CIT) frequently complicates cancer treatment causing chemotherapy treatment delays, dose reductions, and discontinuation. There is no US Food and Drug Administration (FDA)-approved agent available to manage CIT. This study retrospectively evaluated patients with CIT treated on institutional romiplostim treatment pathways at four US centers. The primary outcome was achievement of a romiplostim response (median on-romiplostim platelet count ≥75x10^9/L and ≥30x10^9/L above baseline). Secondary outcomes included time to platelet count ≥100x10^9/L and rates of the following: platelet count <100×10^9/L, platelet count <75x10^9/L, platelet count <50x10^9/L, thrombocytosis, chemotherapy dose reduction/treatment delay, platelet transfusion, bleeding, and thromboembolism. Multivariable regression was used to identify predictors of romiplostim non-response and compare weekly dosing with intracycle/intermittent dosing. A total of 173 patients (153 solid tumor, 20 lymphoma or myeloma) were treated, with 170 (98%) receiving a median of four (range: 1-36) additional chemotherapy cycles on romiplostim. Romiplostim was effective in solid tumor patients: 71% of patients achieved a romiplostim response, 79% avoided chemotherapy dose reductions/treatment delays, and 89% avoided platelet transfusions. Median per-patient platelet count on romiplostim was significantly higher than baseline (116x10^9/L *vs.* 60x10^9/L; P<0.001). Bone marrow (BM) tumor invasion, prior pelvic irradiation, and prior temozolomide exposure predicted romiplostim non-response. Bleeding rates were lower than historical CIT cohorts and thrombosis rates were not elevated. Weekly dosing was superior to intracycle dosing with higher response rates and less chemotherapy dose reductions/treatment delays/bleeding; intracycle dosing had an incidence rate ratio (IRR) for dose reduction/treatment delay of 3.00 (95%CI: 1.30-6.91; P=0.010) and an IRR for bleeding of 4.84 (95%CI: 1.18-19.89, P=0.029) compared with weekly dosing. Blunted response (10% response rate) was seen in non-myeloid hematologic malignancy patients with BM involvement. In conclusion, romiplostim was safe and effective for CIT in most solid tumor patients.

Correspondence:

HANNY AL-SAMKARI
hal-samkari@mgh.harvard.edu

Received: March 5, 2020.

Accepted: May 27, 2020.

Pre-published: June 4, 2020.

https://doi.org/10.3324/haematol.2020.251900

©2021 Ferrata Storti Foundation

Material published in Haematologica is covered by copyright. All rights are reserved to the Ferrata Storti Foundation. Use of published material is allowed under the following terms and conditions: https://creativecommons.org/licenses/by-nc/4.0/legalcode. Copies of published material are allowed for personal or internal use. Sharing published material for non-commercial purposes is subject to the following conditions: https://creativecommons.org/licenses/by-nc/4.0/legalcode, sect. 3. Reproducing and sharing published material for commercial purposes is not allowed without permission in writing from the publisher.

Introduction

Thrombocytopenia is frequent in cancer patients, usually due to myelosuppressive chemotherapy, tumor infiltration of the bone marrow (BM), or infection.[1] Chemotherapy-induced thrombocytopenia (CIT) is a common complication of cytotoxic chemotherapy and many targeted therapies, occurring in approximately 15-25% of patients receiving platinum, taxane, and/or gemcitabine-based regimens.[2] Currently there is no US Food and Drug Administration (FDA)-approved agent for CIT management. Platelet transfusion offers only temporary, unreliable

improvement that is often impractical or impossible to continue for extended periods. Therefore, chemotherapy dose reductions and treatment delays are the current standard of care for the management of CIT, allowing platelet count to recover to the desired count for subsequent administration of cancer-directed treatment. Reduced relative dose intensity (RDI) that results from CIT-related treatment delays and dose reductions may reduce progression-free survival (PFS) and overall survival (OS).[3,4] Conversely, management or prevention of CIT with thrombopoietic agents may maintain RDI and improve OS, particularly in curable malignancies.[5-8] Bleeding in CIT has major consequences for patient outcomes; patients with CIT who develop major bleeding have been shown to have substantially lower OS.[4]

Thrombopoietin receptor agonists (TPO-RA) have been developed and approved for use in immune thrombocytopenia (ITP),[9] aplastic anemia,[10] hepatitis C-associated thrombocytopenia,[11] and perioperative thrombocytopenia.[12-14] Romiplostim is a weekly subcutaneously-administered TPO-RA currently approved to treat ITP. Maximal doses of romiplostim are considerably more potent in raising the platelet count than the oral small molecule TPO-RA in healthy subjects and possibly in ITP,[15-17] making this an ideal agent for investigation into myelosuppressive thrombocytopenias such as CIT. To date, studies of romiplostim to manage CIT have been limited to case series and small single-center studies.[18-21] These studies suggest that romiplostim is effective in raising the platelet count in patients with solid tumors. Predictors of romiplostim non-response, optimal dosing regimens, and use in non-myeloid hematologic malignancies (lymphoma and myeloma) have not been evaluated. Clinical outcomes data more relevant than simple platelet count measurements, such as resumption of treatment without further chemotherapy dose reductions or treatment delays, bleeding, or thrombosis, are limited. The safety of TPO-RA in cancer patients is a concern, as TPO-RA carry an associated risk for venous thromboembolism (VTE), which could add to the baseline risk associated with malignancy.

The present study aims to address these questions and evaluate romiplostim to manage CIT in a large cohort of both solid tumor and hematologic malignancy patients treated at four affiliated US academic cancer centers. Institutional pathways guided administration of romiplostim at each center. Management of CIT remains an off-label use of romiplostim.

Methods

Patients and data collection

This study was approved by the Institutional Review Board of Partners Healthcare (approval PHS/2015000152). All patients aged ≥18 years with thrombocytopenia treated with romiplostim to support administration of chemotherapy to treat solid tumors or non-myeloid hematologic malignancies (multiple myeloma, Hodgkin lymphoma or aggressive non-Hodgkin lymphoma) between July 1st 2009 and July 1st 2019 at the four participating institutions (Massachusetts General Hospital, Brigham and Women's Hospital, Dana-Farber Cancer Institute, and Newton-Wellesley Hospital) were identified using the Research Patient Data Registry at Partners Healthcare. The specific patient data collected are available in the *Online Supplementary Methods*.

Institutional romiplostim chemotherapy-induced thrombocytopenia pathways: weekly *versus* intracycle dosing

Patients qualified to enter their institutional romiplostim CIT pathway after persistent thrombocytopenia (platelet count <100x10^9/L) at least 3 weeks from the date of last chemotherapy administration or after a delay in chemotherapy regimen initiation ≥1 week due to thrombocytopenia. For solid tumor patients, two institutions utilized a weekly romiplostim CIT pathway in which romiplostim was administered weekly irrespective of timing of chemotherapy administration and two utilized an intracycle romiplostim CIT pathway in which romiplostim was administered primarily on chemotherapy off-weeks, on average twice per month (see Figure 1 for dosing pathways). Regardless of pathway, platelet counts were obtained weekly. All hematologic malignancy patients were treated at institutions that employed the weekly romiplostim treatment pathway.

Effectiveness and safety measures

The primary outcome was achievement of a romiplostim response, defined as a median on-romiplostim platelet count ≥75x10^9/L and at least 30x10^9/L higher than the pretreatment baseline. Median on-romiplostim platelet counts were used in all analyses comparing individual patient baseline platelet count to individual patient on-romiplostim platelet count. As romiplostim response is a measure of effectiveness over the entire duration of romiplostim treatment, the time from romiplostim initiation to first achievement of platelet count ≥100x10^9/L was also evaluated. Because there is no universally accepted platelet count threshold that defines CIT recurrence, incidence rates of all measured platelet counts below thresholds of 50x10^9/L, 75x10^9/L, and 100x10^9/L were also evaluated. Similarly, thrombocytosis was defined as >400x10^9/L and incidence rates were evaluated.

Other clinical outcomes included rates of chemotherapy intensity reduction (dose reduction or treatment delay) specifically for thrombocytopenia and rates of platelet transfusion, bleeding, and arterial or venous thromboembolic events.

Patients treated with romiplostim for CIT but not able to resume chemotherapy were included in analyses of bleeding, VTE, and platelet count outcomes while on romiplostim treatment but not analyses of chemotherapy intensity reduction or platelet transfusion.

Predictors of romiplostim non-response

Predictors of failure to achieve a romiplostim response (referred to hereafter as "predictors of romiplostim non-response") were evaluated using a multivariable logistic model (see *Online Supplementary Methods* for development of the model).

Statistical analysis

Median individual patient platelet counts on romiplostim support were compared with the pre-romiplostim baseline platelet count with the Wilcoxon signed-rank test. Predictors of romiplostim non-response were identified using a multivariable logistic model (see *Online Supplementary Methods*).

Solid tumor patients receiving weekly *versus* intracycle dosing were compared. Rates of thrombosis, bleeding, chemotherapy delay/dose reduction, platelet transfusion, and platelet counts <50x10^9/L, <75x10^9/L, <100x10^9/L, and >400x10^9/L were compared in the two groups with negative binomial regression models (see *Online Supplementary Methods*). Baseline and median on-romiplostim platelet counts for each group were compared with the Mann-Whitney U test.

Results

Patients' characteristics

A total of 173 patients (153 solid tumor, 20 hematologic malignancy) were treated for CIT with romiplostim to facilitate ongoing chemotherapy administration. Table 1 lists patients' baseline characteristics. Colorectal, hepatobiliary, pancreatic, and gastroesophageal cancers were the most common malignancies in the cohort, accounting for half of all patients treated. A total of 170 patients (98%; 150 solid tumor and 20 hematologic malignancy) were able to receive additional chemotherapy, receiving a median of four (range: 1-36) additional chemotherapy cycles over a median of 10 (range: 2-125) weeks of romiplostim support. This totaled 60.7 patient-years (3,163 patient-weeks) of romiplostim treatment of CIT and 1,063 supported cycles of chemotherapy in the entire cohort. Of the hematologic malignancy patients, 13 had aggressive lymphoma and seven had multiple myeloma; all had known BM involvement by tumor.

Platinum, gemcitabine, temozolomide, and taxane-based regimens most commonly precipitated CIT and were most frequently supported with romiplostim. *Online Supplementary Table S1* details chemotherapy regimens precipitating CIT and supported on romiplostim.

Romiplostim dosing

For the entire cohort as well as solid tumor patients only, the median starting dose of romiplostim was 3 μg/kg (interquartile range [IQR], 2-3 μg/kg) and the median optimized dose of romiplostim (the dose at which platelet count ≥100x10^9/L was achieved in patients achieving this threshold) was 3 μg/kg (IQR: 2-5 μg/kg).

The median starting dose for hematologic malignancy patients was 2 μg/kg (IQR: 2-4 μg/kg) and median optimized dose was 3 μg/kg (IQR: 2-5 μg/kg). Only seven (30%) hematologic malignancy patients achieved platelet count ≥100x10^9/L and were therefore included in this median. Of the 13 hematologic malignancy patients not achieving platelet count ≥100x10^9/L, only one was titrated to maximum dose romiplostim (10 μg/kg).

Effect of romiplostim on platelet counts and rates of romiplostim response in solid tumor patients

Median individual patient platelet counts on romiplostim were significantly higher than at baseline in the entire cohort (112x10^9/L *vs.* 54x10^9/L; *P*<0.001) and in solid tumor patients alone (116x10^9/L *vs.* 60x109/L; *P*<0.001). Figure 2A illustrates median weekly platelet counts on romiplostim support for solid tumor patients.

The rate of romiplostim response (achieving a median on-romiplostim platelet count ≥75x10^9/L and at least 30x10^9/L higher than the pretreatment baseline) was 71% for all solid tumor patients and 82% for those patients without predictors of romiplostim non-response (see "Predictors of romiplostim non-response in solid tumor patients" below).

Of all 153 solid tumor patients, 130 (85%) achieved platelet count ≥100x10^9/L on romiplostim therapy, with a median time from romiplostim initiation to achievement of these values of 9 days (interquartile range [IQR] 7-15 days). After excluding patients with predictors of romiplostim non-response (see below), 116 of 122 solid tumor patients (95%) achieved a platelet count ≥100x10^9/L on romiplostim therapy, with a median time to platelet count ≥100x10^9/L of 9 days (IQR 7-14 days). Statistics of additional time to platelet count ≥100x10^9/L are listed in *Online Supplementary Table S2*.

Table 1. Baseline characteristics of patients (n=173) treated with romiplostim for chemotherapy-induced thrombocytopenia (CIT) and American Joint Committee on Cancer (AJCC) staging.

Characteristic	Value
Age (years), mean (range)	60 (19-85)
% female	45
AJCC[a] stage	I: 2 (1%) II: 4 (2%) III: 17 (10%) IV: 128 (74%) Not AJCC staged:[b] 22 (13%)
Duration of chemotherapy delay due to CIT prior to romiplostim (weeks), median (range)	3 (1-15)
Prior chemotherapy regimens, median (range)	2 (1-11)
Cycles of current regimen prior to romiplostim initiation, median (range)	2 (1-55)
Tumor type, N (%)	Breast 11 (6%) CNS 15 (9%)[c] Colorectal 23 (13%) Gastroesophageal 18 (10%) Genitourinary 2 (1%) Gynecologic 11 (6%) Head and neck 5 (3%) Hepatobiliary 22 (13%) Lung 13 (8%) Lymphoma 13 (8%) Myeloma 7 (4%) Neuroendocrine 6 (4%) Pancreatic 22 (13%) Sarcoma 5 (3%)

[a]AJCC staging for solid tumors, Lugano modification of Ann Arbor staging for lymphomas. [b]Includes 15 patients with primary central nervous system (CNS) tumors and seven patients with myeloma. [c]Patients with primary CNS lymphoma are classified as part of this group.

Predictors of romiplostim non-response in solid tumor patients

Eight different chemotherapeutics administered to patients prior to development of CIT met criteria for inclusion in the multivariable logistic model evaluating predictors of romiplostim non-response: cisplatin, carboplatin, oxaliplatin, gemcitabine, fluorouracil, irinotecan, temozolomide, and the taxane class (paclitaxel, docetaxel, or cabazitaxel). In a multivariable logistic model with romiplostim response as the dependent variable, and age, sex, biopsy-proven tumor BM invasion, prior pelvic irradiation, and these chemotherapeutics as independent variables, three variables predicted a significantly lower likelihood of romiplostim response: BM invasion (odds ratio [OR] 0.029, 95% confidence interval [CI]: 0.0046-0.18; *P*<0.001), prior pelvic irradiation (OR 0.078, 95%CI: 0.0062-0.98; *P*=0.048), and prior exposure to temozolomide (OR 0.24, 95%CI: 0.061-0.96; *P*=0.043). On-romiplostim platelet counts were considerably lower in patients with these characteristics (Figure 2B) and were reflected in rates of romiplostim response of 23%, 20%, and 46%, respectively. Taken together, 14 of 31 of these

Table 2. Venous thromboembolic events in cohort while on romiplostim treatment for chemotherapy-induced thrombocytopenia (CIT) and within 30 days of romiplostim discontinuation.

Patient information	Type of VTE	Platelet count at VTE	Notes
46 y M, Astrocytoma	Proximal lower extremity DVT	150×10^9/L	
61 y M, Pancreatic Ca Stage IIB	Peripherally inserted central venous catheter-associated upper extremity DVT	119×10^9/L	
49 y F, Cervical Ca Stage IV	Renal vein thrombosis	147×10^9/L	
58 y M, Pancreatic Ca Stage III	Segmental PE, splenic infarct	146×10^9/L	
67 y M, Pancreatic Ca Stage IV	Proximal lower extremity DVT	156×10^9/L	
67 y M, Cholangiocarcinoma Stage IV	Central venous catheter-associated internal jugular vein thrombus	65×10^9/L	
53 y M, Cholangiocarcinoma Stage IV	Bilateral distal lower extremity DVT	307×10^9/L	Occurred in setting of hospitalization, following T4 compression fracture, bilateral thoracic decompression surgery; thrombocytosis with platelet count in 500-600x10^9/L range present the week prior
59 y M, Pancreatic Ca Stage IV	Segmental PE	118×10^9/L	

Plt: platelet count; Ca: cancer; VTE: venous thromboembolism; y: years; M: male; F: female; DVT: deep venous thrombosis; PE: pulmonary embolus.

Table 3. Bleeding events in cohort while on romiplostim treatment for chemotherapy-induced thrombocytopenia (CIT).

Patient information	Type of bleed	Platelet count at bleed	On anticoagulation at bleed?	WHO grade	CTCAE v.4.03 grade	Red cell transfusion requirements	Notes
84 y M, DLBCL Stage IV	Subdural hematoma	198×10^9/L	No	4	2	None	Occurred after a fall and strike to the head
61 y M, Pancreatic Ca Stage IIB	Upper GI bleed	142×10^9/L	No	4	4	9 units pRBC	Bleeding from duodenal ulcer
63 y F, SCLC Stage IV	Hemorrhagic brain metastases	55×10^9/L	No	4	1	None	Asymptomatic, incidentally discovered
59 y M, GIST Stage IV	Upper GI bleed	115×10^9/L	Yes (fondaparinux)	4	4	6 units pRBC	
85 y M, Pancreatic Ca Stage IIB	Oral mucosa bleeding	19×10^9/L	Yes (rivaroxaban)	1	1	None	
74 y M, NSCLC Stage IV	Upper GI bleed	80×10^9/L	Yes (aspirin)	3	3	3 units pRBC	
40 y F, Endometrial Ca Stage IV[a]	Lower GI bleed	49×10^9/L	No	3	3	4 units pRBC	In setting of radiation proctitis
40 y F, Endometrial Ca Stage IV[a]	Lower GI bleed	49×10^9/L	No	3	3	9 units pRBC	In setting of radiation proctitis
60 y F, Lung Ca Stage IV	Cutaneous ecchymoses	11×10^9/L	No	2	2	None	
72 y F, Endometrial Ca Stage IV	Vaginal bleeding	10×10^9/L	No	3	3	2 units pRBC	
61 y M, Colorectal Ca Stage IV	GI bleed	170×10^9/L	No	3	3	2 units pRBC	
58 y M, Pancreatic Ca Stage III	Upper GI bleed	82×10^9/L	No	2	2	None	
66 y M, Cholangiocarcinoma Stage IV	Epistaxis	79×10^9/L	Yes (rivaroxaban)	3	3	1 unit pRBC	
39 y M, Colorectal Ca Stage IV	GI bleed	239×10^9/L	No	3	3	3 units pRBC	

Ca: cancer; CTCAE: Common Terminology Criteria for Adverse Events; DLBCL: diffuse large B-cell lymphoma; GI: gastrointestinal; NSCLC: non-small cell lung cancer; Plt: platelet count; pRBC: packed red blood cells; SCLC: small cell lung cancer; WHO: World Health Organization. [a]Same patient, two separate bleeding events (separated by 2 months) that each occurred at the same platelet count.

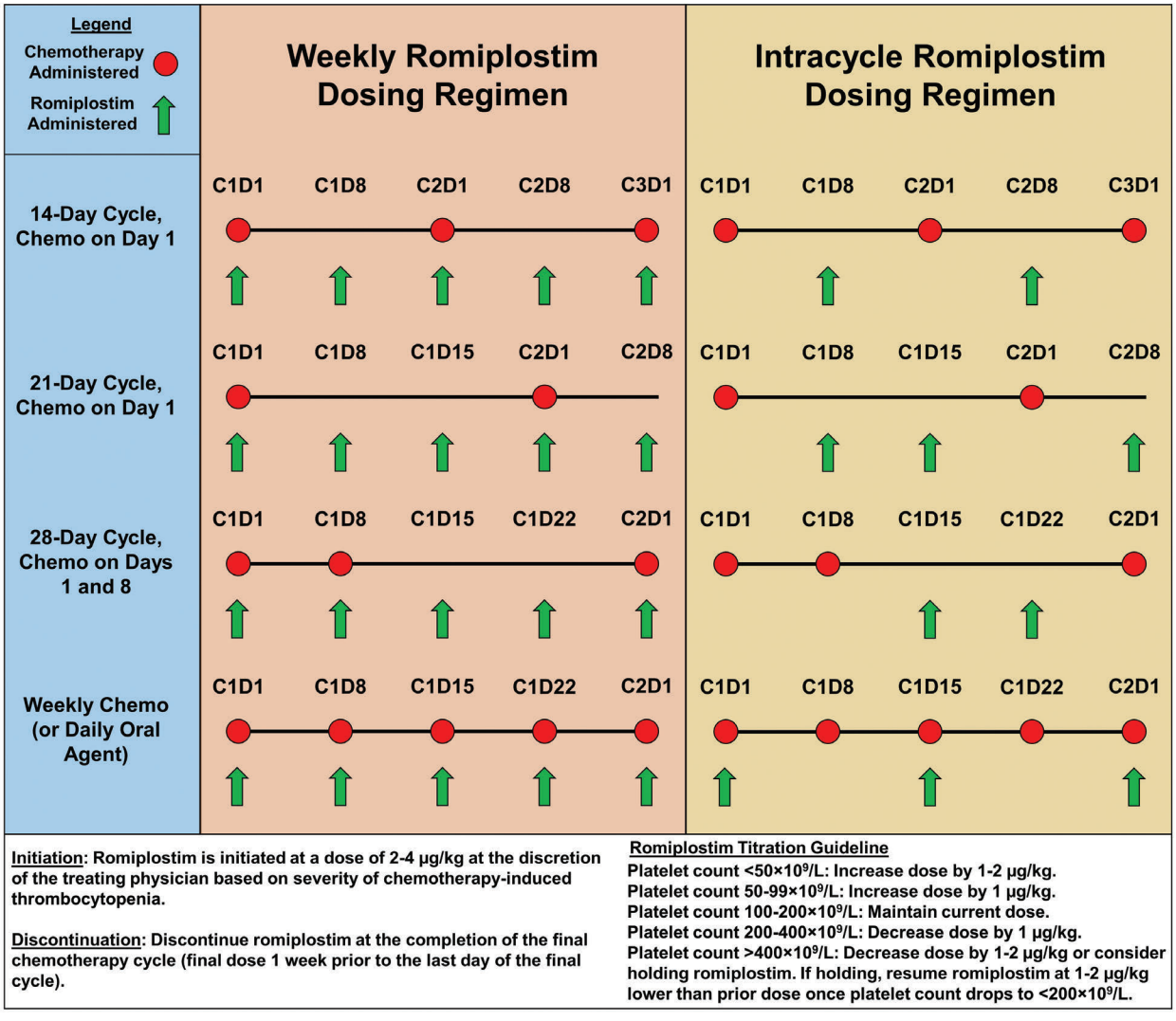


Figure 1. Chemotherapy-induced thrombocytopenia (CIT) romiplostim treatment pathways. In the weekly romiplostim dosing pathway, romiplostim is administered weekly irrespective of treatment schedule. In the intracycle romiplostim dosing pathway, romiplostim is dosed on chemotherapy off-weeks, except for chemotherapy regimens employing regular treatment without off-weeks in which case romiplostim is administered every other week. Platelet counts are obtained weekly in both pathways.

patients (45%) achieved platelet count ≥100x10^9/L on romiplostim therapy, with a median time to platelet count ≥100x10^9/L of 17 days (IQR 8-24 days). This poor rate of response was observed despite substantial romiplostim dose-escalation in these patients (median romiplostim dose, 8 µg/kg [IQR, 5-10 µg/kg]).

Clinical effectiveness and safety outcomes in solid tumor patients

In the 150 solid tumor patients able to continue chemotherapy with romiplostim treatment, number of events and event rates over the 57.7 patient-years at risk were as follows: chemotherapy intensity reduction, 89 events resulting in a rate of 154 events per 100 patient-years at risk; bleeding, 13 events resulting in a rate of 23 events per 100 patient-years at risk; VTE, eight events resulting in a rate of 14 events per 100 patient-years at risk; and platelet transfusion, 62 events resulting in a rate of 107 events per 100 patient-years at risk. Excluding patients with predictors of romiplostim non-response (50.0 patient-years at risk), number and rates of these outcomes declined as follows: chemotherapy intensity reduction, 65 events, rate 130 per 100 patient-years at risk; bleeding, eight events, rate 16 per 100 patient-years at risk; VTE, seven events, rate 14 per 100 patient-years at risk; and platelet transfusion, 13 events, rate 26 events per 100 patient-years at risk. Of all solid tumor patients 118 out of 150 (79%) had no chemotherapy intensity reductions and 133 out of 150 (89%) required no platelet transfusions while on romiplostim. There were no arterial thromboembolic events. Tables 2 and 3, respectively, describe the individual VTE and bleeding events in the patient cohort. No patient died of bleeding or thrombosis. The three patients given romiplostim but not able to resume chemotherapy did not experience bleeding or thrombotic events on romiplostim.

Comparison of weekly romiplostim dosing *versus* intracycle romiplostim dosing in solid tumor patients

Of the solid tumor patients, 80 were treated on the

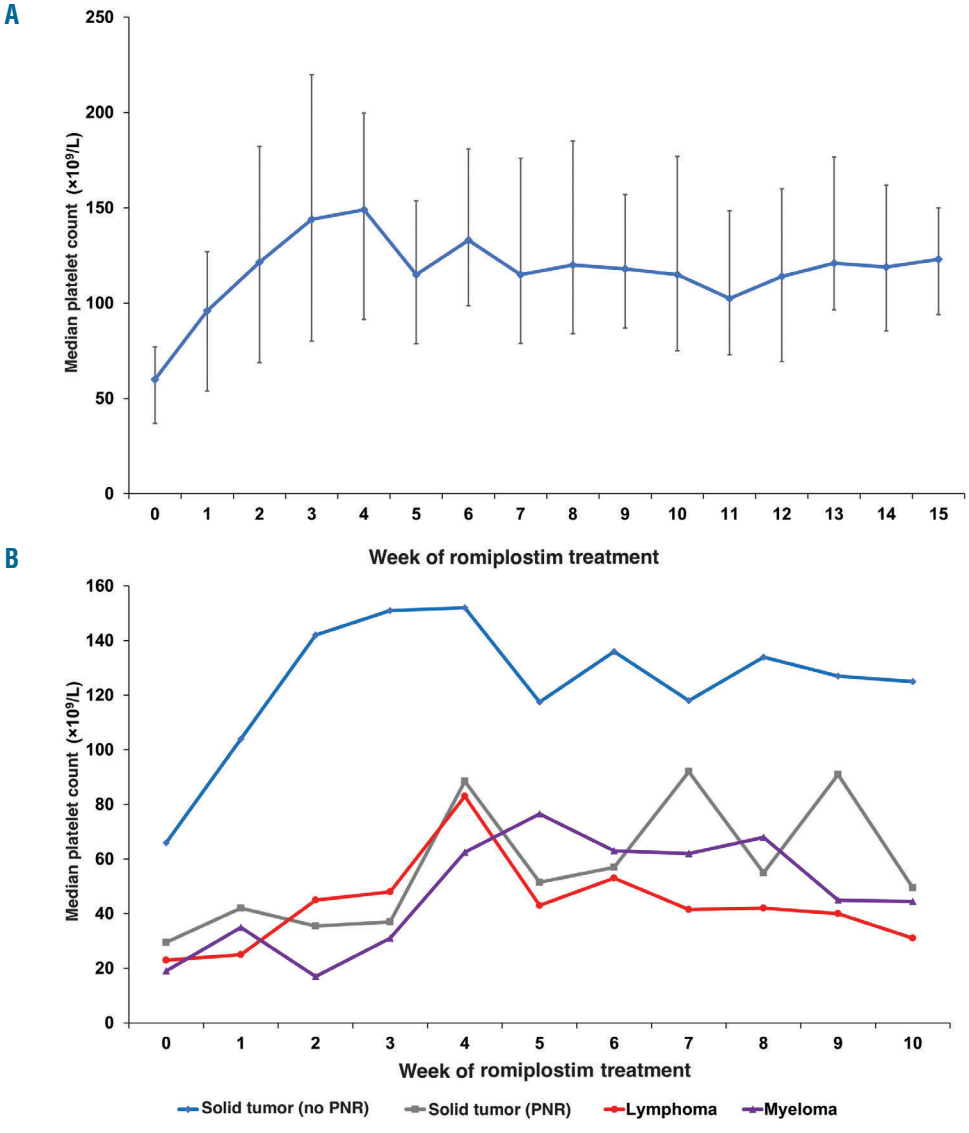


Figure 2. Median weekly platelet counts for patients on romiplostim chemotherapy-induced thrombocytopenia (CIT) treatment pathway. (A) Solid tumor patients (n=153). Error bars represent interquartile ranges. (B) Solid tumor patients with no predictors of romiplostim non-response (n=122, blue); solid tumor patients with predictors of romiplostim non-response (n=31, gray) including bone marrow (BM) invasion by tumor, prior pelvic irradiation, or prior temozolomide treatment; aggressive lymphoma patients (n=13, red); and myeloma patients (n=7, purple). Error bars omitted for figure clarity. PNR: predictors of romiplostim non-response (includes BM invasion by tumor, prior temozolomide exposure, or prior pelvic irradiation).

weekly romiplostim dosing pathway and 73 were treated on the intracycle romiplostim dosing pathway (Figure 1). Table 4 describes differences in clinical and platelet count outcome between the two groups. Patients receiving weekly dosing had a significantly higher median platelet count on romiplostim (143x10^9/L *vs.* 106x10^9/L; P<0.001) and a higher rate of achieving a romiplostim response (81% *vs.* 63%; P=0.006). Figure 3 illustrates the difference in median weekly platelet counts for each cohort. Using negative binomial regression modeling controlling for demographics and predictors of romiplostim non-response, intracycle dosing had higher rates of platelet counts measured <50x10^9/L, <75x10^9/L, or <100x10^9/L (see Table 4 for details), chemotherapy intensity reduction (incidence rate ratio [IRR] 3.00, 95%CI: 1.30-6.91; P=0.010), and bleeding (IRR 4.84, 95%CI: 1.18-19.89; P=0.029) compared with weekly dosing, with similar rates of thromboembolism and platelet transfusion for chemotherapy administration.

Outcomes in hematologic malignancy patients

Median individual patient platelet counts on romiplostim were significantly higher than at baseline: 46x10^9/L *vs.* 21x10^9/L; P=0.003. Figure 2B illustrates median weekly platelet counts on romiplostim support for hematologic malignancy patients. The rate of romiplostim response in hematologic malignancy patients was 10%. Seven of 20 hematologic malignancy patients (35%) achieved a platelet count ≥100x10^9/L on romiplostim therapy, with a median time to platelet count ≥100x10^9/L of 24 days (IQR 19-36 days).

In the 20 hematologic malignancy patients treated (for 3.0 patient-years), there were nine chemotherapy intensity reduction events, one bleeding event (which was not fatal), 44 platelet transfusion events, and no thrombotic events.

Additional data on platelet count outcomes and the bleeding event in hematologic malignancy patients are given in *Online Supplementary Tables S2* and *S3*, respectively.

Discussion

Initial studies of platelet growth factors to manage CIT utilized the first-generation thrombopoietic agents rhIL-11

Table 4. Solid tumor patient dosing strategy comparison. Rates of platelet count measurements describe the fraction of counts measured beyond a given platelet count threshold (mean rates for all patients in each group are given). Rates of clinical outcomes are exposure-adjusted (given as rates per 100 patient-years at risk).

Outcome	Weekly regimen		Intracycle regimen		Intracycle vs. weekly	P
	All (N=80[a])	No PNR (N=65[b])	All (N=73[c])	No PNR (N=57)		
Weekly platelet count measurements[#]	1,154	1,049	1,287	1,142		
Baseline median platelet count	54×10^9/L	61×10^9/L	66×10^9/L	70×10^9/L		All: 0.27* No PNR: 0.35*
On-romiplostim median platelet count	143×10^9/L	146×10^9/L	106×10^9/L	110×10^9/L		All: <0.001* No PNR: <0.001*
Achieved romiplostim response (%)	63 (81%)	61 (95%)	45 (63%)	39 (68%)	0.28 (0.11-0.69)[†]	0.006
Mean rate of platelet count measurements beyond thresholds on romiplostim						
Platelet count measured $<50\times10^9$/L	0.13	0.032	0.18	0.090	1.72 (1.01-2.90)[†]	0.043
Platelet count measured $<75\times10^9$/L	0.21	0.10	0.32	0.24	1.72 (1.26-2.35)[†]	0.001
Platelet count measured $<100\times10^9$/L	0.31	0.21	0.49	0.44	1.74 (1.38-2.20)[†]	<0.001
Platelet count measured $>400\times10^9$/L	0.050	0.060	0.029	0.026	0.39 (0.11-1.40)[†]	0.14
Rates of clinical outcomes per 100 patient-years at risk (100 patient-years on romiplostim support)						
Chemotherapy intensity reduction (dose reduction or treatment delay)	82	76	224	178	3.00 (1.30-6.91)[§]	0.010
Platelet transfusion	96	38	118	15	0.89 (0.19-4.23)[§]	0.89
Bleeding event	11	13	34	19	4.84 (1.18-19.89)[§]	0.029
Venous thromboembolic event	7.1	8.4	20	19	2.60 (0.51-13.25)[§]	0.25

PNR: predictors of romiplostim non-response (includes bone marrow [BM] invasion by tumor, prior temozolomide exposure, or prior pelvic irradiation). [a]80 patients received weekly dosing, of which two could not resume chemotherapy. All 80 are included in the platelet count outcome analyses but only the 78 able to restart chemotherapy are included in the clinical outcome analyses. [b]Sixty-five patients without predictors of romiplostim non-response received weekly dosing, of which one could not resume chemotherapy. All 65 are included in the platelet count outcome analyses but only the 64 able to restart chemotherapy are included in the clinical outcome analyses. [c]Seventy-three patients without predictors of romiplostim non-response received intracycle dosing, of which one could not resume chemotherapy. All 73 are included in the platelet count outcome analyses but only the 72 able to restart chemotherapy are included in the clinical outcome analyses. *By Mann-Whitney U Test. [†]The value is the odds ratio with a 95% confidence interval, calculated from a multivariable logistic regression model with romiplostim response as the dependent variable and age, dosing regimen, BM invasion, prior pelvic irradiation, and prior temozolomide exposure as independent variables. [‡]The value is the rate ratio with a 95% confidence interval, calculated from multivariable negative binomial regression models with the given platelet count threshold as the dependent variable, number of platelet count measurements as the exposure variable, and age, dosing regimen, BM invasion by tumor, prior pelvic irradiation, and prior temozolomide exposure as independent variables. [§]The value is the rate ratio with a 95% confidence interval, calculated from multivariable negative binomial regression models with the given clinical outcome as the dependent variable, duration of romiplostim support as the exposure variable, and age, sex, dosing regimen, BM invasion by tumor, prior pelvic irradiation, and prior temozolomide exposure as independent variables.

(oprelvekin), rhTPO (recombinant human thrombopoietin), and PEG-rhMGDF (pegylated recombinant human megakaryocyte growth and development factor). These agents demonstrated efficacy in CIT management in clinical studies, reducing need for platelet transfusions, increasing overall and nadir platelet counts, and allowing for improved relative dose intensity.[5,22-24] Unfortunately, development of recombinant thrombopoietins was halted in the West due to occurrence of antibodies to PEG-rhMGDF with cross-reactivity to native TPO.[25] Oprelvekin was FDA-approved for CIT but use was limited due to an unfavorable side-effect profile; this agent is no longer available from the manufacturer. Notably, rhTPO, which is not associated with cross-reactive antibodies, completed development in China where it is a routine component of supportive care in cancer patients.[26] More recent emergence of the TPO-RAs romiplostim, eltrombopag, and avatrombopag has renewed interest in pharmacologic CIT management in the West.

Four single-center studies, each evaluating between 20-52 solid tumor patients receiving romiplostim for CIT,[18-21] concluded that romiplostim is effective in raising the platelet count in CIT but did not compare different dosing strategies or characterize predictors of romiplostim non-response. None of these studies evaluated bleeding, the primary hazard of thrombocytopenia, and only limited data on the impact of romiplostim treatment on chemotherapy dose reductions and treatment delays were described.[20,21] Treatment of CIT with romiplostim in non-myeloid hematologic malignancy is currently limited to case reports.[27] These factors provided the rationale behind the present study which aimed to address each of these important questions.

We found that romiplostim was effective for the management of CIT in solid tumor patients receiving a variety of different chemotherapy regimens, with 98% (150 of 153) able to continue receiving chemotherapy with romiplostim support. Romiplostim treatment more than doubled the median platelet count of the cohort (from $54x10^9$/L to $112x10^9$/L) enabling 79% of solid tumor patients to proceed without further chemotherapy dose reductions or treatment delays due to thrombocytopenia and 89% to proceed without platelet transfusions. The use of romiplostim for CIT in patients with solid tumors may improve outcomes of cancer treatment by allowing maintenance of dose intensity. Weekly romiplostim dosing, as compared with intracycle romiplostim dosing, resulted in fewer recurrences of CIT, chemotherapy dose reductions/treatment delays, and bleeding events (Table 4). Thrombocytosis rates were higher but VTE rates were similar. The lower overall exposure to romiplostim in patients treated with intracycle dosing as compared with weekly dosing may account for the differences in the observed outcomes between these two groups. Of note, intracycle dosing was still an effective strategy and could be considered as this reduces drug-associated costs.

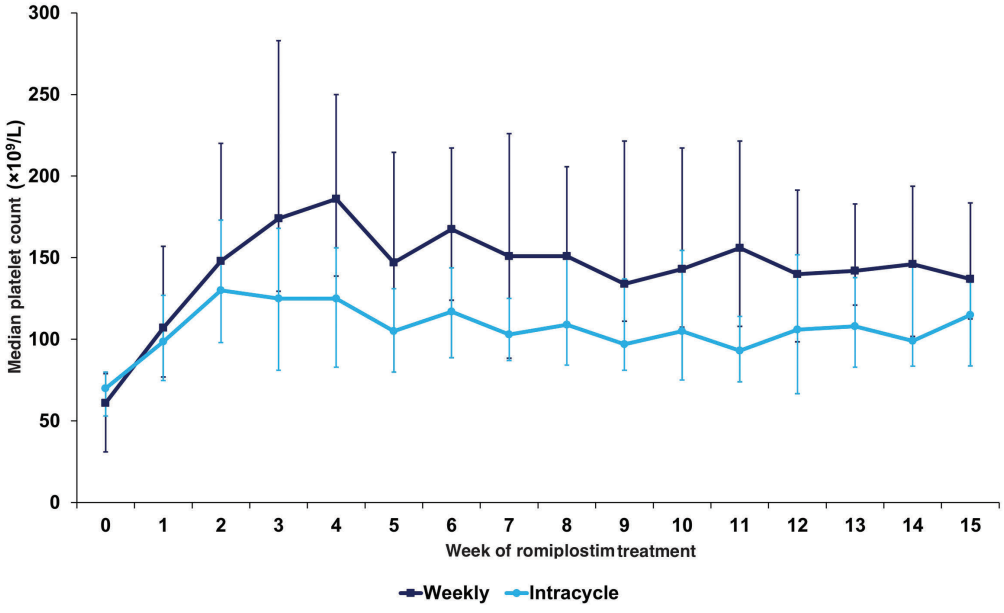


Figure 3. Median weekly platelet counts for solid tumor patients receiving standard weekly romiplostim dosing (n=65, dark blue) *versus* intracycle romiplostim dosing (n=57, light blue). Patients with predictors of romiplostim non-response (bone marrow invasion, prior pelvic irradiation, or prior temozolomide) were excluded from this figure to emphasize the difference specifically attributable to dosing regimen. Error bars represent interquartile ranges.

Given our large sample size, we were able to evaluate predictors of romiplostim non-response using multivariable logistic modeling; we found that BM invasion by tumor, prior pelvic irradiation, and prior exposure to temozolomide predict poor response to romiplostim treatment. The latter finding is consistent with the distinct risk of temozolomide resulting in severe marrow toxicity,[28] made manifest by prolonged cytopenias or even aplastic anemia. Our findings suggest evaluation of CIT patients at high risk for BM involvement by tumor (such as patients with metastatic breast, prostate, or lung cancer with known bony involvement) with a BM biopsy may be appropriate before considering romiplostim treatment. Similarly, patients previously treated with pelvic irradiation or temozolomide may be better served with alternative approaches to CIT management. Studies of other thrombopoietic agents have demonstrated efficacy in treatment of CIT in lymphoma[5] and demonstrated BM invasion by tumor as a predictor of romiplostim non-response in solid tumor patients. Given this, in this study, the overall subpar response of non-myeloid hematologic malignancy patients to romiplostim observed is likely secondary to known BM infiltration by malignancy, although many of these patients were not escalated to maximal doses of romiplostim. Additional studies of romiplostim to treat CIT in lymphoma patients without significant BM involvement are needed to better assess its utility in this population.

With 60.7 patient-years at risk of romiplostim treatment in this study, we were able to meaningfully evaluate rates of thromboembolic and bleeding events on romiplostim treatment. Eight patients developed a VTE event on romiplostim treatment, a rate of 14 VTE events per 100 patient-years. Given that 75% of our patients had metastatic disease (with one-third of those with localized disease having primary central nervous system malignancies which impart a high VTE risk) and approximately half had tumor types associated with higher VTE risk, this rate is consistent with VTE rates of 10-14 events per 100 patient-years described in epidemiologic studies of similar populations.[29,30] No patient developing VTE had thrombocytosis at the time of VTE diagnosis, with platelet counts ranging between 65-307x10^9/L (Table 2). Solid tumor patients without predictors of romiplostim non-response had an overall bleeding rate of 16 events per 100 patient-years at risk, consistent with rates in the non-anti-coagulated, non-thrombocytopenic metastatic cancer population.[31,32] This rate is considerably lower than rates in prior studies of CIT patients not treated with thrombopoietic agents. In a large retrospective study of 609 solid tumor and lymphoma patients with 1,262 chemotherapy cycles complicated by CIT, World Health Organization (WHO) grade 3 or 4 bleeding occurred in 43 (3.4%) of cycles.[4] The rate of WHO grade 3 or 4 bleeding in this study was just 11 out of 1,063 cycles supported with romiplostim (1.0%), and many of these bleeds were likely unrelated to thrombocytopenia (only six occurred at platelet counts <100x10^9/L and only three occurred at platelet counts <50x10^9/L) (Table 3). This same retrospective study also found dramatically higher rates of platelet transfusion and chemotherapy dose reduction and treatment delay than those observed in the present study.[4]

Our study has several limitations. As a retrospective, observational study, patients were treated with romiplostim according to institutional pathways that did not mandate strict adherence to treatment parameters. The overall study population was heterogeneous, including a number of different tumor types and chemotherapy regimens. As with many retrospective studies, there is the possibility of selection bias as the patient cohort was defined by those patients enrolled on the romiplostim treatment pathway without evaluating those that were not enrolled. The study was not randomized so cannot quantify the impact of romiplostim treatment compared with a placebo or platelet transfusion-only control group. Although this is the largest study of thrombopoietic growth factor treatment of CIT to date, and the first to include patients with non-myeloid hematologic malignancy, the number of patients with hematologic malignancy was low.

In conclusion, romiplostim is effective for the management of CIT in patients with solid tumors, as demonstrat-

ed by improved platelet counts and low rates of chemotherapy dose reductions and treatment delays, bleeding, and platelet transfusions. VTE rates approximated rates in similar cancer populations not receiving romiplostim. Weekly dosing resulted in improved outcomes as compared with more intermittent intracycle dosing. Romiplostim was generally ineffective in patients with BM invasion by tumor, prior pelvic irradiation, and prior exposure to temozolomide.

Disclosures

HA-S has had a consultancy role for Agios, Dova, Rigel, Argenx, and Sobi, and has received research funding from Agios, Dova, and Amgen; ADP has had a consultancy role for Sunovion, has received research funding from Genentech/Hoffman LaRoche, and Shire/Takeda, and sits on the scientific advisory boards of Bayer, and Shire/Takeda; JIW has had a consultancy role for AbbVie; JMC sits on the scientific advisory boards of Bristol-Myers Squibb, and Portola, has had a consultancy role for Bristol-Myers Squibb, has received personal fees from Bristol-Myers Squibb, and sits on the data safety monitoring board of Unum Therapeutics; DJK has received research funding from Protalex, Bristol-Myers Squibb, Rigel, Bioverativ, Agios, Syntimmune, Principia, and Alnylam, and has had a consultancy role for ONO, Pfizer, 3SBios, Eisai, GlaxoSmithKline, Genzyme, Shire, Amgen, Shionogi, Rigel, Syntimmune, MedImmune, Novartis, Alexion, Bioverativ, Argenx, Zafgen, Fujifilm, Principia, Kyowa Kirin, Takeda, and the Platelet Disorders Support Association.

Contributions

HA-S wrote the first draft of the manuscript and contributed to study design, data collection, data analysis, creation of tables and figures, critical revision of the manuscript, and final approval of the manuscript for publication; ADP contributed to romiplostim treatment pathway design, data collection, revision of the manuscript, and final approval of the manuscript for publication; KG, JIW and JMC contributed to romiplostim treatment pathway design, revision of the manuscript, and final approval of the manuscript for publication; DJK contributed to romiplostim treatment pathway design, critical revision of the manuscript, and final approval of the manuscript for publication.

Acknowledgments

Hemophilia Foundation-Shire Clinical Fellowship Award, the Harvard Catalyst Medical Research Investigator Training Award, and the American Society of Hematology Scholar Award. We also acknowledge the Harvard Catalyst Biostatistics Team, and in particular Dr. Douglas Hayden, for biostatistical support in this study.

References

1. Kuter DJ. Managing thrombocytopenia associated with cancer chemotherapy. Oncology (Williston Park). 2015;29(4):282-294.
2. Wu Y, Aravind S, Ranganathan G, Martin A, Nalysnyk L. Anemia and thrombocytopenia in patients undergoing chemotherapy for solid tumors: a descriptive study of a large outpatient oncology practice database, 2000-2007. Clin Ther. 2009;31 Pt 2:2416-2432.
3. Denduluri N, Patt DA, Wang Y, et al. Dose delays, dose reductions, and relative dose intensity in patients with cancer who received adjuvant or neoadjuvant chemotherapy in community oncology practices. J Natl Compr Canc Netw. 2015;13(11):1383-1393.
4. Elting LS, Rubenstein EB, Martin CG, et al. Incidence, cost, and outcomes of bleeding and chemotherapy dose modification among solid tumor patients with chemotherapy-induced thrombocytopenia. J Clin Oncol. 2001;19(4):1137-1146.
5. Moskowitz CH, Hamlin PA, Gabrilove J, et al. Maintaining the dose intensity of ICE chemotherapy with a thrombopoietic agent, PEG-rHuMGDF, may confer a survival advantage in relapsed and refractory aggressive non-Hodgkin lymphoma. Ann Oncol. 2007;18(11):1842-1850.
6. Aspinall SL, Good CB, Zhao X, et al. Adjuvant chemotherapy for stage III colon cancer: relative dose intensity and survival among veterans. BMC Cancer. 2015;15:62.
7. Havrilesky LJ, Reiner M, Morrow PK, Watson H, Crawford J. A review of relative dose intensity and survival in patients with metastatic solid tumors. Crit Rev Oncol Hematol. 2015;93(3):203-210.
8. Hanna RK, Poniewierski MS, Laskey RA, et al. Predictors of reduced relative dose intensity and its relationship to mortality in women receiving multi-agent chemotherapy for epithelial ovarian cancer. Gynecol Oncol. 2013;129(1):74-80.
9. Kuter DJ, Rummel M, Boccia R, et al. Romiplostim or standard of care in patients with immune thrombocytopenia. N Engl J Med. 2010;363(20):1889-1899.
10. Townsley DM, Scheinberg P, Winkler T, et al. Eltrombopag added to standard immunosuppression for aplastic anemia. N Engl J Med. 2017;376(16):1540-1550.
11. Afdhal NH, Dusheiko GM, Giannini EG, et al. Eltrombopag increases platelet numbers in thrombocytopenic patients with HCV infection and cirrhosis, allowing for effective antiviral therapy. Gastroenterology. 2014;146(2):442-452 e441.
12. Al-Samkari H, Marshall AL, Goodarzi K, Kuter DJ. Romiplostim for the management of perioperative thrombocytopenia. Br J Haematol. 2018;182(1):106-113.
13. Terrault N, Chen YC, Izumi N, et al. Avatrombopag before procedures reduces need for platelet transfusion in patients with chronic liver disease and thrombocytopenia. Gastroenterology. 2018;155(3):705-718.
14. Tateishi R, Seike M, Kudo M, et al. A randomized controlled trial of lusutrombopag in Japanese patients with chronic liver disease undergoing radiofrequency ablation. J Gastroenterol. 2018;54(2):171-181.
15. Kumagai Y, Fujita T, Ozaki M, et al. Pharmacodynamics and pharmacokinetics of AMG 531, a thrombopoiesis-stimulating peptibody, in healthy Japanese subjects: a randomized, placebo-controlled study. J Clin Pharmacol. 2007;47(12):1489-1497.
16. Jenkins JM, Williams D, Deng Y, et al. Phase 1 clinical study of eltrombopag, an oral, nonpeptide thrombopoietin receptor agonist. Blood. 2007;109(11):4739-4741.
17. Nomoto M, Pastino G, Rege B, Aluri J, Ferry J, Han D. Pharmacokinetics, pharmacodynamics, pharmacogenomics, safety, and tolerability of avatrombopag in healthy Japanese and white subjects. Clin Pharmacol Drug Dev. 2018;7(2):188-195.
18. Parameswaran R, Lunning M, Mantha S, et al. Romiplostim for management of chemotherapy-induced thrombocytopenia. Support Care Cancer. 2014;22(5):1217-1222.
19. Miao J, Leblebjian H, Scullion B, Parnes A. A single center experience with romiplostim for the management of chemotherapy-induced thrombocytopenia. Am J Hematol. 2018;93(4):E86-E88.
20. Al-Samkari H, Marshall AL, Goodarzi K, Kuter DJ. The use of romiplostim in treating chemotherapy-induced thrombocytopenia in patients with solid tumors. Haematologica. 2018;103(4):e169-e172.
21. Soff GA, Miao Y, Bendheim G, et al. Romiplostim treatment of chemotherapy-induced thrombocytopenia. J Clin Oncol. 2019;37(31):2892-2898.
22. Tepler I, Elias L, Smith JW 2nd, et al. A randomized placebo-controlled trial of recombinant human interleukin-11 in cancer patients with severe thrombocytopenia due to chemotherapy. Blood. 1996;87(9):3607-3614.
23. Vadhan-Raj S, Verschraegen CF, Bueso-Ramos C, et al. Recombinant human thrombopoietin attenuates carboplatin-induced severe thrombocytopenia and the need for platelet transfusions in patients with gynecologic cancer. Ann Intern Med. 2000;132(5):364-368.
24. Basser RL, Underhill C, Davis I, et al. Enhancement of platelet recovery after myelosuppressive chemotherapy by recombinant human megakaryocyte growth and development factor in patients with advanced cancer. J Clin Oncol. 2000;18(15):2852-2861.
25. Neumann TA, Foote M. Megakaryocyte growth and development factor (MGDF): an Mpl ligand and cytokine that regulates thrombopoiesis. Cytokines Cell Mol Ther. 2000;6(1):47-56.

26. Consensus Committee of Chemotherapy Induced Thrombocytopenia CSoCO. [Consensus on clinical diagnosis, treatment and prevention management of chemotherapy induced thrombocytopenia in China(2018)]. Zhonghua Zhong Liu Za Zhi. 2018;40(9):714-720.
27. Demeter J, Istenes I, Fodor A, et al. Efficacy of romiplostim in the treatment of chemotherapy induced thrombocytopenia (CIT) in a patient with mantle cell lymphoma. Pathol Oncol Res. 2011;17(1):141-143.
28. Villano JL, Letarte N, Yu JM, Abdur S, Bressler LR. Hematologic adverse events associated with temozolomide. Cancer Chemother Pharmacol. 2012;69(1):107-113.
29. Wun T, White RH. Epidemiology of cancer-related venous thromboembolism. Best Pract Res Clin Haematol. 2009;22(1):9-23.
30. Khorana AA, Dalal M, Lin J, Connolly GC. Incidence and predictors of venous thromboembolism (VTE) among ambulatory high-risk cancer patients undergoing chemotherapy in the United States. Cancer. 2013;119(3):648-655.
31. Haas SK, Freund M, Heigener D, et al. Low-molecular-weight heparin versus placebo for the prevention of venous thromboembolism in metastatic breast cancer or stage III/IV lung cancer. Clin Appl Thromb Hemost. 2012;18(2):159-165.
32. Carrier M, Abou-Nassar K, Mallick R, et al. Apixaban to prevent venous thromboembolism in patients with cancer. N Engl J Med. 2019;380(8):711-719.

Concomitant constitutive LNK and NFE2 mutation with loss of sumoylation in a case of hereditary thrombocythemia

The vast majority of patients with myeloproliferative neoplasms (MPN), polycythemia vera, essential thrombocythemia (ET), and primary myelofibrosis acquire driver mutations in the *JAK2, MPL* or *CALR* gene. Clustering of MPN is seen in select families, but in most pedigrees the MPN-predisposing change has not been determined and affected individuals somatically acquire one of the three above-mentioned driver mutations. In contrast, a small number of individuals with hereditary thrombocythemia (HT) carry constitutive alterations, e.g., in the *TPO* or the *LNK* (*SH2B3*) gene.[1-4] Acquired mutations in *LNK*, a negative regulator of JAK2 signaling, rarely occur in both sporadic and familial MPN cases.[1,2] In the latter, they do not segregate with disease phenotype and diseased individuals acquire a concomitant MPN driver mutation.[2] It, therefore, appears unlikely that mutant LNK acts as a driver in MPN.

We have shown that the transcription factor Nuclear Factor Erythroid-derived-2 (NFE2) is overexpressed in the vast majority of MPN patients, independent of other molecular aberrations.[5] In addition, we have identified *NFE2* mutations in MPN and acute myeloid leukemia (AML) patients, that enhance the activity of wild-type (WT) NFE2.[6,7] In several murine models, elevated NFE2 activity causes pathognomonic features of MPN.[6-8] The molecular mechanisms by which NFE2 mutants exert their effect remain unclear since the regulation of NFE2 transcriptional activity is poorly understood. Various post-translational modifications have been described, including ubiquitination, phosphorylation, and sumoylation but their functional role remains elusive.[9]

Here, we identified a 74-year-old female patient given the diagnosis of ET by World Health Organization criteria (*Online Supplementary Table S1*), who tested negative for the three MPN driver mutations, *JAK2, CALR*, and *MPL*. Sequencing 36 myeloid neoplasms associated genes (*Online Supplementary Tables S2 and S3*) revealed both a previously described p.E208Q point-mutation in *LNK* as well as a novel mutation in *NFE2* (c.1102A>T) that prematurely truncates the protein at lysine 368 (p.K368X, Figure 1A). Buccal swab DNA analysis determined that both mutations were heterozygously present in the germline. Because of the constitutive nature of both mutations, this patient should be designated as having hereditary thrombocythemia.

The p.K368X mutation leaves almost the entire NFE2 protein, including the bZIP domain and the N-terminal activation domain, intact. Only the terminal 4 amino acids are lost. Notably, this mutation deletes the ψKXE sumoylation consensus motif identified at lysine 368 and shown to be sumoylated by SUMO1 *in vitro* and *in vivo*.[10] The LNK p.E208Q mutation retains near-complete inhibitory capacity and did not confer significantly higher TPO-hypersensitivity in cell proliferation assays than WT-LNK, suggesting only a subtle loss of function.[3] Therefore, we hypothesized that the loss of sumoylation increases NFE2 activity, which, in co-operation with mutant LNK, drives thrombocytosis in this patient.

To test whether NFE2-K368X retains binding to its cognate DNA motif, we performed an electromobility shift assay (EMSA) using a consensus NFE2 binding site from the human PBGD promoter. DNA binding is preserved in the NFE2-K368X mutant (Figure 1B), consistent with retention of the complete DNA binding and heterodimerization domains.

We subsequently examined the ability of NFE2-K368X to transactivate transcription using a luciferase reporter assay. Heterodimerization with MafG is required for optimal NFE2 activity (*Online Supplementary Figure S1*). The NFE2-K368X mutant was more than twice as active at promoting reporter gene expression than WT-NFE2 (Figure 1C). Because transcription off a plasmid DNA template does not model intact chromatin, we used endogenous gene activation in a cell line as a second read-out. CB3 cells are devoid of NFE2 expression due to viral integration but express β-globin upon re-introduction of NFE2. We therefore lentivirally transduced CB3 cells with either WT-NFE2 or NFE2-K368X and determined β-globin expression by quantitative reverse transcriptase-polymerase chain reaction (qRT-PCR). Again, NFE2-K368X, present in the same amount, was two times more active than its WT counterpart in directing transcription, demonstrating that the mutation results in a protein with supraphysiological activity on intact chromatin (Figure 1D). NFE2-K368X thus constitutes a novel Type Ia mutation, DNA–binding and activating, according to the classification of NFE2 mutations we proposed.[7]

To investigate sumoylation of the NFE2-K368X mutant, we conducted *in vitro* sumoylation assays using recombinantly expressed proteins. SUMO is attached to proteins by hierarchical action of the E1-activating enzyme Aos1/Uba2, the E2-conjugating enzyme UBC9, and a substrate-specific E3-ligase. Sumoylation of WT-NFE2 with SUMO1 has been shown in assays that contained Aos1/Uba2 and UBC9 but lacked an E3-ligase.[10] Under these conditions, we could not detect SUMO1 modification of NFE2 (*Online Supplementary Figure S2*). Substrate recognition is accomplished by UBC9, but E1 and E2 enzymes have poor transfer efficiency, which is stimulated by E3-ligases. Addition of the E3-ligases IR1+M,[11] PIAS1,[12] or ZNF451-N,[13] led to sumoylation of GST-NFE2-WT but not the NFE2-K368X mutant (Figure 2, top).

IR1+M, the catalytic core domain of the E3-enzyme RanBP2, has high SUMO ligase activity but low substrate specificity.[11] Unphysiological *in vitro* conditions can facilitate sumoylation of non-canonical lysine residues, which may facilitate both the observed IR1+M mediated sumoylation of WT-NFE2 (Figure 2, lane 1, marked*) as well as unspecific modification of the NFE2-K368X mutant (Figure 2, lane 6, marked**). The RanBP2 fragment RanBP2ΔFG has a higher substrate specificity,[11] and did not sumoylate either GST-NFE2-WT or NFE2-K368X (Figure 2, lanes 2 and 7). These data suggest that while NFE2 sumoylation is facilitated by the minimal catalytic activity of the IR1+M fragment,[11] NFE2 is not a substrate of the RanBP2 E3-ligase itself. Presence of the small subunit MafG does not influence the sumoylation efficacy of NFE2 by IR1+M with SUMO1 (*Online Supplementary Figure S3*).

Two additional E3-ligases modified NFE2: PIAS1 and ZNF451-N, both with either SUMO1 or SUMO2/3 (Figure 2, top and bottom, lanes 3 and 4). The ZNF451-N ligase has been described as specific for SUMO2/3,[13] but modified GST-NFE2-WT with SUMO1 in our study. This activity may result from the high concentration of the components and the unphysiological conditions *in vitro*. PIAS1 is a member of the PIAS family class of E3-ligases and was described to facilitate MafG sumoylation by

SUMO2/3.[14] PIAS1 is also involved in the negative regulation of the JAK/STAT signaling pathway,[12] which is aberrantly upregulated in MPN patients and constitutes a central molecular hallmark of MPN pathogenesis.

Negative regulation of transcription factors by sumoylation has previously been described and can occur through several distinct mechanisms.[15] For example, sumoylation can compete with acetylation or phosphorylation of nearby residues. While the acetylated or phosphorylated transcription factor is active, the sumoylated form is not. NFE2 activity is regulated by phosphorylation, but the precise molecular mechanisms have not been defined.[9] We, therefore, propose that sumoylation may negatively regulate NFE2 by interfering with other post-translational modifications, such as acetylation, methylation or phosphorylation, required for full activity.

Alternatively, rather than controlling the placement of other post-transcriptional modifications, NFE2 sumoylation may regulate nuclear localization. PIAS1 and ZNF451-N sumoylate the tumor suppressor PML, the main component of PML nuclear bodies (PML-NBs).[12] PML-NB control gene expression by sequestering transcriptions factors in a SUMO-dependent manner.[15] WT-NFE2 and PML co-localize in the nucleus of K562 cells, while sumoylation-deficient NFE2 did not.[10] Sumoylated WT-NFE2 might, therefore, become

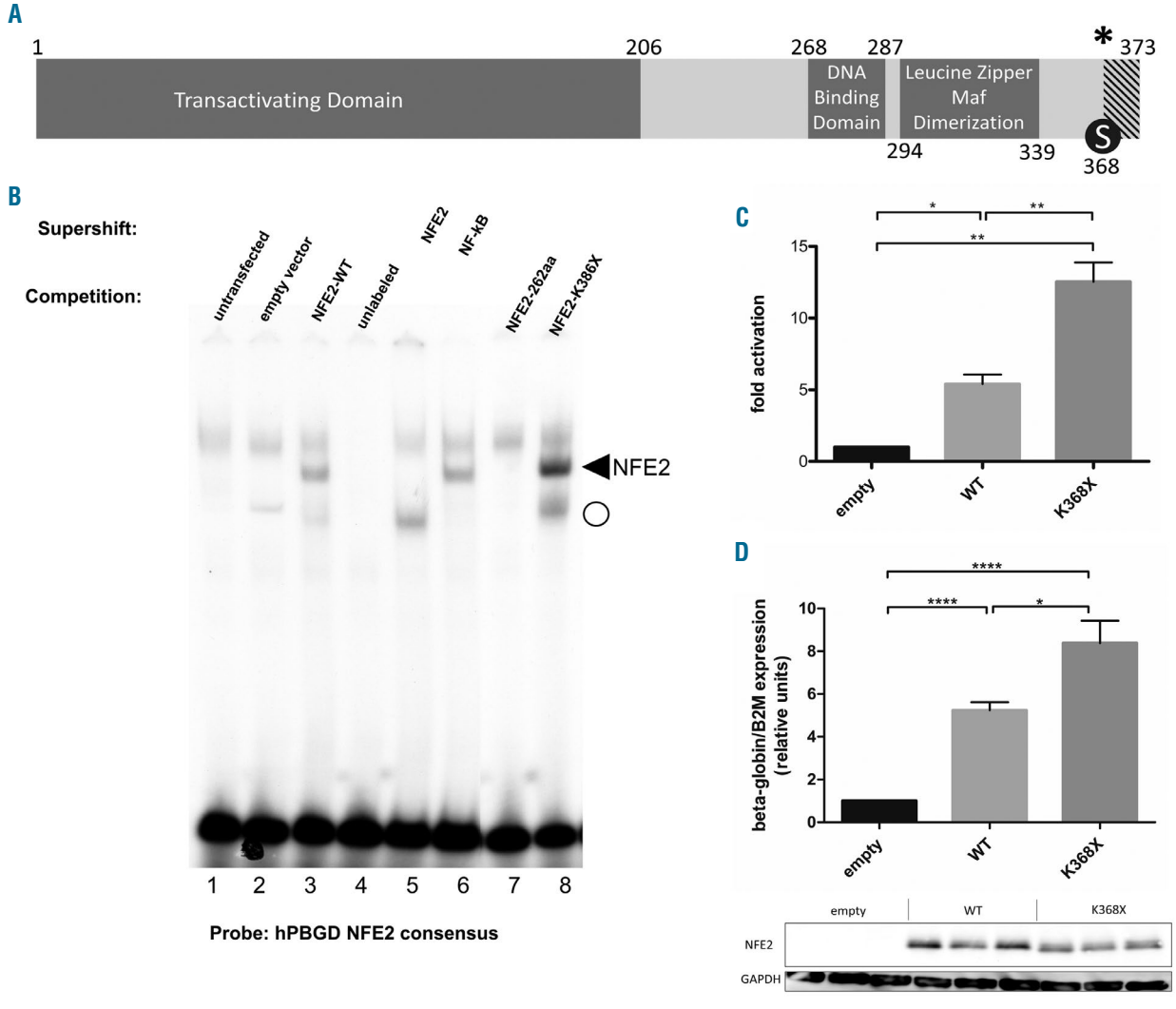


Figure 1. DNA binding affinity and transcriptional activity of the NFE2-K368X mutant. (A) Schematic representation of the NFE2 protein. The location of the K368X mutation is indicated by an asterisk, the sumoylation site at K368 is marked by a circle. (B) EMSA of wild-type (WT) NFE2 and the NFE2-K368X mutant. Nuclear extracts from HEK293T cells transduced with expression vectors encoding MafG as well as NFE2-WT (lane 3), NFE2-K368X (lane 8), or the NFE2-262aa truncation mutant (lane 7) were incubated with a ^{32}P-labeled oligonucleotide containing an NFE2 binding site. In lane 4, a 100x excess of a nonradioactive oligonucleotide was added. Alternatively, an antibody to NFE2 (lane 5) or a control NF-κB antibody (lane 6) was added. The NFE2-262aa truncation mutant, lacking the bZIP domain with consecutive loss of DNA binding, serves as a negative control (lane 7).[6] The arrowhead points to the position of NFE2/DNA complexes on the gel, the open circle indicates nonspecific bands. (C) Dual luciferase reporter assay. HEK293T cells were co-transfected with a pRBGP2-luciferase reporter construct that contains tandemly arranged NFE2 binding sites driving a minimal chicken β-globin promoter together with expression vectors for NFE2, either WT or the K368X mutant, and MafG as indicated. Experiments were carried out with a ratio of 1:8 MafG:NFE2. Firefly luciferase activity was measured 24 h after transfection and was normalized to constitutively expressed renilla luciferase activity. Activity for transfection with MafG alone was set as one and fold activity relative to this control is depicted. Bar graphs represent the mean + SEM. (D) Rescue of β-globin expression. CB3 cells were infected with lentiviral (pLeGO-iG) constructs encoding NFE2-WT, NFE2-K368X, or an empty control virus as indicated. 72 h after infection, RNA was harvested and assayed for β-globin and β2-microglobulin housekeeping gene mRNA expression by qRT-PCR. Results represent the mean + SEM of three independent experiments and are reported as relative expression levels setting β-globin expression for the empty virus as 1. Protein expression in transduced CB3 cells was assessed by western blot. Whole cell extracts, prepared from each of the three independent experiments, were probed for NFE2 and stripped blots reprobed for GAPDH as a loading control. All data were analyzed for statistical significance by two-tailed Student's *t*-test. *P<0.05; **P<0.01; ****P<0.0001.

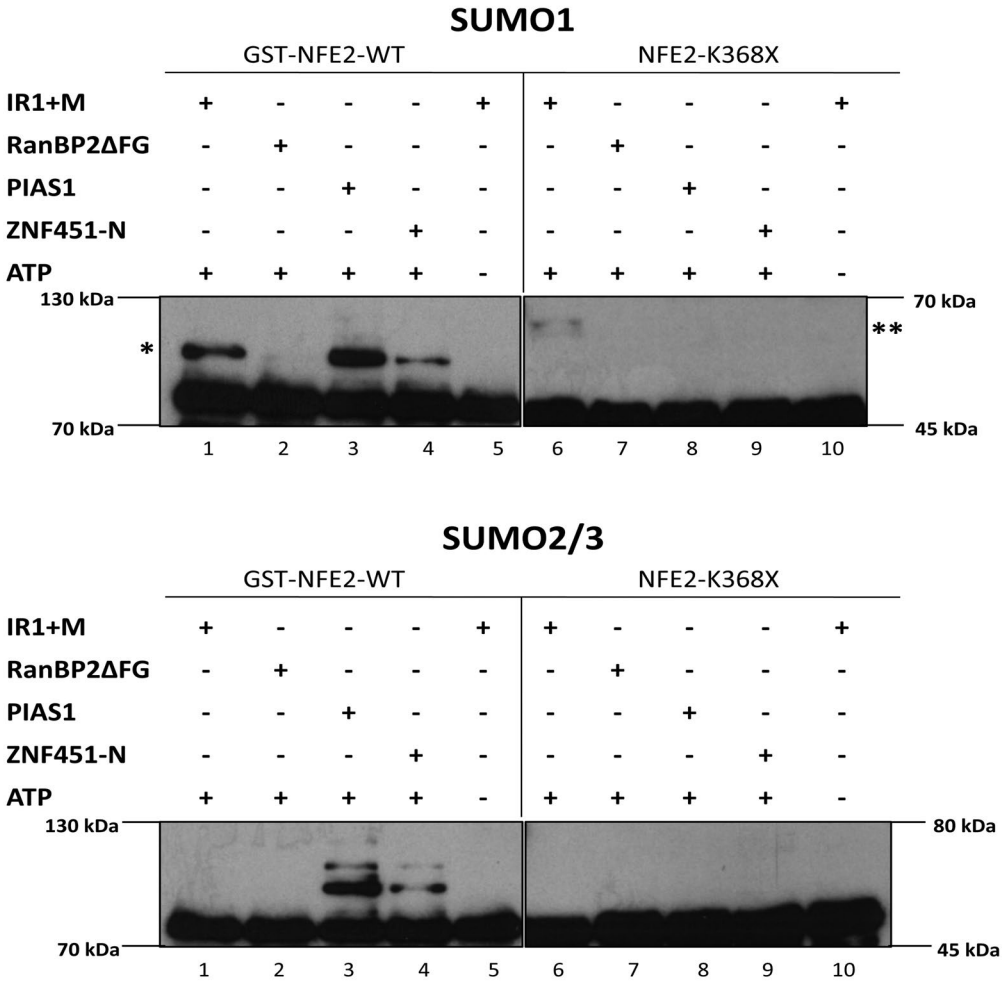


Figure 2. *In vitro* sumoylation assay of NFE2-WT and the NFE2-K368X mutant. Recombinantly expressed GST-NFE2-WT (WT, wild-type) (72 kDa) and NFE2-K368X (45 kDa) were tested for modification with the SUMO1 (top) or the SUMO2/3 (bottom) peptide by different E3 ligases, as indicated. The GST tag was proteolytically cleaved from NFE2-K368X to exclude any potential influence on protein conformation and overall charge. The reaction mixture was subjected to SDS-PAGE and immunoblotting using an anti-NFE2 antibody. Following modification with SUMO2/3, two bands appear as SUMO2/3 is capable of forming chains by self-sumoylation. *The IR1+M mediated modification of GST-NFE2-WT with SUMO1. **The IR1+M mediated modification of NFE2-K368X with SUMO1.

sequestered in PML nuclear bodies, leaving non-sumoylatable NFE2-K368X available to exert the observed, unphysiologically high transcriptional activity.

To test the physiological effect of the K368X mutation, we employed a murine bone marrow (BM) transplantation model. FVB/N-45.2 donor BM was lentivirally infected to express either NFE2-K368X or NFE2-WT and transplanted into FVB/N-45.1 recipient mice. No significant difference in CBC between mice expressing NFE2-K368X, NFE2-WT, or an empty control construct was observed, although a trend towards an elevated thrombocyte count at older age was noted in mice expressing NFE2-K368X (Figure 3A). This observation is consistent with the very late disease onset in our patient, who only manifested clinical signs of thrombocytosis at the age of 74, despite having carried the *LNK* and *NFE2* mutations since birth.

Because of the mild platelet phenotype observed, we morphologically evaluated megakaryopoiesis in histological BM sections of the transplanted mice. We defined three size categories for megakaryocytes (large, middle and small) and enumerated them in five high power fields each of 5 mice of each genotype. The total number of megakaryocytes was increased 50% in NFE2-K368X transplanted mice compared to WT controls (Figure 3B). Moreover, the fraction of small and large megakaryocytes was significantly increased compared to WT, while the fraction of middle-sized megakaryocytes decreased, suggesting alterations in megakaryocyte maturation (Figure 3B). Polymorphic and pleomorphic megakaryocytes, visible in our murine BM histologies (Figure 3C and D), are also typically observed in BM sections of MPN patients.

In conclusion, this report constitutes the first description of a constitutional *NFE2* mutation. Since in a murine model, the NFE2-K368X mutant is sufficient to cause thrombocytosis with a long latency similar to that observed in our patient, and since the LNK-E208Q-mutation was hypothesized to require co-operation with an MPN-driver mutation to produce an MPN phenotype, we now propose that the NFE2-K368X mutation constitutes such an MPN-driver. Our findings provide a rationale for investigating possible NFE2 mutations in triple-negative MPN patients. The observation that the NFE2-K368X mutation abrogates NFE2 sumoylation by either SUMO1

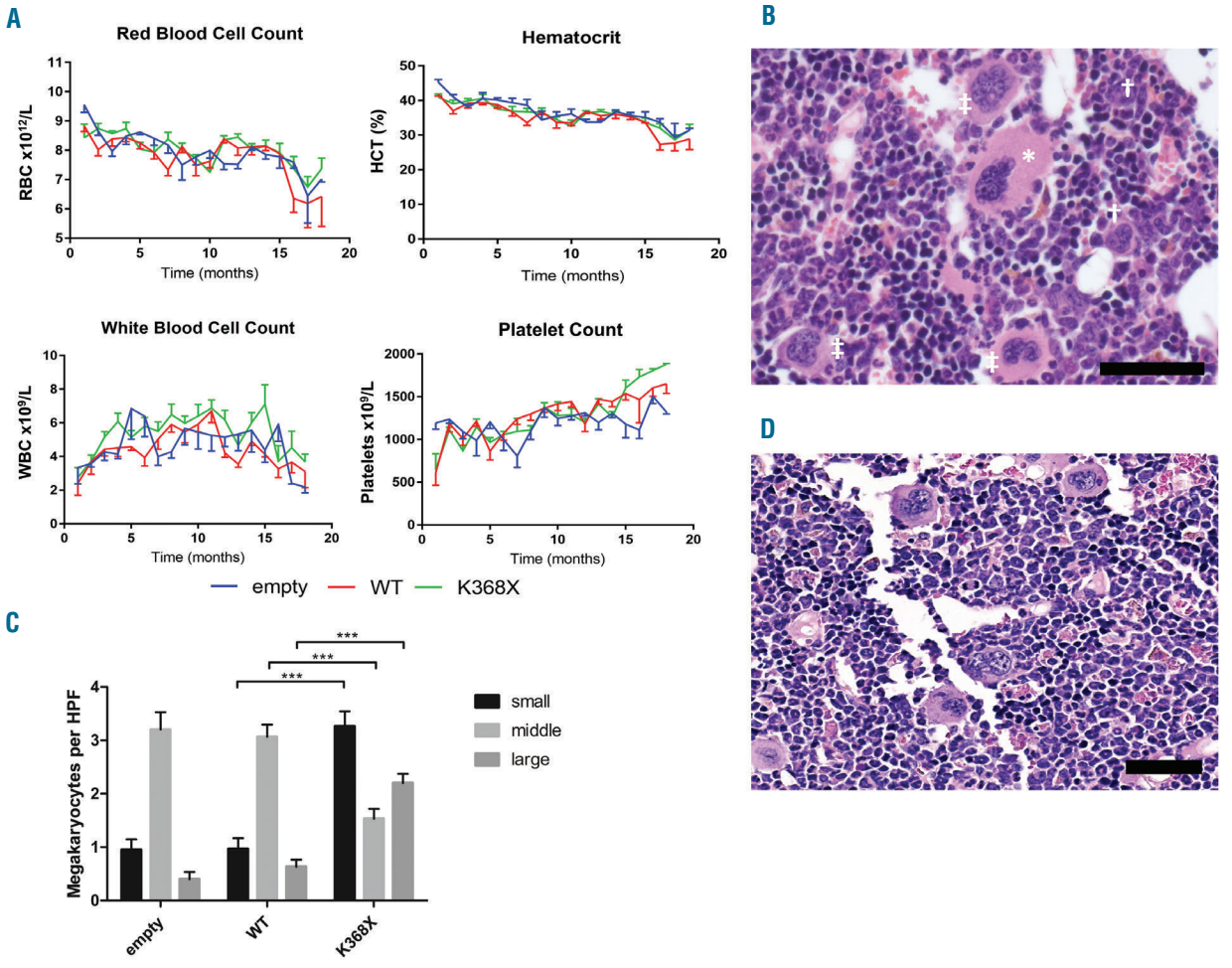


Figure 3. Effect of NFE2-K368X expression on megakaryopoiesis *in vivo*. FVB/N-45.1 acceptor mice were lethally irradiated (2x5 Gy given 4 hours apart) and transplanted with bone marrow (BM) from FVB/N-45.2 donor mice, lentivirally transduced either with an empty vector (n=5), or with a vector expressing wildtype (WT) NFE2 (n=6), or the NFE2-K368X mutant (n=6) (*Online Supplementary Figure S4*). Twelve weeks after the transplantation, engraftment exceeded 90% in all cases (*Online Supplementary Figure S5*). The expression level of NFE2 was doubled in transplanted BM compared to the endogenous level (*Online Supplementary Figure S6*). (A) Complete blood count. Mean±standard error of mean (SEM) are shown. (B) Representative Hematoxylin & Eosin (H&E) stained BM section of a mouse expressing the NFE2-K368X mutation, demonstrating the high variability in megakaryocyte size. *Large size; †middle size; ‡small size. Scale bar=50 μm. (C) H&E stained BM sections morphologically evaluated for megakaryopoiesis and enumerated for five mice of each genotype. Results represent the mean+SEM per five HPF per mouse (400x magnification). Grouped data were analyzed for statistical significance by two-way ANOVA with Bonferroni post tests. ***P<0.001. (D) Representative BM section (H&E) of a mouse expressing NFE2-WT. Scale bar=50 μm.

or SUMO2/3 suggests a previously unrecognized function of sumoylation in negatively regulating NFE2 function.

Lukas Clemens Böckelmann,[1] Titiksha Basu,[1] Albert Gründer,[1] Wei Wang,[1] Jan Breucker,[2] Sandra Kaiser,[1] Andrea Pichler[2] and Heike Luise Pahl[1]

[1]Department of Medicine I, Medical Center, University of Freiburg, Faculty of Medicine, University of Freiburg and [2]Department of Epigenetics, Max Planck Institute of Immunobiology and Epigenetics, Freiburg, Germany

Correspondence:

HEIKE L. PAHL - heike.pahl@uniklinik-freiburg.de

doi:10.3324/haematol.2020.246587

Disclosures: no conflicts of interest to disclose.

Contributions: LCB conceived and designed experiments, performed experiments, analyzed data and wrote the paper; TB performed sequencing and analyzed data; AG performed experiments and analyzed data; WW performed experiments and analyzed data; JB and SK performed experiments; AP conceived and designed experiments, and analyzed data; HLP conceived and designed experiments, analyzed data, and wrote the paper.

Acknowledgments: the authors sincerely thank Prof. Dr. Torsten Haferlach, Munich Leukemia Laboratory (MLL), for providing patients' samples and molecular diagnostics.

Funding: this work was supported by grants from the Mildred-Scheel-Doktorandenprogramm of the Deutsche Krebshilfe (70110768 to LCB) and by the Deutsche Forschungsgemeinschaft (Pa 611/5-3 to HLP).

References

1. McMullin MF, Cario H. LNK mutations and myeloproliferative disorders. Am J Hematol. 2016;91(2):248-251.
2. Rumi E, Harutyunyan AS, Pietra D, et al. LNK mutations in familial myeloproliferative neoplasms. Blood. 2016;128(1):144-145.
3. Oh ST, Simonds EF, Jones C, et al. Novel mutations in the inhibitory adaptor protein LNK drive JAK-STAT signaling in patients with myeloproliferative neoplasms. Blood. 2010;116(6):988-992.
4. Wiestner A, Schlemper RJ, van der Maas APC, Skoda RC. An acti-

vating splice donor mutation in the thrombopoietin gene causes hereditary thrombocythaemia. Nat Genet. 1998;18(1):49-52.
5. Goerttler PS, Kreutz C, Donauer J, et al. Gene expression profiling in polycythaemia vera: overexpression of transcription factor NF-E2. Br J Haematol. 2005;129(1):138-150.
6. Jutzi JS, Bogeska R, Nikoloski G, et al. MPN patients harbor recurrent truncating mutations in transcription factor NF-E2. J Exp Med. 2013;210(5):1003-1019.
7. Jutzi JS, Basu T, Pellmann M, et al. Altered NFE2 activity predisposes to leukemic transformation and myelosarcoma with AML-specific aberrations. Blood. 2019;133(16):1766-1777.
8. Kaufmann KB, Gründer A, Hadlich T, et al. A novel murine model of myeloproliferative disorders generated by overexpression of the transcription factor NF-E2. J Exp Med. 2012;209(1):35-50.
9. Gasiorek JJ, Blank V. Regulation and function of the NFE2 transcription factor in hematopoietic and non-hematopoietic cells. Cell Mol Life Sci. 2015;72(12):2323-2335.
10. Shyu Y-C, Lee T-L, Ting C-Y, et al. Sumoylation of p45/NF-E2: nuclear positioning and transcriptional activation of the mammalian β-like globin gene locus. Mol Cell Biol. 2005;25(23):10365-10378.
11. Pichler A, Knipscheer P, Saitoh H, Sixma TK, Melchior F. The RanBP2 SUMO E3 ligase is neither HECT- nor RING-type. Nat Struct Mol Biol. 2004;11(10):984-991.
12. Rabellino A, Andreani C, Scaglioni PP. The role of PIAS SUMO E3-ligases in cancer. Cancer Res. 2017;77(7):1542-1547.
13. Koidl S, Eisenhardt N, Fatouros C, Droescher M, Chaugule VK, Pichler A. The SUMO2/3 specific E3 ligase ZNF451-1 regulates PML stability. Int J Biochem Cell Biol. 2016;79:478-487.
14. Motohashi H, Katsuoka F, Miyoshi C, et al. MafG sumoylation is required for active transcriptional repression. Mol Cell Biol. 2006;26(12):4652-4663.
15. Lallemand-Breitenbach V, de Thé H. PML nuclear bodies: from architecture to function. Curr Opin Cell Biol. 2018;52:154-161.

Targeting GLUT1 in acute myeloid leukemia to overcome cytarabine resistance

A key alteration in cancer metabolism is an increase in glucose uptake mediated by the glucose transporters (GLUT). Otto Warburg observed already in the 1950s that glycolysis was increased in many tumors, and this is now called the Warburg effect.[1] Interestingly, a distinct glucose metabolic signature was recently described for acute myeloid leukemia (AML), showing that enhanced glycolysis correlates with decreased sensitivity for chemotherapy (cytarabine, Ara-C) and poor prognosis.[2] AML is the most common acute leukemia in adults and is associated with poor survival, especially in patients >60 years, an age group in which only 5-15% are cured. Moreover, older patients who cannot tolerate intensive chemotherapy have a median overall survival of only 5-10 months. Thus, novel therapeutic approaches are needed to improve the cure rates of AML. Interestingly, defective GLUT1-mediated glucose uptake was shown to impair AML cell proliferation, and transplantation of GLUT1-deleted murine AML cells attenuated AML development in mice, suggesting that GLUT1 plays an important role in AML.[3] Thus, targeting GLUT1 may represent a novel therapeutic vulnerability in AML by overcoming Ara-C resistance. However, there are still no clinically available drugs targeting GLUT, which may partly be due to the lack of suitable *in vitro* drug-screening systems. Here we present a detailed structural and functional analysis of compounds that inhibit glucose transporters and sensitize AML cells for chemotherapy.

GLUT1 is an integral membrane protein consisting of 12 transmembrane helices and an intracellular domain, which transports glucose depending on the concentration gradient (Figure 1A).[4] Measuring the activity of membrane proteins such as GLUT1, which transport uncharged substrates, is challenging due to the lack of an easily accessible readout. However, we have developed a system by which purified glucose transporters are reconstituted in vitro into giant vesicles reporting their transport activity using fluorescence microscopy.[5] This allows glucose uptake to be measured without any interference from other proteins by having the purified transporters imbedded in a lipid-bilayer mimicking the size and curvature of mammalian cells. Applying this method, putative GLUT1 inhibitors PGL-13, PGL-14 and PGL-27 (Figure 1B),[6] were validated and benchmarked against the well-known GLUT1 inhibitors WZB-117 and cytochalasin B (CB). A clear decrease in glucose uptake was detected for PGL-13 and PGL-14, but not for PGL-27 (Figure 1C).

To rationalize these results, molecular modeling studies including docking, molecular dynamics (MD) simulations and ligand-protein binding energy evaluations were carried out. The structure of GLUT1 has previously been determined in complex with CB and phenylalanine amide-based inhibitor[7] displaying binding to the central substrate-binding site (Figure 1A). To evaluate whether PGL-13 and PGL-14 also interact at the substrate-binding site, PGL-14 was docked into that site of GLUT1 in an inward-open conformation.[7] The docking solutions could be clustered into three binding poses and for each cluster the docking solution with the best estimated binding energy was selected as a representative potential binding mode. To assess the reliability of the predicted binding modes, the three ligand-protein complexes (complex 1-3, *Online Supplementary Figure S1A-C*) were subjected to MD simulations. In parallel, the same MD protocol was applied to the GLUT1-PGL-14 complex predicted from our previous docking studies based on the GLUT1 homology model in a partially occluded inward-facing conformation, where the ligand is bound to the intracellular domain of GLUT1 (complex 4, *Online Supplementary Figure S1D*).[8] In 3 out of 4 GLUT1-PGL-14 complexes studied (complex 2-4), the ligand maintained its binding mode predicted by docking showing an average root-mean square deviation (RMSD) of its disposition during the MD simulations below 1.5 Å (Figure 1D). In particular, the binding disposition of compound PGL-14 in the intracellular site (complex 4) was remarkably stable, with an average RMSD of about 0.7 Å. Combined, these analyses suggest that PGL-14 likely interacts with GLUT1 in a partially occluded, inward-facing conformation at the intracellular domain. This is an interesting feature that distinguishes the PGL from competitive inhibitors of GLUT1, for instance CB that is known to bind to the transmembrane area.[7] However, we cannot exclude the possibility of PGL compounds having two potential GLUT1 binding sites: the transmembrane and the intracellular binding site (Figure 1E). A refined binding mode was generated for PGL-14, revealing that the interactions are essentially as previously described,[7] with a salicylketoxime ring sandwiched between the side chains of E146 and R212, forming a π-π stacking interaction with the latter residue, as well as H-bond interactions by the functional groups of the ligand to the backbone of the protein (Figure 1F). As PGL-27 did not have inhibitory effects (Figure 1C), the presence of a meta-methyl group in the terminal phenolic ring of PGL-27 (Figure 1B) could result in less favorable binding affinity as it requires displacement of the water molecule that is forming a water-bridged interaction between the ligand and the protein (Figure 1F), and might additionally result in steric clashes.

To experimentally investigate the modeled binding sites, we monitored intrinsic fluorescence quenching for the two binding-site tryptophans upon PGL binding.[9] Measurements showed a decrease in fluorescence intensity, suggesting binding to the transmembrane domain (Figure 1G and H). However, at higher concentrations, a red shift in the emission spectra and an increase in fluorescence intensity was observed (Figure 1G and H). Based on the MD simulations, such behavior could imply PGL binding at two sites (Figure 1D and E) with different affinities. The decrease in fluorescence shows binding in the transmembrane part, while the red shift could result from a secondary conformational event in the intracellular domain, as structural changes accompanying PGL binding could have an overall effect. Indeed, a recent study demonstrated that the intracellular domain of GLUT1 is highly mobile and that its conformational flexibility is strongly coupled to other parts of the protein.[10]

To evaluate whether the PGL compounds are specific for GLUT1, and if targeting GLUT1 can sensitize AML cells for chemotherapy, myeloid leukemia-derived cell lines were screened for GLUT1 expression (*Online Supplementary Figure S2*). THP-1 cells expressed significant amounts of GLUT1 in contrast to KG-1 cells (Figure 2A and B). Thus, comparison between THP-1 and KG-1 cells is an applicable model system to validate the specificity of PGL towards GLUT1 and their sensitization effects for Ara-C treatment. First, the effect on cell viability by Ara-C, PGL-13 and PGL-14 was assessed at increasing concentrations in THP-1 and KG-1 cells (by ATP-assay) and IC25 values were determined (*Online Supplementary Figure S3A-C*). Subsequently, co-treatments with Ara-C and PGLs at IC25 were evaluated for potential synergistic or additive effects. The combinatory

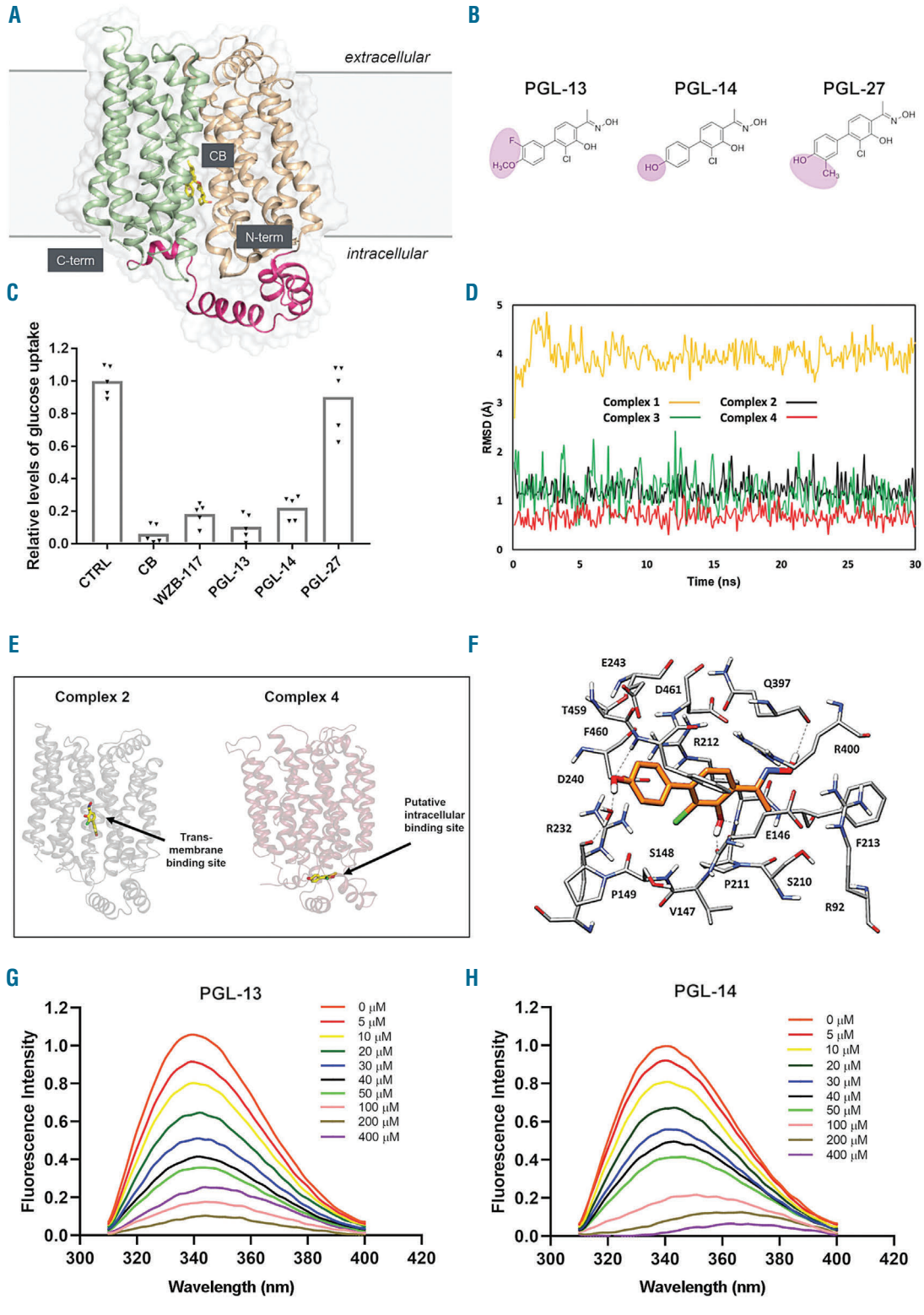


Figure 1. Inhibition of glucose uptake via GLUT1 by PGL compounds through interference with the intracellular domain. (A) Cartoon representation of GLUT1 in complex with cytochalasin B (CB) (PDB ID 5EQI). N- and C-terminal domains are colored in wheat and green, respectively, and the intracellular domain is shown in magenta. The bound CB is shown in stick representation in yellow. (B) Structures of PGL-13, PGL-14 and PGL-27. (C) Inhibition of glucose uptake by selected compounds measured in giant vesicles. Results demonstrate mean normalized to the DMSO control (CTRL), n=5. (D) Molecular dynamics (MD) simulation of representative binding modes of PGL-14 at GLUT1 (complex 1-3) and at homology model of GLUT1 (complex 4). (E) Two PGL binding sites, transmembrane and intracellular, predicted by docking of PGL-14. Complex 2 with predicted inhibitor binding site at GLUT1 inward open conformation overlapping with a glucose/CB binding site (PDB ID 5EQI). Complex 4 with a predicted intracellular binding site at homology model of GLUT1 in a partially occluded inward-facing conformation. (F) Minimized average structure of PGL-14 within the intracellular binding site of GLUT1, derived from the last 15 ns of MD simulation. Hydrogen bonds are represented as dashed lines. (G and H) Intrinsic fluorescence spectra for purified GLUT1 at different concentrations of the inhibitors (G) PGL-13 and (H) PGL-14, with excitation wavelength at 295 nm.

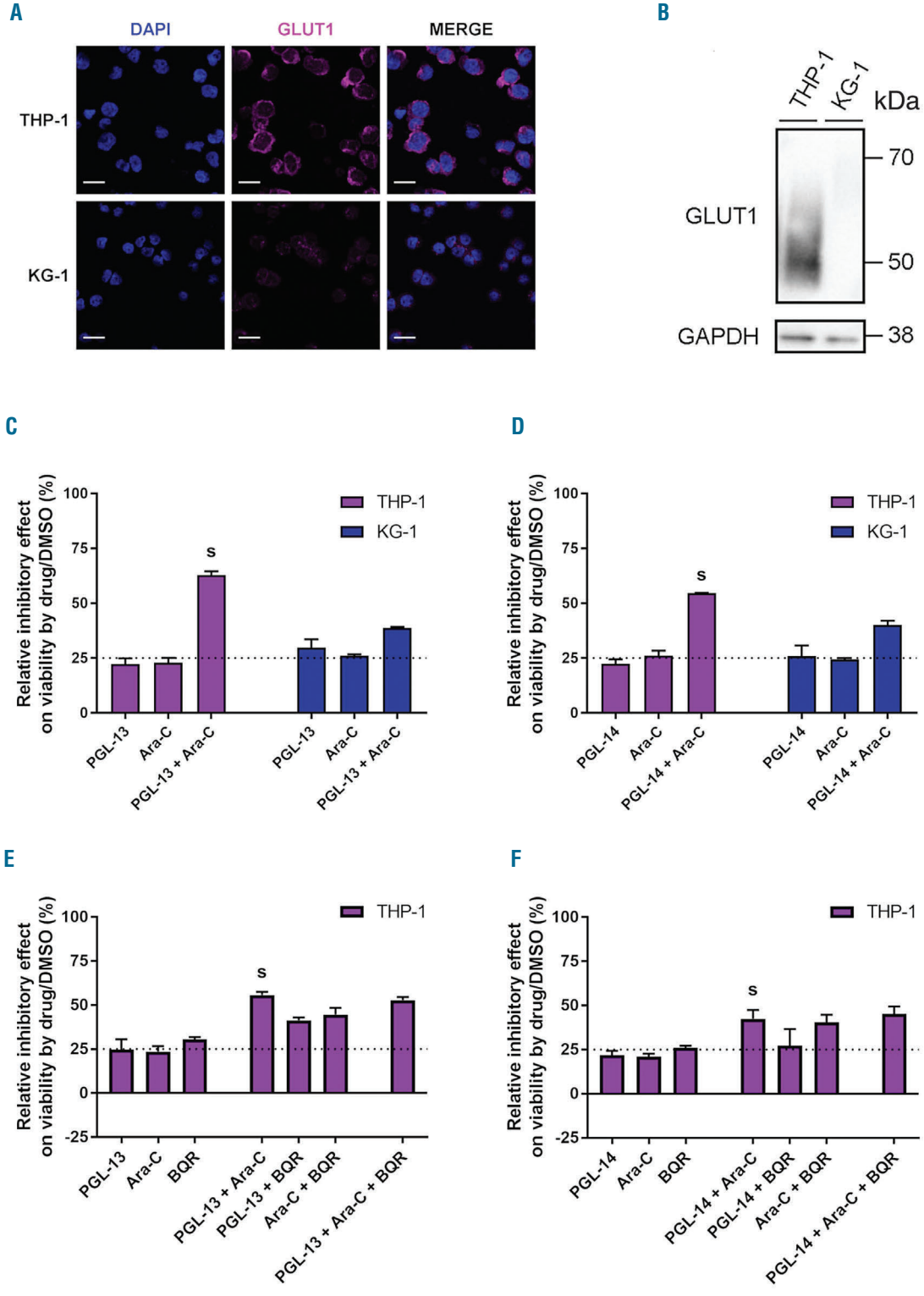


Figure 2. Sensitization to cytarabine (Ara-C) by inhibition of glucose uptake. (A) Immunofluorescence of GLUT1 expression (magenta) in THP-1 cells and KG-1 cells. Nucleus stained with DAPI. 60x magnification, scale bars=30 μm. (B) Western blot of THP-1 and KG-1 whole lysates; GAPDH as the loading control. (C and D) Relative inhibition of cell viability in THP-1 (magenta) and KG-1 (blue) cells using Ara-C and (C) PGL-13 or (D) PGL-14, alone or in combination at IC25. Co-treatment effects were destined synergistic or additive/no effect as determined by the Bliss independence model through calculation of the combination index (CI). SSynergy (CI<1) and is based on CI-values (C) 0.64 and (D) 0.78. (E and F) Relative inhibition of cell viability in THP-1 cells using Ara-C, Brequinar (BQR) and (E) PGL-13 or (F) PGL-14, alone or in combination. Combination of PGL with Ara-C gave values (E) CI=0.76 and (F) CI=0.90. All co-treatment values show mean+standard deviation normalized to a DMSO control, n=3-5. Dotted lines show theoretical IC_{25} values.

effect was considered synergistic when the combination index (CI) had a value <1. An inhibitory synergistic effect was detected for PGL-13 (CI=0.64) and PGL-14 (CI=0.78) in combination with Ara-C for THP-1, but not for KG-1 (CI=1.24 and CI=1.10 for PGL-13 and PGL-14, respectively) (Figure 2C and D and *Online Supplementary Figure S4A and B*). A similar inhibitory effect for the combination of doxorubicin with PGL-13 (CI=0.53) or PGL-14 (CI=0.76) was detected in THP-1 cells (*Online Supplementary Figures S3D and S4C and D*). To confirm the specificity of the PGL, THP-1 cells were also co-treated with maltose (a disaccharide known to bind to GLUT1 but which is non-transportable) and Ara-C, showing a clear inhibitory synergistic effect (CI=0.82) (*Online Supplementary Figures S3E and S4E*). This suggests a sensitization effect by both PGL compounds in myeloid leukemia cells with high GLUT1 expression. However, also Mono-Mac-6 (MM6) cells with a clear but lower GLUT1 expression level compared to THP-1 (*Online Supplementary Figure S2A and B*) displayed synergistic inhibitory effects for the PGL with Ara-C (CI=0.62 and CI=0.53, for PGL-13 and PGL-14, respectively), suggesting that the presence of GLUT1, rather than the amounts, is contributing to sensitization effects (*Online Supplementary Figures S3A-C and S4F and G*).

A mechanistic explanation for the observed synergistic effects could be that Ara-C inhibits the Akt-pathway resulting in increased dependence on aerobic glycolysis that in turn is inhibited by PGL. This is supported by the observations that PGL-13 can restore repression of increased glycolysis caused by Akt inhibitors,[11] and by the suggestions that Ara-C can inhibit phosphorylation of Akt and the downstream mTOR pathway in AML.[12] However, Ara-C resistant AML cells have been shown to rather be dependent on oxidative phosphorylation (OXPHOS) than glycolysis.[13] Thus, to validate the hypothesis, we also targeted dihydroorotate dehydrogenase (DHODH) a known putative metabolic target for AML therapy and a potent regulator of AML cell growth, apoptosis and differentiation.[14,15] Specifically, the oxidation of dihydroorotate via the activity of DHODH provides electrons for OXPHOS. A distinct inhibition of proliferation by Brequinar, a well-studied DHODH inhibitor, was detected. However, although the combination index was close to 1 (CI values ranging from 1.00 to 1.20), no synergistic effects were displayed when combined with Ara-C (Figure 2E and F, and *Online Supplementary Figures S3F and S5A-D*). In addition, when combining PGL, Brequinar and Ara-C the outcome was similar as to when only PGL and Ara-C were combined (Figure 2E and F, and *Online Supplementary Figures S3F and S5A-D*). Taken together, this suggests that AML cells with high levels of glucose transporters are particularly vulnerable towards blocking glycolysis in combination with chemotherapy, suggesting that the PGL class of compounds should be further evaluated for AML therapy.

Hannah Åbacka,[1] Jesper S. Hansen,[1] Peng Huang,[1] Raminta Venskutonytė,[1] Axel Hyrenius-Wittsten,[2] Giulio Poli,[3] Tiziano Tuccinardi,[3] Carlotta Granchi,[3] Filippo Minutolo,[3] Anna K. Hagström-Andersson[2] and Karin Lindkvist-Petersson[1,4]

[1]Department of Experimental Medical Science, Medical Structural Biology, BMC C13, Lund University, Lund, Sweden; [2]Department of Laboratory Medicine, Division of Clinical Genetics, BMC C13, Lund University, Lund, Sweden; [3]Department of Pharmacy, University of Pisa, Pisa, Italy and [4]LINXS - Lund Institute of Advanced Neutron and X-ray Science, Scheelevägen 19, SE-223 70, Lund, Sweden

Correspondence:

KARIN LINDKVIST-PETERSSON - karin.lindkvist@med.lu.se

doi:10.3324/haematol.2020.246843

Disclosures: no conflicts of interest to disclose.

Contributions: HÅ, JH, AH-W, TT, FM, AKH-A and KL-P designed the experiments; HÅ, JH, PH, RV, AH-W, GP and CG conducted the experiments; HÅ, JH, RV, TT, FM, AKH-A and KL-P analyzed the data; HÅ, RV, TT, FM, AKH-A and KL-P wrote the manuscript.

Funding: this work was supported by Swedish Research Council (2016-01319 and 2017-05816) and the Swedish Cancer Society (2017/307).

References

1. Warburg O. On respiratory impairment in cancer cells. Science. 1956;124(3215):269-270.
2. Chen WL, Wang JH, Zhao AH, et al. A distinct glucose metabolism signature of acute myeloid leukemia with prognostic value. Blood. 2014;124(10):1645-1654.
3. Saito Y, Chapple RH, Lin A, Kitano A, Nakada D. AMPK protects leukemia-initiating cells in myeloid leukemias from metabolic stress in the bone marrow. Cell Stem Cell. 2015;17(5):585-596.
4. Deng D, Xu C, Sun P, et al. Crystal structure of the human glucose transporter GLUT1. Nature. 2014;510(7503):121-125.
5. Hansen JS, Elbing K, Thompson JR, Malmstadt N, Lindkvist-Petersson K. Glucose transport machinery reconstituted in cell models. Chem Commun (Camb). 2015;51(12):2316-2319.
6. Granchi C, Qian Y, Lee HY, et al. Salicylketoximes that target glucose transporter 1 restrict energy supply to lung cancer cells. ChemMedChem. 2015;10(11):1892-1900.
7. Kapoor K, Finer-Moore JS, Pedersen BP, et al. Mechanism of inhibition of human glucose transporter GLUT1 is conserved between cytochalasin B and phenylalanine amides. Proc Natl Acad Sci U S A. 2016;113(17):4711-4716.
8. Tuccinardi T, Granchi C, Iegre J, et al. Oxime-based inhibitors of glucose transporter 1 displaying antiproliferative effects in cancer cells. Bioorg Med Chem Lett. 2013;23(24):6923-6927.
9. Carruthers A. ATP regulation of the human red cell sugar transporter. J Biol Chem. 1986;261(24):11028-11037.
10. Galochkina T, Ng Fuk Chong M, Challali L, Abbar S, Etchebest C. New insights into GluT1 mechanics during glucose transfer. Sci Rep. 2019;9(1):998.
11. Massihnia D, Avan A, Funel N, et al. Phospho-Akt overexpression is prognostic and can be used to tailor the synergistic interaction of Akt inhibitors with gemcitabine in pancreatic cancer. J Hematol Oncol. 2017;10(1):9.
12. Chen L, Guo P, Zhang Y, et al. Autophagy is an important event for low-dose cytarabine treatment in acute myeloid leukemia cells. Leuk Res. 2017;60:44-52.
13. Farge T, Saland E, de Toni F, et al. Chemotherapy-resistant human acute myeloid leukemia cells are not enriched for leukemic stem cells but require oxidative metabolism. Cancer Discov. 2017;7(7):716-735.
14. Sykes DB, Kfoury YS, Mercier FE, et al. Inhibition of dihydroorotate dehydrogenase overcomes differentiation blockade in acute myeloid leukemia. Cell. 2016;167(1):171-186.e15.
15. Wu D, Wang W, Chen W, et al. Pharmacological inhibition of dihydroorotate dehydrogenase induces apoptosis and differentiation in acute myeloid leukemia cells. Haematologica. 2018;103(9):1472-1483.

Anemia and hemodilution: analysis of a single center cohort based on 2,858 red cell mass measurements

Anemia is the most frequent hematologic disorder worldwide. It was biologically defined many years ago by the World Health Organization (WHO) as a decrease in circulating hemoglobin concentration [Hb] to <120 g/L in women and <130 g/L in men.[1] In severe anemia (i.e., anemia causing symptoms or when [Hb] <70-80 g/L), curative treatments (e.g., iron, folates, vitamin B12 supplementation or erythropoiesis stimulating agents [ESA]) or transfusions are typically used. Approximately 85 million red blood cell (RBC) units are transfused per year worldwide.[2]

In a recent study, Otto *et al.*[3] reported that in approximately half the cases anemia can be explained as a result of hemodilution (increased plasma volume [PV]) rather than by a reduction in red cell mass (RCM), especially in chronic heart and liver diseases. These results, obtained by using total hemoglobin mass measurement with carbon monoxide rebreathing method and PV indirect calculation, suggest that treatment of anemias could be over-prescribed for hemodiluted patients.

In order to determine whether anemia-related treatment could be over-prescribed for "anemic" patients in our institution, we retrospectively analyzed RCM and PV from normal, anemic and polycythemic patients using direct measurements of red cell and plasma volumes (Cr^{51}-labeled RBC and I^{125}-labeled albumin). Briefly, 2,858 RCM and PV performed concomitantly in our department between 2010 and 2017 (mostly for suspected myeloproliferative diseases) were retrospectively analyzed in addition to [Hb] and hematocrit (Hct) determination. These measurements were performed in different situations: i) looking for real RCM decrease in case of low [Hb] in presence of possible cause of hemodilution or in absence of other obvious causes of [Hb] decrease; ii) looking for "masked" RCM increase in presence of known myeloproliferative neoplasm in case of low or normal [Hb]; or iii) confirming polycythemia in case of elevated [Hb]. We then selected a group of "anemic" patients with low [Hb] (<120 g/L in women and <130 g/L in men) and classified them according to the severity of the anemia (WHO classification of anemia[4]): mild anemia (110-119 g/L for women and 110-129 g/L for men, n=27), moderate anemia (80-109 g/L, n=27) and severe anemia (< 80 g/L, n=9). We also selected a control group (n=97) defined as follow: [Hb] 120-160 g/L in women and 130-165 g/L in men, Hct ≤48% in women and ≤49% in men, mean corpuscular volume 80-100 fL, RCM ≤ +25% of normal value, absence of *JAK2*V617F mutation, no splenomegaly, white blood cell (WBC) count 4-10x10^9/L and platelet count 150-450x10^9/L, and a group of "polycythemic" patients with increased [Hb] (>160 g/L in women and >165 g/L in men) (n=1,815). Patients' characteristics are summarized in Table 1 and a flow chart of the study is shown in *Online Supplementary Figure S1*.

PV categories had previously been defined according to Otto *et al.*[3]: plasmatic contraction if PV < -8% of the expected theoretical value, normal if ≥ -8% and ≤ +8%, moderate expansion if > +8% and ≤ +25%, and severe expansion if > +25%. RCM was considered as normal when varying between -25% and +25% of the theoretical value, increased (polycythemia) when RCM > +25% of the theoretical normal RCM, and reduced when RCM < -25% of the theoretical normal RCM according to Pearson *et al.*[5]

We first focused on anemic and control subjects. Anemic patients had a significantly higher PV than the control group (mean PV +41% *vs.* -5%; P<0.0001) (Figure 1A), 94% of them had PV > +8% (*vs.* 9% in the control group) and 73% PV > +25% (*vs.* 0% in the control group) (Table 2), confirming with direct measurement previous findings from Otto *et al.*[3] about the high frequency of hemodilution in anemic patients. There was also a statistical difference in RCM between the control group and the anemic group (mean RCM -12.7% *vs.* +8.8% for anemic and control groups, respectively; P<0.0001) (Figure 1B). Only 24% (n=15) of anemic patients had RCM < -25% of the expected theoretical value (Table 2 and Figure 1C), confirming that, in our cohort, a decrease in [Hb] may be due more often to an increase in PV rather than related to a decrease in RCM in clinical practice. Among anemic patients, no patient with mild anemia had RCM < -25%, while patients with moderate anemia presented a 25.9% risk of RCM < -25% and those with severe anemia a risk of 88.9% (Table 2), suggesting that even in severe anemic patients, patients may have hemodilution rather than an important reduction in the RCM. Moreover, 77.8% (n=7) of the severe anemic patients with RCM < -25% also have increased PV > +25%. This suggests that, in the vast majority of cases, severe anemia is related to both reduced RCM and increased PV.

We then focused on the correlations between [Hb], PV and RCM. Studying the whole cohort according to the [Hb] revealed a direct correlation between [Hb] level and PV (P=0.0006). This was also observed when focusing on anemic (P<0.0001) and control patients (P=0.0006) (*data not shown*). A direct correlation between [Hb] and RCM was found in the whole cohort: the lower the [Hb] level, the lower the RCM (P<0.0001). This correlation between

Table 1. Characteristics of anemic patients, control subjects, and of patients with increased hemoglobin concentration.

	All	"Anemic"			Control	"Polycythemic"
		Mild	Moderate	Severe		
N	63	27	27	9	97	1,815
Age (years)	61.0±19.4	61.0±17.2	63.9±21.1	52.5±19.8	52.4±16.8	56.7±15.2
M/F	1.4	1.7	1.1	2.0	2.7	5.8
WBC (x10^9/L)	8.7±8.3	8.5±4.6	9.2±11.3	7.6±7.1	6.7±1.5	8.0±4.3
[Hb] (g/L)	103±20	120±6	97±8	67±6	158±7	177±9
Hct (%)	31.7±5.9	36.9±2.0	29.8±3.2	21.6±3.4	46.1±2.0	51.4±3.1
Platelets (x10^9/L)	322±329	490±430	207±116	152±117	247±69	256±153

M/F: sex ratio male/female; WBC: white blood cell count; [Hb]: hemoglobin concentration; Hct: hematocrit. Polycythemic patients in this table are all patients with increased [Hb] whatever the cause: red cell mass increase (real polycythemia) or plasma volume decrease (hemoconcentration).

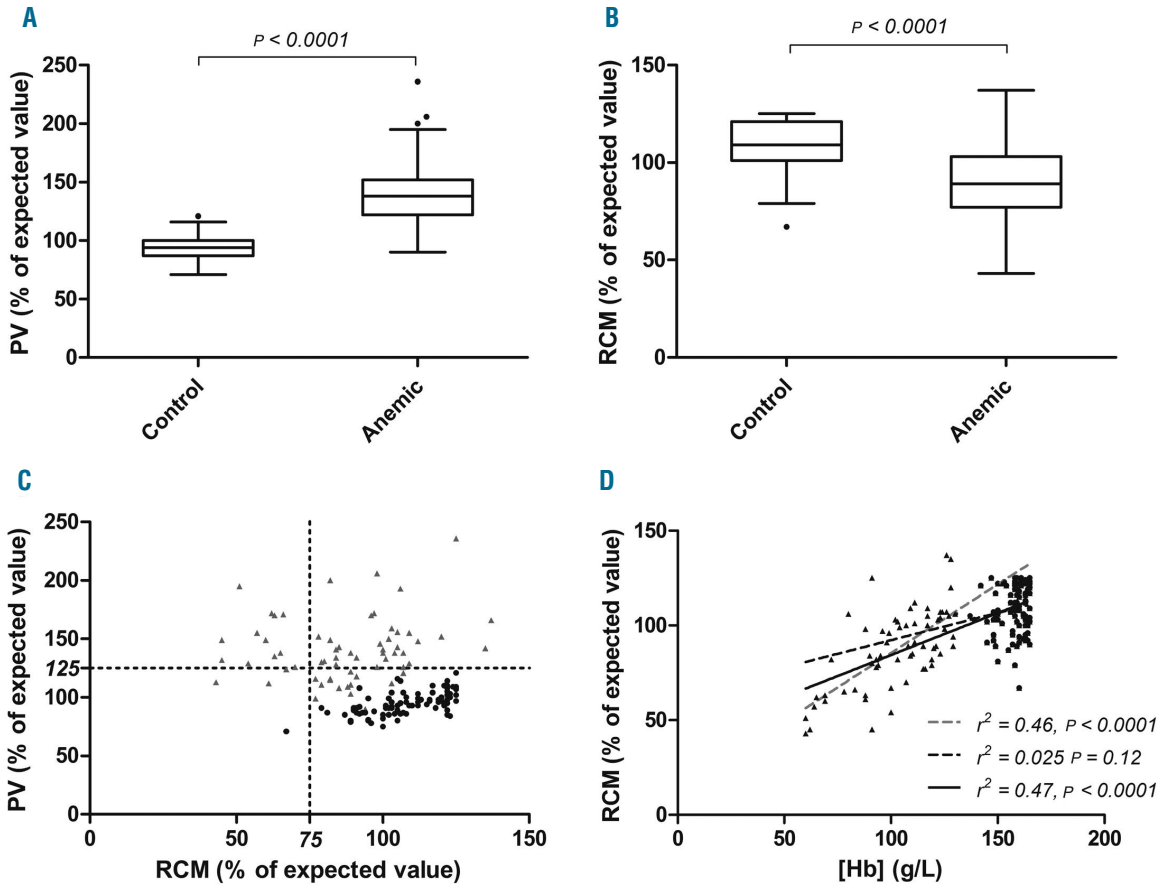


Figure 1. Plasma volume (PV), red cell mass (RCM) and hemoglobin concentration [Hb] in control subjects and anemic patients. Box-and-Whisker plot of (A) PV and (B) RCM (in % of expected theoretical value) in control and anemic patients. (C) Correlations of PV and RCM in control and anemic patients. (D) Correlations of RCM and [Hb] (g/L) in control and anemic patients. Black points and discontinued line represent control patients, gray triangles and discontinued line represent anemic patients, black continuous line represents both anemic and control patients.

RCM and [Hb] level was found in anemic patients (P<0.0001) but, interestingly, not in control patients (P=0.12) (Figure 1D).

We then analyzed in more detail the levels of [Hb] according to PV measurements. We observed higher mean [Hb] in patients with normal PV (156 g/L) compared to moderately expanded (126 g/L; P<0.0001) or severely expanded (99 g/L; P<0.0001) PV (Figure 2A). Conversely, mean PV was lower for the control group (-5%) than in mild "anemia" (+26%; P<0.0001), moderate "anemia" (+49%; P<0.0001) or severe "anemia" (+60%; P=0.0001) groups (Figure 2B). In contrast to the results of Otto *et al.*[3], in which correlation between [Hb] and total hemoglobin mass (measured with respiratory test) weakened as PV rose, we found a positive correlation between [Hb] and RCM whatever the PV status (normal, moderately or severely expanded), and this did not weaken as PV increased (Figure 2C). In order to define whether these correlations were only found for anemic and normal subjects, we also analyzed the correlation for patients with increased [Hb]. For those patients, correlations between [Hb] and PV or RCM were also significant (P<0.0001 in both cases) (*data not shown*).

Lastly, since spleen enlargement is considered to be the main cause of an increase in PV in hematologic disorders, we compared anemic patients with or without spleen enlargement and normal subjects. Twenty-nine out of 63 (46%) anemic patients presented splenomegaly and these had a significantly higher PV than anemic patients without spleen enlargement (+49% *vs.* +34%; P=0.03) (Figure 2D). Surprisingly, comparison between anemic patients without spleen enlargement and control patients also revealed a significantly higher PV in the anemic group (+34% *vs.* -5%; P<0.0001), suggesting that anemia due to hemodilution is not only associated to spleen enlargement and that there could be other causes of hemodilution in these patients.

We decided to verify whether the causes of anemia (heart disease, renal failure, hypergammaglobulinemia, portal thrombosis, primary myelofibrosis, other myeloproliferative neoplasms) could be associated with differences in PV, RCM or [Hb] in anemic patients. However, we failed to find any difference according to disease; this was probably due to the low number of patients in each group (*data not shown*).

Here we retrospectively analyzed RCM measurements in a single center cohort of patients with a focus on anemic patients. RCM and PV determinations are rarely performed in these patients. We assume a study bias in this patient cohort as clinicians asking for RCM measurement probably hypothesize that their patients would present a hemodilution rather than a true anemia. Measurement of RCM was performed here using standard recommendations (Cr^{51}-labeled RBC) and direct PV was measured using the dilution method based on I^{125}-labeled albumin. Then, using a different technical approach, and despite the probable bias in patient selection that may have artificially increased the hemodilution rate compared to

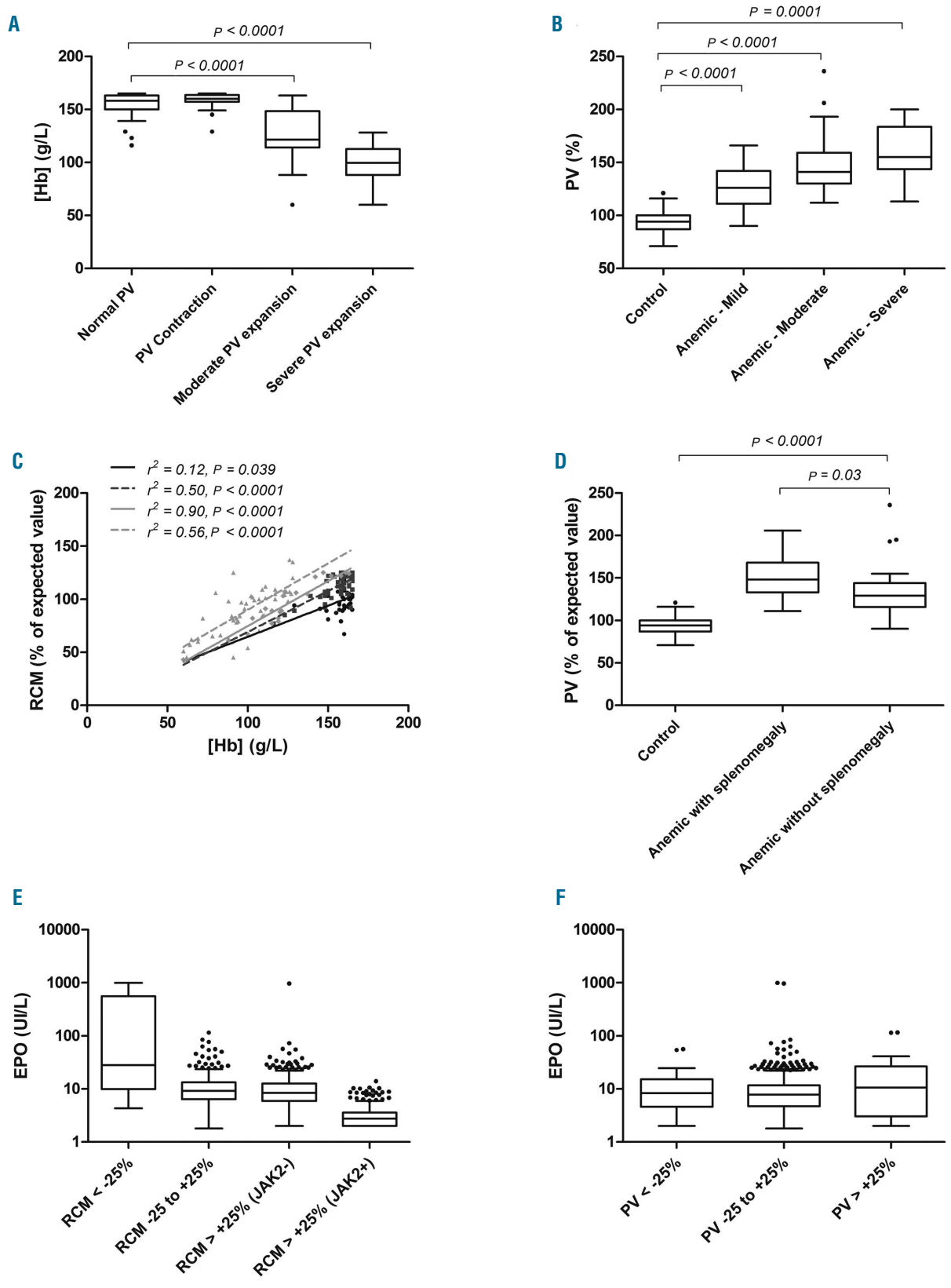


Figure 2. Correlations between hemoglobin concentration [Hb], plasma volume (PV), red cell mass (RCM), splenomegaly, and erythropoietin (EPO) concentrations. (A) [Hb] (g/L) according to PV groups of patients. (B) PV (in % of expected theoretical value) in the anemic groups of patients (World Health Organization definition). (C) Correlations of RCM (in % of expected theoretical value) and [Hb] in different PV groups: black points and continuous line represents a group of PV contraction patients, dark gray squares and discontinued line represent a group of normal PV patients, light gray diamonds and continuous line represent a group of moderate PV expansion patients, light gray triangles and discontinued line represent a group of severe PV expansion patients. (D) PV in anemic patients according to spleen enlargement. (E) EPO concentrations according to RCM groups or (F) PV groups (in % of expected theoretical value).

Table 2. Red cell mass and plasma volume in anemic patients, control subjects, and patients with increased hemoglobin concentration.

		Anemic (%)			Control (%)	Polycythemic (%)
	All	Mild	Moderate	Severe		
Total, n	63	27	27	9	97	1,815
RCM < -25%	15 (23.8)	0 (0)	7 (25.9)	8 (88.9)	1 (1.0)	3 (0.2)
and PV < -25%	0 (0)	0 (0)	0 (0)	0 (0)	1 (1.0)	1 (0.1)
and PV ≥ -25% and < -8%	0 (0)	0 (0)	0 (0)	0 (0)	0 (0)	2 (0.1)
and PV ≥ -8% and ≤ +8%	0 (0)	0 (0)	0 (0)	0 (0)	0 (0)	0 (0)
and PV > +8% and ≤ +25%	3 (4.8)	0 (0)	2 (7.4)	1 (11.1)	0 (0)	0 (0)
and PV > +25%	12 (19.0)	0 (0)	5 (18.5)	7 (77.8)	0 (0)	0 (0)
RCM ≥ -25% and ≤ +25%	46 (73.0)	25 (92.6)	20 (74.1)	1 (11.1)	96 (99.0)	1,004 (55.3)
and PV < -25%	0 (0)	0 (0)	0 (0)	0 (0)	0 (0)	75 (4.1)
and PV ≥ -25% and < -8%	1 (1.6)	1 (3.7)	0 (0)	0 (0)	35 (36.1)	614 (33.8)
and PV ≥ -8% and ≤ +8%	3 (4.8)	3 (11.1)	0 (0)	0 (0)	52 (53.6)	297 (16.4)
and PV > +8% and ≤ +25%	10 (15.9)	9 (33.3)	1 (3.7)	0 (0)	9 (9.3)	16 (0.9)
and PV > +25%	32 (50.8)	12 (44.4)	19 (70.4)	1 (11.1)	0 (0)	2 (0.1)
RCM > +25%	2 (3.2)	2 (7.4)	0 (0)	0 (0)	–	808 (44.5)
and PV < -25%	0 (0)	0 (0)	0 (0)	0 (0)	–	13 (0.7)
and PV ≥ -25% and < -8%	0 (0)	0 (0)	0 (0)	0 (0)	–	283 (15.6)
and PV ≥ -8% and ≤ +8%	0 (0)	0 (0)	0 (0)	0 (0)	–	414 (22.8)
and PV > +8% and ≤ +25%	0 (0)	0 (0)	0 (0)	0 (0)	–	83 (4.6)
and PV > +25%	2 (3.2)	2 (7.4)	0 (0)	0 (0)	–	15 (0.8)

n: number; RCM: red cell mass; PV: plasma volume.

unselected anemic patients of other clinical centers, we confirmed the results from Otto *et al.*[3] showing the high proportion of anemic patients who, in fact, present a hemodilution rather than a reduction in RCM. However, and for clinical purposes, our study demonstrates that when a patient presents severe anemia (i.e., [Hb] <80 g/L), RCM is decreased in around 90%, thus justifying therapeutic intervention (such as transfusion or ESA) whatever the cause of the anemia. However, therapeutic interventions for patients with mild or moderate anemia have to be discussed since we noticed that over half the patients were hemodiluted and did not have a decrease in RCM. In order to distinguish hemodiluted from "real anemic" patients in the moderate and mild groups of patients, we analyzed erythropoietin (EPO) level measured in the different cohorts. Our data, as previously reported,[6] demonstrated that only truly anemic patients presented increased circulating EPO concentrations. However, the overlap in EPO concentrations among the different groups suggested that as a marker this was not sufficiently discriminative (Figure 2E and F).

RCM and PV measurement are currently performed for polycythemic patients since the correlation between [Hb] or [Hct] and RCM is relatively low in these patients. We previously reported that, even in *JAK2*V617F mutated myeloproliferative neoplasm patients, the RCM was consistently increased over +25% only for patients presenting Hct >55%.[7]

Here we demonstrate that [Hb] is a good surrogate marker of decreased RCM for severe anemic patients but not for moderate or mild anemic patients. Therefore, for this last category of patients, measurement of RCM and PV to clearly differentiate RCM decrease and hemodilution could only be useful before therapeutic intervention. Based on these results, a prospective study in anemic patients may confirm these findings and thus help in treatment decisions.

Louis Drevon,[1,2,3] Nabih Maslah,[1,2,3] Juliette Soret-Dulphy,[2,4] Christine Dosquet,[1,2,3] Odno Ravdan,[1] Laetitia Vercellino,[5] Celia Belkhodja,[1,2,3] Nathalie Parquet,[6] Anne C. Brignier,[6] Marie-Hélène Schlageter,[1,2,3] Bruno Cassinat,[1,2,3] Jean-Jacques Kiladjian,[2,3,4] Christine Chomienne[1,2,3] and Stéphane Giraudier[1,2,3]

[1]APHP, Service de Biologie Cellulaire, Hôpital Saint-Louis, F-75010 Paris; [2]France Intergroupe des Syndromes Myéloproliferatifs (FIM); [3]Université de Paris, U1131 INSERM, IRSL, F-75010 Paris; [4]APHP, Centre d'Investigations Cliniques, Hôpital Saint-Louis, F-75010 Paris; [5]APHP, Service de Médecine Nucléaire, Hôpital Saint-Louis, F-75010 Paris and [6]APHP, Service d'Aphérèse Thérapeutique, Hôpital Saint-Louis, F-75010 Paris, France

Correspondence:
STEPHANE GIRAUDIER - stephane.giraudier@aphp.fr

doi:10.3324/haematol.2020.249409

Disclosures: no conflicts of interest to disclose.

Contributions: LD, OR, JS, CC, CD, NP, AB, JJK and SG followed the patients; LD, CB and SG collected data; MHS, NM and BC performed biological analysis; LD, BC, JJK and SG analyzed the data and wrote the paper.

Acknowledgments: the authors particularly thank Veronique Lenoble, Veronique Tran and Armelle Yollant for their technical assistance and commitment during this work. They also thank the local tumor biobank of Saint Louis Hospital for providing high quality samples.

Funding: this work was also supported by a grant from the National Institute of Cancer (INCa, TRANSLA CTIM3).

References

1. Nutritional anaemias. Report of a WHO scientific group. World Health Organ Tech Rep Ser. 1968;405:5-37.
2. Takei T, Amin NA, Schmid G, Dhingra-Kumar N, Rugg D. Progress in global blood safety for HIV. J Acquir Immune Defic Syndr. 2009; 52 Suppl 2:S127-S131.
3. Otto JM, Plumb JOM, Clissold E, et al. Hemoglobin concentration, total hemoglobin mass and plasma volume in patients: implications

for anemia. Haematologica. 2017;102(9):1477-1485.
4. WHO. Haemoglobin concentrations for the diagnosis of anaemia and assessment of severity. WHO. Available from: http://www.who.int/vmnis/indicators/haemoglobin/en/
5. Pearson TC, Guthrie DL, Simpson J, et al. Interpretation of measured red cell mass and plasma volume in adults: Expert Panel on Radionuclides of the International Council for Standardization in Haematology. Br J Haematol. 1995;89(4):748-756.
6. Beguin Y, Clemons GK, Pootrakul P, Fillet G. Quantitative assessment of erythropoiesis and functional classification of anemia based on measurements of serum transferrin receptor and erythropoietin. Blood. 1993;81(4):1067-1076.
7. Maslah N, Soret J, Dosquet C, et al. Masked polycythemia vera: analysis of a single center cohort of 2480 red cell masses. Haematologica. 2020;105(3):e95-e97.

Reveromycin A, a novel acid-seeking agent, ameliorates bone destruction and tumor growth in multiple myeloma

Along with the progression of bone disease, the bone marrow (BM) microenvironment is skewed in multiple myeloma (MM). This underlies the unique pathophysiology of MM, and confers aggressiveness and drug resistance. Receptor activator of NF-κB ligand (RANKL), a critical mediator of osteoclastogenesis, is upregulated to extensively enhance osteoclastogenesis and bone resorption in MM. Importantly, activated osteoclasts (OC) in turn enhance glycolysis in MM cells and thereby MM cell proliferation, leading to the formation of a vicious cycle between MM tumor expansion and osteoclastic bone destruction.[1-3] OC should therefore be targeted to improve treatment efficacy, especially in MM cells

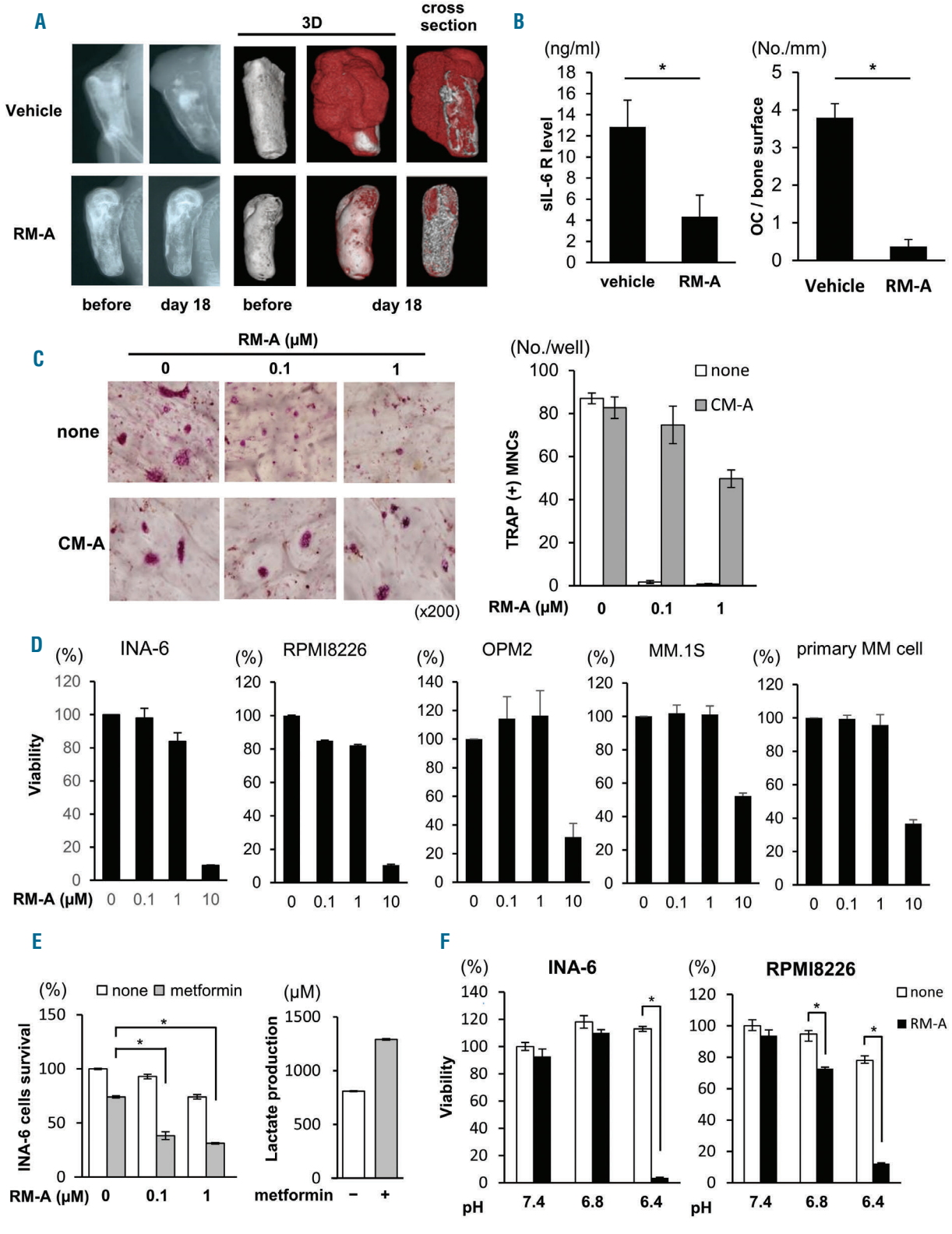


Figure 1. Effects of reveromycin A (RM-A) on osteoclasts (OC) and multiple myeloma (MM) cell viability. (A) Effects of RM-A on MM cell-bearing SCID-rab models. To prepare SCID-rab mice, rabbit femurs were cut into two and implanted subcutaneously in SCID mice. A month later the human MM cell line INA6 was inoculated directly into the bone marrow (BM) cavity in the rabbit bones implanted in SCID mice. After confirming the MM cell growth at 4 weeks after the MM cell inoculation, we started to inject RM-A at 4 mg/kg or a vehicle (saline) to the mice (n=5 for each treatment) intraperitoneally twice daily for 18 days. Soft X-ray and micro-computed tomography (μCT) images of the implanted rabbit femurs were taken before and after the treatment with RM-A or a vehicle. Representative images of soft X-ray (left panels) and μCT (right panels) are shown. MM tumor lesions are shown in red in 3D and cross sections of the rabbit bones in μCT images. (B) INA-6 cell-derived human soluble IL-6 receptor (sIL-6R) levels in mouse sera were measured as a marker for MM tumor burden after the treatment for 18 days with RM-A or a vehicle. The rabbit bones were taken out and analyzed to count the numbers of OC over bone surface (OC/bone surface). Data are expressed as the mean±standard error (SE). (C) Rabbit BM cells were cultured on the bovine bone slice in 96-well culture plates in RPMI1640 containing 10% fetal bovine serum with 20 ng/mL soluble receptor activator of NF-κB ligand (RANKL) for 4 days. After washing, RM-A at the indicated concentrations was added in triplicate for 24 hours (h) in the presence or absence of concanamycin A (CM-A) at 100 nM. The cells were then stained with tartrate-resistant acid phosphatase (TRAP), and photos were taken (original magnitude, x200) (left). The numbers of TRAP-positive multinucleated cells (MNC) with three and more nuclei were counted (right). Data were expressed as % changes from the baseline (mean±SE). (D) INA-6, RPMI8226, OPM2 and MM.1S MM cell lines and primary MM cells were cultured at $2x10^5$/mL for 24 h at the indicated concentrations of RM-A. Viable cell numbers were counted with a WST-8 assay. The data were expressed as % changes from the baseline (mean±SE). (E) INA-6 cells were cultured in triplicate for 24 h in the presence of RM-A at the indicated concentrations with or without 5 mM metformin. Cell viability was analyzed by a WST-8 assay (left). The results were expressed as % changes from the baseline without any treatment (mean±SE. *P<0.05). Lactate levels in the culture supernatants were measured after the treatment with metformin for 24 h. (F) INA-6 and RPMI8226 MM cells were cultured in triplicate in the media whose pH values were adjusted by sodium hydroxide or lactic acid. RM-A was added at 1.0 μM. After culturing for 24 h, cell viability was analyzed by a WST-8 assay. Results were expressed as mean±SE. *P<0.05.

expanding in the BM with enhanced osteoclastogenesis.

Under low O_2 conditions, and as a consequence of glycolysis (the Warburg effect), cancer cells highly produce protons and lactate, leading to an extracellular acidification to pH 6.4-7.0, while pH values are 7.2-7.4 in normal tissues.[4] Activated OC on the bone surface abundantly secrete protons into excavated pits (~pH 4-5) to resorb bone while acidifying their close vicinity.[5] In osteolytic bone lesions in MM, therefore, the MM cell-OC interaction appears to create a highly acidic milieu by protons produced by OC and lactate by proliferating glycolytic MM cells. We reported that acid activates the PI3K-Akt signaling to upregulate the acid sensor TRPV1 in MM cells, thereby forming a positive feedback loop between acid sensing and the PI3K-Akt survival signaling.[6] In addition, tumor acidity has been demonstrated to blunt cytotoxic effects of various chemotherapeutic agents as well as the activity of immune effecter cells.[7,8] Therefore, acidic conditions should be targeted to improve the therapeutic efficacy against MM.

Reveromycin A (RM-A) is a small microbial metabolite with three carboxylic groups, isolated from *Streptomyces* sp. SN-593.[9,10] In an acidic microenvironment, RM-A becomes a non-polar form, which is able to permeate a cell membrane and induce apoptosis by inhibiting isoleucine tRNA synthesis.[9,10] As such, RM-A has been demonstrated to preferentially induce apoptosis in acid-producing OC but not in other types of normal cells.[9-11] In the present study, we explored whether RM-A targets an acidic condition induced by the MM cell-OC interaction to alleviate tumor expansion and bone destruction in MM.

To clarify anti-tumor activity of RM-A against MM, we examined the *in vivo* effects of RM-A in animal models mimicking MM bone lesions. The human MM cell line INA6 was inoculated into rabbit femurs subcutaneously implanted in SCID mice (SCID-rab), as previously reported.[12] SCID-rab mice have been demonstrated to allow human MM cells to grow within the rabbit bones and induce bone destructive lesions as in patients with MM. In vehicle-treated mice, marked radiolucent osteolytic lesions were observed in the implanted rabbit bones on X-ray and micro-computed tomography (μCT) images, and MM tumor was packed in the BM cavity and expanded outside the rabbit bones (Figure 1A). However, in RM-A-treated mice, MM tumor markedly decreased in size without apparent bone destruction in rabbit bones. The levels of human soluble IL-6 receptor in mouse sera, a marker of human MM tumor burden, were also substantially reduced in the RM-A-treated mice (Figure 1B). OC numbers were increased in bone specimens from vehicle-treated SCID-rab mice; however, they were markedly reduced in RM-A-treated mice (Figure 1B). These results suggest that RM-A can suppress MM cell growth in the BM along with preventing bone destruction and loss *in vivo*.

To further investigate the effects of RM-A, we first generated OC on bone slices from whole rabbit BM cells, and then treated them with RM-A. Large multinucleated tartrate-resistant acid phosphatase (TRAP)-positive mature OC almost completely disappeared upon treatment with RM-A at 100 nM for 12 hours (h) (Figure 1C). Interestingly, blockade of acid release from OC by the proton pump inhibitor concanamycin A abolished the cytotoxic effect of RM-A on OC, indicating the critical role of acid released from OC in triggering the cytotoxic activity of RM-A. In contrast to OC, RM-A did not affect the viability of MM cell lines and primary MM cells even at higher concentrations up to 1 μM at 24 h (Figure 1D). However, RM-A was able to induce MM cell death even at concentrations as low as 100 nM when lactate production from MM cells was enhanced by metformin (Figure 1E). Furthermore, RM-A at 1 μM was able to induce cell death in MM cells when culture media were acidified to be at pH6.4 with exogenously added lactic acid (Figure 1F). These results suggest that acid-producing OC are highly susceptible to RM-A, and that an acidic milieu with lactate can trigger the cytocidal effects of RM-A against MM cells.

We next dissected the mechanisms of the MM cell death in acidic conditions by RM-A. RM-A induced apoptosis in MM cells at pH6.4 but not at pH7.4, as indicated with annexin V-propidium iodine dual staining (Figure 2A). RM-A activated caspase-8 as well as caspase-9 in MM cells at pH6.4 (Figure 2B andC), indicating the induction of caspase-dependent apoptosis. The transcription factor Sp1 has been demonstrated to be overexpressed and to act as a critical pro-survival mediator in MM cells.[13,14] In parallel with the caspase-8 activation, the protein levels of Sp1 were reduced in MM cells at pH6.4 but not at pH6.8 nor pH7.4 (Figure 2B). However, Sp1 mRNA was not decreased in MM cells even at pH6.4. We previously reported that Sp1 protein is subject to enzymatic degradation by caspase-8, thereby inducing MM cell death.[14] Consistent with the previous observation,[14] treatment with the caspase-8 inhibitor z-IETD-FMK abolished the reduction of Sp1 protein at pH6.4 (Figure 2D), indicating caspase-8-mediated degradation of Sp1 protein. Furthermore, treatment with the Sp1 inhibitor terameprocol was able to reduce its target molecules critical for MM cell growth and survival, PIM2[15] and MYC[14,15] (Figure 2E). Consistently, PIM2 and MYC levels were decreased

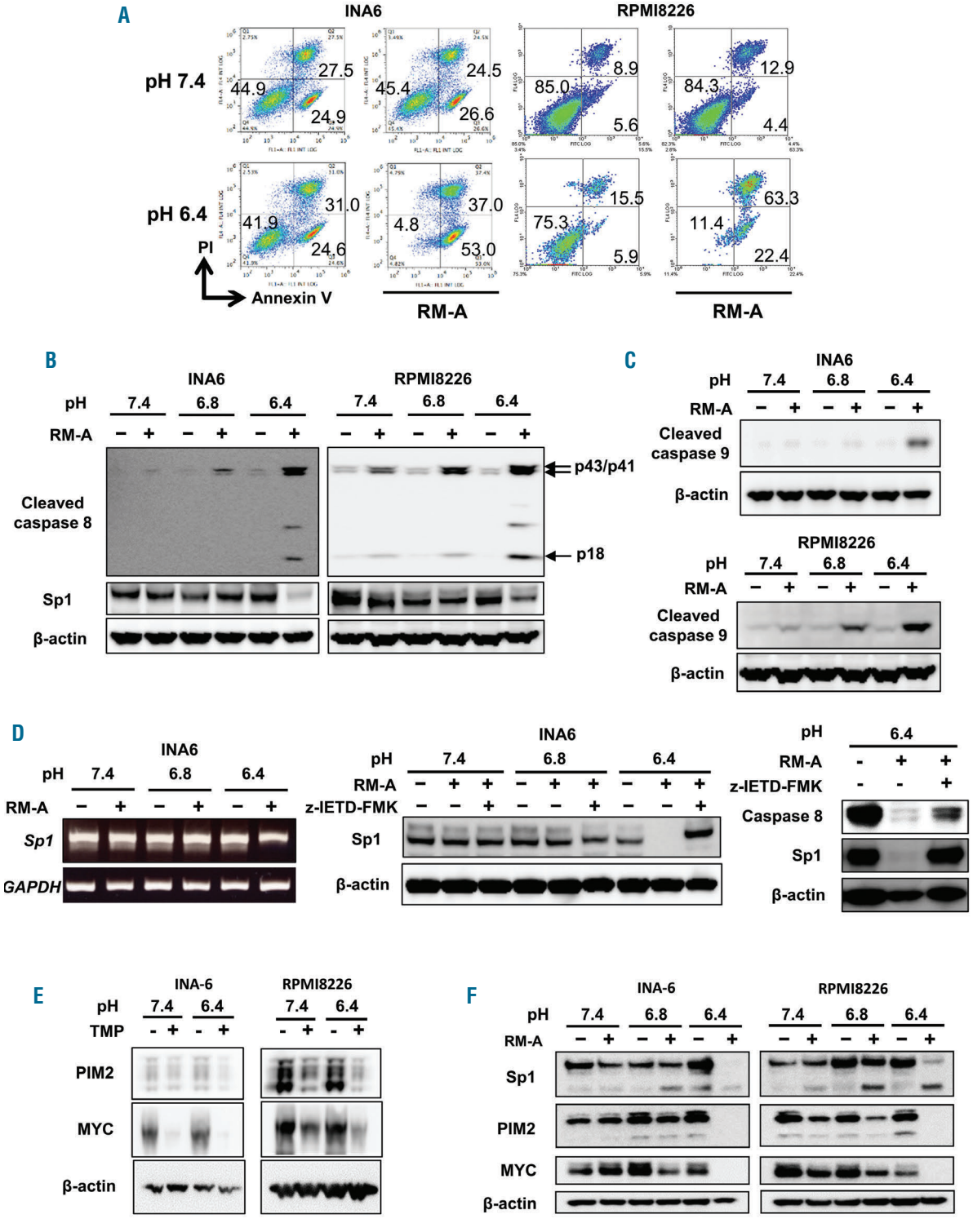


Figure 2. Induction of multiple myeloma (MM) cell apoptosis by reveromycin A (RM-A). (A) INA-6 and RPMI8226 MM cells were cultured for 24 hours (h) at pH 7.4 or 6.4 in the presence or absence of RM-A at 1 μM. Apoptotic cells were evaluated with annexin V and propidium iodide staining by flow cytometry. Distributions (%) of cells in each column are indicated. (B and C) INA-6 and RPMI8226 MM cells were cultured for 24 h at different pH values as indicated in the presence or absence of RM-A at 1 μM. The protein levels of cleaved caspase-8 and Sp1 (B) and cleaved caspase-9 (C) were analyzed by western blotting. β-actin was used as a protein loading control. (D) INA-6 cells were cultured for 24 h at the indicated pH values in the presence or absence of RM-A at 1 μM. *Sp1* mRNA levels were analyzed by reverse transcription-polymerase chain reaction (RT-PCR) (left). *GAPDH* served as an internal control. The caspase-8 inhibitor z-IETD-FMK at 100 μM was added together with RM-A as indicated. Sp1 and caspase 8 protein levels were analyzed by western blotting (right). β-actin was used as a protein loading control. (E) INA-6 and RPMI8226 MM cells were cultured for 24 h at pH 7.4 or 6.4 in the presence or absence of the Sp1 inhibitor terameprocol (TMP) at 50 μM. PIM2 and MYC protein levels were analyzed by western blotting. β-actin was used as a protein loading control. (F) INA-6 and RPMI8226 cells were cultured for 24 h at the indicated pH values in the presence or absence of RM-A at 1 μM. The protein levels of Sp1, PIM2 and MYC were analyzed by western blotting. β-actin was used as a protein loading control.

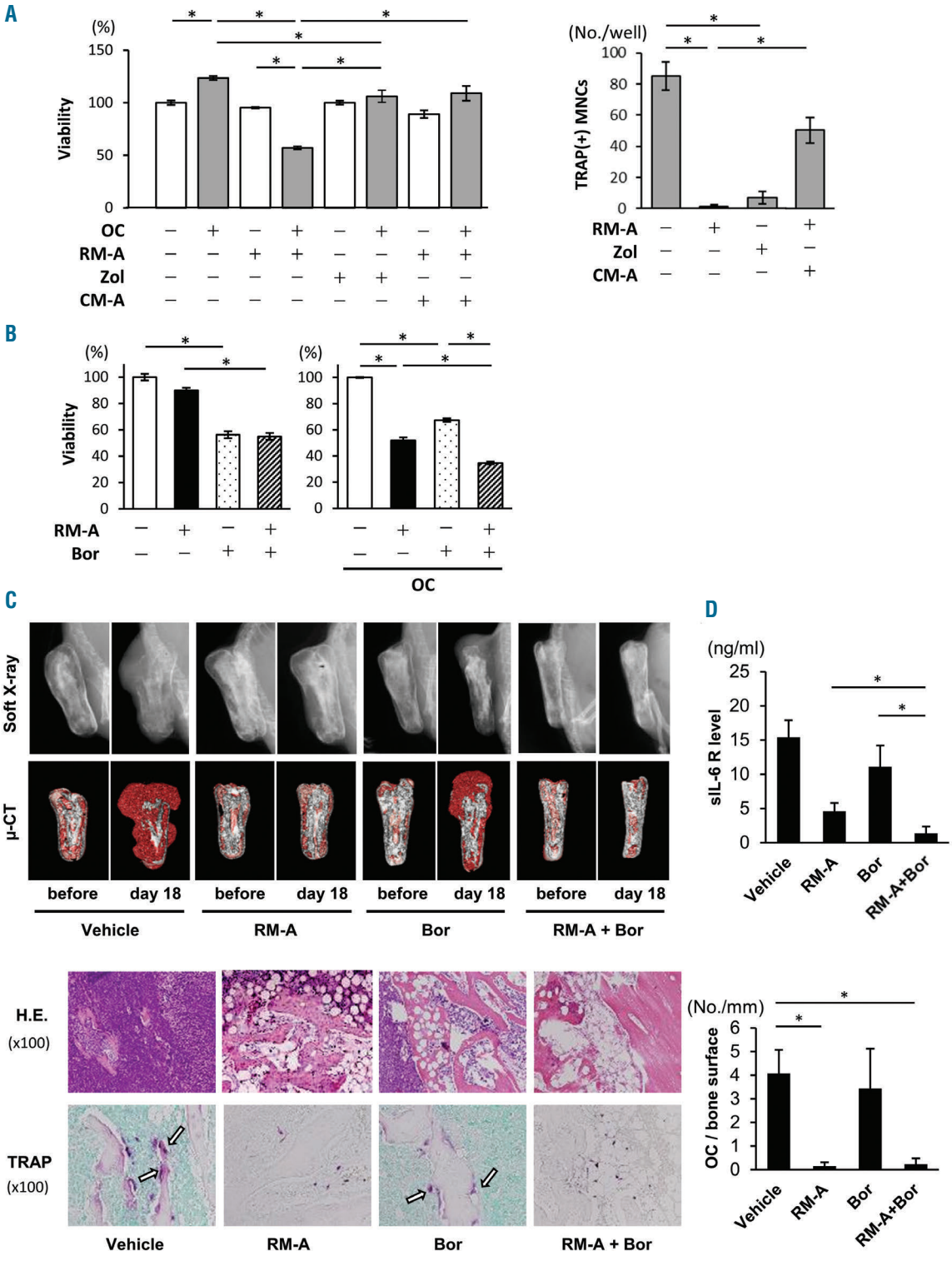


Figure 3. Cytotoxic effects of reveromycin A (RM-A) on multiple myeloma (MM) cells in combination with bortezomib. (A) Rabbit bone marrow cells were cultured on bone slices in the presence of soluble receptor activator of NF-κB ligand (RANKL) to generate osteoclasts (OC). INA-6 cells labeled with the fluorescein dye PKH26 at $1x10^6$/mL were co-cultured with the OC generated on bone slices or cultured alone on bone slices. RM-A (1 μM), zoledronic acid (Zol) (5 μM), or CM-A (100 nM) were added as indicated. After culturing for 12 hours (h), 7-AAD was added to stain dead cells. (B) RM-A at 1 μM and/or bortezomib (Bor) at 5 nM were added as indicated. After culturing for 24 h, 7-AAD was added to stain dead cells. The distribution of 7-AAD-negative alive cells was counted within PKH-labeled MM cells in flow cytometry. Results were expressed as % changes from the baselines. (C) INA6 cell-bearing SCID-rab models as described in Figure 1A were prepared. RM-A (4 mg/kg, twice a day) and/or bortezomib (Bor) (0.5 mg/kg, twice a week) were intraperitoneally injected for 18 days (n=5 for each treatment). Saline was injected as a vehicle. Soft X-ray and micro-computed tomography (μCT) images ware taken before and after the treatment. Representative images of soft X-ray (upper panels) and μCT (lower panels) are shown. Soft tissue area is shown in red in cross sections of the rabbit bones in μCT images. (D) INA-6 cell-derived sIL-6R levels in mouse sera were measured after the treatment. (E) Hematoxylin and eosin (H&E) (upper) and tartrate-resistant acid phosphatase (TRAP) (lower) staining was performed in the rabbit bones resected from SCID-rab mice. White arrows indicate TRAP-positive OC. The rabbit bones were further analyzed to count the numbers of OC over bone surface (OC/bone surface). Data are expressed as the mean ± standard error..

in MM cells preferentially at pH6.4 in parallel with the reduction of Sp1 protein by RM-A.

Because an extracellular acidification makes RM-A permeate cell membrane to induce apoptosis, it is plausible that an acidic milieu created by the OC-MM cell interaction rather induces cytotoxic activity by RM-A against MM cells as well as acid-producing OC. To clarify whether RM-A affects MM cell viability in the presence of OC, we next examined the cytotoxic effects of RM-A on MM cells in co-cultures with OC on bone slices generated from rabbit BM cells. RM-A at 1 μM was able to decrease the MM cell viability in the co-cultures with OC, although RM-A at this concentration did not affect MM cell viability when MM cells were cultured alone (Figure 3A, left). When the bisphosphonate zoledronic acid was added to deplete mature OC, viable INA6 cells were decreased in number in co-cultures with OC to the levels observed in the cultures of INA6 cells alone. RM-A reduced the viability of INA6 cells more potently than zoledronic acid in the presence of OC, although RM-A and zoledronic acid similarly reduced the numbers of TRAP-positive multinucleated OC (Figure 3A, right), suggesting that the anti-MM effects of RM-A is not merely due to depletion of mature OC. Blockade of acid release by the proton pump inhibitor concanamycin A abolished the cytotoxic effects of RM-A on MM cells in the co-cultures with OC. These results suggest that RM-A not only impairs OC but also disrupts the OC-MM cell interaction.

We next examined the combinatory effects of RM-A with the proteasome inhibitor bortezomib. Although bortezomib was able to induce MM cell death, the cytotoxic effects of bortezomib on MM cells were mitigated in co-cultures with OC (Figure 3B), indicating drug resistance by OC. However, RM-A impaired the viability of MM cells cultured in the presence of OC; and further potentiated the cytotoxic effects on MM cells in combination with bortezomib, suggesting that RM-A overcomes the drug resistance induced by OC. Finally, we validated the combinatory therapeutic effects of RM-A and bortezomib *in vivo*, using human MM cell-bearing SCID-rab models. Treatment with RM-A suppressed bone destruction and MM tumor growth; importantly, the suppressive effects of RM-A on MM tumor growth and bone destruction was further enhanced in combination with bortezomib, as shown in X-ray and μCT images and the levels of human soluble IL-6 receptor in mouse sera, a marker of MM tumor burden (Figure 3D). In histological analyses, MM cells were tightly packed in the BM cavity of the rabbit bones while bone trabeculae decreased in size with the appearance of multinucleated OC on the surfaces of the remaining bone (Figure 3E). RM-A, but not bortezomib, markedly reduced the number of OC in the SCID-rab mouse MM lesions (Figure 3E). However, treatment with RM-A and bortezomib cooperatively reduced MM tumors along with the disappearance of TRAP-positive large OC on the bone surface.

These results collectively suggest that the acidic microenvironment produced by the MM-OC interaction enhances MM tumor progression but can trigger the cytotoxic effects of RM-A on MM cells as well as acid-producing OC. Given that an acidic condition makes MM cells resistant to chemotherapeutic agents, RM-A could be a candidate to target MM cells at acidic bone lesions, and augment the therapeutic efficacy of currently available anti-MM agents which are active at non-acidic sites.

Keiichiro Watanabe,[1,2] Ariunzaya Bat-Erdene,[3*] Hirofumi Tenshin,[1,2*] Qu Cui,[4] Jumpei Teramachi,[5] Masahiro Hiasa,[2] Asuka Oda,[1] Takeshi Harada,[1] Hirokazu Miki,[6] Kimiko Sogabe,[1] Masahiro Oura,[1] Ryohei Sumitani,[1] Yukari Mitsui,[1] Itsuro Endo,[1] Eiji Tanaka,[2] Makoto Kawatani,[7] Hiroyuki Osada,[7] Toshio Matsumoto[8] and Masahiro Abe[1]*

[1]*Department of Hematology, Endocrinology and Metabolism, Institute of Biomedical Sciences, Tokushima University Graduate School, Tokushima, Japan;* [2]*Department of Orthodontics and Dentofacial Orthopedics, Institute of Biomedical Sciences, Tokushima University Graduate School, Tokushima, Japan;* [3]*Department of Immunology, School of Bio-Medicine, Mongolian National University of Medical Sciences, Ulaanbaatar, Mongolia;* [4]*Department of Hematology, Beijing Tiantan Hospital, Capital Medical University, Beijing, China;* [5]*Department of Tissue Regeneration, Institute of Biomedical Sciences, Tokushima University Graduate School, Japan;* [6]*Division of Transfusion Medicine and Cell Therapy, Tokushima University Hospital, Tokushima, Japan;* [7]*RIKEN Center for Sustainable Resource Science, Chemical Biology Research Group, Saitama, Japan and* [8]*Fujii Memorial Institute of Medical Sciences, Tokushima University, Tokushima, Japan*

**KW, AB and HT contributed equally as co-first authors.*

Correspondence:
MASAHIRO ABE - masabe@tokushima-u.ac.jp

doi:10.3324/haematol.2019.244418

Disclosures: MA received research funding from Chugai Pharmaceutical, Sanofi KK, Pfizer Seiyaku KK, Kyowa Hakko Kirin, MSD KK, Astellas Pharma, Takeda Pharmaceutical, Teijin Pharma and Ono Pharmaceutical, and honoraria from Daiichi Sankyo Company. The other authors declare no competing financial interests.

Contributions: KW, AB, HT, MK, HO and MA designed the research and conceived the project. Animal experiments were performed by KW, QC, HT, TH, HM, KS, MO, RS and JT; cell cultures by KW, AB, HT, AO, TH, KS, MO and RS; immunoblotting by AB, JT, HT, AO and MH; and bone analyses by KW, QC, YM, MH, IE, and ET. KW, AB, HT, MK, HO, TM and MA analyzed and discussed the data, and wrote the manuscript.

Funding: this work was supported in part by JSPS KAKENHI grant ns. JP15K20536, JP16K11504, JP17KK0169, JP17K09956, JP17H05104, JP18K08329, JP18K16118, and JP18H06294, and the Research Clusters program of Tokushima University. The funders had no role in study design, data collection and analysis, the decision to publish or the preparation of the manuscript. The authors would like to thank Dr. Toshihiko Nogawa (RIKEN) for preparing reveromycin A.

References

1. Abe M, Hiura K, Wilde J, et al. Osteoclasts enhance myeloma cell growth and survival via cell-cell contact: a vicious cycle between bone destruction and myeloma expansion. Blood. 2004;104(8):2484-2491.
2. Lawson MA, McDonald MM, Kovacic N, et al. Osteoclasts control reactivation of dormant myeloma cells by remodelling the endosteal niche. Nat Commun. 2015;6:8983.
3. Nakano A, Miki H, Nakamura S, et al. Up-regulation of hexokinase II in myeloma cells: targeting myeloma cells with 3-bromopyruvate. J Bioenerg Biomembr. 2012;44(1):31-38.
4. Ji K, Mayernik L, Moin K, Sloane BF. Acidosis and proteolysis in the tumor microenvironment. Cancer Metastasis Rev. 2019;38(1-2):103-112.
5. Teitelbaum SL. Bone resorption by osteoclasts. Science. 2000; 289(5484):1504-1508.
6. Amachi R, Hiasa M, Teramachi J, et al. A vicious cycle between acid sensing and survival signaling in myeloma cells: acid-induced epigenetic alteration. Oncotarget. 2016;7(43):70447-70461.
7. Gerweck LE, Vijayappa S, Kozin S. Tumor pH controls the in vivo efficacy of weak acid and base chemotherapeutics. Mol Cancer Ther. 2006;5(5):1275-1279.
8. Tannock IF, Rotin D. Acid pH in tumors and its potential for therapeutic exploitation. Cancer Res. 1989;49(16):4373-4384.
9. Kawatani M, Osada H. Osteoclast-targeting small molecules for the

treatment of neoplastic bone metastases. Cancer Sci. 2009; 100(11): 1999-2005.
10. Woo JT, Kawatani M, Kato M, et al. Reveromycin A, an agent for osteoporosis, inhibits bone resorption by inducing apoptosis specifically in osteoclasts. Proc Natl Acad Sci U S A. 2006;103(12):4729-4734.
11. Muguruma H, Yano S, Kakiuchi S, et al. Reveromycin A inhibits osteolytic bone metastasis of small-cell lung cancer cells, SBC-5, through an antiosteoclastic activity. Clin Cancer Res. 2005;11(24 Pt 1):8822-8828.
12. Takeuchi K, Abe M, Hiasa M, et al. Tgf-Beta inhibition restores terminal osteoblast differentiation to suppress myeloma growth. PLoS One. 2010;5(3):e9870.
13. Fulciniti M, Amin S, Nanjappa P, et al. Significant biological role of sp1 transactivation in multiple myeloma. Clin Cancer Res. 2011; 17(20):6500-6509.
14. Bat-Erdene A, Miki H, Oda A, et al. Synergistic targeting of Sp1, a critical transcription factor for myeloma cell growth and survival, by panobinostat and proteasome inhibitors. Oncotarget. 2016;7(48): 79064-79075.
15. Asano J, Nakano A, Oda A, et al. The serine/threonine kinase Pim-2 is a novel anti-apoptotic mediator in myeloma cells. Leukemia. 2011;25(7):1182-1188.

Infrequent "chronic lymphocytic leukemia-specific" immunoglobulin stereotypes in aged individuals with or without low-count monoclonal B-cell lymphocytosis

Chronic lymphocytic leukemia (CLL) is a chronic, incurable malignancy of antigen-experienced B cells, mainly affecting the aged population.[1] Immunogenetic analysis in CLL revealed the existence of subsets of patients expressing stereotyped B-cell receptor immunoglobulins (BcR IG),[2] which represent homogeneous CLL variants with distinct biological and clinical characteristics.[3] Little is known regarding the presence of "CLL-specific", stereotyped BcR IG within the repertoire of healthy individuals. Low-throughput studies[4] led to the identification of cases with stereotyped BcR IG, followed by next-generation sequencing studies that found CLL stereotypes in normal B-cell populations, albeit at very low frequencies.[5]

This issue is more pertinent to monoclonal B-cell lymphocytosis (MBL), characterized by clonal "CLL-like" B-cell expansions detected in 3-12% of the population.[6] "CLL-like" MBL is categorized into high-count (HC-MBL) and low-count (LC-MBL) forms, based on a cutoff of $0.5x10^9$ cells/L.[6] Previously, we showed that HC-MBL was immunogenetically similar to CLL, whereas LC-MBL was characterized by low frequency and different characteristics of stereotyped BcR IG.[7] However, this evidence derived from low-throughput data and was, thus, inherently limited with regards to reflecting the complexity of the BcR IG repertoire.

Here, using a high-throughput methodology we analyzed the composition of the BcR IG repertoire expressed by: (i) clonal and normal B cells from individuals with "CLL-like" LC-MBL (n=23), as well as (ii) naïve and memory B cells from age-matched, healthy individuals (n=6) (*Online Supplementary Table S1*).

Blood samples (5 mL) were obtained from all individuals and cell-sorted within 24 hours. IGHV-IGHD-IGHJ gene rearrangements were amplified by polymerase chain reaction, sequenced on the MiSeq platform and bioinformatically processed (*Online Supplementary Methods*).

Overall, we identified 592,023 unique BcR IG clonotypes. Of these, 238,075 (40.2%) were expanded (>1 read) and distributed across sample categories as follows: (i) individuals with LC-MBL: 9,014 clonotypes in MBL cell samples (mean: 751/sample); 29,587 clonotypes in peripheral blood mononuclear cell (PBMC) samples (mean: 2,690/sample); and 88,366 clonotypes in normal B-cell samples (mean: 11,046/sample); (ii) healthy individuals: 67,358 clonotypes in naïve B-cell samples (mean: 11,226/sample); and 43,750 clonotypes in memory B-cell samples (mean: 8,750/sample) (*Online Supplementary Table S2*). The presence of stronger biases in the normal B-cell compartment of individuals with LC-MBL compared to that of healthy donors is in line with the hypothesis of an impaired pre-germinal center B-cell production in LC-MBL, which would lead to a limited B-cell repertoire.[8]

Clonality assessment focused on abundant clonotypes (individual frequency >0.92%; *Online Supplementary Methods*). In total, 222 abundant clonotypes were identi-

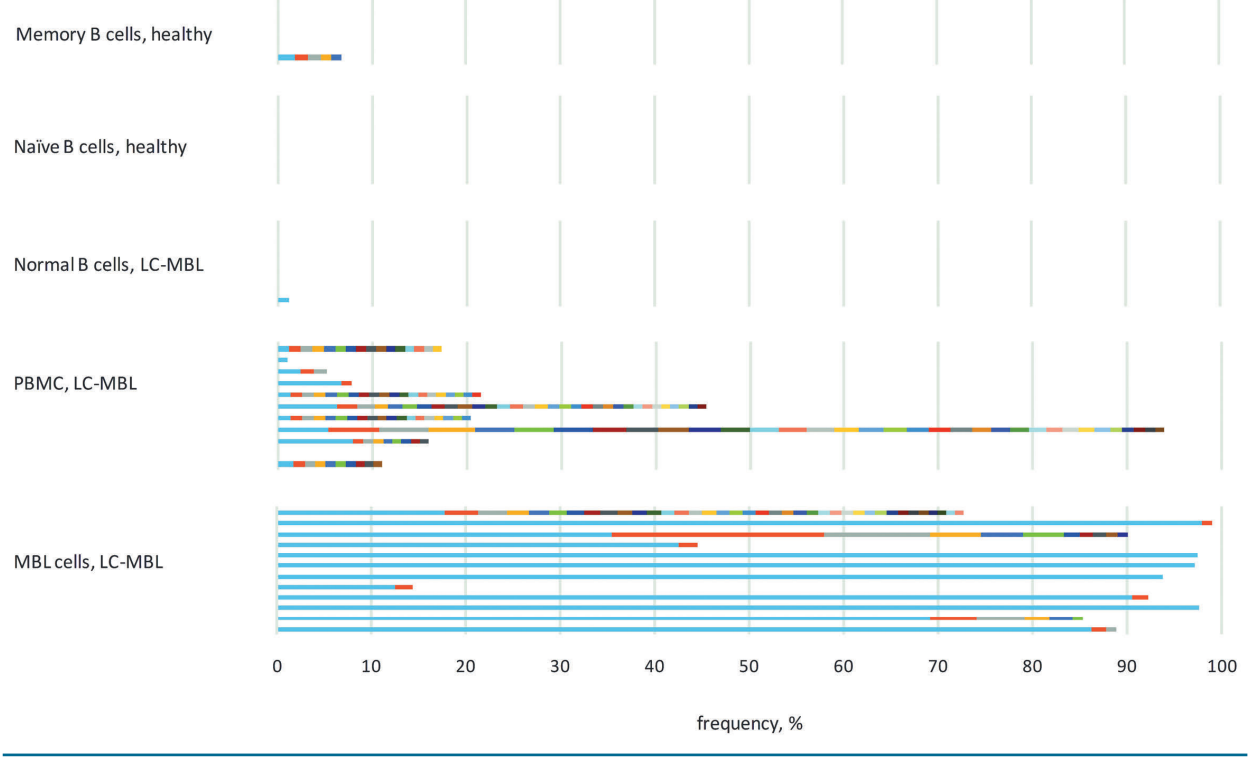


Figure 1. The B-cell receptor immunoglobulin clonotype repertoire. The B-cell receptor immunoglobulin clonotype repertoire is more clonal in monoclonal B-cell lymphocytosis (MBL) cell samples, albeit at heterogeneous levels. MBL cell samples displayed either monoclonal or oligoclonal immunoglobulin gene repertoire profiles. Heterogeneity was also evident in peripheral blood mononuclear cell samples from individuals with MBL in whom both oligo- and polyclonal cases were evident. All normal B-cell populations were polyclonal and essentially devoid of abundant clonotypes. Each lane corresponds to an individual sample, whereas the color code represents the ranking of abundant clonotypes (individual frequency of >0.92%) based on their relative frequency. LC: low count; MBL: monoclonal B-cell lymphocytosis; PBMC: peripheral blood mononuclear cells.

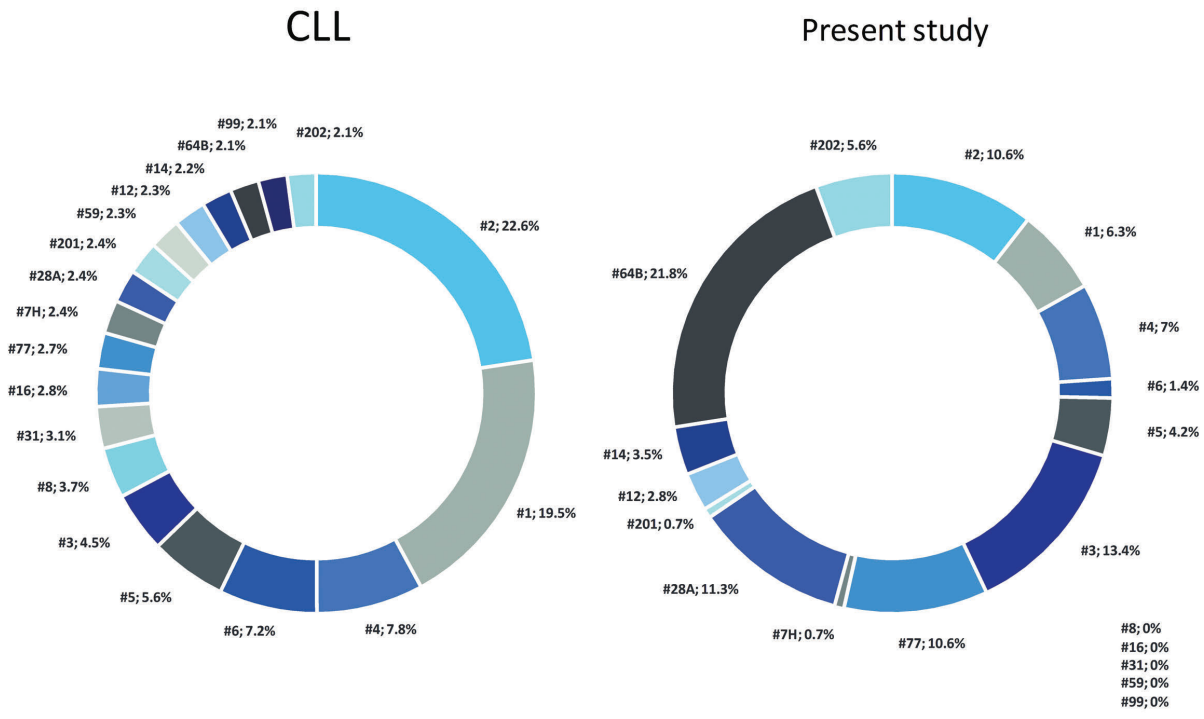


Figure 2. Frequencies of major chronic lymphocytic leukemia stereotyped clonotypes. The major chronic lymphocytic leukemia (CLL) stereotyped clonotypes were few, expressed at very low frequencies and did not follow the trend observed in CLL. The relative frequencies of major stereotypes in the present study was distinct from the one we previously reported in CLL.[5] Characteristic examples were the low relative frequencies of subsets #1 and #2 as well as the complete absence of B-cell receptor immunoglobulins belonging to subsets #8, #16, #31, #59 and #99.

fied (*Online Supplementary Table S3*), of which 216 (97.3%) belonged to either the MBL (70/222, 31.5%) or the PBMC samples (146/222, 65.8%) from LC-MBL. The average number of abundant clonotypes per sample was 6.4 for the MBL cell samples, 9.8 for the PBMC samples and ≤1 for all sample categories of normal B cells.

With regards to clonality, the majority of samples (9/12, 75%) displayed a monoclonal pattern characterized by the presence of a single abundant clonotype dominating the repertoire (frequency range, 42.5-97.9%). The remaining three samples (MBL-5, MBL-10 and MBL-12) were characterized by an oligoclonal pattern. The median LC-MBL clone size was large (6.5 cells/μL), especially when compared to that in populations of Asian origin (median: 0.12 cells/μL),[9] perhaps linked to the low prevalence of oligoclonality in our cohort. The assessment of the relation between the size of the MBL clone and the level of clonality (Spearman rho correlation coefficient) showed a positive trend, in line with previous studies showing a lower frequency of oligoclonality along the spectrum from LC-MBL to HC-MBL and, eventually, CLL.[9] However, results were not statistically significant (P=0.18), perhaps because of the small size of the cohort. No correlations were found between clone size and age, sex or cytogenetic aberrations.

All but one PBMC sample from LC-MBL carried abundant clonotypes (10/11, 90.9%), yet a relatively high-frequency clonotype (individual frequency of >6%) was identified in 3/11 samples (27.3%). Finally, normal B-cell samples were clearly polyclonal without significant expansions; only four abundant clonotypes were identified in two samples, but with very low frequencies (range, 1.1-1.8%). Figure 1 illustrates the clonality patterns in all sample groups. As expected, LC-MBL cell populations displayed high levels of clonality, thus clearly differing from the polyclonal normal B-cell populations. Such differences in clonality patterns among LC-MBL cell samples may reflect different timepoints in the process of clonal evolution. In other words, LC-MBL could initially involve a polyclonal B-cell population that at some point acquires the CLL phenotype due to sustained antigenic stimulation. The specific immunogenetic characteristics of the BcR IG along with the progressive acquisition of genetic lesions, e.g., cytogenetic alterations,[10] by individual MBL clones could drive their expansion, thus leading to oligoclonal and, eventually, monoclonal LC-MBL cell populations, as proposed previously.[9]

The IGHV gene repertoire was characterized by significant restrictions in all sample categories (*Online Supplementary Table S4*). The application of a 5% frequency cutoff led to the identification of seven frequent IGHV genes in the MBL cell category, which collectively accounted for 38.1% of the total repertoire. With regard to normal B cells from individuals with and without LC-MBL, restrictions were less pronounced with four and three frequent IGHV genes, respectively. Analysis at the individual IGHV gene level revealed statistically significant differences in the expression of two frequent genes (*IGHV3-23, IGHV3-30*) and ten low-frequency IGHV genes (analysis of variance, P<0.05) (*Online Supplementary Table S5*, Figure 2). These differences concerned mostly the category of normal B cells from healthy individuals who, overall, displayed a distinct IGHV repertoire compared to that of individuals with LC-MBL. Biases in the IGHD and IGHJ gene repertoires were evident in all sample categories (*Online Supplementary Tables S6* and *S7*). Overall, the existence of distinct biases in the IGHV gene repertoire, especially between $CD5^+$ CLL-like cells from individuals with LC-MBL and normal (mostly $CD5^-$) B cells, point towards different selection processes and

functions of these B-cell subpopulations. In order to identify BcR IG stereotypes, we applied our purpose-built algorithm[2] on all abundant BcR IG clonotypes (frequency of >0.92%) of the present cohort along with 30,221 CLL clonotypes from the IMGT/CLL-DB (*http://www.imgt.org/CLLDBInterface/query*). According to our findings, 43/222 (19.4%) abundant clonotypes were assigned to 42 distinct clusters (*Online Supplementary Table S8*).

The vast majority of abundant clonotypes with stereotyped VH CDR3 (42/43, 97.7%) were found in samples from individuals with LC-MBL (12 in MBL cell samples and 30 in PBMC samples). Virtually all abundant stereotyped LC-MBL clonotypes (47/48, 97.9%) were assigned to minor clusters with a mean size of four clonotypes (range, 2-22 clonotypes). Only a single abundant clonotype was assigned to a large CLL subset, namely subset #148B[11] (CLUSTER-4-0003), which contained 150 clonotypes in the current analysis. Hence, "CLL-specific" stereotyped clonotypes were observed in most samples, yet these were scant and, for the most part, exhibited low frequency. In the case of subset #148B, which was the only well-documented CLL subset from the present analysis, its biological and clinical characteristics were "compatible" with LC-MBL: a high frequency of del(13q), low frequency of CD38 positivity, young age at diagnosis and a long time to first treatment (9.2 years).[11]

The complete absence of "CLL-specific" BcR IG stereotypes belonging to major CLL stereotyped subsets[2] prompted us to search for such sequences among all expanded BcR IG clonotypes (>1 sequence), irrespective of individual clonotype frequency. We identified 142 of 238,075 (0.0006%) clonotypes belonging to 14 major CLL subsets (*Online Supplementary Table S9*) in 27/42 samples (64.3%) from all sample categories, although at very low frequencies (range, 0.0002-0.28%). Most "CLL-specific" BcR IG stereotypes were found in naïve B-cell samples (average: 8.5); in contrast, MBL and PBMC samples from LC-MBL had the fewest (averages: 1.3 and 1.1, respectively).

Interestingly, the distribution of "CLL-specific" BcR IG stereotypes differed from that reported in CLL[2] (Figure 2) as shown by the low incidence of subsets #1 and #2, the largest in CLL, and the absence of rearrangements similar to those of CLL subsets #8, #31, #59 and #99, all associated with aggressive disease.[11] Furthermore, stereotyped clonotypes typical of CLL subset #4[2] were significantly (P<0.05) biased to naïve B-cell populations. This BcR IG stereotype is distinctive for utilizing the *IGHV4-34* gene, notable for its germline-encoded autoreactive potential.[12] This gene is frequent in naïve B cells but suppressed in classical memory B cells and, instead, enriched in autoimmune repertoires and certain lymphoproliferations,[13] prompting an argument for stringent censoring of IGHV4-34 B cells in healthy individuals. This appears to be supported by the present study as well, in which we found that LC-MBL is devoid of CLL stereotypes related to aggressive disease and that the subset #4 stereotype is confined to the naïve B-cell repertoire.

In conclusion, in the first next-generation sequencing immunoprofiling study of LC-MBL we report differences from age-matched individuals without MBL. Critically, the very low incidence of "CLL-specific" stereotyped BcR IG in LC-MBL (as well as in elderly individuals without LC-MBL) further attests to the unique immunogenetic signature of CLL while also highlighting the role of microenvironmental triggering, mediated through the BcR, as a major driver even before the onset of CLL.[14] This could also explain the low incidence of CLL in the East, since not only the genetic background but also environmental triggers could differ between Asian and Caucasian populations.[9,15]

Andreas Agathangelidis,[1,2] Chrysi Galigalidou,[2,3] Lydia Scarfò,[1] Theodoros Moysiadis,[2,4] Alessandra Rovida,[1] Maria Gounari,[2] Fotis Psomopoulos,[2] Pamela Ranghetti,[1] Alex Galanis,[3] Frederic Davi,[5] Kostas Stamatopoulos,[2,4] Anastasia Chatzidimitriou[2,4#] and Paolo Ghia[1#] also on behalf of the Euroclonality NGS Working Group

[1]*Strategic Research Program on CLL and B-Cell Neoplasia Unit, Division of Experimental Oncology, Università Vita-Salute San Raffaele and IRCCS Ospedale San Raffaele, Milan, Italy;* [2]*Institute of Applied Biosciences, Center for Research and Technology Hellas, Thessaloniki, Greece;* [3]*Department of Molecular Biology and Genetics (MBG), Democritus University of Thrace, Alexandroupolis, Greece;* [4]*Department of Molecular Medicine and Surgery, Karolinska Institute, Stockholm, Sweden and* [5]*Assistance Publique - Hôpitaux de Paris (AP-HP), Hôpital Pitié-Salpêtrière, Department of Biological Hematology, Sorbonne Université, UMR_S 1138, Centre de Recherche des Cordeliers, Paris, France*

[#]*AC and PG contributed equally as co-senior authors.*

Correspondence:
ANASTASIA CHATZIDIMITRIOU - achatzidimitriou@certh.gr

doi:10.3324/haematol.2020.247908

Disclosures: AA has received funding from Gilead. KS has received honoraria from AbbVie, Gilead Science, Janssen and reseach funding from AbbVie and Janssen. PG has received honoraria from AbbVie, Acerta, BeiGene, Gilead, Janssen, Sunesis and reseach funding from AbbVie, Gilead, Janssen, Novartis, and Sunesis.

Contributions: AA designed the research, performed the experiments, analyzed the data and wrote the manuscript; CG analyzed the data and wrote the manuscript; LS, AR, MG and PR assisted with the experiments; TM performed the statistical analysis; FP assisted with the data analysis; AG and FD supervised the research and wrote the manuscript; KS, AH and PG designed and supervised the research and wrote the manuscript. All authors provided final approval of the manuscript.

Funding: this project received funding from the Hellenic Foundation for Research and Innovation (HFRI) and the General Secretariat for Research and Technology (GSRT), under grant agreement n. 336 (Project CLLon); the TRANSCAN-2 Joint Transnational Call for Proposals 2014 (JTC 2014) by the European Commission/DG Research and Innovation; the TRANSCAN-2: Employing next-generation sequencing technology for improved, non-invasive early detection, staging and prediction of progression in lymphoma patients (NOVEL/MIS 5041673); the project "KRIPIS II ODYSSEUS" funded by the Operational Programme "Competitiveness, Entrepreneurship and Innovation" (NSRF 2014-2020) and co-financed by Greece and the European Union (European Regional Development Fund); the Italian Association for Cancer Research (AIRC, Special Program on Metastasis, 5 per mille #21198 to PG); PRIN 2015ZMRFEA, Italian Ministry of University and Research - MIUR, Roma, Italy; open access project, ID number LM2011020, funded by the Ministry of Education, Youth and Sports of the Czech Republic under the activity "Projects of major infrastructures for research, development and innovations"; the Greek Precision Medicine Network, a mission of the Research and Innovation sector of the Ministry of Education, Research and Religious Affairs of Greece; the Asklepios Grant Programme grant from Gilead Hellas. MG is recipient of a Marie Sklodowska-Curie individual fellowship (grant agreement n. 796491), funded by the European Union's Horizon 2020 research and innovation programme.

References

1. Hallek M. Chronic lymphocytic leukemia: 2015 update on diagnosis, risk stratification, and treatment. Am J Hematol. 2015;90(5):446-460.

2. Agathangelidis A, Darzentas N, Hadzidimitriou A, et al. Stereotyped B-cell receptors in one-third of chronic lymphocytic leukemia: a molecular classification with implications for targeted therapies. Blood. 2012;119(19):4467-4475.
3. Stamatopoulos K, Agathangelidis A, Rosenquist R, Ghia P. Antigen receptor stereotypy in chronic lymphocytic leukemia. Leukemia. 2017;31(2):282-291.
4. Forconi F, Potter KN, Wheatley I, et al. The normal IGHV1-69-derived B-cell repertoire contains stereotypic patterns characteristic of unmutated CLL. Blood. 2010;115(1):71-77.
5. Colombo M, Bagnara D, Reverberi D, et al. Tracing CLL-biased stereotyped immunoglobulin gene rearrangements in normal B cell subsets using a high-throughput immunogenetic approach. Mol Med. 2020;10(26(1):25.
6. Scarfo L, Ghia P. What does it mean I have a monoclonal B-cell lymphocytosis? Recent insights and new challenges. Semin Oncol. 2016;43(2):201-208.
7. Vardi A, Dagklis A, Scarfo L, et al. Immunogenetics shows that not all MBL are equal: the larger the clone, the more similar to CLL. Blood. 2013;121(22):4521-4528.
8. Criado I, Blanco E, Rodriguez-Caballero A, et al. Residual normal B-cell profiles in monoclonal B-cell lymphocytosis versus chronic lymphocytic leukemia. Leukemia. 2018;32(12):2701-2705.
9. de Faria-Moss M, Yamamoto M, Arrais-Rodrigues C, et al. High frequency of chronic lymphocytic leukemia-like low-count monoclonal B-cell lymphocytosis in Japanese descendants living in Brazil. Haematologica. 2020;105(6):e298-e301.
10. Criado I, Rodriguez-Caballero A, Gutierrez ML, et al. Low-count monoclonal B-cell lymphocytosis persists after seven years of follow up and is associated with a poorer outcome. Haematologica. 2018;103(7):1198-1208.
11. Baliakas P, Hadzidimitriou A, Sutton LA, et al. Clinical effect of stereotyped B-cell receptor immunoglobulins in chronic lymphocytic leukaemia: a retrospective multicentre study. Lancet Haematol. 2014;1(2):e74-84.
12. Potter KN, Hobby P, Klijn S, Stevenson FK, Sutton BJ. Evidence for involvement of a hydrophobic patch in framework region 1 of human V4-34-encoded Igs in recognition of the red blood cell I antigen. J Immunol. 2002;169(7):3777-3782.
13. Tipton CM, Hom JR, Fucile CF, Rosenberg AF, Sanz I. Understanding B-cell activation and autoantibody repertoire selection in systemic lupus erythematosus: a B-cell immunomics approach. Immunol Rev. 2018;284(1):120-131.
14. Agathangelidis A, Ljungstrom V, Scarfo L, et al. Highly similar genomic landscapes in monoclonal B-cell lymphocytosis and ultra-stable chronic lymphocytic leukemia with low frequency of driver mutations. Haematologica. 2018;103(5):865-873.
15. Wu SJ, Lin CT, Lin SC, et al. Similar epidemiological trends of preneoplastic precursors and their respective lymphoid malignancies in Taiwan. Ann Hematol. 2016;95(10):1727-1729.

Isatuximab plus pomalidomide and dexamethasone in elderly patients with relapsed/refractory multiple myeloma: ICARIA-MM subgroup analysis

Multiple myeloma (MM) typically affects elderly patients, with a median age at diagnosis of 69 years.[1] Treatment of elderly patients is challenging due to frailty, comorbidities, and decreased resilience to treatment-related toxicity.[2] Furthermore, advanced age has a negative impact on the prognosis of patients with MM.[3,4] Considering these challenges, new, well-tolerated treatment options for this age group are needed.

Isatuximab is a monoclonal antibody that targets a specific epitope on CD38 and triggers MM cell death via multiple mechanisms.[5-7] Isatuximab-irfc is approved in the USA for use in combination with pomalidomide and dexamethasone (Pd) to treat patients with relapsed/refractory MM (RRMM) patients who have received at least two prior therapies, including lenalidomide and a proteasome inhibitor.[8]

ICARIA-MM (ClinicalTrials.gov, number NCT02990338) was a randomized, open-label, multicenter phase III study of isatuximab in combination with Pd (Isa-Pd) that showed significantly improved progression-free survival in heavily treated patients with RRMM with a manageable safety profile compared with that of Pd alone.[9,10] Due to its prognostic relevance, age (<75 *versus* ≥75 years) was one of the stratification factors in ICARIA-MM. As the population <75 years was very large, it was further divided into 65-74 and <65 years subpopulations in this pre-specified subgroup analysis of ICARIA-MM, comparing efficacy and safety in these three age groups.

The baseline characteristics of the patients, divided by age group, are shown in Table 1, and were generally balanced across arms.

The median progression-free survival was significantly prolonged with Isa-Pd and was similar in all three age subgroups (Figure 1A-C). In the age group ≥75 years old it was 11.40 months (Isa-Pd; n=32) *versus* 4.47 months (Pd; n=29), hazard ratio (HR)=0.479; 95% confidence interval (95% CI): 0.242-0.946. In the age group 65-74 years old it was 11.57 months (Isa-Pd; n=68) *versus* 8.58 months (Pd; n=54), HR=0.638; 95% CI: 0.385-1.059. In the age group <65 years old it was 11.53 months (Isa-Pd; n=54) *versus* 5.03 months (Pd; n=70), HR=0.656; 95% CI: 0.401-1.074.

The overall response rate was also improved with Isa-Pd *versus* Pd in all three age subgroups (Figure 1D). In the age group ≥75 years old the overall response rate was 53.1% *versus* 31.0%, respectively (odds ratio [OR] 2.52; 95% CI: 0.79-8.26). In the subgroup 65-74 years old it was 64.7% *versus* 38.9% (OR 2.88; 95% CI: 1.29-6.46). In the age group <65 years old it was 59.3% *versus* 34.3% (OR 2.79; 95% CI: 1.26–6.20). Across age groups, the proportion of patients who achieved a very good partial response (VGPR) or better rate was consistently higher with Isa-Pd than with Pd (Figure 1D): ≥75 years, 31.2% *versus* 0% (OR not calculable); 65-74 years, 32.3% *versus* 13.0% (OR 3.21; 95% CI: 1.17-9.70); and <65 years 31.5% *versus* 8.6% (OR 4.90; 95% CI: 1.64-16.35).

Eight patients in the Isa-Pd arm have minimal residual disease negativity rate (at a sensitivity level of 10-5 assessed by next-generation sequencing): two were ≥75 years old, two were 65-74 years old and four were <65 years. No patients in the Pd arm achieved minimal residual disease negativity.

In patients ≥75 years, eight of 32 (25.0%) in the Isa-Pd arm died *versus* 15 of 29 (51.7%) in the Pd arm. The median overall survival in these patients was not reached in the Isa-Pd arm and was 10.3 months in the Pd arm with a CI for the HR that does not cross 1 (HR=0.40; 95% CI: 0.17-0.96). Among patients 65-74 years old, the median overall survival was not reached in the Isa-Pd arm and was 14.5 months in the Pd arm (HR 0.75; 95% CI: 0.38-1.45). The median overall survival was not reached in either treatment arm in patients <65 years old (HR 0.85; 95% CI: 0.46-1.59).

Multivariate analyses adjusting progression-free survival and overall survival for International Staging System stage at study entry in the three age groups were performed and suggest that the imbalance in the International Staging System stage at study entry did not influence the treatment effect in favor of Isa-Pd for progression-free or overall survival outcomes (*Online Supplementary Table 1*).

Health-related quality of life parameters were better maintained in the Isa-Pd arm among patients aged ≥75 years, *versus* 65-74 years and <65 years (*Online Supplementary Figures S1, S2* and *S3*, respectively), as demonstrated by the results of Global Health Status/Quality of Life, Physical Functioning and Role Functioning scores and no worsening of Fatigue, C30 Pain, and MY20 Disease Symptoms. The maintenance of quality of life in elderly MM patients is important because (i) while younger patients with MM are usually more concerned with achieving a complete response or minimal residual disease negativity, older patients want to have their disease controlled while maintaining their quality of life;[11] and (ii) MM-related complications tend to be more severe and debilitating in older patients, and therefore treatments that preserve quality of life are particularly desired in this group of patients.[2]

As indicated in *Online Supplementary Table S2*, the treatment duration was longer with Isa-Pd than with Pd, independently of age. In the Isa-Pd arm, treatment exposure was longer and higher numbers of cycles were started in patients ≥75 years old compared with the other two age groups. Additionally, a tendency towards lower relative dose intensity was observed for patients ≥75 years old, followed by patients aged 65-74 years and <65 years in both treatment arms.

The number of patients with any treatment-emergent adverse event (TEAE) was similar in the Isa-Pd and Pd arms (Table 2). The incidences of grade ≥3 TEAE, serious TEAE, and discontinuations due to TEAE were higher in patients ≥75 years old than in younger patients with both Isa-Pd and Pd, but there was no increase in fatal TEAE in the Isa-Pd arm or impact on median treatment duration (*Online Supplementary Table 2*). The most common any-grade non-hematologic TEAE with Isa-Pd were infusion reactions, regardless of age group (Table 2). Infusion reactions were mostly grade 1-2, reversible, and occurred with the first infusion. Interestingly, fewer infusion reactions were observed in patients ≥75 years (28.1%) than in those 65-74 years (36.4%) or <65 years (42.6%). The underlying mechanism of anti-CD38 infusion reactions is not currently understood; it is possible that cytokine release by involved immune cell subset(s) is less pronounced in elderly patients due to their impaired immune function.

The most common grade ≥3 non-hematologic TEAE was pneumonia, regardless of patients' age or treatment group (Table 2). In the Isa-Pd arm, the incidence of pneumonia was lower in patients ≥75 years (12.5%), followed by those <65 (16.7%) and 65-74 years (27.3%). This might be explained by a higher percentage of older

Table 1. Patients' baseline characteristics at study entry by age group in the intent-to-treat population.

	≥75 years (n=61)		65–74 years (n=122)		<65 years (n=124)	
	Isa-Pd (n=32)	Pd (n=29)	Isa-Pd (n=68)	Pd (n=54)	Isa-Pd (n=54)	Pd (n=70)
Age (years)						
Mean (SD)	77.9 (2.0)	78.3 (3.2)	69.4 (2.9)	69.0 (2.5)	56.5 (5.9)	57.0 (6.1)
Median (range)	77 (75-83)	78 (75-86)	69 (65-74)	69 (65-74)	57.5 (36-64)	58 (41-64)
MM subtype, n (%)						
IgG	21 (65.6)	22 (75.9)	45 (66.2)	32 (59.3)	38 (70.4)	47 (67.1)
IgA	9 (28.1)	4 (13.8)	17 (25.0)	19 (35.2)	7 (13.0)	18 (25.7)
IgM	0	0	1 (1.5)	0	1 (1.9)	0
Kappa light chain only	1 (3.1)	2 (6.9)	2 (2.9)	1 (1.9)	5 (9.3)	4 (5.7)
Lambda light chain only	1 (3.1)	1 (3.4)	3 (4.4)	2 (3.7)	3 (5.6)	1 (1.4)
ISS stage*, n (%)						
Stage I	7 (21.9)	4 (13.8)	31 (45.6)	18 (33.3)	26 (48.1)	29 (41 .4)
Stage II	12 (37.5)	12 (41.4)	22 (32.4)	23 (42.6)	19 (35.2)	21 (30.0)
Stage III	13 (40.6)	12 (41.4)	14 (20.6)	13 (24.1)	7 (13.0)	18 (25.7)
Unknown	0	1 (3.4)	1 (1.5)	0	2 (3.7)	2 (2.9)
ECOG Performance Status, n (%)						
0	9 (28.1)	14 (48.3)	24 (35.3)	18 (33.3)	22 (40.7)	37 (52.9)
1	18 (56.3)	8 (27.6)	36 (52.9)	31 (57.4)	29 (53.7)	29 (41.4)
2	5 (15.6)	7 (24.1)	8 (11.8)	5 (9.3)	3 (5.6)	4 (5.7)
Cytogenetic risk†, n (%)						
High-risk CA	7 (21.9)	11 (37.9)	9 (13.2)	6 (11.1)	8 (14.8)	19 (27.1)
Standard-risk CA	20 (62.5)	9 (31.0)	47 (69.1)	32 (59.3)	36 (66.7)	37 (52.9)
Unknown or missing	5 (15.6)	9 (31.0)	12 (17.6)	16 (29.6)	10 (18.5)	14 (20.0)
N. of patients with a medical history of Asthma or COPD, n (%)	5 (15.6)	5 (17.2)	7 (10.3)	8 (14.8)	4 (7.4)	4 (5.7)
N. of patients with renal impairment‡, n (%)	30 (93.8)	27 (93.1)	63 (92.6)	51 (94.4)	49 (90.7)	67 (95.7)
eGFR, n (%)						
≥60-<90 mL/min/1.73 m² (mild impairment)	10 (33.3)	11 (40.7)	31 (49.2)	25 (49.0)	20 (40.8)	33 (49.3)
≥45-<60 mL/min/1.73 m²	13 (43.3)	9 (33.3)	14 (22.2)	12 (23.5)	8 (16.3)	11 (16.4)
≥30-<45 mL/min/1.73 m²	6 (20.0)	5 (18.5)	7 (11.1)	4 (7.8)	6 (12.2)	7 (10.4)
≥15-<30 mL/min/1.73 m² (severe impairment)	0	1 (3.7)	0	0	1 (2.0)	0
N. of prior lines of therapy, Median (range)	3 (2–11)	3 (2–10)	3 (2–8)	3 (2–6)	3 (2–10)	3 (2–7)
Prior therapy, n (%)						
Alkylating agent	27 (84.4)	29 (100)	60 (88.2)	51 (94.4)	52 (96.3)	68 (97.1)
Proteasome inhibitor	32 (100)	29 (100)	68 (100)	54 (100)	54 (100)	70 (100)
Lenalidomide	32 (100)	29 (100)	68 (100)	54 (100)	54 (100)	70 (100)
Refractory status, n (%)						
Lenalidomide refractory	7 (21.9)	3 (10.3)	1 (1.5)	7 (13.0)	2 (3.7)	2 (2.9)
PI refractory	6 (18.8)	4 (13.8)	7 (10.3)	9 (16.7)	6 (11.1)	8 (11.4)
Lenalidomide and PI refractory	3 (9.4)	0	0	3 (5.6)	1 (1.9)	1 (1.4)

*International Staging System staging was derived based on the combination of serum β_2-microglobulin and albumin concentrations. †High risk chromosomal abnormalities were defined as the presence of del(17p), and/or t(4;14), and/or t(14;16) by fluorescence *in situ* hybridization. Cytogenetics was performed by a central laboratory with a cut-off of analyzed plasma cells of 50% for del(17p), and of 30% for t(4;14) and t(14;16). ‡Renal impairment was defined as an estimated glomerular filtration rate <60 mL/min/1.73 m² as determined using the Modification of Diet in Renal Disease (MDRD) equation. Isa: isatuximab: Pd: pomalidine and dexamethasone; SD: standard deviation; MM: multiple myeloma; Ig: immunoglobulin; ISS: International Staging System; ECOG: Eastern Cooperative Oncology Group; CA: chromosomal abnormalities; COPD: chronic obstructive pulmonary disease; eGFR: estimated glomerular filtration rate; PI: proteasome inhibitor.

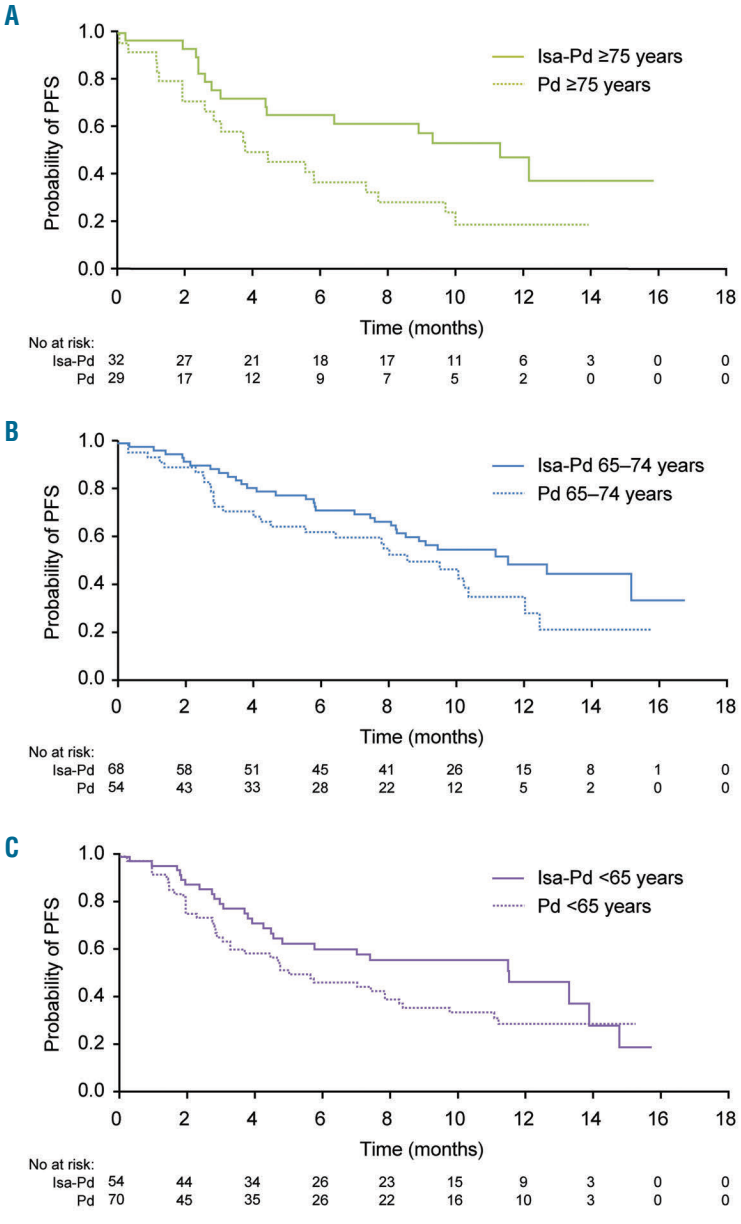


Figure 1. Progression-free survival and response to therapy in the different treatment arms in patients divided by age group. (A-C) Kaplan-Meier analysis of progression-free survival in the isatuximab plus pomalidine and dexamethasone treatment arm *versus* the pomalidine and dexamethasone treatment arm in patients ≥75 years (A), 65-74 years (B), and <65 years (C), as assessed by an independent response assessment committee. The hazard ratios and corresponding 95% confidence intervals are from a Cox proportional hazard model. (D) Overall response rate by age group as assessed by an independent response assessment committee using the International Myeloma Working Group uniform response criteria for evaluating response in patients with multiple myeloma. A stratified Cochran-Mantel-Haenszel χ^2 test measured treatment differences in overall response rates, rates of very good partial response or better, and rates of complete response or better. PFS: progression-free survival; Isa: isatuximab; Pd: pomalidomide and dexamethasone; ORR: overall response rate; PR: partial response; VGPR: very good partial response; CR: complete response; sCR: stringent complete response.

patients receiving prophylactic antibiotic treatment (*Online Supplementary Table S3*). In the Isa-Pd arm, the TEAE with the greatest differences in incidences in patients ≥75 *versus* <65 years were infusion reaction (28.1% *versus* 42.6%) and acute kidney injury (15.6% *versus* 1.9% [10.7% *versus* 5.9% in the Pd arm], possibly because elderly patients have less renal buffer). Hematologic laboratory abnormalities were assessed during the study (Table 2) and were recorded as TEAE only if they were serious or led to a modification or discontinuation of study treatment. Grade 3-4 neutropenia was more common with Isa-Pd than with Pd, regardless of

Table 2. Most common treatment-emergent adverse events and hematologic laboratory abnormalities while on treatment by patient age group and treatment arm in the safety population.

	≥75 years (n=60)		65–74 years (n=119)		<65 years (n=122)	
	Isa-Pd (n=32)	Pd (n=28)	Isa-Pd (n=66)	Pd (n=53)	Isa-Pd (n=54)	Pd (n=68)
Any TEAE*, n (%)	32 (100)	28 (100)	66 (100)	52 (98.1)	53 (98.1)	66 (97.1)
Infections	26 (81.3)	19 (67.9)	57 (86.4)	30 (56.6)	40 (74.1)	47 (69.1)
Upper respiratory tract infection	10 (31.3)	1 (3.6)	22 (33.3)	8 (15.1)	11 (20.4)	17 (25.0)
Pneumonia	4 (12.5)	2 (7.1)	18 (27.3)	7 (13.2)	9 (16.7)	17 (25.0)
Blood and lymphatic system disorders	22 (68.8)	15 (53.6)	38 (57.6)	25 (47.2)	29 (53.7)	25 (36.8)
Neutropenia	17 (53.1)	13 (46.4)	30 (45.5)	18 (34.0)	24 (44.4)	19 (27.9)
Thrombocytopenia	6 (18.8)	3 (10.7)	9 (13.6)	7 (13.2)	4 (7.4)	8 (11.8)
Gastrointestinal disorders	19 (59.4)	17 (60.7)	33 (50.0)	23 (43.4)	29 (53.7)	34 (50.0)
Diarrhea	12 (37.5)	7 (25.0)	14 (21.2)	10 (18.9)	13 (24.1)	12 (17.6)
Constipation	4 (12.5)	7 (25.0)	11 (16.7)	7 (13.2)	9 (16.7)	12 (17.6)
Musculoskeletal disorders	19 (59.4)	13 (46.4)	38 (57.6)	29 (54.7)	29 (53.7)	32 (47.1)
Back pain	6 (18.8)	6 (21.4)	10 (15.2)	4 (7.5)	9 (16.7)	12 (17.6)
Arthralgia	4 (12.5)	1 (3.6)	7 (10.6)	7 (13.2)	5 (9.3)	5 (7.4)
Others						
Fatigue	19 (59.4)	20 (71.4)	35 (53.0)	30 (56.6)	28 (51.9)	39 (57.4)
Acute kidney injury	5 (15.6)	3 (10.7)	1 (1.5)	1 (1.9)	1 (1.9)	4 (5.9)
Infusion reaction	9 (28.1)	0	24 (36.4)	1 (1.9)	23 (42.6)	1 (1.5)
Grade ≥3 TEAE†, n (%)	30 (93.8)	21 (75.0)	56 (84.8)	40 (75.5)	46 (85.2)	44 (64.7)
Infections	15 (46.9)	10 (35.7)	30 (45.5)	14 (26.4)	20 (37.0)	21 (30.9)
Upper respiratory tract infection	1 (3.1)	0	1 (1.5)	1 (1.9)	3 (5.6)	0
Pneumonia	4 (12.5)	2 (7.1)	14 (21.2)	7 (13.2)	7 (13.0)	14 (20.6)
Blood and lymphatic system disorders	22 (68.8)	15 (53.6)	36 (54.5)	22 (41.5)	29 (53.7)	22 (41.5)
Neutropenia	16 (50.0)	13 (46.4)	30 (45.5)	17 (32.1)	24 (44.4)	18 (26.5)
Thrombocytopenia	5 (15.6)	3 (10.7)	9 (13.6)	7 (13.2)	4 (7.4)	8 (11.8)
Gastrointestinal disorders	3 (9.4)	0	2 (3.0)	2 (3.8)	4 (7.4)	1 (1.5)
Diarrhea	1 (3.1)	0	1 (1.5)	1 (1.9)	1 (1.9)	0
Constipation	0	0	0	0	0	0
Musculoskeletal disorders	2 (6.3)	2 (7.1)	3 (4.5)	3 (5.7)	7 (13.0)	3 (4.4)
Back pain	0	1 (3.6)	1 (1.5)	0	2 (3.7)	1 (1.5)
Arthralgia	2 (6.3)	0	1 (1.5)	1 (1.9)	1 (1.9)	0
Others						
Fatigue	2 (6.3)	0	3 (4.5)	0	1 (1.9)	0
Acute kidney injury	2 (6.3)	2 (7.1)	1 (1.5)	1 (1.9)	1 (1.9)	3 (4.4)
Infusion reaction	1 (3.1)	0	2 (3.0)	0	1 (1.9)	0
Grade 5 (fatal) TEAE	2 (6.3)	4 (14.3)	3 (4.5)	5 (9.4)	6 (11.1)	4 (5.9)
Serious TEAE	22 (68.8)	16 (57.1)	41 (62.1)	32 (60.4)	31 (57.4)	32 (47.1)
TEAE leading to definitive discontinuation	5 (15.6)	4 (14.3)	2 (3.0)	8 (15.1)	4 (7.4)	7 (10.3)
Hematologic laboratory abnormalities‡ (grade 3-4)						
Neutropenia	28 (87.5)	18 (64.3)	53 (80.3)	38 (71.7)	48 (88.9)	47 (69.1)
Anemia	14 (43.8)	12 (42.9)	20 (30.3)	11 (20.8)	14 (25.9)	18 (26.5)
Thrombocytopenia	11 (34.4)	8 (28.6)	20 (30.3)	13 (24.5)	16 (29.6)	15 (22.1)

*System Organ Class with treatment-emergent adverse events (TEAE) with an incidence of ≥15%. †System Organ Class with grade ≥3 TEAE with an incidence of ≥10%. ‡Derived from clinical laboratory analysis, including complete blood count, neutrophil count, platelet count, and hemoglobin values. Clinical laboratory abnormalities were recorded as TEAE only if they were serious or led to modification or discontinuation of the study treatment. Isa: isatuximab: Pd: pomalidine and dexamethasone; TEAE: treatment-emergent adverse event.

age group (Table 2). Grade 3-4 anemia was more common in older patients and was observed at comparable rates in both arms, except among patients aged 65-74 years. Patients ≥75 years required more red blood cell transfusions and treatment with erythropoiesis-stimulating agents than younger patients, with older Pd patients requiring these interventions more than Isa-Pd patients (*Online Supplementary Table S4*). The incidence of grade 4 thrombocytopenia was similar in the two arms across age groups, except for patients ≥75 years (18.8% with Isa-Pd *versus* 10.7% with Pd) (*Online Supplementary Table S5*). The need for platelet transfusions was low for all subpopulations and in both treatment arms. Neutropenia and infections were reversible and manageable with supportive care (granulocyte colony-stimulating factor/granulocyte-macrophage colony-stimulating factor and antibiotics, respectively).

As shown in *Online Supplementary Table S6*, the majority of TEAE leading to treatment discontinuation were grade ≥3. Infections were the most common TEAE leading to treatment discontinuation in patients ≥75 years in both arms: 9.4% in the Isa-Pd arm and 14.3% in the Pd arm. In the Isa-Pd arm, one patient aged 65-74 (1.5%) and two aged <65 years (3.7%) discontinued treatment due to general disorders. Among patients aged 65-74 and <65 years in the Pd arm, thrombocytopenia was the most frequent TEAE leading to treatment discontinuation (5.7% and 5.9%, respectively).

One limitation of the current ICARIA-MM sub-analysis is that the subgroup of patients ≥75 years in ICARIA-MM was about half the size of the other two age groups. Comorbidities and other illnesses that frequently accompany elderly patients may have compromised their eligibility for the study. However, the same limitation is present in many MM clinical trials.[12] Nonetheless, both study arms had around 20% of patients aged ≥75 years and the oldest patient enrolled in ICARIA-MM was 86 years old, a very advanced age for a third-line trial. Furthermore, the ICARIA-MM study did not assess frailty.[13]

In contrast to the general observation of a negative prognosis of elderly age in MM, the addition of isatuximab to pomalidomide and dexamethasone improved progression-free survival, overall response rate, very good partial responses or better rate, and overall survival in elderly patients, consistent with the benefit observed in the overall ICARIA-MM study population. Moreover, isatuximab was well tolerated in older patients (≥75 years), whose treatment lasted longer than that in younger patients, with no increase in fatal TEAE in the Isa-Pd arm *versus* the Pd arm. A consistent trend toward higher rates of serious TEAE and discontinuation due to TEAE in patients ≥75 years was evident in both arms. Our findings support the use of Isa-Pd in RRMM patients regardless of age.

Fredrik Schjesvold,[1] Paul G. Richardson,[2] Thierry Facon,[3] Adrián Alegre,[4] Andrew Spencer,[5] Artur Jurczyszyn,[6] Kazutaka Sunami,[7] Laurent Frenzel,[8] Chang-Ki Min,[9] Sophie Guillonneau,[10] Peggy L. Lin,[11] Solenn Le-Guennec,[12] Frank Campana,[13] Helgi van de Velde,[13] Samira Bensfia[11] and Sara Bringhen[14]

[1]Oslo Myeloma Center, Oslo University Hospital and KG Jebsen Center for B Cell Malignancies, University of Oslo, Oslo, Norway; [2]Dana-Farber Cancer Institute, Boston, MA, USA; [3]Lille University Hospital, Lille, France; [4]Hospital Universitario La Princesa & Hospital Quironsalud, Madrid, Spain; [5]Department of Clinical Hematology, Alfred Health-Monash University, Melbourne, Australia; [6]Department of Hematology, Jagiellonian University Medical College, Krakow, Poland; [7]Department of Hematology, National Hospital Organization Okayama Medical Center, Okayama, Japan; [8]Hôpital Necker-Enfants Malades, Paris, France; [9]Department of Hematology, Catholic Hematology Hospital and Leukemia Research Institute, Seoul St. Mary's Hospital, College of Medicine, The Catholic University of Korea, Seoul, Republic of South Korea; [10]Sanofi CMO, Chilly-Mazarin, France; [11]Sanofi Global Oncology, Cambridge, MA, USA; [12]Sanofi R&D, Vitry-sur-Seine, France; [13]Sanofi R&D, Cambridge, MA, USA and [14]Myeloma Unit, Division of Hematology, University of Torino, Azienda-Ospedaliero Universitaria Città della Salute e della Scienza di Torino, Torino, Italy

Correspondence:
SARA BRINGHEN - sarabringhen@yahoo.com

doi:10.3324/haematol.2020.253450

Disclosures: FS: honoraria – Amgen, Celgene, Janssen, MSD, Novartis, Oncopeptides, Sanofi, SkyliteDX and Takeda; membership on an entity's Board of Directors or advisory committees – Amgen, Celgene, Janssen, MSD, Novartis, Oncopeptides, Sanofi and Takeda. PGR: research funding – Bristol-Myers Squibb, Celgene, Oncopeptides and Takeda; honoraria – Celgene, Janssen, Karyopharm, Oncopeptides, Sanofi and Takeda. TF: membership on an entity's Board of Directors or advisory committees – Amgen, Celgene, Janssen, Karyopharm, Oncopeptides, Roche and Takeda. AA: honoraria – Amgen, Celgene, Janssen, Sanofi and Takeda; membership on an entity's Board of Directors or advisory committees – Amgen, Celgene, Janssen, Sanofi and Takeda. AS: research funding – Amgen, Celgene, Haemalogix, Janssen Servier and Takeda; honoraria – AbbVie, Amgen, Celgene, Haemalogix, Janssen, Sanofi, SecuraBio, Specialised Therapeutics Australia, Servier and Takeda; consultancy – AbbVie, Celgene, Haemalogix, Janssen, Sanofi, SecuraBio, Specialised Therapeutics Australia, Servier and Takeda; speakers' bureau – Celgene, Janssen and Takeda. AJ: honoraria – Amgen, Celgene, Janssen-Cilag, Karyopharm and Takeda; membership on an entity's Board of Directors or advisory committees – Karyopharm. KS: research funding – AbbVie, Alexion Pharma, Bristol-Myers Squibb, Celgene, Daiichi Sankyo, MSD, Ono Pharmaceutical, Sanofi and Takeda Pharmaceutical; honoraria – Bristol-Myers Squibb, Celgene, Ono Pharmaceutical and Takeda Pharmaceutical. LF: honoraria – Amgen, Celgene, Janssen-CILAG and Takeda. SBr: honoraria – Amgen, Bristol-Myers Squibb, Celgene and Janssen; membership on an entity's Board of Directors or advisory committees – Amgen, Celgene, Janssen and Karyopharm; consultancy – Janssen and Takeda. SG, PLL, SL-G, FC, HvdV and SBe are employed by Sanofi. CKM has no relevant financial relationships to disclose.

Qualified researchers can request access to patient-level data and related study documents including the clinical study report, study protocol with any amendments, blank case report forms, statistical analysis plan, and dataset specifications. Patient-level data are anonymized, and study documents are redacted to protect the privacy of the trial participants. Further details on Sanofi's data-sharing criteria and the process for requesting access are available at: https://www.clinicalstudydatarequest.com.

Contributions: FC: the funder's clinical study director, was responsible for overseeing the ICARIA-MM study. PGR was a co-primary investigator of this study. FS, PGR, TF, AA, AS, AJ, KS, LF, C-KM and SBr were investigators in the study and contributed to data acquisition. PGR, FC and SL-G designed the study. SG and PLL processed the health-related quality of life data and performed the analysis. SL-G, FC, HvdV and SBe contributed to the analysis and interpretation of data for the work. All authors revised the work for important intellectual content and assume responsibility for data integrity and the decision to submit this manuscript for publication; they had full access to the study data, edited and reviewed the manuscript drafts, and approved the final version for submission.

Acknowledgments: the authors thank the participating patients and their families, and the study centers and investigators for their contributions to the study. We specially thank Professor Michel Attal from the

Institut Universitaire du Cancer de Toulouse-Oncopole, Toulouse, France, a co-primary investigator of the ICARIA-MM study, for reviewing this manuscript. We thank Medha Sasane, Wahidullah Noori and Denise Bury for their contributions to the Patient Reported Outcomes and Health-Related Quality of Life data collection and interpretation. Medical writing support was provided by Camile Semighini Grubor, PhD of Elevate Medical Affairs, contracted by Sanofi Genzyme for publication support services.

Funding: the ICARIA-MM study was sponsored by Sanofi.

References

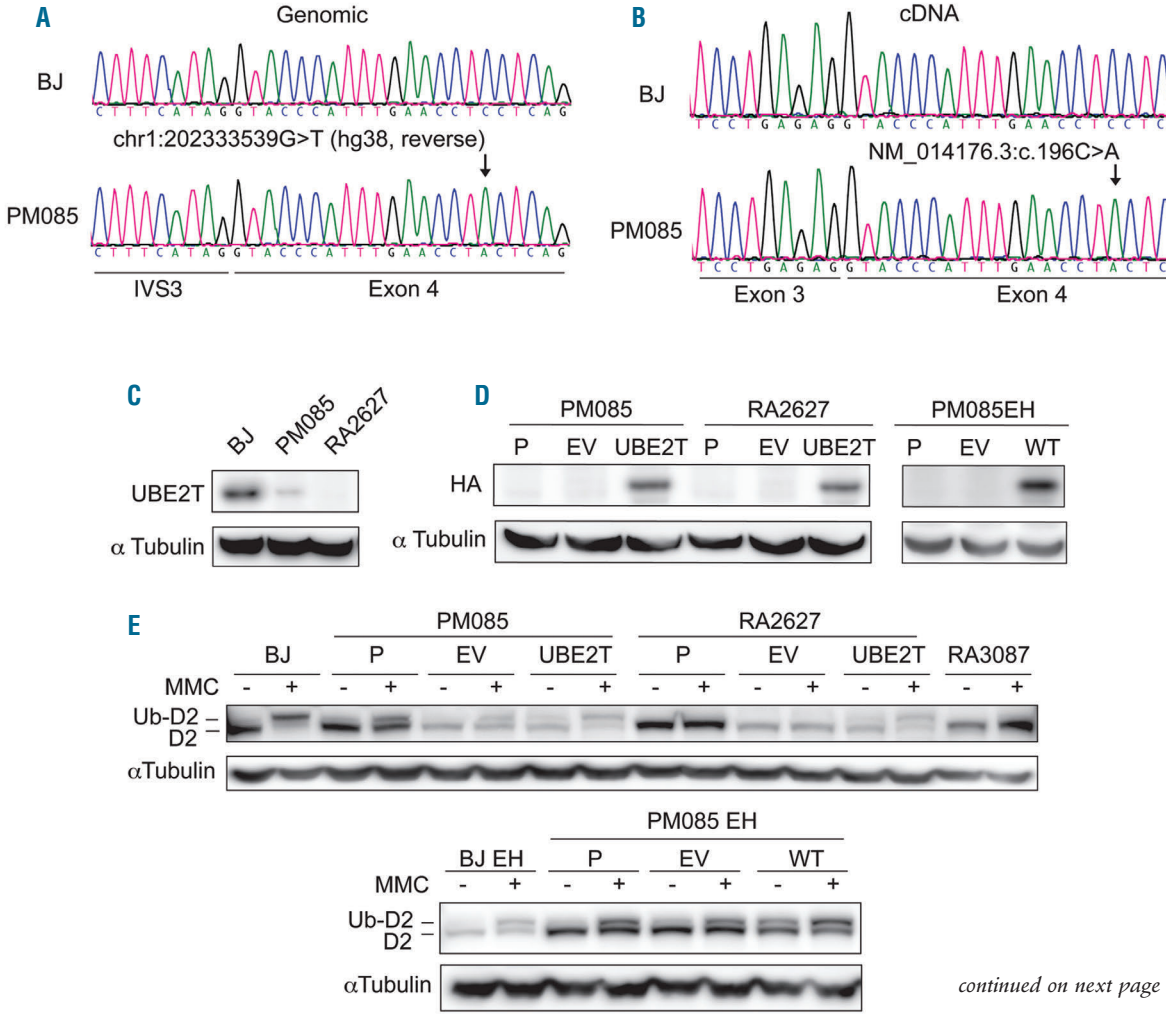
1. Howlader N, Noone A, Krapcho M, et al. SEER Cancer Statistics Review, 1975-2016, National Cancer Institute. Bethesda, MD. https://seer.cancer.gov/csr/1975_2016/, based on November 2018 SEER data submission, posted to the SEER web site, April 2019. Accessed December 16, 2019.
2. Willan J, Eyre TA, Sharpley F, Watson C, King AJ, Ramasamy K. Multiple myeloma in the very elderly patient: challenges and solutions. Clin Interv Aging. 2016;11:423-435.
3. Bringhen S, Mateos MV, Zweegman S, et al. Age and organ damage correlate with poor survival in myeloma patients: meta-analysis of 1435 individual patient data from 4 randomized trials. Haematologica. 2013;98(6):980-987.
4. Dimopoulos MA, Kastritis E, Delimpasi S, et al. Multiple myeloma in octogenarians: clinical features and outcome in the novel agent era. Eur J Haematol. 2012;89(1):10-15.
5. Deckert J, Wetzel MC, Bartle LM, et al. SAR650984, a novel humanized CD38-targeting antibody, demonstrates potent antitumor activity in models of multiple myeloma and other CD38+ hematologic malignancies. Clin Cancer Res. 2014;20(17):4574-4583.
6. Jiang H, Acharya C, An G, et al. SAR650984 directly induces multiple myeloma cell death via lysosomal-associated and apoptotic pathways, which is further enhanced by pomalidomide. Leukemia. 2016;30(2):399-408.
7. Moreno L, Perez C, Zabaleta A, et al. The mechanism of action of the anti-CD38 monoclonal antibody isatuximab in multiple myeloma. Clin Cancer Res. 2019;25(10):3176-3187.
8. Sanofi. SARCLISA [Package Insert]. Bridgewater, NJ 2020.
9. Attal M, Richardson PG, Rajkumar SV, et al. Isatuximab plus pomalidomide and low-dose dexamethasone versus pomalidomide and low-dose dexamethasone in patients with relapsed and refractory multiple myeloma (ICARIA-MM): a randomised, multicentre, open-label, phase 3 study. Lancet. 2019;394(10214):2096-2107.
10. Richardson PG, Attal M, Campana F, et al. Isatuximab plus pomalidomide/dexamethasone versus pomalidomide/dexamethasone in relapsed/refractory multiple myeloma: ICARIA phase III study design. Future Oncol. 2018;14(11):1035-1047.
11. Anderson KC. Insights into the management of older patients with multiple myeloma. Clin Adv Hematol Oncol. 2019;17(7):390-392.
12. van de Donk N, Richardson PG, Malavasi F. CD38 antibodies in multiple myeloma: back to the future. Blood. 2018;131(1):13-29.
13. Palumbo A, Avet-Loiseau H, Oliva S, et al. Revised International Staging System for multiple myeloma: a report from International Myeloma Working Group. J Clin Oncol. 2015;33(26):2863-2869.

A homozygous missense variant in *UBE2T* is associated with a mild Fanconi anemia phenotype

Fanconi anemia (FA) is a rare multi-system disorder characterized by bone marrow failure, congenital abnormalities, and cancer predisposition.[1] Pathogenic variants have been described in 22 known FA genes (*FANCA-FANCW*) that are required for the proper repair of DNA interstrand crosslinks.[2,3] A key step in the repair of interstrand crosslinks is FA pathway activation via monoubiquitination of FANCD2 and FANCI by FANCL, an E3 ubiquitin-ligase working with UBE2T/FANCT, an E2 ubiquitin-conjugating enzyme.[4-7] Pathogenic germline variants in *UBE2T* have been described in three individuals with FA;[6-8] thus, the knowledge of the phenotypic spectrum is limited for the FA-T complementation group. Here we describe a mild presentation of FA resulting from a hypomorphic missense variant in *UBE2T* that partially disrupts the function of the encoded protein. This report highlights the importance of an algorithmic approach to bone marrow failure that combines genetic testing and functional cellular assays.[9]

Three patients have previously been reported with biallelic pathogenic variants in *UBE2T* consistent with an autosomal recessive disease. All three patients presented with the classic features of FA (*Online Supplementary Table S1*).[6-8] Hira *et al*. reported two unrelated patients both harboring a c.4C>G, p.Gln2Glu missense variant *in trans* with either a 23 kb whole gene deletion (patient 1) or a c.180+5G>A, p.Gln37Argfs*47 frameshift variant (patient 2). Both patients developed hematologic abnormalities and bone marrow failure. Patient 2 developed myelodysplastic syndrome which evolved to acute myeloid leukemia. Both patients required hematopoietic stem cell transplantation.[7] Rickman *et al*. and Virts *et al*. reported the findings of a maternally inherited Alu-mediated duplication, c.-64_468dup, producing an unstable transcript and a paternally inherited Alu-mediated deletion, c.-64_468del, leading to loss of the majority of the gene. However, this patient did not develop bone marrow failure as a result of somatic mosaicism identified in his peripheral blood.[6,8]

The patient reported here is a 22-year-old Hispanic female who was unaffected at birth, had a normal developmental history, and a negative family history with no reported consanguinity. She originally presented to an another institution at 8 years of age and was reported to have mild neutropenia and thrombocytopenia; a bone marrow biopsy at that time was non-diagnostic. At 21 years, the patient presented with persistent neutropenia and macrocytosis, intermittent thrombocytopenia, episodic fevers, an urticarial erythematous rash, and metromenorrhagia (*Online Supplementary Tables S1* and *S2*). No developmental anomalies or cutaneous hypo/hyperpigmentation were noted. Chromosomal



continued on next page

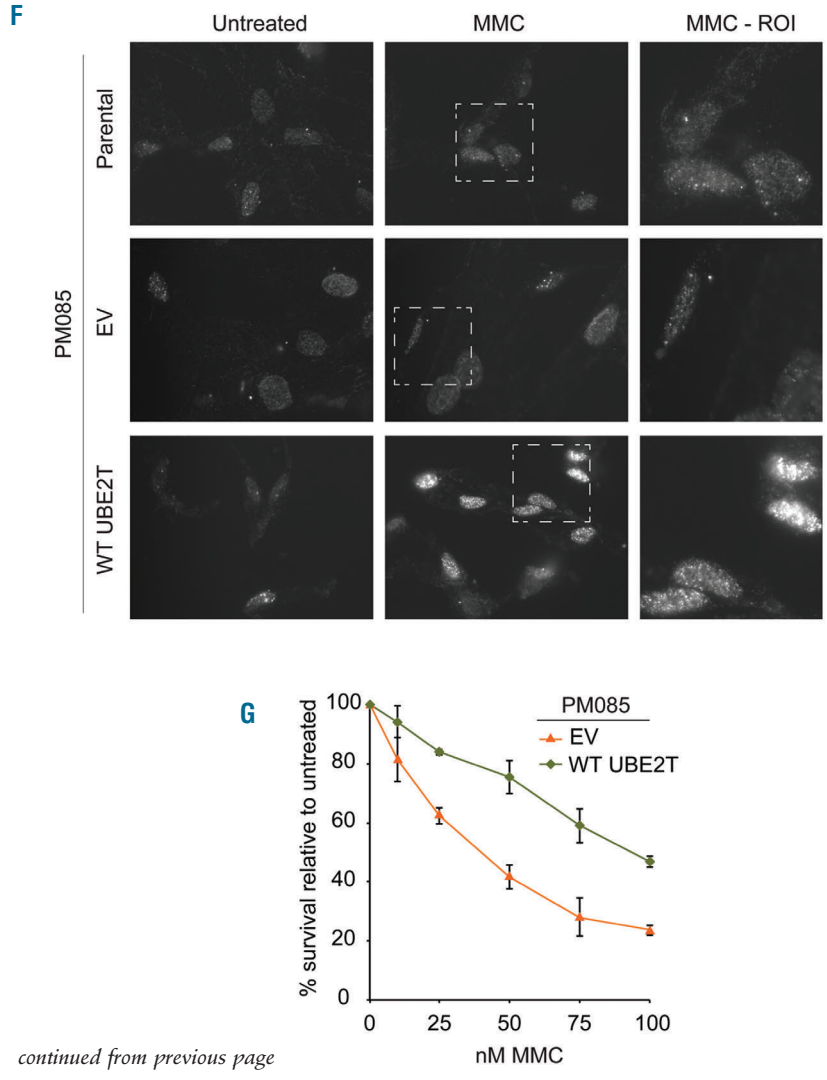


Figure 1. The proband carries a likely pathogenic *UBE2T* variant expressed at low levels conferring defective interstrand crosslink repair. (A) Sequencing of genomic DNA extracted from primary fibroblasts (PM085) of the affected individual indicating a homozygous chr1:202333539G>T variant (hg38, reverse). (B) Sequencing of complementary DNA (cDNA) from the proband's fibroblasts indicating the presence of a variant NM_014176.3:c.196C>A and no evidence of aberrant splicing. Exon numbering reflects ref seq NM_014176.3 since the primers were designed against this transcript.[6] (C) Immunoblot with anti-UBE2T antibody in whole cell extract from the proband's primary fibroblasts (PM085), wild-type BJ fibroblasts (from the American Type Culture Collection) and fibroblasts from an UBE2T/FANCT-null Fanconi anemia patient (RA2627).[6] (D) Immunoblot with anti-HA antibody in PM085 (proband) and RA2627 (*UBE2T*$^{-/-}$) primary fibroblasts and PM085 EH (immortalized fibroblasts) expressing C-HA-FLAG empty vector (EV) or wild-type (WT) UBE2T. HA expression in parental (P) (non-transduced) cells and cells expressing EV or WT UBE2T. (E) Immunoblot with anti-FANCD2 antibody on whole cell extracts of cells treated or not with mitomycin C (MMC). Ub-D2 indicates the monoubiquitinated band. (F) Formation of foci of FANCD2 after MMC treatment in patient-derived PM085 cells (non-transduced parental cells) or cells expressing EV, or WT UBE2T. (G) Cell survival of the proband's PM085 fibroblasts expressing EV or WT UBE2T after treatment with MMC.

continued from previous page

breakage assays performed on peripheral blood lymphocytes showed increased breakage (*Online Supplementary Table S1*). A repeat bone marrow biopsy revealed moderate hypocellularity (40-50%) with no evidence of dysplasia or a lymphoproliferative process and a normal karyotype. A gene panel to investigate periodic fever was negative (*Online Supplementary Table S3*). Due to the patient's undiagnosed neutropenia, panel-based next-generation sequencing was performed on whole blood (*Online Supplementary Table S4*) and revealed a homozygous c.196C>A, p.P66T (NM_014176.3, Chr1(GRCh37): 202302667G>T) missense variant of uncertain significance in UBE2T. This variant is absent from the gnomAD database. GeneDx exon level deletion/duplication calling from sequencing data (with manual verification) did not detect any evidence of a multi-exon copy number variant in *UBE2T*, suggesting the patient is not hemizygous. Parental samples were not available for testing.

The p.P66T variant identified causes a substitution of a hydrophobic to polar uncharged amino acid at a highly conserved position in the UBC fold domain (*Online Supplementary Figure S1*). Multiple *in silico* tools predict that this variant is likely to be damaging (*Online Supplementary Table S5*). The proline 66 resides at the base of one of multiple loops comprising the FANCL binding region[10] (*Online Supplementary Figure S2A* and *B*). When modeled, P66T is predicted to change the position of the loop because of changes in the backbone phi/psi (φ/ψ) angles. The loop is moved out, as compared to the wild-type (WT) structure, and the interacting residues are moved away from the UBE2T and FANCL interface (*Online Supplementary Figure S2C*). As P66T changes the range of peptide backbone flexibility, making the base of the loop much more flexible, the binding with FANCL is expected to be dysregulated from a stricter *cis/trans* switch.

In order to confirm the pathogenicity of the c.196C>A (p.P66T) variant in *UBE2T*, functional *in vitro* studies were performed. Sanger sequencing of genomic DNA and complementary DNA from patient-derived fibroblasts (PM085) confirmed the presence of this variant and absence of splicing defects (Figure 1A and B). Immunoblotting of whole cell extract from these cells demonstrated decreased, but not absent, UBE2T protein expression (Figure 1C). This is consistent with the p.P66T missense variant causing instability in the UBE2T protein, resulting in the observed decrease in protein level.

To determine whether the c.196C>A (p.P66T) variant affects the E2 function of UBE2T, FANCD2 monoubiquitination was assessed after treatment with the DNA

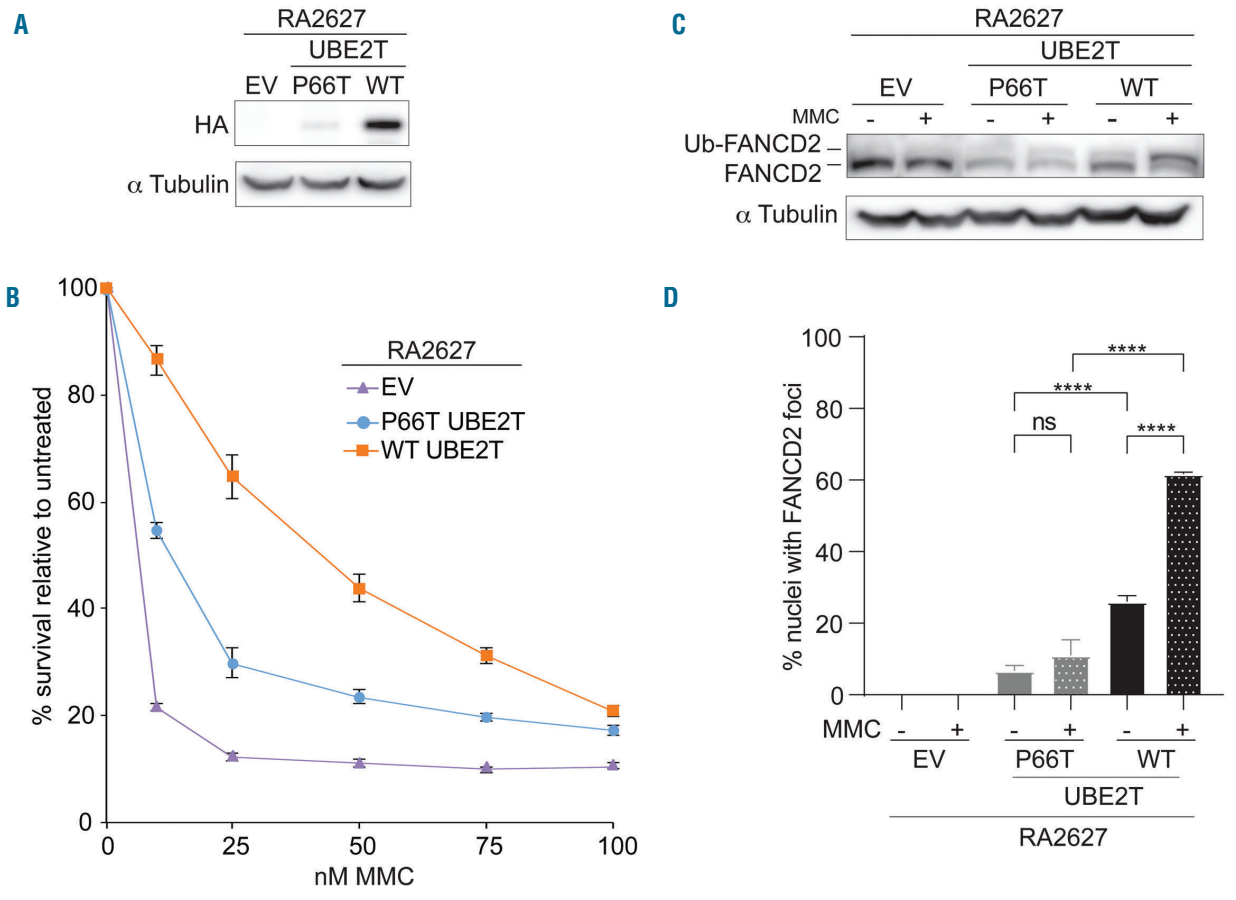


Figure 2. P66T UBE2T is a partial loss-of-function variant. (A) Immunoblot with anti-HA antibody of RA2627 (*UBE2T*$^{-/-}$) primary fibroblasts expressing empty vector (EV) or C-HA-FLAG P66T UBE2T or wild-type (WT) UBE2T. (B) Cell survival of RA2627 (*UBE2T*$^{-/-}$) fibroblasts expressing EV, P66T UBE2T, or WT UBE2T after treatment with mitomycin C (MMC). (C) FANCD2 ubiquitination with and without MMC treatment in RA2627 (*UBE2T*$^{-/-}$) fibroblasts expressing EV, P66T UBE2T, or WT UBE2T. (D) Quantification of FANCD2 foci formation after MMC treatment in RA2627 (*UBE2T*$^{-/-}$) fibroblasts expressing EV, P66T UBE2T, or WT UBE2T. Approximately 300 HA-expressing cells were analyzed for the presence of FANCD2 foci in three separate coverslips. The mean percent nuclei with FANCD2 foci was plotted and tested for significance using one-way analysis of variance with multiple comparisons. ns: not significant, ****P=≤0.0001.

interstrand crosslinking agent mitomycin C. Normal FANCD2 monoubiquitination was observed in the WT control cell line (BJ fibroblasts), was absent in UBE2T$^{-/-}$ (RA2627) and FANCA$^{-/-}$ (RA3087) fibroblasts and was reduced in the proband's fibroblasts (Figure 1E). Expression of WT UBE2T in the patient's fibroblasts fully rescued FANCD2 monoubiquitination (Figure 1D and E), recruitment of FANCD2 to chromatin after mitomycin C treatment, and sensitivity of the proband's fibroblasts to mitomycin C (Figure 1F-H). These results indicate that the proband belongs to FA-T complementation group and suggest that the patient's missense variant is hypomorphic, resulting in reduced function.

To further demonstrate that the missense variant reduces UBE2T function and is indeed likely pathogenic, UBE2T$^{-/-}$ cells were transduced with either WT or P66T HA-tagged UBE2T (Figure 2A). The P66T variant expressed at a lower level compared to WT UBE2T, consistent with decreased stability of UBE2T carrying that variant. Expression of P66T UBE2T also only partially rescued cell survival, FANCD2 ubiquitination, and FANCD2 foci formation upon treatment with mitomycin C compared to WT UBE2T expression (Figure 3B-D). This provides further evidence that the missense variant is a likely pathogenic hypomorph.

The cellular and patients' phenotypes described for the FA-T complementation group are thus far consistent with defective FA pathway activation and a defect in interstrand crosslink repair. However, it was previously reported that UBE2T-deficient DT40 cells were sensitive to ultraviolet irradiation and the replication stress-inducing agent, hydroxyurea.[11] To determine whether UBE2T is important for resistance to other types of DNA damage, RA2627 cells were tested for sensitivity to a number of other genotoxic agents. RA2627 cells were not found to be hypersensitive to ultraviolet irradiation, ionizing radiation, camptothecin, hydroxyurea, or the PARP inhibitor olaparib (Figure 3A-E). These data suggest that UBE2T does not have a major role in responding to DNA lesions or replication stress produced by these agents and its primary function is in interstrand crosslink repair and that the patients' phenotypes reflect defects in the repair of interstrand crosslink lesions.

In conclusion, we report a novel presentation of FA-T complementation group resulting from a likely pathogenic missense variant (c.196C>A) in *UBE2T*. The patient presented with atypical, mild FA, characterized by persistent macrocytosis and neutropenia with intermittent thrombocytopenia but no severe bone marrow failure (without evidence of somatic reversion in blood) or congenital abnormalities common to FA. Clinical chromosomal breakage assays were consistent with a diagnosis of FA and subsequent functional analysis of patient-derived

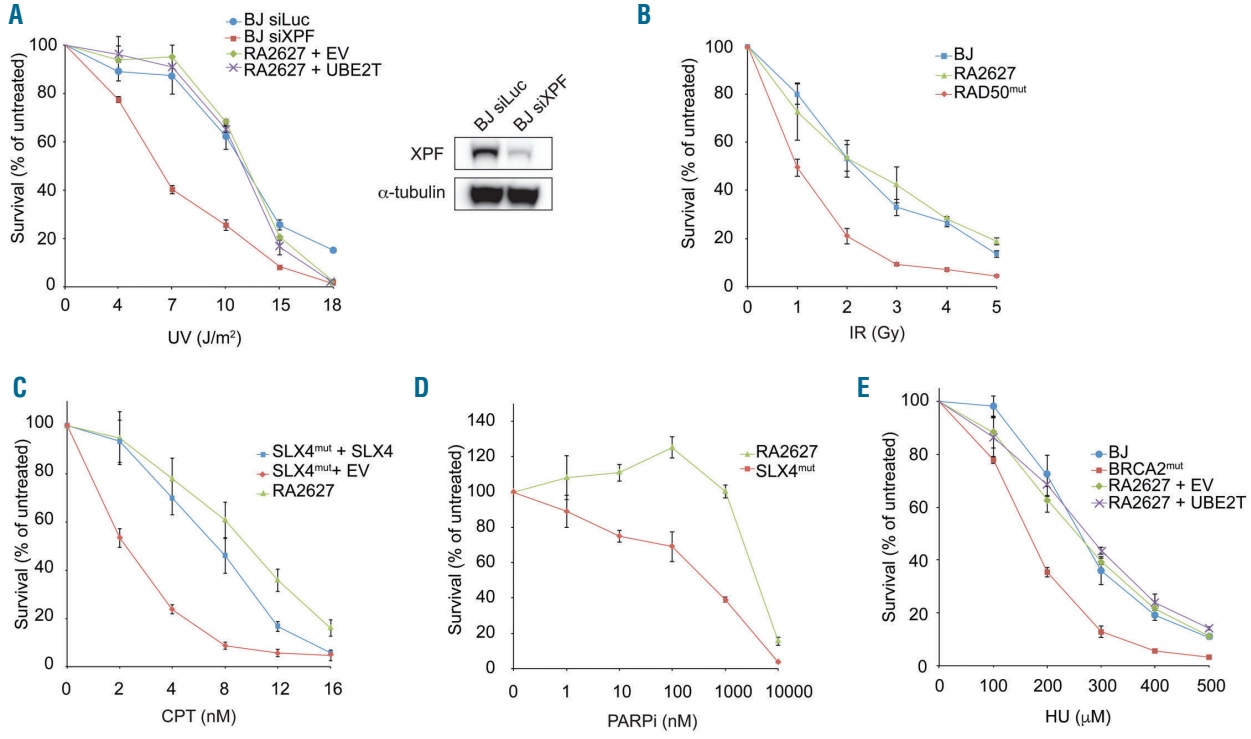


Figure 3. UBE2T does not have a major role in the repair of non-interstrand crosslink DNA lesions. (A) Cell survival assay after ultraviolet treatment of complemented pairs of RA2627 fibroblasts compared to BJ wild-type (WT) fibroblasts depleted of XPF used as a positive control. The immunoblot shows decreased XPF levels after siRNA depletion. (B) Cell survival assay of RA2627 fibroblasts after treatment with irradiation. HA239F fibroblasts with *RAD50* mutations are sensitive to irradiation and act as a positive control (RAD50^{mut}). (C, D) Cell sensitivity assays comparing RA2627 fibroblasts to RA3331 Fanconi anemia patient-derived fibroblasts with *SLX4* mutations (SLX4^{mut}) expressing WT SLX4 or empty vector exposed to camptothecin (C) and the PARP inhibitor, olaparib (D). (E) Cell survival assay after hydroxyurea treatment of RA2627 cells compared to the RA3226 BRCA2 patient cell line (BRCA2^{mut}). Error bars indicate the standard deviation. EV: empty vector; UV: ultraviolet irradiation; IR: irradiation; CPT: camptothecin; PARPi: PARP inhibitor; HU: hydroxyurea.

fibroblasts and the p.P66T UBE2T variant performed here demonstrate that the hypomorphic variant is the likely cause of disease in this patient and can be classified as likely pathogenic following the recommendations of the American College of Medical Genetics and Genomics and the Association for Molecular Pathology.[12]

The c.196C>A (p.Pro66Thr) *UBE2T* variant is likely damaging to UBE2T function by conferring both reduced E2 activity and reduced stability as immunoblotting demonstrated decreased protein levels. The p.P66T variant affects a residue highly conserved across various E2 and likely affects the interaction with FANCL due to the amino acid residue substitution being at the hydrophobic E2-E3 interface.[10] The patients previously reported by Hira *et al*. who also had a missense variant, p.Q2E, were likewise demonstrated to be hypomorphic in RA2627 cells,[13] but heterozygous and *in trans* to loss of function variants suggesting the possibility of UBE2T dosage sensitivity, as the two patients presented with more severe disease. Disease severity may also be increased in those two patients because of the presence of the ALDH2* variant which is known to interact genetically with the FA pathway.[14]

We hypothesize that the hypomorphic variant and resulting residual function of the c.196C>A (p.P66T) variant in *UBE2T* explains our patient's mild phenotype. This case adds to the limited knowledge regarding this rare FA-T complementation group. It is possible that there are other undiagnosed patients with mild phenotypes, emphasizing the utility of an algorithmic approach utilizing genomic sequencing and functional analysis for patients with non-specific hematologic phenotypes.

Laura Schultz-Rogers,[1] Francis P. Lach,[2*] Kimberly A. Rickman,[2] Alejandro Ferrer,[1] Abhishek A. Mangaonkar,[3] Tanya L. Schwab,[4] Christopher T. Schmitz,[4] Karl J. Clark,[4] Nikita R. Dsouza,[5] Michael T. Zimmermann,[5,6] Mark Litzow,[3] Nicole Jacobi,[7] Eric W. Klee,[1,8] Agata Smogorzewska[2#] and Mrinal M. Patnaik[3#]*

[1]Center for Individualized Medicine, Mayo Clinic, Rochester, MN; [2]Laboratory of Genome Maintenance, The Rockefeller University, New York, NY; [3]Department of Hematology, Mayo Clinic, Rochester, MN; [4]Department of Biochemistry and Molecular Biology, Mayo Clinic, Rochester, MN; [5]Bioinformatics Research and Development Laboratory, Genomics Sciences and Precision Medicine Center, Medical College of Wisconsin, Milwaukee, WI; [6]Clinical and Translational Sciences Institute, Medical College of Wisconsin, Milwaukee, WI; [7]Department of Hematology Oncology, Hennepin County Medical Center, Minneapolis, MN and [8]Department of Clinical Genomics, Mayo Clinic, Rochester, MN, USA

**LS-R and FPL contributed equally as co-first authors.*

#EWK, AS and MMP contributed equally as co-senior authors.

Correspondence:
MRINAL PATNAIK - patnaik.mrinal@mayo.edu
AGATA SMOGORZEWSKA - asmogorzewska@rockefeller.edu

doi:10.3324/haematol.2020.259275

Disclosures: no conflicts of interest to disclose.

Contributions: FPL, KAR, LSR, AF, KJC, EWK and AS designed the study and interpreted the results. FPL, KAR, TLS and CTS performed the study. MMP, AM and ML were the treating team at the Mayo Clinic where the patient was seen in the institutional inherited bone marrow failure clinic. NJ oversaw the patient's care at Hennepin

County Medical Center. NRD. and MTZ performed in silico protein modeling. LSR, KAR, FPL, MMP and AS wrote the manuscript with input from the other authors.

Acknowledgments: we thank the proband for participating in this study.

Funding: this work was supported in part by the Mayo Clinic Center for Individualized Medicine and the "Henry Predolin Leukemia Foundation" and by a Starr Cancer Consortium grant (to AS), National Institutes of Health (NIH) RO1 HL120922 (to AS), and grant # UL1TR001866 from the National Center for Advancing Translational Sciences, NIH Clinical and Translational Science Award program. KAR was supported by a Medical Scientist Training Program grant from the National Institute of General Medical Sciences of the NIH under award number T32GM007739 to the Weill Cornell/Rockefeller/Sloan-Kettering Tri-Institutional MD-PhD Program. AS is a Howard Hughes Medical Institute.Faculty Scholar. The content of this study is solely the responsibility of the authors and does not necessarily represent the official views of the NIH.

References

1. Fiesco-Roa MO, Giri N, McReynolds LJ, Best AF, Alter BP. Genotype-phenotype associations in Fanconi anemia: a literature review. Blood Rev. 2019;37:100589.
2. Kottemann MC, Smogorzewska A. Fanconi anaemia and the repair of Watson and Crick DNA crosslinks. Nature. 2013;493(7432):356-363.
3. Niraj J, Farkkila A, D'Andrea AD. The Fanconi anemia pathway in cancer. Annu Rev Cancer Biol. 2019;3:457-478.
4. Meetei AR, de Winter JP, Medhurst AL, et al. A novel ubiquitin ligase is deficient in Fanconi anemia. Nat Genet. 2003;35(2):165-170.
5. Machida YJ, Machida Y, Chen Y, et al. UBE2T is the E2 in the Fanconi anemia pathway and undergoes negative autoregulation. Mol Cell. 2006;23(4):589-596.
6. Rickman KA, Lach FP, Abhyankar A, et al. Deficiency of UBE2T, the E2 ubiquitin ligase necessary for FANCD2 and FANCI ubiquitination, causes FA-T subtype of Fanconi anemia. Cell Rep. 2015;12(1):35-41.
7. Hira A, Yoshida K, Sato K, et al. Mutations in the gene encoding the E2 conjugating enzyme UBE2T cause Fanconi anemia. Am J Hum Genet. 2015;96(6):1001-1007.
8. Virts EL, Jankowska A, Mackay C, et al. AluY-mediated germline deletion, duplication and somatic stem cell reversion in UBE2T defines a new subtype of Fanconi anemia. Hum Mol Genet. 2015;24(18):5093-5108.
9. Mangaonkar AA, Ferrer A, Pinto EVF, et al. Clinical applications and utility of a precision medicine approach for patients with unexplained cytopenias. Mayo Clin Proc. 2019;94(9):1753-1768.
10. Hodson C, Purkiss A, Miles JA, Walden H. Structure of the human FANCL RING-Ube2T complex reveals determinants of cognate E3-E2 selection. Structure. 2014;22(2):337-344.
11. Kelsall IR, Langenick J, MacKay C, Patel KJ, Alpi AF. The Fanconi anaemia components UBE2T and FANCM are functionally linked to nucleotide excision repair. PLoS One. 2012;7(5):e36970.
12. Richards S, Aziz N, Bale S, et al. Standards and guidelines for the interpretation of sequence variants: a joint consensus recommendation of the American College of Medical Genetics and Genomics and the Association for Molecular Pathology. Genet Med. 2015;17(5):405-424.
13. Lv Z, Rickman KA, Yuan L, et al. S. pombe Uba1-Ubc15 structure reveals a novel regulatory mechanism of ubiquitin E2 activity. Mol Cell. 2017;65(4):699-714.e6.
14. Hira A, Yabe H, Yoshida K, et al. Variant ALDH2 is associated with accelerated progression of bone marrow failure in Japanese Fanconi anemia patients. Blood. 2013;122(18):3206-3209.

Bi38-3 is a novel CD38/CD3 bispecific T-cell engager with low toxicity for the treatment of multiple myeloma

Monoclonal antibodies targeting CD38, such as daratumumab, have shown good therapeutic efficacy in multiple myeloma (MM), both alone[1] and in combination with normal standard-of-care regimens.[2,3] However, many patients eventually relapse because of resistance mechanisms, including FcγR-dependent downregulation of CD38 on tumor cells as well as inhibition of complement-dependent cytotoxicity, antibody-dependent cell-mediated cytotoxicity and antibody-dependent cellular phagocytosis.[4]

Bispecific T-cell engaging (BiTE) antibodies belong to a new class of immunotherapeutic agents that can recognize, on the one hand, a specific antigen on the surface of the target cells (i.e., tumor antigen) and, on the other hand, the CD3ε chain on T lymphocytes.[5] By activating T cells via the CD3 complex and recruiting them in proximity of target cells, BiTE antibodies efficiently induce T-cell-mediated cytotoxicity.[6] In MM, bispecific antibodies recognizing B-cell maturation antigen or FcRH5 (CD307) have been shown to eliminate tumor plasma cells in preclinical models.[7-9] However, FcRH5 expression is not limited to tumor plasma cells and B-cell maturation antigen is abundantly secreted in MM patients.[10,11] These two features may limit the specificity or efficiency of these cognate bispecific antibodies *in vivo*. Recently, an anti-CD38 bispecific antibody, AMG424, was shown to eliminate MM cells in preclinical models, but also to trigger "off tumor" T-cell cytotoxicity on B, T and NK cells *in vitro*,[12] Thus, development of an efficient and safer bispecific antibody could contribute to improve the treatment of MM.

We have developed a new BiTE (Bi38-3) that consists of two single-chain variable fragments derived from mouse hybridomas, producing anti-human CD38 and CD3ε (*Online Supplementary Figure S1A* and *B*). Purified Bi38-3 efficiently and specifically recognizes CD38 on MM cells and binds CD3ε–expressing Jurkat T cells (*Online Supplementary Figure S1C* and *D*). To assess the effect of Bi38-3 on the cytotoxic activity of T cells, we performed co-culture assays with effector T cells, isolated from peripheral blood mononuclear cells of healthy donors, on firefly luciferase-expressing target KMS11 and MM.1S MM cell lines. We observed that T cells readily killed KMS11 cells (as measured by luciferase activity) in a Bi38-3 dose-dependent manner, with a half maximal effective concentration (EC_{50}) around 5 ng/mL, the equivalent of 0.09 nM for this 55.6 Kda protein (Figure 1A). Bi38-3-mediated T-cell cytotoxic activity was also observed in co-culture with MM.1S cells (Figure 1B). However, in this cell line, which expresses heterogeneous levels of CD38, the EC_{50} was 10-fold lower (0.5 ng/mL), indicating that Bi38-3 also triggered strong T-cell cytotoxicity in MM cells with weaker CD38 expression. In line with this, stimulation of donor T cells with Bi38-3 in the presence of MM.1S cells led to robust proliferation, expression of activation markers CD25 and CD69, as well as production of interferon-γ, tumor necrosis factor-α and interleukin-2 in a Bi38-3 dose-dependent manner (*Online Supplementary Figure S1E-H*). The viability of MM.1S or KMS11 MM cells was not affected by co-culture with T cells or Bi38-3 alone (Figure 1A and B, right). In addition, Bi38-3 induced poor T-cell-mediated killing of CD38-deficient MM.1S cells (MM1.S-KO), with around half of CD38-deficient MM.1S cells surviving the co-culture even at the highest dose of Bi38-3 (1 μg/mL) (Figure 1C). These results indicate that, at lower doses, similar to those that are expected in patients, Bi38-3 directs efficient T-cell cytotoxic activity specifically towards CD38-expressing MM cells.

We next analyzed the potential of Bi38-3 to induce lysis of target tumor plasma cells, isolated from four patients at diagnosis, by autologous effector T cells. Fluorescence-activated cell sorting (FACS) analysis of overnight effector cell:target cell (E:T) co-cultures revealed that the numbers of viable $CD138^+$ MM cells were reduced in a Bi38-3 dose-dependent manner, with the EC_{50} ranging from 0.028 to 1.29 ng/mL, depending on the patient (Figure 1D and *Online Supplementary Figure S2*). Importantly, in the absence of T cells, Bi38-3 exhibited no toxicity against fresh tumor cells. Bi38-3-induced cytotoxicity of autologous T cells was further investigated on tumor plasma cells from three MM patients at relapse and demonstrated similar efficacy, with EC_{50} values ranging from 0.2 to 0.86 ng/mL (Figure 1E). These results indicate that Bi38-3 triggered autologous T-cell-mediated killing of tumor plasma cells from patients both at diagnosis and at relapse.

To investigate potential toxic effects of Bi38-3 on blood cells, peripheral blood mononuclear cells from donors were treated with various concentrations of Bi38-3 for 24 h and the mononuclear cell populations were individually analyzed by FACS (*Online Supplementary Figure S3*). We observed that the percentages of CD14-expressing monocytes included in the live gate were markedly reduced in a Bi38-3 dose-dependent manner (Figure 2A). In contrast, the percentages of CD4 and CD8 T lymphocytes, which together represented around 60% of total peripheral blood mononuclear cells, slightly increased in response to Bi38-3, probably due to the decrease in live $CD14^+$ cells. Similarly, the B ($CD19^+$) and NK ($CD56^+$) cell populations remained at similar levels (around 10% and 5%, respectively), even at high concentrations of Bi38-3 (100 ng/mL) (Figure 2A).

Next, we investigated whether expression of CD38 at the surface of blood cells was downregulated by Bi38-3. FACS analysis indicated that CD38 mean fluorescence intensity on T, B and NK cells remained similar in cultures containing increasing doses of Bi38-3 (Figure 2B). In line with this, CD38 expression was not dramatically reduced on $CD14^+$ monocytes. Of note, this analysis could not be performed at high doses because these cells, which express higher levels of CD38, were sensitive to elevated concentrations of Bi38-3 (above 1 ng/mL). To compare the activity of Bi38-3 on $CD38^{high}$ MM *versus* $CD38^{int}$ cells, we performed co-culture assays with MM.1S, expressing high levels of CD38, freshly isolated B cells, expressing intermediate levels of CD38 (Figure 2C) and autologous T cells. Following overnight culture, the percentages of viable $CD20^+$ B cells and $CD138^+$ MM.1S cells were analyzed by flow cytometry (*Online Supplementary Figure S4A*). We observed that the percentages of MM.1S cells dropped at Bi38-3 concentrations of 0.1 ng/mL and this reduction was more dramatic at higher doses (Figure 2C). In contrast, compared to untreated conditions, the percentages of viable $CD20^+$ B cells remained unchanged even at high concentrations of Bi38-3 (Figure 2C).

We developed a similar autologous tri-culture assay to investigate potential toxic effects of Bi38-3 on $CD34^+$ bone marrow hematopoietic progenitors and on regulatory T cells, which both express low levels of CD38. While Bi38-3 readily induced MM cell killing at low concentrations (10^{-2} ng/mL and above), we found that it did not trigger significant T-cell-mediated cytotoxicity on

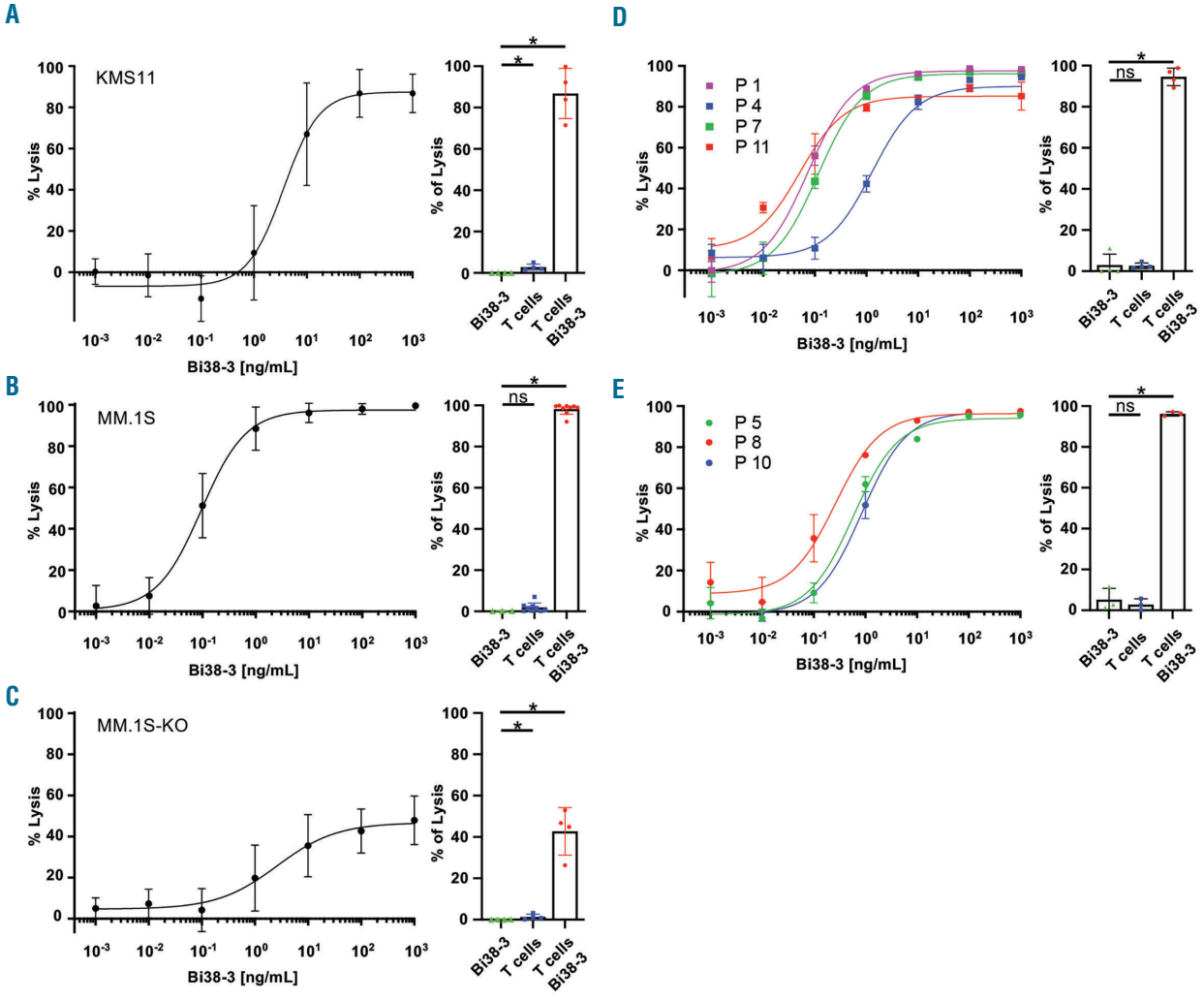


Figure 1. Bi38-3 induces CD38-dependent T-cell-mediated lysis of multiple myeloma cells *in vitro*. (A-C) KMS11-luc (A), MM.1S-luc (B) and CD38-deficient MM.1S-luc (MM.1S-KO-luc) (C) multiple myeloma cell lines were co-cultured with T cells, isolated from peripheral blood samples from healthy donors, at an effector:target (E:T) cell ratio of 5:1 with increasing concentrations of Bi38-3 for 24 h. Curves represent target cell lysis, monitored by luciferase activity and expressed as the percentage of the untreated condition (0% lysis). Data are the means of independent experiments with four (A), nine (B) and four (C) different donors. Standard deviations (SD) are shown for each concentration. Histograms on the left show target cell lysis induced by Bi38-3 alone, donor T cells alone and T cells with Bi38-3 (10^1 ng/mL) on KMS11-luc (A), MM.1S-luc (B) and MM1.S-KO-luc (C). (D and E) Fresh tumor plasma cells were collected from buffy coat of bone marrow aspirates from myeloma patients, then $CD138^+$ cells were purified and co-cultured with autologous $CD3^+$ T cells isolated from peripheral blood mononuclear cells at an E:T cell ratio of 5:1 for 24 h. Cultures were analyzed by fluorescence-activated cell sorting (FACS) to monitor the number of $CD138^+$ cells falling into the live gate. The average percentages of lysis of $CD138^+$ cells (relative to the untreated condition) in four different patients at diagnosis (D) and three different patients at relapse (E) are shown. The error bars indicate the SD. Histograms show the average effects of Bi38-3 alone, T cells alone and T cells with Bi38-3 (10^2 ng/mL) on tumor plasma cells from the same four patients at diagnosis (D) and three patients at relapse (E). SD are shown and *P* values were determined by a two-sided Mann–Whitney U-test (*P<0.05; **P<0.01; ***P<0.001).

$Foxp3^+$ regulatory T cells (Figure 2D). Similarly, there was no significant toxicity on $CD34^+$ hematopoietic progenitors at concentrations below 10 ng/mL and moderate toxicity (>40% survival) at the highest concentrations (Figure 2E). Collectively, our results indicate that Bi38-3 does not impair the surface expression of CD38 and only triggers T-cell-mediated killing of cells expressing high levels of CD38 with no or limited toxicity against cells expressing intermediate levels of CD38, such as hematopoietic progenitors, B, T or NK cells.

The antitumor activity of Bi38-3 was further assessed *in vivo* using a human MM xenograft mouse model. MM.1S cells expressing luciferase (MM.1Sluc) were injected into the tail vein of immunodeficient (NSG) mice and luciferase levels were measured using an IVIS Imaging System every 3 or 4 days. Thirteen days after MM.1S injection, purified human T cells were transplanted intravenously with or without Bi38-3 (0.1 mg/kg). Treatments with Bi38-3 or vehicle were repeated daily for 9 days (Figure 3A). Seven days after tumor cell injection, all mice showed similar levels of radiance (luciferase), indicating that MM cells had effectively engrafted in host animals prior to Bi38-3 treatment (Figure 3B). While control mice showed rapid tumor progression, all Bi38-3-treated animals displayed a marked reduction in tumor growth within the first 5 days of Bi38-3 treatment (Figure 3C). At the end of the treatments, the level of luciferase-expressing MM cells in Bi38-3-treated mice was only one tenth of the initial level and was on average 30-fold lower than that in untreated controls (Figure 3C). These results show that Bi38-3 is able to efficiently control MM tumor progression *in vivo*.

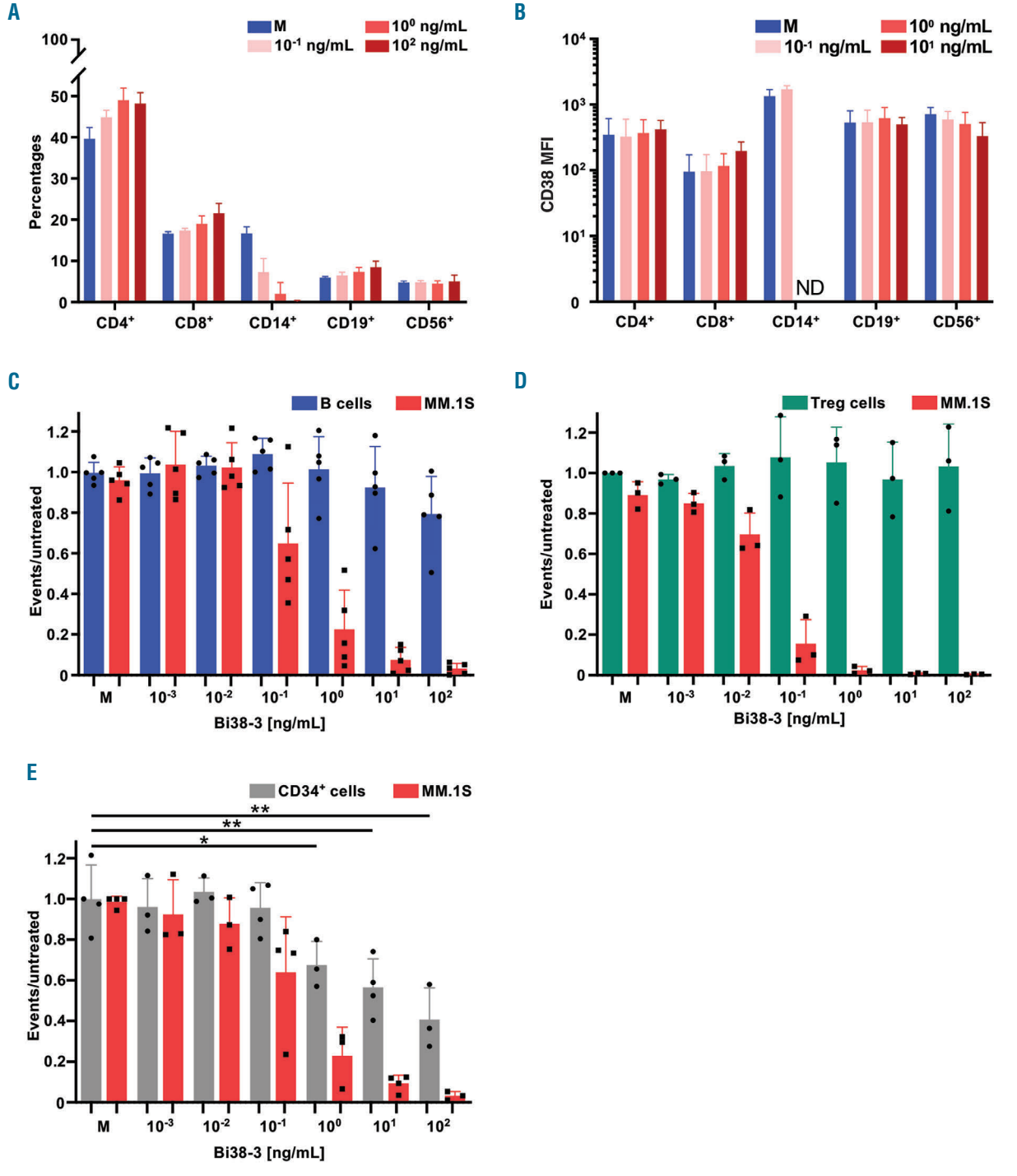


Figure 2. Sensitivity of blood cells and bone marrow hematopoietic progenitors to Bi38-3. (A) Peripheral blood mononuclear cells (PBMC) from healthy donors (n=3) were cultured with medium (M) or various concentrations of Bi38-3 for 24 h and the percentages of live T, myeloid, B and NK cells were determined by fluorescence-activated cell sorting (FACS) analysis. Histograms show the average percentages of live $CD4^+$ T cells, $CD8^+$ T cells, $CD14^+$ monocytes, $CD19^+$ B cells and $CD56^+$ NK cells in Bi38-3 cultures compared to untreated controls from three independent donors. The error bars indicate the standard deviation (SD). (B) Mean fluorescence intensity (MFI) was measured in MM.1S wild-type (WT) cells and in subsets of cells expressing CD4, CD8, CD14, CD19 and CD56, based on FACS analysis of CD38 expression levels in PBMC cell populations cultured with various concentrations of Bi38-3 as in (A). Histograms show average CD38 MFI of MM.1S cells and PBMC populations and error bars indicate the SD. ND: not determined because there were too few events. (C) Relative Bi38-3-mediated T-cell lysis of B *versus* MM.1S cells. Purified paired B and T cells from healthy donors (n=5) were co-cultured with increasing concentrations of Bi38-3 for 24 h in the presence of MM.1S cells. (D) Relative Bi38-3-mediated T-cell lysis of regulatory T cells (Treg) *versus* MM.1S cells. Purified T cells from healthy donors (n=3) were co-cultured with increasing concentrations of Bi38-3 for 24 h in the presence of MM.1S cells. (E) Relative Bi38-3-mediated T-cell lysis of $CD34^+$ bone marrow hematopoietic progenitors *versus* MM.1S cells. Paired $CD34^+$ hematopoietic progenitors and T cells purified from the bone marrow of healthy donors (taken during hip surgery) (n=4) were co-cultured with increasing concentrations of Bi38-3 for 24 h in the presence of MM.1S cells. In (C-E), the numbers of live $CD20^+$ (B cells), $FoxP3^+$ (Treg cells), $CD34^+$(hematopoietic progenitors) and $CD138^+$ (MM.1S cells) were calculated by FACS using counting beads and expressed as a ratio to untreated controls. Histograms show the ratios of B, Treg, $CD34^+$ hematopoietic progenitor and MM.1S cells for each Bi38-3 concentrations and error bars indicate the SD. The normality of the $CD34^+$ populations was established with a Shapiro-Wilk normality test and *P*-values were determined by an unpaired Student *t* test (**P*<0.05; ***P*<0.01; ****P*<0.001).

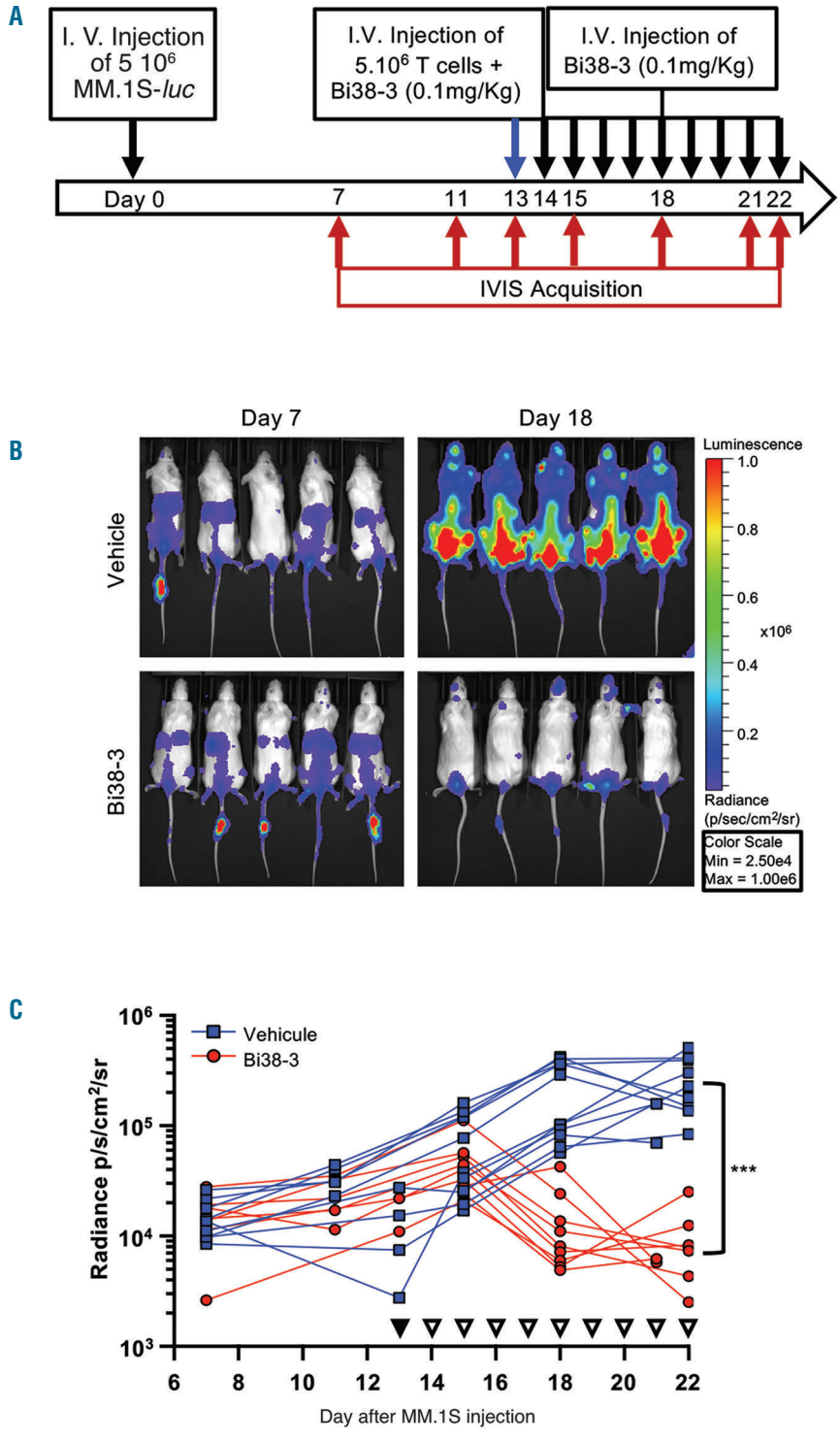


Figure 3. *In vivo* activity of Bi38-3 in the MM.1Sluc xenograft mouse model. (A) Treatment schedule. Six- to 12-week-old NOD/SCID/IL-2Rγnull mice were inoculated with $5x10^6$ MM.1SLuc cells by tail vein injection (i.v) at day 0, followed, 13 days later, by infusion of $5x10^6$ purified human T cells, isolated from healthy donors, with (or without) Bi38-3 at a dose of 0.1 mg/kg (blue arrow). Treatment was initiated at day 13 when similar levels of luciferase-expressing MM cells were detected in all mice. Tail vein injections of Bi38-3 (0.1 mg/Kg) or phosphate-buffered saline (PBS, for controls) were repeated daily for 9 days (black arrows). Bioluminescence was measured with the IVIS Imaging System on days 7, 11, 13, 15, 18 and 21 (or 22) after tumor injection (red arrows). (B) Serial bioluminescence imaging was performed to assess myeloma progression/regression. Radiance was measured on the entire body of mice. Images on the left show bioluminescence at 7 days after inoculation with MM.1S myeloma cells and before the beginning of the treatment. Images on the right indicate bioluminescence 18 days after inoculation with MM.1S cells and 4 days after treatment with Bi38-3 (lower panel) or with vehicle (upper panel). The radiance color scale is represented on the right. (C) Longitudinal radiance levels of mice treated with vehicle (blue lines) or Bi38-3 (red lines). Red and blue curves represent groups of nine and 11 mice inoculated with MM.1SLuc and T cells and then treated with Bi38-3 (0.1 mg/kg) and PBS, respectively. Black filled triangles indicate the first injection of Bi38-3 or PBS with T cells and white filled triangles indicate Bi-38 or PBS injections every day for 9 days. These experiments were performed with T cells isolated from two independent donors. The normality of populations was established with the Shapiro-Wilk normality test, and *P*-values were calculated based on an unpaired Student *t* test (*P<0.05; **P<0.01; ***P<0.001).

We report here the development of Bi38-3, a new anti-CD38/CD3 BiTE, which triggers T-cell-mediated lysis of $CD38^+$ MM cells *in vitro, ex vivo* and *in vivo*. Interestingly, Bi38-3 provokes no toxicity on B, T and NK cells *in vitro* and is, therefore, likely to have less "off tumor" effects than AMG424, a recently developed anti-CD38 bispecific antibody.[12] Importantly, Bi38-3 efficiently triggers killing of MM cells from patients who are resistant to standard treatments. Furthermore, because it recognizes a specific epitope on CD38 and is devoid of the Fc region, Bi38-3 is expected to be efficient also in relapsed patients following daratumumab therapy. Collectively, the data presented in this study identifies Bi38-3 as a selective and efficient compound for the treatment of MM, which could be used as a front-line agent or at relapse (alone or in combination with other drugs), and which should be evaluated further in MM patients.

Maxime Fayon,[1] Carolina Martinez-Cingolani,[1] Audrey Abecassis,[1] Nathalie Roders,[1] Elisabeth Nelson,[1] Caroline Choisy,[1] Alexis Talbot,[1,2] Armand Bensussan,[1] Jean-Paul Fermand,[1,2] Bertrand Arnulf[1,2] and Jean-Christophe Bories[1]

[1]INSERM, UMR 976, Institut de Recherche Saint-Louis, Université de Paris and [2]Immuno-Hematology, Saint-Louis Hospital, Paris, France.

Correspondence:
JEAN-CHRISTOPHE BORIES - jean-christophe.bories@inserm.fr

doi:10.3324/haematol.2019.242453

Disclosures: AA has received funds from Servier. Some of the work described in this letter is covered by a patent (international patent application number PCT/EP2020/070057).

Contributions: MF, CM-C and JCB designed the study; MF and CM-C performed all the experiments; AB provided the anti-CD38 hybridoma; AA and NR contributed to the functional assay; EN and CC performed the mouse studies; AT, JPF and BA provided samples from patients with multiple myeloma; MF, CM-C and JCB interpreted the data, designed the figures, and drafted the manuscript.

Acknowledgments: we thank M. Goodhardt, and D. Garrick for their critique of the manuscript. We are also grateful to the animal facility and to the pole of cytometry of the "Institut de Recherche Saint-Louis" for technical help.

Funding: this work was supported by grants from the "Cancéropole Ile de France" and from the "Fondation Française pour la Recherche contre le Myélome et les Gammapathies monoclonales". MF and CM-C were supported by fellowships from the French "Agence National pour la Recherche", programme d'Investissements d'avenir (ANR-10-IDEX-03-02). MF was also supported by a fellowship from the "Société Française d'Hématologie". AA was supported by a fellowship from the "Agence Nationale pour la Recherche Scientifique, CIFRE" in partnership with Servier.

References

1. Usmani SZ, Weiss BM, Plesner T, et al. Clinical efficacy of daratumumab monotherapy in patients with heavily pretreated relapsed or refractory multiple myeloma. Blood. 2016;128(1):37-44.
2. Dimopoulos MA, Oriol A, Nahi H, et al. Daratumumab, lenalidomide, and dexamethasone for multiple myeloma. N Engl J Med. 2016;375(14):1319-1331.
3. Palumbo A, Chanan-Khan A, Weisel K, et al. Daratumumab, bortezomib, and dexamethasone for multiple myeloma. N Engl J Med. 2016;375(8):754-766.
4. van de Donk N, Usmani SZ. CD38 antibodies in multiple myeloma: mechanisms of action and modes of resistance. Front Immunol. 2018;9:2134.
5. Bannas P, Hambach J, Koch-Nolte F. Nanobodies and nanobody-based human heavy chain antibodies as antitumor therapeutics. Front Immunol. 2017;8:1603.
6. Brischwein K, Schlereth B, Guller B, et al. MT110: a novel bispecific single-chain antibody construct with high efficacy in eradicating established tumors. Mol Immunol. 2006;43(8):1129-1143.
7. Hipp S, Tai YT, Blanset D, et al. A novel BCMA/CD3 bispecific T-cell engager for the treatment of multiple myeloma induces selective lysis in vitro and in vivo. Leukemia. 2017;31(10):2278.
8. Li J, Stagg NJ, Johnston J, et al. Membrane-proximal epitope facilitates efficient T cell synapse formation by anti-FcRH5/CD3 and Is a requirement for myeloma cell killing. Cancer Cell. 2017;31(3):383-395.
9. Seckinger A, Delgado JA, Moser S, et al. Target expression, generation, preclinical activity, and pharmacokinetics of the BCMA-T cell bispecific antibody EM801 for multiple myeloma treatment. Cancer Cell. 2017;31(3):396-410.
10. Ise T, Nagata S, Kreitman RJ, et al. Elevation of soluble CD307 (IRTA2/FcRH5) protein in the blood and expression on malignant cells of patients with multiple myeloma, chronic lymphocytic leukemia, and mantle cell lymphoma. Leukemia. 2007;21(1):169-174.
11. Sanchez E, Li M, Kitto A, et al. Serum B-cell maturation antigen is elevated in multiple myeloma and correlates with disease status and survival. Br J Haematol. 2012;158(6):727-738.
12. Zuch de Zafra CL, Fajardo F, Zhong W, et al. Targeting multiple myeloma with AMG 424, a novel anti-CD38/CD3 bispecific T-cell-recruiting antibody optimized for cytotoxicity and cytokine release. Clin Cancer Res. 2019;25(13):3921-3933.

Effect of post-consolidation regimen on symptomatic osteonecrosis in three DCOG acute lymphoblastic leukemia protocols

Symptomatic osteonecrosis is a serious side effect of childhood acute lymphoblastic leukemia (ALL) treatment. In affected children, the blood supply to especially the epiphysis of weight-bearing bones is insufficient.[1] Osteonecrosis may resolve completely with conservative treatment or may result in debilitating long-term sequelae such as articular collapse, ultimately leading to joint replacement at an early age.[2,3]

Corticosteroids, used to treat ALL, largely contribute to osteonecrosis development.[4] Moreover, higher cumulative corticosteroid doses may be associated with an elevated risk of osteonecrosis. A large trial from the Children's Oncology Group (CCG-1961) showed that shorter corticosteroid pulses decreased the risk of osteonecrosis despite a higher cumulative dose in adolescents.[5] This strategy has been widely adopted in other pediatric ALL protocols.[6] However, asparaginase has been shown to increase the risk of osteonecrosis especially when administered concurrently with corticosteroids,[1,7] and its administration has been intensified in recent ALL protocols, which contributed to increased survival rates.[8] The benefit of shorter pulses dexamethasone on osteonecrosis development in the context of recent asparaginase intensified regimens remains unclear.

The primary aim of this study was to compare the cumulative incidence of osteonecrosis (CION) in children treated with long (Dutch Childhood Oncology Group [DCOG] ALL-9) *versus* short pulses dexamethasone (asparaginase intensified ALL-10/11 medium risk group [MRG]). The secondary aim was to investigate the associations between risk factors and osteonecrosis and to assess the characteristics of patients with severe osteonecrosis.

Children aged 1-18 years with newly diagnosed ALL between January 1997 to March 2015 treated according to the DCOG ALL-9 or ALL-10/11 MRG protocol were eligible for this study. Detailed information on patient selection and data collection is provided in the *Online Supplementary Appendix*. For our primary aim, the CION was estimated from start post-consolidation (landmark analysis), since dexamethasone pulses started from this timepoint onwards. Consent from patients and/or legal guides for data collection had been previously obtained.

Patients were treated with dexamethasone during induction and with long pulses dexamethasone (14 days 6 mg/m^2/day every 7 weeks, cumulative dose non-high risk group, 1,370 mg/m^2; high risk group, 1,244 mg/m^2) without concurrent asparaginase during post-consolidation in ALL-9 (*Online Supplementary Table S1*). Patients in ALL-10/11 MRG were treated with prednisone during induction and with short pulses dexamethasone (5 days 6 mg/m^2/day every 3 weeks, cumulative dose, 1,115 mg/m^2) with 18 or 30 weeks concurrent PEG-asparaginase (2,500 IU/m^2 [ALL-10] or an individualized dose [ALL-11] every 2 weeks) during post-consolidation, resulting in six or ten dexamethasone pulses that were administered concomitantly with PEG-asparaginase.

Osteonecrosis was defined as persistent pain in joints and/or limbs (not resulting from vincristine neuropathy) developed during or in the first year after ALL treatment and confirmed by magnetic resonance imaging (and/or X-ray, see the *Online Supplementary Appendix*). Severe osteonecrosis was defined as Ponte di Legno (PdL) grade 4 (*Online Supplementary Table S2*) in ALL-10/11 MRG.[9]

The CION since start post-consolidation therapy was estimated for patients treated in ALL-10/11 MRG *versus* ALL-9 using competing risk models with stem cell transplantation, second malignancy, relapse and death as competing event. In this analysis, only the subset of patients who reached post-consolidation per protocol was included. The CION since ALL diagnosis was estimated for different age categories in the total cohort. Fine and Gray's test was used to assess the difference between the CION. A univariable and multivariable Cox proportional hazard regression model was used to estimate the effect of risk factors on osteonecrosis (see the *Online Supplementary Appendix* for details).

Of 1,612 patients eligible for ALL-9 (n=886) and ALL-10/11 MRG (n=726), 1,470 (91%) were included in this study (*Online Supplementary Figure S1*). Thirteen hundred eighty-four (94%) of these patients reached the start of post-consolidation therapy per protocol and were included in the landmark analysis. The baseline characteristics of patients treated in ALL-9 *versus* ALL-10/11 MRG were not significantly different (*Online Supplementary Table S3*).

In total, 79 (5%) of 1,470 patients developed osteonecrosis during the study. Thirty-six (5%) of 731 children in ALL-9 and 38 (6%) of 652 children in ALL-10/11 MRG who were included in the landmark analysis developed osteonecrosis, respectively. No statistically significant difference between the CION since start post-consolidation therapy for the two groups was found (P=0.54, Figure 1); at 3 years since the start of post-consolidation therapy, the CION was 4.9% (95% Confidence Interval [CI]=3.4-6.5) and 5.4% (95% CI=3.6-7.1) in ALL-9 *versus* ALL-10/11 MRG, respectively. In addition, the CION since ALL diagnosis was estimated, which showed no statistically significant difference (P=0.80, *Online Supplementary Figure S2*).

Table 1. Cause-specific hazard ratio estimates along with their 95% Confidence Intervals for the risk of symptomatic osteonecrosis since start post-consolidation therapy from a univariable and multivariable Cox proportional hazard regression model.

	Univariable model n=1,383			Multivariable model n=1,383		
	HR_{cs}	95% CI	*P*	HR_{cs}	95% CI	*P*
Post-consolidation regimen (ALL-10/11 MRG *vs.* ALL-9)	1.21	0.76-1.92	0.416	0.69	0.43-1.11	0.123
Age (yrs)	1.38	1.30-1.46	<0.001	1.40	1.32-1.49	<0.001
Sex (male *vs.* female)	1.18	0.75-1.87	0.479	1.53	0.97-2.44	0.070
BMI (SDS)	1.01	0.82-1.24	0.942	0.90	0.73-1.10	0.289

ALL: acute lymphoblastic leukemia; BMI: body mass index; CI: Confidence Interval; DEXA: dexamethasone; HR_{cs}: cause-specific hazard ratio; MRG: medium risk group; SDS: standard deviation score; yrs: years.

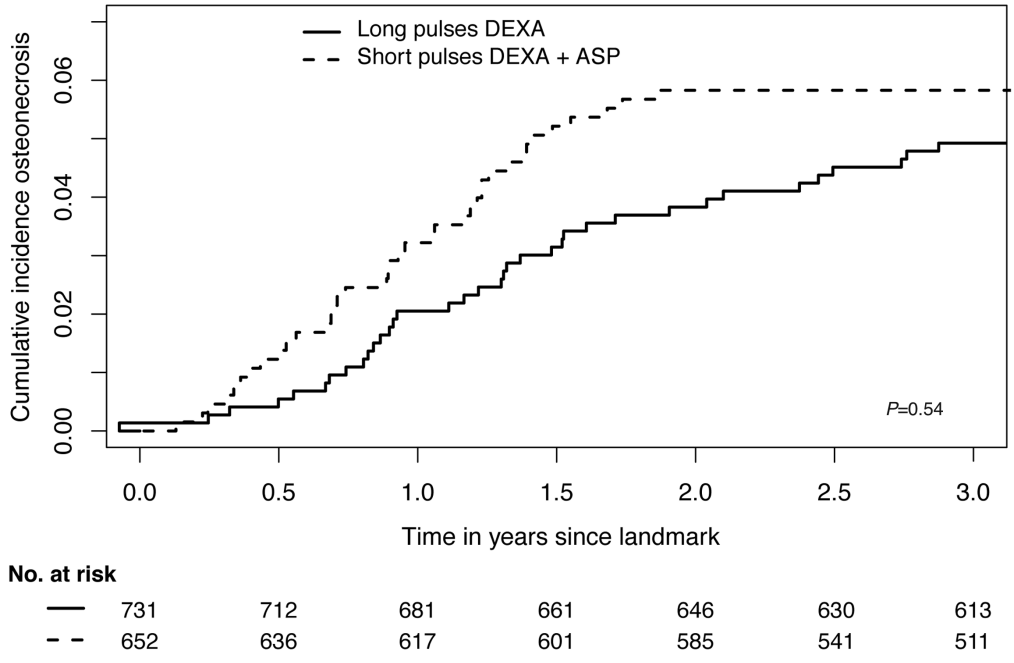


Figure 1. Cumulative incidence of symptomatic osteonecrosis for patients treated with long pulses dexamethasone (n=731) and patients treated with short pulses dexamethasone plus asparaginase (n=652) since start post-consolidation therapy (landmark). ASP: asparaginase; DEXA: dexamethasone.

In multivariable analysis including type of post-consolidation treatment regimen, age at ALL diagnosis, sex and body mass index standard deviation score, age was the only significant independent risk factor (cause-specific hazard ratio [HR_{CS}]=1.40; 95% CI=1.32-1.50; P<0.001, Table 1).

A statistically significant difference between the CION for different age categories at ALL diagnosis was observed (P<0.001, Figure 2). At 3 years since ALL diagnosis, the CION was 1.2% (95% CI=0-2.3), 14.3% (95% CI=10.0-18.5) and 31.4% (95% CI=30.9-31.9%) for children aged (years) 1-9, 10-14, and 15-18, respectively.

Fifteen of 38 children (39%) with osteonecrosis in ALL-10/11 MRG experienced severe osteonecrosis. Severe osteonecrosis occurred in none of the 6 children with osteonecrosis aged (years) 1-9, in 5 of the 15 (33%) aged 10-14, and in 10 of the 17 (59%) aged 15-18.

For detailed information on the site and management of osteonecrosis, refer to the *Online Supplementary Appendix*.

In this study, no statistically significant difference in the CION for children treated with short versus long pulses dexamethasone was found. Based on the findings of the CCG-1961 trial,[5] we hypothesized that patients treated with short pulses dexamethasone would have a lower CION. This hypothesis was consistent with a recent preclinical study which showed that asparaginase added to a discontinuous dexamethasone regimen did not increase osteonecrosis occurrence in mice.[10]

We realized however, that to increase the survival of children with ALL over the past decades, asparaginase intensification has played an important role. Although the combined administration of dexamethasone and asparaginase in our protocols does not allow to prove the relative contribution of asparaginase to osteonecrosis development, we think it is conceivable that intensification of ALL treatment components other than dexamethasone regimens such as asparaginase may explain our findings. There is evidence that asparaginase is associated with osteonecrosis, especially when administered concurrently with dexamethasone.[1,7] We have previously shown that in patients with osteonecrosis, a hypercoagulable state may result from a lower dexamethasone-related increase of anticoagulants in combination with a subsequent decline of these anticoagulants after asparaginase introduction.[1] Furthermore, asparaginase increases the plasma concentration of dexamethasone, and in particular PEG-asparaginase may increase triglyceride levels (associated with osteonecrosis) especially in combination with dexamethasone.[7,11,12] In a controlled pre-clinical model, mice receiving asparaginase plus continuous dexamethasone experienced osteonecrosis more often than those receiving dexamethasone alone.[13] Furthermore, discontinuous dexamethasone reduced the risk of osteonecrosis compared to continuous dexamethasone in the CCG-1961 trial more in patients who received intensified *versus* standard treatment, also suggesting that other treatment components may play a role in the effect of dexamethasone pulses duration.[5] Other explanations for our finding could be that the long pulses dexamethasone in the DCOG ALL-9 protocol were already shorter than the continuous dexamethasone in the CCG-1961 trial, and administered throughout maintenance compared to during delayed intensification only, respectively.

Our results highlight the relevance of therapeutic context when interpreting results of treatment-related toxicity. Further research addressing the effect of dexamethasone and asparaginase schedules on osteonecrosis occurrence is needed. This is of interest since older children who are at highest risk of (severe) osteonecrosis are also most likely to have an unfavorable leukemia outcome, which raises serious cautiousness towards ALL treatment reduction because of toxicity.[14] Furthermore, adequate treatment of osteonecrosis remains an issue: overall success of conservative treatment is limited since about 50% of patients reported persistent symptoms after 5 years of

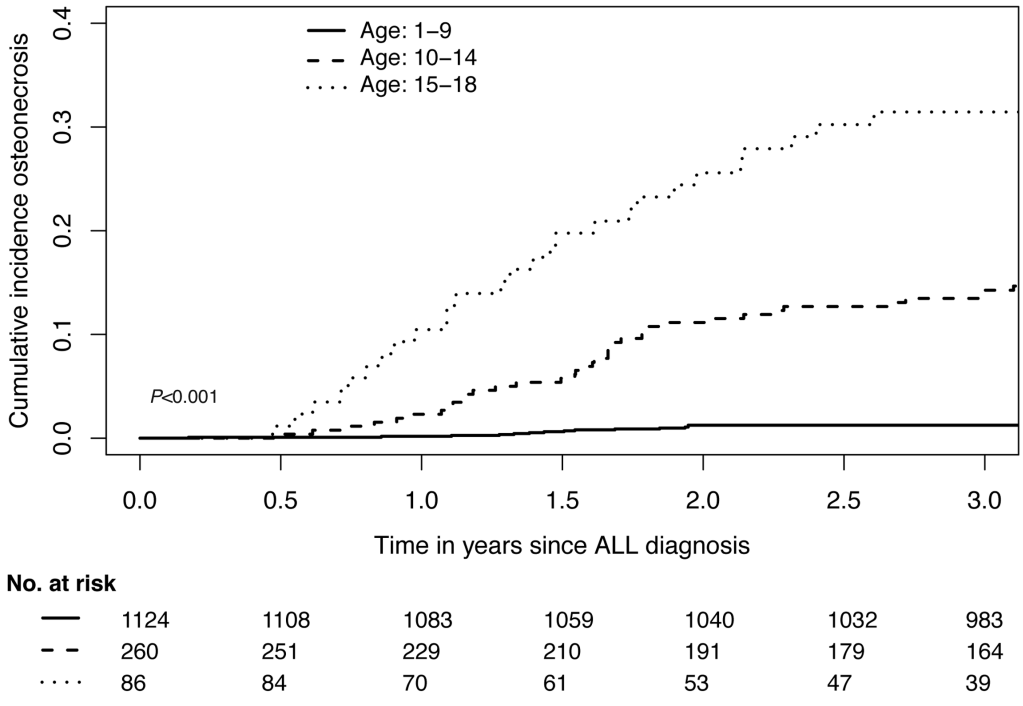


Figure 2. Cumulative incidence of symptomatic osteonecrosis for children aged 1-9 years (n=1,124), 10-14 years (n=260) and 15-18 years (n=86) since acute lymphoblastic leukemia diagnosis. ALL: acute lymphoblastic leukemia.

follow-up.[2] Hence, prevention of osteonecrosis by treatment scheduling modification seems preferable since it could possibly decrease osteonecrosis associated morbidity without jeopardizing leukemia outcome.

The association between age and the risk of osteonecrosis has been thoroughly studied. Adolescents are disproportionally affected by this toxicity relative to younger children and adults.[15] We here confirmed findings from other large studies,[5,16] and showed in addition that the 3-year CION was significantly different in children aged (years) 1-9 (1.2%), 10-14 (14.3%), and 15-18 (31.4%). This means that among children older than 10 years, an age group that most studies have focused on,[4,7,15] children aged 15-18 seem to develop osteonecrosis most often, even relative to children aged 10-14 years. This is especially important since our study for the first time shows that in these 15-18-year-old patients, the osteonecrosis is more often severe. Of all patients affected by severe osteonecrosis, 67% ultimately required joint replacement and 20% still experienced chronic pain at follow-up, indicating the clinical relevance of this complication. Our finding is in line with previous studies that showed an increased risk of severe osteonecrosis and hip replacement among older children.[5,17] More studies are needed to better understand the occurrence of severe and progressive osteonecrosis.

The results of our study must be interpreted in light of several limitations. We did not perform a randomized controlled trial, so differences between the cohorts other than those adjusted for may exist. We think limiting our analysis to the MRG in ALL-10/11 was justified, but could have introduced bias. However, an overall analysis comparing the CION of ALL-9 *versus* the entire ALL-10/11 cohort showed similar results. Although we attempted to rule out differences in induction therapy by employing a landmark analysis, this protocol variation, as well as differences in asparaginase formulation, should be appreciated. Furthermore, all patients in ALL-10/11 received both short pulses dexamethasone and asparaginase, so assessing the effect of each treatment component separately was not possible.

We conclude that no statistically significant difference in the CION for children treated with short pulses dexamethasone plus asparaginase *versus* long pulses of dexamethasone alone during ALL post-consolidation therapy was found. We postulate that the protective effect of shorter pulses dexamethasone on osteonecrosis occurrence may be attenuated by recent intensification of other treatment components such as asparaginase. Among children older than 10 years, especially children aged 15-18 years developed symptomatic, in particular severe osteonecrosis.

Jenneke E. van Atteveld,[1] Hester A. de Groot-Kruseman,[2] Marta Fiocco,[1,3,4] Maarten H. Lequin,[1,5] Sebastian J.C.M.M. Neggers,[1] Saskia M.F. Pluijm,[1] Inge M. van der Sluis,[1] Rob Pieters[1] and Marry M. van den Heuvel-Eibrink[1]

[1]Princess Máxima Center for Pediatric Oncology, Utrecht; [2]Dutch Childhood Oncology Group (DCOG), Utrecht; [3]Medical Statistics Unit, Department of Biomedical Data Science, Leiden University Medical Center, Leiden; [4]Mathematical Institute, Leiden University, Leiden and [5]Department of Radiology, University Medical Center Utrecht, Utrecht, the Netherlands

Correspondence: JENNEKE E. VAN ATTEVELD
j.e.vanatteveld@prinsesmaximacentrum.nl

doi:10.3324/haematol.2020.257550

Disclosures: no conflicts of interest to disclose.

Contributions: JEvA study design, data collection, data analysis, data interpretation, manuscript writing; HAdG-K data collection, data analysis, data interpretation, manuscript writing; MF data analysis, data interpretation, manuscript writing; MHL data interpretation, manuscript writing; SJCMMN data interpretation, manuscript writing; SMFP data interpretation, manuscript writing;

IMvdS data interpretation, manuscript writing; RP study design, data interpretation, manuscript writing; MMvdH-E study design, data interpretation, manuscript writing.

References

1. te Winkel ML, Appel IM, Pieters R, van den Heuvel-Eibrink MM. Impaired dexamethasone-related increase of anticoagulants is associated with the development of osteonecrosis in childhood acute lymphoblastic leukemia. Haematologica. 2008;93(10):1570-1574.
2. te Winkel ML, Pieters R, Hop WCJ, et al. Prospective study on incidence, risk factors, and long-term outcome of osteonecrosis in pediatric acute lymphoblastic leukemia. J Clin Oncol. 2011;29(31):4143-4150.
3. Mattano LA, Sather HN, Trigg ME, Nachman JB. Osteonecrosis as a complication of treating acute lymphoblastic leukemia in children: a report from the Children's Cancer Group. J Clin Oncol. 2000; 18(18):3262-3272.
4. Girard P, Auquier P, Barlogis V, et al. Symptomatic osteonecrosis in childhood leukaemia survivors: prevalence, risk factors and impact of quality of life in adulthood. Haematologica. 2013;98(7):1089-1097.
5. Mattano LA, Devidas M, Nachman JB, et al. Effect of alternate-week versus continuous dexamethasone scheduling on the risk of osteonecrosis in paediatric patients with acute lymphoblastic leukaemia: results from the CCG-1961 randomised cohort trial. Lancet Oncol. 2012;13(9):906-915.
6. Toft N, Birgens H, Abrahamsson J, et al. Results of NOPHO ALL2008 treatment for patients aged 1-45 years with acute lymphoblastic leukemia. Leukemia. 2018;32(3):606-615.
7. Kawedia JD, Kaste SC, Pei D, et al. Pharmacokinetic, pharmacodynamic, and pharmacogenetic determinants of osteonecrosis in children with acute lymphoblastic leukemia. Blood. 2011;117(8):2340-2347; quiz 2556.
8. Pieters R, Hunger SP, Boos J, et al. L-asp treatment in ALL: a focus on erwinia. Cancer. 2011;117(2):238-249.
9. Schmiegelow K, Attarbaschi A, Barzilai S, et al. Consensus definitions of 14 severe acute toxic effects for childhood lymphoblastic leukaemia treatment: a Delphi consensus. Lancet Oncol. 2016;17(6):e231-e239.
10. Karol SE, Janke LJ, Panetta JC, et al. Asparaginase combined with discontinuous dexamethasone improves antileukemic efficacy without increasing osteonecrosis in preclinical models. PLoS One. 2019;14(5):e0216328.
11. Yang L, Panetta JC, Cai X, et al. Asparaginase may influence dexamethasone pharmacokinetics in acute lymphoblastic leukemia. J Clin Oncol. 2008;26(12):1932-1939.
12. Finch ER, Smith CA, Yang W, et al. Asparaginase formulation impacts hypertriglyceridemia during therapy for acute lymphoblastic leukemia. Pediatr Blood Cancer. 2019;(Aug 2019):1-10.
13. Liu C, Janke LJ, Kawedia JD, et al. Asparaginase potentiates glucocorticoid-induced osteonecrosis in a mouse model. PLoS One. 2016;11(3):1-13.
14. Pieters R, de Groot-kruseman H, Van Der Velden V, et al. Successful therapy reduction and intensification for childhood acute lymphoblastic leukemia based on minimal residual disease monitoring: study ALL10 from the Dutch Childhood Oncology Group. J Clin Oncol. 2016;34(22):2591-2601.
15. Toft N, Birgens H, Abrahamsson J, et al. Toxicity profile and treatment delays in NOPHO ALL2008-comparing adults and children with Philadelphia chromosome-negative acute lymphoblastic leukemia. Eur J Haematol. 2016;96(2):160-169.
16. Möricke A, Zimmermann M, Valsecchi MG, et al. Dexamethasone vs prednisone in induction treatment of pediatric ALL: results of the randomized trial AIEOP-BFM ALL 2000. Blood. 2016;127(17):2101-2112.
17. Mogensen SS, Harila-Saari A, Makitie O, et al. Comparing osteonecrosis clinical phenotype, timing, and risk factors in children and young adults treated for acute lymphoblastic leukemia. Pediatr Blood Cancer. 2018;65(10):e27300.

Endoplasmic reticulum stress controls iron metabolism through *TMPRSS6* repression and hepcidin mRNA stabilization by RNA-binding protein HuR

The liver hormone hepcidin controls the main inflows of iron into plasma by binding to and inducing the degradation or the occlusion of the iron export activity of ferroportin, the only known cellular exporter of iron.[1,2] When hepcidin concentrations are high, iron is trapped in enterocytes of the duodenum, hepatocytes, and macrophages. Hepcidin production by the hepatocytes is induced by a number of stimuli, most notably iron, through the BMP-SMAD signaling pathway,[3] and inflammatory signals, through the IL-6/ STAT3 signaling axis.[4] In addition, hepcidin has also been reported to respond to intracellular stress, namely endoplasmic reticulum (ER) stress which is involved in a number of pathophysiological states, including the inflammatory response, nutrient disorders and viral infection. A previous study has suggested that hepcidin induction by ER stress is controlled by the BMP-SMAD pathway,[5] but the exact mechanism is still uncertain.

ER stress may have an important role in the development of nonalcoholic fatty liver disease (NAFLD).[6] Indeed, hepatic lipid accumulation induces ER stress, and, in turn, the ER stress response promotes hepatic lipogenesis, thus creating a positive-feedback loop, which may contribute to the development of hepatic steatosis.[6] ER stress has also been implicated in the development of hepatocellular injury and fibrosis and the progression of simple steatosis to nonalcoholic steatohepatitis (NASH). Interestingly, approximately one third of patients with NAFLD show signs of disturbed iron homeostasis as indicated by elevated serum ferritin with normal or mildly elevated transferrin saturation, mild hepatic iron deposition[7] and increased hepcidin production.[8] Excess iron is proposed to aggravate the natural course of NAFLD because of its capability to catalyze the formation of toxic hydroxyl radicals that cause cellular damage. Iron accumulation in NAFLD is mainly due to impaired iron export from hepatocytes and Kupffer cells[7] which might well be the consequence of hepcidin induction by ER stress.

Given the potential impact of ER stress-induced hepcidin on hepatic iron deposition in NAFLD patients, it is essential to better understand the molecular mechanisms leading to the induction of hepcidin in this context. In order to definitely elucidate these mechanisms, we used a model of acute ER stress induced in mice by tunicamycin. We demonstrated that induction of hepcidin by ER stress requires repression of *TMPRSS6*, the gene coding for the inhibitor of BMP-SMAD1/5/8 signaling, matriptase-2, and stabilization of hepcidin mRNA by the RNA-binding protein, HuR.

In order to investigate the kinetics of hepcidin induction by ER stress over time, wild-type (WT) mice received one intraperitoneal (IP) injection of tunicamycin (Tm) (2 mg/kg), a well-known ER stress inducer, and were sacrificed at time points ranging from 3 to 24 hours after injection. As expected, Tm injection triggered ER stress in the liver (*Online Supplementary Figures S1A-B, S2A-B*). As shown in *Online Supplementary Figure S1C*, hepcidin gene expression progressively increased and reached a maximum 6 hours after Tm injection. Therefore, this time point was chosen for performing all the following experiments.

As expected, we show that hepcidin induction coincides with an activation of the BMP-SMAD pathway (Figure 1A-C; Online *Supplementary Figure S1D*) which is dependent on the Bmp type 1 receptor Bmpr1a (*Online Supplementary Figure S3*) 6 hours after Tm injection. In this study, our objective was to find out the mechanisms that activate BMP-SMAD signaling during ER stress, leading to excessive hepcidin production. As shown in the *Online Supplementary Figure S4A-H*, Tm did not increase the expression of the ligands known to activate Bmp-Smad signaling and hepcidin gene expression in circumstances other than ER stress, i.e., Bmp6[3] and Bmp2[9] and does not modulate the expression of other genes belonging to this pathway. Another ligand of the TGF-β family, activin B, was suggested to induce hepcidin in ER stress5 but, as shown in the *Online Supplementary Figure S4I-J*, Tm similarly induced *Id1* and hepcidin gene expression in *Inhbb*$^{-/-}$ mice, lacking activin B, and in WT controls. A role for activin B in this process is thus unlikely.

Matriptase-2, encoded by the *TMPRSS6* gene, is a strong inhibitor of the BMP-SMAD signaling pathway and of hepcidin expression.[10] Interestingly, Tm injection significantly suppressed matriptase-2 at mRNA (Figure 1D; *Online Supplementary Figure S1E*) and protein (*Online Supplementary Figure S5*) levels, which could explain the observed activation of BMP-SMAD signaling and induction of hepcidin expression in these mice. In order to confirm this hypothesis, we assessed the response of *Tmprss6*$^{-/-}$ mice to Tm. Notably, in the absence of stimulation, Smad5 phosphorylation and *Id1* expression are, as expected, constitutively high in *Tmprss6*$^{-/-}$ mice, but they have not reached their peak and can still be further induced by iron dextran (*Online Supplementary Figure S6F-G*). This demonstrates that *Tmprss6*$^{-/-}$ mice have the ability to activate the BMP-SMAD signaling in response to external stimuli. However, although ER stress was similarly induced in both *Tmprss6*$^{-/-}$ and WT mice (*Online Supplementary Figure S6A-D*), Smad5 phosphorylation (Figure 1E) and *Id1* expression (Figure 1F) were not further increased by Tm in *Tmprss6*$^{-/-}$ mice. In order to determine if the loss of BMP-SMAD activation was not blunted by the iron deficiency anemia of *Tmprss6*$^{-/-}$ mice, we used *Bmp6*$^{-/-}$ - *Tmprss6*$^{-/-}$ mice which have a BMP signaling similar to WT mice and no iron deficiency anemia.[11] In this mouse model, BMP signaling is not induced by Tm injection either (*Online Supplementary Figure S7A-B*) confirming that repression of matriptase-2 is required for activation of BMP-SMAD signaling by ER stress. Of note, lack of Bmp6 only does not prevent the induction of BMP signaling and hepcidin expression in response to ER stress (*Online Supplementary Figure S8*).

Quite surprisingly though, and despite the lack of further Smad5 activation, hepcidin induction was not totally abolished in mice lacking matriptase-2 (Figure 1G; *Online Supplementary Figure S7C*), suggesting that a second mechanism contributes to the whole magnitude of hepcidin upregulation in ER stress.

In order to characterize this additional mechanism observed in *Tmprss6*$^{-/-}$ mice, we used the HepG2 hepatoma cell line that expresses *TMPRSS6* mRNA at a level so low that a siRNA directed against it is unable to promote any activation of BMP-SMAD signaling (data not shown). The HepG2 cell line is thus a good model to characterize hepcidin regulation by ER stress independently of matriptase-2 and BMP-SMAD signaling. Treatment of HepG2 cells with Tm induces ER stress (Figure 2A) and hepcidin (Figure 2B; *Online Supplementary Figure S9A*) even in the absence of Smad5 activation or *ID1* mRNA induction (Figures 5C-D; *Online Supplementary Figure S9B*).

The cytoplasmic level of a messenger RNA relies not only on its rate of synthesis but also on its decay rate. Therefore, in order to determine if the hepcidin level in response to Tm is regulated through induction of its transcription or through increased stability of its mRNA, HepG2 cells were treated with the transcriptional inhibitor actinomycin D. As expected, treatment with actinomycin D significantly reduced hepcidin mRNA levels in these cells (Figure 2E). However, when treated with Tm in the presence of actinomycin D, HepG2 cells still exhibited a significant increase in hepcidin mRNA expression (Figure 2E), clearly demonstrating that ER stress controls hepcidin gene expression through post-transcriptional mechanisms.

Interestingly, ELAVL1/HuR was recently described as a protein stabilizing hepcidin mRNA in response to satu-

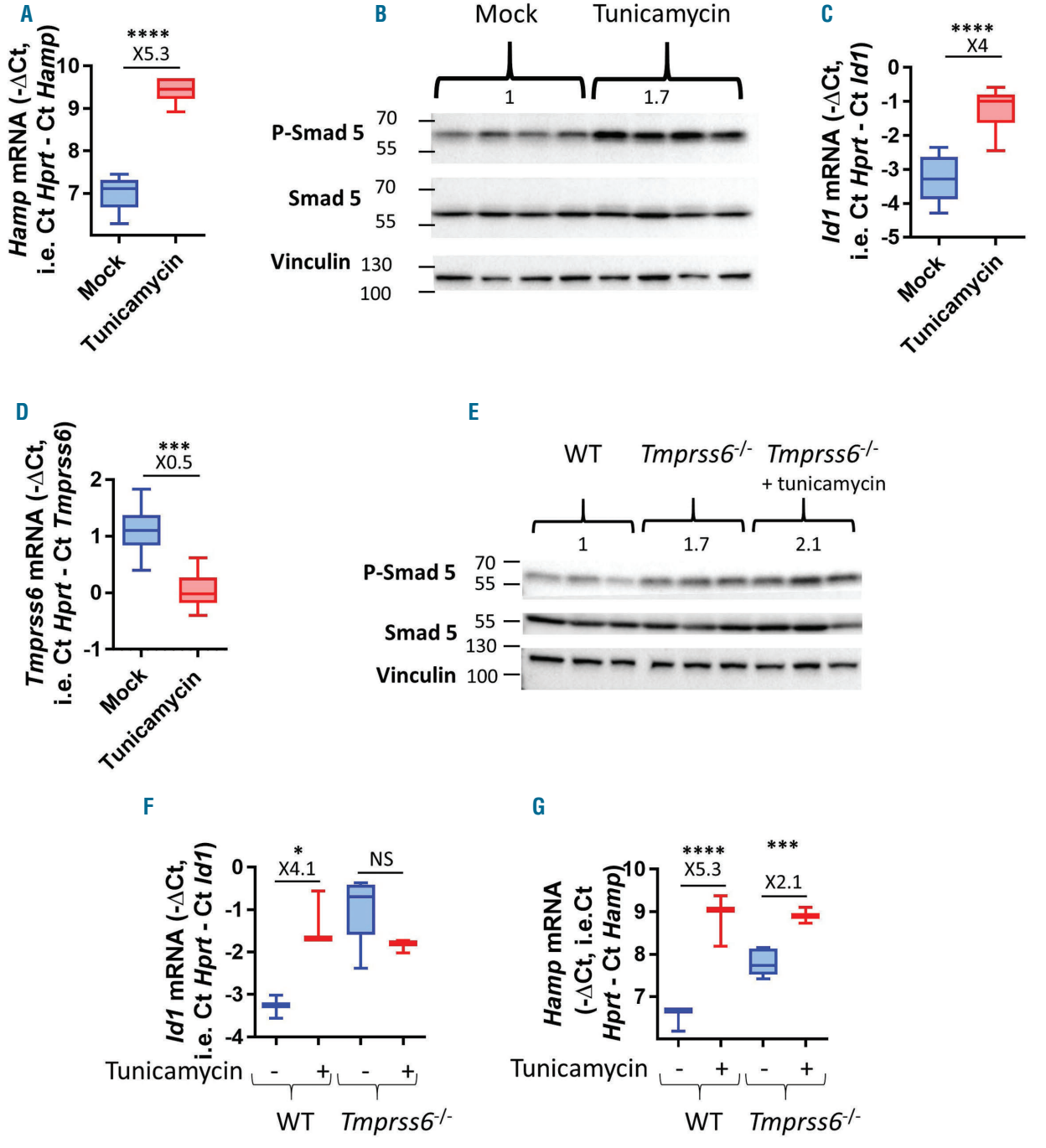


Figure 1. Endoplasmic reticulum stress upregulates hepcidin expression and activates the BMP-SMAD signaling pathway partially through matriptase-2. Wild-type (WT) CD1 mice (6-9/group) were injected with mock (blue boxes) or tunicamycin (red boxes) and were analyzed 6 hours (h) later for liver (A) *Hamp* mRNA expression; (B) P-Smad 5 relative to total Smad5 protein expression; (C) *Id1* mRNA expression and (D) *Tmprss6* mRNA expression. C57Bl/6 WT mice and *Tmprss6*$^{-/-}$ mice (3-4/group) were injected with mock (blue boxes) or tunicamycin (red boxes) and were analyzed 6 h later for liver (E) P-Smad 5 relative to total Smad 5 protein expression; (F) *Id1* mRNA expression and (G) *Hamp* mRNA expression. Estimates of the fold changes in gene expression ($2^{-\Delta\Delta Ct}$) are shown on the graphs. *P<0.05; ***P<0.001; ****P<0.0001.

rated fatty acids. It acts through a direct interaction with the AU-rich elements (ARE) located in the 3'UTR of hepcidin mRNA.[12] Importantly, we observed that HuR mRNA expression is increased in the liver in response to Tm treatment (*Online Supplementary Figure S1F*). HuR was thus a good candidate for the control of hepcidin mRNA stability not only in response to fatty acids but also to ER stress. In HepG2 cells transfected with a siRNA pool directed against human HuR, HuR silencing reduced *HuR* mRNA expression (Figure 2F) and, prevented a significant increase of hepcidin mRNA in response to Tm (Figure 2G). In order to determine if, in response to Tm, HuR regulates hepcidin mRNA stability through direct binding to hepcidin 3'UTR, we performed RNA-CLIP experiments with HuR or IgG control antibodies followed by quantitative RT-PCR with primers specific for the hep-

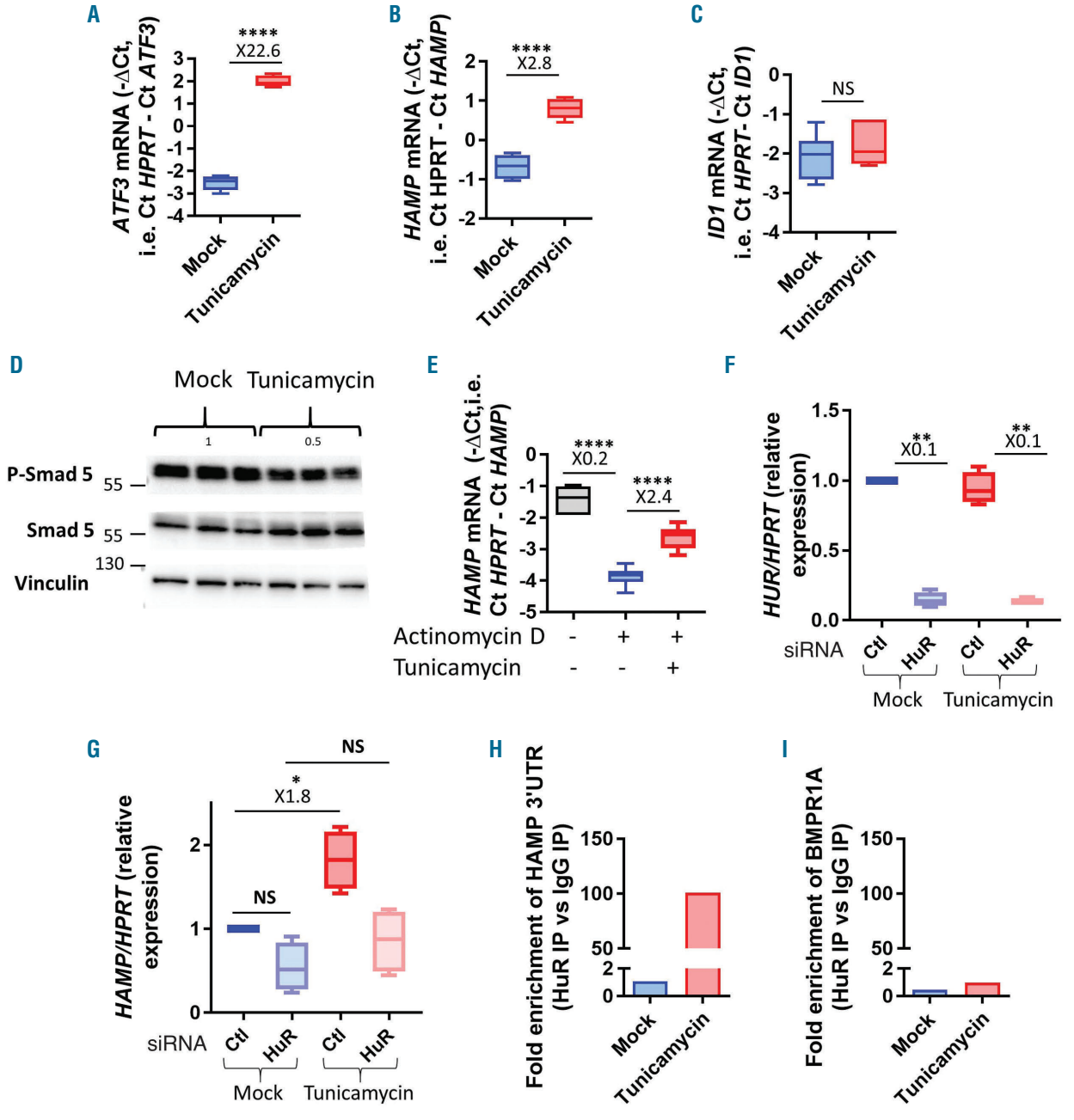


Figure 2. Endoplasmic reticulum stress stabilizes hepcidin mRNA through HuR *in vitro*. HepG2 cells were treated with mock (blue boxes) or tunicamycin (Tm) (red boxes) and analyzed for (A) *ATF3* mRNA expression; (B) *HAMP* mRNA expression; (C) *ID1* mRNA expression and (D) P-Smad 5 relative to total Smad 5 protein expression. Values shown are the result of three independent experiments performed in duplicate. (E) HepG2 cells were treated with mock (black box) or actinomycin D alone (blue box) or together with Tm (red box) for 6 hours (h) and analyzed for *HAMP* mRNA expression. (F-G) HepG2 cells were transfected either with a control pool of small interfering RNA (siRNA) or a pool of siRNA designed to silence human HuR and subjected to either treatment with mock (blue box) or Tm (red box) for 6 h. The results of four experiments were analyzed by repeated measures one-way ANOVA. Fold-change compared to cells transfected with siRNA control (ctl) and treated with mock are shown on the graphs. Total lysates from HepG2 cells treated with mock or Tm were subjected to cross-linking immunoprecipitation CLIP-seq RNA-CLIP with either HuR or control normal IgG antibodies. RNA was collected from the immunoprecipitates and analyzed for (H) HAMP 3'untranslated region (UTR) sequence and (I) a non-relevant sequence (BMPR1A) enrichment by quantitative RT-PCR. One representative experiment over three independent experiments is presented. Estimates of the fold changes in gene expression ($2^{-\Delta\Delta Ct}$) are shown on the graphs. **P*<0.05; ***P*<0.01; *****P*<0.0001. NS: not significant.

cidin 3'UTR sequence or a non-relevant sequence in the *BMPR1A* gene. In cells treated with Tm, the level of hepcidin 3'UTR measured in the immunoprecipitate collected with HuR antibody was increased 20 to 6,700-fold relative to that in the immunoprecipitate collected with control IgG (Figure 2H; *Online Supplementary Figure S10A-B*). No such enrichment of hepcidin 3'UTR is seen in cells treated with mock. Furthermore, there was no enrichment of the non-relevant sequence in the immunoprecipitate collected with HuR antibody (Figure 2I; *Online Supplementary Figure S10C-D*), indicating that Tm treatment specifically promotes binding of the RNA stabilizer HuR to hepcidin 3'UTR.

Interestingly, while HuR mRNA expression is stimulated in response to ER stress in WT and *Tmprss6*$^{-/-}$ mice (*Online Supplementary Figures S1F, S6E*), it is blunted when *Bmpr1A* is missing (*Online Supplementary Figure S3H*). This is consistent with the previously reported transcriptional control of HuR by BMP-SMAD signaling.[13] Accordingly, hepcidin mRNA expression is not stabilized in *Bmpr1A*$^{hep/hep}$ mice.

In the present study, we showed that ER stress up-regulates the iron-regulatory hormone hepcidin through two complementary mechanisms. The first involves the inhibition of matriptase-2, which activates BMP-SMAD signaling without the induction of Bmp2 and Bmp6 or the requirement for activin B. The second is the stabilization of hepcidin mRNA by the RNA-binding protein, HuR. These two mechanisms appear to act sequentially. Indeed, whereas the induction of another target of BMP-SMAD signaling, Id1, reached a plateau 3 hours after Tm injection (*Online Supplementary Figure S1D*), hepcidin mRNA did not achieve its maximal level at this time point and continued to rise at least 2-fold between 3 and 6 hours (*Online Supplementary Figure S1C*). This coincided with the induction of Hur expression in the liver (*Online Supplementary Figure S1F*). Thus, the effect of HuR on hepcidin mRNA stabilization is very likely secondary to the activation of BMP-SMAD signaling. Moreover, in WT mice, in which both mechanisms are functional, hepcidin is increased 5.3 times whereas in *Bmp6*$^{-/-}$*-Tmprss6*$^{-/-}$ mice in which the BMP signaling is not activated, hepcidin expression is only induced 2.8 times. This suggests that both mechanisms each contribute to half of the whole magnitude of hepcidin induction in response to ER stress. Interestingly, *HuR* mRNA is not increased in mice lacking *Bmpr1A* specifically in hepatocytes. A functional BMP-SMAD signaling pathway is thus necessary for the induction of hepcidin by ER stress.

Chronic liver ER stress, promoted at least in part by liver fatty acid accumulation,[6] contributes to the progression of NAFLD towards NASH.[14-16] Mild to moderate hepatic iron accumulation, seen in hepatocytes and/or in cells of the reticuloendothelial system of one third of the patients with NAFLD,[7] is also a factor of poor prognosis. Finally, NAFLD patients often have high levels of hepcidin.[8] *In vitro*, HuR stabilizes hepcidin mRNA in response not only to ER stress as demonstrated here but also to saturated fatty acids.[12] As saturated fatty acids accumulate in the liver in NAFLD and induce ER stress, it is highly likely that ER stress is the intermediary between fatty acids and activation of HuR and that HuR also participates in hepcidin regulation in patients with NAFLD. Nonetheless, the role of HuR on the stabilization of hepcidin *in vivo* will need to be confirmed by further studies.

Audrey Belot,[1] Ophélie Gourbeyre,[1] Anais Palin,[1] Aude Rubio,[1] Amélie Largounez,[1] Céline Besson-Fournier,[1] Chloé Latour,[1] Megane Lorgouilloux,[1] Inka Gallitz,[2] Alexandra Montagner,[3] Arnaud Polizzi,[3] Marion Régnier,[3] Sarra Smati,[3] An-Sheng Zhang,[4] Manuel D. Diaz-Munoz,[5] Andrea U. Steinbicker,[2] Hervé Guillou,[3] Marie-Paule Roth,[1] Hélène Coppin[1] and Delphine Meynard[1]

[1]IRSD, Université de Toulouse, INSERM, INRA, ENVT, UPS, Toulouse, France; [2]Department of Anesthesiology, Intensive Care and Pain Medicine, University Hospital Muenster, University of Muenster, Muenster, Germany; [3]Institut National de La Recherche Agronomique (INRA), UMR1331 ToxAlim, Toulouse, France and [4]Cell, Developmental, and Cancer Biology, Oregon Health & Science University, Portland, OR, USA and [5]CPTP, INSERM UMR1043/CNRS U5282, Toulouse, France

Correspondence:
DELPHINE MEYNARD - delphine.meynard@inserm.fr

doi:10.3324/haematol.2019.237321

Disclosures: no conflicts of interest to disclose.

Contributions: AB, OG, AP, AR, and AL performed experiments, analyzed, and discussed results; CB-F, CL, ML, IG, AM, AP, MR, SS and AUS performed experiments; MD-M, AUS, HG analyzed and discussed results; A-SZ provided antibody against matriptase-2, DM, HC, and M-PR discussed data and wrote the manuscript; DM designed research, performed experiments, analyzed and discussed data, and wrote the manuscript; and all authors reviewed and approved the final manuscript.

Acknowledgments: the authors are grateful to Carlos Lopez Otin (University of Oviedo, Oviedo, Spain) for kindly providing the original *Tmprss6*$^{-/-}$ mice on a mixed genetic background. They also thank Florence Capilla (Experimental Histopathology Platform, Toulouse Purpan), and members of the INSERM US006 facility (Toulouse) for their technical assistance and help in the mouse breeding..

Funding: DM was supported by the Cooley's Anemia Foundation, the French Foundation for Rare Diseases, the Région Midi-Pyrénées and ANR (ANR-17-CE14-0036-01 and ANR-17-CE14-0031-01). AUS was supported by a research grant of the German Research Foundation (DFG, STE-1985/4-1). HG was supported by grants from Région Occitanie and ANR (ANR-15-CE14-0026-Hepatokind). MDD-M was supported by ATIP-AVENIR (INSERM/CNRS) program and by Plan-Cancer (C18003BS). A-SZ was supported by a grant from NIH (R01DK102791). This work was also supported by the "Programme des Investissements d'Avenir" ANINFIMIP (ANR-11EQPX-0003).

References

1. Nemeth E, Tuttle MS, Powelson J, et al. Hepcidin regulates cellular iron efflux by binding to ferroportin and inducing its internalization. Science. 2004;306(5704):2090-2093.
2. Aschemeyer S, Qiao B, Stefanova D, et al. Structure-function analysis of ferroportin defines the binding site and an alternative mechanism of action of hepcidin. Blood. 2018;131(8):899-910.
3. Meynard D, Kautz L, Darnaud V, Canonne-Hergaux F, Coppin H, Roth MP. Lack of the bone morphogenetic protein BMP6 induces massive iron overload. Nat Genet. 2009;41(4):478-481.
4. Nemeth E, Rivera S, Gabayan V, et al. IL-6 mediates hypoferremia of inflammation by inducing the synthesis of the iron regulatory hormone hepcidin. J Clin Invest. 2004;113(9):1271-1276.
5. Canali S, Vecchi C, Garuti C, Montosi G, Babitt JL, Pietrangelo A. The SMAD pathway is required for hepcidin response during endoplasmic reticulum stress. Endocrinology. 2016;157(10):3935-3945.
6. Wang D, Wei Y, Pagliassotti MJ. Saturated fatty acids promote endoplasmic reticulum stress and liver injury in rats with hepatic steatosis. Endocrinology. 2006;147(2):943-951.
7. Nelson JE, Wilson L, Brunt EM, et al. Relationship between the pattern of hepatic iron deposition and histological severity in nonalcoholic fatty liver disease. Hepatology. 2011;53(2):448-457.
8. Nelson JE, Klintworth H, Kowdley KV. Iron metabolism in Nonalcoholic Fatty Liver Disease. Curr Gastroenterol Rep. 2012; 14(1):8-16.
9. Koch PS, Olsavszky V, Ulbrich F, et al. Angiocrine Bmp2 signaling in murine liver controls normal iron homeostasis. Blood. 2017;

129(4):415-419.
10. Du X, She E, Gelbart T, et al. The serine protease TMPRSS6 is required to sense iron deficiency. Science. 2008;320(5879):1088-1092.
11. Nai A, Rubio A, Campanella A, et al. Limiting hepatic Bmp-Smad signaling by matriptase-2 is required for erythropoietin-mediated hepcidin suppression in mice. Blood. 2016;127(19):2327-2336.
12. Lu S, Mott JL, Harrison-Findik DD. Saturated fatty acids induce post-transcriptional regulation of HAMP mRNA via AU-rich element-binding protein, human antigen R (HuR). J Biol Chem. 2015; 290(40):24178-24189.
13. Jeyaraj SC, Singh M, Ayupova DA, Govindaraju S, Lee BS. Transcriptional control of human antigen R by bone morphogenetic protein. J Biol Chem. 2010 2;285(7):4432-4440.
14. Kammoun HL, Chabanon H, Hainault I, et al. GRP78 expression inhibits insulin and ER stress-induced SREBP-1c activation and reduces hepatic steatosis in mice. J Clin Invest. 2009;119(5):1201-1215.
15. Oyadomari S, Harding HP, Zhang Y, Oyadomari M, Ron D. Dephosphorylation of translation initiation factor 2alpha enhances glucose tolerance and attenuates hepatosteatosis in mice. Cell Metab. 2008;7(6):520-532.
16. Xiao G, Zhang T, Yu S, et al. ATF4 protein deficiency protects against high fructose-induced hypertriglyceridemia in mice. J Biol Chem. 2013;288(35):25350-25361.

Sex-specific transcriptional profiles identified in β-thalassemia patients

β-thalassemia comprises a group of heterogeneous autosomal recessive hereditary anemias characterized by the reduction or absence of β-globin chain synthesis, and it is a highly prevalent disease affecting 1.5% of the global population.[1] Three different clinical conditions are recognized in patients with β-thalassemia minor (trait) being the asymptomatic form, β-thalassemia major (TM) being the most severe form of the disease and β-thalassemia intermedia (TI) presenting with variable severity. Despite extensive characterization of the genetic basis of disease pathogenesis,[2] currently the classification of patients relies on the severity of symptoms and hemoglobin (Hb) F levels regardless of the underlying genotype. Thus, the aim of the study was to develop an approach for patient stratification based on gene expression, to pinpoint the targets that dictate each phenotype and to provide a framework for the development of therapeutic strategies focused on these targets. To this end, we have analyzed the gene expression profiles of TI, TM and healthy individuals using RNA sequencing (RNAseq) (National Center for Biotechnology Information [NCBI], GSE117221) and we have studied the differentially expressed genes (DEG) and pathways irrespective to patient genotype. Interestingly, after analysis of various confounding factors, we identified sex differences in the patients' expression profiles suggesting that males and females are differentially affected by β-thalassemia. Thus, taking sex into account might benefit prognosis, diagnosis, stratification and therapeutic management of the disease.

In particular, 49 subjects (after exclusion of low quality samples) were included in the analysis and organized in groups of three age- and sex-matched samples within each group (*Online Supplementary Tables S1-2*). RNAseq libraries were generated from erythroid precursor cell cultures after the isolation of peripheral blood mononuclear cells from all participants, as previously described.[3] We identified 716 genes with aberrant expression between TI patients and healthy subjects, and 2,885 between TM patients and healthy subjects with most of DEG seen in TI patients being also present in TM patients when compared to healthy subjects, albeit with more pronounced changes (Figure 1A; Table 1; *Online Supplementary Tables S3-5*). However, no significantly DEG were found when TM patients were compared directly to TI patients suggesting that either the global gene expression profile was very similar between the two types of the disease or that substantial variability in expression did not allow the identification of consistent changes, or both (*Online Supplementary Table S6*). In general, only small changes were detected when TM and TI were directly compared (Figure 1B) and the increased gene expression variability seen in TI patients, which did not allow the identification of the same number of significantly DEG as in the case of TM patients, also hindered the identification of DEG between TI and TM patients. Increased gene expression variability in TI potentially reflects the high level of phenotypic heterogeneity for TI patients.

Nonetheless, the expression profiles accurately portrayed the clinical observations of β-thalassemia. The severe TM phenotype was associated with induction of organismal injuries, as well as inhibition of key hematological system genes and inflammatory response molecules compared to the less severe type of the disease (TI) (Figure 1C-D; *Online Supplementary Table S7*). Moderate changes were seen in the expression levels of various globin and other interacting proteins in TI patients, whereas in TM patients the data portrayed the marked repression of β-thalassemia-related proteins with concomitant upregulation of other globin proteins as a means of compensating for the ineffective erythropoiesis (*Online Supplementary Figure S1*). Focusing on molecular pathways affected by the disease, gene set enrichment analysis (GSEA) revealed very similar pathways in both TI and TM patients as differentially represented when compared to healthy participants, in accordance with the gene expression profiles (*Online Supplementary Figure S2*). Several of the pathways identified have been previously linked to β-thalassemia validating our results, such as the impaired packaging of telomere ends,[4] impaired unfolded protein response (UPR) pathway[5] and lipid abnormalities.[6,7] Nonetheless, the lack of significant changes between TI and TM patients in terms of global gene expression profiles or molecular pathways suggest that a continuous spectrum describes the disease and not distinct conditions.

We then searched for other biological confounders that could affect global expression patterns allowing patient stratification, since the study was designed to limit as much as possible all technical sources of variation (balanced groups in terms of sex and age, standardized cell culture protocol in all centers with the matched samples being cultured at the same time, library construction per-

Table 1. Numbers of significantly differentially expressed genes.

Analysis		All	Males	Females
TI *vs.* H	Samples	16 TI *vs.* 17 H	7 TI *vs.* 8 H	9 TI *vs.* 9 H
	Up-regulated	147	315	5
	Down-regulated	569	1,244	9
	Total	**716**	**1,559**	**14**
TM *vs.* H	Samples	16 TM *vs.* 17 H	8 TM *vs.* 8 H	8 TM *vs.* 9 H
	Up-regulated	939	40	100
	Down-regulated	1,946	401	210
	Total	**2,885**	**441**	**310**
TM *vs.* TI	Samples	16 TI *vs.* 16 TM	8 TM *vs.* 7 TI	8 TM *vs.* 9 TI
	Up-regulated	0	0	0
	Down-regulated	0	0	1
	Total	**0**	**0**	**1**

TI: β-thalassemia intermedia; TM: β-thalassemia major; H: healthy. Numbers of significantly differentially expressed genes are shown for all comparisons performed. The analysis is produced by DESeq2 and differentially expressed genes were defined as significant when *Padj*<0.1.

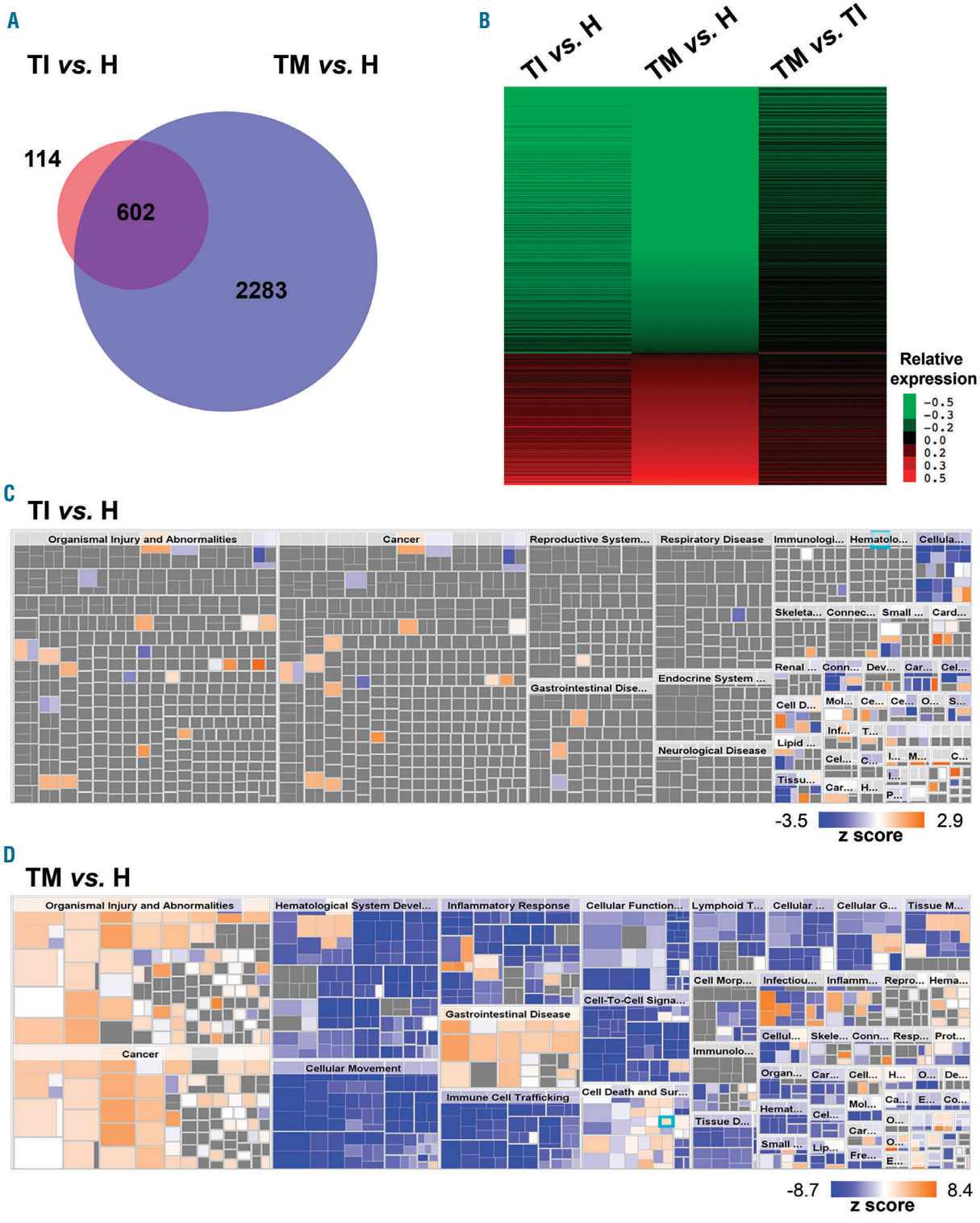


Figure 1. Differential gene expression analysis of β-thalassemia intermedia or β-thalassemia major patients against healthy participants. (A) Venn diagram depicting common significantly differentially expressed genes (DEG) when β-thalassemia intermedia (TI) (n=16) or β-thalassemia major (TM) (n=16) patients were compared to healthy (H) participants (n=17). (B) Heatmap depicting relative normalized gene expression levels (z score) of all 2,999 genes that were found significantly differentially expressed in TI or TM patients when compared to healthy participants. The $\log_2$fold change values of the genes used range from -3.0 to 3.0. (C-D) Mosaic graphs produced by Ingenuity Pathway Analysis (IPA) depicting enriched terms regarding diseases and biological functions when TI patients were compared to healthy participants (C) or when TM patients were compared to healthy participants (D). The z score depicts predicted inhibition or activation of disease/function, whereas the size of the box represents the significance of each identified term ($-\log_{10}$ *P*-value). Due to visualization purposes, category labels are not shown in full, but detailed enrichment terms can be found in the *Online Supplementary Table S7*.

formed by a single user and balanced sequencing runs). Distinct analyses performed per research center, age group and other clinical characteristics of the patients (such as HbF levels and presence or absence of splenectomy, hepatomegaly, extramedullary hematopoiesis or bone deformities) were unable to detect any major differences in the expression profiles. In order to further explore the data, we performed Principal Component Analysis (PCA), which visualizes strong patterns in a dataset by reducing the dimensionality of the dataset and clustering of samples based on their similarity. PCA did not yield clear clustering when taken into account all the different patient characteristics, with the striking exception of sex, where all samples were clustered into two distinct groups representing males and females irrespective of the disease status (Figure 2A). Although a clear dis-

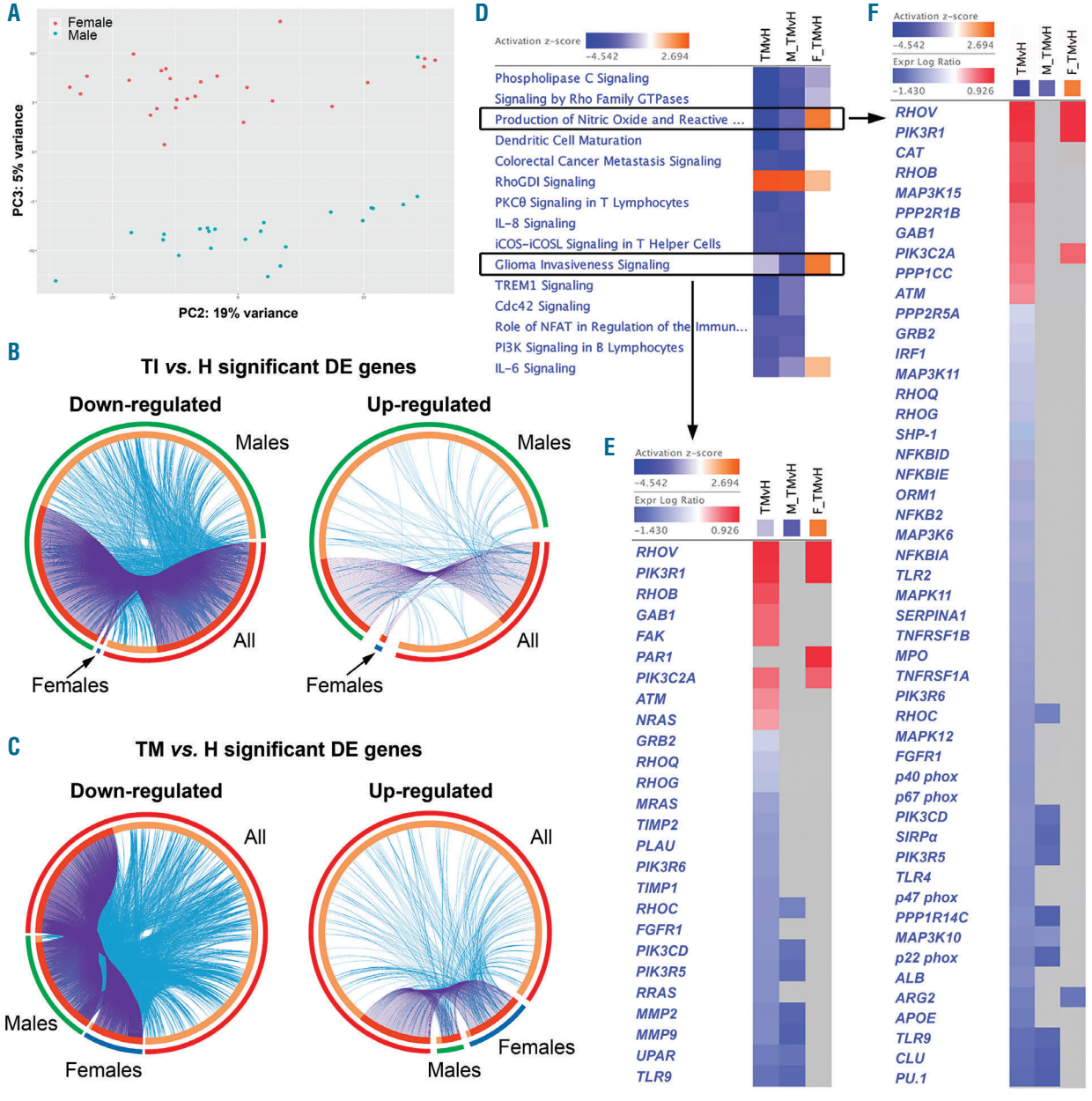


Figure 2. Differential gene expression analysis of β-thalassemia patients against healthy participants according to sex. (A) Principal Component Analysis (PCA) graph showing clustering of samples according to sex irrespective of disease status. (B-C) Circos plots depicting the down-regulated (left) and up-regulated (right) significantly differentially expressed genes (DEG) when β-thalassemia intermedia (TI) (B) or β-thalassemia major (TM) (C) patients were analysed against healthy participants. Outer circle represents the type of analysis with red depicting analysis of all samples (sixteen TI or sixteen TM samples), green depicting analysis of male samples only (seven TI or eight TM samples) and blue depicting analysis of female samples only (nine TI or eight TM samples). Inner circle represents the overlap with dark orange depicting genes that exist in multiple lists and light orange depicting genes that are unique to that particular list. Purple lines link the same genes when shared by multiple lists, whereas blue lines link different genes that fall into the same ontology term. (D) Heatmap produced by Ingenuity Pathway Analysis (IPA) depicting enriched terms regarding canonical pathways when all TM patients were analyzed against healthy participants, male only TM patients were analyzed against healthy males or female only TM patients were analyzed against healthy females. The activation z-score depicts predicted inhibition or activation of the pathway. (E-F) Heatmaps produced by IPA for two example canonical pathways; glioma invasiveness signaling (E) and production of nitric oxide and reactive oxygen species in macrophages (F). The heatmaps depict gene expression levels (expression log ratio, i.e., $\log_2$fold change), whereas the boxes above the heatmaps depict the z-score corresponding to panel D and showing the predicted inhibition or activation of the pathway.

tinction between sexes was anticipated, it raised the question whether males and females were affected in distinctive ways by the disease. In order to examine such a possibility, same sex analysis between healthy participants and patients was performed expecting fewer changes due to the lower number of samples used per differential expression analysis (from 49 participants, 23 were males and 26 were females) and similar DEG between males and females, as β-thalassemia presents with similar phenotype in both sexes and has not been linked to sex-defining genes. Interestingly, very different results were obtained for males and females suffering from TI against healthy participants, with 1,559 DEG in males, but only 14 DEG in females (Table 1; *Online Supplementary Tables S8-S9*). The very low number of DEG in females highlights the increased biological variability seen in females and suggests that other factors might play an important role in determining the disease outcome. When comparing the significantly DEG identified in both male and female TI patients with the genes identified only in male TI patients, a significant overlap was seen in down-regulated genes, not only in terms of specific genes, but also in terms of gene functionality through Gene Ontology (GO) terms (Figure 2B; *Online Supplementary Figure S3A-B; Online Supplementary Table S5*). In contrast, in up-regulated genes, fewer common genes were identified and fewer similarities in their functionality suggesting less conserved changes. Different results were also found for males and females suffering from TM when compared to healthy participants, albeit less prominent, with 441 DEG identified in males and 310 DEG in females (Table 1; *Online Supplementary Tables S10-S11*). Furthermore, the overwhelming majority of genes identified in either male or female TM patients were also yielded when all TM patients were analysed against healthy subjects irrespective of their sex (Figure 2C; *Online Supplementary Figure S3C-D; Online Supplementary Table S5*). The limited number of deregulated genes in common between female and male TM patients could demonstrate sex-specific differences, further supported by the association of different terms related to diseases and body functions in male and female patients when compared to same sex healthy subjects (*Online Supplementary Figure S4*). Dissection of the molecular pathways involved through pathway and GO analysis revealed pathways with opposing status between males and females, such as the production of nitric oxide and reactive oxygen species in macrophages, and glioma invasiveness signalling (Figure 2D-F; *Online Supplementary Figure S4*). Per sex, all the significant DEG identified exhibited a unanimous direction of transcription, but different members of the pathway were differentially expressed in males and females. The DEG identified in male or female TI and TM patients could be potentially invaluable for the development of sex-specific treatment options and stratification strategies (*Online Supplementary Tables S5, S12-S13; Online Supplementary Figure S5*).

To our knowledge no other studies comparing gene expression profiles in males and females suffering from β-thalassemia currently exist, however, there have been reports of correlations of disease symptoms or complications related to sex. For instance, HbF levels have been found significantly higher in the female population of TM patients and this difference became more apparent after the age of 30 years.[8] When considering complications of the disease, male TM patients have shown a strong association with diabetes[9] and although no clear reason currently exists for such an association, it can be partly attributed to increased sensitivity of males to iron overload.[10] Better survival rate has also been reported in females rather than males with fewer occurrences of cardiac complications and cardiac-based morbidities.[11] In terms of development of osteoporosis and osteopenia in TM patients, a sex difference was seen in the prevalence and the severity of the disorder with males being more frequently and severely affected than females.[12] In general, various pathways have been found to exhibit sex-related differences, many of which are linked to β-thalassemia, such as oxidative stress defense,[13] lipid metabolism[14] and erythropoietin activity.[15] The present study, besides the identification of sex-specific transcriptional profiles in β-thalassemia through public availability of our data, represents a novel resource for meta-analyses and follow-up studies. In conclusion, our data highlight the need for considering sex as an important variable of the disease, which should be taken into account when developing differential diagnostic and therapeutic strategies.

Aikaterini Nanou,[1] Chrisavgi Toumpeki,[1] Pavlos Fanis,[2] Nicoletta Bianchi,[3] Lucia Carmela Cosenza,[3] Cristina Zuccato,[3] George Sentis,[1] Giorgos Giagkas,[1] Coralea Stephanou,[2] Marios Phylactides,[2] Soteroula Christou,[4] Michalis Hadjigavriel,[5] Maria Sitarou,[6] Carsten W. Lederer,[2] Roberto Gambari,[3] Marina Kleanthous[2] and Eleni Katsantoni[1]

[1]Basic Research Center, Biomedical Research Foundation, Academy of Athens, Athens, Greece; [2]Molecular Genetics Thalassaemia Department, The Cyprus Institute of Neurology and Genetics, Nicosia, Cyprus; [3]Department of Life Sciences and Biotechnology, Ferrara University, Ferrara, Italy; [4]Thalassaemia Clinic, Archbishop Makarios III Hospital, Nicosia, Cyprus; [5]Limassol General Hospital, Department of Internal Medicine, Limassol, Cyprus and [6]Thalassemia Clinic Larnaca, Larnaca General Hospital, Larnaca, Cyprus

Correspondence:
ELENI KATSANTONI - ekatsantoni@bioacademy.gr

doi:10.3324/haematol.2020.248013

Disclosures: no conflicts of interest to disclose.

Contributions: AN performed experiments, analyzed results and wrote the paper; CT, PF, NB, LCC, CZ and CS performed experiments; GS analyzed results and performed experiments; GG analyzed results; SC, MH and MS provided patient samples and evaluated the clinical picture of the patients; MP, CWL, RG and MK designed the research; EK designed the research, performed experiments, analyzed results and wrote the paper

Acknowledgments: the authors would like to thank Dr. Sjaak Philipsen for critical reading of the manuscript, GeneCore/EMBL for sequencing support and Panayiota Papasavva for helpful discussions.

Funding: this work was supported by the European Union's FP7 THALAMOSS (Project no. 306201 to E.K., R.G., M.K.), the European Union's Horizon 2020 research and innovation programme under the Marie Skłodowska-Curie grant agreement No 813091 (E.K.) and by the Republic of Cyprus through the Research Promotion Foundation under grants agreements ΥΓΕΙΑ/ΒΙΟΣ*0609 (*ΒΕ*)/01 (EK, M.K.) and* ΥΓΕΙΑ/ΒΙΟΣ*/0311(*ΒΕ*)/20 (M.K.).*

References

1. Colah R, Gorakshakar A, Nadkarni A. Global burden, distribution and prevention of β-thalassemias and hemoglobin E disorders. Expert Rev Hematol. 2010;3(1):103-117.
2. Thein SL. Genetic basis and genetic modifiers of β-thalassemia and sickle cell disease. Adv Exp Med Biol. 2017;1013:27-57.
3. Cosenza LC, Breda L, Breveglieri G, et al. A validated cellular biobank for β-thalassemia. J Transl Med. 2016;14(1):255.
4. Chaichompoo P, Pattanapanyasat K, Winichagoon P, Fucharoen S, Svasti S. Accelerated telomere shortening in β-thalassemia/HbE patients. Blood Cells Mol Dis. 2015;55(2):173-179.
5. Lithanatudom P, Leecharoenkiat A, Wannatung T, Svasti S,

Fucharoen S, Smith DR. A mechanism of ineffective erythropoiesis in β-thalassemia/Hb E disease. Haematologica. 2010;95(5):716-723.
6. Amendola G, Danise P, Todisco N, D'Urzo G, Di Palma A, Di Concilio R. Lipid profile in β-thalassemia intermedia patients: correlation with erythroid bone marrow activity. Int J Lab Hematol. 2007; 29(3):172-176.
7. Livrea MA, Tesoriere L, Maggio A, D'Arpa D, Pintaudi AM, Pedone E. Oxidative modification of low-density lipoprotein and atherogenetic risk in beta-thalassemia. Blood. 1998;92(10):3936-3942.
8. el-Hazmi MA, Warsy AS, Addar MH, Babae Z. Fetal haemoglobin level-effect of gender, age and haemoglobin disorders. Mol Cell Biochem. 1994;135(2):181-186.
9. Pes GM, Tolu F, Dore MP. Anti-thyroid peroxidase antibodies and male gender are associated with diabetes occurrence in patients with β-thalassemia major. J Diabetes Res. 2016;2016:1401829.
10. Marsella M, Borgna-Pignatti C, Meloni A, et al. Cardiac iron and cardiac disease in males and females with transfusion-dependent thalassemia major: a T2* magnetic resonance imaging study. Haematologica. 2011;96(4):515-520.
11. Marsella M, Pepe A, Borgna-Pignatti C. Better survival and less cardiac morbidity in female patients with thalassemia major: a review of the literature. Ann N Y Acad Sci. 2010;1202:129-133.
12. Kyriakou A, Savva SC, Savvides I, et al. Gender differences in the prevalence and severity of bone disease in thalassaemia. Pediatr Endocrinol Rev. 2008;6(Suppl 1):S116-122.
13. Kander MC, Cui Y, Liu Z. Gender difference in oxidative stress: a new look at the mechanisms for cardiovascular diseases. J Cell Mol Med. 2017;21(5):1024-1032.
14. Link JC, Reue K. Genetic basis for sex differences in obesity and lipid metabolism. Annu Rev Nutr. 2017;37:225-245.
15. Soliz J, Khemiri H, Caravagna C, Seaborn T. Erythropoietin and the sex-dimorphic chemoreflex pathway. Adv Exp Med Biol. 2012; 758:55-62.

Lack of activation-induced cytidine deaminase expression in *in situ* follicular neoplasia

The immunoglobulin heavy chain (*IGH*) genes undergo class switch recombination (CSR) and somatic hypermutation (SHM) to produce a diverse repertoire of high affinity antibodies. CSR and SHM occur in mature B lymphocytes in the highly specialized microenvironment of germinal centers (GC) and depend on activation-induced cytidine deaminase (AID), an enzyme present in germinal center B cells. AID mediates deamination of cytosine (C) to uracil (U) at cytosine:guanine (C:G) base pairs to generate uracil:guanine (U:G) mismatch, and double-strand DNA breaks (DSB) into switch (S) region sequences of *IGH*. This process introduces point mutations at a high frequency in *IGHV* and *IGLV* genes, allowing for affinity maturation of the antibody response, and replaces the heavy chain constant region of the antibody from the default IgM to IgG, IgA or IgE isotypes.[1]

In addition to *IGH*, endogenous AID affects numerous genes across the B-cell genome but at much lower levels than the immunoglobulin loci. Off target AID activity during the germinal center reaction contributes to lymphomagenesis.[2] In malignancies of mature B-cell origin, recurrent translocations often arise as a result of DSB within the *IGH* switch region and a partner gene. These translocations arise as a result of aberrant AID mediated CSR.[2] Mutations in various oncogenes implicated in the pathogenesis of B-cell lymphomas like *BCL6, PAX5, MYC* and *BCL2* share features similar to immunoglobulin gene mutations suggesting a role for aberrant *SHM*.[1]

Based on RNA expression data, AID appears to be selectively expressed in GC B cells and GC-derived malignancies.[3] Follicular lymphoma (FL) originates from GC B cells and shows heterogeneity in the SHM pattern, suggesting the possible heterogeneous expression of AID in this entity. The reported expression of AID in FL by immunohistochemistry (IHC) varies from 25% to 100%, acknowledging that some of this variation may be due to technical and definitional differences.[3,4,5] More recently, Scherer and colleagues demonstrated that AID messenger RNA (mRNA) and protein expression were highly correlated in FL by quantitative reverse transcriptase polymerase chain reaction (RT-PCR) and IHC, respectively. However, there was great variability with 38% of cases showing less than ten IHC-positive cells/high power field (hpf).[6] This translates to 1% or less of cells in a hpf of small lymphocytes. Interestingly, duodenal-type FL (DFL) lacks AID expression, which has been postulated to be related to its extremely indolent clinical behavior.[7] Immunophenotypically, DFL cells typically strongly co-express CD10 and BCL2 proteins. *In situ* follicular neoplasia (ISFN) is characterized by partial or total colonization of reactive germinal centers by $BCL2^{+}/CD10^{+}$ co-expressing B cells harboring *IGH-BCL2* fusions in an otherwise architecturally preserved lymph node. BCL2 and CD10 IHC staining is characteristically intense and is higher than that seen in systemic FL cells, much like DFL. Given all the overlapping characteristics of these entities, we explored AID expression in ISFN.

Institutional pathology archives (2002-2017) were searched for cases of ISFN and re-reviewed to confirm diagnosis. We identified 16 patients with ISFN (six male, ten female) with adequate tissue for study. The median age was 66 years (range, 50–83 years) at the time of diagnosis. Additional clinical information was obtained by review of the medical records and was available for 13 patients. The ISFN was discovered incidentally in all the cases, during pathologic review of biopsies performed for a variety of clinical indications. Ten patients had other hematolymphoid or non-hematolymphoid neoplasms at some point in time. Two patients had a history of preceding FL, and one patient had concurrent FL at another anatomic site. Of the non-FL patients, none developed subsequent FL on median follow-up of 43.5 months (range, 13-97 months). 11 patients were alive at last the follow-up, one was lost to follow-up and one patient died from complications of chronic myelomonocytic leukemia and related treatment. The clinicopathologic features are summarized in the *Online Supplementary Table S1*.

Morphologically, the lymphoid and immune architecture was preserved in all ISFN cases, with a few follicles demonstrating BCL2 highly overexpressing GC B cells. Initially, six ISFN cases were subjected to immunohistochemical staining with AID which suggested lack of staining in ISFN cells compared to the expression in reac-

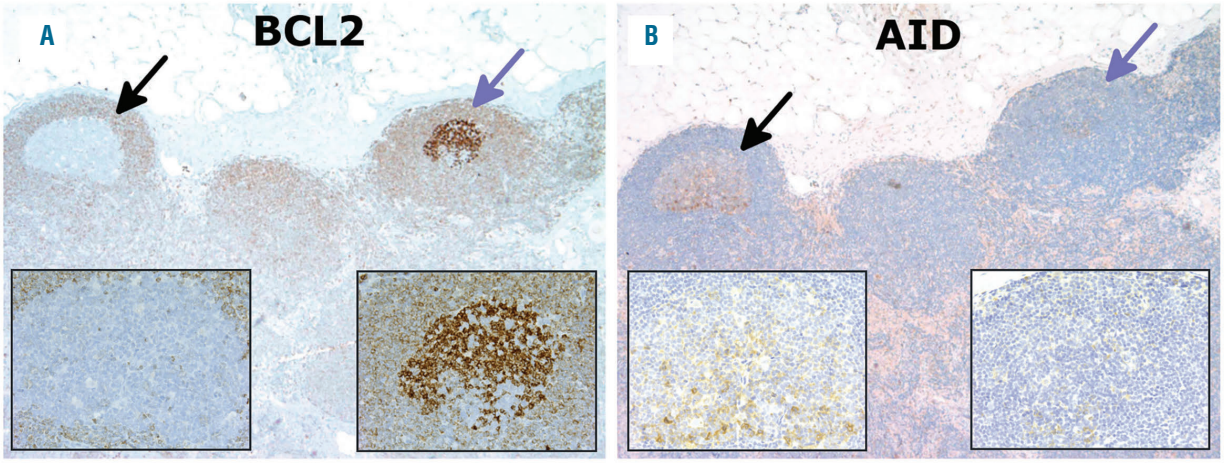


Figure 1. BCL2 and AID immunohistochemistry. (A) Intense BCL2 staining in follicle involved by *in situ* follicular neoplasia (ISFN) (blue arrow) and negative BCL2 staining in reactive follicle (black arrow). (B) In contrast, ISFN follicle (blue arrow) lacks activation-induced cytidine deaminase (AID) , and reactive follicle (black arrow) is positive for AID.

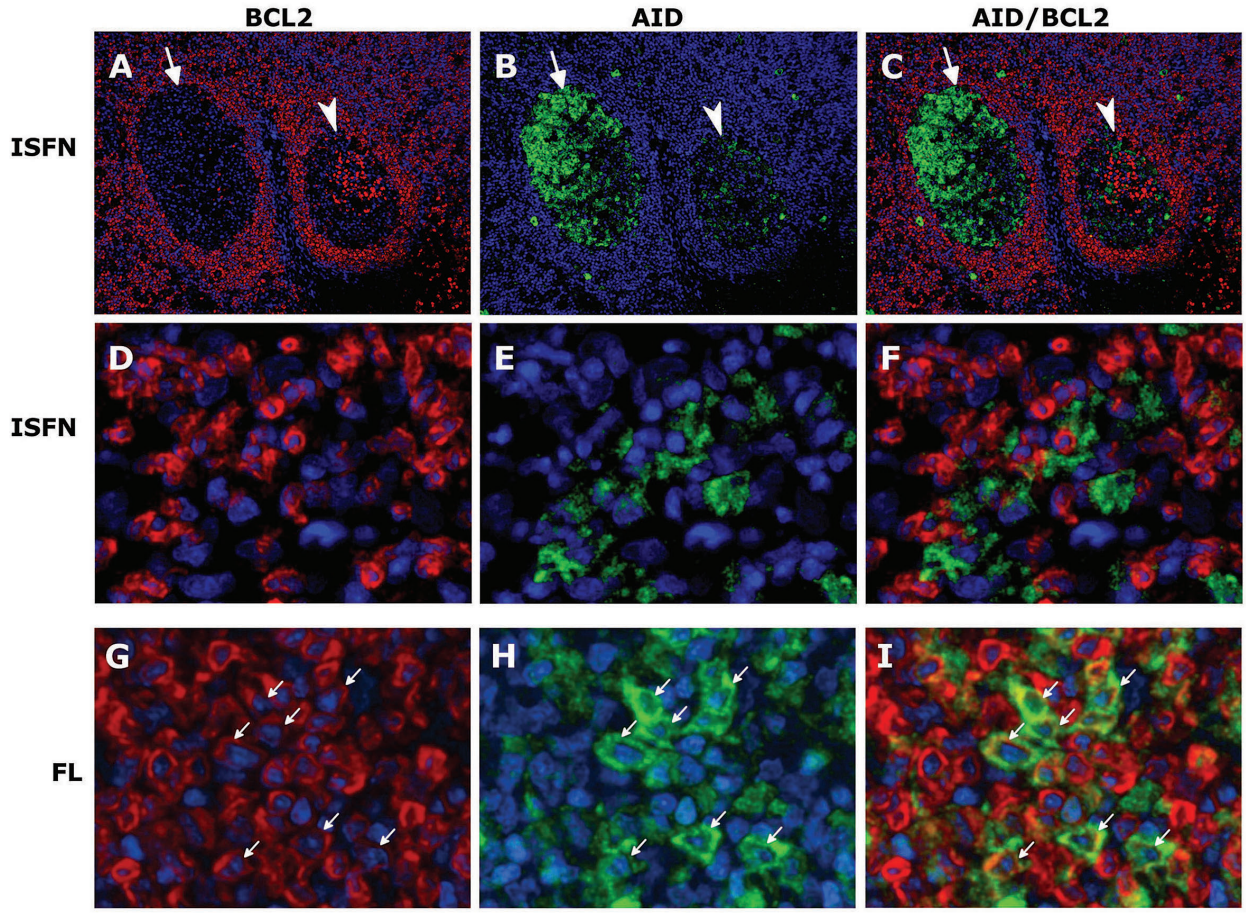


Figure 2. Immunofluorescent AID/BCL2 double staining. (A-C) Follicle (arrowhead) involved by *in situ* follicular neoplasia (ISFN) with BCL2 staining red cells (A) and few activation-induced cytidine deaminase (AID) staining green cells (B) shows lack of AID/BCL2 double staining cells(C). A nearby reactive follicle (arrow) is negative for BCL2 (A), positive for AID (B) and shows lack of AID/BCL2 double staining cells (C). (D-F) High magnification of the ISFN follicle showing BCL2 (D) positive cells (red), fewer AID (E) staining cells (green), and absence of AID/BCL2 double staining cells (F). (G-I) High magnification of a follicle from lymph node with FL: BCL2 (red) is diffusely positive in lymphoma cells (G) and AID (green) is positive in scattered lymphoma cells (H). AID/BCL2 double staining highlights many dual positive (arrows) lymphoma cells (I).

tive GC cells (Figure 1). In order to confirm this impression, we then performed AID/BCL2 double immunofluorescent (IF) staining on 16 ISFN cases. Double IF staining showed lack of AID expression in strongly BCL2 expressing cells in the ISFN follicles in all the cases (Figure 2). Thus, all cases were considered AID-negative. Internal positive controls (nearby reactive follicles and cells within the same follicle) stained appropriately ($BCL2^{-}$, AID^{+}). In order to compare the AID expression pattern seen in ISFN to that of typical systemic nodal FL, we also evaluated 15 cases of low grade FL for AID expression using double IF from a tissue microarray constructed during the same time period. Seven of 15 (47%) low grade FL cases demonstrated co-expression of BCL2 and AID in 10% or more of neoplastic cells within follicles on double IF staining (Figure 2). This difference between systemic nodal FL and ISFN was statistically significant ($P<0.001$). We could not evaluate *AID* expression in three cases with manifest FL at other time points/sites due to the lack of availability of these specimens. Given the known correlation between *AID* mRNA and protein levels by IHC,[6] we further verified the lack of *AID* expression at mRNA level on two cases each of ISFN and FL by performing RNAscope *in situ* hybridization. The findings in ISFN were similar to both the IHC and double IF results, confirming the absence (or extremely low levels) of AID in ISFN follicles, compared to manifest FL (Figure 3). Methodological details are presented in the accompanying *Online Supplementary Appendix*.

ISFN is an indolent condition with a very low risk (<5%) of progression to FL.[8] The ISFN cells carry a t(14;18)(q32;q21), similar to usual-type FL.[9] This abnormality leads to constitutive overexpression of BCL2, inhibition of apoptosis and accumulation of inappropriately rescued B cells with a prolonged life span. This event is believed to be the first genetic hit in the natural history of FL pathogenesis, but additional genetic hits are required for progression to malignant follicular lymphoma.[10] ISFN carries few secondary genetic changes.[9] In contrast, secondary genetic alterations are found in 70–90% of FL at initial diagnosis in addition to the t(14;18)/*IGH-BCL2* fusion.[11] AID expression is a marker of the germinal center reaction. The additional genetic hits in follicular lymphoma B cells are postulated to be facilitated by AID, contributing to genomic instability.[10] A subset of FL cases (25-100%) has been shown to express AID.[3,4,5] We confirm this in our study by showing that approximately half of the low grade FL cases expressed high level AID in neoplastic follicles by double IF. In our study, none of the ISFN cases expressed detectable AID in BCL2 intensely positive neoplastic cells in GC. The absence of detectable AID in IFSN may be related to greater genetic stability and its generally benign behavior. We cannot exclude very low levels of AID expression,

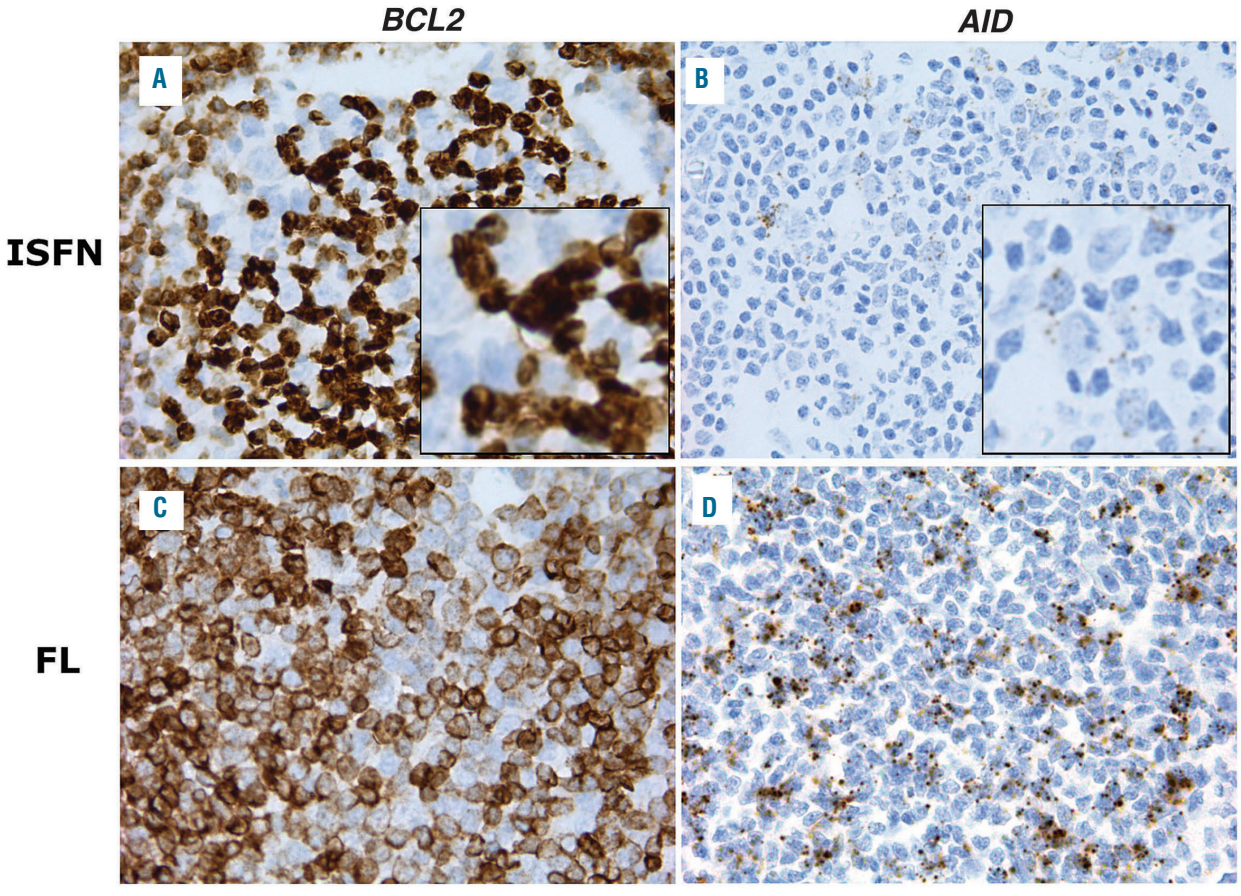


Figure 3. RNAscope, *in situ* hybridization for *AID* in *in situ* follicular neoplasia (results in punctate staining). (A-B) Follicle involved by *in situ* follicular neoplasia (ISFN) - strongly positive for *BCL2* messenger RNA (mRNA) (A) and negative for activation-induced cytidine deaminase (*AID*) mRNA (B). The few *AID* positive cells are residual benign germinal center cells which are larger than the small cleaved ISFN cells. Insets are from exactly the same field on serial section. (C-D) Follicular lymphoma- positive for both *BCL2* (C) and *AID* mRNA (D).

below the technical limits of our assays. Indeed, it has been shown that levels of AID in non-isotype switched FL cells correlate with *IGHV* mutations and aberrant SHM in *BCL6*.[6] Interestingly, circulating follicular lymphoma-like and ISFN cells, by virtue of the "allelic paradox" phenomenon, are IgM-expressing and show much lower levels of genomic alterations compared to overt FL, consistent with the theory of very low or near absent AID activity at this "early lesion" stage.[9]

The AID expression results in our study are similar to the findings described by Katsuyoshi *et al*. in duodenal-type FL.[7] All 17 studied cases of duodenal-type FL lacked expression of AID. Interestingly, a clonal relationship has been proven in a recent case report of ISFN and duodenal-type FL in the same patient.[12] Our study further demonstrates commonalities between these two entities and reinforce the hypothesis that these two entities might represent different tissue manifestations of a single precursor lesion.[12] Despite the lack of AID expression, duodenal-type FL B cells have been shown to be at the memory B-cell stage with somatic and ongoing mutations, which later was suggested to be a consequence of BACH2 expression in tumor cells.[7,13] This may be worth exploring given copy number gains of the BACH2 locus in ISFN cells.[9] Interestingly, there is emerging evidence of ongoing IGH SHM in ISFN as recently shown by Kosmidis *et al*.[14] Ongoing SHM in ISFN despite the absence of AID expression is not without precedent in typical FL. Ongoing mutations and intraclonal heterogeneity was detected in AID-negative FL samples, albeit at significantly lower levels than AID-positive cases.[4] The regulation of AID expression is complex, involving transcription, posttranscription, and posttranslational mechanisms.[15] This provides for many avenues to explore the mechanism behind ongoing mutations, mechanism for downregulated AID, and the global genetic profile of ISFN that will enhance our understanding of this entity.

Tanu Goyal, Sarah L. Ondrejka , Juraj Bodo, Lisa Durkin and Eric D. Hsi

Cleveland Clinic Robert J. Tomsich Pathology and Laboratory Medicine Institute, Cleveland, OH, USA

Correspondence: ERIC D. HSI - hsie@ccf.org

doi:10.3324/haematol.2020.249342

Disclosures: EDS has received the following support, unrelated to the submitted work: research sponsorship from Abbvie, Eli LIlly as well as honoraria from Jazz, Seattle Genetics and Miltenyi; all other authors have no conflicats of interest to disclose.

Contributions: EDH, TG, SLO prepared the manuscript, JB and LD performed the laboratory work, EDH coordinated reseach.

References

1. Gu X, Shivarov V, Strout MP. The role of activation-induced cytidine deaminase in lymphomagenesis. Curr Opin Hematol. 2012; 19(4):292-298.
2. Yamane A, Resch W, Kuo N, et al. Deep-sequencing identification of the genomic targets of the cytidine deaminase AID and its cofactor

RPA in B lymphocytes. Nat Immunol. 2011;12(1):62-69.
3. Smit LA, BendeR, Aten J, Guikema JEJ, Aarts WM, Van Noesel CJM. Expression of activation-induced cytidine deaminase is confined to B-cell non-Hodgkin's lymphomas of germinal-center phenotype. Cancer Res. 2003;63(14):3894-3898.
4. Hardianti MS, Tatsumi E, Syampumawati M, et al. Activation-induced cytidine deaminase expression in follicular lymphoma: association between AID expression and ongoing mutation in FL. Leukemia. 2004;18(4):826-831.
5. Greeve J, Philipsen A, Krause K, et al. Expression of activation-induced cytidine deaminase in human B-cell non-hodgkin lymphomas. Blood. 2003;101(9):3574-3580.
6. Shrerer F, Navarrete MA, Bertinetti-Lapatki C, Boehm J, Schmitt-Graeff A, Veelken H. Isotype-switched follicular lymphoma displays dissociation between activation-induced cytidine deaminase expression and somatic hypermutation. Leuk Lymphoma. 2016; 57(1):151-160.
7. Takata K, Sato Y, Nakamura N, et al. Duodenal and nodal follicular lymphomas are distinct: the former lacks activation-induced cytidine deaminase and follicular dendritic cells despite ongoing somatic hypermutations. Mod Pathol. 2009;22(7):940-949.
8. Jegalian AG, Sato Y, Nakamura N, et al. Follicular lymphoma in situ: Clinical implications and comparisons with partial involvement by follicular lymphoma. Blood. 2011;118(11):2976-2984.
9. Mamessier E, Song JY, Eberle FC, et al. Early lesions of follicular lymphoma: A genetic perspective. Haematologica 2014;99(3):481-488.
10. Ott G, Rosenwald A. Molecular pathogenesis of follicular lymphoma. Haematologica 2008 Dec;93(12):1773-6.
11. Schmidt J, Salaverria I, Haake A, et al. Increasing genomic and epigenomic complexity in the clonal evolution from in situ to manifest t(14;18)-positive follicular lymphoma. Leukemia. 2014;28(5):1103-1112.
12. Nann D, Bonzheim I, Müller I, et al. Clonally related duodenal-type follicular lymphoma and in situ follicular neoplasia. Haematologica. 2019;104(11):e537-e539.
13. Takata K, SatoY, Nakamura N, et al. Duodenal follicular lymphoma lacks AID but expresses BACH2 and has memory B-cell characteristics. Mod Pathol. 2013;26(1):22-31.
14. Kosmidis P, Bonzheim I, Dufke C, et al. Next generation sequencing of the clonal IGH rearrangement detects ongoing mutations and interfollicular trafficking in in situ follicular neoplasia. PLoS One. 2017;12(6):e0178503.
15. Lou Y, Liu Y, Wu L, et al. CUL7 E3 ubiquitin ligase mediates the recombination in B lymphocytes deaminase and regulates the Ig class switch degradation of activation-induced cytidine. J Immunol. 2019;203(1):269-281.

Identification of biallelic germline variants of *SRP68* in a sporadic case with severe congenital neutropenia

Congenital neutropenia (CN) are a heterogeneous group of very rare diseases characterized by profound and chronic neutropenia possibly associated with co-morbidities.[1] Variants in about 25 genes implicating distinct pathophysiological pathways have been identified in CN.[1] Recently, co-translational targeting of nascent secretory and membrane proteins to the endoplasmic reticulum (ER) mediated by the signal recognition particle (SRP) complex has been implicated in the pathogenesis of both CN and Shwachman-Diamond-like syndrome.[2,3] In humans, the SRP complex is composed of six proteins (SRP9, SRP14, SRP19, SRP54, SRP68, and SRP72) assembled on a 7S RNA molecule.[4] The SRP54 protein with its GTPase activity constitutes the key element of this complex and regulates the entire physiological process.[5] We recently reported germline *SRP54* variants in a large number of sporadic and familial cases with autosomal dominant CN.[3] Apart from *SRP54*, germline heterozygous variants of *SRP72* have been described in a few cases with aplastic anemia and myelodysplasia.[6,7]

Here, we report a sporadic case of severe CN associated with biallelic pathogenic variants of *SRP68*, implicating for the first time the SRP68 protein in the pathogenesis of CN. Specifically, we investigated the functional consequences of SRP68 defect on granulopoiesis and on ER homeostasis (see the *Online Supplementary Appendix*). The patient is a Caucasian boy referred for an anal abscess at 6 weeks of age. Blood counts showed severe neutropenia (white blood cells $6.1x10^9$/L, neutrophils $0.2x10^9$/L), elevated monocyte count ($1.7x10^9$/L), anemia (hemoglobin 7.5 g/dL) associated with iron deficiency and moderate thrombocytopenia (platelets $149x10^9$/L). Serial blood counts (n=41) confirmed the persistent and profound neutropenia ($0.200x10^9$/L [range: 0-1.800]). The bone marrow examination showed a maturation arrest at the promyelocytic stage and major features of dysgranulopoiesis. Promyelocytes displayed numerous condensed granulations, abnormal nuclei, clumped chromatin and the absence of cytoplasmic vacuoles; the remaining neutrophils were highly dystrophic (Figure 1A). In the first year of life, neutropenia was associated with profound anemia and thrombocytopenia which recovered later. The level of hemoglobin and the platelet count were respectively 8.7 g/dL [range, 5.5-11.3] and $132x10^9$/L [range, 43-318]). From diagnosis to the last follow-up at the age of 5 years, he had a prophylactic antibiotherapy and was treated with granulocyte colony-stimulating fac-

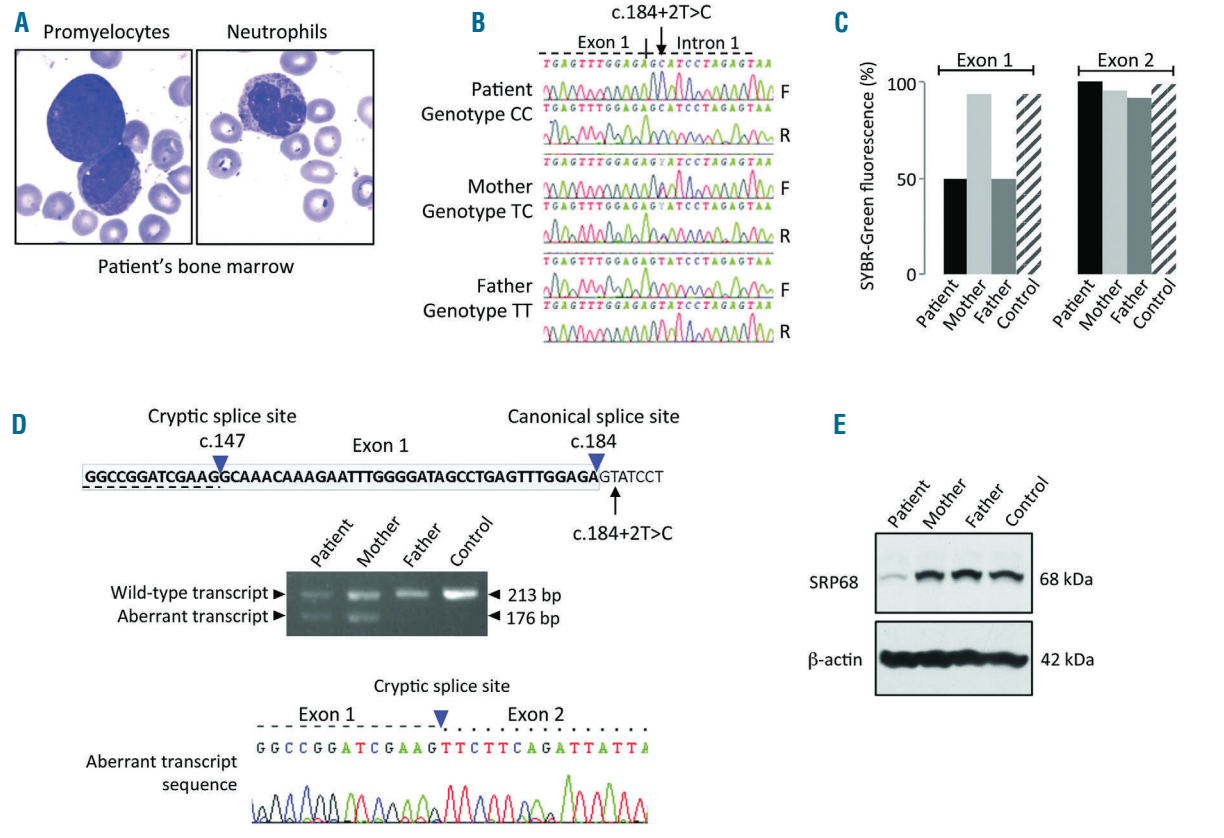


Figure 1. A sporadic case with severe congenital neutropenia and loss-of-function variants of *SRP68*. (A) Cytology analysis after May Grunwald-Giemsa staining of patient's bone marrow. Pictures represent granulocytic precursors (left) and neutrophils (right) (original magnification x100). (B) Sanger sequencing confirmation of the splice site variant c.184+2T>C located in intron 1 of *SRP68*. F: forward strand; R: reverse strand. (C) Confirmation of the deletion of exon 1 of *SRP68* by quantitative polymerase chain reaction (PCR) using SYBR-Green. (D) Predicted alternate cryptic splice site located 37 bp upstream of the splice donor site shown on *SRP68* sequence and confirmed by RT-PCR using RNA extracted from fibroblasts and Sanger sequencing of the shorter product (176 bp). (E) Expression level of *SRP68* protein in fibroblasts evaluated by western blot analysis

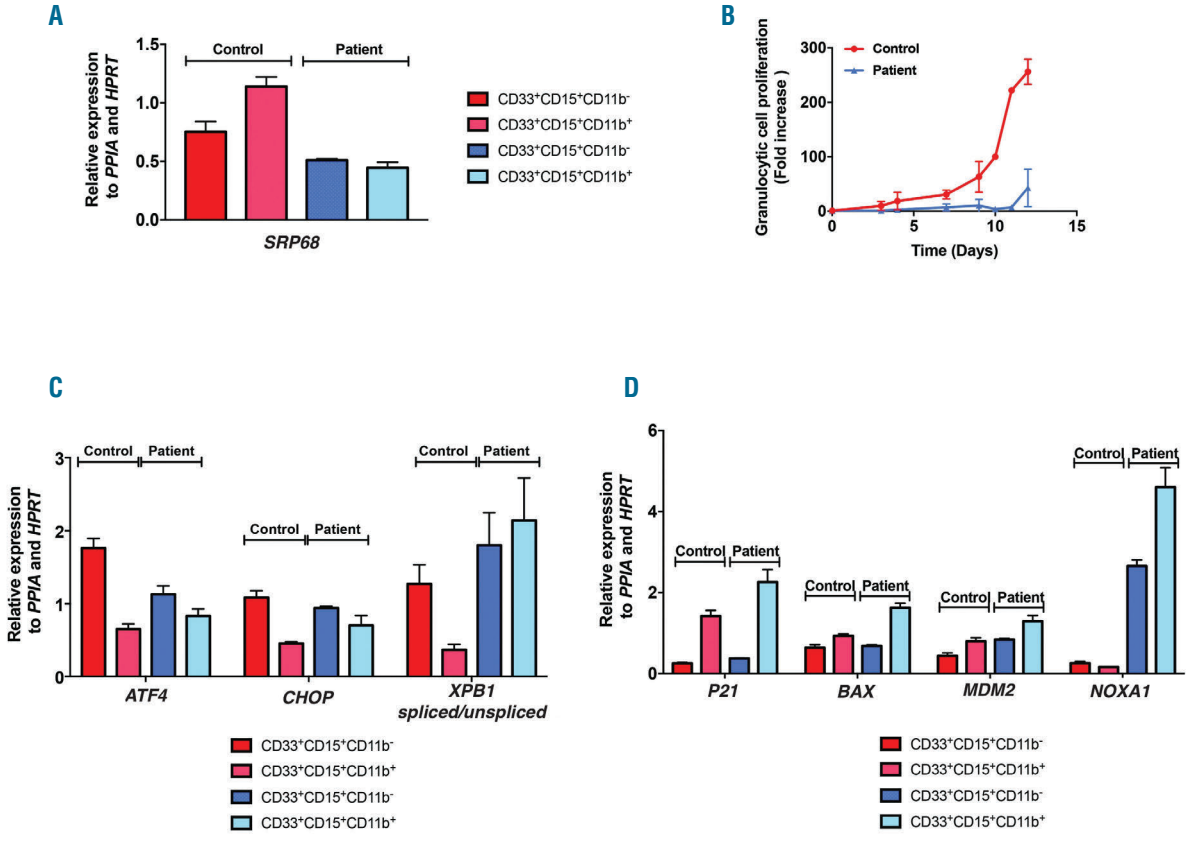


Figure 2. *SRP68* biallelic variants induce a defect in granulocytic differentiation and endoplasmic reticulum stress and increase P53-dependent apoptosis of granulocytic precursors and neutrophils. CD34$^+$ cells from the patient and the control donor were purified from blood and cultured for 12 days in serum free-medium with stem cell factor, interleukin 3 and granulocyte colony-stimulating factor. Sorted granulocytic cells CD33$^+$15$^+$11b$^-$ and CD33$^+$15$^+$11b$^+$ were sorted on day 12. Expression levels were determined by quantitative everse transcription polymerase chain reaction related to *PPIA* and *HPRT* on day 12. (A) Expression level of SRP68 (n=1 in triplicate; mean±standard deviation [SD]). (B) Fold increase in cell proliferation during granulocytic differentiation (n=2; mean±SD). (C) Expression level of *ATF4, CHOP* and ratio spliced/unspliced *XBP1* (n=1 in triplicate; mean±SD). (D) Expression level of *P21, BAX, MDM2 and NOXA1* (n=1 in triplicate; mean±SD).

tor (5 to 10 μg/kg/day). With this treatment and despite the persistent severe neutropenia, the patient has not presented severe bacterial infections. There was no familial medical history. After excluding the genes classically involved in CN by targeted high throughput sequencing, we performed whole exome sequencing (WES) on a trio-based approach (*Online Supplementary Appendix*). WES diagnosed an intronic homozygous point substitution affecting the splice donor site of exon 1 (c.184+2T>C) of the *SRP68* gene. This variant was detected at a heterozygous state in his mother and was absent in his father suggesting the presence in trans of a large deletion (*Online Supplementary Table S1*). Sanger sequencing and quantitative polymerase chain reaction (PCR) confirmed the splice site variant and the deletion of exon 1 of *SRP68* (Figure 1B-C; *Online Supplementary Table S2*). This latter was inherited from his father confirming the compound heterozygous *SRP68* genotype (c.184+2T>C) (exon 1 deletion) of the patient.

In order to determine the consequences of the intronic *SRP68* variant on splicing, we performed reverse transcription PCR (RT-PCR) using primary fibroblasts from the patient, his parents, and a control donor. Agarose gel electrophoresis indicated that the patient and his mother harbor both the expected 213 bp fragment and a shorter product (176 bp). Sequencing of this fragment revealed the use of a predicted cryptic splice donor site located 37 bases upstream (c.147) and resulting in the premature truncation of the mutated protein (Ala50Phefs*52) (Figure 1D). By western blot analysis, we found a drastic decrease of SRP68 protein expression in fibroblasts of the patient compared to his parents (Figure 1E) demonstrating the loss-of-function effect of the SRP68 defects. Nevertheless, we observed a residual protein expression in the patient that may be due to a partial splicing defect as suggested by the semi-quantitative analysis of *SRP68* transcripts in the mother (ratio 65%/35% for both 213 bp/176 bp fragments, Figure 1D). This finding was also consistent with the *SRP68* transcript expression level determined from patient's granulocytic cells. The residual expression of *SRP68* could be explained by the specific post-transcriptional splicing mechanism related to GT>GC variants affecting the canonical 5' donor splice site as identified in our patient (c.184+2T>C). In fact, 5' splice site GT>GC variants may retain their ability to generate normal transcripts and be associated with a milder than expected clinical phenotype.[8] SRP68 functions only as a heterodimeric structure with the SRP72 protein.[9] We could speculate that null *SRP68* variants would be lethal on the basis of what was recently shown in Srp72$^{-/-}$ mice.[10]

We purified CD34$^+$ progenitor cells from peripheral blood and cultured them in serum-free medium supplemented with stem cell factor (25 ng/mL), interleukin 3 (10 ng/mL) and granulocyte colony-stimulating factor (20 ng/mL) for 12 days. The level of *SRP68* expression on day

12 was reduced to 68% in immature $CD33^+CD15^+CD11b^-$ cells and to 39% in the more mature $CD33^+CD15^+CD11b^+$ cells of the patient compared with control cells (Figure 2A). We also analyzed the consequences of SRP68 defect on granulocyte proliferation. In the same experimental conditions, we cultured $CD34^+$ cells purified from blood samples and observed nearly six-times less granulocytic cell proliferation in the patient compared to $CD34^+$ cells from healthy control (Figure 2B).

These results highlight the major role of the SRP complex during granulocytic differentiation. This physiological process requires the production and maturation of a huge number of granule proteins.[11] This context explains why granulocytic precursors and neutrophils are highly sensitive to alterations of protein synthesis, protein transport into ER/Golgi and ER protein misfolding. A defective co-translational targeting of nascent proteins may either affect the level of ER resident proteins as chaperones and glycosylases or lead to incorrectly translocated proteins essential for granulocytic precursor maturation as the neutrophil elastase ELANE.[12] Both hypotheses will result in ER stress, activation of the unfolded protein response (UPR) and finally, to cycle cell arrest, senescence and/or death by apoptosis or necrosis of granulocytic cells. In mammals, the SRP68/SRP72 heterodimer plays an essential role in the recognition of the signal peptide of nascent proteins and in their translocation through the SRP receptor located at the ER membrane.[13] As we previously showed that SRP54 variants induce an ER stress and activate the UPR pathway, we investigated several markers of UPR activation (ATF4, CHOP and spliced XBP1).[3] Using *in vitro* sorted granulocytic cells, we found a significant increase in spliced *XBP1* expression level in both immature and mature granulocytic cells of the patient in comparison with control cells pointing out the specific activation of the IRE1 ER stress sensor of the UPR signaling (Figure 2C).[14] In contrast to SRP54, no activation of the PERK pathway, another distinct ER sensor, was observed by analyzing ATF4 and CHOP UPR-target genes.[14] Under ER stress conditions, the induction of UPR leads to enhanced apoptosis reducing the number of granulocytic precursors and neutrophils. In most CN, including *SRP54*-related CN, apoptosis seems to be dependent on p53 pathway activation.[3] We analyzed, by quantitative RT-PCR, the expression level of several P53 target genes (*BAX, NOXA1, P21* and *MDM2*) in sorted granulocytic cells (Figure 2D). The patient displayed a higher expression level of P53 target genes than in control and the activation was more pronounced in the more mature granulocytic $CD33^+CD15^+CD11b^+$ cells. However, we could not definitively exclude P53-independent pathways that also lead to cell cycle arrest and apoptosis.[15] Of note, P53-independent nucleolar stress has been reported in animal models of bone marrow failure syndromes caused by impaired ribosomal biogenesis and function.[15]

Besides the profound neutropenia, this patient presented transient severe anemia and thrombocytopenia as also reported in patients harboring SRP54 and SRP72 defects.[3,6] We could hypothesize that an aberrant SRP complex, regardless of the implicated defective SRP protein, may have consequences on the targeting of proteins essential for hematopoietic stem cells or erythroid, megakaryocytic and granuloytic progenitor/precursors. Further studies are needed to characterize the mechanisms leading to impaired differentiation of hematopoietic lineages and to identify the protein partners of the SRP complex.

In conclusion, we have identified a novel genetic entity of CN affecting another protein of the SRP complex underlying the major implication of the universally conserved co-translational targeting machinery of proteins in the pathogenesis of CN. These first observations show that loss-of-function *SRP58* variants trigger an ER stress resulting in an increased P53-dependent apoptosis of granulocytic precursors and neutrophils.

Barbara Schmaltz-Panneau,[1,2] Anne Pagnier,[3] Séverine Clauin,[4] Julien Buratti,[3] Caroline Marty,[1,2] Odile Fenneteau,[5] Klaus Dieterich,[6] Blandine Beaupain,[7,8] Jean Donadieu,[7,8,9] Isabelle Plo[1,2] and Christine Bellanné-Chantelot[1,4,8]

[1]Gustave Roussy Cancer Center, INSERM U1287, Villejuif; [2]Paris Saclay University, U1287, Villejuif; [3]Department of Pediatric Hematology and Oncology, CHU Grenoble Alpes, Grenoble, GIN, Grenoble; [4]AP-HP, Pitié-Salpêtrière Hospital, DMU BioGeM, Department of Genetics, Sorbonne University, Paris; [5]AP-HP, Robert Debré Hospital, Laboratory of Hematology, University of Paris, Paris; [6]Department of Medical Genetics, Univsersity Grenoble Alpes, INSERM U1216, CHU Grenoble Alpes, GIN, Grenoble; [7]French Registry of Chronic Neutropenia, Trousseau Hospital, Paris; [8]Reference Center for Chronic Neutropenia, Paris and [9]AP-HP, Trousseau Hospital, Department of Pediatric Hematology and Oncology, Paris, France

Correspondence: CHRISTINE BELLANNE'-CHANTELOT christine.bellanne-chantelot@aphp.fr

doi:10.3324/haematol.2020.247825

Disclosures: no conflicts of interest to disclose

Contributions: BSP performed most of the research and analyzed functional data; AP provided samples and clinical data; SC performed and analyzed molecular experiments; JB performed bioinformatics analysis; CM performed fibroblast culture and western blot; OF performed cytological analysis; KD provided samples and clinical data; BB collected clinical data; JD involved in the clinical part and contributed to intellectual input; IP designed the study, analyzed the data and critically reviewed the paper; CB-C designed the study, analyzed the data and wrote the paper.

Acknowledgments: the authors would like to thank the family involved in the study. The authors also thank the Cytometry Platform (PFIC) of Gustave Roussy, especially Philippe Rameau and Yann Lecluse.

Funding: the whole-exome sequencing was funded by the Foundation for rare diseases (AO9102LS) and the research was supported by grants from INCA-PLBIO 2017 (I Plo). The French Registry is supported by grants from X4 pharma, Prolong Pharma and Chugai SA to BB and JD.

References

1. Donadieu J, Beaupain B, Fenneteau O, Bellanne-Chantelot C. Congenital neutropenia in the era of genomics: classification, diagnosis, and natural history. Br J Haematol. 2017;179 (4):557-574.
2. Carapito R, Konantz M, Paillard C, et al. Mutations in signal recognition particle SRP54 cause syndromic neutropenia with Shwachman-Diamond-like features. J Clin Invest. 2017;127 11):4090-4103.
3. Bellanne-Chantelot C, Schmaltz-Panneau B, Marty C, et al. Mutations in the SRP54 gene cause severe congenital neutropenia as well as Shwachman-Diamond-like syndrome. Blood. 2018; 132(12):1318-1331.
4. Wild K, Juaire KD, Soni K, et al. Reconstitution of the human SRP system and quantitative and systematic analysis of its ribosome interactions. Nucleic Acids Res. 2019;47 (6):3184-3196.
5. Focia PJ, Shepotinovskaya IV, Seidler JA, Freymann DM. Heterodimeric GTPase core of the SRP targeting complex. Science. 2004;303(5656):373-377.
6. Kirwan M, Walne AJ, Plagnol V, et al. Exome sequencing identifies autosomal-dominant SRP72 mutations associated with familial aplasia and myelodysplasia. Am J Hum Genet. 2012;90(5):888-892.

7. Bluteau O, Sebert M, Leblanc T, et al. A landscape of germ line mutations in a cohort of inherited bone marrow failure patients. Blood. 2018;131(7):717-732.
8. Lin JH, Tang XY, Boulling A, et al. First estimate of the scale of canonical 5' splice site GT>GC variants capable of generating wild-type transcripts. Hum Mutat. 2019;40(10):1856-1873.
9. Gao Y, Zhang Q, Lang Y, et al. Human apo-SRP72 and SRP68/72 complex structures reveal the molecular basis of protein translocation. J Mol Cell Biol. 2017;9(3):220-230.
10. D'Altri T, Schuster MB, Wenzel A, Porse BT. Heterozygous loss of Srp72 in mice is not associated with major hematological phenotypes. Eur J Haematol. 2019;103(4):319-328.
11. Cowland JB, Borregaard N. Granulopoiesis and granules of human neutrophils. Immunol Rev. 2016;273(1):11-28.
12. Grenda DS, Murakami M, Ghatak J, et al. Mutations of the ELA2 gene found in patients with severe congenital neutropenia induce the unfolded protein response and cellular apoptosis. Blood. 2007; 110(13):4179-4187.
13. Elvekrog MM, Walter P. Dynamics of co-translational protein targeting. Curr Opin Chem Biol. 2015;29:79-86.
14. Walter P, Ron D. The unfolded protein response: from stress pathway to homeostatic regulation. Science. 2011;334(6059):1081-1086.
15. James A, Wang Y, Raje H, Rosby R, DiMario P. Nucleolar stress with and without p53. Nucleus. 2014;5(5):402-426.

Biallelic *IARS2* mutations presenting as sideroblastic anemia

Aminoacyl-tRNA synthetases (ARS) are evolutionarily conserved enzymes that catalyze amino acid attachment to their cognate transfer RNA (tRNA), ensuring accuracy of the translation process. Two separate sets of cellular ARS are required, as translation takes place in two distinct compartments, namely cytosol and mitochondria. Eighteen ARS act exclusively in the cytosol (ARS1), 17 act exclusively in the mitochondria (ARS2) and two ARS are bifunctional, as they act in both compartments.[1] Mutations in the nuclear genes encoding ARS2 have emerged as a new group of mitochondrial diseases, inconsistently impairing oxidative phosphorylation.[2] Among them, pathogenic variants in the *IARS2* gene (Online Mendelian Inheritance in Man [OMIM] 612801) have been reported to cause overlapping clinical phenotypes ranging from isolated cataract to a syndromic condition with cataract (CA), growth hormone deficiency (G), sensory neuropathy (S), sensorineural hearing loss (S), and skeletal dysplasia syndrome (CAGSSS) OMIM 616007) and Leigh syndrome (Table).[3-8]

Here, we report on biallelic pathogenic *IARS2* variants in three unrelated siblings presenting with neonatal sideroblastic anemia mimicking Pearson syndrome.

Patient 1, the third child of non-consanguineous healthy parents of French origin, was born after a normal full-term pregnancy with normal birth parameters. His older sister and brother are healthy (Figure 2). At birth, he presented with severe sideroblastic anemia (hemoglobin 5.1 g/dL, normal>14.5 g/dL) with normal mean corpuscular volume (MCV). Myelogram showed 2% of ring sideroblasts (Figure 1D). Search for B19 parvovirus, Coombs test and Kleinhauer test were negative. Plasma B12 and folate were normal. He required two red blood cell transfusions during the first month and thrombopenia reached a nadir of 80.000 platelets/mm^3 normal >150.000 platelets/mm^3). Plasma lactate (3.8-5.3 mmol/L, normal <2 mmol/L), lactate/pyruvate ratios (33, normal <20) and cerebrospinal fluid (CSF) lactate were elevated (3.9 mmol/L, normal <2 mmol/L). The child had exocrine pancreatic dysfunction with decreased fecal elastase (75 µg/g, normal 200-500 µg/g) and hypoparathyroidism (plasma calcium 1.24 mmol/L, normal 2.2-2.7 mmol/L; plasma phosphate 2.8 mmol/L, normal 1.12-1.45 mmol/L; parathormone 3 pg/mL, normal: 10-55 pg/mL). He presented with congenital bilateral cataract, axial hypotonia, peripheral dystonia and motor delay. At 6 months, he developed pharmaco-resistant infantile spasms with hypsarrhythmia on electroencephalogram (EEG) and vigabatrin and topiramate were started. Metabolic work-up, including plasma amino acids and liver enzymes (aspartate amino transferase/alanine amino transferase [ASAT/ALAT]), urinary organic acids and skeletal X-ray were normal. Brain magnetic resonance imaging (MRI) (3 months) was normal except for a lactate peak on spectroscopy (Figure 1A). The child died at 16 months due to respiratory distress in a context of inhalation pneumonia.

A next-generation sequencing panel targeting genes involved in mitochondrial disorders showed two compound heterozygous *IARS2* variants: a novel nonsense variant inherited from his father (c.891G>A; p. Trp297*), predicted to result in either nonsense-mediated (NMD) or loss of the terminal two thirds of the protein including

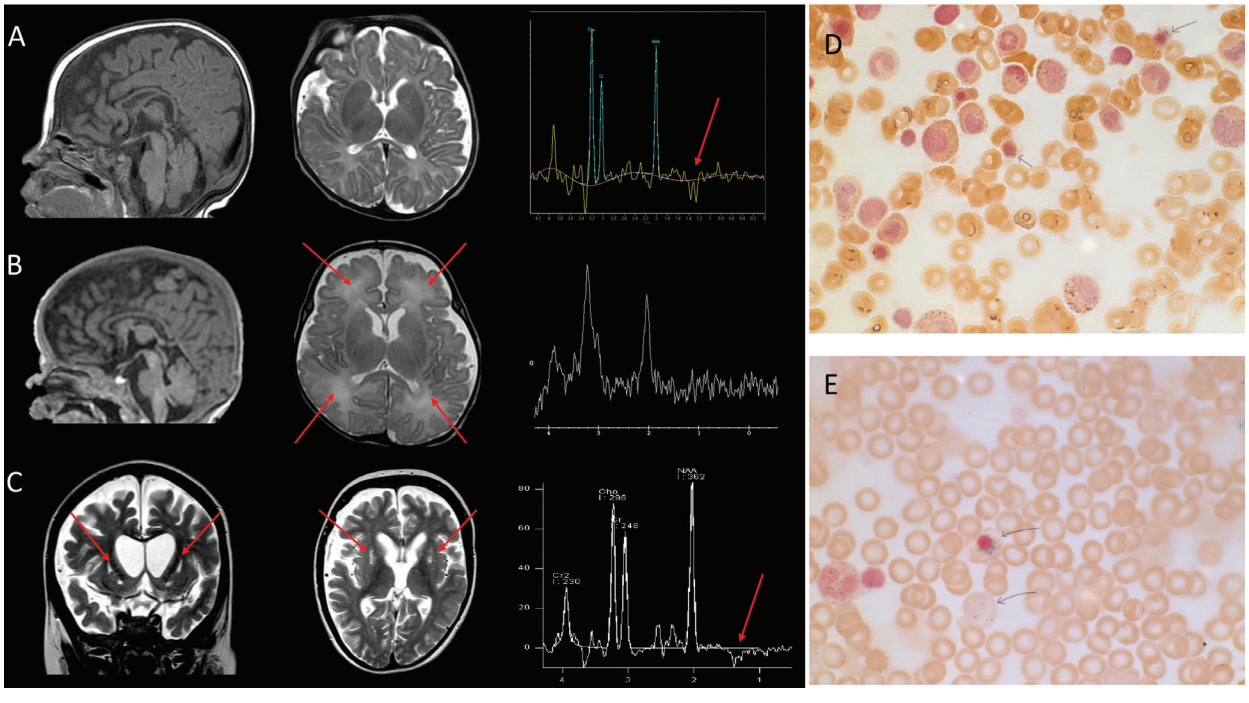


Figure 1. Brain magnetic resonance imaging anomalies in three patients carrying biallelic pathogenic *IARS2* variants and bone marrow aspiration from patients 1 and 2. (A) Patient 1 (3 months): sagittal T1, axial T2 weighted images and magnetic resonance spectroscopy (MRS) showing no anomalies other than a lactate peak (arrow). (B) Patient 2 (2 months): sagittal T1, axial T2 weighted images and MRS showing no lactate peak but mild and diffuse white matter hyperintensities (arrows). (C) Patient 3 (7 years): coronal T2, axial T2 weighted images and MRS showing bilateral cavitations in putamen characteristic of Leigh disease (arrows), frank and diffuse cerebral atrophy, white matter loss and a lactate peak. (D, E) Bone marrow aspiration from patient 1 (D) and 2 (E) showing ring sideroblasts on iron stain.

Table 1. Clinical, neuroimaging and molecular findings in patients carrying pathogenic *IARS2* variants.

Authors, year	Pt	Sex	Family	Diagnosis	Age at onset	Neurological findings and development	Ocular findings	Endocrinological findings and growth	Skeletal	Brain MRI	Auditory features	Follow-up	*IARS2* mutations	Other
Schwartzentruber *et al.*, 2014	1	F	1	CAGSSS	Birth	DD, distal sensory neuropathy (9,5 y)	Cataract (17 m), corneal opacification (5y), orbital myopathy (32 y)	GH deficiency (15 y) Short stature	Bilateral hip dislocation, SEMD (2 y)	Atrophied pituitary adenohypophysis and small neurohypophysis	hearing loss (2 y)	33 y No ID	Homozygous c.2726C>T (p.Pro909Leu)	Dysmorphic features. Type 2 achalasia
	2	F	1	CAGSSS	Birth	DD, distal sensory neuropathy (8 m)	Cataract (3 m), corneal opacification (17y)	GH deficiency (4 y) Short stature	Bilateral hip dislocation, SEMD (18 m)		Hearing loss	6 y No ID	Homozygous c.2726C>T (p.Pro909Leu)	Dysmorphic features
	3	M	1	CAGSSS	Birth	DD, distal sensory neuropathy	Cataract (5 m), corneal opacifications (5 y)	GH deficiency (5 y) Short stature	Bilateral hip dislocation (at birth), SEMD		Hearing loss (21 m)	17 y No ID	Homozygous c.2726C>T (p.Pro909Leu)	Dysmorphic features
	4	M	2	Leigh syndrome	1 m	No	No	No	No	Diffuse atrophy and hyperintensities on T2 in the basal ganglia and thalami	No	18 m (deceased)	Compound heterozygous c.1821G>A (p.Trp607*) and c.2122G>A	Increased CSF L
Moosa *et al.*, 2017	1	F	1	CAGSSS	Birth	Hypotonia, peripheral neuropathy	Cataract (3 y)	Normal GH Short stature (-6SD)	Bilateral hip dislocation (at birth), SEMD (18 m)	Mild hydrocephalus and narrow foramen magnum	Hearing loss (8 y)	8 y No ID	(p.Glu708Lys) Homozygous c.2620G>A (p.Gly874Arg)	Dysmorphic features Telangiectasia
Takezawa *et al.*, 2018	1	F	1	CAGSSS, Leigh and West syndrome	5 m	Infantile spasms, DD	Cataract (8 y)	Short stature (-5 SD)	NK	Mild cortical atrophy (8 m); severe cortical atrophy and atrophy and bilateral hyperintensity in the basal ganglia on T2 (21 m)	NK	8 y Hypotonic quadriplegia and bedridden	Compound heterozygous c.680T>C (p.Phe227Ser) and c.2450G>A (p.Arg817His)	Increased L and L/P in blood and CSF
	2	F	1	CAGSSS, Leigh and West syndrome	7 m	Infantile spasms	No	NK Short stature (-5 SD)	NK	Diffuse cortical atrophy (7 m) bilateral hyperintensity in the basal ganglia on T2 (18 m)	NK	5 y Hypotonic quadriplegia, bedridden (1 y)	Compound heterozygous c.680T>C (p.Phe227Ser) and c.2450G>A (p.Arg817His)	Increased L and L/P in blood and CSF
Vona *et al.*, 2018	1	M	1	CAGSSS	Birth	Spasticity	Congenital cataract, nystagmus, corneal opacification	GH deficiency Short stature (-3.5 SD)	SEMD (18 y)	Normal	Hearing loss (13 y)	20 y No ID	Homozygous c.2725C > T (p.Pro909Ser)	Type 2 achalasia, dysmorphic features
	2	F	2	CAGSSS	Birth	No	Congenital cataract, corneal opacification	No	SEMD	NK	No	35 y No ID	Homozygous c.2282A > G (p.His761Arg)	Dysmorphic features
	3	F	2	CAGSSS	Birth	No	Congenital cataract	No	NK	NK	No	27 y No ID	Homozygous c.2282A > G (p.His761Arg)	Dysmorphic features
Li *et al.*, 2018	1	M	1	Cataract	5 m	No (5 m)	Cataract	No	No	NK	No	NK	Compound heterozygous c.607G>C (p.Gly203Arg) and c.2575T>C (p.Phe859Leu)	
	2	M	2	Cataract	6 m	No (6 m)	Cataract	No	No	NK	No	NK	Compound heterozygous c.2446C>T	Increased serum L

continued on the next page

continued from previous page

														(p.Arg816*) and c.2575T>C (p.Phe859Leu)
	3	M	2	Cataract	NK	No	Cataract	No	No	NK	No	NK	Compound heterozygous c.2446C>T (p.Arg816*) and c.2575T>C (p.Phe859Leu)	
Lee *et al*., 2019	1	F	1	Leigh syndrome	18 m	Development regression	No	NK	No	T2 hyperintensity involving both the caudate nucleus and basal ganglia with swelling and a lactate peak in the basal ganglia lesion (42m)	No	13 y Walks with assistance; no speech	Compound heterozygous c.1195A> G (p.Met399Val) and c.2052delT (p.Gln685Lysfs*15)	
	2	F	2	Leigh syndrome	11 m	DD, hypotonia	No	NK	No	T2 hyperintensity in the periaqueductal area and midline of the midbrain, together with diffuse brain atrophy	NA	16 m (deceased)	Compound heterozygous c.550G> A (p.Ala184Thr) and c.1967T>C (p.Phe656Ser)	NK
	3	M	3	Leigh syndrome	11 m	DD	Nystagmus, cataract	NK	No	T2 hyperintensity in both the basal ganglia (putamen) and a lactate peak in the putamen (37 m)	No	8 y Walks alone; No speech	Compound heterozygous c.314_318del (p.Val105Aspfs*7) and c.2450G>A (p.Arg817His)	Increased serum L
	4	M	4	Leigh syndrome	9 m	DD, Microcephaly, Seizures (spasms)	Cataract	Short stature	No	Bilateral symmetric T1- weighted low and T2- hyperintensity in the putamen and delayed myelination (22 m)	No	3 y Sit up and stand with assistance, no speech	Compound heterozygous c.971_972del (p.Ser324*) and c.2450G> A (p.Arg817His)	Increased serum L
	5	M	5	Leigh syndrome	5 m	DD, Microcephaly, seizures	Cataract	Hypopara-thyroidism Short stature	No	Bilateral symmetric T2 hyperintensity and atrophic changes in both the putamen and caudate nucleus, diffuse cerebral atrophy, and loss of WM volume	NK	5 y Nearly bedridden; no babbling	Compound heterozygous c.314_318del (p.Val105Aspfs*7) and c.2450G>A (p.Arg817His)	Increased serum L
This article	1	M	1	Leigh syndrome, anemia	Birth	DD, seizures (spasms)	Cataract	Hypopara-thyroidism	No	Bilateral basal ganglia hyperintensity on T2-weighted images	No	16 m (deceased)	Compound heterozygous c.891G>A (p.Trp297*) c.2450G>A (p.Arg817His)	Increased serum and CSF L
	2	M	2	Anemia, cardiomyopathy	Birth	DD	No	No	No	Bilateral basal ganglia hyperintensity on T2-weighted images (1 m)	No	2 m (deceased)	Homozygous c.199C>T (p.Pro67Ser)	Increased serum L
	3	M	3	Anemia, cardiomyopathy	Birth	DD, Anemia, cardiomyopathy	Cataract (4,5m) Glaucoma 4 y	No	scoliosis	bilateral caudate nuclei and putamen hyperintensities (16 m). Subsequent global cerebral and basal ganglia volume loss with a small lactate peak on MR spectroscopy in the basal ganglia.	No	14 y (deceased), profound ID (no walking, no language), pharmaco-resistant epilepsy, NGF	Compound heterozygous c.2025dup; p.Asp676* c.986T>C; p.Leu329 Pro	Intermittently increased serum L
	4	F	3	DD, right mild hemiplegia	Birth	DD, Seizures (spasms),	Cataract (6 m) Glaucoma 26 y	No	scoliosis	Volume loss involving the caudate nuclei, globus pallidi and putamina. T2 flair hyperintensities involving the basal ganglia	No	26 y, profound ID (no walking, no language), pharmaco-resistant seizures.	Compound heterozygous c.2025dup; p.Asp676* c.986T>C; p.Leu329 Pro	Increased serum and CSF L

CAGSSS: cataracts, growth hormone deficiency, sensory neuropathy, sensorineural hearing loss, and skeletal dysplasia syndrome; CC: corpus callosum; CSF: cerebrospinal fluid; DD: developmental delay; F: female; GH: growth hormone; ID: intellectual disability; L: lactate; M: male; m: months; NGF: naso-gastric feeding; NK: not known; P: pyruvate; SD: standard deviation; SEMD: Spondylo-epi-metaphyseal dysplasia; WM: white matter; y: years. *IARS2* cDNA accession number is NM_018060.3.

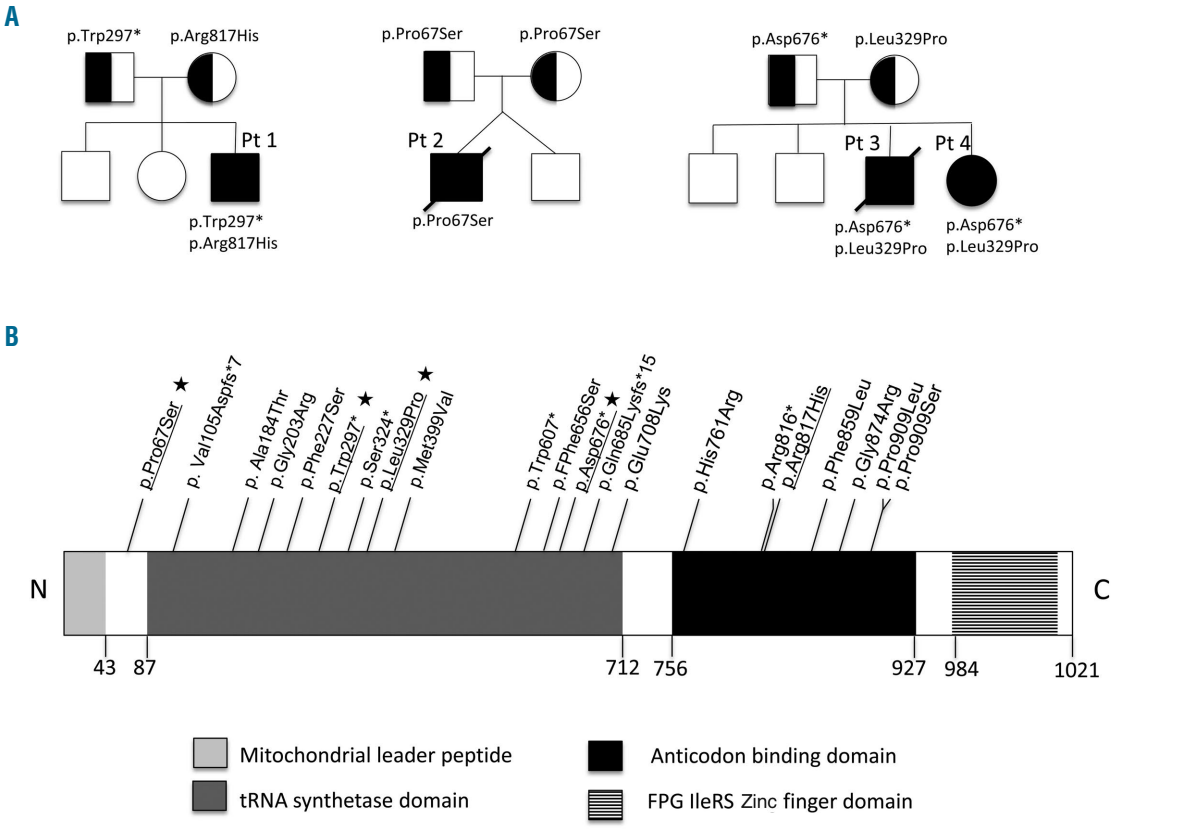


Figure 2. Pedigrees of the reported families and pathogenic variants described in the *IARS2* gene. (A) Pedigrees, segregation and localization of the pathogenic *IARS2* variants. (B) Linear map of the reported pathogenic *IARS2* variants. Important structural domains and their locations on the protein map are shown. Amino acid location of each reported pathogenic variant is indicated (NM_018060.3). The likely pathogenic variants reported in this article are underlined and, if novel, indicated by a star.

the anticodon binding domain, and a missense variant inherited from his mother (c.2450G>A, p. Arg817His). The p. Arg817His variant has been previously reported in four patients with Leigh syndrome.[5,8]

Patient 2 was born from non-consanguineous healthy parents from Sri Lanka, at 31 weeks of gestation by cesarean section for cardiac rhythm anomalies after a dichorionic twin pregnancy (Apgar score 3, 6 and 7). His brother had no fetal distress and was healthy. He presented with respiratory distress and anemia at birth (hemoglobin 3.9 g/dL, normal 9-14 g/dL; MCV 84 fl). He needed transfusions at days 54, 69, 76 and 79. Thrombocytopenia was also present at birth (115 platelets/mm^3 with a nadir at 50, normal >150.000) and myelogram showed 3.7% of ringed sideroblasts (Figure 1E). His plasma lactate was elevated (3.6-9.7 mmol/L, normal <2 mmol/L). A complete metabolic work-up, including plasma amino acids and vitamin B12 and urinary organic acids was normal. Brain MRI showed mild, diffuse white matter hyperintensities (Figure 1B). He was referred to the intensive care unit for mechanical ventilation. At day 54, he presented with pericardial effusion in the context of severe biventricular hypertrophic cardiomyopathy. He died at 2,5 months due to bradycardia.

Whole exome sequencing identified a homozygous variant in the IARS2 gene (c.199C>T; p. Pro67Ser). This variant, absent in publicly available databases, is highly conserved through evolution and predicted to be damaging by *in silico* softwares (Figure 1B).

Patient 3, the last of four siblings, was born at 33 weeks gestation by emergency caesarean section due to reduced fetal movements (Apgar score 1, 5 and 6). His elder sister (patient 4, see pedigree in Figure 2) had a mild left intra-ventricular bleed on an early cranial ultrasound and was diagnosed with bilateral cataracts at 6 months. She was found to have global developmental delay and infantile spasms at 32 months of age with hypsarrhythmia on EEG. Her MRI neuroimaging showed volume loss involving caudate nuclei, globi pallidi and putamina, T2 flair hyperintensities of basal ganglia with no evidence of lactate doublet on nuclear magnetic resonance (NMR) spectroscopy. No cardiac or hematological involvement were noted and her bone marrow biopsy was unremarkable.

Patient 3 required ventilation for 2 weeks and developed profound anemia (hemoglobin nadir 3.1g/dL) and severe cardiomegaly with poor cardiac function. At 4.5 months (11 weeks corrected), he was diagnosed with bilateral cataracts. At 18 months of age, he presented with a first metabolic crisis in the context of pneumonia associated with profound hypotonia, severe anemia and elevated lactate. He developed persistent oropharyngeal incoordination that necessitated gastrostomy. At 2.5 years, he developed refractory tonic seizures and an EEG demonstrated frequent bilateral spike-wave discharges. He was able to smile and acquired head control but was unable to sit unsupported.

At 4 years of age, the transfusion-dependent anaemia relapsed (hemoglobin nadir 3.5g/dL). Bone marrow aspiration showed subnormal myelopoiesis and megakaryopoiesis but marked erythroid hypoplasia and dysplasia with an increased number of progenitors, vacuolation

and basophilic stippling. Iron staining showed ring sideroblasts in 10% of erythroid cells. He went on to develop mild concentric left ventricular hypertrophy, glaucoma, constipation, scoliosis and mixed central/obstructive sleep apnoea requiring non-invasive ventilation therapy. Brain MRI at 16 months of age demonstrated bilateral hyperintensities of caudate nuclei and putamen. Subsequent neuroimaging showed global cerebral and basal ganglia volume loss with bilateral putamina cavitation, characteristic of Leigh disease and a small lactate peak on NMR spectroscopy in basal ganglia (Figure 1C). Plasma lactate was intermittently elevated (up to 3.3 mmol/L, normal 0.6-2.4 mmol/L) but biochemical work-up was otherwise normal. He died from central respiratory failure at the age of 14 years. In patient 3 and 4, whole exome sequencing identified two compound heterozygous variants in *IARS2*; a paternally inherited nonsense variant (c.2025dup; p. Asp676*) predicted to result in either NMD or loss of the terminal two thirds of the protein including anticodon binding domain; and a maternally inherited missense variant (c.986T>C; p. Leu329Pro) modifying a mildly conserved residue. Neither of these variants have been reported to date.

Respiratory chain enzyme activities were normal in the liver, skeletal muscle or lymphocytes of patients 1 and 3 (Table). Blue native polyacrylamide gel electrophoresis of respiratory enzyme chain complexes was normal in cultured skin fibroblasts of patient 1 (*not shown*). No mitochondrial DNA (mtDNA) deletions or rearrangements were found in circulating leukocytes and bone marrow of patients 1 to 3 (Table).

Here, we report on three unrelated patients presenting with sideroblastic anemia, initially suggestive of Pearson Marrow-Pancreas syndrome. The absence of mtDNA deletion or complex rearrangements prompted to reconsider this diagnosis and to eventually identify biallelic pathogenic *IARS2* variants in the three patients. Children with Pearson syndrome usually present with bone marrow failure and exocrine pancreatic dysfunction in the first year of life. They have macrocytic sideroblastic anemia with ringed sideroblasts detected by iron staining of the bone marrow. This transfusion-dependent condition is accompanied by thrombocytopenia and neutropenia. The disease gradually worsens and multisystem involvement occurs, including failure to thrive, liver failure, hypotonia and lactic acidosis. Survival and spontaneous recovery from bone marrow dysfunction after several years is possible, with a transition to clinical manifestations of Kearns-Sayre syndrome.[9] Pearson syndrome is caused by a single large-scale mitochondrial DNA deletion.[10]

At variance with Pearson syndrome, our patients had a low level of ring sideroblasts in blood marrow aspiration, and presented with an early extra-hematological involvement (cardiomyopathy, cataract, and neurological involvement).

Pearson syndrome is not the unique cause of sideroblastic anemia in respiratory chain deficiency. In fact, sideroblastic anemia has been associated with pathogenic variants in other mitochondrial proteins, namely SLC25A38, PUS1, ABCB7, GLRX5, NDUFB11, COX10, HSPA9, TRNT1 and ATP6.[11] Moreover, congenital sideroblastic anemia has been associated with mutations in two other mitochondrial *ARS2* genes, namely *YARS2* and *LARS2*.[12-14]

IARS2 mutations were first identified in patients with CAGSSS, then in patients with Leigh syndrome, and more recently in patients with cataract. To date, 18 patients have been reported with a broad range of partially overlapping symptoms (Table 1).[3-8]

Our report expands the clinical spectrum of *IARS2*-related disorders to early-onset sideroblastic anemia mimicking Pearson syndrome. It adds *IARS2* to the list of mitochondrial disease genes underlying sideroblastic anemia in early childhood. Future studies will hopefully help in identifying the actual impact of respiratory chain deficiency on human erythropoiesis and explaining why sideroblastic anemia is a frequent, yet inconstant feature in mitochondrial disorders.

Giulia Barcia,[1] Dinusha Panditha[2] Benedetta Ruzzenente,[3] Zahra Assouline,[1] Alessandra Pennisi,[1] Clothilde Ormieres,[1] Claude Besmond,[4] Charles-Joris Roux,[5] Nathalie Boddaert,[5] Isabelle Desguerre,[6] David R. Thorburn,[7,8] Drago Bratkovic,[2] Arnold Munnich,[1-3] Jean-Paul Bonnefont,[1-3] Agnès Rötig[3] and Julie Steffann[1-3]

[1]Federation of Medical Genetics and Reference Center for Mitochondrial Diseases (CARAMMEL), Hospital Necker - Enfants Malades, Paris, France; [2]Metabolic Clinic, Women's and Children's Hospital, North Adelaide, South Australia, Australia; [3]Laboratory for Genetics of Mitochondrial Disorders, UMR 1163, Université de Paris, Institut Imagine, Paris, France; [4]Translational Genetics Laboratory, UMR U1163, Institut Imagine, Université Paris Descartes-Sorbonne Paris Cité, Paris, France; [5]Department of Pediatric Radiology, Hospital Necker Enfants Malades, Paris, France; [6]Department of Pediatric Neurology, Hospital Necker-Enfants Malades, Paris, France; [7]Murdoch Children's Research Institute and Victorian Clinical Genetics Services, Royal Children's Hospital, Melbourne, Victoria, Australia and [8]Department of Pediatrics, University of Melbourne, Melbourne, Victoria, Australia

Correspondence: GIULIA BARCIA - giulia.barcia@aphp.fr

doi:10.3324/haematol.2020.270710

Disclosures: no conflicts of interest to disclose.

Contributions: GB performed molecular researchs, data analysis and wrote the manuscript; AM supervised this study, performed clinical evaluation, and wrote the manuscript. BR performed data analysis; ZA and CB performed the molecular study; DP, AP, CO, ID performed clinical follow-up; CJR and NB performed neuro-imaging analysis; DRT, DB, JPB, AR, JS performed data analysis and supervised the study.

References

1. Meyer-Schuman R, Antonellis A. Emerging mechanisms of aminoacyl-tRNA synthetase mutations in recessive and dominant human disease. Hum Mol Genet. 2017;26(R2):R114-R127.
2. Konovalova S, Tyynismaa H. 2013. Mitochondrial aminoacyl-tRNA synthetases in human disease. Mol Genet Metab. 2013;108(4):206-211.
3. Schwartzentruber J, Buhas D, Majewski J, et al. Mutation in the nuclear-encoded mitochondrial isoleucyl-tRNA synthetase IARS2 in patients with cataracts, growth hormone deficiency with short stature, partial sensorineural deafness, and peripheral neuropathy or with Leigh syndrome. Hum Mutat. 2014;35(11):1285-1289.
4. Moosa S, Haagerup A, Gregersen PA, et al. Confirmation of CAGSSS syndrome as a distinct entity in a Danish patient with a novel homozygous mutation in IARS2. Am J Med Genet A. 2017; 173(4):1102-1108.
5. Takezawa Y, Fujie H, Kikuchi A, et al. Novel IARS2 mutations in Japanese siblings with CAGSSS, Leigh, and West syndrome. Brain Dev. 2018;40(10):934-938.
6. Vona B, Maroofian R, Bellacchio E, et al. Expanding the clinical phenotype of IARS2-related mitochondrial disease. BMC Med Genet. 2018;19(1):196.
7. Li J, Leng Y, Han S, et al. Clinical and genetic characteristics of Chinese patients with familial or sporadic pediatric cataract. Orphanet J Rare Dis. 2018;13(1):94.
8. Lee JS, Kim MJ, Kim SY, et al. Clinical and genetic characteristics of Korean patients with IARS2 related disorders. J Genet Med. 2019;16(2):55-61.
9. Pearson HA, Lobel JS, Kocoshis SA, et al. A new syndrome of refrac-

tory sideroblastic anemia with vacuolization of marrow precursors and exocrine pancreatic dysfunction. J Pediatr. 1979;95(6):976-984.
10. Rotig A, Colonna M, Bonnefont P, et al. Mitochondrial DNA deletion in Pearson's marrow/pancreas syndrome. Lancet. 1989; 333 (8643):902-903.
11. Tesarova M, Vondrackova A, Stufkova H, et al. Sideroblastic anemia associated with multisystem mitochondrial disorders. Pediatr Blood Cancer. 2019;66(4):e27591.
12. Riley LG, Cooper S, Hickey P, et al. Mutation of the mitochondrial tyrosyl−tRNA synthetase gene, YARS2, causes myopathy, lactic acidosis, and sideroblastic anemia–MLASA syndrome. Am J Hum Genet. 2010;87(1):52-59.
13. Riley LG, Rudinger-Thirion J, Schmitz-Abe K, et al. LARS2 variants associated with hydrops, lactic acidosis, sideroblastic anemia, and multisystem failure. JIMD Rep. 2016;28:49-57.
14. Long Z, Li H, Du Y, Han B. Congenital sideroblastic anemia: advances in gene mutations and pathophysiology. Gene. 2018; 668:182-189.

Comment on "Combining brentuximab vedotin with dexamethasone, high-dose cytarabine and cisplatin as salvage treatment in relapsed or refractory Hodgkin lymphoma: the phase II HOVON/LLPC Transplant BRaVE study."

The high-dose cytarabine-containing regimen with dexamethasone, cytarabine and cisplatin (DHAP) had been predominantly used in Europe as standard salvage chemotherapy for relapsed or refractory (R/R) classical Hodgkin lymphoma (c-HL) until the recent introduction of brentuximab vedotin (Bv), an anti-CD30 antibody conjugated to the potent antimicrotubule agent monomethyl auristatin-E.[1] Real-world experience shows a gradual transition from traditional cytotoxic agent-based treatment to selectively active agent-based treatment for R/R c-HL;[2] in clinical practice, Bv was the first agent to be used for this purpose. However, the slight decline in the number of increased rates of metabolic complete response (mCR), as assessed by [18F] fluorodeoxyglucose (FDG)-positron emission tomography (PET)/computed tomography (CT) scan, after Bv exposure as single agent, has raised questions about its efficacy and widespread adoption in the R/R c-HL setting.[2]

We read with great interest the study by Kersten *et al*. published ahead of print in this journal.[3] In their multicenter, international phase II study, between 2014 and 2017, 52 adult patients (median age: 29 years) with R/R c-HL received Bv plus DHAP with the aim of testing the possibly enhanced cyto-destructive potency against Hodgkin and Reed-Sternberg (HRS) cells from this combination. Hospitalized patients received three 21-day cycles of Bv 1.8 mg/kg on day 1 and DHAP (dexamethasone 40 mg on days 1-4, cisplatin 100 mg/m^2 in continuous intravenous infusion [i.v.] for 24 hours on day 1 and cytarabine 2 x 2 g/m^2) on day 2; treatment-related adverse events were also evaluated. Despite several adverse prognostic factors (advanced-stage disease in 54% of patients, primary refractory disease in 43% of patients, and relapses within 1-year from first-line treatment in 29% of patients), Bv combined with DHAP resulted in mCR rates (according to the Lugano classification, 2014 criteria) of 81%, and grade ≥3 toxicity (prevalently consisting of febrile neutropenia according to the National Cancer Institute Common Terminology Criteria for Adverse Events [CTCAE], version 4.03) in only 22% of patients. Subsequently, 47 of 52 patients (90%) received high-dose chemotherapy and hematopoietic stem cell transplantation (HSCT); after a median follow up of 27 months, the progression-free survival (PFS) was 74%. The authors, supported by the evidence of a higher proportion of patients with mCR at 2-years than traditional salvage regimens, concluded that, in R/R c-HL, three cycles of Bv-DHAP are impressively effective and greatly lower costs (using only 3 administrations of Bv).

Several attempts have been made in the R/R c-HL setting to define the best partner(s) that could synergize with Bv.[4-6] Clinical trials conducted in this setting present convincing evidence that increasing the dosage of bendamustine had good anti-cancer activity with no dose-limiting toxicity.[7] Improvements in anti-lymphomatous potency occurred especially when Bv infusion was followed by increasing doses of bendamustine, most likely due to an enhanced synergistic effect which was perceived as a great advantage in this subset. Emerging *in vitro* data suggest that high-dose bendamustine administered immediately after Bv facilitated intracellular trafficking, internalization, and metabolism of antiCD30-auristatin conjugates, and thus targeted delivery of anticancer therapeutics.[8] We have published[9,10] encouraging preliminary single-center efficacy and safety results of a new salvage regimen named Bv+Bs-21 for R/R c-HL; this consists of 3-days outpatient i.v. infusions of 1.8 mg/kg of brentuximab vedotin on day 1 of each 3-week cycle combined in sequence to bendamustine supercharge on days 2 and 3 of the treatment cycle at a fixed dose of 120 mg/m^2 per day, for a total of four courses. Mature results (in terms of larger patient numbers and longer follow-up than in the previously published study[9,10]) are now available. These are characterized by a prospective series of 30 patients (median age: 44 years; range: 23-59 years) receiving Bv+Bs-21 for R/R c-HL during the period from 2013 to 2020 at the Hematology Unit of the Federico II University of Naples, Italy, whose clinical presentations were more aggressive (>3 lines of previous treatment in 75% of patients, primary refractory disease in 70% of patients, autologous HSCT failure in 35% of patients) compared to those in the Kersten *et al*.[3] study. All patients underwent four courses of Bv+Bs-21; median-dose intensity during sequential therapy was 100% (range: 88.6-102.4%) for Bv and 100% (range: 88.7-102.4%) for Bs. A vigorous support drug treatment (especially premedication prior to Bs administration, and antimicrobial drugs) and clinical and laboratory monitoring were systematically performed in all cases. Ten patients (33%) experienced grade ≥3 treatment-related adverse events (according to the CTCAE, version 4.03) consisting of cytomegalovirus reactivation (with viremia [median CMV-DNA: 1,810 IU/mL; range: 620-170,000 IU/mL] with fever, which was successfully treated with pre-emptive therapy with valganciclovir) in seven cases and neutropenia in three cases; all resolved without requiring hospitalization. At post-Bv+Bs-21 re-evaluation, 100% of patients had deep metabolic responses with Deauville 5-point scale scores ≤3 at FDG-PET/CT scans. Thereafter, four patients (13%) received two additional courses of Bv+Bs-21, five patients (17%) received allogeneic HSCT, and the remaining 21 patients (70%) received autologous HSCT. In this last sub-group, for 12 patients, peripheral blood stem cells (PBSC) were previously harvested after two courses of ifosfamide, gemcitabine, vinorelbine and prednisolone; in the remaining nine cases, PBSC were successfully collected after Bv+Bs-21, with mobilization with G-CSF, vinorelbine-cyclophosphamide and/or plerixafor regimen. The median peak value of CD34$^+$ cells was reached on day 12 after mobilization (median number of harvested CD34$^+$ cells: 3.1x10^6 per kilogram of body weight; range: 1.6-4.2x10^6). After HSCT, the median day of engraftment of neutrophils and platelets was recorded on day 11 (range: 9-21 days) and day 12 (range: 9-25 days), respectively. At a median follow up of 36 months (range: 1-83 months) from the end of the Bv+Bs-21 regimen, the estimated 3-year PFS of the entire population was 94% (95% confidence interval: 84.4-100%).

In conclusion, our clinical data indicate that bendamustine (an old and low-cost cytotoxic agent) used in a new schedule modality (i.e., administered at increased dose and after the first-in-class antibody drug conjugate targeting CD30) has highly synergistic activity in outpatient salvage regimen against R/R HRS cells of patients aged <60 years.

Marco Picardi and Claudia Giordano

Department of Clinical Medicine and Surgery, Hematology Unit, Federico II University Medical School, Naples, Italy

Correspondence: CLAUDIA GIORDANO -

claudiagiordano91@hotmail.com

doi:10.3324/haematol.2020.278203

Disclosures: no conflicts of interest to disclose.

Contributions: MP and CG performed research; MP wrote the manuscript; FP supervised the study.

References

1. Younes A, Bartlett NL, Leonard JP, et al. Brentuximab vedotin (SGN-35) for relapsed CD30-positive lymphomas. N Engl J Med. 2010;363(19):1812-1821.
2. Connors JM. Hodgkin lymphoma: outsmarting HRS cells. Blood. 2020;136(21):2362-2364.
3. Kersten MJ, Driessen J, Zijlstra JM, et al. Combining brentuximab vedotin with dexamethasone, high-dose cytarabine and cisplatin as salvage treatment in relapsed or refractory Hodgkin lymphoma: the phase II HOVON/LLPC Transplant BRaVE study. Haematologica. 2020 Apr 9. [Epub ahead of print] doi:haematol.2019.243238.
4. Moskowitz AJ, Schröder H, Yahalom J, et al. PET-adapted sequential salvage therapy with brentuximab vedotin followed by augmented ifosfamide, carboplatin, and etoposide for patients with relapsed and refractory Hodgkin's lymphoma: a non-randomised, open-label, single-centre, phase 2 study. Lancet Oncol. 2015;16(3):284-292.
5. LaCasce AS, Bociek RG, Sawas A, et al. Brentuximab vedotin plus bendamustine: a highly active first salvage regimen for relapsed or refractory Hodgkin lymphoma. Blood. 2018;132(1):40-48.
6. Garcia-Sanz R, Sureda A, de la Cruz F, et al. Brentuximab vedotin and ESHAP is highly effective as second-line therapy for Hodgkin lymphoma patients (long-term results of a trial by the Spanish GELTAMO Group). Ann Oncol. 2019;30(4):612-620.
7. Cohen JB, Wei L, Maddocks KJ, et al. Gemcitabine and bendamustine is a safe and effective salvage regimen for patients with recurrent/refractory Hodgkin lymphoma: results of a phase 1/2 study. Cancer. 2020;126(6):1235-1242.
8. De Filippi R, Cillo M, Crisci S, et al. Continuous exposure to bendamustine (BDM) results in stable upregulation of CD30 and increased sensitivity to brentuximab vedotin (BV) in tumor cells of Hodgkin lymphoma (HL). Blood. 2015;126(23):2479.
9. Picardi M, Della Pepa R, Giordano C, et al. Brentuximab vedotin followed by bendamustine supercharge for refractory or relapsed Hodgkin lymphoma. Blood Adv. 2019;3(9):1546-1552.
10. Della Pepa R, Picardi M, Pugliese N, et al. Brentuximab vedotin followed by bendamustine supercharge for refractory or relapsed Hodgkin lymphoma: mature results of a monocentric prospective trial. Haematologica. 2020;105(s2):S101-102.

A real world multicenter retrospective study on extramedullary disease from Balkan Myeloma Study Group and Barcelona University: analysis of parameters that improve outcome

Meral Beksac,[1] Guldane Cengiz Seval,[1] Nicholas Kanellias,[2] Daniel Coriu,[3] Laura Rosiñol,[4] Gulsum Ozet,[5] Vesselina Goranova-Marinova,[6] Ali Unal,[7] Jelena Bila,[8] Hayri Ozsan,[9] Arben Ivanaj,[10] Lejla Ibricevic Balić,[11] Efstathios Kastritis,[2] Joan Bladé,[4] Meletios Athanasios Dimopoulos[2]

[1]Department of Hematology, School of Medicine, Ankara University, Ankara, Turkey; [2]Department of Clinical Therapeutics, National and Kapodistrian University of Athens, School of Medicine, Athens, Greece; [3]University of Medicine and Pharmacy "Carol Davila", Fundeni Clinical Institute, Bucharest, Romania; [4]Hospital Clinic, IDIBAPS, Barcelona, Spain; [5]Clinic of Hematology, Ankara Numune Education and Research Hospital, Ankara, Turkey; [6]University Hospital "Sv. Georgi" and Medical University Plovdiv, Plovdiv, Bulgaria; [7]Department of Hematology, School of Medicine, Erciyes University, Kayseri, Turkey; [8]Faculty of Medicine, University of Belgrade, Belgrade, Serbia; [9]Department of Hematology, School of Medicine, Dokuz Eylül University, Izmir, Turkey; [10]University of Medicine Tirana, Tirana, Albania and [11]Clinical Center of Sarajevo University, Sarajevo, Bosnia and Herzegovina

Published in Haematologica 2020;105(1):201-208.

doi:10.3324/haematol.2020.278272

©2021 Ferrata Storti Foundation

We have noticed an error in the progression-free survival of patients with extramedullary plasmacytoma in our article published in Haematologica in January 2020 (doi: HAEMATOL/2019/219295).

The following sentence in the abstract:

"Extramedullary plasmacytoma at relapse had the worst prognosis with a PFS of 13.6 months and overall survival of 11.4 months."

Should be replaced by:

"Extramedullary plasmacytoma at relapse had the worst prognosis with a PFS of 9.1 months and overall survival of 11.4 months."

Likewise, on page 205, the following sentence:

"However, if diagnosed at relapse, PFS and OS were 13.6 months and 11.4 months for EMP compared to 20.9 months (*P*=0.249) and 39.8 months (*P*=0.093) for PO, respectively (Table 2 and Figure 1)."

Should be replaced by:

"However, if diagnosed at relapse, PFS and OS were 9.1 months and 11.4 months for EMP compared to 20.9 months (*P*=0.249) and 39.8 months (*P*=0.093) for PO, respectively (Table 2 and Figure 1)."

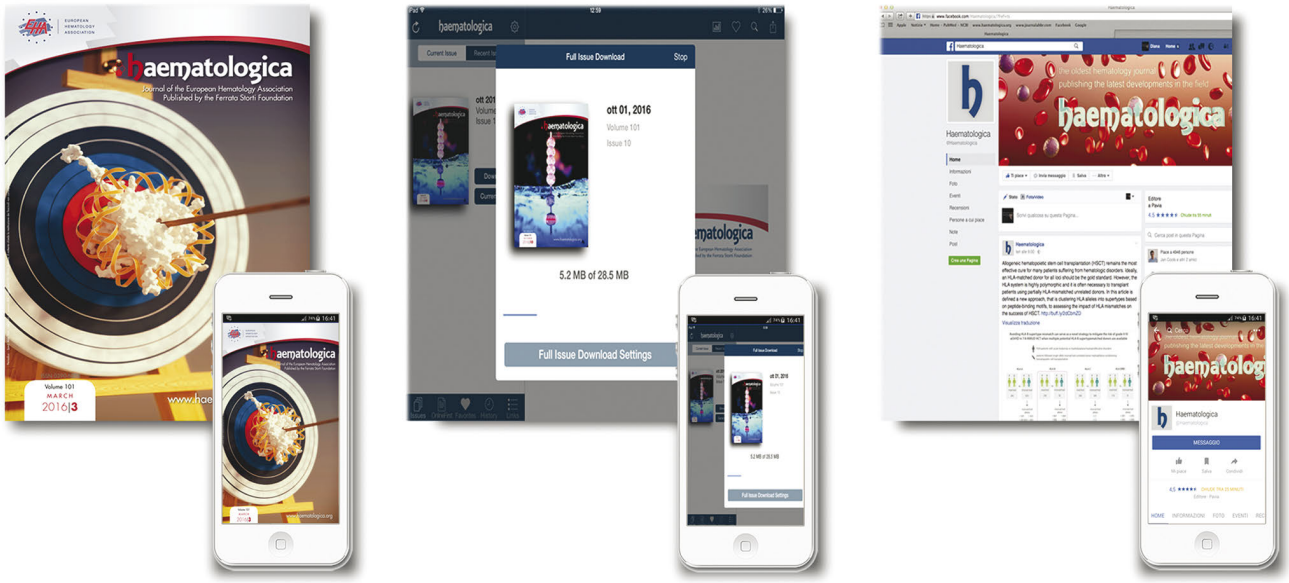
The error was also present in Table 2.
The corrected Table 2 is shown below.

Table 2. Comparison of response, survival outcomes of extramedullary plasmacytomas (EMP) or paraosseous (PO) patients either at diagnosis or at relapse.

	CR (%)		PFS (mos)		OS (mos)	
EMP						
diagnosis (n=92)	19.3		38.9 (95% CI: 23.6-54.2)	*P*<0.001	46.5 (95% CI: 25.5-67.5)	*P*<0.001
relapse (n=84)	9	*P*=0.034	9.1 (95% CI: 11.6-15.6)		11.4 (95% CI:*.6-16.2)	
PO						
diagnosis (n=38)	34.2	*P*=0.001	51.7 95% CI: 13.5-89.9)	*P*=0.005	NR	*P*<0.001
relapse (n=12)	54.5		20.9 (95% CI: 10.3-31.5)		39.8 (95% CI: 12.7-66.9)	

CR: complete remission; PFS: progression-free survival; OS: overall survival; n: number.

RESEARCH, READ & CONNECT



We reach more than
6 hundred thousand readers each year

The first Hematology Journal in Europe

Impressions YTD

14,171,734

Digital Readers

4,908

Total Audience

558,982

Worldwide rank	Impact factor	Total citations
7 th	7.116	10,831

haematologica

Journal of the Ferrata Storti Foundation

www.haematologica.org

haematologica — Vol. 106 n. 4 — April 2021 — 925-1228